

EMF-2103(NP)(A)
Revision 0

Realistic Large Break LOCA Methodology for Pressurized Water Reactors

April 2003

Framatome ANP Richland, Inc.

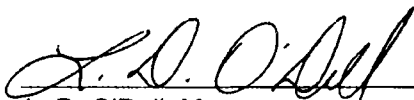
ISSUED IN FRA-ANP ON-LINE
DOCUMENT SYSTEM
DATE: 08/23/01

ISSUED IN FRA-ANP ON-LINE
DOCUMENT SYSTEM
DATE: 9-15-03

EMF-2103(NP)
Revision 0

**Realistic Large Break LOCA Methodology for
Pressurized Water Reactors**

Prepared:



L. D. O'Dell, Manager
U.S. and Far East Research & Technology

8/22/01
Date

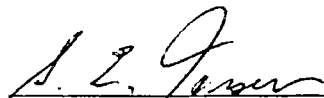
Concurred:



R. P. Martin, Engineer
Safety Analysis Methods

8/22/01
Date

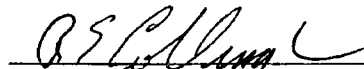
Concurred:



S. E. Jensen, Team Leader
Safety Analysis Methods

8/22/01
Date

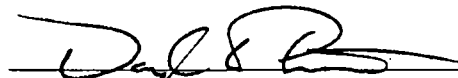
Approved:



R. E. Collingham, Manager
BWR Reload Engineering & Methods Development

8/22/01
Date

Approved:



D. W. Pruitt, Manager
Safety Analysis Methods

8/22/01
Date

Approved:



R. C. Gottula, Manager
PWR Safety Analysis

8/22/01
Date

Approved:



J. F. Mallay, Director
Regulatory Affairs

8/22/01
Date

/lmk

U.S. Nuclear Regulatory Commission Report Disclaimer

Important Notice Regarding the Contents and Use of This Document

Please Read Carefully

This technical report was derived through research and development programs sponsored by Framatome ANP Richland, Inc. It is being submitted by Framatome ANP Richland, Inc. to the U.S. Nuclear Regulatory Commission as part of a technical contribution to facilitate safety analyses by licensees of the U.S. Nuclear Regulatory Commission which utilize Framatome ANP Richland, Inc. fabricated reload fuel or technical services provided by Framatome ANP Richland, Inc. for light water power reactors and it is true and correct to the best of Framatome ANP Richland, Inc.'s knowledge, information, and belief. The information contained herein may be used by the U.S. Nuclear Regulatory Commission in its review of this report and, under the terms of the respective agreements, by licensees or applicants before the U.S. Nuclear Regulatory Commission which are customers of Framatome ANP Richland, Inc. in their demonstration of compliance with the U.S. Nuclear Regulatory Commission's regulations.

Framatome ANP Richland, Inc.'s warranties and representations concerning the subject matter of this document are those set forth in the agreement between Framatome ANP Richland, Inc. and the Customer pursuant to which this document is issued. Accordingly, except as otherwise expressly provided in such agreement, neither Framatome ANP Richland, Inc. nor any person acting on its behalf:

- a. makes any warranty, or representation, express or implied, with respect to the accuracy, completeness, or usefulness of the information contained in this document, or that the use of any information, apparatus, method, or process disclosed in this document will not infringe privately owned rights;
- or
- b. assumes any liabilities with respect to the use of, or for damages resulting from the use of, any information, apparatus, method, or process disclosed in this document.



UNITED STATES
NUCLEAR REGULATORY COMMISSION

WASHINGTON, D.C. 20555-0001

April 9, 2003

Mr. James F. Mallay
Director, Regulatory Affairs
Framatome ANP, Richland, Inc.
2101 Horn Rapids Road
Richland, WA 99352

SUBJECT: SAFETY EVALUATION ON FRAMATOME ANP TOPICAL REPORT
EMF-2103(P), REVISION 0, "REALISTIC LARGE BREAK LOSS-OF-COOLANT
ACCIDENT METHODOLOGY FOR PRESSURIZED WATER REACTORS"
(TAC NO. MB7554)

Dear Mr. Mallay:

By letter dated August 20, 2001, Framatome ANP submitted Topical Report EMF-2103(P), Revision 0, "Realistic Large Break LOCA Methodology for Pressurized Water Reactors," for NRC staff review and approval.

The NRC staff has completed its review of the topical report and Framatome ANP's response to the staff's request for additional information (RAI) with regard to the analysis of large break loss-of-coolant accident (LOCA) events in pressurized water reactors of the Westinghouse 3- and 4-loop and Combustion Engineering 2x4 designs. The NRC staff's safety evaluation describes the S-RELAP5 analysis code and the assessment of the code's capabilities based on application of the Code Scaling, Applicability, and Uncertainty (CSAU) evaluation methodology. The report is acceptable for referencing in licensing applications to the extent specified and under the limitations delineated in the report and in the associated NRC staff's safety evaluation, which is enclosed. The safety evaluation defines the basis for acceptance of the topical report.

The subject topical report and supporting documentation has been reviewed by the Advisory Committee on Reactor Safeguards which has agreed with the staff's recommendation for approval by its letter of December 20, 2002.

If the NRC staff's criteria or regulations change so that its conclusion in this letter, that the topical report is acceptable, is invalidated, Framatome ANP and/or the applicant or licensee referencing the topical report will be expected to revise and resubmit its respective documentation, or submit justification for the continued applicability of the topical report without revision of the respective documentation.

Accordingly, use of the subject Framatome ANP methodology is acceptable for referencing in licensing submittals subject to the following conditions and limitations as discussed in the safety evaluation:

- The model applies to 3 and 4 loop Westinghouse- and CE-designed nuclear steam systems.

- The model applies to bottom reflood plants only (cold side injection into the cold legs at the reactor coolant discharge piping).
- The model is valid as long as blowdown quench does not occur. If blowdown quench occurs, additional justification for the blowdown heat transfer model and uncertainty are needed if the calculation is corrected. A blowdown quench is characterized by a temperature reduction of the peak cladding temperature (PCT) node to saturation temperature during the blowdown period.
- The reflood model applies to bottom-up quench behavior. If a top-down quench occurs, the model is to be justified or corrected to remove top quench. A top-down quench is characterized by the quench front moving from the top to the bottom of the hot assembly.
- The model does not determine whether Criterion 5 of 10 CFR 50.46, long term cooling, has been satisfied. This will be determined by each applicant or licensee as part of its application of this methodology.
- Specific guidelines must be used to develop the plant-specific nodalization. Deviations from the reference plant must be addressed.
- A table that contains the plant-specific parameters and the range of the values considered for the selected parameter during the topical report approval process must be provided. When plant-specific parameters are outside the range used in demonstrating acceptable code performance, the licensee or applicant will submit sensitivity studies to show the effects of that deviation.
- The licensee or applicant using the approved methodology must submit the results of the plant-specific analyses, including the calculated worst break size, PCT, and local and total oxidation.
- Applicants or licensees wishing to apply the Framatome ANP realistic large break loss-of-coolant accident (RLBLOCA) methodology to M5 clad fuel must request an exemption for its use until the planned rulemaking to modify 10 CFR 50.46(a)(i) to include M5 cladding material has been completed.

The review of the models and benchmarks noted concerns and deficiencies resulting in conditions of use of S-RELAP5 as follow, which have been committed to in a letter from Framatome ANP to NRC dated December 20, 2002:

- A CCFL violation warning will be added to alert the analyst to CCFL violation in the downcomer should such occur.
- Framatome ANP has agreed that it is not to use nodalization with hot leg to downcomer nozzle gaps.
- If Framatome ANP applies the RLBLOCA methodology to plants using a higher planar linear heat generation rate (PLHGR) than used in the current analysis, or if the

methodology is to be applied to an end-of-life analysis for which the pin pressure is significantly higher, then the need for a blowdown clad rupture model will be reevaluated. The evaluation may be based on relevant engineering experience and should be documented in either the RLBLOCA guideline or plant specific calculation file.

- Slot breaks on the top of the pipe have not been evaluated. These breaks could cause the loop seals to refill during late reflood and the core to uncover again. These break locations are an oxidation concern as opposed to a PCT concern, since the top of the core can remain uncovered for extended periods of time. Should an analysis be performed for a plant with loop seals with bottom elevations that are below the top elevation of the core, Framatome ANP will evaluate the effect of the deep loop seal on the slot breaks. The evaluation may be based on relevant engineering experience and should be documented in either the RLBLOCA guideline or plant-specific calculation file.


In accordance with the guidance provided on the NRC's website, we request that Framatome ANP publish an accepted version within 3 months of receipt of this letter. The accepted version shall incorporate (1) this letter and the enclosed SE between the title page and the abstract, (2) all RAIs from the NRC staff and all associated responses, and (3) a "-A" (designating accepted") following the report identification symbol.

We have determined that the enclosed safety evaluation does not contain proprietary information as defined in 10 CFR 2.790. However, we will delay placing the safety evaluation in the public document room for a period of ten working days from the date of this letter to provide you with the opportunity to comment on the proprietary aspects only. If you believe that any information in the enclosure is proprietary, please identify such information line by line and define the basis for such claim pursuant to 10 CFR 2.790.

Our acceptance applies only to matters approved in the report. On the basis of our review of the topical report and our finding as to its acceptability, we will review license applications that reference the report to ensure that the material presented applies to the specific plant involved.

In the event that any comments or questions arise, please contact Drew Holland at (301) 415-1436.

Sincerely,



Herbert N. Berkow, Director
Project Directorate IV
Division of Licensing Project Management
Office of Nuclear Reactor Regulation

Project No. 693

Enclosure: Safety Evaluation



UNITED STATES
NUCLEAR REGULATORY COMMISSION
WASHINGTON, D.C. 20555-0001

SAFETY EVALUATION BY THE OFFICE OF NUCLEAR REACTOR REGULATION

TOPICAL REPORT EMF-2103(P), REVISION 0

"REALISTIC LARGE BREAK LOCA METHODOLOGY FOR
PRESSURIZED WATER REACTORS"

PROJECT NO. 693

1.0 INTRODUCTION

On August 20, 2001, Framatome ANP submitted EMF-2103(P), Revision 0 (Reference 1), for NRC staff review and approval for application of the S-RELAP5 thermal-hydraulic analysis computer code to the realistic large break loss-of-coolant accident (RLBLOCA) in Westinghouse and Combustion Engineering (CE) pressurized water reactors (PWRs) as detailed in References 3 through 7.

Framatome ANP stated that its goal is to apply a single computer code to the analysis of both LOCA and non-LOCA transient events. The NRC staff has previously reviewed and approved application of the S-RELAP5 code to Title 10, *Code of Federal Regulations* (10 CFR) Part 50, Appendix K, small break LOCA (SBLOCA) events (Reference 8), as well as certain non-LOCA Standard Review Plan (SRP) Chapter 15 events (Reference 9).

This safety evaluation (SE) addresses application of the S-RELAP5 code in a realistic manner in which the uncertainties in estimating the necessary parameters to satisfy the requirements of 10 CFR 50.46(b) are determined for the large break LOCA (LBLOCA).

2.0 REGULATORY BASIS

The requirements of 10 CFR 50.46 specify that each boiling or pressurized light-water nuclear power reactor fueled with uranium oxide pellets within cylindrical zircaloy or ZIRLO cladding must be provided with an emergency core cooling system (ECCS) that must be designed so that the calculated cooling performance following a postulated LOCA conforms to the criteria contained within the paragraph.

The stated requirement can be met through an evaluation model for which an uncertainty analysis has been performed as follows:

...the evaluation model must include sufficient supporting justification to show that the analytical technique realistically describes the behavior of the reactor system during a loss-of-coolant accident. Comparisons to applicable experimental data must be made and uncertainties in the analysis method and inputs must be identified and assessed so that the uncertainty in the calculated results can be estimated. This uncertainty must be

accounted for, so that, when the calculated ECCS cooling performance is compared to the criteria set forth in paragraph (b) of this section, there is a high level of probability that the criteria would not be exceeded.

Paragraph (b) specifies that the peak cladding temperature (PCT) must not be calculated to exceed 2,200°F, the maximum cladding oxidation must not exceed 0.17 times the total cladding thickness before oxidation, the maximum hydrogen generation must not exceed 0.01 times the hypothetical amount that would be generated if all of the metal in the cladding surrounding the fuel pellets were to react, the core must remain in a coolable geometry, and the core temperature shall be maintained at an acceptably low level and decay heat shall be removed for the extended period of time required by the long-lived radioactivity remaining in the core.

The NRC has suggested certain means by which the above regulatory criteria can be met. References 10 and 11 describe acceptable approaches to determine the calculated uncertainty in the 10 CFR 50.46(b) parameters.

3.0 REGULATORY EVALUATION

The Framatome ANP S-RELAP5 code is based on the RELAP5/MOD2 (References 14 and 15), RODEX3A fuel models (References 16 through 18), ICECON containment code (References 19 and 20), and RELAP5/MOD3 code (Reference 21). The NRC staff became familiar with many of the modifications made to the RELAP5/MOD2 and RELAP5/MOD3 codes during its S-RELAP5 SBLOCA review. That review focused on the conservative nature of the models necessary to satisfy the requirements of 10 CFR Part 50, Appendix K. The requirements of a realistic code are somewhat different in that many of the prescriptive conservative models can be replaced by more realistic models. Doing so necessitates evaluation of the uncertainty in the calculated results. Various means of achieving an estimate of uncertainty are available in the realm of statistical analysis. Framatome ANP has chosen to follow the basic Code Scaling, Applicability and Uncertainty (CSAU) evaluation methodology outlined in NUREG/CR-5249 (Reference 11). While the CSAU approach defines the process by which an uncertainty analysis is performed, it leaves room for the applicant to determine the specific statistical methodology to be applied. Framatome ANP has chosen the non-parametric order statistics methodology. An expanded explanation of the statistics involved is presented throughout this SE.

The following chronology describes the milestones in the NRC staff's review:

- Request for review of S-RELAP5 for RLBLOCA: August 20, 2001. Receipt of code and documentation: August 2001 (Reference 1).
- Acceptance of code for review by the NRC staff: October 3, 2001 (Reference 2).
- Presentation to the staff describing code material and approach to uncertainty analysis: October 30, 2001 (Reference 12).
- Presentation to the Advisory Committee on Reactor Safeguards (ACRS) Thermal-Hydraulic Subcommittee regarding code methodology and uncertainty analysis methodology: January 17/18, 2002 (Reference 13).

- NRC requests for additional information (RAIs): July 2002 (Reference 22).
- Framatome ANP response to the staff's RAIs: August 2002 (Reference 23).
- ACRS Thermal-Hydraulic Subcommittee meeting: November 2002.
- ACRS Full Committee meeting: December 2002.

Sections 3.1 through 3.14 of this SE describe a comparison of the Framatome ANP methodology with the CSAU methodology.

3.1 Step 1 - Scenario Selection

The processes and phenomena that can occur during an accident or transient vary considerably depending upon the specific event being analyzed. Framatome ANP has identified the LBLOCA as the event to which the methodology under review will be applied.

Framatome ANP is consistent with this step in the CSAU approach.

3.2 Step 2 - Nuclear Power Plant (NPP) Selection

The dominant phenomenon and timing for an event can vary significantly from one nuclear power plant design to another. Framatome ANP has specified the nuclear power plant applicability for the methodology under review to be the Westinghouse 3- and 4-loop designs and the CE 2-loop (4 pumps) design.

Framatome ANP is consistent with this step in the CSAU approach.

3.3 Step 3 - Phenomena Identification and Ranking

The behavior of a nuclear power plant undergoing an accident or transient is not influenced in an equal manner by all phenomena that occur during the event. A determination must be made to establish those phenomena that are important for each event and various phases within an event. Development of a Phenomena Identification and Ranking Table (PIRT) establishes those phases and phenomena that are significant to the progress of the event being evaluated.

The Framatome ANP PIRT differs from that in NUREG/CR-5249 (Reference 11) in describing the CSAU approach. NUREG/CR-5249 omitted the following items from the PIRT:

- There was no hot bundle region. Consequently, the calculated sink temperatures were too low, lowering the PCT. The hot rod was incorrectly contained in the average core region.
- The plant calculations were not performed at realistic peak linear heat rates (PLHR). A PLHR of 9.5 kilowatts per foot (kw/ft) was used whereas a more realistic upper bound to the PLHRs fall in the range 12.0 to 13.0 kw/ft. This low PLHR lowers the PCT.

- The effects of containment pressure were not evaluated, so the impact of steam binding and the potential for downcomer boiling were missed. These effects will also tend to increase the PCT.

The PIRT developed in support of the Framatome ANP RLBLOCA methodology addresses each of these areas in addition to identifying the phases of the LBLOCA and the phenomena occurring in each phase. All phenomena ranking high and medium are addressed in the code assessment process.

The specific phases described in the Framatome ANP PIRT are:

- Blowdown - The phase of the LOCA defined as the time period from initiation of the break until flow from the accumulators or safety injection tanks begins.
- Refill - The phase of the LOCA from the time accumulators or flooding tanks begin injecting until the mixture level in the vessel refills the lower plenum and begins to flow into the core.
- Reflood - The phase of the LOCA from the lower plenum filling and emergency core cooling (ECC) flow into the bottom of the core until the temperature transient throughout the core has been terminated.
- Post-Critical Heat Flux (CHF) Heat Transfer - Defined according to the transient phase. During blowdown, high pressure, high mass flux, low vapor superheat film boiling. During refill, a combination of dispersed flow film boiling and natural convection to single-phase vapor. During reflood, dispersed flow film boiling.
- Reflood Heat Transfer - Defined for the reflood period as convection to single-phase steam, wall-to-fluid radiation, film boiling, and transition boiling.
- Rewet - Defined according to transient phase. During blowdown, quench associated with high heat transfer rates near the quench front during high liquid flow. During refill and reflood, limited to top-down quenching due to falling liquid films.

The Framatome ANP methodology incorporates a hot bundle in addition to the hot rod, and plant calculations are performed at realistic, representative peak linear heat generation rates. The ability to address containment back pressure has been addressed through interfacing the S-RELAP5 capability with the ICECON containment analysis code previously approved by the NRC.

Framatome ANP is consistent with the PIRT guidelines and the specifications of this step in the CSAU approach.

3.4 Step 4 - Frozen Code Version Selection

The version of a code, or codes, reviewed for acceptance must be "frozen" to ensure that after an evaluation has been completed, changes to the code do not impact the conclusions and that changes occur in an auditable and traceable manner. Framatome ANP has specified that the

S-RELAP5 version UJUL00 code, and the UMAR01 version of the code incorporating the corrected RODEX3A code, which are frozen, were used for the uncertainty analysis.

Framatome ANP is consistent with this step in the CSAU approach.

3.5 Step 5 - Provision of Complete Code Documentation

This step is to provide documentation on the frozen code version such that evaluation of the code's applicability to postulated transient or accident scenarios for a specific plant design can be performed through a traceable record. Framatome ANP has provided the necessary documentation in References 3 through 7 and 16 through 20.

Framatome ANP is consistent with this step in the CSAU approach.

3.6 Step 6 - Determination of Code Applicability

The applicability of the Framatome ANP methodology is addressed in the following evaluation of the technical content of the documentation.

3.6.1 Heat Transfer Models

In its review of the heat transfer models within the RLBLOCA model (Reference 4), the NRC staff proceeded by first identifying the differences (modifications) in the heat transfer models and CHF correlations between the previously reviewed SBLOCA models in S-RELAP5 (Reference 8), and the RLBLOCA model. For example, Framatome ANP pointed out that in the heatup/dry-out period of the SBLOCA, the core can essentially be characterized by a single-phase steam region above a two-phase mixture region. Therefore, its PCT is mainly determined by the single-phase vapor heat transfer and will not be significantly impacted by small changes in other heat transfer models.

Due to the large number of different heat transfer correlations used in analyzing a particular transient, and in order to obtain a better understanding of such subtle differences and other differences between the two models, the NRC staff chose to investigate one particular transient from its initiation to its termination, carefully analyzing the various heat transfer correlations (Biasi, modified Zuber, etc.) used in the methodology. The review consisted of carefully reviewing the applicability of each particular correlation as the transient unfolded.

The NRC staff requested additional information from the vendor in Reference 22 and asked Framatome ANP to choose a transient and identify all the different correlations that are used from the beginning of the transient to the end. The NRC staff asked Framatome ANP to state the particular correlation used, its applicable range (in terms of the Reynolds Number, flow rates, etc.), and validation of its use in the applicable range.

3.6.1.1 Transient Simulation

The transient chosen for simulation is a limiting transient in terms of PCT for a 3- and 4-loop Westinghouse plant. To demonstrate the capability of S-RELAP5 to simulate a LBLOCA transient, Framatome ANP constructed a test-matrix composed of key correlation dependent

parameters (such as pressure, mass flow, temperature, range of applicability, etc.) based on validation studies (benchmarks such as those from the Thermal-Hydraulic Test Facility [THTF] tests and the FLECHT-SEASET tests) and published correlation reports. The key parameters that were identified are those parameters that are typically used to define the thermal-hydraulic behavior and correlation development. The test-matrix defined the space in which the selected transient is expected to exist. Ideally, the test-matrix should span the simulation-space; however, realistically, there may be holes in the test-matrix which Framatome ANP does not expect to fill in because of the lack of available data and test facilities.

Consequently, Framatome ANP constructed a PIRT for the LBLOCA to demonstrate adequate coverage of the test-space (Reference 23). The PIRT identified and ranked the relevant phenomena identified as being important for LBLOCA. Table 1 of Reference 1 highlights the core heat transfer phenomena identified as being important for the LBLOCA. Table 1 of Reference 1 does not explicitly identify all the important heat transfer regimes or correlations. However, this information is provided in Reference 3. Table 1 of Reference 1 does provide a tabulation of the ranking of important heat transfer regimes, such as the nucleate boiling, CHF, departure from nucleate boiling (DNB), transition boiling and the film boiling regimes. The Framatome ANP PIRT team concluded, and the NRC staff agrees, that other heat transfer regimes were either not present or had negligible impact on the peak clad temperatures. Data (Figures 1, 2, 3 and 4 provided in Reference 23 for the 3- and 4-loop sample plants), indicates that the core heat transfer around the hot rod is limited to the heat transfer regimes stated above.

In Reference 23, Framatome ANP provided a time-line of the chosen PCT event as it unfolded, including clad temperature plots from the 3- and 4-loop sample problems, as well as the respective LBLOCA phases (see Table 3 in Reference 23). The complexity of the PCT scenarios are evident as multiple heat transfer correlations are called upon at the various stages, based upon appropriate applicable ranges of the respective heat transfer correlation. Results of the analyses indicate that with the exception of the period from the onset of quenching to the end of the calculation, the dominant heat transfer mode is the Sleicher-Rouse correlation, representative of single phase convection. In addition, the results of the analyses also show that for the majority of the transient, the hot rod is in film boiling, which is consistent with the PIRT results of Table 1 of Reference 1.

Reference 23 also included a chronological presentation of each of the heat transfer correlations in terms of the range of applicability and validation as applied to the hot rod.

The system of heat transfer correlations in S-RELAP5 includes the range of applicability of the individual correlations, as well as the expanded ranges of applicability of correlations beyond their published ranges. The expanded range of applicability is provided by the uncertainty analysis using the THTF and the FLECHT-SEASET data sets and the RLBLOCA analysis methodology, resulting in a bias calculation used to validate the calculated uncertainty bias.

Tables comparing pressure and heat flux (the heat flux was translated into linear heat generation rate [LHGR]) are provided and compared to published ranges for each of the correlations in the simulated space. Where gaps existed between the range of applicability in matrix space and simulated space, a statistical uncertainty was applied to the data for the range of applicability. To bridge the gap in the void fractions for application of the Forslund-Rohsenow

and the modified Bromley correlations, linear interpolation was utilized to extend the applicability of these correlations. The NRC staff would have preferred a more physical solution to this situation; however, the NRC staff also recognizes the fact that large uncertainties do exist in thermal-hydraulic formulation and there is a shortage of relevant data in this subject. Given the limited availability of data to fill in these gaps, and the acceptable predictions of the most important phenomena in the assessment cases described below, the staff finds this linear interpolation to be acceptable.

3.6.1.2 Reflood Heat Transfer

In computing the heat transfer to the liquid, Framatome ANP uses the Bromley correlation and the Forslund-Rohsenow correlation to cover parts of the anticipated range of void fraction. Linear interpolation between the two correlations is used to obtain the heat transfer coefficient between applicable ranges of void fraction. Framatome ANP is, in effect, interpolating between two correlations to determine the heat transfer along a major portion of the fuel rod for a sustained period of time during reflood. The NRC staff and Framatome ANP do not agree on understanding the nature of the Forslund-Rohsenow model with regard to wall-droplet contact heat transfer when the wall temperature is above the minimum film boiling temperature, that is, $T_w > T_{min}$, the Leidenfrost temperature. The NRC staff understands the Forslund-Rohsenow correlation to be primarily a vapor de-superheating effect and secondarily a combination of a wet contact model and a dry contact model that should only be applied above the quench region where the wall is below the minimum film boiling temperature. Reference 26 states, "...heat is transferred from the wall to a possibly superheated vapor to liquid droplets. Superimposed on this two-step process is an additional amount of heat that is transferred from the tube wall directly to the liquid droplets, a kind of Leidenfrost effect." The NRC staff believes that References 24 through 32 further support this position. Framatome ANP, on the other hand, believes the Forslund-Rohsenow model is a dry contact model which can be applied when the wall temperature is greater than the minimum film boiling temperature. In addition, the NRC staff notes that the Forslund-Rohsenow model was developed from data taken for mass fluxes 10 to 100 times the mass flux typical of low flooding rate reflood conditions.

The NRC staff and Framatome ANP studied the Forslund-Rohsenow correlation's effect further through several assessment calculations using the S-RELAP5 code. Assessment cases were recalculated with a multiplier set to multiply the Forslund-Rohsenow equation by a factor of zero (0) when $T_w > T_{min}$. When this was done, the assessments showed that this limitation on Forslund-Rohsenow had no effect on the peak cladding temperature or its time of occurrence. This is to be expected since the void fraction in the period leading up to the PCT is predominantly above 0.995. When the void fraction is above 0.995, the dominant heat transfer is single-phase vapor determined by the Sleicher-Rouse correlation.

Beyond the time of PCT, the void fraction is lower than 0.995 so that either the modified Bromley, Forslund-Rohsenow, or an interpolation between the two is used. This results in temperature response beyond the point of PCT that was slightly higher and the quench time delayed. The overall effect on temperature beyond the PCT point and the quench point was a change in temperature ranging from -24°F to +20°F. Since this temperature variation is within the experimental uncertainty for temperature measurements, the NRC staff concludes that while the staff disagrees with Framatome ANP on the applicability of the Forslund-Rohsenow model for wall temperatures above the minimum film boiling temperature, its use does not play

a significant role in the temperature response of the transient. The NRC staff, therefore, accepts the modeling included in the Framatome ANP RLBLOCA methodology.

An overall comparison of the performance of the steam cooling model can be seen in Figure 1 (attached to this SE); the steam temperature at the time of PCT for FLECHT-SEASET Test 31302. The steam temperature predicted by S-RELAP5 is conservative relative to the measured steam temperature. The higher predicted steam temperature results in lower, conservative, heat transfer from the fuel rod simulators.

3.6.1.3 Minimum Film Boiling Temperature

S-RELAP5 employs a conservatively low minimum film boiling temperature and uses this temperature limit for both blowdown and reflood. This temperature does not bound the lower range of T_{min} for blowdown suggested in NUREG/CR-5249 (i.e., 600°K). However, since the NUREG/CR-5249 report was prepared, experience with various vendor analyses, and staff analyses using its own suite of codes show that T_{min} in the range 600 to 750°F is not expected to have a strong sensitivity to PCT. Therefore, the model is adequate since it does not impact the PCT.

3.6.1.4 Heat Transfer Models Summary

The NRC staff agrees with the Framatome ANP conclusion that the post-CHF heat transfer is the dominant influence on the clad temperatures of the fuel rod. The submitted analysis demonstrated that although multiple CHF correlations are employed (programmed into S-RELAP5) simultaneously during a LBLOCA calculation, a single phase vapor provides the primary heat transfer sink for the hot fuel rods. It is the interplay between these different correlations (superpositioning, overlapping of correlations, etc.) that actually forms the overall post-CHF heat transfer correlation in S-RELAP5.

The NRC staff also reviewed the range of applicability and the expanded range, based on the statistical treatment and code to data comparisons. The NRC staff agrees with Framatome ANP that in general, the FLECHT-SEASET and the THTF data sets used to expand the range of applicability encompass the original derived range of applicability. However, there remained regions in the test-matrix (assessment-space) where the range of applicability of certain correlations and associated uncertainty analysis still contained some gaps. To account for these gaps, Framatome ANP assessed the code against a series of integral tests, including LOFT, CCTF, and Semiscale (References 3 and 5). The analyses showed good agreement with the test data and the uncertainty analysis thereby enabling Framatome ANP to complete the test-matrix (assessment space) and cover the simulation space.

The NRC staff notes that there is disagreement regarding the application of the Forslund-Rohsenow model when the wall temperature exceeds the minimum film boiling temperature. Since the effect of the correlation when used within the overall heat transfer model has been shown to be negligible under the conditions existing in both experimental comparisons and in predicted full plant conditions, the NRC staff accepts the overall reflood heat transfer modeling in the S-RELAP5 code.

3.6.2 Decay Heat Model

Framatome ANP employs conservative assumptions to compute the decay heat using the ANSI/ANS-5.1-1979 standard (Reference 34). The ANSI/ANS-5.1-1979 standard is applicable where U235 is the principal fissile material, but does consider fission contributions from Pu239 and U238. Framatome ANP has assumed infinite reactor operating time, all fissions are from U235, a fission energy of 200 MeV/fission, and one standard deviation total decay heat uncertainty. Actinide capture decay power is also computed using the ANSI/ANS-5.1-1979 standard equations, along with the addition of decay heat from neutron capture in fission products. The NRC staff concludes that the decay heat model used in the Framatome ANP RLBLOCA methodology is conservative and acceptable.

3.6.3 Counter-current Flow (CCFL) Model

The S-RELAP5 Code employs a CCFL model to limit the flow of liquid into the core through the fuel alignment plate. Since the CCFL model is not used in the downcomer, there are no controls to assure that future plant calculations will not result in violations of the CCFL or unrealistic co-current downflow in this region. Furthermore, the drag and entrainment models in the original RELAP5 code were not developed specifically to accommodate countercurrent flow. In response to the staff's RAIs, Framatome ANP calculations of the Wallis parameters from the 3-loop sample problem show that there is not a violation of the CCFL in the downcomer. The 4-loop sample problem, however, shows a CCFL violation three times during the transient simulation. The staff agrees with Framatome ANP that this is a minor effect and does not affect the overall success of the calculation. To preclude excessive CCFL violation in future applications, Framatome ANP has agreed to have the code provide a warning message to the analyst if a CCFL violation in the downcomer occurs. The code user will then determine if the transient is being influenced by the CCFL violation or whether the violation is insignificant. The NRC staff accepts this code addition in lieu of the addition of a CCFL model to the downcomer.

3.6.4 Break Type and Size

The requirements of 10 CFR 50.46(a)(1)(i) state, in part:

ECCS cooling performance must be calculated in accordance with an acceptable evaluation model and must be calculated for a number of postulated loss-of-coolant accidents of different sizes, locations, and other properties sufficient to provide assurance that the most severe postulated loss-of-coolant accidents are calculated.

Framatome ANP has interpreted the above requirements to mean that the break size can be sampled as one of the variable parameters treated statistically by random sampling. The NRC staff has studied the position proposed by Framatome ANP and accepts its approach on the basis of the break type and size distributions assumed in its analysis. Specifically, the methodology applies a binomial distribution to the break type sampling, that is, the two break types, Double Ended Guillotine and Slot, are treated as equally probable. In addition, the entire break size distribution is uniform from the largest to the smallest size. Thus, the break type and size selection is of uniform probability for the entire spectrum.

In response to an NRC staff request for additional information, Framatome ANP performed a complete set of analyses while fixing the break size at the worst calculated size. That is, for the 0.66 DEG CL break in a 3-loop Westinghouse plant (the case that resulted in the worst PCT calculated at 1853°F), the remaining parameters treated statistically were chosen by Monte Carlo sampling to establish the 59 sample cases. The calculations resulted in two (2) PCTs calculated above the base worst case and 57 PCTs below the base case. The two PCTs above the base case were 20°F and 76°F above the base case. The NRC staff finds the break spectrum as calculated by Framatome ANP in support of its RLBLOCA methodology acceptable.

Should Framatome ANP elect to alter this distribution specification to one with a bias on size or type, the NRC staff will require further review of that approach.

3.6.5 Critical Flow Model

The critical flow model in S-RELAP5 utilizes the Trapp-Ransom model for subcooled flow and homogeneous equilibrium model (HEM) for two-phase flow. The model does not model non-equilibrium critical flow through the break and therefore does not address the guidance in items b and c in Section 3.4.1.1 of Regulatory Guide 1.157, "Best-Estimate Calculations of Emergency Core Cooling System Performance," which states that the critical flow model should (b) provide thermal non-equilibrium conditions when the fluid is subcooled, and (c) provide a means of transition from non-equilibrium to equilibrium conditions.

Framatome ANP responded to an NRC staff question on the subject of the transition region between subcooled and saturated fluid conditions lasting 5 – 15 seconds in the Marviken tests and less than 5 seconds in plant calculations. The Marviken test comparisons showed good agreement with the data except in the transition region. Since the transition region is of short duration, this calculation discrepancy has an insignificant effect on the calculation and is considered acceptable.

3.6.6 Multi-Dimensional Downcomer Model

To demonstrate momentum conservation and to assist in understanding the behavior of the 2-D downcomer model, the NRC staff requested that Framatome ANP present the results of several simple test models. The RELAP5 code, as well as other similar codes such as TRAC and RETRAN, can produce anomalous flow circulations, for example, between parallel pipes. These anomalies are of a numerical nature and cannot easily be corrected without the use of additional artificial form losses (Reference 33). Framatome ANP provided the results of a calculation of the sample flow problem presented in Reference 33 and described how the S-RELAP5 code resolves this anomalous flow behavior. The NRC staff finds Framatome ANP's response to this concern is acceptable because it demonstrates that the Framatome ANP multidimensional downcomer model addition does not exhibit anomalous circulatory flow.

3.6.7 Downcomer Boiling

Framatome ANP presented the results of a downcomer boiling study performed for the three-loop plant, including eight variations of the nodalization, cross-flow form loss, and containment pressure.

Since the sensitivity studies performed include containment back pressure as low as 10 psia, along with the effect of single failure, the methodology has been shown to be applicable to subatmospheric containment, including ice condenser plants.

The sensitivity studies were compared to the base case PCT and the variations resulted in an increase of less than 100°F. The NRC staff concludes that the effect of downcomer boiling has been properly accounted for in the analysis.

The sensitivity studies performed demonstrate applicability of the methodology to containment pressures as low as 10 psia. Thus, the methodology is applicable to subatmospheric containment designs, including ice condenser containments, to a containment back pressure of 10 psia. Application to containments with a back pressure lower than that value will require further justification.

3.6.8 ECC Bypass

ECC bypass is calculated by the interaction of the interfacial friction, wall drag, and condensation models. Framatome ANP confirmed that no credit is taken for the bypass conservatism in the uncertainty analysis. That is, there is no direct, negative bias in the uncertainty methods simulating ECC bypass. This is conservative and acceptable to the NRC staff.

Framatome ANP is consistent with this step in the CSAU approach since the models used in the methodology adequately represent physical phenomena identified in the PIRT, or are conservative relative to available data.

3.6.9 Two-Phase Pump Degradation Model

An evaluation of the use of either the Semiscale or EPRI-CE two-phase pump degradation model in the RLBLOCA methodology is presented in Appendix B of Reference 3. Sensitivity studies show an 18°F higher PCT using the Semiscale model than the PCT using the EPRI-CE model. Since the expected variability in an S-RELAP5 calculation is 30°F, this level of variation indicates that either model will produce essentially the same result in a RLBLOCA analysis. Framatome ANP uses the EPRI-CE two-phase pump degradation model in its SEM/PWR-98 10 CFR Part 50, Appendix K model, as well as the other applications of the S-RELAP5 model (References 8 and 9). The NRC staff finds the change to consistently use the EPRI-CE two-phase pump degradation model in the RLBLOCA methodology to be acceptable.

3.6.10 Gadolinia Bearing Fuel Rod Modeling

In the performance of sensitivity studies required to respond to an RAI on the RLBLOCA methodology, Framatome ANP discovered that the modeling of Gadolinia bearing fuel rods had

been performed incorrectly. The modeling of Gadolinia bearing fuel rods was corrected and the results showed about a 63°F reduction in the 95/95 PCT for the three-loop sample problem and a 66°F reduction in the four-loop sample problem.

The correction to the Gadolinia bearing fuel rod modeling was to consider a set of Uranium Oxide (UO₂) and Gadolinia bearing fuel rods for each of the 59 cases analyzed. In the sample problems, this meant analyzing a UO₂ rod and a 2 weight percent (w%), 4 w%, 6 w%, and 8 w% Gadolinia bearing fuel rod for each case. The power in the Gadolinia bearing fuel rod is reduced relative to the UO₂ rod at the statistically selected point in time for each case. The PCT established for each case is the highest of the PCTs for all of the rods modeled.

Framatome ANP is consistent with this step in the CSAU approach. The NRC staff finds the sensitivity studies performed acceptable.

3.7 Step 7 - Establish Assessment Matrix

Framatome ANP established an assessment matrix of separate effects tests and integral system tests, summarized in Table 1 attached to this SE, to address the important phenomena identified in the PIRT. The NRC staff review of several of the tests used in the assessment matrix follows, along with some specific staff experience and observations while using the S-RELAP5 code on NRC's computers.

While the staff reviewed all of the assessments performed in support of the RLBLOCA methodology, the following discussion will emphasize those assessments performed against the 2D/3D test program data. The most recent generic PWR test program in the public domain was sponsored by the NRC Office of Nuclear Regulatory Research during the 1980-90 timeframe. Much of the work done at those test facilities used full-scale, or nearly full-scale, reactor component simulation components. In addition, the data are considered to be of high quality. For this reason they are considered to be highly appropriate for code assessment.

Before discussing the results of the review of the 2D/3D assessments, two examples are given of the assessments presented by Framatome ANP. Figure 2, Framatome ANP RLBLOCA Figure 4.35 taken from Reference 3, attached to this SE, shows the comparison of the S-RELAP5 maximum cladding temperature calculation versus the measured temperature for FLECHT-SEASET Test 31504. The figure shows that the code is conservative with respect to the measured cladding temperature throughout the length of the test assembly. Figure 3, Framatome ANP RLBLOCA Figure 4.194 taken from Reference 3, attached to this SE, shows the comparison between the S-RELAP5 predicted cladding temperature and the measured cladding temperature for LOFT test LP-LB-1. Two S-RELAP5 predictions are shown, one made without accounting for the code biases determined from the separate effects test assessments, and one made with the biases taken into account. Again, the code predicted cladding temperature is conservative relative to the measured temperature throughout the test assembly except at the very top of the fuel assembly. At that point, the temperature is significantly below the PCT. It is also noted in the LOFT assessment that the effect of considering the biases is to bring the code predicted temperature into close agreement with the measured temperature with the attendant data error bands.

3.7.1 Upper Plenum Test Facility (UPTF)

Framatome ANP compared RLBLOCA S-RELAP5 calculational results to seven UPTF tests. The UPTF tests were performed to provide full-scale simulation of the primary system phenomena occurring during three phases of a PWR LBLOCA. The phases investigated were end-of-blowdown, refill and reflood. The phenomena that the code calculations must realistically represent in this assessment include countercurrent flow in the downcomer, upper tie plate, upper plenum and hot leg, CCFL, refill behavior, condensation induced pressure and fluid oscillations, entrainment/de-entrainment, steam binding, and carryout. Discussion of the specific tests follows.

3.7.1.1 UPTF Tests 6 and 7

Five calculations of UPTF Test 6 and one calculation of UPTF Test 7 were designed to examine downcomer countercurrent flow during blowdown, ECC bypass, and lower plenum refill with cold leg injection. The RLBLOCA S-RELAP5 calculations were assessed against the data to determine the code's ability to predict them.

The tests simulated late blowdown and refill phases of a PWR cold leg LBLOCA. The Test series 6 calculations were initiated with very little or no lower plenum water inventory, and nitrogen injection with ECCS injection. The Test series 7 calculation was initiated with the lower plenum partially filled. A lower plenum drain valve operated by a level-controller allowed the observation of lower steam injection rates to further extend the Test 6 series. Nitrogen was not injected with the ECCS flow in Test 7.

A constant steam flow rate was injected into the core and steam generator simulators for each test calculation, but the injection rate varied by test. The lowest steam injection rate data was gathered from Test 7. A constant ECCS injection was delivered into the three intact cold legs in all the tests.

Steam injected into the core traveled downward to the lower plenum, up the downcomer and out the broken cold leg. Depending on the downcomer steam flow rate, the ECCS water entering the downcomer either bypassed to the broken cold leg, or penetrated downward to fill the lower plenum. The lower plenum water level determined the amount of ECCS water reaching the lower plenum.

Framatome ANP noted that there was very little water delivery to the downcomer until the cold legs were completely filled with water. Further, the rate of penetration varied inversely with the steam flow rate. The ECC water penetrated the downcomer opposite the broken cold leg, but the water from the intact cold leg adjacent to the broken leg was bypassed to the break, as expected. However, the calculated end of bypass occurred later than it did in the experiment. It is not clear whether this was due to the calculation missing the initial high flowrate, or whether it results from the delay due to filling the cold legs before penetration.

The downcomer pressure increased with increasing steam flowrate. Pressure drop due to condensation was captured by the code in most cases. The code predicts a pressure increase due to ECC water entrainment to the broken cold leg, producing two-phase critical flow at the break. However, it was not clear how the mixture level tracking influenced the flow at the break.

Framatome ANP stated that S-RELAP5 overpredicts lower plenum sweep-out. It concluded that the steam velocity increased through the downcomer and that the overprediction of liquid sweep-out reduces the lower plenum refill rate and will conservatively delay core recovery and quench.

The positive slope of the lower plenum mass inventory curve indicates ECC water penetration into the downcomer. Underprediction of the initial high refill rate results in a lower ECC penetration rate.

Two sensitivity studies, lower plenum oscillations and a 2D lower plenum model, were performed. These studies were performed to investigate the large oscillations of pressure, lower plenum level and lower plenum mass.

As a result of the studies, Framatome ANP suggested that the large oscillations were due to the level tracking in the bottom node of the lower plenum model. When the level tracking model was turned off, the large oscillations dampened, and the mass and level remained significantly lower than the data. To investigate this, the 2D lower plenum model was implemented. Results were improved by implementing the 2D model.

3.7.1.2 UPTF Test 8

The purpose of Test 8 was to investigate condensation-induced pressure and fluid oscillations in the cold legs due to ECCS injection. Overall, the code closely predicted the flow regime transition between slug flow and stratified flow. However the downcomer temperature plots when S-RELAP5 changes from slug to stratified flow, were not in good agreement with the data.

3.7.1.3 UPTF Tests 10 and 29

The purpose of Tests 10 and 29 was to verify the ability of a code to properly predict entrainment/de-entrainment and to limit countercurrent flow at the upper tie plate and upper plenum regions for a LBLOCA during reflood. The downcomer and lower vessel were filled with water to prevent steam flow between the core and the downcomer.

When using the CCFL inputs recommended by the RLBLOCA methodology, Framatome ANP observed that overall predictions of total water carryover to the steam generator simulators indicated that the code overpredicts the liquid carryover to the steam generators. It concluded that this would result in an overprediction of the steam binding effect which would reduce the reflood rate. Related to the overprediction of the liquid carryover, Framatome ANP further suggested that the fallback to the core was underpredicted. The results improved when using the CCFL input parameters suggested by KWU for UPTF tests, rather than the CCFL model values specified in the RLBLOCA methodology.

3.7.1.4 UPTF Tests 10 and 12

These tests were similar to the previous set, except flow was allowed between the core and the downcomer and nitrogen was included in Test 12. Similar results were obtained for these tests as the previous set. Nitrogen did not appear to have a significant impact on CCFL.

3.7.1.5 UPTF Test 11

Test 11 was composed of a series of quasi-steady-state separate effects tests to investigate countercurrent flow in the hot leg. Flow conditions were changed to develop a set of countercurrent flow curves at low and high pressure. Further, the models for these tests were built with and without CCFL models at the junction between the hot leg and inlet plenum.

The results of these tests show that the interfacial friction package alone cannot properly calculate the countercurrent flow at the steam generator inlet plenum. Therefore, as concluded by Framatome ANP, the CCFL model must be applied at the junction between the hot leg and the steam generator inlet plenum. The CCFL coefficients for the Wallis form result in good agreement with the data.

3.7.2 Cylindrical Core Facility (CCF) Test

Framatome ANP compared the S-RELAP5 calculational results to 4 CCF tests. The CCF tests were intended to provide full-scale simulation of the primary system phenomena occurring during reflood after a PWR LBLOCA. The phenomena that the code calculations realistically represented in these assessment cases include ECC flow behavior in the downcomer, and reactor core responses during reflood. The NRC staff concludes that the code performed acceptably in the CCF assessment test cases.

3.7.3 Code Internals and Experience

The NRC staff compared a few selections from the RLBLOCA coding to the documentation provided. Five subroutines were reviewed. They were CHFCAL, DITTSG, DITTUS, FILMBL, and PREDNB. The purpose of the comparison was to determine consistency, soundness of approach and completeness between the documentation and the code. The results of this review follow.

3.7.3.1 Subroutine CHFCAL

Subroutine CHFCAL calculates the CHF using the Zuber and Biasi CHF correlations. Many of the NRC staff's questions involved only minor clarification in the documentation. In some cases, correlation descriptions which appeared in the code did not appear in the documentation. For example, the description of the "Extended Biasi" was not included in Reference 4. However, Framatome ANP stated, and the NRC staff confirmed, that the Extended Biasi is not applied to RLBLOCA, SBLOCA and other Chapter 15 non-LOCA methodologies. In another case, the interpolation scheme found in the coding used to smooth the transition between two correlations for mass flux from 100 to 200 kg/m²s had not been updated in Reference 4. Framatome ANP is aware of this, and correction will be made in a documentation revision. The NRC staff also checked for unit consistency and found that units had been accounted for correctly.

3.7.3.2 Subroutine DITTSG

Subroutine DITTSG codes the implementation of either the Dittus Boelter or Sleicher Rouse convective heat transfer correlations. Again, many of the staff's questions involved only minor

clarifications. Some terms in the correlations needed to be completely accounted for in the text, and an equation reference error was corrected. Framatome ANP will correct inconsistencies in the documentation in a subsequent version of the document.

3.7.3.3 Subroutine DITTUS

Subroutine DITTUS calculates the forced convection heat transfer correlation only for liquid. One line of code in the natural convection correlation within DITTUS did not appear in the documentation. Framatome ANP stated that this coding was added to smooth the transition between the forced convection correlation and the natural convection correlation. This oversight will be corrected in the approved documentation.

3.7.3.4 Subroutine FILMBL

The FILMBL routine computes the heat transfer coefficients for film boiling. Framatome ANP provided the NRC staff with some minor clarification about the continuity between the documentation and the coding. As a result, the NRC staff found the subroutine to be correctly coded.

3.7.3.5 Subroutine PREDNB

This subroutine calculates the pre-DNB forced convection heat transfer correlations. As with the other subroutines, Framatome ANP provided the NRC staff with some minor clarification. The NRC staff concludes that the subroutine is correctly coded.

Framatome ANP provided the NRC staff with the necessary clarification leading to establishing consistency between the code and documentation and an understanding of the soundness of its approach. The NRC staff concludes from its review of the selected subroutines that the coding is correct.

3.7.4 NRC Staff Studies of Effects on PCT

The NRC staff investigated PCT changes for the Framatome ANP 3-loop PWR model due to code changes to 3 subroutines and 6 variations in the reflood rate. The three modifications investigated by the staff included an increase in the post-DNB forced convection heat transfer correlation (PSTDNB) by a factor of two, an increase in the liquid water viscosity (VISCOL) by a factor of five, and multiplication of the wall drag (FWDRAG), for both liquid and vapor phases, by factors of 0.1, 2, and 10. The unmodified calculation predicted a PCT of 1663°F at 232 seconds, with quench at 199 seconds.

Neither the change in post-DNB forced convection heat transfer nor the change in the liquid viscosity had a significant effect on the predicted PCT. The increase in the forced convection heat transfer correlation, alone, lowered the PCT to 1582°F, and the increase in liquid viscosity, alone, lowered the PCT to 1564°F. In both cases the quench time changed less than 40 seconds.

The variations in the wall drag had a much more significant effect on the PCT, as would be expected since changing the wall drag alters the reflood rate. The base case used for the wall

drag study had a PCT of 1577°F with a quench time of 232 seconds. Increasing the wall drag by a factor of 2 increased the PCT to 1617° and delayed quench by 50 seconds. Increasing the wall drag by a factor of 10 resulted in an entirely different transient. In this case, there was a blowdown quench on the order of 400°F along with a delay in the PCT, now occurring at 150 seconds versus 30 seconds in the original calculation. In this case, the PCT reached 1686°F with a steadily decreasing clad temperature, but no quench at the time of problem termination at 370 seconds.

Figure 4 (attached to this SE), illustrates the effects of multiplying the liquid viscosity by a factor of 10, multiplying the post-DNB forced convection heat transfer by a factor of 10, and multiplying the wall drag by a factor of 10 for a PWR model. A comparison of the results obtained by ranging the multiplier on the wall drag from 1 to 2 to 10 is shown in Figure 5 (attached to this SE), for the PWR model.

An additional study was performed based on the model for the FLECHT-SEASET Test 31504. FLECHT-SEASET Test 31504 was a low flooding rate test, fixed as a boundary condition at 0.972 in/sec. Thus, the test assembly was controlled in reflooding by a prescribed liquid and vapor velocity which was then influenced by the fuel simulator power profile. The test assembly model consists of a lower plenum, heated core volume, unheated core volume, and an upper plenum. The 12-foot heated core is divided into 20 equal length axial nodes with a cosine power shape.

Since the forced convection heat transfer and liquid viscosity were determined to be less important than the wall drag, only the wall drag was modified for this study. Three cases were calculated: wall drag unmodified, and wall drag multiplied by 0.1, 2, and 10, as can be noted in Figure 6 (attached to this SE), with the base case calculated with a multiplier of 10 on the liquid viscosity for comparison. The first three cases had little effect on the overall progress of the transient. The calculated PCTs were 2168°F, 2132°F, and 2096°F, for the multipliers of 0.1, 1, and 2, respectively. The multiplier of 10, however, again altered the shape of the temperature plot significantly. The PCT in this case was reduced to 1969°F with a later quench.

Close examination of the cases indicates that when the wall drag is increased, with a fixed coolant boundary condition, more water mass is retained in the lower portion of the core allowing the quench front to progress, combined with an increase in the steam flow rate. Thus the heat transfer is improved under these conditions. When the reduced wall drag is used, there is a higher mass flow out of the core, a higher carryout fraction, but less liquid in the core to allow advancement of the quench front. In addition, the flow regime map indicates that the flow is inverted annular flow, a less efficient mode for heat removal.

These analyses performed by the NRC staff with the Framatome ANP S-RELAP5 code confirm the importance of reflood heat transfer in the analysis of the large break LOCA.

The NRC staff concludes that for the parametric studies it performed, the relative importance of the phenomena are consistent with the identified PIRT rankings.

3.7.5 Cladding Material Applicability

Framatome ANP incorporated the NRC-approved M5 cladding material properties into the S-RELAP5 methodology (References 35 and 36). Sensitivity studies were performed to investigate the sensitivity of PCT and oxidation with the substitution of M5 for Zircaloy cladding. The studies show that no unique phenomenological differences are introduced with the M5 cladding.

Differences in the cladding material properties do cause differences in the fuel pellet behavior due to differences in the gap width, thus affecting pellet temperature and pellet-cladding interaction. The resulting increase in fuel centerline temperature, increased gap heat transfer resistance, and removal of stored energy produced a PCT that is 40°F higher for M5 clad fuel, and a maximum change in oxidation of +0.04%. The M5 cladding material properties approved by the NRC have been properly incorporated in the Framatome ANP RLBLOCA methodology.

Under existing NRC regulations, applicants wishing to apply the Framatome ANP RLBLOCA methodology to M5 clad fuel must request an exemption for its use (prior to a rulemaking to modify 10 CFR 50.46(a)(1)(i) to include M5 cladding material).

The staff concludes that Framatome ANP is consistent with this step in the CSAU approach based on a broad assessment of the code against accepted separate effects tests and integral systems tests, with the addition of the most recent test facility results that were performed at full- and nearly full-scale models.

3.8 Step 8 - NPP Nodalization Definition

Reference 11 discusses the tradeoffs in determining an adequate NPP nodalization. Framatome ANP developed guidelines for its RLBLOCA methodology that are as explicit as possible to remove nodalization as a contributor to calculational uncertainty. The guidelines provide rules for deriving the appropriate nodalization, thus defining a method for automating the generation of input for a RLBLOCA analysis that maintains consistency in approach from one analysis to another. Development of the guidelines has relied heavily on past experience with the S-RELAP5 code and its predecessor code versions.

The NRC staff has noted that NPP nodalization should not consider gaps between the hot leg nozzles and the downcomer in the plant model. The leakage from these nozzle gaps relieves the steam pressure/steam binding effect during reflood and is, therefore, beneficial to reflooding the core and reducing the PCT. There is no evidence to support the view that the nozzle gaps would remain open under the high temperatures present due to the steam exiting the core under transient conditions. Framatome ANP has agreed that it is not to use nodalization with hot leg to downcomer nozzle gaps.

Framatome ANP is consistent with this step in the CSAU approach by specifying a nodalization approach that maintains consistency between the application of the methodology and the assessment of the methodology.

3.9 Step 9 - Definition of Code and Experimental Accuracy

Simulation of the experiments developed from Step 7 using the NPP nodalization from Step 8 provides checks to determine code accuracy. The differences between the code calculated results and the test data provide bias and deviation information. Code scale-up capability can also be evaluated from separate effects data through full-scale data when they are available. Overall code capabilities are assessed from integral systems test data. In addition to these assessment tools, the code uncertainty determination must also use additional techniques to determine the uncertainty in the individual contributions arising from both code and experiment, along with a range of uncertainty for each of the individual contributors.

Framatome ANP used comparisons of code predictions to test data for 15 different separate effects test facilities to determine code biases in correlations and models, which were then applied to the assessments performed for the integral systems test facilities.

Framatome ANP is consistent with this step in the CSAU approach since the uncertainties in experimental data have been accounted for in determining the biases identified for use with the methodology.

3.10 Step 10 - Determination of Effect of Scale

Various physical processes may give different results as components or facilities vary in scale from small to full size. The effect of scale must be included in the quantification of bias and deviation to determine the potential for scale-up effects. The effect of scale was addressed by Framatome ANP with regard to each of the phases of the transient described in the PIRT along with the discussion of test scaling, code scaling and specific phenomena scaling. In a departure from the discussion in Reference 11, Framatome ANP has included in the scale determination for S-RELAP5, the full-scale UPTF test data, which became available after the preparation of Reference 11. This is an enhancement to the methodology identified in Reference 11.

Framatome ANP is consistent with this step in the CSAU approach since the recommendation provided in Reference 11 has been used and enhanced by inclusion of full-scale facility test data where available.

3.11 Step 11 - Determination of the Effect of Reactor Input Parameters and State

The purpose of this step is to determine the effect that variations in the plant operating parameters have on the uncertainty analysis. Plant process parameters characterize the state of operation and are controllable by the plant operators to a certain degree. Framatome ANP performed a review to identify the NPP parameters that are to be addressed when performing a LBLOCA analysis. The parameters identified come from the PIRT, plant-specific technical specifications, and utility input. Components, or operating parameters, and the associated parameters and ranges were addressed by Framatome ANP.

Sensitivity studies were performed to establish a requirement on the level of importance an analyst might give when quantifying process parameter uncertainties. The results from a set of sensitivity studies performed for process parameters for the 3- and 4-loop PWRs were given.

Sensitivity studies are also useful in determining if certain parameters need not be treated statistically, can be treated conservatively instead, or can be treated as insignificant.

Framatome ANP is consistent with this step in the CSAU approach since the effect of reactor input parameters has been considered in the sensitivity studies performed in support of the methodology.

3.12 Step 12 - Performance of NPP Sensitivity Calculations

Sensitivity calculations are performed to evaluate methodology sensitivity to parameters such as PCT or metal-water reaction, and to various plant operating conditions that arise from uncertainties in the reactor state at the initiation of the transient, in addition to sensitivity to plant configuration.

Framatome ANP is consistent with this step in the CSAU approach since adequate sensitivity studies have been performed.

3.13 Step 13 - Determination of Combined Bias and Uncertainty

The individual uncertainties resulting from code models of important phenomena, scale effects, and NPP input parameter variations must be combined to obtain an overall bias and uncertainty.

Framatome ANP provided sample RLBLOCA analyses for 3- and 4-loop PWRs following the framework described in Reference 3. Base input models were developed to describe the NPP and fuel behavior based upon information obtained from several different 3- and 4-loop plants. Consequently, the analyses are considered representative of typical 3- and 4-loop PWR designs, rather than specific representations of specific plants. The models used, in general, are taken as demonstrations of the applicability of the RLBLOCA methodology to the 3- and 4-loop PWR designs.

Framatome ANP is consistent with this step in the CSAU approach.

3.14 Step 14 - Determination of Total Uncertainty

The first few steps in the CSAU methodology identify and rank the physical phenomena important to judging the performance of the safety systems and margins in the design. The phenomena are compared to the modeling capability of the code to assess whether the code has the necessary models to simulate the phenomena. Most important, the range of the identified phenomena covered in experiments is compared to the corresponding range of the intended application to assure that the code has been qualified for the most significant phenomena, as reflected in the ranking process, over the appropriate range. The result is then provided in a PIRT. The NRC staff has reviewed the PIRT provided for S-RELAP5 in Reference 3, and finds it acceptable and consistent with the NRC staff's experience in judging the important phenomena associated with the LBLOCA.

The discussion of the uncertainty analysis approach presented in NUREG/CR-5249 and in Regulatory Guide 1.157 envisioned the use of response surfaces for quantifying uncertainty in

the calculated PCT. The NRC staff recognizes that there are other valid and acceptable means by which the uncertainty can be assessed. Framatome ANP has chosen to use a method based on non-parametric order statistics which follows the development by Wilks (Reference 37) and others.

The Framatome ANP methodology as described in Reference 3, applies a statistical method based on order statistics to demonstrate that S-RELAP5 meets the acceptance criteria for RLBLOCA analyses of pressurized water reactors. These are

1. High probability that the calculated maximum PCT value is less than 2200°F.
2. High probability that the calculated maximum nodal oxidation is less than 17 percent.
3. High probability that the calculated maximum total core oxidation is less than 1 percent.

The methodology adopted by Framatome ANP is based on combining the individual biases and uncertainties in the S-RELAP5 model and plant parameters to infer the uncertainty associated with the parameters in the above acceptance criteria via Monte Carlo sampling. That is, the distributions of the model parameters and plant parameters are sampled at random; and for each sample of parameters, a RLBLOCA calculation is performed. The three parameters in the acceptance criterion are scored. The Framatome ANP methodology claims that 59 cases are sufficient to show that the value of the 59th order statistic associated with the peak cladding temperature can be used to show that the acceptance criteria for all three parameters are met.

A 95% probability at 95% confidence (95/95) inference with regard to a random variable based on a sample size of 59 is valid in the case of a univariate distribution. Satisfaction of the above acceptance criteria at a uniform probability and confidence level of 95/95 implies a trivariate distribution is necessary. A trivariate distribution requires performing additional calculations. This has not been done by Framatome ANP.

Instead, Framatome ANP has referred to Regulatory Guide 1.157 for clarification of the acceptance criterion. Specifically:

The revised paragraph 50.46(a)(1) (i) requires that it be shown with a high probability that none of the criteria of paragraph 50.46(b) will be exceeded, and is not limited to the peak cladding temperature criterion. However, since the other criteria are strongly dependent on peak cladding temperature, explicit consideration of the probability of exceeding the other criteria may not be required if it can be demonstrated that meeting the temperature criterion at the 95% probability level ensures with an equal or greater probability that the other criteria will not be exceeded.

Rather than performing the number of calculations needed to support a trivariate analysis, Framatome ANP has used a mixture of classical statistics in support of a univariate analysis combined with engineering knowledge in support of the remaining two criteria. That is, the 59 cases performed provide the PCT at the 95/95 level. Since the PCT is below the criterion of 2,200°F, and the cladding oxidation is a strong function of temperature, there is a high probability that the cladding oxidation will be below the acceptance criteria. Information provided by Framatome ANP indicates that the local and total oxidation level at the calculated

PCT are 0.8 percent and 0.02 percent, respectively, for the 4-loop plant, and 1.3 percent and 0.04 percent, respectively, for the 3-loop plant. These oxidation levels are significantly below the acceptance criteria cited above. Thus, combining classical statistics with engineering knowledge provides reasonable assurance at a high probability that the acceptance criteria will not be exceeded.

The NRC staff has studied the position proposed by Framatome ANP that break type and size be treated statistically, and accepts its approach on the basis of the break type and size distributions assumed in its analysis. Specifically, the methodology applies a binomial distribution to the break type sampling, that is, the two break types (double-ended guillotine and slot breaks) are equally probable. In addition, a uniform distribution is applied to the entire break size spectrum from the largest to the smallest size. Thus, the break type and size selection is of uniform probability for the entire spectrum.

The NRC staff finds that the Framatome ANP methodology for the statistical results of an analysis of a RLBLOCA of a PWR meets the acceptance criteria stated in 10 CFR 50.46 and Regulatory Guide 1.157.

Framatome ANP is consistent with this step in the CSAU approach.

4.0 CONCLUSIONS

The NRC staff concludes from its review of the documentation, code and input models submitted that the S-RELAP5 RLBLOCA methodology is structured consistent with the CSAU methodological process, and satisfactorily reflects the intended use of the methodology to address licensing requirements for a variety of similarly designed nuclear power plants.

The NRC staff concludes that the approach proposed by Framatome ANP for selection of break type and size is acceptable since it assumes a binomial distribution of break type and uniform distribution of break size. Should Framatome ANP choose to change from this approach, the NRC staff will review the proposed changes.

The review of the models and benchmarks noted concerns and deficiencies resulting in conditions of use of S-RELAP5 as follows, which have been committed to in Reference 38:

- A CCFL violation warning will be added to alert the analyst to CCFL violation in the downcomer should such occur.
- Framatome ANP has agreed that it is not to use nodalization with hot leg to downcomer nozzle gaps.
- If Framatome ANP applies the RLBLOCA methodology to plants using a higher planar linear heat generation rate (PLHGR) than used in the current analysis, or if the methodology is to be applied to an end-of-life analysis for which the pin pressure is significantly higher, then the need for a blowdown clad rupture model will be reevaluated. The evaluation may be based on relevant engineering experience and should be documented in either the RLBLOCA guideline or plant specific calculation file.

- Slot breaks on the top of the pipe have not been evaluated. These breaks could cause the loop seals to refill during late reflood and the core to uncover again. These break locations are an oxidation concern as opposed to a PCT concern, since the top of the core can remain uncovered for extended periods of time. Should an analysis be performed for a plant with loop seals with bottom elevations that are below the top elevation of the core, Framatome ANP will evaluate the effect of the deep loop seal on the slot breaks. The evaluation may be based on relevant engineering experience and should be documented in either the RLBLOCA guideline or plant-specific calculation file.

The following restrictions apply when the Framatome ANP methodology is used for analysis of RLBLOCA.

- The model applies to 3 and 4 loop Westinghouse and CE-designed nuclear steam systems.
- The model applies to bottom reflood plants only (cold side injection into the cold legs at the reactor coolant discharge piping).
- The model is valid as long as blowdown quench does not occur. If blowdown quench occurs, additional justification for the blowdown heat transfer model and uncertainty are needed or the calculation is corrected. A blowdown quench is characterized by a temperature reduction of the PCT node to saturation temperature during the blowdown period.
- The reflood model applies to bottom up quench behavior. If a top-down quench occurs, the model is to be justified or corrected to remove top quench. A top-down quench is characterized by the quench front moving from the top to the bottom of the hot assembly.
- The model does not determine whether Criterion 5 of 10 CFR 50.46, long term cooling, has been satisfied. This will be determined by each applicant or licensee as part of the application of this methodology.

The NRC staff also notes that a generic topical report describing a code such as S-RELAP5 cannot provide full justification for each specific individual plant application. When a license amendment is necessary in order to use the S-RELAP5-based RLBLOCA methodology, the individual licensee or applicant must provide justification for the specific application of the code which is expected to include:

- Nodalization: Specific guidelines used to develop the plant-specific nodalization. Deviations from the reference plant must be addressed.
- Chosen Parameters and Conservative Nature of Input Parameters: A table that contains the plant-specific parameters and the range of the values considered for the selected parameter during the topical report approval process. When plant-specific parameters are outside the range used in demonstrating acceptable code performance, the licensee or applicant will submit sensitivity studies to show the effects of that deviation.

- Calculated Results: The licensee or applicant using the approved methodology must submit the results of the plant-specific analyses, including the calculated worst break size, PCT, and local and total oxidation.

5.0 REFERENCES

1. Letter, J. Mallay (Framatome ANP) to Document Control Desk (NRC), dated August 20, 2001.
2. Letter, J. Cushing (NRC) to J. Mallay (Framatome ANP), dated October 3, 2001.
3. EMF-2103(P), Rev. 0, Realistic Large Break LOCA Methodology for Pressurized Water Reactors, Framatome ANP, August 2001.
4. EMF-2100(P), Rev. 4, S-RELAP5 Models and Correlations Code Manual, Framatome ANP, May 2001.
5. EMF-2102(P), Rev. 0, S-RELAP5: Code Verification and Validation, Framatome ANP, August 2001.
6. EMF-2058(P), Rev. 1, S-RELAP5 Realistic Large Break LOCA Analysis Guidelines, Framatome ANP, August 2001.
7. EMF-2101(P), Rev. 2, S-RELAP5 Programmers Guide, Framatome ANP, January 2001.
8. Safety Evaluation by the Office of Nuclear Reactor Regulation for EMF-2328(P), PWR Small Break LOCA Evaluation Model, S-RELAP5 Based, June 2001.
9. Safety Evaluation by the Office of Nuclear Reactor Regulation for EMF-2310(P), SRP Chapter 15 Non-LOCA Methodology for Pressurized Water Reactors, August 2001.
10. Regulatory Guide 1.157, Best-Estimate Calculations of Emergency Core Cooling System Performance, May 1999.
11. NUREG/CR-5249, Quantifying Reactor Safety Margins, Application of Code Scaling, Applicability, and Uncertainty Evaluation Methodology to a Large-Break, Loss-of-Coolant Accident, December 1989.
12. Framatome ANP Presentation, Realistic Large Break LOCA Methodology for Pressurized Water Reactors, for NRR staff, October 30, 2001.
13. Framatome ANP Presentation, Realistic Large Break LOCA Methodology for Pressurized Water Reactors, for ACRS Thermal-Hydraulic Phenomena Subcommittee, January 17-18, 2002.
14. Ransom, V. H., et al, RELAP5/MOD2 Code Manual, NUREG/CR, EGG-2396, Rev. 1, March 1987.

15. Dimenna, R. A., et al, RELAP5/MOD2 Models and Correlations, NUREG/CR-5194, EGG-2531, August 1988.
16. ANF-90-145(P)(A), RODEX3 Fuel Rod Thermal-Mechanical Response Evaluation Model, Volumes 1 and 2, April 1996.
17. EMF-1557(P), Rev. 4, RODEX3A: Theory and User's Manual, November 2000.
18. EMF-2417(P), Rev. 0, RODEX3A Code Verification and Programmers Guide for Version USEP98, July 2000.
19. EMF-CC-039(P), Rev. 2, ICECON Code User's Manual: A Computer Program Used to Calculate Containment Back Pressure for LOCA Analysis (Including Ice Condenser Plants), March 1999.
20. EMF-CC-039(P), Rev. 2, Supplement 1, ICECON Code User's Manual: A Computer Program Used to Calculate Containment Back Pressure for LOCA Analysis (Including Ice Condenser Plants), December 1999.
21. Ransom, V. H., et al, RELAP5/MOD3 Code Manual, NUREG/CR-5535, INEL-95/0174, August 1995.
22. Request for Additional Information, Letter, NRC to Framatome ANP, dated June 24, 2002.
23. Response to Request for Additional Information, Letter, Framatome ANP to NRC, dated December 20, 2002.
24. Andreani, M, Studies of Dispersed Flow Film Boiling with 3-D Lagrangian Hydrodynamics and 2 2-D Eulerian Vapor Field, Swiss Federal Institute of Technology Zurich, Diss Ethz Nr. 9794, 1992.
25. Kirchner, W. L, Reflood Heat Transfer in a Light Water Reactor, NUREG-0106, Vol. I and II, MIT, August 1976.
26. Forslund, R. P. and W. M. Rosenow, Dispersed Flow Film Boiling, J. of Heat Transfer, pp. 399-407, November 1968.
27. Varone, A. F., and Rosenow, W. M., Post Dryout Heat Transfer Prediction, Nucl. Engr. And Design 95, pp. 315-327, 1986.
28. Yadigaroglu, G. et al, Modeling of Reflood, Nucl. Engr. and Design 145, pp. 1-35, (1993).
29. Andreani, M. and Yadigaroglu, G., Dispersed Flow Film Boiling, NUREG/IA-0042, August 1992.

30. Webb, S. W. and Chen, J. C., A Numerical Model for Turbulent Non-Equilibrium Dispersed Flow Heat Transfer, Int. J. Heat Mass Transfer, Vol.25, No.3, pp. 325-335, 1982.
31. Bajorek, S. and Young, M., Direct-Contact Heat Transfer Model for Dispersed-Flow Film Boiling, Nuclear Technology, Vol. 132, December 2000.
32. Yoder, G.L. and Rosenow, W. M., A Solution for Dispersed Flow Heat Transfer Using Equilibrium Fluid Conditions, J. of Heat Transfer, Vol. 105, pp.11-17, February 1983.
33. Lucas, S., Recirculating Flow Anomaly Problem Solution Method, Proceedings of ICONE8, 8th International Conference on Nuclear Engineering, paper # 8479, April 2-6, 2000.
34. ANSI/ANS-5.1-1979, American National Standard for Decay Heat Power in Light Water Reactors, approved August 29, 1979.
35. BAW-10227P-A, Evaluation of Advanced Cladding and Structural Material (M5) in PWR Reactor Fuel, Framatome Cogema Fuels, February 2000.
36. BAW-10231P-A, COPENIC Fuel Rod Design Computer Code, Framatome Cogema Fuels, April 2002.
37. Wilks, S.S., Determination of Sample Sizes for Setting Tolerance Limits, Ann. Math. Stat., Vol. 12, 1941.
38. Letter, Framatome ANP to NRC dated December 20, 2002.

Attachments: 1. Table 1 - S-RELAP5 Assessment Matrix
2. Figure 1 - FLECHT-SEASET Test 31302
3. Figure 2 - FLECHT-SEASET Test 31504
4. Figure 3 - LOFT LP-LB-1 S-RELAP5 Analysis
5. Figure 4 - PCT Independent of Location - PWR
6. Figure 5 - PCT Independent of Location - PWR
7. Figure 6 - Peak Clad Temperature - FS 31504

Principal Contributor: R. Landry

Date: April 9, 2003

Table 1

S-RELAP5 ASSESSMENT MATRIX		
Facility	Tests	Purpose
THTF Heat Transfer	35	Heat Transfer
THTF Level Swell	3	Void Distribution
GE Level Swell	1	Void Distribution
FRIGG-2	27	Void Distribution
Bennet Tube	2	Heat Transfer
FLECHT & FLECHT-SEASET	9	Heat Transfer, Nodalization, Axial Power Distribution, Scalability, Entrainment
PDTF/SMART	4	Spacer Effects
Marviken	9	Break Flow
W/EPRI 1/3 Scale	9	Cold Leg Condensation, Interfacial Heat Transfer
Mini-Loop CCFL	3	Upper Tie Plate CCFL
Multi-dimensional Flow	3	Core Flow Distribution
UPTF	14	ECCS Bypass, Steam Binding, CCFL, Scalability, Nodalization
CCF	4	Steam Binding, Nodalization, Scalability
SCTF	6	Nodalization
ACHILLES	1	Accumulator Nitrogen Disch.
LOFT	4	Overall Code Performance, Nodalization, Scalability
Semiscale	2	Blowdown Heat Transfer, Nodalization, SCALABILITY, Compensating Errors

FLECHT-SEASET Test 31302

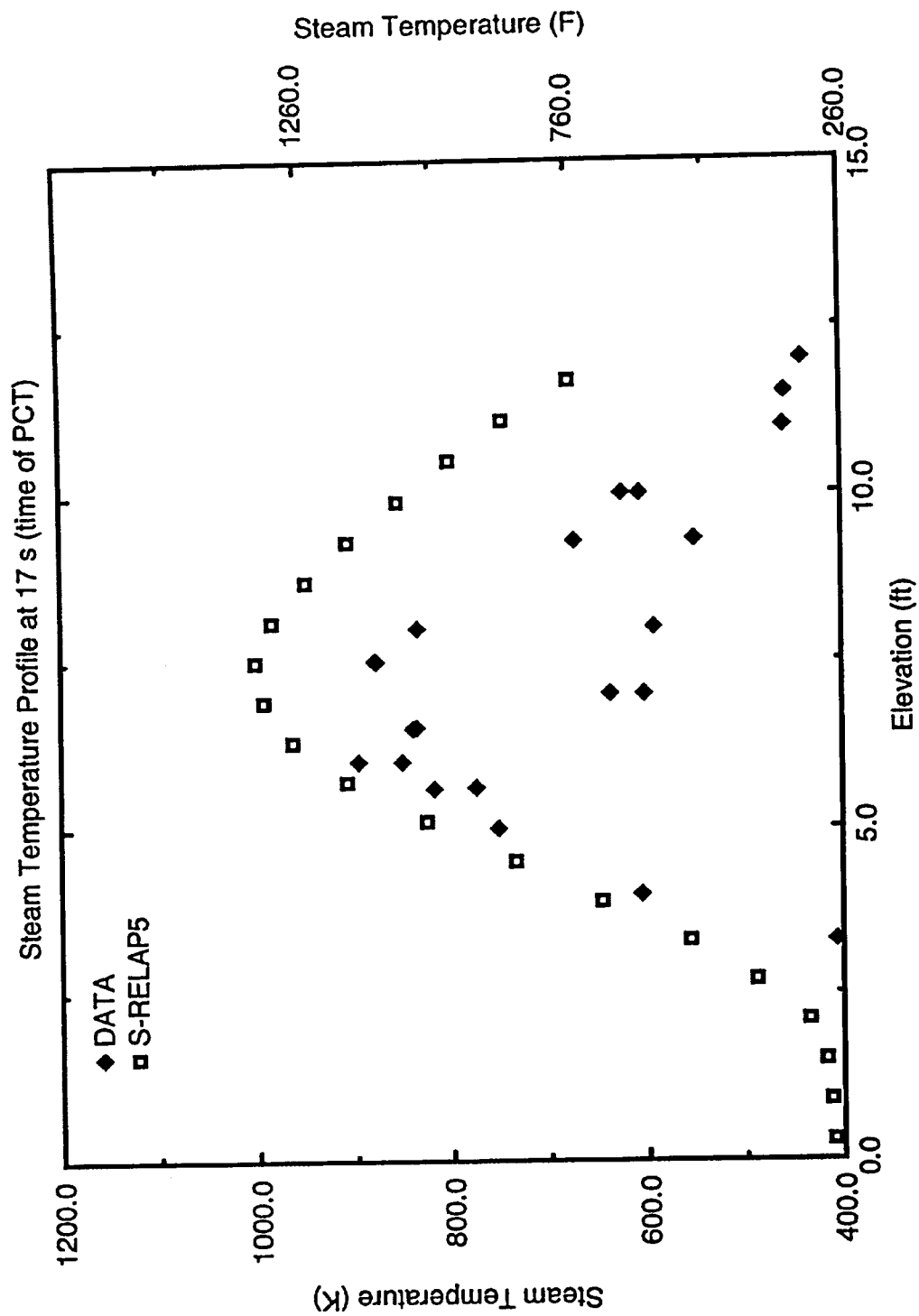


Figure 1

Figure 2

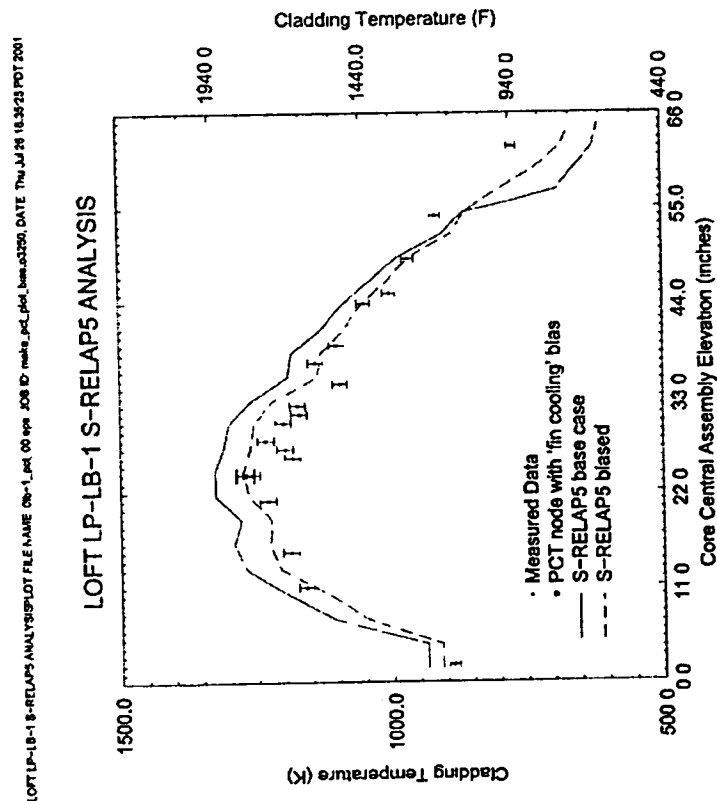


Figure 4.194 LOFT LP-LB-1 PCT Profile

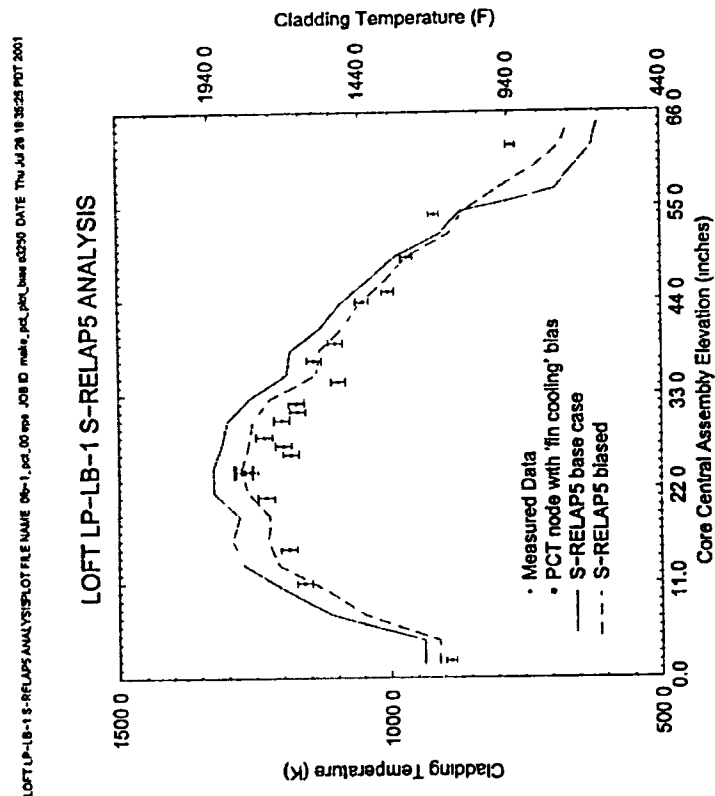


Figure 4.194 LOFT LP-LB-1 PCT Profile

PCT Independent of Location - PWR

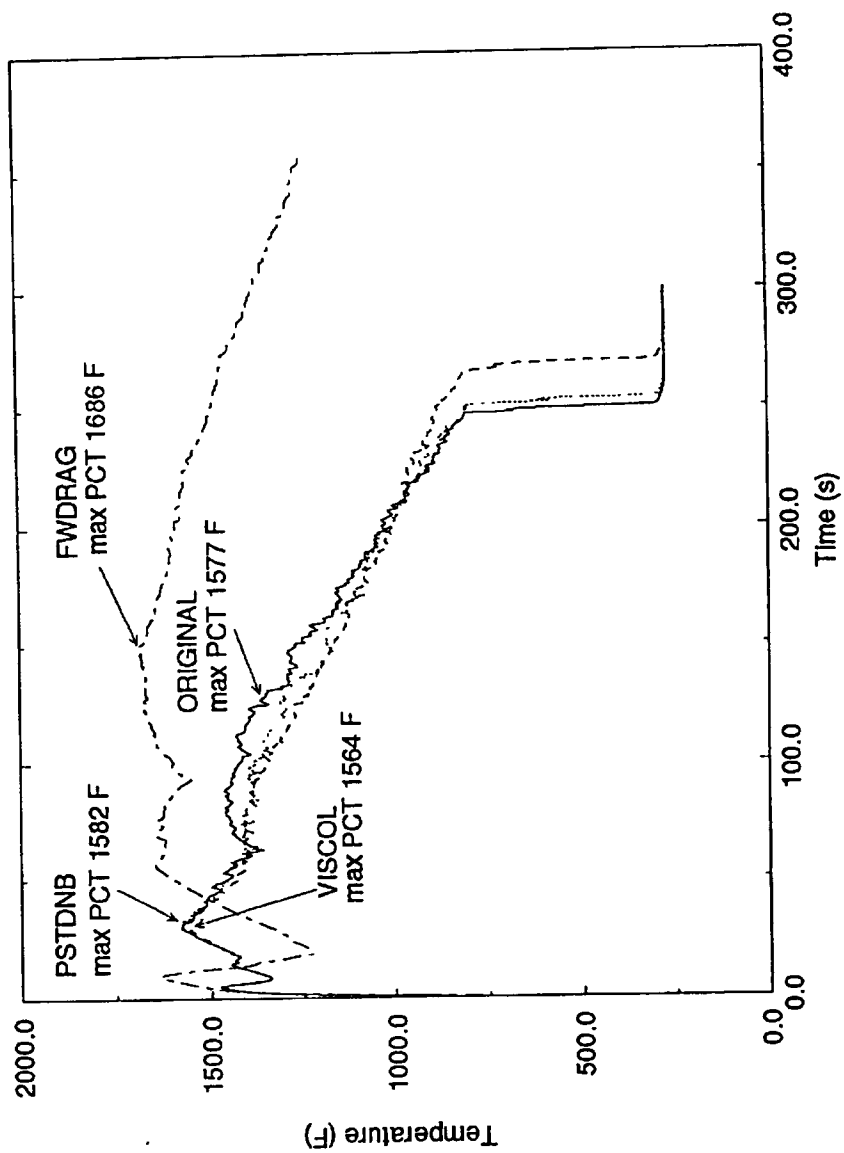


Figure 4

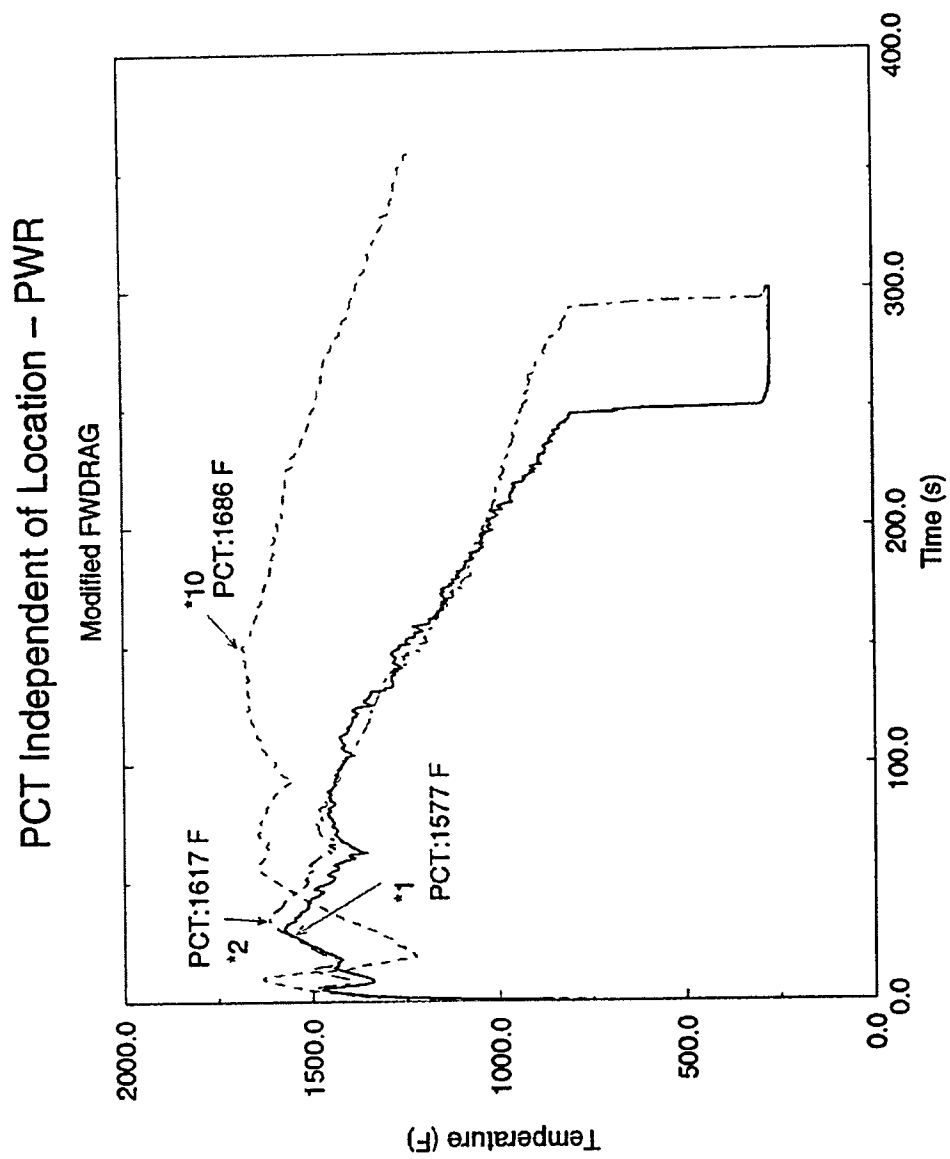


Figure 5

Peak Clad Temperature – FS 31504

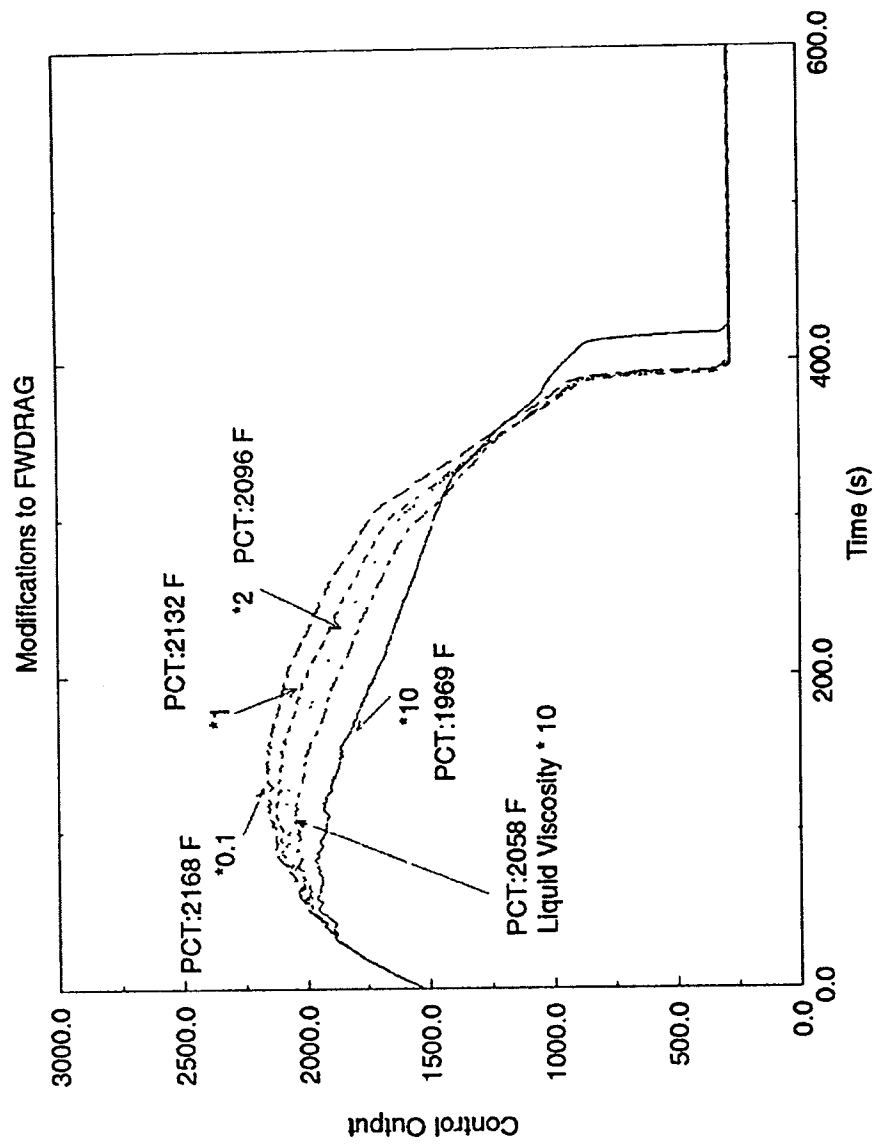


Figure 6



August 20, 2001
NRC:01:035

Document Control Desk
ATTN: Chief, Planning, Program and Management Support Branch
U.S. Nuclear Regulatory Commission
Washington, D.C. 20555-0001

Request for Review of EMF-2103(P) Revision 0, Realistic Large Break LOCA Methodology for Pressurized Water Reactors

Framatome ANP requests the NRC's review and approval for referencing in licensing actions the topical report EMF-2103(P) Revision 0, Realistic Large Break LOCA Methodology for Pressurized Water Reactors. One CD containing a proprietary version of the report and one CD containing the non-proprietary version of the report are enclosed. We request that the NRC approve this report by September 1, 2002. Framatome ANP plans to apply this methodology to the analysis of the H. B. Robinson plant.

Several documents referenced in the topical report are being provided in a separate transmittal. These documents are intended to facilitate the NRC's review and approval. The computer codes used to execute the methodology and input for a sample problem are also being provided separately.

Framatome ANP intends to make minor modifications to the methodology described in the topical report after its approval. These modifications will facilitate the integration of the fuel designs developed by Siemens Power Corporation and Framatome Cogema Fuels. These changes will extend the range of applicability of the methodology to other plants types (B&W), another fuel cladding type (M5), and an additional fuel rod code (COPERNIC). Since these modifications will be submitted for review and approval soon after the base methodology has been accepted, these planned modifications should be taken into account during the review.

Framatome ANP considers some of the information contained in the enclosed report to be proprietary. As required by 10 CFR 2.790(b), an affidavit is enclosed to support the withholding of the information from public disclosure.

Very truly yours,

A handwritten signature in black ink, appearing to read 'James F. Mallay', written over a horizontal line.

James F. Mallay, Director
Regulatory Affairs

cc: R. Caruso
R. Landry (w/enclosures)
N. Kalyanam (w/enclosures)
J. S. Wermiel Project 702

Framatome ANP Richland, Inc.

2101 Horn Rapids Road
Richland, WA 99352

Tel: (509) 375-8100
Fax: (509) 375-8402

AFFIDAVIT

STATE OF WASHINGTON)
) ss.
COUNTY OF BENTON)

1. My name is James F. Mallay. I am Director, Regulatory Affairs, for Framatome ANP ("FRA-ANP"), and as such I am authorized to execute this Affidavit.

2. I am familiar with the criteria applied by FRA-ANP to determine whether certain FRA-ANP information is proprietary. I am familiar with the policies established by FRA-ANP to ensure the proper application of these criteria.

3. I am familiar with the FRA-ANP material enclosed in report EMF-2103(P), Revision 0, "Realistic Large Break LOCA Methodology for Pressurized Water Reactors," transmitted with letter NRC:01:035, and referred to herein as "Document." Information contained in this Document has been classified by FRA-ANP as proprietary in accordance with the policies established by FRA-ANP for the control and protection of proprietary and confidential information.

4. This Document contains information of a proprietary and confidential nature and is of the type customarily held in confidence by FRA-ANP and not made available to the public. Based on my experience, I am aware that other companies regard information of the kind contained in this Document as proprietary and confidential.

5. This Document has been made available to the U.S. Nuclear Regulatory Commission in confidence with the request that the information contained in the Document be withheld from public disclosure.

6. The following criteria are customarily applied by FRA-ANP to determine whether information should be classified as proprietary:

- (a) The information reveals details of FRA-ANP's research and development plans and programs or their results.
- (b) Use of the information by a competitor would permit the competitor to significantly reduce its expenditures, in time or resources, to design, produce, or market a similar product or service.
- (c) The information includes test data or analytical techniques concerning a process, methodology, or component, the application of which results in a competitive advantage for FRA-ANP.
- (d) The information reveals certain distinguishing aspects of a process, methodology, or component, the exclusive use of which provides a competitive advantage for FRA-ANP in product optimization or marketability.
- (e) The information is vital to a competitive advantage held by FRA-ANP, would be helpful to competitors to FRA-ANP, and would likely cause substantial harm to the competitive position of FRA-ANP.

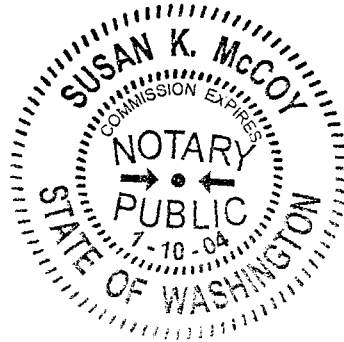
7. In accordance with FRA-ANP's policies governing the protection and control of information, proprietary information contained in this Document has been made available, on a limited basis, to others outside FRA-ANP only as required and under suitable agreement providing for nondisclosure and limited use of the information.

8. FRA-ANP policy requires that proprietary information be kept in a secured file or area and distributed on a need-to-know basis.

9. The foregoing statements are true and correct to the best of my knowledge,
information, and belief.

James P. Mally

SUBSCRIBED before me this 23rd
day of August, 2001.



Susan K. McCoy

Susan K. McCoy
NOTARY PUBLIC, STATE OF WASHINGTON
MY COMMISSION EXPIRES: 1/10/04



March 1, 2002
NRC:02:015

Document Control Desk
ATTN: Chief, Planning, Program and Management Support Branch
U.S. Nuclear Regulatory Commission
Washington, D.C. 20555-0001

NRC Review of EMF-2103(P) Revision 0, Realistic Large Break LOCA Methodology for Pressurized Water Reactors

Ref.: 1. Letter, J. F. Mallay (FRA-ANP) to Document Control Desk (NRC), "Request for Review of EMF-2103(P) Revision 0, Realistic Large Break LOCA Methodology for Pressurized Water Reactors," NRC:01:035, August 2001 (Accession #ML012400042).

Framatome ANP requested the NRC's acceptance for referencing in licensing actions the topical report EMF-2103(P) Revision 0, "Realistic Large Break LOCA Methodology for Pressurized Water Reactors" in Reference 1. Two documentation errors have been identified since the submittal of Reference 1. The attachment to this letter contains two corrected pages which Framatome ANP proposes to use when the A version of EMF-2103 is issued following NRC review and approval.

The change on page 4-97 deletes the following sentences:

As this value was based solely on data at 40 psia (2.76 bar), a penalty bias was included to cover the possibility of the system pressure falling below this value. The hydrodynamic film instability theory of Berenson was used to develop this pressure bias (Reference 5).

The use of a pressure bias was considered during the development of the methodology but was determined to be unnecessary due to the extensive conservatism inherent in the base model. The primary conservatism derives from basing the T_{min} model on tests using stainless steel clad. Comparison of quench data for zircaloy clad quantify this conservatism to be around 200°F. A complete discussion of this model and the inherent conservatism is given in EMF-2102.

The change on page 5-22 deletes the entry "ECCS Losses" from the table. The ECCS losses are dominated by variations in break size and are therefore not treated separately. In addition, data from a series of accumulator drain down tests showed only a $\pm 3\%$ variation.

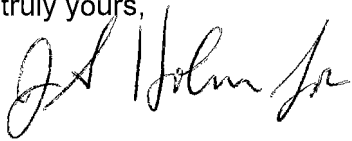
Framatome ANP, Inc.

2101 Horn Rapids Road
Richland, WA 99352

Tel: (509) 375-8100
Fax: (509) 375-8402

Framatome ANP considers some of the information contained in the enclosure to this letter to be proprietary. The affidavit provided with the original submittal of EMF-2103(P) Revision 0 (Reference 1) satisfies the requirements of 10 CFR 2.790(b) to support the withholding of this information from public disclosure.

Very truly yours,

A handwritten signature in black ink, appearing to read "J. F. Mallay".

James F. Mallay, Director
Regulatory Affairs

lmk

Enclosure

cc: R. R. Landry
J. S. Cushing
D. G. Holland
Project 693

]

The probability density functions are defined by the following two equations. The coefficients for the equations vary depending on whether they are to be applied to FILMBL (low void fraction) or FRHTC (high void fraction).

[

]

[

]

These are given in Table 4.20.

4.3.3.2.6 T_{min}

A set of seven FLECHT SEASET tests was used to evaluate the trends in T_{min} at low pressure. Quench temperatures improve at higher pressures; hence, a T_{min} uncertainty based on low pressure data was expected to bound high pressure data. This was validated with data from ROSA/TPTF, the ORNL/THTF and the Westinghouse G1/G2 tests. Examination of FLECHT SEASET data showed that based on observable conservatisms, only the 3 in/s reflood rate test (Test #31302) was necessary to evaluate a bounding T_{min} uncertainty (Reference 5).

From the FLECHT SEASET data and from an evaluation of code uncertainty with regard to how the LBLOCA multiplier relates to T_{min}, [

] The uncertainty evaluation has been

demonstrated to be a conservative bounding distribution relative to other datasets.

4.3.3.2.7 Break Flow

Break flow is a function of break area and critical flow uncertainty. [

Table 5.6 Relationship of Uncertainty Parameters to Computer Code Input



May 1, 2002
NRC:02:024

Document Control Desk
ATTN: Chief, Planning, Program and Management Support Branch
U.S. Nuclear Regulatory Commission
Washington, D.C. 20555-0001

NRC Review of EMF-2103(P) Revision 0, Realistic Large Break LOCA Methodology for Pressurized Water Reactors – Appendices D and E

Ref.: 1 Letter, J. F. Mallay (FRA-ANP) to Document Control Desk (NRC), "Request for Review of EMF-2103(P) Revision 0, Realistic Large Break LOCA Methodology for Pressurized Water Reactors," NRC:01:035, August 20, 2001

Framatome ANP requested the NRC's acceptance for referencing in licensing actions the topical report EMF-2103(P) Revision 0, "Realistic Large Break LOCA Methodology for Pressurized Water Reactors" in Reference 1. The purpose of this letter is to submit two appendices (D and E) to EMF-2103(P). We request that these appendices be included in the NRC's review and approval of EMF-2103 (P). Appendix D provides a sample application of the EMF-2103 methodology to a 3-loop Westinghouse plant. Appendix E describes the incorporation of M5 cladding properties into the realistic methodology.

A CD containing proprietary and non-proprietary versions of Appendix D and Appendix E is enclosed. The attachment to this letter provides a list of the files contained on the CD.

Framatome plans to include Appendices D and E in the approved version of EMF-2103(P) following receipt of the NRC safety evaluation report. The table of contents in the approved version of EMF-2103(P) will be modified to reflect these appendices.

Framatome ANP considers some of the information contained in the enclosure to be proprietary. The affidavit provided, with Reference 1, satisfies the requirements of 10 CFR 2.790(b) to support withholding of this information from public disclosure

Very truly yours,

A handwritten signature in black ink, appearing to read 'James F. Mallay'.

James F. Mallay, Director
Regulatory Affairs

Attachment/Enclosures

cc: R. Caruso
D. G. Holland
Project 693

Attachment A

Listing of files contained on the enclosed CD

Readme.txt	File containing listing and description of files on the CD.
EMF-2103(P)_Appendix_D_Sample_Westinghouse_3_Loop_PWR_Licensing_Analysis.pdf	Sample Westinghouse 3-loop PWR Licensing Analysis, Appendix D to EMF-2103 (Proprietary Version)
EMF-2103(P)_Appendix_E_Incorporation_of_M5_Cladding_Properties.pdf	Incorporation of M5 cladding Properties, Appendix E to EMF- 2103 (Proprietary Version)
EMF-2103(P)_TOC.pdf	Updated table of contents and nomenclature for EMF-2103 that includes Appendix D and Appendix E. (Proprietary Version)
EMF-2103(P)_TOC.pdf	Updated table of contents and nomenclature for EMF-2103 that includes Appendix D and Appendix E. (Proprietary Version)
EMF-2103(NP)_Appendix_E_Incorporation_of_M5_Cladding_Properties.pdf	Incorporation of M5 cladding properties, Appendix E to EMF- 2103 (Nonproprietary Version)
EMF-2103(NP)_TOC.pdf	Updated table of contents and nomenclature for EMF-2103 that includes Appendix D and Appendix E. (Nonproprietary Version)



UNITED STATES
NUCLEAR REGULATORY COMMISSION

WASHINGTON, D.C. 20555-0001

June 24, 2002

Mr. James Mallay
Director, Regulatory Affairs
Framatome ANP, Richland, Inc.
2101 Horn Rapids Road
Richland, WA 99352

SUBJECT: REQUEST FOR ADDITIONAL INFORMATION ON EMF-2103(P), REV. 0,
"REALISTIC LARGE BREAK LOCA METHODOLOGY FOR PRESSURIZED
WATER REACTORS" (TAC NO. MB2865)

Dear Mr. Mallay:

By letter dated August 20, 2001, Framatome ANP submitted for staff review Topical Report EMF-2103(P), Rev. 0, "Realistic Large Break LOCA Methodology for Pressurized Water Reactors." The staff has completed its preliminary review of EMF-2103(P), Rev. 0 and has identified a number of items for which additional information is needed to continue its review. The enclosed request for additional information (RAI) was discussed with your staff on May 13, 2002. A mutually agreeable target date of July 19, 2002, was established for responding to the RAI. Please provide the requested information so that the review can be completed in a timely manner. Partial submittals would be welcomed to minimize delays.

Pursuant to 10 CFR 2.790, we have determined that the RAI provided as Enclosure 1 contains proprietary information. Proprietary information contained in Enclosure 1 is indicated by marginal lines. We have prepared a non-proprietary version of the RAI (Enclosure 2) that we have determined does not contain proprietary information. However, we will delay placing Enclosure 2 in the public document room for a period of ten (10) working days from the date of this letter to provide you with the opportunity to comment on the proprietary aspects only. If you believe that any information in Enclosure 2 is proprietary, please identify such information line by line and define the basis pursuant to the criteria of 10 CFR 2.790.

If you have any questions, please call me at (301) 415-1436.

Sincerely,

A handwritten signature in black ink, appearing to read "Drew Holland", is written over the word "Sincerely,".

Drew Holland, Project Manager, Section 2
Project Directorate IV
Division of Licensing Project Management
Office of Nuclear Reactor Regulation

Project No. 693

Enclosures: 1. Request for Additional Information (Proprietary)
2. Request for Additional Information (Non-proprietary)

REQUEST FOR ADDITIONAL INFORMATION

TOPICAL REPORT EMF-2103(P), REV. 0, " REALISTIC LARGE BREAK LOCA METHODOLOGY FOR PRESSURIZED WATER REACTORS"

FRAMATOME, ANP

PROJECT NO. 693

Heat Transfer

1. Please provide a list of differences in the heat transfer models and the critical heat flux (CHF) correlations as utilized in the realistic large break loss-of-coolant accident (RLBLOCA) to those utilized in the small break loss-of-coolant accident (SBLOCA) models.
2. In the analysis of the large break loss-of-coolant accident (LBLOCA) transient, there are a number of different correlations that are used as the transient unfolds (Biasi, modified Zuber, Sleicher and Rouse, Dittus-Boelter, etc.). Please choose a typical LBLOCA transient and map out all the different correlations that are used along the way, from the beginning of the transient to the end. State the particular correlation used, its applicable range (in terms of Reynold No., flow rates, etc.), and validation of its use in the applicable range.
3. Subroutine CHFCAL has the ICHF options for either Biasi and Zuber (ICHF=0), or the Extended Biasi (ICHF=1). EMF-CC-097(P), Rev. 7, page 7-2 also mentions the correlation for the Extended Biasi and choosing this will use the correlation for all flow conditions. However, EMF-2100(P), Section 4.4 does not mention the "Extended" Biasi, but the Biasi and Zuber correlations. There is also a note that the Biasi correlation is not used for $G < 100 \text{ kg/m}^2\text{s}$. Is this Biasi correlation the "Extended Biasi"?
4. Subroutine CHFCAL appears to contain the Modified Zuber CHF correlation beginning at 300. Line 300 and its uncommented continuation and Equation 4.32 of EMF-2100(P) appear to match up if MHTCHF is equal to F. However, it does not appear that was the intention given the code which follows.
 - a. What are MHTCHF and XBIASI and where do they come from?
 - b. The second option for F in Equation 4.33 of EMF-2100(P) is similar, but different than the first uncommented line after what appears to be the modified Zuber CHF correlation. Please clarify the differences and the apparent absence of the first option for F (commented out on the second continuation line after 300).
 - c. The three lines of coding before the last END IF of subroutine CHFCAL appear similar but different than the linear interpolation for mass flux between 100 and 200 $\text{kg/m}^2\text{s}$ of Equation 4.34 of EMF-2100(P). Please explain the apparent differences between the coding and the code manual documentation.

Enclosure 2

- d. Parameter HTHDMO(LS) appears to be in units of meters given the logic question: IF (HTHDMO(LS) .LT. 0.01DO) THEN in the Biasi correlation coding. However, the next line multiplies HTHDMO(LS) by 100 possibly to convert to meters from centimeters before raising it to the "n" power (either 0.4 or 0.6 based on the conditions on page 4-12 of EMF-2100(P)). The documentation states that the hydraulic diameter is in units of cm and is not multiplied by 100 in either Equation 4.28 or 4.29. Please clarify.
 - e. Is the mass flux parameter "G" brought into the CHF calculation in units of gm/cm²s, or kg/m²s?
 - f. Clarify why MAXimums and MINimums are taken throughout the subroutine CHFCAL. How does this affect the uncertainty of the CHF value? For example, if ICHF=1 and G=20 kg/m²s, G is changed to 100 kg/m²s since the Biasi correlation is not used for G<100 kg/m²s. However, Biasi is used when the ICHF overrides that applicability where the Zuber correlation should be used. This also occurs if G is 120 kg/m²s and ICHF=1. It does not appear that the interpolation on the mass flux with the Biasi and Zuber correlations will not be implemented as described in the documentation. Is this Biasi correlation the Extended Biasi? Where did the parameter XBIASI come from?
- 5. In the Sleicher and Rouse heat transfer correlation, please clarify how the coded parameter XTF in subroutine DITTSG matches the documentation of Equation (4.36) in EMF-2100(P), page 4-15.
 - 6. Account for the VOIDG term which appears in the coding for the natural convection term, but does not appear in the documentation.
 - 7. Please clarify what is meant by, "The equation is independent of the characteristic length due to the 1/3 power dependency of the Grashof number given in Equation (4.35)." Equation (4.35) gives the heat transfer coefficient as the MAX of the Sleicher Rouse and the natural convection heat transfer coefficients with no mention of the Grashof number (pages 4-14 and 4-15 of EMF-2100(P), Rev. 4).
 - 8. The documentation on page 4-15 of EMF-2100(P), Rev. 4 includes the addition of radiation heat transfer from the wall to the single phase vapor fluid if the surface temperature is greater than 650K. Identify where this is accounted for in the code.
 - 9. It appears that a modified Dittus-Boelter correlation or the Sleicher and Rouse correlation is chosen based on the IF statement:


```
IF (IAND(IDNGAP(2,IH),256) .NE. 0) THEN.....modified (?) Dittus-Boelter  
else Sleicher Rouse.
```
 - a. Please clarify why in the documentation of page 4-14 of EMF-2100(P), the Sleicher Rouse correlation is said to be selected because it has a smaller uncertainty than the Dittus-Boelter correlation, but in the code the IF statement results in a choice between the two. Please clarify the meaning of the IF statement.

- b. The Dittus-Boelter heat transfer correlation coded in the DITTSG subroutine does not appear to be the same as that documented in Equation (4.16) of EMF-2100(P). Please clarify the differences.
10. The 'nature' convection correlation coding of subroutine DITTUS includes:
$$HTCOEF = \text{MAX}(\text{HMAC}, 0.59\text{DO}*(\text{PRGR})^{**0.25}\text{DO}*\text{PRGR}*\text{COHDM}/\text{TERM})$$
which occurs if PRGR is less than the Reynolds number squared. Please identify the discussion of this in the documentation of EMF-2100(P), or include it as needed.
11. Is the modified Bromley from the documentation (EMF-2100(P), Rev. 4, page 4-18) the same as the Bromley correlation of the FILMBL subroutine?
12. Please describe how the interpolation of the last line of FILMBL is the same as Equation 4.50 of EMF-2100(P), Rev. 4, page 4-19.
13. Please include @@ in the documentation description above Equation 4.50 of EMF-2100(P), Rev. 4, page 4-19 to describe use of the Forslund-Rohsenow and modified Bromley correlations if that was the intent as coded.
14. Please explain why in the code the BROMLEY correlation is calculated for a void fraction less than or equal to [], and the FORSLUND-ROHSENOW is calculated for a void fraction greater than or equal to [] as documented in EMF-2100(P), Rev. 4, page 4-19. The void fractions appear consistent with the documentation beginning at line 208.
15. What does CFR, the first term in HDF, account for in the Forslund-Rohsenow correlation?
16. In the "NATURE" convection correlation, HMAC is defined if (PRGR.LT.TERM) as the []. Please discuss the appearance of the "PRGR/TERM" in the natural convection heat transfer coefficient, which appeared similarly in subroutine DITTUS, which the staff has not yet found described in the documentation.
17. Please include discussion of the scaling of the natural convection heat transfer correlations by the void fraction in the PREDNB subroutine by $\text{COHDMF}=\text{COHDM}*\text{VOIDF}$.
18. Please explain why the suppression factor is coded to be 0.0797 of $\text{ReTP}@70$ instead of 0.1 as documented in Equation 4.21 of EMF-2100(P).
19. What is the ICHF=2 option and where is that described?
20. Many of the test programs used in the assessment of S-RELAP5 inherently incorporated radiation heat transfer between hot rods and colder components. Please discuss and justify exclusion of a specific radiation heat transfer model in the Framatome-ANP RLBLOCA methodology. Include in the discussion the manner in which the methodology accounts for radiation heat transfer during those portions of the analyzed

event for which radiation heat transfer would be expected to play a significant role. Also discuss and justify known compensating errors introduced in the methodology that account for this effect.

21. Please explain and justify the basis for choosing the Forslund-Rosenow correlation for void fractions [] and the Bromley at [] for dispersed flow film boiling. Since the Bromley correlation can result in high heat transfer coefficients during dispersed flow, extrapolating the Bromley correlation between 0.7 and 0.9 can result in applying extrapolated HTC's over large regions of the bundle. Please justify this extrapolation range and show that it does not influence the heat transfer coefficient at or near the PCT location.
22. The Forslund Rosenow correlation for dispersed flow film boiling consists of a droplet wall contact model developed for low quality, high mass flux conditions in a small diameter tube. The model is applicable only to a small localized region just above the quench front, where the wall temperatures are below the rewet temperature. Physically, the droplet wall contact begins at the inverted annular regime and increases through to the agitated inverted annular regime where the effect is at a maximum due to either high turbulence or some possible droplet wall contact. Downstream of the agitated region, this droplet wall contact affect decreases rapidly and becomes non-existent once the highly dispersed flow region develops. The computed heat transfer multiplier of [] indicates that the correlation may not present a true best-estimate representation. Since the Forslund-Rosenow correlation is highly dependent on void fraction, over-estimation of the entrainment can propagate large errors into the heat transfer during reflood.
23. It appears that the data for elevations above 8 ft in the tests used for determining the film boiling heat transfer multipliers were discarded during the data reduction process. Please discuss and justify the applicability of the film boiling heat transfer multiplier at all elevations along the fuel rod and for various power shapes. Include in the discussion, justification for applicability of the film.

PIRT

24. The Framatome-ANP PIRT is similar to the NUREG/CR 5249 PIRT. This PIRT does not address the following:
 - a. Relative location of the hot assembly in the core.
 - b. Uncertainty in the single phase pump performance.
 - c. Uncertainty in the broken nozzle k-factor.

Please clarify how these contributors are addressed in the RLBLOCA methodology.

Break Flow Modeling

25. The orientation and location of the postulated pipe breaks are not explicitly addressed. Please discuss the following:

- a. The choice of break location, such as cold leg versus hot leg and hot leg both with and without pressurizer, and location of slot breaks, such as top, side and bottom of the pipe. In addition, why were other locations than those presented not considered, or if they were considered, why were they not analyzed?
- b. The smallest break size analyzed using the RLBLOCA methodology. Also discuss the definitions used by Framatome-ANP in determining the boundaries between the large and small break methodologies and how a single calculational tool such as S-RELAP5 is applicable over the entire range of break sizes.

Containment Modeling

26. Although the Framatome-ANP RLBLOCA methodology uses the ICECON methodology to perform the containment back pressure to the reactor coolant system analysis, the methodology still uses a simplified component system model of the containment. Please discuss how a single comparison of ICECON with GOTHIC is sufficient demonstration of applicability to the range of Westinghouse and Combustion Engineering containment configurations.

Downcomer Boiling

27. The brief overview and description of LBLOCA behavior on page 3-4 does not mention the potential for downcomer boiling. Downcomer boiling has been shown to be important in the transport of coolant to the core in the LBLOCA. Discuss the basis for the applicability of the S-RELAP5 simulation of the effects of downcomer boiling and the manner in which downcomer boiling has been treated in the RLBLOCA methodology. Include in the discussion the roll of the downcomer wall initial temperature in downcomer boiling.

The PIRT in Table 3.3 does not include downcomer boiling. Please include in the discussion the exclusion of downcomer boiling from the PIRT.

Fuel Swelling and Rupture, Relocation and Metal/Water Reaction

28. On page 3-7 it is noted that fuel rod rupture is not included in the calculations, and possibly the peak local clad oxidation calculation will not include inside oxidation as well as outside oxidation. In addition, there is some confusion regarding the metal/water reaction model being used.
 - a. Please clarify and discuss why the fuel swelling and rupture model is not used. The discussion should include consideration of the effects of burnup. The discussion should also include justification for neglecting fuel swelling and rupture in the calculations and the effect this has on producing a lower oxidation potential since inner cladding surface oxidation is not considered.
 - b. Fuel pellet relocation has been observed which can cause pellets to fill the space created by swelling and ballooning cladding. Please discuss why Framatome-ANP has not included this effect and the basis for that decision.

- c. Please clarify why the Cathcart-Pawel model is used in S-RELAP5 model as described in the Methodology document, EMF-2103, while the Models and Correlations document, EMF-2100 describes the Baker-Just model. Also, there appear to be better models than the Cathcart-Pawel metal/water reaction model for temperatures below 1900°F. Please discuss the basis for not choosing another metal/water reaction model for the lower temperature range and also include in the discussion a justification for the assumptions applied for the initial condition.
- d. In the time-in-life study, what inside and outside initial oxidation thicknesses were used for the BOL analysis. What oxide thickness is used for once and twice burned fuel?

Decay Heat

- 29. Section 4.3.3.2.3 of EMF-2103 discusses the decay heat standard but does not show the calculated decay curve used in the analyses. Please compare the decay heat model with uncertainty applied to the ANSI/ANS-5.1-1979 standard to show that the S-RELAP5 model predicts or bounds the data in the standard for the simulation period. Include in the discussion the treatment of gamma redistribution uncertainty.

Assessment

- 30. Numerous tests cited in the methodology assessment, such as FRIGG2, THTF, GE level swell, FLECHT and FLECHT-SEASET are valid under specific pressure conditions. Please clarify and assess the applicability of the tests used in the assessment program to the ranges of conditions in which they were used. Include in the discussion the assessment of void distribution and subcooled boiling via high pressure data and the applicability of these models to low pressures.

Please discuss and justify use of the Forslund-Rosenow correlation to determine PCT. Justification is needed to assure that errors in other models and the thermal hydraulics will not produce heat transfer coefficients that are beyond the range of the intended correlation.

Long-Term Coolability

- 31. Please discuss how the Framatome-ANP RLBLOCA methodology addresses the element of long-term coolability as required in the regulatory acceptance criteria.
- 32. Please describe the methods and analyses that will be employed to demonstrate that boric acid precipitation is assessed or neglected in the methodology.

Entrainment and 2-D Effects

- 33. The S-RELAP5 liquid entrainment predictions overpredict the data by a factor of 2 for the FLECHT-SEASET and skewed tests. However, S-RELAP5 overpredicts the clad temperatures at the upper elevations. Please discuss this apparent anomaly and also discuss the capability of the 2-D model in S-RELAP5 to simulate the super heat near the wall and account for the radial steam temperature profile across the channel in the tests.

Void Fraction

34. Page 4-97 discusses T_{min} but does not describe the conditions as to how the correlation is applied in the code. Please discuss and justify the effect of void fraction on the application, effect of its exclusion, and the application of T_{min} in the Framatome-ANP RLBLOCA methodology.
35. Page 5-2 of EMF-2103(P) states that "the plant process parameters are treated statistically, however conservative methods also can be used in the absence of adequate data to support the statistical use." Table 5.1 also does not indicate the following parameters. Please discuss which have been treated statistically and which conservatively in the methodology.

Initial Conditions:

RCS Temperature

Accumulator line resistance

Safety injection temperature

Peripheral assembly power (how is this bounded?)

Also please discuss how the following model uncertainties are handled and/or justify their omission from the analysis:

Broken nozzle resistance, K-factor

Broken loop pump resistance

Condensation

Fuel conductivity (before and after burst)

Fuel density (packing fraction after burst)

Rod internal pressure

Cladding burst temperature

Cladding Burst strain and average strain

Metal/water reaction

Since different plant designs will have different values and ranges for many of the parameters in the above lists, will the various parameters be identified in the plant-specific submittals giving the distributions or conservative limits?

36. Please discuss the procedures which will be used to ensure that the range of conditions in the plants for which the Framatome-ANP RLBLOCA methodology is used are consistent with those in the test programs used to assess the code and determine the code uncertainties.
37. Figure 4.4 shows the leakage paths connecting from the upper head to the upper downcomer. Please discuss the effect of the geometry, resistance and flow rates through these junctions on the LBLOCA response expected in the plant designs for which the methodology will be used. Specifically, what is the impact of modeling this leakage on blowdown temperatures and PCT?
38. Figure 4.7 shows four half assemblies surrounding the hot assembly. Please discuss the use of [] assemblies versus [] assemblies since the power level of these adjacent

assemblies would affect the thermal conditions and cross flow in these outer assemblies. A comparison of the effect of this modeling on blowdown temperatures and PCT would be helpful.

39. Please provide the nodalization sensitivity study results used to arrive at the upper plenum and core nodalizations shown in Figures 4-4 through 4-8. Please discuss the level of nodal detail needed to show PCT convergence. Also discuss how the alignment of key leakage paths influences the chimney effects observed in the upper plenum studies and noted in Table A.2.
40. Please discuss the sensitivity of PCT to the cross flow resistance in the core and describe how these resistances are calculated.
41. Regulatory Guide (RG) 1.157, "Best-Estimate Calculations of Emergency Core Cooling System Performance," states that "A distinction from, and transition to laminar convection (i.e. $Re < 2000$) should be made, with a value of the laminar heat transfer for rod bundles that is appropriate for the applicable bundle geometry and flow conditions." Please discuss how the models in Section 4.0 of EMF-2100(P) meet RG 1.157. Also, does the heat transfer model for single phase vapor which considers the Sleicher-Rouse correlation and a separate natural circulation correlation result in the appropriate heat transfer for Re numbers less than 10,000 since the lower limit for this correlation is 10,000 (page 4-115, EMF-2103(P))? Please discuss the use of the Sleicher-Rouse correlation and the steam cooling model for transition and laminar flow.
42. How does the critical flow model address RG 1.157, Section 3.4.1.1, items b and c?
43. How does the frictional pressure drop model address RG 1.157, item 3.6.1, which states: "A model for frictional pressure drop to be used in ECCS evaluations should: b) be consistent with models used for calculating gravitational and acceleration pressure drops. If void fraction models or correlations used to calculate the three components of the total pressure drop differ from one another, a quantitative justification must be provided?"
44. How does the post CHF heat transfer model address RG 1.157, item 3.9.1 b), which states a post-CHF flow model should "recognize effects of liquid entrainment, thermal radiation, thermal non-equilibrium, low and high mass flow rates, low and high power densities, and saturated and subcooled inlet conditions?"
45. To understand the two-dimensional model behavior, please show the results of a test problem to verify the convection of lateral momentum by the vertical velocity. A simple ring noding problem can be developed that represents the flow from a downcomer and a break in a hot leg which shows flows for both vapor and liquid.
46. Anomalous flow circulation has been shown to develop, for example, between parallel pipes, that are of a numerical nature and cannot easily be corrected without the aid of additional form losses (see Proceedings of ICONE8, 8th International Conference on Nuclear Engineering, "Recirculating Flow Anomaly Problem Solution Method," D. Lucas, April 2-6, 2000, paper # 8479). Please discuss the capabilities of S-RELAP5 with regard to the sample flow problem presented in this paper and steps to resolve this anomalous

flow behavior potential. In addition, discuss whether or not the new 2-D model introduces these numerical anomalies as seen in 1-D formulations.

47. Recent reviews of thermal-hydraulic analysis computer codes have questioned the accuracy of momentum flux terms such as given by Equation 2.116 in EMF-2100(P). Please provide and discuss:
 - The numerical form of the momentum equations in S-RELAP5 and their reduction to the Bernoulli "type" equation.
 - The S-RELAP5 calculated Bernoulli expression versus flow channel cell number for a 1-D and 2-D pipe with and without a contraction and an expansion. A simple problem can be defined having a constant flow area and variable flow area and elevation change with the pressure, kinetic, and potential energy terms calculated by S-RELAP5 for both vapor and liquid.
 - Application of S-RELAP5 to the Ferrell-McGee data for flow through a pipe with expansions and contractions. (See Ferrell, J. K. and McGee, J. W. , "Two-phase Flow through Abrupt Expansions and Contractions," TID-23394, 1966.)
48. Please discuss the stability analysis for the numerical scheme presented in Section 2.6.5 of EMF-2100(P). Include a discussion of a consistency analysis of the finite difference equations and, as discussed in Section 2.6.4, justification of the use of the value of $C = 0.35$ when evaluating Equations 2.124 and 2.125. Include in the discussion the reason why the value of C must be within the range 0.0 to 0.5 for stability.
49. During the review of S-RELAP5 for application to 10 CFR Part 50, Appendix K small-break LOCA analysis, concerns were raised regarding the completeness of the formulation of the momentum equation. Specifically, the momentum equation as formulated is a vector equation that can only be reduced to 1-D if the flows and forces act in a single direction and hard surface reaction forces have also been omitted. Also, the momentum equation can only be reduced to Bernoulli's equation for pipes by integrating the differential form of the momentum balance along a streamline. Please discuss the momentum equation and its application to the reactor coolant system when major portions are modeled as a series of variable flow areas, 1-D straight pipes, and flow channels with bends.
50. Please discuss the manner in which S-RELAP5 indicates to the user that mass, energy, and momentum are conserved in a plant application. Is there a measure that shows in the code output that the above parameters are conserved?
51. Please discuss the omission of the viscous shear term in the 2-D formulation. Include a discussion of the consequence of the omission of this term, for example, in the hot bundle and hot channel during early reflood when the Re numbers are in the range 1,000 to 2,000. Are there low flow conditions during the LOCA (blowdown, refill, reflood, long term during downcomer boiling) where omission of this term would affect the hot channel thermal behavior and/or hot rod PCT?
52. Please discuss the numerical solution strategy described in Section 2.6.5.1 for a single 1-D pipe and a second system using a 1-D loop connected to a 2-D component. Include

a discussion of the development of the coefficients from the numerical approximation to the conservation equations and the tri-diagonal matrix, along with the column vectors containing the source terms.

53. Please discuss the method and model used to simulate the emergency core cooling entering and mixing in the discharge legs? Also, since emergency core cooling water can enter the loop seal during rapid safety injection tank (SIT) injection, please discuss how S-RELAP5 captures this behavior. What is the effect of loop seal refill on steam binding, the reflood rate, and the PCT?
54. Please provide the comparisons of the S-RELAP5 predictions to the Marviken test system pressure for the tests presented in EMF-2102, Section 3.5. Discuss how the uncertainty in break flow was determined. Does the S-RELAP5 model include wall heat structures? If not, discuss the effect of the omission of wall heat on the results.
55. What is the cause of the drop in mass flow rate at 75 seconds in Figure 3.5.18 and at 20 seconds in Figure 3.5.22 presented in EMF-2102? Why was the S-RELAP5 prediction not shown for completion in Figures 14, 15, 18, 21, and 22?
56. The comparisons to the data show that the transition from single-phase to two-phase conditions is not well predicted. Please discuss the expected transition in the plant calculations, including effect of persistence of the duration of the transition period for an extended time and the error introduced in the calculation that is not captured by the uncertainty evaluated from the Marviken test comparisons. Include a discussion of the effect of the duration of the transition period on the uncertainty in the break flow model determined from the Marviken tests.
57. Does the critical flow model uncertainty show a dependence on L/D for all fluid conditions? Please discuss the lack of this effect in the uncertainty evaluation.
58. How is the critical flow rate calculated when superheated steam exits the break? Please discuss the uncertainty in the break flow model under these conditions.
59. No tests were provided to show the capability of the code to predict pure steam flow out of the break. Were comparisons of S-RELAP5 with data for saturated steam flow, to Marviken Test 11, performed? Please discuss the uncertainty in the break flow model for saturated steam.
60. Were comparisons performed between S-RELAP5 and data for vessel blowdown, such as Allemann, "Experimental High Enthalpy Blowdown from a Simple Vessel through a Bottom Outlet," BNWL-1111, Battelle Northwest Laboratory, 1970? If so, please discuss the results of the comparisons.
61. HEM is an equilibrium break flow model. Since HEM is applied to two-phase conditions, and since non-equilibrium conditions can exist at the break with combinations of subcooled liquid with saturated or superheated steam (or saturated liquid with superheated steam) exiting the system, how are these conditions handled with the S-RELAP5 critical flow model? What is the uncertainty in the break flow model under non-equilibrium conditions?

62. What is the uncertainty in the critical flow model when the flow is no longer critical and may contain superheated steam or non-equilibrium two-phase conditions? Please discuss benchmarks that were used to evaluate the break flow model under these conditions and include results of the transition from critical to non-critical conditions and discuss how the model works.
63. Section 3.5.4 states that a break flow multiplier of [] was used to predict these tests. Uncertainty in the model is typically determined with a value of 1.0. Use of a multiplier in the range [], implies that S-RELAP5 tends to overpredict break flow for the Marviken tests. Discuss how this additional bias has been taken into account in the uncertainty analysis when the bias was varied for the Marviken tests? How is the break discharge coefficient then modeled when performing plant calculations? What is the uncertainty in the break model if a discharge coefficient of 1.0 is used? Please discuss how, in light of this initial assumed bias in the break multiplier input, the 25 percent error calculated for the break flow model bounds the data.
64. The break nodalization of the discharge leg in Figure 4.3 of EMF-2103(P) shows [] in the discharge leg while the nodalization of the break in the Marviken test shows [] in the exit pipe. In Section 3.5.6 of EMF-2102, it is noted that "the fine nodalization was used to mitigate numerical diffusion which may send hotter water or vapor prematurely to the discharge pipe." The modeling philosophy given in Section 4.2.3.5, entitled Cold Leg and Break, seems to contradict the statements in Section 3.5.6. Please discuss and justify the differences in the modeling philosophy applied to the Marviken test and that applied to plant calculations. Include a discussion of the effect of finer nodalization on break flow and PCT in the plant calculations and the effect of the use of a crude nodalization on break flow uncertainty.
65. Section 4.3.1.10 discusses the CCFL model applied to the upper tie plate and compares test data against the theoretical flooding curve to bound the air – water flow rates. The performance of the code has not been demonstrated against test data to show that the model is performing correctly, especially under saturated and subcooled fluid conditions. To demonstrate the capability of the model, please show comparisons of code predictions to test data, such as the Northwestern data (Bankoff, 1981), to show the condensation effects on the CCFL predictions and the model's performance. How does S-RELAP5 prevent unrealistic concurrent down flow of liquid and steam into the core? Does countercurrent flow or concurrent downward flow produce upper core cooling or a top down quench for any of the separate effects, integral tests, or plant calculations?

Discuss how the two fluid models have been assessed for CCFL behavior since the flooding point is determined entirely by the interfacial drag and entrainment models in the code. Has the CCFL model in S-RELAP5 demonstrated its ability to reproduce flooding behavior which is consistent with scaling laws. Has a comparison been performed for the S-RELAP5 model to tests such as the Creare 1/15th and 1/5th scale data. Are there continuous liquid and steam velocity plots in the downcomer verifying that CCFL is preserved by the S-RELAP5 interfacial drag model for saturated and subcooled conditions? Since the CCFL limit model [], what controls are used to assure that plant calculations will not result in violations of CCFL or unrealistic concurrent downflow in this region? Also please discuss what special interfacial drag, film droplet, entrainment/de-entrainment, drop size models were added

or modifications/provisions to RELAP5 to properly deal with countercurrent flow in the downcomer in the [].

66. Page 4-4 of EMF-2103(P) briefly states how compensating errors are handled in the assessment matrix for FLECHT, SCTF, CCTF, and THTF. However, there are no detailed discussions of compensating errors relative to the separate effects and integral tests. Please discuss compensating errors relative to the separate effects and integral experiments. The discussion should include post CHF heat transfer, emergency core cooling bypass/condensation, and blowdown/post-blowdown thermal hydraulics and entrainment.
67. Please identify a reference discussing error propagation and how this is handled in the uncertainty methodology.
68. The Achilles Test in EMF-2102 showed that S-RELAP5 underpredicted the core liquid level, the PCT by about 125°F, and the downcomer level. Please discuss possible reasons for these differences. The effect of the nitrogen on condensation was not measured in this test. How is the effect of nitrogen on condensation determined in S-RELAP5? Also, please discuss the sensitivity of the PCT to condensation efficiency. How does S-RELAP5 compute entrainment of liquid by the nitrogen and, if so, how does this influence the calculations? What is the sensitivity of full scale plant PCT to condensation efficiency?
69. Section 4.3.3.2.6 of EMF-2103(P) identifies a T_{min} of [] is used in the analysis based on comparison to FLECHT reflood data while page 4-20 of EMF-2100(P) identifies a T_{min} of [] as used to establish the boiling curve. Please clarify and discuss the impact on the test comparisons and plant calculations.
70. Regarding modeling of transition boiling heat transfer at the lower limit, S-RELAP5 uses the maximum of the Sleicher-Rouse steam cooling correlation and a free convection correlation; Forslund-Rosenow or Bromley is used for film boiling depending on the void fraction. Please discuss the lower limit of the transition correlations with regard to consistency with the lower limit on the film boiling correlations. Please discuss code stability with regard to the heat transfer coefficient at T_{min} during the switch from transition boiling to film boiling.
71. General comments regarding code assessment:
 - a. Core 3-D Flow and Void Distribution (page 4-85, EMF 2103(P)). Comparison to the THTF and GE level swell data, for example, are high pressure tests and do not represent PWR reflood conditions. The GE data does not apply to rod bundle drag. On the other hand, specific FLECHT boil-off or reflood data are applicable to voids in bundles at low pressure (FLECHT-SEASET Test 35658, for example).
 - b. Regarding Core 3-D flow distribution, the SCTF comparisons, especially at the higher elevations, indicate underprediction of peak temperatures and quench times that are early by 200 –300 seconds for transients with 500 second heat-up times. Additional justification is needed to demonstrate that the clad oxidation is bounded. While these are low temperature tests, the early quench time

predictions will significantly affect oxidation and the uncertainty may effect the error methodology. Discussion is needed regarding how the 200–300 second early quench predictions are factored into the uncertainty in oxidation calculations. There should also be discussion of the lack of a model for film boiling as a function of distance from the quench front which would improve the quench time predictions. This discussion should also address the reasons for the discrepancies in quench time predictions and underprediction of PCTs. The S-RELAP5 code predicts large oscillations in the void fractions in the core (see Figure 3.11.47 of EMF-2102, for example). Discussion is needed regarding the oscillations and their effect on super heat and clad temperature underprediction. The discussion should also address the consequences of the oscillations with respect to the reflood behavior the potential bias of these oscillations to lower PCT.

- c. Liquid Entrainment. While the entrainment is overpredicted for the CCTF tests, overprediction coupled with drop size could bias the steam temperatures in the channel to low values if the drop size is too small. Please discuss how the S-RELAP5 model predicts the steam super heat for these tests (at selected elevations starting at locations near the quench front) and the reflood data presented in EMF-2102. How does the void fraction influence the steam super heat and dispersed flow film boiling heat transfer when the entrainment is overpredicted for the tests? Included in the discussion should be the topic that excess entrainment does not lead to propagating errors into the film boiling model and a non-conservative impact on PCT.
- d. Upper Plenum Entrainment/De-entrainment. Please discuss the manner in which de-entrainment in the upper plenum is calculated. Is there a model for de-entrainment on structures? How is entrainment to the hot legs and steam generator calculated? It should be shown that the S-RELAP5 overprediction of liquid buildup in the upper plenum is not due to underprediction of entrainment to the hot legs and steam generators. Also since the code allows a second top down quench, does CCFL in any of the SETs, integral tests, and plant calculations reduce the clad temperatures or affect clad oxidation in the top of the core?
- e. CCFL. There are no special drag models in the downcomer specifically designed to treat CCFL. Without these comparisons, there is no assurance that the CCFL limit will not be violated during a plant calculation. Comparisons to countercurrent flow data would demonstrate that the liquid down flows in the downcomer do not violate CCFL. Figures 4.116 and 4.117 show that the CCFL model is limiting the liquid downflow for many of the test points. This suggests the drag model tends to produce too high a liquid down flow for a given steam flow. Unless the drag model is different in the downcomer, these results suggest that the drag model will produce excessive liquid down flows in the downcomer. Please discuss the omission of the CCFL model or drag model specifically designed to model CCF in the downcomer.
- f. CCFL. Since the S-RELAP5 code does not use a CCF limit model, interfacial and wall drag modeling is key to predicting CCF. Application of concurrent up-flow correlations for interfacial and wall friction to countercurrent flow tend to

over-estimate the downflow of liquid. It appears that wall shear is neglected during countercurrent flow which would produce over-estimated liquid downflows in the low gas velocity region. Wall shear stress acting on falling water is almost the same order of magnitude as interfacial shear stress, making it inappropriate to ignore this stress. Since RELAP5 ignores wall shear during annular flow and EMF-2100 Section 3.0 does not show the details of the wall shear, discussion is needed that describes how wall shear is computed during CCF. This discussion should also compare the friction factor with data and show the behavior at low velocities/Reynolds numbers.

- g. CCF. How is CCF modeled in the 2-D downcomer and how are the flow regime maps applied in this region?
- h. Hot Leg Entrainment. Hot leg entrainment is underpredicted in Figures 4.165-4.167, 4.173, 4.177, and 4.179, and, thereby it is not supported that hot leg entrainment is calculated conservatively. In some cases entrainment is not predicted until late in the test. Does the underprediction lead to a beneficial effect on PCT for the tests which offsets another conservatism elsewhere in the methodology? Figure 4.173 shows no entrainment was calculated for the entire test. If the entrainment is calculated to match the data late in the test, this does not support the model being conservative as stated on page 4-90 of EMF-2103(P).
- i. Two-Phase Pump Model. The pump resistance and broken cold leg nozzle typically represent the largest resistances in the loop which determines the core flow (and hence fuel stored energy/PCT, during blowdown. It should be shown how the uncertainty in the relative resistances between the core and break through the downcomer and hot leg paths are taken into account and that the pump resistance, broken nozzle resistance, and the other loop resistances conservatively bound the expected variation (or are insignificant) in these path resistances from the core to the break.
- j. Pump Differential Pressure Loss. How is the pump coastdown verified in the case where there is no plant data? What is done in the modeling to assure the coast down is bounded?
- k. Non-Condensable Transport. The Achilles Test # 25 underpredicted the PCT later in the event. While the effect of the nitrogen is to initially force additional water onto the core providing some early limited core cooling, the later overall effect is to reduce core cooling since the higher initial steaming reduces the liquid inventory in the core causing a late heat-up of the core. S-RELAP5 underpredicted the negative effects while capturing some of the early beneficial effects. Please discuss the basis for including the early beneficial effects of nitrogen in plant calculations and not considering this parameter in the uncertainty methodology and imposing it as a penalty on PCT.
- l. Downcomer Entrainment. Please identify the correct section in Reference 5 for the downcomer entrainment tests and discussion referred to in Section 4.3.3.1.10 of EMF-2103(P). Please discuss the cause of the lower plenum liquid level oscillations in Figures 4.106 through 4.110, including the flow regimes

predicted by S-RELAP5 during this period, and the steam and liquid velocities in the downcomer and exiting the lower plenum during these tests. Does the underprediction of the liquid inventory in the lower plenum enhance the steam downflow in the core during blowdown and produce a beneficial effect on PCT? Does boiling occur in the lower downcomer and lower plenum in these tests and what effect does boiling versus no boiling have on the entrainment?

- m. Downcomer Level Oscillations. Figure 3.11.47 of EMF-2102, shows large oscillations in void fraction. Please discuss the model conservatism as stated in Section 4.3.3.1.11, since the core in these tests shows large void oscillations which can "provide additional core cooling" as pointed out on page 4-92. If downcomer boiling occurs during accumulator discharge, what is the effect on PCT after the accumulators empty.
- o. Lower Plenum Sweepout. Oscillations suggest that the sweepout of the liquid from the lower plenum is retained in the downcomer and immediately flows back into the lower plenum periodically. In such a case, please discuss the model conservatism regarding the lower plenum liquid level test predictions. Should there be flow of liquid back into the lower plenum? Does this result in entrained liquid entering the core and providing additional cooling? Discuss the need for bias in the uncertainty evaluations if the lower plenum oscillations cool the core.

Uncertainty Analysis

Reference EMF-2102(P)

72. 5.1.1 - Data Set Adequacy

With regard to Table 5.1 it appears that not only the maximum pressure data, but also the mass flux of the vapor and liquid do not bound the intended application. Please justify in greater detail the statement that the data set on which film boiling multipliers, bias, and uncertainty are determined adequately cover the intended application.

73. 5.1.2 - Inferring Heat Transfer Coefficients from Experimental Data

Please describe mathematically the inverse conduction algorithm (flow diagram and a few equations) used in computing the boiling heat transfer coefficient from the thermocouple data.

In Figure 5.1 is this the numerical node scheme for the inverse algorithm? If so, at what node is the thermocouple?

Specifically, how is the surface heat flux a function of the derivative with respect to time, as stated in Section 5.1.2.1?

The thermocouple measures the temperature $T(r_0, z_0, t)$ (i.e. at some fixed point (r_0, z_0) as a function of time t (as in Figures 5.2 and 5.3). The objective seems to be to compute the surface temperature at the same elevation at the same time points as the thermocouple measurements. So where is the time derivative necessary? Where is the source of the amplification?

74. 5.1.2.1 - Signal Filtering

What is the t between thermocouple signals?

What is the thermocouple instrument error?

The thermocouple reading has two sources of variation:

- a. the instrument error
- b. a variance due to the fluctuations in the underlying physical process. (If we had a perfect instrument, this variance would still be there.)

Do you estimate these effects?

What is your stopping rule with regard to smoothing of the thermocouple readings with respect to the above variances?

What is your stopping rule with regard to smoothing the inferred heat transfer coefficients (as in Figures 5.4 and 5.5)?

Do you apply any quantitative measure to claim that "the underlying features of the signal are intact"?

Comment: Figure 5.6 is irrelevant.

75. 5.1.3 - Data Consistency Check

Since the test data provide multiple estimates of HTC for common times and elevations, is the mean computed at some specific time and elevation the "truth" with respect to which you compute the bias in the computed value at that time and elevation; and the standard deviation the uncertainty?

How do you assure that the data was not oversmoothed? (That is only the instrument error and outliers were removed.)

76. 5.1.4 - Partitioning the Data

The data is partitioned into two sets. What is being validating? Are the THTF and FLECHT - SEASET data considered initially as one set and then split into two through random selection?

77. 5.1.5 - S-RELAP5 Calculated HTC

5.1.5.1 - Data Averaging

The oscillations in the computed values of void fraction, heat transfer coefficient and clad temperature are attributed to changes in the heat transfer mode in the course of the

c computation(i.e., film boiling @ single-phase vapor) c omputation(i.e., film boiling @ single-phase vapor).

- a. What is the variable and its value that determines which mode to assume?
- b. What is the time increment in the computation and what is the average cycle length of the oscillation in the void fraction, and T_{clad} ?

78. a. Is it correct that RELAP computes the void fraction (@), the heat transfer coefficient (h) and the clad temperature (T_{clad}) sequentially as follows:

@ @ h @ T_{clad}

If so, is the same algorithm applied with the 8 second window? How does the window size compare to the computational time step?

How does it compare to the time step in the T_{clad} measured values?

- b. Is the following sequence of computations during processing of the data correct?

Let $D(t)$ be the original values at time t . Assume $w = 3$. Then

$$\bar{f}_3(4) = (1/3) [D(1) + D(2) + D(3) + D(4)]$$

$$\bar{f}_3(5) = (1/3) [D(2) + D(3) + D(4) + D(5)]$$

etc.

Then $f_{smooth}(t-w/2) @ f_w(t)$ for each $t @ w/2$.

Is it correct to say that you compute a moving average with a lag of w and then shift the value back by $w/2$ in time?

79. In reference to the comparison shown in Figures 5.18 through 5.20.

- a. Are you applying the same algorithm (i.e., w) in the vapor and quench parts of the curves as in the transition region?
- b. How would enlarging the window result in larger segments of unsmoothed data in the film boiling regime?
- c. How is stopping the smoothing at the level where the amount of ripple remaining is on the order of what might be expected as experimental uncertainty relevant? The computation is deterministic, therefore, experimental uncertainty cannot be reproduced. By not smoothing "completely" how can you be sure you are not

skewing the distribution on which your uncertainty estimate in the multiplier is based?

- d. Therefore, what harm is there in smoothing completely, in view of the comparisons shown in Figures 5.18 through 5.20?
- e. 5.1.6 - Multiplier Correlation

Two heat transfer coefficient correlation multipliers are being determined in this section: M_{FILMBL} and M_{FRHTC} . Correct?

M is a function of z (fuel height) and t the time in the transient, since $h_{meas}(z_0, t)$ and $h_{calc}(z, t)$, where z_0 is the thermocouple location. Correct?

80. How do you define quench front?

- a. At a thermocouple location z_0 how do you determine the time of the quench front at that location from the measured data?
- b. How are M_{FILMBL} and M_{FRHTC} related to the definition of quench front?
- c. In aligning the quench fronts to a common location (say z_0), what parameters are you equating (i.e., $P_{meas}(z_0, t_{meas}) = P_{calc}(z_0, t_{calc})$?

81. You state "Temporal displacements between THTF measured data and code calculations were ignored. The transients are sufficiently short in duration that the temporal differences are expected to be small."

In principle, is it not the relationship between the time step size in the transient calculation in relation to the temporal differences that is the issue, and not the duration of the transient? Please explain your reasoning in greater detail.

Note: Since

$$M(t) = h_{meas}(t) / h_{calc}(t)$$

a misalignment of h_{meas} and h_{calc} with respect to time will introduce a bias in the distribution of $M(t)$ (which t will be used in $M(t)$, the one from the measurements or from the calculation?)

82. 5.1.7 - Film Boiling Multiplier Statistics

5.1.7.1 - Defining Data Set

Is this the same partitioned set as described in Section 5.1.4?

83. The first paragraph is not clear.

- a. Does "multiplier pairs" mean M_{FILMBL} and M_{FRHTC} ?

meas@LOCA measured result of a !LOCA

calc@LOCA S-RELAP5 calculated result of a LOCA

Of the above four the only one the staff cannot do is the meas@LOCA, yet it is what the staff wants to estimate since it is considered the "truth".

Let P be a variable of interest such as peak clad temperature.

@ P(@) where @ @ set of independent variables defined by PIRT and for which the sensitivities have been quantified.

So, scaling issues deal with the effect of @|_{test} @ @₀ @ @|_{LOCA} @ @₀ + @ @ on P(@).

If scaling holds

$$P(@_0 + @ @) - P(@_0) @ @ @ .$$

The question then is what are the conditions on test scaling and code scaling so that we can get an estimate of the "truth" in terms of meas@test, calc@test, and calc@LOCA.

Consider the following relationships:

Test Scaling:

$$p \text{ meas@test}(@_0) @ \text{ meas@LOCA}(@)$$

Under the assumption that the tests are scalable

$$p \text{ meas@LOCA}(@) @ p \text{ meas@test} (@_0) + @P/@@| \text{meas@test} @ @$$

$$@ \quad p \text{ meas@LOCA}(@)/p \text{ meas@test}(@_0) @ \{ 1 + 1/P @P/@@| \text{meas@test} @ @ \}$$

Similarly for

Code scaling:

$$p \text{ calc@LOCA}(@)/p \text{ calc@test}(@_0) @ \{ 1 + 1/P @P/@@| \text{calc@test} @ @ \}$$

What we want to estimate is the "true" value of P(@) at LOCA conditions, i.e. we want to compute P meas@LOCA(@) at some level of confidence.

From the above expressions we form

$$\frac{p \text{ meas@LOCA}(@)/p \text{ meas@test}(@_0)}{p \text{ calc@LOCA}(@)/p \text{ calc@test}(@_0)} @ \frac{\{ 1 + 1/P @P/@@| \text{meas@test} @ @ \}}{\{ 1 + 1/P @P/@@| \text{calc@test} @ @ \}}$$

$$p \text{ calc@LOCA}(@)/p \text{ calc@test}(@_0) @ \{ 1 + 1/P @P/@@| \text{calc@test} @ @ \}$$

Rearranging terms we obtain

$$P_{meas@LOCA} @ P_{calc@LOCA} * (P_{meas@test}/P_{calc@test}) * \{ 1 + 1/P_{@P/@@|meas@test @ @} \{ 1 + 1/P_{@P/@@|calc@test @ @} \}^{-1}$$

for $| 1/P_{@P/@@|calc@test @ @} | @ 1$ we can write

$$P_{meas@LOCA} @ P_{calc@LOCA} * (P_{meas@test}/P_{calc@test}) * SF$$

where we define a scaling factor (SF) as

$$SF @ (1 + 1/P_{@P/@@|meas@test @ @} - 1/P_{@P/@@|calc@test @ @})$$

$@@@$
test scaling
 $@@@$
code scaling

So, the estimate of the "true" RLBLOCA value of some parameter P has the following components:

- a. $P_{calc@LOCA}$ - the S-Relap5 computed parameter for the LOCA.
- b. $P_{meas@test}/P_{calc@test}$ - the bias estimated by comparing computed and measured values of the parameter from tests. This is the sole source of variation that contributes to the computation of the confidence level in the estimate of $P_{meas@LOCA}(@)$.
- c. SF is a factor that accounts for scaling effects.

The analysis implies that $SF @ 1.0$. The above discussion implies that for this to be true we must fulfill the following conditions:

- a. $| 1/P_{@P/@@|calc@test @ @} | @ 1$
- b. $1/P_{@P/@@|meas@test @ @} @ 1/P_{@P/@@|calc@test @ @}$

The first implies that the sensitivities of the computed results of the tests to changes in the independent variables are small. The second that the sensitivity of the measured results for the tests are comparable in size to those computed.

How do your conclusions with regard to test scaling for blowdown, refill and reflood fit into the above scheme?

Similarly, how do your conclusions with regard to code scaling fit into the above scheme?

89. 5.1.1 - Determining Important Process Parameters

You state "In contrast, treating these process parameters statistically accounts for higher order behavior by including all possible combinations in the sample space."

- a. What exactly are you referring to by higher order behavior? Give an illustrative example.
- b. To get "all possible combinations in the sample space" would require n^9 (from Table 5.1) uniformly distributed sample points, where n is some appropriate number of observations for each variable. Is this what was in mind? This gets big very quickly!

90. 5.1.2 - Role of Sensitivity Studies

"Parameters can be demonstrated to be insignificant by sensitivity studies and/or by their relationship to low-ranked PIRT parameters."

- a. What exactly is meant by sensitivity studies in this context? That is, are these S-RELAP5 calculations of a full scale RLBLOCA wherein input parameters are varied? Give an example.
- b. Have you shown that the results of a S-RELAP5 calculation for sensitivity at full scale is valid?

91. 5.1.3 - Quantifying Statistical Quantities

Why are there no measurement uncertainties associated with the parameters - accumulator level through core flow in Table 5.4?

92. How are the operational and measurement uncertainties combined to give the distribution for the parameters in Table 5.4?

93. 5.2 - Performance of NPP Sensitivity Calculations

5.2.1 - Statistical Approach

The statement "Non-parametric statistical techniques are useful in situations where acceptance or rejection is based on meeting a tolerance limit and where you do not need the probability distribution itself." is misleading. The analytic form of the probability distribution function need not be known, but the function must be continuous. In the current context, the distribution function is the S-RELAP5 code. What evidence do you give that S-RELAP5 computed PTC and cladding oxidation are continuous in the independent random variables for RLBLOCA analysis conditions?

94. Define your use of the term "outlier" in the current context of your application, i.e. given 59 observations of PCT, what makes you call the 59th term in the order statistic and outlier? What statistical test do you apply and what makes you think it is appropriate, i.e. not due to some deterministic quirk in the computation? Please formulate your test for an outlier in terms of a statistical hypothesis test.

95. 5.4 - Determination of Total Uncertainty

The final results for the 4-loop sample problem are summarized as:

- The 95/95 calculated PCT was 1635°F
 - The 95/95 calculated maximum nodal oxidation was 1.1%
 - The 95/95 calculated maximum total oxidation was 0.02%
- a. Are these joint estimates based on the same $n = 59$ S-RELAP5 runs?
 - b. If yes, please explain why. The 95/95 for the joint estimation of three dependent variables requires far more than $n = 59$.
 - c. Physically PCT and oxidation rates should be correlated. Do you account for that and if so how?
96. Stored energy in the fuel is treated, however pin pressure is not. Please describe the methods used to assess the potential for blowdown ruptures and how fuel rod gap pressures are calculated and treated statistically.
 97. Please explain how the uncertainty in the gap gas conductance is accounted for. Please explain how variations due to fuel relocation are treated and included in the uncertainty in the stored energy of the fuel.
 98. What is the initial oxide layer thickness assumed on the inside and outside of the rod. Please explain how this is treated and justify the initial oxide layer thicknesses.
 99. On page 4-94, the 90 percent confidence limit was used to evaluate the constant and exponential terms in the oxidation model. As described in RG 1.157, please use the 95 percentile confidence limits to evaluate these terms. Also, was the uncertainty on the predicted mean of the data in the Cathcart-Pawel cited reference verified.
 100. Cold leg condensation only, is discussed on page 4-99. Please explain how downcomer condensation was ranged and applied in the methodology.
 101. Downcomer entrainment was not discussed in the statistically treated section. Please explain how downcomer entrainment was ranged.
 102. The refill heatup period heat transfer multipliers were also not discussed. Please show the S-RELAP5 code predictions to data during refill and show the heat transfer multipliers applicable to refill.
 103. Please explain the "Comparison with Adjusted Accumulator" in Figure 4.152.
 104. LOFT L2-3 predictions capture the second peak due to the lack of quench during blowdown. If quench occurs, how well does S-RELAP predict the second peak? Do the plant calculations always show a failure to quench during blowdown? If not what is the effect on the reflood PCT?
 105. Explain why the methodology does not contain an uncertainty assessment regarding peak local oxidation. At the higher PLHGRs and with downcomer boiling, what is the core wide oxidation.

106. What is the basis of the moderator-density feedback curve employed in the analysis? Is the most positive MTC allowed by the technical specifications used? Please explain and show the reactivity versus density curve used in the demonstration analysis. What doppler feedback curve is used? What is the uncertainty in these curves applied to the analysis?
107. In Table 5.7 on page 5-23 of EMF-2103, how was the lower limit on T inlet determined? Will the analysis be applied to plants during an end of cycle coastdown? If so, what is the sensitivity of the methodology to T inlet and how would the evaluation be performed?
108. In Figure 5.2 on page 5-29 of EMF-2103, which peak temperatures are due to first peaks and which are due to reflood peaks? The peaks corresponding to times beyond 100 seconds are very low. These appear to be reflood peaks; please explain why the reflood peaks are so low when linear heat rates are based on peaking factors in the range 2.4 to 2.6? Why do the guillotine breaks appear to be all first peak limited?
109. Figure 5.3 shows break areas of 1.0 ft² and less. What is the effect on the PCT distribution if breaks 1.0 ft² and smaller are thrown out? The upper limit on the break size is about 4.0 ft². What are the break multipliers for the largest sizes in Figure 5.3? How are the multipliers applied to each side of the break? Please explain.
110. What does the scatter plot for PCT versus reflood rate look like?
111. Table 5.7 identifies the failure of 1 LPSI and 1HPSI. Please show the PCTs for a diesel failure, a LPSI failure, and no failure on the same plot.
112. In Table 5.7, why is steam generator plugging limited to 10 percent since the average for operating plants is 15 percent? How is the plugging distributed among the steam generators? How are asymmetries in plugging handled?
113. Table 5.7 lists the hot assembly to be anywhere in the core? Please show the core flow and PCT for the hot assembly placed in the most limiting position which minimizes blowdown cooling.
114. Minimum EC boron of 2925 is used in the analysis. What is the minimum time to boron precipitation for this boron concentration? Show that the switch to simultaneous injection occurs before precipitation for the limiting large break and location.
115. Please explain why the PCT is not skewed toward the higher values as power is increased in Figure 5.6 of EMF-2103 and Fq is increased in Figure 5.7?
116. How is the ASI chosen in the analysis? Are power distributions with power skewed toward the top most likely and how does the ASI chosen reflect the most likely distribution?
117. Please explain why the trend in PCT is not increasing with increasing inner ring and cold ring power? Are these PCTs determined with the hot assembly located in the position which minimizes core flow and cooling during blowdown? Which PCTs are first peaks?

118. What do the PCT scatter plots look like if they are separated into first peaks and second peaks?
119. Why does the PCT turn around so quickly in Figure 5.18? What is the reflood rate versus time for this break? Please explain why the quench occurs so early since downcomer boiling should initiate following discharge of the SITs.
120. What is the cause of the spike in flow at about 7.5 seconds in Figure 5.20? What is the PCT if this flow spike is eliminated?
121. What is the cause of the downcomer level increase just after 50 seconds in Figure 5.25? What causes the drop in level at 225 seconds? Please show a plot of the downcomer void fractions versus time. Also show a plot of the downcomer temperatures for these locations versus time compared to the saturation temperature.
122. Show a plot of the core flow at the PCT location.
123. Please show the heat transfer coefficient and steam temperatures corresponding to Figure 5.18. Also show the core void fraction versus time for these locations and the droplet size at the hot spot versus time. What is the reflood rate versus time?
124. Why does the PCT show the rapid temperature decrease just after the safety injection tanks empty? What are the low pressure safety injection and high pressure safety injection flow rates after safety injection tank exhaustion?
125. Why is the lower plenum liquid solid at about 75 seconds? Why is there no boiling in this region? How is wall heat modeled in the lower plenum? Please explain
126. What is the source of the pressure spike in Figure 5.28 at 70 seconds? Please explain.
127. What is the sensitivity of PCT to the expected variation in containment pressure? What is the uncertainty in containment pressure?
128. Page A-4 of EMF-2103 states that a discussion of each study is not practical. In order to demonstrate the basis for these studies, plots of key parameters are needed along with a discussion of the results. The basis for each sensitivity needs to be explained and the key plots presented with comparisons to the base case to provide the technical justification for the choices for the parameters listed in the sensitivity studies given in Table A.2.
129. The discussion in Section A.2 refers to core flow stagnation, reduced heat transfer and many other phenomenological behaviors but does not show any plots other than PCT. Figures A.1 through A.4 do not display quench. Please show the quench for these cases. What is the impact on clad oxidation for these cases? Comparison of Figure A.3 with A.1 shows an increase in PCT of 500°F. Given this large change in PCT and the fact that the S-RELAP5 did not capture the effects of nitrogen which was to subsequently increase PCT after the initial decrease, please provide the justification for including this PCT benefit in the methodology. Is Figure A.2 incorrectly labeled as this plot for the 4-loop plant? Why does the PCT increase substantially beyond that for the 3-loop plant compared to the 4-loop plant when nitrogen injection is precluded.

130. How does low rod pressure produce more conservative PCTs as indicated in Table A.2? Higher rod pressures at higher linear heat rates will eventually cause blowdown ruptures increasing the stored energy at end of blowdown that will increase PCTs. Please explain.
131. In the rupture sensitivities given in Figures B.3 and B.4, how was fuel relocation and the subsequent heat generation in the ruptured zone modeled? If this was not taken into account, please justify the omission of fuel relocation effects in the ruptured region. How does blowdown rupture influence the conclusions of the rupture study? What assumptions are made regarding rupture of the surrounding rods in the rupture study. Are touching strains predicted and what conditions are needed for this condition? What is the justification for the blockages calculated that show rupture reduces PCT? What is the PCT sensitivity to percent blockage up to the maximum? What test data was used to justify the less limiting nature of rod rupture and show S-RELAP5 comparisons to the data?
132. Please show the heat transfer coefficient vs. time for Figures B.3 and B.4. Also show the temperature of the node just above the ruptured region and it's corresponding heat transfer coefficient. Also show the gap conductance vs time for the ruptured and unruptured region just above. Are the drop sizes affected by the ruptured region. What is the void fraction and corresponding drop sizes versus time at the hot spot?
133. Figure B.13 shows an increasing PCT at the end of the plot. Please show the transient until quench.
134. Figure C.1 shows a variation of about 50 K during reflood with time step. Please discuss the effect of smaller time steps on PCT.
135. Please support the basis for the uncertainty, especially the difference between the 95/95 and 50/50 and the data base used to assess the code predictive capability (for example, there are many more FLECHT-SEASET, FLECHT Cosine and FLECHT Skewed tests with PCT between 2000 and 2200 F that were not used in the S-RELAP5 comparisons). This would include the sensitivity of PCT to nitrogen injection, fuel swell and rupture modeling, sensitivity to time step, downcomer boiling sensitivities, etc. If a larger data base was used, how would the uncertainty be impacted?
136. As identified on page 3-17 of EMF-2100, the Weber number is used to define the maximum bubble size. For reflood calculations, Wallis has proposed a formula based on the Taylor instability theory. Please discuss the impact of the Wallis approach for choosing bubble size on level swell and reflood behavior and justify the model.
137. Regarding the critical Weber number of 4.0 for droplets in dispersed flow (page 3-17 of EMF-2100), Wallis recommends that a Weber number of 12 be used to define the maximum drop diameter for viscous fluid droplets. Drop diameters of about 1/10 inch characterize LOCA reflood behavior and have been used to capture the PCT in the FLECHT tests. Please justify the Weber number used to compute the drop size for the FLECHT tests. What is the lower limit on drop size in the S-RELAP5 methodology and how does this value compare to the data base?

138. How are the flow regime maps applied to the 2-D downcomer model?
139. Since flow regimes affect entrainment and ECC bypass, how was the uncertainty in the flow regime maps included in the methodology?



FRAMATOME ANP

An AREVA and Siemens company

FRAMATOME ANP, Inc.

October 30, 2002
NRC:02:049

Document Control Desk
ATTN: Chief, Planning, Program and Management Support Branch
U.S. Nuclear Regulatory Commission
Washington, D.C. 20555-0001

NRC Review of EMF-2103(P) Revision 0, Realistic Large Break LOCA Methodology for Pressurized Water Reactors

Ref.: 1. Letter, Framatome ANP, Inc. (James F. Mallay) to NRC (Document Control),
"Request for Review of EMF-2103(P) Revision 0, Realistic Large Break LOCA
Methodology for Pressurized Water Reactors," NRC:01:035, August 20, 2001.

Enclosed are revised pages to be inserted into EMF-2103(P) Revision 0. This revision was developed to reflect two corrections to the calculations performed for the LOFT assessments. The first correction was to the RODEX3 input decks for the LOFT assessments. The RODEX3 code truncates data that exceed 80 columns, and some of the input data went beyond column 80. The second correction was to the zirc-oxide thermal conductivity in S-RELAP5 in which an incorrect unit conversion factor was used.

As a result of making this correction, new PCTs were calculated for the LOFT assessments. The PCT changes ranged from 1°F lower for the L2-3 test to 20°F lower for the LP-LB-1 test. Nearly all the impact was due to the RODEX3 input error. The correction to the zirc-oxide thermal conductivity in S-RELAP5 was insignificant. These minor changes do not affect any of the conclusions in the report. A vertical line in the right hand margin of each revised page signifies the revisions made, which include new plots.

The revised pages will be included in the approved versions of the proprietary and nonproprietary topical reports, which will be issued following NRC approval of the topical report. Since the revised pages do not contain any proprietary information, only non-proprietary pages are enclosed.

Very truly yours,

James F. Mallay, Director
Regulatory Affairs

Enclosures

cc: D. G. Holland
R. R. Landry
Project 693

measured temperatures below the 15-in elevation, much greater than the measurements from 15-in to 44-in elevation, and much lower than measurements above the 44-in elevation. The comparison can be considered acceptable because the calculated temperature trends followed the data trends, although the magnitudes did not compare well, and the calculated temperatures were overpredicted for the high power region. The highest PCT of 942 K (1236 F) was measured at the 15-in elevation while the calculated PCT was 1005 K (1350 F).

4.3.2.1.5 LOFT Test L2-5 Assessment

Test L2-5 was the third LBLOCA test conducted in the LOFT facility in which the reactor core power provided the primary heat source. The test represented a hypothetical cold leg guillotine break that simulated a double-ended, offset, shear break in a commercial (1000 MWe) 4-loop PWR. The test was initiated at 75% thermal power (36 MWt) and a 12.22 kW/ft maximum LHGR.

Operation of the LOFT PCPs differs from a typical PWR in that the LOFT pump rotors are electromagnetically coupled to their flywheel system. It is normal during LOFT tests to uncouple the pumps from their flywheels whenever the pump speed falls below 750 rpm (78.54 rad/s). During the L2-5 test, the two PCPs were tripped at 1 second and disconnected from their flywheels. This provided a rapid pump coast down. This operation of the pumps reduced the flow into the vessel to less than the flow to the break, thus preventing an early bottom-up fuel rod rewet. These simulated conditions are more typical of a 3-loop PWR than a 4-loop PWR. LOFT pumps normally coast down while connected to their flywheels that were designed to represent the normal pump coast down of commercial W 4-loop PWRs.

The Test L2-5 HPIS flow is 58% of Test L2-3 HPIS flow and is 75% of Test LP-02-6 HPIS flow because an improper small break HPIS flow condition was inadvertently specified for Test L2-5. The injections of high and low pressure ECCSs were delayed to 23.9 and 37.32 seconds, respectively, to simulate the expected delay in starting up the emergency power diesel generator to run the ECCS.

Before the transient started, the power level in the reactor core was steadily increased, then held at 36 MW \pm 1.2 MW for about 28 hours. This ensured that an appropriate decay heat power level would be obtained once the control rods were inserted into the reactor core. Test conditions before the beginning of the L2-5 test were as follows.

leg and 558.0 K for the hot leg come very close to measured values considering the large error bands quoted for the measured data, namely $554.3 \text{ K} \pm 4.2 \text{ }^\circ\text{K}$ for the cold leg and $561.9 \text{ K} \pm 4.3 \text{ }^\circ\text{K}$ for the hot leg. The desired steady-state conditions were successfully achieved and the calculation accurately reached the L2-5 test initial conditions.

For the transient calculation, a short steady-state calculation before the break opening is carried out to ensure that the steady-state initial condition is properly maintained when switching from the steady-state input model to the transient simulation. The calculation for this analysis is a simulation of Test L2-5 from 10 seconds before the break initiation at 0 seconds up to 140 seconds. This time interval was chosen because the important phenomena and significant events of Test L2-5 occurred during this period.

The assessment of S-RELAP5 to predict each of the important LOCA phenomena is presented in detail in Reference 5. Figure 4.149 depicts the final comparison of the calculated and measured PCT versus core elevation. In this figure, the PCT is referred to as a maximum cladding surface temperature, either calculated or measured at the various locations, during the LOCA transient history. The comparison generally shows very good agreement and the differences between the calculated and measured PCT in the high power region between 15-in to 44-in elevations are quite small. Calculations and measurements both show a plateau region between the 15-in and 28-in elevations where maximum PCT occurs. The highest PCT of 1105.4 K (1530.1 F) was measured at the 24-in elevation and the calculated PCT was 1102 K (1524 F).

4.3.2.1.6 LOFT LP-02-6 Assessment

LOFT LP-02-6 was the fourth LOFT nuclear powered core LBLOCA test conducted with pressurized nuclear fuel rods and with a specification of minimum U.S. ECC injection rates. The maximum LHGR of 14.87 kW/ft was above the typical technical specifications currently used for licensing analyses of PWR fuel rods with the same approximate pellet diameter used in a 15 x 15 fuel pin array. Test LP-02-6 represented an NRC "design basis accident" test and was supposed to run at 100% power, 50 MWt, but because of questions concerning the integrity of the pressurized fuel rods in the central hot assembly, the power level was reduced to mitigate possible safety problems. LP-02-6 is an important LBLOCA test for code assessment because it addresses the issues relating to safety margins associated with the response of a PWR to the NRC "design basis accident" scenario, including delayed minimum ECC safeguards.

agree quite well and the calculated initial conditions are generally within the uncertainty band of the measured quantities. The calculated initial broken loop temperature of 557.6 K for the cold leg and 558.3 K for the hot leg come very close to measured values considering the large error bands quoted for the measured data, namely $553.0\text{ K} \pm 6.0\text{ }^{\circ}\text{K}$ for the cold leg and $560.0\text{ K} \pm 6.0\text{ }^{\circ}\text{K}$ for the hot leg. The desired steady-state conditions were achieved and the calculation accurately reached the LP-02-6 test initial conditions.

A short, steady-state calculation before the break opening is carried out to ensure that the steady-state initial condition is properly maintained when switching from the steady-state input model to the transient simulation. The calculation for this analysis is a simulation of Test LP-02-6 from 10 seconds before the break initiation at 0 second up to 140 seconds. This time interval was chosen because the important phenomena and significant events of Test LP-02-6 occurred during this period.

The assessment of S-RELAP5 to predict each of the important LOCA phenomena for LOFT LP-02-6 is presented in detail in Reference 5. Figure 4.150 compares the calculated and measured PCT versus core elevation. This figure refers to the PCT as a maximum cladding surface temperature, either calculated or measured at the various elevations, during the LOCA transient history. The comparison shows that the code overpredicted the measured temperatures except at the low power region near the core exit. The greatest differences between the calculated and measured PCT occur in the high power region between the 15 in and 44 in elevations. The highest PCT of 1104.8 K (1529 F) was measured at the 26-in elevation. The comparison shows that the calculated PCT of 1159 K (1627 F) is in good agreement with data and conservatively exceeds the measured PCT in the high power core region.

4.3.2.1.7 LOFT Test LP-LB-1 Assessment

The fifth LOFT LOCE, Test LP-LB-1, simulated a hypothetical double-ended cold leg guillotine break initiated from conditions representative of a PWR operating near its licensing limits. The initial core power was near the facility design limit of 50 MWt with maximum LHGR of 15.8 kW/ft. Included in the test's boundary conditions were loss-of-offsite power coincident with the LOCE, a rapid PCP coastdown, and a minimum safeguard ECCS injection assumption from a European PWR. To minimize possible fuel pin damage, all of the fuel rods in the core were initially unpressurized.

From Reference 5, a bias of $11.4^{\circ}\text{K} \pm 16.2^{\circ}\text{K}$ ($20.5^{\circ}\text{F} \pm 29.2^{\circ}\text{F}$) should be applied to the measured PCT to account for the 'fin cooling' effects on the surface mounted thermocouples. Thus, the reportable PCT for LOFT LP-LB-1 is 1284.0 K (1851.5 F).

A steady-state initialization calculation was performed to reach the desired steady-state conditions for initiating the LOCA calculation. The calculated and measured initial conditions agree quite well and the calculated initial conditions are generally within the uncertainty band of the measured quantities. The calculated initial broken loop temperature of 560.0 K for the cold leg and 558.3 K for the hot leg come very close to measured values considering the large error bands quoted for the measured data, namely $552.0\text{ K} \pm 6.0\text{ K}$ for the cold leg and $561.0\text{ K} \pm 6.0\text{ K}$ for the hot leg. The desired steady-state conditions were achieved and the calculation accurately reached the LP-LB-1 test initial conditions.

A short steady-state calculation before the break opening is carried out to ensure that the steady-state initial condition is properly maintained when switching from the steady-state input model to the transient simulation. The calculation for this analysis is a simulation of Test LP-LB-1 from 10 seconds before the break initiation at 0 second up to 240 seconds. This time interval was chosen because, although most the important phenomena and significant events of Test LP-LB-1 occur before 100 seconds, the quenching of the core occurred much later in the calculation.

The assessment of S-RELAP5 to predict each of the important LOCA phenomena for LOFT test LP-LB-1 is presented in detail in Reference 5. Figure 4.151 compares the calculated and measured PCT versus core elevation. In this figure, the PCT is referred to as a maximum cladding surface temperature, either calculated or measured at the various elevations, during the LOCA transient history. The comparison shows that S-RELAP5 overpredicted temperatures in the high power region up to the 44-in elevation, and slightly underpredicted temperatures above 44 in. The measured PCT is 1284.0 K (1851.5 °F) at the 24-in elevation. That measurement includes a bias and uncertainty of $11.4^{\circ}\text{K} \pm 16.2^{\circ}\text{K}$ ($20.5^{\circ}\text{F} \pm 29.2^{\circ}\text{F}$) caused by the fin cooling effects on the surface mounted thermocouple. The calculated maximum PCT of 1310 K (1899 F) also occurred at the 24-in core level and is in good agreement with the measured PCT. Based on Figure 4.151, the PCT at any elevation is within approximately 20% of the data, which is reasonable agreement.

LOFT L2-3 S-RELAP5 ANALYSIS PLOT FILE NAME: 012-3_pct_00.eps, JOB ID: make_pct_plot.o3570, DATE: Tue May 21 08:46:34 PDT 2002

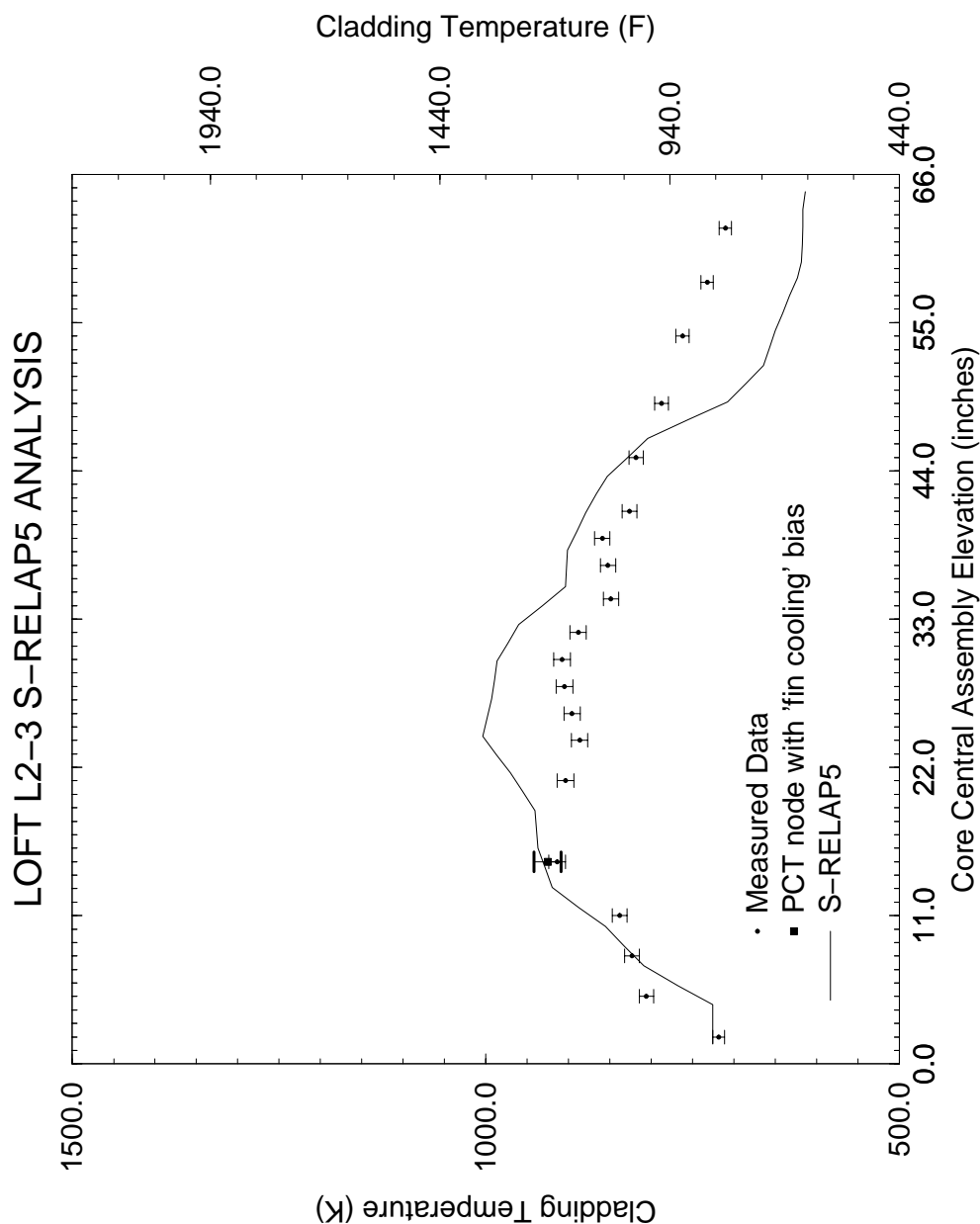


**Figure 4.148 Comparison of PCTs Versus Core Elevations LOFT
Test L2-3 with S-RELAP5**

LOFT L2-5 S-RELAP5 ANALYSIS PLOT FILE NAME: 012-5_pct_00.eps, JOB ID: make_pct_plot.03858, DATE: Tue Sep 10 15:04:54 PDT 2002

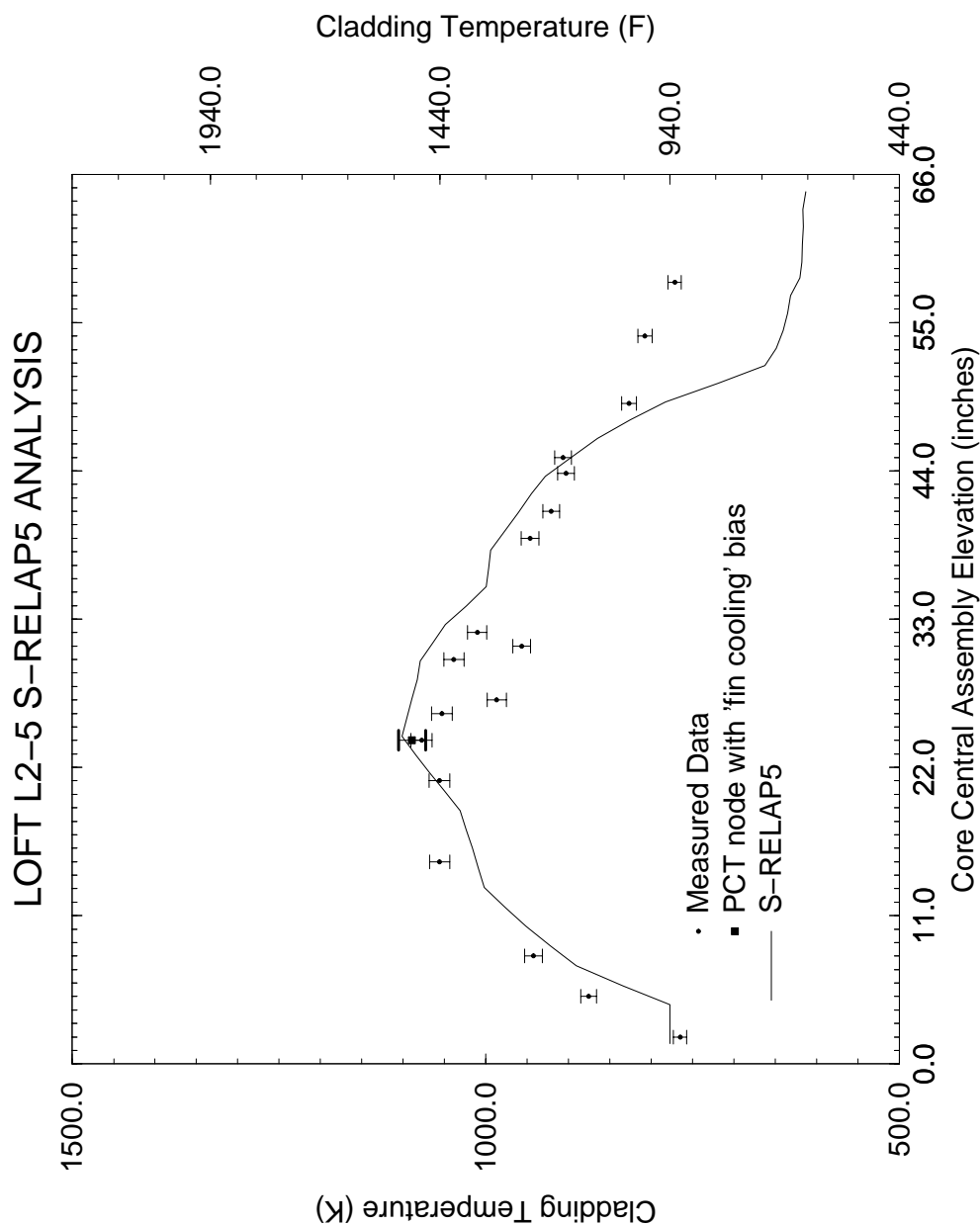


**Figure 4.149 Comparison of PCTs Versus Core Elevations LOFT
Test L2-5 with S-RELAP5**

LOFT LP-02-6 S-RELAP5 ANALYSIS PLOT FILE NAME: 012-6_pct_00.eps, JOB ID: make_pct_plot.03857, DATE: Tue Sep 10 15:04:09 PDT 2002

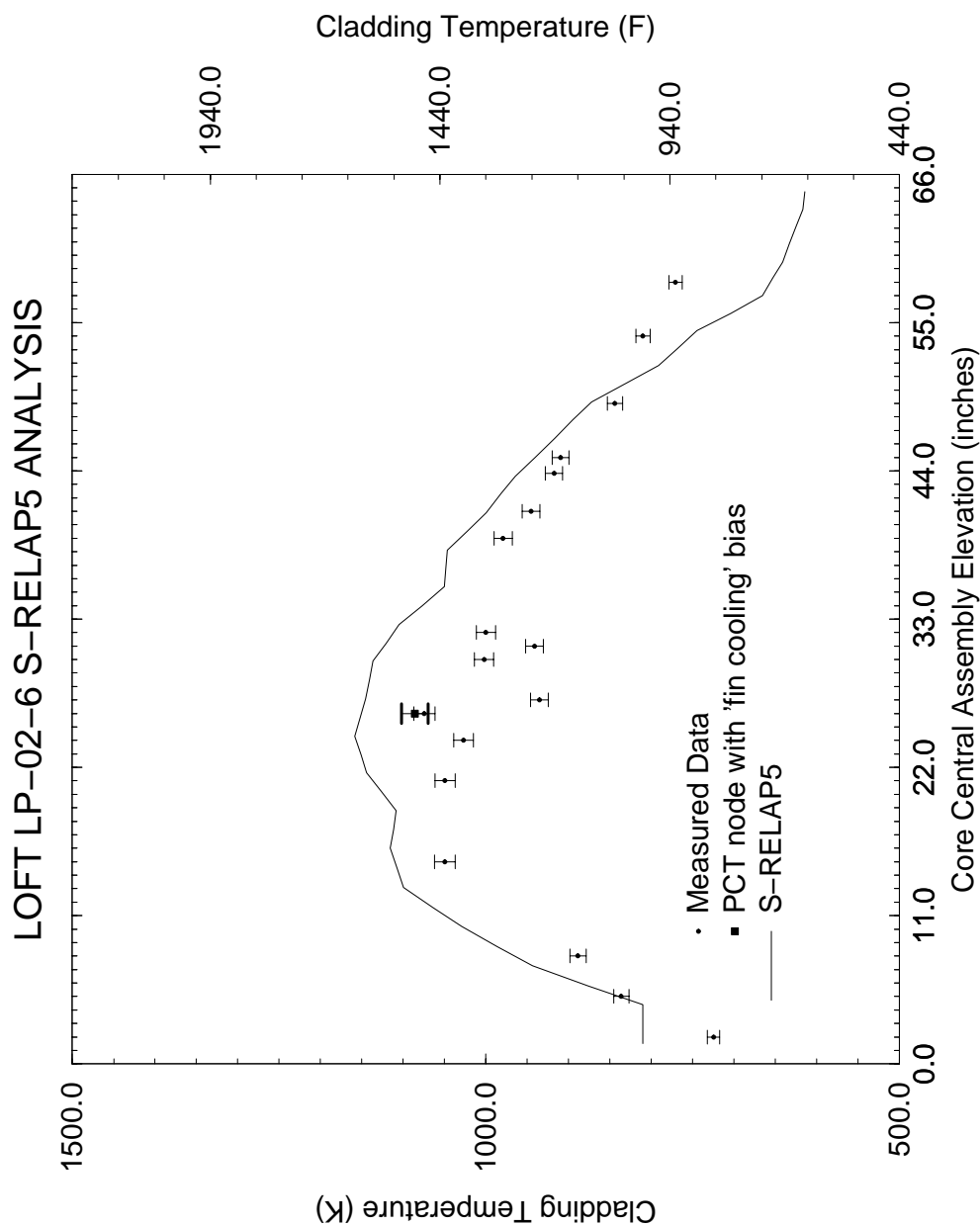


Figure 4.150 LOFT Test LP-02-6 Comparison of PCTs Versus Core Elevations

LOFT LP-LB-1 S-RELAP5 ANALYSIS PLOT FILE NAME: 0lb-1_pct_00.eps, JOB ID: make_pct_plot.o3587, DATE: Wed May 22 08:57:30 PDT 2002

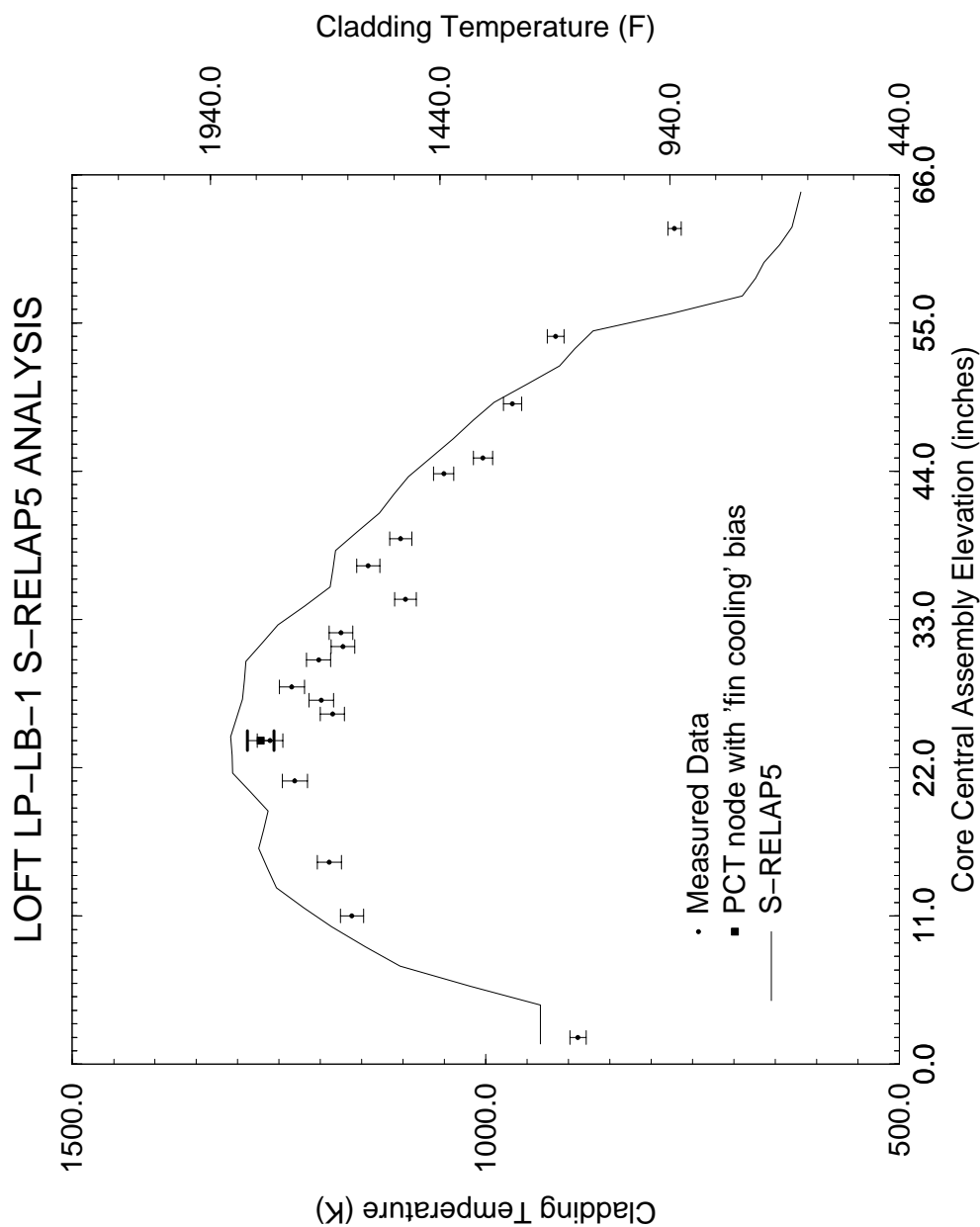


Figure 4.151 LOFT Test LP-LB-1 Comparison of PCTs Versus Core Elevations

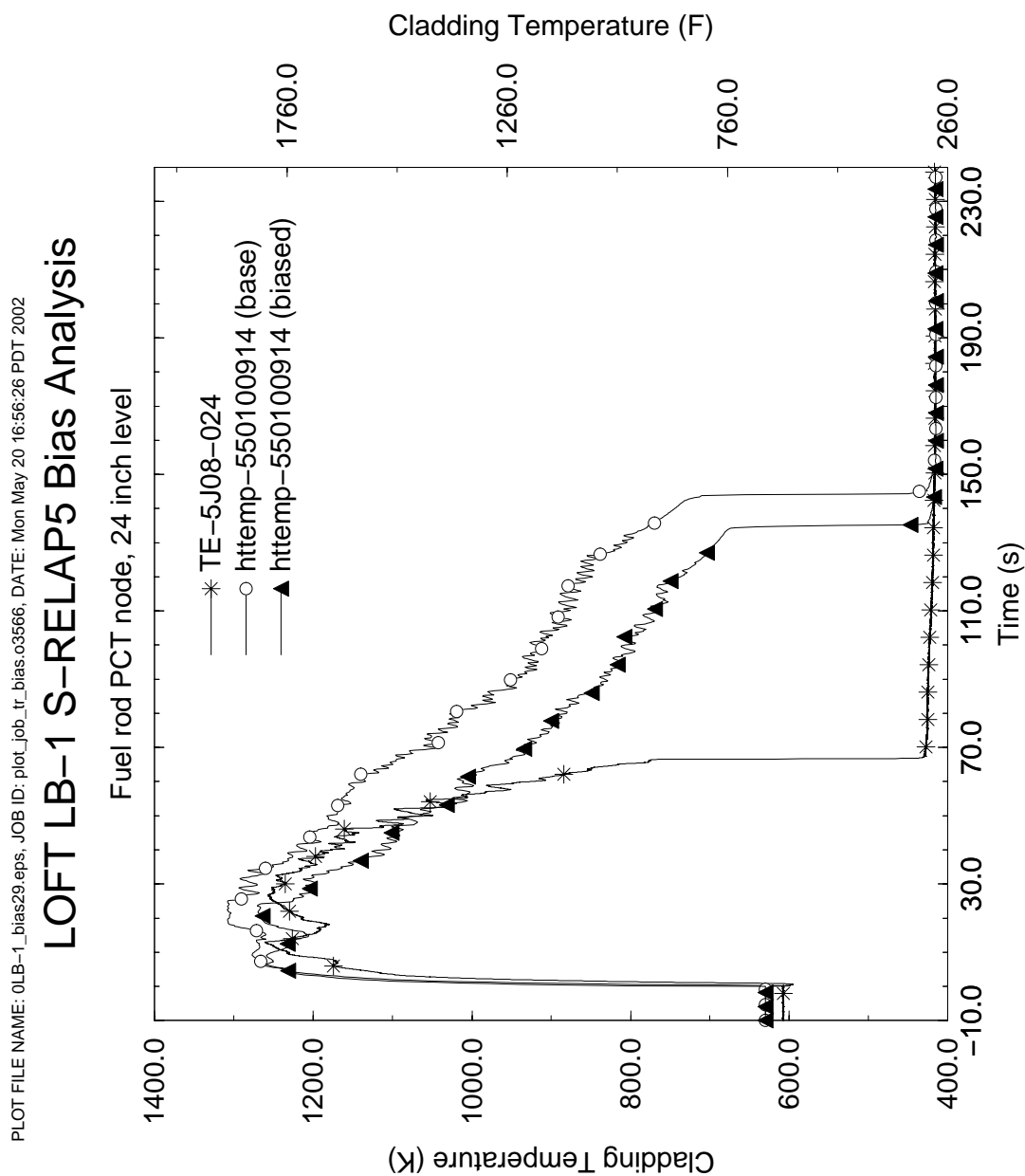


Figure 4.193 LOFT LP-LB-1 Temperatures at Measured PCT Node

LOFT LP-LB-1 S-RELAP5 ANALYSIS PLOT FILE NAME: 0lb-1_pct_00.eps, JOB ID: make_pct_plot_bias.o3588, DATE: Wed May 22 08:58:28 PDT 2002

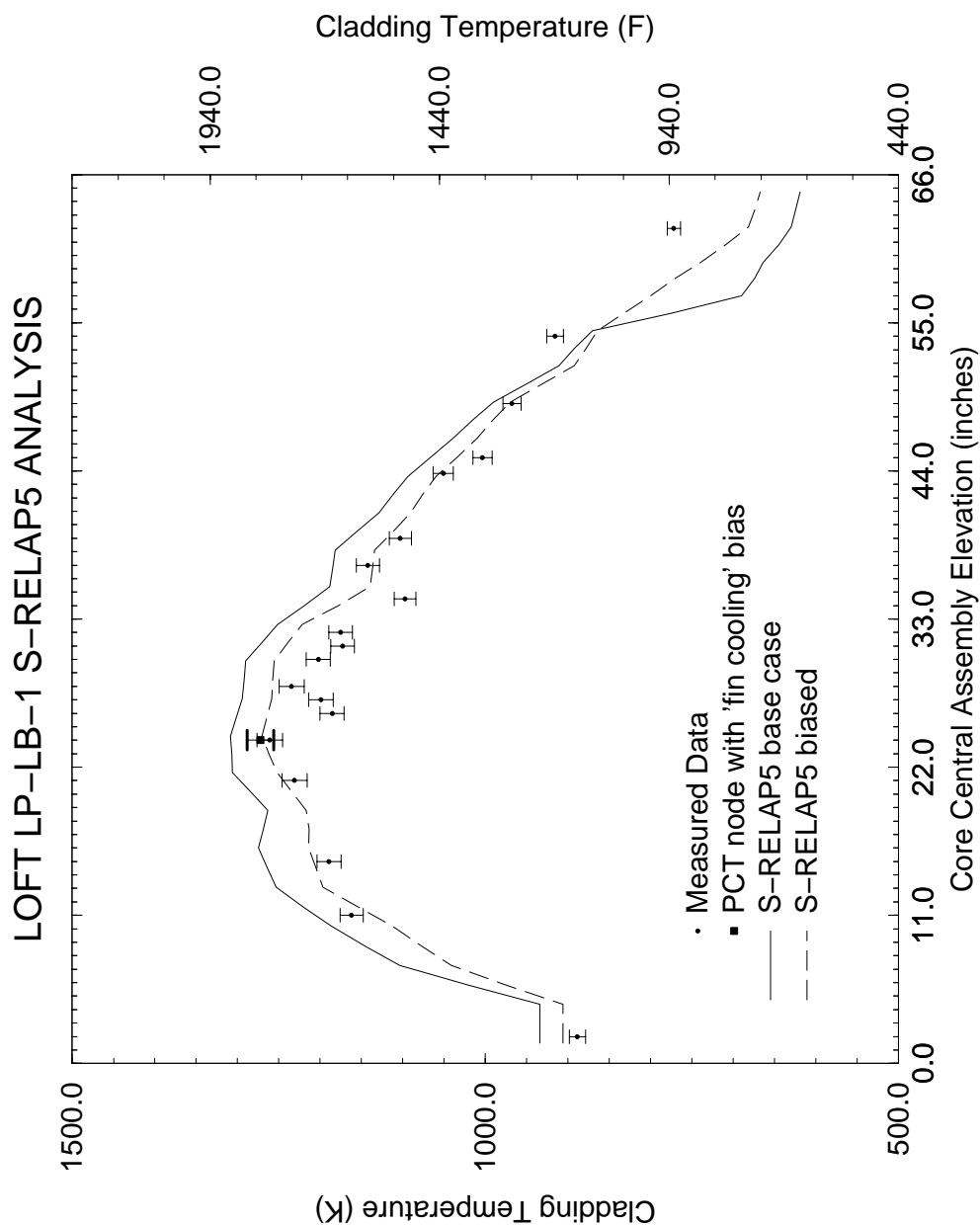


Figure 4.194 LOFT LP-LB-1 PCT Profile

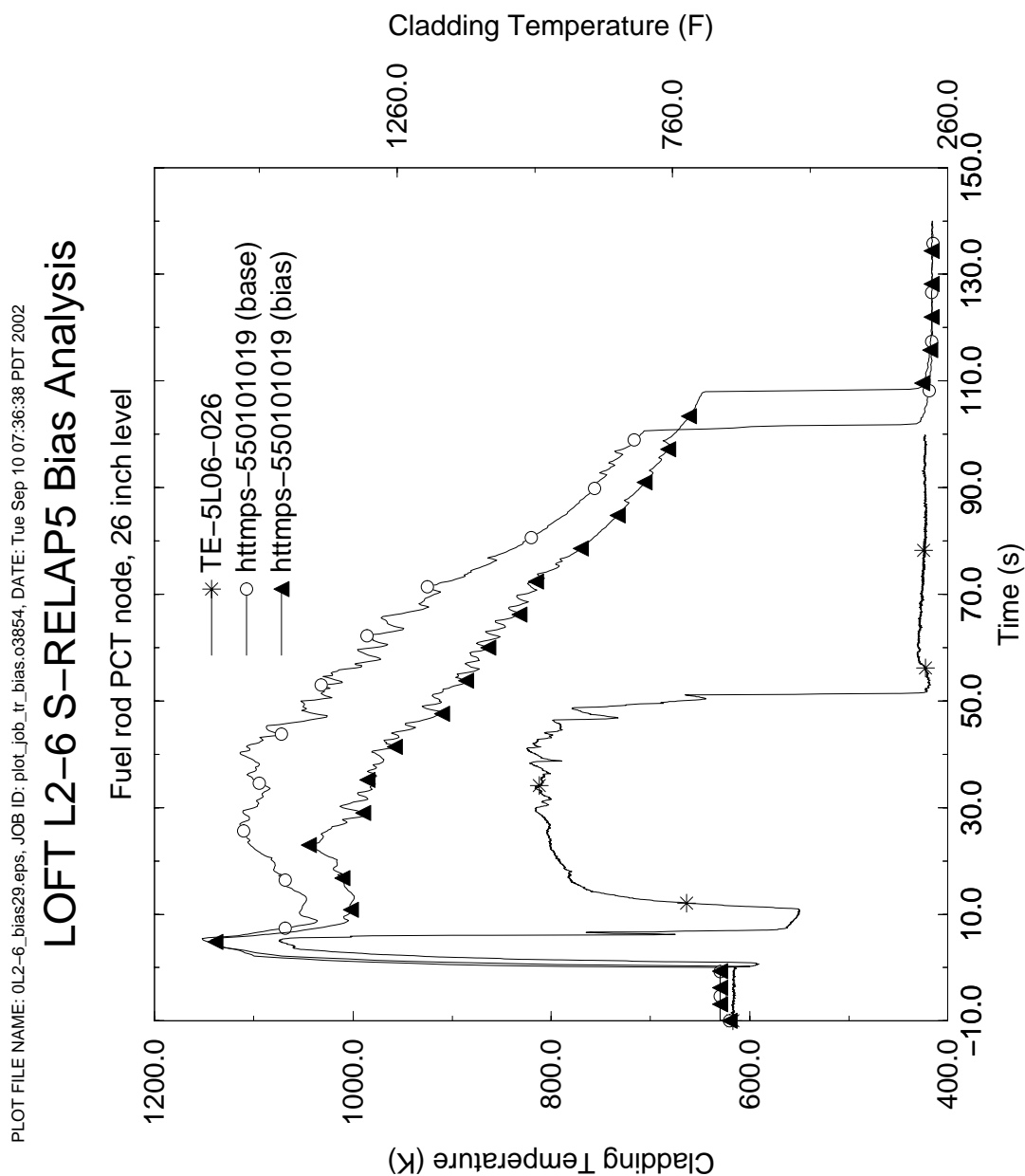


Figure 4.195 LOFT LP-02-6 Temperatures at Measured PCT Node

LOFT LP-02-6 S-RELAP5 ANALYSIS PLOT FILE NAME: 012-6_pct_00.eps, JOB ID: make_pct_plot_bias.o3856, DATE: Tue Sep 10 10:22:30 PDT 2002

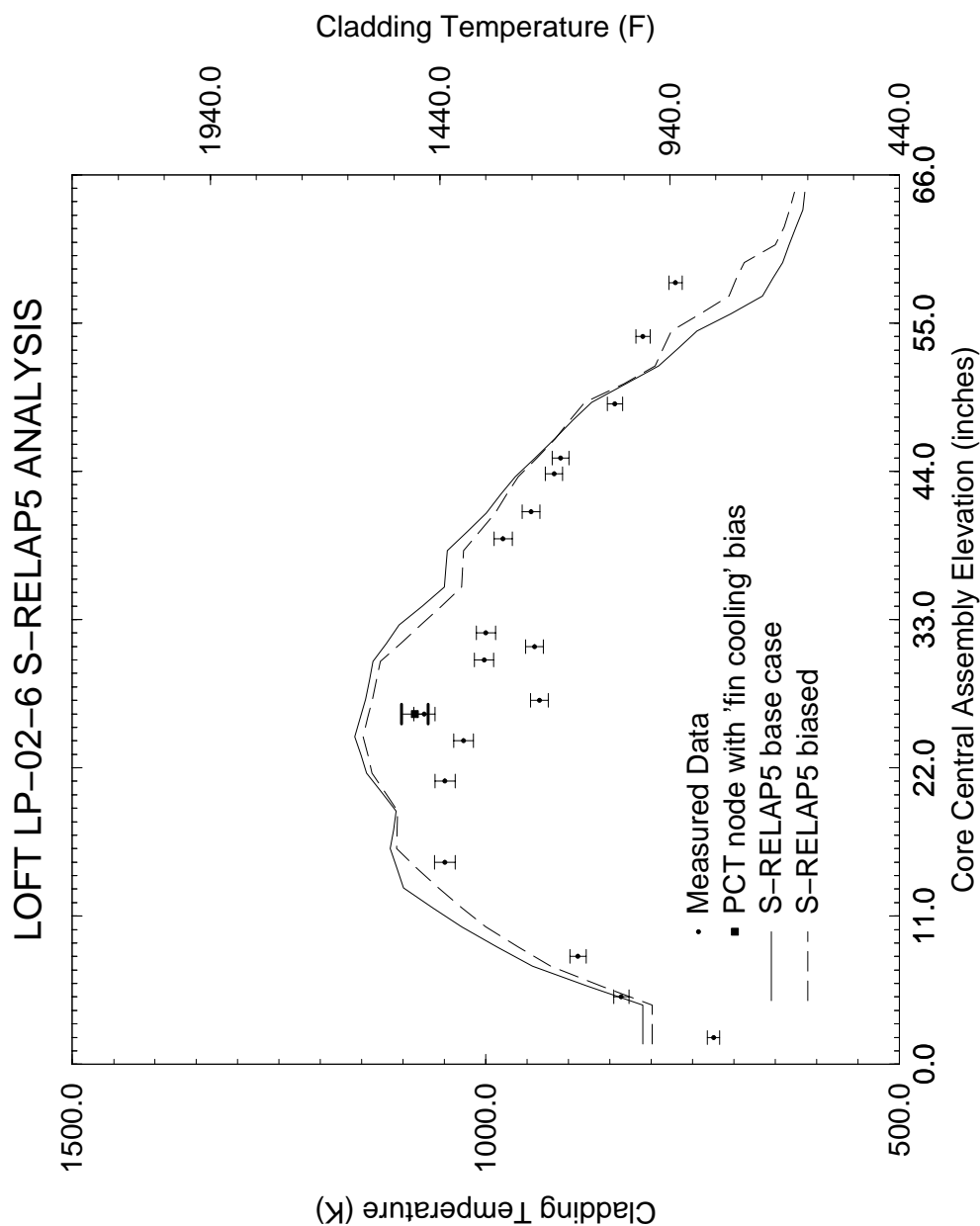


Figure 4.196 LOFT LP-02-6 PCT Profile

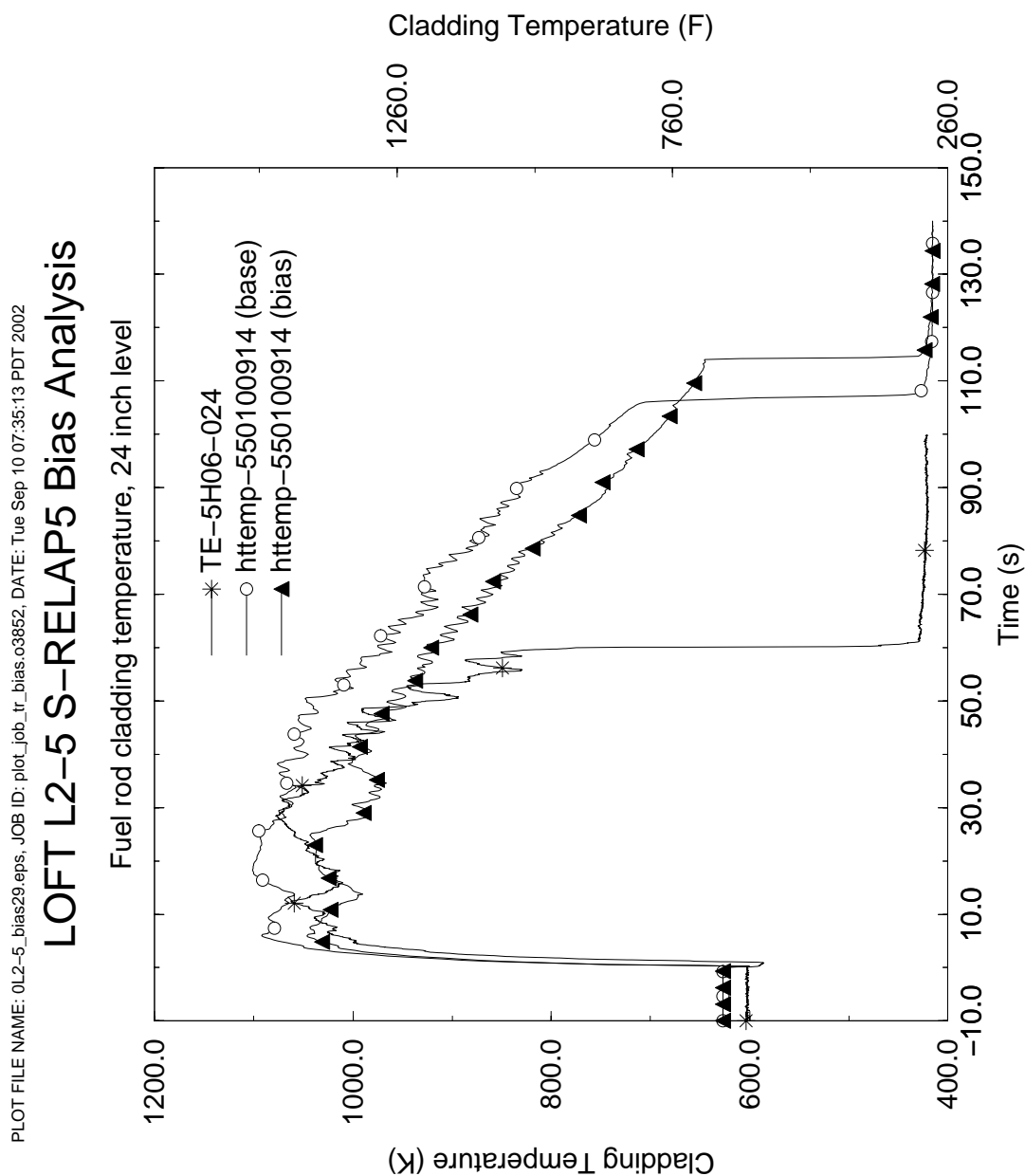


Figure 4.197 LOFT L2-5 Temperatures at Measured PCT Node

LOFT L2-5 S-RELAP5 ANALYSIS PLOT FILE NAME: 012-5_pct_00.eps, JOB ID: make_pct_plot_bias.o3859, DATE: Tue Sep 10 15:05:32 PDT 2002

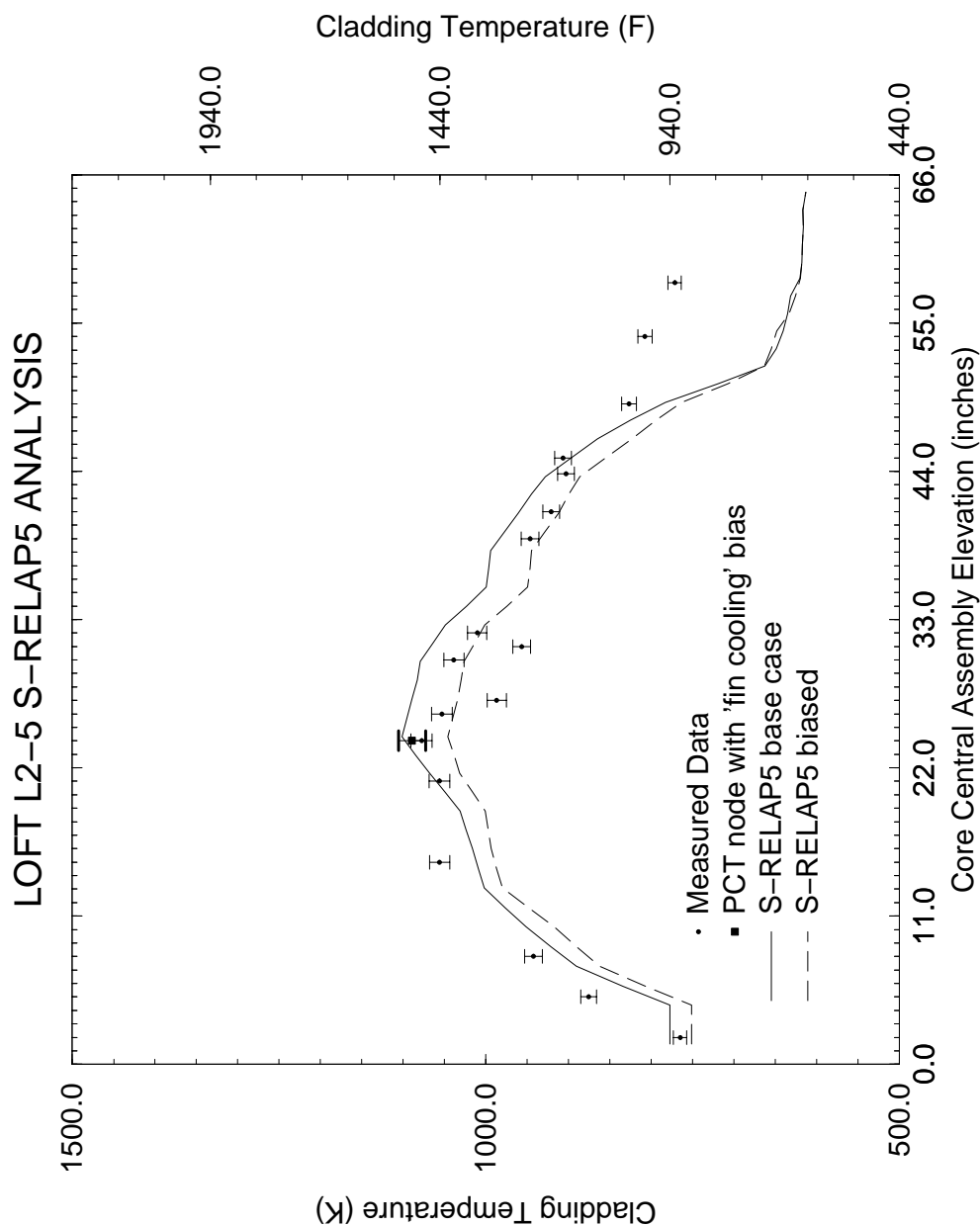


Figure 4.198 LOFT L2-5 PCT Profile

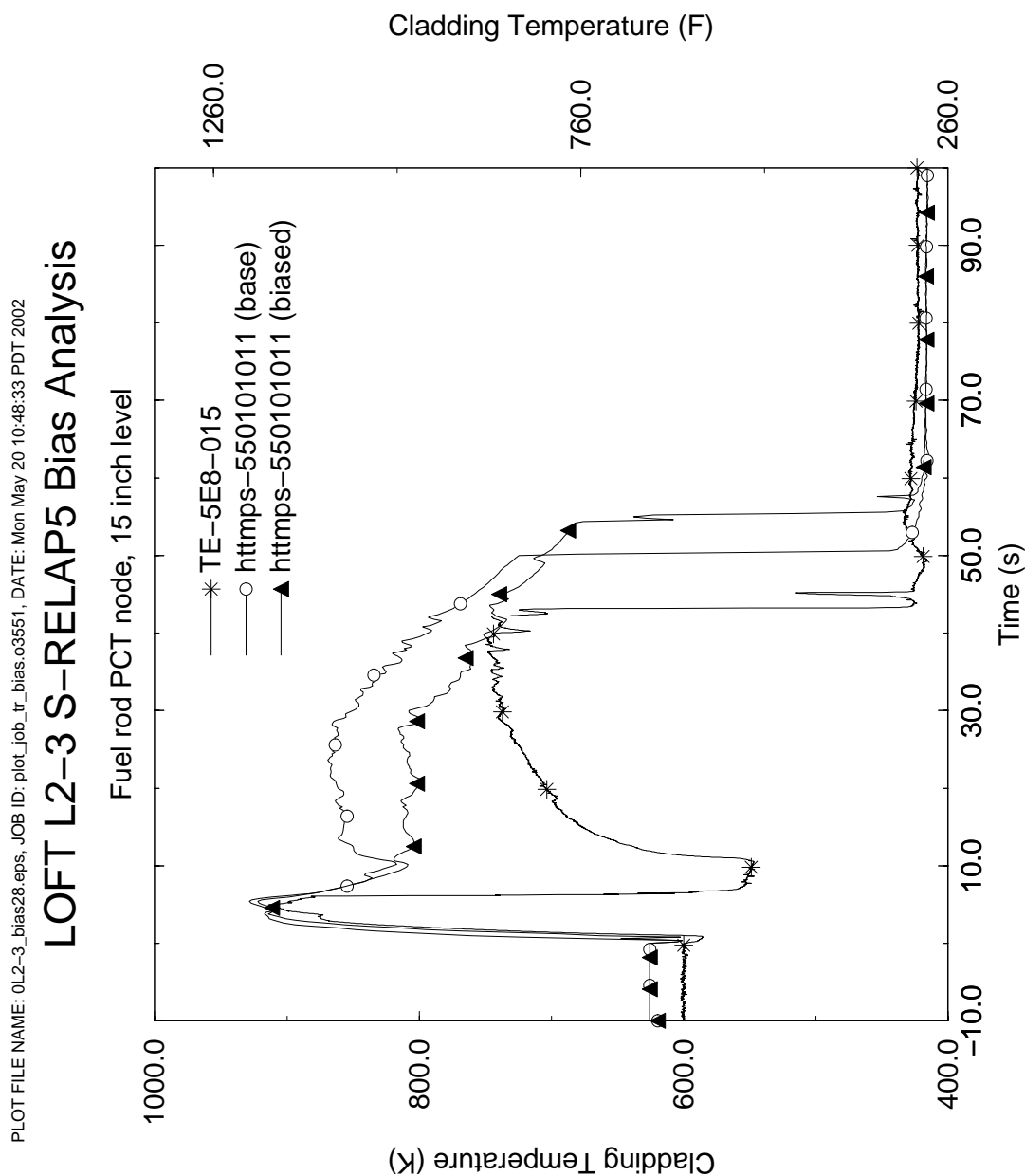


Figure 4.199 LOFT L2-3 Temperatures at Measured PCT Node

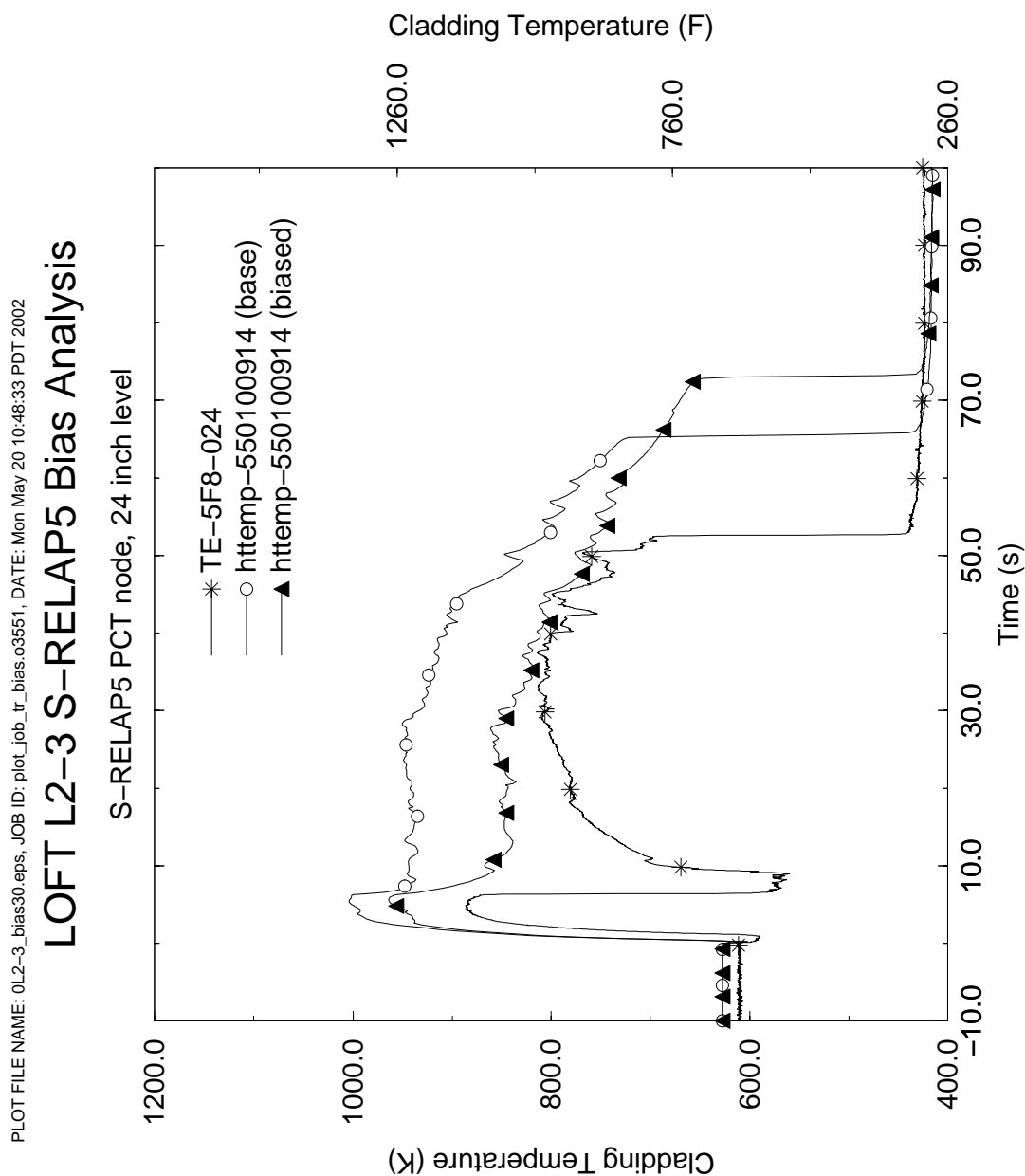


Figure 4.200 LOFT L2-3 Temperatures at Calculated PCT Node

LOFT L2-3 S-RELAP5 ANALYSIS PLOT FILE NAME: 012-3_pct_00.eps, JOB ID: make_pct_plot_bias.o3571, DATE: Tue May 21 08:48:21 PDT 2002

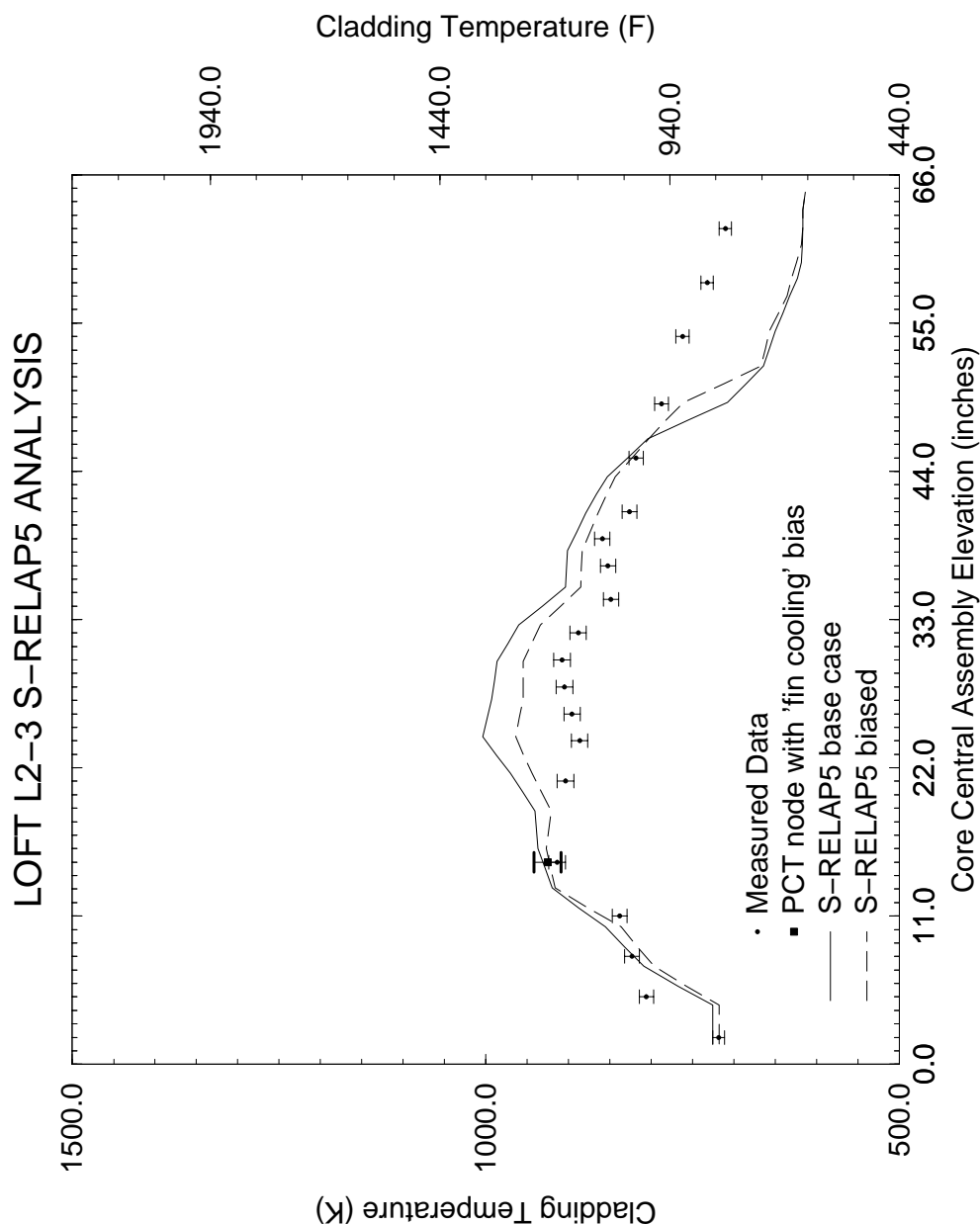


Figure 4.201 LOFT L2-3 PCT Profile

FRAMATOME ANP, Inc.

December 20, 2002
NRC:02:062

Document Control Desk
ATTN: Chief, Planning, Program and Management Support Branch
U.S. Nuclear Regulatory Commission
Washington, D.C. 20555-0001

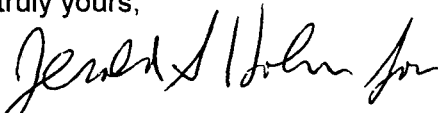
Responses to a Request for Additional Information on EMF-2103(P) Revision 0, "Realistic Large Break LOCA Methodology for Pressurized Water Reactors," (TAC No. MB2865)

Ref.: 1. Letter, Drew Holland (NRC) to James Mallay (Framatome ANP), "Request for Additional Information on EMF-2103(P), Rev. 0, "Realistic Large Break LOCA Methodology for Pressurized Water Reactors" (TAC No. MB2865), June 24, 2002.

In Reference 1, the NRC requested additional information to facilitate the completion of its review of the Framatome ANP topical report EMF-2103(P) Revision 0, "Realistic Large Break LOCA Methodology for Pressurized Water Reactors." Proprietary and non-proprietary versions of the response to this request are provided on the enclosed CDs.

Framatome ANP considers some of the information contained in the enclosure to be proprietary. This information has been noted by enclosing it within brackets. The affidavit provided with the original submittal of the referenced topical report satisfies the requirements of 10 CFR 2.790(b) to support the withholding of this information from public disclosure.

Very truly yours,


James F. Mallay, Director
Regulatory Affairs

Enclosures

cc: R. Caruso
D. G. Holland (w/enclosures)
R. Landry (w/enclosures)
J. S. Wermiel
Project 728

S-RELAP5 REALISTIC LARGE BREAK LOCA

Request for Additional Information

Heat Transfer

Question 1: Please provide a list of differences in the heat transfer models and CHF correlations as utilized in the Realistic Large Break LOCA to those utilized in Small Break LOCA models.

Response 1: The differences in the heat transfer models and CHF correlations utilized in the RLBLOCA methodology relative to those utilized in the SBLOCA methodology are summarized in Table 1.1 below.

Table 1.1 Differences Between SBLOCA and LBLOCA Models

Heat Transfer Model	Changes from SBLOCA to LBLOCA	References	
		EMF-2100, Revision 2	EMF-2100, Revision 4
Minimum Film Boiling Temperature, $T_{min} = 700 \text{ K}$	New Model	Figure 4.1	Figure 4.1
Transition Boiling	The F_r factor in the modified Chen's transition boiling correlation is changed for smoothness	Equation (4.36)	Equation (4.41)
Forslund-Rohsenow Dispersed Film Boiling	The value for the coefficient K is changed from 0.4 to 0.2	Page 4-17, second sentence from the end of the first paragraph	Page 4-18, the last sentence of second paragraph
Modified Bromley Film Boiling	The $(1 - \alpha_g)^{1/4}$ factor is dropped	Equation (4.45)	Equation (4.47)
Modified Zuber Critical Heat Flux (CHF)	Zuber CHF is used for void fraction below 0.74 and the modification factor is applied for void fraction above 0.74	Equation (4.32)	Equations (4.32) and (4.33)

The minimum film boiling temperature [] was implemented to improve the calculated quench temperature and quench behavior during reflood. The T_{min} model practically eliminates the role played by the transition boiling correlation to determine whether the heat transfer mode is in transition boiling or film boiling. Consequently, the transition boiling correlation can be modified for smoothness without significant impact on the calculated results.

The changes in the film boiling correlations were made in an attempt to improve code-data comparisons for tube data.

The change in the modified Zuber critical heat flux is partly based on experimental data and partly intended to smooth the reflood calculations.

The heat transfer modifications between the SBLOCA and the RLBLOCA code versions are improvements for LBLOCA. In the heat-up/dry-out period of a SBLOCA, the core can essentially be characterized by a single-phase steam region above a two-phase mixture region. Therefore, its PCT is mainly determined by the single-phase vapor heat transfer and will not be significantly impacted by small changes in other heat transfer models. Undocumented calculations did demonstrate that both SBLOCA and RLBLOCA code versions produce about the same PCTs for SBLOCA.

Question 2: *In the analysis of the LBLOCA transient, there are a number of different correlations that are used as the transient unfolds, (Biasi, modified Zuber, Sleicher and Rouse, Dittus-Boelter, etc.). Please choose a typical LBLOCA transient and map out all the different correlations that are used along the way, from the beginning of the transient to the end. Stating the particular correlation used, its applicable range (in terms of Reynolds No., flow rates, etc.), and validation of its use in the applicable range.*

Response 2: During a transient simulation, different heat transfer correlations may be applied at any given time. The best way to demonstrate how the S-RELAP5 simulation of a LBLOCA is supported by correlation development and validation studies is to first identify (or map) the "simulation-space" and compare it to the "assessment-space." The "assessment -space" represents the combination of the applicability range from separate-effects investigation (i.e., correlation development or derivation), the expanded applicability range from uncertainty analysis, and validation from integral-effects benchmark calculations. The simulation-space is evaluated through the examination of the limiting calculations (in terms of PCT) for the 3- and 4-loop sample problems for key correlation dependent parameters. The key parameters are defined as those engineered parameters that can be designed into a thermal-hydraulic test matrix. The most common engineered parameters used in thermal-hydraulic testing and correlation development are pressure, power (in terms of linear heat generation rate, or heat flux), and mass flux (may be also given as Reynolds number or mass flow).

The comparison of the simulation-space and assessment-space provides quantitative support to Step 6, Determination of Code Applicability, in the Code Scaling, Applicability, and Uncertainty (CSAU) methodology (Reference 1). As stated in Reference 1, "if inadequacies are noted, they should be fully documented and, if possible, quantified." Ideally, the assessment-space will span the simulation space; however, realistically, there will likely be holes in the assessment-space. To prioritize the effort in demonstrating adequate coverage, Framatome ANP presented a PIRT for the LBLOCA in Reference 2. This PIRT identified and ranked the relevant phenomena of importance for a LBLOCA. Table 2.1 highlights just the core heat transfer phenomena identified as being important for LBLOCA from the PIRT. This table does not explicitly identify all the heat transfer regimes or correlations of importance. This information is given in Reference 3. The important heat transfer regimes are nucleate boiling, CHF (DNB), transition boiling, and film boiling. As can be seen from the PCT response in Figures 2.1 and 2.3 for the 3- and 4-loop sample problems, respectively, core heat transfer around the hot rod is limited to these heat transfer regimes. Figures 2.2 and 2.4 provide the corresponding heat transfer coefficient near the PCT node. It was the conclusion of the Framatome ANP PIRT team that the other heat transfer regimes were either not present or had negligible impact on peak clad temperatures. In fact, it was concluded that nucleate boiling has a relatively low ranking during the LBLOCA event (see Table 2.1).

The best resource for information about the heat transfer regimes and their application can be found in Section 4 for the S-RELAP5 Models and Correlations Code Manual (EMF-2100, Reference 3). The selection logic for each heat transfer regime is presented in Figure 4.1 of that document. As a summary Table 2.2 highlights the heat transfer correlations used in S-RELAP5.

The transient history at the PCT node for the 3- and 4-loop limiting PCT calculations (Case 41 and Case 22, respectively as given in Reference 2) are used as an example to show the heat transfer models invoked during the entire transient and to define the example problem simulation-space. The heat structures at the PCT locations pass through the CHF point almost immediately (~ 0.03 s) after the break is initiated and the mass flux drops rapidly from over 3000 kg/s-m². Table 2.3 defines the simulation-space from the 3- and 4-loop sample problems for the duration of the transient simulation by presenting the different heat transfer regimes, the heat transfer correlations used and approximate parameter ranges. (Note: the chronology presented in this table is the traditional LBLOCA phases. The LBLOCA phases map well to the heat transfer region numbers highlighted in Figures 2.1 and 2.3 and referenced in Table 2.3.)

Figures 2.1 and 2.3 show clad temperature plots from the 3- and 4-loop sample problems, respectively with the LBLOCA phases in Table 2.3 identified. The heat transfer modes during the LBLOCA are identified in this figure. During most of the LOCA calculation, multiple heat transfer modes are present. However, with the exception of the period from just prior to quench to the end of the calculation, the dominant heat transfer mode is convection to single phase vapor (Sleicher-Rouse correlation). It should be noted that the heat transfer to vapor is calculated by the Sleicher-Rouse correlation during the film boiling period. Unlike the 4-loop sample problem, the 3-loop sample problem shows a late reflood heat up (Figure 2.1 vs. 2.3). As identified in Table 2.3, this is a period of film boiling with the void fraction generally greater than 0.995. The most obvious observation that can be made from these figures is that for the majority of the transient the hot rod is in film boiling. This is consistent with the expectation presented in the PIRT.

Definition of the assessment-space in terms of the range of applicability and validation of the relevant heat transfer correlations applied to the hot rod is given in the following paragraphs. This discussion is presented in the chronological order anticipated during a LBLOCA. Pressure and heat flux (heat flux is translated into linear heat generation rate, LHGR, by assuming a typical fuel rod diameter) are easily compared to the simulation-space; however, reported flow rates are given in either mass flux, velocity (aka, reflood rate), or Reynolds number. A simple approximation for reflood rate is 1 in/s \approx 25 kg/s-m².

Time Period: Early Blowdown (0.0 – 0.03 s)

Immediately following the postulated LBLOCA, portions of the core will, for a very brief time, be in the nucleate boiling heat transfer regime until critical heat flux (CHF) is achieved. The duration of this period depends on the size of the break; however, for the typical limiting PCT break, this period will last only a fraction of a second. This period is more influenced by the CHF correlation, rather than the nucleate boiling heat transfer correlation, because CHF triggers the time of transition to the low heat transfer regimes (post-CHF).

S-RELAP5 Implementation of CHF

Correlation: Modified Zuber [] and Biasi []

Formulation: See Section 4.4 of Reference 3.

Derived Range of Applicability: During this early portion of the LBLOCA transient, core mass fluxes are generally high as fluid is beginning to move rapidly towards the break planes. For these higher mass fluxes, the Biasi correlation will apply. The Biasi correlation is empirical. For LBLOCA simulation with S-RELAP5, the Biasi correlation is applied only immediately following the transient initiation until the beginning of reflood. Sensitivity studies have shown that CHF is reached so quickly after a break, that clad temperatures are unaffected by a large uncertainty in CHF. The applicability range for the Biasi correlation is published in Reference 19 as:

- $2.7 \text{ bar} < \text{Pressure (P)} < 140 \text{ bar}$ (approx. $40 \text{ psia} < P < 2050 \text{ psia}$)
- $100 \text{ kg/m}^2\text{-s} < \text{Mass Flux (G)} < 6000 \text{ kg/m}^2\text{-s}$ (S-RELAP5 constrains to $G > 200 \text{ kg/m}^2\text{-s}$, typical of blowdown phase of LBLOCA)

In general, the conditions for which the Zuber correlation is applied are not expected during this early period. Nonetheless, the Zuber correlation was derived theoretically for pool boiling conditions with well-wetted horizontal surfaces; however, the formulations for other geometries range within +/- 12% of the Zuber values (Reference 17). It is applied for very low mass fluxes and when the reflood heat transfer model is activated. The S-RELAP5 mass flux constraint was recommended in Reference 18.

Validation/Assessment/Expanded Range of Applicability: Sensitivity of PCT to CHF was determined to be minimal in LBLOCA sensitivity studies. Early in the transient, heat transfer in the core rapidly advances to post-CHF conditions. Nonetheless, the Biasi correlation was assessed against the tests performed on the THTF at Oak Ridge National Laboratory and a bounding bias was determined for application in the RLBLOCA methodology. This study is presented in EMF-2102 (Reference 15). Further discussion is provided in Section 4.13 of EMF-2100 (Reference 3).

Table 2.4 provides a comparison of the simulation-space (taken from Table 2.3) and the range of applicability evaluated for the assessment-space for the Biasi CHF correlation. [Note: the assessment-space includes three components as previously described: the test conditions used in correlation development, relevant uncertainty analysis, and integral-effects validation.]

Time Period: Blowdown (0.03 – 20 s)

As the RCS depressurizes and CHF is reached in the core, vapor generation is rapid and the steam quality increases. This post-CHF period is characterized by film boiling, single-phase steam convection, and radiation (although radiation isn't expected to be significant; hence, it doesn't appear in the PIRT). As long as the steam maintains some wetness, the total heat transfer includes all three heat transfer mechanisms; however, single phase steam convection dominates heat transfer when void fractions are above about 0.75. Post-CHF heat transfer includes uncertainty not only from the application of the correlations, but also from contributions of interfacial drag and heat transfer phenomena. For this reason, total post-CHF heat transfer, rather than the individual correlations, is a statistically treated parameter.

S-RELAP5 Implementation of Film Boiling Heat Transfer

Correlation: Modified Bromley [], Forslund-Rohsenow [], Sleicher-Rouse ($\alpha = 1$)

Formulation: See Section 4.7 of Reference 3.

Derived Range of Applicability: The modified Bromley correlation was analytically derived to be generally applicable in the film boiling regime. Nonetheless, the Bromley model was assessed with datasets covering a range of working fluids. The published database ranges for this correlation is:

- $0.1 \text{ Mpa} < \text{Pressure (P)} < 0.7 \text{ Mpa}$ (or $14.7 \text{ psia} < P < 102.9 \text{ psia}$, bounds reflood pressures)
- $0 < \text{Velocity (V)} < 0.3 \text{ m/s}$ (approx. $0 < G < 300 \text{ kg/s-m}^2$, typical of reflood conditions)
- $30.0 \text{ kW/m}^2 < \text{Heat Flux (q'')} < 130 \text{ kW/m}^2$ and $0.25 \text{ in} < D(\text{rod}) < .5 \text{ in}$
(or $\sim 0.16 \text{ kW/ft} < \text{LHGR} < 0.7 \text{ kW/ft}$, typical decay heat during reflood)
- $\text{Void} < 0.4$

The Forslund-Rohsenow correlation was derived experimentally using only nitrogen as the working fluid.

- $\text{Pressure} = 25 \text{ psia}$ (below reflood)
- $70,000 \text{ lbm/hr-ft}^2 < G < 190,000 \text{ lbm/hr-ft}^2$ ($0.82 \text{ kg/s-m}^2 < G < 2.23 \text{ kg/s-m}^2$, a very low flow rate)
- $q'' < 25000 \text{ Btu/hr-ft}^2$ ($q'' < 79 \text{ kW/m}^2$, $.228 \text{ in} < D < .462 \text{ in}$, hence, $0.44 \text{ kW/ft} < \text{LHGR} < 0.88 \text{ kW/ft}$, approximately, typical decay power range)

The Sleicher-Rouse correlation is discussed separately in the next section.

Validation/Assessment/Expanded Range of Applicability: Within S-RELAP5 both the modified Bromley and Forslund-Rohsenow correlations may be used outside their derived range of applicability; however, applied statistical uncertainty on the total heat transfer provides the means for expanding the range of applicability. The primary deviations from the original range of applicability are:

- The modified Bromley correlation is limited to the condition where vapor void fraction is less than [], rather than 0.4.
- The Forslund-Rohsenow correlation was developed using nitrogen as the working fluid.
- The Forslund-Rohsenow correlation is applied when the volume void fraction is above [].
- For void fractions between [], both the Forslund-Rohsenow and modified Bromley correlations are smoothly weighted to cover this transition region.
- Full range of pressure from 2250 psia to atmospheric.
- Full range of mass fluxes expected during reflood.

A discussion on the statistical treatment of total heat transfer is presented in S-RELAP5 Verification and Validation document, EMF-2102 (Reference 15). The uncertainty analysis applies data from the Thermal-Hydraulic Test Facility (THTF) tests and from FLECHT-SEASET tests. The applicability of these tests was evaluated by analysis of the breadth of the data in terms of key correlation parameters and the density of the data in terms of the parameters for which the correlation is most sensitive, pressure and void fraction. A comparison of the data density from the simulation- and test-space over the Bromley and Forslund-Rohsenow void range of applicability are given in Figures 2.5 and 2.6. The experimental ranges for the key test parameters for each test are:

THTF: Transient reflood tests and full height

- 404 psia < P < 1195 psia (typical during blowdown)
- $G < 4250 \text{ kg/s-m}^2$ (typical during steady-state and blowdown)
- $0.8 \text{ kW/ft} < \text{LHGR} < 2.2 \text{ kW/ft}$ (typical during blowdown)

FLECHT-SEASET: Transient reflood tests and full height

- 20 psia < P < 60 psia (typical reflood range)
- $.8 \text{ in/s} < \text{flooding rate} < 6 \text{ in/s}$ (approx. $20 \text{ kg/s-m}^2 < G < 150 \text{ kg/s-m}^2$, typical reflood range)
- $\text{LHGR} < .7 \text{ kW/ft}$ (typical decay power)

Since steady-state pressure will always be near 2250 psia, there will be a short period of time in which the system pressure will be above the range of applicability. However, additional coverage is supported through the "Evaluation of Bias" calculations using the LOFT and SemiScale benchmarks that show good or conservative agreement. These are integral tests that are initiated from full pressure conditions.

S-RELAP5 Implementation of Single-Phase Vapor Convection

Correlation: Sleicher-Rouse

Formulation: See Section 4.5 of Reference 3.

Derived Range of Applicability: The Sleicher-Rouse correlation was developed for single-phase heat transfer for both liquids and gases over the following parameter ranges:

$0.1 < Pr < 10^5$ ($0.6 < Pr < 0.9$, typical for single phase water vapor)
 $10^4 < Re < 10^6$ (typical of blowdown phase, high for refill and reflood period)

The form of the correlation is a summation of both a turbulent and laminar convection term. The laminar convection term is $Nu(\text{lam}) = 5.0$. This is below the best-estimate value of 7.86 for rod pitch to diameter of 1.33 (see Section 4.2 of Reference 3).

Validation/Assessment/Expanded Range of Applicability: Single-phase vapor heat transfer has been assessed using the 161-rod bundle FLECHT-SEASET steam cooling tests (Reference 16, also see RAI Response 41). The range of the key design parameters for these tests is:

- Pressure = 40 psia (typical of post-blowdown periods)
- $3000 < Re < 20000$ (typical of reflood period)
- $0.006 \text{ kW/ft} < \text{Rod Power } (q') < 0.24 \text{ kW/ft}$ (below typical decay heat powers)

The LOFT and Semiscale integral tests during the refill period and the separate effect assessments, including FLECHT-SEASET and CCTF, during the early period of adiabatic heat-up were used to validate single-phase heat transfer at very low flows. The range of the key design parameters for these tests are:

- Pressure = 20-60 psia
- $0 < Re < 3000$
- $\text{LHGR} < .7 \text{ kW/ft}$ (typical decay power)

Low flows that directionally oscillate are characteristic during this period in both the tests and the calculations (i.e., Re will be as low as zero). In LBLOCA calculations during vessel refill, vapor flow rates decelerate and directionally oscillate as a result of the transition to refill. This will last

until the beginning of core reflood which is a period typically less than 15 s. During this unsettled period, core flow will likely remain turbulent; however, vapor Reynolds numbers will be low.

In general, the S-RELAP5 results conservatively bound the measured results (higher clad temperatures). While the results of the assessments demonstrated that the Sleicher-Rouse correlation is adequate for post-blowdown periods during a LOCA (and lower Reynolds numbers), single-phase vapor heat transfer is treated implicitly in the evaluation of uncertainty in the total post-CHF heat transfer (see previous section).

S-RELAP5 Implementation of Radiation

Correlation: Sun (for rod-to-fluid, based on Stephan-Boltzman)

Formulation: See Section 4.8 of Reference 3

Derived Range of Applicability: The Stephan-Boltzman correlation was derived to be generally applicable for radiation calculations. Radiation heat transfer in S-RELAP5 is limited to rod-to-fluid phenomenon. The key addition of the Sun correlation is the development of separate emissivities for vapor and liquid droplets. Since radiation is a relative small contributor to heat transfer, this model is not invoked until rod temperature is both above 650 K and the steam temperature.

Validation/Assessment/Expanded Range of Applicability: Since radiation is such a small component to total heat transfer, this model has not been explicitly assessed by separate effects tests; however, this model is activated in the majority of assessments presented in the S-RELAP5 Code Verification and Validation document (Reference 15). This includes both the THTF and FLECHT-SEASET test suites used to derive the post-CHF total heat transfer uncertainty.

Table 2.5 provides a comparison of the simulation-space (taken from Table 2.3) and the range of applicability evaluated for the assessment-space for the film boiling correlation. (Note: the assessment-space includes three components as previously described: the test conditions used in correlation development, relevant uncertainty analysis, and integral-effects validation.)

Time Period: Refill (20 s – 32 s)

During the refill period, the RCS has nearly depressurized and the core region is devoid of coolant. Heat transfer in the core is almost all from single phase vapor. As previously stated, single phase vapor heat transfer is predicted using the Sleicher-Rouse correlation. The core conditions during this time are consistent with both the derived range of applicability and the FLECHT-SEASET steam cooling tests. While post-CHF total heat transfer is a statistically treated parameter, there is no bias or uncertainty applied when void fraction equals 1.0. As assessed from the FLECHT-SEASET steam cooling tests, the Sleicher-Rouse correlation is slightly conservative relative to the data. Analysis of the "Evaluation of Bias" integral tests assessment cases support this finding.

Since the single-phase vapor heat transfer is a component of film boiling, refer to Table 2.5 for a comparison of the simulation-space (taken from Table 2.3) and the range of applicability evaluated for the assessment-space for the Sleicher-Rouse single-phase vapor heat transfer correlation.

Time Period: Reflood (32 s – Quench)

By this time, RCS pressure has established some equilibrium with the relative low pressure containment. ECCS coolant from the accumulator begins to reach the lower portions of the core and a definite two-phase mixture is present throughout the core region. With the constant supply of coolant, a quench front is established at the bottom of the core that slowly moves upward. At some point the coolant supply from the accumulator ends and core heat removal relies solely on that provided by the low pressure injection system. This may result in a late reflood heat up. Nonetheless, in time this supply of coolant will be able to completely quench all the fuel rods in the core.

For the duration of this period, the heat structure nodes with the highest temperatures are removing heat by film boiling. Table 2.5 provides a comparison of the simulation-space (taken from Table 2.3) and the range of applicability evaluated for the assessment-space for the film boiling. This period ends with the fuel rod quench, which will occur shortly after meeting the conditions for transition boiling.

S-RELAP5 Implementation of Reflood Heat Transfer

Correlation: All

Formulation: See Section 4.12 in Reference 3.

Derived Range of Applicability: Refer to the discussion on the suite of heat transfer correlations presented in this RAI response.

Validation/Assessment/Expanded Range of Applicability: When core reflood is enabled in S-RELAP5 (provided in the input model), a heat transfer regime profile covering the entire boiling curve is established along the modeled heat structure. Proceeding from the bottom of the core, this will be single-phase liquid and/or nucleate boiling, transition boiling, and single-phase vapor and/or film boiling. The same heat transfer correlations apply that would apply otherwise; the only major difference is the forced mapping of the heat transfer profile that keys on the calculation of CHF wall temperature from the Zuber CHF correlation.

The uncertainty and bias for the total post-CHF heat transfer includes data from THTF and FLECHT-SEASET simulations that modeled reflood heat transfer. This expanded range of applicability was presented previously in the discussion on film boiling.

S-RELAP5 Implementation of Transition Boiling

Correlation: Modified Chen

Formulation: See Section 4.6 of Reference 3.

Derived Range of Applicability: Chen reports the following parameter ranges for which the correlation was assessed:

- $61 \text{ psia} < \text{Pressure (P)} < 2830 \text{ psia}$
- $1.221 \times 10^4 \text{ lbm/hr-ft}^2 < G < 2.22 \times 10^6 \text{ lbm/hr-ft}^2$ ($0.143 \text{ kg/s-m}^2 < G < 26.0 \text{ kg/s-m}^2$, approx. 0-1.0 in/s reflood rate)
- $1.07 \times 10^4 \text{ Btu/hr-ft}^2 < \text{Heat Flux (q'')} < 5.236 \times 10^6 \text{ Btu/hr-ft}^2$ (approx. LHGR $< 13.5 \text{ kW/ft}$)

Validation/Assessment/Expanded Range of Applicability: In general, the application of the modified Chen correlation is within the range of applicability; however, system pressures will likely be lower than the 61 psia used in the derived range of applicability. In limiting RLBLOCA simulations (high clad temperatures), the PCT sensitivity to transition boiling is minimal. This is because the location of PCT in these limiting cases is well above the quench plane (see Figures 2.1 and 2.3). Once heat transfer moves into the transition boiling regime, the feedback from the cooler cladding temperature enhances heat transfer rapidly and within only a few seconds heat transfer moves into the nucleate boiling regime. Considering the distance between the quench location and the PCT location, heat transfer below the quench front has little direct influence on PCT.

Indirectly, the quench phenomenon does enhance liquid entrainment which may influence PCT. This implies that the timing of quench is more important than transition boiling heat transfer. For this reason, a T_{min} model defining the transition from film boiling to transition boiling is used in S-RELAP5. For RLBLOCA applications T_{min} []. This value was derived using FLECHT-SEASET test 31302 which was performed at a pressure of 40 psia, a peak power of 0.7 kW/ft and a flooding rate of ~ 75 kg/s-m². This is a very conservative value (see Reference 15). Examination of the integral test validation problems presented in Reference 15 (LOFT, CCTF, and Semiscale) provides evidence of this conclusion.

Table 2.6 provides a comparison of the simulation-space (taken from Table 2.3) and the range of applicability evaluated for the assessment-space for the Modified Chen transition boiling correlation. (Note: the assessment-space includes three components as previously described: the test conditions used in correlation development, relevant uncertainty analysis, and integral-effects validation.)

Time Period: Long Term Cooling (Quench – End of Simulation)

This period is characterized by single-phase liquid convection or nucleate boiling. Peak clad temperatures are not influence by this condition. Calculations are terminated after whole core quench.

S-RELAP5 Implementation of Nucleate Boiling Heat Transfer

Correlation: Chen

Formulation: See Section 4.3 of Reference 3.

Derived Range of Applicability: The Chen correlation is based on several datasets with a broad range of applicability. A discussion of the applicability range of the datasets is provided in Reference 19. The pressure range included in the derivation of the Chen correlation extends up to about 510 psia.

Validation/Assessment/Expanded Range of Applicability: Since nucleate boiling is not considered to have a significant influence on clad temperatures, no formal assessment has been performed. S-RELAP5 has been assessed for the few high pressure boil-off tests presented in Reference 15; however, the focus of these other tests is the more dominant film boiling phenomena.

Table 2.7 provides a comparison of the simulation-space (taken from Table 2.3) and the range of applicability evaluated for the assessment-space for the Chen nucleate boiling correlation. (Note: the assessment-space includes three components as previously described: the test

conditions used in correlation development, relevant uncertainty analysis, and integral-effects validation.)

Summary

A discussion has been presented on the mapping of heat transfer regimes to the chronology of the limiting LOCA calculation. It has been emphasized that post-CHF heat transfer has the dominant influence on clad temperatures. In addition, among the post-CHF heat transfer mechanisms, heat transfer to single phase vapor provides the primary heat sink for fuel rods. As has been presented, individual correlations have been programmed into S-RELAP5; however, during a LBLOCA calculation multiple correlations will be employed simultaneously to calculate a total heat transfer during post-CHF conditions. In addition, correlations for interfacial phenomena will also influence this calculation. For this reason it is the superposition of these individual correlations that becomes the post-CHF heat transfer correlation in S-RELAP5. The pedigree of this "correlation" must rely on the range of applicability of the individual correlations; the expanded range of applicability provided by the uncertainty analysis using the THTF and FLECHT-SEASET datasets and the RLBLOCA analysis methodology; and the "Evaluation of Bias" calculations used to validate the calculated uncertainty bias. Discussion on the details of this work has been provided in the methodology document (Reference 2), the S-RELAP5 Code Verification and Validation document (Reference 15), and this RAI response.

Table 2.8 presents a collective summary of the coverage of the assessment-space provided in the discussion of the heat transfer regimes (including data provided in Tables 2.4-2.7). This includes the derived range of applicability, the expanded range of applicability based on statistical treatment (the uncertainty analysis), and code-to-data comparisons. In general, the FLECHT-SEASET and THTF test-spaces, used to expand the range of applicability, encompass the original derived range of applicability. Nonetheless, between the range of applicability of the correlations and the uncertainty analysis, some holes still remain. To account for holes, a number of integral test simulations were performed and are presented in References 2 and 15. The integral tests, including LOFT, CCTF, and Semiscale, provide the largest coverage of the assessment-space; that is, they were performed at conditions typical for LBLOCA. The demonstration of good agreement among these validation cases sufficiently completes the assessment-space and the assessment-space provides sufficient coverage over the simulation-space.

For certain nuclear power plants, aggressive containment cooling mechanisms exist to rapidly lower containment pressure to atmospheric or subatmospheric conditions. No useful test data exists for this range, but no new phenomena are expected as a result of the lower pressure. The dominant LBLOCA phenomena strongly dependent on pressure, steam binding and downcomer boiling, will be enhanced by lower pressures. Nonetheless, the dynamics of these phenomena are dependent on steam and water properties; hence, the uncertainty associated with low pressure conditions is that associated with the water property tables applied. S-RELAP5 incorporates the 1967 ASME steam tables. Uncertainty is reported there to be within a very tight tolerance. In RLBLOCA analyses containment back pressure is conservatively derived by using a hypothetical worst single failure and by statistically ranging containment volume (see RAI #26).

Table 2.1 Final PIRT for PWR LBLOCA (Core Heat Transfer Only)

Core	DNB	7	-	-
	Post CHF	8	8	9
	Rewet	8	6	-
	Reflood HT plus Quench	-	-	9
	Nucleate Boiling	4	2	2

Table 2.2 Summary of Heat Transfer Regimes

Heat Transfer Regime	Correlations	Reference #
Single-phase liquid convection	Dittus-Boelter	4
Nucleate boiling	Chen	5
Critical Heat Flux, []	Modified Zuber	6
Critical Heat Flux, []	Biasi	7
Transition boiling	Modified Chen	8
Film boiling, []	Modified Bromley	9
Film boiling, []	Forslund-Rohsenow	10
Single-phase vapor convection	Sleicher-Rouse	11
Condensation	Carpenter and Colburn	12
Convection to noncondensable-water mixture	RELAP5/MOD2	13
Radiation	Sun (Stefan-Boltzman)	14

**Table 2.3 Identification of Heat Transfer Parameters During a
Limiting LBLOCA Simulation**



Table 2.4 Simulation- and Application-Space for CHF

Table 2.5 Simulation- and Application -Space for Film Boiling Heat Transfer

Table 2.6 Simulation- and Application -Space for Transition Boiling Heat Transfer

Table 2.7 Simulation- and Application-Space for Nucleate Boiling Heat Transfer (late reflood)

Table 2.8 Summary of Full Range of Applicability

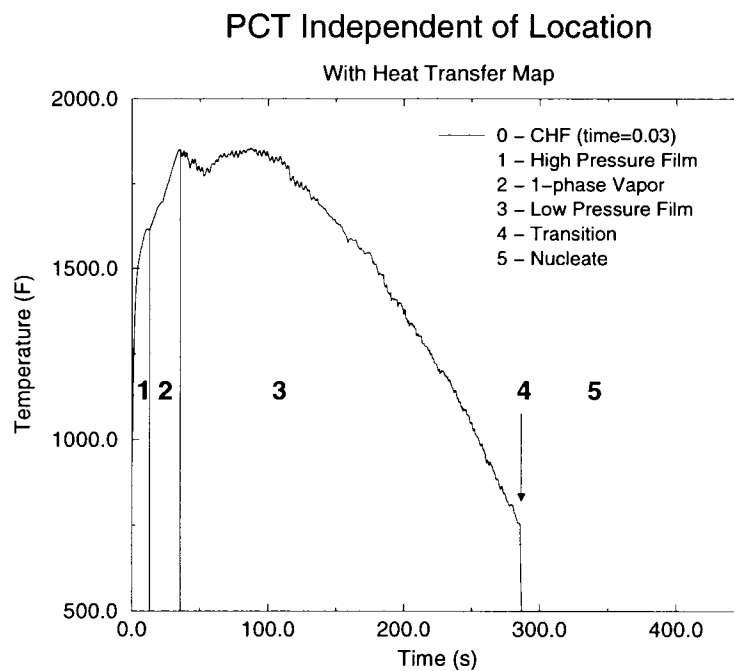
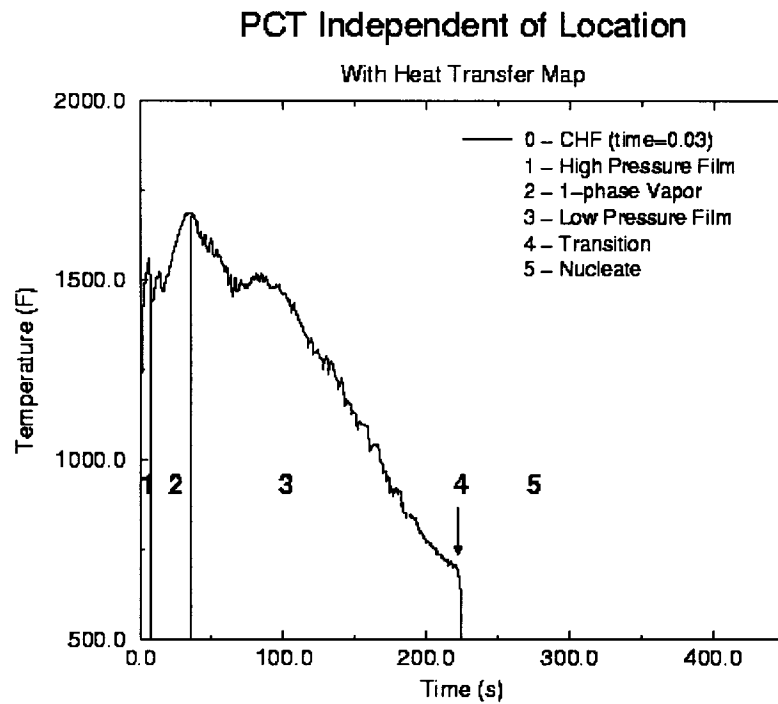


Figure 2.1 Heat Transfer Map for PCT Node Independent of Location for 3-Loop Sample Problem



**Figure 2.2 Corresponding Heat Transfer Coefficient at PCT Node (Node 33)
for 3-Loop Sample Problem**



**Figure 2.3 Heat Transfer Map for PCT Node Independent of Location
for 4-Loop Sample Problem**



**Figure 2.4 Corresponding Heat Transfer Coefficient Near PCT Node (Node 33)
for 4-Loop Sample Problem**

Figure 2.5 Comparison of Density of Pressure and Void Fraction for the LBLOCA Application (left) and the Test Data (right) in the Modified Bromley Region

Figure 2.6 Comparison of Density of Pressure and Void Fraction for the LBLOCA Application (left) and the Test Data (right) in the Forslund-Rohsenow Region

References

1. Technical Program Group, *Quantifying Reactor Safety Margins*, NUREG/CR-5249, EGG-2552, October 1989.
2. EMF-2103(P) Revision 0, *Realistic Large Break LOCA Methodology*, Framatome ANP Richland, Inc., August 2001.
3. EMF-2100(P) Revision 4, *S-RELAP5 Models and Correlations Code Manual*, May 2001.
4. F. W. Dittus and L. M. K. Boelter, "Heat Transfer in Automobile Radiators of the Tubular Type," *Publications in Engineering*, Volume 2, pp. 443-461, University of California, Berkeley, 1930.
5. J. C. Chen, "A Correlation for Boiling Heat Transfer to Saturated Fluids in Convective Flow," *Process Design and Development*, Volume 5, pp. 322-327, 1966.
6. N. Zuber, M. Tribus and J. W. Westwater, "Hydrodynamic Crisis in Pool Boiling of Saturated and Subcooled Liquid," *2nd International Heat Transfer Conference*, Denver, Colorado, 1961.
7. Biasi et. al., "Studies on Burnout Part 3 - A New Correlation for Round Ducts and Uniform Heating and Its Comparison with World Data," *Energia Nucleare*, Volume 14, pp. 530-536, 1967.
8. J. C. Chen, R. K. Sundaram, F. T. Ozkaynak, *A Phenomenological Correlation for Post-CHF Heat Transfer*, NUREG-0237, June 1977.
9. L. A. Bromley, "Heat Transfer in Stable Film Boiling," *Chemical Engineering Progress* Volume 46, pp. 221-227, 1950.
10. R. P. Forslund and W. M. Rohsenow, "Dispersed Flow Film Boiling," *Journal of Heat Transfer* Volume 90 (6), pp. 399-407, 1968.
11. C. A. Sleicher and M. W. Rouse, "A Convenient Correlation for Heat Transfer to Constant and Variable Property Fluids in Turbulent Pipe Flow," *International Journal of Heat and Mass Transfer*, Volume 18, pp. 677-683, 1975.
12. E. F. Carpenter and A. P. Colburn, "The Effect of Vapor Velocity on Condensation Inside Tubes," *Proceedings of General Discussion on Heat Transfer, Institute Mechanical Engineering/American Society of Mechanical Engineers*, pp. 20-26, 1951.
13. V. H. Ransom et al., *RELAP5/MOD2 Code Manual, Volume 1: Code Structure, Systems Models, and Solution Methods*, NUREG/CR-4312, EGG-2396, Revision 1, March 1987.
14. K. H. Sun, J. M. Gonzales-Santalo, and C. L. Tien, "Calculations of Combined Radiation and Convection Heat Transfer in Rod Bundles Under Emergency Cooling Conditions," *Journal of Heat Transfer*, pp. 414-420, 1976.
15. EMF-2102(P) Revision 0, *S-RELAP5 Code Verification and Validation Document*, August 2001.
16. "Analysis of the FLECHT-SEASET Unblocked Bundle Steam-Cooling and Boiloff Tests," EPRI NP-1460, May 1981.

17. Y. Y. Hsu and R. W. Graham, "Transport Processes in Boiling and Two-Phase Systems," Hemisphere Publishing Corporation, 1976.
18. T. A. Bjomard and P. Griffith, "PWR Blowdown Heat Transfer," Symposium on the Thermal and Hydraulic Aspects of Nuclear Reactor Safety, 1977 ASME Winter Annual Meeting, Atlanta, GA, Nov. 1977.
19. J. G. Collier, *Convective Boiling and Condensation*, 2nd edition, McGraw-Hill, New York, 1981.
20. P. Griffith, J. F. Pearson, and R. J. Lepkowski, "Critical Heat Flux During a Loss-of Coolant Accident," *Nuclear Safety* Volume 18, pp. 298-309, 1977.

Question 3: Subroutine CHFCAL has the ICHF options for either Biasi and Zuber (ICHF=0), or the Extended Biasi (ICHF=1). EMF-CC-097(P), Rev. 7, page 7-2 also mentions the option for the Extended Biasi and choosing this will use the correlation for all flow conditions. However, EMF-2100(P), Section 4.4 does not mention the "Extended" Biasi, but the Biasi and Zuber correlations. There is also a note that the Biasi correlation is not used for $G < 100 \text{ kg/m}^2\text{s}$. Is this Biasi correlation the "Extended Biasi"?

Response 3: The Extended Biasi (ICHF=1) is only used in the steam line break methodology for the steam generator secondary side to provide a conservative heat transfer treatment. The option is not applied to RLBLOCA, SBLOCA, and other Chapter 15 non-LOCA methodologies. It is an oversight that a description of the Extended Biasi is not included in EMF-2100. The Extended Biasi option uses only the Biasi correlation for CHF calculations under all flow conditions. With the Extended Biasi, the mass flux, G , in the Biasi correlation is set to [].

Question 4: Subroutine CHFCAL appears to contain the Modified Zuber CHF correlation beginning at 300. Line 300 and its uncommented continuation, and Equation 4.32 of EMF-2100(P) appear to match up if MHTCHF is equal to F . However it does not appear that was the intention given the code which follows.

Question 4a: What are MHTCHF and XBIASI and where do they come from?

Response 4a: MHTCHF and XBIASI are RLBLOCA uncertainty analysis multipliers for the modified Zuber and the Biasi CHF correlation, respectively. The default value for all multipliers is 1.0. The multipliers are for RLBLOCA sensitivity studies and statistical analyses. The input formats for the multipliers are described in Section 2.9 (Page 2-4) of EMF-CC-097(P), Rev.7.

Question 4b: The second option for F in Equation 4.33 of EMF-2100(P) is similar but different than the first uncommented line after what appears to be the modified Zuber CHF correlation. Please clarify the differences and the apparent absence of the first option for F (commented out on the second continuation line after 300?).

Response 4b: [

1

Question 4c: *The 3 lines of coding before the last END IF of subroutine CHFCAL appear similar but different than the linear interpolation for mass flux between 100 and 200 kg/m²s of Equation 4.34 of EMF-2100. Please explain the apparent differences between the coding and the code manual documentation.*

Response 4c: The interpolation scheme was modified in the S-RELAP5 code version for the proposed RLBLOCA methodology. It is an oversight that the change did not get in EMF-2100. The interpolation scheme is for smoothing the transition between two correlations. The new scheme places more weight on the modified Zuber correlation in computing the CHF in the transition region.

Question 4d: *Parameter HTHDMO(LS) appears to be in units of meters given the logic question: IF (HTHDMO(LS) .LT. 0.01DO) THEN in the Biasi correlation coding. However, the next line multiplies HTHDMO(LS) by 100 possibly to convert to meters from centimeters before raising it to the "n" power (either 0.4 or 0.6 based on the conditions on page 4-12 of EMF-2100(P)). The documentation states that the hydraulic diameter is in units of cm and is not multiplied by 100 in either Equation 4.28 or 4.29. Please clarify.*

Response 4d: As stated on page 4-12 of EMF-2100(P), the hydraulic diameter in Equations (4.28) and (4.29) is in units of centimeters (cm). The equations have not been changed to be in the Standard SI units generally used by S-RELAP5. The variable HTHDMO, which holds the value of hydraulic diameter, is in units of meters (m). In the expression IF (HTHDMO(LS) .LT. 0.01DO) THEN, 1 cm is converted to 0.01 m to be compared with HTHDMO. In computing the CHF, HTHDMO is multiplied by 100 to be in units of cm, for use by the equations for the Biasi correlation.

Question 4e: *Is the mass flux parameter "G" brought into the CHF calculation in units of gm/cm²s, or kg/m²s?*

Response 4e: The mass flux G, is in kg/m²s.

Question 4f: *Clarify why MAXimums and MINimums are taken throughout the subroutine CHFCAL. How does this affect the uncertainty of the CHF value? For example, if ICHF=1 and G=20 kg/m²s, G is changed to 100 kg/m²s since the Biasi correlation is not used for G<100 kg/m²s. However, Biasi is used when the ICHF overrides that applicability where the Zuber correlation should be used. This also occurs if G is 120 kg/m²s and ICHF=1. It does not appear*

that the interpolation on the mass flux with the Biasi and Zuber correlations will not be implemented as described in the documentation. Is this Biasi correlation the Extended Biasi? Where did the parameter XBIASI come from?

Response 4f: The MAX and MIN are generic FORTRAN Intrinsics. They are used in S-RELAP5 in two ways: (1) to set physical limits and (2) to combine IF-THEN statements, as demonstrated in the Question 4b responses. The multipliers for the uncertainty analysis are applied after the MAX and MIN functions are applied; therefore, their effects are taken into account implicitly. As described in the response to Question 3, the option ICHF=1, which is called the Extended Biasi, is not used in the proposed RLBLOCA methodology. The interpolation scheme is described in the response to Question 4c and XBIASI is discussed in the response to Question 4a.

Question 5: *In the Sleicher and Rouse heat transfer correlation, please clarify how the coded parameter XTF in subroutine DITTSG matches the documentation of Equation (4.36) in EMF-2100, P. 4-15.*

Response 5: XTF corresponds to the factor:

$$\left(\frac{\log_{10} X}{\log_{10} 10} \right)^{1/4}$$

The coding uses conversion from common logarithm (\log_{10}) to natural logarithm (\ln):

$$\log_{10} X^{1/4} = 0.25 \frac{\ln X}{\ln 10} = \frac{0.25}{\ln 10} \ln X = 0.1085736 \ln X$$

LOG is the FORTRAN generic function for \ln .

Question 6: *Account for the VOIDG term which appears in the coding for the natural convection term but does not appear in the documentation.*

Response 6: The text below Equation (4.44) will be modified as follows: "The heat transfer coefficient, h_{cg} , is given in Equation (4.35) with the natural convection heat transfer coefficient of Equation (4.37) multiplied by a void fraction factor to approximately account for the effective vapor area."

Question 7: *Please clarify what is meant by, "The equation is independent of the characteristic length due to the 1/3 power dependency of the Grashof number given in Equation (4.35)." Equation (4.35) gives the heat transfer coefficient as the MAX of the Sleicher Rouse and the natural convection heat transfer coefficients with no mention of the Grashof number. (Pages 4-14,15 of EMF-2100(P), Rev. 4)*

Response 7: The reference to Equation (4.35) is incorrect. The reference should be to Equation (4.37). Equation (4.37) is equal to Equation (4.7) with the definition of Grashof number, Equation (4.5), inserted into the equation and with the subscript f (for liquid phase) changed to g (for vapor phase). The Grashof number contains a factor D_h^3 and $(D_h^3)^{1/3} / D_h = 1$.

Question 8: *The documentation on Page 4-15 of EMF-2100(P), Rev. 4 includes the addition of radiation heat transfer from the wall to the single phase vapor fluid if the surface temperature is greater than 650K. Identify where this is accounted for in the code.*

Response 8: [

]
[

]

The coding is for heat transfer coefficient and is Equation (4.59) of EMF 2100(P) divided by $(T_w - T_g)$.

Question 9: *It appears that a modified Dittus-Boelter correlation or the Sleicher and Rouse correlation is chosen based on the IF statement:*

IF (IAND(IDNGAP(2,IH),256) .NE. 0) THEN.....modified (?) Dittus-Boelter else Sleicher Rouse.

Question 9a: *Please clarify why in the documentation of Page 4-14 of EMF-2100(P) the Sleicher Rouse correlation is said to be selected because it has a smaller uncertainty than the Dittus-Boelter correlation, but in the code, the IF statement results in a choice between the two. Please clarify the meaning of the IF statement.*

Question 9b: *The Dittus-Boelter heat transfer correlation coded in the DITTSG subroutine does not appear to be the same as that documented in Equation (4.16) of EMF-2100(P). Please clarify the differences.*

Response 9, 9a, and 9b: The Dittus-Boelter correlation was used in the past for the approved methodologies using ANF-RELAP (RELAP5/MOD2 with limited improvements) and is no longer used in any approved or proposed methodology based on S-RELAP5. The coding was used to assess the effects of changing the correlation in the transition from the ANF-RELAP-based methodologies to the S-RELAP5-based methodologies. The integer 256 ($=2^8=2^{9-1}$) corresponds to the binary number 100000000. The "1" in the 9th digit can only be set by the user, as described in Section 7.2.6 of EMF-CC-097(P) Revision 7, to purposely select the Dittus-Boelter correlation. Section 7.2.6 of EMF-CC-097(P) clearly states that the input card should be used for code verification purposes only. At the present, there is no use for the vapor phase Dittus-Boelter correlation. Ideally, it should have been removed, but in practice, there always are some leftovers of previously used coding. This can have an advantage of easy restoration of old models in the future if necessary.

The Dittus-Boelter correlation used in the DITTSG subroutine is in the same form as Equation (4.16) of EMF-2100(P) with liquid properties changed to vapor properties. The difference is in the (forced) laminar flow Nusselt number, which is not part of the Dittus-Boelter (forced) turbulent convection correlation. The laminar flow Nusselt number is 7.86 for liquid and 4.36 for vapor.

Question 10: *The 'nature' convection correlation coding of subroutine DITTUS includes: $HTCOEF = MAX(HMAC, 0.59DO*(PRGR)**0.25DO*PRGR*COHDM/TERM)$ which occurs if PRGR is less than the Reynolds number squared. Please identify the discussion of this in the documentation of EMF-2100, or include it as needed.*

Response 10: "Nature" is a typo in a FORTRAN comment statement. The coding is not discussed in EMF-2100(P) but in an ANF-RELAP SDR (Software Development Record). It was added in an attempt to smooth the transition between the forced convection correlation and the natural convection correlation. Because of the use of MAX function, its effect is minimal. Discussion of the coding will be added to EMF-2100(P).

Question 11: *Is the modified Bromley from the documentation (EMF-2100, Rev.4, P.4-18) the same as the Bromley correlation of the FILMBL subroutine?*

Response 11: Yes. The constant CB in the coding represents



and is given a data value of 0.92163 in the code.

Question 12: *Please describe how the interpolation of the last line of FILMBL is the same as Equation 4.50 of EMF-2100(P), Rev.4, P 4-19.*

Response 12: The coding for Equation (4.50) along with Equation (4.51) of EMF-2100(P), Rev. 4 is





Question 13: Please include \leq or \geq in the documentation description above Equation 4.50 of EMF-2100(P), Rev.4, P 4-19 to describe use of the Forslund-Rohsenow and modified Bromley correlations if that was the intent as coded.

Response 13: To be precise, \leq or \geq should be used for one of the two branches of $<$ and $>$ in order to have complete consistency with the coding. However, other than to avoid dividing by zero, the coding can go either way, depending on personal preference. Numerically, exact equality hardly occurs unless due to an assignment statement; therefore, it really does not matter in which branch the equality is placed.

Question 14: Please explain why in the code the BROMLEY correlation is calculated for a void fraction less than or equal to [], and the FORSLUND-ROHSENOW is calculated for a void fraction greater than or equal to [] as documented in EMF-2100(P), Rev.4, Page 4-19. The void fractions appear consistent with the documentation beginning at line 208.

Response 14: The heat transfer coefficient values from the two correlations are quite different in magnitude. It is necessary to have a transition region to bridge the two correlations. It is also necessary that the two correlations be calculated at the boundaries of the transition region to facilitate the interpolation; otherwise, there will be no heat transfer coefficient values at void fractions between []. As the void fraction is selected as an interpolation parameter, the transition boundaries are defined at the void fraction of []. Only the FORSLUND-ROHSENOW correlation is explicitly dependent on the void fraction and the void fraction is set at [] in the transition region calculation.

Question 15: What does CFR, the first term in HDF, account for in the Forslund-Rohsenow correlation?

Response 15: []

and assigned a value of 0.4515 in the code.

Question 16: In the "NATURE" convection correlation, H_{MAC} is defined if (PRGR.LT.TERM) as the [

], which appeared similarly in subroutine DITTUS, which the staff hasn't yet found described in the documentation.

Response 16: See responses provided for the DITTUS question (Question 9) and the next question. The Nusselt number of 7.86 is for the forced laminar flow.

Question 17: *Please include discussion of the scaling of the natural convection heat transfer correlations by the void fraction in the PREDNB subroutine by COHDMF=COHDM* VOIDF.*

Response 17: Natural (or free) convection heat transfer comes from the motion of fluid due to density changes caused by the heating process under gravity force (or body force) conditions. Natural convection heat transfer is negligible in comparison with other heat transfer processes, except for the laminar (forced) flow convection. The coding of natural convection is copied from Subroutine DITTUS to Subroutine PREDNB to provide continuity in the bordering region for numerical reasons rather than for physical reality. It is trivial to use liquid fraction and void fraction to weight the contribution from liquid and from vapor under two-phase conditions. The natural convection heat transfer is not treated as additive, but as a "floor value," i.e., the lowest possible value; therefore, its accuracy is not greatly important and a crude approximation to extend it to two-phase is acceptable. In any case, the natural convection heat transfer for liquid is negligibly small compared with the nucleate boiling heat transfer, it does not matter what form of natural convection is used to supply a reasonable "floor value." Additional discussion of natural convection will be added to the code manual EMF-2100(P).

Question 18: *Please explain why the suppression factor is coded to be 0.0797 if the $Re_{TP} \geq 70$ instead of 0.1 as documented in Equation 4.21 of EMF-2100(P).*

Response 18: The upper limit of Re_{TP} (i.e., maximum value) is 70. Substituting 70 for Re_{TP} in

$$\left[1 + 0.42 Re_{TP}^{0.78}\right]^{-1}$$

yields 0.0797. The coding is correct. The value in the document (EMF-2100(P)) is a rounded-off number.

Question 19: *What is the ICHF=2 option, and where is that described?*

Response 19: ICHF=2 is for the Framatome ANP XNB correlation, which was installed and removed. The statement

IF (ICHF.EQ.2) GO TO 314

was a leftover. It should have been removed along with the XNB correlation coding, but it is harmless, since the model for ICHF = 2 is no longer in existence. To avoid confusion, the statement will be deleted in a future code revision.

Question 20: *Many of the test programs used in the assessment of S-RELAP5 inherently incorporated radiation heat transfer between hot rods and colder components. Please discuss and justify exclusion of a specific radiation heat transfer model in the Framatome-ANP RLBLOCA methodology. Include in the discussion the manner in which the methodology accounts for radiation heat transfer during those portions of the analyzed event for which radiation heat transfer would be expected to play a significant role. Also discuss and justify known compensating errors introduced in the methodology that account for this effect.*

Response 20: The exclusion of rod-to-rod and rod-to-wall radiation heat transfer was a decision that came out of the Framatome ANP PIRT-development team. When ranked in importance to other core heat transfer phenomena, radiation heat transfer was judged to be negligible for all phases of the PWR LBLOCA problem. For that reason it was not included in the methodology PIRT. S-RELAP5 does consider rod-to-fluid radiation heat transfer. This is the largest component of radiation heat transfer occurring in the core since the temperature differences are the largest. Since no effort was made to separate the influence of radiation heat transfer in filtering test data, radiation heat transfer is implicitly treated in the uncertainty analysis for film boiling heat transfer. The development of any post-CHF heat transfer correlation will contain a degree of compensating error because it is difficult, if not impossible, to separate the influences such as fluid state, two-phase flow regime and interfacial drag. Nonetheless, for statistically treated parameters the issue of compensating error is considerably less important because the model error is captured in the application of the statistics in the final analysis.

In addition, the following three points should be made:

Point 1: There are many factors that cause variation in the observed temperatures and heat transfer coefficients in reflood tests. Consider the variation in temperature at the midplane of FSS-31504. For test 31504, the temperature profiles for several rods at elevation 72 inches are shown in Figure 20.2. Prior to the adiabatic heatup, the radial temperature distribution already has a variation of 10 K (-80 sec). The temperatures at this time are sufficiently small that the radiation heat flux may be assumed to be negligible. The heat transfer due to convection is also very small because the flow rate is nominally zero (steam pre-heat has been terminated and reflood has not been initiated). The test is initiated with an adiabatic heatup that begins at approximately -85 seconds and ends at 0 seconds. Notice that at the end of this adiabatic heatup, a period when convective heat transfer rates should be very small, there is considerable variation in the radial temperature distribution, with the maximum difference on the order of 43 K. This difference is caused by several factors, including

- Variations in rod to rod electrical resistivity causing slightly different power and therefore different deposited energies (~0.5%).
- Boron nitride rod to rod property variations in thermal conductivity (10% uncertainty), density (3% uncertainty), and specific heat (5% uncertainty).
- Variation in SS-347 properties of density (1% uncertainty), thermal conductivity (3% uncertainty), and specific heat (3% uncertainty).
- Uncertainty in the temperature measurement (~ ±5 K uncertainty).
- Effects of rod to rod radiative heat transfer (effects reduced by not considering rods in outer two rows, see Figure 1).

Each of these items contributes to the variation in measured heat transfer coefficients and to the uncertainty that is applied. At the time the temperature is near the peak in each rod at the midplane (77 seconds), the maximum observed temperature is 1388 K and the minimum is 1305 K, a difference of 83 K. In addition to the above causes for variation in temperature, the following factors contribute to variation after the onset of reflood:

- Subchannel to subchannel variation in the steam flow rate

- Variations in the void fraction caused by subchannel variations
- Variations in droplet size and velocity
- Variations in local pressure
- Oscillations in the local flow rate
- Variations caused by non-uniform spacer interactions with droplets and with steam flow
- Variations caused by minor rod bow, causing asymmetries between adjacent subchannels
- Inaccuracies caused by rod thermal expansion
- Quenching effects on the rod power through changes in resistivity that cause a redistribution of the rod power

The conclusion is that rod to rod radiative heat transfer is but one of many different factors that affect the PCT observed in reflood tests.

Point 2: The code's package of equations and relations that compute the film boiling regime multiplier in dispersed flow produce a total effective film boiling heat transfer coefficient – one that includes the effects of conduction, convection, and radiation. The total effective heat transfer model is adjusted, through the development of the multiplier, to provide a reasonable estimate of the total effective heat transfer for the FLECHT-SEASET and THTF experiments. The adjusted model implemented in S-RELAP5 is then benchmarked and validated against the measured data and provides a very good estimate of the total effective heat transfer coefficient. The quality of that estimate is defined by the uncertainty obtained from the fit to the FLECHT-SEASET and THTF data.

The measured data used to qualify the model includes all of the mechanisms of heat transfer – radiation, convection, and conduction, between the participating components. Each data point or thermocouple measurement represents the thermal state of a specific rod, at a specific elevation, and at a specific azimuthal location. For a rod that is adjacent to a thimble, some of the thermocouples will have a view factor relative to the cooler thimble and the remaining thermocouples will see only heated rods. Thus, the adjusted model has been developed using data which has differing rates of rod to rod radiation heat transfer between hot and cold surfaces.

In conclusion, the multiplier adjusts the S-RELAP5 total effective heat transfer model to agree with the FLECHT-SEASET and THTF data, and the calculated uncertainty accounts for the degree of fit of the adjusted model to the data. In the actual plant analysis, the uncertainty is applied and will account for the observed variation between the adjusted model with the multiplier and the measured data. The rod to rod radiation is implicitly accounted for.

Point 3: The adjusted S-RELAP5 film boiling heat transfer model is appropriate and correct. The need for the multiplier and the consequent improvement in the prediction of temperatures is illustrated clearly in Figure 20.3 and Figure 20.4. These figures present the PCT by axial elevation for the two hottest CCTF tests assessed with S-RELAP5. Note that this data was not used in the development of the film boiling heat transfer multiplier and provides an

independent check of the multiplier. The temperature is clearly over-predicted when the multiplier is set to the nominal value of 1.0, indicating that the total film boiling heat transfer model needs to be adjusted. When the multiplier is set to 1.75, as determined from the FLECHT-SEASET and THTF tests, the agreement between the measured temperature and the calculated temperature is significantly improved, with the S-RELAP5 model still remaining slightly conservative.

It is also important to note that in this test there are significant differences in powers between assemblies and thus rod to rod radiative heat exchange. Yet the model implemented in S-RELAP5, and adjusted to appropriate data, provides a good estimate of the heat transfer coefficient, and therefore a good estimate of the peak clad temperature.

Conclusion: The film boiling heat transfer coefficient multiplier and uncertainty were determined from the FLECHT-SEASET and THTF data sets. The adjusted S-RELAP5 film boiling heat transfer model has been demonstrated to be correct and applicable for predicting RLBLOCA film boiling heat transfer by validation against the independent CCTF data set. Since the measured data includes all heat transfer components, including rod to rod radiation, the model validation addresses this effect.

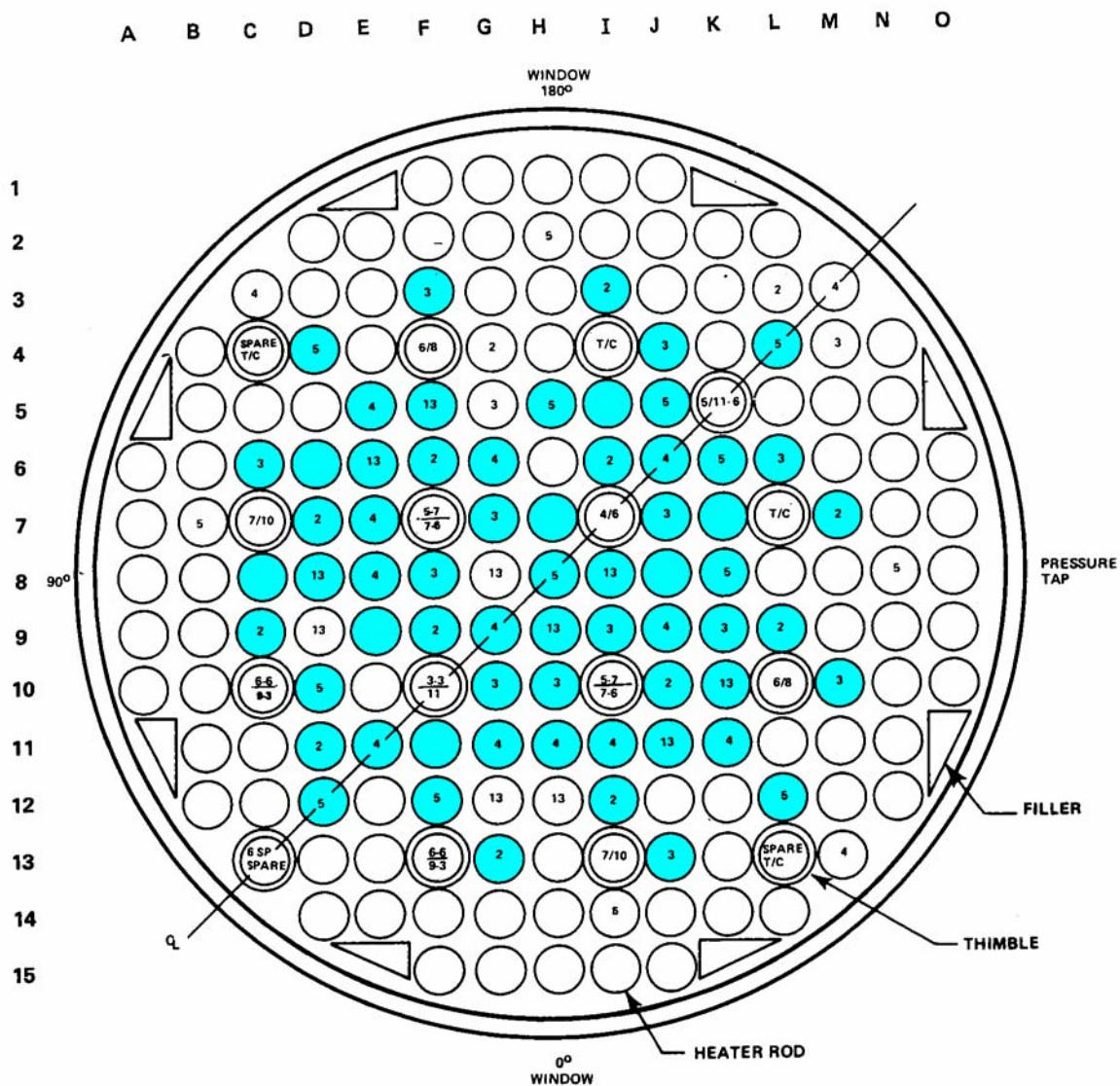


Figure 20.1 FLECHT-SEASET Rods Used for Film Boiling Multipliers

FSS-31504

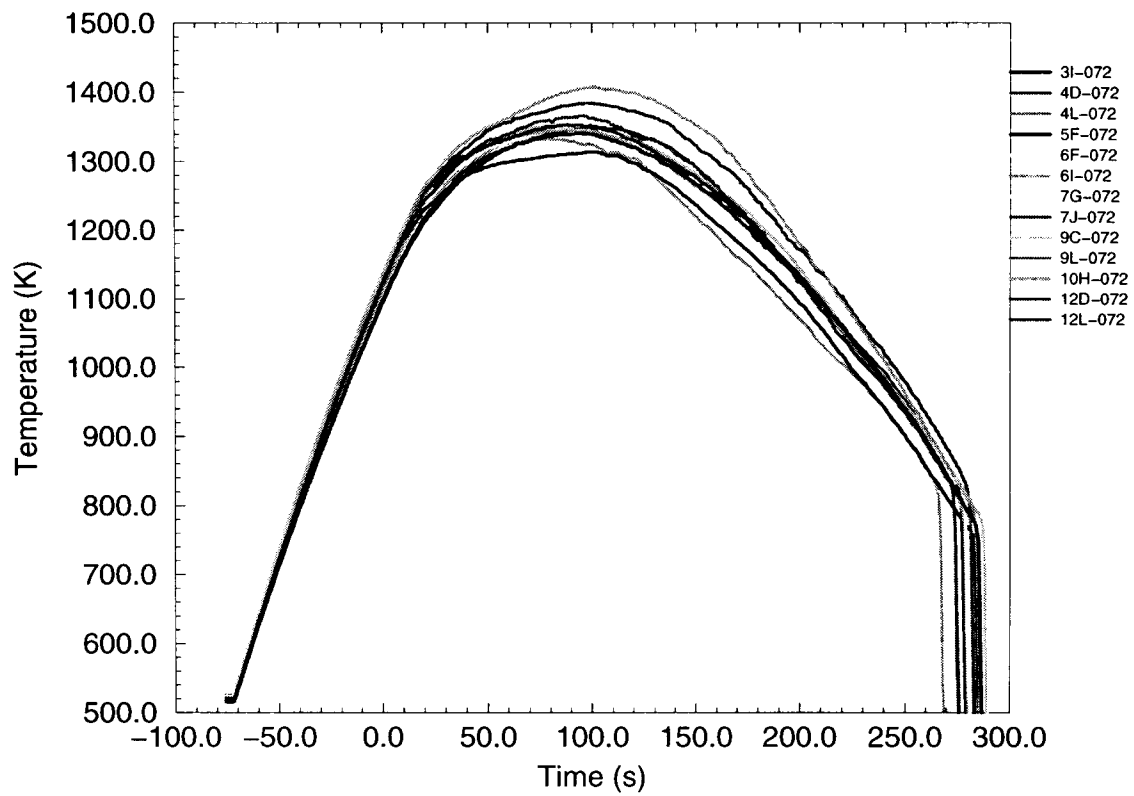


Figure 20.2 Temperature Distribution at 72 in Plane (FSS-31504)

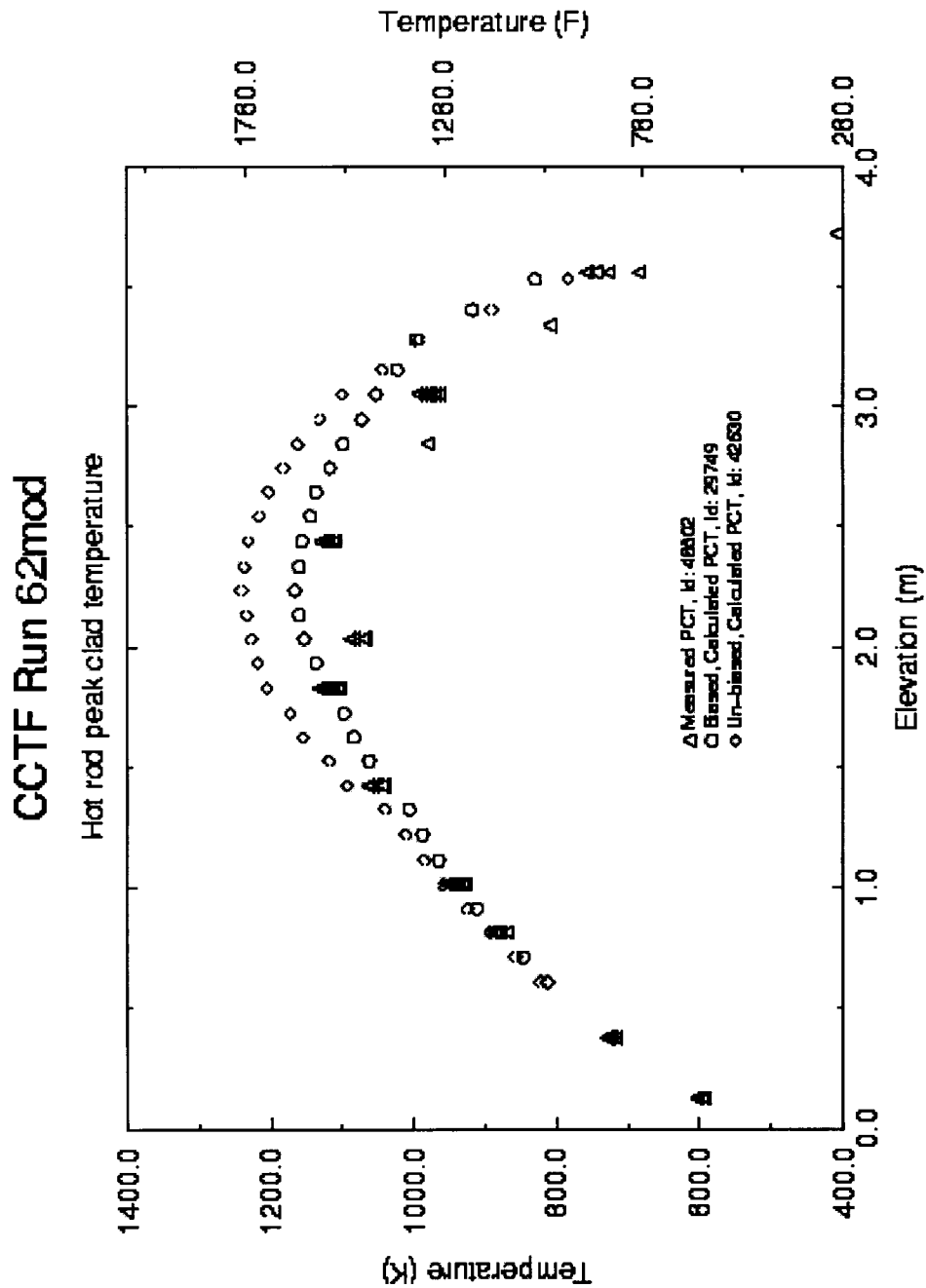


Figure 20.3 PCT by Axial Location (CCTF-62)

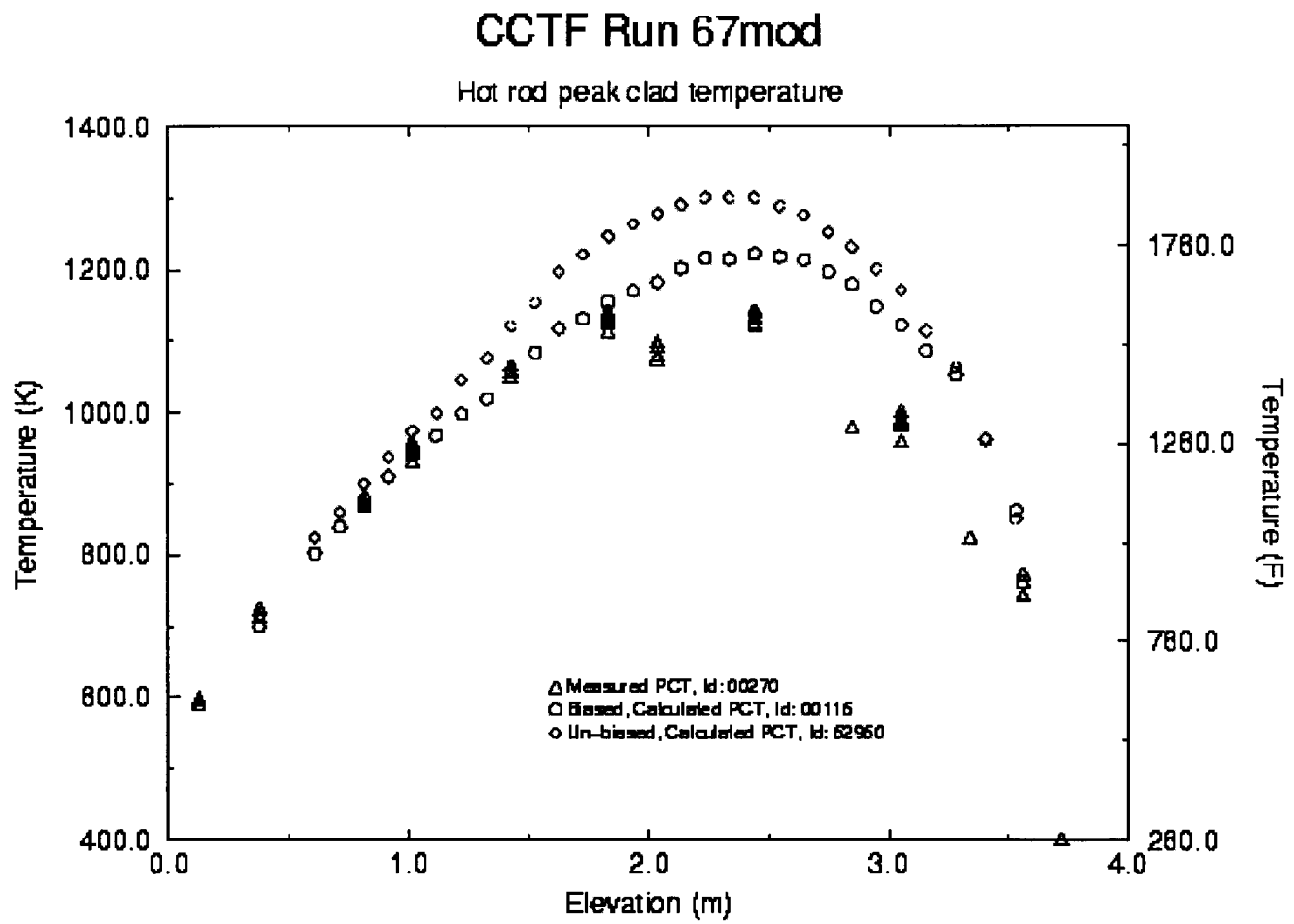


Figure 20.4 PCT by Axial Location (CCTF Test 67)

Question 21: Please explain and justify the basis for choosing the Forslund-Rohsenow correlation for void fractions [] and the Bromley at [] for dispersed flow film boiling. Since the Bromley correlation can result in high heat transfer coefficients during dispersed flow, extrapolating the Bromley correlation between [] can result in applying extrapolated HTC's over large regions of the bundle. Please justify this extrapolation range and show that it does not influence the heat transfer coefficient at or near the PCT location.

Question 22: The Forslund Rohsenow correlation for dispersed flow film boiling consists of a droplet wall contact model developed for low quality, high mass flux conditions in a small diameter tube. The model is applicable only to a small localized region just above the quench front, where the wall temperatures are below the rewet temperature. Physically, the droplet wall contact begins at the inverted annular regime and increases through to the agitated inverted annular regime where the effect is at a maximum due to either high turbulence or some possible droplet wall contact. Downstream of the agitated region, this droplet wall contact affect decreases rapidly and becomes non-existent once the highly dispersed flow region develops. The computed heat transfer multiplier of [] indicates that the correlation may not present a true best-estimate representation. Since the Forslund –Rohsenow correlation is highly dependent on void fraction, over-estimation of the entrainment can propagate large errors into the heat transfer during reflood.

Response 21 and 22: In S-RELAP5, the film boiling heat transfer is modeled as described in EMF-2100, Sections 4.6-4.9. No single correlation has been developed to effectively cover the range of boiling conditions in this heat transfer regime. Instead, Framatome ANP has chosen a suite of correlations developed from various investigations over a broad range of fluid conditions (see response to RAI #2). In calculating film boiling heat transfer, the individual contributors of heat transfer (liquid and vapor convection, radiation to liquid) are calculated independently and summed for the total heat transfer. Liquid convection is described by either the Bromley or Forslund-Rohsenow correlation, vapor convection is described by the Sleicher-Rouse correlation and radiation is described by the Stefan-Boltzman equation. Collectively, these correlations represent the S-RELAP5 model for total heat transfer under film boiling conditions. The choice of these correlations is based on Framatome ANP experience and the recognition of merit given by the thermal-hydraulics community for these correlations.

In the development of the RLBLOCA methodology, uncertainties have been determined for various correlations based on their planned range of applicability. That is, in the development of the assessment matrix various experimental assessments were selected to cover the range of a LBLOCA (LBLOCA-space). These assessments were then used to determine the uncertainty for specific code correlations over the range covered by the assessments (Test space). Thus, in effect extending the range of applicability of those correlations to the assessment range. For the Forslund-Rohsenow correlation this is discussed in some detail in the response to RAI #2 above.

Since post-CHF heat transfer has been determined to have a strong influence on PCTs, the CSAU approach requires that this phenomena be treated statistically. The FILMBL and FRHTC uncertainty are actually determined for the total heat transfer, rather than just for the liquid convection term. This is necessary since any procedure to separate the effects of the other heat transfer mechanisms in the test data inherits an additional measure of uncertainty, thus, negating the value of this task. The uncertainty has been calculated as described in the

methodology report and the uncertainty is applied in a Monte-Carlo sense in the RLBLOCA analysis. Given that the total heat transfer is treated statistically, the emphasis on having perfect models becomes less important. The penalty of not having a perfect model is measured by the uncertainty derived and applied.

The best validation of the heat transfer correlation is presented in EMF-2102. Figures 5.27 and 5.28 present the cumulative probability distribution function applied in the RLBLOCA application. When a parameter is treated statistically, the derived probability distribution function becomes part of the correlation. In comparing the probability distribution function over the void fraction range treated by Bromley and Forslund-Rohsenow to the data, it is obvious that the chosen distributions bound the data. For the void fraction range not explicitly covered by either Bromley or Forslund-Rohsenow, the probability distribution function used is weighted by a smoothing function dependent only on void fraction. Because of the variation in void fraction, this void range has a large uncertainty band. Figure 21.1 below shows how the FLECHT-SEASET and THTF data fall between the two probability density functions. As seen from the figure the data falls between the two functions as would be expected.



Figure 21.1 Cumulative PDF for Interpolated Region

With respect to the applicability of the Forslund-Rohsenow correlation for predicting wall-to-fluid heat transfer for dispersed flow film boiling at void fractions greater than [

], Framatome ANP does not agree that the Forslund-Rohsenow correlation, as presented in their original paper, is applicable as only a droplet wall contact model and, thus, only applicable to a small localized region above the quench front. The description of the Forslund-Rohsenow heat transfer model is provided in the S-RELAP5 Models and Correlations document and by the authors in their paper entitled "Dispersed Flow Film Boiling," presented in the Journal of Heat Transfer, November 1968.

Like the Bromley expression, the form of this heat transfer expression has been derived from a force balance on "droplet on a [sic] hot surface in a gravity field;" however, this does not imply a droplet wall contact model typically associated with two-phase turbulence modeling. There is nothing unique in the derivation of this correlation that binds it to any more restrictive wall or fluid condition. The authors reference an earlier publication entitled "A Generalized Correlation of Vaporization Times of Drops in Film Boiling on a Flat Plate" (Reference 1) as providing this basic component. From this formulation, Forslund and Rohsenow translate the flat plate assumption

to be applicable for tubes, thus providing the final form. The expressions dependency on vapor quality is translated to void fraction by assuming no slip. This is the form referenced in S-RELAP5. Before the correlation is finally applied, two parameters must first be determined: the correction factor K and the mean droplet diameter.

As with the correlation presented by Forslund-Rohsenow, S-RELAP5 has set $K = 0.2$. This value was experimentally derived from tests using nitrogen. As is stated in the S-RELAP5 Models and Correlations document (Section 4.7), other investigators have evaluated this constant to be anywhere between 0.2 and 2.0 for various fluids. The mean droplet diameter calculation in S-RELAP5 is evaluated somewhat differently than by Forslund-Rohsenow as necessitated by the calculational environment; however, both methods are constrained to the calculation of the critical Weber number. The Forslund-Rohsenow calculation of the mean droplet diameter is solved simultaneously with the drift-flux; while S-RELAP5 calculates it explicitly since the momentum equations with interfacial drag are solved directly in the finite difference formulation.

In addition, too much credit has been given to the role of the Forslund-Rohsenow correlation in the Framatome RLBLOCA methodology. As indicated in EMF-2100 a number of other models are provided in S-RELAP5 to account for various important phenomena. Specifically,

Phenomena	S-RELAP5 Models and Correlation Reference
Interfacial heat transfer	Section 3.4.7 (Inverted Slug/Inverted Annular Flow)
Turbulence in center core due to drop flow	No credit taken
Radiation heat transfer between vapor and droplets	Negligible to convection
Evaporation of droplets	Section 2.1 and 3.4.7 (Mass transfer is an explicit function of interfacial heat transfer)
Droplet breakup (non impact)	Section 3.2.1
Droplet breakup (spacer effect)	No credit taken
Rod-to-rod radiation	Negligible to convection
Interfacial drag	Section 3.2.1

As previously stated above, the primary contributors of film boiling heat transfer (liquid and vapor convection, radiation to liquid) are:

Phenomena	S-RELAP5 Models and Correlation Reference
Liquid convection (Bromley, Forslund-Rohsenow)	Section 4.7
Single-phase vapor convection (Sleicher-Rouse)	Section 4.5
Wall-to-fluid radiation	Section 4.8

Physically, fuel clad heat transfer is explicitly and simultaneously dependent on these three primary mechanisms. Collectively, they form the total heat transfer correlation in S-RELAP5. The form of the correlation is given as

$$q'' = q''_r + q''_g + q''_{\text{rad}}$$

Framatome ANP recognizes that uncertainty could be attributed to each primary heat transfer mechanism as well as the seven implicit contributors to heat transfer previously highlighted. In addition, that this uncertainty is dependent on the assumptions associated with each correlation applied (e.g., 1-D, average properties). Nonetheless, what is relevant to cladding temperature is the total heat transfer. This is a variable that can be measured with good-to-excellent fidelity. Conversely, the separation of the total heat transfer into these components is extremely difficult, requires numerous assumptions, and, in general, has not been done in the complex test programs used to support nuclear safety research. Thus, the database to support the development of the individual uncertainties across the range of a LBLOCA is unavailable.

Therefore, the most straight forward approach is to use test data such as that provided by FLECHT-SEASET and THTF (i.e., supporting the expected parameter-space of a LBLOCA) for the derivation of heat transfer uncertainties. In addition, it is also correct to validate these uncertainties against independent test data equally supporting the parameter-space of a LBLOCA as presented in Section 4.3.4, "Evaluation of Code Bias," in the RLBLOCA methodology document, EMF-2103. These calculations using the LOFT, CCTF, and Semi-Scale test series show that the biases, including the heat transfer bias, brings the estimation of clad temperatures in line with the test measurements.

By ensuring (1) that the experimental data base used to develop correlation statistics provides adequate coverage over its expected range of application, and (2) that the correlation uncertainty is supported by comparison with data not used in its generation, than in the statistical framework in which this correlation is applied, the uncertainties have been demonstrated to be acceptable.

The above discussion addresses the majority of the points given in this RAI. With the exception of droplet diameters, the range of applicability and the corresponding LBLOCA parameter space was provided in the response to RAI #2. Droplet diameters are constrained in the code to be between [] m. A plot of droplet diameters for the 4-loop sample problem has been provided in the response to RAI #123. Figure 4.208 in the RLBLOCA methodology document provides a scatter plot of single-phase vapor heat transfer coefficients from the Sleicher-Rouse correlation as a function of Reynolds number from the data originally used to develop the correlation.

The heat transfer coefficients as a function of void fraction at the PCT node and the two nodes immediately upstream are provided in Figures 21.1 and 21.2. Note the film boiling HTC approaches zero as void approaches 1.0. This is due to Forslund-Rohsenow being dependent on void fraction. As void decreases, Forslund-Rohsenow increases slightly until the transition to modified Bromley which starts at a void fraction of []. The transition is shallow until a void fraction of [], then increases rapidly to the modified Bromley at a void fraction of []. The scattering of total and film boiling HTCs occurring below a void fraction of [] is from transition boiling during the quenching process. Overall, these plots show that the heat transfer to the liquid is minimal in the dispersed flow regime.

A sensitivity study was performed to evaluate the impact of the Forslund-Rohsenow correlation on PCT. Table 21.1 compares the PCT values for $K=0$ and $K=0.2$, where K is the coefficient for the Forslund-Rohsenow correlation ($K=K_1K_2$), for the seven FLECHT-SEASET tests used in the derivation of the heat transfer uncertainties. Setting the coefficient K to zero increases PCT in four tests and decreases PCT in the other three tests. The maximum PCT decrease is -24 °F for Test 31203 with a flooding rate of 1.5 in/sec. The maximum PCT increase is +20 °F for Test

31701 with 6.1 in/sec flooding rate. The average PCT change for the seven tests is -2 °F (decrease). The results are within the code accuracy. Thus, the calculated PCT values for $K=0$ and $K=0.2$ can be considered as the same. It is concluded that the Forslund-Rohsenow correlation does not play a significant role in determining PCT.

**Table 21.1 Comparison of PCT values for the Forslund-Rohsenow
Correlation with $K=0$ and $K=0.2$**

Reference 1) Baumeister, et.al, "A Generalized Correlation of Vaporization Times of Drops in Film Boiling on a Flat Plate," 3rd International Heat Transfer Conference and Exhibit, August 1966.



**Figure 21.1 Heat Transfer Coefficient vs. Void Fraction from
FLECHT-SEASET 31302 Calculation**





**Figure 21.2 Heat Transfer Coefficient vs. Void Fraction from
FLECHT-SEASET 31805 Calculation**

Question 23: *It appears that the data for elevations above 8 ft in the tests used for determining the film boiling heat transfer multipliers were discarded during the data reduction process. Please discuss and justify the applicability of the film boiling heat transfer multiplier at all elevations along the fuel rod and for various power shapes. Include in the discussion justification for applicability of the film boiling multipliers for all LBLOCA phases. The discussion should include an explanation of why separate multipliers for the different LBLOCA phases are not obtained using phase-specific test data, such as THTF data for the blowdown phase and FLECHT-SEASET data for the reflood phase.*

Response 23: The FLECHT-SEASET series of tests that were used have cosine axial power shapes. During the preheat of the assembly to the initial condition, this axial power profile causes the initial temperature distribution to be roughly cosine shaped also. As the superheated steam transits the assembly from the bottom to the top, its temperature rises. It is quite probable that by the time this superheated steam reaches the upper parts of the assembly, the temperature of the steam is actually hotter than the rod surface temperature and that the heat transfer is in the reverse direction, that is, the steam is heating the rod. Since the local steam temperature is not easy to measure, the reference saturation temperature is conventionally chosen in analytical models and in data reduction. Thus, it is not easy to determine if reverse heat transfer is occurring.

The data above 8 feet in the FLECHT-SEASET data were discarded in the determination of the film boiling multipliers. The purpose in removing these data was to avoid the possibility of a model with non-physical behavior (negative or reverse heat transfer). This is not the only data that were removed. Also removed from consideration were data that were next to cold surfaces. Retaining these data would have resulted in higher measured heat transfer coefficients. The objective in discarding data was to ensure that the limiting rod was adequately modeled with suitably conservative heat transfer coefficients. The method developed and applied satisfies this requirement.

The film boiling heat transfer coefficient correlation is a local conditions correlation. It was developed using a wide range of local conditions including pressure, power, void fraction, and flow rates, in determining the heat transfer coefficient. In all cases, the location where PCT occurred is included in the data sets that were evaluated. But to ensure that wide ranges of variables could be supported, the development included data from the bottom and midsection of assemblies (FLECHT-SEASET) as well as data from the upper part of an assembly (THTF). Explicit treatment of the axial effects was not necessary.

We chose to not use phase specific treatment of the film boiling multipliers. This simplifies the code logic and avoids complications associated with determining when one phase begins and another ends. Provided the database on which the correlation is developed and validated includes data that covers both the blowdown and reflood phases, the correlation is adequate. It is acknowledged that by having a LBLOCA phase specific correlation, one might be able to reduce the standard deviation on the film boiling multiplier; however, the uncertainties that were obtained are reasonable.

PIRT

Question 24: *The Framatome ANP PIRT is similar to the NUREG/CR 5249 PIRT. This PIRT does not address the following:*

Question 24a: *Relative location of the hot assembly in the core.*

Question 24b: *Uncertainty in the single phase pump performance*

Question 24c: *Uncertainty in the broken nozzle k-factor*

Please clarify how these contributors are addressed in the RLBLOCA methodology.

Response 24: The relative location of the hot assembly is not considered a phenomenon. The methodology guideline specifies that the hot assembly must be modeled under a mixer vane, rather than an open hole. A sensitivity study was performed to address this specific issue that demonstrated that clad temperature calculations for hot assemblies located under a mixer vane or standpipe bounded those located under an open hole.

[

] The RCS temperature and flow is adjusted through a control system acting on the pumps and steam generator feedwater and steam flow. Relevant documentation on this point can be found in EMF-2054, Section 7.4.2 and Appendix A, and in EMF-2058, Section 6.2.2.4.

[

] An overview discussion on break flow treatment can be found in EMF-2103, Section 4.3.3.2.7. Details on statistical treatment of critical flow can be found in Section 4.3.1.8.

It is agreed that variations in the nozzle loss coefficient will impact break flow – a PIRT phenomenon. In RLBLOCA analyses, break flow is varied by both a sampling of break size, over the full LBLOCA spectrum, []. Sensitivity to loss coefficients will only impact break flow during refill and reflood, i.e., when break flow is unchoked. In RLBLOCA analyses, loss coefficients at the break planes are assumed to be 1.0, which is the limit of the classical abrupt area change formula for single-phase flow. During two-phase fluid flow conditions, the losses will be higher. Clad temperatures would be reduced for higher break nozzle losses as a result of less ECCS water being lost during the LBLOCA. Hence, using the single-phase assumption provides a conservative bound for the duration of the LBLOCA.

Variations of loop resistance will also impact the PIRT phenomena break flow and, to a lesser extent, core flow stagnation. There is little uncertainty in total loop resistance since this parameter must be fairly accurate to ensure good steady-state agreement of reactor vessel and core pressure drops; however, a flow split uncertainty may exist that is associated with break configuration and/or relative break location. [

]

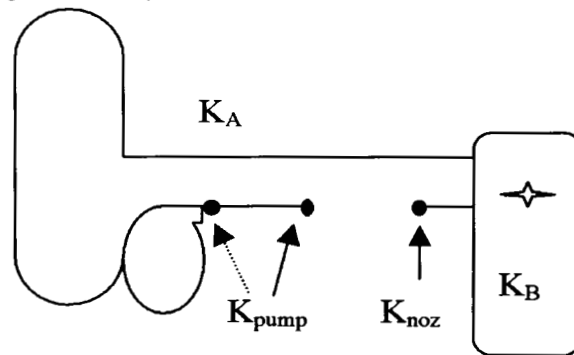
It is agreed that if you look at a single break size and vary the loop resistances and break loss coefficient, a variation in PCT will be observed. However, the proposed methodology performs a full break spectrum. This break spectrum covers the range of possible break flow rates during the LBLOCA. In the Appendix K approach where the break spectrum is looked at in a deterministic manner, one break size and associated break flow is found to be limiting over the others. In general, this break size and associated flow produce the limiting PCT because it produces the longest time of flow stagnation in the core.

The impact of including the uncertainties in the loop resistances would be to change the break flow rate from both sides of the break and, consequently, the total break flow rate for a given break size. The change in total flow rate has the same effect as varying the break size and is

therefore covered by performing the full break spectrum. [

] Thus, the flow rate from each side of the break is already treated statistically in the methodology.

To demonstrate this, a suite of calculations has been performed to assess clad temperature sensitivity to realistic variations in loop resistances. Two specific parameters, K_{pump} and K_{noz} , are the focal point of the study. Two interpretations of K_{pump} were considered, a form loss on the pump component or a modification to rated head. To be consistent with the modification of K_{noz} (a form loss), K_{pump} will be interpreted as a form loss. Since the base model has zero form losses explicitly applied in the pump (all losses captured in pump curves and friction model), the form loss modifications have been made downstream (about 12 ft) of the pump, at the break junction (see figure below), which has a form loss 1.0 in the base model.

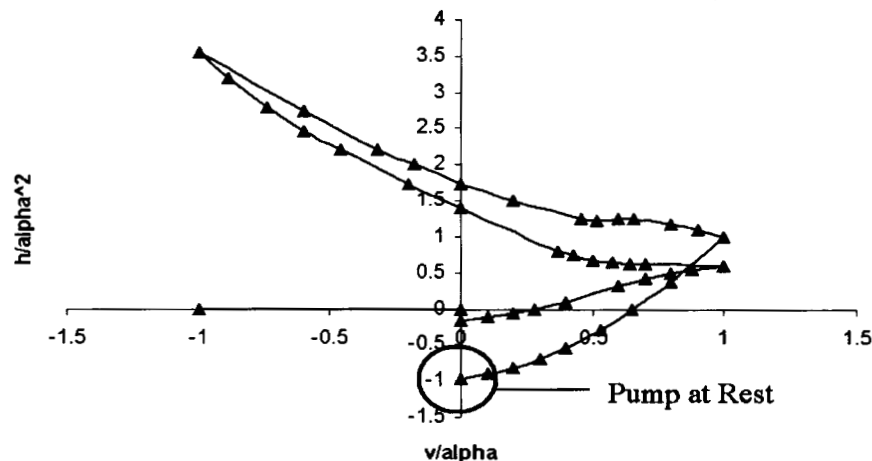


The pump resistance at rest was calculated as follows:

$$K := (2g \cdot AA \cdot K_{LR} \cdot H_r) / Q_r \quad \text{Form loss formula}$$

where

$K_{LR} = 0.96$ Pump at rest loss coefficient from normalized pump head curves (below)



$H_r = 266.0$ ft Rated pump head

$Q_r = 88500$ gal/min Rated pump flow

AA:= 9.09 ft² Pump volume area
K=35.06 Solution
K(2σ):=K*0.02=0.7 Form loss uncertainty

Based on Appendix L of NUREG/CR-5249, the 2σ uncertainty is taken as 2%. Applying this uncertainty to the pump at rest resistance results in a form loss of 0.7. A secondary method of determining this uncertainty can be made by evaluating the form losses applied in the code assessment calculations provided in EMF-2102. Examination of the UPTF, Marviken, LOFT, and SemiScale tests produces values between 0.0 and 1.5; hence, a value of 0.7 for the uncertainty is consistent with how the assessments have been performed.

Four base calculations were performed:

- a) Increase Knoz and decrease Kpump by the 2σ uncertainty (Knoz = 1.7, Kpump = 0.3).
- b) Decrease Kpump and increase Knoz by the 2σ uncertainty (Knoz = 0.3, Kpump = 1.7).
- c) Increase Knoz and increase Kpump by the 2σ uncertainty (set to 1.7).
- d) Decrease Knoz and decrease Kpump by the 2σ uncertainty (set to 0.0).

Additional calculations are included to ensure completeness of the assessment. These are:

- e) Increase Knoz and increase Kpump to 5.0
- f) Increase Knoz and increase Kpump to 10.0
- g) Cd = 1.4 (Knoz = 1.0, Kpump = 1.0).
- h) Cd = 1.4, Increase Knoz and decrease Kpump by the 2σ uncertainty (Knoz = 1.7, Kpump = 0.3).
- i) Cd = 1.4, Decrease Kpump and increase Knoz by the 2σ uncertainty (Knoz = 0.3, Kpump = 1.7).

This set of calculations will bound the expected uncertainty.

For each calculation the following key variables are provided to support the analysis: peak clad temperature, heat transfer coefficient at the high power node, void and quality at the vessel-side break plane, break flow, downcomer liquid and saturation temperatures, downcomer and core liquid levels, and approximate reflood rate. A complete set of plots is provided at the end of this response.

The table below summarizes the key parameter values and results from the base case (case 41) and the nine sensitivity cases. (Note: The case number is used to identify calculations in the figures presented in this summary). With the exception of cases 62,69-71, the PCT results are within 30 F of the base case results and with the exception of case 64, the base case PCT bounds the results of all the cases.



The peak clad temperature is the key measure of interest in licensing calculations and; hence, it is the key measure in this study. Comparisons of the base case peak clad temperature (case 41) are made against the nine sensitivity calculations in Figures 24.1-24.3. The grouping of calculations in Figure 24.1 is symmetric variations of both the K_{pump} and K_{noz} loss coefficients so that break resistance ratio remains constant. The values range from $K_{\text{pump}}, K_{\text{noz}} = 0$ to $K_{\text{pump}}, K_{\text{noz}} = 10$. The grouping of calculations in Figure 24.2 is a simultaneous increase/decrease in form loss between K_{pump} and K_{noz} (break resistance ratio not constant). The grouping of calculations in Figure 24.3 is equivalent to Figure 24.2 except that the vessel-side break discharge coefficient is set to 1.4 in these calculations and the base case calculation (41) is included in the figure.

**Figure 24.1 Clad temperature Sensitivity to Increasing Form Loss Variations
on K_{pump} and K_{noz} (R_{break} constant)**



Figure 24.2 Clad Temperature Sensitivity to 2σ Form Loss Variations on K_{pump} and K_{noz}



**Figure 24.3 Clad Temperature Sensitivity to 2σ Form Loss Variations
on K_{pump} and K_{noz} with $C_d=1.4$**

Analysis of the first grouping of calculations suggests the conclusion that clad temperatures decrease with increasing form loss. This is driven by a reduction in coolant lost out the break. Because the relative amounts of liquid coolant loss are small compared to the total break flow, the break flow plots are not a good indication of this; however, plots of the downcomer and core liquid levels in Figures 24.4-24.6 do show that as the form losses increase more liquid is present in the downcomer. Outside these differences, the results from these cases are relatively similar.



**Figure 24.4 Downcomer and Core Liquid Level Sensitivity to Increasing Form Loss
Variations on K_{pump} and K_{noz} (R_{break} Constant)**

**Figure 24.5 Downcomer and Core Liquid Level Sensitivity
to 2σ Form Loss Variations on K_{pump} and K_{noz}**

**Figure 24.6 Downcomer and Core Liquid Level Sensitivity
to 2σ Form Loss Variations on K_{pump} and K_{noz} with $C_d=1.4$**

Analysis of the second and third grouping of calculations suggests the conclusion that the peak clad temperatures are relatively insensitive to realistic variations in form loss ($\pm 2\%$). Comparison of cases 63 and 64 to the base case 41 and case 70 and 71 to case 69 show PCT variations $< 5^\circ\text{F}$. This is well within the numerical uncertainty of S-RELAP5 and statistically insignificant in the computation of uncertainties. [

] Case 64 does show some delay to quench; however, the delay in quench had no impact on clad temperatures.

The general conclusion from the calculation is that the designation of form losses provided in the base model is conservative with respect to clad temperatures and that realistic variations in loop resistances produce only a relatively minor variation on clad temperatures.

Question 25: *The orientation and location of the postulated pipe breaks are not explicitly addressed. Please discuss the following:*

Question 25a: *The choice of break location, such as cold leg versus hot leg and hot leg both with and without pressurizer, and location of slot breaks, such as top, side and bottom of the pipe. In addition, why were other locations than those presented not considered, or if they were considered, why were they not analyzed?*

Question 25b: *The smallest break size analyzed using the RLBLOCA methodology. Also discuss the definitions used by Framatome ANP in determining the boundaries between the large and small break methodologies and how is a single calculational tool such as S-RELAP5 applicable over the entire range of break sizes.*

Response 25: The choice of break location is addressed in the methodology as part of the scenario specification in Section 3.1. It is stated that "For a LBLOCA, the most limiting break typically occurs in a cold leg pipe between the pump discharge and the reactor vessel." The scenario specification and the PIRT phenomena for this scenario are those associated with the cold leg break location.

There are several reasons why this break location is most severe for a LBLOCA and why it was chosen for the scenario. (1) The cold leg break location has the lowest resistance for flow from the core inlet to the vessel end of the break, and the highest resistance for flow from the core outlet to the loop end of the break. This fact maximizes the potential for early core flow reversal and flow stagnation, which traps initial stored energy in the fuel and results in heatup beginning from a higher temperature level and ultimately higher PCTs. (2) The cold leg break location is between the vessel and the broken loop ECC injection location, and is immediately adjacent to the ECC injection. This break location virtually assures that all of the ECC injection fluid from the broken loop flooding tank or accumulator and from the broken loop pumped ECC injection are lost through the break and cannot contribute to core reflooding. For other break locations, much if not all of this ECC fluid will remain in the system and be available to aid reflooding. (3) The cold leg break location maximizes the flow resistance and pressure drop for steam generated during reflooding to exit the vessel which reduces the reflood rate and increases the PCT.

These factors are all associated with current PWR systems and are independent of the analysis methodology being used. The limiting cold leg break location has been demonstrated many times by various analysts using different codes. Therefore, the writers of the ECCS compendium and the CSAU also limited the worst LBLOCA scenario to the cold leg break location as was done by Framatome ANP.

Break orientation is not considered to be a significant contributor to PCT for LBLOCA simulations because the break size is large by definition which results in high and well mixed break flow. For these conditions, calculated critical flow would not vary with orientation. Also because of the rapid depressurization associated with large breaks, the issue of loop seal plugging is not a concern. This depressurization assures that either the water has flashed or has escaped out the break. Without the plugging in the loop seals, the severe steam binding capable of depressing the core level cannot occur. Spot checks on S-RELAP5 calculations using break sizes near the SBLOCA range have been performed to verify this.

The break size spectrum is designed to interface with the Framatome ANP Small Break LOCA methodology. The SBLOCA methodology, using S-RELAP5, was qualified for breaks up to 10% of the cross-sectional area of the cold leg pipe. Breaks larger than this will be analyzed with the LBLOCA methodology. Thus, the full range of LOCA break sizes is considered.

Containment Modeling

Question 26: *Although the Framatome-ANP RLBLOCA methodology uses the ICECON methodology to perform the containment back pressure to the reactor coolant system analysis, the methodology still uses a simplified component system model of the containment. Please discuss how a single comparison of ICECON with GOTHIC is sufficient demonstration of applicability to the range of Westinghouse and CE containment configurations.*

Response 26: The role of the containment model for LBLOCA simulation is to provide an adequate back pressure calculation. The containment pressure will influence break flow and steam binding phenomena during the simulation. For the types of containment used in PWRs, this space is well modeled by a single large volume with mass and energy transport. S-RELAP5 uses a total energy equation required for accurate energy transport during the early phases of a LBLOCA when large pressure differences between a plant's RCS and the containment exist. Energy removal characteristics from the containment is modeled on a component basis (i.e., sprays, fan coolers, or ice condensers) with data provided by the specific plant to be analyzed. Sensitivity studies have shown that under prediction of containment pressure is generally conservative. This RLBLOCA methodology allows that these parameters may either be treated statistically or using a conservative bound (i.e. maximum energy removal). Containment pressure has been identified as a PIRT parameter of high importance. [

]

Containment pressure during a LBLOCA is largely dependent on mass and energy inputs (primarily boundary conditions) and air/water properties, rather than empirical models. Therefore, the S-RELAP5 containment model has the capability to predict the dominant phenomena which affect containment pressure during a LOCA. For this reason, the two calculations examining a dry containment and an ice containment serve the purpose of validation of the S-RELAP5 models against a containment code which has been assessed against experimental data. Containment codes like GOTHIC do provide a more detailed

physical modeling capable of capturing thermodynamic conditions that can degrade containment systems or challenge containment licensing criteria outside the scope of LOCA analysis. Typically, the routine use of these codes is performed to address licensing concerns documented in NUREG-0800 Section 6.2 (Standard Review Plan for Containments) and NUREG-0588 (Environmental Qualification).

The containment analysis performed as part of the RLBLOCA analysis is not used to support licensing analyses of the plant containment. The only purpose of this containment analysis is to provide a back pressure to the primary reactor coolant system throughout the LBLOCA. Based on sensitivity studies it was concluded that a low containment pressure resulted in higher PCTs. It was also recognized that the utility would, to some extent be moving equipment in and out of containment. [

]

The actual containment for a plant will be addressed in the plant specific RLBLOCA analysis. This includes the impact of the plants actual containment volume, containment sprays, fan coolers, and ice condensers, if present. [

]

[

]

In addition, the containment pressure calculated from two Appendix K simulations for the same 3-loop plant are included in the figure. These Appendix K simulations are for a 0.8 double-ended guillotine break with two different single failure assumptions. In one case a loss of diesel generator (-DG) is the assumed single failure and in the other case a loss of low-pressure injection system (-LPSI) is the assumed single failure. The loss of diesel generator case reported the highest clad temperature; however, containment cooling in this simulation was limited by the loss of some containment spray. The loss of LPSI calculations does not directly impact the designed containment cooling and therefore has a lower containment pressure response than the loss of diesel generator case. Regardless, Figure 26.1 demonstrates that the lower bound from the RLBLOCA calculation is more conservative than either Appendix K result.

[

1

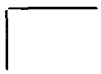


Figure 26.1 Containment Pressure Response from RBLOCA Simulations

Downcomer Boiling

Question 27: *The brief overview and description of large break LOCA behavior on Page 3-4 does not mention the potential for downcomer boiling. Downcomer boiling has been shown to be important in the transport of coolant to the core in the LBLOCA. Discuss the basis for the applicability of the S-RELAP5 simulation of the effects of downcomer boiling and the manner in which downcomer boiling has been treated in the RLBLOCA methodology. Include in the discussion the roll of the downcomer wall initial temperature in downcomer boiling.*

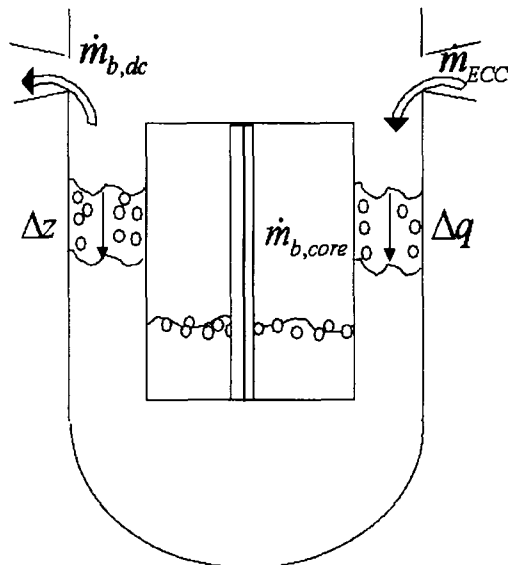
The PIRT in Table 3.3 does not include downcomer boiling. Please include in the discussion the exclusion of downcomer boiling from the PIRT.

Response 27: The downcomer boiling issue is included in the Framatome ANP PIRT under the label "Hot wall" phenomenon; in addition, downcomer boiling is also highly dependent on containment pressure, which is also a phenomenon appearing on the PIRT. Unlike many 10 CFR 50, Appendix K methodologies, S-RELAP5 simulates this phenomenon and its detrimental effects on core reflooding. [

Downcomer wall temperature is initialized both in input and by a long steady-state calculation (800 s). Examination of wall temperatures following the steady-state calculation has shown good convergence.

Boiling is a phenomenon that codes like S-RELAP5 have been developed to predict and boiling in the downcomer is an observed phenomenon in S-RELAP5 LBLOCA simulations. Downcomer boiling is the result of the release of stored energy in vessel metal mass. Unlike many legacy LBLOCA methodologies, surface boiling is a modeled phenomenon for all components in an RLBLOCA analysis. Specifically, downcomer boiling is in the nucleate boiling regime and in S-RELAP5, nucleate boiling heat transfer is modeled using the Chen correlation. The implementation of the nucleate boiling model in S-RELAP5 has been validated through the prediction of several assessments on boiling phenomenon provided in the S-RELAP5 Code Verification and Validation document (EMF-2102).

Hot downcomer walls penalize PCT by two mechanisms: reducing subcooling of coolant entering the core and by the loss of coolant mass out the break from boiling along the downcomer ($\dot{m}_{b,dc}$, see figure at right). These processes reduce the density of the downcomer fluid and effectively lower the height of the liquid column in the downcomer which reduces the pressure driving force for reflooding the core. While boiling in the downcomer may occur at anytime during a LBLOCA transient, the biggest impact on clad temperatures will occur during late reflood following the end of accumulator injection. At this time there is a large step reduction in coolant flow from the ECC system (\dot{m}_{ECC} in figure) and at this same time the coolant subcooling is being lost due to heat input from the downcomer metal mass. When this coolant becomes saturated, boiloff occurs which further reduces the effective downcomer level. With the



reduction of the downcomer liquid level, the core reflood rates will be reduced and the clad temperatures will increase.

While this phenomenon can impact clad temperatures, it is a self-limiting process. As the downcomer liquid level decreases, less energy is released from the downcomer walls and the liquid level eventually stabilizes. (Note: the core liquid level will move with the downcomer level which will further contribute to this stabilizing effect.) This stable level is a function of the total energy release to the coolant. The largest component of the total energy is not from the downcomer; but, rather, from the core to the coolant.

To what extent the liquid level decreases to a new stable level is dependent on the same characteristics that encourage boiling. Many of these factors, such as geometry, coolant flow rates, and power, are dependent on plant design and operation. Phenomenologically, boiling is most dependent on coolant properties, of which, pressure is the key characteristic. (Note: calculations with S-RELAP5 show that heat transfer from the downcomer metal mass becomes conduction-limited, resulting in heat fluxes that are insensitive to hydraulic variations.) The extent of the downcomer liquid level reduction is strongly correlated to the amount of coolant at the beginning of downcomer boiling, i.e., the maximum liquid level following the step change in ECCS flow and prior to boiling. Downcomer liquid level (collapsed) is directly related to how much coolant mass is lost out the break. This implies that the smaller breaks will have the higher pre-downcomer boiling liquid level and the larger downcomer liquid level reduction during downcomer boiling. Thus, downcomer boiling will have the largest impact on clad temperatures for the smaller breaks.

Several sensitivity studies have been performed using S-RELAP5 to demonstrate the primary simulation sensitivities to downcomer boiling phenomena and to establish a pedigree for S-RELAP5's capability to simulate downcomer boiling. These studies are summarized in the table below.

Study #	Description
1	W/ vs. W/O DC Walls
2	Low Containment Pressure Plant RLBLOCA Analysis
3	SemiScale S-06-3 Benchmark
4	Finer Azimuthal Nodalization (6 axial x 9 azimuthal)
5	DC Cross Flow Form Loss (based on Idelchek formulation)

Study #1

Heat structures attached to the downcomer and lower plenum fluid volumes were decoupled so that heat released from these heat structures would not contribute to heating liquid in these regions (the decoupling was assumed to occur following accumulator discharge). Removing the heat structures will both prevent the reduction in subcooling and the boiling of coolant entering the reactor vessel. The base calculation was extracted from a preliminary RLBLOCA analysis of a 3-loop plant. Figure 27.1 compares the PCT from these calculations for the condition with and without downcomer boiling for the case with the highest PCT, 1826°F. This break is best described as a 93% double-end guillotine break to a dry containment. (Note: Generally, dry containment pressures during LBLOCAs are usually greater than 30 psia.)

Shortly after the accumulator discharges, boiling was observed along the downcomer sector adjacent to the broken loop, as seen in Figure 27.2; however, sustained downcomer boiling was

not observed in the other two sectors until after 100 s. These two sectors received LPSI driven ECCS coolant that offset some of the heatup in the downcomer in this area. In comparing the "W/ DC walls" case to the "W/O DC walls" case, the collapsed liquid level shown in Figure 27.3 for the "W/ DC walls" case changes very little; however, it is obvious from the divergence in the liquid level results that at about 100 s downcomer boiling is removing a significant amount of liquid from the downcomer. This level differential represents the dominant condition influencing core reflood rate and it is obvious in Figure 27.1 that downcomer boiling is a factor in raising clad temperature beginning after accumulator discharge. In fact, in this sensitivity study, the PCT contribution from downcomer boiling is about [].



Figure 27.1 PCT Trends with Downcomer Boiling



Figure 27.2 Vapor Generation Rate in Downcomer Broken Loop Sector



**Figure 27.3 Core Collapsed Liquid Level Trends with
Downcomer Boiling**

It is Framatome's experience that the PCT impact of downcomer boiling is predominantly the consequence of plant type, break size and containment pressure. In the above sensitivity study on a 3-loop plant, containment pressure was no lower than 30 psia at anytime during the late reflood period. This is relatively high compared to plants that incorporate ice condensers or more aggressive containment spray systems.

Study #2

To evaluate the effect of containment pressure, a complete RLBLOCA analysis was performed for a 3-loop plant designed with a very aggressive containment cooling system capable of rapidly returning the containment pressure to near atmospheric conditions following a LBLOCA. To demonstrate the downcomer boiling sensitivity to break size, the worst split break and the worst guillotine break were identified. The break size of these cases was determined to be 36% and 89% for the split and guillotine break, respectively. The worst case guillotine break calculation was modified in a special calculation to be similar to the "W/O DC walls" calculation in Study #1. This calculation also modeled an increase in the ECCS coolant temperature to simulate the loss of subcooling that would occur from the downcomer walls.

Figure 27.4 shows a comparison of the PCT response from the limiting LBLOCA simulation (89% DEGB) for the low containment pressure plant and a "No Downcomer Boiling" calculation (no wall heat structures, elevated ECCS coolant temperature). The effect of downcomer boiling is dramatic; however, it only accounts for about a [] impact on PCT. The most noticeable difference is the time-at-temperature condition of the base case. For this reason the effect of downcomer boiling and the low containment temperature will likely have a significant impact on oxidation. Figure 27.5 shows the collapsed liquid level response from these two calculations. In these calculations the accumulator discharge ends near 60 s. At that time both calculations show a dramatic decrease in collapsed liquid level as a result of the drop in coolant flow. (Note: the liquid level is also depressed somewhat from the nitrogen bubble that flows from the accumulator to the break.) After this initial drop, both calculations recover somewhat until subcooling is lost in the base case. At that time, the downcomer collapsed liquid level drops to about 9 ft and stabilizes. The calculation without the wall heat structures shows a relatively consistent increase in the liquid level.

Figure 27.6 shows the PCT response for the limiting split break. Through the end of accumulator discharge, clad temperature remains lower than the DEGB, as would be expected for smaller LOCAs that leave more coolant in the reactor vessel. After this time, there is a significant heat up of the hot pin (300°F over the early reflood peak). In this calculation the downcomer collapsed liquid level drops to about 12.5 ft, prompting the temperature excursion observed during the late reflood.

Figures 27.7 and 27.8 show PCT vs. Time of PCT graphs for the 3-loop sample problem and the low containment pressure RLBLOCA analyses. The key distinction between these two graphs is in the preferences for the Time of PCT. For the dry containment there are two distinct groupings around the early (30 s) and late (90 s) reflood periods. In the low pressure containment analysis there is a distinct grouping during the early reflood period; however, an effect of the low pressure containment is an apparent spreading out of the late reflood grouping. Comparing the early reflood grouping between the two graphs, calculated PCTs are similar (although the dry containment results tend to be higher). However, there is little similarity between the late reflood groupings. The delayed cooldown predicted for the low containment pressure analysis clearly contributes to higher PCTs. In particular, split breaks are noticeably higher.



Figure 27.4 PCT from Worst Guillotine and “W/O DC Walls” Calculation



Figure 27.5 Collapsed Liquid Level from Calculations on Worst Guillotine Break



Figure 27.6 PCT from Worst Split Break Calculation



Figure 27.7 PCT vs. Time of PCT for 3-Loop Sample RLBLOCA Analysis



Figure 27.8 PCT vs. Time of PCT for Low Containment Pressure RLBLOCA Analysis

Framatome is aware of a LBLOCA simulation for the 4-loop Westinghouse Watts Bar plant that attributes about 400°F to a PCT penalty from downcomer boiling. We are unaware of all the assumptions applied in this simulation; however, there are a couple of aspects to this calculation that are unique: specifically, low pressure and break sizes that approach the small break region. As shown in this RLBLOCA analysis on the low containment pressure plant, S-RELAP5 has predicted similar characteristics with a downcomer boiling penalty as high as [] or more for smaller break sizes and low pressure. To date, none of these calculations have been a limiting analysis; however, the design of this RLBLOCA methodology does not preclude this possibility.

Study #3

No specific test program has explicitly addressed downcomer boiling; however, CCTF, LOFT, and SemiScale have all performed tests with hot downcomer walls. All the CCTF, LOFT, and SemiScale assessments performed for the "Evaluation of Code Bias" include hot downcomer walls. In addition, such scaled tests tend to over emphasize metal mass since it is impossible to scale down such structure without distorting hydraulic scaling. Generally, S-RELAP5 has been shown to match or bound clad temperature predictions. The main limitation of these tests is that the minimum pressure among these tests is about 30 psia. Similar containment pressure profiles were used in the PWR sample problems.

Possibly the best benchmark available for examining downcomer boiling is the SemiScale S-06-3 test. This test was included in the S-RELAP5 Code Verification and Validation. Unfortunately, that calculation as presented did not show significant downcomer boiling. For this reason the modeling of this calculation was reevaluated with the aid of one of the original SemiScale engineers (Tom Larson). His suggestion was to reexamine the modeling of the downcomer filler component and its contact with the downcomer vessel wall. This is primarily concerned with how to model the "filler gap," a space located between a filler mass and the vessel wall. Original documentation indicated that this filler gap was filled with air; however,

according to the SemiScale engineer and verified through thermocouple measurements, this space filled with water during the transient and greatly enhanced the release of metal mass energy to the downcomer inventory.

Figures 27.9 and 27.10 show a calculation vs. test comparison of the peak clad temperature and liquid level (in terms of differential pressure) response, respectively. The liquid level specifically shows the post-accident refill, followed by a rapid boil off that stabilizes to about 2.5 psid. The downcomer boiling phenomena doesn't actually contribute to a higher peak clad temperature; however, it does extend the cool down period.



Figure 27.9 Semiscale S-06-3 Peak Clad Temperature Comparison to Data



Figure 27.10 Semiscale S-06-3 Downcomer Liquid Level Comparison to Data

Study #4

This sensitivity study consists of four calculations examining clad temperature sensitivity to downcomer nodalization. The base model, with 6 axial by 3 azimuthal regions (Figure 27.11), has been expanded to 6 axial by 9 azimuthal regions (Figure 27.12). The first calculation simulated is designed to be equivalent to the limiting PCT calculation given for the 3-loop sample problem. The second calculation simulated increases the vessel side break flow discharge coefficients. The third and fourth calculations repeat the first two calculations using a low containment pressure plant (3-loop sample problem).

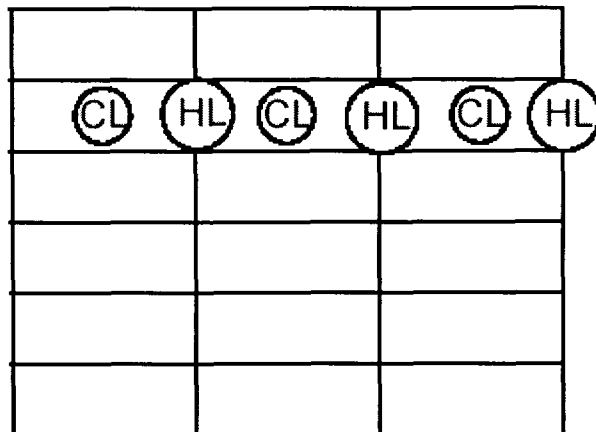


Figure 27.11 Base Model Nodalization Around Cold Leg Nozzles

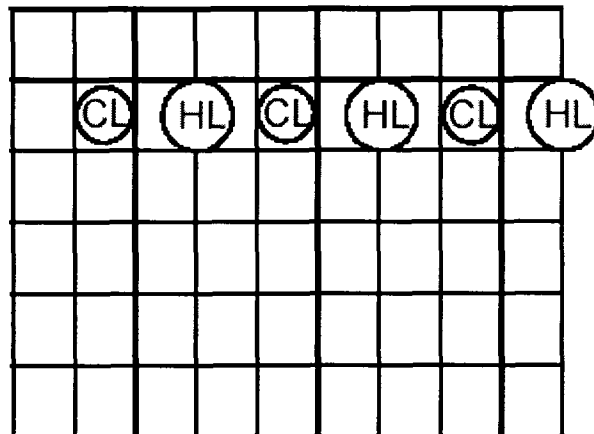


Figure 27.12 Renodalized Model Around Cold Leg Nozzles

Figure 27.13 presents the peak clad temperature responses for the conditions representing the 3-loop sample problem from the renodalized and base models. The renodalized model has a significantly different response beginning at the end of blowdown. The clad temperature response shows a distinct blowdown peak in the sensitivity study that was not present in the base case. From the break flow and downcomer liquid level plots (Figure 27.15 and 27.15), it is obvious that in the sensitivity study that less RCS and ECCS coolant is going out the break during the early phases of the transient and is staying in the downcomer instead.

With basically equivalent models except for the nodalization in the downcomer, the source of this discrepancy is found in understanding how the nodalization influences the result. Referring to the Figures 27.11 and 27.12, the pathways from the intact loops to the broken loop can be traced out by following each optional pathway from the two sources to the one sink. In the base model the pathways are few; flow moves from the source volumes in the downcomer to either up or down, then over to the broken loop sector, and out the sink volume. In the renodalized model, there are more pathways possible. The effect is an increase in the mean free path between the source to the sink volumes for the model with the finer nodalization. By moving to finer and finer nodalization, the change in the mean free path would evidently become negligible; however, there is a penalty in code runtime.

For LBLOCA applications, the remarkable characteristics of the simpler nodalization scheme is that it contributes to a conservative clad temperature bias. Downcomer phenomena impacting clad temperatures are many, including hotwall, boiling, CCFL, condensation, and multi-dimensional effects, and the relative contributions of each of these phenomena are difficult to separate and assess. This was the conclusion of the Technical Program Group that developed the CSAU methodology. Like the TPG the Framatome RLBLOCA methodology has demonstrated the conservatism of the simple nodalization through assessment (primarily against full-scale UPTF tests) and sensitivity study (this nodalization study). By consistently applying this nodalization in assessments and in licensing calculations, the code bias and uncertainty associated with nodalization is passed to all similar calculations. This was the conclusion of the TPG.

Nonetheless, maintaining the simpler nodalization does not fully address downcomer boiling sensitivity to nodalization. For this reason a second calculation was performed using the renodalized model in which the break flow discharge coefficients were increased so that the break flow during the early phase of the transient would be nearly equivalent to that in the base model calculation. By doing this, downcomer inventory at the beginning of reflood would be approximately the same as the base case, thus, providing for the key boundary condition for assessing boiling in the downcomer. Figure 27.16 provides the peak clad temperature response from this calculation compared to the base case. Figures 27.17 and 27.18 present break flow and downcomer liquid level plots that demonstrate that similar beginning of reflood conditions for downcomer inventory exist as the result of increased break flow.

From the peak clad temperature plot it is seen that the two cases present very similar results. The finer nodalization model is still impacted by the longer mean free paths as observed in the first sensitivity calculation; hence clad temperatures are still lower. Relevant to the downcomer boiling issue was whether having more modeled heat structure surfaces cooled by ECCS (i.e., not directly under the cold leg nozzles) would in some way influence how the bulk rate of boiling in the downcomer was calculated. The key measures addressing this concern are downcomer liquid level, downcomer temperatures, and, by virtue of the application, clad temperatures.

No indication of a phenomenological discrepancy is discernable from the downcomer liquid level response in Figure 27.18 and the clad temperature response shown in Figure 27.16. Figure 27.19 shows the coolant liquid temperature vs. saturation temperature for an azimuthal slice in the downcomer between the broken loop and the intact loop. It can be seen that as one moves away from the broken loop, the subcooling of the liquid increases. Comparison of this figure to Figure 27.20 presenting the same temperatures for the base case shows that in the simpler nodalization subcooling is less for the nodes directly under the intact loops and more for the nodes directly under the broken loop; hence, on the average, the same amount of heat is being removed in both calculations. In both calculations it is shown that boiling diminishes with time. Heat transfer out of the downcomer walls becomes conduction-limited and despite the large amount of stored energy remaining in the heat structures, the heat transfer at the wall surface is adequately handled by the flow of LPSI-supplied ECC and subcooling returns.



Figure 27.13 Peak Clad Temperature Comparison of the Renodalization Model to the Base Model



Figure 27.14 Break Flow Comparison of the Renodalization Model and the Base Model



**Figure 27.15 Downcomer Collapsed Liquid Level Comparison of the
Renodalization Model and the Base Model**



**Figure 27.16 Peak Clad Temperature Comparison of the Modified
Renodalization Model to the Base Model**



Figure 27.17 Break Flow Comparison of the Renodalization Model and the Base Model



Figure 27.18 Downcomer Collapsed Liquid Level Comparison of the Modified Renodalization Model and the Base Model



Figure 27.19 Downcomer Saturation and Liquid Temperatures in Second Renodalization Sensitivity Study Calculation



Figure 27.20 Downcomer Saturation and Liquid Temperatures in the Base Case

Downcomer boiling is known to be highly sensitive to containment pressure. For this reason, the two nodalization sensitivity calculations were performed for a plant with an aggressive containment cooling system. Figure 27.21 provides the peak clad temperature response from the “renodalized-only” calculation (74) compared to the low containment pressure base case (16) for this separate RLBLOCA analysis. As with the first calculation, the break flow and downcomer liquid level plots (Figure 27.22 and 27.23) show that less RCS and ECCS coolant is going out the break during the early phases of the transient and staying in the downcomer.

Figure 27.24 compares the peak clad temperature response for the “renodalized + flow” calculation (75) with that from the low containment pressure base case (16). Like the second calculation, the key measures addressing this concern are downcomer liquid level, downcomer temperatures, and clad temperatures. Comparison of these measures provided in Figures 27.24-27.26 to those provided for the 3-loop sample problem show similar characteristics. There is no indication of any phenomenological discrepancies related to the prediction of downcomer boiling between these calculations.



**Figure 27.21 Peak Clad Temperature Comparison of the Renodalization
Model to the Base Model (Low Pressure Plant Analysis)**



Figure 27.22 Break Flow Comparison of the Renodalization Model and the Base Model (Low Pressure Plant Analysis)



Figure 27.23 Downcomer Collapsed Liquid Level Comparison of the Renodalization Model and the Base Model (Low Pressure Plant Analysis)



Figure 27.24 Peak Clad Temperature Comparison of the "Renodalized + Flow" Model to the Base Model (Low Pressure Plant Analysis)



Figure 27.25 Break Flow Comparison of the “Renodalized + Flow” Model and the Base Model (Low Containment Pressure Plant)



Figure 27.26 Downcomer Collapsed Liquid Level Comparison of the “Renodalized + Flow” Model and the Base Model (Low Containment Pressure Plant)

Study #5

Two calculations have been performed to determine clad temperature sensitivity to best-estimate cross flow form loss resistances (friction is inherently treated in S-RELAP5). The form loss calculation applies the Idelchek reference for flow through a curved pipe or rectangular duct. Using an angle of curvature of 120° , this results in a form loss of 0.1167. This loss is applied along the junctions of the three azimuthal sectors in the base case model (not the renodalized model). The two calculations are derived from the limiting calculations for the 3-loop sample problem (in figures, case 66 vs. 41) and from a RLBLOCA analysis of a low containment pressure plant (in figures, case 80 vs. 16). Figures 27.27 and 27.28 show the clad temperature results for these two calculations.

The dominant result in the first calculation is that beginning-of-reflood occurs earlier as a result of less fluid lost from the break. Outside of the clad temperature and downcomer liquid level plots, other key variables are very similar to the base case. The early beginning-of-reflood was not observed in the second calculation. This may be related to differences in the influence of steam binding related to the different containment pressures. A comparison of reflood rates between the two calculations shows that during the early reflood period, the reflood rate from the low pressure plant calculation is significantly lower. The lower reflood rate is indicative of a

greater resistance to flow from the downcomer to the upper plenum and out the break. This resistance is likely the dominant resistance to flow into the reactor vessel rather than the effect of the added cross sectional form losses. As a consequence, the effect of the added cross sectional form loss on clad temperatures is minimal, about 14 F.

The sensitivity calculation does show a later quench time. However, comparison of the total oxidation actually shows that the base case is somewhat higher than the sensitivity calculation. This suggests that for the majority of the transient, the calculations are very similar. There is an accumulative effect from the inclusion of the cross flow form losses that limits how much heat is being removed from the downcomer walls in the form of steam. The result is a delayed quench.

This can be seen in the downcomer collapsed liquid level (Figure 27.29). The base case calculation clearly shows that near the end of the calculation, the rise in the downcomer liquid level is more rapid than in the sensitivity calculation. Measuring the importance of these differences relative to the primary acceptance criteria, PCT, for a LBLOCA, these differences are minor.



Figure 27.27 Peak Clad Temperature Results from Cross Flow Resistance Study



**Figure 27.28 Peak Clad Temperature Results from the Cross Flow Resistance Study
on the Low Pressure Containment Plant**



Figure 27.29 Downcomer Collapsed Liquid Level Responses for the Cross Flow Resistance Sensitivity Study and the Base Case for a Low Containment Pressure Plant

Downcomer Boiling Summary

The key sensitivities for downcomer boiling are break size and containment pressure. Sensitivity studies have been done for both of these parameters during the development of this RLBLOCA methodology. In all the studies performed for lowered containment pressure, clad temperature increased. Studies on break size showed that there tends to be a break size that minimizes blowdown heat transfer and that tends to provide the highest clad temperatures. Sensitivity studies on interfacial drag have not shown a strong influence on clad temperatures. Injection subcooling is considered a Plant Parameter that is treated on a plant specific basis. In sample problems it has been conservatively treated (minimized). A time step sensitivity study is presented in Appendix C of EMF-2103 Revision 1.

Fuel Swelling and Rupture, Relocation and Metal/Water Reaction

Question 28: *On page 3-7 it is noted that fuel rod rupture is not included in the calculations, and possibly the peak local clad oxidation calculation will not include inside oxidation as well as outside oxidation. In addition, there is some confusion regarding the metal/water reaction model being used.*

Question 28a: *Please clarify and discuss why the fuel swelling and rupture model is not used. The discussion should include consideration of the effects of burnup. The discussion should also include justification for neglecting fuel swelling and rupture in the calculations and the effect this has on producing a lower oxidation potential since inner cladding surface oxidation is not considered.*

Response 28a: Swelling and rupture models were not used in the Framatome methodology because use of the swelling and rupture models based on NUREG 0630 would yield slightly reduced PCTs and reduced total metal-water reaction (oxidation) compared to the same calculations without using the swelling and rupture models.

As a fuel rod heats up, the internal pressure will increase and the strength of the zircaloy cladding will decrease. At temperatures usually in excess of 1600F, the cladding will begin to experience plastic strain at which time the cladding begins to move away from the internal fuel, i.e. the gap size increases. This swelling effect is beneficial with regard to the cladding temperature, in that the gap thermal resistance is increasing and any available cooling is now more effective in removing energy from the cladding and reducing the cladding temperature.

With swelling, the external area increases which enhances both the surface heat transfer and the metal-water reaction. As temperature increases further, the NUREG-0630 models predict rupture of the cladding. At rupture, there is a further expansion of the cladding with associated increase in heat transfer area. The metal-water reaction area also increases and at rupture is nearly doubled with the addition of the internal cladding surface for reaction.

In this process, there are competing phenomena some of which tend to increase PCT while others tend to decrease PCT. Therefore, Framatome ANP performed calculations to quantify the overall effect. The results of the calculations showed that for approximately limiting LOCA conditions, the calculated PCT and total local metal-water reaction was highest for the calculated cases without use of the swelling and rupture model. The exponential temperature dependence of the metal-water reaction caused more reaction to be calculated for the rod which did not experience swelling due to the higher temperature than was calculated for the case using the swelling and rupture model. Appendix B.2 of the methodology report EMF-2103 provides some discussion on this issue.

In sensitivity studies examining fuel swelling and rupture, PCTs always went down when swelling and rupture was calculated. Since data from studies on this issue is sparse and the uncertainty large, the decision to not use the fuel swelling and rupture model was logical since PCT predictions without these effects represented a bounding model.

Burnup affects possible fuel rod rupture in two ways: (1) fuel rod initial stored energy, and (2) fuel rod pressure. Fuel rod initial stored energy is highest at near BOL exposure, but then decreases rapidly with burnup. A minimum value is reached and then at higher exposures the initial stored energy increases, but for exposures at which the rod power can be limiting, the stored energy never recovers to the maximum BOL value. The second effect, fuel rod initial operating pressure, increases with burnup. Framatome ANP calculations indicate that the increased temperatures associated with the higher initial stored energy has a much greater effect on PCT and extent of metal-water reaction than does the internal rod pressure. Hence, first cycle high stored energy conditions are most limiting with respect to burnup. (Also see response to Question 131.)

Question 28b: *Fuel pellet relocation has been observed which can cause pellets to fill the space created by swelling and ballooning cladding. Please discuss why Framatome-ANP has not included this effect and the basis for that decision.*

Response 28b: The response to Question 131 shows observed temperature behavior during fuel rod swelling, and rupture with fuel relocation. These results show cooling effects due to swelling and rupture which are not calculated as part of the Framatome model. The fuel relocation occurred but did not adversely affect the subsequent temperature behavior. Thus, a LOCA analysis of the fuel rod with the Framatome model, which ignores the beneficial effects of swelling and rupture, provides a bounding cladding temperature calculation even in the event rod swelling, rupture, and pellet relocation were to occur.

Rupture would not be calculated to occur during the blowdown phase of the LOCA because the external pressure is high during this time and rupture could only occur for very high internal gas pressures. At high burnups when the internal pressure is high, the rod LHGR is too low, due to burnup, to be limiting, and the LOCA transient temperature for this rod does not reach the rupture level during the blowdown phase. [

]

Question 28c: *Please clarify why the Cathcart-Pawel model is used in S-RELAP5 model described in the Methodology document, EMF-2103, while the Models and Correlations document, EMF-2100 describes the Baker-Just model. Also, there appear to be better models than the Cathcart-Pawel metal/water reaction model for temperatures below 1900°F. Please discuss the basis for not choosing another metal/water reaction model for the lower temperature range and also include in the discussion a justification for the assumptions applied for the initial condition.*

Response 28c: The Cathcart-Pawel reaction rate equation is used for S-RELAP5 applications in the Realistic LOCA methodology as described in EMF-2103. For small break LOCA applications using S-RELAP5, calculations are performed according to the requirements of 10 CFR 50 Appendix K. These requirements specify that the Baker-Just reaction rate equation must be used. Report EMF-2103 presents the Realistic LOCA methodology. EMF-2328(P)(A) presents the SBLOCA methodology. EMF-2100 is not specific to either methodology but is a support document for the S-RELAP5 code and thus, is intended to describe the overall code capabilities for all applications. Hence, EMF-2100 documents and presents both models.

The Cathcart-Pawel reaction rate equation is used for the calculation of high temperature oxidation of zircaloy with steam. Experimenters generally note that this high temperature reaction has a negligible rate at temperatures of 1000°C (about 1800°F) and below. The ECCS criteria limit maximum cladding temperatures to less than 2200°F (1200°C). Thus, the temperature range for the high temperature oxidation is limited to 1800–2200°F. Cathcart-Pawel was chosen for this range because it already existed in the RELAP5 code, and the consensus of the ECCS compendium was that this equation was a good best estimate of the reaction rate for this range of temperatures.

It is generally accepted that the reaction rate of zircaloy with steam is insignificant at temperatures below 1000°C (1832°F) (Reference ORNL-NSIC-23). Above this temperature, various reaction rate equations have been formulated. Cathcart-Pawel was chosen for the realistic LOCA model because it is recommended in the ECCS Compendium (NUREG/1230) for application between temperatures of 1000 - 1300°C (1832 - 2372°F) and is given as an

acceptable correlation in Reg. Guide 1.157 for temperatures above 1900°F. The metal-water reaction is best estimate and is appropriately applied over the temperature range where the reaction rate is significant.

The Cathcart-Pawel expression is also extended to lower temperatures. Significant reaction does not occur and is not calculated by the Cathcart-Pawel equation at the lower temperatures. Conclusion 4 from ORNL/NUREG-17 states: "Oxide layer growth at 900 and 950°C (1652 - 1742°F) is not describable in terms of parabolic kinetics. Extrapolation below ~ 1000°C (1832°F) of high temperature rate constant data for oxide or Xi layer growth or total oxygen consumption will yield overpredictions of these quantities. However, the error resulting from such an extrapolation is likely to be negligible if the time of oxidation at the lower temperatures does not exceed ~ 100 s." Thus, the extrapolation of Cathcart-Pawel below 1000°C is conservative and insignificant compared to reaction at higher temperatures.

The oxidation due to corrosion affects the initial cladding state at the initiation of the LBLOCA. The corrosion oxidation is calculated as a function of burnup using the NRC approved RODEX3 code. The RODEX3 initial condition oxidation values are transferred directly to the S-RELAP5 code for use in the LBLOCA calculation. (See response to Question 28d.)

Question 28d: *In the time-in-life study, what inside and outside initial oxidation thickness were used for the BOL analysis. What oxide thickness is used for once and twice burned fuel?*

Response 28d: The NRC reviewed and approved RODEX3A code is used to calculate an exposure dependent oxidation thickness that is transferred to S-RELAP5. S-RELAP5 uses this information for calculating cladding thermal conductivity which affects the initial stored energy results. However, a zero oxidation thickness is assumed to initialize the metal-water reaction rate calculation. Framatome ANP experience with regard to oxidation calculations has been that the oxidation calculated for a zero initial oxide thickness provides the largest oxidation thickness increase during the transient simulation. The results shown for maximum local and core-wide oxidation are those computed for the high temperature metal-water reaction. This is the same approach taken for Framatome ANP Appendix K methodologies.

The response to this question was initially provided in response to an RAI on the topical report EMF-2328PA, "PWR Small Break LOCA Evaluation Model, S-RELAP5 Based". The response provided and accepted by the NRC is shown below followed by some additional comments.

"The Framatome ANP methodology described in EMF-2328(P), "PWR Small Break LOCA Evaluation Model, S-RELAP5 Based," results in a conservative calculation of peak local oxidation for comparison to the 17% oxidation criteria of 10 CFR 50.46. The methodology assumes that the pre-accident cladding oxidation is zero in order to maximize the rate and extent of oxidation during a LOCA. This assumption results in higher peak cladding temperatures and higher peak local oxidation than assuming a non-zero pre-accident oxidation value.

Cladding oxidation from two sources is considered: (1) pre-accident or pre-transient oxidation due to corrosion at operating conditions, and (2) transient oxidation which occurs at high temperature during the LOCA. Pre-transient oxidation is determined by a fuel performance calculation and is a function of burnup. Over the burnup range that the fuel rod is at high power and can approach technical specification peaking limits, the pre-transient oxidation is small; however, at high burnups, pre-transient oxidation can become significant.

Transient oxidation is calculated as part of the LOCA analyses. By rule, this oxidation must be computed using the Baker-Just reaction rate equation. Using this equation, the calculated reaction rate decreases in direct proportion to the increase in thickness of the layer oxidized and increases exponentially with absolute temperature. Therefore, the transient oxidation is maximized by minimizing the initial oxidation layer which yields the highest reaction rate. The increased reaction rate produces higher temperatures which further increases the reaction rate, thus compounding the effect.

The reason that the assumption of zero pre-accident oxidation value results in a conservative calculation of peak cladding temperature and total peak local oxidation is that Framatome's calculations show that a non-zero pre-accident oxidation assumption reduces the transient oxidation by an amount greater than the pre-accident oxidation. Therefore, the maximum oxidation; i.e., the sum of both pre-transient and transient oxidation is greatest when zero pre-transient oxidation is assumed. These results apply for conditions where the transient oxidation is the dominant contributor to the total oxidation, which is the case for calculated PCTs in excess of 2000°F and for burnups at which peaking can approach the technical specification limits. These are the most limiting cases for both LBLOCA and SBLOCA.

Framatome also recognizes that conditions exist where the total oxidation is dominated by the pre-transient oxidation. This situation occurs when lower PCTs are calculated and at high burnups. For cases with low PCTs, the pre-accident oxidation becomes dominant because the transient oxidation is substantially reduced or effectively eliminated due to the low absolute temperature. For high burnups, the transient oxidation is reduced or effectively eliminated due to the inherent low power and associated low transient temperatures, and is further reduced by the presence of a significant initial oxide layer. For these cases, the maximum total oxidation is essentially equal to the initial pre-accident oxidation value. This oxidation value can exceed the value calculated using a zero initial pre-accident oxidation for these conditions; however, the total oxidation is precluded from approaching or exceeding the 17% value by the design limit on pre-accident oxidation. Framatome has a design limit on pre-transient oxidation of [] microns defined on a 95/95 basis that cannot be exceeded. This limit corresponds to [] of the thinnest cladding currently used by Framatome."

The above response is also applicable to the Realistic Large Break LOCA evaluation model. The key concept is that the metal water reaction rate models, Baker-Just and Cathcart-Pawel, are highly oxidation level dependent. If the transient starts with an oxidation level the subsequent oxidation formation is significantly reduced, the larger the initial level the more the formation of additional oxidation during the transient is reduced. The reduction of the oxidation formation during the transient then leads to a reduction in the cladding temperature since a heat source, oxidation formation, is reduced.

Decay Heat

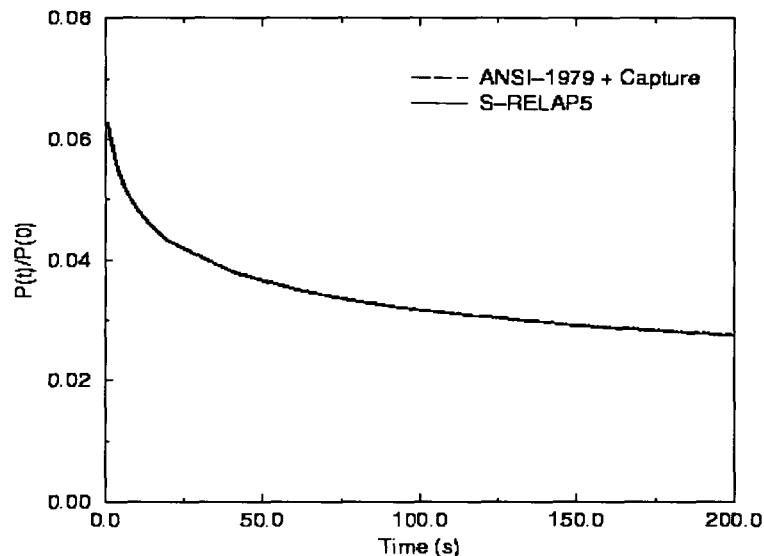
Question 29: Section 4.3.3.2.3 of EMF-2103 discusses the decay heat standard but does not show the calculated decay curve used in the analyses. Please compare the decay heat model with uncertainty applied to the ANSI/ANS-5.1-1979 standard to show that the S-RELAP5 model predicts or bounds the data in the standard for the simulation period. Include in the discussion the treatment of gamma redistribution uncertainty?

Response 29: The decay heat calculations made by the realistic LOCA methodology include contributions from (1) fission power decay, (2) power from fission product decay, (3) power from

actinide product decay, and (4) power from decay due to neutron capture in fission products. The fission power decay is computed by the reactor point kinetics model in S-RELAP5, and will be unique for each LOCA calculation; however, this term is important for only the first second or two of the LOCA transient and vanishes as the reactor fission process is rapidly shut down. The remaining decay power terms are calculated using features of the 1979 ANSI/ANS standard for decay heat, as recommended in Regulatory Guide 1.157. More specifically, the decay heat used is the ANSI/ANS-1979 "Simplified Method" using the ANSI standard tabulation. Inherent in the "Simplified Method" are the assumptions of infinite operating time at full power, all fissions from U-235, and 200 MeV/fission (conservatively low value which yields a higher fission rate—more fission products). In addition, actinide decay is included which represents about 6%-15% additional decay heat. [

] The results are a virtual overlay.

Decay Power Comparison



The distribution of the fission product decay heat source is assumed to follow the distribution of the initial operating power. Diffusion of the decay heat source due to redistribution of the gamma radiation energy is conservatively neglected in the methodology, and no uncertainty is applied due to this effect.

Assessment

Question 30: Numerous tests cited in the methodology assessment, such as FRIGG2, THTF, GE level swell, FLECHT and FLECHT-SEASET are valid under specific pressure conditions. Please clarify and discuss the applicability of the tests used in the assessment program to the ranges of conditions in which they were used. Include in the discussion the assessment of void distribution and subcooled boiling via high pressure data and the applicability of these models to low pressures.

Please discuss and justify use of the Forslund –Rohsenow correlation to determine PCT. Justification is needed to assure that errors in other models and the thermal hydraulics will not produce heat transfer coefficients that are beyond the range of the intended correlation.

Response 30: The set of assessments (FRIGG2, THTF, GE level swell, FLECHT-SEASET, etc.) define the whole test- and simulation-space for code validation. Pressure, void fraction, mass flows, etc. define these spaces as was shown in the response to Question 2. This is useful for defining the limits of a correlation or an analysis. A second purpose is the evaluation of uncertainties for dominant LBLOCA phenomena. The THTF and FLECHT-SEASET series of tests was used to cover the application ranges of the film boiling heat transfer correlations. A discussion of the role of these tests, as well as the concern of potential compensating error, has been provided in the responses to Questions #2 and #20-#23, (NOTE: the responses to these questions also address the second part of this question on the Forslund-Rohsenow correlation).

The GE level swell and FRIGG2 assessment are high pressure tests (at typical BWR full pressure). Their purpose is to evaluate void distribution, interfacial friction and subcooled boiling. The conclusions from these assessments are most relevant during the blowdown phase when pressures are still high and the primary phenomenon of interest is interfacial friction. The void distribution is dependent on both the interfacial friction and boiling models. In addition, subcooled boiling was not judged to be a relevant LBLOCA phenomenon and, consequently was not included in the PIRT.

In addition to the high pressure void distribution comparisons for the THTF and GE level swell tests, void distribution comparisons have been made for low pressure reflood tests. The void distribution comparisons for FLECHT-SEASET and FLECHT SKEWED reflood tests are represented by the calculated and measured differential pressures between 72 and 84 in. displayed in Figures 3.3.71 to 3.3.79 of EMF-2102(P) Revision 0. Note particularly that code-data agreement is excellent after the region between 72 and 84 in. is completely quenched. This demonstrates the wet-wall (pre-CHF) interphase friction model is applicable and adequate for both high pressures (THTF Tests) and low pressures.

The void fraction data for the FLECHT-SEASET tests are derived data from differential pressure measurements with assumptions and approximations made for the computation of frictional pressure losses. The derived data have to be digitized from the data report for use in comparison plots. Framatome ANP, therefore, considers the differential pressure data to be more appropriate for assessing the code performance on the void distribution. In general, the reflood process at a particular elevation roughly goes through three stages: far away from the quench front, close to the quench front and below the quench front. Since the differential pressure behaves similarly at all elevations, it is sufficient to show the code-data comparison at the hot spot (between 72 and 84 in) for all tests.

As presented in Section 4.7 of EMF-2100(P) Revision 4, the film boiling heat transfer in S-RELAP5 includes three components: convective heat transfer to steam, boiling heat transfer to liquid, and wall-to-fluid heat transfer (see also response to RAI Questions 21 and 22). Semi-theoretical correlations and models developed under specially designed configurations are used for the three heat transfer components. The separation of these components has not been done in the complex test programs used to support nuclear safety research. Specifically for FLECHT-SEASET tests, the only heat transfer data available are those for the effective heat transfer coefficient with respect to saturation temperature, i.e., heat flux divided by (wall temperature – saturation temperature). Accordingly, the film boiling heat transfer model can only be and is

validated as the collective effects of all the components. Framatome ANP has demonstrated through various assessments that the film boiling heat transfer model as a whole performs properly and adequately for the intended applications. Sufficient data does not exist and it is not necessary to analyze each individual submodel separately.

The plots of the calculated and measured differential pressures between 72 and 84 in. displayed in Figures 3.3.71 to 3.3.79 of EMF-2102(P) Revision 0 indicate that the calculated liquid fraction far above the quench front is lower than the measured. The lower accumulation of liquid at the position far above the quench front and the generally lower core inventory calculated (Figures 3.3.89 -3.3.97 of EMF-2102(P) Revision 0) are responsible for the calculation of higher clad temperatures during the temperature rise period and conservatively high PCT. The higher PCT calculated in the FLECHT-SEASET, FLECHT Skewed, and CCTF tests are due to the right reason – lower calculated liquid fraction at elevations far above the quench front.

The calculated steam temperatures are higher than the data for the two FLECHT Skewed tests and are lower than the data for the FLECHT-SEASET tests. In general, the two most important factors influencing the steam superheat are (1) net heat transfer to steam and (2) the vapor generation rate. A lower calculated steam temperature may be caused by lower heat transfer to steam or higher vapor generation rate or a combination of the two. In spite of a lower calculated steam temperature, the calculated effective (overall) heat transfer coefficient is not higher than the data during the temperature rise period, as shown in Figures 3.3.80 through 3.3.88 of EMF-2102(P) Revision 0. This is a result of the right reason, as explained in the above paragraph.

The oscillations in the calculated steam temperature comes from the interfacial area enhancement factor given in Equations (3.43) and (3.44) of EMF-2100(P), Revision 4. This is part of the droplet model changes for the post-CHF dispersed flow regime (see Pages 3-18 and 3-19 of EMF-2100(P) Revision 4). The oscillations are accounted for in the developed code heat transfer uncertainty. For this methodology there are no current plans to try to improve this model. However, development of the S-RELAP5 code will continue and this is one of the models which will be examined in this future development. This is consistent with the CSAU methodology, which indicates that one of the side benefits of applying the methodology is that it indicates the areas of the code where future development should take place.

In the development of the RLBLOCA methodology the CSAU approach was followed. As part of this approach there is a direct flow from the PIRT to the development of the assessment matrix. This flow is from the identification of the important phenomena to those experimental assessments which address these phenomena. Sufficient data is then required to develop the uncertainties for these phenomena. We believe that sufficient assessments have been performed to meet the requirements of the methodology development process that was followed.

With respect to performing additional assessments, it should be pointed out that assessments have already been performed for the FLECHT SKEWED tests 13914 and 13609. The results of these assessments are reported in EMF-2102(P) Revision 0 Section 3.3 and summarized in EMF-2103(P) Revision 0 Section 4.3.1.6. Unfortunately for the other assessments we do not have the electronic data currently available to run these assessments. The ability to obtain assessment data for this project has been one of the biggest impediments to its performance in a timely fashion. In addition, as indicated in the first paragraph, it is felt that sufficient assessments have been performed and that additional assessment are unnecessary.

S-RELAP5 uses Lahey's mechanistic subcooled boiling model to calculate subcooled boiling phenomena. The Lahey model is not based on experimental data with certain fixed ranges; therefore, its applicability is not limited to within a certain pressure range. As it is pointed out in Section 3.10 of EMF-2102(P) Revision 0, strong subcooled boiling phenomena are present in 10 out of the 27 tests considered. The assessment was performed partly in response to ACRS' concern about whether S-RELAP5 produces a correct void distribution curve shape for subcooled boiling. The assessment is included in EMF-2103(P) Revision 0 to demonstrate the S-RELAP5 code's general capability to properly calculate the void distribution in heated rod bundles for void fractions up to around 80% under the pre-CHF (wet wall) flow conditions, including subcooled boiling. For LBLOCA events, the pre-CHF flow regime and the subcooled boiling occur below the quench front for the rod bundle geometry and have little or no effect on the temperature rise and PCT. Furthermore, the comparison plots of differential pressure in Figures 3.3.71 to 3.3.79 of EMF-2102(P) Revision 0 show that the void fraction below the quench front is well calculated. This demonstrates the capability to calculate the pre-CHF flow void distribution under low pressure conditions.

The GE level swell test was performed to evaluate S-RELAP5 capability to predict transient void fraction conditions. The assessment was included in the Realistic LOCA model submittal because it demonstrates the S-RELAP5 code capabilities to predict this behavior. The pressure is within the 2200 psi to atmospheric range encountered during the PWR LBLOCA. No uncertainties were derived from this assessment. Use of S-RELAP5 is not limited to LBLOCA, and the conditions of this assessment are more applicable to SBLOCA. This same assessment was presented and referenced in support of the use of S-RELAP5 for the SBLOCA methodology.

Framatome ANP does not use FLECHT Skewed Tests 13609 and 13914 in the uncertainty analysis and the calculation of the film boiling heat transfer coefficient multipliers. The FLECHT-SEASET assessments performed were selected to cover the range of possible PCT's. Figure 5.3 of EMF-2103(P) shows that the PCT values for the 59 cases ranges from 1000°F to 1700°F.

THTF and GE level swell data are for the pre-CHF (wet wall) flow regime. The wet wall flow regime does not play a significant role in LBLOCA. As indicated previously, the FLECHT-SEASET differential pressure code-data comparisons show that the S-RELAP5 code does very well in calculating the void distribution in the pre-CHF regime under low pressure.

Long-Term Coolability

Question 31: *Please discuss how the Framatome-ANP RLBLOCA methodology addresses the element of long-term coolability as required in the regulatory acceptance criteria.*

Response 31: The analysis of a LOCA is continued until the cladding temperature at all locations in the core is decreasing, and the fluid level in the core is rising. At this time, the path to long-term cooling is established. The fluid within the core will continue to rise and the cladding at all elevations quench without further excursions. Once quenched, the core is maintained within a few degrees of the coolant temperature through a continuous flow of water maintained by the ECCS.

Procedures have been established and approved by the NRC for the smooth transition to long-term cooling during which water is recirculated from the reactor building sump through a heat exchanger to the reactor vessel. For hot leg breaks, the establishment of recirculation is the

final requirement for long-term stable cooling. For cold leg breaks, however, coolant supplied to the vessel may not flow to the core. In the most severe case, the core continues to boil for an extended period and only sufficient water to make up for the boiloff is actually passed to the core. Boiling, without throughput of water, will concentrate boric acid. To prevent the crystallization of boric acid within the core, a throughput flow is assured by operator action. The final computation is to demonstrate that this action is timely, assuring the effective establishment of long-term cooling.

The plant licensing basis includes an evaluation of long-term cooling. The evaluation is only repeated if the change being made has an adverse impact on long-term cooling.

Question 32: *Please describe the methods and analyses that will be employed to demonstrate that boric acid precipitation is assessed or neglected in the methodology.*

Response 32: Since all ECC systems inject borated water, salts could build up, precipitate, and block core channels during long-term cooling. To prevent this, operator action is taken to establish a flow of water through the core regardless of the type or location of the break. A simple concentration calculation that assumes boiling at the decay heat rate and no core throughput (water passed through the core) is made from the initiation of the event to the time of operator action. The concentration calculated must be shown to be below the saturation limit of boric acid for the core conditions. The rate of concentration at the time of operator action is shown to be less than the loss of boric acid caused by the throughput flow. This assures that the concentration will thereafter decrease.

The plant licensing bases include an evaluation of the potential for boric acid precipitation. The evaluation is only repeated if the change being made has an adverse impact on the potential for boric acid precipitation.

Entrainment and 2-D Effects

Question 33: *The S-RELAP5 liquid entrainment predictions overpredict the data by a factor of 2 for the FLECHT-SEASET and skewed tests. However, S-RELAP5 overpredicts the clad temperatures at the upper elevations. Please discuss this apparent anomaly and also discuss the capability of the 2-D model in S-RELAP5 simulate the super heat near the wall and account for the radial steam temperature profile across the channel in the tests.*

Response 33: (Information relative to this question is also provided in the response to Question 71a.) The comparison plots for liquid carry-over are not the best indicator for liquid entrainment. The mass in the test section is a better indicator for liquid entrainment because the data and the calculation clearly represent the same thing. Figures 3.3.89 through 3.3.97 of EMF-2102(P) Revision 0 provide comparisons of the calculated and measured mass in the test section for the analyzed FLECHT-SEASET and FLECHT SKEWED tests. While Figure 3.3.89 for test 31805 shows good agreement between the measured and predicted mass in the test assembly, all of the other plots clearly show that the S-RELAP5 predictions have less mass in the test assembly through the time of PCT. It is estimated that this underprediction of mass in the test assembly is from 0 to 20%. In addition, as discussed in the response to Question 71a, the calculated liquid fraction is less than the data at elevations sufficiently above the quench front. This is shown in the code to data comparisons of the differential pressure near the 78 in elevation, and the result of the code calculating the lower liquid fractions is higher rod temperatures.

The nodalization used for the FLECHT-SEASET and FLECHT SKEWED tests is one-dimensional, as discussed in Section 3.3.5 of EMF 2102(P) Revision 0. The tests were not modeled as a 2D component since the FLECHT-SEASET tests have a uniform radial power profile and the radial power distribution is roughly uniform for FLECHT SKEWED tests.

This question refers to film boiling assumptions applied in the prediction of heat transfer in this regime. The heat sink temperature assumed by S-RELAP5 is the film temperature calculated as the average of the wall and saturation temperatures. The assumption of average hydraulic volume properties will contribute to the code uncertainty for film boiling; however, this is an independent contributor to uncertainty that is directly captured in the uncertainty analysis.

Void Fraction

Question 34: *Page 4-97 discusses T_{min} but does not describe the conditions as to how the correlation is applied in the code. Please discuss and justify the effect of void fraction on the application, effect of its exclusion, and the application of T_{min} in the Framatome-ANP RLBLOCA methodology.*

Response 34: The technical discussion on the implementation of the T_{min} model can be found in Section 4.7 in the S-RELAP5 Models and Correlations Code Manual (EMF-2100). Basically, when $T_w < T_{min}$, the heat transfer mode is selected based on the larger of the heat fluxes from transition and film boiling. [

] The S-RELAP5 T_{min} model does not have an explicit dependency on void fraction. The most often referenced T_{min} model was developed for the TRAC code. That model is presented as a best-estimate model and is functionally dependent on pressure (Berenson model). Void fraction is highly correlated with pressure; hence, modeling the pressure dependence will compensate for some effects of void fraction. The uncertainties determined for the S-RELAP5 T_{min} model remove the need to treat pressure and material type by basing the uncertainty on a bounding data set as mentioned in Section 4.3.3.2.6 of EMF-2103. A more rigorous treatment was judged to be unnecessary based on sensitivity studies that showed that variations in T_{min} have a minimal effect on PCT and oxidation.

The T_{min} of [] K used in the plant applications is extremely conservative for the early blowdown quench. Consequently, no early blowdown quench is calculated. Therefore, T_{min} does not affect the stored energy at the end of blowdown.

All of the reflood test assessments indicate that the temperature rise period and the PCT depend strongly on the film boiling heat transfer and are relatively insensitive to the quench times. Furthermore, the calculated quench times for FLECHT-SEASET and CCTF low reflood tests are mostly later than the data, regardless of what void fraction is calculated at the onset of quench. It should also be pointed out that in S-RELAP5 the onset of quench requires two conditions: (1) surface temperature must be below T_{min} and (2) transition boiling heat transfer rate must exceed the film boiling heat transfer rate.

Question 35: *Page 5-2 of EMF-2103 states that "the plant process parameters are treated statistically, however conservative methods also can be used in the absence of adequate data to support the statistical use." Table 5.1 also does not indicate the following parameters. Please discuss which have been treated statistically and which conservatively in the methodology.*

Initial Conditions:

*RCS Temperature
Accumulator line resistance
Safety Injection Temperature
Peripheral Assembly Power (how is this bounded)*

Also please discuss how the following model uncertainties are handled and/or justify their omission from the analysis:

*Broken nozzle resistance, K-factor
Broken loop pump resistance
Condensation
Fuel conductivity (before and after burst)
Fuel density (packing fraction after burst)
Rod internal pressure
Cladding burst temperature
Cladding Burst Strain and average strain
Metal/Water Reaction*

Since different plant designs will have different values and ranges for many of the parameters in the above lists, will the various parameters be identified in the plant-specific submittals giving the distributions or conservative limits?

Response 35: [

1

Included in EMF-2103 Revision 0 Section 5 is a sample problem presenting results from a 4-loop Westinghouse PWR. As part of the discussion, Table 5.7 is provided showing an example of the coverage of specific plant process parameters used in a RLBLOCA analysis.

Question 36: *Please discuss the procedures which will be used to insure that the range of conditions in the plants for which the Framatome-ANP RLBLOCA methodology is used are consistent with those in the test programs used to assess the code and determine the code uncertainties.*

Response 36: In the CSAU methodology, the intent is to develop a PIRT which defines the phenomena which are important for the transient event and plant types being considered. From this PIRT an assessment matrix is defined to address the defined important phenomena. Thus, the assessment matrix is intended to cover the ranges of the important phenomena for the transient event and plant types. However, in practice there is generally insufficient applicable test data to fully cover all possible ranges for all important phenomena. Framatome ANP believes that a sufficient data range has been covered by the test matrix presented in Tables 4.2 and 4.3 of EMF-2103(P) to support application of the methodology to the LBLOCA transient for W 3 and 4-loop plants and CE 2x4 loop plants. Based on the provided PIRT, heat transfer, break flow, and ECCS bypass (described by multiple downcomer phenomena) are the dominant phenomena influencing clad temperature response in a LBLOCA. The primary components of these phenomena are either treated statistically or conservatively and are specifically discussed in either the RLBLOCA methodology document (EMF-2103) or the S-RELAP5 Code V&V document (EMF-2102). In addition, a detailed analysis of specific plant results vs the assessment matrix ranges has been provided for the primary heat transfer modes in the response to RAI #2.

Question 37: *Fig. 4.4 shows the leakage paths connecting from the upper head to the upper downcomer. Please discuss the effect of the geometry, resistance and flow rates through these junctions on the LBLOCA response expected in the plant designs for which the methodology will be used. Specifically, what is the impact of modeling this leakage on blowdown temperatures and PCT?*

Response 37: The leakage flow paths shown correspond to flow holes drilled in the plate between the upper downcomer and the upper head in Westinghouse design plants. It is believed that the original intent of the design was to provide a small coolant flow through the upper head region to cool components in or connected to this region. The flow holes exist and their dimensions are well known. Plants can often provide data on upper downcomer to upper head bypass flow. This information is used during input model development for calculating the flow resistance that provides the expected bypass. The uncertainty of this bypass is considered to be small and it has been judged to have a minor influence on PCT and oxidation.

The dominant PIRT phenomenon associated with this leakage flow is the fluid temperature in the upper head region. The upper head contains a significant amount of liquid and the path of least resistance for this liquid during the LOCA is downward through support or guide tubes to the top of the core and possibly into the core where it can provide significant cooling. The temperature of the upper head fluid determines when this fluid reaches saturation pressure and begins to flash thus providing the driving force for flow to the core and upper plenum.

PCTs have been shown to be sensitive to upper head temperature perturbations in sensitivity studies. [

]

The major PIRT-related phenomenon of concern is core flow stagnation which is closely associated with upper head temperature. Once the steady-state condition has been established, the relatively small leakage that occurs between these components is not expected to impact clad temperatures. If for a given plant, this leak path has some unique dynamics, this will be modeled on a plant-specific basis.

A relatively simple bypass model is used for leakage between the downcomer and the upper head. A junction is applied from the upper head to each radial sector in the downcomer using a code calculated flow area option. This produces a relatively large flow area. Loss coefficients are then tuned to the plant supplied bypass fraction. Ultimately, this bypass along with flow from the exit of the core and/or upper plenum provide the conditions to tune the steady state upper head temperature for the specific plant. The rather large bypass flow area provides essentially no momentum flux between these volumes and is necessary to avoid Courant limiting conditions in adjacent fluid volumes.

Question 38: *Fig 4.7 shows four half assemblies surrounding the hot assembly. Please discuss the use of [] assemblies versus [] assemblies since the power level of these adjacent assemblies would affect the thermal conditions and cross flow in these outer assemblies. A comparison of the effect of this modeling on blowdown temperatures and PCT would be helpful.*

Response 38: [

]

Question 39: *Please provide the nodalization sensitivity study results used to arrive at the upper plenum and core nodalizations shown in Figs. 4-4 through 4-8. Please discuss the level of nodal detail needed to show PCT convergence. Also discuss how the alignment of key leakage paths influences the chimney effects observed in the upper plenum studies and noted in Table A.2.*

Response 39: Nodalization convergence of the upper plenum is difficult to demonstrate because of the need for multi-dimensional thermal-hydraulics and the inherent asymmetry of the structure. For this reason, the approach taken in establishing the nodalization guidelines for the reactor vessel internals was to examine possible options and choose the most conservative configuration. The most important characteristics of nodalization is that it captures the dominant phenomenological characteristics and that it accurately describe the structure while ensuring practical runtimes. In the upper plenum the key LBLOCA parameters are liquid fallback and carryover. [

]

[

]

Question 40: *Please discuss the sensitivity of PCT to the cross flow resistance in the core and how are these resistances are calculated.*

Response 40: The cross flow resistances in the core have been judged to have low importance on PCT and, for this reason, have not been included in the PIRT given in Table 3.4 of the methodology document (EMF-2103). The Westinghouse Flow Blockage tests were used to assess S-RELAP5's capability at predicting cross flow using the TWODEE component applied where two-dimensional hydraulic modeling is necessary. This assessment is documented in Section 3.13 of EMF-2102.

EMF-2054 does reference a proprietary method (EMF-2328(P)(A)) for calculating cross flow resistances across rod bundles. The formulation for cross flow resistances in the core is the same as that currently used in Framatome ANP's NRC-approved SBLOCA methodology. [

]

Question 41: *Reg. Guide 1.157 states that "A distinction from, and transition to laminar convection (i.e. $Re < 2000$) should be made, with a value of the laminar heat transfer for rod*

bundles that is appropriate for the applicable bundle geometry and flow conditions.” Please discuss how the models in Section 4.0 of EMF-2100 meet Reg. Guide 1.157. Also, does the heat transfer model for single phase vapor which considers the Sleicher-Rouse correlation and a separate natural circulation correlation result in the appropriate heat transfer for Re numbers less than 10,000 since the lower limit for this correlation is 10,000 (page 4-115, EMF-2103)? Please discuss the use of the Sleicher-Rouse correlation and the steam cooling model for transition and laminar flow.

Response 41: The methodology addresses the Reg. Guide 1.157 requirements implicitly in the correlations applied for single-phase heat transfer which are described in Sections 4.2 and 4.5 of EMF-2100(P). The correlation for single-phase liquid heat transfer at very low flows is the maximum of the Dittus-Boelter correlation and the laminar flow correlation. S-RELAP5 uses a Nusselt number of [] for forced convection in the laminar region. EMF-2100 references the COBRA/TRAC code; however, it has its origin with work first presented in Rohsenow and Choi's *Heat, Mass, and Momentum Transfer* (1961) and also presented in Tong and Weisman's *Thermal Analysis of PWRs* (1996). For laminar flow around a cylindrical rod, the minimum Nusselt number has been derived as 4.0. However, in a rod bundle this is dependent on the pitch-to-diameter ratio. For most fuel assembly designs for PWRs, this ratio is about 1.3. At these dimensions the laminar flow heat transfer Nusselt number is bounded by the value of [] used in S-RELAP5.

The Sleicher-Rouse correlation is a composite of a turbulent correlation and laminar correlation. The laminar component is simply $Nu(lam) = 5.0$. This is less than the [] value expected for laminar flows in typical PWR rod bundle geometries; however, the turbulent component is applied for the full range of Reynolds number. To address the turbulent Reynolds number range below 10000, the Sleicher-Rouse correlation was assessed using the 161-rod bundle FLECHT-SEASET Steam Cooling Tests. Figure 41.1 shows that S-RELAP5 (i.e., Sleicher-Rouse) conservatively estimates heat transfer in this Reynolds number range. [

] To address the laminar range, the coincident periods of laminar forced convection from LOFT, Semiscale, FLECHT-SEASET and CCTF test were evaluated to validate the applicability of the correlation. Code-to-data comparisons during these periods show similar clad temperature responses with the code generally predicting higher clad temperature increases. This trend is consistent with best-estimate to conservative prediction of single-phase vapor heat transfer in the laminar flow range. [

]

**Figure 41.1 Calculated to measure single-phase vapor heat transfer
for low Reynolds numbers**

Question 42: *How does the critical flow model address Reg. Guide 1.157, Section 3.4.1.1 items b and c?*

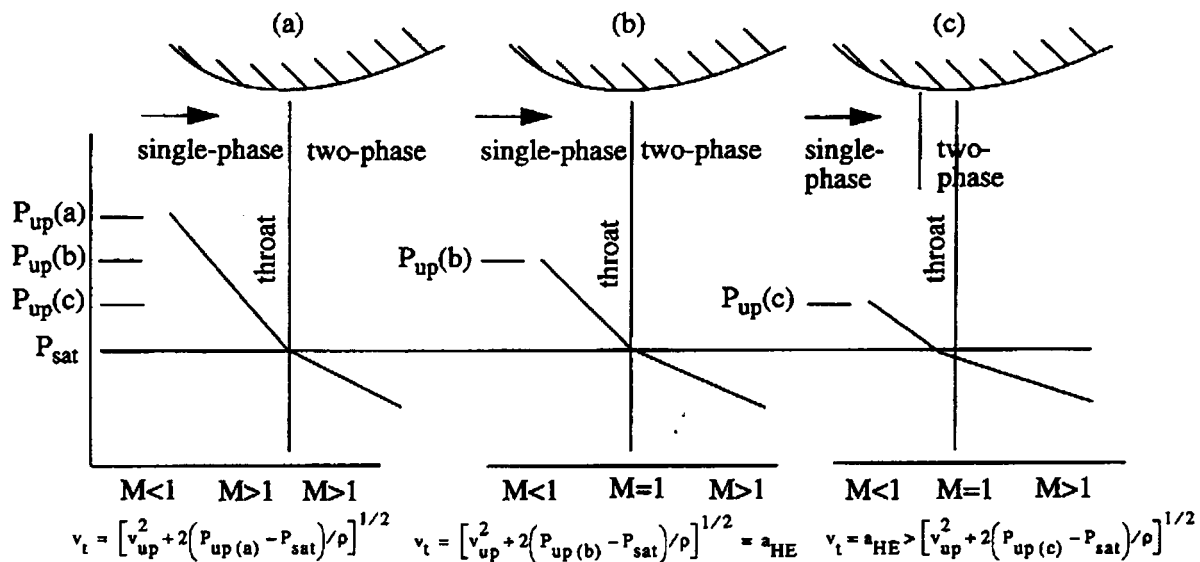
Response 42: (Additional discussion of the S-RELAP5 critical flow model is given in Response to Question 58 and 61.) Item b states "Recognize thermal nonequilibrium conditions when the fluid is subcooled." A subcooled critical flow model based on Almagir-Lienhard-Jones correlation for the onset of vaporization is implemented in S-RELAP5 (see Section 5.1.2.1 of EMF-2100(P) Revision 4) to handle the thermal non-equilibrium conditions when the fluid is subcooled.

Item c states "Provide a means of transition from nonequilibrium to equilibrium conditions." A transition region is set up to bridge the subcooled non-equilibrium conditions to the two-phase equilibrium conditions (item c). The transition from the subcooled model to the two-phase HEM model is discussed in Equations (5.50) to (5.52) of EMF-2100(P) Revision 4. The basic design is to smooth the rapid change in magnitude of the critical mass flow rate and to take care of the under prediction of mass flow rate at very low quality by the HEM critical flow model.

The S-RELAP5 critical mass flow rate is evaluated using the equation of state at the throat. The equation of state at the throat is derived from the flow and (non-equilibrium) state conditions at the volume center, assuming complete mixing of liquid and vapor phase at the throat. The resultant equation of state at the throat can be single phase (subcooled) liquid (equilibrium quality less than or equal to 0), two-phase liquid and vapor mixture (equilibrium quality between

0 and 1), or single phase vapor (equilibrium quality greater than or equal to 1). The critical flow for subcooled liquid is calculated by the Bernoulli equation with pressure undershoot at the throat given by the Alamgir-Lienhard-Jones correlation (Section 5.1.2.1 of EMF-2100(P) Revision 4). The HEM critical flow model is applied when the state at the throat is a two-phase mixture (equilibrium quality between 0 and 1).

The transition from subcooled choking to two-phase choking can be pictorially represented, using the saturation pressure (P_{sat}) as onset of vaporization, in three stages as follows:



(see Section 5.1.1.2 of EMF-2100(P) Revision 4 for a detailed discussion.) In the code, a transition region between single phase subcooled and two-phase choking is set up and an interpolation scheme is used to calculate the critical flow. The transition region is extended sufficiently far into the two-phase region to approximately account for the under prediction of mass flow rate at very low quality by the HEM critical flow model. An under-relaxation scheme is applied in the transition region to further smooth the solution (see Equation (5.53) of EMF-2100(P) Revision 4).

The critical mass flow rate for single-phase steam is calculated based on the well-established formulation for single phase sound speed (see Response to Question 58). The discontinuity between the two-phase HEM sound speed as quality approaches 1 and the single phase steam sound speed is not significant; therefore, special treatment is not needed for the transition from two-phase to single phase steam.

Question 43: *How does the frictional pressure drop model address Reg. Guide 1.157 item 3.6.1, which states: "A model for frictional pressure drop to be used in ECCS evaluations should: b) be consistent with models used for calculating gravitational and acceleration pressure drops. If void fraction models or correlations used to calculate the three components of the total pressure drop differ from one another, a quantitative justification must be provided?"*

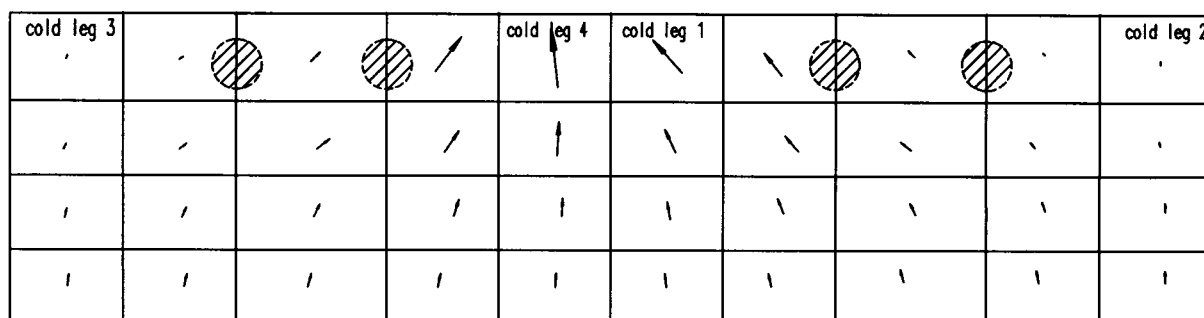
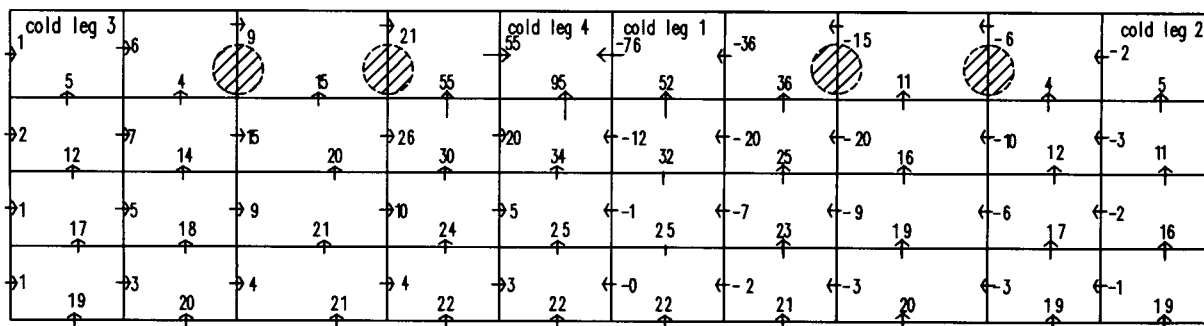
Response 43: The pressure drops from friction, gravitation and acceleration are calculated consistently through the basic fluid field equations. There are no separate correlations used for computing the gravitational and acceleration pressure drops. The frictional pressure drop is computed from the correlations based on experimental data since it is well recognized that the frictional pressure drop is too complex to calculate from first principles.

Question 44: *How does the post CHF heat transfer model address Reg, Guide 1.157? Item 3.9.1 b), which states a post-CHF flow model should "recognize effects of liquid entrainment, thermal radiation, thermal non-equilibrium, low and high mass flow rates, low and high power densities, and saturated and subcooled inlet conditions?"*

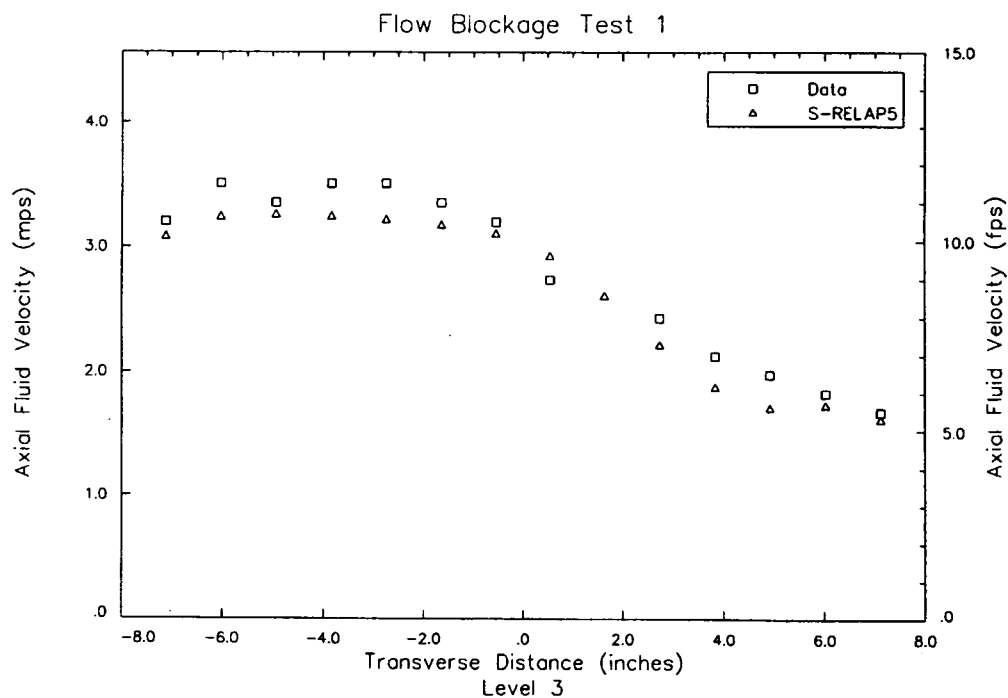
Response 44: The applicability of the post-CHF heat transfer model is presented in the Response to Question 2. The liquid entrainment is treated through the interphase friction package. The wall-fluid radiation is explicitly modeled. S-RELAP5 is a two-fluid, non-equilibrium system code and the heat transfer to two phases at different temperatures is explicitly modeled. All correlations are functions of local conditions (i.e., parameter values at the same location). The dependent parameters for the post-CHF correlations are usually void fraction, phasic density, phasic temperature, phasic thermal conductivity and heat capacity, Reynolds number, mass flow rate, hydraulic diameter, droplet diameter and etc. The location conditions are affected by the inlet conditions, power distributions, and parameter values at other locations. Therefore, the mass flow rate, power density and inlet conditions are either explicitly included or implicitly treated in the post-CHF heat transfer modeling. Test data of various power distributions and different inlet conditions are used to validate the applicability and capability of the model.

Question 45: *To understand the two-dimensional model behavior, please show the results of a test problem to verify the convection of lateral momentum by the vertical velocity. A simple ring noding problem can be developed that represents the flow from a downcomer and a break in a hot leg which shows flows for both vapor and liquid.*

Response 45: There is a two-dimensional gas velocity profile shown on Page 5-50 of EMF-2100(P) Revision 4. The profile is reproduced in the following.



Also, in Section 3.13 of EMF-2102(P) Revision 0, there are a number of plots (Figures 3.13.6 to 3.13.11, 3.13.13 to 3.13.18, and 3.13.20 to 3.13.25) showing the axial fluid velocity vs. transverse distance. Shown below is an example of the figures.



The above two sets of figures demonstrate that under single phase conditions, where the numerics is not affected by the interphase friction model, S-RELAP5 produces correct two-dimensional flow patterns, either as expected or in good agreement with the data. Examples of the two-dimensional flow solution for two-phase are given and discussed in the response to Question 122.

Question 46: *Anomalous flow circulation has been shown to develop, for example, between parallel pipes, that are of a numerical nature and cannot easily be corrected without the aid of additional form losses (see Proceedings of ICONES, 8th International Conference on Nuclear Engineering, "Recirculating Flow Anomaly Problem Solution Method," D. Lucas, April 2-6, 2000, paper # 8479). Please discuss the capabilities of S-RELAP5 with regard to the sample flow problem presented in this paper and steps to resolve this anomalous flow behavior potential. In addition, discuss whether or not the new 2-D model introduces these numerical anomalies as seen in 1-D formulations.*

Response 46: One of the purposes of implementing the two-dimensional numerics in S-RELAP5 is to prevent the anomalous flow behavior between parallel pipes. In hundreds of assessment and plant calculations, no recirculating flow anomalies are observed in the two-dimensional nodalizations. The 2-D model was developed explicitly to be used in the simulation of downcomer regions and the core region. Consistent with the design of the model, it has been assessed using data from downcomer and core tests. The 2-D model applied in the downcomer applications was assessed using data from the full scale UPTF Test 6. The 2-D model as used in the core was assessed using data from flow blockage tests. The results of those comparisons were discussed in EMF-2102 and EMF-2103.

Figure 46.1 shows the nodalization for the recirculating flow anomaly problem from the input deck supplied by NRC. Volume 710 is a time-dependent volume, representing the ECC source. Junction 711 is a time-dependent junction, providing the ECC injection into Volume 175. Junctions 17501 and 17502 connect two parallel volumes (pipes), Volume 160 and Volume 130. Volume 715 is another time-dependent volume which served as the sink for the system. All volumes are vertically oriented. Except for Volume 710, all volumes are initialized with liquid at 2200 psia and 550°F.

In the original problem (base case), the condition for the ECC source volume 710 is liquid at 2200 psia and 90°F. The 90°F cold water is injected into Volume 175 at a rate of 96 lbm/sec through Junction 711. Figure 46.2 shows the flow distribution into the two parallel pipes. After the cold water enters Volume 175, the water in Volume 175 becomes colder than the water in the two pipes (i.e., Volume 130 and 160) below. The tendency for the cold water to move down and warm water to move up produces the initial period of recirculation flow pattern. Eventually, the flow becomes steady to an asymmetric pattern with all water flowing into one pipe and none flowing into the other pipe. The initial recirculating flow pattern establishes the density difference between the two pipes (Volume 160 and Volume 130). The gravity head difference from the density difference balances the pressure difference for the flow and the final flow becomes asymmetric: the flow rate at Junction 17502 is 96 lbm/sec and that at junction 17501 is zero, i.e., all cold water flows into the Volume 130 and none into Volume 160. The asymmetric solution is physically possible due to the small flow rate and the temperature difference present in the system.

To further explain the phenomenon exhibited in the base case calculation, three sensitivity calculations were performed. In the first sensitivity calculation, the injection rate is unchanged

(i.e., 96 lbm/sec), but the ECC temperature (Volume 710 temperature) is set at 550°F, same as the rest of the system. Shown in Figure 46.3 is the flow distribution for this calculation. There is no initial recirculation period and the flow is evenly split: each of the two junctions, 17501 and 17502, has a flow rate of 48 lbm/sec. Thus, if there is no temperature difference between the injection water and the water in the rest of the system, the asymmetric flow pattern will not occur.

In the second sensitivity calculation, 90°F water is injected into Volume 175 at a rate of 300 lbm/sec. Figure 46.4 shows the results for this case. Again, the initial period of recirculation is not present and the flow is symmetric. This demonstrates that the asymmetric solution is not possible if the injection rate is sufficiently high to overcome the thermal head.

For the third sensitivity calculation, the ECC temperature is at 90°F and the injection is at 300 lbm/sec for the first 200 seconds and then reduced to 96 lbm/sec for the rest of the time. Figure 46.5 shows the flow pattern for this case. During the first 200 seconds of the transient, the flow rate is equal into the two parallel pipes, each having 150 lbm/sec. Also the temperature of the system excluding the ECC source volume is reduced from 550°F to close to 90°F at the end of the first 200 second period. When the flow rate is reduced to 96 lbm/sec after 200 seconds, a small recirculation occurs for a short time period. However, the temperature imbalance is not large enough to produce permanent asymmetric flow and the flow becomes equal in the two directions at about 1200 seconds into the transient. These three cases demonstrate that the symmetric steady flow pattern for the parallel pipes can be obtained under suitable conditions.

Finally, an additional calculation was made to demonstrate the effect of replacing the parallel pipes by a 2-D component. In this case, Volume 160 and 130 are replaced by a 2-D annulus (TWODEE-A) component, similar to the nodalization used for a downcomer. The 2-D component has 6 axial levels and 2 azimuthal sectors. The two azimuthal sectors are identical and have the same flow area as that for the parallel pipes. The total length of the six axial levels is equal to the length of Volume 130 (or 160) in the base input deck. All volumes excluding Volume 710 are set at 2200 psia and 550°F at the beginning of the transient. The ECC source volume (Volume 710) is at 2200 psia and 90°F at all times. Figure 46.6 shows the flow distribution with the 2-D component. The slow injection of cold water on top of warm water still produces an initial recirculating flow pattern, similar to that for the parallel pipes. The recirculation ceases at about 1200 seconds and the flow becomes evenly distributed. Thus, the difference between the 2-D component and the parallel pipes is that the steady state flow is symmetric for the 2D component and is asymmetric for the parallel pipes.

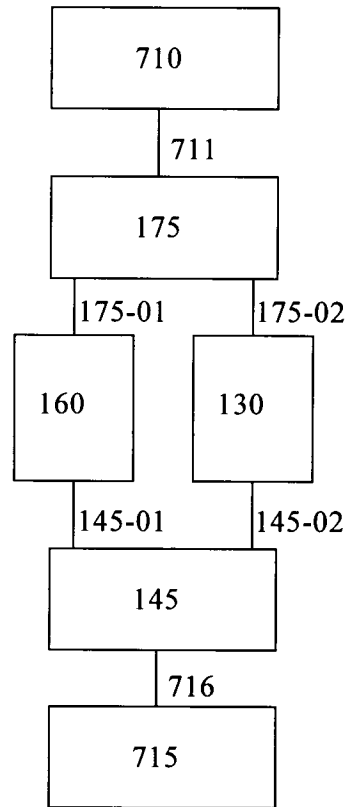
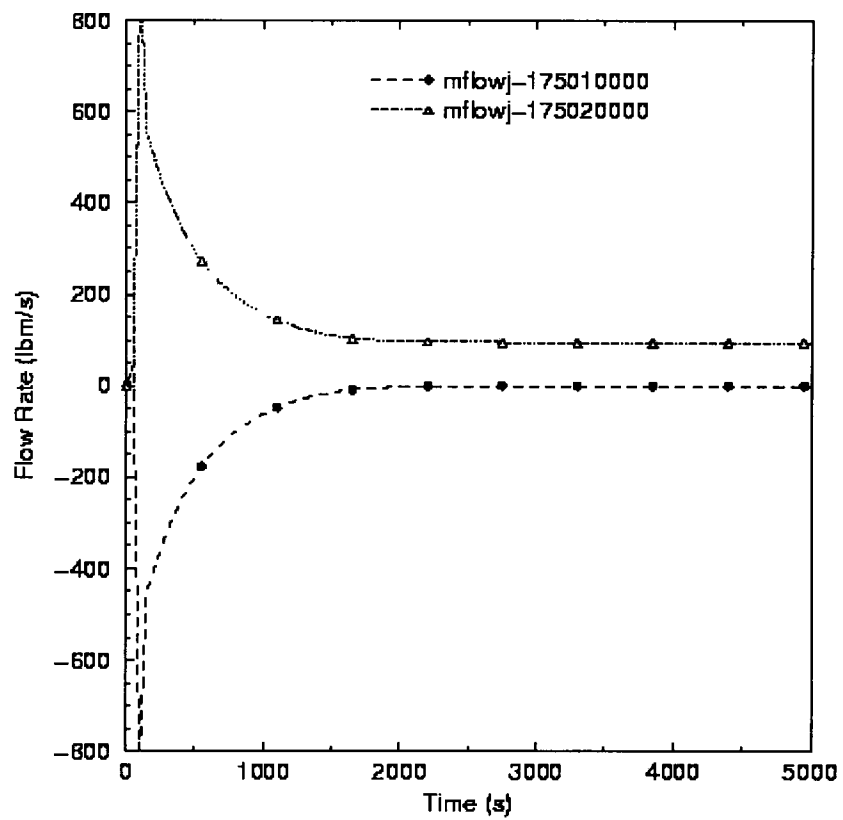
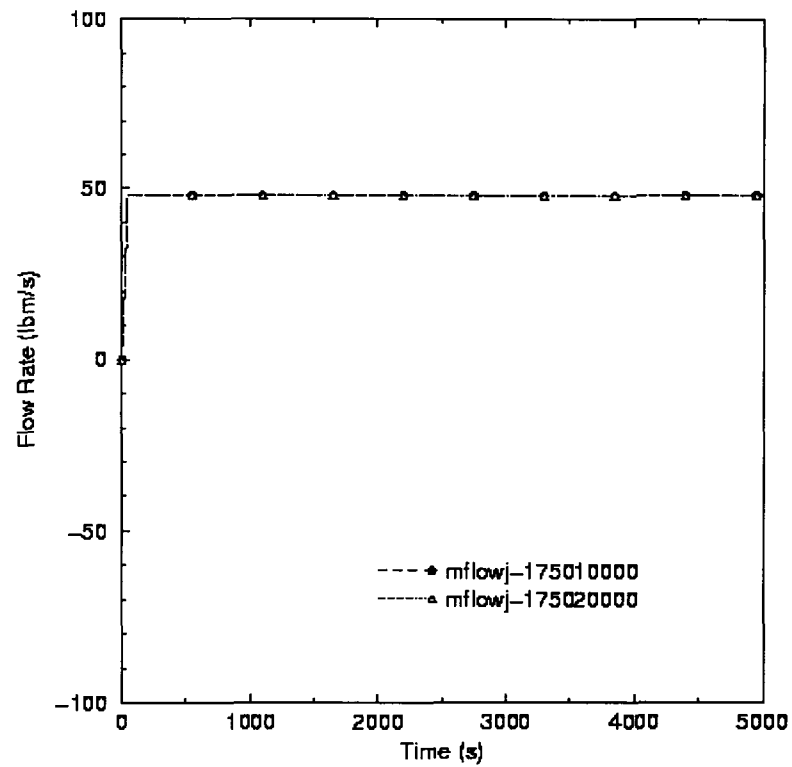


Figure 46.1 Sketch of Nodalization



**Figure 46.2 Flow Split for the (base) Case of Cold Water (90 F)
Injecting into Volume 175 at 96 lbm/sec**



**Figure 46.3 Flow Split for the Case of Warm Water (550 F)
Injecting into Volume 175 at 96 lbm/sec**

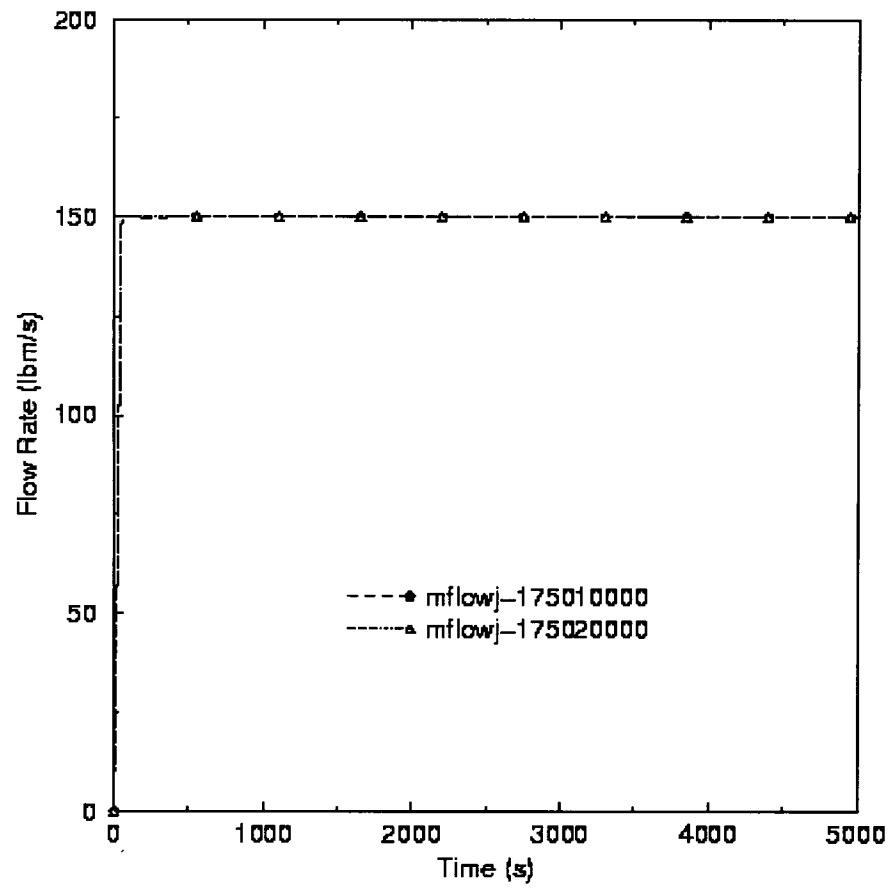


**Figure 46.4 Flow Split for the Case of Cold Water (90 F)
Injecting into Volume 175 at 300 lbm/sec**

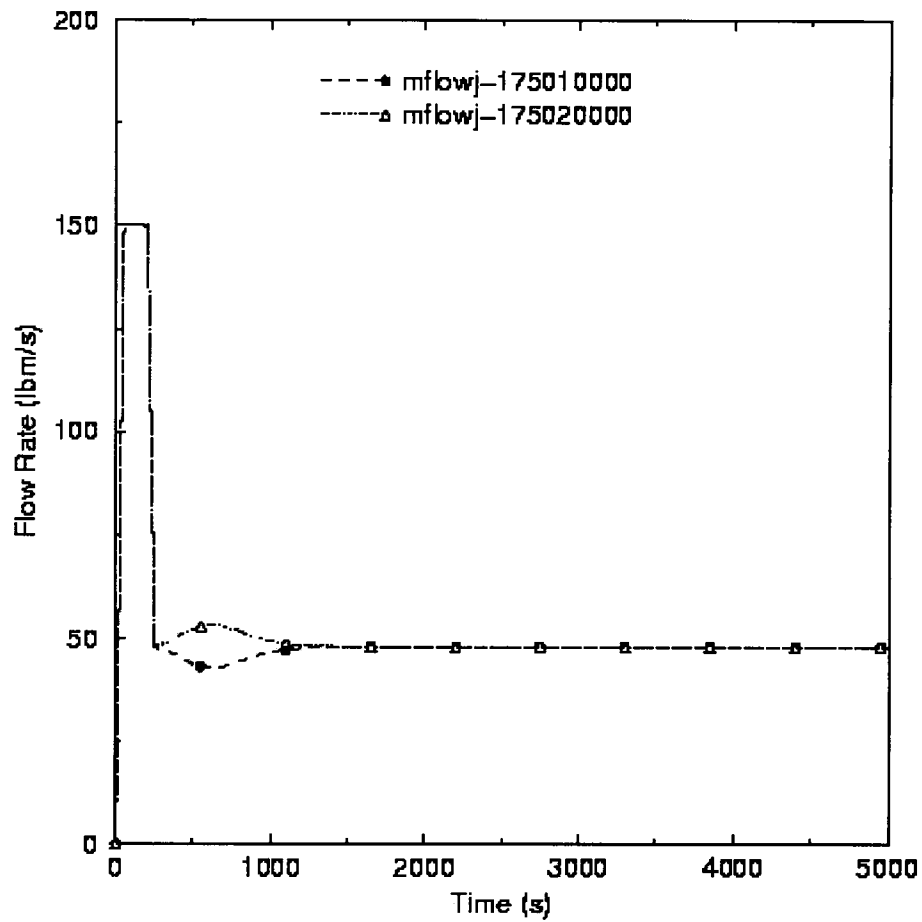


Figure 46.5 Flow Split for the Case of Cold Water (90 F) Injecting into Volume 175 at 300 lbm/sec for the First 200 sec and at 96 lbm/sec for the Remaining Time

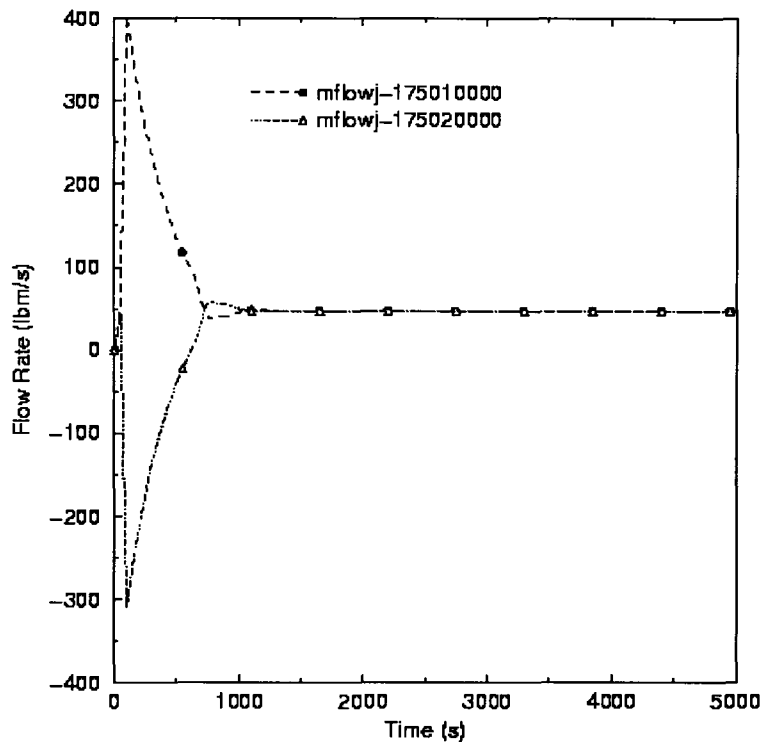


Figure 46.6 Flow Split for the Case of Cold Water (90 F) Injecting into Volume 175 at 96 lbm/sec with the Parallel Pipes Replaced by a 2-D Component

Question 47: Recent reviews of thermal-hydraulic analysis computer codes have questioned the accuracy of momentum flux terms such as given by Eq. 2.116 in EMF-2100. Please provide and discuss:

-The numerical form of the momentum equations in S-RELAP5 their reduction to the Bernoulli "type" equation,

-The S-RELAP5 calculated Bernoulli expression versus flow channel cell number for a 1-D and 2-D pipe with and without a contraction and an expansion. A simple problem can be defined having a constant flow area and variable flow area and elevation change with the pressure, kinetic, and potential energy terms calculated by S-RELAP5 for both vapor and liquid.

-Application of S-RELAP5 to the Ferrell-McGee data for flow through a pipe with expansions and contractions. (see Ferrell, J. K. and McGee, J. W. , "Two-phase Flow through Abrupt Expansions and Contractions", TID-23394, 1966.)

Response 47: The momentum flux terms are described in the fluid field equations as

$$\mathbf{v} \cdot \nabla \mathbf{v} \quad (47.1)$$

For a 1-D pipe, the flux terms are of the form:

$$v \frac{dv}{dx} = \frac{d}{dx} \left(\frac{1}{2} v^2 \right) \quad (47.2)$$

Expressing in the finite difference form over a momentum cell j connecting Volume K and L, the above equation becomes

$$\frac{1}{2} \frac{v_L^2 - v_K^2}{\Delta x_j} \quad (47.3)$$

where the subscripts K and L denote the “volume” velocities at the centers of Volume K and L, respectively, and Δx_j is the length (straight line distance) between the two volume centers. The volume velocities are defined in Equations (2.106) through (2.108) of EMF-2100(P) Revision 4. In a semi-implicit scheme, the volume velocities are evaluated at the old time (n -th time-step). The expression (47.3) is unstable. Consequently, the flux terms are approximated by a donor-like formation:

$$\frac{1}{2} \left(\frac{1}{\Delta x_j} \right) \left[\dot{v}_L^n v_L^n - \dot{v}_K^n v_K^n \right] \quad (47.4)$$

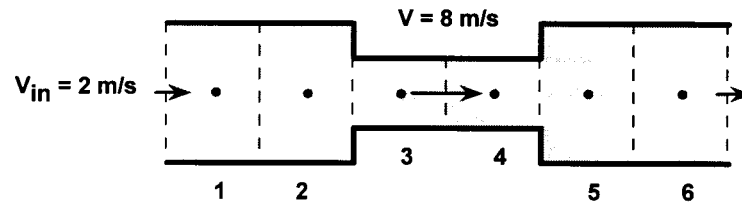
The donor-like velocity \dot{v}_L^n is the velocity at the outlet side of Volume L if v_L^n is positive and is the velocity at the inlet side of Volume L if v_L^n is negative (see Equations (2.117), (2.106) and (2.107) of EMF-2100(P) Revision 4). The expression (47.4) is a hybrid of central difference and upwind difference, and is equivalent to the momentum flux formulation used in RELAP5/MOD3:

$$\frac{1}{2} \left(\frac{1}{\Delta x_j} \right) \left[(v^2)_L^n - (v^2)_K^n + \text{viscous term} \right] \quad (47.5)$$

(see Equations (3.1-103) through (3.1-106) of NUREG/CR-5535 RELAP5/MOD3 Code Manual Vol.1). The above equation indicates that the finite difference representation is dissipative. The RELAP5 numerical solution methods have been well established over the course of about 30 years' development and improvement. Verification work has also been performed at Framatome ANP to show that the numerical schemes are implemented properly. An example to demonstrate the accuracy of the expression (47.4) for the momentum flux is depicted in the following three slides, which were presented in the review meeting for Framatome ANP (Siemens) Appendix-K SBLOCA methodology (August 8-9, 2000).

SIEMENS

Momentum Conservation Equations Expansion-Contraction Test Problem



- Motivation
 - Check accuracy of momentum flux terms
- Test Geometry
 - Tube with 4:1 area contraction and expansion
- Test Conditions
 - Single-phase liquid (~incompressible) with no wall friction or irreversible losses

SIEMENS

Momentum Conservation Equations Expansion-Contraction Test Problem

- Differencing Schemes

- Central Difference

- Second order accuracy but unstable

$$\Delta P = -(\rho v)_j \left(\frac{v_{j+1} - v_{j-1}}{2} \right)$$

- Upwind Difference

- First order accuracy (i.e. dissipative) but stable

$$\Delta P = -(\rho v)_j (v_j - v_{j-1})$$

- S-RELAP5

- Stable, high accuracy for area changes but can be dissipative

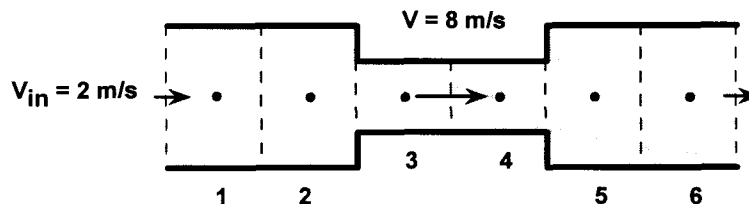
$$\Delta P = -\frac{1}{2} \rho_j (\dot{v}_L v_L - \dot{v}_K v_K)$$

118

RA-MTG:00:025
8/3/00

SIEMENS

Momentum Conservation Equations Expansion-Contraction Test Problem



	Pressure: $(P_0 - P) / \rho$					
Bernoulli	0	0	30	30	0	0
Central Difference	0	6	30	30	6	0
Upwind Difference	0	0	48	48	48	36
S-RELAP5	0	0	30.0001	30.0011	0	0

119

RA-MTG:00:025
8/3/00

The last slide shows that the S-RELAP5 approximation to the Bernoulli form is quite accurate. It should be pointed out that Volume K and Volume L may not have the same flow area and there may be a bend between the two volumes. S-RELAP5 does not explicitly treat the force balances around the bend and at the abrupt area change. The flow restrictions (bends and area changes) are approximated by using energy-loss coefficients, which are generally obtained from Idelchik's Handbook or Crane's Handbook.

[

]

The Ferrel-McGee Test 2C-7 was simulated using S-RELAP5. The test conditions were:

Pressure	120 psia
Flow Rate	1150 lb/hr
Quality	0.076

The test section geometry modeled was:

Lower	Length	24 in
	Diameter	0.46 in
	ϵ/D	0.00005
Upper	Length	48 in
	Diameter	0.59 in
	ϵ/D	0.00002

The RLBLOCA Methodology specifies that abrupt area changes be modeled using the abrupt area change model without code-computed form loss terms. The terms are required to be specified by other means. For the Ferrel-McGee problem, the form losses were computed from Crane (Reference 2) and are computed (using diameters) as:

$$K_{\text{expansion}} = \left(1 - \frac{A_{\text{small}}}{A_{\text{large}}}\right)^2 = \left(1 - \frac{0.46^2}{0.59^2}\right)^2 = 0.154$$

$$K_{\text{contraction}} = 0.5 \left(1 - \frac{A_{\text{small}}}{A_{\text{large}}}\right) = 0.5 \left(1 - \frac{0.46^2}{0.59^2}\right) = 0.196$$

The S-RELAP5 nodalization diagram for the Ferrel-McGee experiment is shown in Figure 47.1. With the exception of the test pressure, the problem was run to steady conditions with the above specified input. The system pressure was set to 118 psia to better approximate the 117.976 psia measured pressure at the test section exit. At the end of the calculation, the pressures were recorded and plotted as a function of test section length, shown in Figure 47.2. The filled circles are the measured data at the specified measurement locations while the S-RELAP5 results are the open squares representing the cell centered pressures. Note that if the S-RELAP5 momentum equation was integrated continuously over the test section, the pressures at the 24 in level would overlay the data. Since the pressure drop through the test section depends on the two phase friction and the two phase pressure drop through the expansion, the good agreement of S-RELAP5 to the measurements show that the two-phase wall friction is acceptable, especially at low pressures, and that using the single phase loss coefficient for abrupt area changes under two phase conditions is acceptable.

References

- 1) Ferrel, JK and McGee, JW, US AEC Report, "Two Phase Flow Through Abrupt Expansions and Contractions", TID-23394 Volume 3 (1966).
- 2) Crane Co., "Flow of Fluids Through Valve and Fittings", Tech. Paper 410, 1982.

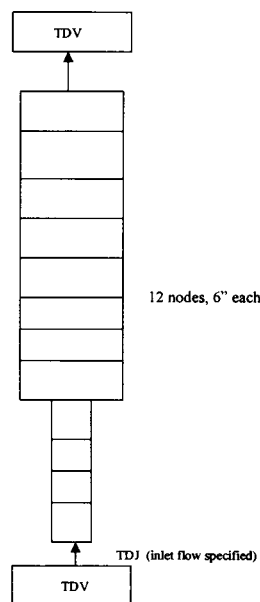


Figure 47.1 S-RELAP5 Nodalization for the Ferrel-McGee Experiment

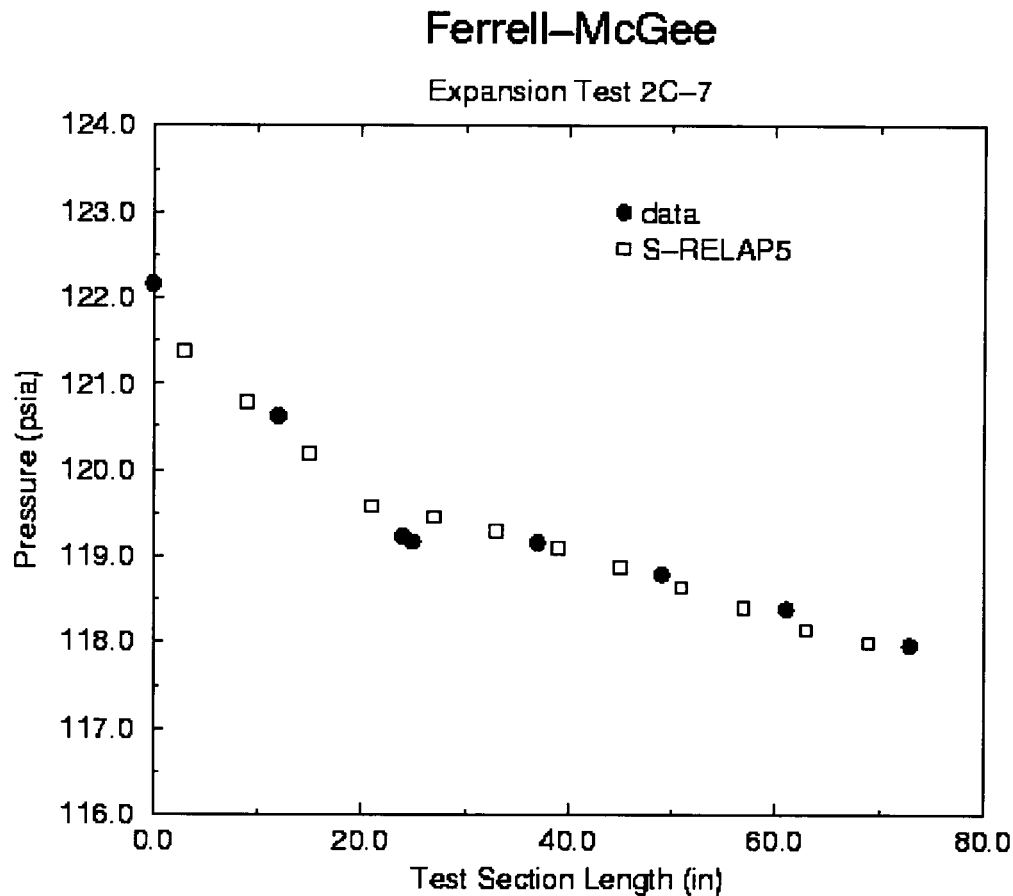


Figure 47.2 Comparison of Measured and Calculated Pressures from the S-RELAP5 Simulation of the Ferrel-McGee Test 2C-7

Question 48: *Please discuss the stability analysis for the numerical scheme presented in Section 2.6.5 of EMF-2100. Include a discussion of a consistency analysis of the finite difference equations and, as discussed in Section 2.6.4, justification of the use of the value of $C = 0.35$ when evaluating Eqs. 2.124 and 2.125. Include in the discussion the reason why the value of C must be within the range 0.0 to 0.5 for stability.*

Response 48: A general discussion of stability of the semi-implicit numerical solution scheme is presented in Section 2.6 of EMF-2100(P) Revision 4. Comprehensive stability analysis for the complex two-phase flow system is not possible. The S-RELAP5 numerical scheme is essentially the same as the RELAP5 scheme and has been empirically proven to be stable. The adequacy of the S-RELAP5 numerical scheme has also been demonstrated by the ability of the code to simulate the tests reported in EMF-2102(P) Revision 0.

The central difference scheme is second-order accuracy and unstable and the upwind difference (donor) scheme is stable with first-order accuracy (see the response to Question 47). The S-RELAP5 difference scheme for the direct and cross-product momentum flux terms:

$$\frac{\partial}{\partial x} \left(\frac{1}{2} v_x^2 \right) \text{ and } v_y \frac{\partial v_x}{\partial y}$$

is a hybrid of the central difference and upwind difference schemes. The hybrid scheme has high accuracy and is stable as demonstrated in Response to Question 47. The upwind difference part does introduce some dissipation, which is necessary for stability. The use of "volume-average" velocities (see Sections 2.6.2, 2.6.3 and 2.6.4 of EMF-2100), instead of junction velocities, enables the code to treat consistently the multiple junctions connecting to a side of a volume, which can be used for connections between 1-D and 2-D components. The weighting factors used in the "volume-average" velocities (see Equations 2.106 to 2.108 of EMF-2100(P) Revision 4) imply that the fluid does not come to rest at the "wall", i.e., the inviscid fluid assumption is invoked, and the flow resistances, such as wall friction, are modeled as "added-on" by using friction factor correlations.

The downstream (acceptor) difference is used only when the upstream difference is not present. This is not necessary and is performed only to improve the accuracy. The criterion of $0 < C < 0.5$ is based on the analysis of the mixing upwind (upstream) difference and downstream difference for the first order linear hyperbolic partial differential equation. Since the downstream difference is used under special circumstance and the difference scheme for momentum flux terms is expressed in a more complex form, the simple criterion may not be applicable. Experience indicates that there is no stability problem for any value of $0 \leq C \leq 1$. The value of $C=0.35$ is empirically determined to be preferable based on certain sensitivity studies performed years ago. The scheme has been demonstrated to be adequate in the performance of the assessments reported in EMF-2102(P) Revision 0.

A stability analysis was performed by Stewart (Journal of Computational Physics, 33, 259-270, 1979) on an equation set similar to that found in RELAP5 and S-RELAP5. In that analysis, Stewart stated that a "Lax-Richtmyer type of stability analysis cannot be performed" due to the equation set having complex characteristics. Stewart then showed stability for the two-phase equation set was achieved under two conditions: 1) the combination of time step, node size and

velocity must satisfy $v \frac{\Delta t}{\Delta x} < 1$, i.e. the Courant limit, and 2) momentum exchange. Stewart

further showed numerical experiments which indicated that there are minimum node sizes where high frequency instabilities may occur. Based on Stewart's work, Shieh, et.al, (NUREG/CR-5535, Volume 6, October 1994) performed a similar stability demonstration with RELAP5/MOD3.

Framatome purposely sought an existing code to form the basis of the RLBLOCA methodology. The significant advantages for adopting an existing code include model and theory development, assessment, and documentation. Having adopted RELAP5, additional model development, assessments, and documentation efforts were made to support the RLBLOCA methodology. Consequently, there are several sources of information available to Framatome in support of the RLBLOCA submittal. Since the semi-implicit numerical scheme in S-RELAP5 is identical to the one used in RELAP5/MOD3, the stability analysis presented in NUREG/CR-5535, Volume 6, is

applicable and therefore satisfies the stability and consistency issues contained in RAI number 48.

The next discussion concerns the multiplier $C = 0.35$. This multiplier is applied to specific occurrences where upwind differencing is not available, such as node boundaries representing walls and velocity direction is away from the wall. Ignoring the cross derivative would be acceptable under these conditions, however increased accuracy was desired. In lieu of using center differencing, a method for using combined upwind and downwind differencing by Murray was investigated. Murray (RELAP5 International Users Seminar, Boston, 1993) developed a method for using a weighted combination of upstream and downstream differencing:

$$\left(\frac{\Delta V}{\Delta \theta} \right)_{\theta=\theta_j} = \left((\omega) \frac{V_j - V_{Uj}}{\theta_j - \theta_{Uj}} + (1 - \omega) \frac{V_j - V_{Dj}}{\theta_j - \theta_{Dj}} \right)$$

Murray performed a stability analysis using a linear Euler equation, and determined the criteria for stability was:

$$\eta = 1 - (2\omega - 1) \frac{v\Delta t}{\Delta x}$$

where

$$0 < \frac{v\Delta t}{\Delta x} < 1$$

$$\frac{1}{2} < \omega \leq 1$$

In S-RELAP5, the upwind difference is set to zero and $C = 1 - \omega = 0.35$. The value of 0.35 was determined by the best fit to LOFT L2-6 clad temperatures, specifically the early quenching immediately after the blowdown peak. However, the code version and system model that were used in the testing are no longer applicable. In the current code version and LOFT model, the effects of using this model are not readily apparent.

Question 49: *During the review of S-RELAP5 for application to 10 CFR Part 50, Appendix K small-break LOCA analysis, concerns were raised regarding the completeness of the formulation of the momentum equation. Specifically, the momentum equation as formulated is a vector equation that can only be reduced to 1-D if the flows and forces act in a single direction and hard surface reaction forces have also been omitted. Also, the momentum equation can only be reduced to Bernoulli's equation for pipes by integrating the differential form of the momentum balance along a streamline. Please discuss the momentum equation and its application to the reactor coolant system when major portions are modeled as a series of variable flow areas, 1-D straight pipes, and flow channels with bends.*

Response 49: The S-RELAP5 field equations are written for a space filled with fluid. The structures are not explicitly considered. The nodalization consists of volumes (cells) and junctions (with no length) forming straight pipes and two-dimensional grids. The fluid is assumed to be inviscid. The effects from walls, bends, and abrupt area changes are superimposed (or added-on) to the field equations by using friction factor correlations for volume wall frictions, and energy-loss coefficients on junctions for bends and abrupt area changes. The energy-loss coefficients for flow restrictions (i.e., bends and abrupt area changes) are generally obtained from Idelchik's Handbook or Crane's Handbook. The approach has been widely used in the industry for the modeling of reactor systems and its adequacy has been demonstrated by the ability of the code to simulate the tests reported in EMF-2102(P) Revision 0.

The momentum flux term

$$\frac{\partial}{\partial x} \left(\frac{1}{2} v_x^2 \right)$$

for the 1-D component or the x-direction of a 2-D component is in the Bernoulli form. It can be expressed in finite-difference form over a momentum cell j connecting Volume K and L (see Figure 2.2 or 2.3 of EMF-2100(P) Revision 4) as

$$\frac{1}{2} \frac{(v_x^2)_L - (v_x^2)_K}{\Delta x_j}$$

where Δx_j is the momentum cell length (in the x-direction), which is equal to half of the sum of the two volume lengths (in the x-direction), and the subscripts K and L denote the velocities at the centers of the two volumes (i.e., the two ends of the junction) respectively. Of course, the above equation is known to be unstable and donor-like velocities as shown in Equations (2.116) and (2.117) of EMF-2100(P) Revision 4 must be used. The point to be stressed is that streamline integration is not required to obtain the momentum equation in the Bernoulli form, even though integration is used in Equation (2.115) of EMF-2100(P) Revision 4.

Question 50: *Please discuss the manner in which S-RELAP5 indicates to the user that mass, energy, and momentum are conserved in a plant application. Is there a measure that shows in the code output that the above parameters are conserved?*

Response 50: Mass conservation is shown on the S-RELAP5 output. However, there is currently no direct printout in the S-RELAP5 output that indicates whether energy or momentum have been conserved. This would require significant additional calculations in the code, increasing run time and finally the cost of using the code. Therefore, the conservation of momentum and energy are only indirectly evaluated.

Momentum equations are force equations and show up on the output as pressure drops across various portions of the systems. They can be checked against plant data in a steady-state calculation. For transient calculations, the calculated differential pressures can be checked against test data. S-RELAP5 output does not display any measure of energy conservation.

Users can use control variables to set up the measure to check the energy conservation for the entire system or parts of the system.

As indicated, the conservation of momentum and energy are not directly checked in the code but can be evaluated based on the following. First there is the results of all the assessments. For each of these assessments the code is first brought to a steady state which is checked against the initial conditions for the assessment. The fact that the code is able to attain steady state conditions that are in agreement with measured data indicates that the momentum and energy are being conserved. If not, and they were constantly being perturbed, the code would not settle out to a steady state, let alone one that was in agreement with the measured conditions.

Secondly, the execution of the assessment transients provide a comparison of the calculated and measured pressure profiles during the transient. The pressure profiles are dependent upon both the momentum and the energy and if either were not being conserved then poor agreement would be expected between the data and the calculation. However, for the four LOFT and two Semiscale assessments, the agreement between the calculated and measured pressure profiles are good to excellent (See Figures 4.1.5, 4.1.37, 4.1.74, 4.1.111, 4.2.6, and 4.2.30 of EMF-2102(P) Revision 0). This good agreement indicates that the code treatment of both the momentum and energy equations is adequate for use in the performance of LBLOCA analyses.

With respect to the actual plant calculations, the code is driven to a steady state condition and this steady state condition is checked against the plant operating conditions. In addition, the primary to secondary energy balance is also checked. These checks provide the assurance that the code and plant specific model is adequately modeling the plant. The fact that the code attains a steady state condition that corresponds to the actual plant operating conditions is the primary indication to the analyst that the code is functioning as intended.

An example demonstrating that S-RELAP5 numerics conserved energy was presented during the August 8 and 9, 2000 presentation of the SBLOCA methodology and is reproduced below.

SIEMENS

Energy Conservation Equations Vessel Blowdown Example Problem

• Motivation

- Check energy conservation for flow across a large pressure drop (e.g., choke plane)

• Initial Conditions

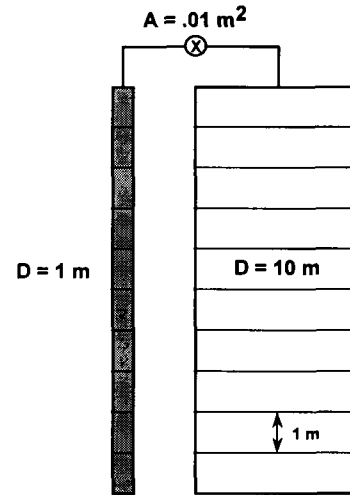
- Vessel - saturated water at 150 bar
- Containment - steam at 1 bar

• Test Parameter

- Sum of internal energy for system with KE and PE assumed negligible

$$\Delta E = [E(t) - E_0] / E_0$$

$$E(t) = \sum_{i=1}^{20} [(\alpha_f \rho_f U_f)_i + (\alpha_g \rho_g U_g)_i] V_i$$

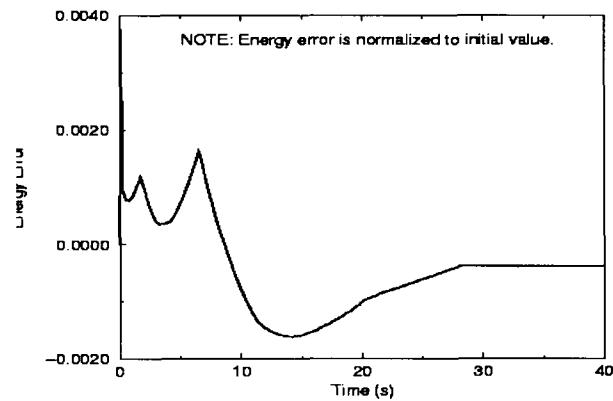


80

RA-MTG-00.025
8/3/00

SIEMENS

Energy Conservation Equations Vessel Blowdown Example Problem



Siemens Power Corporation Proprietary

81

RA-MTG-00.025
8/3/00

Question 51: *Please discuss the omission of the viscous shear term in the 2-D formulation. Include a discussion of the consequence of the omission of this term, for example, in the hot bundle and hot channel during early reflood when the Re numbers are in the range 1,000 to 2,000. Are there low flow conditions during the LOCA (blowdown, refill, reflood, long term during downcomer boiling) where omission of this term would affect the hot channel thermal behavior and/or hot rod PCT?*

Response 51: The discussion of omission of the viscous shear terms has been presented on Page 2-5 of EMF-2100(P) Revision 4. In the reactor vessel, the dominating surface stress forces are wall friction in single phase flow and wall friction and interphase friction in two phase flow; the viscous shear is insignificant relative to those forces, and thus not important. The conclusion of the PIRT was that wall friction did not have a sufficiently significant effect to be considered for uncertainty analysis; therefore there was no reason to consider the effect of viscous shear. The low flow conditions are treated in the wall friction and heat transfer coefficient correlations. Furthermore, unless sufficiently fine nodes are used, such as those for CFD codes, inclusion of the viscous shear terms in a system code only contributes to background noise.

Question 52: *Please discuss the numerical solution strategy described in Section 2.6.5.1 for a single 1-D pipe and a second system using a 1-D loop connected to a 2-D component. Include a discussion of the development of the coefficients from the numerical approximation to the conservation equations and the tri-diagonal matrix, along with the column vectors containing the source terms.*

Response 52: In S-RELAP5, all volumes and junctions, regardless of what components they belong to, are treated equally in the solution scheme. The overall solution strategy is to reduce the conservation equations into a set of linearly independent equations where there is only one equation and one unknown per hydrodynamic volume. The process is described in EMF-2100 Sections 2.6.5.1 and 2.6.5.2. In Section 2.6.5.1, the first transformation using the momentum equation is described. The key point is the reduction of Equations 2.120 and 2.121 into Equation 2.135. Briefly, the process consists of adding and subtracting the old time pressure drop

$$(P_L^n - P_K^n) - (P_L^n - P_K^n)$$

into Equations 2.120 and 2.121, thus forming Equation 2.127. Using matrix notation, Equation 2.127 can be written as:

$$A\bar{x} = \bar{b} + \bar{c}$$

solving for velocity (\bar{x})

$$\bar{x} = A^{-1}\bar{b} + A^{-1}\bar{c}$$

where \bar{x} is the left hand side, while $A^{-1}\bar{b}$ and $A^{-1}\bar{c}$ are the right hand terms (old time velocity and pressure drop, respectively) of Equation 2.135. Substituting Equation 2.135 into the mass and energy equations (described in Section 2.6.5.2) results in one equation for change in

pressure ($P_L^{n+1} - P_L^n$) per hydrodynamic volume, hence a set of 'N' equations with 'N' unknowns. It is easily shown that they form a linearly independent set of equations. Thus, the concept of tri-diagonal is immaterial. Also, since the orthogonal derivatives that appear in the 2-D momentum equation are old time terms and are contained in \bar{b} , no additional development is required.

Thus, the S-RELAP5 solution scheme is entirely different from that of TRAC-M. The derivation is described in Section 2.6 which demonstrates that the derivation of the S-RELAP5 numerical scheme is the most complete when compared to TRAC and other system codes. The TRAC-M manual describes the matrix in general form without specifying the coefficients. S-RELAP5 provides all the actual coefficients.

The S-RELAP5 solution scheme does not solve the 1-D and 2-D components separately. Once the finite difference terms are obtained, the basic elements are volumes and junctions. There is no distinction between 2-D and 1-D junctions or volumes in the finite difference equations. Each junction has two momentum equations (vapor and liquid velocities). Section 2.6.5.1 solves the liquid and vapor velocities in terms of pressure changes of the connection volumes. Section 2.6.5.2 describes the analytical steps to eliminate the void fraction, liquid internal energy, vapor internal energy, and noncondensable quality from the two mass balances, one noncondensable, and two energy balance equations to obtain a pressure equation for each volume. The resultant pressure equation is shown in Equation (2.208) with all the terms described in Equations (2.209) through (2.215). The text in the last paragraph describes how a system of NxN sparse matrix is obtained for a problem with N volumes. In general form, the pressure equations for an N-volume problem are:

$$Ax = b$$

or

$$\begin{bmatrix} a_{11} & a_{12} & \dots & a_{1N} \\ a_{21} & a_{22} & \dots & a_{2N} \\ \dots & \dots & \dots & \dots \\ a_{N1} & a_{N2} & \dots & a_{NN} \end{bmatrix} \begin{bmatrix} \Delta P_1 \\ \Delta P_2 \\ \dots \\ \Delta P_N \end{bmatrix} = \begin{bmatrix} b_1 \\ b_2 \\ \dots \\ b_N \end{bmatrix}$$

where a_{ij} ($i \neq j$) is zero if no junction connects volume i and volume j . The elements b_i and nonzero a_{ij} 's are the terms given in Equations (2.209) through (2.215) of EMF-2100 (P) Revision 4. The pressure matrix subroutine PRESEQ is coded in accordance with the steps and the terms developed in Section 2.6.5.2.

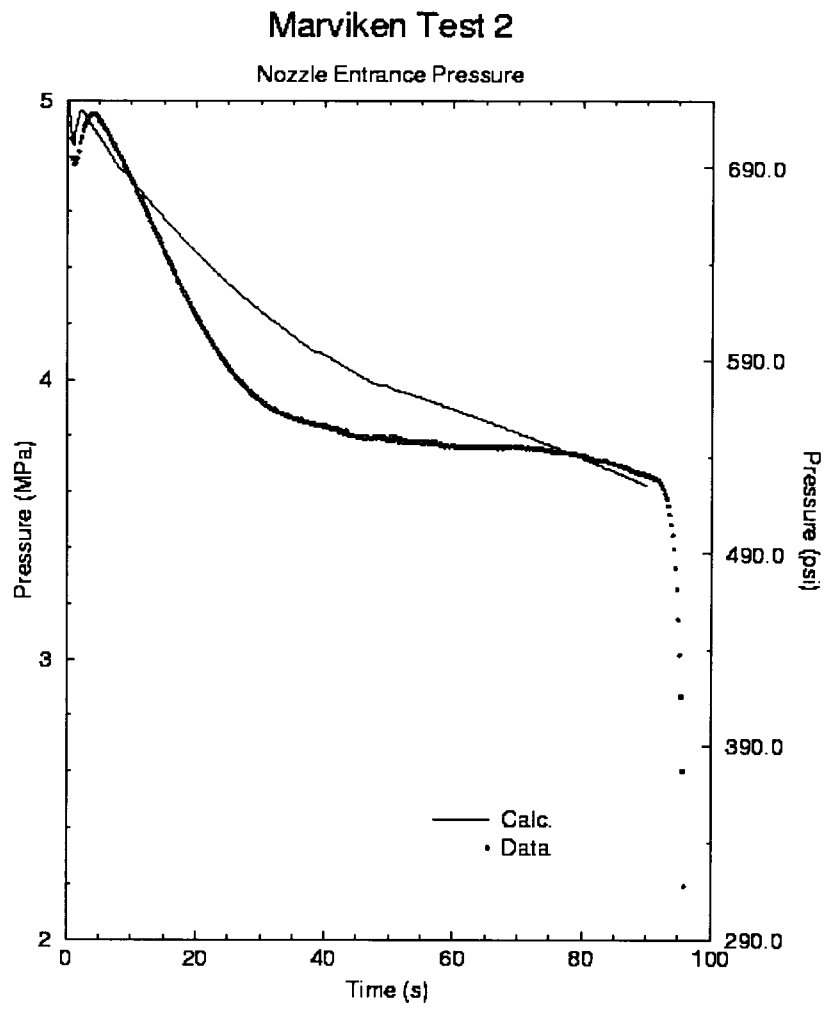
Question 53: *Please discuss the method and model used to simulate the ECC entering and mixing in the discharge legs? Also, since ECC water can enter the loop seal during rapid SIT injection, please discuss how S-RELAP5 captures this behavior. What is the effect of loop seal refill on steam binding, the reflood rate, and the PCT?*

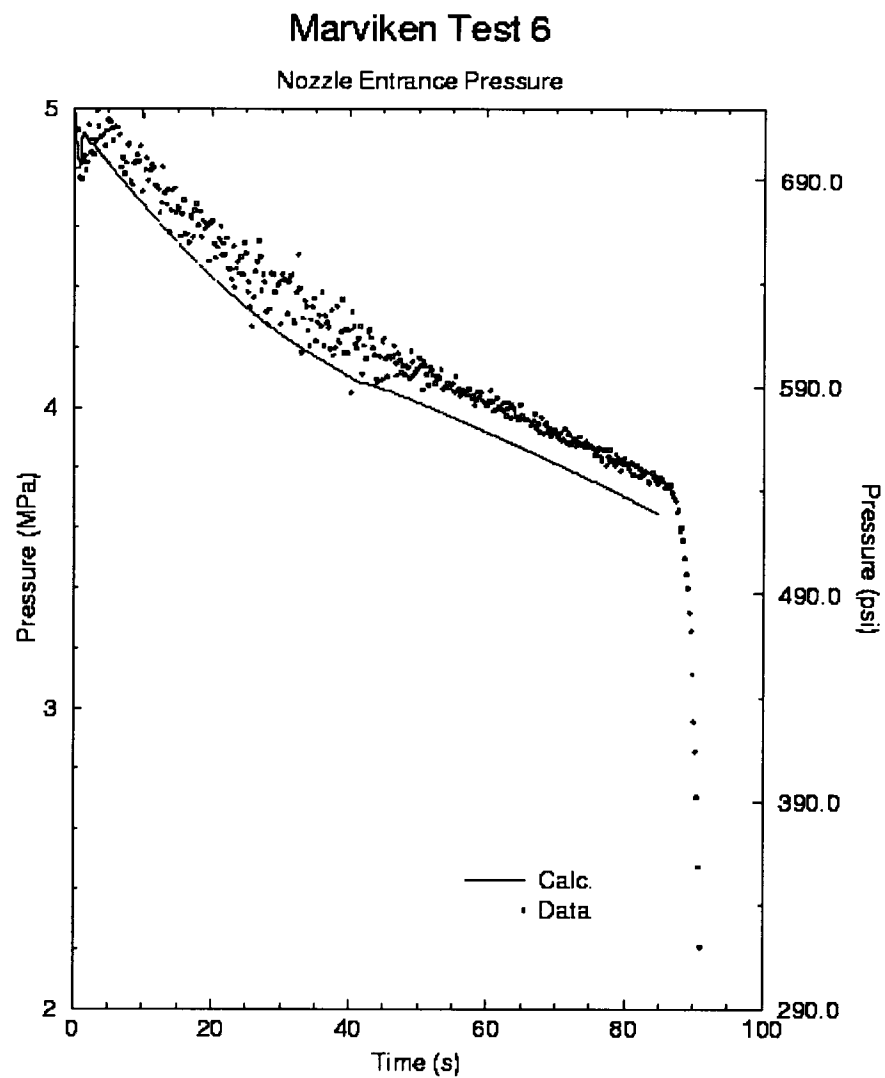
Response 53: There is no special component or process model for the ECC mixing. The applicability and adequacy of S-RELAP5 to simulate ECC mixing have been shown in the assessments of UPTF test 8, Westinghouse/EPRI One-Third Scale Test, and LOFT LBLOCA Tests. The back flow of SIT ECC water either does not occur or is not significant in LOCA events due to (1) the pump design provides physical barriers to hinder or prevent back flow into

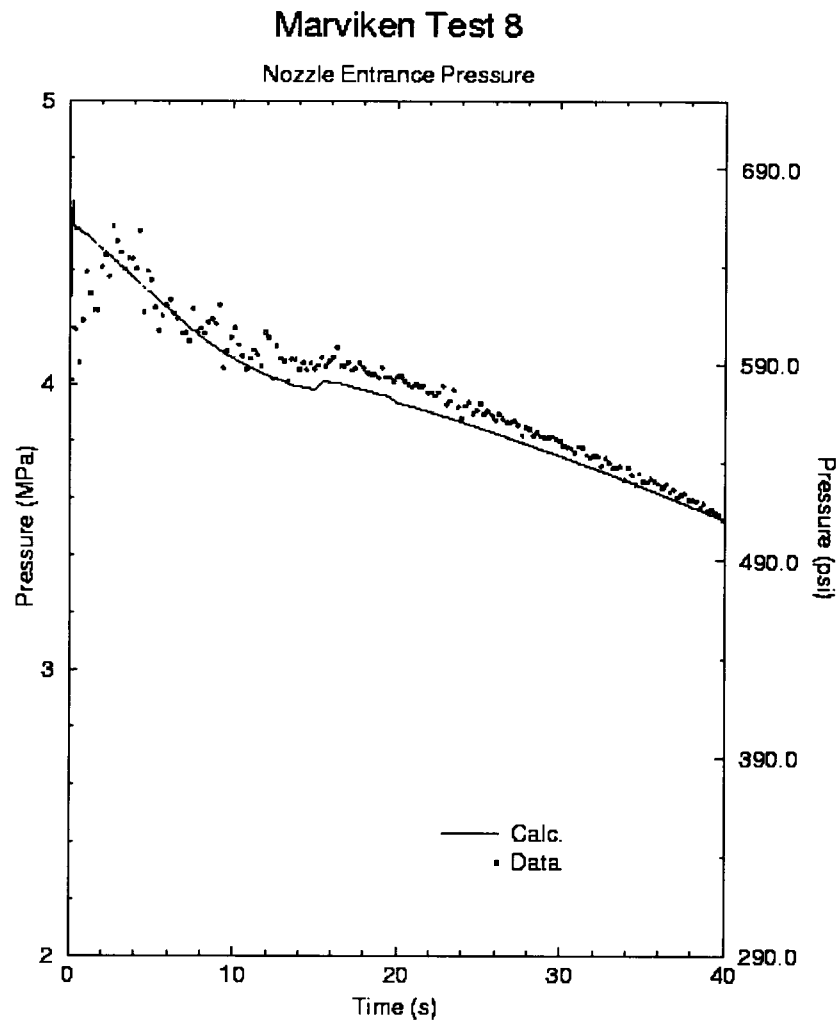
the loop seal and (2) the steam flow from the core to steam generator and then to cold leg is sufficiently strong and the pressure drop due to condensation is sufficiently large to prevent back flow. In UPTF Test 8, there is no evidence of any significant back flow to the loop seal in either the calculations or the data.

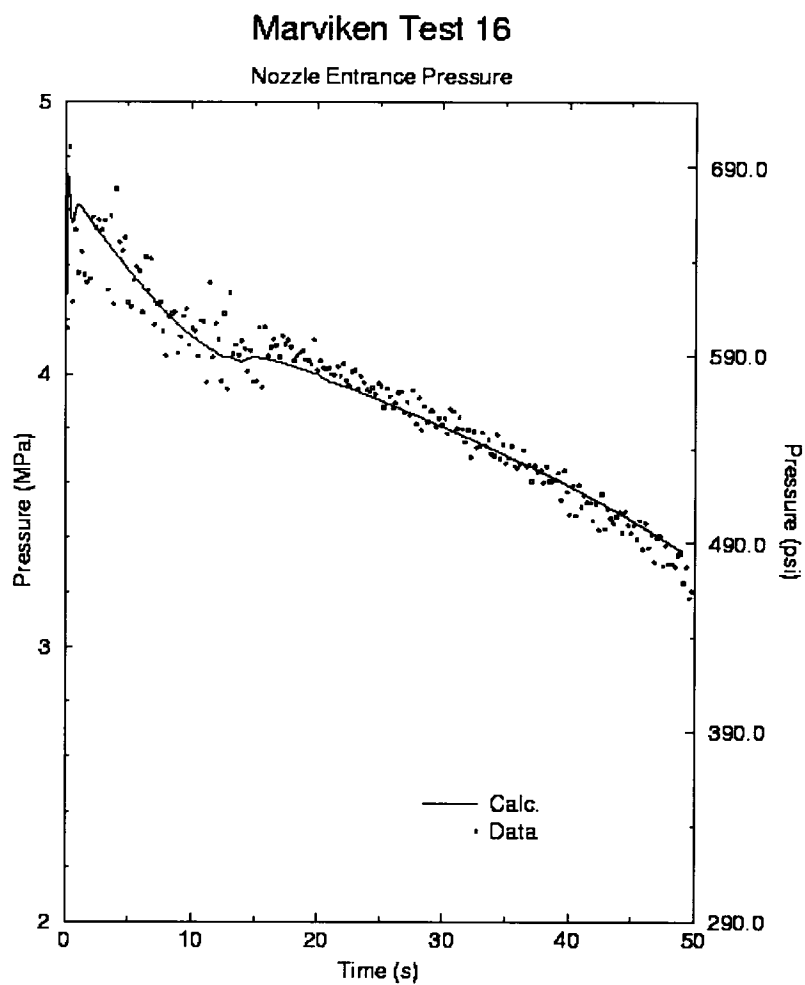
Question 54: *Please provide the comparisons of the S-RELAP5 predictions to the Marviken test system pressure for the tests presented in EMF-2102, Section 3.5. Discuss how the uncertainty in break flow was determined. Does the S-RELAP5 model include wall heat structures? If not, discuss the effect of the omission of wall heat on the results.*

Response 54: The following nine figures show the comparison of pressure near the nozzle entrance for the nine tests. The measured pressures exhibit some fluctuations, except for Test 2. The calculation of break flow uncertainty is discussed on Section 3.5.5 of EMF-2102. The wall heat structures are not included. There are no accurate data available for wall heat structure modeling. In any case, the contribution from the walls to the critical flow calculation is insignificant since the wall and fluid are roughly at the same temperature initially and the fluid temperature change during the very short transient is rather small, particularly in the discharge pipe and nozzle section. The key point is to obtain sufficiently accurate fluid conditions upstream of the break.



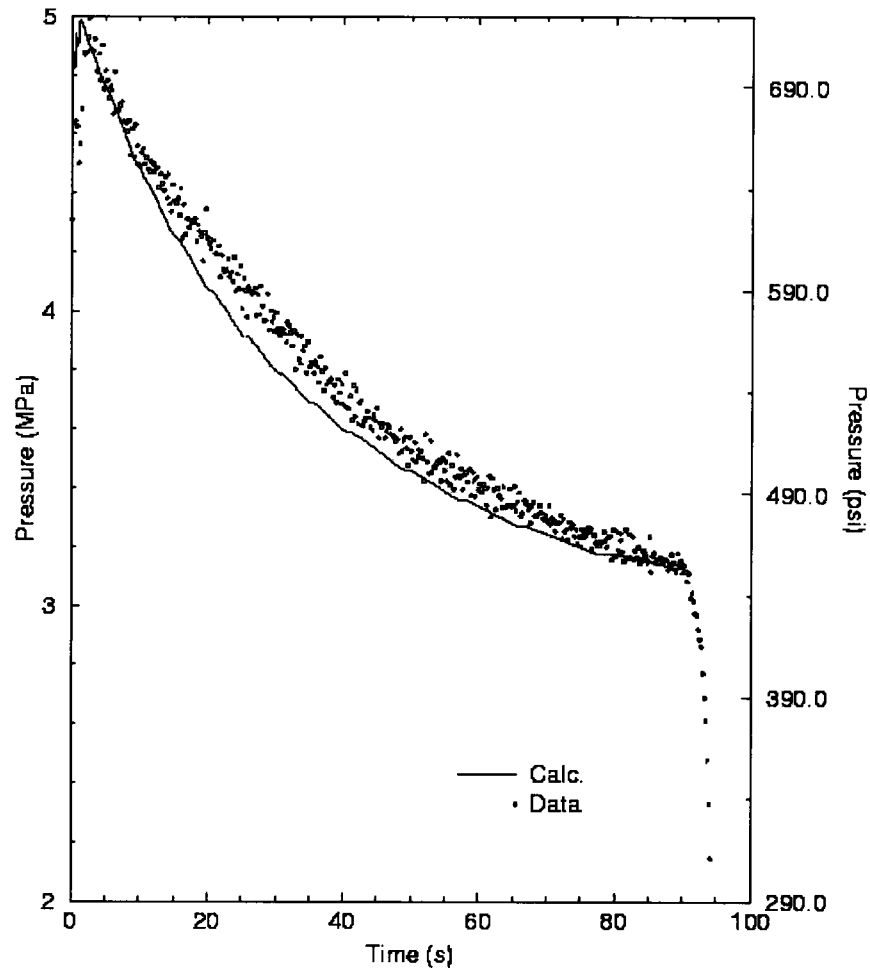


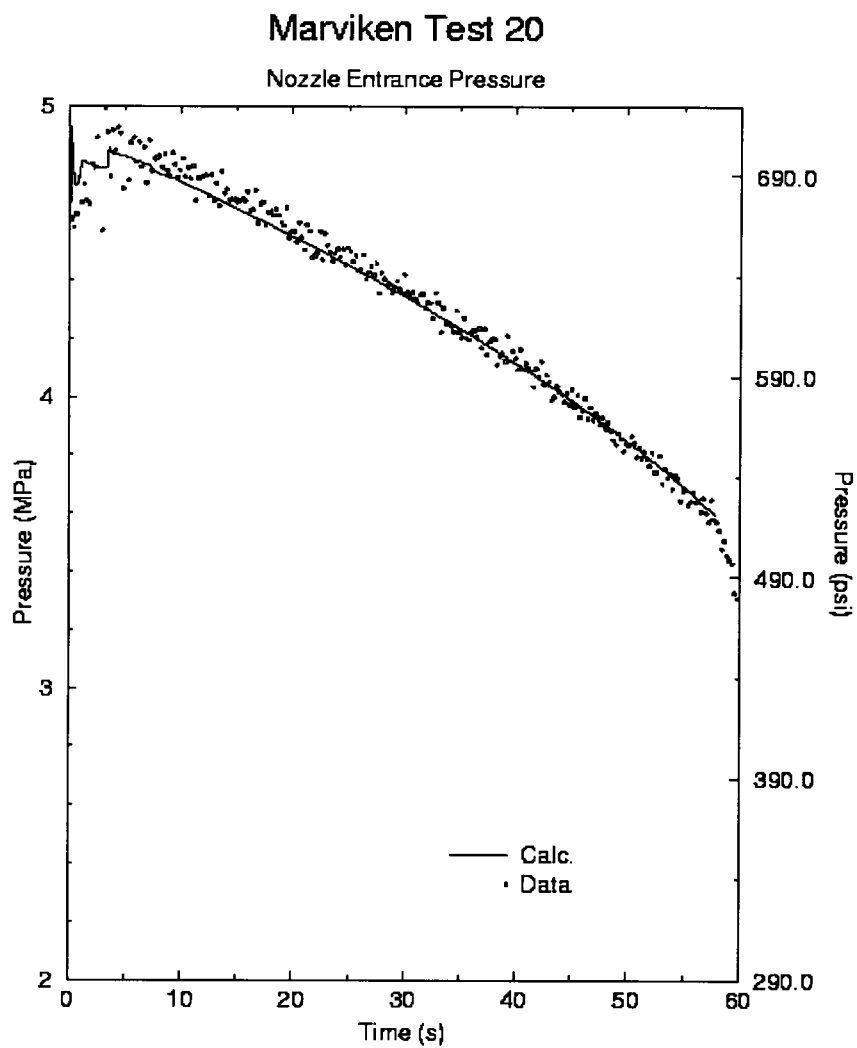


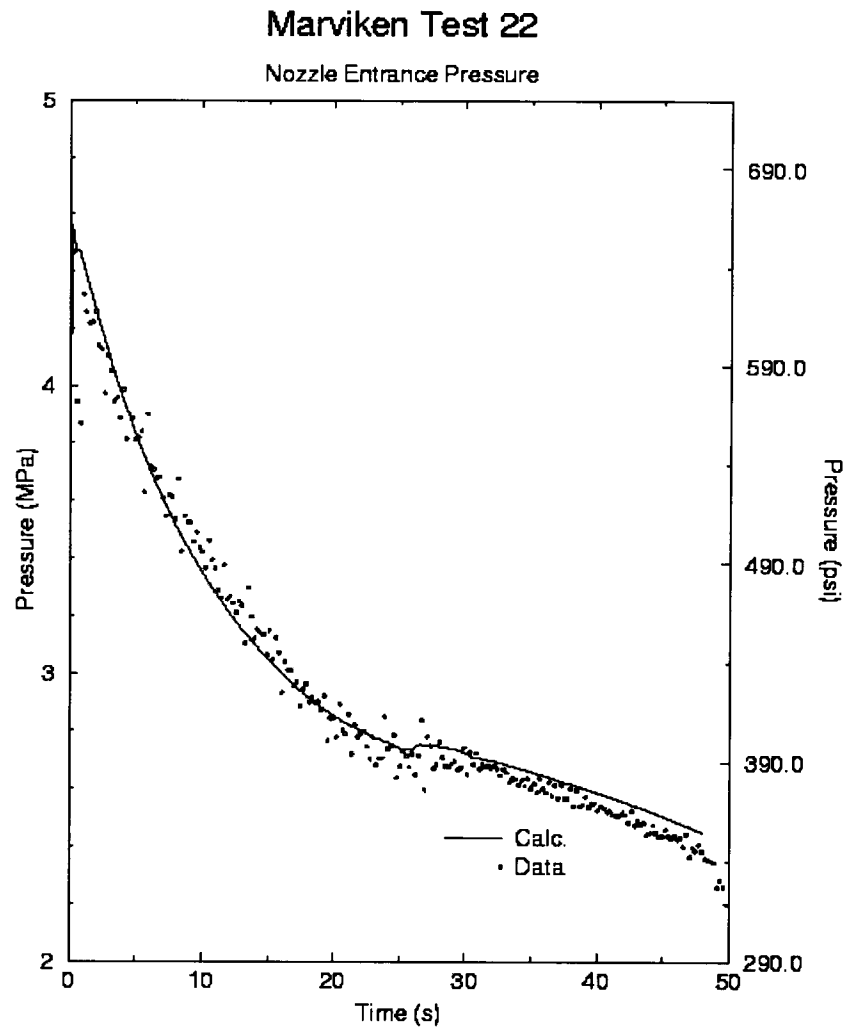


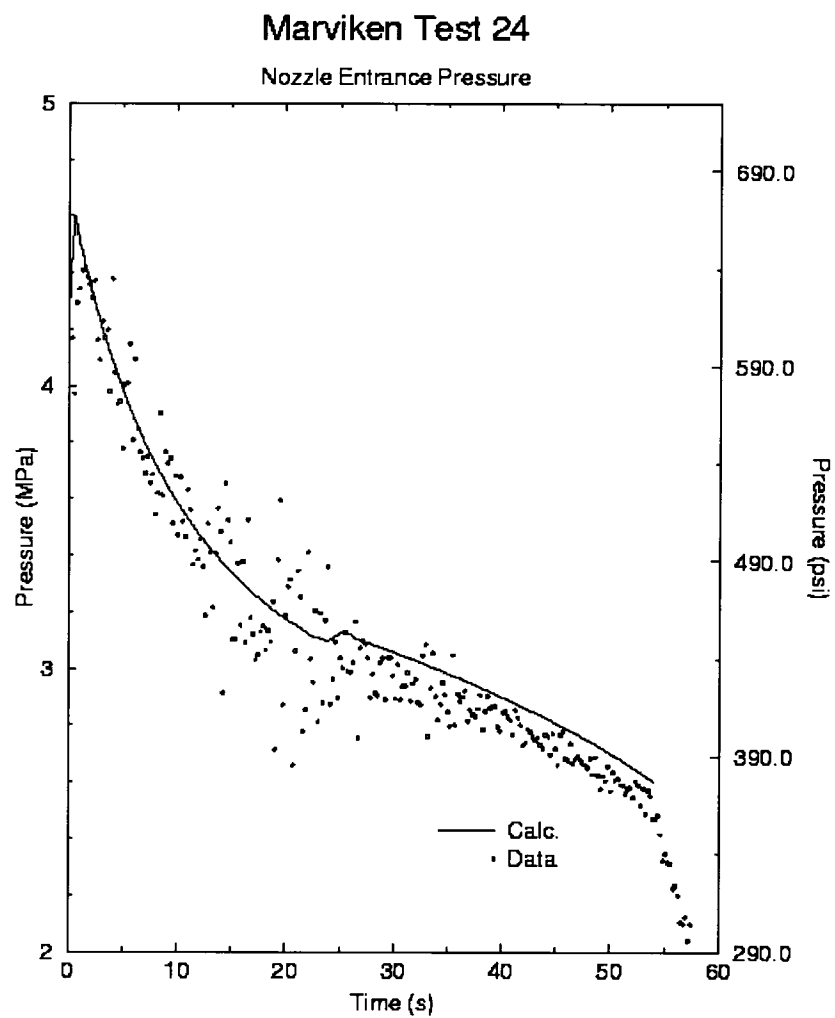
Marviken Test 17

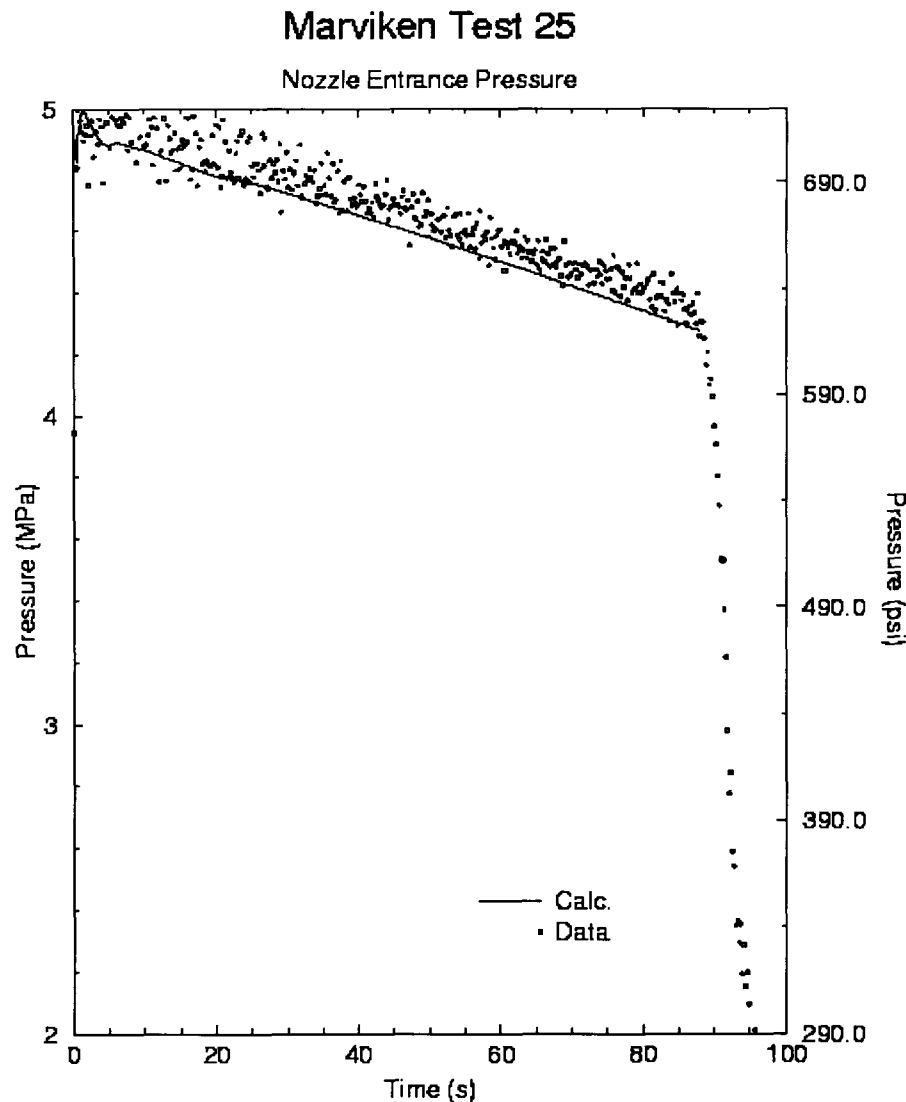
Nozzle Entrance Pressure











Question 55: *What is the cause of the drop in mass flow rate at 75 seconds in Fig. 3.5.18 and at 20 seconds in Fig. 3.5.22 presented in EMF-2102? Why was the S-RELAP5 prediction not shown to completion in Figs.14, 15, 18, 21, and 22?*

Response 55: The mass flow rate drops at 75 seconds because steam has reached the bottom of the vessel in the calculation earlier than the test. As discussed in the last sentence of Section 3.5.4 of EMF-2102(P) Revision 0, the calculation time for all tests are the same or close to the duration of the experiment as specified in NUREG/CR-2671 (Reference 3.5.3 of EMF-2102(P) Revision 0). The test was terminated when the ball valve began to close or when steam entered the discharge pipe (the last sentence of the paragraph next to the last on Page 3.5-3 of EMF-2102(P) Revision 0). Apparently, the flow measurement was not stopped at the termination of

the test. The closure of the ball valve is not simulated in the calculation; therefore, there is no point to carry out the calculation further than the specified test period.

Question 56: *The comparisons to the data show that the transition from single-phase to two-phase conditions is not well predicted. Please discuss the expected transition in the plant calculations, including effect of persistence of the duration of the transition period for an extended time and the error introduced in the calculation that is not captured by the uncertainty evaluated from the Marviken test comparisons. Include a discussion of the effect of the duration of the transition period the uncertainty in the break flow model determined from the Marviken tests.*

Response 56: [

The duration of the transition period is typically 5-15 seconds in the Marviken tests and is typically less than 5 sec in the plant calculations. Therefore, the Marviken transition period data are more than sufficient to cover the plant applications.

Question 57: *Does the critical flow model uncertainty show a dependence on L/D for all fluid conditions? Please discuss the lack of this effect in the uncertainty evaluation.*

Response 57: The critical flow uncertainty does not have a dependence on L/D. Any geometry dependence, including L/D, of the critical flow model is implicitly taken into account in the critical flow uncertainty analysis. In the plant applications, the geometry dependence is accounted for mainly through the break size spectrum analysis.

Question 58: *How is the critical flow rate calculated when superheated steam exits the break? Please discuss the uncertainty in the break flow model under these conditions.*

Question 59: *No tests were provided to show the capability of the code to predict pure steam flow out the break. Were comparisons of S-RELAP5 with data for saturated steam flow, to Marviken Test 11, performed? Please discuss the uncertainty in the break flow model for saturated steam.*

Response to 58 and 59: The single-phase steam critical flow is calculated based on the sound speed formulation:

$$a^2 = \left(\frac{\partial P}{\partial \rho} \right)_s = - \frac{V^2}{\left(\frac{\partial V}{\partial P} \right)_s}$$

where a, P, S, ρ, and V are, respectively, sound speed, pressure, entropy, and specific volume. This theoretical model for single-phase vapor choking has been well established. In plant calculations with cold leg breaks, steam always mixes with subcooled water before going out of the breaks; therefore, single phase steam choking does not occur. Thus, during the period when the break flow is choked, the two-phase critical flow model as exhibited in the Marviken Critical Flow Tests is applicable to plant calculations.

Question 60: *Were comparisons performed between S-RELAP5 and data for vessel blowdown, such as Allemann, "Experimental High Enthalpy Blowdown from a Simple Vessel through a Bottom Outlet," BNWL-1111, Battelle Northwest Laboratory, 1970? If so, please discuss the results of the comparisons.*

Response 60: The particular test has not been used for assessment by system codes such as COBRA/TRAC, TRAC and RELAP5. Framatome ANP has no data available to perform the assessment of the test. Furthermore, the Full Scale Marviken Critical Flow Tests used for critical flow uncertainty analysis are essentially blowdown tests from the vessel bottom.

Question 61: *HEM is an equilibrium break flow model. Since HEM is applied to two-phase conditions, and since non-equilibrium conditions can exist at the break with combinations of subcooled liquid with saturated or superheated steam (or saturated liquid with superheated steam) exiting the system, how are these conditions handled with the S-RELAP5 critical flow model? What is the uncertainty in the break flow model under non-equilibrium conditions?*

Response 61: In evaluating the critical mass flow rate, S-RELAP5 derives the equation of state at the throat from the flow and state conditions at the volume center, assuming complete mixing of liquid and vapor phase at the throat. At the volume center upstream of the break, the flow is non-homogeneous (vapor velocity \neq liquid) and non-equilibrium (vapor temperature \neq liquid temperature). With the equilibrium assumption, the resultant equation of state at the throat can be single-phase (subcooled) liquid (equilibrium quality less than or equal to 0), two-phase liquid and vapor mixture (equilibrium quality between 0 and 1), or single-phase vapor (equilibrium quality greater than or equal to 1). The HEM critical flow model is applied when the state at the throat is a two-phase mixture (equilibrium quality between 0 and 1).

During the reflood period of a LBLOCA superheated steam and subcooled liquid can exit the break together. Since there is sufficient amount of highly subcooled ECC water to bring down the superheated steam to saturation, the equilibrium quality of the two-phase mixture at the volume is less than 1, particularly during the period when the break is choked. Therefore, the critical mass rate computation is within the range of the subcooled single phase and two-phase HEM critical flow model. It should be pointed out that the HEM critical flow model assumes complete mixing of vapor and liquid to compute the maximum allowable mass flow rate through the break, but it does not really turn the non-equilibrium conditions into equilibrium conditions. If the steam is superheated at the volume center, it will exit the break with the same amount of superheat whether the break is choked or not.

The critical flow uncertainty for the subcooled single-phase and two-phase choking is obtained from the analysis of nine Marviken Full Scale Critical Flow Tests, which Framatome, ANP has data for. Since the steam in the Marviken Critical Flow Tests is saturated, the concern is: what is the critical flow uncertainty if the upstream steam is superheated? There are insufficient separate-effects data available to perform uncertainty analysis for such conditions. It is believed that the uncertainty analysis from the Marviken Critical Flow Tests is applicable due to the following reasons. First, as discussed above, the equilibrium quality for the two-phase mixture of subcooled liquid and superheated steam is below 1; therefore, the HEM critical flow model can be used. Second, the period for which the break flow is critical with superheated steam is extremely short or not present during a LBLOCA; therefore, its overall contribution is insignificant. Third, in LOFT and Semiscale LBLOCA assessments, there is no apparent difference in break flow behavior when the steam upstream of the break becomes superheated.

Question 62: *What is the uncertainty in the critical flow model when the flow is no longer critical and may contain superheated steam or non-equilibrium two-phase conditions? Please discuss benchmarks that were used to evaluate the break flow model under these conditions and include results of the transition from critical to non-critical conditions and discuss how the model works.*

Response 62: []

When the break flow is not choked, the critical flow model uncertainty does not apply. Under such circumstances, the break flow is the same as any flow through a junction and is calculated by the field equations and constitutive models. Many of the analyzed separate effects tests, such as CCTF, UPTF, THTF, FRIGG-2, Westinghouse/EPRI and FLECHT-SEASET, have breaks without choking.

The treatment for transition from choked to unchoked flow is discussed in Section 5.1.2.3 of EMF-2100(P) Revision 4. For LBLOCA the transition (from choking to not choking) is not important since the period is extremely short. The Semiscale LBLOCA and LOFT LBLOCA Tests are assessment examples where the transition occurs and the code performs well. The transition treatment has also been validated with SBLOCA Tests (see EMF-2328(P)(A) Rev. 0). An assessment of the methodology assumptions for broken nozzle and loop resistance form loss has been provided in RAI #24.

Question 63: *Section 3.5.4 states that a break flow multiplier of [] was used to predict these tests. Uncertainty in the model is typically determined with a value of 1.0. Use of a multiplier in the range [], implies that S-RELAP5 tends to overpredict break flow for the Marviken tests. Discuss how this additional bias has been taken into account in the uncertainty analysis when the bias was varied for the Marviken tests? How is the break discharge coefficient then modeled when performing plant calculations? What is the uncertainty in the break model if a discharge coefficient of 1.0 is used? Please discuss how in light of this initial assumed bias in the break multiplier input, the 25 percent error calculated for the break flow model bounds the data.*

Response 63: There is clearly a misunderstanding with respect to the information conveyed. In order to model the Marviken nozzles a geometry or K factor was required to match the test depressurization. This geometry factor varied between [] depending on the particular test and nozzle. []

]

Question 64: *The break nodalization of the discharge leg in Fig. 4.3 of EMF-2103 shows [] in the discharge leg while the nodalization of the break in the Marviken test shows [] in the exit pipe. In Section 3.5.6 of EMF-2102, it is noted that "the fine nodalization was used to mitigate numerical diffusion which may send hotter water or vapor prematurely to the discharge pipe." The modeling philosophy given in Section 4.2.3.5, entitled Cold Leg and Break, seems to contradict the statements in Section 3.5.6. Please discuss and justify the differences in the modeling philosophy applied to the Marviken test and that applied to plant calculations. Include a discussion of the effect of finer nodalization on break flow and PCT in the plant calculations and the effect of the use of a crude nodalization on break flow uncertainty.*

Response 64: It is not appropriate to compare the flow path from the top of the vessel to the nozzle in the Marviken Tests with the flow length between the vessel and the break in the plant nodalization. []

】 The same strategy is used in nodalizing the vessel-side break. Therefore, a consistent philosophy is applied in the break upstream nodalization for both the Marviken and the plants.

In plant calculations, there are two possible paths that allow steam from the top of the core to exit the vessel-side break. One path is going up through the intact loop hot leg, steam generator, intact loop cold leg and top of the downcomer; the other path is going down through the lower plenum and then up through the downcomer. In both flow directions, liquid entrained by steam affects the state conditions of the break upstream volume. In the Marviken Tests, steam at the top of the volume propagates slowly downwards to the bottom of the vessel, discharge pipe and the nozzle to the break. The state conditions of the break upstream volume are affected by the vapor pulled through by the liquid. Since two distinct processes (liquid entrainment vs. vapor pull-through) affect the state conditions of the break upstream volume, the vapor propagation in the Marviken vessel has to be simulated as accurately as possible in order not to add improper bias to the critical flow uncertainty. Furthermore, the experiment stipulated that the test was terminated when the steam entered the discharge pipe. Therefore, the state conditions at the bottom of the vessel must be calculated accurately to prevent premature delivery of steam to the discharge pipe. Summarizing, the essential point is to obtain accurate state conditions for the volume upstream of the break in order to reduce to the minimum the dependency of critical flow uncertainty on the numerical schemes and constitutive relations.

Question 65: *Section 4.3.1.10 discusses the CCFL (countercurrent flow limit) model applied to the upper tie plate and compares test data against the theoretical flooding curve to bound the air – water flow rates. The performance of the code has not been demonstrated against test data to show that the model is performing correctly, especially under saturated and subcooled fluid conditions. To demonstrate the capability of the model, please show comparisons of code predictions to test data, such as the Northwestern data (Bankoff, 1981), to show the condensation effects on the CCFL predictions and the model's performance. How does S-RELAP5 prevent unrealistic concurrent down flow of liquid and steam into the core? Does countercurrent flow or concurrent downward flow produce upper core cooling or a top down quench for any of the separate effects, integral tests, or plant calculations?*

Discuss how the two fluid models have been assessed for CCFL behavior since the flooding point is determined entirely by the interfacial drag and entrainment models in the code. Has the CCFL model in S-RELAP5 demonstrated its ability to reproduce flooding behavior which is consistent with scaling laws. Has a comparison been performed for the S-RELAP5 model to tests such as the Creare 1/15th and 1/5th scale data. Are there continuous liquid and steam velocity plots in the downcomer verifying that CCFL is preserved by the S-RELAP5 interfacial drag model for saturated and subcooled conditions? Since the CCFL limit model [

], what controls are used to assure that plant calculations will not result in violations of CCFL or unrealistic concurrent downflow in this region? Also please discuss what special interfacial drag, film droplet, entrainment/de-entrainment, drop size models were added or modifications/provisions to RELAP5 to properly deal with countercurrent flow in the downcomer in the [

Response 65: The code performance on the CCFL phenomena has been demonstrated in the assessments of UPTF Tests 10, 12 and 29 (upper tie plate), FRA-ANP CCFL Tests (upper tie plate), UPTF Test 11 (steam generator inlet plenum), UPTF downcomer penetration tests 6 and

7, CCTF tests (upper tie plate, steam generator inlet plenum, upper core cooling and downcomer) Semiscale and LOFT LBLOCA tests (upper tie plate, steam generator inlet plenum, upper core cooling and downcomer). The fluid conditions in these tests range from highly subcooled to saturated.

S-RELAP5 uses a CCFL correlation of Bankoff-type. Users have the option to input the coefficients in the correlation and to select where the correlation is applied. The correlation can be reduced to Wallis form or Kutateladze form by input. The counter-current flow limiting is invoked only when the model is selected by the user and the calculated countercurrent flow from the interphase friction model exceeds the down flow limit. [

]

The CCFL at the upper tie plate depends strongly on the geometrical configuration of the tie plate region. The coefficients in the CCFL correlation depend on the geometry of the flow restriction and can only be determined by experiment. Framatome ANP performed CCFL tests on several types of upper tie plates (Section 3.9 of EMF-2102(P)). Figure 65.1 (from Figure 3.9.5 of EMF-2102(P) Revision 0) shows the data against the Kutateladze flooding curve for a Framatome ANP BWR ATRIUM-9 UTP (upper tie plate). The data were for the same UTP installed in two different test facilities: Mini-Loop and FCTF. The Mini-Loop data are close to but conservative with respect to the Kutateladze flooding curve:



The FCTF data is also conservative with respect to the above curve and overlay the Mini-Loop data in the range where the data overlap. Translating the above curve in the CCFL correlation form used by S-RELAP5 (Equations (5.106) and (5.510) of EMF-2100(P) Revision 4) yields the set of coefficients:

$$[\quad] \quad (65.2)$$

This set of coefficients is then used to assess other Framatome ANP CCFL Tests. The results show that all data are conservative with respect to the UTP CCFL correlation.

It is not possible to determine a set of coefficient values that best fits the data because of the large variations in data for different types of tie plates. On the other hand, it is not practical to define a set of coefficient values for each type of tie plate. One particular reason is that Framatome ANP has to deal with tie plates manufactured by other vendors in a mixed-core configuration. Therefore, the most appropriate approach is to use a set of coefficient values that bound the data, i.e., it is more restrictive on limiting the down flow of water. Accordingly, the set of coefficients obtained from the Framatome ANP CCFL Tests and described above is used for the upper tie plate CCFL correlation in all assessment and plant application calculations.

The UPTF tests are more appropriate than the Northwestern data to further assess the upper tie plate CCFL model because UPTF is a full scale facility with real plant tie plates and subcooled water and superheated steam were used. The assessments of UPTF Tests 10, 12 and 29 demonstrate that the CCFL correlation with the specified coefficients bounds all the data (Section 3.7 of EMF-2102(P) Revision 0). As an example, a plot of Kutateladze parameters calculated from the S-RELAP5 results compared with the UPTF CCFL correlation is presented

in Figure 65.2. The plot demonstrates three things: (1) S-RELAP5 CCFL model behaves correctly as shown by the linear upper limit of \sqrt{Kg} , (2) The CCFL correlation using the specified set of coefficients is conservative relative to the CCFL correlation derived from the UPTF data (solid line), and (3) a lot of calculation points are below the specified CCFL line. Also, the calculation points with co-current flow solution are not shown in the plot.

In the reflood assessment and plant application cases, the flow solutions calculated at the upper tie plate junctions above the hot bundles are mostly co-current (an example is shown in Response 122). Even if counter-current flow solutions are calculated, they are likely to be below the already conservative down flow limit. Therefore, a certain degree of top down cooling limited to near the top end of the rods is possible, but top down quench is highly unlikely. The rod temperature histories shown in Figures 65.3 and 65.4 demonstrate that top down cooling is insignificant.

Discussion of the downcomer ECC water penetration and CCFL, including suitability of using scaled data such as those of the Creare 1/15th and 1/5th tests, is presented in Section 5.5.2 of EMF-2100(P) Revision 4. In essence, the relative distance between the broken cold leg and each of the intact loop cold legs is an important parameter in determining the downcomer penetration but is poorly represented in the scaled data. The UPTF data showed that the downward flow of ECC water in the downcomer is nonsymmetrical and heterogeneous. The multi-dimensional characteristics of heterogeneous penetration of ECC water was not observed in the earlier small scale tests. [

] Framatome ANP uses the full scale UPTF downcomer penetration test data to assess the performance of the S-RELAP5 downcomer model. [

]

The Kutateladze parameters from the UPTF Test 6 calculations are plotted below and compared to the Glaeser correlation (as shown in Takeuchi and Young, 1998). Since the UPTF correlation was developed from averaged data measured from the lower plenum fill rate, the S-RELAP5 liquid flows for comparison are averaged lower plenum fill rates converted to Kutateladze parameters. A discussion is presented on the Glaeser correlation.

The measured and calculated steam up flows verses lower plenum fill rates are shown in Figure 65.5 and the associated Wallis parameters in Figure 65.6. Each point on the graph represents a particular run from UPTF Test 6. The following table, Table 65.1, lists the run number, the steam injection rate, the lower plenum fill rate, and the test run pressure. The test runs are listed in descending order based on steam flow, which corresponds to the plotted points from top to bottom. The accumulator injection flows are presented to show the amount of bypass measured and calculated for each test run. The total accumulator flow ranged from 1440 to 1480 kg/s.

Table 65.1 UPTF Test 6 Measured Flows and Pressures

Run No.	Steam Flow Rate (kg/s)	Liquid Flow Rate (kg/s)	Pressure (kPa)
135	436	548	360
131	396	570	295
132	295	898	310
133	202	975	250
136	102	875	265

The UPTF correlation by Glaeser was developed to describe the nonsymmetric heterogeneous gas/liquid countercurrent flow in the reactor scale tie plate and downcomer regions. Glaeser extended the Kutateladze-type flooding equation to do so. The flow is nonsymmetric if the ECC water is injected via the hot or cold legs, and the steam/water mixture is flowing out of one broken hot or cold leg. The use of either Wallis or Kutateladze parameters implies the assumption that the important gas velocity at the gas/liquid interface is approximately equal to the superficial gas velocity, i.e. an average gas velocity within the flow channel. This is not the case for large scale nonsymmetric flows.

Since the gas momentum at the interface influences the amount of water flowing downward, a ratio of the gas velocity at the interface to the superficial gas velocity has to be introduced. This gas velocity ratio is mainly determined by the distance 'L' between the respective intact leg, with ECC injection, and the broken leg, where the gas/liquid outflow occurs. The largest upward gas velocity compared to the average gas velocity occurs close to the broken leg due to the lowest pressure in the vicinity of the broken leg. Consequently, the largest build-up of a pressure difference in the gas flow occurs in the vicinity of the broken leg, if ECC water is injected into the gas upflow. The closer that the ECC injection leg is located to the broken leg, the smaller the average gas velocity (superficial gas velocity) for the same interfacial gas velocity, which determines the liquid down-flow rate.

The distance 'L' between the broken leg and the ECC injection leg is defined as:

$$L = \frac{1}{2} \pi D_{\text{outer}} \sin^2 \left(\frac{\theta_{\text{max}}}{2} \right) \quad (65.3)$$

where D_{outer} is the outer diameter of the downcomer interior and

where θ_{max} is the angle between the broken leg and the most distant ECC injection leg.

Another important parameter is the slope of the gas velocity profile, which is determined by the gas viscosity. The correlation defines the reciprocal dimensionless length as:

$$f_{\text{KG}} = \frac{j_i}{j_g} \approx \frac{L}{L^*} = \frac{v^{\frac{2}{3}}}{g^{\frac{1}{3}} L} \quad (65.4)$$

Therefore, the UPTF CCFL correlation, in terms of Kutateladze numbers, is:

$$\left(f_{KG} K_g\right)^{\frac{1}{2}} + 0.011 \left(K_f\right)^{\frac{1}{2}} = 0.0245 \quad (65.5)$$

where

$$K_x = \frac{\rho_x^{\frac{1}{2}} j_x}{\left(\sigma g (\rho_f - \rho_g)\right)^{\frac{1}{4}}} \quad (65.6)$$

and $x = f$ or g .

Note that the correlation is applicable to the later portion of the blow-down period near the 'end-of-blowdown'. The reason for this restriction is that the correlation is only applicable when there is a large pressure drop between the broken leg and an ECC injection leg. These conditions are no longer met after the break unchokes.

The results from applying the UPTF CCFL correlation to both the measured and S-RELAP5 calculated results from Test 6 are shown in Figure 65.7. The correlation was applied to the 3-loop and 4-loop sample problems for comparison purposes. The correlation was applied to the later stages of the 'end-of-blowdown' period where the break was still choked and where the substantial reverse core flow started to decay and positive core flow was re-established. Also, note that the 3-loop sample problem had no counter-current flow during this period.

The results from the 3-loop and 4-loop transients are shown in Figures 65.8 and 65.9. In those figures, the Wallis parameters are presented. [

] However, this occurs at the lower vapor velocities and the occurrences are few in number.

Overall, these results show that S-RELAP5 under-predicts downcomer flow. This is also evidenced from the higher than measured temperatures from the integral tests (EMF-2102) and the RAI responses concerning the downcomer nodalization studies. This is the expected result since the assessments indicate that the combination of the code and nodalization consistently over predict core bypass. Given that core bypass is over predicted, it is highly unlikely that too much downcomer flow is being predicted.

To assure that too much downcomer flow is not predicted, the limiting break case from the RLBLOCA analysis will be analyzed with the following methodology. The time period before reflood will not be analyzed. In blowdown the water in the system is flashing and downcomer flow is not important to core cooling. In the refill phase the full scale UPTF tests have shown that the model is conservative. For the reflood phase of the LBLOCA, a check on CCFL in the downcomer will be implemented using the Wallis correlation. Since a CCFL model is not being directly applied to limit flow in the downcomer, it is expected that there will be some calculated points that exceed the Wallis correlation. Based on the results of the assessments, which indicate that the overall prediction of ECCS bypass is conservative, if a significant percent of the calculated points exceed the criteria, the analyst will review the analysis in detail.

References

- 65.1 2D/3D Program Upper Plenum Test Facility, *UPTF Test No. 6 Downcomer Separate Effects Tests, Quick Look Report*, U9 316/89/2, Siemens AG, March 1989.
- 65.2 H. Glaeser, "Analysis of Downcomer and Tie Plate Countercurrent Flow in the Upper Plenum Test Facility," *Proceedings of 4th International Topical Meeting on Reactor Thermal Hydraulics*, Volume 1, pp. 75-81, October 1989.



**Figure 65.1 Comparison of FCTF Data and Mini-Loop Data Using an ATRIUM-9 UTP
(Figure 3.9.5 of EMF-2102(P) Revision 0)**



**Figure 65.2 Calculated Kutateladze Parameters Test 10 Run 080
(Figure 3.7.141 of EMF-2102(P) Revision 0)**

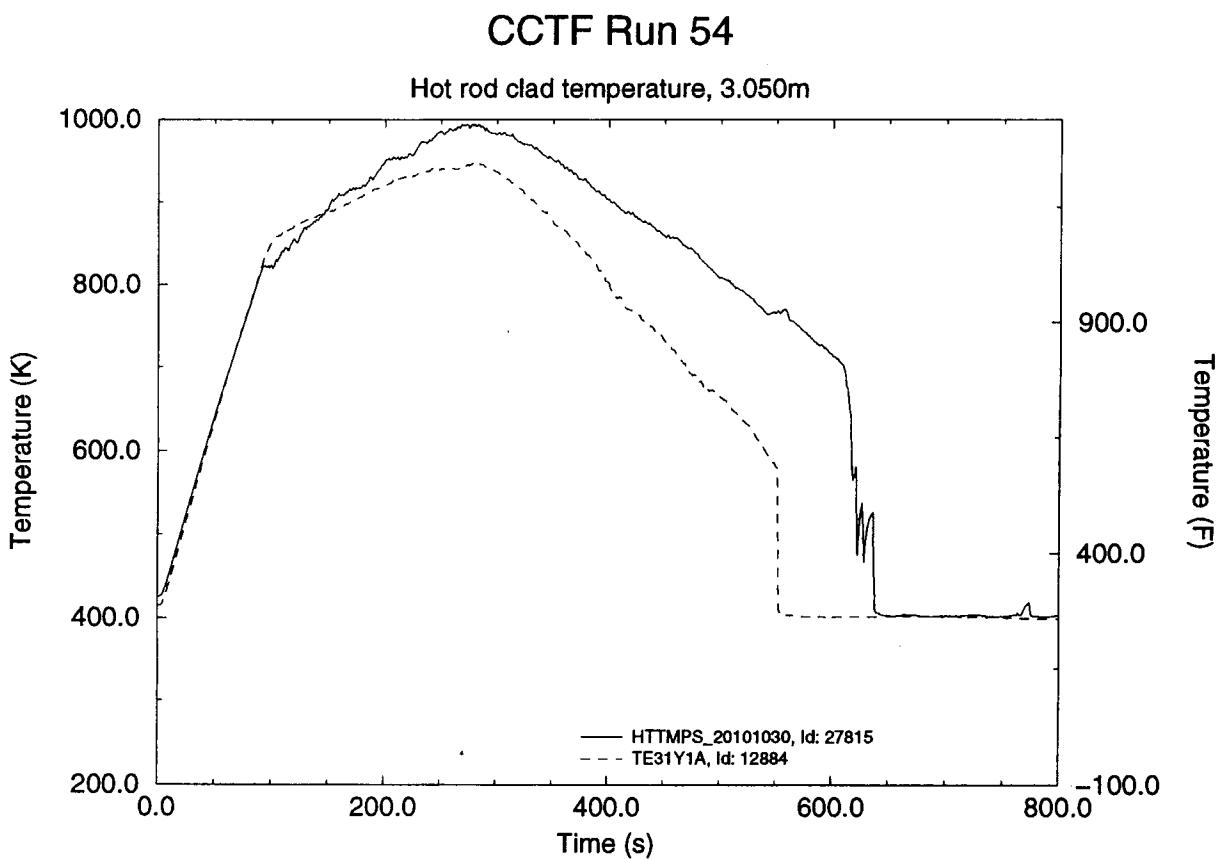


Figure 65.3 Comparison of Rod Surface Temperatures for High Power Bundles at 3.1m Elevation, CCTF Test Run 54 (Figure 3.12.31 of EMF-2102(P) Revision 0)

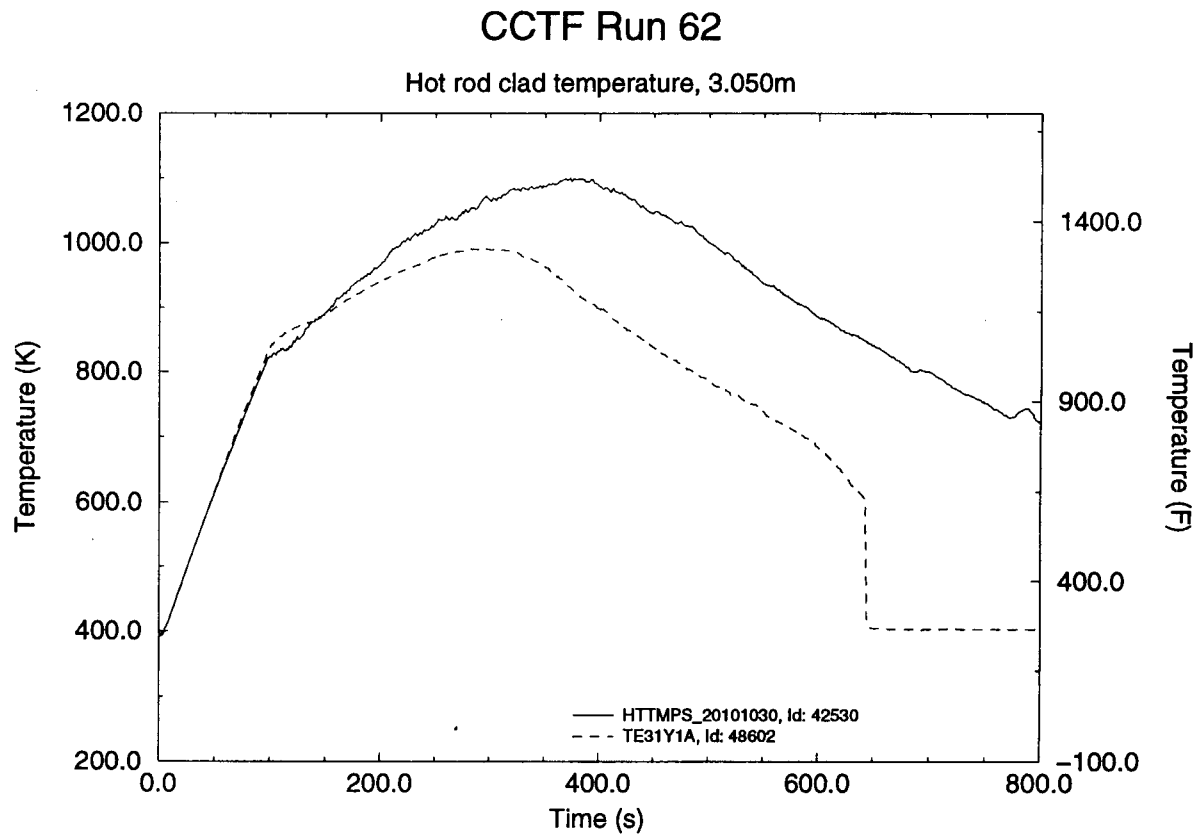


Figure 65.4 Comparison of Rod Surface Temperatures for High Power Bundles at 3.1m Elevation, CCTF Test Run 62 (Figure 3.12.58 of EMF-2102(P) Revision 0)

UPTF Test 6

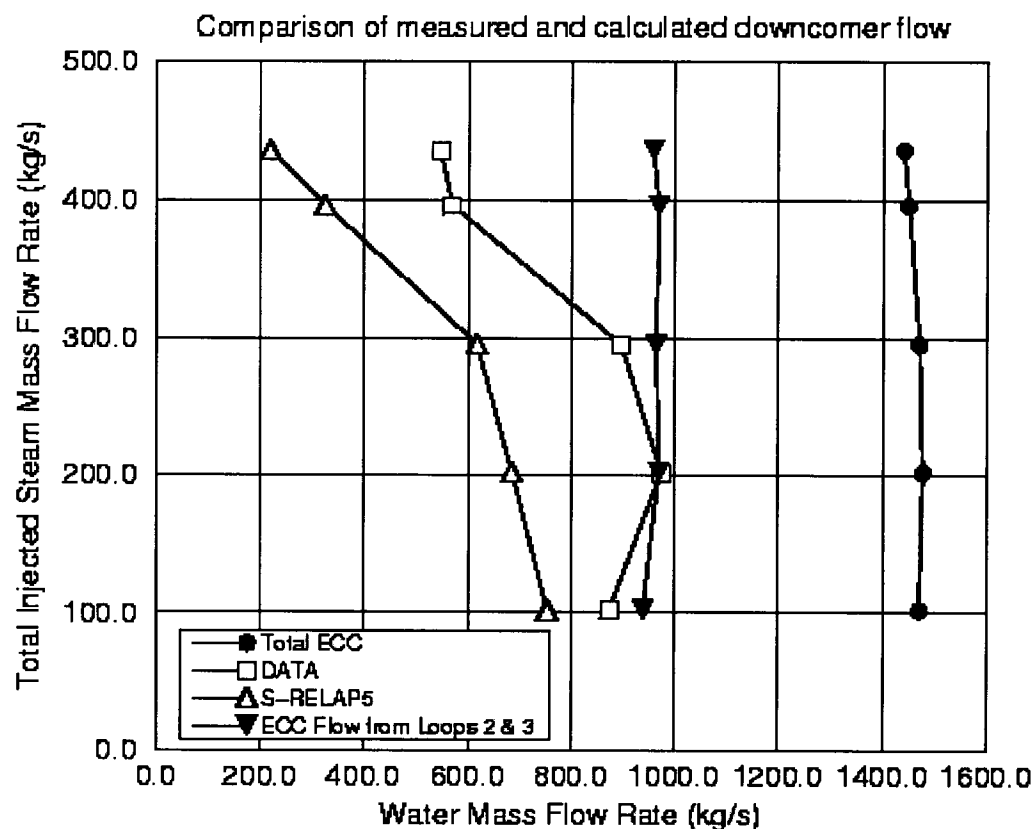


Figure 65.5 Comparison of Downcomer ECC Water Penetration in Terms of Mass Flow Rates for UPTF Test 6

UPTF Test 6

Comparison of measured and calculated Wallis parameters

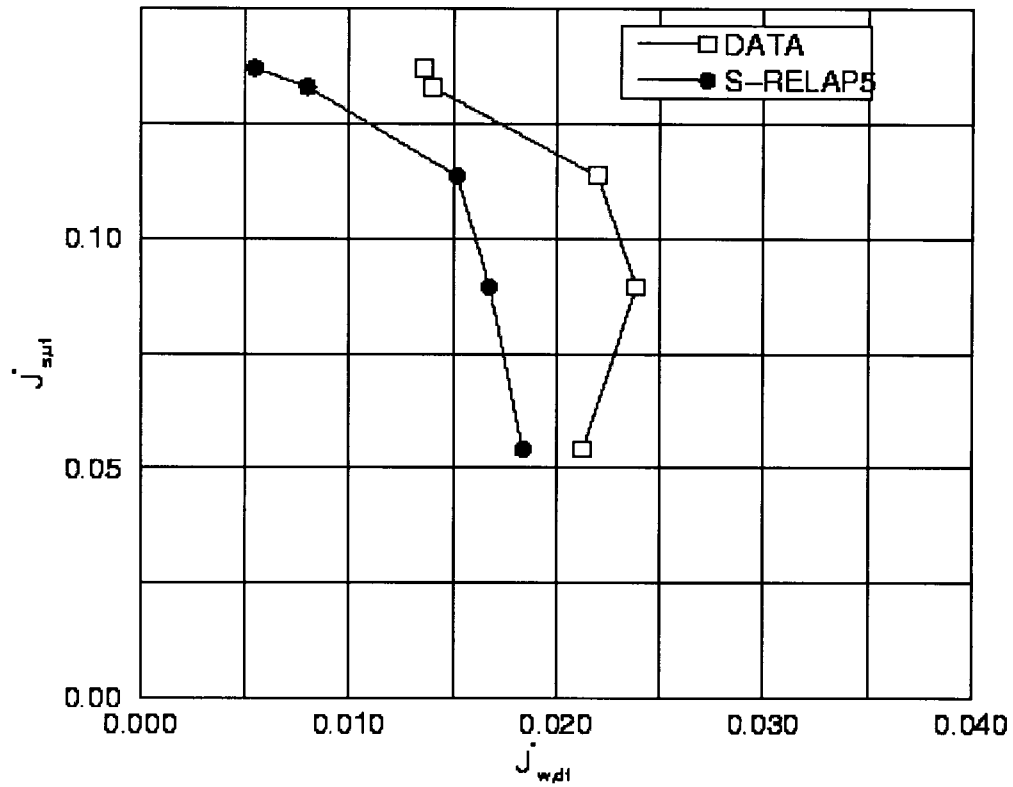


Figure 65.6 Comparison of Downcomer ECC Water Penetration in Terms of Wallis Parameters Using the Creare Correlation

UPTF CCFL Correlation

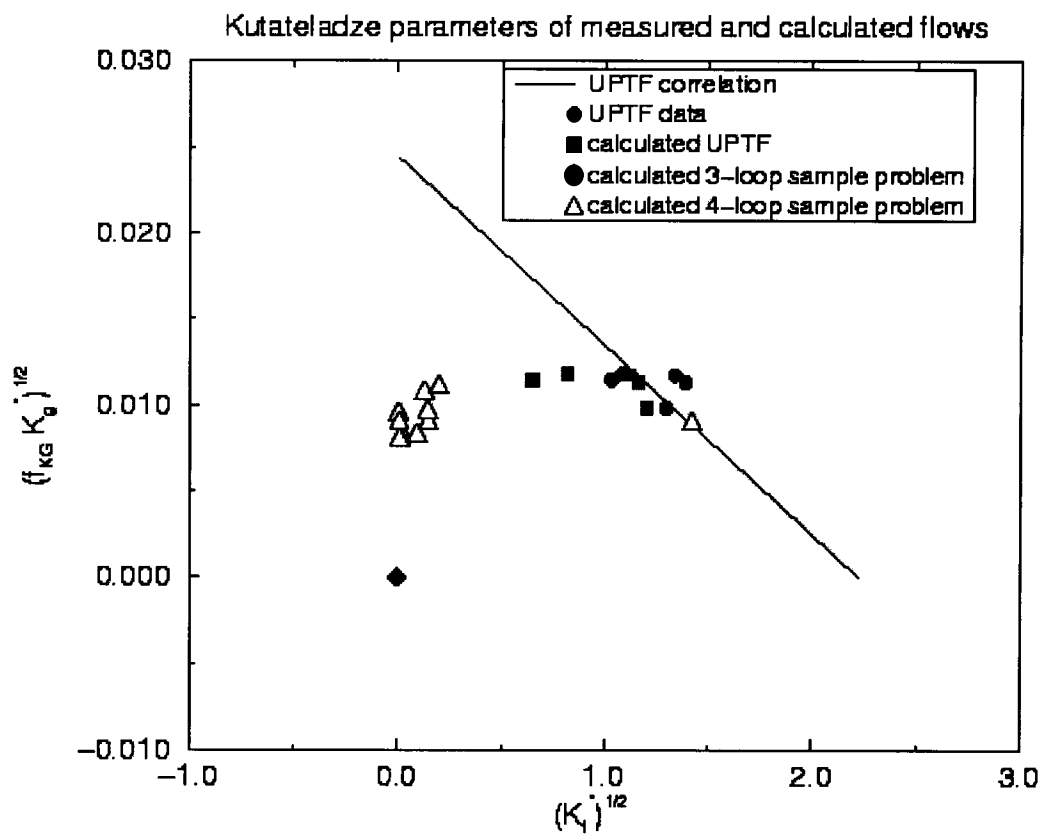


Figure 65.7 Comparison of Data and Calculations to the UPTF CCFL Correlation

3 Loop Sample Problem

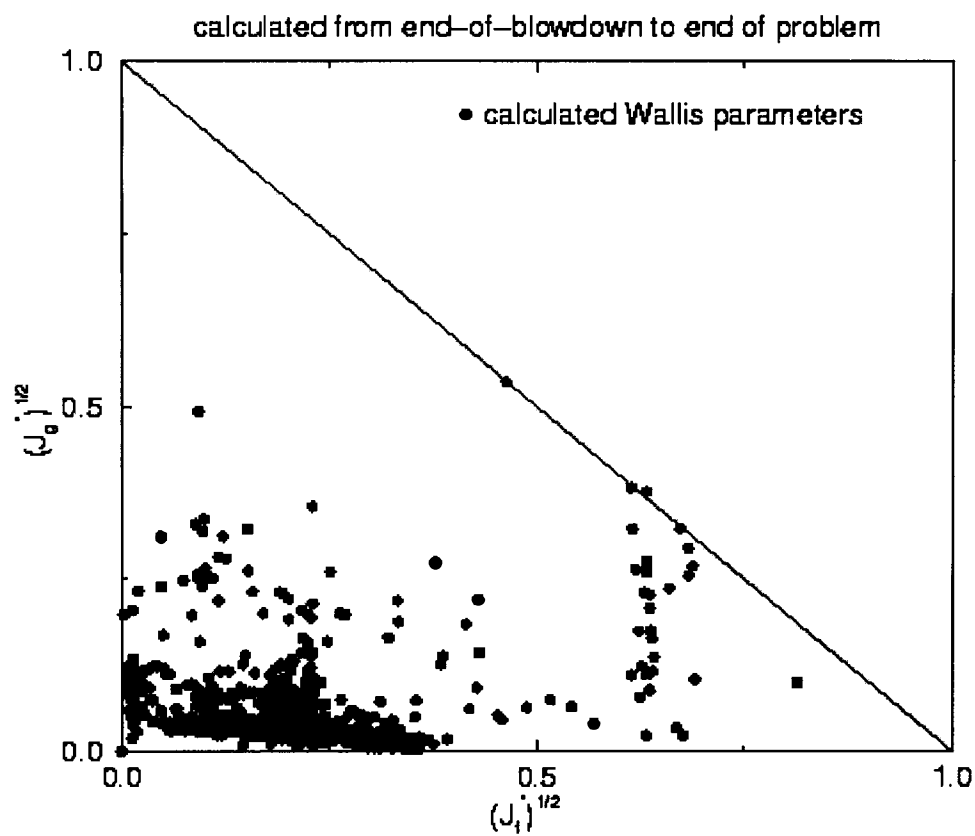


Figure 65.8 Wallis Parameters from 3-Loop Sample Problem

4 Loop Sample Problem

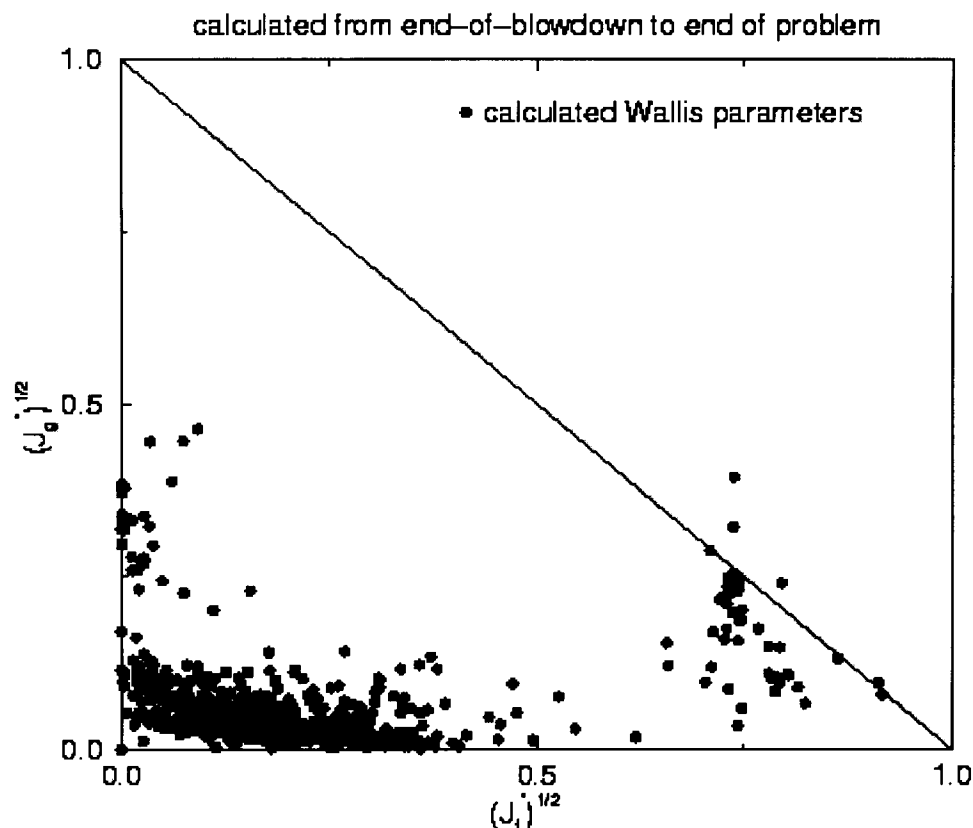


Figure 65.9 Wallis Parameters from 4-Loop Sample Problem

Question 66: Page 4-4 of EMF-2103 briefly states how compensating errors are handled in the assessment matrix for FLECHT, SCTF, CCTF, and THTF. However, there are no detailed discussions of compensating errors relative to the separate effects and integral tests. Please discuss compensating errors relative to the separate effects and integral experiments. The discussion should include Post CHF heat transfer, ECC bypass/condensation, and blowdown/post-blowdown thermal hydraulics and entrainment.

Response 66: The concern with compensating errors is that they may result in the code being able to predict some experimental assessments accurately but not be able to predict others due to changes in conditions or scale. While it is recognized that there may be compensating errors in large system analysis codes, it is also recognized that there is no practical method for proving or disproving the existence of these compensating errors. Thus, the most practical approach for dealing with compensating errors is to perform a wide range of experimental assessments to show that these compensating errors do not impact the code results.

The large number of test facilities and tests in those facilities that have been analyzed are shown in Tables 4.2 and 4.3 of EMF-2103(P). This assessment matrix included tests ranging in scale from as small as the Bennett Tube tests to full scale facilities such as UPTF. In addition, facilities such as FLECHT, FLECHT-SEASET, CCTF, and SCTF included essentially full-length fuel assemblies and in the case of the CCTF and SCTF full scale fuel assemblies. The tests in these facilities covered a wide range of test conditions and the S-RELAP5 code was capable of consistently predicting the test results in these facilities.

As an additional check, the LOFT, Semiscale, and CCTF assessments were re-run with the code model biases removed. The code model biases were determined by comparisons of the code with various SET assessments at varying scale. The use of these biases in a set of independent assessments of different scale provides a level of confidence that the code, even if there are compensating errors, can be expected to predict the important phenomena of the LBLOCA. The removal of the code model biases for the LOFT, Semiscale, and CCTF assessments consistently improved the comparison of code prediction and experimental data. While this does not prove there are no compensating errors in S-RELAP5 it does indicate that any compensating errors that exist in the code will not impact the codes ability to predict the results of a LBLOCA.

In general, the issue of compensating error is only relevant for dominant LOCA phenomena. Two key areas of concern with regard to compensating errors are core heat transfer and ECCS bypass. Core heat transfer is dependent on the suite of heat transfer correlations and interfacial friction. In the response to Question 20, a discussion is provided that explains that the approach to evaluating film boiling uncertainties inherently accounts for compensating error present from the inseparability of heat transfer and interfacial friction.

ECCS bypass is dependent on the separable phenomena including condensation of ECCS water, lower plenum sweepout, downcomer boiling, and downcomer counter current flow.

[

]

Question 67: *Please identify a reference discussing error propagation and how this is handled in the uncertainty methodology.*

Response 67: The non-parametric statistical approach directly propagates the uncertainties and there is no special treatment required for error propagation.

Question 68: *The Achilles Test in EMF-2102 showed that S-RELAP5 underpredicted the core liquid level, the PCT by about 125F, and the downcomer level. Please discuss possible reasons for these differences. The effect of the nitrogen on condensation was not measured in this test. How is the effect of nitrogen on condensation determined in S-RELAP5? Also, please discuss the sensitivity of the PCT to condensation efficiency. How does S-RELAP5 compute entrainment of liquid by the nitrogen and, if so, how does this influence the calculations? What is the sensitivity of full scale plant PCT to condensation efficiency?*

Response 68: The Achilles test simulation was performed to confirm the ability of S-RELAP5 to simulate the effects of nitrogen injection on core cooling following the emptying of the accumulators. The test assembly consisted of an array of rods, arranged in an x-y grid, inserted in a cylindrical pipe. This resulted in an extremely large degree of radial inhomogeneity in the fuel rods. Figure 3.15.5 of EMF-2102(P) Revision 0 shows the radial variation in temperatures at the PCT elevation. From this figure, it is obvious that an accurate modeling of the gaps between the fuel rods and the pipe would be required to predict temperatures accurately. The model flow areas and flow resistances were adjusted to account for the very large by-pass areas in the core in an approximate way. Two different groups of rods were considered: those on the inside area and those on the periphery. The flow areas for the rods on the periphery were adjusted to account for the open flow area and the flow resistance was reduced to account for the open flow paths on the periphery. Considering the approximate nature of the modeling for the fuel rod array, a reasonable agreement between the calculated PCT and the measurements was deemed sufficient for the evaluation of S-RELAP5.

With regard to the liquid levels, the comparison of the core liquid level shown in Figure 3.15.11 seems to reflect quite good agreement between S-RELAP5 and the test. The downcomer level is somewhat bizarre, in that it would seem to require about 20 kPa more dynamic pressure drop during reflood. By varying the losses between the exit of the simulated fuel rods and the exit of the test assembly, it is possible to increase the downcomer level slightly. However, dramatic increases in resistances result in too much expansion cooling downstream and the code "crashes" when the water freezes. In fact, during the test, there was significant freezing of suspended water. (See Figure 3.15.6, where the venturi was reduced by ice, causing an anomalous indication of higher flow.) In the end, since the nitrogen had left the system by 25 seconds, it was not really essential to resolve the level anomalies, since they arose after this time and were not considered to be related to the presence of nitrogen in the system.

The model describing the effect of nitrogen on condensation is presented in Section 3.4.9 of EMF-2100(P) Revision 4. This is discussed below. In general, the presence of the noncondensable gases reduces the condensation rate and the higher the quality of the noncondensable gases, the lower the condensation rate. The formulation in S-RELAP5 reduces the liquid-side heat transfer coefficient by a factor, F , when liquid is subcooled.

$$H_{f,n} = H_f F$$

where the subscript n denotes the heat transfer coefficient in the presence of noncondensable gases and F is given by,

$$F = \left[a + 0.366(1-a) \left(\frac{G_g}{X_n G_f} \right)^{0.2} \right] (1-X_n)^{0.4}$$

The mass fluxes of the gas phase (steam + noncondensable gases) and fluid phase are denoted by G_g and G_f , respectively, X_n denotes the quality of the noncondensable gas and the correction factor for very low qualities is given by

$$a = \text{MAX}[10(0.1 - X_n), 0]$$

The overall effect of condensation was addressed in a sensitivity study and the conclusion was that the effect of nitrogen on condensation was not a significant contributor to PCT. A multiplier is provided in S-RELAP5 for the effect of the reduction in the condensation rate in the presence of noncondensable gases [see Section 2.9 of EMF-CC-097(P) Revision 7] and it was used in plant calculations to address the sensitivity of the model. The sensitivity of the PCT to varying this multiplier was about $\pm 30^\circ\text{F}$. [

]

Entrainment by noncondensable gases (nitrogen) is considered and the models are the same as those for steam entrainment, except for the differences in the properties of the two gases.

Question 69: *Section 4.3.3.2.6 of EMF-2103 identifies a T_{\min} of [] is used in the analysis based on comparison to FLECHT reflood data while Page 4-20 of EMF-2100 identifies a T_{\min} of [] as used to establish the boiling curve. Please clarify discuss the impact on the test comparisons and plant calculations.*

Response 69: EMF-2100, Section 4.7 summarizes the T_{\min} model used in S-RELAP5. [

]

Reference

1) J. Zhang, S. M. Bajorek, R. M. Kemper, and L. E. Hochreiter, "WCOBRA/TRAC Analysis of ORNL High Flow Rod Bundle Film Boiling Tests," 1997 National Heat Transfer Conference, Baltimore, MD, August 1997.

Question 70: *Regarding modeling of transition boiling heat transfer, at the lower limit S-RELAP5 uses the maximum of the Sleicher-Rouse steam cooling correlation and a free convection correlation, Forslund-Rohsenow or Bromely is used for film boiling depending on the void fraction. Please discuss the lower limit of the transition correlations with regard to consistency with the lower limit on the film boiling correlations. Please discuss code stability with regard to the heat transfer coefficient at T_{\min} during the switch from transition boiling to film boiling.*

Response 70: The switch from transition boiling to film boiling rarely occurs in transient calculations. The most likely scenario is from nucleate boiling (pre-CHF) to film boiling (post-CHF) and then remaining in film boiling. The switch from film boiling to transition boiling is responsible for the rod temperature quench behavior (rapid decrease in temperature) shown in both the data and the calculations. Since oscillations are not observed in either the data or the calculations; the large difference in the magnitudes of transition boiling and film boiling heat transfer does not create a problem with respect to code stability.

Question 71: *General comments regarding code assessment:*

Question 71a: *Core 3-D Flow and Void Distribution (Page 4-85, EMF 2103). Comparison to the THTF and GE Level Swell data, for example, are high pressure tests and do not represent PWR reflood conditions. The GE data does not apply to rod bundle drag. On the other hand, specific FLECHT boil-off or reflood data are applicable to voids in bundles at low pressure (FLECHT-SEASET Test 35658, for example).*

Response 71a: In addition to the high pressure void distribution comparisons for the THTF and GE level swell tests, void distribution comparisons have been made for low pressure reflood tests. The void distribution comparisons for FLECHT-SEASET and FLECHT SKEWED reflood tests are represented by the calculated and measured differential pressures between 72 and 84 in. displayed in Figures 3.3.71 to 3.3.79 of EMF-2102(P) Revision 0. Note particularly that code-data agreement is excellent after the region between 72 and 84 in. is completely quenched. This demonstrates the wet-wall (pre-CHF) interphase friction model is applicable and adequate for both high pressures (THTF Tests) and low pressures. The void distribution above the quench front is dominated by the dry-wall (post-CHF) interphase friction model. The differential pressure plots show that (1) the calculated liquid fraction far above the quench front is lower than the measured and (2) the calculated liquid fraction near the quench front is higher than the data for injection rates below 1.5 in/sec and lower than the data for injection rates higher than 3.0 in/sec. This void distribution pattern is consistent with the clad temperature history at around the 78 in. elevation.

The key factor in determining the clad temperature (and PCT) is the void (or more properly, liquid) distribution. The key question to ask is, "Where is the water?" The lower liquid fraction (in comparison with the data) far above the quench front and the generally lower core inventory calculated (Figures 3.3.89 -3.3.97 of EMF-2102(P) Revision 0) indicates that insufficient liquid is retained at elevations far above the quench front and most of the liquid drops carried away from the quench front are carried out of the core. This tends to produce higher clad temperatures during the temperature rise period and hence, conservative (high) PCT as demonstrated by most of the assessments of the reflood separate-effects and integral effects tests reported in EMF-2102(P) Revision 0. The accumulation of more liquid in the region immediately above the quench front results in a quench time closer to the data (Figures 3.3.104 -3.3.109), in spite of higher PCT. The picture of void distribution for the post-CHF region is not perfect and is not as good as that for the pre-CHF region, but it is adequate and conservative for licensing applications.

Question 71b: *Regarding Core 3-D flow distribution, the SCTF comparisons, especially at the higher elevations, indicate underprediction of peak temperatures and quench times that are early by 200 – 300 seconds for transients with 500 second heat-up times. Additional justification is needed to demonstrate that the clad oxidation is bounded. While these are low temperature tests, the early quench time predictions will significantly affect oxidation and the uncertainty may effect the error methodology. Discussion is needed regarding how the 200 – 300 second early quench predictions are factored into the uncertainty in oxidation calculations. There should also be discussion of the lack of a model for film boiling as a function of distance from the quench front which would improve the quench time predictions. This discussion should also address the reasons for the discrepancies in quench time predictions and underprediction of PCTs. The S-RELAP5 code predicts large oscillations in the void fractions in the core (see Fig. 3.11.47 of EMF-2102, for example). Discussion is needed regarding the oscillations and their effect on super heat and clad temperature underprediction. The discussion should also address the*

consequences of the oscillations with respect to the reflood behavior the potential bias of these oscillations to lower PCT.

Response 71b: Framatome ANP has limited the use of the SCTF comparisons to demonstration of the adequacy of the code to calculate radial power distribution effects. The reason for this is that many assessments of S-RELAP5 against experimental data were made, and for essentially all assessments except the SCTF, the code results versus measured data exhibited a consistent conservative pattern for predicting heat transfer and PCT. For reasons not yet understood, the SCTF assessment yielded acceptable PCT comparisons but did not show the same prediction pattern for heat transfer. Framatome ANP believes the predictive capability of S-RELAP5 should be established based on the consistent predictive trends with other assessments and not the SCTF tests.

Question 71c: Liquid Entrainment. *While the entrainment is overpredicted for the CCTF tests, overprediction coupled with drop size could bias the steam temperatures in the channel to low values if the drop size is too small. Please discuss how the S-RELAP5 model predicts the steam super heat for these tests (at selected elevations starting at locations near the quench front) and the reflood data presented in EMF-2102. How does the void fraction influence the steam super heat and dispersed flow film boiling heat transfer when the entrainment is over-predicted for the tests? Included in the discussion should be the topic that excess entrainment does not lead to propagating errors into the film boiling model and a non-conservative impact on PCT.*

Response 71c: The tendency and consequence of the post-CHF interphase friction model to retain less liquid at elevations sufficiently far above the quench front are discussed in the Response to Question #71.a. Such a tendency is the most significant contributor to the calculated higher PCT in most assessment cases, regardless of whether excessive liquid entrainment is present in a calculation.

For the four CCTF tests, the good agreement between the calculated and measured core differential pressure (Figures 3.12.29, 3.12.56, 3.12.84 and 3.12.112 of EMF-2102(P) Revision 0) suggests that the overall void (or liquid) distribution is properly calculated and the liquid carry-out is not excessive. Because the steam temperature instrumentation did not correctly measure the superheated steam temperature in a steam-water mixture environment, as pointed out in Section 4.3.1.12 of EMF-2103(P) Revision 0 and Section 3.12 of EMF-2102 (P) Revision 0, it is not possible to assess the performance of the code calculation of steam temperature against the data.

Generally speaking, the two most important factors influencing the steam superheat are (1) the heat transfer to steam and (2) the vapor generation rate. A lower calculated steam temperature may be caused by lower heat transfer to steam or higher vapor generation rate or a combination of the two. The vapor generation rate depends on the interphase heat transfer model and the amount of liquid; therefore, excessive entrainment, even if calculated, does not necessarily imply higher vapor generation rate or lower steam temperature. Also, a lower steam temperature does not necessarily imply a higher heat transfer rate and a lower PCT. The two-fluid heat transfer model requires the partition of heat transfer to liquid and vapor, but currently there are no data or theory available for accurate modeling of the partition. Forslund and Rohsenow (Dispersed Flow Film Boiling, J. of Heat transfer, p.399, November 1968) cited the two-step process - heat transfer from wall to superheated steam and then from the superheated steam to liquid droplets - proposed by Laverty. The reality is that there are several direct and indirect processes

governing the heat transfer from the wall to the vapor and liquid in the dispersed film boiling and there is no accurate information to determine which portion of the heat transfer in the end goes to which particular phase. Therefore, accurate calculation of steam temperature may not be possible with present knowledge of wall to fluid heat transfer.

The uncertainty in the steam temperature calculation does not necessarily lead to a non-conservative impact on PCT. The key factors are total heat flux from the wall to the fluid and the liquid fraction in the dispersed film boiling flow. The steam temperature, which depends on the assumption of indirect heat transfer processes, is of secondary importance. Of primary importance is to model reasonably well the two key factors. It is concluded, from the inspection of all reflood assessments, that the combined effects of the interphase friction model, vapor generation (or interphase heat transfer) model, heat transfer model and conservative upper tie plate CCFL model, produce higher clad temperatures compared to data in the upper core region (from around 6 to 10 ft) where the PCT occurs and thus, have a conservative impact on PCT.

Question 71d: *Upper Plenum Entrainment/De-entrainment. Please discuss the manner in which de-entrainment in the upper plenum is calculated. Is there a model for de-entrainment on structures? How is entrainment to the hot legs and steam generator calculated? It should be shown that the S-RELAP5 over prediction of liquid buildup in the upper plenum is not due to under-prediction of entrainment to the hot legs and steam generators. Also since the code allows a second top down quench, does counter-current flow in any of the SETs, integral tests, and plant calculations reduce the clad temperatures or affect clad oxidation in the top of the core?*

Response 71d: There is no specific model for de-entrainment of liquid from any reactor component. In vertical components, a co-current (upward) flow solution implies entrainment of liquid and a counter-current flow solution implies de-entrainment of liquid. Among the various force terms in the momentum equations, the interphase friction is the primary factor in determining the flow directions between the two phases. Thus, liquid entrainment/de-entrainment is primarily a function of the interphase friction model. However, at the upper tie plate and steam generator inlet plenum junctions, a CCFL model is applied to limit the liquid down flow; therefore, entrainment/de-entrainment of liquid in the upper plenum is also affected by the CCFL model.

As discussed in Section 3.2.3, particularly, Equation (3.62), of EMF-2100(P) Revision 4, the interphase friction for the upper plenum component is enhanced to increase the liquid entrainment. Also, bounding values of CCFL input are used to hinder the liquid down flow to the core (see Response to Question 65 and discussion below). These two things insure that the down flow of liquid from upper plenum to core is conservatively calculated. The assessment of CCTF tests indicates that the top down quench range is much shorter than the data. Response to Question 122 presents a figure showing that there is no liquid down flow at the upper tie plate junction above the hot assembly.

On page 4-43 of EMF-2103, there is a discussion concerning the effects of CCFL input on the results from UPTF Test 29. The plotted results were not included in EMF-2103, but can be found in Figures 3.7.124 through 3.7.128 on pages 3.7-191 through 3.7-195 in EMF-2102. Those figures show that liquid hold-up in the upper plenum, as well as carry-over to the steam generators, varies with CCFL prediction. Since bounding values of CCFL input are used in the plant models, similar results are expected.

Question 71e: CCFL. *There are no special drag models in the downcomer specifically designed to treat countercurrent flow. Without these comparisons, there is no assurance that the CCF limit will not be violated during a plant calculation. Comparisons to countercurrent flow data would demonstrate that the liquid down flows in the downcomer do not violate CCFL. Figs. 4.116 and 4.117 show that the CCFL model is limiting the liquid downflow for many of the test points. This suggests the drag model tends to produce too high a liquid down flow for a given steam flow. Unless the drag model is different in the downcomer, these results suggest that the drag model will produce excessive liquid down flows in the downcomer. Please discuss the omission of the CCFL model or drag model specifically designed to model CCF in the downcomer.*

Response 71e: (See response to Question 65)

Question 71f: CCFL. *Since the S-RELAP5 code does not use a CCF limit model, interfacial and wall drag modeling is key to predicting CCF. Application of concurrent up-flow correlations for interfacial and wall friction to countercurrent flow tend to over-estimate the downflow of liquid. It appears that wall shear is neglected during countercurrent flow which would produce over-estimated liquid downflows in the low gas velocity region. Wall shear stress acting on falling water is almost the same order of magnitude as interfacial shear stress, making it inappropriate to ignore this stress. Since RELAP5 ignores wall shear during annular flow and EMF-2100 Section 3.0 did not show the details of the wall shear, discussion is needed that describes how wall shear is computed during CCF. This discussion should also compare the friction factor with data and show the behavior at low velocities/Reynolds numbers.*

Response 71f: S-RELAP5 does not ignore the wall shear under counter-current flow conditions and during annular flow. The description of S-RELAP5 wall friction is presented in Section 3.5 of EMF-2100(P) Revision 4. Unless the user purposely turns off the wall friction via input options, the wall friction is always evaluated under all flow conditions. (See response to Question 23).

Question 71g: CCF. *How is CCF modeled in the 2-D downcomer and how are the flow regime maps applied in this region?*

Response 71g: (see response to Question 65)

Question 71h: Hot Leg Entrainment. *Hot leg entrainment is underpredicted in Figs. 4.165-4.167, 4.173, 4.177, and 4.179, and, thereby it is not supported that hot leg entrainment is calculated conservatively. In some cases entrainment is not predicted until late in the test. Does the underprediction lead to a beneficial effect on PCT for the tests which offsets another conservatism elsewhere in the methodology? Fig. 4.173 shows no entrainment was calculated for the entire test. If the entrainment is calculated to match the data late in the test, this does not the model being conservative as stated on page 4-90 of EMF-2103.*

Response 71h: First, the assessment of the conservatism of carryover calculations was based on the accumulated results from three sets of tests. The carryover was dramatically over-predicted in full-scale, UPTF tests. The comparison in EMF-2103 Revision 0 Figures 4.164-4.167 are to levels in a catch tank downstream of the steam generator in the broken loop. Steam and liquid exiting the broken hot leg enter a separator at the top of this catch tank and the liquid is dropped into the tank. The level measurement is quite noisy – the plots have been smoothed significantly. In most cases, the measured level even indicates a level reduction in the early part of the transient. The measured values have a significant amount of uncertainty. In addition, the flow exited from the steam generator and traveled through fairly long pipes that

were modeled as having adiabatic boundaries. Heat transfer to the liquid on the secondary side of the steam generator and in the piping also contributed to additional uncertainties. As with the FLECHT-SEASET data, S-RELAP5 tended to under-predict the carryover when the rates were very low and to over-predict when they got higher. Test 54 (Figure 4.164) had somewhat higher flow rates than did Tests 62 and 68 and it was used to set the scaling factor for the interphasic drag at the inlet to the steam generator tubes. Test 68 also had high calculated carryover, although the data showed only a very small level change. Making a precise statement about the carryover calculations for these four tests is somewhat difficult and the adjustment of the drag was based on a comparison to test 54.

In Figures 4.168-4.171, the levels in the catch tanks downstream of the steam generator simulators were compared to calculated values for the full-scale facility, UPTF. For these tests, the carryover in the broken legs and in the intact legs was measured. Using the enhanced interfacial drag determined by CCTF test 54 resulted in a conservative prediction for the broken and intact legs. Using a nominal value of drag caused a slight under-prediction of levels in certain cases.

Figures 4.172-4.179 compare the levels in the separator tank and in the drain for the separator tank. The carryover is the sum of the two amounts. Test 31805 had very small carryover flows (the level in the separator didn't change and the level change in the drain tank was only about 2"), but Test 31203 had a more substantial amount of carryover and S-RELAP5 over-predicted the levels as long as the carryover was large. During the period from 150 seconds to 350 seconds, there was carryover, but it was not sufficient to show up as a level change in the main tank. Similarly, for Test 31302, S-RELAP5 under-predicted the carryover for low carryover rates. Once the flow became appreciable (~120 seconds), the calculated carryover was significantly higher than the measured. In this case, the modeling of the flow from the separator tank to the separator drain tank affects the filling of the drain tank at 130 seconds. A CCFL model was used in the drain and it held up the water flow to the drainage tank far more than the data would indicate. Removing the CCFL limit would result in a better fit to the level in the drain tank after 130 seconds, but the period before with the low carryover rates would still be under-predicted. Essentially the same comments apply to test 31701, except for the timing. There is a spurious level change in the drain tank when the operators intervened.

Overall, the conclusion reached was that for very low carryover rates, S-RELAP5 under-predicted the carryover. Once carryover became significant, particularly for the issue of steam binding in the steam generator, S-RELAP5 over-predicted the carryover. The under-prediction when carryover was very small was considered to be far less significant than the over-prediction during high carryover. The tendency of S-RELAP5 to over-predict in the strong steam-binding region was the basis for concluding that the modeling was conservative.

Question 71i: *Two-Phase Pump Model. The pump resistance and broken cold leg nozzle typically represent the largest resistances in the loop which determines the core flow (and hence fuel stored energy/PCT) during blowdown. It should be shown how the uncertainty in the relative resistances between the core and break through the downcomer and hot leg paths are taken into account and that the pump resistance, broken nozzle resistance, and the other loop resistances conservatively bound the expected variation (or are insignificant) in these path resistances from the core to the break.*

Question 71j: *Pump Differential Pressure Loss. How is the pump coastdown verified in the case there is no plant data? What is done in the modeling to assure the coast down is bounded?*

Response 71i & 71j: As stated in RAI response #24, the pump model is treated as best-estimate. This is necessary since control systems applied to pump speed (coupled with control systems on steam generator feedwater flow) are used to steady-state the plant model prior to a transient calculation. Without a reasonably accurate pump definition, code prediction of plant steady-state conditions will not agree with measured plant conditions. The figure-of-merit for pump performance is based on agreement of key steady-state operation variables including loop temperatures, flow rates, and pump speed.

Pump coastdown is not explicitly addressed in this methodology's PIRT given in Table 3.4 of the methodology document. As may be inferred from the PIRT, the two-phase pump degradation was ranked as having a strong phenomenological impact on PCT during blowdown, while the pump differential pressure loss has a strong impact on PCT during reflood. However, in the sensitivity study shown in Appendix B.4, the PCT impact of two-phase pump degradation was much less than anticipated by the PIRT team. During reflood, S-RELAP5 evaluates the pump differential pressure loss directly from the single-phase pump performance characteristics required in the pump model. Pump seizure is not considered part of a best-estimate LBLOCA scenario; and, for this reason, it is not considered in this methodology.

Pump performance (including pump differential pressure loss) during single-phase conditions is based on best-estimate pump-specific performance data. It has been Framatome's experience that most plants have this single-phase pump data available for modeling purposes and usually have pump coastdown data for model benchmarking. Large disparities from actual and calculated pump characteristics are unlikely since the steady-state simulation would fail to show loop temperatures and flow rates consistent with plant data. The CE/EPRI two-phase pump degradation model will be used in the RLBLOCA methodology and the methodology document, EMF-2103, will be revised to indicate this (see Appendix D).

As stated in RAI response #24 and #35, the uncertainty in the broken nozzle k-factor and the relative resistances from the core to the two ends of the break is a break flow/flow split issue.

[

]

Question 71k: *Non-Condensable Transport. The Achilles Test # 25 under-predicted the PCT later in the event. While the effect of the nitrogen is to initially force additional water onto the core providing some early limited core cooling, the later overall effect is to reduce core cooling since the higher initial steaming reduces the liquid inventory in the core causing a late heat-up of the core. S-RELAP5 under-predicted the negative effects while capturing some of the early beneficial effects. Please discuss the basis for including the early beneficial effects of nitrogen in plant calculations and not considering this parameter in the uncertainty methodology and imposing it as a penalty on PCT.*

Response 71k: The Achilles test (ISP #25) simulation was performed to confirm the ability of S-RELAP5 and the RBLOCA methodology (including modeling assumptions) to simulate the effects of nitrogen injection on core cooling following the emptying of the accumulators. The test assembly consisted of an array of rods, arranged in a Cartesian x-y grid, inserted in a cylindrical pipe. This resulted in an extremely large degree of radial and azimuthal inhomogeneity in the fuel rod flow areas. For the outside rows of rods, there were fairly significant gaps where the Cartesian rod array could not be forced to match the round tube. As a result, many of the rods near these gaps quenched very quickly. See the temperature traces in Figure 3.15.5 of EMF-2102. It was apparent that water was coming up the bundle through these gaps and quenching at fairly high elevations very quickly. An accurate modeling of the gaps between the fuel rods and the pipe would have been required to predict temperatures accurately. The degree of inhomogeneity far exceeds that present in a PWR core and the model would have had to differ fairly significantly from the core model to be used in the methodology. By adjusting the model carefully it would have been possible to get a better fit to later PCTs, but the comparison would not have used the core model appropriate for the methodology. Therefore, an accurate model was not created.

For the approximate model based on the methodology, the core was broken into two areas and the flow areas and flow resistances were adjusted to account for the very large by-pass areas in the outer portion of the core in an approximate way. Two different groups of rods were considered: those on the inside area and those on the periphery. The flow areas for the rods on the periphery were adjusted to account for the open flow area and the flow resistance was reduced to account for the open flow paths on the periphery. Given the model simplifications of a very complicated flow pattern in the test assembly, the under-prediction of the PCT at the PCT node is not particularly meaningful. If one refers to Figures 3.15.12 through 3.15.17 of EMF-2102, the PCT elevation is the elevation where the predicted temperature falls below the measured. For the neighboring measurements (within about 8"-10" of the PCT elevation), S-RELAP5 over-predicts the temperatures. In addition, note that the temperatures show far less variability at the other elevations than is seen at the PCT elevation (with the possible exception of the temperatures at 3.18 m). Thus, some fairly complicated three-dimensional flow effects that would not be modeled in a LBLOCA are determining the PCT for this test.

Considering the approximate nature of the modeling for the fuel rod array, a reasonable agreement between the calculated PCT and the measurements was deemed sufficient for the evaluation of S-RELAP5.

With this test, the trade-off of early cooling and late heating is fairly obvious. One can force the nitrogen to go through the core by increasing the resistance in its alternate flow path. The effect is a quick flushing of all of the liquid in the downcomer and "lower plenum" as well as the core. This results in a rapid cool-down of the fuel rods. When the initial surge of cooling is past, the liquid inventory is nearly gone from the region below the core and the rods begin an adiabatic heat-up until the liquid finally fills the "lower plenum" region and enters the core. This results in a more rapid heat-up until the liquid reaches the core again, after which the heat-up is in pretty good agreement with the data. However, the fast heat-up more than offsets the initial cooldown and results in a slightly higher PCT than was observed. For a LBLOCA, one does not experience this range of variability in the modeling. The amount of early cool-down in ISP #25 was just a consequence of adjusting the resistance in the escape path for the nitrogen so that it would match the rate of escape of the nitrogen.

[

] The effect of the nitrogen injection can be seen in the core level plot (Figure 5.27) and on the fuel rod temperature plot (Figure 5.18) for the sample case shown in EMF-2103. There is clearly an effect on the temperatures when the nitrogen enters the system. It has been shown in the analysis of Achilles ISP #25 that S-RELAP5 under-predicts any initial beneficial effects of the nitrogen on the PCT. Since S-RELAP5 is conservative with regard to this aspect of nitrogen injection and since it generally over-predicts temperatures in the test assembly, with the exception of the PCT elevation, which has large variability in the measured temperatures; there is no need for a penalty.

Question 71I: *Downcomer Entrainment.* Please identify the correct section in Ref. 5 for the downcomer entrainment tests and discussion referred to in Section 4.3.3.1.10 of EMF-2103. Please discuss the cause of the lower plenum liquid level oscillations in Figs. 4.106 through 4.110, including the flow regimes predicted by S-RELAP5 during this period, and the steam and liquid velocities in the downcomer and exiting the lower plenum during these tests. Does the under-prediction of the liquid inventory in the lower plenum enhance the steam downflow in the core during blowdown and produce a beneficial effect on PCT? Does boiling occur in the lower downcomer and lower plenum in these tests and what effect does boiling versus no boiling have on the entrainment?

Response 71I: The reference indicated in EMF-2103 is correct. The reference is "Section 4.3.1 and Reference 5" where the section referred to is in EMF-2103. In Reference 5 the section of interest is Section 3.7.4.

The lower plenum liquid level oscillations are described in Section 3.7.4.4.1 and the steam and liquid mass flows are provided in Table 3.7.5 of EMF-2102, Revision 0. There were also two sensitivity studies performed to look at these oscillations and they are reported in Section 3.7.4.4 of EMF-2102, Revision 0. The first sensitivity study looked at turning off the mixture level model in the lower plenum and the second sensitivity study looked at using a 2D component in the lower plenum. With the mixture level turned off the oscillations were significantly reduced but the lower plenum liquid level was in worse agreement with the data and even more conservative. With the use of a 2D component in the lower plenum, the comparison to data was significantly improved. However, there was a new set of oscillations in the predictions relative to the data. An undocumented calculation was also performed to look at the use of the 2D lower plenum model in the sample plant calculation. This calculation indicated that the 2D lower plenum model provided a less conservative PCT but significantly increased the run time. Based on this evaluation it was decided to go forward with the lower plenum model reported in EMF-2103, Revision 0.

With respect to the possibility of enhanced steam down flow in the core with a potential benefit on PCT, a lower liquid level in the lower plenum would tend to amplify this possibility. However, this effect, if it did occur, would have a secondary influence on the PCT relative to the delay in the initiation of reflood. The increase in predicted bypass flow and associated decrease in lower plenum fill rate has a direct impact on the predicted PCT. The overall conservatism of the methodology (code and nodalization) is clearly demonstrated in the conservative PCT's calculated for both the LOFT and Semiscale integral assessments.

Very little if any boiling would have occurred in these tests. The tests were conducted by first bringing the system temperature up to that of the steam temperature and then initiating the flow

of the ECCS water. The tests were specifically designed to look at downcomer and bypass flow versus steam flow up the downcomer. The expected impact of boiling in the downcomer in these tests would be to further impede the liquid flow down the downcomer and to increase the bypass flow.

Question 71m: *Downcomer Level Oscillations. Fig. 3.11.47 of EMF-2102, shows large oscillations in void fraction. Please discuss the model conservatism as stated in Section 4.3.3.1.11, since the core in these tests shows large void oscillations which can "provide additional core cooling" as pointed out on page 4-92. If downcomer boiling occurs during accumulator discharge, what is the effect on PCT after the accumulators empty.*

Response 71m: The indicated figure does show large oscillations in the core void fraction. However, the figure also shows that while the code does under predict the void fraction for short periods of time during these oscillations, on average the code conservatively over predicts the void fraction relative to the measured data. This general over prediction of the core void fraction will lead to the prediction of higher conservative PCTs. This conservatism is clearly shown by the over prediction of the temperatures demonstrated in Figures 3.11.36 through 3.11.45.

In general, the impact of downcomer boiling is to delay the flow of water down the downcomer and into the lower plenum. Given this, if downcomer boiling occurs during accumulator discharge the impact would likely be an increase in the amount of accumulator water that would bypass the core and be lost out the break. Given the loss of additional accumulator water, the PCTs would be expected to increase.

Question 71o: *Lower Plenum Sweepout. Oscillations suggest that the sweep out of the liquid from the lower plenum is retained in the downcomer and immediately flows back into the lower plenum periodically. In such a case, please discuss the model conservatism regarding the lower plenum liquid level test predictions. Should there be flow of liquid back into the lower plenum, does this result in entrained liquid entering the core and providing additional cooling? Discuss the need for bias in the uncertainty evaluations if the lower plenum oscillations cool the core.*

Response 71o: The UPTF ECC penetration tests were designed to simulate ECC flow in the downcomer during the LBLOCA blowdown-refill period when the accumulator ECC water penetrates the downcomer and the steam flows down the core and up the downcomer to carry out the water to the break. Under such circumstances, steam flow is in the wrong direction to entrain water to the core. Furthermore, a very strong steam flow is required to produce such large oscillations. For a cold leg break with pump off, the steam flow from the lower plenum to the core, if present, can never be strong enough to produce lower plenum level oscillations of significant amplitudes. Accordingly, the situation of large lower plenum oscillations enhancing liquid entrainment to the core does not exist and is not calculated to occur in plant applications; therefore, there is no need to evaluate the bias or uncertainty for such an event that either does not exist or is of no significance.

It should be pointed out that the large lower plenum oscillations are due to the conditions peculiar to the UPTF Test 6 series and are not observed in plant applications. As discussed in Section 3.7.4.4.1 of EMF-2102(P) Revision 0, the large oscillations go away if the mixture level model is turned off in the bottom volume of the lower plenum. With reference to the nodalization showing in Figure 3.7.4 of EMF-2102(P) Revision 0, the conditions for improper appearing and disappearing of mixture level (more precisely liquid level) in the bottom volume for the Test 6

series are: (1) the lower plenum is initially empty, and (2) no significant amount of steam flows to the bottom volume and the liquid drains slowly to the bottom; therefore, the fluid velocities in the bottom volume are low. These conditions are not present in the plant calculations, since the lower plenum is initially full of water and the void fraction difference between the two lower levels is never large enough to produce a liquid level in the bottom volume.

Therefore, in plant calculations, the lower plenum sweep-out behaves like those shown in Figures 3.7.38, 3.7.41, 3.7.44, 3.7.47 and 3.7.50 of EMF-2102(P) Revision 0. Thus, all liquid above a certain level, which depends on the vapor velocity, of the upper lower plenum volume is carried out of the lower plenum by the vapor, and large oscillations are not present. Note that if the lower plenum is nodalized with more axial levels and with a narrow upper flow path to allow vapor to flow through the lower plenum without much liquid entrainment, no significant sweep-out will occur. The results will be similar to those obtained with the 2-D horizontal component discussed in Section 3.7.4.4.2 of EMF-2102(P) Revision 0. The present two axial level 1-D lower plenum nodalization is a necessary compromise to satisfy certain steady-state requirements. With such a nodalization, conservative lower plenum sweep-out is calculated. However, the sweep-out does not lead to liquid entrainment into the core since the vapor flow either is in the wrong direction or is not strong enough to cause significant entrainment.

Uncertainty Analysis

Ref: EMF - 2102(P)

Question 72: 5.1.1 Data Set Adequacy

With regard to Table 5.1 it appears that not only the maximum pressure data, but also the mass flux of the vapor and liquid do not bound the intended application. Please justify in greater detail your statement that the data set on which film boiling multipliers, bias, and uncertainty are determined adequately cover the intended application.

Response 72: [

]

Question 73 (Part 1): 5.1.2 Inferring Heat Transfer Coefficients from Experimental Data

Please describe mathematically the inverse conduction algorithm (flow diagram and a few equations) used in computing the boiling heat transfer coefficient from the thermocouple data.

Response 73 (Part 1): The requested material is provided (see Appendix A).

Question 73 (Part 2): *In Fig. 5.1 is this the numerical node scheme for the inverse algorithm? If so, at what node is the thermocouple?*

Response 73 (Part 2): In Figure 5.1, the thermocouple is at the boundary between the boron nitride and the clad inside surface.

Question 73 (Part 3): *Specifically, how is the surface heat flux a function of the derivative with respect to time, as stated in sec. 5.1.2.1?*

Response 73 (Part 3): The transient heat conduction equation (one-dimensional, cylindrical geometry) is solved to determine the heat flux at the clad surface.

$$\rho c_p \frac{\partial T}{\partial t} = \frac{1}{r} \frac{\partial}{\partial r} \left(kr \frac{\partial T}{\partial r} \right) + \dot{q}'''$$

The first term in this equation contains the temporal derivative. The term in parenthesis, when divided by the area, is the heat flux. Thus, the heat flux will vary with time.

Question 73 (Part 4): *The thermocouple measures the temperature $T(r_o, z_o, t)$ (i.e. at some fixed point (r_o, z_o) as a function of time t (as in Figs. 5.2 and 5.3). The objective seems to be to compute the surface temperature at the same elevation at the same time points as the thermocouple measurements. So where is the time derivative necessary? Where is the source of the amplification?*

Response 73 (Part 4): The time derivative is necessary to capture the effects of stored energy in the electrically heated rod during the transient test. Failure to include this term will cause the derived convective heat transfer coefficients to have a bias that is related to the lag of the transfer of stored energy to the coolant.

The experimental measurement is of temperature. These measurements are taken discretely, at intervals that are on the order of 0.5 second (FLECHT-SEASET). To obtain the heat transfer coefficient, the heat flux must be inferred (calculated) from these temperature measurements. The heat flux is a function of the derivative of the temperature, which, mathematically, is the slope. The slope is quite small in magnitude so slight variations in the temperature will cause apparently large variations in the heat flux.

Question 74: *5.1.2.1 Signal Filtering*

Question 74 (Part 1) *What is the t between thermocouple signals?*

Response 74 (Part 1): FLECHT-SEASET Tests: 0 to 200 seconds (0.5 sec between samples); after 200 seconds (1.0 sec between samples).

Question 74 (Part 2): *What is the thermocouple instrument error?*

Response 74 (Part 2): The 2-sigma uncertainty of rod sheath thermocouples in THTF is reported by the experimenters to be 10.3 K. An additional 0.3 K is added to this to obtain the nominal transient uncertainty, applicable except at the time of quench.

For FLECHT-SEASET, the thermocouple instrument error is 3/8% of reading between 277 C and 1316 C. This is combined with a conditioner error of $\pm 1.01^\circ\text{C}$ and a readout error of $\pm 2.03^\circ\text{C}$.

Question 74 (Part 3): *The thermocouple reading has two sources of variation:*

i) the instrument error

ii) a variance due to the fluctuations in the underlying physical process. (If we had a perfect instrument, this variance would still be there.)

Do you estimate these effects?

Response 74 (Part 3): Fluctuations in the underlying process were treated qualitatively by filtering the data. Of primary interest is the modeling of the limiting hot rod and the conditions surrounding it. Test data associated with rods within 2 rows of the shroud (channel wall) were removed from consideration because they exhibit cold wall effects that would skew the results.

Question 74 (Part 4): *What is your stopping rule with regard to smoothing of the thermocouple readings with respect to the above variances?*

Response 74 (Part 4): The above variances were not used to establish an acceptance criteria for smoothing the thermocouple readings. The thermocouple data were filtered first with the median filter, then with the binomial filter.

Question 74 (Part 5): *What is your stopping rule with regard to smoothing the inferred heat transfer coefficients (as in Figs. 5.4 and 5.5)?*

Response 74 (Part 5): The above variances were not used to establish an acceptance criteria for smoothing the heat transfer coefficients. The heat transfer coefficient data were filtered first with the median filter, then with the binomial filter.

Question 74 (Part 6): *Do you apply any quantitative measure to claim that "the underlying features of the signal are intact"?*

Response 74 (Part 6): No. This was performed visually by examining sample thermocouple signals processed by the algorithm. As a check that the procedure works acceptably, the results were compared with qualified published results, a sample of which is shown in Figure 5.6.

Question 74 (Part 7): *Comment: Fig. 5.6 is irrelevant.*

Response 74 (Part 7): Agreed, it may not be necessary to retain this figure in EMF-2102.

Question 75 (Part 1): *5.1.3 Data Consistency Check*

Question 75 (Part 1): *Since the test data provide multiple estimates of HTC for common times and elevations, is the mean computed at some specific time and elevation the "truth" with respect to which you compute the bias in the computed value at that time and elevation; and the standard deviation the uncertainty?*

Response 75 (Part 1): We take the values which remain after evaluation of the data and average them. The purpose of the averaging is to obtain a value comparable to the calculated value from S-RELAP5 that represents a nodal volume average.

Question 75 (Part 2): *How do you assure that the data were not oversmoothed? (That is only the instrument error and outliers were removed.)*

Response 75 (Part 2): Smoothing does not necessarily remove the instrument error. It does, however, help remove a part of the truncation error that is part of the analog to digital conversion (this causes the flat spots of apparent zero slope). In THTF, the smoothing of the median filter also removed the sharp temperature spikes that occurred in the data (the experimenters attributed this non-physical behavior to the power supply). Because the same smoothed data was used for analysis of T_{min} and quench time (described in Appendix B), and excess smoothing would round the "knee" in the thermocouple trace, minimal smoothing was applied to the data. The largest effect of smoothing occurs near quench and this effect is discussed in Appendix B to these RAIs.

Question 76: *5.1.4 Partitioning the Data*

The data are partitioned into two sets. What are you validating? Are the THTF and FLECHT - SEASET data considered initially as one set and then split into two through random selection?

Response 76: The data that we have are sampled from the population of possible values. In order to ensure that our result (the curve fit) applies to the population as a whole, and not just to the sample, we divide the sample randomly into two parts. One part is used to develop the curve fit (the multipliers). The other part serves as a check that our curve fit applies more generally to the population.

Question 77: *5.1.5 S-RELAP5 Calculated HTC*

5.1.5.1 Data Averaging

The oscillations in the computed values of void fraction, heat transfer coefficient and clad temperature are attributed to changes in the heat transfer mode in the course of the computation (i.e. film boiling, single-phase vapor)

Question 77i: *What is the variable and its value that determines which mode to assume?*

Response 77i: The S-RELAP5 variable is RFLMOD. The value is the same as for variable HTMODE described in EMF-CC-097 in Section 4.5. Film boiling is identified by HTMODE=7. Single-phase steam is identified by HTMODE=9.

Question 77ii: *What is the time increment in the computation and what is the average cycle length of the oscillation in the void fraction, and T_{clad} ?*

Response 77ii: The S-RELAP5 time step is dynamically determined during the course of the transient to satisfy numeric stability requirements. The maximum allowable time step is input by the user. The user also determines the frequency of writing data to the plot file. This frequency was chosen to correspond to the smallest time step in the measured data. For FLECHT-SEASET, the time increment in the plot file is 0.5 seconds. For THTF, the time increment in the plot file is 0.05 seconds. An analytical computation of the average cycle length in the oscillations in the code was not computed. The cycle length changes as the transient evolves, but is about 2 to 6 seconds per cycle prior to the time of quench.

Question 78a (Part 1):

Is it correct that RELAP computes the void fraction (α), the heat transfer coefficient (h) and the clad temperature (T_{clad}) sequentially as follows:

$$\alpha - h = T_{clad}$$

Response 78a (Part 1): No. The calculation is $h \rightarrow T_{cl} \rightarrow \alpha$.

Question 78a (Part 2): *If so, is the same algorithm applied with the 8 sec. window? How does the window size compare to the computational time step?*

Response 78a (Part 2): Yes, the same algorithm is applied with the 8 sec window. The window size is larger than the calculation time step.

Question 78a (Part 3): *How does it compare to the time step in the T_{clad} measured values?*

Response 78a (Part 3): The window size is larger than the Δt between measured values of temperature.

Question 78b (Part 1): *Is the following sequence of computations during processing of the data correct?*

Let $D(t)$ be the original values at time t . Assume $w = 3$. Then

$$\bar{f}_3(4) = (1/3) (D(1) + D(2) + D(3) + D(4))$$

$$\bar{f}_3(5) = (1/3) (D(2) + D(3) + D(4) + D(5))$$

etc.

Then $f_{smooth}(t-w/2) \leftarrow f_w(t)$ for each $t \geq w/2$.

Response 78b (Part 1): The description of the averaging of the described S-RELAP5 values is the following:

A running average is used to smooth the S-RELAP5 calculated data. It is applied to the void fraction, the clad surface temperature, and the heat transfer coefficient. Through use of control variables it is possible for S-RELAP5 to compute a running average. Part of this running average is computed with S-RELAP5 control variables. The final construction of the running average is performed by post-processing. The S-RELAP5 integrating component computes:

$$I(t) = \int_0^t f(t) dt$$

In S-RELAP5, a delay component may be used to save results of the integration for states that occurred w seconds in the past. Effectively,

$$I(t-w) = \int_0^{t-w} f(t) dt$$

The running average is obtained by taking the difference between these two equations and dividing by the difference in time.

$$\bar{f}_w(t) = \frac{1}{w} [I(t) - I(t-w)] = \frac{1}{w} \left[\int_{t-w}^t f(t) dt \right]$$

The running average generated by this algorithm is a “trailing” average. That is, the average lags the physical behavior. During post-processing of the data, each of the running averages is further refined to generate a central running average. The changes made are:

- Shift the averaged data to the left by $\frac{1}{2}$ of the window width w . This is effectively accomplished by discarding the first half of a windows width of averaged data.
- Second, do not average over the quench front. Therefore, from the quench time less a window width, replace averaged data with raw data.
- Third, patch the first part of the running average by using raw data instead of averaged data. This is necessary because the delay component results in averaging of zeros until the time reaches the window width. The window width, w , is 8 seconds.

Question 78b (Part 2): *Is it correct to say that you compute a moving average with a lag of w and then shift the value back by $w/2$ in time?*

Response 78b (Part 2): S-RELAP5, with the use of control variables, is able to compute a moving average that is based on the recorded data over the previous w seconds. For a function $f(t)$, this average, $f(t)_{avg}$, lags the actual system behavior $f(t)$. This average can be translated into a central average by shifting the time scale by $w/2$ so that half of the interval is in the past, and half of the interval is in the future. On this basis, the answer to the question is yes.

Question 79: *In reference to the comparison shown in Figs. 5.18 through 5.20.*

Question 79a: *Are you applying the same algorithm (i.e. w) in the vapor and quench parts of the curves as in the transition region?*

Response 79a: The algorithm is being applied to the vapor parts but not to the quenched parts. Treatment near the quench front was described in another response above.

Question 79b: *How would enlarging the window result in larger segments of unsmoothed data in the film boiling regime?*

Response 79b: Under some conditions, the inverted annular flow regime (associated with FILMBL) is very short, only a few inches in length. To avoid imparting a bias that includes nucleate boiling (high heat transfer coefficients) that occur at the quench front, it is important that averaging not be applied across the quench front. The calculated data that is within $w/2$ of the quench front is not averaged. A larger w would mean that more of the data is not averaged and more oscillations in the calculation that is to be compared to data. A larger window also results in more of the calculated data at the start of the transient not being smoothed, by width w .

Question 79c: *How is stopping the smoothing at the level where the amount of ripple remaining is on the order of what might be expected as experimental uncertainty relevant? The computation is deterministic, therefore, experimental uncertainty cannot be reproduced. By not smoothing "completely" how can you be sure you are not skewing the distribution on which your uncertainty estimate in the multiplier is based?*

Response 79c: When it was determined that smoothing was necessary, it was applied with the intent to use the minimal amount of smoothing necessary to provide a calculated value that would be comparable to a measured value.

Clearly, the fluctuations observed in the S-RELAP5 calculated void fraction and heat transfer coefficient are not observed physically and are artifacts of the code model. To not smooth would cause very large (and unacceptable) uncertainties.

On the other hand, smoothing causes curvature of gradients to be reduced. If the gradient is "real," then excess smoothing would introduce a bias in the results. Therefore, a compromise was struck. The smoothing, although essential, should be minimized, and consideration of experimental uncertainty was used only to establish a rough estimate for assessing if the amount of smoothing applied was adequate.

Question 79d: *Therefore, what harm is there in smoothing completely, in view of the comparisons shown in Figs. 5.18 through 5.20?*

Response 79d: Additional smoothing in this case would be acceptable.

Question 79e: *5.1.6 Multiplier Correlation*

You are determining two heat transfer coefficient correlation multipliers in this section

M_{FILMBL} and M_{FRHTC}

Correct?

M is a function of z (fuel height) and t the time in the transient, since $h_{\text{meas}}(z_0, t)$ and $h_{\text{calc}}(z, t)$, where z_0 is the thermocouple location. Correct?

Response 79e: It is correct that two heat transfer coefficient correlation multipliers are being defined.

It is possible for M to be a function of the elevation, as an artifact of experiment design. But the correlation and the multipliers are functions of local conditions and do not include the elevation as an explicit parameter.

Question 80: *How do you define quench front?*

Question 80i: *At a thermocouple location z_0 how do you determine the time of the quench front at that location from the measured data?*

Response 80i: The determination of quench in the measured data is based on the FLECHT-SEASET algorithm for the low pressure data. This algorithm was not directly applicable to the

high pressure test data in THTF. The higher sampling rate in THTF made it possible to devise an algorithm that uses the maximum negative curvature in the thermocouple trace (a mathematical way of finding the "knee" in the curve). The mathematical algorithms and description are presented in Appendix B to these RAIs.

Question 80ii: *How are M_{FILMBL} and M_{FRHTC} related to the definition of quench front?*

Response 80ii: The quench front identifies the boundary between nucleate boiling and film boiling in the test section and in the code calculation. The multipliers apply only to film boiling.

Question 80iii: *In aligning the quench fronts to a common location (say z_0), what parameters are you equating? (i.e. $P_{meas}(z_0, t_{meas}) = P_{calc}(z_0, t_{calc})$?)*

Response 80iii: The quench fronts identify a point of commonality between the calculation and the measurement. By using the quench front (instead of time) as the basis for comparison, the section of the heated length that is in nucleate boiling is common between the measurement and calculation and the section of the heated length that is in stable film boiling is common between the measurement and calculation. By aligning these features, the void fraction distribution as a function of elevation above the quench front should be comparable between the measurements and the calculation, and the axial pressure profile should also be close. This means the local conditions on which the film boiling heat transfer coefficient is based will also be closely similar between the measurement and the calculation.

Question 81 (Part 1): *You state "Temporal displacements between THTF measured data and code calculations were ignored. The transients are sufficiently short in duration that the temporal differences are expected to be small."*

In principle, is it not the relationship between the time step size in the transient calculation in relation to the temporal differences that is the issue, and not the duration of the transient? Please explain your reasoning in greater detail.

Response 81 (Part 1): The transient begins with virtually identical conditions between the measurements and the calculation. However, minor differences between the state of the calculation and the measurement will grow as the transient progresses. In a shorter transient, the differences are insignificant. For a longer transient, this will not necessarily be the case. For example, in a rod temperature plot from a long transient, the small differences in heat transfer rate cause the location of the peak clad temperature and the quench front to shift significantly. Many of the observed differences can be removed by applying a small temporal shift to the calculated data.

The heat transfer correlations are evaluated based on "local conditions." To obtain the best possible basis for comparison, the local conditions need to be comparable, with temporal differences removed. The results would be heavily skewed if, for example, the measured point of comparison was quenched and the calculated value was not quenched.

Question 81 (Part 2): *Note: Since*

$$M(t) = h_{meas}(t) / h_{calc}(t)$$

a misalignment of h_{meas} and h_{calc} with respect to time will introduce a bias in the distribution of $M(t)$ (which t will be used in $M(t)$, the one from the measurements or from the calculation?)

Response 81 (Part 2): M was not correlated to be a function of time. A value of M was chosen that applies independent of time. To remove the temporal differences in the FLECHT-SEASET data, the location of the quench front as a function of time was examined. Times were chosen that correspond to when the quench front was just below a differential pressure measurement location. This choice affects the measurement of the void fraction. The time associated with that measurement was used to obtain a snapshot of the measured data. Then, the S-RELAP5 calculation was examined. When the quench front reached the same location as that in the test, the time was noted and a snapshot of the calculated values was obtained. These were then compared directly to the measurements. Therefore, the expression above for M should be written

$$M = \frac{h_{meas} \left[t_{meas} (z_{quench}) \right]}{h_{calc} \left[t_{calc} (z_{quench}) \right]}$$

Question 82: *5.1.7 Film Boiling Multiplier Statistics*

5.1.7.1 Defining Data Set

Is this the same partitioned set as described in sec. 5.1.4?

Response 82: Yes.

Question 83: *I do not understand the first paragraph!*

Question 83i: *Does “multiplier pairs” mean M_{FILMBL} and M_{FRHTC} ?*

Response 83i: Yes.

Question 83ii: *How were $M_{FILMBL} = [\quad]$ and $M_{FRHTC} = [\quad]$ determined?*

Response 83ii: The multipliers were determined by trial and error. Values were chosen and code calculations performed. The calculated values were then compared to the measured values and the mean and standard deviation calculated. A mean of 1.0 corresponds to the desired solution.

Question 83iii: *What does “The correlating set had a mean of 1.00 and a standard deviation of 0.373.” mean? In particular, what is the “correlating set”?*

Response 83iii: As explained, the data which has been collected in experiments represents a sample of the population. This sample was randomly divided into two parts. The first part, the defining data set, (used for correlation, hence the name correlating set) is used to determine the multipliers. The validating set is not used to develop the multipliers.

Question 84: *Please explain the rest of this section more clearly.*

Question 84i: *Figs 5.21 through 5.23 refer to frequencies of measured-to-calculated HTC ratios. what happened to the distinction between FILMBL and FRHTC?*

Response 84i: M_{FILMBL} and M_{FRHTC} were not independently determined. They were determined together, and are part of the code model. In the model, M_{FILMBL} is applied when the void fraction is less than []. M_{FRHTC} is applied when the void fraction is greater than []. Some combination of these two multipliers, as determined by the interpolating function, is applied between void fractions of [].

Because of the oscillatory behavior of the code heat transfer mode, and a transition region where both multipliers apply, an integral approach to the determination of film boiling heat transfer multipliers was required. The figure of merit on the fit is the ratio of the measured to calculated heat transfer coefficient. For both the inverted annular film boiling regime and the dispersed flow regime, this heat transfer coefficient ratio should have a value of 1.0. The interpolating region between the two regimes should also have a ratio whose value is 1.0. Therefore, this is what is reported, for all of the data.

Question 84ii: *Similarly, in the fit of M vs. α , what heat transfer regime is assumed and why?*

Response 84ii: The data has been filtered so only data which is in stable film boiling is considered. The curve fit of M vs. α considers all of the measured data - some of which is inverted annular film boiling, some of which is dispersed flow film boiling, and the remainder of which is in the transition between inverted annular and dispersed flow. The expression indicates that there is not a significant bias in the heat transfer coefficient ratio associated with either multiplier or the combination of the multipliers.

Question 85: *5.1.7.2 Validating Data Set*

Is it not true that both the correlating set and the validating set are random samples from the same data set? I fail to see what you are validating in that case.

Response 85: The collective set of test data represents a sample of the population. Each one of the points in the data set represents a sample from this population. In an ideal world, one would collect data by sampling the population and then develop a model which describes the population from the sample. Then, to demonstrate that the model applies to the population, additional data would be collected by sampling from the same population. This additional data is evaluated with the model to determine if the model provides an adequate simulation of the population. In our development, the ideal world does not exist because the data has already all been collected. So the process must be emulated. This is performed as follows.

Formal methods were applied to develop the multipliers (develop the correlation). Since all of the data was already collected, each of the data points were treated as a sample from the population. The samples were randomly divided into two parts. The first part, the correlating data set, was used to develop the multipliers. The validating data set was set aside, to be used later after the correlation development (the multipliers) is complete. The validating set is used to extend the applicability of the model to the population, which is more than the set of data that has been collected, separately or collectively.

Question 86: 5.1.7.3 Probability Distributions for Film Boiling

It seems to me that a lognormal distribution would be more appropriate for $f(x)$. There is no reason a priori to separate $f(x)$ into two terms based on low and high void fraction. Moreover a discontinuity in the derivative with respect to void fraction is introduced. Please explain.

Response 86: A log-normal distribution for $f(x)$ could be used. However, it doesn't fit the data as well. As a first step in selecting the appropriate empirical distribution for the data, two parameters were calculated based on the data:

$$\beta_1 \equiv \frac{\mu_3^2}{\mu_2^3}$$

and

$$\beta_2 \equiv \frac{\mu_4}{\mu_2^2}$$

where

$$\mu_n \equiv E[(x - \mu_1')^n]$$

These values, which depend on the skew and kurtosis of the distribution, were then plotted on a chart (see for example, Figure 6.1 of "Statistical Models in Engineering," Gerald J. Hahn and Samuel S. Shapiro, John Wiley & Sons, 1967) which was marked into various regions in which different types of empirical distributions were best choices.

The calculated values of the parameters clearly excluded the Log-normal distribution, the Normal distribution and the Gamma distribution. The Log-normal is excluded because the data show a much lower value of β_2 , corresponding to greater peakedness. The Normal distribution was excluded based on the amount of skew. The Gamma distribution was excluded because the skew was too small for the kurtosis. The best candidate was a Beta distribution, with the preferred choice of parameters corresponding to a J-shaped distribution. This distribution is a simple polynomial form, applying over a range of the parameter. The only problem with a reverse J-shaped Beta distribution is that it goes to infinity as the argument goes to zero. The distribution chosen was a simple polynomial form, applied to a finite range of the variable, and it was designed to bound the probability distribution, fit the probability density as well as possible and provide a simple algorithm for use in the Monte Carlo calculations.

By changing the functional form at the peak, a discontinuity in the derivative of the probability density is introduced. However, there is no reason to avoid a discontinuity in the derivative of a probability density or distribution. These occur all the time. In fact, discontinuities in the distribution itself are not uncommon. The only requirements of a probability density function are that it be positive definite and that the integral from negative ∞ to positive ∞ be unity.

Ref: EMF - 2103(P) Rev. 0

Question 87: 4.3.4 Evaluation of Code Biases

In the first paragraph you state that "..., the evaluation of the biases does not include uncertainties."

The biases do have uncertainties associated with them as you have quantified in Table 4.19. In order to make the conclusion in section 4.3.4.4 "The application of the biases resulted in a reduction in the maximum PCT predicted by the code,". Therefore, the bias corrected value of the code is a prediction. This in my view requires that the uncertainty in the bias be taken into account. Please explain.

Response 87: The evaluation of the impact of the calculated biases for the code was based on the mean values of the biases and did not include the uncertainties. This was done for two reasons: the first was that inclusion of the uncertainties would have necessitated a statistical analysis of each of the tests; and second, having done a couple of the LOFT tests statistically, it was found that making the comparison to data was a little more difficult.

The comparison of the code predictions to the data, using a statistical analysis results in a family of predicted cladding temperatures. Many of these predicted temperatures fall above the data. Many are below the data. Thus, the result of considering the uncertainties is a band of predicted temperatures that encompass the assessment data. It can be concluded from these comparisons that there is enough uncertainty in the calculational model to bound the data, high or low, but it does not provide a clear indication of the impact of removing the code model biases.

When the calculation is based on only the mean values of the biases, it can be seen that the biases determined in the separate effects tests have not degraded the ability of the code to predict integrated tests. This point is important in that values inferred from a set of small-scale, separate-effects tests do not a priori have to result in anything meaningful for larger-scale integral-effects tests. If the model is applicable and scalable, the biases will be meaningful for the large scale tests. Thus, comparing the code prediction with the model biases removed to the data supports the bias determination and the scalability of S-RELAP5. The fact that in virtually all cases, the predicted values improved when the model biases were removed provides even more support for the applicability and scalability of the S-RELAP5 code.

Question 88: 4.4 Determination of Effect on Scale (CASU Step 10)

Please comment on the following argument and how your conclusions with regard to the ability of S-Relap5 to scale the requisite phenomena with regard to a RLBLOCA are valid in this context.

A Heuristic Analysis of the Effect of Scale

Notation:

<i>meas@test</i>	<i>measured result of a test</i>
<i>calc@test</i>	<i>S-Relap5 calculated result of a test</i>

meas@LOCA *measured result of a LOCA*

calc@LOCA *S-Relap5 calculated result of a LOCA*

Of the above four the only one we cannot do is the *meas@LOCA*, yet it is what we want to estimate since it is considered the "truth".

Let P be a variable of interest such as peak clad temperature.

$\therefore P(\underline{\theta})$ where $\underline{\theta} \equiv$ set of independent variables defined by PIRT and for which the sensitivities have been quantified.

So, scaling issues deal with the effect of $\underline{\theta}_{test} \equiv \underline{\theta}_0 \rightarrow \underline{\theta}_{LOCA} \equiv \underline{\theta}_0 + \Delta \underline{\theta}$ on $P(\underline{\theta})$.

If scaling holds ∞

$$P(\underline{\theta}_0 + \Delta \underline{\theta}) - P(\underline{\theta}_0) \propto \Delta \underline{\theta}.$$

The question then is what are the conditions on test scaling and code scaling so that we can get an estimate of the "truth" in terms of *meas@test*, *calc@test*, and *calc@LOCA*.

Consider the following relationships:

Test Scaling:

$$P^{meas@test}(\underline{\theta}_0) \rightarrow P^{meas@LOCA}(\underline{\theta})$$

Under the assumption that the tests are scalable

$$P^{meas@LOCA}(\underline{\theta}) \equiv P^{meas@test}(\underline{\theta}_0) + \partial P / \partial \underline{\theta}_{meas@test} \Delta \underline{\theta}$$

$$\square \quad P^{meas@LOCA}(\underline{\theta}) / P^{meas@test}(\underline{\theta}_0) \equiv \{ 1 + 1/P \partial P / \partial \underline{\theta}_{meas@test} \Delta \underline{\theta} \}$$

Similarly for

Code Scaling:

$$P^{calc@LOCA}(\underline{\theta}) / P^{calc@test}(\underline{\theta}_0) \equiv \{ 1 + 1/P \partial P / \partial \underline{\theta}_{calc@test} \Delta \underline{\theta} \}$$

What we want to estimate is the "true" value of $P(\underline{\theta})$ at LOCA conditions, i.e., we want to compute $P^{meas@LOCA}(\underline{\theta})$ at some level of confidence.

From the above expressions we form

$$\frac{P^{meas@LOCA}(\underline{\theta}) / P^{meas@test}(\underline{\theta}_0)}{P^{calc@LOCA}(\underline{\theta}) / P^{calc@test}(\underline{\theta}_0)} \equiv \frac{\{ 1 + 1/P \partial P / \partial \underline{\theta}_{meas@test} \Delta \underline{\theta} \}}{\{ 1 + 1/P \partial P / \partial \underline{\theta}_{calc@test} \Delta \underline{\theta} \}}$$

Rearranging terms we obtain

$$P^{meas@LOCA} \cong P^{calc@LOCA} * (P^{meas@test}/P^{calc@test}) * \{1 + 1/P \partial P / \partial \theta_{meas@test} \Delta \theta\} \{1 + 1/P \partial P / \partial \theta_{calc@test} \Delta \theta\}^{-1}$$

for $|1/P \partial P / \partial \theta_{calc@test} \Delta \theta| < 1$ we can write

$$P^{meas@LOCA} \cong P^{calc@LOCA} * (P^{meas@test}/P^{calc@test}) * SF$$

where we define a scaling factor (SF) as

$$SF = \left(\overbrace{1 + 1/P \partial P / \partial \theta_{meas@test} \Delta \theta}^{\text{test scaling}} - \overbrace{1/P \partial P / \partial \theta_{calc@test} \Delta \theta}^{\text{code scaling}} \right)$$

So, the estimate of the "true" RLBLOCA value of some parameter P has the following components:

- a) $P^{calc@LOCA}$ - the S-Relap5 computed parameter for the LOCA.
- b) $P^{meas@test}/P^{calc@test}$ - the bias estimated by comparing computed and measured values of the parameter from tests. This is the sole source of variation that contributes to the computation of the confidence level in the estimate of $P^{meas@LOCA}(\theta)$.
- c) SF is a factor that accounts for scaling effects.

In my view your analysis implies that $SF = 1.0$. The above discussion implies that for this to be true we must fulfill the following conditions:

- a) $|1/P \partial P / \partial \theta_{calc@test} \Delta \theta| \ll 1$
- b) $1/P \partial P / \partial \theta_{meas@test} \Delta \theta \cong 1/P \partial P / \partial \theta_{calc@test} \Delta \theta$

The first implies that the sensitivities of the computed results of the tests to changes in the independent variables are small. The second that the sensitivity of the measured results for the tests are comparable in size to those computed.

How do your conclusions with regard to test scaling for blowdown, refill and reflood fit into the above scheme?

Similarly, how do your conclusions with regard to code scaling fit into the above scheme?

Response 88: Scaling discussions were separated into test scaling and code scaling in the documentation. The purpose of the discussion with regard to tests was to show that the tests, as they were scaled (or not in the case of the UPTF tests), could predict the LBLOCA phenomena equally well and that there were no discernible effects attributable to the scale of the test facility. For the blowdown phase, it was shown that the peak temperature during the

blowdown was independent of test scale for tests from about 1/6 full scale to tests that were 1/17,000 of full scale. For reflood, a comparison to a similar range of scaled facilities was used to show the independence of the heat-up during reflood (beginning with the liquid at the bottom of the core). For the refill period, full-scale tests were used.

The test scaling condition can be expressed mathematically as

$$P_{Test}(\vec{\theta}') = P_{LOCA}(\vec{\theta})$$

where the $\vec{\theta}$ denotes the parameters which enter into the calculation of the parameter of interest, P . The arrow above is used to indicate a vector. These parameters include those listed in the PIRT table as well as some dimensions. The prime on the vector indicates that it is the vector for the scaled test.

$$\vec{\theta}' \equiv S \cdot \vec{\theta}$$

where S is a matrix which scales the parameter vector. The scaling matrix is by nature a fairly sparse matrix, as the scaling effects need to be applied only to the extensive parameters. The scaling equation then asserts that the measured value of P in the scaled system must be the same as that in the full-scale system for a comparable range of conditions. Only tests for which the scaling condition applies are useful in establishing the test database for the LBLOCA.

The formulation presented in the reviewer's question assumes that the conditions of the tests differ from those in the LBLOCA and that these differences exclude extensive properties that were scaled for the test. This is, in all probability, true. Although scaling of extensive parameters may have been intended, the use of a first-order estimate seems to argue against such an interpretation. Many of the tests were designed to span the conditions that would be expected to occur in a LBLOCA, thereby establishing a basis for analyzing the LBLOCA, provided the analysis tool also scales. For tests consisting of a small number of runs, or even a single run, the conditions were selected to be most representative of the LBLOCA.

Code scaling is important because the code predictions are validated based on small-scale tests and then applied to the full-scale LBLOCA. Scaling discussions in the documentation for S-RELAP5 addressed the extent to which the code predictions might be scale dependent. Several tests with different scaling were evaluated to demonstrate that the code predictions were insensitive to the scale of these tests. In addition, various elements of the code were examined for possible scale effects.

The code scaling relationship can be expressed mathematically as

$$P_{Calc}(\vec{\theta}) = P_{Calc}(\vec{\theta}')$$

where the subscript "Calc" denotes the S-RELAP5 value. This relationship says that the code calculations for scaled test conditions will be the same as the predictions for the full-scale LBLOCA. In this case, the scaled test has to satisfy the test scaling condition.

S-RELAP5 is compared to the test data and biases are determined. Denoting the matrix of biases by M , this process can be summarized by the expression

$$\bar{P}_{Calc}(M \cdot \vec{\theta}') = \bar{P}_{Test}(\vec{\theta}')$$

where the subscript "Calc" denotes the S-RELAP5 value and the bar indicates the mean. Note that the biases have resulted in the code predictions matching the test data in an average sense. Taking into account the uncertainties, the expression can be written as

$$P_{Calc}(\vec{\psi}') = P_{Test}(\vec{\theta}')$$

where

$$\vec{\psi}' \equiv (M + \varepsilon) \cdot \vec{\theta}'$$

and ε is a matrix of random variables representing the uncertainties in the biases. This relationship applies in a statistical sense. That is to say, when the S-RELAP5 calculations are performed using the statistically-varying parameter vector, the probability distribution of the calculated P match those of the test data.

Now, if the code (and the model) with the biases can be scaled from the test conditions to the full-scale, the following relationship can be written

$$P_{LOCA}(\vec{\theta}) = P_{Calc}(\vec{\mathcal{G}})$$

where

$$\vec{\mathcal{G}} \equiv (M + \varepsilon) \cdot \vec{\theta}$$

and the relationship is again understood to apply in a statistical sense.

While the above cannot be expressed as a simple ratio, the points regarding conditions to be met remain valid. The first condition the reviewer places requires the fractional change of the calculated P at LBLOCA conditions from that at test conditions to be small. In addition to requiring a well-behaved calculational tool, it also places a requirement on the sufficiency of the data. The requirement is that the test cases be sufficiently close to the conditions found in the LBLOCA that the fractional variation in the calculated P from the measured P be small. This requirement is met by the use of multiple prototypic tests to evaluate the LBLOCA.

The second condition requires that the predictive model (S-RELAP5 and methodology) display the same dependence on the independent variables as does the test data. This is verified by comparison to a large number of tests, both separate effects and integral, at a large range of scales.

Question 89: 5.1.1 Determining Important Process Parameters

You state "In contrast, treating these process parameters statistically accounts for higher order behavior by including all possible combinations in the sample space."

Question 89a: *What exactly are you referring to by higher order behavior? Give an illustrative example.*

Response 89a: In a typical deterministic assessment, the sensitivity of one parameter is studied at one condition. The choice is often comparable to retaining the linear term in a Taylor series. At points away from that condition, the quadratic term, cubic term, etc. start to have an impact. In addition, the cross-terms with other variables may arise. Then the sensitivity in the variable becomes much different. Consider decay heat sensitivity. At very low PCTs it has one value. Now let the metal-water reaction begin. The sensitivity is suddenly much larger. The higher order behavior in this case refers to all those things in the LBLOCA that make the linearized sensitivity result, taken at one condition, not fully applicable.

Question 89b: *To get "all possible combinations in the sample space" would require n^9 (from Table 5.1) uniformly distributed sample points, where n is some appropriate number of observations for each variable. Is this what you have in mind? This gets big very quickly!*

Response 89b: True. If a census is performed on these combinations the numbers become unmanageable very quickly. In fact, the number of variables in Table 5.1 is much larger than 9. There are 9 categories, but at least 21 variables. So the number is even larger than you have suggested. In the statistical method used for LBLOCA, the presence of a continuum of levels is implicit. By randomly sampling them, the potential for any of the possible combinations of input variables exists. Since the sample size is limited, not all are used to get the final result. However, no combinations are excluded.

Question 90: *5.1.2 Role of Sensitivity Studies*

"Parameters can be demonstrated to be insignificant by sensitivity studies and/or by their relationship to low-ranked PIRT parameters."

Question 90a: *What exactly is meant by sensitivity studies in this context? That is, are these S-Relap5 calculations of a full scale RLBLOCA wherein input parameters are varied? Give an example.*

Response 90a: A large collection (>50) of uncertain parameters (some from the PIRT and some from Plant operation) were identified early on. Estimates of the range of uncertainty that should be associated with each of these were made. A 3-loop Westinghouse Plant model was then run first nominal, then with each of the uncertain parameters adjusted to its maximum (one run per parameter) and then with each adjusted to its minimum. The variation of the PCT for each of these cases was used as a basis for setting the sensitivity. This same process was repeated at an overpower condition to get the PCTs closer to 2200°F to see if the sensitivities were that much different and finally again with a 4-loop Westinghouse plant.

Question 90b: *Have you shown that the results of a S-Relap5 calculation for sensitivity at full scale is valid?*

Response 90b: This question raises the issue of the scalability of sensitivities again. The scalability of the tests used and the scalability of the models within S-RELAP5 were evaluated. In addition, the full-scale model was checked to assure that it conforms to the methodology. The runs were checked and all appear to be acceptable. A series of tests for code stability and repeatability were made to confirm that the variations in the code from numerics and

convergence are small compared to the significant contributors to the PCT changes. These things together support the validity of the S-RELAP5 sensitivities for a full-scale LBLOCA.

Question 91: *5.1.3 Quantifying Statistical Quantities*

Why are there no measurement uncertainties associated with the parameters - accumulator level through core flow in Table 5.4?

Response 91: [

]

Question 92: *How are the operational and measurement uncertainties combined to give the distribution for the parameters in Table 5.4?*

Response 92: [

]

Question 93: *5.2 Performance of NPP Sensitivity Calculations*

5.2.1 Statistical Approach

Your statement "Non-parametric statistical techniques are useful in situations where acceptance or rejection is based on meeting a tolerance limit and where you do not need the probability distribution itself." is misleading. The analytic form of the probability distribution function need not be known, but the function must be continuous. In the current context, the distribution function is the S-Relap5 code. What evidence do you give that S-Relap5 computed PCT and cladding oxidation are continuous in the independent random variables for RLBLOCA analysis conditions?

Response 93: There are two pieces of evidence which suggest that the S-RELAP5 computed PCT and oxidation are continuous in the independent random variables for RLBLOCA conditions. The first is that the underlying correlations used in the code are continuous. Framatome ANP spent considerable effort to assure that the intersection of different correlations for the same parameter was smooth and continuous. The second piece of evidence is that the PCT as a function of time for each of the 59 cases is continuous. The independent variables experience large changes in value as a function of time during each case. If significant discontinuities existed they would be expected to be visible during at least some of the cases.

Question 94: *Define your use of the term "outlier" in the current context of your application, i.e. given 59 observations of PCT, what makes you call the 59th term in the order statistic and outlier? What statistical test do you apply and what make you think it is appropriate, i.e. not due to some deterministic quirk in the computation? Please formulate your test for an outlier in terms of a statistical hypothesis test.*

Response 94: The use of the term outlier in Section 5.2.1 is misleading since the term outlier has a specific meaning in the statistical sense which is not meant in this section. Framatome ANP proposes to delete the paragraph where the term outlier is used.

The following paragraphs will be inserted in place of the current paragraph on page 5-11 which contains the term outlier. A replacement paragraph is needed because the actions described in the paragraph are still necessary.

It is possible that the result of the 95/95 estimate from the 59 cases will be a PCT that exceeds the 2200 F limit. There are two actions that can be taken in this situation. First a change in the reactor conditions that are being evaluated can be made in an effort to create a set of conditions where the 2200 F limit will not be violated. The changed reactors conditions could consist of a revised total peaking factor limit, or a revised accumulator level, or a revised ECCS injection rates.

A second approach would be to run an additional 34 cases generated with the same seed as the previous 59 cases to obtain a total of 93 cases. For 93 cases the 95/95 estimate is the second highest value rather than the highest value (as it is for 59 cases). Experience with order statistics shows that the 95/95 estimate from 59 cases is, in general, more conservative than the 95/95 estimate from 93 cases. This second approach is only useful for those cases where the 95/95 estimate of the PCT from 59 cases is significantly higher than the PCTs for all the other 58 cases. . Framatome ANP does not plan to use more than 93 cases since we believe that the potential for a conservative answer from 93 cases is too low to warrant the expense of additional cases.

Question 95: *5.4 Determination of Total Uncertainty*

The final results for the 4-loop sample problem are summarized as:

- *The 95/95 calculated PCT was 1635 F*
- *The 95/95 calculated maximum nodal oxidation was 1.1%*
- *The 95/95 calculated maximum total oxidation was 0.02%*

Question 95a: *Are these joint estimates based on the same $n = 59$ S-Relap5 runs?*

Response 95a: The estimates for PCT, maximum nodal oxidation and maximum total oxidation are not joint probability estimates.

The following statement is made in Regulatory Guide 1.157 with respect to the estimates to be made for the three criteria together.

"The revised paragraph 50.46(a) (1) (i) requires that it be shown with a high probability that none of the criteria of paragraph 50.46(b) will be exceeded, and is not limited to the peak cladding temperature criterion. However, since the other criteria are strongly dependent on peak cladding temperature, explicit consideration of the probability of exceeding the other criteria may not be required if it can be demonstrated that meeting the temperature criterion at the 95% probability level ensures with an equal or greater probability that the other criteria will not be exceeded."

Framatome ANP will modify the submitted methodology to calculate the 95/95 PCT value and report the other two parameters for this case consistent with the Regulatory Guide. Demonstration that the PCT is met with 95% probability and 95% confidence assures that the two criteria related to oxidation will be met with an equal or greater probability. This is because of the strong correlation between cladding temperature and oxidation and because the margin to the criteria limits is much greater for the oxidation criteria than for the temperature criteria (see Table 5.9).

Section 5.2 of EMF-2103 will be revised to reflect this change in statistical approach. The change pages for Section 5 are presented in Appendix C. Changes to the text will be made on the original pages 5-11, 5-15, 5-16, 5-17, and 5-18. Tables 5.10, 5.11, and 5.12 will be deleted. Figures 5.4 and 5.5 will be deleted. Appendix D will be revised in a similar manner when the approved document is issued.

Question 95b: *If yes, please explain why. The 95/95 for the joint estimation of three dependent variables requires far more than $n = 59$.*

Response 95b: That is generally true, but these are not joint estimates.

Question 95c: *Physically PCT and oxidation rates should be correlated. Do you account for that and if so how?*

Response 95c: S-RELAP5 calculates oxidation rate using the Cathcart-Pawel equation which correlates oxidation rate as a function of absolute temperature. Therefore, the oxidation rate is functionally dependent on the cladding temperature in S-RELAP5. As a result, PCT and oxidation are highly correlated.

Question 96: *Stored energy in the fuel is treated, however pin pressure is not. Please describe the methods used to assess the potential for blowdown ruptures and how fuel rod gap pressures are calculated and treated statistically.*

Response 96: Fuel pin pressure is treated by the methodology; initial fuel rod pressure is calculated with RODEX3A and transient fuel rod pressure is calculated with S-RELAP5 using the same fuel models as RODEX3A. A principal reason for incorporation of the RODEX3A fuel models into S-RELAP5 was to provide a fuel rod pressure calculation consistent with the initial

conditions from the approved RODEX3A model. S-RELAP5 and RODEX3A account for pin pressure variations as a result of changes in pellet and clad dimensions and gas composition.

Pin pressure can influence two LOCA phenomena given in the PIRT in Table 3.4 in the methodology document: stored energy and gap conductance. Table 4.18 briefly lists how each phenomena is treated. [

]

Fuel rupture is not treated in this methodology as is discussed in Appendix B.2. Rupture of fuel rods, when predicted, does not occur during blowdown, because the relatively high system pressure reduces the pressure differential across the cladding during this phase of a LOCA. If calculated, fuel rod rupture typically occurs during reflood and possibly could occur late in the refill phase of a LOCA. Framatome ANP showed that fuel rupture, when calculated, has the beneficial effect of slightly reducing PCT. Since the general influence of fuel swelling and rupture was relatively small and beneficial, we chose to be conservative and ignore this effect and to focus on other methodology development areas. (Also see response to Questions 28a and 131)

Question 97: *Please explain how the uncertainty in the gap gas conductance is accounted for. Please explain how variations due to fuel relocation are treated and included in the uncertainty in the stored energy of the fuel.*

Response 97: [

]

Question 98: *What is the initial oxide layer thickness assumed on the inside and out side of the rod. Please explain how this is treated and justify the initial oxide layer thicknesses.*

Response 98: The initial oxide layer thicknesses on the outside and inside of the cladding are calculated as a function of burnup for each axial node in the RODEX3A calculation. The axially dependent oxide layers are then passed to the S-RELAP5 calculation and are used in the calculation of cladding thermal conductivity which affects the initial stored energy. [

]

Question 99: *On page 4-94, the 90% confidence limit was used to evaluate the constant and exponential terms in the oxidation model. As described in Regulatory Guide 1.157, please use the 95 percentile confidence limits to evaluate these terms. Also, was the uncertainty on the predicted mean of the data in the Cathcart-Pawel cited reference verified.*

Response 99: The 95% limit was obtained by noting that for a normal distribution, the two-sided 90% limits correspond to the 95% upper limit and the 95% lower limit. The statistics on the Cathcart-Pawel model were not reevaluated. This reference is heavily cited and has been reviewed by the NRC as documented in NUREG-1230, Compendium of ECCS Research for Realistic LOCA Analysis.

Question 100: *Cold leg condensation, only, is discussed on page 499. Please explain how downcomer condensation was ranged and applied in the methodology.*

Response 100: [

]

Question 101: *Downcomer entrainment was not discussed in the statistically treated section. Please explain how downcomer entrainment was ranged.*

Response 101: The code calculation of downcomer entrainment is addressed in the methodology by demonstrating that the combination of code models and plant nodalization used in the methodology results in a conservative prediction of the lower plenum fill rate. This conservatism was demonstrated by comparison with the UPTF Tests 6 and 7 and is discussed in Section 4.3.3.1.10 of EMF-2103.

Question 102: *The refill heatup period heat transfer multipliers were also not discussed. Please show the S-RELAP5 code predictions to data during refill and show the heat transfer multipliers applicable to refill.*

Response 102: As part of determining the film boiling heat transfer multipliers, it was necessary to consider the application in which those multipliers are used and compare this range to the available data. The summary results of this evaluation were presented in Table 5.1 of EMF-2102, which identifies the range of key parameters needed for the RLBLOCA application, as compared to the range that is available from the data used to develop the film boiling heat transfer multipliers. The information in this table were derived independent of the transient phase, that is, they represent conditions from blowdown, heatup, and reflood. This was important because in S-RELAP5, the core film boiling heat transfer models are applied any time film boiling is indicated – the same models are used for blowdown, heatup, and reflood. Figures 1 and 3 of RAI Response #2 show the clad rod temperature response during blowdown, heat-up, and reflood at two different PCT locations. The void fractions in the heatup region are well within the range supported by the film boiling multipliers. The pressures observed during the heat-up are also supported. On this basis, the heat transfer multipliers that support heat-up are FILMBL=1.00 and FRHTC=1.75.

The S-RELAP5 predictions to data during refill are shown in the following figure. [

]



Question 103: *Please explain the “Comparison with Adjusted Accumulator” in Fig. 4.152.*

Response 103: In the original data obtained by Framatome, the measured accumulator volumetric flow rate was provided. In the initial performance of the analysis, the analyst missed the fact that when the accumulator emptied the flow switched from liquid to nitrogen. The title on the plot simply reflected the fact that the final analysis had accounted for this switch from liquid to nitrogen flow.

Question 104: *LOFT L2-3 predictions capture the second peak due to the lack of quench during blowdown. If quench occurs, how well does S-RELAP predict the second peak? Do the plant calculations always show a failure to quench during blowdown? If not what is the effect on the reflood PCT?*

Response 104: Since the code under-predicts heat transfer under low void conditions, a second heat-up should over-predict the data. Of the 3-loop and 4-loop plants, the 4-loop plant is most likely to experience quenching immediately after the blowdown peak. The submitted 4-loop plant calculation does not show that behavior.

Question 105: *Explain why the methodology does not contain an uncertainty assessment regarding peak local oxidation. At the higher PLHGRs and with downcomer boiling, what is the core wide oxidation.*

Response 105: In the last paragraph of Section 5.4 (EMF-2103) a statement is provided specifying an uncertainty assessment of PCT, peak local oxidation (a.k.a. maximum nodal oxidation), and core wide oxidation. This is provided in terms of the 95/95 and 50/50 results. In general PCT results are emphasized since the temperature limit is much closer to calculated PCT results likely from an LBLOCA analysis and since the oxidation variables are primarily dependent on clad temperature.

Other conditions being equal, at higher PLHGRs and at low containment pressures in which the effects of downcomer boiling would be expected to be the strongest, clad temperatures would likely remain high for a longer period of time. To ensure an accurate accounting of oxidation variables, a calculation is not terminated until the clad temperature at the peak power node drops below 1200°F and the transient time is greater than 300 s (guillotine breaks) or 400 s (split breaks). At temperatures below 1200°F, oxidation rates are not significant enough to appreciably increase the total oxidation. Nonetheless, most cases run out to total core quench.

Question 106: *What is the basis of the moderator-density feedback curve employed in the analysis? Is the most positive MTC allowed by the Tech. Specs. used? Please explain and show the reactivity versus density curve used in the demonstration analysis. What doppler feedback curve is used? What is the uncertainty in these curves applied to the analysis?*

Response 106: [

Question 107: *In Table 5.7 on page 5-23 of EMF-2103, how was the lower limit on T inlet determined? Will the analysis be applied to plants during an end of cycle coastdown? If so, what is the sensitivity of the methodology to T inlet and how would the evaluation be performed?*

Response 107: Core inlet temperature is a plant parameter which is sampled over the range of operation of the plant. It is expected that the utility customer will supply this information and supporting data to Framatome. Sensitivity studies on the effect of perturbations of this parameter on PCT showed that PCT was relatively insensitive to core inlet temperature over the normal operational range. For the 3- and 4-loop sample problems, no account has been made for end-of-cycle coastdown; however, because of the power coastdown, conditions typical of end-of-cycle coastdown are not expected to challenge LOCA acceptance criteria as much as earlier periods in the cycle.

For plants that apply an end of cycle coastdown, a number of parameter ranges may change during this period. This RLBLOCA methodology already addresses time-in-cycle variations from a neutronics and burnup perspective. Hence, the end of cycle coastdown will be addressed through the sampling of time-in-cycle dependencies and programming the model changes that correspond to that coastdown period.

Question 108: *In Fig. 5.2 on page 5-29 of EMF-2103, which peak temperatures are due to first peaks and which are due to reflood peaks? The peaks corresponding to times beyond 100 seconds are very low. These appear to be reflood peaks; please explain why the reflood peaks are so low when linear heat rates are based on peaking factors in the range 2.4 to 2.6? Why do the guillotine breaks appear to be all first peak limited?*

Response 108: This sample problem is representative of a 4-loop PWR. The PCT signature predicted by S-RELAP5 for the 4-loop problem will typically show a blowdown peak within the first 10-15 s and then a single reflood peak between 30-60 s. With emergency core cooling coming from 3 intact loops, the two-peak characteristic is not a surprising result. For the smaller split breaks the emergency core cooling is more than adequate to suppress clad temperatures; hence, those cases showing a late reflood peak (> 100 s) will typically be those smaller split breaks. A 3-loop PWR sample problem has been supplied as Appendix D of EMF-2103 Revision 0. The PCT signature from the 3-loop problem does show cases having either a blowdown peak, an early reflood peak, or a late reflood peak.

Question 109: *Fig. 5.3 show break areas of 1.0 ft^2 and less. What is the effect on the PCT distribution if breaks 1.0 ft^2 and smaller are thrown out? The upper limit on the break size is about 4.0 ft^2 . What are the break multipliers for the largest sizes in Fig. 5.3? How are the multipliers applied to each side of the break? Please explain.*

Response 109: Following the statistical discussion provided in Section 5.2.1, if, for example, the 10 cases with break sizes less than 1.0 ft^2 were removed, the limiting calculation would still represent about a 94/95 coverage/confidence (i.e., $(0.94)^{49}=0.05$). Performing the 59 cases excluding breaks smaller than 1.0 ft^2 would have some likelihood ($10/59 = 17\%$) of exceeding the limiting PCT calculation; however, the probability that the resulting PCT would be significantly greater than the next highest PCT would be small.

[

]

Question 110: *What does the scatter plot for PCT versus reflood rate look like?*

Response 110: The reflood rate varies over a very wide range during the LBLOCA and one would have to define some sort of weighted average of the time-dependent reflood rate values to create the requested plot. Reflood rate is not a parameter that Framatome ANP considers in the LBLOCA, other than to assure that the range of reflood rates experienced during a LBLOCA are covered in the validation database. Since the dependence on axial power shape, film boiling heat transfer, and break size are so strong, it is likely that if the requested plot were created, it would look like a typical random scatter plot. Such a plot would not have much value from an analytical point of view.

Question 111: *Table 5.7 identifies the failure of 1 LPSI and 1HPSI. Please show the PCTs for a diesel failure, an LPSI failure, and no failure on the same plot.*

Response 111: [

]

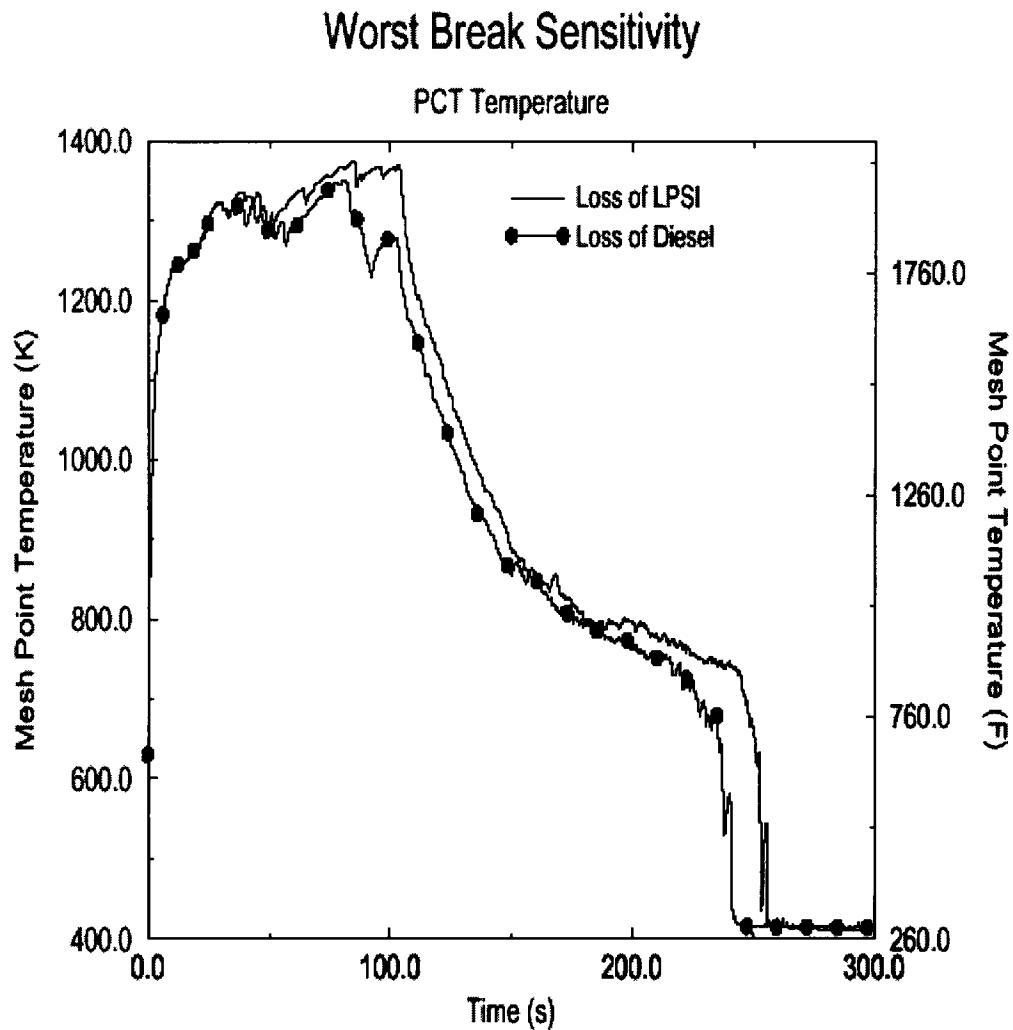


Figure 111.1 Clad Temperature Response from Single-Failure Study

As a followup to this study, another study has been performed analyzing a suite of single-failure assumptions including the no failure assumption. This study has been applied to a low containment pressure plant simulation. The specific calculations are summarized in the following table:

[

[]

]



Figure 111.2 Clad Temperature Response from Single-Failure Study

Figure 111.3 Containment Pressure Response from Single-Failure Study



Figure 111.4 Liquid Level Response from No Failure Simulation

Question 112: *In Table 5.7, why is SG plugging limited to 10% since the average for operating plants is 15%? How is the plugging distributed among the SG? How are asymmetries in plugging handled?*

Response 112: In the sample problems, steam generator tube plugging has been set to 10%. This value is arbitrary for this analysis. For an actual analysis, this information would be provided from the utility customer and likely be adjusted to meet the demands of plant operation. Sensitivity studies on tube plugging show very little impact on PCTs; however, the increased flow resistances do contribute to somewhat lower reflood rates and, hence, core cooling precedes at a rate slower than with steam generators with no plugging. To support subsequent fuel cycles, utility customers usually request that steam generator tube plugging be set higher than current cycle conditions. If steady-state loop flows are significantly impacted, asymmetry in steam generator tube plugging must be considered. Since each steam generator is modeled separately, asymmetric plugging levels can be incorporated by adjusting geometries and flow losses as appropriate in each steam generator.

Question 113: *Table 5.7 lists the hot assembly to be anywhere in the core? Please show the core flow and PCT for the hot assembly placed in the most limiting position which minimizes blowdown cooling.*

Response 113: The position of the hot assembly in the core refers to its placement relative to other assemblies in the core and structure in the upper plenum. For LOCA, the influence of the other assemblies is driven by the radial power distribution in the core. The radial core nodalization is always as that shown in Figure 4.7 of the methodology document. [

]

Question 114: *Minimum EC boron of 2925 is used in the analysis. What is the minimum time to boron precipitation for this boron concentration? Show that the switch to simultaneous injection occurs before precipitation for the limiting large break and location.*

Response 114: See the response to Question 32.

Question 115: *Please explain why the PCT is not skewed toward the higher values as power is increased in Fig. 5.6 of EMF-2103 and F_q is increased in Fig. 5.7?*

Response 115: In most of the PCT scatter plots in Figures 5.2-5.16, an obvious trend is difficult to discern. These figures are presenting the PCT results from the same set of 59 calculations through many different "filters." Because so many parameters are being varied, only the few most dominant parameters will show a correlation with PCT. [

]

Question 116: *How is the ASI chosen in the analysis? Are power distributions with power skewed toward the top most likely and how does the ASI chosen reflect the most likely distribution?*

Response 116: [

]

Question 117: *Please explain why the trend in PCT is not increasing with increasing inner ring and cold ring power? Are these PCTs determined with the hot assembly located in the position which minimizes core flow and cooling during blowdown? Which PCTs are first peaks?*

Question 118: *What do the PCT scatter plots look like if they are separated into first peaks and second peaks?*

Response 117 and 118: [

]

Figure 5.2, which shows the PCT vs. Time-of-PCT, can be used to differentiate first versus second peaks. There are about 10 cases showing a blowdown PCT in Figure 5.2. These all occur before 20 s. The break area has such a strong influence on the time of PCT (blowdown PCT and first or second reflood peak) that it masks any other potential trends.

Question 119: *Why does the PCT turn around so quickly in Fig. 5.18? What is the reflood rate versus time for this break? Please explain why the quench occurs so early since downcomer*

boiling should initiate following discharge of the SITs.

Response 119: The PCT turns around quickly because there is water in the core. The 4-loop PWR LBLOCA benefits from the early blowdown cooling (see Response to Question 120), which removes considerable stored energy from the rods at lower elevations. Consequently, the core is “easier” to quench during the reflood phase. Figure 119.1 shows the core average reflood rate. The ECC water from the intact loop accumulators reaches the cold legs at about 14 seconds. At about 32 seconds, the water reaches the bottom of the core. During the rest of the accumulator injection period (up to about 60 seconds), the ECC water injection rate to the core (reflood rate) is about 12 cm/s (4.7 in/sec). The reflood rate drops to about 2.5 cm/s (1 in/s) after the accumulators are empty. The blowdown cooling and the flow of the accumulator ECC water into the core are responsible for the early quench of the lower part of the core. Figure 119.2 shows the heat transfer rate from the downcomer walls and other structures to the fluid in the downcomer. It is seen that the heat transfer rate to fluid is over 50 MW during the accumulator injection period. However, boiling is limited to near the surface region since the ECC water and, therefore, the bulk of the fluid is highly subcooled as depicted in Figure 119.3, which shows the liquid subcooling at the axial level (Level 3) below the ECC injection level (Level 2).

Note: A short period of negative reflood rate occurs around 270 s. As a consequence of core quench at around 220 s, there is a period of increased vapor flow. As this period of increased vapor dissipates, there is significant liquid fall back to the core from the upper plenum. Using the simple reflood rate approximation applied to generate Figure 119.1, this appears as a period of negative reflood rate.



Figure 119.1 Average ECC Water Injection Rate into the Core



Figure 119.2 Heat Transfer Rate to Downcomer Fluid from Walls and Structures



Figure 119.3 Liquid Subcooling in Downcomer at Axial Level 3 from the Top (One level Below the ECC Entrance to Downcomer)

Question 120: *What is the cause of the spike in flow at about 7.5 seconds in Fig. 5.20? What is the PCT if this flow spike is eliminated?*

Response 120: Figure 120.1 shows the sum of mass flow rates from the four cold legs to the downcomer and the mass flow rate from the lower plenum to the core. The flow from the broken cold leg to the downcomer is negative (out of the downcomer). At the beginning of the transient, the magnitude of the broken loop flow is much larger than the sum of the three intact cold leg

flows and the net flow to the downcomer is negative. Thus, liquid flows from the downcomer and three intact loops to the break. To supply the additional break flow, liquid also flows downward from the core to the lower plenum and up the downcomer to the break. This produces the early core flow reversal. As the system pressure rapidly decreases, the magnitude of the critical flow at the break decreases substantially due to the change in upstream conditions as depicted in Figure 5.19 of EMF-2103(P). During this time, the flow from the three intact cold legs does not change much due to the flow inertia and the short available time for pump coastdown. Consequently after the early core flow reversal, there is a short time period during which the net flow to the downcomer and lower plenum regions is positive. Furthermore, the intact cold legs, downcomer, and lower plenum are still full of liquid. This forces an upward flow through the core. This is a well-known characteristic of the 4-loop plant LBLOCA. For this particular calculation, the positive flow period is between 3.3 seconds and 5.6 seconds. The positive flow reaches the core at about 5 seconds. This positive core flow is real and can produce core quench during the blowdown period, as experimentally observed in the LOFT L2-3 and L2-6 tests. However, S-RELAP5 calculates enhanced blowdown cooling but no quenching due to this effect. The positive flow into the core during this blowdown period is a real physical phenomenon; it cannot be eliminated.



Figure 120.1 Sum of Mass Flow Rates from Cold Legs to Downcomer and Mass Flow Rate from Lower Plenum to Core

Question 121: *What is the cause of the downcomer level increase just after 50 seconds in Fig. 5.25? What causes the drop in level at 225 seconds? Please show a plot of the downcomer void fractions versus time. Also show a plot of the downcomer temperatures for these locations versus time compared to the saturation temperature.*

Response 121: Continuing accumulation of ECC water in the downcomer is the cause of the downcomer level increase. The quenching of the bottom of the core retards the water flowing into the core and the accumulator water flowing into the downcomer is rather strong; therefore, more water is accumulated in the downcomer. At around 200 seconds, the high power region (middle upper elevations) of the average and hot channels quenches within a few seconds between different axial elevations. The extra steam generated flows through the intact loop cold legs to the downcomer and carries more water from the downcomer out to the break. This causes the downcomer level to drop. Figure 121.1 shows a plot of downcomer void fraction at axial level 3 (the ECC water entering the downcomer at axial level 2). The water subcooling (saturation temperature – liquid temperature) at the same axial level is shown in Figure 119.3.



Figure 121.1 Void Fractions at Third Axial Level from the Top of the Downcomer

Question 122: *Show a plot of the core flow at the PCT location.*

Response 122: Figure 122.1 shows the vapor mass flow rate at the PCT node (9.4 ft) in both axial and radial directions. The flow in the radial direction is much lower than the axial flow and is positive (flowing out of the volume) during the reflood period. The corresponding liquid mass flow rates are shown in Figure 122.2. The axial flow is rather chaotic. The radial flow is positive before the region is quenched. The chaotic axial liquid flow is inherent with the reflood calculation. The large amount of vapor generated in the quenching volume causes a temporary pressure increase in the volume, which in turn throws chunks of the liquid up and down into the neighboring volumes. A portion of the liquid thrown upward falls back down and some gets carried out of the core by the vapor. Figure 122.3 shows that at the upper tie-plate junction above the hot assembly the liquid flow is always upward and there is no liquid falling down from the upper plenum into the hot assembly.



Figure 122.1 Axial and Radial Vapor Mass Flow Rate at the PCT Node (9.4 ft)



Figure 122.2 Axial and Radial Liquid Mass Flow Rate at PCT Node (9.4 ft)



**Figure 122.3 Liquid Mass Flow Rate at the Upper Tie Plate Junction
Above the Hot Assembly**

Question 123: *Please show the heat transfer coefficient and steam temperatures corresponding to Fig. 5.18. Also show the core void fraction versus time for these locations and the droplet size at the hot spot versus time. What is the reflood rate versus time?*

Response 123: Heat transfer coefficient, steam temperature, void fraction and droplet size are shown, respectively, in Figures 123.1 through 123.4. The reflood rate is shown in Figure 119.1 (see Response to Question 119). Note that the droplet diameter is not used after an elevation is quenched.



Figure 123.1 Heat Transfer Coefficient at Four Elevations



Figure 123.2 Steam Temperature at Four Elevations



Figure 123.3 Void Fraction at Four Elevations



Figure 123.4 Droplet Diameter at PCT Node

Question 124: *Why does the PCT show the rapid temperature decrease just after the SITs empty? What are the LPSI and HPSI flow rates after SIT exhaustion?*

Response 124: (See Responses to Questions 119 and 120 for more detail.) The clad temperature decrease is due to the presence of water in the region. The blowdown cooling discussed in Response to Question 120 contributes to a reduction in PCT. The flow of the accumulator ECC water into the core discussed in Response to Question 119 accounts for about a 30 second period of higher reflood rate. As a consequence, the clad temperature is not too high and there is water in the core. The LPSI and HPSI flow rates are shown in Figure 124.1

In addition, the following phenomena are associated with the emptying of the SITs that contribute to higher ECCS flow and a pressure pulse at this time. As the SITs empty, the ECC lines connecting them must also be cleared. When this happens, the effective pressure drop resistance of the lines (portion in liquid flow) decreases faster than the gas expansion driving the injection. This results in an unbalanced force that accelerates the ECC injection rate as the lines clear. When the lines are cleared, a pressure pulse follows due to the nitrogen when it enters the vessel (see response to Question 126). These two phenomena enhance cooling just as the SITs clear.



Figure 124.1 LPSI and HPSI Mass Flow Rates

Question 125: *Why is the lower plenum liquid solid at about 75 seconds? Why is there no boiling in this region? How is wall heat modeled in the lower plenum? Please explain.*

Response 125: Lower plenum walls and internal structures are modeled. Figure 125.1 shows the total heat power released to the lower plenum fluid from these structures. The heating power to fluid is still about 9 MW at 75 seconds and decreases rather slowly. However, the bulk liquid is highly subcooled, as indicated in Figure 125.2; therefore, boiling is limited to the region close to structure surfaces.



**Figure 125.1 Heat Transfer Rate to Lower Plenum Fluid
from Walls and other Structures**



**Figure 125.2 Liquid Subcooling (Saturation Temperature – Liquid Temperature)
in the Lower Plenum**

Question 126: *What is the source of the pressure spike in Fig. 5.28 at 70 seconds? Please explain.*

Response 126: The pressure rise starts at 60 seconds and reaches a maximum value at 63 seconds. The start of the pressure rise coincides with the emptying of the accumulators. The nitrogen in the accumulators begins to flow into the system when the accumulators are nearly empty. The pressure associated with the nitrogen gas is determined by the initial amount of gas present and the volume to which this gas has expanded. As the nitrogen enters the system its pressure is above that of the system. At this time the system pressure is near the containment pressure. Thus, the calculated system pressure at the injection point rises rapidly to the nitrogen pressure, then decreases as the nitrogen gas is dissipated. The flow of nitrogen into the cold legs also reduces the condensation rate and thus increases the pressure. Nitrogen bubbles can also be trapped between liquid regions and cause pressure to increase.

Question 127: *What is the sensitivity of PCT to the expected variation in containment pressure? What is the uncertainty in containment pressure?*

Response 127: [

1

Question 128: *Page A-4 of EMF-2103 states that a discussion of each study is not practical. In order to demonstrate the basis for these studies plots of key parameters are needed along with a discussion of the results. The basis for each sensitivity needs to be explained and the key plots presented with comparisons to the base case to provide the technical justification for the choices for the parameters listed in the sensitivity studies given in Table A.2.*

Response 128: Sections 4.1.1, 4.2, 5.1.2 and Appendix A discuss the role of sensitivity studies in the development of this methodology. Section 4.1.1 provides detail on how most of these sensitivity studies were performed for the purpose of establishing the Assessment Matrix. Section 4.2 refers to the role of sensitivity studies in the nodalization definition. Section 5.1.2 clarifies the use of results from sensitivity studies within the non-parametric statistical methodology. Appendix A provides an overview of how the sensitivity studies were designed.

In non-parametric statistics, sensitivity studies are not used to develop a response surface. The role of sensitivity studies is basically to confirm the importance of the highly ranked PIRT phenomena and to determine which of the plant parameters are important. Those phenomena and parameters demonstrated through the sensitivity studies to actually impact the predicted PCT are those which will be addressed statistically in the methodology. This list of important phenomena and parameters are then used to define the assessment matrix for determining uncertainties and to define which plant parameters will require data to support their statistical treatment. Thus, the importance of the sensitivity studies in non-parametric statistics is significantly less than in the response surface approach.

Overall, at least 10 calculational notebooks were created documenting approximately 400 sensitivity studies. This documentation is about 3000 pages worth of information and includes the calculational detail requested. If this detail is of interest to the NRC it is available for their review at the Framatome ANP offices.

Question 129: *The discussion in Section A.2 refers to core flow stagnation, reduced heat transfer and many other phenomenological behaviors but does not show any plots other than PCT. Figs A.1 through A.4 do not display quench. Please show the quench for these cases. What is the impact on clad oxidation for these cases? Comparison of Fig. A.3 with A.1 show an increase in PCT of 500 F. Given this large change in PCT and the fact that the SRELAP5 did not capture the effects of nitrogen which was to subsequently increase PCT after the initial decrease, please provide the justification for including this PCT benefit in the methodology. Is Fig. A.2 incorrectly labeled as this plot for the 4-loop plant? Why does the PCT increase substantially beyond that for the 3-loop plant compared to the 4-loop plant when nitrogen*

injection is precluded.

Response 129: Unlike the parametric statistical approach taken in the CSAU sample problem given in NUREG/CR-5249, sensitivity studies are not used in the development of a PCT response surface. This is not required in a non-parametric approach. The primary application of these sensitivity studies was to determine a relative PCT sensitivity to the many LOCA parameters identified in the PIRT (and from plant operation considerations) and to determine which parameters should be treated statistically. This information serves to define the assessment matrix. The figure-of-merit in this process was chosen to be PCT. For this reason, in the sensitivity studies performed, only PCT vs. time information was recorded. Once PCT sensitivity was determined, the calculation could be terminated. Core quench time is not included in the PIRT; hence, it wasn't necessary to run the calculations out to core quench. Clad oxidation is dependent on clad temperatures and thus does not need to be evaluated separately.

Clad oxidation and accumulator nitrogen were not included in many of the sensitivity studies because they can potentially introduce nonlinear PCT sensitivities that might disguise the true sensitivity of the studied parameters. This is discussed in Section 4.1.1. (Note: one set of 72 sensitivity studies included accumulator nitrogen and another ~35 sensitivity studies were done examining PCT fuel rod parameters such as clad oxidation, these are mentioned in Table A.2.)

Nonetheless, both clad oxidation and accumulator nitrogen are applied in this RLBLOCA methodology (i.e., no benefit has been taken). As a method to evaluate PCT sensitivities to serve in the CSAU decision-making process, this action was judged to be appropriate.

Figure A.2 is incorrectly labeled. It should read "PCT independent of elevation for the 3-loop plant at nominal power without accumulator nitrogen effects". This will be corrected in the document. Three of the four sets of sensitivity studies were performed without including accumulator nitrogen. The cases shown in Figure A.3 and A.4 are described in the third and fourth bullets in the first paragraph of Section A.1.

For the cases referred to by Figures A.3 and A.4, a top skewed axial power profile and an increase in both core and decay power were made to force PCT to occur during late reflood. The relatively higher PCT in the 3-loop base case is the result of a number of differences between the 3- and 4-loop problems; however, the biggest player is probably that emergency core cooling is served through only 2 intact loops in a 3-loop PWR vs. 3 intact loops in the 4-loop PWR.

Question 130: *How does low rod pressure produce more conservative PCTs as indicated in Table A.2? Higher rod pressures at higher linear heat rates will eventually cause blowdown ruptures increasing the stored energy at end of blowdown that will increase PCTs. Please explain.*

Response 130: Table A.2 states that the low rod pressure sensitivity study "produces slightly more conservative PCTs – not significant to range, use nominal values." The actual difference in PCT was 17.3°F. This is within the normal code numerical uncertainty given as [] in Appendix C; hence, the conclusion was that this is not a significant difference and that, for this reason, it is unnecessary to range this parameter.

The likelihood of blowdown ruptures is consistent with the condition of higher rod pressure which is characteristic of high burnup fuel rods. Framatome's experience is that such fuel rods are

present for latter cycle fuel, i.e., once- or twice-burned fuel. Sensitivity studies examining clad temperature sensitivity relative to burnup have shown that sampling from first cycle fuel assemblies, will produce clad temperature predictions which will bound the clad temperatures predictions for previously burned fuel. This has been attributed to the lower power densities characteristic for previously burned fuel.

Question 131: *In the rupture sensitivities given in Figs. B.3 and B.4, how was fuel relocation and the subsequent heat generation in the ruptured zone modeled? If this was not taken into account, please justify the omission of fuel relocation effects in the ruptured region. How does blowdown rupture influence the conclusions of the rupture study? What assumptions are made regarding rupture of the surrounding rods in the rupture study. Are touching strains predicted and what conditions are needed for this condition? What is the justification for the blockages calculated that show rupture reduces PCT? What is the PCT sensitivity to percent blockage up to the maximum? What test data was used to justify the less limiting nature of rod rupture and show S-RELAP5 comparisons to the data?*

Response 131: [

]

[

]





[

]

References

131.1 E. H. Karb et al., *KfK In Pile Tests on LWR Fuel Rod Behavior During the Heatup Phase of a LOCA*, KfK 3028, Kernforschungszentrum Karlsruhe GmbH, Karlsruhe.

Question 132: *Please show the heat transfer coefficient vs time for Figs. B.3 and B.4. Also show the temperature of the node just above the ruptured region and its corresponding heat transfer coefficient. Also show the gap conductance vs time for the ruptured and unruptured region just above. Are the drop sizes affected by the ruptured region. What is the void fraction and corresponding drop sizes versus time at the hot spot?*

Response 132: A sensitivity study of the effect of using a swelling and rupture model is presented in Appendix B of EMF-2103(P). In this study, the rod swelled but did not rupture, though this may not be clear from the discussion. The intent of the original calculations was to examine the rod performance issues in a "bounding manner". Applying the method described in Section 5.1.3.2 of the methodology document (EMF-2103(P)), a limiting hot rod was identified from a large set of neutronics calculations designed to analyze the specific reload cycle. This limiting rod is the rod that is expected to have the highest peak LHGR rate. In the study, the highest LHGR calculated using the method from Section 5.1.3.2 was 11.5 kW/ft. After this rod was identified, the LHGR was increased so that the rod-averaged power (i.e., radial peaking factor) was 80% greater than core average (a bounding value for most, if not all, currently operating PWRs). In the sensitivity studies, this raised the peak LHGR to ~12.5-13 kW/ft, which varies depending on burnup. The specific sensitivity studies presented in Section B.2 were designed to examine the effects of the swelling and rupture model in the S-RELAP5 code. This is the NUREG-0630 model most commonly used in LOCA analyses. In both instances, the use of this model provided a benefit in terms of PCT and oxidation criteria. The conclusion from this study is that it is conservative to neglect swelling and rupture in the methodology. The complexity of the swelling and rupture phenomena is such that it was decided to accept this conservatism in the methodology.

In response to this question an additional analysis has been performed applying the swelling and rupture model (based on NUREG-630) to the limiting PCT calculation presented in Appendix D. The purpose of this was to perform a sensitivity study where rupture did occur. The following

figures provide the requested results from the additional sensitivity study. The first figure presents a PCT comparison for a calculation including the swelling and rupture model vs. the base case. As with the calculations given in Section B.2, PCT is reduced relative to the base case. In addition, examination of the oxidation criteria shows that the base case results also bound the swelling and rupture case. The second figure shows the heat transfer coefficient vs. time for the two cases at node 28 which is the rupture node when the swelling and rupture model is enabled (indicated as "Modeled Enabled" on the figures). Also, from the "Model Enabled" calculation, the heat transfer coefficient is shown for the node immediately above the rupture node. The third figure shows the clad temperature traces at these same three nodes. The last figure shows the gap conductance. The drop in gap conductance which begins around 13 s is from the rod swell. Around 18 s the rod ruptures and the gap conductance drops to its eventual minimum value.

The swelling and rupture model does not take credit for the likely liquid deentrainment that would occur as a result of this condition. In addition, the Forslund-Rohsenow dispersed flow film boiling correlation is unmodified for this condition. The deentrainment phenomenon is expected to be a PCT benefit and by not considering its effects in S-RELAP5, the analyses possess this conservatism. A discussion of void fraction and droplet size at the hot spot is presented in the response to Question 123.

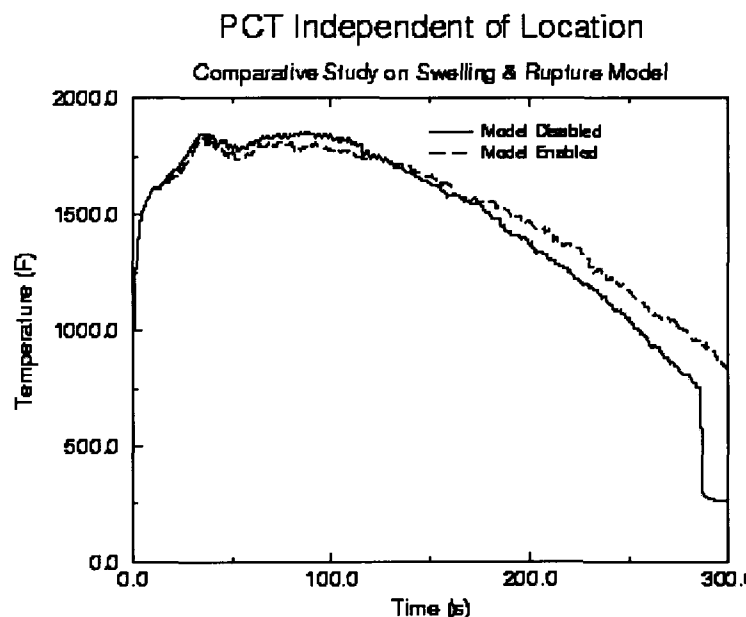


Figure 132.1 Swelling and Rupture Model: PCT Independent of Location



Figure 132.2 Swelling and Rupture Model: Heat Transfer Coefficient



Figure 132.3 Swelling and Rupture Model: Clad Temperatures Near Rupture Node



Figure 132.4 Swelling and Rupture Model: Gap Conductance

Question 133: *Fig. B.13 shows an increasing PCT at the end of the plot. Please show the transient until quench.*

Response 133: The purpose of the sensitivity study presented in Figure B.13 was to assess the impact of pump two-phase degradation model by replacing the best-estimate EPRI model with the Semiscale model (with greater degradation). Following the reasoning used to develop the PIRT ranking for this parameter, the period of interest is blowdown. The phenomenological expectation was that with increased pump degradation, the pumps influence on blowdown cooling would be minimized and that this should be observable in the first 20-50 s; hence, this figure was made to highlight this period of interest.

As mentioned in RAI response #129, the objective of the sensitivity studies was to determine PCT sensitivity to perturbations in a set of PIRT and plant parameters. Due to the volume of sensitivity studies required to support the CSAU step on defining the assessment matrix, minimizing the calculational run time allowed us to be more efficient in this task. Appendix D presents the 3-loop sample problem, this calculation provides the LOCA simulation through whole core quench.

Question 134: *Fig C.1 shows a variation of about 50 K during reflood with time step. Please discuss the effect of smaller time steps on PCT.*

Response 134: In reading Figure C.1, clad temperatures do vary within a band of about 50 K (90°F). As reported in Appendix C, the actual variation of PCT is only []. PCT is the figure of merit in this study. Basically, the current time steps used for RLBLOCA analysis is at the tolerance threshold for reasonable run times. Smaller time steps have been investigated; however, no improvement in numerical uncertainty has been observed.

Question 135: *Please support the basis for the uncertainty, especially the difference between the 95/95 and 50/50 and the data base used to assess the code predictive capability (for example, there are many more FLECHT-SEASET, FLECHT Cosine and FLECHT Skewed tests with PCT between 2000 and 2200 F that were not used in the S-RELAP5 comparisons). This would include the sensitivity of PCT to nitrogen injection, fuel swell and rupture modeling, sensitivity to time step, downcomer boiling sensitivities, etc. If a larger database was used, how would the uncertainty be impacted?*

Response 135: It is fully recognized that there are a significant number of tests that have been performed that were not modeled and analyzed in this methodology submittal. The submittal followed the CSAU approach of identifying the important transient and plant phenomena through the PIRT process. Following the completion of the PIRT an assessment matrix was developed to support evaluation of the important PIRT phenomena, defined as those ranked 5 or higher. This assessment matrix was then evaluated and uncertainties developed and conservatism justified. The most likely result of using a larger database is that the uncertainties would decrease.

Question 136: *As identified on page 3-17 of EMF-2100, the Weber number is used to define the maximum bubble size. For reflood calculations, Wallis has proposed a formula-based on Taylor instability theory. Please discuss the impact of the Wallis approach for choosing bubble size on level swell and reflood behavior and justify the model.*

Response 136: The bubble size is of little importance for the reflood since the bubbly-slug flow occurs only below the quench front. Also, as is pointed out in Response to Question 71a, the adequacy and applicability of the bubbly-slug interphase model for the reflood calculation has been demonstrated in the excellent code-data comparison of the differential pressure below the quench front (Figures 3.3.71 to 3.3.79 of EMF-2102(P) Revision 0). Since the effects are of little importance and the existing model is shown to be adequate, Framatome ANP does not feel that the effort of incorporating a new model such as proposed by Wallis is warranted.

Question 137: *Regarding the critical Weber number of 4.0 for droplets in dispersed flow (page 3-17 of EMF-2100), Wallis recommends that a Weber number of 12 be used to define the maximum drop diameter for viscous fluid droplets. Drop diameters of about 1/10 inch characterize LOCA reflood behavior and have been used to capture the PCT in the FLECHT tests. Please justify the Weber number used to compute the drop size for the FLECHT tests. What is the lower limit on drop size in the S-RELAP5 methodology and how does this value compare to the database?*

Response 137: The critical Weber number and the size of droplets/bubbles are hypothetical processes to obtain reasonable values for interphase friction and interphase heat transfer. The ultimate justification is how good are the code-data comparisons of void distribution, and fluid and surface temperatures. The exact form and interpretation of the critical Weber number relation may vary depending on the application intent and the definition of droplet diameter. In S-RELAP5, the critical Weber number is used to determine a reasonable average droplet diameter. Also, as discussed in Section 3.2.1 of EMF-2100 (P) Revision 4, the critical Weber number is not the only criterion for determining the droplet diameter. An example of droplet diameters calculated by S-RELAP5 during the reflood period is shown in Figure 123.4 (see Response to Question 123). The droplet diameters are mostly in the range between 0.5 mm

and 2.0 mm. Figure 137.1 is a reproduction of a droplet diameter plot for FLECHT-SEASET 31504 from NUREG/CR-2256, "PWR FLECHT SEASET Unblocked Bundle, Forced and Gravity Reflood Task Data Evaluation and Analysis Report," November 1981. It is seen that the S-RELAP5 calculated values, ranging from 0.5 to 2.0mm, are within the data range shown in this figure. Note that the legend "PREDICTION" in the figure is not an S-RELAP5 prediction. The S-RELAP5 calculation is shown in Figure 123.4 (Response to Question 123).

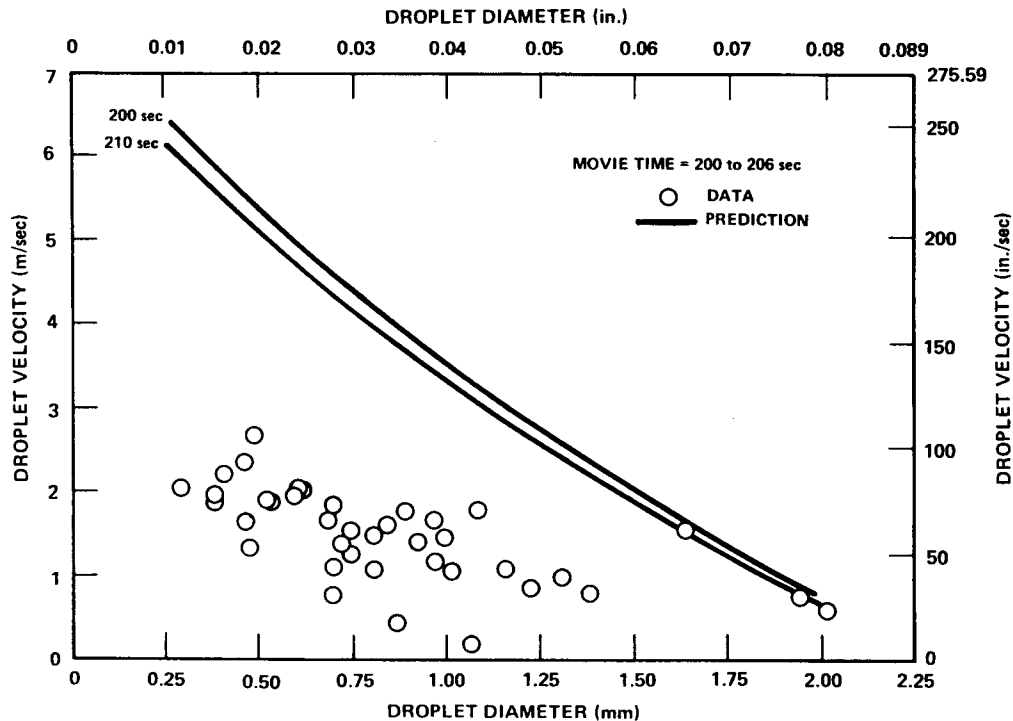


Figure 137.1 Reproduction of Plot of Comparison of Calculated and Measured Drop Velocities, Run 31504, 1.83 m (72 in.) Elevation, Page F20 of NUREG/CR-2256

Question 138: *How are the flow regime maps applied to the 2-D downcomer model?*

Response 138: The flow regime map for 2-D components is discussed in Section 3.1 and in the text below Equation (3.11) of EMF-2100(P) Revision 4. In essence, for the 2-D downcomer, the axial direction parameters are used for determining the flow regime map and the range of the annular-mist regime is expanded.

Question 139: *Since flow regimes affect entrainment and ECC bypass, how was the uncertainty in the flow regime maps included in the methodology?*

Response 139: There is no direct treatment of the uncertainty in the flow regime maps used in the code. Variations between the code predicted flow regime and the actual flow regime is included in the uncertainties generated and conservatisms demonstrated in the other parameters, for example heat transfer coefficients. In the development of the code uncertainties the differences between the code prediction and the experimental data would include differences in the flow regime map. Thus, the uncertainty in the flow regime maps is indirectly included in the statistical treatment.

Additional Items.

Item 1: Two Phase Pump Degradation Model

An evaluation of the use of either the Semiscale or EPRI-CE two phase pump degradation model in the RLBLOCA methodology is presented in Appendix B of EMF-2103(P). The original decision was to use the Semiscale two phase pump degradation model. This decision was based on the fact that the sensitivity study showed an 18 degree F higher PCT using the Semiscale model than the PCT using the EPRI-CE model. Since the expected variability in an S-RELAP5 calculation is approximately 30 degrees F this degree of variation, 18 degrees, indicates that either model will produce the same result in a LBLOCA analyses. Framatome ANP uses the EPRI-CE two phase pump degradation model in its SEMPWR-98 evaluation model and other S-RELAP5 based models. In order to use consistent models in the future, Framatome ANP will use the EPRI-CE two phase pump degradation model in the RLBLOCA methodology.

Item 2: Gadolinia Bearing Fuel Rod Modeling

In the performance of sensitivity studies required to respond to the RAI on the realistic LBLOCA, Framatome ANP discovered that the modeling of gadolinia bearing fuel rods had been performed incorrectly. The modeling of gadolinia fuel rods was corrected and the results showed about a 63F reduction in the 95/95 PCT for the three loop sample problem and a 66F reduction in the four loop sample problem.

[

]

Item 3: NRC Requested Break Size Evaluation

To evaluate the impact of statistically treating the break size in the Framatome ANP proposed Realistic large break LOCA methodology the NRC requested that a sensitivity study on the calculated highest PCT case for the 3-loop plant be performed. The staff specifically requested that the break size associated with the highest reported PCT in EMF-2103 Appendix D, the 3-loop 0.66 DEG cold leg break, be fixed and that the 59 cases be rerun with the other parameters selected by Monte Carlo methods as specified in the methodology.

The 59 cases have been run as requested and the resulting PCTs are provided in Table 1. These cases have all been run with the same break size as EMF-2103 Appendix D case 41, which is the limiting case from the reported 3-loop sample problem with a break size of .66 DEG and a PCT of 1853 F. As shown in the table only two cases from the sensitivity study, case 11 and case 51, have higher PCTs than the limiting case 41 in EMF-2103 Appendix D. The sensitivity study case 51 has a PCT of 1873 F, which is 20 F higher, and case 11 has a PCT of 1929 F, which is 76 F higher.

A comparison was made between EMF-2103 Appendix D case 41 and the sensitivity study case 11 to determine the principle parameters contributing to this difference. The comparison is provided in Table 2 for the most important parameters with respect to their contribution to the PCT. These parameters were selected because they have been shown, based on sensitivity studies, to have the largest impact on PCT. As shown in Table 2, the primary differences which contributed to the higher PCT in the sensitivity study case 11 are the power parameters. Case 11 has a higher Fq and a higher peaked axial shape than the limiting case 41 in EMF-2103 Appendix D.

An additional break spectrum study was also performed by Framatome ANP to look at variations in the break size for EMF-2103 Appendix D case 41, the limiting case from the 3-loop sample problem. The results of this study are provided in Table 3 which looks at a range of guillotine and split breaks. As shown in Table 3, the PCT was reduced for all larger and smaller break sizes relative to the 0.66 guillotine break in EMF-2103 Appendix D case 41. This shows that the EMF-2103 Appendix D case 41 break size is the limiting break size for the statistically selected conditions.

In conclusion, it has been demonstrated for the 3-loop sample problem, that performing a statistical analysis around the break size for the limiting PCT case, EMF-2103 Appendix D case 41, results in only a 76 F change in the maximum PCT. This change is due to a more conservative selection of the Fq and ASI. It has also been demonstrated, that the limiting case for the 3-loop sample problem was associated with the limiting break size given the other selected statistical conditions in EMF-2103 Appendix D case 41.

Table 1 Peak Clad Temperatures for 59 Cases with Constant Break Size – Sensitivity Study

Case Number	Peak Clad Temperature, F
1	1671.4
2	1448.7
3	1675.3
4	1501.4
5	1655.5
6	1651.1
7	1679.1
8	1647.5
9	1733.5
10	1673.9
11	1929.0
12	1802.6
13	1746.8
14	1655.6
15	1720.8
16	1634.1
17	1539.3
18	1588.6
19	1618.1
20	1658.7
21	1515.3

Case Number	Peak Clad Temperature, F
22	1532.1
23	1827.5
24	1477.5
25	1560.1
26	1729.6
27	1504.4
28	1849.9
29	1647.7
30	1358.1
31	1610.5
32	1538.4
33	1685.7
34	1482.5
35	1638.6
36	1675.2
37	1435.6
38	1534.5
39	1584.3
40	1645.1
41	1852.8
42	1804.5
43	1468.5
44	1674.0
45	1628.0
46	1718.0
47	1658.3
48	1720.4
49	1654.9
50	1662.4
51	1872.1
52	1579.2
53	1559.5
54	1517.4
55	1676.4
56	1563.7
57	1619.8
58	1502.0
59	1352.0

Table 2 Comparison of Sensitivity Study Case 11 and EMF-2103 Appendix D Case 41 Parameters

Statistical Parameter	EMF-2103 Appendix D Case 41	Sensitivity Study Case 11
Axial Shape Index (ASI)	-0.0088	-0.1361
Fq	2.28	2.38
Heat Transfer Multiplier, FILMBL	0.8813	1.274
Heat Transfer Multiplier, FRHTC	1.059	1.492

Table 3 Break Spectrum Study for EMF-2103 Appendix D Case 41

Break Type	Break Size	Peak Clad Temperature, F
Guillotine	1.0	1703
Guillotine	0.9	1708
Guillotine	0.8	1742
Guillotine	0.66	1853
Guillotine	0.5	1617
Split	1.0	1607
Split	0.7	1687
Split	0.4	1313
Split	0.1	1226

Appendix A Inverse Heat Conduction Model

Due to the complications resulting from the heater rods being constructed of multiple material layers and the specification of an internal boundary condition via a table of measured values, it is necessary to use a numerical solution to infer the transient surface heat flux. Also, due to the large axial spacing of the rod thermocouples, it is only practical to employ a one-dimensional treatment of conduction within the rod. Thus, all effects of axial conduction will be ignored. This assumption is reasonable under most conditions but it will lead to potential errors in the estimation of the surface heat flux in the vicinity of the quench front. However, because the focus here is to determine heat transfer coefficients in the film boiling region, this assumption is not a major limitation.

There are four principal steps in developing a generalized form for the numerical implementation of the inverse conduction algorithm. First, the transient conduction equation must be put into finite difference form (Section 1.0), then the appropriate internal boundary conditions must be applied (Section 2.0). The resulting matrix solved (Section 3.0) for the transient radial temperature profile. Finally, from the calculated radial temperature profile, the surface heat flux and the heat transfer coefficient are determined. However, as described in EMF-2102, Section 5.1.2.1, it is beneficial (if not necessary) to first pre-condition the thermocouple signal to reduce noise and to also smooth the resulting heat transfer coefficient.

2.0 Finite Difference Equation

The one-dimensional transient radial conduction equation is

$$\rho c_p \frac{\partial T}{\partial t} = \frac{1}{r} \frac{\partial}{\partial r} \left(kr \frac{\partial T}{\partial r} \right) + q'''' \quad (1)$$

where

- ρ = Material density, kg/m³
- c_p = Material specific heat, J/kg-K
- k = Material thermal conductivity, W/m-K
- r = Radial location from rod center, m
- $T(r)$ = Material temperature, K
- q'''' = Volumetric heat generation rate within the material, W/m³

To formulate a numerical model, a radial noding scheme must be chosen and the conduction equation volume (or area) averaged for each of the nodes. One way of accomplishing this is to divide the conductor into a number of concentric radial rings. For accuracy, the nodal points are placed at the geometric centers of each radial ring. Also, when multiple material regions exist, as

is the case in fuel rod simulators, the radial rings are chosen so that their boundaries coincide with the material boundaries. Within each material region, however, any integral number of radial rings can be specified in order to provide for a finer discretization in regions of sharp temperature gradients.

An important assumption in the implementation of the inverse heat conduction equation calculations is that the presence of the thermocouples within the test rods does not have a major impact on the radial temperature profile in the rods.

An exception to the above is made for the radial ring at the external surface of the fuel rod simulator. This last node is taken to be of "half-thickness" so that the actual nodal point is located on the surface. A typical noding scheme for a fuel rod simulator is given in EMF-2102, Figure 5.1. In this example, there are four material regions with a varying number of radial nodes for each region. Note the placement of the last node on the rod external surface.

For the i th radial ring, the cross-sectional area averaged transient conduction equation becomes

$$(\rho c_p A)_i \frac{\partial T_i}{\partial t} = K_{i+1/2} (T_{i+1} - T_i) + K_{i-1/2} (T_{i-1} - T_i) + q'_i \quad (2)$$

where

A_i = Cross-sectional area of the i th ring, m^2

K = Inter-node conductance, $W/m-K$

q'_i = Linear heat generation rate for the i th radial ring, W/m

The inclusion of the subscript " i " indicates that the value is either the nodal value (in the case of temperature) or is the area averaged value for that radial ring. The inter-node conductance between node " i " and node " $i+1$ ", denoted as $K_{i+1/2}$, is defined in terms of the thermal resistance as

$$K_{i+1/2} = \frac{1}{R_{i,j+1/2} + R_{i+1,j+1/2}} \quad (3)$$

where $R_{i,j+1/2}$ is the resistance to heat flow from node " i " to the boundary between nodes " i " and " $i+1$ " which is indicated by the subscript " $i+1/2$ ". Similarly, $R_{i+1,j+1/2}$ is the thermal resistance between node " $i+1$ " and the boundary between nodes " i " and " $i+1$ ". It remains to define the values for these thermal resistances.

To rigorously formulate these resistances, one must know the radial temperature distribution. Since this is the quantity we wish to solve for, a way to approximate these resistances is required. The method used here is to approximate the transient thermal resistance by its steady state value. Thus,

$$R_{i+1/2} = \frac{\ln\left(\frac{r_{i+1/2}}{r_i}\right)}{2\pi k_i} \quad (4)$$

where

r_i = The radius of the node center, m

$r_{i+1/2}$ = Radius of the boundary, m

The inter-node conductances are then

$$K_{i+1/2} = \frac{2\pi k_i k_{i+1}}{k_{i+1} \ln\left(\frac{r_{i+1/2}}{r_i}\right) + k_i \ln\left(\frac{r_{i+1}}{r_{i+1/2}}\right)} \quad (5)$$

and

$$K_{i-1/2} = \frac{2\pi k_i k_{i-1}}{k_i \ln\left(\frac{r_{i-1/2}}{r_{i-1}}\right) + k_{i-1} \ln\left(\frac{r_i}{r_{i-1/2}}\right)} \quad (6)$$

To complete the numerical model, it remains to specify the temporal discretization and to state how the material properties are to be evaluated.

A fully implicit scheme for temporal discretization was implemented. The discretized transient heat conduction equation is

$$(\rho^n c_p^n A)_i \frac{T_i^{n+1} - T_i^n}{\Delta t} = K_{i+1/2}^n (T_{i+1}^{n+1} - T_i^{n+1}) + K_{i-1/2}^n (T_{i-1}^{n+1} - T_i^{n+1}) + (q')_i^n \quad (7)$$

where the superscript "n+1" indicates that the quantity is to be evaluated at the new time and "n" at the old time. As indicated above, the material properties are evaluated at the old time value of the nodal temperature.

3.0 Inverse Heat Conduction Equation Boundary Conditions

In a normal transient conduction solution of a fuel rod simulator (cylindrical geometry), there are two boundary conditions: an adiabatic boundary condition for the heater rod centerline and a heat transfer coefficient on the external surface. For the inverse conduction solution, the adiabatic centerline boundary condition is retained. An internal temperature boundary condition is applied at the location of the thermocouple of interest. Implicit to the use of an internal temperature boundary condition is the observation that the thermocouple is present within the test rod. It is assumed that the presence of thermocouples within the test rod does not have a

significant effect on the radial temperature profile. The surface heat flux (or heat transfer coefficient) is one of the unknowns to be determined.

To simplify the discussion, introduce the following notation for the transient conduction equation for the i th node

$$a_i T_{i-1}^{n+1} + b_i T_i^{n+1} + c_i T_{i+1}^{n+1} = d_i \quad (8)$$

where all of the temperatures are at new time and their coefficients are

$$\begin{aligned} a_i &= -K_{i-1/2} \\ c_i &= -K_{i+1/2} \\ b_i &= \frac{(\rho c_p A)_i}{\Delta t} - a_i - c_i \end{aligned}$$

The explicit right-hand-side term is given by

$$d_i = \frac{(\rho c_p A)_i}{\Delta t} T_i^n + q_i'$$

Let the nodes be numbered from 1 to N , where N is the index of the node on the clad exterior surface. The adiabatic centerline boundary condition is applied to the first node by setting

$$a_1 = 0 \quad (9)$$

so that the first conduction equation is reduced to

$$b_1 T_1 + c_1 T_2 = d_1 \quad (10)$$

For the last node, the conduction equation becomes

$$a_N T_{N-1} + b_N T_N = d_N - q_w'' P \quad (11)$$

where the wall heat flux, q_w'' , and perimeter, P , have been introduced.

If the wall heat flux (or equivalently the heat transfer coefficient) were known, we would now have a set of N equations with N unknown values of the new time temperature forming a tri-diagonal matrix. The solution would then be performed by a straightforward Gaussian elimination and back-substitution. However, because the wall heat flux is one of our unknowns, another boundary condition must be introduced.

Typically, the rod thermocouple would be attached to the inside clad surface. That is, it would be at the boundary between two material regions and hence at the boundary between two

cylindrical rings. Let the ring just inside this boundary be denoted by the subscript "n", so that the boundary is at "n+1/2" and the first node within the clad has the subscript "n+1". Since the location of the measured temperature, T_{meas} , to be used as a boundary condition does not coincide with the location of one of our nodes, it cannot be used directly as a temperature boundary condition. Instead, because a boundary cannot store energy, a constant heat flux boundary condition across this interface is applied. That is,

$$q''_{n,n+1/2} = q''_{n+1/2,n+1} \quad (12)$$

where

$$q''_{n,n+1/2} = \text{heat flux from node "n" to the boundary}$$

$$q''_{n+1/2,n+1} = \text{heat flux from the boundary to node "n+1".}$$

In terms of the thermal resistances introduced above,

$$\frac{T_n - T_{meas}}{R_{n,n+1/2}} = \frac{T_{meas} - T_{n+1}}{R_{n+1/2,n+1}} \quad (13)$$

where all of the temperatures are at the new time. Equation (13) can be recast as

$$b'_n T_n + c'_n T_{n+1} = d'_n \quad (14)$$

where

$$b'_n = \frac{1}{R_{n,n+1/2}}$$

$$c'_n = \frac{1}{R_{n+1/2,n+1}}$$

$$d'_n = (b'_n + c'_n) T_{meas}$$

Equation (14) is the implementation of the internal boundary necessary to provide for the determination of the surface heat flux. Section 4.0 describes the solution procedure for the new time nodal temperatures.

4.0 Inverse Heat Conduction Equation Solution Procedure

There are N+1 equations (N transient conduction equations plus the interface heat flux constraint) and N+1 unknowns (N new time temperatures and the surface heat flux). Therefore, the system is solvable. To do so, the solution is divided into two parts.

First, construct a matrix consisting of the conduction equations for the first n nodes and the interface boundary condition. This gives

$$\mathbf{b}'_n \mathbf{T}_n + \mathbf{c}'_n \mathbf{T}_{n+1} = \mathbf{d}'_n$$

which has $n+1$ equations and $n+1$ unknown temperatures. Using standard Gaussian elimination and back substitution, we now have values for the new time temperatures of the first $n+1$ nodes.

The temperature, T_{n+1} , corresponds to the first node within the cladding (i.e., outside of the imposed thermocouple temperature boundary condition). It remains to calculate the new time temperatures for the remaining clad nodes and the wall heat flux. This system of equations is

$$a_N T_{N-1} + b_N T_N = d_N - q_w'' P$$

If there are n_c nodes in the clad, then we have n_c conduction equations in the above system for $n_c - 1$ unknown temperatures and the surface heat flux. Considering the first equation, both T_n and T_{n+1} are known. Therefore,

$$T_{n+2} = \frac{(d_{n+1} - a_{n+1}T_n - b_{n+1}T_{n+1})}{c_{n+1}} \quad (17)$$

Similarly, back-substitution is used for all of the clad temperatures. The remaining equation is then solved for the surface heat flux

$$q_w'' = \frac{d_N - a_N T_{N-1} - b_N T_N}{P} \quad (18)$$

All of the information required to compute the heat transfer coefficient is now known. The heat transfer coefficient is defined relative to the saturation temperature as

$$h = \frac{q_w''}{T_N - T_{sat}} \quad (19)$$

where the saturation temperature is taken to be that corresponding to the upper plenum pressure. Note that the calculated value for the rod surface temperature, T_N , is used to calculate

the heat transfer coefficient rather than the measured thermocouple temperature. Thus, the resulting heat transfer coefficient is consistent with that computed in S-RELAP5.

Appendix B Quench Time Determination in Measured Data

The criteria applied to determine quench time in the THTF and FLECHT-SEASET tests are different. The differences are caused by the difference in data sampling rates and also because the FLECHT-SEASET algorithm was optimized for low pressure reflood conditions.

FLECHT-SEASET Quench Determination

The FLECHT-SEASET criteria are taken from Reference 1 (from page E-26 of the report). The algorithm examines five sequential data points at a time. These temperature points are identified by index, i.e., $T(i)$, $T(i+1)$, $T(i+2)$, $T(i+3)$, and $T(i+4)$. They are associated with time $t(i)$, $t(i+1)$, $t(i+2)$, $t(i+3)$, and $t(i+4)$, as shown in Figure B.1.

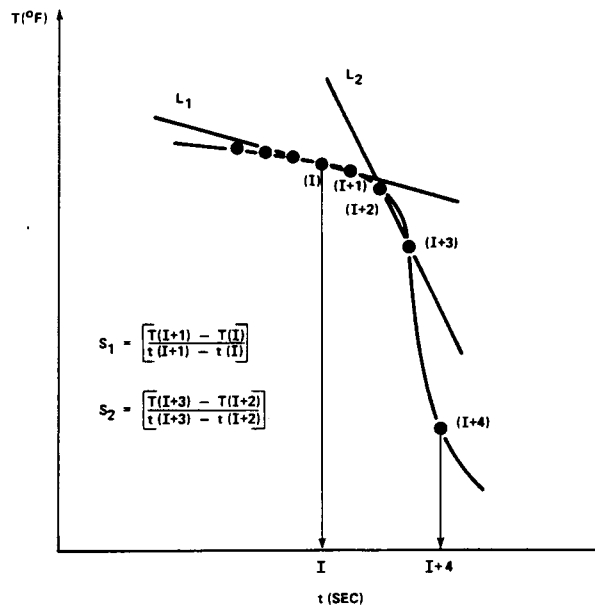


Figure B.1 FLECHT-SEASET Quench Analysis (Figure E-1 from Ref. 1)

The algorithm is performed in steps. In the first step, the temperature $T(i)$ must be greater than 149°C for a potential quench condition to exist.

In the second step, quench may exist if the slope of the temperature time curve between the third and fourth points is greater than 28°C/S .

$$S_{L2} = \frac{T(i+3) - T(i+2)}{t(i+3) - t(i+2)} < -28 \text{ } ^\circ\text{C/s}$$

In the third step, if the absolute value of the slope between the third and fourth points is more than two times greater than the absolute value of the slope between the first two points, then a potential quench condition exists.

$$S_{L1} = \frac{T(i+1) - T(i)}{t(i+1) - t(i)}$$

$$|S_{L2}| > 2|S_{L1}|$$

In the fourth step, provided all of the above criteria have been satisfied, and if the slope between the fourth and fifth points is greater than the slope between the third and fourth points, then quench is determined to have occurred.

$$S_{L3} = \frac{T(i+4) - T(i+3)}{t(i+4) - t(i+3)}$$

$$|S_{L3}| > |S_{L2}|$$

In the fifth step, the time and temperature of quench is calculated to be the intersection between the lines L_1 and L_2 .

THTF Quench Determination

The FLECHT-SEASET algorithm was specifically developed for low pressure reflood conditions and for thermocouple traces with low sampling frequencies. Indeed, several of the criteria used to find the quench condition are, in effect, hardwired for the conditions expected in FLECHT. Consequently, they do not work at all for the high pressure conditions of the THTF reflood tests.

One possible approach would be to find another set of hardwired criteria to be implemented in a THTF version of the algorithm. But the relatively high sampling frequencies of the THTF data, 20-100 Hz, allows another, more mathematical, approach.

For pool boiling, T_{min} is defined to occur at a local minimum in the surface heat flux for which the heat flux begins to increase as the wall temperature is reduced. For this special case (constant fluid conditions), the criteria for T_{min} can be expressed as:

$$\frac{dq''}{dT_w} = 0 \text{ with } T_w > T_{CHF}$$

In theory, one could perform just such a test for the THTF data. However, in quenching tests, the fluid conditions change dramatically with time, i.e., from superheated vapor to subcooled liquid, and so the derivative of the surface heat flux can be confounded due to the change in fluid conditions. Therefore, another set of criteria is needed.

In a quenching test, the quench temperature is associated with the "knee" in the thermocouple trace (Figure B.2).

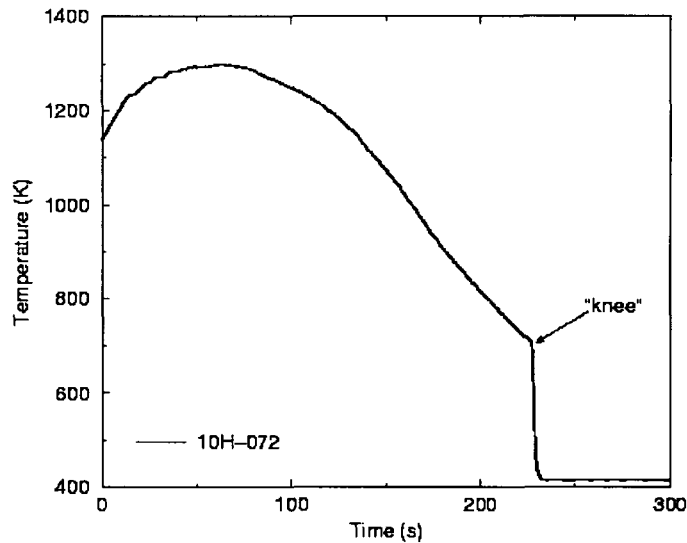


Figure B.2 Illustration of the "Knee" in a Thermocouple Trace

The physical reason for this "knee" is that as the wall temperature decreases, it reaches a point where heat transfer to the liquid can begin and subsequent decreases in the wall temperature accelerate the process. The result is a pronounced change in the slope of the thermocouple trace thereby creating the "knee" in the curve. The quench condition can then be identified by searching for the location of the maximum change in slope of the thermocouple trace, or in other words, by finding the location of the most negative value of the curvature:

$$\min \left[\frac{\partial^2 T_w}{\partial t^2} \right] \Rightarrow t_Q \text{ and } T_Q$$

The second derivative of temperature with respect to time for the i th data point is then approximated by the finite difference form:

$$\frac{\partial^2 T_w}{\partial t^2} \approx \frac{T_{i+1} - 2 \cdot T_i + T_{i-1}}{2 \cdot \Delta t}$$

where, T_i is value of thermocouple temperature for the i th data point and Δt is the time step size between data points.

Using this criteria, the time, t_{\max} , for which the maximum negative value of the curvature has been found indicates that the rod has already begun quenching by this time in the transient. So, if the quench time and quench temperature are assigned as the recorded values at this point, that is, $t_Q = t_{\max}$ and $T_Q = T_{\max}$, then the calculated quench time should be slightly later than the actual quench time and the quench temperature slightly below its actual value. The time differential is minimal as the time step size in THTF is either 0.01 or 0.05 seconds. However,

despite the miniscule difference in quench time, due to the extremely high rate at which the clad temperature is decreasing (> 400 K per second), the under-estimation of the quench temperature can be on the order of 25 K.

In calculating the quench temperature there are two other complications that should be considered:

- The thermocouple signal is noisy and to prevent false indications of quenching, the signal has been filtered before it was analyzed. How much does this filtering distort the value of the quench temperature?
- The quench temperature is based on the filtered thermocouple signal and the thermocouple is located on the interior of the clad surface. How much does the actual clad surface temperature differ from the thermocouple reading?

The following two figures illustrate the temperature differences that can result from filtering the thermocouple signal. In the first, Figure B.3, there is no discernable difference between the original and the filtered signal. At an extremely fine scale focused on the quench point (Figure B.4), it is observed that the filtered signal has a smoother shape and under-predicts the temperature at the point of maximum negative curvature. For this particular example, the temperature difference is ~ 9 K. Of course, the exact value of this under-prediction varies from thermocouple to thermocouple and from test to test, however, this example gives a good indication of the trend towards under-prediction and its approximate magnitude.

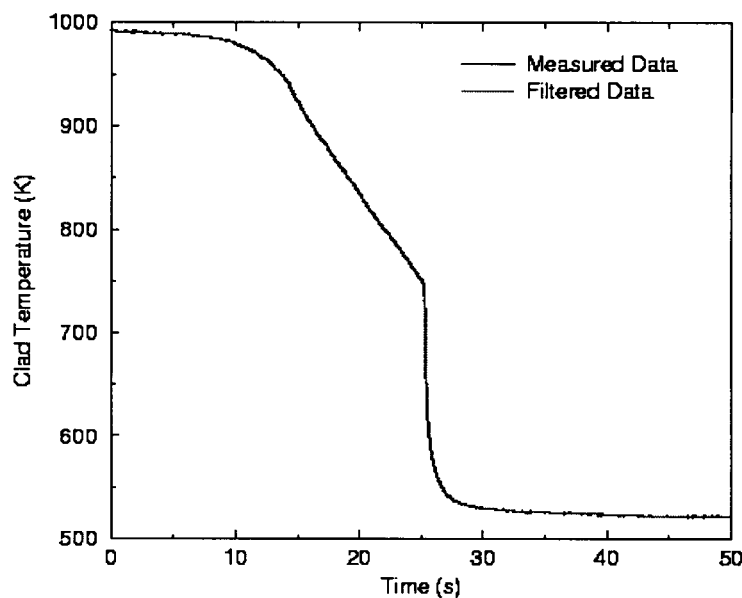


Figure B.3 Comparison of Original Thermocouple Signal and the Filtered Signal for Thermocouple TE-320AG of Test 3.02.10C

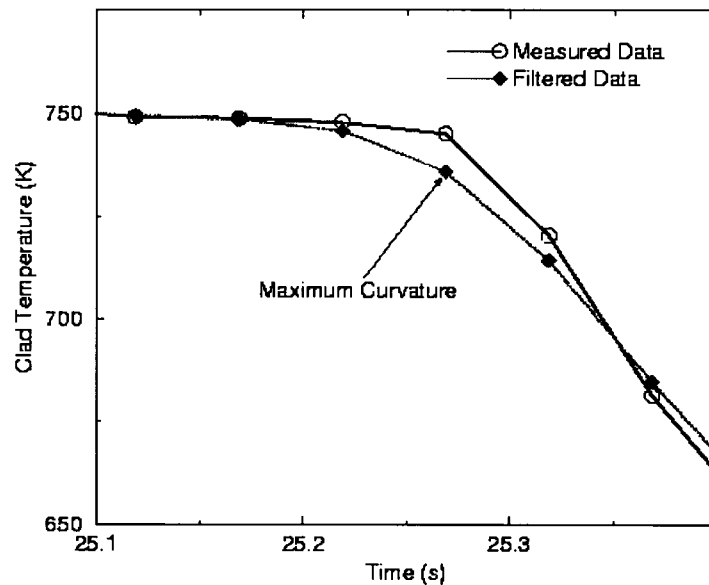


Figure B.4 Detail of the Comparison of Original Thermocouple Signal and the Filtered Signal for Thermocouple TE-320AG of Test 3.02.10C Showing Location of the Point of Maximum Negative Curvature

In the S-RELAP5 heat transfer package, the wall temperature criterion for the transition from the film boiling regime to transition boiling is based on the temperature of a node located on the rod surface. In contrast, reported quench temperatures are normally based on a thermocouple reading where the thermocouple is attached to the clad interior. This was the case for the quench temperatures computed by the data analysis program for the FLECHT-SEASET tests and is also the case for the high pressure THTF reflood tests. Consequently, there is the potential to introduce a non-conservative bias as the measured temperature will always be greater than the actual clad surface temperature.

Usually, it is argued that up until the time of quench the rod heat flux is low (on the order of the decay heat) and this, combined with the high thermal conductivity of the clad material, results in a small temperature drop across the clad that is negligible compared to the uncertainty in determining the quench temperature. That this is indeed the case is illustrated in Figure B.5. The plotted thermocouple signal is the same filtered signal that is used in both the quench temperature analysis and as the boundary condition in the inverse conduction solution for the heat transfer coefficient. The plotted surface temperature is that which results from the inverse conduction solution.

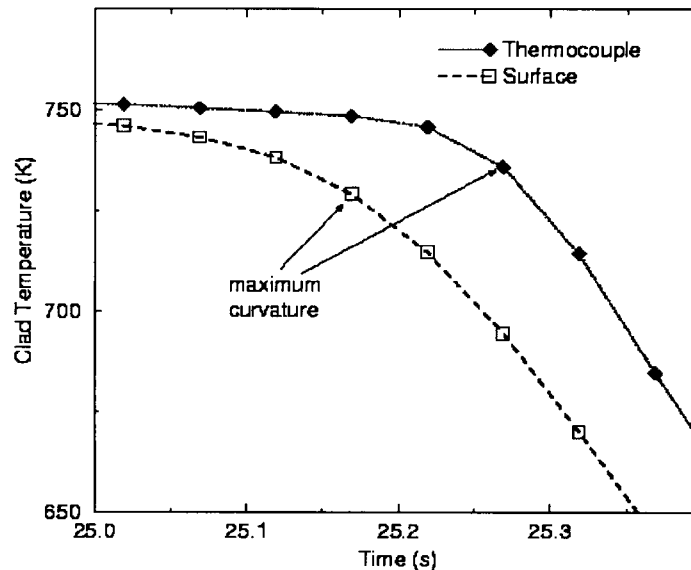


Figure B.5 Comparison of Calculated Surface Temperature with Thermocouple Response for Thermocouple TE-320AG of Test 3.02.10C at the Onset of Quenching

Before the arrival of the quench front, the temperature drop across the clad is on the order of 5 K. During quenching, the thermocouple response lags behind the surface response by about 0.1 seconds. So, at any given point in time, the clad temperature drop can approach 50 K. However, if one compares the points of maximum negative curvature on the two curves, there is a time shift of 0.1 seconds but the calculated quench temperature differs by less than 10 K. To some extent, this over-prediction counter balances the bias towards under-prediction introduced by the signal filtering and by selecting the point with maximum curvature as the quench point. Although it would be a difficult exercise to quantify the magnitude of each of these three effects, based on the above, it appears reasonable to take the quench temperatures calculated by the data analysis program as a lower bound to the actual quench temperatures and to use the spread in the data as an estimate of their uncertainty.

Reference

1. "PWR FLECHT-SEASET Unblocked Bundle, Forced and Gravity Reflood Task Data Report, Volume 1," NUREG/CR-1532, June 1980.

Appendix C
Changed Pages for Section 5 of EMF-2103

]

[

]

5.2.2 Application of Methodology

The FRA-ANP RLBLOCA methodology is a statistics-based methodology; therefore, the application does not involve the evaluation of different deterministic calculations. [

] The methodology results in a bounding value with 95% probability and 95% confidence in the PCT.

The PCT criterion is shown to be met with at least 95% probability and 95% confidence by comparing the 95/95 PCT value to the PCT criterion. Regulatory Guide 1.157 states that it is not necessary to explicitly consider the probability of meeting the other 10 CFR 50.46 criteria due to the strong dependence of the other criteria on PCT. Demonstration that the PCT criterion is met with 95% probability and 95% confidence shows that the other criteria are also met with high probability as required by the regulation. In order to define values for peak local oxidation and total core oxidation, these values will be reported from the 95/95 PCT case.

Application of this methodology relies on two computer codes: RODEX3A and S-RELAP5. All key LBLOCA parameters are calculated from S-RELAP5; RODEX3A is used to generate the initial fuel properties to be used by the fuel performance models in S-RELAP5. Performance of the RLBLOCA calculations relies on three analyst-created code input files describing the fuel, plant thermal-hydraulics, and containment thermal-hydraulics. The fuel model input is

The parameters treated statistically are listed in Table 5.6 and the values for the specific parameters and ranges addressed are given in Table 5.7. The distributions assumed for this sample problem are those given in Table 5.4. [

] The results of these calculations are presented in Figures 5.2 through 5.28.

Figures 5.2 through 5.16 present scatter plots for the more important phenomena/parameters in the analysis. These scatter plots are provided to demonstrate that the methodology does select input which covers the phenomena/parameter ranges and associated distributions. In general, it is difficult to see the PCT dependence of an individual parameter from these scatter plots. This is primarily due to the fact that there are several major parameters and a conservative combination of these parameters is required to obtain the higher values of PCT. Based on this the following paragraphs will concentrate on a discussion of the LBLOCA criteria as addressed by the analysis.

[

]

[

]

[

]

[

]

[

]

[

]

[

]

[

]

[

]

[

]

5.4 ***Determination of Total Uncertainty (CSAU Step 14)***

[] the biases and uncertainties determined during the code assessments are either directly addressed in the statistical analysis or demonstrated to be a code conservatism which adds an additional unquantified conservatism to the reported results. The final results for the 4-loop sample problem can be summarized as follows:

- The 95/95 calculated PCT was 1686 F which compares to the criterion for maximum PCT of 2200°F.
- The maximum nodal oxidation for the 95/95 PCT case was 0.8% which compares to the criterion for maximum nodal oxidation of 17%.
- The maximum total oxidation for the 95/95 PCT case was 0.02% which compares to the criterion for maximum total core oxidation of 1%.

Based on these results, it is concluded that the LBLOCA analysis for the sample W 4-loop plant meets the criteria for the LBLOCA event.

With respect to the identification of the degree of conservatism in the analysis, a comparison can be made to the 50/50 probability value for the PCT. The 50/50 PCT at 1375°F is 311°F less than the 95/95 PCT.

Appendix D
Changed Pages for Two-Phase Pump Degradation Model

with higher flows (54 and 68) the predicted levels are either conservative or in reasonable agreement.

For the UPTF tests, the liquid is separated in the steam generator simulator. For the two tests, the calculated liquid accumulating in the catch tanks is quite conservative (See Figures 4.168 through 4.171).

For the FLECHT-SEASET tests, there is no steam generator. The hot-leg piping terminates in a separator, which has a tank with a pipe in the bottom leading to a drain tank. Figures 4.172 through 4.179 compare the calculated levels in the separator tank and the separator drain tank with the measured levels. Because of the tendency of the model to hold a larger quantity of liquid in the upper plenum initially than would be indicated by measurements (See Section 4.3.3.1.4), the calculated carry-over to the separator is delayed. The bottom line for these figures is that the calculation has the liquid carried over to these tanks arriving slightly later than the measurements would indicate, with the overall carry-over from the calculation being greater. This latter point shows that the liquid entrained and carried over by the hot-leg model is conservative.

4.3.3.1.7 Two Phase Pump Degradation

The pump two phase degradation is addressed in the methodology as a best estimate input. Based on the sensitivity study described in Appendix B for a limiting break on both a 3-loop and a 4-loop plant, it is shown that this is not an important phenomenon for the limiting LBLOCA case. The use of the Semiscale two-phase degradation instead of the CE/EPRI two-phase degradation model produced essentially no impact on the 3-loop results and only an 18 F (10 K) for the 4-loop plant. Thus, the best estimate CE/EPRI model will be used in the RLBLOCA methodology.

4.3.3.1.8 Pump Differential Pressure Loss

The pump differential pressure loss is addressed in the methodology strictly as a best estimate. The S-RELAP5 code has the ability to input the pump specific homologous curves for the NPP being analyzed and this option is used. The homologous curves for the specific NPP pumps are obtained from the utility and, if plant data is available, a pump coast down is modeled to ensure that the curves are consistent with the plant data.

region was tested at full scale in the UPTF, as were the hot legs and the steam generator inlet plenum. The steam generator tubing geometry is prototypic in the CCTF (although the number of tubes is smaller). All these tests in the three facilities collected water carried over from the core under conditions representing the reflood phase of the LBLOCA and all three have additional collapsed liquid level measurements. As presented in Section 4.3, a study on carryover to the steam generator was performed using the CCTF. From that study, a bias on interfacial drag was determined to conservatively bound this phenomenon. The results of the CCTF (with bias), UPTF, and FLECHT-SEASET evaluations indicate that S-RELAP5 overpredicts the entrainment of liquid from the test bundle (Section 5.6 and Reference 5). While each test by itself has some deficiencies in terms of simulating a PWR and in terms of scale, the combination of the three tests provides a substantial basis for evaluating modeling of the drag between the two phases during reflood at full scale.

4.4.2.2.5 Pump Scaling

The S-RELAP5 code has normalized single phase homologous curves for a full scale W reactor coolant pump as code default. The use of full scale data for the pump makes code scaling moot for the pump. These homologous curves are set to applicable values by entering plant specific values for rated head, torque, moment of inertia, etc. The coastdown of the pump is driven by the torque and moment of inertia of the rotating mass. The torque includes the effects of friction and back EMF (pump torque) and of the loop pressure losses (hydraulic torque). The single phase pump head and torque curves are adjusted for two-phase degradation based on experimental data. The EPRI two-phase degradation data (Reference 54) is based on pumps that are similar to PWR coolant pumps and represent best estimate parameters.

4.4.2.2.6 Cold Leg Condensation

Cold leg condensation was evaluated at a scaled EPRI test facility (Reference 55) to determine the accuracy of the calculated interfacial heat transfer between the ECC water and the steam in the cold leg. The principal portion of the test apparatus was the simulated cold leg, which was fabricated from straight pipe with an ID of 10.42 in. Two injection points were provided so that the pipe lengths downstream of the injection point approximated either a typical PWR cold leg scaled down to about one-third or the full length of the cold leg. The cold leg pipe length

Table 4.1 Parameters Perturbed for PIRT Sensitivity Studies (*Continued*)

Table 4.18 Important PIRT Phenomena and Methodology Treatment



In the sensitivity studies the single-phase homologous curves ($H_{1\phi}$) used for all cases are supplied by the default Westinghouse pump data that is coded in S-RELAP5. The model describing two-phase degradation (H_{DEGRAD} and $M(\alpha)$) is entered as tabular input to S-RELAP5. For the base case, the default EPRI-CE data (Reference 59) for two-phase degradation is specified. The sensitivity study examined replacing the EPRI-CE degradation model with the Semiscale degradation model. The degradation model is only applied when two-phase conditions are present in the pump. During the rapid blowdown resulting from a LBLOCA, this period lasts about 10-15s following the break.

The PCT results, relative to the three base cases without accumulator nitrogen, are shown in Figures B.13 - B.15 (extracted for the time period of interest). For the 3-loop plant cases, no sensitivity is evident. This is the expected result, since the break size chosen was selected to minimize the enhanced blowdown heat transfer provided by the pumps. The 4-loop plant case does show an increase in the blowdown peak PCT of about 18 °F (10 K).

The PCT change of 18 °F well within the expected variability of the results which is about 30 °F (see Appendix C). In hindsight the pump degradation does not appear to be as significant of a parameter as originally anticipated. This result is consistent with the original work performed on the CSAU methodology (Reference 4). Since it has been demonstrated that increased pump degradation is not an important PIRT phenomena, the best-estimate EPRI-CE degradation model will be used in the RLBLOCA methodology.



FRAMATOME ANP

An AREVA and Siemens company

FRAMATOME ANP, Inc.

December 20, 2002
NRC:02:063

Document Control Desk
ATTN: Chief, Planning, Program and Management Support Branch
U.S. Nuclear Regulatory Commission
Washington, D.C. 20555-0001

**Conditions for Safety Evaluation on EMF-2103(P), "Realistic Large Break LOCA
Methodology for Pressurized Water Reactors"**

In drafting the safety evaluation for EMF-2103(P), the NRC developed a number of conditions on its acceptance of this methodology for application to licensed activities. Framatome ANP expressed its concerns about including some of these provisions in the SE, which led to a series of discussions with the NRC.

Framatome ANP has agreed to the conditions set forth in Attachment 1. We believe these limitations and requirements accurately reflect the understanding reached in our most recent technical discussions.

Very truly yours,

James F. Mallay, Director
Regulatory Affairs

Enclosure

cc: w/attachments
R. Caruso
D. G. Holland
R. Landry
J. S. Wermiel
Project 728

Attachment 1

Conditions on EMF-2103(P) Accepted by Framatome ANP

1. The model applies to 3 and 4 loop Westinghouse and CE designed NSSSs.
2. The model applies to bottom reflood plants only (cold side injection into the cold legs at the reactor coolant discharge piping).
3. The model is valid as long as blowdown quench does not occur. If blowdown quench occurs, additional justification for the blowdown heat transfer model and uncertainty are needed or the run corrected. A blowdown quench is characterized by a temperature reduction of the PCT node to saturation temperature during the blowdown period.
4. The reflood model applies to bottom up quench behavior. If a top-down quench occurs, the model will be justified or corrected to remove top quench. A topdown quench is characterized by the quench front moving from the top to the bottom of the hot assembly.
5. A counter-current flow limit violation warning will be added to alert the analyst to the occurrence of a CCFL violation in the downcomer.
6. Framatome ANP will not include the hot leg nozzle gaps.
7. If Framatome ANP applies the RLBLOCA methodology to plants using a higher Peak Linear Heat Generation Rate than used in the current analysis, or if the methodology is to be applied to an end-of-life analysis for which the pin pressure is significantly higher, then the need for a blowdown clad rupture model will be reevaluated. The evaluation may be based on relevant engineering experience and will be documented in either the RLBLOCA guideline or the plant specific calculation file.
8. Slot breaks on the top of the pipe have not been evaluated. If an analysis is performed for a plant with loop seals with bottom elevations that are below the top elevation of the core, Framatome ANP will evaluate the effect of the deep loop seal on the slot breaks. The evaluation may be based on relevant engineering experience and will be documented in either the RLBLOCA guideline or the plant specific calculation file.
9. The staff also notes that a generic topical report describing a code such as S-RELAP5 can not provide full justification for each specific individual plant application. When a license amendment is necessary in order to use this S-RELAP5 topical report, the individual applicant must provide justification for the specific application of the code. The justification is intended to ensure that the methodology has been applied to a specific plant within the conditions of this SE and within the stated limitations of the topical report. The justification may be in the form of a checklist that is provided to the NRC for information. The checklist should consist of the identification of an item with a statement by the licensee that the item has been (or will be) satisfied consistent with the topical report.

EMF-2103(NP)
Revision 0

Realistic Large Break LOCA Methodology for Pressurized Water Reactors

August 2001

Nature of Changes

Item	Page	Description and Justification
1.	All	This is a new document.

Contents

1.0	Introduction	1-1
2.0	Methodology Roadmap	2-1
2.1	Requirements and Code Capabilities	2-1
2.2	Assessment and Ranging of Parameters	2-3
2.3	Sensitivity and Uncertainty Analysis.....	2-4
3.0	Requirements and Capabilities	3-1
3.1	Scenario Specification (CSAU Step 1)	3-1
3.2	Nuclear Power Plant Selection (CSAU Step 2)	3-4
3.3	Phenomena Identification and Ranking (CSAU Step 3)	3-5
3.4	Frozen Code Version Selection (CSAU Step 4)	3-10
3.4.1	RODEX3A.....	3-12
3.4.2	S-RELAP5	3-14
3.4.3	New Product Support	3-16
3.5	Code Documentation (CSAU Step 5).....	3-17
3.6	Determination of Code Applicability (CSAU Step 6)	3-18
3.6.1	Field Equations	3-18
3.6.2	Closure Equations.....	3-19
3.6.3	Code Numerics	3-19
3.6.4	Structure and Nodalization	3-19
4.0	Assessment and Ranging of Parameters.....	4-1
4.1	Establishment of Assessment Matrix (CSAU Step 7)	4-1
4.1.1	PIRT Considerations	4-2
4.1.2	Nodalization Considerations.....	4-4
4.1.3	Scaling Considerations	4-4
4.1.4	Compensating Errors	4-4
4.1.5	Summary	4-4
4.2	Nuclear Power Plant Nodalization Definition (CSAU Step 8).....	4-5
4.2.1	Nodalization Methodology	4-6
4.2.2	Numerical Considerations	4-8
4.2.3	Loop Model	4-9
4.2.3.1	Hot Leg	4-9
4.2.3.2	Steam Generator	4-10
4.2.3.3	Pump Suction	4-11
4.2.3.4	Reactor Coolant Pump.....	4-11
4.2.3.5	Cold Leg and Break	4-11
4.2.3.6	ECCS.....	4-12
4.2.3.7	Pressurizer.....	4-13
4.2.4	Reactor Vessel Model	4-13
4.2.4.1	Downcomer.....	4-13
4.2.4.2	Lower Vessel	4-15
4.2.4.3	Core, Core Bypass, and Fuel.....	4-16
4.2.4.4	Upper Plenum/Upper Head	4-17

4.2.5	Containment Model	4-18
4.2.6	Plant Model Summary	4-18
4.3	Definition of Code and Experimental Accuracy (CSAU Step 9)	4-19
4.3.1	Separate Effects Tests (SET).....	4-20
4.3.1.1	THTF Heat Transfer	4-20
4.3.1.2	THTF Level Swell.....	4-21
4.3.1.3	GE Level Swell	4-22
4.3.1.4	FRIGG2	4-23
4.3.1.5	Bennett Tube	4-24
4.3.1.6	FLECHT and FLECHT SEASET	4-24
4.3.1.7	PDTF/SMART Tests	4-29
4.3.1.8	Marviken Tests	4-31
4.3.1.9	Westinghouse/EPRI 1/3 Scale Tests	4-32
4.3.1.10	FRA-ANP CCFL Tests	4-35
4.3.1.11	UPTF Tests.....	4-37
4.3.1.11.1	UPTF Tests 6 and 7	4-38
4.3.1.11.2	UPTF Test 8.....	4-40
4.3.1.11.3	UPTF Tests 10 and 29	4-41
4.3.1.11.4	UPTF Tests 10 and 12	4-43
4.3.1.11.5	UPTF Test 11	4-45
4.3.1.12	CCTF Tests	4-47
4.3.1.13	SCTF Tests.....	4-54
4.3.1.14	ACHILLES Tests.....	4-58
4.3.1.15	Multi-Dimensional Flow Testing	4-61
4.3.1.15.1	Summary	4-62
4.3.1.15.2	Test Descriptions.....	4-62
4.3.1.15.3	Input Description	4-63
4.3.1.15.4	Results	4-63
4.3.1.15.5	Conclusions.....	4-64
4.3.2	Integral Effects Tests (IET).....	4-64
4.3.2.1	LOFT Assessments	4-65
4.3.2.1.1	LOFT Facility	4-65
4.3.2.1.2	LOFT Test Descriptions.....	4-68
4.3.2.1.3	LOFT Assessment Summary.....	4-69
4.3.2.1.4	LOFT L2-3 Assessment.....	4-70
4.3.2.1.5	LOFT Test L2-5 Assessment.....	4-73
4.3.2.1.6	LOFT LP-02-6 Assessment	4-75
4.3.2.1.7	LOFT Test LP-LB-1 Assessment.....	4-77
4.3.2.2	Semiscale Tests	4-80
4.3.2.2.1	Semiscale Facilities.....	4-80
4.3.2.2.2	Semiscale Test Descriptions	4-82
4.3.2.2.3	Test S-06-3 Assessment	4-84
4.3.2.2.4	Test S-07-1 Assessment	4-84
4.3.3	Methodology Treatment of PIRT Phenomena	4-85
4.3.3.1	PIRT Phenomena Not Treated Statistically	4-85
4.3.3.1.1	Core 3-D Flow and Void Distributions	4-85
4.3.3.1.2	Liquid Entrainment in Core	4-86
4.3.3.1.3	Core Flow Reversal/Stagnation	4-87

	4.3.3.1.4	Upper Plenum Liquid Entrainment/de-entrainment	4-88
	4.3.3.1.5	Counter Current Flow Limit (CCFL)	4-88
	4.3.3.1.6	Hot Leg Entrainment/de-entrainment	4-89
	4.3.3.1.7	Two Phase Pump Degradation	4-90
	4.3.3.1.8	Pump Differential Pressure Loss	4-90
	4.3.3.1.9	Non-Condensable Transport	4-91
	4.3.3.1.10	Downcomer Entrainment	4-91
	4.3.3.1.11	Downcomer Liquid Level Oscillations	4-91
	4.3.3.1.12	Lower Plenum Sweepout	4-92
4.3.3.2		PIRT Phenomena Treated Statistically	4-92
	4.3.3.2.1	Stored Energy	4-93
	4.3.3.2.2	Oxidation	4-93
	4.3.3.2.3	Decay Heat	4-94
	4.3.3.2.4	Departure from Nucleate Boiling	4-96
	4.3.3.2.5	Core Post-CHF Heat Transfer	4-96
	4.3.3.2.6	T _{min}	4-97
	4.3.3.2.7	Break Flow	4-97
	4.3.3.2.8	Steam Binding	4-98
	4.3.3.2.9	Cold Leg Condensation	4-99
	4.3.3.2.10	Accumulator Discharge	4-99
	4.3.3.2.11	Reactor Vessel Hot Walls	4-100
	4.3.3.2.12	Containment Pressure	4-100
4.3.4		Evaluation of Code Biases	4-100
	4.3.4.1	Evaluation of Biases with CCTF	4-101
	4.3.4.1.1	Summary and Conclusions	4-101
	4.3.4.1.2	Test 54	4-101
	4.3.4.1.3	Test 62	4-102
	4.3.4.1.4	Test 67	4-103
	4.3.4.1.5	Test 68	4-103
	4.3.4.1.6	Conclusion Regarding Bias Evaluation in CCTF	4-104
	4.3.4.2	Evaluation of Biases with LOFT	4-104
	4.3.4.2.1	Summary and Conclusions	4-105
	4.3.4.2.2	LOFT Test LP-LB-1	4-105
	4.3.4.2.3	LOFT Test LP-02-6	4-106
	4.3.4.2.4	LOFT Test L2-5	4-107
	4.3.4.2.5	LOFT Test L2-3	4-108
	4.3.4.2.6	Conclusions	4-109
	4.3.4.3	Evaluation of Biases with Semiscale	4-109
	4.3.4.3.1	Summary and Conclusions	4-109
	4.3.4.3.2	Semiscale Test S-06-3	4-109
	4.3.4.3.3	Semiscale Test S-07-1	4-110
	4.3.4.3.4	Conclusions	4-110
	4.3.4.4	Conclusions from Bias Evaluation	4-111

4.4	Determination of Effect of Scale (CSAU Step 10)	4-111
4.4.1	Test Scaling	4-111
4.4.1.1	Blowdown	4-112
4.4.1.2	Refill	4-112
4.4.1.3	Reflood	4-113
4.4.2	Code Scaling	4-113
4.4.2.1	Post-CHF and Reflood Heat Transfer	4-114
4.4.2.2	Scaling from Tests	4-117
4.4.2.2.1	Film Boiling Heat Transfer	4-117
4.4.2.2.2	Core Entrainment	4-118
4.4.2.2.3	Critical Flow at Break	4-119
4.4.2.2.4	Carry-over to Steam Generator	4-119
4.4.2.2.5	Pump Scaling	4-120
4.4.2.2.6	Cold Leg Condensation	4-120
4.4.2.2.7	Bypass of Downcomer by ECC Water and Lower Plenum Sweep-Out	4-121
4.4.2.2.8	Loop Oscillations	4-122
5.0	Sensitivity and Uncertainty Analysis	5-1
5.1	Determination of Effect of Reactor Input Parameters and State (CSAU Step 11)	5-1
5.1.1	Determining Important Process Parameters	5-1
5.1.2	Role of Sensitivity Studies	5-2
5.1.3	Quantifying Statistical Quantities	5-3
5.1.3.1	General	5-3
5.1.3.2	Treatment of Time in Cycle	5-4
5.1.3.3	Treatment of Axial and Radial Power Shapes	5-5
5.1.4	Supporting Ranges Without Data	5-7
5.1.5	Reporting of Treatment of Process Parameters	5-7
5.2	Performance of NPP Sensitivity Calculations (CSAU Step 12)	5-7
5.2.1	Statistical Approach	5-7
5.2.2	Application of Methodology	5-11
5.2.3	New RLBLOCA Analyses	5-12
5.2.4	Ranging Uncertainty	5-12
5.2.5	Parameter Initialization	5-14
5.2.6	Calculation Order	5-14
5.2.7	Subsequent RLBLOCA Analyses	5-14
5.3	Determination of combined Bias and Uncertainty (CSAU Step 13)	5-14
5.4	Determination of Total Uncertainty (CSAU Step 14)	5-17
6.0	References	6-1
Appendix A	Overview of Base Case and Sensitivity Studies	A-1
A.1	Base Case Analyses Description	A-1
A.2	LBLOCA Calculation and Event Description	A-2
A.3	Sensitivity Studies Overview	A-4

Appendix B	Conservatisms	B-1
B.1	Analysis for Fresh Fuel Assemblies Only	B-1
B.2	Analysis without Clad Swelling and Rupture	B-2
B.3	Radial Power Distributions	B-3
B.4	Pump Two-Phase Degradation	B-5
Appendix C	Time Step Sensitivity	C-1
Appendix D	Sample Westinghouse 3-Loop PWR Licensing Analysis	D-1
D.1	Introduction	D-1
D.2	Summary	D-1
D.3	Analysis	D-2
D.3.1	Description of the LBLOCA Event	D-3
D.3.2	Description of Analytical Models	D-4
D.3.3	Plant Description and Summary of Analysis Parameters	D-6
D.3.4	Realistic Large Break LOCA Results	D-7
D.4	Conclusions	D-32
D.5	References	D-32
Appendix E	Incorporation of M5 Cladding Properties	E-1
E.1	Introduction	E-1
E.2	Summary	E-1
E.3	Implementation of M5 Cladding Properties in RODEX3A	E-2
E.3.1	Summary of Cladding Related Models in the Fuel Performance Evaluation Model	E-2
E.3.1.1	M5 Cladding Creep Correlation	E-2
E.3.1.2	M5 Cladding Free Growth Correlation	E-5
E.3.1.3	M5 Cladding Thermal Conductivity	E-6
E.3.1.4	M5 Cladding Zirconium Oxide Thermal Conductivity	E-7
E.3.1.5	M5 Cladding Specific Heat	E-7
E.3.1.6	M5 Cladding Density	E-7
E.3.1.7	M5 Cladding Thermal Expansion	E-7
E.3.1.8	M5 Cladding Elastic Modulus	E-9
E.3.1.9	M5 Cladding Poisson's Ratio	E-9
E.3.1.10	M5 Cladding Emissivity	E-9
E.3.1.11	M5 Cladding Corrosion	E-10
E.3.1.12	M5 Cladding Hydrogen Pick-up	E-11
E.3.1.13	High Temperature M5/Steam Reaction Kinetics	E-11
E.3.1.14	M5 Cladding Swelling and Rupture / Blockage	E-12
E.3.2	Creep Benchmark Calculations	E-17
E.3.2.1	Introduction	E-17
E.3.2.2	Creep Benchmark Results	E-18
E.4	Implementation of M5 Properties in S-RELAP5	E-24
E.4.1	Summary of Cladding Related Models in the Thermal- Hydraulic Performance Evaluation Model	E-24
E.4.1.1	M5 Cladding Creep Correlation	E-24
E.4.1.2	M5 Cladding Free Growth Correlation	E-24
E.4.1.3	M5 Cladding Thermal Conductivity	E-24
E.4.1.4	M5 Cladding Oxide Thermal Conductivity	E-24

E.4.1.5	M5 Cladding Specific Heat.....	E-24
E.4.1.6	M5 Cladding Density.....	E-25
E.4.1.7	M5 Cladding Thermal Expansion.....	E-25
E.4.1.8	M5 Cladding Elastic Modulus.....	E-25
E.4.1.9	M5 Cladding Poisson's Ratio.....	E-27
E.4.1.10	M5 Cladding Emissivity.....	E-27
E.4.1.11	M5 Cladding Corrosion.....	E-27
E.4.1.12	M5 Cladding Hydrogen Pick-up.....	E-27
E.4.1.13	High Temperature M5/Steam Reaction Kinetics.....	E-28
E.4.1.14	M5 Cladding Swelling and Rupture / Blockage.....	E-29
E.4.2	3-Loop Sample Problem with M5 Cladding.....	E-31
E.5	References.....	E-32

Tables

3.1	Approximate Values of Key Large Break LOCA Plant Analysis Parameters.....	3-20
3.2	Appendix K Large Break LOCA Approximate Sequence of Events Timing	3-21
3.3	Preliminary Process Identification and Ranking Table (PIRT) for PWR Large Break Loss-of-Coolant Accident	3-22
3.4	Final Process Identification and Ranking Table (PIRT) for PWR Large Break Loss-of-Coolant Accident.....	3-24
3.5	Frozen Code Versions Used in the Methodology Development.....	3-26
3.6	Field Equations/Models in S-RELAP5.....	3-27
3.7	Phenomena/Processes in S-RELAP5.....	3-28
3.8	Component Modeling Requirements for PWR	3-31
4.1	Parameters Perturbed for PIRT Sensitivity Studies	4-124
4.2	Assessment Matrix.....	4-127
4.3	Assessment Matrix Tests and Phenomena Addressed.....	4-128
4.4	Large Break LOCA Nodalization	4-130
4.5	PDTF SMART Tests Chosen for S-RELAP5 Verification and Validation	4-131
4.6	Comparison of Effluent Temperature for the Plant-Consistent Model, Westinghouse/EPRI	4-132
4.7	Test Phase Parameters for Test 10 Run 081.....	4-133
4.8	Test Phase Parameters for Test 29 Run 212/211.....	4-133
4.9	Calculated Water Downflow Rates for the 0.3 MPa Test Series	4-134
4.10	Calculated Water Downflow Rates for the 1.5 MPa Test Series	4-135

4.11	CCTF Test Conditions.....	4-136
4.12	Summary Comparison of Measured and Calculated PCT, CCTF Tests 54, 62, 67, and 68	4-136
4.13	Test Data for SCTF-II Tests Modeled	4-137
4.14	Phase I Assessment Results, SCTF Tests	4-139
4.15	Phase II Assessment Results, SCTF Tests	4-139
4.16	PWR-LOFT Scaling Ratios	4-140
4.17	LOFT Nuclear Large Break Test Parameters.....	4-141
4.18	Important PIRT Phenomena and Methodology Treatment.....	4-142
4.19	Summary of Evaluated Uncertainties of key PIRT Parameters.....	4-144
4.20	Film Boiling HTC Distribution Fit Parameters.....	4-145
4.21	Test Ranges for Film Boiling Heat Transfer Test Comparison.....	4-146
5.1	NPP Parameters for Consideration in the Performance of a Realistic LBLOCA Analysis.....	5-19
5.2	Relationship of PIRT to Operational Parameters	5-20
5.3	Ranked Importance of Process Parameters Relative to Plant Type	5-20
5.4	Statistical Distributions Used for a Sample 3-Loop PWR.....	5-20
5.5	[]	5-21
5.6	Relationship of Uncertainty Parameters to Computer Code Input	5-22
5.7	Plant Operating Range and Fuel Design Supported by the LOCA Analysis	5-23
5.8	Summary of Major Parameters Describing Limiting PCT Case (Case 22).....	5-25
5.9	Summary of Results for the Limiting PCT Case (22)	5-25

Figures

2.1	Code Scaling, Applicability, and Uncertainty Methodology Flow Chart.....	2-6
4.1	PCT Signature for 3- and 4-Loop NPP Base Case	4-147
4.2	PIRT Sensitivity Histogram	4-148
4.3	Loop Nodalization for NPP	4-149
4.4	Reactor Vessel Nodalization for NPP	4-150
4.5	CE 2x4 and Westinghouse 3- and 4-Loop Plant Vessel Downcomer Configurations	4-151
4.6	NPP Core Nodalization – Axial Plane	4-152
4.7	NPP Core Nodalization – Cross-Sectional Plane.....	4-153
4.8	NPP Upper Plenum Nodalization – Axial Plane	4-154
4.9	NPP Upper Plenum Nodalization – Cross-Sectional Plane.....	4-155
4.10	NPP Emergency Core Cooling System Nodalization	4-156
4.11	Double-Ended Guillotine Break Nodalization	4-157
4.12	Double-Ended Split Break Nodalization	4-157
4.13	Comparison of Calculated HTC to Measured HTC, ORNL THTF	4-158
4.14	Frequency Distribution for Scale Factor for HTC, ORNL THTF	4-159
4.15	Bounding Distribution for HTC Scaling, ORNL THTF.....	4-160
4.16	Comparisons of Void Profiles, ORNL THTF Test 3.09.10j.....	4-161
4.17	Comparison of Void Profiles, ORNL THTF Test 3.09.10 m.....	4-162
4.18	Comparison of Void Profiles, ORNL THTF Test 3.09.10dd.....	4-163
4.19	Void Profiles at 40 Seconds for the 1 ft GE Test 1004-3.....	4-164
4.20	Void Profiles at 100 Seconds for the 1 ft GE Test 1004-3.....	4-165
4.21	Comparison of Calculated and Measured Void Fraction, Frigg-2 Test 313007	4-166
4.22	Comparison of Calculated and Measured Void Fraction, Frigg-2 Test 313014	4-167
4.23	Comparison of Calculated and Measured Void Fraction, Frigg-2 Test 313016	4-168
4.24	Comparison of Calculated and Measured Void Fraction, Frigg-2 Test 313020	4-169
4.25	Comparison of Calculated and Measured Void Fraction, Frigg-2 Test 313060	4-170
4.26	Comparison of Calculated and Measured Void Fraction, Frigg-2 Test 313010	4-171

4.27	Comparison of Calculated and Measured Void Fraction, Frigg-2 Test 313013	4-172
4.28	Comparison of Calculated and Measured Void Fraction, Frigg-2 Test 313017	4-173
4.29	Comparison of Calculated and Measured Void Fraction, Frigg-2 Test 313019	4-174
4.30	Comparison of Calculated and Measured Void Fraction, Frigg-2 Test 313030	4-175
4.31	Comparison of Calculated and Measured Void Fraction at the Same Location for all 27 FRIGG Tests.....	4-176
4.32	Wall Temperature Profiles, Bennett Heated Tube Test 5358.....	4-177
4.33	Wall Temperature Profiles, Bennett Heated Tube Test 5379.....	4-178
4.34	Maximum Clad Temperature at All Measured Elevations, FLECHT SEASET Test 31805	4-179
4.35	Maximum Clad Temperature at All Measured Elevations, FLECHT SEASET Test 31504	4-180
4.36	Maximum Clad Temperature at All Measured Elevations, FLECHT SEASET Test 31203	4-181
4.37	Maximum Clad Temperature at All Measured Elevations, FLECHT SEASET Test 31302	4-182
4.38	Maximum Clad Temperature at All Measured Elevations, FLECHT SEASET Test 31701	4-183
4.39	Maximum Clad Temperature at All Measured Elevations, FLECHT SEASET Test 34209	4-184
4.40	Maximum Clad Temperature at All Measured Elevations, FLECHT SEASET Test 32013	4-185
4.41	Maximum Clad Temperature at All Measured Elevations, FLECHT Skewed Test 13609	4-186
4.42	Maximum Clad Temperature at All Measured Elevations, FLECHT Skewed Test 13914	4-187
4.43	Steam Temperatures Calculated at 75.6 in and Measured at 72 in, FLECHT SEASET Test 31805	4-188
4.44	Steam Temperatures Calculated at 75.6 in and Measured at 72 in, FLECHT SEASET Test 31504	4-189
4.45	Steam Temperatures Calculated at 75.6 in and Measured at 72 in, FLECHT SEASET Test 31203	4-190
4.46	Steam Temperatures Calculated at 75.6 in and Measured at 72 in, FLECHT SEASET Test 31302	4-191
4.47	Steam Temperatures Calculated at 75.6 in and Measured at 72 in, FLECHT SEASET Test 31701	4-192

4.48	Steam Temperatures Calculated at 75.6 in and Measured at 72 in, FLECHT SEASET Test 34209	4-193
4.49	Steam Temperatures Calculated at 75.6 in and Measured at 72 in, FLECHT SEASET Test 32013	4-194
4.50	Steam Temperatures Calculated at 82.8 in and Measured at 84 in, FLECHT Skewed Test 13609	4-195
4.51	Steam Temperatures Calculated at 82.8 in and Measured at 84 in, FLECHT Skewed Test 13914	4-196
4.52	Comparison of Calculated and Measured Heat Transfer Coefficient, FLECHT SEASET Test 31805	4-197
4.53	Comparison of Calculated and Measured Heat Transfer Coefficient, FLECHT SEASET Test 31504	4-198
4.54	Comparison of Calculated and Measured Heat Transfer Coefficient, FLECHT SEASET Test 31203	4-199
4.55	Comparison of Calculated and Measured Heat Transfer Coefficient, FLECHT SEASET Test 31302	4-200
4.56	Comparison of Calculated and Measured Heat Transfer Coefficient, FLECHT SEASET Test 31701	4-201
4.57	Comparison of Calculated and Measured Heat Transfer Coefficient, FLECHT SEASET Test 34209	4-202
4.58	Comparison of Calculated and Measured Heat Transfer Coefficient, FLECHT SEASET Test 32013	4-203
4.59	Comparison of Calculated and Measured Heat Transfer Coefficient, FLECHT Skewed Test 13609	4-204
4.60	Comparison of Calculated and Measured Heat Transfer Coefficient, FLECHT Skewed Test 13914	4-205
4.61	Accumulated Water Mass in the Test Section, FLECHT SEASET Test 31805	4-206
4.62	Accumulated Water Mass in the Test Section, FLECHT SEASET Test 31504	4-207
4.63	Accumulated Water Mass in the Test Section, FLECHT SEASET Test 31203	4-208
4.64	Accumulated Water Mass in the Test Section, FLECHT SEASET Test 31302	4-209
4.65	Accumulated Water Mass in the Test Section, FLECHT SEASET Test 31701	4-210
4.66	Accumulated Water Mass in the Test Section, FLECHT SEASET Test 34209	4-211
4.67	Accumulated Water Mass in the Test Section, FLECHT SEASET Test 32013	4-212

4.68	Accumulated Water Mass in the Test Section, FLECHT Skewed Test 13609	4-213
4.69	Accumulated Water Mass in the Test Section, FLECHT Skewed Test 13914	4-214
4.70	Total Liquid Carryover From Test Assembly, FLECHT SEASET Test 31805	4-215
4.71	Total Liquid Carryover From Test Assembly, FLECHT SEASET Test 31203	4-216
4.72	Total Liquid Carryover From Test Assembly, FLECHT SEASET Test 34209	4-217
4.73	Total Liquid Carryover From Test Assembly, FLECHT SEASET Test 32013	4-218
4.74	Total Liquid Carryover From Test Assembly, FLECHT Skewed Test 13609	4-219
4.75	Total Liquid Carryover From Test Assembly, FLECHT Skewed Test 13914	4-220
4.76	Average Rod Quench Time, FLECHT SEASET Test 31805.....	4-221
4.77	Average Rod Quench Time, FLECHT SEASET Test 31203.....	4-222
4.78	Average Rod Quench Time, FLECHT SEASET Test 31302.....	4-223
4.79	Average Rod Quench Time, FLECHT SEASET Test 31701.....	4-224
4.80	Average Rod Quench Time, FLECHT SEASET Test 34209.....	4-225
4.81	Average Rod Quench Time, FLECHT SEASET Test 32013.....	4-226
4.82	Calculated Rod Surface Temperatures at 79 in for the 20-Volume Test Section Cases With Various Time-Step Sizes, FLECHT SEASET Test 31504	4-227
4.83	Calculated Rod Surface Temperatures at 79 in for the 40-Volume Test Section Cases With Various Time-Step Sizes, FLECHT SEASET Test 31504	4-228
4.84	Maximum Cladding Temperatures vs. Axial Elevation, FLECHT SEASET Test 31504	4-229
4.85	Comparison of Predicted PCT and Measured Data, PDTF SMART	4-230
4.86	MCT vs. Elevation Comparison to Data for 4-in/s-Flooding-Rate Test, PDTF SMART	4-231
4.87	MCT vs. Elevation Comparison to Data for 2-in/s-Flooding-Rate Test, PDTF SMART	4-232
4.88	MCT vs. Elevation Comparison to Data for 1-in/s-Flooding-Rate Test, PDTF SMART	4-233
4.89	MCT vs. Elevation Comparison to Data for Variable-Flooding-Rate Test, PDTF SMART	4-234

4.90	Comparison of Break Mass Flow Rates, Marviken Test 2	4-235
4.91	Comparison of Break Mass Flow Rates, Marviken Test 6	4-236
4.92	Comparison of Break Mass Flow Rates, Marviken Test 8	4-237
4.93	Comparison of Break Mass Flow Rates, Marviken Test 16	4-238
4.94	Comparison of Break Mass Flow Rates, Marviken Test 17	4-239
4.95	Comparison of Break Mass Flow Rates, Marviken Test 20	4-240
4.96	Comparison of Break Mass Flow Rates, Marviken Test 22	4-241
4.97	Comparison of Break Mass Flow Rates, Marviken Test 24	4-242
4.98	Comparison of Break Mass Flow Rates, Marviken Test 25	4-243
4.99	Comparison of Calculated and Measured Mass Fluxes (All Nine Marviken Tests)	4-244
4.100	Break Flow Uncertainty, Marviken Tests.....	4-245
4.101	Comparison of Calculated and Measured Effluent Temperature for the Plant-Specific Model, Westinghouse/EPRI	4-246
4.102	Cumulative Distribution Plots for CONMAS, Westinghouse/EPRI	4-247
4.103	Comparison Between Mini-Loop CCFL Data of a Westinghouse 17 x 17 UTP and Bankoff.....	4-248
4.104	Comparison Between Mini-Loop CCFL Data of a Westinghouse 15 x 15 UTP and Bankoff.....	4-249
4.105	Comparison Between Mini-Loop CCFL Data of a Combustion Engineering 14 x 14 UTP and Bankoff.....	4-250
4.106	Lower Plenum Liquid Level Comparison UPTF Test 6 – Run 131.....	4-251
4.107	Lower Plenum Liquid Level Comparison UPTF Test 6 – Run 132.....	4-252
4.108	Lower Plenum Liquid Level Comparison UPTF Test 6 – Run 133.....	4-253
4.109	Lower Plenum Liquid Level Comparison UPTF Test 6 – Run 135.....	4-254
4.110	Lower Plenum Liquid Level Comparison UPTF Test 6 – Run 136.....	4-255
4.111	Lower Plenum Liquid Level Comparison UPTF Test 7 – Run 203.....	4-256
4.112	UPTF Data/S-RELAP5 Cold Leg Temperature Comparison, UPTF Test 8 Run 111.....	4-257
4.113	UPTF Data/S-RELAP5 Flow Regime Comparison, UPTF Test 8 Run 111.....	4-258
4.114	UPTF Data/S-RELAP5 Cold Leg Temperature Comparison, UPTF Test 8 Run 112.....	4-259
4.115	UPTF Data/S-RELAP5 Flow Regime Comparison, UPTF Test 8 Run 112.....	4-260
4.116	Countercurrent Flow of Steam and Water UPTF Test 10 Run 081.....	4-261
4.117	Countercurrent Flow of Steam and Water UPTF Test 29 Run 212/211.....	4-262
4.118	Carryover to Steam Generators Test 10 Run 081 Beyond 150 sec.....	4-263

4.119	Cumulative Water Carryover to Steam Generators Test 29 Run 212/211	4-264
4.120	Counter Current Flow of Steam and Water, UPTF Test 10, Run 080	4-265
4.121	Upper Plenum Pressure Comparison Test 10, Run 080	4-266
4.122	Calculated Downflow Comparison UPTF Test 10, Run 080 (m=1.0, c=1.8)	4-267
4.123	Counter Current Flow of Steam and Water, UPTF Test 12, Run 014	4-268
4.124	Upper Plenum Pressure Comparison UPTF Test 12, Run 014	4-269
4.125	Calculated Downflow Comparison UPTF Test 12, Run 014 (m=1.0, c=1.8)	4-270
4.126	Steam and Water Injection Rates for UPTF Test 11 1.5 MPa Series	4-271
4.127	Steam and Water Injection Rates for UPTF Test 11 0.3 MPa Series	4-272
4.128	Comparison of UPTF Test 11 Data with S-RELAP5 Calculations	4-273
4.129	Comparison of Peak Surface Temperatures vs. Elevation for High Power Bundles, CCTF Test Run 54	4-274
4.130	Comparison of Peak Surface Temperatures vs. Elevation for High Power Bundles, CCTF Test Run 62	4-275
4.131	Comparison of Peak Surface Temperatures vs. Elevation for High Power Bundles for Test Run 67	4-276
4.132	Comparison of Peak Surface Temperatures vs. Elevation for High Power Bundles, CCTF Test Run 68	4-277
4.133	Temperature Comparison at 1.905 m, SCTF S2-17	4-278
4.134	Temperature Comparison at 1.905 m, SCTF S2-18	4-279
4.135	Thermocouple Variation Range at the PCT Elevation, ACHILLES ISP 25	4-280
4.136	Nitrogen Insurge Impact at 1.08 m, ACHILLES ISP 25	4-281
4.137	Nitrogen Insurge Impact at 1.81 m, ACHILLES ISP 25	4-282
4.138	Nitrogen Insurge Impact at 2.13 m, ACHILLES ISP 25	4-283
4.139	Nitrogen Insurge Impact at 2.33 m, ACHILLES ISP 25	4-284
4.140	Nitrogen Insurge Impact at 2.65 m, ACHILLES ISP 25	4-285
4.141	Nitrogen Insurge Impact at 3.18 m, ACHILLES ISP 25	4-286
4.142	Axial Velocities at 32.5 Inches, Asymmetric Flow - Test 1	4-287
4.143	Axial Flow Fractions for Asymmetric Flow - Test 1	4-288
4.144	Axial Velocities at 32.5 Inches, for Asymmetric Flow - Test 2	4-289
4.145	Axial Flow Fractions for Asymmetric Flow – Test 2	4-290
4.146	Axial Velocities at 32.5 Inches, for Asymmetric Flow - Test 3	4-291
4.147	Comparison of S-RELAP5 with Design Codes for Asymmetric Flow - Test 1	4-292
4.148	Comparison of PCTs Versus Core Elevations LOFT Test L2-3 with S-RELAP5	4-293

4.149	Comparison of PCTs Versus Core Elevations LOFT Test L2-5 with S-RELAP5	4-294
4.150	LOFT Test LP-02-6 Comparison of PCTs Versus Core Elevations	4-295
4.151	LOFT Test LP-LB-1 Comparison of PCTs Versus Core Elevations	4-296
4.152	Assessment of Semiscale LBLOCA Test S-06-3, PCTs	4-297
4.153	Assessment of Semiscale LBLOCA Test S-07-1, PCTs versus Elevation	4-298
4.154	Upper Plenum Level, UPTF Test 10, Run 081	4-299
4.155	Upper Plenum Level, UPTF Test 29 Run 212/211	4-300
4.156	Liquid Level in Upper Plenum CCTF Test 54	4-301
4.157	Liquid Level in Upper Plenum CCTF Test 62	4-302
4.158	Liquid Level in Upper Plenum CCTF Test 67	4-303
4.159	Liquid Level in Upper Plenum CCTF Test 68	4-304
4.160	Upper Plenum Levels for FLECHT-SEASET Test 31805	4-305
4.161	Upper Plenum Levels for FLECHT-SEASET Test 31203	4-306
4.162	Upper Plenum Levels for FLECHT-SEASET Test 31302	4-307
4.163	Upper Plenum Levels for FLECHT-SEASET Test 31701	4-308
4.164	Comparison of Liquid Carryover for CCTF Test 54	4-309
4.165	Comparison of Liquid Carryover for CCTF Test 62	4-310
4.166	Comparison of Liquid Carryover for CCTF Test 67	4-311
4.167	Comparison of Liquid Carryover for CCTF Test 68	4-312
4.168	Level in Broken Loop Catch Tank - UPTF Test 081	4-313
4.169	Level in Intact Loop Catch Tank - UPTF Test 081	4-314
4.170	Level in Broken Loop Catch Tank - UPTF Test 212	4-315
4.171	Level in Intact Loop Catch Tank - UPTF Test 212	4-316
4.172	Level in Separator Tank for FLECHT-SEASET Tests 31805	4-317
4.173	Level in Separator Drain Tank for FLECHT-SEASET Tests 31805	4-318
4.174	Level in Separator Tank for FLECHT-SEASET Tests 31203	4-319
4.175	Level in Separator Drain Tank for FLECHT-SEASET Tests 31203	4-320
4.176	Level in Separator Tank for FLECHT-SEASET Tests 31302	4-321
4.177	Level in Separator Drain Tank for FLECHT-SEASET Tests 31302	4-322
4.178	Level in Separator Tank for FLECHT-SEASET Tests 31701	4-323
4.179	Level in Separator Drain Tank for FLECHT-SEASET Tests 31701	4-324
4.180	CCTF TEST 54 Temperatures at Measured PCT Node	4-325
4.181	CCTF TEST 54 Temperatures Near Calculated PCT Node	4-326

4.182	CCTF TEST 54 PCT Profile	4-327
4.183	CCTF TEST 62 Temperatures at Measured PCT Node	4-328
4.184	CCTF TEST 62 Temperatures Near Calculated PCT Node.....	4-329
4.185	CCTF TEST 62 PCT Profile	4-330
4.186	CCTF TEST 67 Temperatures at Measured PCT Node	4-331
4.187	CCTF TEST 67 Temperatures Near Calculated PCT Node.....	4-332
4.188	CCTF TEST 67 PCT Profile	4-333
4.189	CCTF TEST 68 Temperatures at Measured PCT Node	4-334
4.190	CCTF TEST 68 Temperatures Near Calculated PCT Node.....	4-335
4.191	CCTF TEST 68 PCT Profile	4-336
4.192	CCTF TEST 68 Intact Loop Cold Leg Void Fraction	4-337
4.193	LOFT LP-LB-1 Temperatures at Measured PCT Node.....	4-338
4.194	LOFT LP-LB-1 PCT Profile	4-339
4.195	LOFT LP-02-6 Temperatures at Measured PCT Node	4-340
4.196	LOFT LP-02-6 PCT Profile	4-341
4.197	LOFT L2-5 Temperatures at Measured PCT Node.....	4-342
4.198	LOFT L2-5 PCT Profile	4-343
4.199	LOFT L2-3 Temperatures at Measured PCT Node.....	4-344
4.200	LOFT L2-3 Temperatures at Calculated PCT Node.....	4-345
4.201	LOFT L2-3 PCT Profile	4-346
4.202	Semiscale S-06-3 Temperatures at Measured PCT Node.....	4-347
4.203	Semiscale S-06-3 Temperatures at Calculated PCT Node.....	4-348
4.204	Semiscale S-06-3 PCT Profile	4-349
4.205	Semiscale S-07-1 Temperatures at Measured PCT Node.....	4-350
4.206	Semiscale S-07-1 Temperatures at Calculated PCT Node.....	4-351
4.207	Semiscale S-07-1 PCT Profile	4-352
4.208	Sleicher-Rouse HTC for Steam Compared to Data	4-353
5.1	Calculation Framework	5-26
5.2	[.....].....	5-27
5.3	[.....]	5-28
5.4	[.....].....	5-29
5.5	[.....]	5-30
5.6	[.....].....	5-31
5.7	[.....]	5-32

5.8	[]	5-33
5.9	[
]	5-34
5.10	[
]	5-35
5.11	[
]	5-36
5.12	[
]	5-37
5.13	[
]	5-38
5.14	[
]	5-39
5.15	[
]	5-40
5.16	[
]	5-41
5.17	[
]	5-42
5.18	[
]	5-43
5.19	[
]	5-44
5.20	[
]	5-45
5.21	[
]	5-46
5.22	[
]	5-47
5.23	[
]	5-48
5.24	[
]	5-49
5.25	[
]	5-50
5.26	[
]	5-51

Nomenclature

Acronym	Definition
ACC	accumulator core coolant
ANP	advanced nuclear products
ANS	American Nuclear Society
ASME	American Society of Mechanical Engineers
BHL	beginning of heated length
BLCL	broken loop cold leg
BLHL	broken loop hot leg
BOCREC	bottom of core recovery
BST	blowdown suppression tank
BWR	boiling water reactor
CCFL	countercurrent flow limiting
CCTF	Cylindrical Core Test Facility
CFR	Code of Federal Regulations
CHF	critical heat flux
CONMAS	interfacial condensation heat transfer coefficient multiplier
CSAU	Code Scaling, Applicability, and Uncertainty
DEG	double-ended guillotine
DIW	deionized water tank
DMS	document management system
DNB	departure from nucleate boiling
ECC	emergency core cooling
ECCS	emergency core cooling system
EDR	Experimental Data Report
EHL	end of heated length
EPRI	Electric Power Research Institute
FCTF	Fuel Cooling Test Facility
FIINVS	post-CHF inverted slug regime
FIMIST	post-CHF mist flow regime
FLECHT	Full Length Emergency Cooling Heat Transfer
FLOREG	flow regime
HEM	homogeneous equilibrium model
HPI	high pressure injection
HPIS	high pressure injection system
HTP	high thermal performance
ICAP	International Code Assessment Program
IET	Integral Effects Tests

ILCL	intact loop cold leg
ILHL	intact loop hot leg
INEEL	Idaho National Environmental Engineering Laboratory (formerly INEL)
INEL	Idaho National Engineering Laboratory
JAERI	Japan Atomic Energy Research Institute
KWU	Kraftwerk Union (SPC), now Framatome ANP GmbH
LANL	Los Alamos National Laboratory
LBLOCA	large break loss-of-coolant accident
LHGR	linear heat generation rate
LOCA	loss-of-coolant accident
LOCE	loss-of-coolant experiment
LOFT	Loss of Fluid Test
LPCI	low pressure coolant injection
LPIS	low pressure injection system
MCT	maximum clad temperature
MLHGR	maximum linear heat generation rate
MSIV	main steam isolation valve
NAI	Numerical Applications, Inc.
NPP	nuclear power plant
NRC	United States Nuclear Regulatory Commission
OECD	Organization of Economic Cooperation and Development
ORNL	Oak Ridge National Laboratory
PCP	primary coolant pump
PCS	primary coolant system
PCT	peak cladding temperature
PDTF	Product Development Test Facility
PFM	pipe flow meter
PIRT	Process Identification and Ranking Table
PLC	programmable logic controllers
PWR	pressurized water reactor
QLR	Quick Look Report
QOBV	quick-opening blowdown valve
RABS	reflood assisted bypass system
RABV	reflood assisted bypass valve
RLBLOCA	realistic large break loss-of-coolant accident
SBLOCA	small break loss-of-coolant accident
SCTF	Slab Core Test Facility
SDR	Software Development Record
SEASET	System Effects And Separate Effects Tests

SET	Separate Effects Tests
SMART	SMall Array Reflood Test
SPC	Siemens Power Corporation
S/W	steam/water
THTF	Thermal-Hydraulic Test Facility
TMDPJUN	time-dependent junction
TMDPVOL	time-dependent volume
UCSP	upper core support plate
UPTF	Upper Plenum Test Facility
USNRC	United States Nuclear Regulatory Commission
UTP	upper tie plate
W/EPRI	Westinghouse/Electric Power Research Institute

1.0 Introduction

This report describes the Framatome ANP (FRA-ANP) methodology developed for the realistic evaluation of a large break loss-of-coolant accident (LBLOCA) for pressurized water reactors (PWRs). The methodology complies with the revised LOCA emergency core cooling system (ECCS) rule as issued by the U.S. Nuclear Regulatory Commission (NRC) in 1988 (Reference 1). This rule allows the use of realistic LOCA evaluation models in place of the prescribed conservative evaluation models as specified by 10 CFR 50 Appendix K, provided that it can be established with a high probability that the criteria of 10 CFR 50.46 are not violated.

The basis for the revised rule is a large body of research performed after the 1975 LOCA ECCS rule was implemented, which shows that the prescribed Appendix K analysis methods are unnecessarily conservative. A compendium of ECCS research (Reference 2) was issued that references the relevant thermal-hydraulic research.

The revised rule requires that an acceptable realistic LOCA ECCS evaluation model have sufficient supporting justification to show that the analytical technique realistically describes the behavior of the reactor system during a LOCA. It is expected that the analytical technique will, to the extent practicable, utilize realistic methods and be based upon applicable experimental data.

The amended rule also requires that the uncertainty of the calculation be estimated and accounted for when comparing the results of the calculation to the temperature limits and other criteria of 10 CFR 50.46. The realistic evaluation model will retain a degree of conservatism consistent with the quantified uncertainty of the calculation.

The final rule does not prescribe the analytical methods or uncertainty techniques to be used. However, a Regulatory Guide (Reference 3) was issued to provide guidance for realistic LOCA analyses. The NRC also independently developed and demonstrated the code scaling, applicability and uncertainty (CSAU) methodology (Reference 4) for quantifying uncertainties in realistic codes. The 95th percentile of the probability distribution is accepted (Reference 3) as providing the level of conservatism required by the rule.

The purpose of this report is to provide a description of the FRA-ANP realistic PWR LBLOCA methodology and demonstrate its application to representative nuclear power plants. The

methodology documentation is provided in a format consistent with that outlined in the "CSAU Evaluation Methodology," which specifies that a roadmap be provided for the methodology followed by a detailed discussion. Each of the steps outlined in CSAU is addressed in both the roadmap section (Section 2) and the detailed description section (Section 3, 4, and 5).

As outlined in CSAU the development of this methodology relies on the code documentation. The models and correlations document provides the information to demonstrate the applicability of the codes to the chosen event scenario and Nuclear Power Plant (NPP) types through the use of the phenomena identification and ranking table (PIRT) process. The PIRT identifies the models and correlations in the code for which biases and uncertainties would have to be generated or conservatisms demonstrated.

Finally, the results of the code assessments reported in the verification and validation report (EMF-2102, Reference 5) provides the information required to define how each of the important PIRT phenomena are treated in the uncertainty analysis. This treatment ranges from simply acknowledging that the code is conservative and accepting that conservatism to the definition of a bias and uncertainty, including their distribution, which are required to treat the PIRT phenomena statistically.

2.0 Methodology Roadmap

This section provides an overview of the methodology and points to the detailed discussion of the individual CSAU steps that follow. The CSAU approach to realistic LOCA analysis is diagrammed in Figure 2.1. The CSAU procedure has three major elements:

- Requirements and Code Capabilities (Section 3.0)
- Assessment and Ranging of Parameters (Section 4.0)
- Sensitivity and Uncertainty Analysis (Section 5.0)

FRA-ANP's realistic LBLOCA evaluation methodology is defined and documented consistent with the CSAU procedure as shown in the following three sections. FRA-ANP's CSAU-compliant procedure for PWRs is applicable to Westinghouse (W) 3-loop and 4-loop designs and to Combustion Engineering (CE) 2x4 designs.

2.1 Requirements and Code Capabilities

The requirements and code capabilities discussion identifies and compares scenario-modeling requirements with code capabilities to determine the code's applicability to the particular scenario and to identify potential limitations. This is accomplished through the performance of the following six CSAU steps:

- Scenario Specification (Section 3.1)
- Nuclear Power Plant Selection (Section 3.2)
- Phenomena Identification and Ranking (Section 3.3)
- Frozen Code Version Selection (Section 3.4)
- Provision of Complete Code Documentation (Section 3.5)
- Determination of Code Applicability (Section 3.6)

The scenario being addressed in this report is the LBLOCA. The licensing criteria for this event are:

- The calculated peak cladding temperature (PCT) shall not exceed 2200°F.
- The maximum calculated cladding oxidation shall nowhere exceed 0.17 times the total cladding thickness before oxidation.
- The maximum calculated hydrogen generation from the chemical reaction of the cladding with water or steam shall not exceed 0.01 times the hypothetical amount that would be generated if all of the metal in the cladding cylinders surrounding the fuel, excluding the cladding surrounding the plenum volume, were to react.

- The calculated changes in core geometry shall be such that the core remains amenable to cooling.
- The calculated core temperature shall be maintained at an acceptably low value and decay heat shall be removed for the extended period of time required by the long-lived radioactivity remaining in the core.

These licensing criteria, with the primary focus on the PCT, will be used as the figure-of-merit upon which decisions will be made with respect to the acceptability of the methodology. The PCT is chosen as the primary criteria because all the other criteria are, to some extent, dependent upon or related to it.

The selected NPP types to which the methodology is to be applicable includes those PWRs with U-tube type steam generators and ECCS injection into the cold legs. Provided with the methodology is a sample problem for a (W) 4-loop PWR and a licensing analysis for a (W) 3-loop PWR. The methodology is also applicable to (CE) 2x4 plants (see end of Section 2.0).

A PIRT has been prepared for the LBLOCA and the NPP types. This initial PIRT was developed by FRA-ANP from a combination of published PIRTs (Reference 2), reviews by external experts, and a peer review conducted by FRA-ANP personnel and external experts. The PIRT that resulted from this process is provided in Table 3.4.

The codes selected for the performance of the realistic LBLOCA analysis include the RODEX3A fuel rod code (References 6, 7, and 8) and the S-RELAP5 system code (References 5, 9, 10, and 11). Frozen versions for each of these codes were selected and used to perform the analyses presented in this report. Documents were developed for each of the codes to address the models and correlations used, and include a users manual, an assessment report, and user guidelines to execute the methodology (References 12 and 13). Verification was also performed to confirm that the models reported in the documentation are the models actually contained in the code (Reference 5). In addition, the ICECON code (References 14 and 15) has been incorporated into the S-RELAP5 code, where ICECON subroutines provide the required containment boundary conditions.

The final step in the requirements and code capabilities element is to demonstrate that the code is applicable to the chosen scenario and NPP types. This objective is accomplished by comparing the important scenario phenomena from the PIRT and the selected NPP modeling requirements with the capabilities of the chosen codes. The results of this comparison

demonstrate that the chosen codes are applicable to the LBLOCA and NPP types, as shown in Section 3.6.

2.2 ***Assessment and Ranging of Parameters***

The assessment and ranging of parameters element is used to quantify the uncertainties and biases that are to be addressed in the analysis of the chosen scenario with the chosen codes.

This element includes four steps:

- Establishment of Assessment Matrix (Section 4.1)
- NPP Nodalization Definition (Section 4.2)
- Definition of Code and Experimental Accuracy (Section 4.3)
- Determination of Effect of Scale (Section 4.4)

Implementing this element requires a series of iterations among the several steps. An examination of the PIRT (Table 3.4, Section 3.3) reveals that a large number of potentially important phenomena must be addressed. That is, those phenomena ranked 5 or higher. Assessing so many phenomena would not be manageable. Thus, the following four-step process was used to reduce the number of phenomena to be addressed.

First, the NPP nodalization was defined using the following steps:

- A trial nodalization was developed based on internal FRA-ANP experience using RELAP5 codes.
- A limited number of calculations were performed.
- The NPP nodalization was then adjusted until reasonable trends, based on engineering judgement, were obtained in the results.
- A limited number of experimental assessments was selected and modeled with the nodalization.
- The nodalization was again adjusted until reasonable trends were observed in both the NPP analyses and in the assessment calculations.

A peer review was conducted using internal and external experts, to evaluate the proposed NPP nodalization and the results produced. The peer review concluded that the nodalization of the upper plenum required more detail. This change resulted in a repeat of the above process until a nodalization was obtained that addressed all the issues identified in the peer review.

Second, each of the potentially important phenomena was paired with a parameter in the code that could be varied. Third, a possible range of uncertainty for each of the potentially important

phenomena and the associated parameters that could be varied in the analysis were defined. The uncertainty ranges defined were based on a review of available literature.

Fourth, the nodalization and the identified uncertainty ranges were used to perform sensitivity calculations. Based on the results of these sensitivity studies, the dominant phenomena were identified (Table 4.1, Section 4.1) and an assessment matrix was developed to assess these phenomena (Table 4.3, Section 4.1). In addition, various assessments were chosen to be part of the assessment matrix in order to demonstrate the scalability of the code.

Using the assessment matrix, which includes separate effects (SET) and integral effects tests (IET), each of the assessment test facilities was modeled with S-RELAP5 incorporating the nodalization defined above. The initial results of the assessment calculations required additional modification of both the code and the nodalization. A complete rerun of the PIRT sensitivity calculations and a re-evaluation of the assessment matrix were performed based on the changes made. Once this iterative process had been completed, the final NPP nodalization, assessment matrix, and assessment calculations were produced.

Completion of the assessment calculations provided the uncertainties for use in the plant analyses and also provided the basis for the demonstration of code scalability. The treatment of uncertainties is described and quantified in Section 4.3. The scalability of the code is demonstrated in Section 4.4.

2.3 ***Sensitivity and Uncertainty Analysis***

The sensitivity and uncertainty analysis element combines the code and model uncertainties and the plant specific contributors to obtain a total uncertainty and to provide a basis for making an acceptability statement with respect to the established safety criteria. The following steps are included in this CSAU element:

- Determination of the Effect of Reactor Input Parameters and State (Section 5.1)
- Performance of NPP Sensitivity Calculations (Section 5.2)
- Determination of Combined Bias and Uncertainty (Section 5.3)
- Determination of Total Uncertainty (Section 5.4)

The NPP input parameters and possible operating states were reviewed to determine the applicable input parameters and state. This review identified a list of inputs that might impact

the realistic LBLOCA event. Actual NPP operating conditions and typical technical specifications were assessed to identify allowed operating conditions. Sensitivity studies were performed using the selected NPP model to determine those parameters that impact the realistic LBLOCA event. For the most important parameters additional plant data were obtained, where available, so that actual operational data distributions could be determined.

[

] The identification of the parameters and the results of the parameter studies are provided in Tables 5.1-5.4 and Section 5.1.

The methodology for determination of the combined biases and uncertainties and the development of a final statement of probability for the limiting criteria are addressed in Section 5.2. To perform these last two CSAU steps, [

]

A licensing analysis for a 3-loop (W) designed plant is provided in Reference 16. Section 5.4 provides the final statement of overall conformance to the licensing criteria.

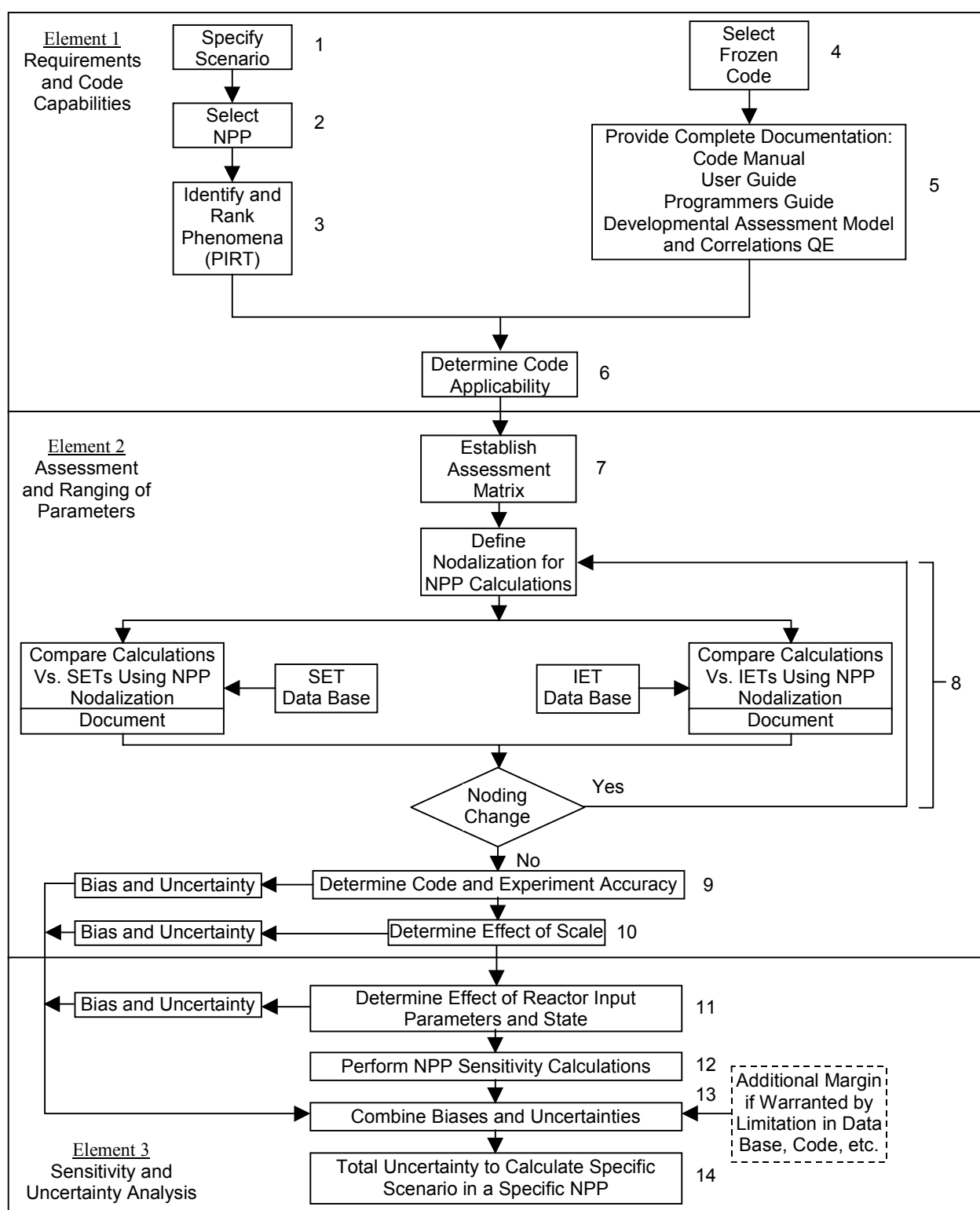


**Figure 2.1 Code Scaling, Applicability, and Uncertainty Methodology
Flow Chart**

3.0 Requirements and Capabilities

The objective of the first element of the CSAU methodology is to establish the analysis requirements and to demonstrate that the chosen codes can address these requirements. The important phenomena are determined from the event scenario and NPP types and documented in the PIRT. The ability of the codes to address the important phenomena must then be demonstrated. Documents must be developed that contain sufficient detail to permit the code models to be correlated with the important PIRT phenomena.

3.1 Scenario Specification (CSAU Step 1)

This report describes methodology for the realistic evaluation of LBLOCAs. The Standard Review Plan (SRP) (Reference 17), Event 15.6.5, defines a LOCA. LOCAs are defined in SRP Event 15.6.5 as follows:

"Loss-of-coolant accidents (LOCA) are postulated accidents that would result from the loss of reactor coolant, at a rate in excess of the capability of the normal reactor coolant makeup system, from piping breaks in the reactor coolant pressure boundary. The piping breaks are postulated to occur at various locations and include a spectrum of break sizes, up to a maximum pipe break equivalent in size to the double-ended rupture of the largest pipe in the reactor coolant pressure boundary. Loss of significant quantities of reactor coolant would prevent heat removal from the reactor core, unless the water is replenished."

PWRs are required to be equipped with an ECCS that satisfies the requirements of 10 CFR Part 50, Section 50.46 (Reference 1).

The LBLOCA event is classified as a Postulated Accident and a Condition IV event (Reference 17). This event is not expected to occur during the lifetime of the plant but is designated a design basis accident. The specific acceptance criteria for performance of the ECCS are:

- The calculated PCT shall not exceed 2200°F.
- The maximum calculated cladding oxidation shall nowhere exceed 0.17 times the total cladding thickness before oxidation.
- The maximum calculated hydrogen generation from the chemical reaction of the cladding and water or steam shall not exceed 0.01 times the hypothetical amount that would be generated if all of the metal in the cladding cylinders surrounding the fuel, excluding the cladding surrounding the plenum volume, were to react.

- The calculated changes in core geometry shall be such that the core remains amenable to cooling.
- The calculated core temperature shall be maintained at an acceptably low value and decay heat shall be removed for the extended period of time required by the long-lived radioactivity remaining in the core.
- The radiological consequences of the most severe LOCA are within the guidelines of 10 CFR 100.
- The TMI Action Plan requirements have been met. (The TMI Action Plan requirements are more specifically related to the Small Break LOCA (SBLOCA) event.)

The methodology described here is shown to be in compliance with the first four criteria above. These criteria, with a primary focus on the PCT, will be used as the figure-of-merit upon which decisions are made with respect to the acceptability of the methodology. The PCT is chosen as the primary criterion because to some extent all the other criteria are dependent upon or related to it.

A hypothetical LOCA is initiated by an instantaneous rupture of a reactor coolant system (RCS) pipe ranging in cross-sectional area up to and including that of the largest pipe in the RCS. A spectrum of breaks for both double-ended guillotine and split break types is analyzed. The spectrum includes double-ended guillotine breaks ranging in size from one to two times the cross sectional area of the largest RCS pipe. The split break spectrum is analyzed for longitudinal split areas ranging in size from the largest small break size (10% of the cross sectional area) to one times the full cross-sectional area of the largest RCS pipe. For a LBLOCA, the most limiting break typically occurs in a cold leg pipe between the pump discharge and the vessel.

Offsite power availability must also be considered in the analysis. If loss-of-offsite power is assumed to occur coincident with the LOCA initiation, RCS pump coastdown will occur with the loss-of-offsite power. For short periods of time following the break and up to about 5 to 8 seconds into the transient, the pump head may be sufficient to maintain positive flow through the core, which can provide significant cooling of the fuel. Due to loss-of-offsite power, an additional time delay for startup of the diesel generators and safety injection system (SIS) pumps must also be accounted for in the analysis. The worst single failure is identified and applied in the analysis. The worse single failure is typically the loss of one low head safety injection (LHSI) pump or the loss of a diesel generator.

A LBLOCA event is typically described in three phases: (1) blowdown, (2) refill, and (3) reflood. The blowdown phase is defined as the time period from initiation of the break until flow from the accumulators or safety injection tanks begins. This definition is somewhat different than the traditional definition of blowdown which extends the blowdown until the RCS pressure approaches containment pressure. The blowdown phase typically lasts about 12 to 25 seconds, depending on the break size. The refill phase lasts from the end of blowdown until fluid from the ECCS has filled the downcomer and lower plenum up to the bottom of the heated length of the fuel. The reflood phase lasts from the end of refill until the core temperatures are reduced.

Following the instantaneous pipe break, the blowdown phase is characterized by a sudden depressurization from operating pressure down to the saturation pressure of the hot leg fluid. An immediate flow reversal and stagnation occurs in the core due to flow out the break which causes the fuel rods to pass through critical heat flux (CHF), usually within 1 second following the break. Following this initial rapid depressurization, the RCS depressurizes at a more gradual rate with the reactor coolant being expelled primarily by vaporization.

A reactor trip signal occurs when either the pressurizer low-pressure trip setpoint or containment vessel high-pressure trip setpoint is reached. However, reactor trip and scram are conservatively neglected in this LOCA methodology, and reactor shutdown is accomplished initially by moderator feedback and maintained by the boron content of the ECCS water. A SIS initiation signal is also actuated when the high containment pressure setpoint is reached.

When the system pressure falls below the accumulator pressure, flow from the accumulator is injected into the cold legs ending the blowdown period and initiating the refill period. Once the system pressure falls below the respective shutoff heads of the high head safety injection (HHSI) pumps and the LHSI pumps and the system startup time delays are met, SIS flows begin injection into the RCS. While some of the ECCS flow bypasses the core and goes directly out the break, the downcomer and lower plenum gradually refill until the liquid level reaches the bottom of the core. During this refill period, heat is primarily transferred from the hotter fuel rods to cooler fuel rods and structures by radiative heat transfer.

Once the lower plenum is refilled to the bottom of the fuel rod heated length, refill ends and the reflood phase begins. The ECCS fluid flowing into the downcomer provides the driving head to move coolant through the core. As the mixture level moves up the core, steam is generated and liquid is entrained. As this entrained liquid passes into the steam generators, and

vaporizes, steam binding may occur, reducing the core reflood rates. However, the fuel rods are eventually cooled and quenched by radiation and convective heat transfer as the quench front moves up the core.

3.2 ***Nuclear Power Plant Selection (CSAU Step 2)***

The selected NPP types to which the methodology is to be applied includes those PWRs with U-tube type steam generators and ECCS injection into the cold leg. This includes W 3- and 4-loop plants and CE 2x4 plants. These three NPP types have very similar hot and cold legs, pressurizers, steam generators, and vessels. The largest difference among the NPP types is the number of hot and cold legs and steam generators. However, experience in the performance of Appendix K large break LOCA analyses for the three NPPs has shown that all three types behave similarly.

All three NPP types have inverted U-tube steam generators, a pressurizer connected to the hot leg, and ECCS injection into the cold legs. The steam generators for all three plant types can all be modeled with a downcomer, boiler, plenum, dryer/separator, and steam dome region. In addition, the main and auxiliary feedwater enters the steam generators in the downcomer for all three-plant types. The pressurizers are essentially the same and can be modeled with axial nodes, associated heat structures, heaters, sprays, and a surge line connected to a hot leg. The plant nodalization for a loop is described in detail in Reference 12 and illustrated in Figure 4.3.

The configuration of the vessels for all three-plant types is also essentially the same and can be modeled in the code with the same major divisions and nodalization schemes. The coolant enters the vessel through the inlet nozzles and flows into the downcomer. In the downcomer a small fraction of the flow leaks into the upper head but the majority of the flow goes down the downcomer into the lower head/plenum region. From here the majority of the flow goes up through the active core with some flow bypassing the core through the baffle and guide tubes. From the core the flow enters the upper plenum and exits the vessel through the hot leg nozzles.

The principal difference in the vessel between the W and CE plants is in the connection between the downcomer and the lower plenum/head. In the CE plants there may be a flow skirt that is intended to force part of the flow to pass through the lower head before going into the

lower plenum region. The NPP model of the lower plenum to be used for both the W and CE plant types has been nodalized to address this vessel configuration difference. The plant nodalization for the vessel is described in detail in Reference 12 and illustrated in Figure 4.4.

As indicated above the principle difference between these NPP types is in the number of hot and cold legs and steam generators. The W 3-loop NPP has 3 hot legs, 3 cold legs and 3 steam generators. The W 4-loop NPP has 4 hot legs, 4 cold legs, and 4 steam generators. The CE 2x4 plant has 2 hot legs, 4 cold legs and 2 steam generators.

A typical vessel loop configuration for the three NPP types is shown in Figure 4.5. This figure shows the location of the cold legs (arrows pointing into vessel) and hot legs (arrows pointing out of vessel) for the three NPP types. Since the hot legs pass through the vessel downcomer region into the upper plenum they essentially provide a flow path blockage at the elevation of the hot and cold legs in all three NPP types. As illustrated in this figure the flow paths for the W 4-loop and the CE 2x4 plants are very similar in relation to the hot and cold legs.

To further demonstrate that these three NPP types are very similar and respond in essentially the same manner, approximate values for some of the important NPP parameters are provided in Table 3.1 and a sequence of events from a typical Appendix K analysis is provided in Table 3.2. As illustrated in Table 3.1 the biggest difference in the important NPP parameters is in the pressure of the accumulators for the W plants and the safety injection tanks (SITs) in the CE plants. The impact of this difference is shown in the sequence of events given in Table 3.2 where the SIT flow initiation is delayed in the CE plants until the pressure in the cold legs drops below the SIT pressure. Taking into account this delay in the SIT delivery, the sequence of events is very similar for the three NPP types.

Provided with the methodology is a sample problem for a W 4-loop PWR NPP. A licensing analysis for a W 3-loop PWR has also been completed and will be submitted on a plant specific basis.

3.3 ***Phenomena Identification and Ranking (CSAU Step 3)***

A key step in the CSAU process is to identify and rank the important phenomena that must be addressed in analyzing a LBLOCA. This step is performed by experts who are knowledgeable of LBLOCA phenomena and who define the important phases of the LBLOCA scenario and identify phenomena that could be important during each phase of the transient. Based on their

knowledge, the experts then rank the phenomena as to their relative importance during each phase of the LOCA transient. The result is a PIRT which ranks the relative importance of the phenomena for each component and phase of the LOCA. The PIRT provides the basis for: (1) determining code applicability (does the code properly model the important phenomena), (2) establishing the assessment matrix (identifying test data that contain the appropriate phenomena during each accident phase), and (3) identifying phenomena parameters to be ranged and quantified for evaluating uncertainties.

A PIRT for a W 4-loop PWR LBLOCA is presented in the Compendium (Reference 2).

Table 3.3 provides an initial PIRT which was developed from the Compendium by averaging the ranking of the experts and the ranking developed by the analytical hierarchy process (AHP) and rounding up when necessary. Each phenomena is given a ranking, where importance is proportional to the numerical value (e.g., 9 = extreme importance, 1 = least importance). The ranking indicates the important phenomena that should be simulated by a realistic LBLOCA evaluation model.

Using Table 3.3 as the starting point, the following process was followed to generate a final PIRT for use in the FRA-ANP CSAU process. The initial PIRT was reviewed by three experts, who offered recommendations for the addition or deletion of phenomena from the PIRT and revisions to the ranking of the phenomena. Following this review, a peer review was held with the three experts and four additional FRA-ANP personnel to derive a final PIRT that incorporated the input from all seven participants. This PIRT is provided in Table 3.4.

To ensure a coherent peer review process, a set of definitions were agreed upon:

1. Blowdown: The blowdown phase of the LOCA is defined as the time period from initiation of the break until flow from the accumulators or safety injection tanks begins. This definition is somewhat different from the traditional definition of blowdown which continues until the RCS pressure approaches containment pressure.
2. Refill: The refill phase of the LOCA begins when the accumulators or flooding tanks begin injecting and continues until the mixture level in the vessel refills the lower plenum and begins to flow into the core.

3. Reflood: The reflood phase of the transient begins when the lower plenum fills and ECC begins flowing into the bottom of the core and continues until the temperature transient throughout the core has been terminated. At this time the LOCA stored energy and decay heat are being removed and the LOCA has been reduced to an issue of maintaining long term cooling.
4. Post-CHF Heat Transfer: Defined according to the transient phase. For blowdown it is the high pressure, high mass flux, low vapor superheat film boiling. During refill, it is a combination of dispersed flow film boiling and natural convection to single-phase vapor. During reflood, it is dispersed flow film boiling.
5. Reflood Heat Transfer: Defined only for the reflood phase as convection to single phase steam, wall to fluid radiation, film boiling, and transition boiling. Thus, includes effects of precursory cooling and quenching.
6. Rewet: Defined according to transient phase. For blowdown this is the quenching (either bottom-up or top-down) associated with high heat transfer rates near the quench front during periods of high liquid flows. For refill and reflood, limit this to top-down quenching due to falling liquid films.

With the above definitions as the basis, the following changes were made to the PIRT for the LBLOCA during the peer review process:

1. []
[]
]
[]
2. []
[]
]

Framatome ANP Richland, Inc.

4. []

[

]

[

]

5. []

[

]

[

]

[

]

6. []

[

]

7. []

[

]

8. []

[

]

[

]

[

]

These results are all shown in the final PIRT given in Table 3.4. This PIRT was used in the demonstration of code applicability and as the basis for performing sensitivity studies and determining the code assessment matrix.

The codes selected for use in the realistic LBLOCA methodology include RODEX3A (References 6, 7, and 8) and S-RELAP5 (References 5, 9, 10, and 11). RODEX3A is a best

estimate fuel rod code which has been approved for use in the performance of realistic LBLOCA (RLBLOCA) analyses (Reference 6). The S-RELAP5 code is a RELAP5 based thermal hydraulic system code for performing LBLOCA analyses. The ICECON code (References 14 and 15) has been incorporated into the S-RELAP5 code to provide the required containment boundary conditions for the LBLOCA analysis. ICECON was developed to predict the long-term behavior of PWR nuclear plant containment systems.

The frozen versions of these codes used in the development of this methodology are defined in Table 3.5. The interpretation of the version designation is described below for the S-RELAP5 code version, UJUL00:

- U signifies that the code is a USE code version which means it has been verified, validated, and documented in conformance with FRA-ANP's quality assurance program. It also indicates that the code has been stored in FRA-ANP's code management system (CMS) where it can be read but not modified and is automatically archived.
- JUL00 is the month and year in which the code version was built and placed in CMS.

Two USE versions of the S-RELAP5 code were used in the development of this methodology, UJUL00 and UMAR01. The differences between these two code versions reflect the addition of the final set of multiplication parameters for use in the uncertainty analysis in UMAR01 and the correction of problems found in the verification of the RODEX3A incorporation into S-RELAP5. The verification of the RODEX3A incorporation into S-RELAP5 occurred late in the methodology development process. During this verification process, several problems were identified and corrected.

In addition, two point releases have been made for the UMAR01 use code versions. These point releases dealt only with the application of the multipliers used in the uncertainty analysis. Consistent with the CSAU definition of a frozen code, these changes do not constitute a code change.

Since a large number of the assessments had already been completed it was decided that only those assessments which actually used RODEX3A would be rerun and the software development record for UMAR01 would document that assessments performed with electrical heater rods were unaffected by the changes to the RODEX3A implementation. The assessments that used electrical heater rods and had already been completed would not be rerun with UMAR01 and would continue to rely on the UJUL00 analyses. On the other hand the

LOFT analyses which used nuclear fuel rods had to be rerun with UMAR01. In addition, all the final plant analyses were run with the UMAR01 code version. Thus, while two code versions of S-RELAP5 have been used in the methodology development, it has been demonstrated that no change in results would occur if everything was rerun with the final UMAR01 code version.

3.4.1 RODEX3A

Key to a realistic LBLOCA analysis is the model used for calculating fuel rod performance. In particular the initial operating temperature of the fuel pellets (stored energy) and the internal fuel rod gas pressure are significant parameters that affect the calculated peak cladding temperature (PCT). These parameters are functions of fuel exposure and power history.

FRA-ANP developed the realistic fuel rod mechanical response model RODEX3A, which provides exposure dependent initial fuel conditions for the realistic LOCA evaluation model. Further, to assure compatibility and consistency between the RODEX3A initial fuel conditions and the initial and transient conditions calculated by S-RELAP5, the appropriate fuel models from RODEX3A were incorporated into S-RELAP5.

The model features included in RODEX3A are:

- A coolant subchannel model to compute the coolant state and cladding surface temperature.
- A model to compute the radial temperature distribution in a fuel rod and adjust the porosity contribution to the fuel thermal conductivity.
- A model to compute gap conductance.
- A model to compute internal rod pressure.
- Models to compute grain size, and fission gas release and redistribution in the fuel microstructure.
- A model to compute pellet-cladding interaction forces.
- Models to compute cladding creep and growth.
- Models to compute cladding oxidation and hydriding.
- A model to calculate elastic response of the cladding.
- A fuel "segment mechanics" model to compute fuel pellet creep, dish filling, cracking, deformations, and mechanical response.
- Models to compute pellet densification, swelling, and hot pressing.
- A pellet flexibility model.
- Material properties models.

- A model to compute the radial dependence of the heat generation.
- Models to calculate the axially dependent exposure and fluence distribution.

To perform a LOCA analysis with the FRA-ANP RLBLOCA evaluation model, RODEX3A calculations are first performed to calculate initial condition inputs for all fuel rods modeled in S-RELAP5. Inputs to RODEX3A describe:

- The cladding geometry, composition and creep coefficients.
- The pellet geometry, composition, density, grain size and open porosity.
- The axial and radial nodalization of the fuel rod.
- The fuel plenum volume(s) and plenum spring(s).
- The initial fuel rod pressure and gas composition.
- The S-RELAP5 axial nodalizations and geometry indices.
- The time dependent power, coolant pressure, and coolant inlet temperature histories.

For each burnup of interest, an electronic transfer of RODEX3A data to S-RELAP5 is made. This transfer includes information needed to describe the exposed state of the fuel and accelerates the convergence of the S-RELAP5 steady state solution. It also ensures that the RODEX3A and S-RELAP5 fuel geometries are identical. The RODEX3A data describe the fuel state at the reference fuel temperature (usually 70 F) and zero power. A steady state S-RELAP5 calculation is required to initialize the S-RELAP5 calculation at the power of interest. The data transferred from RODEX3A to S-RELAP5 include:

- The date and time when the RODEX3A calculation was performed to provide traceability.
- The gas constant, the moles of gas in the fuel rod, the initial internal fuel rod pressure, and the gas coefficients (which are dependent upon the gas composition) which are used to calculate the rod internal pressure and the gap thermal conductivity and viscosity.
- The S-RELAP5 geometry index, the RODEX3A pellet, and cladding node radii. The S-RELAP5 and RODEX3A radial nodalizations must be identical.
- The fuel rod plenum lengths and initial temperature(s), and the plenum spring constant(s) which are used to compute the fuel rod plenum gas temperature(s) and the internal fuel rod pressure.
- The fluence, and the cladding flexibility and yield stress coefficients which are used to compute pellet-cladding contact pressures and changes in the gap width resulting from the "trapped stack" effect.
- The cladding axial/radial elastic deflection coefficients which are used to compute the elastic deformations in the cladding.

- The axial strain distribution resulting from irradiation induced cladding creep and growth which are used to compute the fuel plenum volume and rod internal pressure.
- The pellet composition, the pellet dish volumes, the axial/radial burnup distribution, the axial/radial porosity distribution, and oxygen to fuel ratios. The porosity distribution depends upon the initial pellet density and the amount of pellet densification and swelling with exposure. These data are used to compute pellet thermal properties and the internal rod pressure.
- The exposure dependent radial displacements due to fuel migration, pellet creep, pellet densification, pellet swelling and clad creep which are used to compute the gap dimension, gap thermal properties, gap volume, and rod internal pressure.
- The axial/radial distribution of power (i.e., the flux depression profile) which are used to compute the power distribution in the fuel rod and hence the temperature distribution.
- The initial clad oxide layer thickness which are used to compute cladding temperatures and the amount of energy deposited in the cladding due to the reaction of zirconium with steam (i.e., oxygen).
- The axial/radial temperature distribution, the fuel/cladding slip ratio, and the axial force distribution which are used to help speed the convergence of the S-RELAP5 steady state calculation. These values change with time.

RODEX3 (Reference 6) has been approved for use in providing input to the RLBLOCA analysis under certain conditions. These conditions have been addressed in the methodology and are discussed in Section 4.3. Following the approval of RODEX3, the code was modified to provide the required input to the S-RELAP5 code. At that time the code was renamed to RODEX3A (References 7 and 8). The RODEX3A code provides equivalent results on all benchmarks used for the approved RODEX3 code.

3.4.2 S-RELAP5

S-RELAP5 is an FRA-ANP-modified version of RELAP5/MOD2 (Reference 18) which incorporates the computer portability aspects of RELAP5/MOD3 (Reference 19) and modifications to the constitutive package to provide congruency with literature correlations and to improve the simulation of key large break LOCA experiments. The field equations are basically in the same form as RELAP5/MOD2 with the addition of full two-dimensional momentum equations. This two-dimensional capability is only applied to the downcomer, core and upper plenum regions in the RLBLOCA methodology, but can be applied anywhere in the reactor system through input. The S-RELAP5 code structure was modified to be essentially the same as RELAP5/MOD3. The coding for reactor kinetics, control systems, and trip systems was also replaced by that from RELAP5/MOD3.

The following list summarizes the major modifications and improvements incorporated into S-RELAP5 relative to RELAP5/MOD2:

- **Multi-dimensional Capability.** Full two-dimensional treatment was added to the hydrodynamic field equations.
- **Energy Equations.** The energy equations were modified to better conserve energies transported into and out of a control volume.
- **Numerical Solution of Hydrodynamic Field Equations.** The reduction of the hydrodynamic finite-difference equations to a pressure equation is obtained analytically in S-RELAP5.
- **State of Steam-Noncondensable Mixture.** The state relations were modified to correctly simulate the accumulator depressurization and to prevent code failures during the period of accumulator ECC water injection.
- **Hydrodynamic Constitutive Models.** Significant modifications and enhancements were made to the interphase friction and interphase mass transfer models.
- **Choked Flow.** The computation of the equation of state at the choked plane was modified.
- **Counter-Current Flow Limiting.** A Bankoff form correlation was implemented, which can be reduced to either a Wallis type or Kutateladze type CCFL correlation.
- **Component Models.** A revised two-phase pump degradation model based on EPRI data was implemented.
- **Fuel Model.** Initial fuel conditions are supplied by the realistic fuel performance code, RODEX3A. To be consistent, the fuel deformation and conductivity models from RODEX3A were included in S-RELAP5.
- **Containment Back Pressure.** Capability to interface with a concurrent calculation of containment back pressure using the ICECON code was added.

FRA-ANP performed sensitivity calculations to evaluate the effects of containment back pressure. The results showed that the RLBLOCA model significantly reduces the sensitivity of calculated PCT to containment back pressure, relative to the current Appendix K based ECCS evaluation models, but does not eliminate these effects. A conservatively low (atmospheric) containment back pressure yields an increased PCT. However, varying time dependent containment pressures within a band of a few psi gave little difference in calculated PCTs. Thus, based on these results, FRA-ANP concluded that a containment back pressure calculation which provides a reasonable approximation for the time dependent back pressure is desirable for a RLBLOCA evaluation model.

The conversion from RELAP5/MOD2 includes the capability to interface external calculations with S-RELAP5. With this interface, a containment pressure calculation using a different code can be run concurrently with S-RELAP5. Break flows and enthalpies are transferred to the

containment code, which continuously feeds back calculated pressure and temperature through S-RELAP5 time dependent volumes. The choice for the containment code to use with the RLBLOCA evaluation model is ICECON (References 14 and 15), which is based on CONTEMPT LT-022 (Reference 20). ICECON was originally approved for calculating a conservative containment back pressure under Appendix K rules, but it can be used with realistic input and, with only minor modifications, to give an approximate realistic back pressure calculation. [

]

3.4.3 New Product Support

While it is understood that model enhancements and code improvements are specifically forbidden after a code has been declared frozen, updates supporting the treatment of uncertainty are allowed under the CSAU framework. Circumstances that could lead to code changes include:

- Minor plant design changes (which could introduce other uncertainty parameters)
- New fuel rod or assembly design (such as a new cladding alloy)
- Expanded thermal-hydraulic database
- Uncertainty analysis refinement (e.g., alternative probability distribution function) or error correction

Because of these possibilities, FRA-ANP distinguishes "Code Development" and "Code Maintenance" as distinct activities. Code development encompasses all the activities required to define a "frozen code" version prescribed by the CSAU methodology. This process includes model development, code implementation, developmental assessment, documentation, etc. Code maintenance includes incremental code updates or "point releases" where it is demonstrated that the change has not invalidated the fully qualified software baseline. The qualification of production use codes requires extensive validation through a suite of test cases. Simply stated, any code update that prevents the reproduction of test suite results supporting the baseline or "frozen" code version requires that a full code qualification be performed.

As a nuclear fuel vendor, FRA-ANP continually develops new fuel rod and fuel assembly designs. To support these new designs, upgrades to LOCA methodologies need to be made. Currently, FRA-ANP uses the approved fuel performance code RODEX3A, which supports fuel currently being supplied to customers who own Westinghouse and Combustion Engineering PWRs. As new designs are developed, new models and often new computer codes are developed to model the fuel performance. Even though new or modified fuel performance codes are developed and approved^{*}, the fuel performance code changes will not invalidate the qualification of a "frozen" code. These changes will expand the application of the methodology.

Expansion of the FRA-ANP methodology, which require code updates that do not require requalification of the methodology, will be reported through supplemental documentation or document revision. This documentation will include a statement of application, models and correlations, developmental assessment, a programmer's guide supplement, and user's manual and guidelines.

3.5 **Code Documentation (CSAU Step 5)**

The documentation for the codes used in the development of this methodology is provided in References 6, 7 and 8 for the RODEX3A code, in References 5, 9, 10, and 11 for the S-RELAP5 code, and References 14 and 15 for the ICECON code. This documentation describes the models and correlations used in the codes, defines the code inputs, and provides a description of the code structure. These documents have been verified against the actual coding to ensure that the documentation and coding are consistent (Reference 5).

The code validation is provided in Reference 5, which compares the code predictions to measured data in a number of SET facilities and IET facilities. In addition, the guidelines that will govern the application of the realistic LBLOCA is provided in References 12 and 13. Reference 12 describes how to develop the S-RELAP5 input for the NPP model and Reference 13 describes how to perform the actual analysis.

* For LOCA analyses, this fuel performance information, including fuel and clad material properties, fuel deformation related to burnup, and gap thermal properties, are used as parameters in estimating initial stored energy.

3.6 ***Determination of Code Applicability (CSAU Step 6)***

The objective of the determination and code applicability element of CSAU is to demonstrate that the selected codes are capable of modeling the chosen event for all NPP types. This is accomplished by comparing the event and important phenomena identified in the PIRT with the models and correlations documents for the selected codes. Four attributes are needed to make this comparison:

- Field equations that address global processes.
- Closure (constitutive) equations which support the conservation equations by modeling specific phenomena or processes.
- Code numerics that demonstrate that the code can efficiently and reliably perform the required calculations.
- Structure and nodalization, which address the ability of the code to model the NPP geometry and components and to provide an accurate prediction of the NPP response.

These four attributes are discussed in the following sections.

3.6.1 Field Equations

The field equations (conservation of mass, momentum, and energy) must possess the capability of simulating each of the distinct phases (blowdown, refill, and reflood) of a LBLOCA. During the refill and reflood phases, counter-current flow occurs at various locations in the RCS, and subcooled liquid coexists with superheated steam in parts of the reactor core. Therefore, for realistic analyses the field equations should be non-homogeneous (unequal velocity for each phase) and non-equilibrium (unequal temperature for each phase). The presence of nitrogen in the accumulator requires an additional field equation to model and track the movement of a noncondensable gas.

The S-RELAP5 field equations evaluation against their ability to model all important PIRT phenomena (Table 3.4). The results of this evaluation are summarized in Table 3.6. Additional requirements shown in the table are multi-dimensionality, separation due to gravity, and interphase exchange terms. As indicated in Table 3.6, the S-RELAP5 code has the required field equations to address the important LBLOCA phenomena.

3.6.2 Closure Equations

Closure equations (constitutive models and correlations) are required to support the basic field equations. These closure equations are essential for modeling the processes and phenomena given in the PIRT (Table 3.4). The S-RELAP5 constitutive models and correlations are presented in Reference 9. The verification and validation of the code models and correlations are given in Reference 5. The two documents together demonstrate that the S-RELAP5 code adequately simulates LBLOCA events with a high level of confidence.

The capability of the S-RELAP5 code closure equations to meet the requirements of the PIRT (Table 3.4) is summarized in Table 3.7. The closure equations address wall friction, interphase friction, mass transfer (interphase heat transfer), wall-to-fluid heat transfer, form-losses, and similar functions. The various models require flow regime maps, boiling curves, state relationships, and fluid and material properties for completeness. As indicated in Table 3.7, the S-RELAP5 code has the required closure equations to address the important LBLOCA phenomena.

3.6.3 Code Numerics

The numerical solutions contained in S-RELAP5 has been extensively demonstrated in numerous assessments reported in the literature. These numerics have been improved in S-RELAP5 as described in Section 3.4.2 and in Reference 9. The adequacy of the S-RELAP5 specific numerics has been demonstrated in the performance of the assessments reported in Reference 5 and summarized in Section 4.3. In addition, the adequacy of the numerics has also been demonstrated in the performance of the many sensitivity analyses reported in Section 4.1 and by the time step sensitivity analysis reported in Appendix C.

3.6.4 Structure and Nodalization

To properly model a NPP, a code must be able to adequately model the important components and control systems of the NPP with respect to the chosen accident scenario. The S-RELAP5 code has the ability, as indicated in Table 3.8, to model all the major components and associated control systems of the plant. The modeling of each of the NPP components is discussed in detail in Reference 12 and summarized in Section 4.2. Section 4.2 also describes the studies that were performed to determine the final plant nodalization.

**Table 3.1 Approximate Values of Key Large Break LOCA Plant
Analysis Parameters**

Plant Parameter	<u>W</u> 3-loop	<u>W</u> 4-loop	CE 2x4
Power, MWt	2700	3400	2700
RCS Flow Rate, gpm	275,000	290,000	350,000
Reactor Vessel Volume, ft ³	3600	4950	4500
Primary Coolant Volume, ft ³	9400	12,000	11,000
Core Inlet Temperature, F	545	545	550
Pressurizer Pressure, psia	2250	2250	2250
Pressurizer Liquid Volume, ft ³	750	1100	800
Accumulators/ SIT Water Volume, ft ³	1000	1000	1150
Accumulators/ SIT Water Temperature, F	120	120	120
Accumulators/ SIT Pressure, psia	640	630	230
Containment Volume, ft ³	2,300,000	2,600,000	2,500,000

**Table 3.2 Appendix K Large Break LOCA Approximate Sequence of
Events Timing**

Event	<u>W</u> 3-loop, sec	<u>W</u> 4-loop, sec	CE 2x4, sec
Analysis Initiated	0.00	0.00	0.00
Break Opened	0.05	0.05	0.05
Safety Injection Signal	0.7 to 1.4	0.6 to 1.0	0.7 to 1.0
Broken Loop Accumulator/ SIT Flow Initiated	1 to 3	2 to 7	9 to 10
Intact Loop Accumulator/ SIT Flow Initiated	10 to 15	15 to 18	14 to 16
End of Bypass/Beginning of Refill	15 to 25	20 to 25	15 to 20
Broken Loop Accumulator/ SIT Empties	25 to 35	40 to 50	50 to 60
Beginning of Reflood	25 to 45	30 to 45	30 to 35
Fuel Cladding Rupture	35 to 50	55 to 70	40 to 50
Intact Accumulator/ SIT Empties	32 to 46	45 to 55	50 to 65
PCT Occurred	80 to 135	70 to 235	135 to 155

**Table 3.3 Preliminary Process Identification and Ranking Table
(PIRT) for PWR Large Break Loss-of-Coolant Accident**

Component	Phenomenon	Avg. Ranking		
		BD	RFL	RFD
Fuel Rod	Stored energy	9	2	2
	Oxidation	-	1	8
	Decay heat	2	1	8
	Gap conductance	3	1	7
Core	DNB	6	2	2
	Post CHF	6	8	4
	Rewet	8	7	1
	Reflood HT plus quench	-	-	9
	Nucleate Boiling	4	2	2
	One-phase vapor natural convection	-	6	4
	3-D flow	1	3	8
	Void distribution, generation	4	6	8
	Entrainment/de-entrainment	2	3	6
	Flow reversal, stagnation	3	1	1
Upper Plenum	Entrainment/de-entrainment	1	1	9
	Phase separation	2	1	2
	Countercurrent flow (drain/fallback)	1	2	6
	Two-phase convection	2	1	5
Hot Leg	Entrainment/de-entrainment	1	1	9
	Flow reversal, stagnation	2	1	-
	Void distribution, generation	1	1	4
	Two-phase convection	2	2	3
Pressurizer	Early quench	7	-	-
	Critical flow in surge line	7	-	-
	Flashing, steam expansion	7	2	2
Steam Generator	Steam binding	-	2	9
	Delta-p, form losses	2	2	2

**Table 3.3 Preliminary Process Identification and Ranking Table (PIRT) for PWR
Large Break Loss-of-Coolant Accident (*Continued*)**

Component	Phenomenon	Avg. Ranking		
		BD	RFL	RFD
Pump	Two-phase	9	5	-
	Differential pressure form loss	3	3	8
Cold Leg, Accumulator	Condensation, oscillations	2	9	5
	Noncondensable gas	-	1	9
	HPI mixing	-	3	2
Downcomer	Entrainment/de-entrainment	2	8	2
	Condensation	-	9	2
	Hot wall	-	5	5
	3-D	2	8	2
	Countercurrent, slug, non-equilibrium flow	1	8	2
	Flashing	1	-	-
	Liquid level oscillations	-	3	7
	Two-phase convection	2	3	2
	Saturated nucleate boiling	1	2	2
Lower Plenum	Sweep-out	2	7	5
	Hot wall	1	7	6
	Multi-dimensional effects	1	2	7
Break	Critical flow	9	7	1
	Flashing	3	2	1
	Containment pressure	2	4	2
Loop	Two-phase differential pressure	7	7	6
	Oscillations	-	7	9
	Flow split	7	7	2

Notes

1. BD is blowdown; RFL is refill; RFD is reflood
2. A ranking of 9 is most important; a ranking of 1 is least important
3. A ranking of "-" means that the phenomenon does not occur in the indicated phase of the transient

**Table 3.4 Final Process Identification and Ranking Table (PIRT)
for PWR Large Break Loss-of-Coolant Accident**



**Table 3.4 Final Process Identification and Ranking Table (PIRT)
for PWR Large Break Loss-of-Coolant Accident (*Continued*)**



**Table 3.5 Frozen Code Versions Used in the Methodology
Development**

Code	Version	Function
S-RELAP5	UJUL00	Predict fuel, core, and system performance during transient event including containment response
	UMAR01	
RODEX3A	UJUN00	Predict fuel performance during steady state and transient operation

Table 3.6 Field Equations/Models in S-RELAP5

Scenario and PIRT Requirements	S-RELAP5 Model Existence	Field Equations/Model
Non-equilibrium two-phase flow	Yes	Six equation unequal velocity, unequal temperature
Non-condensable gas flow	Yes	Gas mass balance in vapor flow field
Solute tracking for boron	Yes	Solute mass balance liquid flow field
Multidimensional flow capability	Yes	2-D components available as required
Separation due to gravity	Yes	Gravity pressure differential in flow field equations
Interphase exchange terms	Yes	Mass and energy transfer between phases, vaporization and condensation

Table 3.7 Phenomena/Processes in S-RELAP5

Table 3.7 Phenomena/Processes in S-RELAP5 (*Continued*)

Table 3.7 Phenomena/Processes in S-RELAP5 (*Continued*)

Table 3.8 Component Modeling Requirements for PWR

Required Component	Component Model Existence	Code Component
Pressure Vessel	Yes	1-D and 2-D components: model upper head, upper plenum, core, lower plenum, downcomer, structure, flow paths, elevations, resistances, volumes Heat structures: model vessel walls, internal structures, fuel rods
Hot Leg	Yes	Pipes, volumes, and junctions: model flow areas, lengths, volumes, resistances, elevations Heat structures: model pipe walls
Steam Generator	Yes	Separators, pipes, volumes and junctions: model flow areas, volumes, lengths, resistances, elevations, flow paths, phase separation, recirculation, feedwater, steam flow Heat structures: model generator walls, heat exchange between the primary and secondary system.
Pumps	Yes	Pump: models homologous curves, degradation, flow areas, volumes, losses, suction and discharge flow
Cold Leg	Yes	Pipes, volumes, and junctions: model flow areas, volumes, lengths, resistances, elevations, branches Heat structures: model pipe walls
Pressurizer	Yes	Pipe: models volumes, flow areas, phase separation, lengths, resistances, elevations Heat structures: model vessel walls and heater
Surge Line	Yes	Pipe and junctions: models volumes, flow areas, lengths, resistances, elevations, choked flow Heat structures: model pipe walls

Table 3.8 Component Modeling Requirements for PWR (*Continued*)

Required Component	Component Model Existence	Code Component
Accumulators	Yes	Pipes and junctions: model volumes, flow areas, lengths, elevations, nitrogen, discharge of ECC water and noncondensable gas Heat structures: model accumulator walls
ECC Systems	Yes	Pipes, volumes, and junctions: model flow rates, pressure dependence, volumes, flow areas, lengths, resistances, elevations Heat structures: model pipe walls
Valves	Yes	Valve: models areas, control
Pressure Boundary	Yes	ICECON and junctions: model pressure boundary, break flow, containment volume

4.0 **Assessment and Ranging of Parameters**

The assessment and ranging of parameters element establishes the assessment matrix to be used in defining the NPP nodalization, quantifying the code accuracy, and demonstrating any code or model scaling effects.

4.1 ***Establishment of Assessment Matrix (CSAU Step 7)***

The following four considerations must be taken into account in establishing the assessment matrix. The first consideration is the important phenomena identified in the PIRT process described in Section 3.3 (CSAU step 3) and presented in Table 3.4. The assessment matrix must include experiments that address the important phenomena, defined as those phenomena ranked 5 or higher in Table 3.4. The selected experiments must have taken sufficient data to determine the code accuracy, including bias and uncertainty, for the important phenomena.

The second consideration is that of NPP nodalization. Here experiments must be selected that are representative of the types of NPPs being addressed and cover the identified phases of the selected scenario. Thus, for this application, experiments must be selected that are representative of W 3 and 4-loop plants and CE 2x4 plants. The experiments also should cover one or all of the LBLOCA phases identified in Section 3.1 (CSAU step 1); blowdown, refill, and reflood.

The third consideration is to demonstrate that the code and NPP nodalization have the ability to scale from experiments of different sizes to the full size NPP for which analyses will be performed. Generally this is done by selecting a number of assessments in facilities of different scale and demonstrating that the code and NPP nodalization is capable of consistently predicting the experimental data from all the experiments.

The final consideration is with respect to compensating errors in the code. Because it is extremely difficult, if not impossible, to demonstrate that a code does not contain compensating errors, it should be demonstrated that the compensating errors will not produce erroneous results for the selected scenario and NPP being analyzed. Thus, an attempt must be made to select experiments that cover the range of each important phenomenon observed in the NPP analyses. Analysis of these experiments will demonstrate that, even if the code contains compensating errors, the code as currently configured still is capable of reliably predicting the selected scenario in the selected NPP.

4.1.1 PIRT Considerations

The PIRT presented in Table 3.4 provides a qualitative expression of what is perceived to be the degree of importance of key phenomena present in a LBLOCA. Given the limitations of resources (time, human, and computational) and the incompleteness of the LBLOCA database, not all of the moderately to highly ranked phenomena can be treated as uncertainty parameters. Nonetheless, all these phenomena must be accounted for either statistically or in a bounding application. A bounding application has a major drawback in that the methodology is penalized for not applying a rigorous model. Minimizing this penalty clearly is valuable in making the methodology viable for broad application. Conversely, to treat a parameter statistically, test data must be available so the statistics can be quantified. Clearly, such tests must be included in the assessment matrix.

To optimize the choice of which parameters to treat statistically and which parameters to bound, a large set of PIRT and plant sensitivities studies (~72 calculations/set) was performed to quantify the importance of each moderately to highly ranked phenomenon along with key plant operational parameters. The first column of Table 4.1 lists the moderate and high ranked PIRT phenomena cross referenced to a description of one or more calculations performed in the sensitivity studies. These studies were performed with the 3- and 4-loop sample problems. (Note: Appendix A contains an overview of all documented plant sensitivity studies performed during the development of this methodology.)

While the chronology of the 3- and 4-loop base cases is well described in Table 3.2, some aspects of the LBLOCA model were modified to improve the usefulness of the results (additional discussion on base cases is given in Appendix A, Section A.2). The primary changes in the baseline 3- and 4-loop LBLOCA analyses used in the PIRT sensitivity studies were designed to accentuate PCT sensitivity. This was done by skewing the power profile towards the top of the core and raising core and decay power in such a manner that predicted PCTs approached regulatory limits (2000 F – 2200 F). These modifications enhance the late reflood PCT in such a way that both the 3- and 4-loop models show both an early and late reflood peak. Preceding these sensitivities, a break spectrum was performed to identify the worst break size. This was also used to bias the sensitivity studies. Fuel metal-water reaction and nitrogen transport from the accumulators were removed from the model. These two phenomena have been shown to contribute nonlinear PCT sensitivities that might disguise the sensitivity of the studied

parameters. Figure 4.1 shows the PCT signatures from the 3- and 4-loop sample problems. The integrity of the baseline calculations is built on the rigorous approach to nodalization, which emphasized demonstration of the moderately and highly rank PIRT phenomena as presented in Section 3.3.

In addition to the two baseline studies, two more sets of sensitivities were performed for the 3-loop sample problem at nominal power conditions. The difference between these two sets was whether accumulator nitrogen was allowed into the RCS or valved out. These studies were done to ensure that dominant phenomena, whose influence may diminish at higher temperatures, were considered in this methodology.

For the parameters used in performing the PIRT sensitivities (column 2, Table 4.1), best estimate or conservative parameter range limits were identified. These range limits were derived from expert experience, literature review, or physical bounds. Each sensitivity calculation perturbed the baseline model by modifying the key parameters that drove a particular phenomenon to a range limit. The changes in PCT (Δ PCT) during blowdown, early reflood, and late reflood from the baseline calculation were recorded for each study.

Interpretation of the results of over 250 calculations involved the tabulation and ranking by the magnitude of the Δ PCTs. The degree of sensitivity on PCT for a particular study was classified as either low, medium, or high. The high classification is based on the regulatory definition of "significant change" (i.e., > 50 F). [

] (Appendix C presents a confirmation study examining code variability from a set of 14 time-step sensitivities.)

The bulk of the sensitivity studies confirmed the important PIRT phenomena; however, a few parameters did show only weak sensitivity. Column 3 of Table 4.1 presents the conclusions from these results. For most of the PIRT phenomena, assessment against test program results is indicated. In some cases published uncertainty is available. Phenomena not demonstrating significant LBLOCA PCT sensitivity also are identified in column 3 of Table 4.1. For those PIRT phenomena demonstrating significant LBLOCA PCT, a database is identified, based on test

facility and or plant data, for validating a specific model or quantifying the phenomenon uncertainty.

4.1.2 Nodalization Considerations

Given the extensive experimental facility database developed from the PIRT considerations, only one additional test facility was identified strictly to address nodalization effects. That test facility was the Slab Core Test Facility (SCTF), where specific assessments were performed to address radial nodalization with variations in radial power distributions. However, in the selection of the specific tests to be analyzed in each facility, nodalization was a consideration.

4.1.3 Scaling Considerations

Within the test facility database developed to support the PIRT considerations are facilities that span a scaling range of 1:1500 to 1:1. In addition, some specific tests were performed as a counterpart to tests performed in other facilities. Where data were available, these tests have been added to the assessment matrix.

4.1.4 Compensating Errors

The issue of compensating errors arises primarily from the use of correlations and closure relations in the code. The interaction of the various correlations and closure relations can be such that an error in one of these models is compensated for by an error in another model. These compensating errors can result in the code being able to predict specific tests but incapable of predicting other tests. For the LBLOCA, only those compensating errors which could function in one manner in the assessments and in an entirely different manner in the LBLOCA are a concern. Thus, the assessment matrix must include tests that can be scaled up and that cover the range of the LBLOCA PIRT phenomena. The compensating error issue is addressed in the test matrix through the FLECHT, FLECHT-SEASET, SCTF, CCTF, and THTF for the core phenomena and UPTF for most of the other major reactor coolant system components.

4.1.5 Summary

Given these four considerations, the assessment matrix described in Table 4.2 and Table 4.3 was developed. Table 4.2 lists the test facilities and makes the association between the

selected facilities and the identified parameter groups. The actual tests analyzed from each test facility are provided in Table 4.3, along with the associated phenomena being examined.

4.2 **Nuclear Power Plant Nodalization Definition (CSAU Step 8)**

Reference 4 ("Quantifying Reactor Safety Margins") makes the following statements regarding nodalization:

"The plant model must be nodalized finely enough to represent both the important phenomena and design characteristics of the NPP but coarsely enough to remain economical."

"Thus, the preferred path is to establish a standard NPP nodalization for the subsequent analysis. This minimizes or removes nodalization, and the freedom to manipulate noding, as a contributor to uncertainty."

"Therefore, a nodalization selection procedure defines the minimum noding needed to capture the important phenomena. This procedure starts with analyst experience in previous code assessment and application studies and any documented nodalization studies. Next, nodalization studies are performed during the simulation of separate- and integral-effects code data comparisons. Finally, an iterative process using the NPP model is employed to determine sufficiency of the NPP model nodalization."

Given these general recommendations, the goal of a nodalization methodology is to optimize somewhat independent priorities. These include preserving dominant phenomena, minimizing code uncertainty, conforming to design characteristics, and minimizing computational expense. The guidelines developed for the FRA-ANP RLBLOCA methodology (Reference 12, EMF-2054) are quantitatively explicit wherever possible to remove nodalization as a contributor to uncertainty. Because not all plants of the same type are identical, the guidelines provide rules for deriving the appropriate nodalization. This strategy serves both to remove nodalization as a contributor to uncertainty and to define a method for automating the generation of input for a RLBLOCA analysis.

As described by Step 8 of the CSAU process, "NPP Nodalization Definition," this task is iterative. To minimize the degree of iteration, the baseline nodalization definition originated from user experience with earlier manifestations of S-RELAP5 (i.e., for SBLOCA Reference 21), and RELAP5 (References 22 and 23). The current nodalization has been refined using results from sensitivity studies performed with the current frozen S-RELAP5 code version and its predecessors. Because the nodalization requirements are strictly applied, uncertainty associated with nodalization becomes part of the studies to determine the statistics of key uncertainty parameters. If the results of one or more assessments brought into question the

validity of a particular nodalization, additional studies were performed. For RLBLOCA applications, these guidelines have been developed and refined by sensitivity studies (Appendix A) and/or assessments or they have been constrained to a best fit for a complex structural configuration. Table 4.4 summarizes the guidelines for hydraulic nodalization based on this approach.

The derived input prescription defines the standardized nodalization scheme, specifies a logical numbering system, and recommends key parameter inputs for the S-RELAP5 input model. Details of noding have been determined from experience with simulation of integral- and separate-effects tests (Reference 5) that result in a technically and economically sound nodalization scheme for simulating LBLOCA in a PWR. Assessment calculations of the FLECHT/SEASET reflood experiments provided data for the axial nodalization of the core region. Studies of the Cylindrical Core Test Facility (CCTF) and SCTF were used to identify two-dimensional modeling techniques for the downcomer and core. Analyses of the LOFT and Semiscale experiments gave information on describing the primary coolant loops, reactor coolant pumps, reactor vessel, and steam generators with S-RELAP5. Assessments of Upper Plenum Test Facility (UPTF) tests also were used to identify two-dimensional modeling techniques and provide useful plant information, including experimental data on full-scale downcomer fluid behavior during the blowdown, refill, and reflood phases of a LBLOCA.

Column 1 of Table 4.4 defines a particular NPP component or coolant system region and the S-RELAP5 components generally used for its simulation. Column 2 lists the important phenomena associated with the component as evaluated through the PIRT process (Section 3.3). Column 3 defines the number of cells required, based on user experience and assessment calculations, to provide adequate detail. The source or bases for the selections are given in Column 4.

4.2.1 Nodalization Methodology

The necessary conditions for a satisfactory nodalization methodology are to discriminate key structural characteristics, to obtain reasonable steady-state agreement with plant data, to preserve first order accuracy of dominant phenomena, and to minimize PCT sensitivity to nodalization. The ability of the code and associated nodalization to describe key structural components is addressed in Section 3.6.4, where it is demonstrated that the code is capable of modeling the key components. Obtaining reasonable steady-state results is implicitly aided by

adhering to strict conformance to structural design characteristics (e.g., elevations and volumes). Obtaining reasonable results also is aided by the use of system-initialization control systems.

The most challenging of the necessary conditions is the task to preserve dominant phenomena. A computer code's ability to capture LBLOCA phenomena cannot separate the contributions of the applicable phenomenological models and nodalization. While it was stated that strict adherence to nodalization transfers the burden of code uncertainty to the uncertainty analysis of key LBLOCA parameters, every effort was made to provide a nodalization scheme that minimizes this nodalization uncertainty.

Experience indicates that S-RELAP5 plant models of W 3- and 4-loop PWRs and CE 2x4 loop PWRs will require between 200 and 500 volume component nodes, junction flow paths, and heat structures. The following figures show the modeling techniques.

Figure 4.3, Loop Nodalization

Figure 4.4, Reactor Vessel Nodalization

Figure 4.5, CE 2x4 and Westinghouse 3- and 4-Loop Plant Vessel Downcomer Configuration

Figure 4.6, Core Nodalization - Axial Plane

Figure 4.7, Core Nodalization - Cross-Sectional Plane

Figure 4.8, Upper Plenum Nodalization - Axial Plane

Figure 4.9, Upper Plenum Nodalization - Cross-Sectional Plane

Figure 4.10, Emergency Core Cooling System Nodalization

Figure 4.11, Double-Ended Guillotine Break Nodalization

Figure 4.12, Double-Ended Split Break Nodalization

The following sections discuss the nodalization of each major plant component in the context of the PIRT (as presented in Section 3.3) and describes the evolution of the nodalization schemes.

The nodalization methodology has been derived for LBLOCA. The application of the developed guidelines may not capture expected phenomena or may exhibit unacceptable variability for calculations other than LBLOCA.

4.2.2 Numerical Considerations

The nodalization of a particular model translates into a computational array used to solve the mass, momentum, and energy equations; thus, numerical constraints also must be considered in the sizing and configuration of component volumes. In general, competing criteria exist for defining nodalization. The primary numerical issues of concern are accuracy, numerical stability, and code variability. While optimizing all three is necessary to have useable results, some code variability can be tolerated as long as it is reasonably defined (Appendix C). However, numerical stability must be assured before performing any production calculations to assess accuracy through code/data comparisons.

In general, the RELAP5 series of codes has inherited a solid foundation with regard to numerical stability, as discussed in Reference 9. However, nodalization and time step decisions both can influence numerical stability. It is generally understood that numerical solutions are well behaved if the number of mesh points is sufficiently small. Such small nodes will require equally small time steps to satisfy the Courant stability requirement, leading to long uneconomical code execution times. Conversely, it has been shown that modeling interfacial drag contributes to the stability of coarser mesh models for two-phase flow codes, such as RELAP5 (Reference 24). While this stabilizing condition created by modeling interfacial drag actually works to destabilize the solution for very small mesh sizes, it also supports the coarser mesh models required for economical code execution times. As a result, considering strictly hydraulic phenomena, spatial mesh configuration is not a high concern for numerical stability.

For code accuracy, mesh sizing does become more important for heated surfaces. Steep temperature gradients will influence the adjacent fluid conditions. For this reason, smaller mesh sizes are used on heated surfaces to capture expected phenomena.

The final figure-of-merit for quantifying code variability can come from calculations of hot rod PCT. For a set of equivalent input models, differing only in time step (constrained to be less than the Courant limit), comparisons of PCT traces can be used to evaluate expected code variability. By using this approach, nodalization decisions can be made in an effort to minimize the impact of code variability.

In summary, the iteration process for defining a nodalization methodology included decisions to change a component nodalization based on the analysis of either assessments (integral- and

separate-effects) or plant sensitivity studies. These calculational results were generally used to confirm the adequacy of a chosen nodalization scheme; however, sensitivity studies also were performed to quantify the impact on peak clad temperature. In some instances, the effect of a trial nodalization scheme produced unacceptable variability in PCT results.

4.2.3 Loop Model

The loop includes those components outside the reactor vessel, including the pressurizer and ECCS. For W and CE PWRs supported by this methodology, all loops are modeled individually (i.e., the unbroken loops are not lumped into a single combined loop). Each loop models the hot-leg piping, steam generator primary and secondary fluid volume and heat transfer, pump suction piping, and pump discharge cold-leg piping. Each loop also contains modeling of the accumulator and high- and low-pressure injection ECCSs. The nodalization scheme is presented in Figure 4.3 for a sample loop with the pressurizer.

The following are key features and assumptions for the reactor coolant loops.

- []
- []
- The nodalization detail for the coolant loops, pressurizer, and primary and secondary sides of the steam generators was selected to give consistent results without increasing running time because of excessive nodalization
- []

Assessment of loop nodalization comes from various facility test programs, including SCTF, CCTF, LOFT, Semiscale, and, to a lesser extent, UPTF. In addition, the W/EPRI 1/3 Scale Steam/Water tests, a separate-effects test examining ECC mixing in the cold leg, also is a useful assessment. Acceptance of nodalization schemes was based on the general agreement in code/data comparisons for pressures, differential pressures, mass flow rates, and heat structure temperatures.

4.2.3.1 Hot Leg

The hot leg connects the reactor vessel to the steam generator inlet plenum. [

]

[

] The entrainment of droplets from the reactor vessel will enhance the effect of steam binding, which will inhibit reflood. Code-to-data comparisons of tests performed on the CCTF show that S-RELAP5 overpredicts the entrainment phenomenon from the upper plenum to the hot legs. This is considered acceptable given that over-entrainment will have a conservative influence on PCT and that the relative importance of entrainment in the hot legs is moderate.

4.2.3.2 Steam Generator

The steam generator nodalization scheme is essentially identical to the traditional approach used by other large thermal-hydraulic codes such as TRAC and RELAP5 (References 4 and 23). [

]

The dominant phenomena of importance are the steady-state heat balance and steam binding during reflood. Heat balance is ensured by the use of control systems controlling feed and steam flow depending on liquid level and recirculation ratio. Plant sensitivity studies examining steam generator performance during a LBLOCA have shown that all the liquid that gets carried into the steam generator vaporizes. This is the expected result; hence, this nodalization scheme is considered acceptable.

4.2.3.3 Pump Suction

[

]

4.2.3.4 Reactor Coolant Pump

The pump is a component model, meaning that the pump physics is independent of nodalization; hence, the primary objective of the nodalization scheme is to ensure consistency with the structural characteristics. [

]

4.2.3.5 Cold Leg and Break

The cold leg extends from the RCS pump discharge to and including the reactor vessel inlet nozzle. [

]

[

] The break model is either a double-ended guillotine or a double-ended split. The difference is break size and whether a flow path is modeled across the break. An investigation into code variability showed that the defined break configuration

reduces code variability associated with water property calculations. [

]

Condensation driven by the cold ECCS water coming in contact with steam is the primary phenomenological concern that may be influenced by nodalization. The parameter has been identified as one of the key uncertainty parameters for RLBLOCA; hence, any nodalization dependence is absorbed within the assessment that quantifies this uncertainty.

4.2.3.6 ECCS

The ECCS includes models for the accumulator and the piping connecting it to the RCS with sufficient detail to allow the code to accurately predict coolant flow splits for low-pressure injection flows. Figure 4.10 shows a typical nodalization for the ECCS of a three-loop plant. The dominant component in the ECCS is the accumulators. [

]

The dominant phenomena of importance are the accumulator discharge and the noncondensable gas transport following accumulator discharge. Activity in the accumulator lines can be characterized as a period of single-phase incompressible flow (accumulator water discharge) followed by a brief period of single-phase compressible flow (nitrogen gas) before a two-phase mixture (water-nitrogen) from the accumulator and the low pressure injection system. Accumulator discharge and LPSI flow are governed by Bernoulli physics for incompressible, single phase flows. Noncondensable gases will transport from the accumulator to the RCS by gas expansion and pressure forces. However, as the partial pressure at the ECCS-to-cold-leg junction drops with increasing noncondensable quality, flow will choke for a time and the upstream conditions will become independent of the downstream conditions. For this reason, the important phenomenon, rate of flow into the RCS, is dominated by the choked flow

phenomenon and any special treatment of the compressible flow problem will have a negligible effect on the outcome of the transient.

4.2.3.7 Pressurizer

The pressurizer vessel is modeled with [

] The dominant phenomena of interest are early quench and critical flow in the surgeline. Neither phenomenon will show much sensitivity to nodalization because the surgeline remains choked during the period in which these concerns are important (blowdown).

4.2.4 Reactor Vessel Model

The key components of the reactor vessel are the downcomer, lower head and plenum, core, and upper head and plenum. The nodalization is presented in Figure 4.4. The key features and assumptions for the reactor vessel are as follows:

- []
- []
- []
- []

4.2.4.1 Downcomer

The reactor downcomer is modeled for the RLBLOCA analysis using [

]

For asymmetric cold and hot leg connections to the reactor vessel, the only practical nodalization option is [

]

The dominant downcomer LBLOCA phenomena (condensation, hot wall effects, multi-dimensional flow, CCFL, and entrainment) affect the refill period. These phenomena primarily influence the duration of ECCS bypass. With the exception of multidimensional flow, sensitivity of these phenomena to downcomer nodalization is not expected (condensation and hot wall effects are selected uncertainty parameters). The collective sensitivity of these phenomena was evaluated by varying the azimuthal node sizes in the UPTF input model. The UPTF model for the sensitivity study was simplified by neglecting heat structures; hence, the influence of the hot wall phenomena cannot be determined from this assessment.

The UPTF Test 6 experiments investigated the countercurrent flow of steam and ECC water in the downcomer during the end-of-blowdown and the refill phases of a four-loop PWR LOCA. Test 6 consisted of five separate quasi-steady runs with essentially the same boundary conditions, but with different core steam flows ranging from 100 to 440 kg/s. Run 136 was the lowest steam flow case of the Test 6 series. The ECC water in Test 6 was injected into each of the three intact loops at the same flow rate.

[

] The conclusions from this study were that the lower plenum refill is relatively insensitive to downcomer nodalization for uniform ECC water injection into all intact loops. Both the base and sensitivity calculations showed conservative results when compared to measured data. Additionally, the base case model results with heat structures actually increased the conservative bias in the lower plenum refill.

A similar study was performed for the 3-loop plant model. The trial nodalization doubled the number of azimuthal sectors from [

] This configuration reduced the amount of ECC bypass, which resulted in a less severe transient.

In conclusion, the downcomer model described in Reference 12 was found to provide the best representation of the expected downcomer phenomena.

4.2.4.2 Lower Vessel

The lower vessel includes all volumes [

- []
 - []
 - []
-]
-]
- [
-]

The dominant LBLOCA phenomenon of importance that possibly is influenced by nodalization is liquid sweep-out, although this phenomenon is expected to have only a moderate influence on transient PCT. Because some multidimensional flow is to be expected, [

]

Considering that the UPTF facility is a full scale facility, the conservative bias demonstrated in the UPTF Test 6 assessment is expected to translate into a conservative bias for the sweep-out phenomenon in plant calculations.

4.2.4.3 Core, Core Bypass, and Fuel

The core region extends from the bottom of the active core to the top of the upper core support plate. [

]

The most important contributor to nodalization sensitivity is expected to be the core nodalization because it directly affects the liquid distribution in the core. The key phenomena of importance influenced by nodalization are the convective heat transfer modes, entrainment/deentrainment, multi-dimensional flow, stored energy, oxidation, core power and decay heat. Since the heat transfer modes, entrainment/de-entrainment, core power, decay heat and stored energy phenomena are treated statistically, only the multidimensional flow phenomenon is relevant for nodalization.

Axial core nodalization studies using the 3-loop plant model showed significant variability with coarse models. Given the expense of moving to a finer nodalization, the axial nodalization was defined in the range of [

] These node lengths are the smallest defined for the S-RELAP5 plant model; hence, they will define the Courant limit. [

]

Radial core nodalization studies using the SCTF assessment model has shown that the four radial ring model provides essentially the same results as on the 8 ring model. The [

]

[

]

[

] This configuration was used to give better resolution to the axial power profile. The radial widths used to describe the internals of the fuel rod are on a scale to finely resolve temperature gradients (Reference 12).

4.2.4.4 Upper Plenum/Upper Head

The upper plenum region extends from the top of the upper core support plate to the core support ledge in the vessel wall (the bottom of the upper head wall). [

]

The dominant phenomena of importance are entrainment/deentrainment, fallback (CCFL), and upper head temperature. The entrainment phenomenon is considered in the same manner as it was for the hot legs and the upper head temperature is treated statistically. Nodalization sensitivity to fallback was investigated through sensitivity studies. [

] This configuration captures the preference for fallback to colder assemblies as demonstrated in a 3-loop model test problem. The CCTF assessments were performed with

the multi-dimensional upper plenum. The results from these assessments showed general conservatism to liquid fallback.

In many plants, flow asymmetry into the upper plenum can exist. Flow can travel either directly into the upper plenum or through a support column or mixer vane and then into the middle of the upper plenum. [

] This configuration is necessary to bound the possibility of having the hot assembly under a standpipe. The standpipe will restrict liquid fallback from the upper plenum into the core relative to an open hole. [

]

4.2.5 Containment Model

Nodalization of the containment for the RLBLOCA is defined in a separate input file from the normal S-RELAP5 input. The containment model input is equivalent to the input used for the ICECON code (Reference 14), which is the FRA-ANP proprietary version of the CONTEMPT code (Reference 20). Appended to the S-RELAP5 input file is a description of the link between the S-RELAP5 input and the ICECON input. [

] S-RELAP5 drives the containment calculations with mass flow and enthalpy and the ICECON subroutines return containment pressure and temperature to update the S-RELAP5 time-dependent volumes.

The dominant phenomenon of interest related to the containment model is containment pressure. Containment pressure is treated statistically in this RLBLOCA methodology by ranging the containment volume from the best-estimate value to maximum possible free volume. Because the ICECON models provide only pressure and temperature for S-RELAP5, a simple model is adequate. This model is one volume representing the containment space surrounding the reactor vessel.

4.2.6 Plant Model Summary

The nodalization described in this section has been developed by applying the approach described in Reference 4. This nodalization development methodology was an iterative approach. The base nodalization originated through experience gained by RELAP5 users at the

Idaho National Engineering Laboratory and by ANF-RELAP and S-RELAP5 users at FRA-ANP. Nodalization has been refined from both plant and code assessment tests which, to the extent possible used the same nodalization. These studies were performed to examine the sensitivity of PCT and dominant phenomena to nodalization. Test results were used to justify any nodalization changes.

The final product of the nodalization methodology is a guideline (Reference 12) that when strictly followed defines how a CE 2x4 and W 3- or 4-loop plant should be modeled for S-RELAP5 calculations. While the uncertainty associated with nodalization is minimal, it will be included in the uncertainties determined for key LBLOCA parameters, because the NPP nodalization has been used in determining those uncertainties. Nonetheless, every attempt was made to develop a nodalization with a minimal uncertainty before any uncertainty analysis was performed.

4.3 *Definition of Code and Experimental Accuracy (CSAU Step 9)*

This section provides the evaluation of the code assessments reported in Reference 5 with respect to the RLBLOCA methodology. The code assessments from Reference 5 applicable to the RLBLOCA methodology are those discussed in Section 4.1 and listed in the assessment matrix Tables 4.2 and 4.3. These assessments were chosen to address the important PIRT phenomena identified in Table 3.4. The cross correlation between assessments and PIRT phenomena is provided in Table 4.3. In addition, some assessments were chosen to address issues of code scalability. These assessments and the discussion with respect to scalability are provided in Section 4.4.

One purpose of the assessments is to determine S-RELAP5's capability to predict the important phenomena in the large-scale PWR systems. Section 4.2 discusses appropriate nodalization to represent the PWR system components. For the assessment results to apply to the large-scale PWRs, nodalization used in the assessments must be consistent with the large-scale plant nodalization in the regions where the phenomena are being assessed. As far as possible, FRA-ANP used the plant nodalization described in Section 4.2 and the S-RELAP5 input guidelines (Reference 12) to derive assessment nodalizations which are consistent with the PWR application nodalization. However, unique features of the small-scale facilities sometimes require deviations from the guidelines. The detailed nodalizations for the experimental facility assessments are given for each assessment in Reference 5. For the most part, the assessment

nodalizations are consistent with the plant application, and where deviations have been made, the reasons for the deviations and the effects on results are discussed.

4.3.1 Separate Effects Tests (SET)

Separate effects tests from 15 different facilities have been used to assess the capabilities of the S-RELAP5 and RODEX3A codes to predict LOCA and transient phenomena. The detailed results comparing calculations against measured test data are given in the S-RELAP5 code verification and validation report, Reference 5. The S-RELAP5 code is used in multiple methodologies; therefore, it is appropriate that the code validation assessments are included as part of the code documentation. However, the SET assessments in Reference 5 also provide the information to assess code capability for the RLBLOCA methodology. Detailed results from Reference 5 will not be repeated in this report. Instead the appropriate information will be extracted and summarized with respect to the LBLOCA phenomena addressed. Table 4.3 shows the SET facilities, the tests that were selected, and the phenomena from the PIRT to be addressed. The following sections follow the format of Table 4.3 in providing the results of the assessments in order of the listed facilities.

4.3.1.1 THTF Heat Transfer

The Oak Ridge National Laboratory (ORNL) thermal-hydraulic test facility (THTF) was used to perform numerous heat transfer tests using full-length electrically heated fuel rod simulators. The facility, tests, and assessments are detailed in Section 3.1.2 of Reference 5. The assessment tests consisted of 22 steady-state film boiling tests, three transient boiloff tests, and two sets of reflood tests (11 tests).

The purpose of the assessments using the steady-state tests were to get optimum values of the bias for the CHF correlation and for the post-CHF heat transfer correlation. [

]

The ratio of the measured heat transfer coefficient (HTC) to the calculated HTC (from S-RELAP5) was evaluated statistically (see Figure 4.13). The frequency plot, Figure 4.14, showed the ratio to be non-normal, with a downward skew. The ratio was fit using a conservatively bounding normal distribution. This distribution is slightly conservative with respect to the distribution of measured scaling factors, as shown in Figure 4.15, and the

uncertainty in the post-dryout HTC for S-RELAP5 can be represented by [

]

The range of HTC bias variation was then applied to three sets of transient data: one in blowdown and two in reflood. The range of variation determined in the steady-state analysis was sufficient to allow the predictions by S-RELAP5 to bound the measured data for the blowdown cases and for nearly half the reflood cases. With one exception, for the other reflood cases, the S-RELAP5 predictions for quenching were conservatively slow. [The one case in which the prediction was not slow was the lowest reflood case.] The temperatures predicted by S-RELAP5 for all the other cases in that test series bounded the measured temperatures. The underprediction of the quench time for the one case is quite anomalous and, because of the very low flow rate, could well be an artifact of the boundary conditions.

For the second set of reflood tests, S-RELAP5 somewhat overpredicted the quench time. Overall the results of the transient test predictions by S-RELAP5 are acceptable. In the bulk of the cases, the uncertainties for the HTC bias were sufficient to make the data and the predictions agree. For those reflood cases that had data outside the predicted range, the predictions by S-RELAP5 were conservative.

The CHF bias is applied for RLBLOCA calculations, and the statistical information on heat transfer is used to derive the uncertainty multipliers on heat transfer presented in Section 4.3.3.2.

4.3.1.2 THTF Level Swell

Calculations for the three ORNL THTF Level Swell Tests, 3.09.10j, 3.09.10m, and 3.09.10dd, were carried out with S-RELAP5. Section 3.1.3 of Reference 5 presents the details of these assessments. Comparisons of calculated and measured void fractions for the three tests are shown in Figures 4.16 through 4.18, along with results using RELAP5/MOD3.2. The void fractions calculated by S-RELAP5 are slightly lower than the data in two cases and are very close to the data in the third, Test 3.09.10j. The mixture level lies between the pre-CHF and post-CHF regions. Both the data and the calculations show that the post-CHF region has a void fraction of 1 (single-phase steam) or nearly 1. Such a condition is typical of the core during a SBLOCA.

For S-RELAP5 calculations, the flow regime below the mixture level belongs to slug flow. Therefore, the purpose of this assessment was to validate the constitutive models of the slug flow in the reactor core. The subcooled boiling model is responsible for the starting point of measurable void fraction. The interphase heat transfer model takes care of the vapor generation from heat input to the fluid. The interphase friction correlations for the slug flow determine the void profile in the pre-CHF region.

The small differences between the calculated and measured void fractions indicate that the interphase correlations apply. The agreement is particularly good for Test 3.09.10j, which has the lowest pressure (609 psi) among the three tests. For the two higher pressure cases, Test 3.09.10m (1009 psi) and Test 3.09.10dd (1173 psi), the calculated void fractions are slightly lower than the data. This indicates that the interphase friction is computed somewhat lower than it should be at high pressures. The lower interphase friction tends to result in a longer dryout period and, therefore, higher clad temperatures for a SBLOCA.

4.3.1.3 GE Level Swell

The GE Level Swell Test, 1004-3, is essentially a small break blowdown of a vertical vessel 14 ft high by 1 ft in diameter. The vessel was initially pressurized to 1011 psi and filled with saturated water up to the 10.4 ft elevation. The void fraction distribution was measured axially in the test. This assessment provides a test of the two-fluid interphase models in predicting the flow regimes and void fraction distributions that occur under depressurization conditions. Section 3.6 of Reference 5 gives the detailed assessment results of the GE level swell test.

The purpose of this assessment was to validate some of the interphase heat transfer submodels. The key model affecting these assessments is the interphase friction for the bubbly and slug flows. Comparisons of measured versus calculated void fraction distributions are made at two transient times, 40 and 100 seconds. Figures 4.19 and 4.20 show the S-RELAP5 calculated void fraction results along with data and RELAP5/MOD 3.2 results. Results from S-RELAP5 compare well with the data. The void fractions calculated by S-RELAP5 are within the range of experimental uncertainty, providing excellent agreement. The calculated flow regimes are bubbly flow below the void fraction of 0.25; slug flow from the void fraction of 0.25 up to the two-phase mixture level position, which occurs at around the void fraction of 0.3 to 0.6; and annular-mist flow (very close to single-phase steam) above the mixture level. The results

indicate that, for this slow transient condition, the two-fluid interphase friction model implemented in S-RELAP5 is applicable.

The jump of void fraction from ~ 0.4 to ~ 0.99 within neighboring volumes distinctly defines the location of a two-phase mixture level. The interphase friction models for slug flow, vertical stratification, and annular-mist flow work in harmony to produce a smooth, but sharp transition from a low void fraction region to a very high void fraction (close to 1) region.

In a non-equilibrium code such as S-RELAP5, the phase exchange (vapor generation) process during blowdown is calculated through the use of an interphase heat transfer model. The calculated liquid and vapor (steam) temperatures are close to the saturation temperature. This shows that the interphase heat transfer submodels described in Section 3.4 of the code manual (Reference 9), particularly those for the metastable state conditions, are appropriate and adequate for treating the depressurization phenomena.

4.3.1.4 FRIGG2

The FRIGG2 void distribution experiments were performed in the Caps Loop Facility in the late 1960s. The test section had 36 heated rods and was designed to give a full-scale simulation of a boiling channel for the Marviken reactor. There are 27 axial void distribution tests. The void distribution was measured by the multi-beam gamma method. Section 3.10 of Reference 5 describes the FRIGG2 assessments.

The assessments were run to validate the S-RELAP5 subcooled boiling model and interphase friction model for pre-CHF flow regimes. The tests are steady state and the axial void distribution data are well-suited for the purpose. Calculations of all 27 tests were carried out.

Calculations of the 27 FRIGG2 axial void distribution tests produced good to excellent code-data comparisons, as shown in Figures 4.21 through 4.30. In the plot of calculated versus measured void fraction shown in Figure 4.31, the points are scattered around and close to the diagonal line. The mean of 170 points of calculation over measurement is 0.98 and the standard deviation is 0.096. The results confirm the applicability of the S-RELAP5 interphase friction model for the pre-CHF flow regimes, particularly the slug flow, for the core geometry.

4.3.1.5 Bennett Tube

The Bennett Heated Tube Tests were conducted by the UKAEA Research Group to measure the dry-out [or critical heat flux (CHF)] location and the surface temperature profiles in the region beyond the dry-out point. Calculations for Test Case 5358 and Test Case 5379 were performed. The main purpose of the assessment is to evaluate the applicability of the Biasi CHF correlation. Post-CHF heat transfer also was examined. The detailed assessment results are given in Section 3.2 of Reference 5.

Two Bennett heated tube tests were assessed, a low-flow test (5358) and a high-flow test (5379). As shown in Figures 4.32 and 4.33, the calculated CHF positions agree well with the data for these two cases. For the low-mass-flux case, the wall temperatures in the film boiling region are well predicted. The calculated temperature rise immediately after the CHF is not as high as the measured temperature. For the case of high mass flux, the calculated wall temperature stays rather flat in the post-CHF region and is higher than the data in the top-end region. For the low-mass-flux case, the calculated temperature continues to rise in the post-CHF region and catches up with the data. The mass flux for the high-flow case is well outside the LBLOCA conditions. In conclusion, the results of this assessment validate the S-RELAP5 correlations for predicting CHF and dry-out.

4.3.1.6 FLECHT and FLECHT SEASET

Full Length Emergency Cooling Heat Transfer - System Effects And Separate Effects (FLECHT SEASET) Tests and Full Length Emergency Cooling Heat Transfer (FLECHT) Low-Flooding-Rate Skewed Tests (Skewed) have been widely used to assess system codes. The S-RELAP5 assessments for these facilities are given in Section 3.3 of Reference 5.

The purpose of these assessments was to evaluate the S-RELAP5 code heat transfer and hydrodynamics. In addition, core axial nodalization studies were performed to validate NPP nodalization. The FLECHT SEASET facility used the W 17 x 17 geometry for the reference fuel design; the FLECHT facility used the W 15 x 15 geometry for the reference fuel design. The forced reflood separate-effect tests are with injection or flooding rates that are very demanding for simulations with the realistic system codes. The FRA-ANP selected the FLECHT SEASET tests 31504, 31701, 31302, 31203, 31805, 32013, and 34209, and FLECHT Skewed Tests 13609 and 13914 to validate the reflood modeling capability of S-RELAP5 for the RLBLOCA

methodology. For LBLOCA reflood, the selection covers the whole range of pressure, subcooling, and flooding rate, and includes cosine and skewed axial power profiles.

The important parameters for assessing the code calculation against the measured data are:

- PCT
- Cladding surface temperature history
- Steam temperatures
- Heat transfer coefficients
- Differential pressures
- Mass inventory
- Liquid carryover
- Rod quench time.

The PCT is one of the required criteria for LBLOCA licensing. PCT is the maximum value of all cladding temperatures. With the power specified, the cladding surface temperatures at various elevations depend on the heat transfer rates from the surface to the fluid. The fluid conditions, including the steam temperature and void distribution, determine the heat transfer rates. The differential pressures indirectly measure void distribution under low-flow conditions. The total mass in the test section indicates how much of the injection water stays in the test section to cool the rods and how much is entrained out. The liquid carryover is the amount of liquid entrained out of the test section and is closely related to the mass inventory. The rod quench time depends strongly on the transition boiling correlation used in the code. Information about the eight parameters listed provides a basis for understanding the computed results compared with the measured data.

Conclusions from the FLECHT-SEASET and FLECHT Skewed assessments in terms of the important parameters are provided in the following paragraphs.

Peak Cladding Temperature

Figures 4.34 through 4.42 show the calculated maximum surface temperatures and the measured temperature data at various elevations in the simulated fuel assemblies for the various tests. The S-RELAP5 calculated PCT is in good agreement with or acceptably higher than the measured data. The calculated maximum clad temperature being generally higher than the measured data at all elevations. The calculated maximum clad temperature more

closely matches the measured data below the test section mid-plane. However, the calculated maximum clad temperatures generally are much more conservative above the test section mid-plane. The conservatism above the test section mid-plane is exaggerated even more when the axial power profile is top peaked. The calculated maximum clad temperature conservatism generally increases with decreasing reflood rate, decreasing system pressure, or increasing inlet subcooling

Rod Surface Temperatures

The calculated temperature at a specified elevation has been compared with the measured temperature near the same elevation. The quench times are calculated well at the lower elevations for all tests and at all elevations for the lower flooding rate tests.

The calculated rod surface temperature during the temperature rise portion of the test compares well with the measured data. However, the quenching time is calculated late for the highest reflood rate test, Test 31701. The quenching time is progressively earlier for the tests with lower reflood rates until, at the lowest reflood rate, S-RELAP5 calculates a quenching time that is too early. S-RELAP5 has calculated good agreement of the complete transient at the 78 in elevation for the three intermediate reflood rate tests.

S-RELAP5 calculated rod surface temperatures are in good agreement for the complete transient at all elevations for the high system pressure test, Test 32013, and for elevations below 90 in for the low pressure test, Test 34209. For Test 34209, at elevations at or above 90 in, the rod surface temperature is significantly overpredicted.

For the FLECHT Skewed tests, S-RELAP5 tends to predict a higher maximum clad temperature at all elevations and tends to predict late turnaround. In the low subcooling test, Test 13914, S-RELAP5 tends to predict a late quench time. In the high subcooling test, Test 13609, S-RELAP5 tends to predict an earlier quench time at or below an elevation of 82.8 in.

For FLECHT SEASET Test 31504, the PCT occurs in the region above, but close to, the mid-plane of the test section. The calculated rod surface temperature in the temperature rise period is in good agreement with the measured data.

Steam Temperatures

Steam temperature is one of the important parameters in determining the heat transfer rate during the temperature rise period. Figures 4.43 through 4.51 show the calculated and measured steam temperatures for the FLECHT and FLECHT-SEASET tests. The calculated steam temperature generally is lower than the measured steam temperature for the FLECHT-SEASET tests and higher than measured steam temperature for the FLECHT skewed tests.

Differential Pressures

Differential pressure is an indirect measurement of void distribution, which is an important property for calculating the heat transfer rate. The calculated differential pressures are somewhat higher than the measured data in the period between 200 and 300 seconds for the three lower reflood tests. S-RELAP5 calculates excess liquid accumulation within the region between the 72 and 84in elevations during this period. This happens after the PCT has occurred and thus has no effect on PCT.

Heat Transfer Coefficient

The heat transfer coefficient normally is defined with respect to phase or saturation temperature, depending on the heat transfer mode. This definition is used in S-RELAP5 and the other codes in the RELAP5 series. The heat transfer coefficient data usually are deduced from the heat transfer measurements with reference to the saturation temperature. Good agreement between the calculated and measured data is observed for the dispersed-film-boiling heat transfer regime (before time = 200 s) leading to a good calculation of the PCT. Figures 4.52 through 4.60 show calculated versus measured heat transfer coefficients for the tests.

Mass Inventory

The calculated water mass accumulation generally is less than measured. Most of the mass accumulation occurs early in the transient as the lower half of the test section is filled. Once the water accumulation reaches the high power mid-plane region of the test bundle, the water accumulation becomes a balance between injected water entering and entrained and evaporated water leaving. Figures 4.61 through 4.69 compare calculated versus measured liquid mass inventory.

Liquid Carryover

The calculated carryover generally is greater than the liquid carryover derived from the measured carryover tank level, as shown in Figures 4.70 through 4.75 for the FLECHT-SEASET tests. This is consistent with the lower calculated mass levels in the test bundle and would indicate that S-RELAP5 is overpredicting the entrainment in the bundle.

Rod Quench Time

The calculated quench time generally is greater than the mean quench time derived from measured rod thermocouple data at high elevations in the FLECHT-SEASET test assembly. The magnitude of the delay generally increases with increasing elevation in the test assembly. These trends do not hold true for the lowest (Test 31805) and highest (Test 31701) reflood rate tests. Quench time comparisons are given in Figures 4.76 through 4.81.

Summary

Data comparisons for the eight key parameters were made for all tests calculated. The agreement is good, with S-RELAP5 generally calculating peak cladding temperature (PCT) in agreement with or higher than the measured data. These data will be used to derive the heat transfer parameter multipliers shown later in this section.

Sensitivity Studies

Timestep and nodalization sensitivity studies also were performed using FLECHT SEASET Test 31504 to demonstrate the solution convergence of the S-RELAP5 treatment of the reflood transient. FLECHT SEASET Test 31504 was chosen because it is a demanding low flooding rate (0.97 in/s) [2.46 cm/s] test. High-flooding-rate tests are known to be easier for the advanced system codes to simulate because of early temperature turnover and no sharp discontinuities in the void distribution.

The timestep and nodalization sensitivity studies showed that calculated rod surface temperatures are not sensitive to timestep sizes, particularly in the temperature rise period. The calculated results had some small variations with the node sizes, noticeably in the quench period. The local maximum cladding temperatures (as a function of elevation) computed with different node sizes and different time-step sizes are clustered in an extremely narrow band.

This band is much narrower than the corresponding measured data band. Also, the calculation points are distributed in the high-temperature outer envelope of the measured data.

Figures 4.82 through 4.84 show results from the nodalization and time step calculations.

[

]

4.3.1.7 PDTF/SMART Tests

The Product Development Test Facility (PDTF) Small Array Reflood Test (SMART) tests were performed by FRA-ANP to show that the high thermal performance (HTP)-type (FRA-ANP-type) spacer was thermodynamically equivalent to the FOCUS™ (mixing vane)-type spacer with respect to reflood and PCT. The data from these tests provides simulations of FRA-ANP prototypic fuel rods under LOCA reflood conditions. Therefore, FRA-ANP used the data from the SMART to perform verification and validation assessments on the S-RELAP5 thermal-hydraulic simulation code in support of FRA-ANP's RLBLOCA methodology. The tests are similar to the FLECHT-SEASET tests and assess the same phenomena, except that they were performed in a FRA-ANP facility and used hardware prototypic of FRA-ANP 15 x 15 fuel. The assessments also examined the effects of spacer modeling on reflood phenomena. The details of the assessments are reported in Section 3.4 of Reference 5.

The test assemblies were 6 x 6, full-height, simulated PWR assemblies. The rod diameter and pitch were characteristic of FRA-ANP's 15 x 15 PWR fuel design. The test assembly had a uniform radial power distribution and a chopped cosine axial power distribution. The tests simulated five different flooding conditions. Of the five flooding rate conditions, four were constant-flooding-rate tests and one was a variable-flooding-rate test. The constant-flooding-rate tests had flooding rates of 0.6, 1, 2, and 4 in/s. The variable-flooding-rate tests started at 8 in/s and ramped rapidly to a constant 1-in/s flooding rate. The 0.6-in/s tests were terminated prematurely; therefore, they were eliminated for the verification and validation of S-RELAP5.

* FOCUS is a trademark of Framatome ANP.

Four tests were chosen to evaluate S-RELAP5's ability to predict maximum clad temperature (MCT) at individual elevations and overall PCT. The four tests that were explicitly modeled are listed in Table 4.5.

The current methodology for RLBLOCA does not explicitly model spacers in the core. These assessments are being performed to evaluate the acceptability of this methodology. Therefore, in addition to evaluating the performance of S-RELAP5 with the current spacer-free modeling, a model that incorporates spacer volumes also was created and evaluated. This additional model only addresses the reduction in flow area through the spacer.

Figure 4.85 shows the PCT for each test as predicted by the S-RELAP5 models with and without spacer volumes, as well as the PDTF SMART test data. As can be seen, the simulations without spacer volumes, but with appropriate junction loss coefficients, predict a PCT within the range of the data (excellent agreement) for each flooding condition except for the 4-in/s case. For this test, the prediction is 34 °F (19 °C) below the range of the data. This is not a significant difference (good agreement). The model without spacer volumes represents the current Realistic LBLOCA methodology. The predictions of differential pressure across the test assembly and rod surface temperature versus time for the model without spacer volumes also were found to be adequate when compared to test data.

The effect of spacer heat transfer enhancement can be seen when comparing measured maximum clad temperatures for the 2 peak power nodes at the axial center of the assembly for tests KH02B and KH03B (the 4-in/s flooding rate for test KH01B is large enough such that spacer heat transfer enhancement is not as important). These 2 nodes have identical power peaking and, since they are adjacent nodes, they should see similar heat transfer environments. However, the upper peak power node spans a spacer. Comparison of measured maximum clad temperature data at these nodes shows a temperature differential between the two locations (72 in versus 77 in) of about 110°F (43°C). Therefore, this is the inferred spacer benefit from the measured data.

The model without spacer volumes predicted a more conservative PCT than the model with spacer volumes for every case. Also, the predictions of differential pressure across the test assembly and rod surface temperature versus time showed the simulation predictions to be in

good agreement with each other. Generally, the model without spacers predicted higher rod surface temperatures and a smaller total pressure drop than the model with spacer volumes.

Figures 4.86 through 4.89 show the predicted PCT and the maximum clad temperature (MCT) at each nodal elevation compared to the available data for each test. These figures show that the predicted PCTs and MCTs generally are within the range of the data. Also, it can be seen that while the model with spacer volumes generally predicts lower MCTs and does a better job of predicting rod surface temperature in the vicinity of the spacers, generally little difference is apparent between predictions at locations away from spacers. Because of the enhanced heat transfer associated with the spacer, PCT does not occur at the spacer location. Therefore, the superior ability of the model with spacer volumes to predict rod surface temperatures at spacer locations is unimportant with respect to this key analysis parameter.

In conclusion, this analysis shows that the S-RELAP5 code can adequately predict the reflood thermal-hydraulic behavior for the PDTF SMART reflood tests. Also, the analysis shows that the current methodology, which does not include the flow area restrictions associated with spacer volumes in the core, is an equivalent or conservative model compared to a model that includes spacer volumes.

4.3.1.8 Marviken Tests

The Marviken Test Facility and test data are well documented. The facility has four main parts: a full-scale boiling water reactor (BWR) vessel, a discharge pipe attached to the bottom of the vessel, a test nozzle connected to the downstream end of the discharge pipe, and a rupture disk assembly attached to the downstream end of the nozzle. Nozzles of various length-to-diameter ratios are used in the tests.

The assessment of the Marviken full-scale critical flow tests was performed to provide the uncertainty information for the S-RELAP5 critical flow model to support the S-RELAP5 RLBLOCA project. The Marviken full-scale critical flow test data were used in the CSAU methodology (Reference 4) to determine the critical flow multipliers and uncertainties for the break flow model. The Marviken test data also are widely used in assessing critical flow models for various system codes.

Nine Marviken tests were selected for the assessments based on the availability of electronic data. The test numbers for the nine tests are: 2, 6, 8, 16, 17, 20, 22, 24 and 25. Test 24 has

been used to assess the RELAP5 critical flow model beginning with RELAP5/MOD1 and Test 22 has been used to assess RELAP5/MOD2 and RELAP5/MOD3. The break flow data are assumed to be accurate, (i.e., uncertainties of data are ignored, when the uncertainties of the S-RELAP5 break flow model are computed).

Details of the Marviken assessments are given in Section 3.5 of Reference 5 and are only summarized here. The calculated critical flow mass fluxes and the measured values are sampled at 1-second intervals. A total of 587 pairs of calculated and measured values from the 9 tests are collected. Figures 4.90 to 4.98 show the code-to-data comparisons of mass flow rates at the break. The calculations agree well with the data. The worst situation is in the subcooled-to-two-phase transition region where the differences are larger.

Figure 4.99 shows the comparison of the calculated mass flux versus the data. The figure clearly shows that the comparison points are uniformly scattered around the 45 degree line. The ratios of (calculated mass flux minus data)-to-data are used to compute the statistics. [

]

The ratios given in Figure 4.100 were evaluated first by separating the subcooled choking and two phase choking and then as an overall data set. [

]

4.3.1.9 Westinghouse/EPRI 1/3 Scale Tests

The W/EPRI 1/3-scale test assessments were performed to assess the ECC/steam mixing process during the reflood-accumulator and reflood-safety injection period in a typical PWR LBLOCA scenario.

The principal feature of the test apparatus was a simulated cold leg that was fabricated from a 10.42-in, inside diameter (I.D.) straight pipe. Two ECC injection points were provided so that the pipe lengths downstream of the injection point were either scaled to a typical PWR or were full length. Superheated steam from the boiler flowed through the inlet surge tank and an inlet flow chamber before entering the test section. The inlet flow chamber was designed to yield a uniform velocity profile entering the test section. Cold water from the storage tank entered the test section through either the scaled length ECC injection point or the full length injection point. The effluent fluid exited the test section into the outlet surge tank. The surge tanks upstream and downstream of the test section help maintain constant pressure boundary conditions for circumstances where large pressure oscillations occurred inside the test section. The test section was fitted at the top and bottom with thermocouples. This provided temperature data for both the vapor and liquid phase in the case of stratified flow inside the test section. Pressure drops along the test section also were measured.

One of the important phenomena identified in PWR LBLOCA is the mixing of the ECCS water and the steam in the cold leg during the LBLOCA refill and reflood phases. The controlling parameter is the interfacial condensation heat transfer coefficient. Its impact on the PCT calculation needs to be evaluated. To do this, the uncertainty range in the interfacial condensation heat transfer coefficient for the mixing process must be determined based on an assessment against relevant data. In this study, data from the W/Electric Power Research Institute (EPRI) one-third scale study was selected. This data has been determined to be appropriate and representative of conditions encountered in the reflood and post-reflood phases of a PWR LBLOCA.

Section 3.8 of Reference 5 documents the assessment results and a sensitivity study of the multiplier on the interfacial heat transfer coefficient. The results are used to support the overall application of the RLBLOCA methodology.

To confirm the appropriateness of the data, the results of a typical LBLOCA scenario for a W 3-loop PWR were examined. The range of conditions considered in the test matrix is similar to that found in the sample calculation. Hence, the test matrix selected is appropriate for the present assessment, and can be used to determine the uncertainty associated with the code's capability to predict the ECC/steam mixing process during the reflood period of a LBLOCA.

For the S-RELAP5 assessments, the difference between the liquid effluent temperature and the injection temperature was the primary data because it relates directly to the interfacial condensation heat transfer rate over the entire test section. The capability of S-RELAP5 in predicting the interfacial condensation heat transfer in the mixing of ECCS water and steam can therefore be assessed by calculating this temperature difference and comparing the calculated temperature difference results to measured data.

[] To be consistent with the FRA-ANP guidelines, a plant-consistent model is therefore developed for the assessments. The determination of the interfacial condensation multiplier is based on this plant-consistent model.

Nineteen runs were assessed; 9 correspond to the reflood phase after accumulator injection and the other 10 to the reflood accumulator injection phase. The primary result sought in this study is the effluent liquid temperature (i.e., the liquid phase temperature at the exit of the test section). For all the cases run, the thermal hydraulic variables were sufficiently steady at 100 seconds except for several reflood-accumulator tests. Hence the effluent temperatures at 100 seconds were used to compare with the measured data.

Table 4.6 compares the calculated and measured effluent temperature for all the cases, using the plant-consistent model. The information from Table 4.6 is plotted in Figure 4.101. The total amount of interfacial heat transfer is approximately proportional to the difference between the liquid effluent temperature and the inlet temperature (i.e., ECC liquid temperature). Denote this difference by ΔT . The ratio of the calculated ΔT and the measured ΔT approximates the ratio between the code-predicted condensation heat transfer and the actual value. Hence define R as

$$R = \frac{(T_{\text{effluent}} - T_{\text{in}})_{\text{measured}}}{(T_{\text{effluent}} - T_{\text{in}})_{\text{calculated}}}$$

Deviation from unity of R represents a code bias in predicting the interfacial condensation heat transfer during the ECC/steam mixing process. [

]

S-RELAP5 was assessed against selected tests from the W/EPRI 1/3 scale condensation experiment. A bias was defined that approximately represents the ratio of the experimental and code-calculated interfacial condensation heat transfer. This bias was used to assess the accuracy of the code in predicting the interfacial condensation heat transfer during the ECC/steam mixing process. [

]

4.3.1.10 FRA-ANP CCFL Tests

As described in Section 3.9 of Reference 5, a small-scale test facility was used to flow test the upper tie plates (UTPs) of interest and determine whether or not the S-RELAP5 calculation of CCFL was sufficient (i.e., accurate or conservative). UTPs from FRA-ANP designs for W 15 x 15 and 17 x 17 fuel assemblies and a CE 14 x 14 fuel assembly were obtained and flow tested in the mini-loop of the PDTF. The testing consisted of measuring the liquid penetration in an upflow air channel containing the UTP. Kutateladze parameters were calculated from the measured data and compared to the corresponding flooding curve predicted for the geometry by the S-RELAP5 CCFL model.

The mini-loop is a Lexan test loop designed to do part-array testing for air/water evaluations and/or flow visualization studies. It was configured to spray water into the top of the test chamber while air was injected into the lower portion of the test section. The test chamber was sized to contain a 5 x 5 bundle with four spacers and a UTP. Instrumentation is provided to monitor flows, pressures, temperatures, and water levels.

The generic test bundle consisted of a lower flow straightener, four spacers, and 24 rods in a 5 x 5 array. The bundle was situated in the test channel such that it was held a prototypic distance from the UTP test section. The UTP section was supported by the test channel and

not connected to the bundle. To ensure proper isolation of the UTP effect, the topmost spacer was situated approximately 12 in below the UTP. The same rod and spacer configuration was used throughout the evaluation. Care was taken to seal the edge of the UTP to prevent unintended bypass.

The mini-loop was operated at ambient temperature and atmospheric pressure for all test conditions. Water was inserted in a disperse spray above the top of the bundle. The facility was modified to provide a means to collect the water injected during the test by installing a collection tank.

Countercurrent flow limiting (CCFL) affects the liquid fallback from the upper plenum to the core during the refill and reflood portions of the LBLOCA transient. [

]

The experimental data was converted to Kutateladze parameters for comparison to Bankoff (Reference 9). The Bankoff correlation, as used in S-RELAP5, has provisions for Wallis or Kutateladze weighting, as well as slope and intercept as user input. [

] The intercept

is modified by Tien with:

$$c' = c \left\{ \tanh \left[0.9 \left(\frac{D_i}{L} \right)^{1/4} \right] \right\}^\beta$$

where the characteristic length L is given by

$$L = \sqrt{\frac{\sigma}{g(\rho_f - \rho_g)}},$$

and where

c	1.8 (user input)
β	1.0 (user input to choose Kutateladze weighting)
D_j	tie plate hydraulic diameter
g	gravity
σ	surface tension
ρ_f	liquid density
ρ_g	vapor density

For the geometries used in the experiments, the following hydraulic diameters and resulting c' were used to calculate the Bankoff flooding curves used for comparison purposes:

[]
[]
[]

Figures 4.103, 4.104, and 4.105 compare mini-loop data with Bankoff. In all cases, the measured data is conservative (acceptable agreement) with respect to the flooding curves using the RLBLOCA parameters (Reference 12).

4.3.1.11 UPTF Tests

Section 3.7 of Reference 5 documents assessments of S-RELAP5 using the Upper Plenum Test Facility (UPTF). The UPTF was operated by Kraftwerk Union AG (KWU) in support of the 2D/3D Refill and Reflood Program. It was designed to simulate a four-loop 3900 MWt PWR primary system, and was intended to provide a full-scale simulation of thermal-hydraulic behavior in the primary system during the end-of-blowdown, refill, and reflood phases of a PWR LBLOCA. Note that end-of-blowdown defined by UPTF experimenters differs from the blowdown period defined for the RLBLOCA PIRT and consists of the period when the accumulators are flowing but the system is still depressurizing. The specific tests assessed with S-RELAP5 include selected runs from the following test series, Tests 6, 7, 8, 10, 11, 12, and 29.

4.3.1.11.1 UPTF Tests 6 and 7

UPTF Tests 6 (Runs 131, 132, 133, 135, and 136) and 7 (Run 203) were designed specifically to examine downcomer countercurrent flow behavior during blowdown, ECC bypass, and lower plenum refill with cold-leg ECC injection. The ECC injection is activated in a PWR during the end-of-blowdown and refill phases of a cold-leg break LBLOCA transient. These interactions play a key role in determining the rate at which ECC water is able to refill the lower plenum. The tests were analyzed to demonstrate the ability of S-RELAP5 to self-limit countercurrent flow in the downcomer and predict reasonable refill behavior including ECC bypass compared to experimental data.

The S-RELAP5 assessment calculations included simulations of Test 6, Runs 131, 132, 133, 135, and 136 and Test 7, Run 203. For these runs, the UPTF system was configured to simulate the late blowdown and refill phases of a cold-leg break PWR LBLOCA. These tests all were initiated with no water inventory in the lower plenum. Steam injected in the core region traveled downward to the lower plenum, then exited the vessel via the downcomer and broken cold leg. An identical pattern of ECC injection was used for all the runs analyzed, with a constant injection rate into each of the three intact cold legs. A wide range of steam flow rates was used for the various runs and, depending on the downcomer steam flow rate, the ECC water entering the downcomer either bypassed to the broken cold leg or penetrated downward to fill the lower plenum.

The following general observations regarding UPTF Tests 6 and 7 were found to be true of both the experiments and their corresponding S-RELAP5 simulations.

- Very little water was delivered to the downcomer and lower plenum during the period that the intact cold legs were filling with ECC water. Only after the cold legs were filled did a significant amount of ECC penetration to the downcomer and lower plenum begin.
- When ECC penetration to the lower plenum did occur, the rate of that penetration tended to vary inversely with the rate of steam flow in the downcomer.
- During the period of ECC penetration, ECC water from cold legs 2 and 3 (opposite the broken cold leg) tended to penetrate directly downward to the lower plenum. ECC water from cold leg 1 (immediately adjacent to the broken cold leg) tended to be bypassed to the broken cold leg.
- Highly unstable flow conditions were observed in the downcomer during the entire period of ECC injection.

The specific LBLOCA refill phenomena addressed by the analyses of Tests 6 and 7 include the following:

- Downcomer multi-dimensional effects

Both calculated steam flow and calculated ECC water flow are shown to distribute themselves azimuthally in multi-dimensional patterns that were consistent with test results.

- Downcomer countercurrent and slug flow

The various runs were performed with a wide range of downcomer steam flow rates and with two phase flow conditions including countercurrent and slug flow. In all cases, the code was demonstrated to conservatively (adequate to reasonable agreement with data) predict downcomer penetration of ECC water with the RLBLOCA lower plenum plant nodalization.

- Downcomer condensation and non-equilibrium flow

The various runs were performed with a wide range of ECC subcoolings (and downcomer condensation rates) and in all cases, the code was demonstrated to conservatively predict downcomer penetration of ECC water with the RLBLOCA plant lower plenum nodalization.

- Downcomer entrainment and deentrainment

With the RLBLOCA plant lower plenum nodalization, the code conservatively predicted the entrainment of ECC water from the intact cold legs to the broken cold leg during the cold-leg filling period, and correctly predicted full or partial entrainment of ECC water to the broken cold leg during the lower plenum refill period.

- Lower plenum sweepout

The code was shown to overestimate the lower plenum sweepout rate when the standard RLBLOCA lower plenum nodalization is used (adequate agreement with data). A sensitivity study was performed that indicates that the use of a 2-D lower plenum model improves the code prediction of sweepout and liquid level.

Figures 4.106 through 4.111 show the lower plenum liquid level as calculated by S-RELAP5 with the RLBLOCA plant lower plenum nodalization and as measured for each test run. The

code is shown to consistently underpredict the lower plenum fill rate and overpredict the amount of lower plenum sweep out during the refill period. Underpredicting the lower plenum fill rate indicates that, in the full size UPTF facility, the S-RELAP5 code is overpredicting ECC bypass. Underpredicting the rate of lower plenum fill is conservative because it delays the beginning of core recovery, which will result in the prediction of higher PCTs.

4.3.1.11.2 UPTF Test 8

UPTF Test 8 was performed to investigate the thermal hydraulic behavior of ECC water injection during the end-of-blowdown, refill, and reflood phases of a postulated LOCA. Of particular interest in the test is the pressure and fluid oscillations occurring in the cold legs. These oscillations are induced by condensation of steam from the injection of the subcooled ECC water, the formation of a liquid plug in the cold leg (slug flow regime), and the transition to the stratified flow regime. The code assessment was performed for two Test 8 runs (Run 111 and Run 112) that differed by the value of the resistance to flow applied in the pump simulator of intact loop 2. The different resistance resulted in a different steam rate into the intact loop 2.

The primary results from the comparisons of S-RELAP5 to the UPTF data for Test 8 Run 111 and Run 112 are as follows:

- A key test result was the measurement of a subcooled liquid plug filling the entire cross section of the cold leg (slug flow) at higher ECC injection rates. S-RELAP5 also predicted the plug formation at the start of the test for the higher ECC injection rates consistent with the test results.
- The experimental results and the S-RELAP5 prediction both indicate that condensation occurs at the face of the cold-leg plug.
- When the step change in the ECC flow from 400 to 250 (kg/s) occurs in the experiment, the S-RELAP5 calculation changes from slug flow to stratified flow. This corresponds directly to the start of a transition in the experiment from slug flow to fully developed stratified flow. This transition is marked by a high level of temperature oscillation that in the case of Run 112 clearly reaches the steam temperature.
- The S-RELAP5 cold-leg temperature solution is in good agreement with the measured UPTF data until the point where S-RELAP5 changes from slug flow to stratified flow. At that point, no single S-RELAP5 calculated temperature can be directly compared to the UPTF data.
- For these S-RELAP5 calculations, the predicted behavior was shown to be relatively insensitive for a maximum time step of less than 10 ms.

Figures 4.112 through 4.115 show the results from Test 8 Runs 111 and 112.

4.3.1.11.3 UPTF Tests 10 and 29

UPTF Tests 10, Run 081, and 29, Runs 211 and 212, were specifically designed to simulate upper core, upper plenum, and hot-leg fluid flow behavior during the reflood phase of a LBLOCA transient. These tests were analyzed to demonstrate the ability of S-RELAP5 to properly predict entrainment/deentrainment phenomena and to limit countercurrent flow at the UTP and upper plenum regions of a PWR during the LBLOCA reflood phase. The limiting of down flow into the core is important because water down flow into the core region provides a source of additional core cooling and reduces the likelihood of water carryout to the steam generators. The water carryout to the steam generators affects the predicted steam binding effects because of liquid vaporization in the steam generators

The S-RELAP5 assessment calculations included simulations of Test 10, Run 081, and Test 29 for a combination of Runs 211 and 212. For all of these runs, the UPTF system was configured to simulate the reflood phase of a cold-leg break PWR LBLOCA. UPTF Test 10, Run 081, and 29, Run 211/212, were separate effects tests that investigated core, upper plenum, hot leg and steam generator behavior during the reflood phase of a PWR LBLOCA with a cold-leg break. For these tests, the lower plenum and lower downcomer were filled with water to block steam flow directly from the core to the downcomer and cold legs. A mixture of steam and water was injected into the core simulator to simulate reflood steam generation and water entrainment. The injected steam and entrained water then flowed to the hot legs via the upper core support plate and upper plenum. From the hot legs, the steam/water mixture flowed into the steam generator simulators where water was separated from the mixture by cyclone separators. The separated water was stored and measured in holding tanks, while the steam (and any unseparated water) flowed onward through the pump simulators, intact cold legs, upper annulus and broken cold leg to the break junction.

Each test consisted of a sequence of phases using different steam and water injection rates. Run 081 was a 300-second transient consisting of four different flow phases. This test was flawed during the period from 50 through 150 seconds by the inadvertent leakage of steam from the lower plenum around the core barrel skirt into the downcomer and by accompanying lower plenum flow oscillations observed in the test data. This flawed test period involves the first

three phases of the test, and data from these phases is not compared with S-RELAP5 simulation results. The conditions for the four phases of this test are given in Table 4.7.

Runs 211 and 212 were 900-second transients consisting of six different flow phases. Each phase consisted of a period of constant steam flow rate and water flow rate, followed by a period of no flow. Test 211 was flawed by the inadvertent operation of drain valves in the steam generator simulator during the first two flow phases. Run 212 was a repeat of Run 211 with the drain valve problem fixed. Run 212 was flawed by oscillatory broken loop drain flow during phases 4 through 6. Consequently, the S-RELAP5 predictions will be compared to data from phases 1 and 2 (0 through 300 s) from Run 212, and data from phases 3 through 6 (300 through 900 s) from Run 211. The test parameters for the six phases in combined Run 212/211 are shown in Table 4.8.

The specific LBLOCA reflood phenomena addressed by the Test 10 and 29 analyses include the following:

- Steam generator steam binding
- Upper plenum two-phase convection
- Upper plenum countercurrent flow
- Upper plenum and hot-leg entrainment and deentrainment

The following general observations can be made regarding the S-RELAP5 simulations of UPTF Tests 10 and 29 using the CCFL inputs for the RLBLOCA methodology.

- Overall predictions of total water carryover to the steam generator simulators indicates that the code conservatively overpredicts (adequate agreement with data) the liquid carryover to the steam generators. This is conservative because it will result in an overprediction of the steam binding effect, which in turn reduces the reflood rate.
- Overall predictions of total fallback to the lower vessel region also was shown to be conservative in that the fallback to the core was underpredicted (adequate agreement with data). This is consistent with the overprediction of liquid carryover to the steam generators because more liquid will be present in the upper plenum to be carried over to the steam generators.

For UPTF Test 10 Run 081 the Kutateladze CCFL correlation is used in the S-RELAP5 code to limit down flow at the core UTP. Figure 4.116 presents a plot of Kutateladze parameters calculated from the S-RELAP5 results compared to the UPTF correlation. The comparison

shows that S-RELAP5 is correctly limiting liquid down flow, as noted by the linear upper limit of \sqrt{Kg} . [

] Figure 4.116 clearly shows the S-RELAP5 calculations are conservative relative to the UPTF correlation developed from the UPTF data.

For UPTF Test 29, Run 211/212, Figure 4.117 presents a plot of Kutateladze parameters calculated from the S-RELAP5 results compared to the UPTF correlation derived from the data. This comparison also shows that S-RELAP5 is correctly limiting liquid downflow noted by the linear upper limit of \sqrt{Kg} . Figure 4.117 shows that the S-RELAP5 calculation is conservative relative to the UPTF correlation derived from the data.

Figures 4.118 and 4.119 demonstrate the S-RELAP5 code overprediction of the liquid carryover to the steam generators. Figure 4.118 has been shifted in time to account for Test 10, Run 081, problems in the first part of the test to limit flow between the core and downcomer. Both plots clearly show that S-RELAP5 with the RLBLOCA plant nodalization conservatively overpredicts the carryover of liquid to the steam generators.

An additional set of S-RELAP5 simulations was performed using the CCFL input parameters recommended by KWU for the UPTF tests. These CCFL input parameters significantly reduced the conservatism in the S-RELAP5 predictions, indicating that the code is functioning appropriately with respect to CCFL inputs. The code prediction of carryover to the steam generators still is shown to be conservative relative to the UPTF test data. This indicates that the code entrainment/deentrainment model is conservative when applied with the RLBLOCA Kutateladze parameters in conjunction with the 2D upper plenum model.

4.3.1.11.4 UPTF Tests 10 and 12

UPTF Tests 10, Run 080, and 12, Run 014 were also specifically designed to simulate upper core, upper plenum, and hot-leg fluid flow behavior during the reflood phase of a LBLOCA transient. These tests differed from Test 10, Run 081, and Test 29 in that flow was allowed between the downcomer and core region and Test 12 included nitrogen injection. Analysis of these tests demonstrates the ability of S-RELAP5 to properly limit countercurrent flow at the UTP and upper plenum regions of a PWR during the LBLOCA reflood phase. This limiting of down flow into the core is important because water down flow into the core region provides a

source of additional core cooling and reduces the likelihood of water carryout to the steam generators with the associated steam binding effects.

UPTF Test 10, Run 080, was performed to examine countercurrent flow through the UTP and to examine co-current water down flow. The lower plenum was filled with water to a level of 1.2 m (3.94 ft), steam was injected into the core, and subcooled water was injected into the intact hot legs. The boundary conditions set up countercurrent flow of steam and water through the UTP as well as through regions of co-current water down flow.

UPTF Test 12, Run 014, was performed to examine countercurrent flow between the UTP and the upper plenum. The water level in the lower vessel at the start of the test was low enough (0.56 m, 1.84 ft) to allow steam to flow from the core to the downcomer and broken cold leg. Steam was injected into the core, and subcooled water was injected into the intact hot legs. These boundary conditions setup countercurrent flow of steam and water through the UTP.

The key parameters to be compared between S-RELAP5 simulations and test results are the down flow of water to the lower vessel region, Kutateladze countercurrent flow parameters calculated at the junctions between the upper plenum and core, and the upper plenum pressure. Reduced down flow of water to the lower vessel generally is considered to have a conservative effect because it leads to less core cooling. Figures 4.120 through 4.122 show results for UPTF Test 10, Run 080. Figures 4.123 through 4.125 give similar results for UPTF Test 12, Run 014.

For both tests, data and S-RELAP5 calculations were compared with two different sets of Kutateladze parameters. [

] For both sets of Kutateladze parameters, the S-RELAP5 code is demonstrated to conservatively limit the water downflow in the countercurrent flow mode. The degree of conservatism is significantly reduced when the UPTF experimental data parameters are used, but the code predictions remain conservative relative to the data in both tests (acceptable agreement).

The calculated UPTF water down flow also was compared with the S-RELAP5 calculated water down flow based on the two sets of Kutateladze CCFL input parameters. The results show that overall (co-current and countercurrent) S-RELAP5 conservatively underpredicts down flow. The small difference between the down flow results, despite the change in CCFL parameters,

indicates that the total down flow is primarily caused by co-current flow. This is consistent with the UPTF results which indicate break through of ECC liquid near the hot-leg upper plenum junction. The S-RELAP5 results are based on describing the core to upper plenum junction with the fuel bundle UTP area consistent with the current RLBLOCA methodology.

With respect to upper plenum pressure, the S-RELAP5 calculated upper plenum pressure and the measured data comparisons indicate that the S-RELAP5 code slightly underpredicts the pressure for all cases.

The final observation is that the presence of nitrogen in the system does not appear to have a significant impact on CCFL. One of the differences between Test 12, Run 14, compared to Test 10, Run 080, is that nitrogen was injected into the system. Comparisons of the Kutateladze parameters indicate that the presence of the nitrogen in the system does not affect either the S-RELAP5 calculation or the UPTF experimental results for CCFL.

4.3.1.11.5 UPTF Test 11

Assessment of UPTF Test 11 was made to validate the application of the S-RELAP5 CCFL model to the steam generator inlet plenum junction from the hot leg. UPTF Test 11 is a series of quasi-steady-state SETs conducted to investigate the countercurrent flow of steam and saturated water in the hot leg of a PWR. Countercurrent flow in the hot leg was simulated by venting steam from the primary system through the UPTF broken loop hot leg to the containment simulator downstream from the water separator. Simultaneously, a stream of saturated water was injected into the water separator inlet chamber. The test consisted of a series of flow conditions to map out the countercurrent flow curves at two different pressure conditions, 0.3 MPa (low pressure case) and 1.5 MPa (high pressure case).

The measured water level increase in the lower plenum of the test vessel was used to calculate the mean downflowing water rate by use of the volume versus elevation calibration curve. The upflowing water mass flow rate was separated by the cyclones and measured using the water level outside the cyclones in the water separator. At higher injected steam mass flow rates, a small part of the upflowing water was carried out by the steam to the containment simulator. To check the water mass balance, the water level in the water separator was measured and no water was drained from the water separator or from the lower plenum of the test vessel during the test.

Two S-RELAP5 input decks were created for each test series, one without the CCFL model and one with the CCFL option selected for the junction between the hot leg and inlet plenum. [

] The water and steam injection rates were input as boundary conditions into S-RELAP5 for both the low- and high-pressure test series. Figure 4.126 shows the simulation of the water and steam injection rates for the entire high-pressure (1.5 MPa) test series. At 12 seconds, water injection started and reached 9.8 kg/s within 0.5 second. Between 150 to 200 seconds, the water injection rate increased from 9.8 kg/s to 29.4 kg/s and then remained constant. After the initial ramp-up, the steam injection rate was held constant for 200 seconds and then increased to a higher value within a 50-second interval. This steam injection pattern was repeated for all the high-pressure test steam flow rates. For the low-pressure (0.3 MPa) test series, a similar simulation of the water and steam injection rates was used for the test calculation, as shown in Figure 4.127.

The calculated water downflow rates are listed in Table 4.9 for the low-pressure test series and Table 4.10 for the high-pressure test series. The calculated results, data, and data error bands are shown in Figure 4.128 with the steam injection rate plotted against the liquid mass downflow rate.

When the [

] good agreement between calculation and data is shown. For the high-pressure case (1.5 Mpa), complete carryover of water to the steam generator occurs at a steam flow rate of 40.2 kg/s, which is the same as the experimental value. For the low pressure case (0.3 Mpa), complete carryover occurs at a steam flow rate of 18.5 kg/s, which is lower than the experimental value of 20.5 kg/s (note, however, no experimental data points occur between 15.3 kg/s and 20.5 kg/s). For both test series, the calculated water downflow rates are slightly higher than the data in the region close to complete carryover and lower than the data in the lower steam flow region. [

]

Without the CCFL model, the steam flow rate for complete liquid carryover is calculated to be 55 kg/s and 24 kg/s, respectively, for the high-pressure and low-pressure cases. Complete water downflow is calculated to occur below the steam mass flow rate of 18.5 kg/s for the low-pressure case and below 40.2 kg/s for the high-pressure case. This is not supported by the

experimental data and is not conservative. [

]

The calculated results without the CCFL model show that the interphase friction package alone cannot properly calculate the countercurrent flow phenomena at the steam generator inlet plenum. [

]

4.3.1.12 CCTF Tests

The Cylindrical Core Test Facility (CCTF) Core-II Test Series was undertaken to provide a major and useful data base of LBLOCA reflood behavior in PWRs. Of particular interest were the simulations of reflood behavior after a LBLOCA in W 4-loop PWRs in which ECC is injected into the cold leg. CCTF is a full-height, 1/21 scale model of the primary coolant system of a 4-loop PWR plant. The facility was designed to reasonably simulate the flow conditions, including ECC flow behavior in the downcomer, and reactor core responses in the primary system of a PWR during the refill and reflood phases of a LOCA. Details of the CCTF assessments are reported in Section 3.12 of Reference 5.

The objective of these assessments is to ascertain S-RELAP5's capability to simulate reflood transients in conjunction with FRA-ANP RLBLOCA modeling guidelines. Therefore, the nodalization, time step, and other input parameters are set to those defined in the modeling guidelines (Reference 12) and all LBLOCA uncertainty multipliers are set to the nominal value of 1.0.

Four of the 29 tests (tests 54, 62, 67, and 68) were chosen as a diverse sample of behaviors to evaluate the performance of the model during vessel reflood. These CCTF tests were representative of a series of CCTF system gravity reflood tests with certain aspects of refill included. Calculations of these tests provide an understanding of key reflood phenomena and comparisons of predicted (calculated) and experimental (measured) results for assessment of various S-RELAP5 thermal-hydraulic models and their dynamic interactions. Table 4.11 summarizes the key test parameters of the four tests.

Table 4.12 shows that S-RELAP5 with an input model built on the current RLBLOCA modeling guidelines generates PCT that range from an overprediction by 157 K for the case with the worst agreement to an underprediction of the PCT by 17 K for the case with the best agreement.

4.3.1.12.1 Test Run 54

Test Run 54 simulated the reflood phase of a cold-leg ECC injection PWR LOCA with a nominal decay power (i.e., without augmenting American Nuclear Society (ANS) 1971 draft standard decay power by 20%), a system pressure of 0.2 MPa, and a low-pressure coolant injection (LPCI) flow rate of 0.011 m³/s.

The broken-loop hot-leg (BLHL) mass flow rate is in reasonable agreement with the data, but the calculated pump-side break mass flow rate, on average, is below the data by about 30%. The vessel-side break mass flow rate was not measured. Therefore, it is not possible to use vessel-side break mass flow rate comparisons to assess ECC bypass to the break. The good agreement between the calculated and the measured steam mass flow rates in the intact-loop hot legs (ILHL) indirectly indicates that the appropriate vapor generation rate is calculated in the core region. The calculated void fractions in the ILHLs and BLHLs are lower than the voiding shown by the data. The calculated void fraction in the intact-loop cold legs (ILCL) after the switch of ECC injection from accumulator core coolant (ACC) to LPCI also is lower than the measured data. This may be caused, in part, by observed inconsistencies among measured loop mass flow rates and poor calibrations of void fraction measurement (the void fraction was measured to be below 1.0 in the hot legs during the initial heatup period). Another possible cause could be a slight elevation change in the test facility that allowed the liquid to drain back into the downcomer resulting in a large data uncertainty for a small liquid fraction (below 5%) and stratified flow conditions. Therefore, no conclusion can be drawn about entrainment and deentrainment from the comparison of loop void fractions. In the cold-leg ACC injection period, the calculated void fraction in the ILCL agrees well with the data, indicating that the appropriate condensation rate is calculated in the cold leg under the accumulator ECC injection conditions.

Both the calculations and data show no asymmetrical or multidimensional effects of downcomer ECC penetration, mainly because no back steam flow occurs from the core to the downcomer. The lack of upward steam flow in the downcomer also precludes the issue of scaling on the downcomer ECC penetration behavior. The calculated downcomer differential pressure agrees

reasonably well with the data particularly during the accumulator injection period. Except for a short period of slightly lower calculated values after the switch from ACC injection to LPCI and slightly lower predictions later in the reflood period, the calculated core differential pressure is in good agreement with the data, indicating that the overall liquid inventory in the core is calculated properly. Another important parameter for the reflood process is the steam temperature in the core. Unfortunately, the steam temperature instrumentation did not correctly measure the superheated steam temperature in a steam-water mixture environment.

The heater-rod temperature histories are conservatively calculated, particularly for the high power rod bundles. At elevations above the mid-plane of the high-power rod bundles, the calculated temperature rise is somewhat higher and the calculated temperature rise period is longer, partly because of the over- and undercooling calculated for the accumulator ECC injection. The over- and undercooling sequence is partly attributable to the sudden and large system depressurization caused by the strong condensation associated with the ACC injection. The calculated PCT is 1147 K (1605 F) at 2.44 m elevation at approximately 257 seconds, compared to the measured PCT of 1113 K (1544 F) at 1.83 m at 130 seconds. The higher value of PCT at a higher elevation and later time is consistent with the general hydrodynamic behavior calculated by S-RELAP5. Figure 4.129 compares calculated versus measured maximum temperatures with core elevation for CCTF Test 54.

In summary, the assessment results have shown that the S-RELAP5 code calculates the important reflood phenomena occurring in the CCTF Reflood Test Run 54 well (reasonable or better agreement with data). The assessment demonstrates the successful application of S-RELAP5 to PWR LOCA analyses to support the conclusion that S-RELAP5 will produce acceptable licensing simulations of reflood behavior during the postulated LOCA of a cold-leg-injection PWR.

4.3.1.12.2 Test Run 62

Test Run 62 simulated the reflood phase of a cold-leg ECC injection PWR LOCA with a high decay power (i.e., augmenting ANS 1971 draft standard decay power by 20%), a system pressure of 0.2 MPa, and an LPCI flow rate of 0.011 m³/s.

The calculated pump-side break mass flow rate again is low by about 30% on average. The vessel-side break mass flow rate was not measured. Therefore, using vessel-side break mass

flow rate comparisons to assess ECC bypass to the break is not possible. The good agreement between the calculated and the measured steam mass flow rates in the ILHLs indirectly indicates that the appropriate vapor generation rate is calculated in the core region. The calculated void fractions in the ILHLs and BLHLs are lower than the data void fractions. The calculated void fraction in the ILCLs after the switch of ECC injection from ACC to LPCI also is lower than the measured data. This may be caused, in part, by observed inconsistencies among measured loop mass flow rates and poor calibrations of void fraction measurement (the void fraction was measured to be below 1.0 in the hot legs during the initial heatup period). Another possible cause could be a slight elevation change in the test facility that allows the liquid to drain back into the downcomer, resulting in large data uncertainty for small liquid fraction (less than 5%) and stratified flow conditions. Therefore no conclusion can be drawn about entrainment and deentrainment from the comparison of loop void fractions. In the cold-leg ACC injection period, the calculated void fraction in the ILCL agrees well with the data, indicating that an appropriate condensation rate is calculated in the cold leg under the accumulator ECC injection conditions.

Both the calculations and data show no asymmetrical or multidimensional effects of downcomer ECC penetration, mainly because no back steam flow occurs from the core to the downcomer. The lack of upward steam flow in the downcomer also precludes the issue of scaling on the downcomer ECC penetration behavior. The calculated downcomer differential pressure agrees reasonably well with the data particularly during the accumulator injection period. Except for a short period of slightly lower calculated values after the switch from ACC injection to LPCI, the calculated core differential pressure is in good agreement with the data, indicating that the overall liquid inventory in the core is properly calculated. Another important parameter for the reflood process is the steam temperature in the core. Unfortunately, the steam temperature instrumentation did not correctly measure the superheated steam temperature in a steam-water mixture environment.

The heater-rod temperature histories are well calculated, particularly for the high-power rod bundles. At elevations above the mid-plane of the high-power rod bundles, the calculated temperature rise is somewhat higher and the calculated temperature rise period is longer, partly because of the over- and undercooling calculated for the accumulator ECC injection. The over- and undercooling sequence is partly attributable to the sudden and large system depressurization caused by the strong condensation associated with the ACC injection. The

calculated PCT is 1241 K (1774 F) at 2.44 m elevation and 317 seconds, compared to the measured PCT of 1132 K (1578 F) at 2.38 m and 154 seconds. The higher value of PCT at a higher elevation and later time is consistent with the general hydrodynamic behavior calculated by S-RELAP5. Figure 4.130 shows the comparison of calculated versus measured maximum temperatures with core elevation for CCTF Test 62.

In summary, the assessment results have shown that the S-RELAP5 code calculates the important reflood phenomena occurring in the CCTF Reflood Test Run 62 with reasonable agreement to data. The assessment demonstrates the successful application of S-RELAP5 to PWR LOCA analyses to support the conclusion that S-RELAP5 will produce acceptably conservative licensing simulations of reflood behavior during the postulated LOCA of a cold-leg injection PWR.

4.3.1.12.3 Test Run 67 Description

Test Run 67 simulated the reflood phase of a cold-leg ECC injection PWR LOCA with a high decay power (i.e., augmenting ANS 1971 draft standard decay power by 20%), a lowered system pressure of 0.15 MPa, and an LPCI flow rate of 0.011 m³/s.

Again, the calculated pump-side break mass flow rate is low by about 30% compared with the data. The vessel-side break mass flow rate was not measured. Therefore, vessel-side break mass flow rate comparisons cannot be used to assess ECC bypass to the break. The good agreement between the calculated and the measured steam mass flow rates in the ILHLs indirectly indicates that the appropriate vapor generation rate is calculated in the core region. The calculated void fractions in the ILHLs and BLHLs are lower than the data void fractions. The calculated void fraction in the ILCLs after the switch of ECC injection from ACC to LPCI also is lower than the measured data. This may be caused, in part, by observed inconsistencies among measured loop mass flow rates and poor calibrations of void fraction measurement. The void fraction was measured to be below 1.0 in the hot legs during the initial heatup period. This resulted in a large data uncertainty for a small liquid fraction (below 5%) and stratified flow conditions. Therefore, no conclusion can be drawn about entrainment and deentrainment from the comparison of loop void fractions. In the cold-leg ACC injection period, the calculated void fraction in the ILCL agrees well with the data, indicating that the appropriate condensation rate is calculated in the cold leg under the accumulator ECC injection conditions.

Both the calculations and data show no asymmetrical or multidimensional effects of downcomer ECC penetration, mainly because no back steam flow occurs from the core to the downcomer. The lack of upward steam flow in the downcomer also precludes the issue of scaling on the downcomer ECC penetration behavior. The calculated downcomer differential pressure agrees reasonably well with the data during the accumulator injection period in particular. Except for a short period of slightly lower calculated values after the switch from ACC injection to LPCI, the calculated core differential pressure is in good agreement with the data, indicating that the overall liquid inventory in the core is properly calculated. Another important parameter for the reflood process is the steam temperature in the core. Unfortunately, the steam temperature instrumentation did not correctly measure the superheated steam temperature in a steam-water mixture environment.

The heater-rod temperature histories are conservatively calculated, particularly for the high-power rod bundles. At elevations above the mid-plane of the high-power rod bundles, the calculated temperature rise is much higher and the calculated temperature rise period is longer, partly because of the over- and undercooling calculated for the accumulator ECC injection. The over- and undercooling sequence is partly attributable to the sudden and large system depressurization caused by the strong condensation associated with the ACC injection. The calculated PCT is 1300 K (1880 F) at 2.44 m elevation and 304 seconds, compared to the measured PCT of 1143 K (1598 F) at 1.83 m and 164 seconds. The higher value of PCT at a higher elevation and later time is consistent with the general hydrodynamic behavior calculated by S-RELAP5. Figure 4.131 compares calculated versus measured maximum temperatures with core elevation for CCTF Test 67.

In summary, the assessment results have shown that the S-RELAP5 code calculates the important reflood phenomena occurring in the CCTF Reflood Test Run 67 acceptably well. The assessment demonstrates the successful application of S-RELAP5 to PWR LOCA analyses to support the conclusion that S-RELAP5 will produce acceptable licensing simulations of reflood behavior during the postulated LOCA of a cold-leg injection PWR.

4.1.3.12.4 Test Run 68

Test Run 68 simulated the reflood phase of a cold-leg ECC-injection PWR LOCA with a nominal decay power (without augmenting the ANS 1971 draft standard decay power by 20%), a system pressure of 0.2 MPa, and an increased LPCI flow rate of 0.025 m³/s.

Both the calculated pump-side break mass flow rate and the calculated BLHL mass flow rate are in good agreement with the data, however the measured results are suspect because they show relatively large negative flow rates during the initial heat-up (refill) phase. The vessel-side break mass flow rate was not measured. Therefore, vessel-side break mass flow rate comparisons cannot be used to assess ECC bypass to the break. The good agreement between the calculated and the measured steam mass flow rates in the ILHLs indirectly indicates that the appropriate vapor generation rate is calculated in the core region. The calculated void fractions in the ILHLs and BLHLs are lower than the data void fractions. The calculated void fraction in the ILCLs after the switch of ECC injection from ACC to LPCI also is lower than the measured data. This may be caused, in part, by observed inconsistencies among measured loop mass flow rates and poor calibrations of void fraction measurement. The void fraction was measured to be below 1.0 in the hot legs during the initial heatup period. This resulted in a large data uncertainty for a small liquid fraction (below 5%) and stratified flow conditions. Therefore, no conclusion can be drawn about entrainment and deentrainment from the comparison of loop void fractions. In the cold-leg ACC injection period, the calculated void fraction in the ILCL agrees well with the data, indicating that an appropriate condensation rate is calculated in the cold leg under the accumulator ECC injection conditions.

Both the calculations and data show no asymmetrical or multidimensional effects of downcomer ECC penetration, mainly because no back steam flow occurs from the core to the downcomer. The lack of upward steam flow in the downcomer also precludes the issue of scaling on the downcomer ECC penetration behavior. The calculated downcomer differential pressure agrees reasonably well, $\approx 12\%$ lower than the data shows. The calculated core differential pressure is in good agreement with the data providing an indication that overall liquid inventory in the core is properly calculated. Another important parameter for the reflood process is the steam temperature in the core. Unfortunately, the steam temperature instrumentation did not correctly measure the superheated steam temperature in a steam-water mixture environment.

The heater-rod temperature histories are in excellent agreement, particularly for the high-power rod bundles. At elevations above the mid-plane of the high-power rod bundles, the calculated temperature rise is somewhat lower and the calculated temperature rise period is generally longer, partly because of the over- and undercooling calculated for the accumulator ECC injection. The over- and undercooling sequence is partly attributable to the sudden and large system depressurization caused by the strong condensation associated with the ACC injection.

The calculated PCT is 1105 K (1529 F) at 2.44 m elevation and 210 seconds, compared to the measured PCT of 1122 K (1560 F) at 1.83 m and 164 seconds. The higher value of PCT at a higher elevation and later time is consistent with the general hydrodynamic behavior calculated by S-RELAP5. Figure 4.132 compares the calculated versus measured maximum temperatures with core elevation for CCTF Test 68.

In summary, the assessment results have shown that the S-RELAP5 code calculates the important reflood phenomena occurring in the CCTF Reflood Test Run 68 with reasonable agreement to data. The assessment demonstrates the successful application of S-RELAP5 to PWR LOCA analyses to support the conclusion that S-RELAP5 will produce acceptable licensing simulations of reflood behavior during the postulated LOCA of a cold leg injection PWR.

4.3.1.13 SCTF Tests

The Slab Core Test Facility (SCTF) Core-II Test Series was undertaken in part to obtain information that could be used to assess thermal hydraulic models in best estimate, evaluation models and other computer codes. The intent for these assessments was to use the SCTF-II test series to assess the accuracy of the S-RELAP5 computer code. Six tests from the series of 19 were chosen as a diverse sample of behaviors to evaluate the performance of the model during vessel reflood phenomena. The present study has two objectives: to assess the code's capability of simulating both forced and gravity reflood transients and to study the effect of radial nodalization on reflood behavior. Details of the SCTF assessment calculations are presented in Section 3.11 of Reference 5.

The SCTF test program is designed to investigate the two-dimensional (2D) thermal-hydraulic behaviors in the pressure vessel during the reflood phase of a PWR LBLOCA. To meet this objective, SCTF simulates a full-radius slab section of a PWR with eight bundles arranged in a row. The heating power for each bundle can be controlled independently.

In the SCTF test, the following two test modes were adopted: gravity feed with the ECC injection into the cold leg, and forced feed with ECC injection into the lower plenum by closing the bottom of the downcomer. Although the first mode is considered to be a better simulation of integral reactor behavior, the boundary conditions at the core inlet (mass flow rate and subcooling) are affected by parameter changes (change of system pressure and core heating, etc.). Therefore, to investigate the effect of the parameter changes on the 2D thermal-hydraulic

behaviors in the pressure vessel, the forced feed test mode was adopted to obtain more accurate boundary conditions at the core inlet.

The tests that were modeled in the calculation assessments were two "gravity reflood" tests (Tests S2-SH1 and S2-AC1) and four "forced reflood" tests (Tests S2-10, S2-11, S2-17, and S2-18). The S2-SH1 test is the SCTF-II gravity-reflood base-case test. During Test S2-SH1, the downcomer was not blocked from the lower plenum (i.e., hydraulic communication existed between the lower plenum and the downcomer). A combination of lower plenum injection and cold leg injection was used in Test S2-SH1. Test S2-AC1 differs from Test S2-SH1 in the ACC injection rate and duration.

The S2-10 test is the SCTF-II forced-reflood base case. In Test S2-10, ECC was injected into the lower plenum only, with no hydraulic communication between the lower plenum and the downcomer. The ECC injection rate was specified to match the core inlet flow rate achieved in the gravity feed test S2-SH1. Test S2-11 differs from S2-10 in that a high ACC flow rate was used to simulate test S2-AC1.

Test S2-17 and S2-18 are also forced reflood tests with the primary difference being in the radial power distribution. Test S2-17 has a flat power profile and Test S2-18 has a steep power profile with test conditions similar to a standard plant. The S2-18 test has a power profile that is consistent with the RLBLOCA methodology NPP nodalization (Reference 12). The assessment of these two tests with their widely different radial power distributions provide a good test for the S-RELAP5 code and NPP nodalization.

Table 4.13 shows the test conditions for each of the tests examined. The six SCTF Core-II reflood experiment tests were selected to assess forced reflood, gravity reflood, and the effect of radial nodalization. The assessment matrix is summarized as follows:

- Forced vs. Gravity Reflood (Phase I). In this assessment phase, two sets of counterpart tests were chosen to study the differences between forced and gravity reflood. The first set consists of Tests S2-11 and S2-AC1 and the second set consists of Tests S2-10 and S2-SH1. A nominal nodalization of two bundles per core channel was modeled for this study.
- Effect of Radial Nodalization (Phase II). In this assessment phase, two tests were chosen to study the effect of radial nodalization on reflood behavior. These tests are S2-18 and S2-17. Three different nodalizations were used: the nominal nodalization, a fine-nodalization of one bundle per channel, and a plant-consistent nodalization (Reference 12).

Phase I Assessment Results: Forced vs. Gravity Reflood.

This phase studies the comparison between forced and gravity reflood for the same test conditions. The pair S2-11 and S2-AC1, the flooding rate is about 17.4 cm/s during ACC reflood and 1.6 cm/s during LPCI reflood and represent the highest combined injection rate in the SCTF-II test matrix. For Test S2-11, the calculated responses show reasonable agreement with the data except at the top elevations. At the two topmost elevations, the data show prolonged heat up when the calculation predicted quenching. The vessel pressure agreement is reasonable. The pressure in the vessel increases at the point of ECC injection because of steam generation. The extent of pressurization depends on the rate of steam venting through the hot leg. The vessel void fraction calculated results exhibit large oscillations, typical of reflood simulation. The average behavior follows the data trend.

For Test S2-AC1, the agreement between calculation and data is better than that observed in Test S2-11. In particular, the quench time along the heated length is better predicted at all elevations shown. The cladding temperature prediction at the two uppermost elevations also is better than for S2-11. However, the peak vessel pressure was overpredicted.

For S2-10 and S2-SH1, the flooding rate is about 3.7 cm/s during ACC reflood and 1.8 cm/s during LPCI reflood. These tests represent the lowest combined injection rate in the SCTF-II test matrix. The calculation is in reasonable agreement with the data for both tests.

The comparison of calculated and measured PCT and quench time for the Phase I assessments are presented in Table 4.14. The quench time was predicted to occur earlier than the data for both the high and low flooding rate tests. Thus, the quench front was predicted to advance faster than the data for these tests. For test S2-10, the PCT was overpredicted and for S2-SH1, the PCT was underpredicted. Conversely the time of PCT was overpredicted in S2-10 and underpredicted in S2-SH1.

In summary, the Phase I assessments show that S-REALP5 can simulate both forced and gravity reflood transients. The PCT for counterpart tests, S2-11 and S2-AC1 and Tests S2-10 and S2-SH1, have good agreement with data. For high and low flooding rates, the PCT was predicted within 55 F or less (good agreement with data).

Phase II Assessment Results: Effect of Radial Nodalization

This phase studies the effect of radial nodalization on the reflood behavior during a postulated LBLOCA incident. Tests S2-17 and S2-18 were selected for this study. The ACC flooding rate for Test S2-17 is about half of that for Test S2-18, while the LPCI flooding rates are about the same for both tests. The major difference between these two tests is in the core power distribution. Test S2-17 has uniform power across the core (all at 890 kW). Test S2-18 has a significant radial power distribution, with the peak bundle power (1210 kW) about twice as much as the peripheral bundle power (676 kW). The total power level for the two tests is almost the same (7120 kW for S2-17 versus 7118 kW for S2-18). The distribution of radial power renders these two tests ideal for studying core radial nodalization.

[

]

The input models for the individual nodalization and the plant-consistent nodalization were developed from the base model having the nominal nodalization. Three primary modifications are required:

- [

]

- [

]

• [

]

Figures 4.133 and 4.134 show typical measured temperature transients near the core midplane for SCTF tests 17 and 18, respectively. These figures also compare the calculated temperature transients for the individual assembly and plant consistent nodalizations. These and comparisons of temperature transients at other elevations for both tests show that the differences in radial nodalization have minimal impact on the cladding temperature results (Reference 5). In particular, the fluid conditions seen by the "hot" rod must be similar to produce the similar cladding temperature responses.

Table 4.15 summarizes the Phase II assessment results for the calculation with the highest PCT from the nodalization studies. For Test S2-17 the highest PCT is for the individual assembly nodalization and for Test S2-18 it is the RLBLOCA plant consistent nodalization. For both tests the PCT and bundle quench time is underpredicted relative to the data. However, the time of PCT is underpredicted for Test S2-17 and overpredicted for Test S2-18.

These results confirm that the use of the plant nodalization scheme is adequate to capture the PCT response. [

]

4.3.1.14 ACHILLES Tests

International Standard Problem Number 25 (ISP 25) is based on a test in the ACHILLES facility that simulated the latter phase of accumulator injection during a LOCA. ISP 25 tests the ability of system codes to be evaluated for the impact of the nitrogen cover gas in the accumulator on the LBLOCA. The accumulators in a PWR are pressurized with nitrogen. When the system pressure falls below the nitrogen pressure, the borated water from the accumulator flows into the primary system. When the accumulators empty of liquid, the nitrogen cover gas enters the primary coolant system where it flows to the upper part of the downcomer and causes the pressure to increase. The increased pressure depresses the liquid level in the downcomer, resulting in a surge of water into the core. The nitrogen gas bypasses the core and flows out through the break, and in a few seconds the upper downcomer pressure drops, the downcomer level recovers, and the nitrogen has no further effect on the transient.

The difference between a pressurization surge caused by steam and one caused by nitrogen is that the nitrogen does not condense. Thus, the nitrogen can act like a large piston pushing the fluid into the core. For the realistic LBLOCA methodology, it is important that the code does not overpredict the surge into the core and the transient cooling caused by this in-surge, thereby leading to an underprediction of PCT. The ability of S-RELAP5 to predict both system and fuel temperature responses was confirmed by comparing the calculated values to the measurements.

The ACHILLES test facility is designed to simulate the latter stages of accumulator injection in an LBLOCA. The simulated downcomer is connected to the bottom of the core and a valve is closed, before nitrogen injection begins, to hold the water in the downcomer until injection occurs. Another valve is open before injection begins and provides a flow path for the pumped water so that it does not enter the core. This valve closes on initiation of nitrogen injection. The simulated core has 69 simulated fuel rods with a geometry similar to that of a W 17 x 17 design. The simulation core has 8 spacer grids. The rods are housed in a piece of pipe. The exit region has a centrifugal separator to collect carryover water. The steam then joins the nitrogen bypass flow and exits.

The nitrogen tank is connected to the top of the simulated downcomer, and a valve, which is initially closed, opens to initiate the nitrogen flow. Nitrogen forces flow through the core by increasing the pressure on the downcomer. Nitrogen also flows through a bypass path to join the steam that has passed through the core, then it exits. A flowmeter measures the nitrogen flow from the tank and another flowmeter measures the bypass flow.

Each simulated fuel rod has multiple thermocouples on the surface of the rod. The PCT level (2.13 m) is the most heavily instrumented, with 66 thermocouples.

Achilles ISP 25 was analyzed using S-RELAP5 modeling consistent with the realistic LBLOCA methodology. S-RELAP5 was able to accurately predict the liquid surge into the core, liquid carryover to the upper plenum, and rod thermocouple readings. In particular, the surge into the core when the nitrogen flow is initiated is never overpredicted.

Predicted PCTs are good to excellent, which clearly is an acceptable outcome in light of the radial flow inhomogeneities observed in the Achilles test.

As the appropriate valves are operated to initiate the event, an immediate pressure transient occurs at the top of the downcomer. The initial pressurization of the downcomer causes a rapid surge of liquid into the simulated core. As the nitrogen leaves the system via the bypass, the pressure drops at the top of the downcomer, the levels in the core and downcomer recover, and the core reflooding now depends on the pumped water flow, which is entering both the downcomer and the core.

Figure 4.135 presents the range of variation in the thermocouples at the PCT elevation (2.13 m). The wide variation shown is not a consequence of power variation because the rods all are the same power. Three rods set the lower bound and all three of these rods are located next to the shroud in the test assembly. The early quench indicates that the flow field near the shroud is far different from that in the interior.

The remaining rods can be divided into a group that tracks the maximum fairly well and a group that falls well below the maximum, but not as dramatically as the three rods setting the lower limit. Thus, the test data shows that to get a reasonable prediction of core temperatures requires a multidimensional analysis.

The radial inhomogeneity is greater than would be experienced in a large-scale reactor core because the flow path on the periphery has hydraulic properties that are significantly different from the interior flow paths. While a reactor core is anisotropic and inhomogeneous, it does not have the range of variations this test assembly has. Thus, predicting the reflood behavior for this test assembly is significantly more challenging than for a PWR core.

For the S-RELAP5 assessments, the central 21 rods in the test assembly were modeled as one channel and the remaining 48 rods and the shroud were modeled as the other channel using the TWODEE component. The comparisons to data were made by comparing the predictions for the central channel with the measured values for the same 21 rods.

Calculated nitrogen flow rate was compared to measured results. The agreement is excellent until frost forms in the throat of the venturi at about 7 seconds (Reference 5). The time-to-empty agrees to within about 2 seconds. The calculated flow spikes a little early compared to the measured flow and then is slightly lower for the remainder of the blowdown.

The calculated liquid carryover at the core exit was compared to the measured carryover. The agreement with data is good, with the major discrepancy coming from the measured burst of flow at 20 to 50 seconds and the subsequent cessation of all liquid flow at the exit for nearly 50 seconds. Nothing in the thermocouple data distinguishes this time period.

The steaming rate at the core exit shows good agreement between the calculations and the measured data.

The downcomer level measurements generally are higher than the calculated results, indicating that the pressure drop through the core and the two sets of separators probably is higher than is modeled. No attempt was made to match this level because the core collapsed level, which is not very sensitive to pressure drop variations, matches quite well.

Calculated temperatures for the central region were compared to measured temperatures for the 21 rods in the middle of the assembly. The maximum, minimum, and average temperatures were compared with the calculated temperature for elevations from 1.08 m to 3.18 m. The calculated values are generally in good agreement with the measured values. The PCT elevation is 2.13 m and, at this elevation, the calculated PCT is about 30 K lower than the measured values. At all other elevations, the calculated peak temperature exceeds the measured values.

The impact of the nitrogen injection, which is the focus of this assessment, can be seen in the first 25 seconds of the transient. Figures 4.136 to 4.141 show the temperature comparisons on expanded time and temperature scales to emphasize the nitrogen effects. The rod thermocouples all show a transient temperature reduction at the beginning of the event. This initial cool-down is caused by the nitrogen in-surge that initiates the event. S-RELAP5 calculates a conservatively small cool-down compared to the data. In all cases, the calculated downward temperature transient accompanying the nitrogen injection is smaller than the measured temperature decrease, indicating that S-RELAP5 underpredicts the cool-down due to the nitrogen injection.

4.3.1.15 Multi-Dimensional Flow Testing

Flow blockage tests were performed using simulated pressurized water reactor (PWR) fuel assemblies (Reference 5). These tests provided data on single-phase flow redistribution for non-uniform inlet and outlet conditions. S-RELAP5 has a two-dimensional component used to

model multidimensional flows. These flow blockage tests have been used as a basis for evaluating the two-dimensional component in S-RELAP5. The comparisons to the measured data and to other codes that have been approved for flow distribution calculations show that the two-dimensional component in S-RELAP5 can be used to model multidimensional flow problems.

The S-RELAP5 assessment of these tests are presented in detail in Section 3.13 of Reference 5. No bias or uncertainty is derived from this assessment.

4.3.1.15.1 Summary

The radial flow split distributions of axial velocities calculated by S-RELAP5 show good agreement with data for all three tests considered. The comparison of S-RELAP5 with flow blockage data shows that the two-dimensional model in S-RELAP5 is sufficient to describe flow redistribution in multidimensional problems, and that it does as well as thermal-hydraulic design codes used for PWR core analysis in predicting the flows for these blockage tests (Reference 5).

4.3.1.15.2 Test Descriptions

The test assembly consists of two simulated PWR assemblies with a pin array representative of a 15 x 15 fuel assembly. The simulated assemblies are about 38 in long and are enclosed in a rectangular canister. For the bulk of the testing, the gap between the two simulated fuel assemblies was left open, but for some tests a perforated plate was inserted between the two simulated fuel assemblies. Because of the detail of the measurements and the nearly prototypic geometry (in the radial, or x-y, direction), these tests have become a standard benchmark test for flow redistribution codes.

The tests consisted of introducing asymmetric flow in the inlet region and measuring flow recovery in the bundle with a series of pitot tube arrays. The pitot tubes measure flow velocities at many points in each plane. The first array is 2.5 in above the inlet. The remainder are located at 5-in intervals, with the last one at 32.5 in level.

For the test series without a perforated plate between the two assemblies, two different test configurations were evaluated. The first configuration (Test 1) has a nominal 1100 gpm entering one fuel assembly and 550 gpm in the other. The second configuration (Test 2) has

one inlet blocked and a nominal 1500 gpm entering the other. In both cases, the exits are open. The case with the perforated plate inserted between the two assemblies (Test 3) has the inlet and outlet blocked on one assembly and has a nominal inlet flow of 1300 gpm.

4.3.1.15.3 Input Description

The test section was modeled in S-RELAP5 as a TWODEE component with 10 vertical (x) volumes and 14 horizontal (y) volumes. This, in effect, collapses the test assembly in the direction perpendicular to the asymmetric flows. Selection of 14 horizontal volumes resulted in volumes that corresponded to the pitot tube measurements. The vertical volumes had lengths that made the first volume match the bottom of the rodged region (4.5 in) and each of the others matches the elevation of a velocity measurement point (pitot tube location).

4.3.1.15.4 Results

A review of the data for Test 1 indicates that the real flows were probably 1138 gpm and 512 gpm for Bundles A and B, respectively. Figure 4.142 provides a comparison of the measured and calculated flow distributions at the last set of pitot tubes. The reported axial fluid velocities were calculated by S-RELAP5 with inlet flows of 1138 and 512 gpm. The measured velocities are almost all higher than the S-RELAP5 velocities at this level. Figure 4.143 compares the reported mass flow fraction in the high flow bundle, Bundle A, with that calculated by S-RELAP5.

A review of the data for Test 2 indicates the real inlet flow was probably 1281 gpm, rather than the nominal 1500 gpm for the test. This value was used in the S-RELAP5 model. Figure 4.144 compares the S-RELAP5 velocity distributions with the reported axial fluid velocities at the last set of pitot tubes. In general, the agreement is excellent. The largest discrepancy occurs on the side of the blocked bundle next to the wall. Here, S-RELAP5 calculates more of a tendency to back flow. The measurement velocities, which are based on pitot tube readings, show that the flow stops near the wall.

Figure 4.145 compares the fractional flow in the unblocked bundle, Bundle A. The agreement is good over most of the axial height of the bundle. Near the exit, the measured flow was nearly equal for the two bundles. The calculated flow distribution is still about 60/40 for S-RELAP5. The overall agreement is good.

Figure 4.146 compares the reported axial fluid velocities for Test 3 to those calculated by S-RELAP5. The agreement for these data is excellent for this and all levels. The most notable difference is the tendency of S-RELAP5 to predict reverse flow near the wall in the blocked assembly, very similar to the result in Test 2.

To assess the quality of the comparison to data, the XCOBRA-IIIC and THINC-IV flow predictions for Tests 1 and 2 were compared to the S-RELAP5 flow predictions. Figure 4.145 compares the S-RELAP5 calculations with the XCOBRA-IIIC calculations, the THINC-IV calculations, and the data for Test 1. The flow distribution calculated by S-RELAP5 is clearly in the best agreement with the data.

4.3.1.15.5 Conclusions

A series of flow blockage tests was analyzed using the two-dimensional component in S-RELAP5. S-RELAP5 was able to calculate the axial flow redistribution within the two test assemblies. Overall, S-RELAP5 does as well as, or better than, core flow distribution codes used for core flow and subchannel analysis of PWR cores. Calculated results were generally in reasonable agreement with the data.

4.3.2 Integral Effects Tests (IET)

The SETs presented in Section 4.3.1 assess the code capability and provide information to quantify the uncertainty to predict specific phenomena identified by the PIRT. In addition to the SETs, assessments are performed of integral effects tests (IET) to evaluate the overall code capabilities to predict the integrated LOCA scenario and the interacting phenomena in facilities of differing scale. Some of the facilities discussed with the SETs, such as SCTF, CCTF, and UPTF are large scale and include integral interacting-phenomena effects. However, these tests are still limited in that only a portion of the LOCA scenario is addressed. For this reason, FRA-ANP regarded these as separate effects tests.

Integral tests covering the entire LBLOCA scenario have been performed in the loss-of-fluid test (LOFT) facility, and the smaller scale Semiscale test facility. FRA-ANP has performed assessments of tests from both of these facilities. These assessments are reported in detail in Reference 5 and are summarized in the following sections.

4.3.2.1 LOFT Assessments

Assessments of the LOFT Tests L2-3, L2-5, LP-02-6, and LP-LB-1 were performed to justify the use of FRA-ANP's Realistic LBLOCA methodology and the S-RELAP5 code developed by FRA-ANP for realistic analysis of LBLOCA. This section of the methodology report documents the LOFT assessment calculations with the FRA-ANP RLBLOCA methodology. The assessment results demonstrates the accuracy of the RODEX3A and S-RELAP5 codes and the capability of simulating the LBLOCA phenomena observed during the LOFT tests, and provide assessments of the calculated results versus measured results to satisfy the rule change requirements.

4.3.2.1.1 LOFT Facility

The LOFT facility was designed to simulate a LOCA in a large W 4-loop PWR, and thus, to provide data with which to evaluate the adequacy and to improve analytical methods for analyzing LOCA transient response of a PWR. The LOFT results have been widely used to validate thermal-hydraulic codes that analyze PWR accident and transient phenomena. Key LOFT LBLOCA tests have been included in the CSAU assessment matrix (Reference 4) and RELAP5/MOD3 developmental assessment matrix. LOFT assessments have also been performed to verify RELAP5/MOD2 or MOD3 by various members of the NRC-sponsored International Code Assessment Program (ICAP).

LOFT was an NRC-sponsored nuclear test facility designed to simulate the nuclear and thermal-hydraulic phenomena that take place in a PWR LBLOCA. The LOFT facility was a 50 MWt experimental PWR designed to simulate the system response of a W 4-loop PWR during a hypothetical LBLOCA. The facility included five major subsystems, an intact loop, a broken loop, a reactor vessel, an emergency core cooling system, and a blowdown suppression system. The LOFT facility was instrumented so that system parameters could be measured during the tests.

The LOFT reactor had a single active intact loop that simulated the combined three intact loops of a W 4-loop PWR. The intact loops included an active steam generator, two primary coolant pumps (PCP) in parallel, a pressurizer, a loop seal, and the connecting piping.

The broken loop in the LOFT facility was an inactive flow loop during normal operation. The loop consisted of a hot leg, a steam generator simulator, a pump simulator, and a cold leg. It

became an active flow loop and simulated the broken loop of a 4-loop PWR during LOCA tests. The BLCL was divided into two parts: a pump side, that connected the pump simulator to the blowdown suppression system and the vessel side that connected the vessel downcomer to the blowdown suppression system. The steam generator and pump simulators provided flow resistances representative of a PWR during a LOCA. Both sides of the broken cold legs contained quick-opening blowdown valves (QOBV) that opened to initiate the transient.

The LOFT reactor vessel had an annular downcomer, a lower plenum, below core hardware, a nuclear core, above core hardware, and an upper plenum. The downcomer was connected to the intact and broken cold legs and the upper plenum was connected to the hot legs. The core contained 1300 fuel rods arranged in five square (15 x 15) and four triangular (corner) assemblies with an average linear heat generation rate (LHGR) of about 7.0 kW/ft at full power. The LOFT fuel rods and pitch were typical of a PWR 15 x 15 rod array, except that the active length was 1.68 m (5.5 ft) while that of a PWR is typically 3.66 m (12 ft). For Test LP-02-6, all the fuel rods in the central assembly except the outside row were pressurized with helium to 2.51 MPa (350 psig) and all fuel rods in the peripheral assemblies were unpressurized. In remaining tests, L2-3, L2-5, and LP-LB-1, all of the fuel rods were unpressurized.

The LOFT intact loop had two separate ECCSs connected to the cold leg. Each system contained an accumulator, an HPIS, and an LPIS. Only one ECCS was used during a LOCA test and the other was used as backup for plant protection in case of unplanned emergency situations that might occur during the test. The ECCS was not connected to the broken loop. For the LBLOCA tests, ECC was injected into the ILCL. The HPIS and LPIS were connected to the accumulator injection piping. The LOFT blowdown suppression system consisted of a header and a suppression tank that simulated the PWR containment pressure and temperature environment expected to occur during an LBLOCA.

LOFT was designed with a primary system volume-to-core power ratio similar to that of a PWR. The design objective for the LOFT facility was to produce, on a reduced scale, the significant thermal hydraulic phenomena with representative conditions and a representative sequence of events that could occur in a PWR during postulated LOCAs. Volumetric scaling generally was used for the design of LOFT components. Primary system components (e.g., lower plenum, core region, upper plenum, outlet piping, steam generator, and inlet piping) also were designed with relative volumes equivalent to those in a PWR. LOFT is a reduced-scale facility that is not

uniformly scaled by a consistent scaling criteria. Therefore, scaling distortions exist that must be considered when applying the results of the LOFT tests. Table 4.16 shows the PWR-LOFT scaling ratios to a PWR.

The accumulator gas volume is scaled so that the ratio of accumulator gas volume to accumulator liquid volume injected is made equal to that of a typical 4-loop PWR by adjusting the standpipe height. The LOFT accumulator liquid volume is scaled to represent three of the four accumulators of a typical 4-loop PWR, assuming that the liquid in the fourth accumulator is lost out of the break. The LOFT HPIS flow rate for the LB tests is volume-ratio scaled using the ratio of the LOFT to PWR total primary system fluid volume plus the single failure criterion and the assumption that flow from one of four lines of injection is lost out of the break. The LPIS flow rate is scaled based on the combined downcomer and core flow areas. The single failure criterion and the assumption that flow from one of four injection lines is lost out of the break are also used for LPIS scaling.

The major differences between the LOFT and a 4-loop PWR are summarized as follows:

- The LOFT has one active operating (intact) loop and a passive blowdown (broken) loop with only a steam generator and pump simulator, while a 4-loop PWR has four operating loops.
- The LOFT has two pumps connected in parallel in the operating loop, while a PWR has only a single pump in each loop.
- The LOFT core has a 1.68 m (5.5 ft) active fuel length, while PWR core lengths are at least 3.66 m (12 ft). The axial power distribution of the LOFT core is similar to a beginning-of-life, bottom-skewed power distribution in a PWR core.
- The LOFT has a short steam generator relative to a PWR.
- The LOFT cold leg ECC injection location is very close to the vessel inlet, while the PWR ECC injection lines are located near the pump outlet.
- Axial lengths and elevations of hydraulic components are not preserved relative to a PWR.

The LOFT scaling philosophy was to reduce the component coolant volume and flow areas by the core power ratio. The volume and power scaling was not achieved completely, and vertical scaling was not preserved. Despite these component differences and scaling distortions, the LOFT components were functionally similar to those of a PWR and provide sufficient similarity to permit the LOCA data to be used to validate the S-RELAP5 code for evaluating the PWR LOCA/ECCS performance.

4.3.2.1.2 LOFT Test Descriptions

Between 1976 and 1985, 50 LOFT tests were performed. The LOFT facility was designed primarily for performing LBLOCA tests; however, only five tests, L2-2, L2-3, L2-5, LP-02-6 (L2-6), and LP-LB-1 (LB-1), were LBLOCA tests with a heated nuclear core. The first three LBLOCA tests were sponsored by the NRC and the last two were conducted under the auspices of the OECD sponsored by an international consortium. LP-02-6 was conducted under OECD, but was totally funded and sponsored by the NRC. Test LP-LB-1 was the only LOFT LBLOCA test funded by the OECD consortium. The OECD Test LP-FP-01 also is a LBLOCA test simulating a German-type reactor accident scenario resulting in the fuel rod rupture and gap fission product release. It was therefore categorized as a fission product test rather than an LBLOCA test. Table 4.17 shows the characteristics and parameters of the LOFT nuclear LBLOCA tests.

FRA-ANP selected four LOFT LBLOCEs, L2-3, L2-5, LP-02-6, and LP-LB-1 for assessment with S-RELAP5. All of the selected LOFT tests simulate cold leg guillotine breaks. The major differences between these tests are: L2-3 and L2-5 were initiated from 75% power while LP-02-6 and LP-LB-1 were initiated from near 100% full power and the PCP flywheels were not attached during the coastdown of Tests L2-5 and LP-LB-1, but were attached when the pump speed was above 750 rpm (78.54 rad/s) in Test LP-02-6 and were left running for Test L2-3. These LOFT tests have been used to validate the S-RELAP5 code for the blowdown, refill, and reflood phases of an LBLOCA. The tests were selected for S-RELAP5 assessment for the following reasons.

- The test initial and boundary conditions most closely simulate the "design basis accident" LOCA conditions for typical W 4-loop PWRs.
- Test L2-3 provides scaling data when compared to Semiscale Test S-06-3.
- The LOCA phenomenology for Tests L2-5 and LP-LB-1 are similar to that expected for a W 3-Loop PWR, and the LOCA phenomenology for Test LP-02-6 is similar to that expected for a W 4-Loop PWR.
- Test L2-3 was designated as United States Standard Problem 10 for code assessment by the NRC.
- Test L2-5 was designated as ISP 13 for code assessment by the OECD.

- Other code assessment calculations of L2-5, LP-02-6, LP-LB-1 are available for comparison.

4.3.2.1.3 LOFT Assessment Summary

The LOFT assessment calculations were performed with an input model developed to be consistent with the nodalization used in other assessments and the nodalization to be applied for PWR plant calculations (Reference 12). The philosophy of developing the S-RELAP5 consistent input models is to use a similar nodalization scheme in terms of number and distribution of volumes, junctions, heat structures, and input specifications to represent corresponding components in the LOFT and plant models. Exceptions are made only where significant LOFT geometry differences justify a different, but consistent scheme.

Reference 5 contains detailed comparisons of the results of the LOFT L2-3, L2-5, LP-02-6, and LP-LB-1 tests with calculated results using the FRA-ANP LOCA realistic evaluation model. The LOFT test analytical results demonstrate the ability of S-RELAP5 to realistically simulate the key important system phenomena relevant to an LBLOCA that were observed during the unique LOFT LBLOCA test. These include: (1) system depressurization, (2) core flow reversal and core dry-out, or critical heat flux (CHF), (3) the fuel cladding temperature excursion and peak cladding temperature (PCT), (4) two-phase pump flow and critical flows at the breaks, (5) prevention of core bottom-up quench during the early blowdown period, (6) ECC downcomer penetration and bypass, and (7) core refill, reflood, and final quench.

As shown by the results presented in Reference 5, the FRA-ANP RLBOCA evaluation model produced results in good agreement with the observations for LOFT Tests L2-3, L2-5, LP-02-6, LP-LB-1. The results are summarized as follows:

- The RODEX3A-calculated fuel initial centerline fuel temperatures were within 10% of the measured data.
- The S-RELAP5 code results provide good agreement with the hydraulic responses of the LOFT tests. That is, the calculated results either were within measured uncertainties, followed the major trends of the data if not within measured uncertainties, or were conservative with respect to the data if the phenomena were not simulated. The intact loop mass flow rates, break flow in the broken loop, and loop volume densities were all well-calculated. Coolant temperatures also were well calculated. Pressurizer draining was overpredicted, but because the pressurizer liquid tended to flow to the broken loop and was

removed from the system, that trend produced conservative results. Calculated pump speeds were accurately predicted up to the time where a two-phase mixture appeared. After that time, the pump speeds were lower than measured and, thus, acceptable.

- The code accurately calculated the thermal response (fuel centerline temperature and cladding temperature). The centerline temperatures closely match the data. The cladding temperature results generally were in reasonable agreement with the measured data. The hot rod PCT is very well calculated, considering test measurement uncertainty. The cladding quench times are significantly delayed with respect to the measured data. The early bottom-up core quenching found in Tests L2-3 and LP-02-6 were not simulated in the code calculations. The upper regions of the core showed delayed dry-out with respect to the test data. However, once the upper regions went through dry-out, the calculated rewet was much later than measured. In general, the code predicted higher than measured temperatures in the middle core region, lower than measured temperatures in the upper core region, and approximately measured temperatures in the lower region. In all cases, the calculated PCT was either within or greater than the measured PCT with analytical uncertainties included.
- The calculated ECC injection rates for the low pressure injection system (LPIS) and accumulator tended to underpredict the measured data and, hence, are acceptable.

4.3.2.1.4 LOFT L2-3 Assessment

Test L2-3 was the second LBLOCA test conducted in the LOFT facility in which the reactor core power provided the primary heat source. The test represented a hypothetical cold leg guillotine break that simulated a double-ended, offset, shear break in a commercial (1000 MWe) 4-loop PWR. The test was initiated at 75% thermal power (36 MWt) and a 12.22 kW/ft maximum linear heat generator rate (MLHGR).

The test was initiated by opening the QOBVs. Reactor scram commenced 0.1 seconds into the transient and was completed 1.6 seconds later, HPIS injection was initiated at 14 seconds, accumulator injection at 17 seconds at 4.18 MPa system pressure, and LPIS injection at 29 seconds. The core was reflooded at 55 seconds. During this test, the primary coolant pumps (PCP) operated continuously throughout the transient and were tripped off at 200 seconds.

The cladding temperature started rising as expected and, after 2 to 3 seconds into the transient, the ILCL mass flow exceeded the broken loop mass flow, causing flow diversion to the downcomer. That process eventually caused a bottom-up rewet of the core and the cladding was quenched momentarily. The conditions for core upflow quickly ceased and the core dry-out and heat-up resumed 10 seconds into the blowdown. The core heat-up continued until sufficient ECC injection caused quenching of the core at 55 seconds. The final rewet pattern was first the bottom, then the top, and finally the middle regions of the core.

The measured PCT was 914.0 K (1185.0 F) and occurred at 5 seconds. As indicated in Reference 5, a bias of $11.4 \text{ K} \pm 16.2 \text{ K}$ ($20.5 \text{ F} \pm 29.2 \text{ F}$) should be applied to the measured PCT to account for the 'fin cooling' effects on the surface mounted thermocouples. Thus the reportable PCT for LOFT L2-3 is 941.6 K (1235.2 F).

The S-RELAP5 LOFT input model for FRA-ANP assessments was developed at FRA-ANP. This model provides detailed thermal and hydraulic representations of all the major LOFT system components. It results from developing an LBLOCA analysis input model that is consistent with the nodalization scheme used in all assessment and PWR LBLOCA plant calculations (Reference 12).

The computer codes used to perform the LOFT assessment calculations were RODEX3A and S-RELAP5. RODEX3A is the FRA-ANP realistic fuel rod thermal-mechanical behavior analysis code. S-RELAP5 is an FRA-ANP-modified version of the INEEL RELAP5/MOD2 and MOD3 codes. The RODEX3A code provides input to calculate the fuel conditions and stored energy for all fuel types modeled by S-RELAP5 at the initiation of the realistic LBLOCA calculation. The RODEX3A models have been integrated with S-RELAP5 to provide a consistent realistic calculation of the thermal-mechanical responses of the fuel rods during the LOCA. The FRA-ANP input prescription (Reference 12) defines the acceptable nodalization, numbering system, and parameter inputs for an S-RELAP5 PWR plant or experimental facility input model.

The LOFT core components modeled by the RODEX3A code are the fuel rod coolant channel, the active fuel column, the gap, the cladding, upper fuel rod plenum free volume, and the fill and released fission gases (for pressurized rods only). The four fuel rod types represented by the S-RELAP5 heat structures differ by power level and initial fill gas pressure. The rod powers are modeled in accordance with the core axial and radial power distributions. The two hot rods and

the hot assembly rod are modeled as pressurized rods while the average core rod is unpressurized for Tests L2-5 and LP-02-6. For Test LP-LB-1, all fuel rods are unpressurized. RODEX3A calculations provide exposure-dependent input to the S-RELAP5 fuel model that calculates initial fuel rod conditions and stored energy. Therefore, pretest power and power histories were included in the initial stored energy calculation. For the analysis presented here, fuel information at 50 hours, as calculated by RODEX3A, was transferred to S-RELAP5.

A steady-state initialization calculation was made to obtain the desired initial conditions for the transient simulation. The calculated and measured initial conditions agree quite well and the calculated initial conditions generally are within the uncertainty band of the measured quantities (Reference 5). The calculated initial broken loop temperature of 560.8 K for the cold leg and 560.5 K for the hot leg come very close to measured values considering the large error bands quoted for the measured data, namely $554.3 \text{ K} \pm 1.8 \text{ K}$ for the cold leg and $565.5 \text{ K} \pm 1.8 \text{ K}$ for the hot leg.

The calculation for this analysis is a simulation of Test L2-3 from 10 seconds before the break initiation at 0 seconds up to 100 seconds. This time interval was chosen because the important phenomena and significant events of L2-3 occurred during this period.

For assessment purposes, the LOCA phenomena of primary interest are as follows:

- Fuel initial stored energy
- System blowdown and depressurization
- PCP performance
- DNB or CHF
- Bottom-up or top-down rewet
- Subcooled and two-phase critical flow through the break
- System refill and ECC bypass
- Core reflood and rod quench
- PCT.

Reference 5 discusses the assessed capability to calculate each of these LOCA phenomena; the details are not repeated here. Figure 4.148 compares the calculated and measured PCT versus core elevation. This figure refers to the PCT as a maximum cladding surface temperature, either calculated or measured at the various locations, during the LOCA transient history. The comparison shows that the calculated temperatures are quite close to the

measured temperatures below the 15-in elevation, much greater than the measurements from 15-in to 44-in elevation, and much lower than measurements above the 44-in elevation. The comparison can be considered acceptable because the calculated temperature trends followed the data trends, although the magnitudes did not compare well, and the calculated temperatures were overpredicted for the high power region. The highest PCT of 942 K (1236 F) was measured at the 15-in elevation while the calculated PCT was 1005 K (1350 F).

4.3.2.1.5 LOFT Test L2-5 Assessment

Test L2-5 was the third LBLOCA test conducted in the LOFT facility in which the reactor core power provided the primary heat source. The test represented a hypothetical cold leg guillotine break that simulated a double-ended, offset, shear break in a commercial (1000 MWe) 4-loop PWR. The test was initiated at 75% thermal power (36 MWt) and a 12.22 kW/ft maximum LHGR.

Operation of the LOFT PCPs differs from a typical PWR in that the LOFT pump rotors are electromagnetically coupled to their flywheel system. It is normal during LOFT tests to uncouple the pumps from their flywheels whenever the pump speed falls below 750 rpm (78.54 rad/s). During the L2-5 test, the two PCPs were tripped at 1 second and disconnected from their flywheels. This provided a rapid pump coast down. This operation of the pumps reduced the flow into the vessel to less than the flow to the break, thus preventing an early bottom-up fuel rod rewet. These simulated conditions are more typical of a 3-loop PWR than a 4-loop PWR. LOFT pumps normally coast down while connected to their flywheels that were designed to represent the normal pump coast down of commercial W 4-loop PWRs.

The Test L2-5 HPIS flow is 58% of Test L2-3 HPIS flow and is 75% of Test LP-02-6 HPIS flow because an improper small break HPIS flow condition was inadvertently specified for Test L2-5. The injections of high and low pressure ECCSs were delayed to 23.9 and 37.32 seconds, respectively, to simulate the expected delay in starting up the emergency power diesel generator to run the ECCS.

Before the transient started, the power level in the reactor core was steadily increased, then held at 36 MW \pm 1.2 MW for about 28 hours. This ensured that an appropriate decay heat power level would be obtained once the control rods were inserted into the reactor core. Test conditions before the beginning of the L2-5 test were as follows.

- The primary intact loop mass flow rate was set at $192.4 \text{ kg/s} \pm 7.8 \text{ kg/s}$.
- The hot leg pressure was $14.94 \text{ MPa} \pm 0.06 \text{ MPa}$.
- The primary coolant system hot and cold leg temperature were held at $589.7 \text{ K} \pm 1.6 \text{ K}$ and $556.0 \text{ K} \pm 4.0 \text{ K}$, respectively.

Test L2-5 was conducted to address conservatism in current licensing analyses. Many W plants are limited by Appendix K LOCA analysis results in which the calculated PCTs are predicted to occur during the reflood portion of the transient. Previous LOFT LB Tests L2-2 and L2-3 revealed that Appendix K requirements may be overly conservative because Appendix K criteria preclude the return to nucleate boiling (rewetting) before the end of blowdown. However, Tests L2-2 and L2-3 demonstrated that system hydraulic behavior can lead to an early rewet of the fuel cladding. This early rewet not only limits the PCT during blowdown [], but also removes a significant amount of stored energy from the fuel rod, thus reducing the reflood PCT. The cladding temperatures during reflood after blowdown rewet will be much lower than those occurring without rewet. Preventing the early rewet provides maximum core stored energy at the end of blowdown, and beginning of refill/reflood.

The test results showed that the early bottom-up core wide rewet that occurred in Tests L2-2 and L2-3 did not occur in Test L2-5 as planned. The PCT was 1078 K (1481 F), and because there was no early rewet and the hot rod temperature was fairly constant over a long period of time, there was no clear demarcation of blowdown and the reflood PCT was clearly the maximum. The cladding completely quenched at $65 \text{ seconds} \pm 2 \text{ seconds}$. The test was complete after LPIS was terminated at 107 seconds .

From Reference 5, a bias of $11.4 \text{ K} \pm 16.2 \text{ K}$ ($20.5 \text{ F} \pm 29.2 \text{ F}$) should be applied to the measured PCT to account for the 'fin cooling' effects on the surface mounted thermocouples. Thus, the reportable PCT for LOFT L2-5 is 1105.4 K (1530.1 F).

A steady-state initialization calculation was performed to reach the desired steady-state conditions for initiating the LOCA calculation. The calculated and measured initial conditions agree quite well and the calculated initial conditions generally are within the uncertainty band of the measured quantities. The calculated initial broken loop temperature of 556.0 K for the cold

leg and 558.0 K for the hot leg come very close to measured values considering the large error bands quoted for the measured data, namely $554.3 \text{ K} \pm 4.2 \text{ }^{\circ}\text{K}$ for the cold leg and $561.9 \text{ K} \pm 4.3 \text{ }^{\circ}\text{K}$ for the hot leg. The desired steady-state conditions were successfully achieved and the calculation accurately reached the L2-5 test initial conditions.

For the transient calculation, a short steady-state calculation before the break opening is carried out to ensure that the steady-state initial condition is properly maintained when switching from the steady-state input model to the transient simulation. The calculation for this analysis is a simulation of Test L2-5 from 10 seconds before the break initiation at 0 seconds up to 140 seconds. This time interval was chosen because the important phenomena and significant events of Test L2-5 occurred during this period.

The assessment of S-RELAP5 to predict each of the important LOCA phenomena is presented in detail in Reference 5. Figure 4.149 depicts the final comparison of the calculated and measured PCT versus core elevation. In this figure, the PCT is referred to as a maximum cladding surface temperature, either calculated or measured at the various locations, during the LOCA transient history. The comparison generally shows very good agreement and the differences between the calculated and measured PCT in the high power region between 15-in to 44-in elevations are quite small. Calculations and measurements both show a plateau region between the 15-in and 28-in elevations where maximum PCT occurs. The highest PCT of 1105.4 K (1530.1 F) was measured at the 24-in elevation and the calculated PCT was 1102 K (1524 F).

4.3.2.1.6 LOFT LP-02-6 Assessment

LOFT LP-02-6 was the fourth LOFT nuclear powered core LBLOCA test conducted with pressurized nuclear fuel rods and with a specification of minimum U.S. ECC injection rates. The maximum LHGR of 14.87 kW/ft was above the typical technical specifications currently used for licensing analyses of PWR fuel rods with the same approximate pellet diameter used in a 15 x 15 fuel pin array. Test LP-02-6 represented an NRC "design basis accident" test and was supposed to run at 100% power, 50 MWt, but because of questions concerning the integrity of the pressurized fuel rods in the central hot assembly, the power level was reduced to mitigate possible safety problems. LP-02-6 is an important LBLOCA test for code assessment because it addresses the issues relating to safety margins associated with the response of a PWR to the NRC "design basis accident" scenario, including delayed minimum ECC safeguards.

Test LP-02-6 simulated a cold leg guillotine break coincident with a loss-of-offsite power. It was conducted with a delayed and degraded high and low pressure ECC injection. During the test, the PCPs were tripped and coasted down with their flywheels attached. The result was an early partial core rewet from the bottom up. When PCP speed dropped below 750 rpm (78.54 rad/s), the flywheels were uncoupled from the pumps to increase the pump speed deceleration. The attached flywheels produced pump coastdown characteristics more typical of a commercial W 4-loop PWR.

Before the initiation of blowdown, the power level in the reactor core was steadily increased and then held at $46 \text{ MWt} \pm 1.2 \text{ MWt}$ to ensure that an appropriate decay heat power level would be obtained once the control rods were inserted into the reactor core. Test conditions at the beginning of the LP-02-6 test were as follows:

- The primary intact loop mass flow rate was $248.7 \text{ kg/s} \pm 2.6 \text{ kg/s}$,
- The hot leg pressure was $15.09 \text{ MPa} \pm 0.08 \text{ MPa}$, and
- The primary coolant system hot and cold leg temperatures were $589.0 \text{ K} \pm 1.0 \text{ K}$ and $559.0 \text{ K} \pm 1.1 \text{ K}$, respectively.

The LOFT LP-02-6 results showed the early bottom-up rewet of the fuel rods because the PCPs were allowed to coast down normally and the pump flow exceeded vessel side-break flow during the early part of blowdown, causing the early rewet. The early quench of the fuel rods extended to two-thirds of the core. Following the blowdown, the core underwent a second heat-up caused by a second dry-out. Because of the large fuel rod stored energy removal during blowdown, the PCT of 1074.0 K (1474.0 F) occurred early in the blowdown. The cladding completely quenched at $56 \text{ seconds} \pm 0.2 \text{ seconds}$. The test was complete after core reflood was completed at $59 \text{ seconds} \pm 1.0 \text{ second}$.

From Reference 5, a bias of $11.4 \text{ }^\circ\text{K} \pm 16.2^\circ \text{ K}$ ($20.5 \text{ }^\circ\text{F} \pm 29.2 \text{ }^\circ\text{F}$) should be applied to the measured PCT to account for the 'fin cooling' effects on the surface mounted thermocouples. Thus, the reportable PCT for LOFT Test LP-02-6 is 1104.8 K ($1529 \text{ }^\circ\text{F}$).

A steady-state initialization calculation was performed to reach the desired steady-state conditions for initiating the LOCA calculation. The calculated and measured initial conditions

agree quite well and the calculated initial conditions are generally within the uncertainty band of the measured quantities. The calculated initial broken loop temperature of 557.6 K for the cold leg and 558.3 K for the hot leg come very close to measured values considering the large error bands quoted for the measured data, namely $553.0\text{ K} \pm 6.0\text{ }^{\circ}\text{K}$ for the cold leg and $560.0\text{ K} \pm 6.0\text{ }^{\circ}\text{K}$ for the hot leg. The desired steady-state conditions were achieved and the calculation accurately reached the LP-02-6 test initial conditions.

A short, steady-state calculation before the break opening is carried out to ensure that the steady-state initial condition is properly maintained when switching from the steady-state input model to the transient simulation. The calculation for this analysis is a simulation of Test LP-02-6 from 10 seconds before the break initiation at 0 second up to 140 seconds. This time interval was chosen because the important phenomena and significant events of Test LP-02-6 occurred during this period.

The assessment of S-RELAP5 to predict each of the important LOCA phenomena for LOFT LP-02-6 is presented in detail in Reference 5. Figure 4.150 compares the calculated and measured PCT versus core elevation. This figure refers to the PCT as a maximum cladding surface temperature, either calculated or measured at the various elevations, during the LOCA transient history. The comparison shows that the code overpredicted the measured temperatures except at the low power region near the core exit. The greatest differences between the calculated and measured PCT occur in the high power region between the 15 in and 44 in elevations. The highest PCT of 1104.8 K (1529 F) was measured at the 26-in elevation. The comparison shows that the calculated PCT of 1159 K (1627 F) is in good agreement with data and conservatively exceeds the measured PCT in the high power core region.

4.3.2.1.7 LOFT Test LP-LB-1 Assessment

The fifth LOFT LOCE, Test LP-LB-1, simulated a hypothetical double-ended cold leg guillotine break initiated from conditions representative of a PWR operating near its licensing limits. The initial core power was near the facility design limit of 50 MWt with maximum LHGR of 15.8 kW/ft. Included in the test's boundary conditions were loss-of-offsite power coincident with the LOCE, a rapid PCP coastdown, and a minimum safeguard ECCS injection assumption from a European PWR. To minimize possible fuel pin damage, all of the fuel rods in the core were initially unpressurized.

Similar to LOFT Test L2-5, the PCP flywheels were uncoupled from the pump rotors to affect a rapid pump coastdown and prevent an early bottom-up core rewet. In this test, the PCPs were tripped and uncoupled from their flywheels within 1 second after the start of the transient.

The ECC injection assumption for this test resulted in an accumulator liquid volume that was approximately 70%, and a pumped injection flow rate that was about 50% of that used in Test LP-02-6. The pumped injection was accomplished using the LPIS with a delay of nearly 32 seconds to simulate the delay in starting the emergency power diesel generator.

Before the start of the transient, the power level in the reactor core was steadily increased, then held at $49.3 \text{ MWt} \pm 1.2 \text{ MWt}$ to ensure that an appropriate decay heat power level would be obtained once the control rods were inserted into the reactor core. Test conditions at the beginning of the LP-LB-1 test are as follows.

- The primary intact loop mass flow rate was $305.8 \text{ kg/s} \pm 2.6 \text{ kg/s}$.
- The hot leg pressure was $14.77 \text{ MPa} \pm 0.06 \text{ MPa}$.
- The primary coolant system cold leg temperature was $556.6 \text{ K} \pm 1.0 \text{ K}$ with a fluid temperature increase of $29.5 \text{ K} \pm 1.4 \text{ K}$.

Similar to Test L2-5, Test LP-LB-1 was conducted to produce an LBLOCA that had a maximum of core stored energy at the end of blowdown by preventing an early bottom-up core rewet. Then using the high temperature conditions at the start of reflood, the test explored the reflood behavior of the system and provided information against which best estimate computer code simulations could be evaluated.

As desired, the early bottom-up core-wide rewet did not occur in Test LP-LB-1. By altering the PCP coastdown, an early bottom-up rewet was prevented. The test did have a partial top-down rewet that resulted in two peaks in the cladding temperature history. A blowdown PCT of 1261.0 K (1810.0 F) occurred at about 13 seconds and a refill/reflood peak of 1257.0 K (1803.0 F). The clad temperature at the peak power location remained at an elevated temperature for a long time. The cladding was completely quenched at $72 \text{ seconds} \pm 1 \text{ second}$. The test was terminated at 132 seconds.

From Reference 5, a bias of $11.4^{\circ}\text{K} \pm 16.2^{\circ}\text{K}$ ($20.5^{\circ}\text{F} \pm 29.2^{\circ}\text{F}$) should be applied to the measured PCT to account for the 'fin cooling' effects on the surface mounted thermocouples. Thus, the reportable PCT for LOFT LP-LB-1 is 1284.0 K (1851.5 F).

A steady-state initialization calculation was performed to reach the desired steady-state conditions for initiating the LOCA calculation. The calculated and measured initial conditions agree quite well and the calculated initial conditions are generally within the uncertainty band of the measured quantities. The calculated initial broken loop temperature of 560.0 K for the cold leg and 558.3 K for the hot leg come very close to measured values considering the large error bands quoted for the measured data, namely $552.0 \text{ K} \pm 6.0 \text{ K}$ for the cold leg and $561.0 \text{ K} \pm 6.0 \text{ K}$ for the hot leg. The desired steady-state conditions were achieved and the calculation accurately reached the LP-LB-1 test initial conditions.

A short steady-state calculation before the break opening is carried out to ensure that the steady-state initial condition is properly maintained when switching from the steady-state input model to the transient simulation. The calculation for this analysis is a simulation of Test LP-LB-1 from 10 seconds before the break initiation at 0 second up to 240 seconds. This time interval was chosen because, although most the important phenomena and significant events of Test LP-LB-1 occur before 100 seconds, the quenching of the core occurred much later in the calculation.

The assessment of S-RELAP5 to predict each of the important LOCA phenomena for LOFT test LP-LB-1 is presented in detail in Reference 5. Figure 4.151 compares the calculated and measured PCT versus core elevation. In this figure, the PCT is referred to as a maximum cladding surface temperature, either calculated or measured at the various elevations, during the LOCA transient history. The comparison shows that S-RELAP5 overpredicted temperatures in the high power region up to the 44-in elevation, and slightly underpredicted temperatures above 44 in. The measured PCT is 1284.0 K (1851.5 °F) at the 24-in elevation. That measurement includes a bias and uncertainty of $11.4^{\circ}\text{K} \pm 16.2^{\circ}\text{K}$ ($20.5^{\circ}\text{F} \pm 29.2^{\circ}\text{F}$) caused by the fin cooling effects on the surface mounted thermocouple. The calculated maximum PCT of 1310 K (1899 F) also occurred at the 24-in core level and is in good agreement with the measured PCT. Based on Figure 4.151, the PCT at any elevation is within approximately 20% of the data, which is reasonable agreement.

4.3.2.2 Semiscale Tests

S-RELAP5 was assessed against the Semiscale LBLOCA tests S-06-3 and S-07-1. Test S-06-3 was performed in the Semiscale MOD-1 facility. The MOD-1 facility was scaled from the LOFT facility and Test S-06-3 was performed as a counterpart to LOFT Test L2-3. The results presented for this assessment are used to support the application of S-RELAP5 in PWR LBLOCA analysis and to verify the capability of the S-RELAP5 code to calculate integral LOCA phenomena in facilities of different scale.

Semiscale Test S-07-1 is a blowdown test performed in the Semiscale MOD-3 facility with cold-leg ECC injections. The results presented for this assessment are used to support the application of S-RELAP5 in PWR LBLOCA analysis and to verify the capability of the code to calculate blowdown film boiling heat transfer in the core.

4.3.2.2.1 Semiscale Facilities

MOD-1 Facility

The Semiscale MOD-1, 1½-loop facility was scaled to the LOFT facility, which in turn was scaled to a 4-loop PWR. It is designated a 1½-loop system because it is configured with one active loop and one passive blowdown loop. Subsequent Semiscale facilities have included components that have made the facility more typical of a PWR. All the other Semiscale facilities were designed with 1/1600 to 1/2000 volume scaling, with full height, in reference to a 4-loop, 3400 MWt PWR.

The MOD-1 system contains a reactor vessel with internals, including a 40-rod electrically heated core, an active intact loop scaled to represent three loops of a PWR and a broken loop scaled to a single loop of a PWR. The intact loop contains an active steam generator and an active PCP and is connected to the pressurizer. The broken loop contains hydraulic simulators for the steam generator and pump and break simulators or rupture assemblies connected to a blowdown suppression system. The blowdown suppression system simulates containment pressure.

The 40-rod electrically heated core has a PWR fuel pin pitch (0.563 in) and the heated length (5.5 ft) and outside diameter (0.42 in) are identical to the nuclear fuel rods of the LOFT core.

Semiscale Test Series 6 was performed to assist the LOFT program in planning the first nuclear test series. Test S-06-3 was performed as a counterpart to LOFT Test L2-3. For this test, the four central heater rods were operated at approximately 39.4 kW/m, 32 rods were operated at approximately 24.9 kW/m, and four rods were unpowered to simulate passive rod locations. This configuration yielded a peaked power profile that simulates that of the LOFT facility and provides a total core power of 1.004 MW.

The safety injection includes the HPIS, LPIS, and accumulators. For Test S-06-3, two HPIS pumps and two LPIS pumps delivered flow into the intact-loop cold leg along with the intact-loop accumulator. The primary coolant pump was powered for the entire transient.

MOD-3 Facility

The Semiscale MOD-3 facility is constructed with two fully active coolant loops. The intact loop, retained from the Semiscale MOD-1 system, was scaled to the LOFT facility, which in turn was scaled to a 4-loop PWR. The broken loop, on the other hand, was scaled directly to a 4-loop commercial PWR. The Semiscale MOD-3 facility was designed with 1/1600 to 1/2000 volume scaling and full height, in reference to a 4-loop, 3400 MWt PWR.

The vessel in the MOD-3 system consists of the upper plenum with internals required to represent guide and support tubes, upper head, 25-rod electrically heated core, and an external single pipe downcomer. The active intact loop is scaled to represent three loops of a PWR and the active broken loop is scaled to represent a single loop of a PWR. The intact loop contains a pump and the short Type I steam generator, and is connected to the pressurizer. The broken loop contains the taller Type II steam generator in addition to pump and break simulators or rupture assemblies connected to a blowdown suppression system. The blowdown suppression system simulates containment pressure.

The 25-rod electrically heated core is characterized by fuel pin pitch (0.563 in) and outside diameter (0.422 in) typical of a PWR. The heated length (12 ft) of the MOD-3 core is identical to a 4-loop PWR core.

Test S-07-1 was performed to establish the baseline performance of the MOD-3 system during a blowdown with cold-leg ECC injections. It was conducted to obtain core heat transfer and DNB characteristics of the heater rods. The MOD-3 system was initialized in the experiment to

a primary pressure of 15.95 MPa, total-loop flow of 9.4 kg/s and cold-leg temperatures of 559 K for the intact loop and 557 K for the broken loop at a core power level of 2.01 MW nominal. The system was subjected to a double-ended cold-leg break through a rupture assembly and two non-communicative nozzles. (Reference 5).

4.3.2.2.2 Semiscale Test Descriptions

Test S-06-3

In Test S-06-3, the MOD-1 system was initialized to a primary pressure of 15.769 MPa, cold leg temperature of 563 K, and inlet flow of 6.68 L/s (liters per second) at the initial core power level of 1.004 MWt. The system was subjected to a double-ended cold leg break through two rupture assemblies and two LOFT facility counterpart nozzles, each having a break area of 0.000243 m² (0.00262 ft²). The effluent from the primary system was ejected into the pressure suppression system.

After initiating blowdown, power to the heated core was reduced to simulate the predicted heat flux response of the nuclear fuel rods during a LOCA. Blowdown was accompanied by ECC injection into the cold leg piping of the intact loop. Coolant injection from the HPIS began at blowdown and continued until test termination (300 seconds). Coolant injection from the accumulator started at approximately 18.5 seconds after rupture and terminated at approximately 68.7 seconds. LPIS began at 25.5 seconds after rupture at a pressure of 1900 kPa and continued until test termination.

Test S-07-1

The specific test conditions simulated in the calculation are as follows:

- The 23 rods in the square matrix of the 25-rod electrically heated core were operated at approximately 36.9 kW/m with a flat radial power profile resulting in a total core power level of 2.01 MW nominal. One corner rod (Rod E-5) was unpowered and another corner rod (A-1) was replaced by a liquid level probe. The normalized axial power profile is a chopped cosine with peak axial power factor of 1.55 nominal (Reference 5).
- During the blowdown transient, power to the electrically heated core was automatically controlled to simulate the thermal response of nuclear heated fuel rods. The power history is modeled based on the measured core power decay.

- The accumulators for the intact (IL) and broken (BL) cold legs were pressurized with nitrogen to 4137 kPa (600 psia). IL accumulator injection began at 19 seconds and nitrogen discharge began at 72 seconds. BL accumulator injection began at 12.5 seconds and nitrogen discharge began at 35 seconds. The IL and BL accumulator injected flows are modeled based on the measured data. The accumulators are actuated in the calculation on time, not pressure, to match the injection timing of the experiment.

The simulation will extend from the time of pipe rupture until the time before nitrogen injection. Nitrogen was injected at 35 seconds, originating from the BL accumulator. Therefore, the simulation will extend for 35 seconds transient time after pipe rupture.

- The initial containment pressure is 246 kPa nominal. The transient containment pressure is modeled based on the measured data.
- The maximum break area corresponding to a double-ended break is 0.849 in^2 (5.48 cm^2) and is modeled. This implies that each of the two blowdown nozzles had a break area of $0.849 \div 2$ or 0.424 in^2 ($5.48 \div 2$ or 2.74 cm^2). This maximum break area was determined from the ratio of the maximum break area to the primary liquid volume of a PWR system applied to the primary liquid volume of the Semiscale MOD-3 system.
- The intact- and broken-loop primary coolant pumps coast down during the test. The IL and BL pump are modeled based on the measured data.
- HPIS flow into the intact and broken loops started at 3.5 seconds at a pressure of 12,410 kPa (1800 psia) and continued until test termination. The IL and BL HPIS injected flows are modeled based on the measured data. The HPIS pumps are actuated in the calculation on time, not pressure, to match the injection timing of the experiment.
- The LPIS started into the IL and BL at 27 seconds at a pressure of 2000 kPa (290 psia) and continued until test termination. The IL and BL LPIS injected flows are modeled based on the measured data. The LPIS pumps are actuated in the calculation on time not pressure to match the injection timing of the experiment.
- The measured fluid temperature in the IL and BL ECCS injection lines indicate that the ECCS (HPIS, LPIS and accumulator) water temperature is approximately 300 K (80.6 °F). Therefore, the IL and BL ECCS water are both modeled at a temperature of 300 K.

4.3.2.2.3 Test S-06-3 Assessment

Through a sensitivity study, the "best" discharge coefficients were determined to be 0.8 for the vessel side and 0.7 for the pump side break junctions for both the subcooled and two-phase flows. The nodalization of the input model was developed to be as consistent as possible with the LBLOCA input guidelines (Reference 12).

The S-RELAP5 initial condition results match reasonably well with the Semiscale Test S-06-3 data. The detailed comparisons of predicted versus measured results for the important transient phenomena are shown in Reference 5, and are not repeated here. The calculation results have been compared to test data for the three phases of the test (blowdown, refill, and reflood). While reasonable agreement is obtained between code results and data for the major thermal-hydraulic variables, the MOD-1 Test S-06-3 experienced apparent ECC bypass that could not be caught well by the LBLOCA methodology. This resulted in earlier refill being calculated and consequently earlier calculated reflood and quenching of the heater rods. The PCT of 1152 K in the test occurs at an elevation of 21 in above the bottom of the heated length at 20.7 seconds after pipe rupture. The calculated PCT of 1161 K occurs during blowdown at an elevation of 31.2 in above the bottom of the heated length at 26.5 seconds after pipe rupture. Figure 4.152 shows the calculated versus measured maximum temperatures as a function of elevation in the simulated core for Semiscale Test S-06-3.

4.3.2.2.4 Test S-07-1 Assessment

S-RELAP5 was assessed against Semiscale Test S-07-1. The calculation results have been compared to test data. Reasonable to good agreement is obtained between code results and data for the major thermal hydraulic variables including upper plenum pressure, break flow rates, coolant temperatures, and rod temperatures. The comparison demonstrates that S-RELAP5 is capable of simulating the blowdown film boiling heat transfer phenomena expected of a PWR LBLOCA transient. In particular, the code conservatively predicted the average of measured PCT at all elevations. For instance, the calculated maximum temperature at an elevation of 72.4 in is 1092 K compared to the average measured PCT of 1056 K at this elevation (based on eight thermocouple readings). In addition, the highest calculated PCT is 1108 K, compared to the highest measured (not average) PCT of 1101 K. Figure 4.153 shows the calculated versus measured maximum temperatures as a function of elevation in the simulated core for Semiscale Test S-07-1.

4.3.3 Methodology Treatment of PIRT Phenomena

Sections 4.3.1 and 4.3.2 reviewed the extensive assessment of the S-RELAP5 code with regard to capabilities to predict the important phenomena identified in the LBLOCA PIRT. In some cases statistical information was determined with regard to the mean values and uncertainties for predicting a specific phenomenon. Much of this information also is contained in Section 5 of the S-RELAP5 Code Verification and Validation, Report EMF-2102 (Reference 5). In other cases, the code, in its current configuration, was shown to calculate the phenomenon conservatively and no evaluation of the bias and uncertainty was performed. In these situations the conservatism associated with these phenomena was simply accepted as unquantified conservatism in the methodology. Table 4.18 summarizes the important PIRT phenomenon and how that phenomenon is being addressed in the methodology.

4.3.3.1 PIRT Phenomena Not Treated Statistically

From the comparison of the code predictions and data for both the SET and IET assessments, a number of important PIRT phenomena were found to be predicted conservatively by the code. The conservative prediction was either because of a conservative model in the code or the use of conservative input. These phenomena are indicated in Table 4.19 as being treated in the methodology as an "inherent conservatism" or an "input conservatism". By "inherent conservatism" is meant that a code model or combination of models has been demonstrated to conservatively predict these phenomena. By "input conservatism" is meant that the input being provided to the code has been demonstrated to be conservative and will be used in NPP analyses. These conservatisms are accepted in the methodology as an unquantified conservatism above that indicated by the statistical analysis. These phenomena will be discussed individually in the following sections.

4.3.3.1.1 Core 3-D Flow and Void Distributions

The core flow distribution and void distribution are determined by the initial power distributions and [

] In

effect this will result in a wide variation of calculated flow and void distributions in the core.

The ability of the code to calculate void distributions has been demonstrated in the SET assessments performed for the THTF level swell, GE level swell, and the FRIGG-2 tests. For all these assessments, the agreement between code prediction and measured void fractions was good to excellent (Section 4.3.1 and Reference 5). This indicates that the code is capable of calculating acceptable void distributions in the core.

The ability of the code to calculate flow distributions in the core was demonstrated in the SET assessments (Section 4.3.1 and Reference 5) performed for the multi-dimensional flow tests, CCTF, and SCTF. The multi-dimensional flow tests demonstrated that the code was capable of modeling and predicting the measured flows in these tests. In addition, the assessments performed for SCTF test S2-17 and S2-18 demonstrated that the combined code and core nodalization was capable of predicting the effects of changes in radial power distribution and associated flows during the reflood period of the LBLOCA. This was demonstrated by comparing the calculated with the measured PCTs for those tests.

The CCTF assessments further demonstrated that the combined code and core nodalization was able to predict the core flows and resulting PCTs in a cylindrical facility. The cylindrical facility is consistent with the input modeling used in the methodology NPP nodalization.

Based on the information in the previous paragraph, the combination of these assessments clearly demonstrates that the code is capable of realistically predicting the core flows and void distributions as the statistical parameters are being varied in the statistical analysis of the LBLOCA. In addition, the code prediction of flow and void distributions is an integral part of determining the code heat transfer biases and uncertainties. [

]

4.3.3.1.2 Liquid Entrainment in Core

The liquid entrainment in the core has been demonstrated to be conservatively calculated by the code and methodology nodalization. This is shown in the assessments performed for CCTF, UPTF, and FLECHT-SEASET and reported in Section 5.6 of Reference 5. In the CCTF tests examined, Tests 54, 62, 67, and 68, the conclusion was that the liquid entrained from the core into the upper plenum was overpredicted by the code during the early part of the test. This

overprediction occurred until about 400 to 500 s into the test, after that the code underpredicted the amount of liquid in the upper plenum. Only after quenching occurred in the test did the data indicate higher levels. Both the measured and calculated time of PCT occurred before the calculation began to underpredict the liquid in the upper plenum.

For the FLECHT-SEASET tests, as shown in Figures 4.61 through 4.69, the mass of water in the test section is underpredicted by the code and methodology nodalization. This is consistent with the results provided in Figures 4.70 through 4.75, which show that the code is overpredicting the water carryover from the test assembly.

For UPTF Test 10, Run 081, and Test 29, Run 212/211, the water level in the upper plenum was consistently overpredicted by the code and methodology nodalization. This overprediction by the code is shown clearly in Figures 4.154 and 4.155.

In conclusion, the code predicted liquid carryout from the core to the upper plenum was examined in three different test facilities. In all three test facilities, the amount of liquid carry out of the core into the upper plenum was overpredicted. Given these results from three different test facilities, it is concluded that the code and methodology prediction of core entrainment is conservative and no bias or uncertainty was developed to take credit for this conservatism.

4.3.3.1.3 Core Flow Reversal/Stagnation

The reversal and stagnation of flow in the core is the result of the size of the break and the rate of coolant loss versus the rate of coolant injection from the ECC systems. Generally, a combination of other phenomena occur to determine the limiting set of conditions that result in the worse situation where the flow in the core is essentially stagnant or has a low reflood rate for the longest period of time. This condition is addressed by the random variation of the other dominant phenomena. [

]

4.3.3.1.4 Upper Plenum Liquid Entrainment/de-entrainment

When liquid droplets are entrained in the core and carried up into the upper plenum they can remain there, fall back into the core (de-entrainment) or be carried out into the hot leg (entrainment). The major modeling concern for LBLOCA is that allowing too much liquid to fall back into the core would result in a top-down quench and a significant underprediction of the PCT. It would also reduce steam binding. To demonstrate conservatism, the calculated upper plenum collapsed liquid levels were compared to a series of tests and shown to be higher.

Tests at CCTF (54, 62, 67 and 68), FLECHT-SEASET (31805, 31203, 31302 and 31701) and UPTF (Test 10, Run 081 and Test 29, Run 211/212) were used to evaluate the balance of liquid droplet flows in the upper plenum. These tests simulated a PWR core using either steam and water (UPTF) or electrically heated, simulated fuel rods during the reflood period. The calculated liquid levels were compared to the measured liquid levels in the upper plenum region.

The liquid level in the upper plenum is generally overpredicted by S-RELAP5 for reflood conditions. This seems to be true for the prototypic upper plenum of the UPTF (Section 4.3.3.1.2 above), the scaled upper plenum in the CCTF (see Figures 4.156 through 4.159) and the atypical upper plenum of the FLECHT-SEASET tests (see Figures 4.160 through 4.163).

The conclusion is that, using the RLBLOCA methodology, S-RELAP5 tends to hold the liquid in the upper plenum to a slightly greater degree than testing would indicate when the liquid fractions are low. When substantial amounts of liquid are present, S-RELAP5 tends to carry over more than enough liquid and S-RELAP5 models liquid carry-over for the LBLOCA conservatively.

4.3.3.1.5 Counter Current Flow Limit (CCFL)

The CCFL phenomenon is addressed conservatively in the methodology by applying conservative input to the Kutateladze parameters. For the methodology, the following parameters will be used [] This has been shown to provide a conservative prediction of down flow at the UTP for the FRA-ANP specific UTP designs and in the UPTF assessment.

Figures 4.103 through 4.105 demonstrate the conservative comparison for the FRA-ANP current UTP designs for the W 15x15 and 17x17 fuel designs and for the CE 14x14 fuel design. Figures 4.116 and 4.117 and Figures 4.120 and 123 demonstrate the conservatism for the UPTF Test 10, Runs 080 and 081, Test 29, Run 212/211, and Test 12, Run 014. For all these tests, the selected Kutateladze parameters are demonstrated to be conservative.

This conservative set of Kutateladze weighting parameters were selected primarily to address the issue in the assessments (CCTF, SCTF, FLECHT-SEASET, THTF, Semiscale) where best estimate parameters are unavailable. To be able to use these assessments and still meet the CSAU requirement that the assessments use the same model as the NPP analysis, it was decided to use a conservative set of parameters.

4.3.3.1.6 Hot Leg Entrainment/de-entrainment

Liquid entrained into the upper plenum is carried through the hot leg to the steam generator, where it flashes to steam and increases the pressure drop. The more liquid reaching the steam generator, the more conservative the modeling. The liquid carry-over to the steam generator was calculated using modeling based on the RLBLOCA methodology and compared to measured carry-over values for a series of tests.

Tests at CCTF (54, 62, 67 and 68), FLECHT-SEASET (31805, 31203, 31302 and 31701) and UPTF (Test 10, Run 081 and Test 29, Run 211/212) were used to evaluate the carryover of liquid droplets in the hot leg and the steam generator. These tests simulated reflood conditions for a PWR by either introducing steam and water (UPTF) or by quenching electrically-heated, simulated fuel rods (CCTF and FLECHT-SEASET). CCTF used prototypic U-tubes in the steam generator and had a cyclone separator downstream of the steam generator exit. The UPTF was full scale and used cyclone separators in its steam generator simulators to trap water carried over by the hot leg. FLECHT-SEASET had a smaller (~4") horizontal pipe carrying the steam and water from the upper plenum to a separator and collector.

For the CCTF tests, the liquid is separated well downstream (~30') after the exit of the steam generator. Figures 4.164 through 4.167 compare the calculated level changes in the catch tank with the measured changes. The measurements are somewhat inaccurate (note the level decreases which affect the first three cases) and the piping from the steam generator exit to the catch tank introduces some uncertainties. The predicted trends are correct and for the tests

with higher flows (54 and 68) the predicted levels are either conservative or in reasonable agreement.

For the UPTF tests, the liquid is separated in the steam generator simulator. For the two tests, the calculated liquid accumulating in the catch tanks is quite conservative (See Figures 4.168 through 4.171).

For the FLECHT-SEASET tests, there is no steam generator. The hot-leg piping terminates in a separator, which has a tank with a pipe in the bottom leading to a drain tank. Figures 4.172 through 4.179 compare the calculated levels in the separator tank and the separator drain tank with the measured levels. Because of the tendency of the model to hold a larger quantity of liquid in the upper plenum initially than would be indicated by measurements (See Section 4.3.3.1.4), the calculated carry-over to the separator is delayed. The bottom line for these figures is that the calculation has the liquid carried over to these tanks arriving slightly later than the measurements would indicate, with the overall carry-over from the calculation being greater. This latter point shows that the liquid entrained and carried over by the hot-leg model is conservative.

4.3.3.1.7 Two Phase Pump Degradation

The pump two phase degradation is addressed in the methodology as a best estimate input. Based on the sensitivity study described in Appendix B for a limiting break on both a 3-loop and a 4-loop plant, it is shown that this is not an important phenomenon for the limiting LBLOCA case. The use of the Semiscale two-phase degradation instead of the CE/EPRI two-phase degradation model produced essentially no impact on the 3-loop results and only an 18 F (10 K) for the 4-loop plant. Thus, the best estimate CE/EPRI model will be used in the RLBLOCA methodology.

4.3.3.1.8 Pump Differential Pressure Loss

The pump differential pressure loss is addressed in the methodology strictly as a best estimate. The S-RELAP5 code has the ability to input the pump specific homologous curves for the NPP being analyzed and this option is used. The homologous curves for the specific NPP pumps are obtained from the utility and, if plant data is available, a pump coast down is modeled to ensure that the curves are consistent with the plant data.

4.3.3.1.9 Non-Condensable Transport

The treatment of non-condensibles in the S-RELAP5 code was demonstrated to be conservative by the performance of an assessment of the ACHILLES ISP #25. The rod thermocouples in the test all clearly showed a reduction in temperature following the introduction of nitrogen into the system. The S-RELAP5 code conservatively underpredicted this cooldown, as shown in Figures 4.136 through 4.141. Thus, the impact of the nitrogen injection following the accumulator emptying of water will be conservatively predicted in the NPP analysis. However, as indicated in the sensitivity studies (Appendix A), the injection of nitrogen into the RCS system following the emptying of the accumulators was found to not significantly affect the final predicted LBLOCA event PCT.

4.3.3.1.10 Downcomer Entrainment

The S-RELAP5 prediction of the downcomer entrainment was demonstrated to be conservative through the assessment of UPTF Tests 6 and 7 (Section 4.3.1 and Reference 5). In these essentially full scale tests the lower plenum fill rate was measured as a function of time during the tests. Test 6 consisted of five different test assessments where the steam flow rate up the downcomer was varied with a constant ECC injection rate. One run from Test 7 was used in the assessments to extend the downcomer steam flow rate to a lower value.

The comparison of the lower plenum level for Test 6 is provided in Figures 4.106 through 4.110 and for Test 7 in Figure 4.111. These level comparisons show that S-RELAP5 underpredicts the lower plenum level for all the Test 6 and 7 assessments using the methodology NPP nodalization (Reference 12). This indicates that S-RELAP5 is overpredicting the entrainment of the ECC water and carrying it out the break. Thus, the results clearly indicate that the S-RELAP5 code overpredicts the bypass of ECC water in these full scale tests. Based on these results, it is concluded that the S-RELAP5 predictions will provide a conservative result with respect to ECC bypass, lower plenum fill, and core recovery. (For a discussion of the oscillations in the lower plenum level, see the discussion on lower plenum sweepout.)

4.3.3.1.11 Downcomer Liquid Level Oscillations

The downcomer liquid level oscillation is another phenomenon that is controlled primarily by other important phenomena. The ranging of these phenomena either will or will not produce the oscillations based on their specific ranging.

Manometer type downcomer liquid level oscillations have not been observed to any significant extent in the methodology NPP nodalization models. This appears to be the result of the boiling in the downcomer acting as a stabilizer for the phenomenon. Preliminary undocumented calculations in which the downcomer heat structures were uncoupled were able to produce manometer type downcomer level oscillations. The lack of these oscillations in the methodology NPP nodalization model is conservative because the effect of the oscillations is to drive water up into the core and provide an additional cooling mechanism. Thus, the fact that this phenomenon is not predicted by the methodology NPP model is acceptable.

4.3.3.1.12 Lower Plenum Sweepout

The conservatism of the S-RELAP5 lower plenum sweepout is also demonstrated in the essentially full scale UPTF Test 6 and 7 assessments with the methodology nodalization (Reference 12). Again these tests were performed with a constant ECC injection rate and with various steam flow rates up the downcomer. The measured versus code prediction of the lower plenum level is provided in Figures 4.106 through 4.110 for Test 6 and Figure 4.111 for Test 7.

In these figures the predicted lower plenum level shows a series of decreases. These decreases in the lower plenum level are a result of the prediction of liquid sweepout from the lower plenum. This sweepout is seen to be more pronounced in the higher steam flow rate assessments, Test 6, Runs 131, 132, 133, and 135, and less pronounced in the two lower steam flow rate assessments, Test 6, Run 136 and Test 7, Run 203. The measured data in these figures do not show these large sweepout events.

The large sweepout events predicted in the UPTF Test 6 and 7 assessments is a direct result of the methodology nodalization used in the lower plenum. Sensitivity studies were performed (Reference 5) that clearly showed that this sweepout prediction could be corrected with a more detailed model (i.e., a 2D lower plenum model). However, because many of the other assessments had already been run, it was decided to continue to use this lower plenum model and to simply accept the conservatism in the methodology.

4.3.3.2 PIRT Phenomena Treated Statistically

The parameters presented in this section are to be treated statistically in the FRA-ANP RLBLOCA methodology. The uncertainties developed from S-RELAP5 code assessments have been presented in Section 4.3.2 and Section 5 of Reference 5. For those parameters a

summary is provided giving the parameter bias and uncertainty and how it is to be applied in the methodology. In addition to these parameters, a few other parameters are being treated statistically based on analysis other than code assessment. The discussion on these parameters includes additional background and explanation of the objective of the statistical treatment. Table 4.19 presents a summary of the key statistical characteristics used in the FRA-ANP RLBLOCA methodology. The table provides a list of biases, standard deviations (for parameters treated with a normal probability distribution function), and range boundaries ($\pm 2\sigma$ for normal probability distribution functions).

4.3.3.2.1 Stored Energy

The analysis of stored energy uncertainty was performed by assessing RODEX3A predictions for centerline fuel temperature relative to data taken at the Halden Reactor Project. The results are presented in Section 5.8 of Reference 5. Using a normal probability distribution function, the mean error in centerline fuel temperature is 0.0 with a standard deviation of 130 °F. A bias in centerline temperature has been identified for burnup greater than 10 MWd/kgU. This is given by the expression:

$$Y\{^{\circ}\text{F}\} = -4.2232 * X\{\text{MWd/kgU}\} + 39.183\text{ }^{\circ}\text{F}$$

The parameter is first sampled using a normal distribution with a mean of 0.0 and standard deviation of 130 °F. A test on "Time-of-Cycle" is performed to check if the bias is to be applied. If so, the bias is then added to the sampled centerline fuel temperature. In applying the sampled fuel centerline temperature, the S-RELAP5 multiplier, FUELK, is used in conjunction with a control system that tracks the centerline temperature of the peak power node. The FUELK multiplier is applied to the fuel pellet thermal conductivity. Using a control system applied during a steady-state S-RELAP5 calculation, this multiplier is driven to a value that results in shifting the fuel centerline temperature from a best-estimate value to the best-estimate value plus uncertainties as given by the equation above.

4.3.3.2.2 Oxidation

Energy released through the oxidation of cladding is calculated from the Cathcart-Pawel correlation (Reference 25) for oxide layer growth:

$$\frac{\delta_{\phi}^2}{2} = 0.01126 \exp(-35890 / RT)$$

R is the universal gas constant (1.987 cal/mole-K) and T is clad temperature. This appears in the S-RELAP5 Models and Correlations document (Reference 9) as

$$\frac{\partial \Delta r_{\phi}}{\partial t} = \frac{0.000002252}{2\Delta r_{\phi}} \exp(-18062 / T)$$

In Reference 25, uncertainties are provided for both the constant term and the exponential term. It is reported that the 90% confidence limits on the constant term is -23% to +30% and on the exponential term, it is $\pm 2.2\%$. A standard deviation is calculated from the upper 1-sided 95% probability point (+30%, 2.2%). Assuming a normal distribution, this corresponds to 1.645 standard deviations; hence, the standard deviation is

$$\frac{30\%}{1.645} = 18.237\% \text{ on the constant term and } \frac{2.2\%}{1.645} = 1.337\% \text{ on the exponential term.}$$

4.3.3.2.3 Decay Heat

The FRA-ANP realistic LOCA evaluation model, S-RELAP5, calculates decay heat based on the 1979 ANSI/ANS standard (ANSI/ANS-5.1-1979, Reference 26). This standard is applicable to light water reactors containing Uranium 235 as the principal initial fissile material.

Fission contributions from Plutonium 239 and fast fission of Uranium 238 can be explicitly treated using the standard; other fissionable isotopes are treated as Uranium 235. Methods of accounting for the effect of decay energy from neutron capture in fission products are also described in the standard, and equations for decay of the capture product actinides Uranium 239 and Neptunium 239 are shown. The 1979 standard considers the reactor operating history and the average recoverable energy associated with fission of each of the above isotopes. Two types of reactor operation are presented, a fission pulse and a constant fission rate over an operating time period. Both methods yield decay power but do not account for the spatial distribution of the decay power deposition.

The decay heating described by the standard can be used for many types of calculations including LOCA analysis. However, considerations for LOCA are somewhat different from other

applications. LOCA is a hypothetical event which must be analyzed prior to reactor operation. Thus, the operating history and the concentration of fissionable isotopes will not be known prior to a LOCA. Fortunately, simplifying assumptions can be made which allow calculation of a realistic but slightly conservative decay heat curve as a function of time using the 1979 standard. The decay heat calculated with these assumptions bounds the more detailed decay heat curves that would result if the conditions at the initiation of LOCA were known. The assumptions are:

- infinite operating time at full power.
- All fissions assumed from U 235
- 200 MeV / fission (conservatively low)
- One standard deviation total decay heat of []

LBLOCAs are a short time event with PCT and quenching occurring on the order of 100 seconds and well within 1000 s. For this short decay time, decay energy tends to be dominated by short-lived fission products. A characteristic of short-lived fission products is that they approach equilibrium concentrations within a short operating time. The assumption of infinite operating time is equivalent to assuming equilibrium fission product inventory. While this assumption is bounding, it is also realistic with respect to the dominant short-lived fission product isotopes.

The ANS standard suggests a simplified method of calculating decay heat assuming Uranium 235 as the only fissionable isotope and applying a conservative multiplier. FRA-ANP makes the assumption that all fissions are from Uranium 235, and adjusts the uncertainty to account for the other isotopes.

The assumption of 200 MeV / fission converts power to fission rate. A low value is conservative. The components of this parameter and the uncertainties are described in more detail in following paragraphs.

Total decay heat using these assumptions was compared to more detailed calculations, and it was determined that use of a one standard deviation uncertainty of [] conservatively bounds total decay heat using these assumptions.

In addition to fission product decay heat, actinide capture product decay power is computed using the ANS standard equations, and added to the fission product decay heat.. In this calculation a conversion ratio appropriate for the time in cycle analyzed is obtained from core neutronics calculations. The ANS standard also provides equations to calculate the addition of decay heat from neutron capture in fission products. These equations are included in S-RELAP5 and the contribution to the total decay heat from this source is calculated and included.

4.3.3.2.4 Departure from Nucleate Boiling

Test results from the THTF Heat Transfer separate-effects test contributed to identifying a bias in the Biasi CHF correlation (Reference 5). [

] The CHF scaling is applied for RLBLOCA calculations, and the statistical information on heat transfer is used along with other test data (see next section) to derive the uncertainty parameters on film boiling heat transfer (FILMBL) and the dispersed flow heat transfer (FRHTC). (See following section).

4.3.3.2.5 Core Post-CHF Heat Transfer

The FLECHT-SEASET tests were used to assess S-RELAP5's capability to predict several phenomena associated with reflooding a heated bundle. This facility provided reflood data covering the LBLOCA range of pressures, subcoolings, and reflood rates using an electrically heated bundle with a center-peaked cosine power profile. The FLECHT skewed test data were added to provide additional data for an upskewed axial power profile.

The results (summarized in Section 4.3.1.6) showed that S-RELAP5 calculated maximum surface temperatures are generally higher than the measured data at all elevations. These trends were consistently observed for nearly all assessments of the S-RELAP5 heat transfer.

FLECHT and FLECHT SEASET data and data from THTF reflood tests were used to derive the multipliers to be used for film boiling heat transfer (FILMBL) and dispersed flow forced convection (FRHTC) as shown in Section 5.1 of EMF-2102 (Reference 5). [

]

The probability density functions are defined by the following two equations. The coefficients for the equations vary depending on whether they are to be applied to FILMBL (low void fraction) or FRHTC (high void fraction).

[

]

[

]

These are given in Table 4.20.

4.3.3.2.6 Tmin

A set of seven FLECHT SEASET tests was used to evaluate the trends in Tmin at low pressure. Quench temperatures improve at higher pressures; hence, a Tmin uncertainty based on low pressure data was expected to bound high pressure data. This was validated with data from ROSA/TPTF, the ORNL/THTF and the Westinghouse G1/G2 tests. Examination of FLECHT SEASET data showed that based on observable conservatisms, only the 3 in/s reflood rate test (Test #31302) was necessary to evaluate a bounding Tmin uncertainty (Reference 5).

From the FLECHT SEASET data and from an evaluation of code uncertainty with regard to how the LBLOCA multiplier relates to Tmin, [

] The uncertainty evaluation has been

demonstrated to be a conservative bounding distribution relative to other datasets.

4.3.3.2.7 Break Flow

Break flow is a function of break area and critical flow uncertainty. [

]

The homogeneous-equilibrium critical flow model in S-RELAP5 was assessed by comparison to full-scale critical flow tests at the Marviken facility. This was presented in Section 4.3.1.8. From these assessments, [

]

4.3.3.2.8 Steam Binding

Steam generator liquid entrainment was examined in the code assessments for CCTF and UPTF.

For the purpose of measuring liquid entrainment in the steam generator, the facilities use a steam generator simulator. For the CCTF tests, liquid entrainment into the steam generator is determined by measurements of liquid levels in a collection tank from the separation of the two-phase mixture entering the simulator. The comparisons of measured and calculated liquid levels in the collection tank indicate that the amount of liquid carried over to the steam generator is in reasonably good agreement, given the uncertainties in the modeling. The uncertainty in the heat transferred from the steam generator simulator, the uncertainty in the extent to which the piping is adiabatic (as it is modeled in S-RELAP5), and the uncertainty in the dimensions of collection tank (dimensioned drawings were not available for the analysis) are significant. The assessment of the liquid carryover was based on conservatively low estimates of these uncertain values; even so, the results show reasonably good agreement.

[

]

[

]

Analyses of liquid entrainment from the upper plenum and hot legs (as discussed in Sections 4.3.3.1.2, 4.3.3.1.4, and 4.3.3.1.6) suggest that S-RELAP5 tends to carry over more than enough liquid and that liquid carryover for the LBLOCA is conservative. The large model uncertainty in the CCTF assessment requires the []

This bias is considered an additional conservatism in light of the UPTF results showing that carryover to the steam generator is conservative without the bias. The increased interfacial drag at the steam generator inlet will result in conservative carryover to the SG and will provide a bounding estimate of steam binding during a LBLOCA.

4.3.3.2.9 Cold Leg Condensation

S-RELAP5 was assessed against selected tests from the W/EPRI 1/3 scale condensation experiment. [

] This bias was used to assess the accuracy of the code in predicting the interfacial condensation heat transfer during the ECC/steam mixing process. The results show that the mean bias, based on 19 data points, is [] using a nodalization consistent with plant nodalization. This indicates that S-RELAP5 slightly overpredicts the interfacial condensation rate on the average. For RLBLOCA analyses, a [] bounds the uncertainty range of the interfacial condensation heat transfer coefficient in the ECC/steam mixing process. It is to be applied in the system cold legs and in the downcomer. Condensation in the downcomer should not be that significant; however, sampling of a low condensation factor may prevent sufficient ECC mixing in the cold leg and this mixing would then be completed in the downcomer.

4.3.3.2.10 Accumulator Discharge

Accumulator discharge may be influenced by piping flow resistances and pressure. Most plants have can provide best-estimate data that maybe used to accurately model flow resistance;

hence, the largest uncertainty to accumulator discharge is accumulator pressure. To support a plant technical specification for accumulator pressure ranges, the accumulator pressure is sampled over a range, using a probability distribution developed specifically for the plant of interest. The information on uncertainty for this and other plant process parameters will be reported to the licensee with the safety analysis.

4.3.3.2.11 Reactor Vessel Hot Walls

The results from UPTF Tests 6 and 7 demonstrated that S-RELAP5 will overpredict ECC bypass; however, many parameters may contribute to this phenomena. The hot wall effect can be separated out since it is expected that there is a direct relationship with the degree of nucleate boiling in the downcomer and ECC bypass. To maximize the hot wall effect, heat transfer in the downcomer can be locked into nucleate boiling by raising the CHF point to a high value. In the FRA-ANP methodology, the hot wall effect [

]

4.3.3.2.12 Containment Pressure

Containment pressure is ranged [

] Sensitivity studies

have shown that lower containment pressure reduces PCT margins. [

]

4.3.4 Evaluation of Code Biases

This section assesses the effects of the defined code biases on the LBLOCA assessments. The biases were developed from uncertainty analyses performed on separate-effect tests. Although each bias developed has an uncertainty associated with it, the evaluation of the biases does not include the uncertainties.

Having defined the biases and uncertainties for use with S-RELAP5, an evaluation of the impact of these biases on the assessments was performed for the CCTF, LOFT, and Semiscale. The CCTF facility was selected from the various SET facilities because it is a large facility and has a cylindrical configuration consistent with the NPP core model. The two IET facilities were chosen because they provide a complete assessment for all phases of the LBLOCA scenario.

The following biases were included in all of the evaluation calculations and were taken from Table 4.19:

[]
[]
[]
[]
[]
[]
[]

4.3.4.1 Evaluation of Biases with CCTF

The biases were applied to each of the CCTF tests. The overall effects of the biases are shown by comparisons with unbiased results and measured temperatures. The comparisons are shown at the core elevation where the measured PCT occurred. In all the tests the measured PCT occurred at the 1.83 m elevation, while the calculated PCT in both the base case and the biased calculation occurred between the 2.3 and 2.5 m elevations. Therefore temperature comparison plots will be made at the 1.83 m elevation and at the 2.44 m elevation.

Also presented are rod temperature profile comparisons between measured, unbiased, and biased temperatures. In the profile plots, the temperatures presented are the maximums occurring at each elevation. The maximum temperature profile, referred to as a PCT plot, readily shows how the calculated temperatures compare with the measurements.

4.3.4.1.1 Summary and Conclusions

Inclusion of the biases resulted in improved but conservative PCT calculations in three of the four evaluation tests. In the fourth, which is a low PCT case, the inclusion of the biases improved the calculation of the general trends and produced a good comparison but slightly non-conservative PCT. [

]

4.3.4.1.2 Test 54

This test incorporates best estimate decay power (ANS x 1.0), a nominal cold leg ECC injection rate (0.011 m³/s), and nominal pressure (0.20 Mpa).

The comparison between measured, unbiased, and biased temperatures at the 1.8 m level where the measured PCT occurred is given in CCTF Figure 4.180. From the time reflood starts at 93 seconds up to the time that the rods quench, the heat transfer regime oscillates between dispersed flow film boiling and single phase steam heat transfer. [

] Similar trends are observed in Figure 4.181, where the comparison is made near the calculated PCT elevation. At this elevation, the calculation tracks the measured temperature almost exactly and the measured and calculated quench temperatures are nearly identical.

The PCT versus elevation plot is shown in Figure 4.182, where the biased and unbiased peak temperatures either exceed the measured temperatures or are within the range of the measured temperatures, except at the 1.425 m elevation, where the unbiased calculated temperature fall slightly below the lowest measured temperature. In the upper one third of the heated section, the code calculates higher temperatures than measured in both calculations. However all three figures show the code calculated the trends of the experimental data. Also, both the unbiased and biased calculations tend to overpredict the data near the calculated PCT location. The biased calculation, however, tends to fall between the data and the unbiased results.

4.3.4.1.3 Test 62

This test incorporates Appendix K required decay power (ANS x 1.2), a nominal cold leg ECC injection rate ($0.011 \text{ m}^3/\text{s}$), and nominal pressure (0.20 Mpa).

The comparison between measured, unbiased, and biased temperatures at the 1.8 m level where the measured PCT occurred and at the 2.44 m level where the calculated PCT occurred are given in CCTF Figures 4.183 and 4.184. The trends are similar to those shown for Test 54.

The PCT versus elevation plot is shown in Figure 4.185, where the biased and unbiased peak temperatures either exceed the measured temperatures or are within the range of the measured temperatures without exception. Also, both the unbiased and biased calculations tend to

overpredict the data near the calculated PCT location, but the biased calculation tends to be much closer to the data than do the unbiased results.

4.3.4.1.4 Test 67

This test incorporates Appendix K required decay power (ANS x 1.2), a nominal cold leg ECC injection rate ($0.011 \text{ m}^3/\text{s}$), and reduced pressure (0.15 Mpa). This test produced the greatest PCT in both the tests and in the calculation because of the combination of low pressure and higher decay power.

The comparison between measured, unbiased, and biased temperatures at the 1.8 m level where the measured PCT occurred and at the 2.44 m level where the calculated PCT occurred are given in CCTF Figures 4.186 and 4.187. Again, the trends are similar to those shown previously for Test 54 and 62, but because of the higher temperatures the effects of the biases are magnified.

The PCT versus elevation plot is shown in CCTF Figure 4.188, where, as in test 62, the biased and unbiased peak temperatures either exceed the measured temperatures or are within the range of the measured temperatures without exception. Also, both the unbiased and biased calculations tend to overpredict the data near the top half of the core, but the biased calculation tends to be much closer to the data than do the unbiased results.

4.3.4.1.5 Test 68

This test incorporates best estimate decay power (ANS x 1.0), an increased cold leg ECC injection rate ($0.025 \text{ m}^3/\text{s}$), and nominal pressure (0.20 Mpa). This test produced the best agreement between the calculated PCT and that measured for the unbiased runs.

The comparison between measured, unbiased, and biased temperatures at the 1.8 m level where the measured PCT occurred and at the 2.44 m level where the calculated PCT occurred are given in Figures 4.189 and 4.190. As shown in both of these figures, the addition of the biases tends to produce PCTs at both locations that are slightly non-conservative. However, as shown in Figure 4.190, the underprediction is mainly the result of the initial temperature undershoot at the start of reflood. After the initial under shoot that ends at approximately 130 seconds the slope of the calculated temperature curve tracks that of the measured

temperature until 340 seconds, at which time the biased heat transfer rate becomes larger than that measured rate.

The PCT versus elevation plot for CCTF Test 68 is shown in Figure 4.191. The figure shows that both the biased and unbiased peak temperatures either exceed the measured temperatures or are within the range of the measured temperatures except at the measured PCT location where the biased temperature is under the lowest measured value. Also, both the unbiased and biased calculations tend to overpredict the data near the top third of the core. Because of the discontinuity in the measured temperatures near the core mid plane, visually deciding whether the biased or unbiased calculations produce the best overall comparison is difficult.

This test is the only one in which the biases produced a notable effect on any of the measured loop parameters (pressure drop, flow rate, void fraction, etc.). For this test the steam generator inlet interfacial drag bias of 1.75 produced a noticeable improvement in the agreement between the measured and calculated intact loop cold leg void fraction between the start of reflood and 350 seconds. After 350 seconds the biases produced little difference. The cold leg void fraction comparison is shown in Figure 4.192.

4.3.4.1.6 Conclusion Regarding Bias Evaluation in CCTF

Inclusion of the biases resulted in improved but conservative PCT calculations in three of the four evaluation tests. In the fourth, test which is a low PCT case, the inclusion of the biases improved the calculation of the general trends and produced a good comparison but slightly non-conservative PCT. [

]

4.3.4.2 Evaluation of Biases with LOFT

The integral tests used for the assessment were the LOFT Tests LP-LB-1, LP-02-6, L2-5, and L2-3. These tests were evaluated as part of the S-RELAP5 assessment, which provides a comparative basis.

The biases were applied to each of the LOFT tests. The overall effects of the biases are shown by comparisons with unbiased results and measured temperatures. The comparisons are shown at the core elevation where the measured PCT occurred. In Tests LP-LB-1 and L2-5, the calculated location of the PCT coincided with the measured location. From the Test LP-02-6 results, the elevation of the measured PCT was 26 in, while the calculated PCT occurred at the 24 in level. The difference in elevations is small enough to perform the analysis at the 26 in level. However, simulation of the L2-3 test resulted in a calculated PCT occurring at the 24 in elevation, while the measurements show the PCT occurring at the 15 in level. Thus two comparisons are evaluated, temperature comparisons at 15 in and 24 in.

Also presented are rod temperature profile comparisons between measured, unbiased, and biased temperatures. In the profile plots, the temperatures presented are the maximums occurring at each elevation. The maximum temperature profile, referred to as a PCT versus elevation plot, readily shows how the calculated temperatures compare with the measurements.

4.3.4.2.1 Summary and Conclusions

From the assessment calculations, S-RELAP5 was demonstrated to be conservative with respect to the measured PCT data from LOFT tests LP-LB-1, LP-02-6, L2-5, and L2-3. Those assessment cases were re-run with the code biases applied in the analysis. The S-RELAP5 calculated results from the biased calculations were in better agreement with the data and the PCT results were still conservative.

4.3.4.2.2 LOFT Test LP-LB-1

Figure 4.193 compares the measured, unbiased, and biased temperatures at the 24 in level where the measured PCT occurred. The initial temperature rise is calculated to occur slightly earlier than was measured, and the biased calculation shows an earlier rise than the base calculation. [

]

From 4 s to approximately 35 s, the code calculates the heat structure to be in the dispersed film-boiling regime. The code bias of 1.75 is applied. The biased results show peak temperatures closer to the measured data during this period. The bias calculation underpredicts the measured temperatures slightly between 25 and 35 s. Had the calculated peak temperature

been delayed to the measured value, the calculated temperatures would have been in excellent agreement with the measurement.

After 35 s the heat transfer regimes are predicted to enter the transition region between dispersed flow film boiling ($\alpha > 0.9$) and the Bromley film boiling region ($\alpha < 0.7$). At that point, [

]

Both calculations follow the measured temperature excursion until 50 s. At that time, the measured temperature starts decreasing more rapidly and final quench occurs just before 70 s. The LP-LB-1 transient shows early quenching, primarily caused by top-down quenching in the upper core. The S-RELAP5 calculations do not effectively calculate that phenomenon.

The PCT versus elevation plot is shown in Figure 4.194. In that figure, the unbiased peak temperatures exceed the measured temperatures except at the 54 and 61 in elevations. The results from the biased calculation are shown with a dashed line. Those results are either within the measured uncertainties or exceed the measured temperature peaks except at the upper elevations. In the low power upper region of the core, the calculated dry-out is delayed relative to the data. After dry-out occurs, the code calculates quenching much later than measured. That calculated discrepancy is associated with the inability to adequately predict top-down quenching (see CCFL discussion in Section 4.3.3.1.5).

Except for top-down quenching, both figures show that the code calculated the trends of the experimental data. Also, both the unbiased and biased calculations tend to overpredict the data. The biased calculation, however, tends to fall between the data and the unbiased results, and tends to be within the measured uncertainty for ~20% of the data. [

]

4.3.4.2.3 LOFT Test LP-02-6

The LOFT LP-02-6 experiment is characterized by a short period of core quenching immediately after the blow-down peak temperatures occur because of a slow pump coast down. The

quenching occurred in the lower two-thirds of the core. The S-RELAP5 calculations do not show that brief core quenching.

The calculated temperatures from unbiased and biased cases are compared with measured temperatures at the 26 in core elevation, and are shown in Figure 4.195. The analysis of the effects of the biases on the calculated temperatures is similar to what was discussed for Test LP-LB-1 with alternative timings for the phenomenon occurrence. [

]

The Test LP-02-6 PCT versus elevation plot is shown in Figure 4.196. As was the case in the Test LP-LB-1 PCT plot, the calculated peak temperatures overpredict the measured peak temperatures, except in the upper core region. Unlike the Test LP-LB-1 PCT plot, the biased calculation shows little difference from the unbiased case, although the biased results fall between the measured and unbiased temperatures. The conclusion from the LP-02-6 assessment is that the code still is conservative, even with the application of the biases.

4.3.4.2.4 LOFT Test L2-5

The LOFT L2-5 experiment was designed to provide data for evaluation model assessment. The experiment is characterized by a rapid pump coast down and PCT occurring during the reflood portion of the experiment.

Figure 4.197 shows the calculated temperatures from the unbiased and biased cases compared with the measured temperatures at the 24 in core elevation. The results, and consequent bias analysis, are similar to those from the Test LP-LB-1 comparison except for the calculated overprediction of temperatures. The Test L2-5 experiment has a controversial power associated with it. The core was operated for 28 hours at 38 MW, then reduced to a reported 36 MW over a 2.5 hour period before the test. Additionally, the reported core power with uncertainty was 36 ± 1.2 MW, but the target power for the test had been 37.5 ± 1.0 MW. The calculation was performed using 36 MW. As shown in Figure 4.198, the unbiased calculated temperatures do not greatly exceed the measured temperatures as expected based on the other LOFT assessments.

Based on the current results, time shifting the calculated results so the PCT would occur at the same time as the data, the biased temperature decay would overlay the measured temperature

decay. Also, the unbiased temperature would greatly exceed the measured temperature. The implication is that the biased results are more accurate after PCT is reached.

Figure 4.198 shows the PCT versus elevation plot where the unbiased and biased peak temperatures are compared with the measured peak temperatures. In its present form, the biased calculation is within the measured uncertainties of the data above the 26 in elevation. However at the lower elevations, the figure shows both calculations underpredicting the data.

4.3.4.2.5 LOFT Test L2-3

The LOFT L2-3 test was one of the tests performed early in the LOFT experimental LBLOCA test series with a nuclear core. The prime characteristic of the L2-3 test is the total core quench immediately after the blowdown peak temperature occurred. The quenching was caused by the pumps running at 100% (i.e. no coast down) throughout the transient. The pump operation can cause an early core flow recovery as the pumps cause cold leg flow to exceed break flow. The LOFT facility was highly susceptible to this core quenching phenomenon.

The measured PCT occurred at the 15 in core elevation, as shown in Figure 4.199. That figure includes calculated temperatures from the unbiased and biased transients. The figure shows the blowdown peak well predicted from both calculations, while the reflood portion of the transient was overpredicted. Again, the code does not show the core quenching immediately after the blowdown peak. Missing the core quench immediately after blowdown contributes to the high temperatures calculated during reflood.

The code calculated a much higher PCT for the L2-3 test, which occurred at the 24 in core elevation. Those results are compared with data in Figure 4.200. The calculations show similar behavior as was seen in Figure 4.199. Although the biased results are closer to the data, both calculations overpredict the data and are conservative.

The PCT versus elevation plot is shown in Figure 4.201. From the calculated profile, the calculated results are skewed showing the peak temperatures centered at the 24 in core elevation. The measured results show a flat profile in that region because of the core wide quenching. The temperatures from the biased calculation are lower than the temperatures from the unbiased calculation. Both calculated results overpredict the measured temperatures.

4.3.4.2.6 Conclusions

The evaluation of the S-RELAP5 biases using LOFT shows the expected results from the application of the biases. That is, the biases bring the code predictions more into line with the measured data for all four LOFT tests evaluated. For three of the four tests the code continues to demonstrate conservatism relative to the measured data. For Test L2-5, where the code prediction with biases no longer overpredicts the data, there has always been a concern with respect to the actual power for this test. Most previous analyses of this test have indicated that the power level from which the test was initiated is likely higher than the reported value. Thus, it is concluded that the biases produce the expected improvement in the comparison of calculation and measurement and that the code continues to demonstrate conservatism relative to the measured data.

4.3.4.3 Evaluation of Biases with Semiscale

The code biases were used to make S-RELAP5 assessment calculations of the Semiscale Tests S-06-3 and S-07-1. Previous S-RELAP5 assessment results have shown that the calculated PCT from each Semiscale assessment occurred at a different elevation than was measured. From the S-06-3 assessment, the measured PCT occurred at the 21 in elevation, while the calculated PCT occurred at the 27 and 30 in elevations. From the S-07-1 assessment, the calculated PCT occurred at the 81.5 in elevation, while the measured PCT occurred at the 70.5 in elevation. Comparisons from both locations are presented for consistency.

4.3.4.3.1 Summary and Conclusions

The bias evaluation using the Semiscale tests showed the expected trends because the predicted PCT in the high powered central region of the hot rod was reduced when the biases were applied. However, in test S-06-3, the comparison with data was not improved while for test S-07-1 the comparison with data, particularly in the high power central region of the hot rod, was improved.

4.3.4.3.2 Semiscale Test S-06-3

Figure 4.202 shows the unbiased and biased calculated temperatures compared with data at the 21 in core location where the PCT was measured. At that location, the S-RELAP5 temperature from the assessment (unbiased) underpredicted the measured temperature. The calculated temperature from the bias case is lower than the temperature from the unbiased run,

the expected result. Figure 4.203 shows the calculated temperatures compared with data at the 29 in core elevation, the calculated PCT level. In that figure, both calculated temperatures initially overpredict the measured temperature during the first 50 s of the transient. Because of the [] the temperature from the biased calculation is lower than the temperature from the unbiased calculation.

Figure 4.204 shows the PCT versus elevation plot from the S-06-3 calculation. As shown in the figure, the calculated peak temperature profile is shifted higher in core elevation than was measured. As expected, the biased results are lower than the unbiased results in the vicinity where the calculated PCT occurred. However, the biased profile crossed over and exceeded the unbiased profile above the 2.7 ft core elevation, while the LOFT L2-3 results show the crossover occurring above the 3.6 ft core elevation (Figure 4.201). The biased results are acceptable because they are lower than the unbiased results at the calculated PCT location.

4.3.4.3.3 Semiscale Test S-07-1

Figures 4.205 through 4.207 show the Semiscale S-07-1 temperature comparisons between measured, unbiased, and biased temperatures. Figure 4.205 shows the comparison at the measured PCT node, Figure 4.206 shows the comparison at the calculated PCT location, and Figure 4.207 shows the PCT versus elevation plot. In all figures, the biased results are lower than the unbiased results and both calculations are conservative with respect to the data.

4.3.4.3.4 Conclusions

As expected, for both the Semiscale tests evaluated, application of the biases reduced the calculated PCT. For Test S-06-3, the overall comparison to the data was not improved. This is clearly shown in Figure 4.204 where the temperatures in the lower and upper parts of the rod are further from the data with the application of the biases. The results for Test S-07-1, with a 12 ft core, are more consistent with the expected trends. The PCTs from the biased calculation are lower than the unbiased calculation in the central high power portion of the rod and are in better agreement with the measured data. While the comparison with data at the top and bottom of the rod are essentially unchanged between the biased and unbiased calculations relative to the data, the magnitude of the PCT is in good agreement with the data.

4.3.4.4 Conclusions from Bias Evaluation

Overall the evaluation of the model biases showed the expected trends. The application of the biases resulted in a reduction in the maximum PCT predicted by the code, which is consistent with the observed tendency of the code to overpredict the data. In general, the reduction in PCT improved the comparisons between calculation and data, as should be expected if the developed biases are reasonable. This indicates that the biases developed from comparison of the code predictions and data for the SET assessments are affecting the code predictions consistent with the intent and expectations.

4.4 ***Determination of Effect of Scale (CSAU Step 10)***

The basis for the analysis of a LBLOCA is the entire methodology being used, not just the basecode, S-RELAP5. When S-RELAP5 is referenced in this section, it means the combination of the code and the associated methodology. As noted in Appendix C of Reference 4, there are two premises which the assessment process is based. The first premise is that the tests are scalable to a LBLOCA and the second is that the models in S-RELAP5 and the implementation result in scalability of the code predictions. For the first premise to be true, the selection of tests needs to be such that all of the important phenomena in a PWR LBLOCA are captured by one or more appropriately scaled tests. For the second premise to be true, the phenomenological models in S-RELAP5 should apply to both the PWR LBLOCA and the scaled test. The scaling of the tests and of the phenomenology will be discussed in the following paragraph.

Throughout the assessment program (Reference 5), S-RELAP5 was used to simulate a variety of tests. These tests are a significant portion of the basis for the RLBLOCA methodology, having been used to demonstrate the ability of S-RELAP5 to predict the test outcomes. Because of the cataclysmic nature of a design-basis LBLOCA, no tests exist that replicate it at full scale. All of the integral tests and some of the separate-effects tests are scaled. One exception is the UPTF, which is full-scale, but has no core and no steam generators. The ability of the scaled tests to capture the phenomena of the LBLOCA is then pivotal to the applicability of the assessments for S-RELAP5.

4.4.1 Test Scaling

Tests are scaled to preserve certain features of the full-scale phenomena. For this reason, tests with different scaling are used to address different phases or aspects of an LBLOCA. If a test is

considered appropriately scaled for the phenomena of interest, then assessment conclusions to that data is considered applicable to the full scale NPP.

It has been shown (Reference 28) that scaling a test facility based on preserving the ratio of the power to the volume (power-to-volume scaling) results in substantially the same system response throughout the simulation, except for the behavior in the downcomer. For the downcomer component, the heat transfer with the wall is an important phenomenon, and it does not scale the same way. The SEMISCALE results showed entirely different flow patterns in the downcomer compared to the analogous LOFT. The Ishii-Kataoka scaling laws (Reference 29) are more general and have specific scaling laws for different phenomena.

4.4.1.1 Blowdown

Power-to-volume scaling for the blowdown period was demonstrated in Reference 4. Five system tests with powers from $1/48^{\text{th}}$ of a typical PWR to $1/30,000^{\text{th}}$ were used as a basis for the comparison. Each of these facilities were scaled such that the ratio of power to volume was preserved. The peak temperature during blowdown was plotted as a function of linear power for each of these test facilities. The measured peak temperatures all fell within 350 F of a linear regression line (temperature versus LHGR). The data scatter for a single facility was as great as, or greater than, any differences between facilities. As a result, it is hard to conclude there are any scale effects occur in the blowdown peak. It is concluded that tests that preserve the power-to-volume ratio of a PWR will scale properly for the blowdown phase of the LBLOCA.

4.4.1.2 Refill

During refill and early reflood, scale dependent multi-dimensional flow behavior has been observed in the downcomer for facilities using power-to-volume scaling. The SEMISCALE and LOFT facilities were compared for analogous tests in Reference 28. Under ideal scaling, the two tests should have shown the same behavior. However, during the refill portion of the simulation, the downcomer flow was observed to be generally up for the SEMISCALE test before the pressure increase accompanying the emptying of the accumulator. For the analogous test in the LOFT facility, the flow was asymmetric; down for the regions near the intact loop and up for the region near the broken loop. This has been attributed differences in the downcomer gap and the distance between the cold leg penetrations. This allows multi-dimensional flow effects to dominate the flow in the LOFT facility, whereas they do not occur to the same extent in the SEMISCALE facility. The downcomer gap, volume and surface area-to-

fluid volume ratios do not scale between these two facilities in such a manner to preserve the transit time and the heat transfer to the fluid from the walls.

The UPTF facility (Reference 30) was designed to simulate a four-loop 3900 MWt PWR primary system and to provide a full-scale simulation of thermal-hydraulic behavior in the primary system during the end of blowdown and refill phases of a PWR LBLOCA. The reactor vessel, the core barrel, and the greater part of the vessel internals are full-sized representations of the reference PWR, as are the four hot and cold legs that simulate three intact loops and one broken loop. The dimensions of the test vessel are those of the reactor pressure vessel of the reference PWR, with the exception that the vessel wall is thinner. The downcomer annulus, which is formed by the vessel wall and the core barrel, has a gap width that varies from 0.25 m (0.82 ft) in the lower part down to 0.21 m (0.69 ft) in the upper part. The loop geometry and flow areas correspond to the 4-loop PWR.

With the exception of the wall thickness, the UPTF is full scale. The hot-wall effect should be slightly under estimated, because of the slight reduction in vessel mass and stored energy. However, there is an ample amount of metal in the vessel so that the UPTF tests should be applicable to the refill portion of an LBLOCA.

4.4.1.3 Reflood

Scaling issues associated with reflood were addressed in Reference 4, where the effects of refill scaling were removed from the data by comparing the temperature rise to reflood rates. The temperature rise considered is the change from the beginning of reflood to the PCT.

Temperature rise data were collected for 8 facilities with volumes scaled from 1/21st to 1/1700th, all of which were power-to-volume scaled. Figure 34 of Reference 4 compares the temperature rise for all 8 facilities to the reflood rate. The data were fit with a regression relation and the tolerance bands added. As with the blowdown data, the spread in the data for a single facility was as great as or greater than the difference between the facilities. Tests which scale by maintaining the power-to-volume are applicable to the reflood phase of a LBLOCA.

4.4.2 Code Scaling

The issue of code scaling is primarily determined by the ability of the correlations and closure relations used to describe complicated thermal-hydraulic phenomena that are not treated from a mechanistic, theoretical approach. Generally, phase transitions, heat transfer, phasic

interactions and CHF fall in this category. The models, correlations, and closure relations used in S-RELAP5 are described in Reference 9. To a lesser extent, the numerical implementation may be subject to scaling issues. Generally, issues of numerics are treated by addressing the converged nature of the nodalization and time step criteria. This way, demonstrates that the computer code can solve the mathematical model correctly over the applicable range for the tests and the LBLOCA. This leaves the issue of scaling of the correlations and the closure relations employed in LBLOCA analysis.

Code scaling evaluation will focus on those items identified by the sensitivity studies of PIRT phenomena as having the greatest impact on LBLOCA. Table 4.1 shows the results of sensitivity studies on the PIRT phenomena in a PWR LBLOCA. The models related to these and the scalability of each of these models are discussed in the following paragraphs.

Items related to fuel rod performance are not affected by scaling, because the basis for the fuel-stored energy and dynamic response are based on RODEX3A (Reference 7), which has been benchmarked to fuel rod data. Similarly, decay heat models require no scaling.

4.4.2.1 Post-CHF and Reflood Heat Transfer

When heat flux from the fuel rods and any other metal masses exceed the CHF, the heat transfer is calculated using correlations specific to the heat transfer regimes. The single-phase vapor, transition boiling and film boiling regimes constitute the post-CHF heat transfer regimes. For each of these regimes, the effects of radiation heat transfer also are considered. Single-phase vapor heat transfer is the maximum of the Sleicher-Rouse correlation (Reference 31) for forced flow regimes (turbulent and laminar) and the turbulent natural convection heat transfer recommended by Holman (Reference 32). In general, the Sleicher-Rouse correlation determines the heat transfer.

The natural convection heat transfer model is based on data from the flow between vertical plates. If the boundary layer is small compared to the diameter of the rod, then heat transfer through this layer would be very similar to that through the boundary layer on a plate. With the Prandtl number near unity and the rod diameter large compared to the boundary layer, the Holman formulation for natural convection heat transfer used in S-RELAP5 applies (Reference 33) as long as

$$\frac{D}{L} \geq 35 \cdot (Gr)^{-0.25}$$

where D is the rod diameter, L is the length used in calculating the Grashof number and Gr is the Grashof number. When these conditions are met, the flat plate solution does not differ by more than 5% from the solution for the cylinder. In the turbulent flow regime, this implies $0.02 \leq D/L \leq 0.2$. For a 17x17 fuel design, with a diameter of 0.376 in., the length can be as low as 1.9 in. and as large as 19 in. [

] These fall well within the range of applicability of the natural convection heat transfer correlation.

The Sleicher-Rouse correlation is valid for the following ranges:

$$0.6 < Pr < 0.9$$

$$10^4 < Re < 10^6$$

$$1 < \frac{T_w}{T_g} < 5$$

$$\frac{x}{D} > 40$$

The Prandtl number (Pr) for steam at pressures below 50 psia and temperatures above 1000 F are all less than 0.9 (Reference 34). For lower temperatures, the Prandtl number is around unity. The steam Reynolds number (Re) for a typical limiting LBLOCA is approximately 5,000 during the reflood phase. This falls slightly below the correlation limit for the Sleicher-Rouse correlation. Wall temperatures (T_{av}) easily meet the criterion, as does the length-to-diameter ratio (x/D).

For the Prandtl number and the Reynolds number, the Sleicher-Rouse correlation falls slightly short of covering the conditions present in the LBLOCA. For the Prandtl number, the difference is quite small and the extrapolation should have little effect on the scalability of the calculations. For the Reynolds number, the LBLOCA falls somewhat further outside the region of applicability of the Sleicher-Rouse correlation. Heat transfer correlations such as Seider-Tate (Reference 35), Dittus-Boelter (Reference 36) and Sleicher-Rouse all have nearly the same (linear) Reynolds number dependence. In Reference 31 the Sleicher-Rouse correlation was compared to 120 data points and the standard deviation of the error was 4.2%. The 95%

tolerance range on these data would be $\pm 8.3\%$ ($= t_{119,97.5} \times \sigma_{fit} = 1.98 \times 4.2\%$). Treating the dependence as linear (because it is very nearly so) the tolerances for the ratio of predicted Nusselt number to the measured Nusselt number for a Reynolds number of x_0 would be given by

$$\pm t_{n-2, 1-\alpha/2} \cdot \sigma_{fit} \cdot \sqrt{1 + \frac{1}{n} + \frac{(x_0 - \bar{x})^2}{(n-1) \cdot \sigma_x^2}}$$

Where \bar{x} is the mean of the Reynolds number and σ_x is the standard deviation. Inserting values here for the mean value of Reynolds number and for the standard deviation, the uncertainty in the extrapolated value can be obtained. Figure 4.208 shows the data from Figure 1 of Reference 31 plotted with a linear x-axis. In this figure, the tolerance bands have been included. The uncertainty in the extrapolated value ($Re = 5000$) is not significantly increased as the turbulent regime is still applicable.

In conclusion, the model for single-phase vapor heat transfer used in S-RELAP5 can be applied to a full-scale PWR LBLOCA.

Transition boiling is not really a heat transfer regime in the sense that it can be characterized by a homogeneous, steady, heat transfer mechanism. It is a combination of dynamically varying heat transfer mechanisms, including nucleate boiling, film boiling and vapor heat transfer. The amount of time a region spends in one of these heat transfer modes determines the effective heat transfer rate. Very few measurements are available for transition boiling heat transfer and they do not cover a very wide range. In addition, the unsteady nature of the process makes modeling the process physically very challenging.

Despite the complexity of this regime, exact modeling of the heat transfer is not particularly important for the LBLOCA because most volumes in the core move through this heat transfer regime rather quickly and are not sensitive to the details of the modeling. The main requirement for simulating the LBLOCA is that the point at which the code predicts the beginning and end of the transition region be reliable. In addition, the heat transfer in the transition region should be significantly better than the vapor heat transfer and it should remain below the CHF.

The major assumption in modeling this regime is that it can be modeled by a combination of steady state boiling heat transfer to liquid and convective heat transfer to vapor. In this model,

the heat flux is bounded by the CHF at the lowest wall temperatures and it approaches the flux based on single-phase vapor heat transfer as the wall temperature rises. The heat transfer is based on a modified Chen correlation for transition heat transfer (Reference 18 and 37). This model makes a smooth transition from the CHF to the vapor, with the calculated fraction of liquid heat transfer based on the wall temperature. The Chen correlation has been tested against data and behaves adequately, which is sufficient for LBLOCA transition boiling.

Film boiling occurs when the wall temperature exceeds the minimum temperature for stable film boiling and the void fraction lies in the appropriate range. The coolant consists of vapor and water droplets in this mode. The heat transfer mechanisms consist of boiling heat transfer to liquid droplets, convective heat transfer to vapor, and radiative heat transfer to droplets.

[

]

[

]

4.4.2.2 Scaling from Tests

While analytical arguments (see prior section) can provide a basis for code scaling for selected cases, often the issue of scaling needs to be addressed by a comparison to test data. Code scaling and the tests making up the basis are discussed in the following paragraphs.

4.4.2.2.1 Film Boiling Heat Transfer

A series of tests was performed in the THTF at Oak Ridge National Laboratory to measure heat transfer at higher pressures and flows. These included 22 steady-state dry-out tests (Reference

44), 3 transient boil-off tests (Reference 45) and two sets of transient reflood tests (References 46 and 47). The reactor core was simulated by an 8x8 array of heated rods with dimensions corresponding to those of a W 17x17 fuel assembly. The axial power shape was uniform. The FLECHT-SEASET used 161 full-length simulated fuel rods and axially-dependent power shapes (Reference 48). Based on rod count, these two test facilities differ by a scaling factor of 2.5.

These tests were used to evaluate the film boiling heat transfer. Table 4.21 compares the ranges for LBLOCA calculations for parameters that affect heat transfer with the ranges covered by the THTF tests and FLECHT-SEASET. Given the near prototypic nature of the fuel rod simulators and the extent to which the tests span the applicable ranges for LBLOCA, it is concluded that the heat transfer models, including correlations and closure relations, in S-RELAP5 are sufficient to allow direct application to a PWR LBLOCA and that the uncertainties obtained from these tests are applicable.

4.4.2.2.2 Core Entrainment

Entrainment of water droplets by the steam flow in the core can affect the predicted core cooling flow. The primary determinant of entrainment is the drag exerted on the liquid droplets by the steam flowing up out of the core. This drag, in turn, depends on the vertical flow regime in the core model. The determinants of the model applicability to a PWR LBLOCA are primarily local and, in the core, principally related to the conditions within the flow channel between the fuel rods. The axial effects predominate in this phenomenon. Radial redistribution is a second-order effect, in that it makes fluid available in a channel or removes it. The RLBLOCA methodology makes use of the TWOODEE component in S-RELAP5 to model the radial behavior in the core.

The tests used in the assessments, CCTF (Reference 49), FLECHT-SEASET (Reference 48), and THTF (References 44, 45, 46, and 47), use bundles of full-length fuel rods. Achilles (Reference 50) also used full-length rods, but the gaps between the rods and the piping containing the rods caused some radial flow re-distributions which made it less suitable for confirming scaling of core entrainment. The LOFT and SEMISCALE Test S-06-03 cores were too short for entrainment scaling. Based on the comparisons to CCTF, FLECHT-SEASET and THTF, the core entrainment model in S-RELAP5 is conservative and will scale suitably to a full-scale PWR LBLOCA.

4.4.2.2.3 Critical Flow at Break

The choked flow model used for FRA-ANP RLBLOCA analyses is the homogeneous equilibrium model (HEM) and not the Ransom-Trapp model (Reference 51). Choking for break flow occurs when the flow velocity reaches the speed of sound in the break. The critical flow model is not scale dependent, however, the Marviken Full-Scale Critical Flow Test data were used to determine the S-RELAP5 critical flow multipliers and uncertainties (Reference 5) as discussed in Section 4.3.

The test facility consists of four major components: a full-scale BWR vessel, a discharge pipe attached to the bottom of the vessel, a test nozzle connecting to the downstream end of the discharge pipe and a rupture disk assembly attached to the downstream end of the nozzle. Nozzles of various length-to-diameter ratios are used in the tests. The Marviken test data have been widely used in assessing critical flow models of various system codes over a range of flows to confirm the scalability. The Marviken tests provide a suitable basis for code scaling verification and the determination of uncertainties.

4.4.2.2.4 Carry-over to Steam Generator

Steam binding in a LBLOCA is assumed to occur as a result of steam production in the steam generator. This steam production occurs when water carried over from the core enters the hot steam generator. The resulting vaporization expansion increases the pressure drop through the steam generator and produces steam binding that reduces the core reflood rate.

The results from three test facilities were used to benchmark and verify the RLBLOCA methodology and S-RELAP5: Tests 54, 62, 67 and 68 (Reference 49) at the CCTF, Tests 10 (Reference 52) and 29 (Reference 53) at the UPTF, and Tests 31203, 31302, 31701, and 31805 at FLECHT-SEASET (Reference 48). The FLECHT-SEASET tests have prototypic rods and spacers for PWR fuel, but the balance of the test facility bears little resemblance to a PWR. The UPTF is a full-scale simulation of a German PWR. The steam generators are replaced with steam separators and the pumps are simulated with mechanical resistance. The CCTF is scaled such that it is prototypic of a W PWR in the dimension parallel to flow and scaled down (~ 0.2) in the orthogonal directions.

The UPTF has no core per se, and reflood is simulated with steam and water injection. The CCTF and FLECHT-SEASET have electrically heated rods in the core. The upper plenum

region was tested at full scale in the UPTF, as were the hot legs and the steam generator inlet plenum. The steam generator tubing geometry is prototypic in the CCTF (although the number of tubes is smaller). All these tests in the three facilities collected water carried over from the core under conditions representing the reflood phase of the LBLOCA and all three have additional collapsed liquid level measurements. As presented in Section 4.3, a study on carryover to the steam generator was performed using the CCTF. From that study, a bias on interfacial drag was determined to conservatively bound this phenomenon. The results of the CCTF (with bias), UPTF, and FLECHT-SEASET evaluations indicate that S-RELAP5 overpredicts the entrainment of liquid from the test bundle (Section 5.6 and Reference 5). While each test by itself has some deficiencies in terms of simulating a PWR and in terms of scale, the combination of the three tests provides a substantial basis for evaluating modeling of the drag between the two phases during reflood at full scale.

4.4.2.2.5 Pump Scaling

The S-RELAP5 code has normalized single phase homologous curves for a full scale W reactor coolant pump as code default. The use of full scale data for the pump makes code scaling moot for the pump. These homologous curves are set to applicable values by entering plant specific values for rated head, torque, moment of inertia, etc. The coastdown of the pump is driven by the torque and moment of inertia of the rotating mass. The torque includes the effects of friction and back EMF (pump torque) and of the loop pressure losses (hydraulic torque). The single phase pump head and torque curves are adjusted for two-phase degradation based on experimental data. The EPRI two-phase degradation data (Reference 54) is based on pumps that are similar to PWR coolant pumps and represent best estimate parameters.

4.4.2.2.6 Cold Leg Condensation

Cold leg condensation was evaluated at a scaled EPRI test facility (Reference 55) to determine the accuracy of the calculated interfacial heat transfer between the ECC water and the steam in the cold leg. The principal portion of the test apparatus was the simulated cold leg, which was fabricated from straight pipe with an ID of 10.42 in. Two injection points were provided so that the pipe lengths downstream of the injection point approximated either a typical PWR cold leg scaled down to about one-third or the full length of the cold leg. The cold leg pipe length

downstream of the injection point for a typical Westinghouse PWR is about 16 and the cold leg ID is about 2.7. In the EPRI 1/3 scale test, the full length is approximately 15.6 feet, and the scaled length is 6.

For vertical components and for horizontal components not in either the stratified or slug flow regimes, the condensation model is based on a model by Carpenter and Colburn (Reference 56) as formulated in Collier's book on heat transfer (Reference 57). For stratified and slug flow in horizontal components the heat transfer also is taken from Reference 57. These models are relatively insensitive to geometry and are expected to scale from the 1/3 scale tests to full scale. In addition, these condensation effects were considered in the UPTF (see Section 4.3.1.11.2), which is full scale.

4.4.2.2.7 Bypass of Downcomer by ECC Water and Lower Plenum Sweep-Out

The scalability of the code predictions for the bypass of downcomer water is of particular interest because tests with fixed power-to-volume scaling do not show the same phenomena (LOFT L2-3 versus SEMISCALE counterpart Test, S-06-3, Reference 5). The major difference between these two tests was the behavior of the flow in the downcomer during the accumulator injection phase. In the LOFT test, the flows were down in the region of the downcomer near the intact loop and up near the broken loop before the accumulator empties. In the SEMISCALE test, it was up in both segments until the accumulator emptied. The differences were attributed to the scaling, which preserved power-to-volume but did not preserve downcomer volumes, gaps, and surface area-to-fluid volume ratios between the two tests.

The UPTF test facility has full-scale downcomer, cold legs and hot leg. This makes code scaling a non-issue for this comparison to test data. Test 6 (References 58 and 59), Runs 131, 132, 133, 135, and 136, and Test 7 (References 60 and 61), Run 203, were specifically designed to examine downcomer counter current flow behavior during blowdown, ECC bypass, and lower plenum refill with cold leg ECC injection. These interactions play a key role in determining the rate at which ECC water is able to refill the lower plenum. The tests were analyzed to demonstrate the ability of S-RELAP5 to self-limit counter current flow in the downcomer and predict reasonable refill behavior including ECC bypass compared to experimental data. The code comparisons focused on steam-water flow phenomena in the intact cold legs, the downcomer, and the lower plenum during the end-of-blowdown/refill phases of a LBLOCA.

In these tests, steam was injected in the core region, where it traveled downward to the lower plenum, then into the bottom of the downcomer. It then rose through the downcomer and exited at the broken cold leg. ECC injection (with and without nitrogen) entered from the cold legs at the top of the downcomer. Depending on the upward flow rate of the steam in the downcomer, the ECC water from the cold legs either bypassed to the broken cold leg or flowed down into the lower plenum.

These tests were such that the code modeling for the several important phenomena could be compared to full-scale measurements, for the downcomer, multi-dimensional effects, condensation and non-equilibrium flow, countercurrent and slug flow and entrainment and de-entrainment. Since the steam was flowing out the bottom of the core, these tests also addressed lower plenum sweep out. The results of these assessments indicated that S-RELAP5, with the RLBLOCA nodalization (Reference 12), overpredicted the ECC bypass and lower plenum sweep out.

4.4.2.2.8 Loop Oscillations

Test 8 at the UPTF (References 62 and 63) investigated the behavior during the end-of-blowdown, refill, and reflood phases of a postulated LOCA with ECC injection. The focus of the test evaluations was the pressure and fluid oscillations in the cold legs. These oscillations arise when the steam is condensed by the ECC water and forms a liquid plug in the cold leg. The flow rate falls and the flow in the cold leg transitions to the stratified flow regime, allowing the steam flow to increase again. This sweeps the liquid out again.

Test 8, Runs 111 and 112 was performed by isolating one intact loop at the pump simulator, opening a second intact loop to stabilize the pressure drop between the upper plenum and the downcomer, opening the break valves on the broken loop, injecting steam into the test vessel, and varying ECC water injection into the third intact loop cold leg downstream from the pump simulator. Thus the principle portion of the system relevant to the UPTF Test 8 used in this analysis consists of the cold leg piping for the third loop from the steam generator simulator to the pump simulator (including loop seal), the pump simulator, and the cold leg piping from the pump simulator to the vessel downcomer; all of which are full scale.

The S-RELAP5 calculations for this test indicated that the code predicted the formation of a cold leg sub-cooled liquid plug and condensation at the face of that plug. This was consistent with

the data for the test, indicating that the code is capable of calculating the appropriate phenomena in a full-scale facility.

Table 4.1 Parameters Perturbed for PIRT Sensitivity Studies



Table 4.1 Parameters Perturbed for PIRT Sensitivity Studies (*Continued*)

Table 4.2 Assessment Matrix

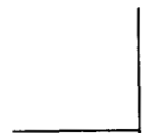


Table 4.3 Assessment Matrix Tests and Phenomena Addressed



Table 4.3 Assessment Matrix Tests and Phenomena Addressed (*Continued*)

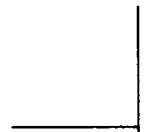


Table 4.4 Large Break LOCA Nodalization



**Table 4.5 PDTF SMART Tests Chosen for S-RELAP5 Verification
and Validation**

Test Designator	Test Description
KH01B	Reported HTP spacer test with constant flooding rate of 4 in/s
KH02B	Reported HTP spacer test with constant flooding rate of 2 in/s
KH03B	Reported HTP spacer test with constant flooding rate of 1 in/s
KH05A	Reported HTP spacer test with variable flooding rate from 8 to 1 in/s

**Table 4.6 Comparison of Effluent Temperature for the Plant-
Consistent Model, Westinghouse/EPRI**

Run Number	Liquid, Data	Liquid, Calculated	Vapor, Data	Vapor, Calculated
5-18	189.0	195.30	188.0	239.61
5-24	222.0	238.65	281.0	280.71
5-25	281.0	268.24	282.0	485.01
5-27	229.0	220.96	226.0	489.91
5-34	228.0	229.35	221.0	415.71
5-52	209.0	200.98	230.0	237.75
5-53	184.0	194.72	184.0	234.22
5-57	280.0	275.63	282.0	489.34
5-60	231.0	220.52	233.0	466.19
6-41	195.0	198.91	197.0	267.11
6-65	182.0	198.95	182.0	226.42
6-67	160.0	154.05 ^a	159.0	235.07
6-69	172.0	173.83	175.0	497.47
6-73	168.0	192.22	169.0	224.37
6-83	174.0	195.14	156.0	223.78
6-88	172.0	170.89	174.0	510.17
6-93	134.0	133.00 ^a	134.0	215.81
6-95	196.0	212.65	198.0	317.74
6-99	151.0	156.63 ^a	153.0	280.97

^a Oscillatory results. Values presented are time-averaged value from 70 to 100 seconds at 4-second intervals.

Table 4.7 Test Phase Parameters for Test 10 Run 081

Phase	Start Time (s)	End Time (s)	Steam Injection Rate (kg/s) (lb _m /s)	Water Injection Rate (kg/s) (lb _m /s)
1	35	75	125 276	60 132
2	75	135	125 276	16 35
3	135	196	110 243	16 35
4	195	255	87 192	16 35

Table 4.8 Test Phase Parameters for Test 29 Run 212/211

Phase	Start Time (s)	End Time (s)	Steam Injection Rate (kg/s) (lb _m /s)	Water Injection Rate (kg/s) (lb _m /s)
1	35	175	102 225	140 309
2	175	320	87 192	153 337
3	320	465	100 221	90 198
4	465	615	85 187	101 223
5	615	770	101 223	47 104
6	770	900	85 187	63 139

**Table 4.9 Calculated Water Downflow Rates for the 0.3 MPa
Test Series**

Steam Injection Rate (kg/s)	Water Injection Rate (kg/s)	Water Downflow Rate w/o CCFL (kg/s)	Water Downflow Rate w/ CCFL (kg/s)
4.6	30.5	30.5	30.5
10.5	30.5	30.5	28.2
11.0	30.5	30.5	25.1
12.4	30.5	30.5	17.9
12.9	30.5	30.5	15.3
15.3	30.5	30.5	5.8
18.5	30.5	30.5	0.0
20.5	30.5	27.0	
21.0	30.5	24.0	
22.0	30.5	20.0	
23.0	30.5	16.0	
24.0	30.5		

**Table 4.10 Calculated Water Downflow Rates for the 1.5 MPa
Test Series**

Steam Injection Rate (kg/s)	Water Injection Rate (kg/s)	Water Downflow Rate w/o CCFL (kg/s)	Water Downflow Rate w/ CCFL (kg/s)
8.3	29.4	29.4	29.4
9.3	29.4	29.4	29.4
18.1	29.4	29.4	29.4
24.0	29.4	29.4	19.1
28.0	29.4	29.4	10.0
31.0	29.4	29.4	5.3
32.6	29.4	29.4	3.5
33.5	29.4	29.4	2.6
36.0	29.4	29.4	1.3
40.2	29.4	29.4	0.0
42.0	29.4	29.0	
45.0	29.4	20.0	
48.0	29.4	15.1	
51.0	29.4	10.3	
53.0	29.4	7.3	
55.0	29.4	0.0	

Table 4.11 CCTF Test Conditions

Run	Core Power	LPCI Flow $\left(\frac{\text{m}^3}{\text{s}}\right)$	System Pressure (MPa)
54	ANSx1.0 + Actinide * 1.1	0.011	0.20
62	ANSx1.2 + Actinide * 1.1	0.011	0.20
67	ANSx1.2 + Actinide * 1.1	0.011	0.15
68	ANSx1.0 + Actinide * 1.1	0.025	0.20

**Table 4.12 Summary Comparison of Measured and Calculated PCT,
CCTF Tests 54, 62, 67, and 68**

Run	Measured PCT (K)	Time of Measured PCT (s)	Calculated PCT (K)	Time of Calculated PCT (s)
54	1113	130	1147	257
62	1132	154	1241	317
67	1143	164	1300	357
68	1122	144	1105	210

Table 4.13 Test Data for SCTF-II Tests Modeled

Table 4.13 Test Data for SCTF-II Tests Modeled (*continued*)

Table 4.14 Phase I Assessment Results, SCTF Tests

		S2-10	S2-11	S2-AC1	S2-SH1
PCT (K)	Data	1168.0	1085.0	1085.0	1166.0
	S-RELAP5	1193.0	1066.0	1073.0	1112.0
Time of PCT (s)	Data	193.5	125.5	127.0	251.5
	S-RELAP5	221.0	123.5	129.0	183.1
Quench Time (s)	Data	564.0	458.5	510.5	628.5
	S-RELAP5	471.0	235.0	309.0	403.0

Table 4.15 Phase II Assessment Results, SCTF Tests

		S2-17	S2-18
PCT (K)	Data	1080.0	1116.0
	S-RELAP5	1034.0	1069.0
Time of PCT (s)	Data	180.0	125.0
	S-RELAP5	168.3	135.7
Quench Time (s)	Data	540.0	500.0
	S-RELAP5	362.0	374.0

Table 4.16 PWR-LOFT Scaling Ratios

Parameters	PWR	LOFT	Ratio
Core Power (MWt)	3411	50	68/1
Total PCS Volume (ft ³)	12540	281	45/1
Upper Plenum/Head Volume (ft ³) (JAERI)*	1959 1450	31.8 31.8	62.1 41/1
Core Height (ft)	12	5.5	2/1
Core and Bypass Volume (ft ³)	920	11.1	83/1
Core Flow Area (ft ²) (JAERI)*	54.1 57.2	1.997 1.997	27/1 29/1
Lower Plenum Volume (ft ³)	1050	25.34	41/1
Downcomer & Inlet Annulus (ft ³)	721	24.25	30/1
Downcomer Flow Area (ft ²) (Including LOFT 0.25 in. Gap)	45.5 45.5	1.527 1.840	36/1 25/1
ILHL Volume (ft ³)	237	13.28	18/1
ILHL Flow Area (ft ²)	13.76	0.682	20/1
Steam Generator Volume (ft ³)	3231	49.4	65/1
Pump Suction Pipe Volume (ft ³)	378	12	32/1
Pump Suction Pipe Area (ft ²)	15.73	0.682	23/1
Pump Volume (ft ³)	168	7	24/1
ILCL Volume (ft ³)	255	15.61	19/1
BLHL Volume (ft ³)**	79	12.65**	6/1
BLHL Flow Area (ft ²)	4.586	0.682	7/1
BL Steam Generator/Simulator Volume (ft ³)	1077	19.4	55/1
Pump Suction Pipe Volume (ft ³)	126	unknown	-
Pump Suction Pipe Area (ft ²)	5.24	unknown	-
BLCL Pump Side Volume (ft ³)**	85	13.19**	6/1
BLCL Vessel Side Volume (ft ³)			
BLCL Vessel Side Flow Area (ft ²)	4.123	2.3	24/1
Break Flow Area (ft ²)	4.123	0.09231	45/1
Total Pressurizer Volume (ft ³)	1800	34	52/1

* JAERI data are given in the noted Reference 49

** LOFT BLHL Volume and BLCL-Pump Side Volume include portions of the RABV line volume.

Table 4.17 LOFT Nuclear Large Break Test Parameters

Test	Power (MWt)	MLHGR (KW/ft)	Pump Operation	Fuel Press- urized	ECC			PCT (K)
					HPIS	LPIS	Accum.	
L2-2 - Double end-cold leg break, with break area scaled to simulate PWR double-end cold leg break, US Appendix K ECC.	25	8	On	No	2/3	1/2	3/4	789
L2-3 - Similar to L2-2, with higher power and increased LHGR.	36	12	On	No	2/3	1/2	3/4	914
L2-5 - Similar to L2-3, with pumps turned off and decoupled from their external flywheels within 1 s, US Appendix K ECC with 58% L2-3 HPIS.	36	12.22	Off(A)	Yes	1/3	1/2	3/4	1078
LP-02-6 - Similar to L2-5, with pumps turned off but initial coast down with external flywheels, US Appendix K ECC, increased core power and MLHGR.	46	14.87	Off(N)	Yes	1/3	1/2	3/4	1077
LP-LB-1 - Similar to LP-02-6, with pump turned off and decoupled from their external flywheels within 1 s, UK minimum safeguards ECC, and slightly increased core power and MLHGR.	49.3	15.8	Off(A)	Yes	0/3	1/2	2/4	1261

A - atypical rapid pump coastdown,
N - normal pump coastdown.

Table 4.18 Important PIRT Phenomena and Methodology Treatment



Table 4.19 Summary of Evaluated Uncertainties of key PIRT Parameters



Table 4.20 Film Boiling HTC Distribution Fit Parameters



Table 4.21 Test Ranges for Film Boiling Heat Transfer Test Comparison

Parameter	Maximum		Minimum	
	Tests	LBLOCA	Tests	LBLOCA
Pressure (MPa)	8.2	10.8	0.13	0.22
Mass Flux Vapor (kg/s-m ²)	907	367	0	0
Mass Flux Liquid (kg/s-m ²)	4254	945	0	0
Void Fraction	1	1	0.13	0.13
Saturation Temperature °K	570	589	381	390
Vapor Temperature °K	1294	1160	384	391
Wall Temperature °K	1525	1400	390	396
Quality	1	1	-0.11	0

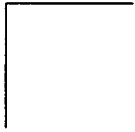


Figure 4.1 PCT Signature for 3- and 4-Loop NPP Base Case

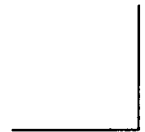


Figure 4.2 PIRT Sensitivity Histogram



Figure 4.3 Loop Nodalization for NPP



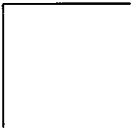


Figure 4.4 Reactor Vessel Nodalization for NPP



**Figure 4.5 CE 2x4 and Westinghouse 3- and 4-Loop Plant Vessel
Downcomer Configurations**



Figure 4.6 NPP Core Nodalization – Axial Plane



Figure 4.7 NPP Core Nodalization – Cross-Sectional Plane

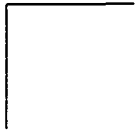


Figure 4.8 NPP Upper Plenum Nodalization – Axial Plane

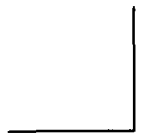
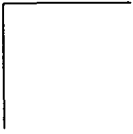


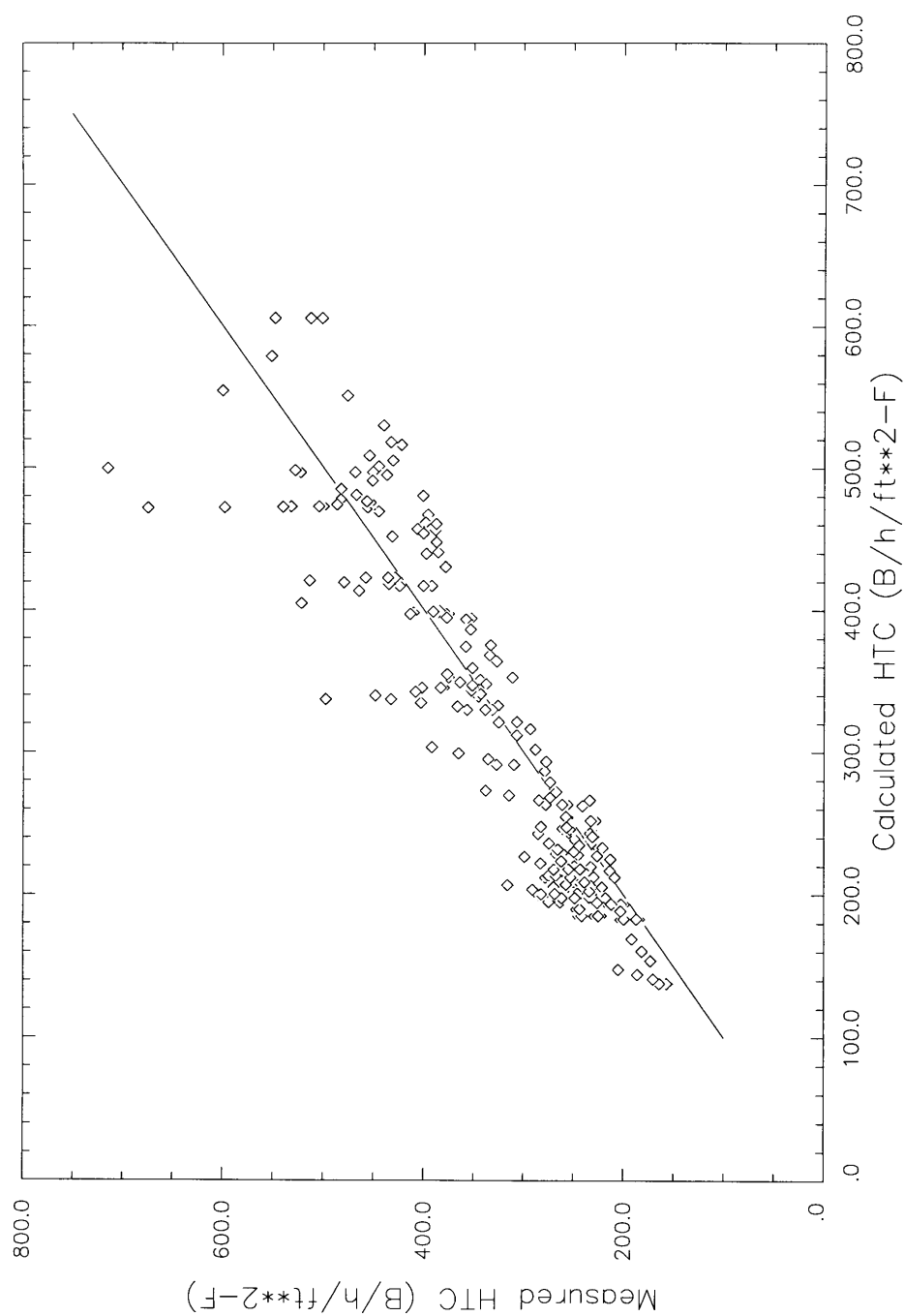
Figure 4.9 NPP Upper Plenum Nodalization – Cross-Sectional Plane



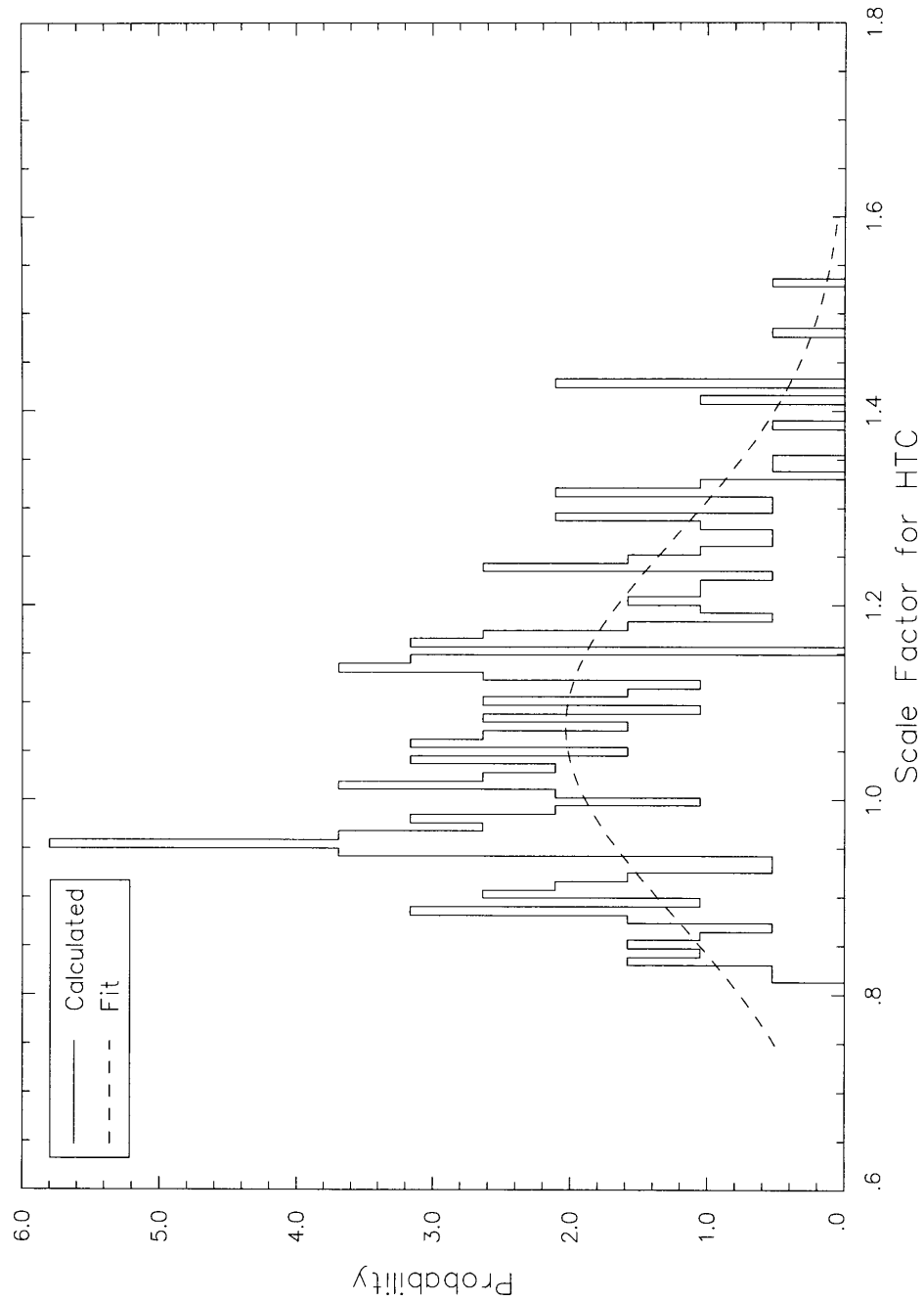
Figure 4.10 NPP Emergency Core Cooling System Nodalization

Figure 4.11 Double-Ended Guillotine Break Nodalization

Figure 4.12 Double-Ended Split Break Nodalization



**Figure 4.13 Comparison of Calculated HTC to Measured HTC, ORNL
THTF**



**Figure 4.14 Frequency Distribution for Scale Factor for HTC, ORNL
THTF**

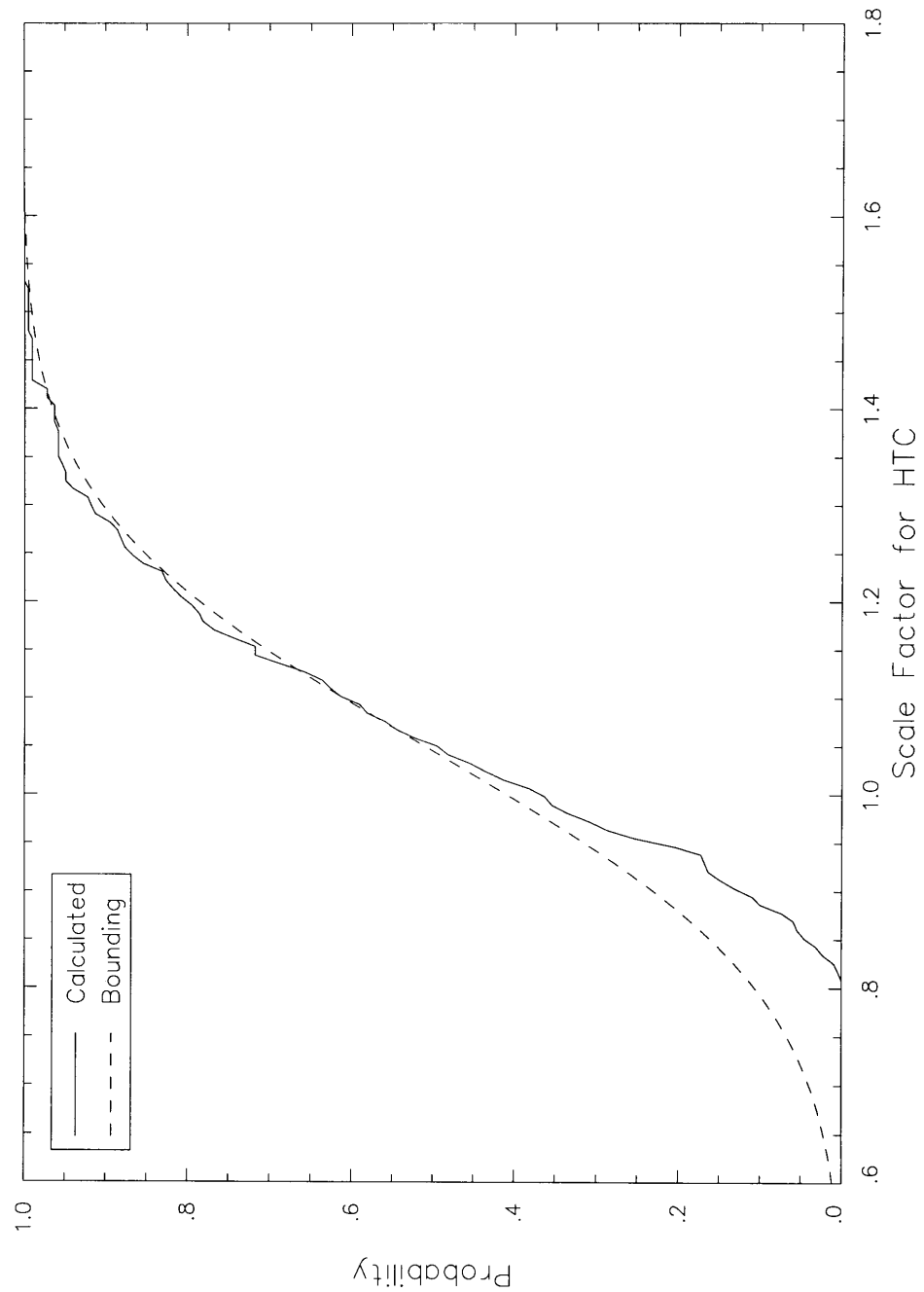


Figure 4.15 Bounding Distribution for HTC Scaling, ORNL THTF

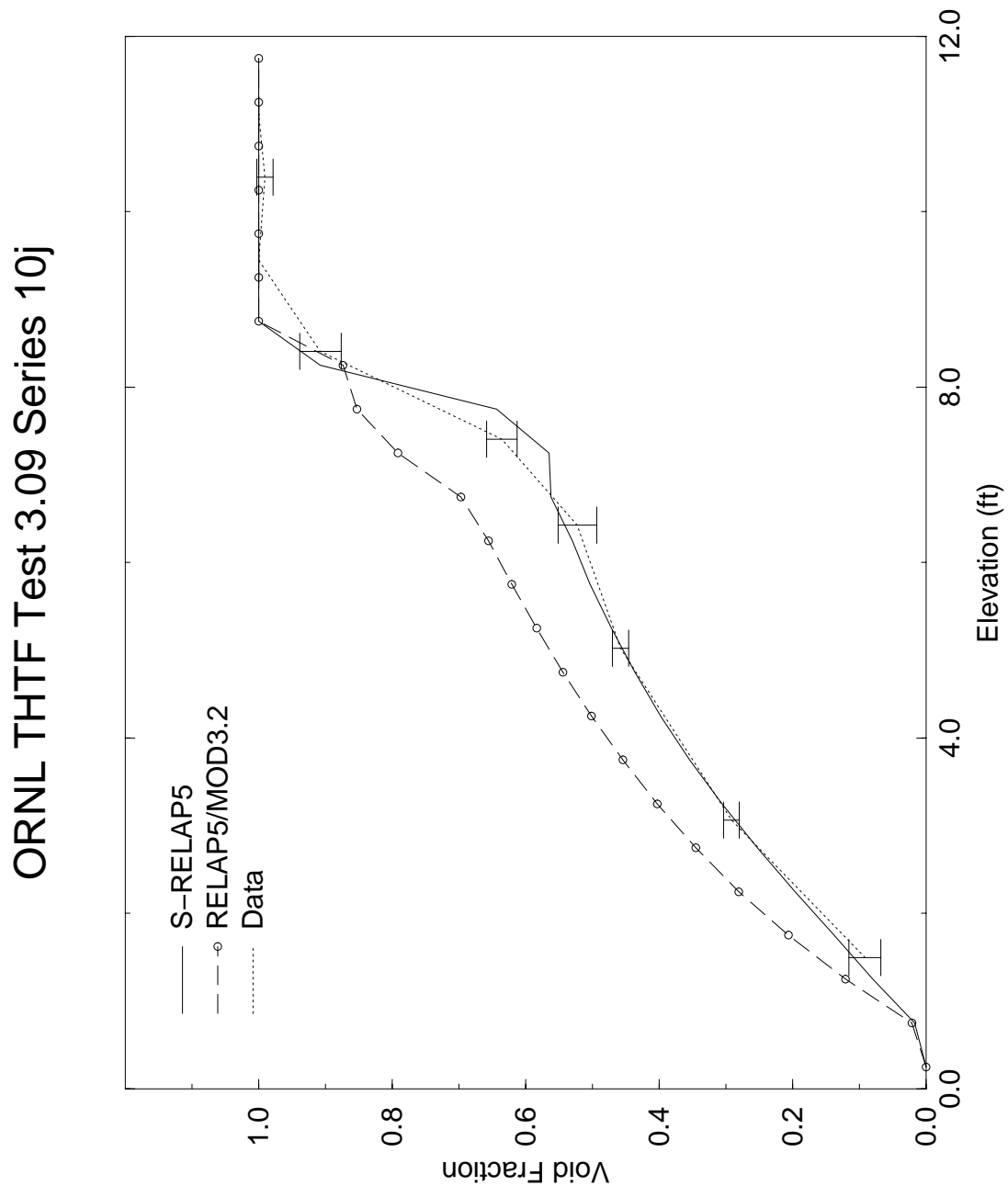


Figure 4.16 Comparisons of Void Profiles, ORNL THTF Test 3.09.10j

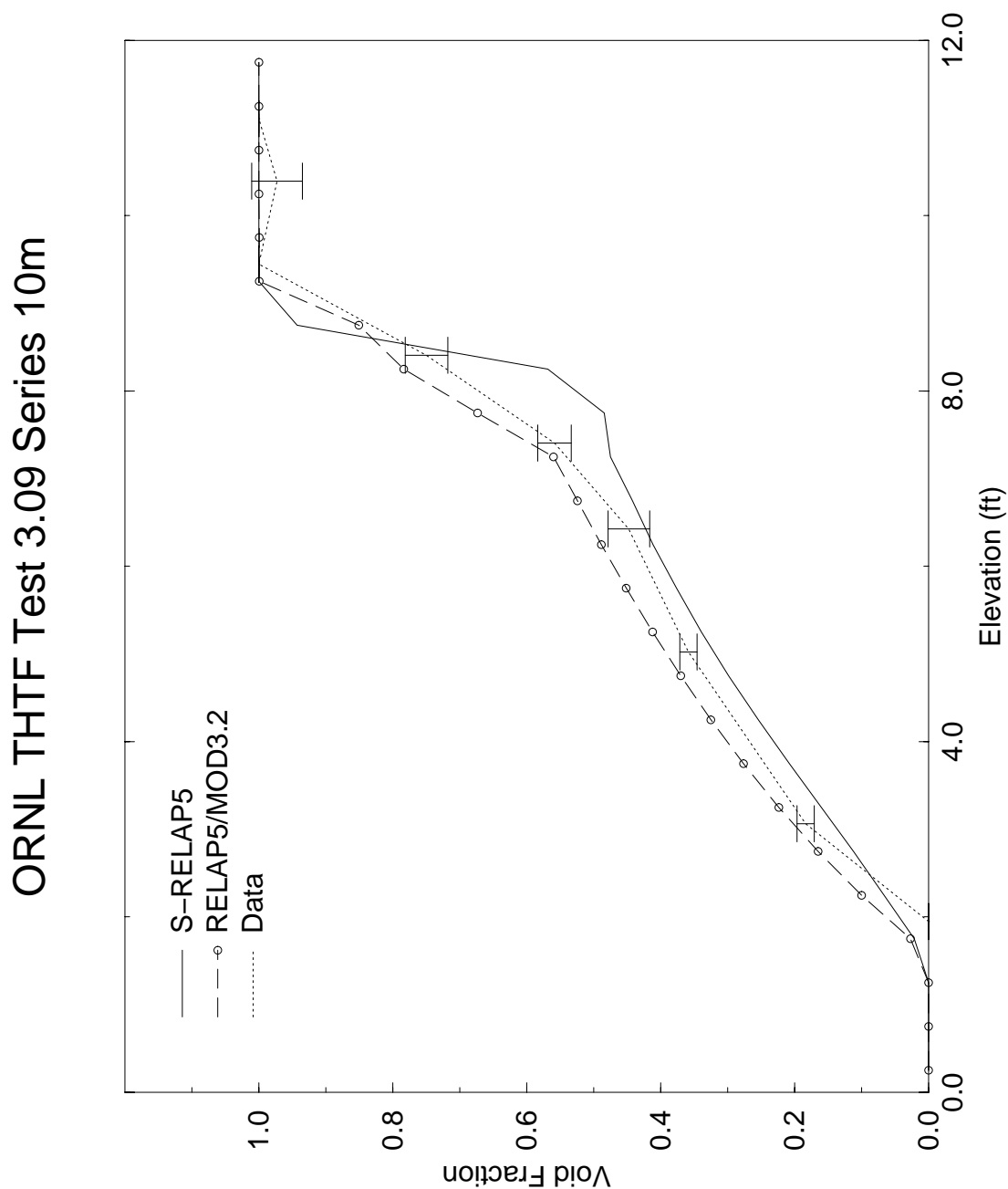


Figure 4.17 Comparison of Void Profiles, ORNL THTF Test 3.09.10 m

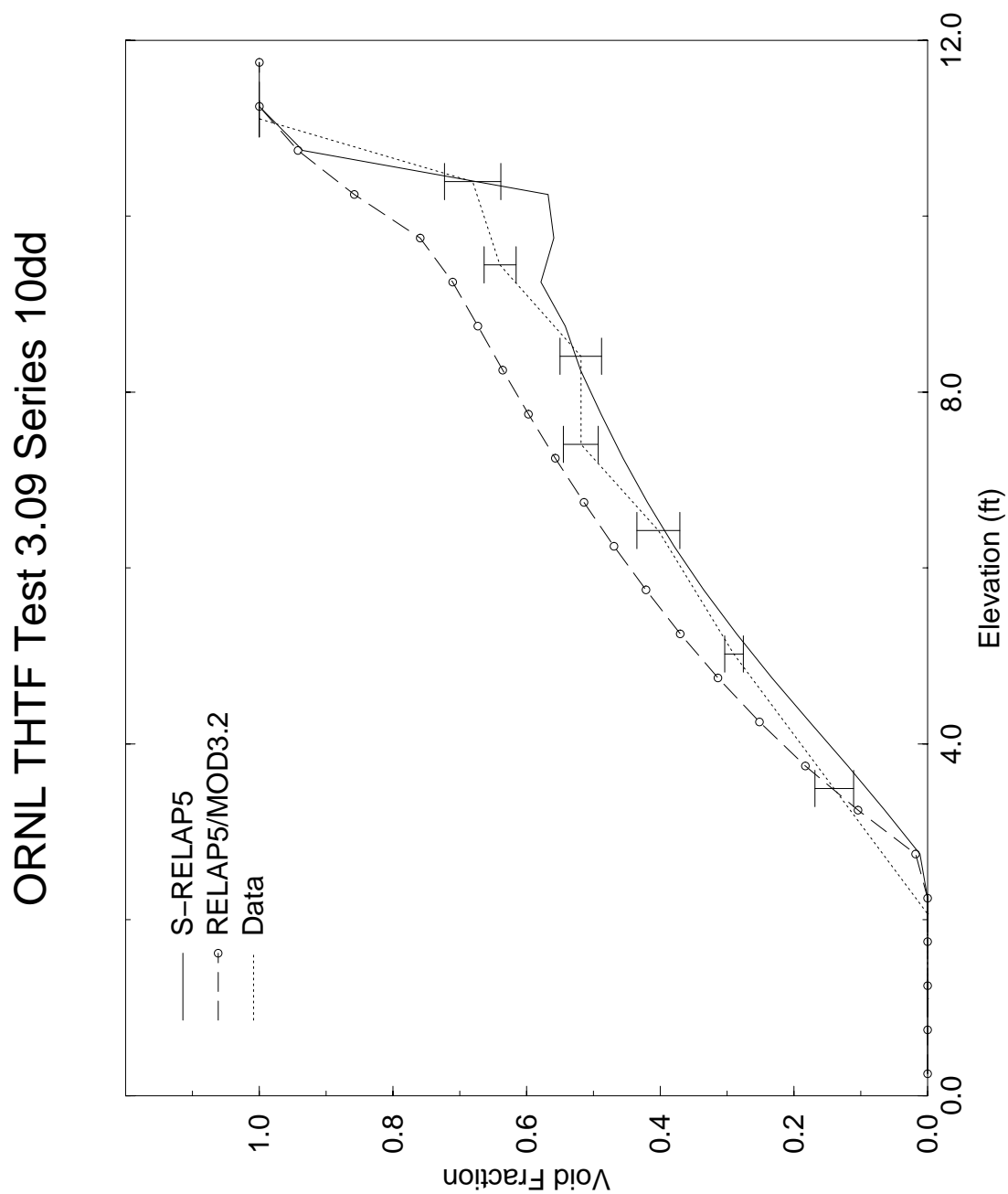


Figure 4.18 Comparison of Void Profiles, ORNL THTF Test 3.09.10dd

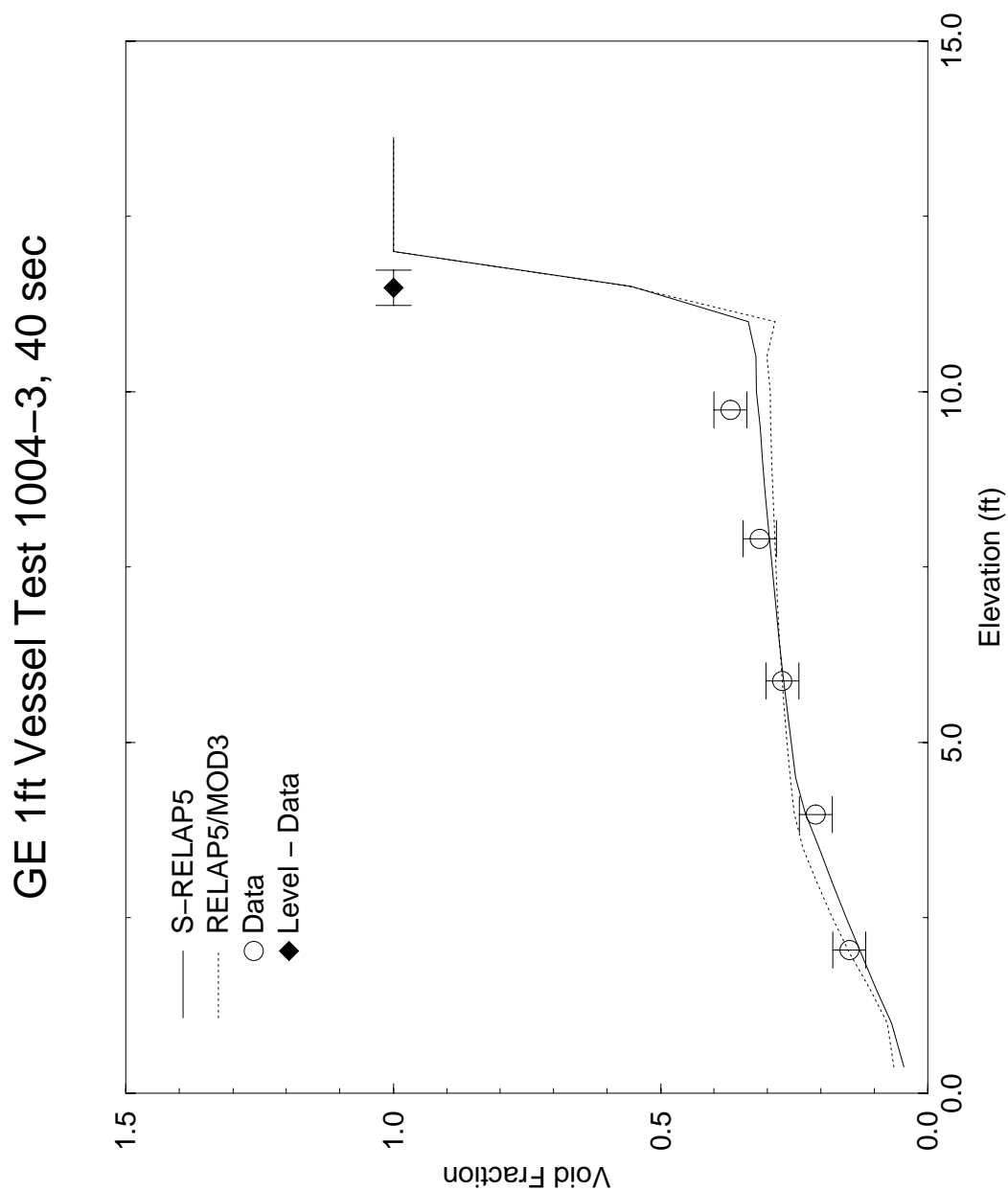


Figure 4.19 Void Profiles at 40 Seconds for the 1 ft GE Test 1004-3

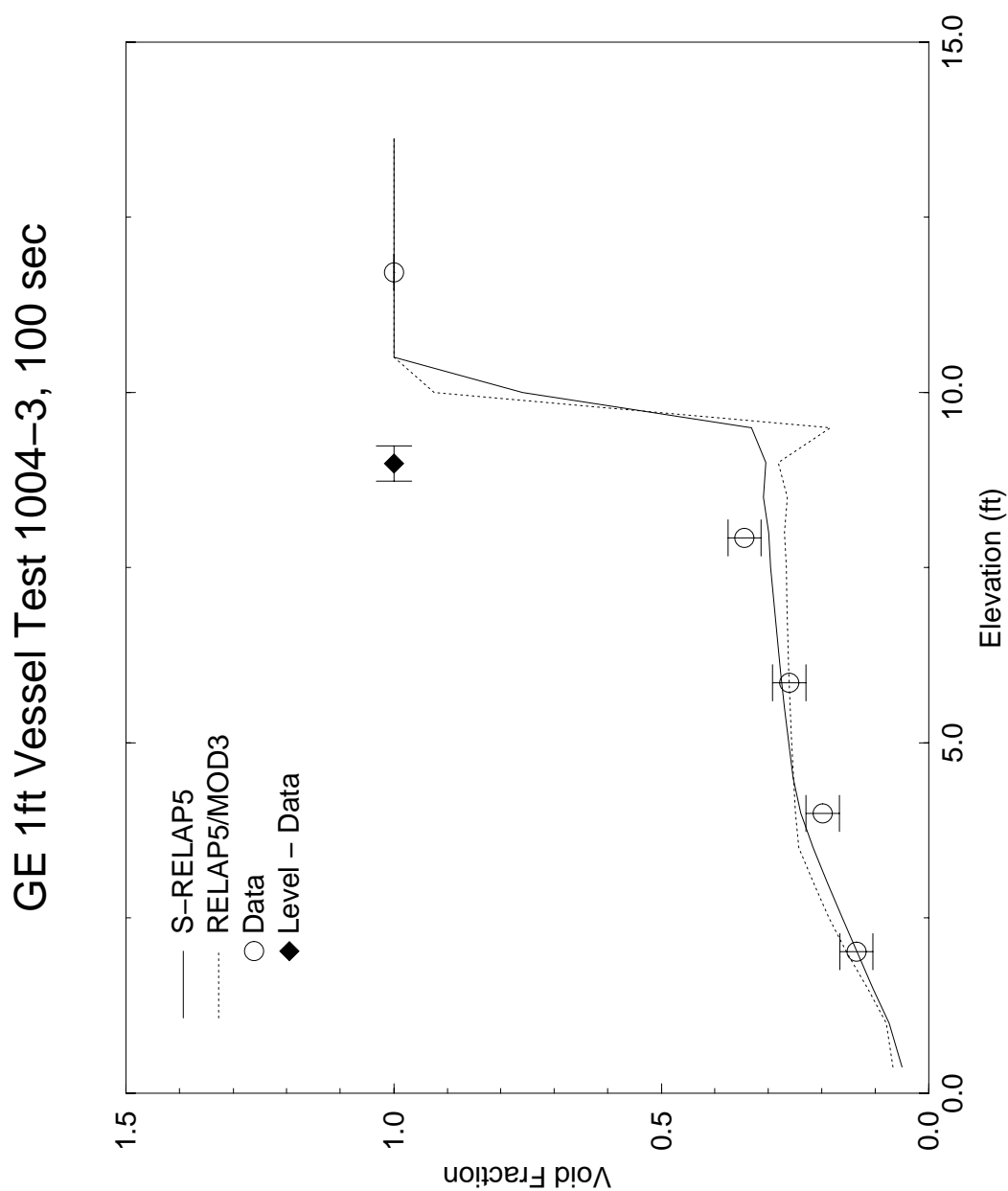
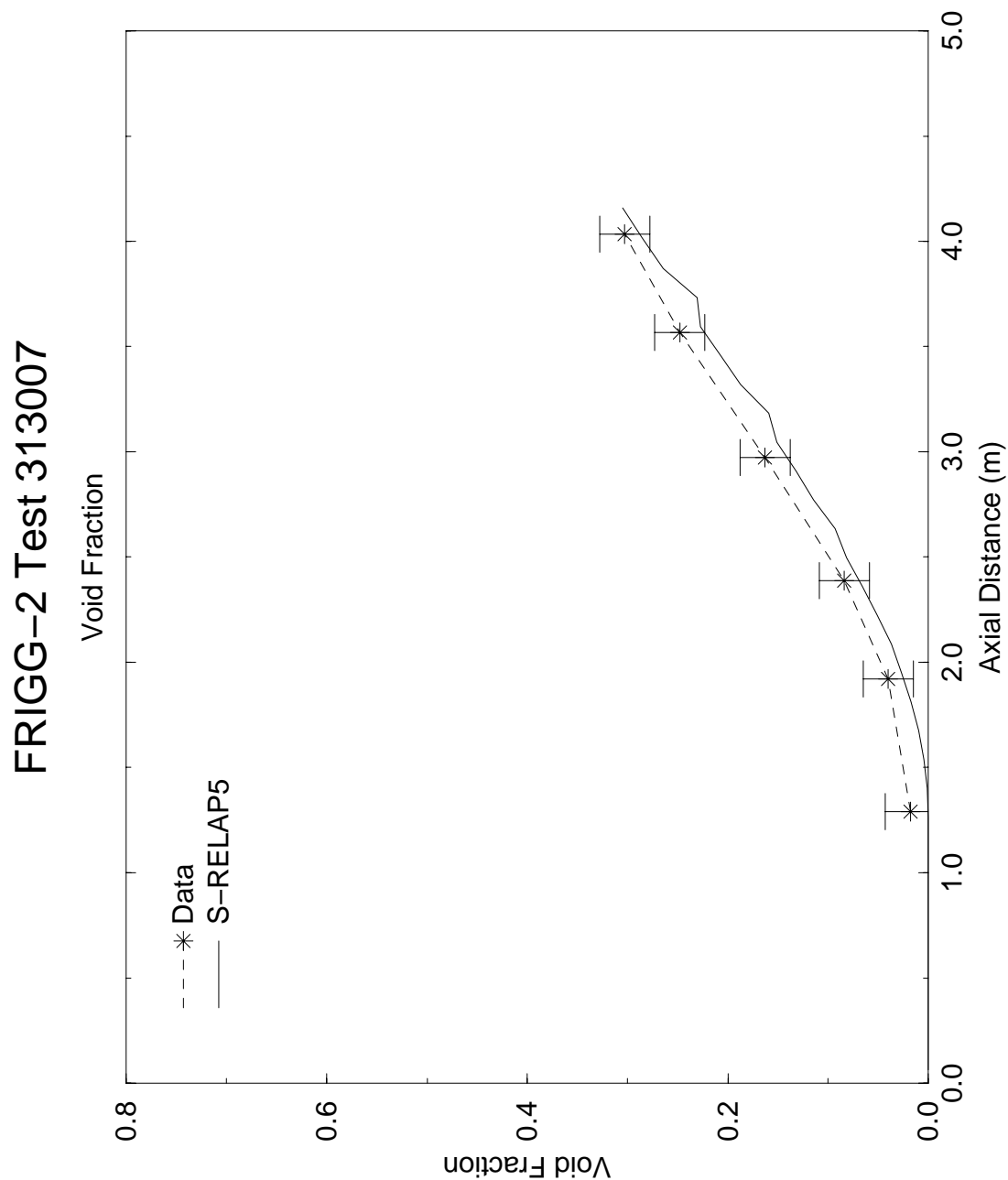
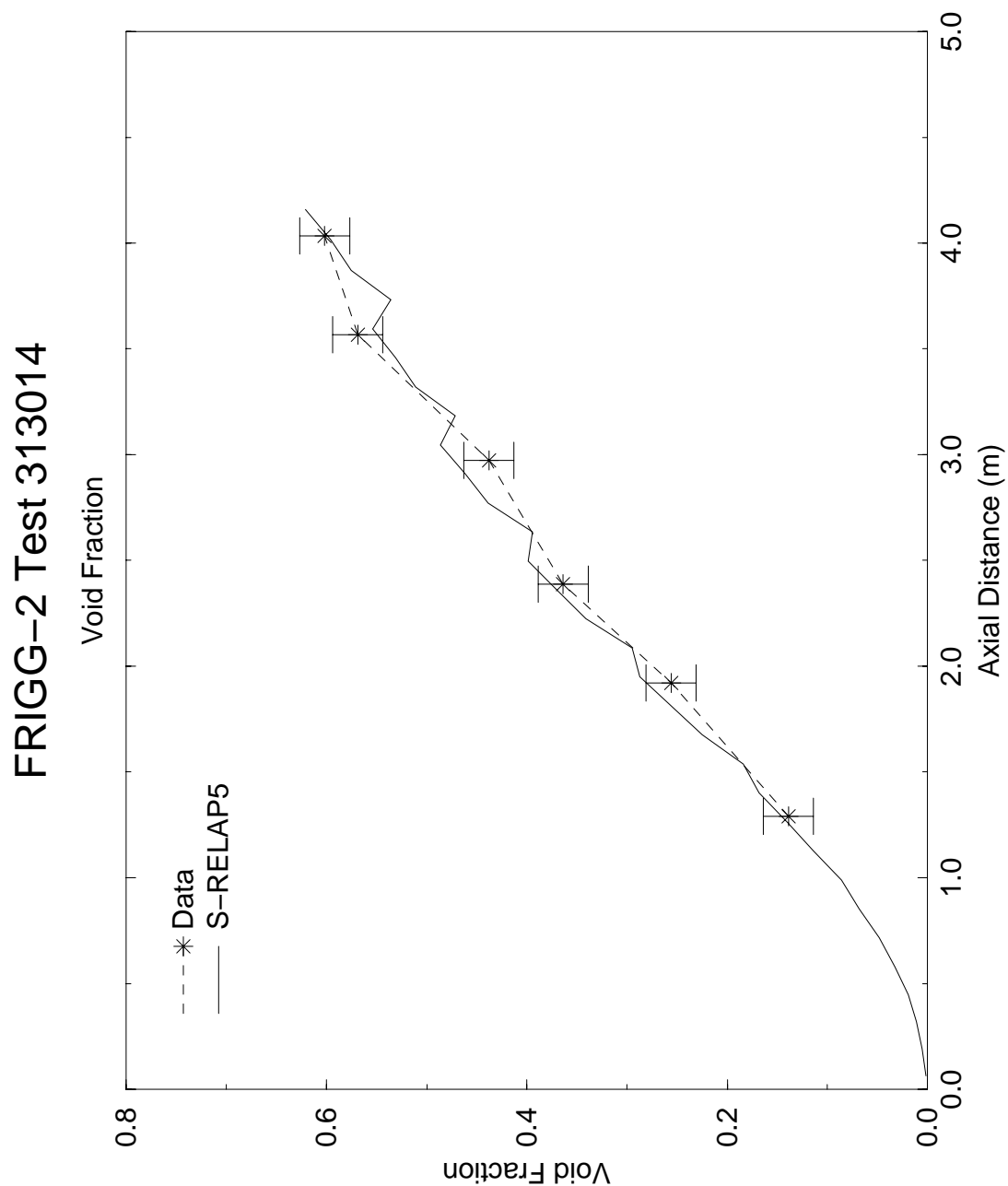


Figure 4.20 Void Profiles at 100 Seconds for the 1 ft GE Test 1004-3



**Figure 4.21 Comparison of Calculated and Measured Void Fraction,
Frigg-2 Test 313007**



**Figure 4.22 Comparison of Calculated and Measured Void Fraction,
Frigg-2 Test 313014**

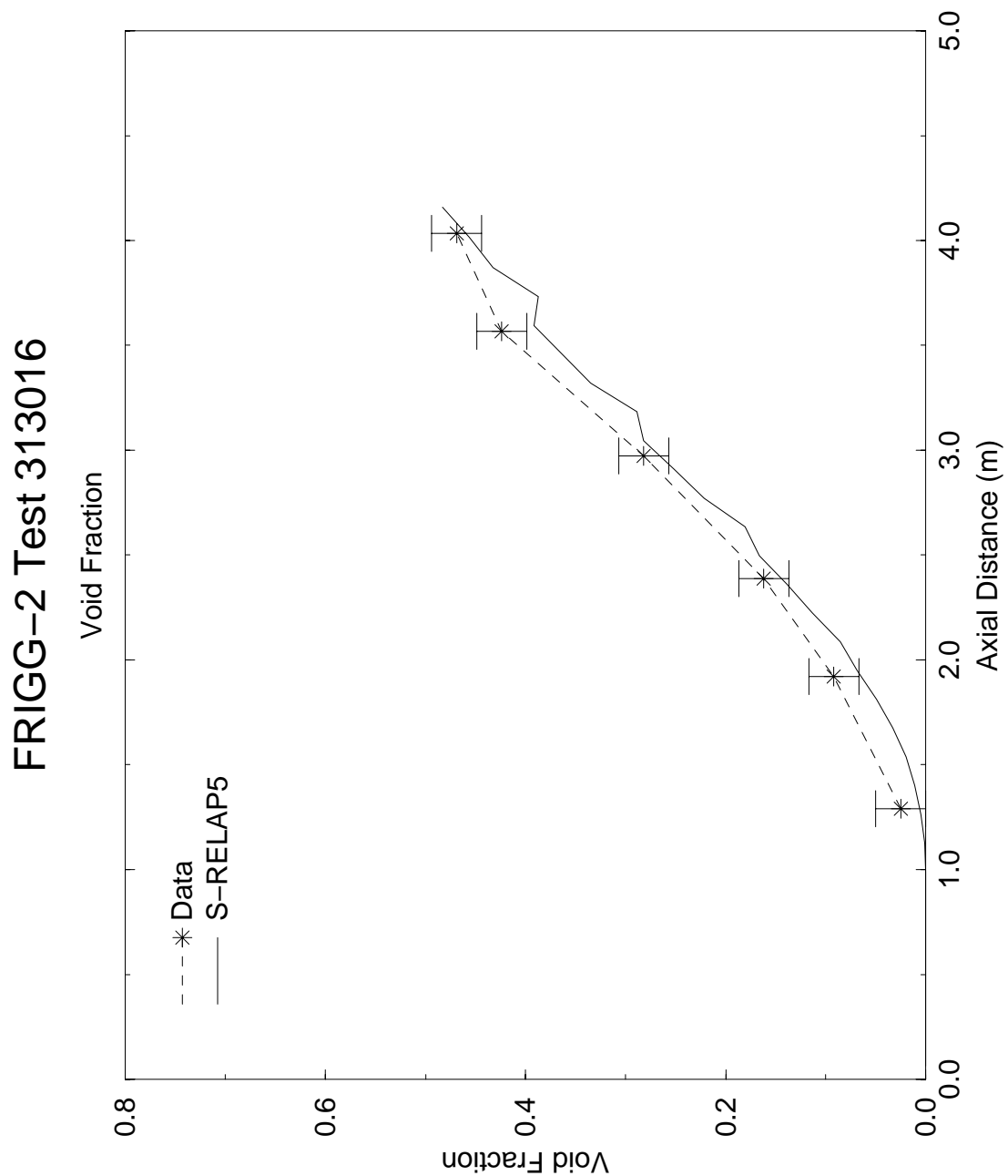


**Figure 4.23 Comparison of Calculated and Measured Void Fraction,
Frigg-2 Test 313016**

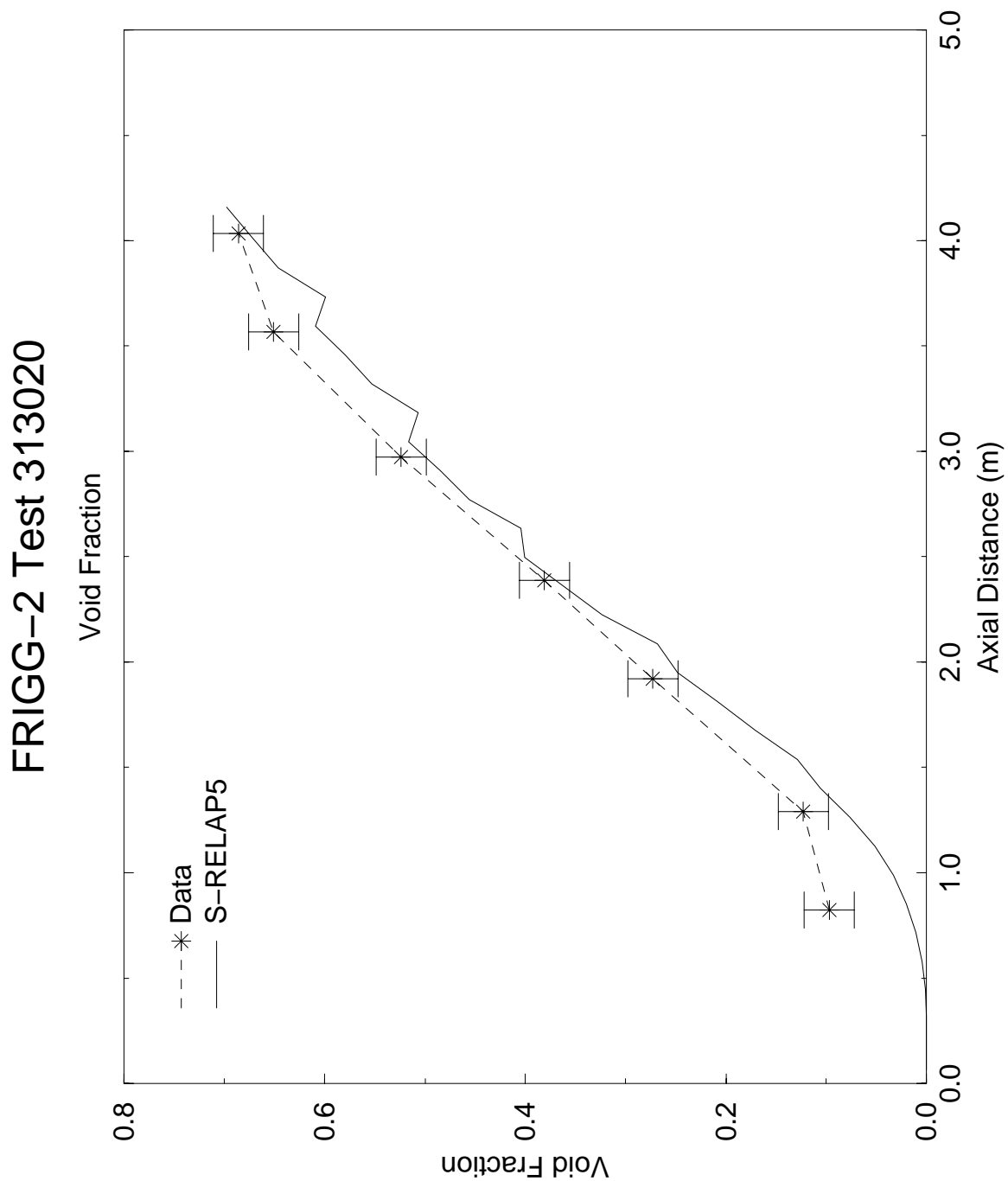
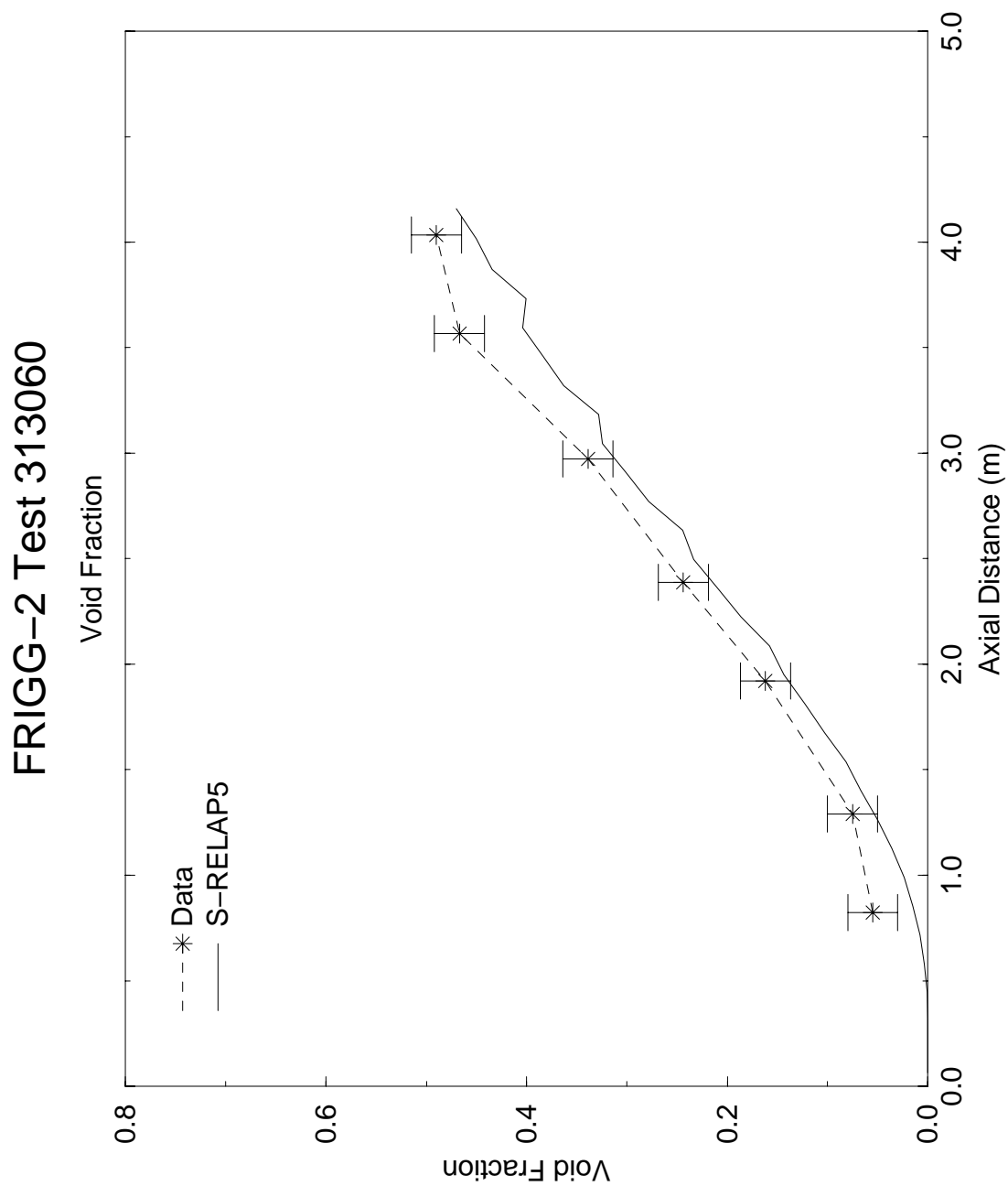
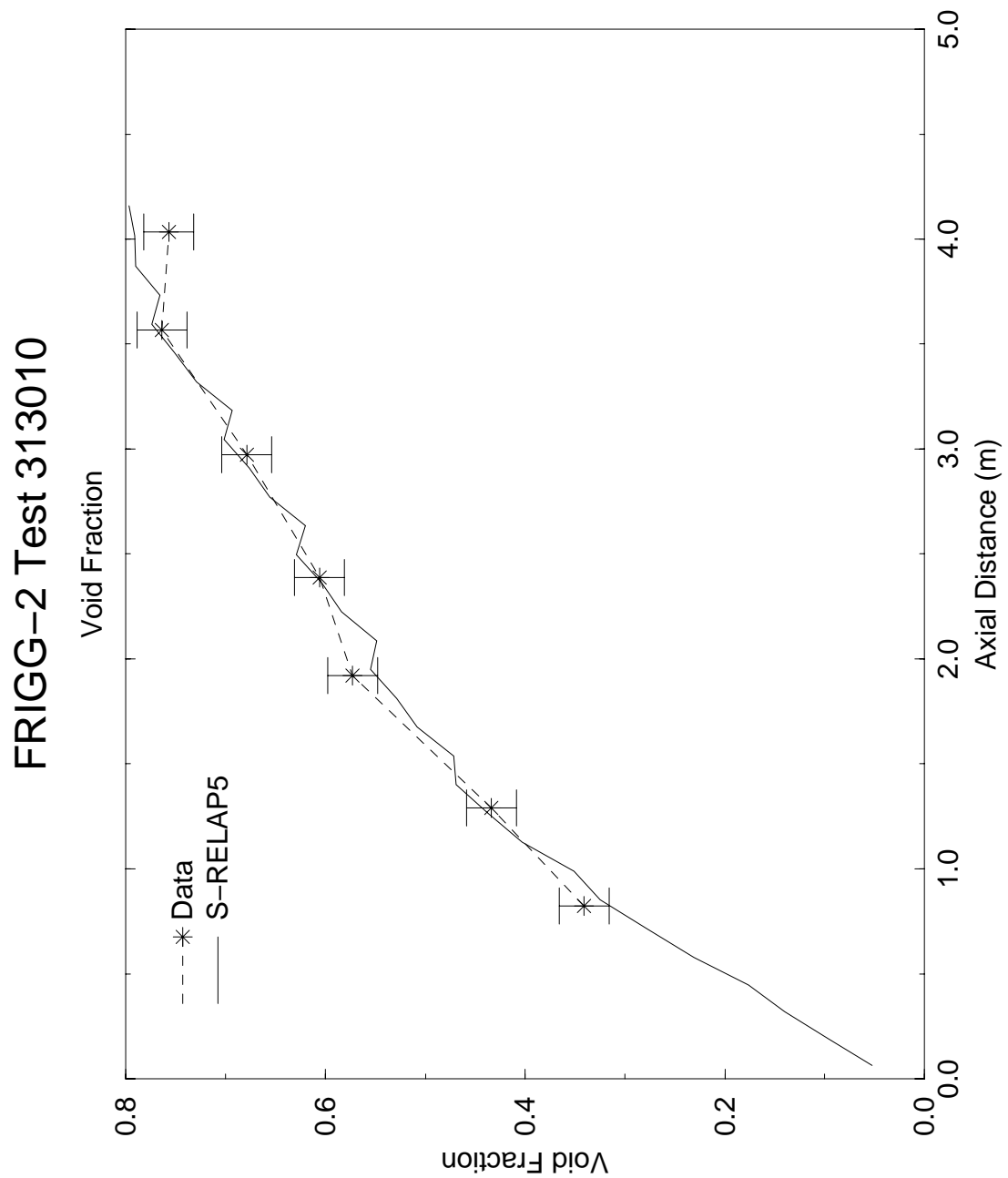


Figure 4.24 Comparison of Calculated and Measured Void Fraction, Frigg-2 Test 313020



**Figure 4.25 Comparison of Calculated and Measured Void Fraction,
Frigg-2 Test 313060**



**Figure 4.26 Comparison of Calculated and Measured Void Fraction,
Frigg-2 Test 313010**

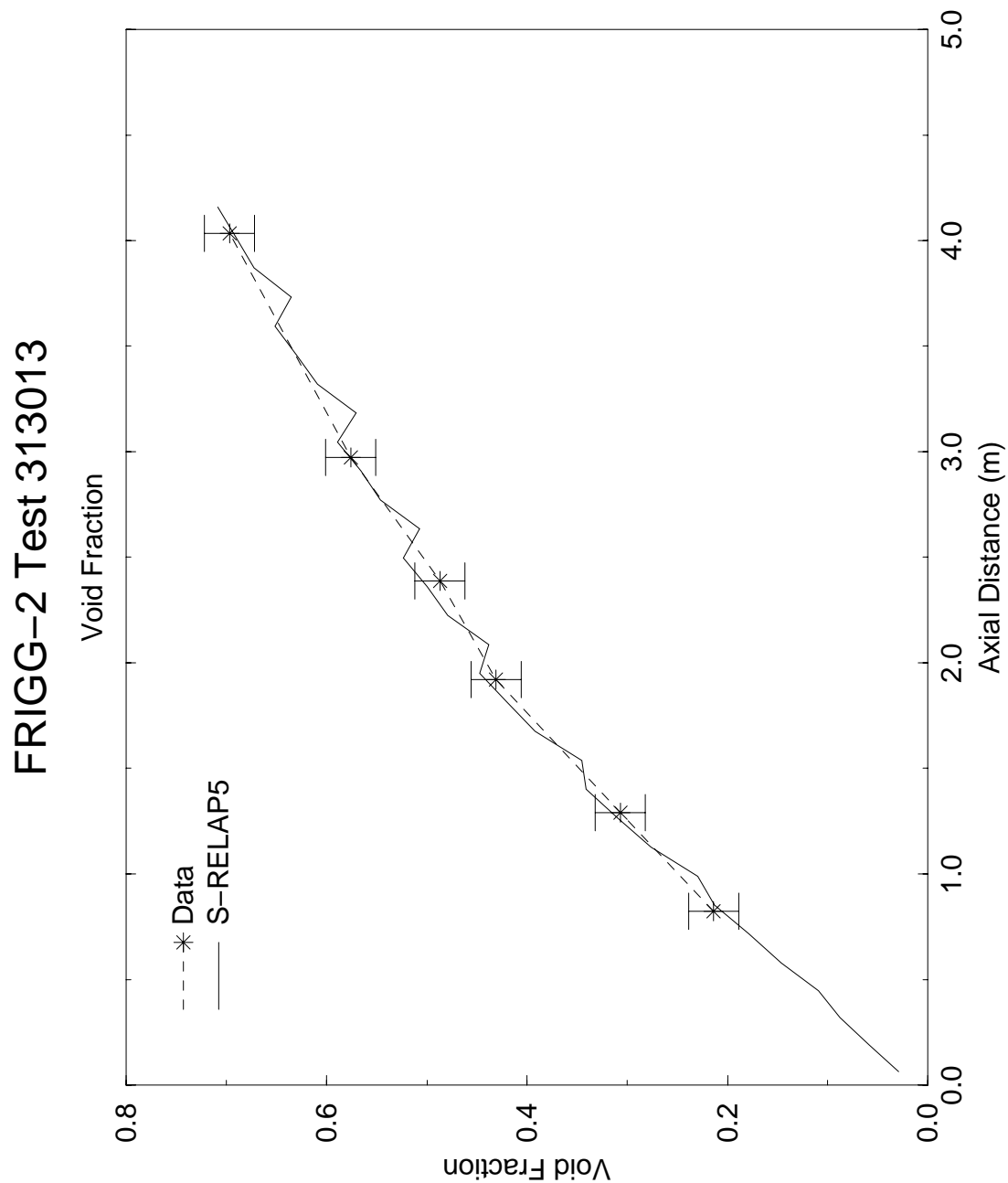


**Figure 4.27 Comparison of Calculated and Measured Void Fraction,
Frigg-2 Test 313013**

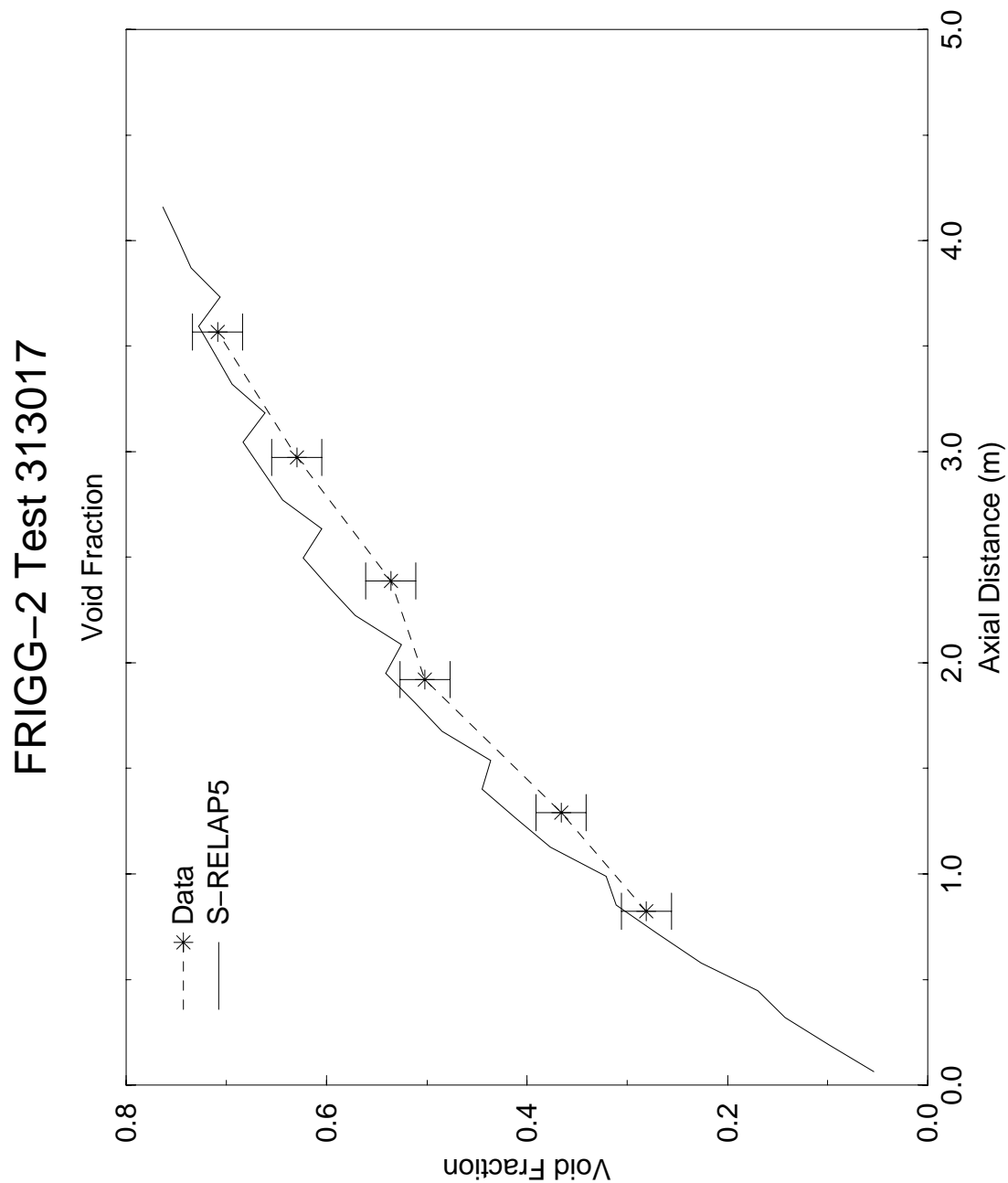


**Figure 4.28 Comparison of Calculated and Measured Void Fraction,
Frigg-2 Test 313017**

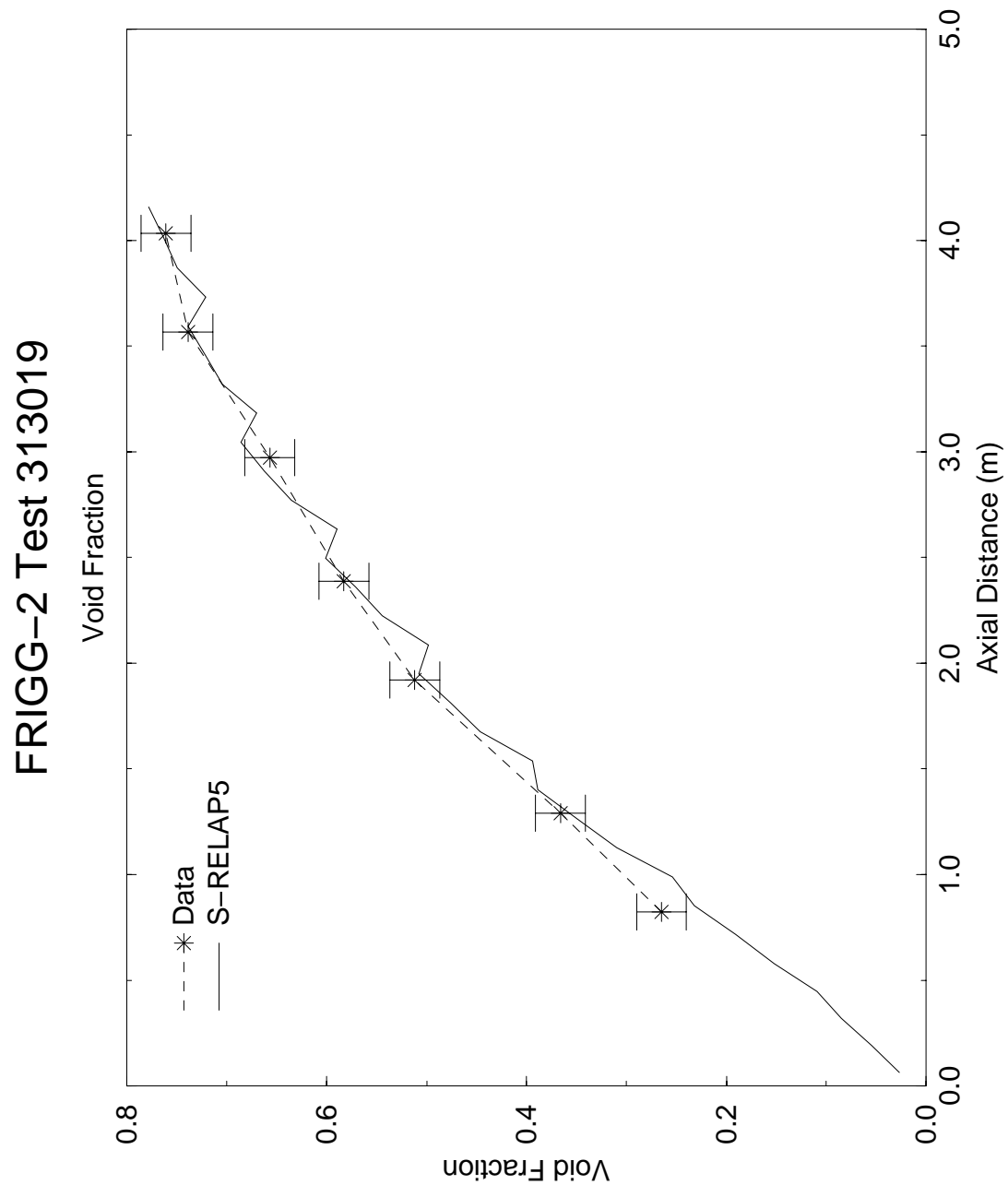


**Figure 4.29 Comparison of Calculated and Measured Void Fraction,
Frigg-2 Test 313019**

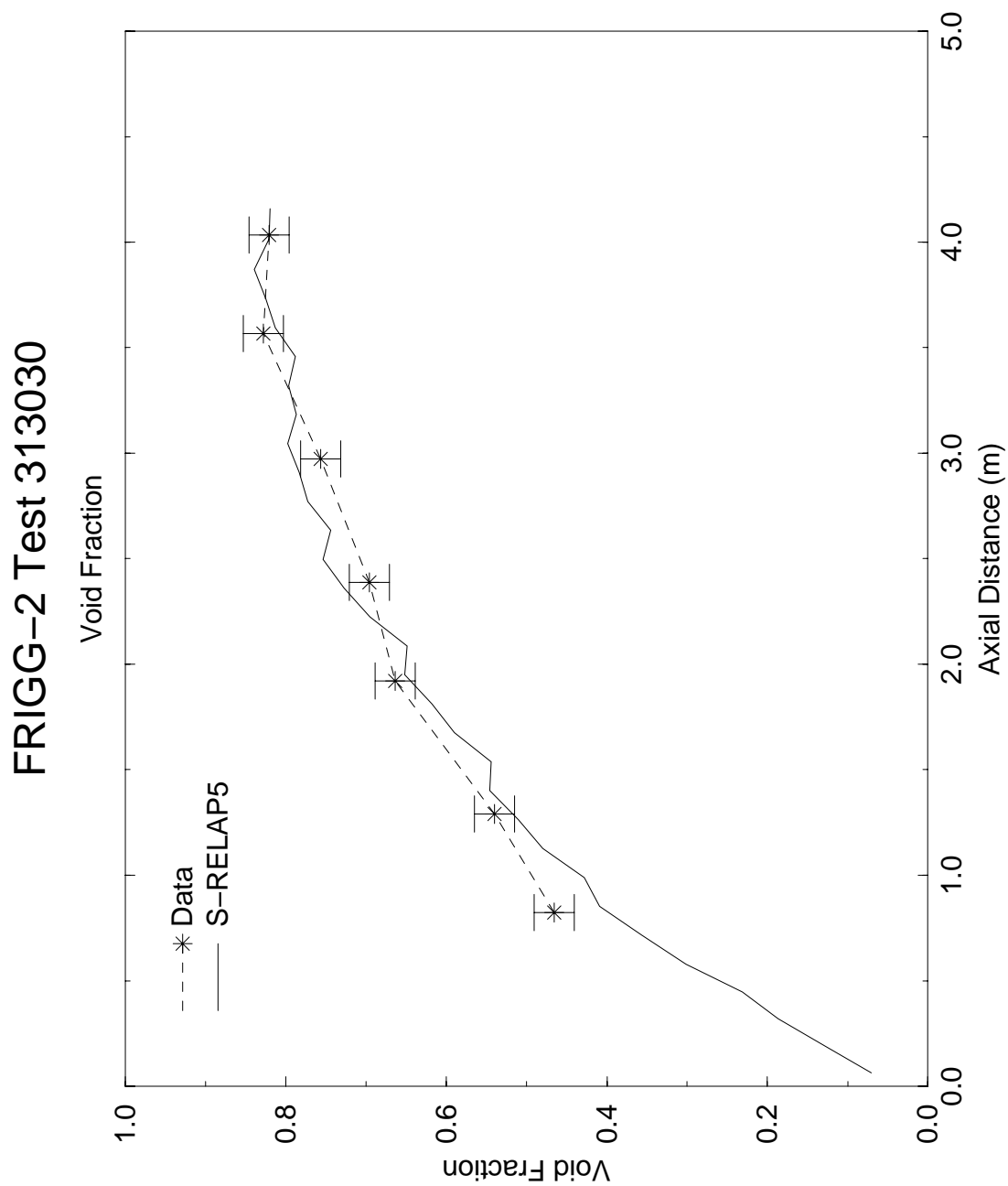


**Figure 4.30 Comparison of Calculated and Measured Void Fraction,
Frigg-2 Test 313030**

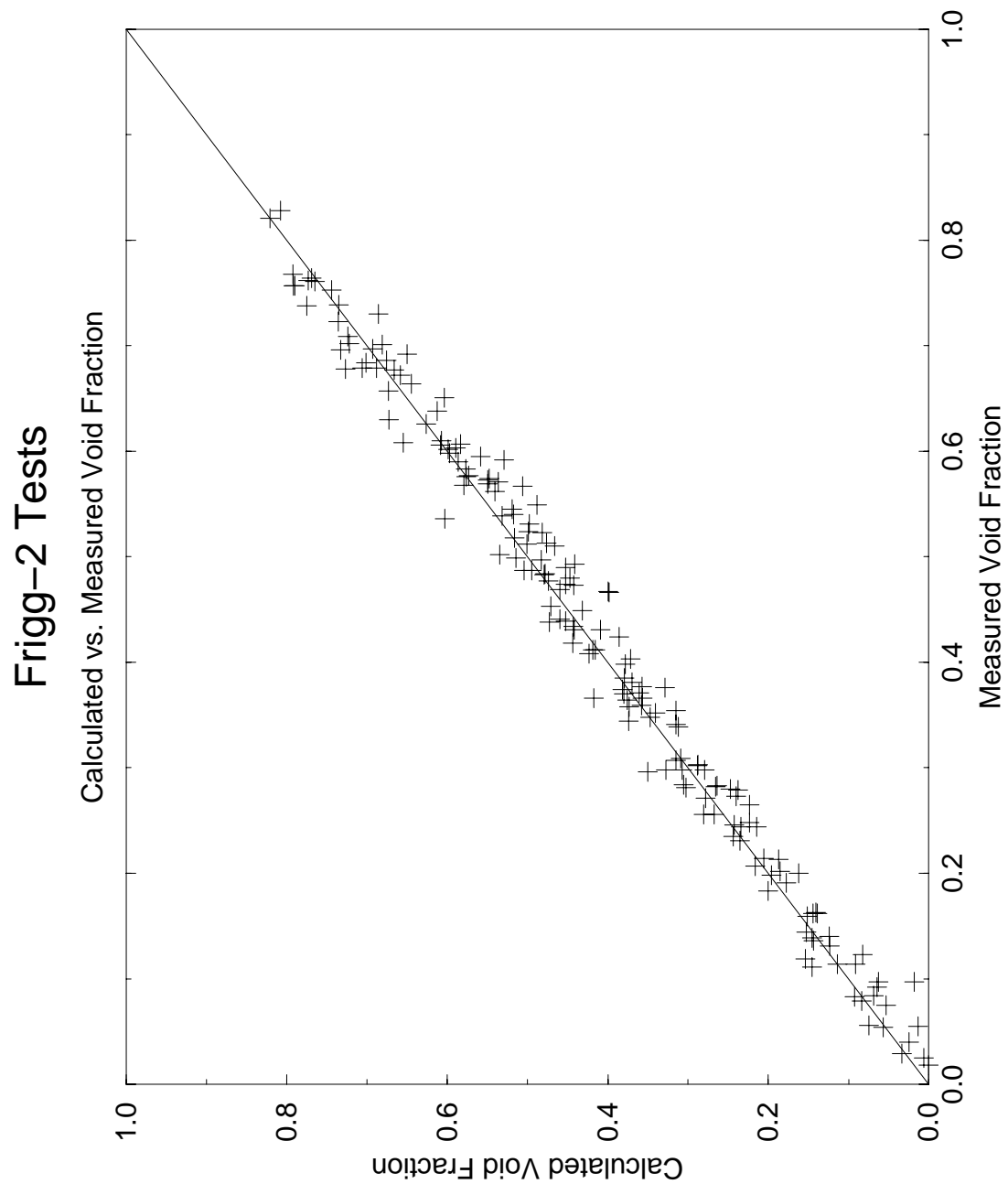


**Figure 4.31 Comparison of Calculated and Measured Void Fraction
at the Same Location for all 27 FRIGG Tests**

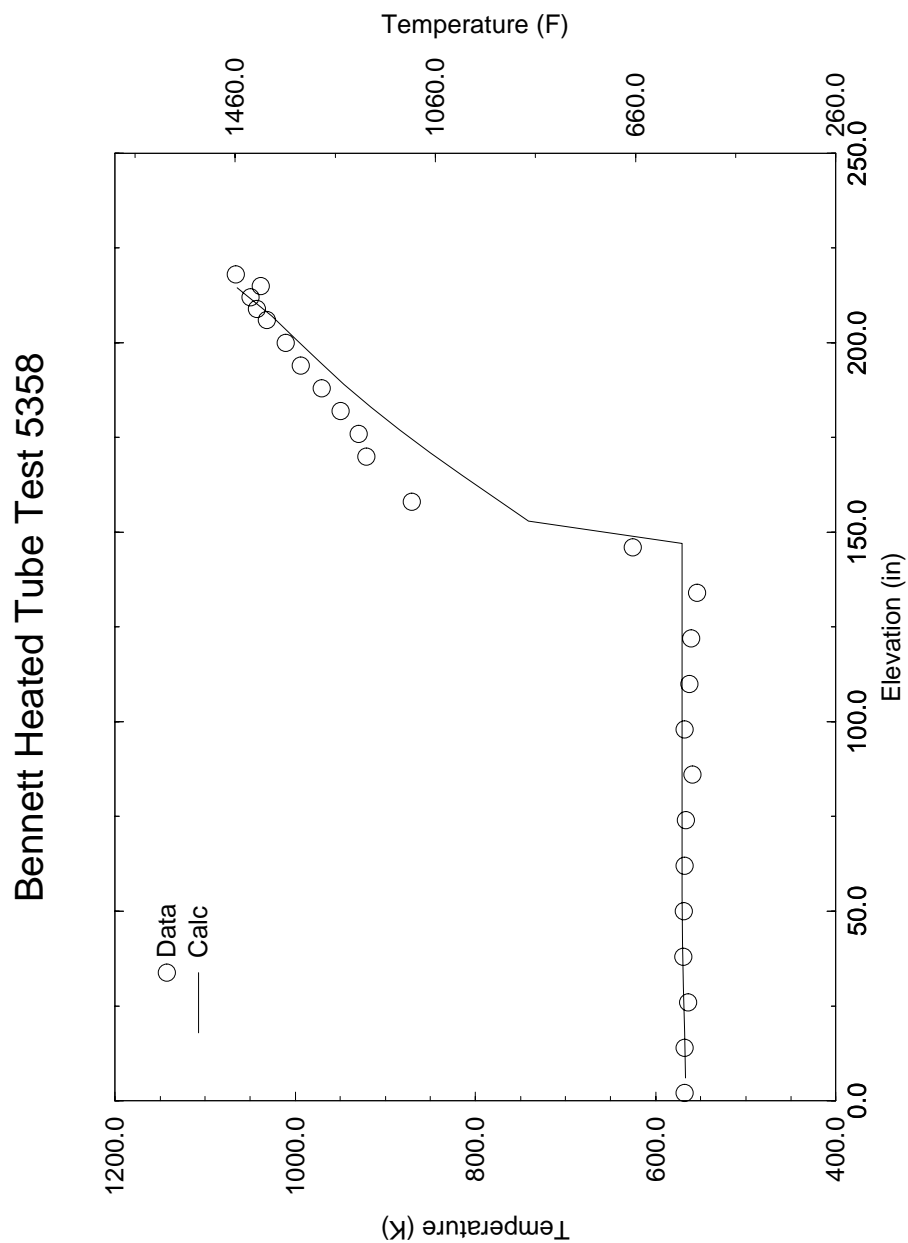


Figure 4.32 Wall Temperature Profiles, Bennett Heated Tube Test 5358

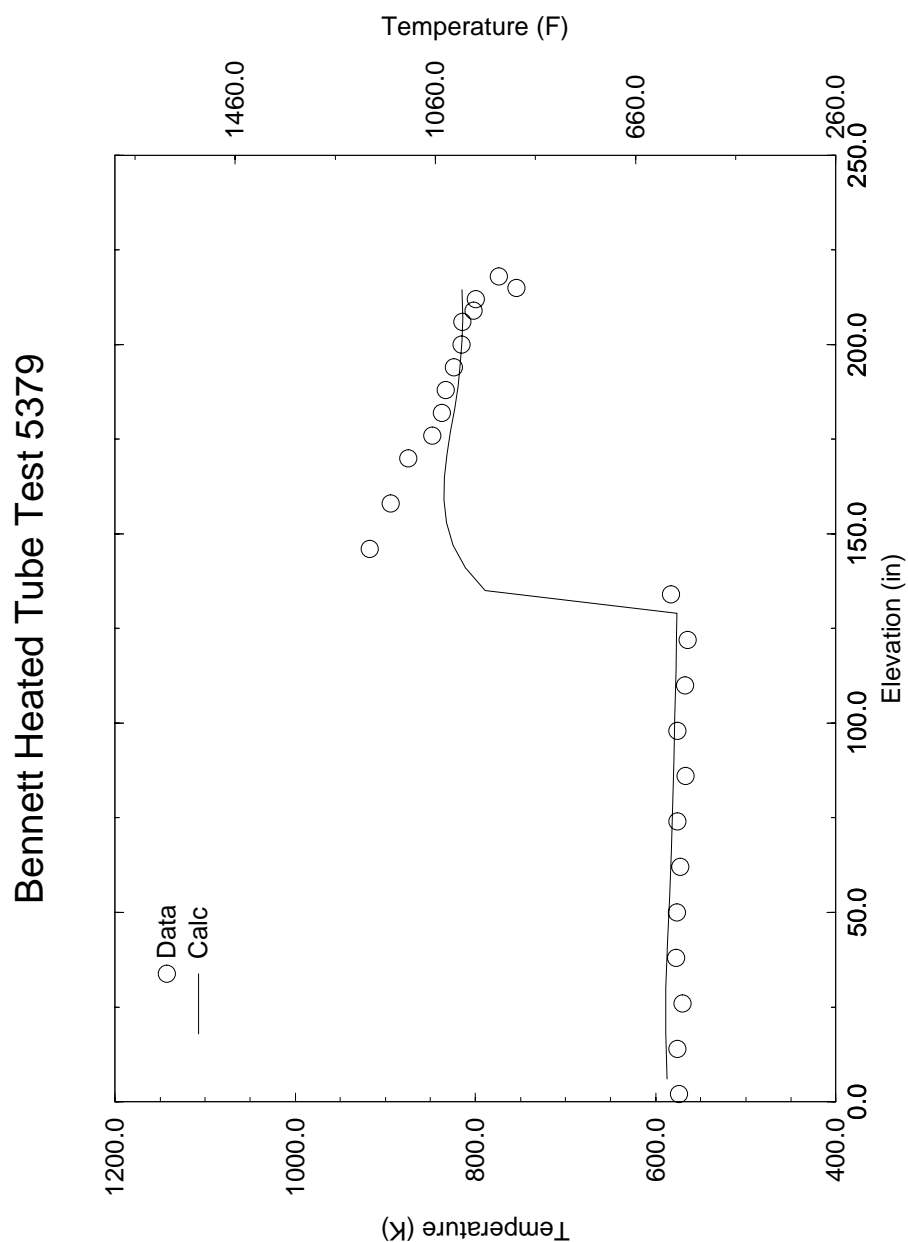
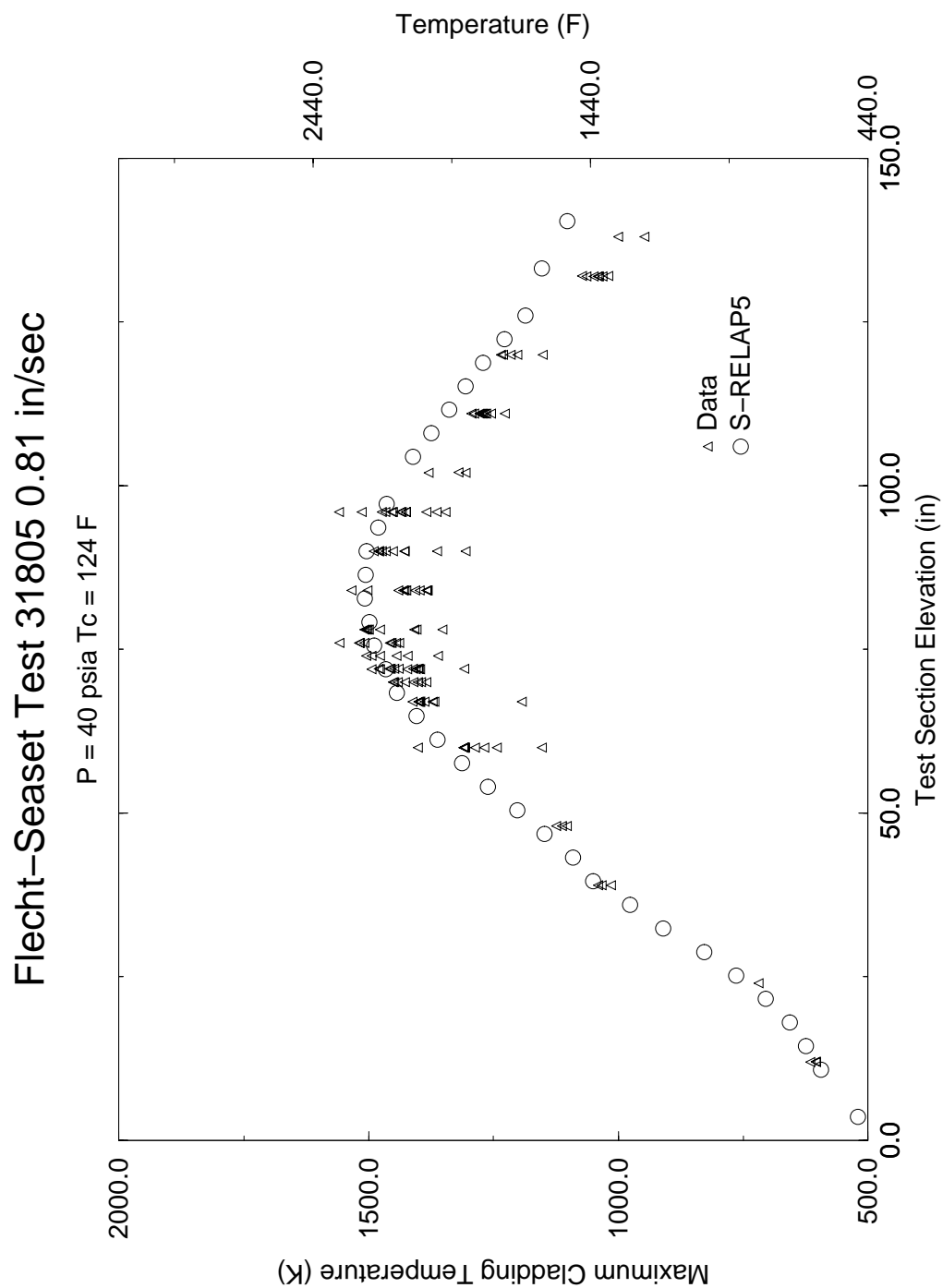
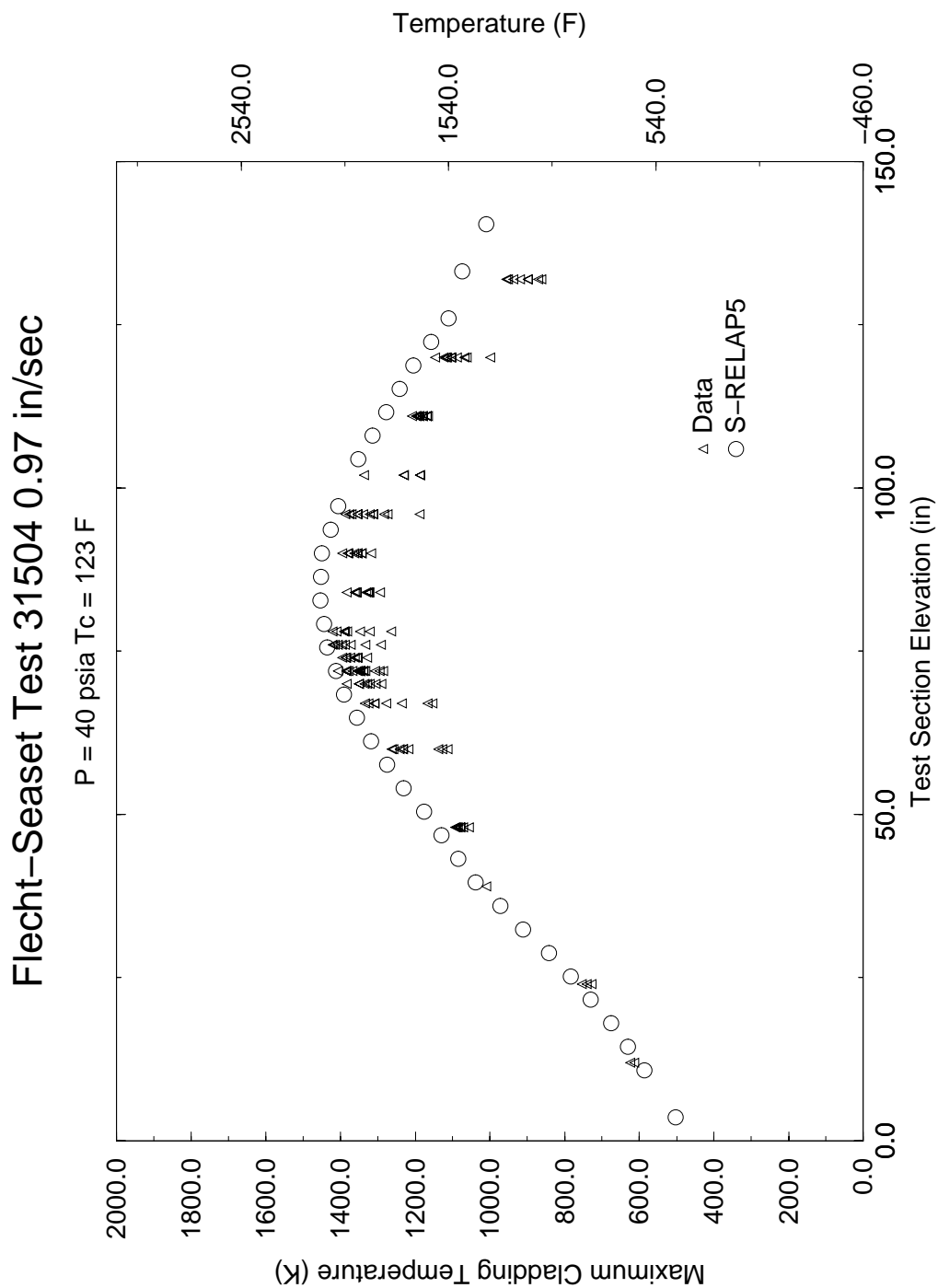


Figure 4.33 Wall Temperature Profiles, Bennett Heated Tube Test 5379



**Figure 4.34 Maximum Clad Temperature at All Measured Elevations,
FLECHT SEASET Test 31805**



**Figure 4.35 Maximum Clad Temperature at All Measured Elevations,
FLECHT SEASET Test 31504**

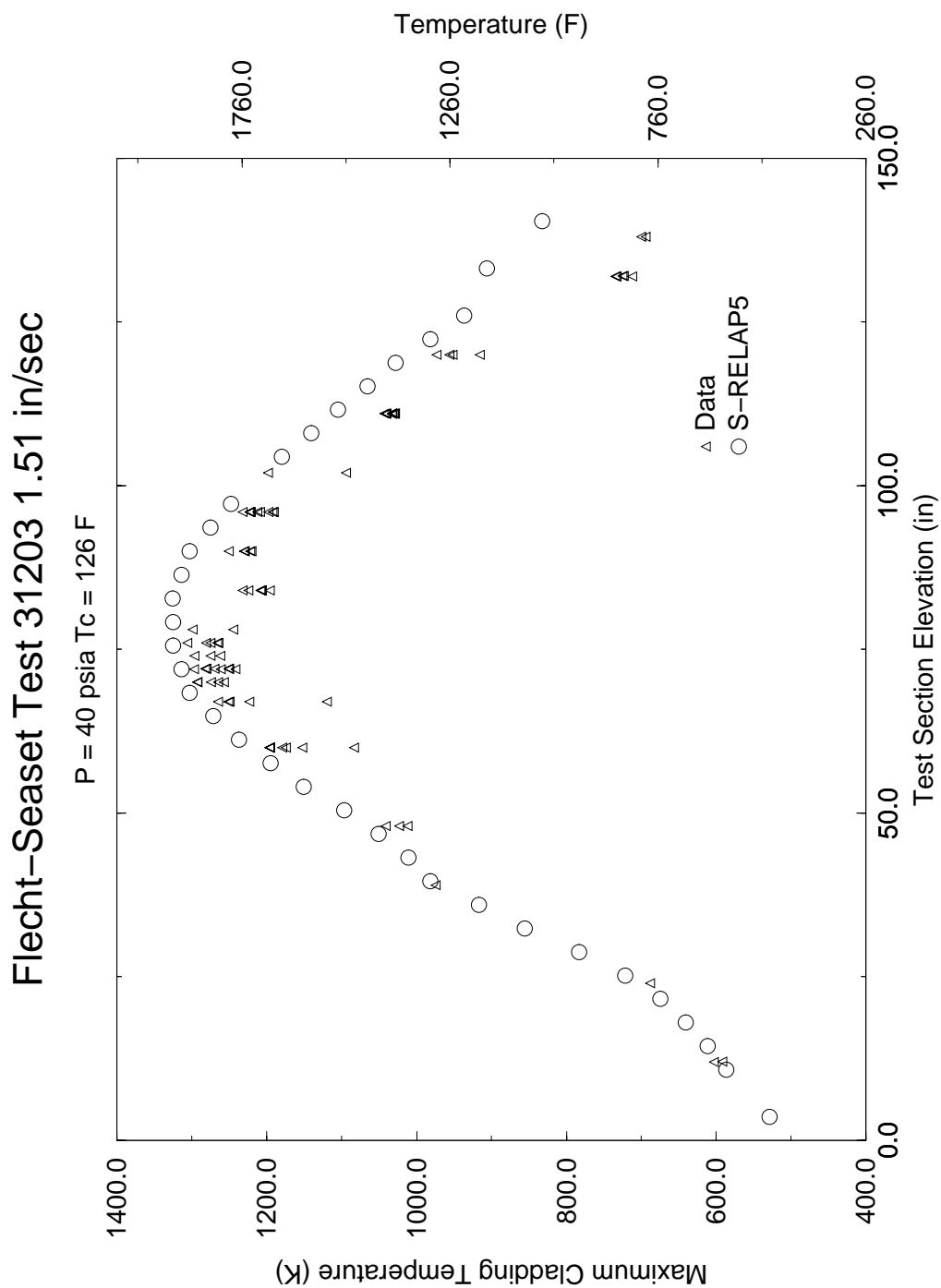


**Figure 4.36 Maximum Clad Temperature at All Measured Elevations,
FLECHT SEASET Test 31203**

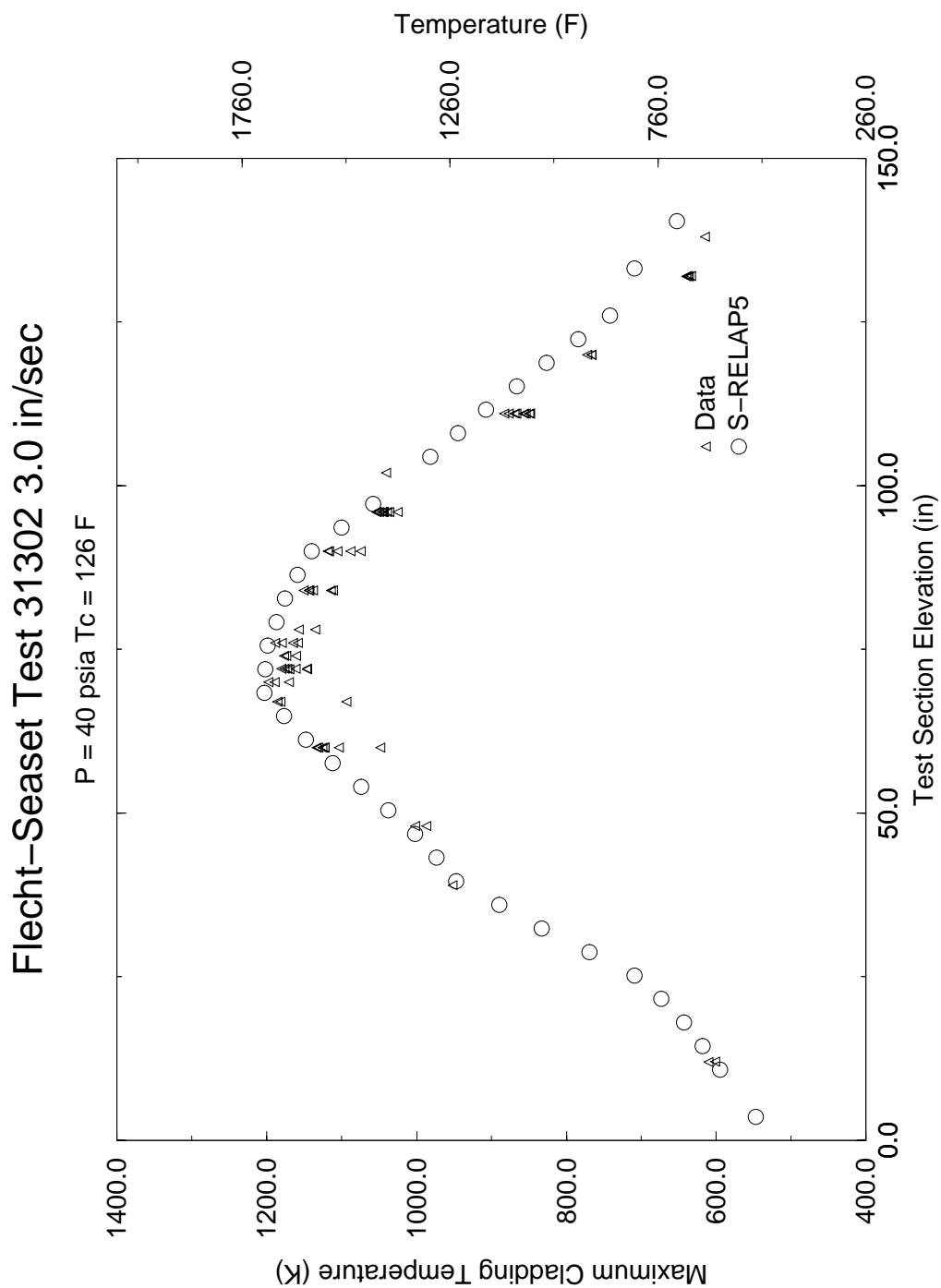


**Figure 4.37 Maximum Clad Temperature at All Measured Elevations,
FLECHT SEASET Test 31302**

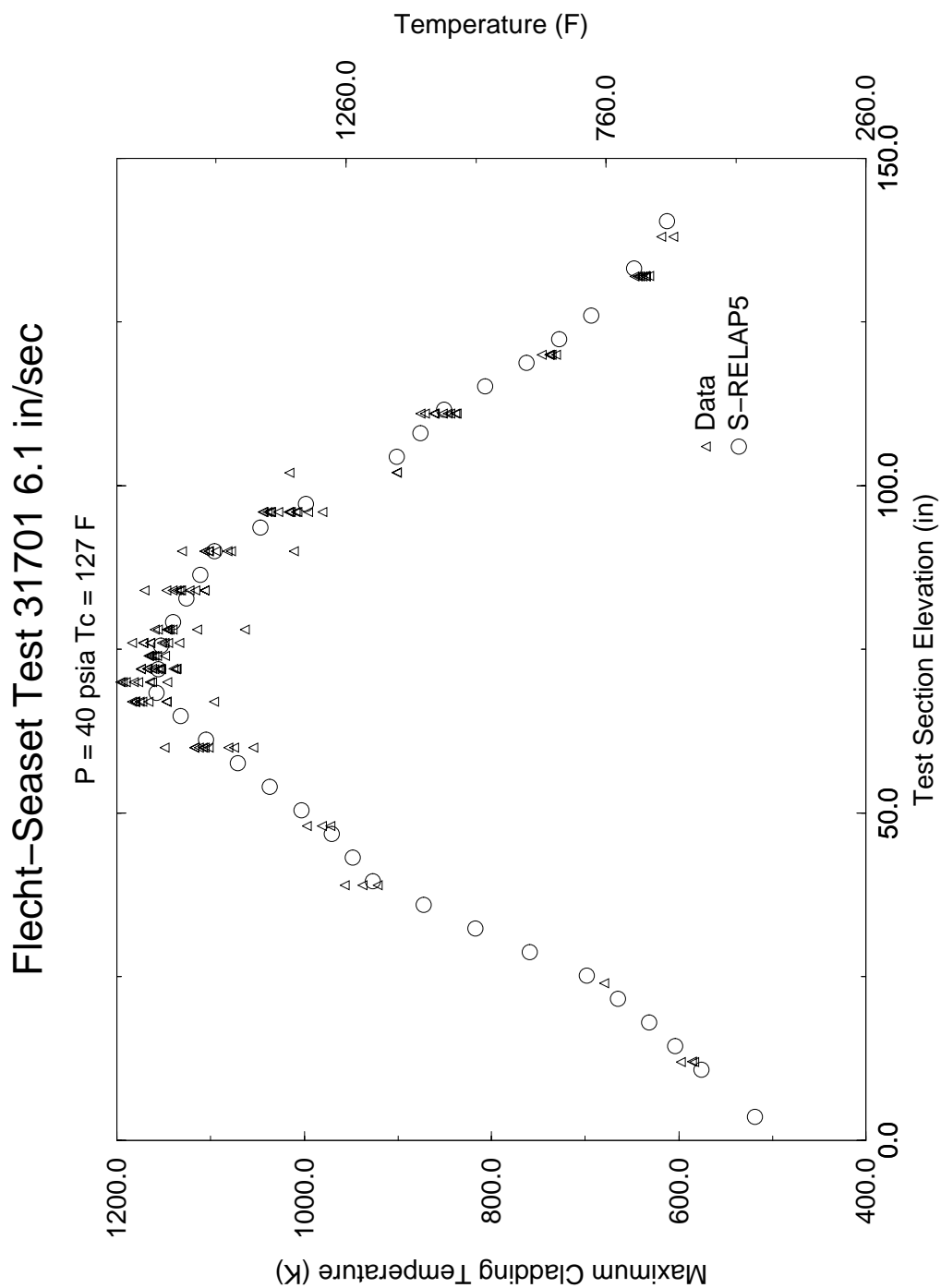


**Figure 4.38 Maximum Clad Temperature at All Measured Elevations,
FLECHT SEASET Test 31701**

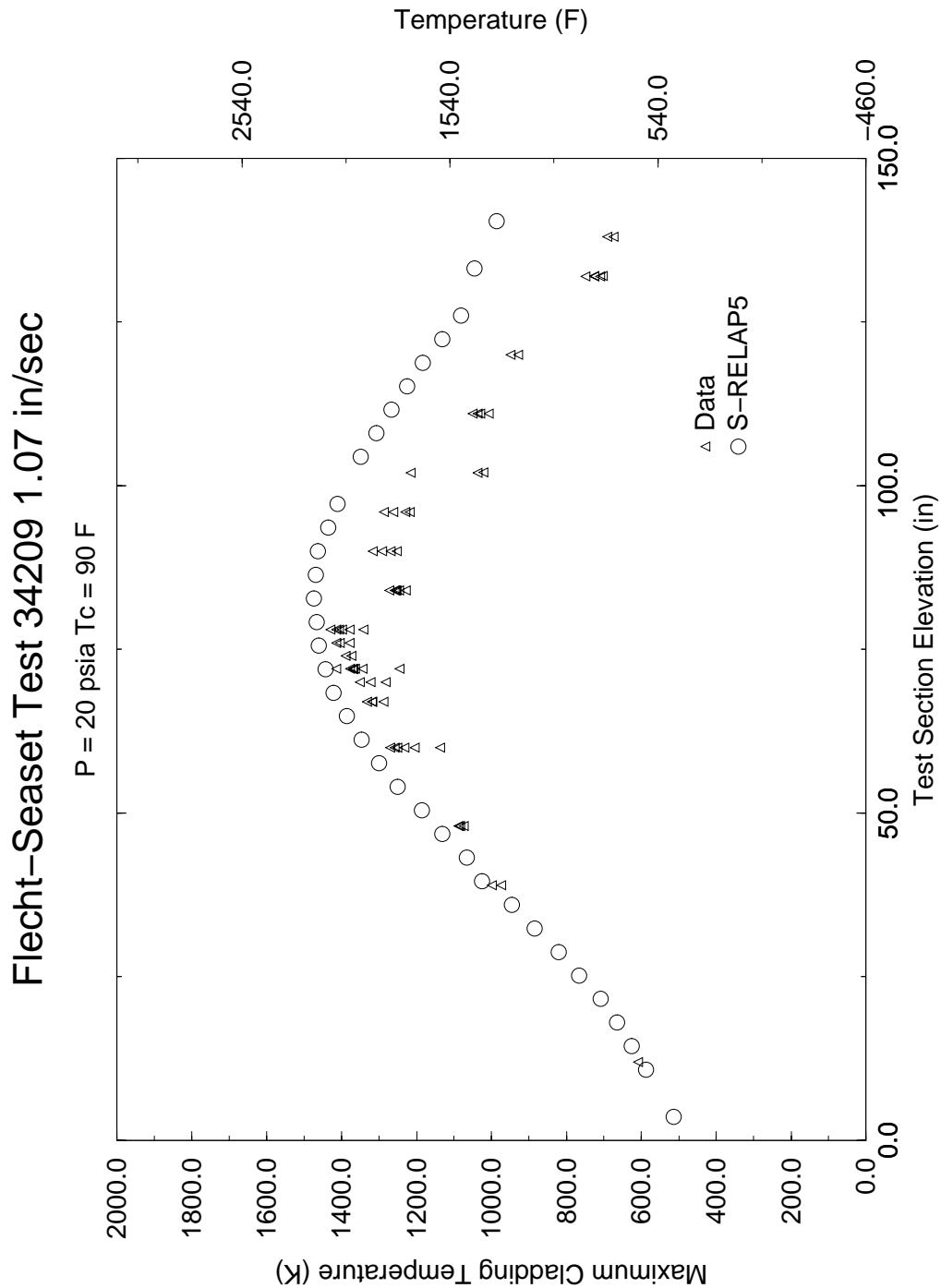


**Figure 4.39 Maximum Clad Temperature at All Measured Elevations,
FLECHT SEASET Test 34209**

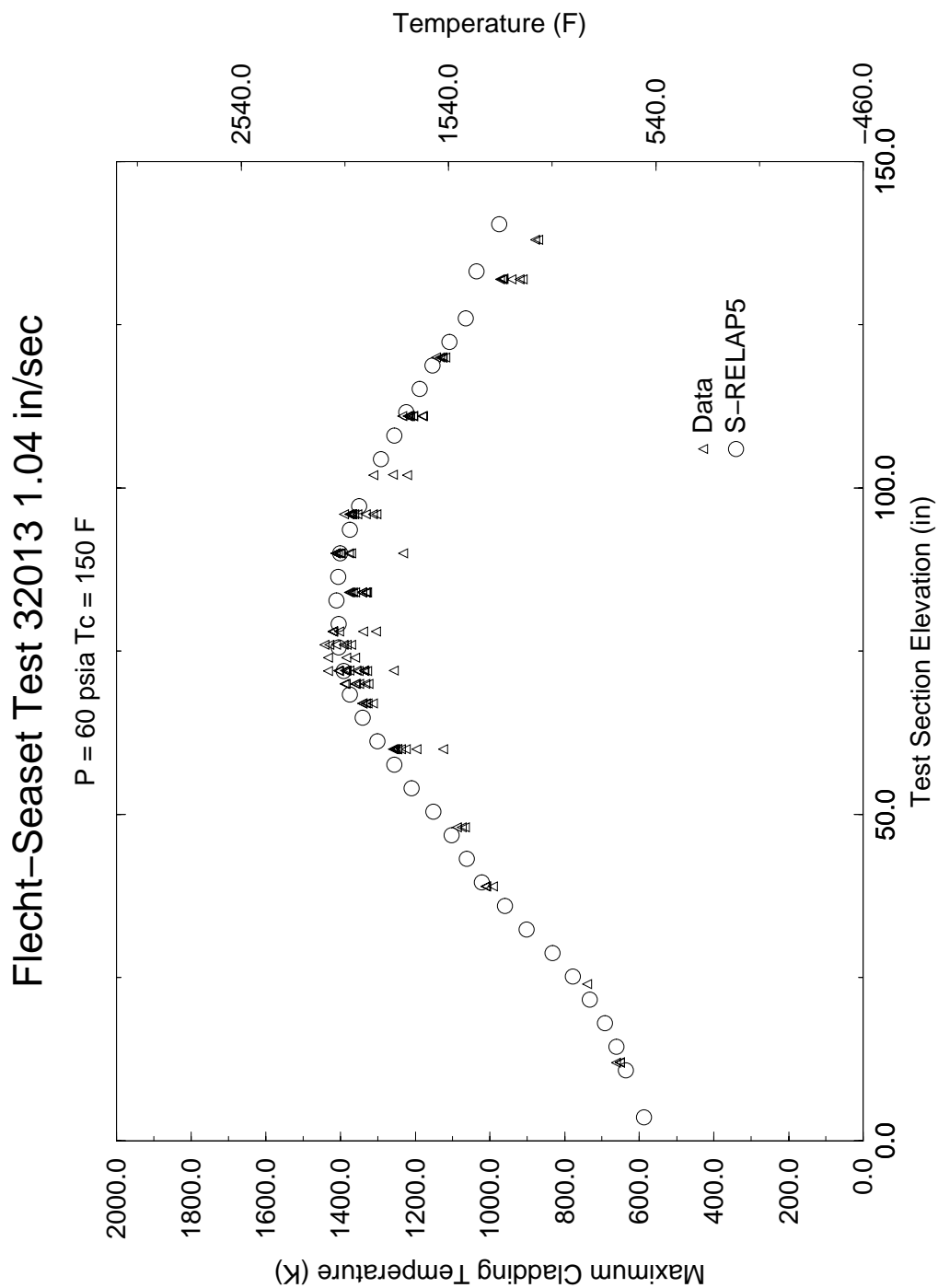


**Figure 4.40 Maximum Clad Temperature at All Measured Elevations,
FLECHT SEASET Test 32013**

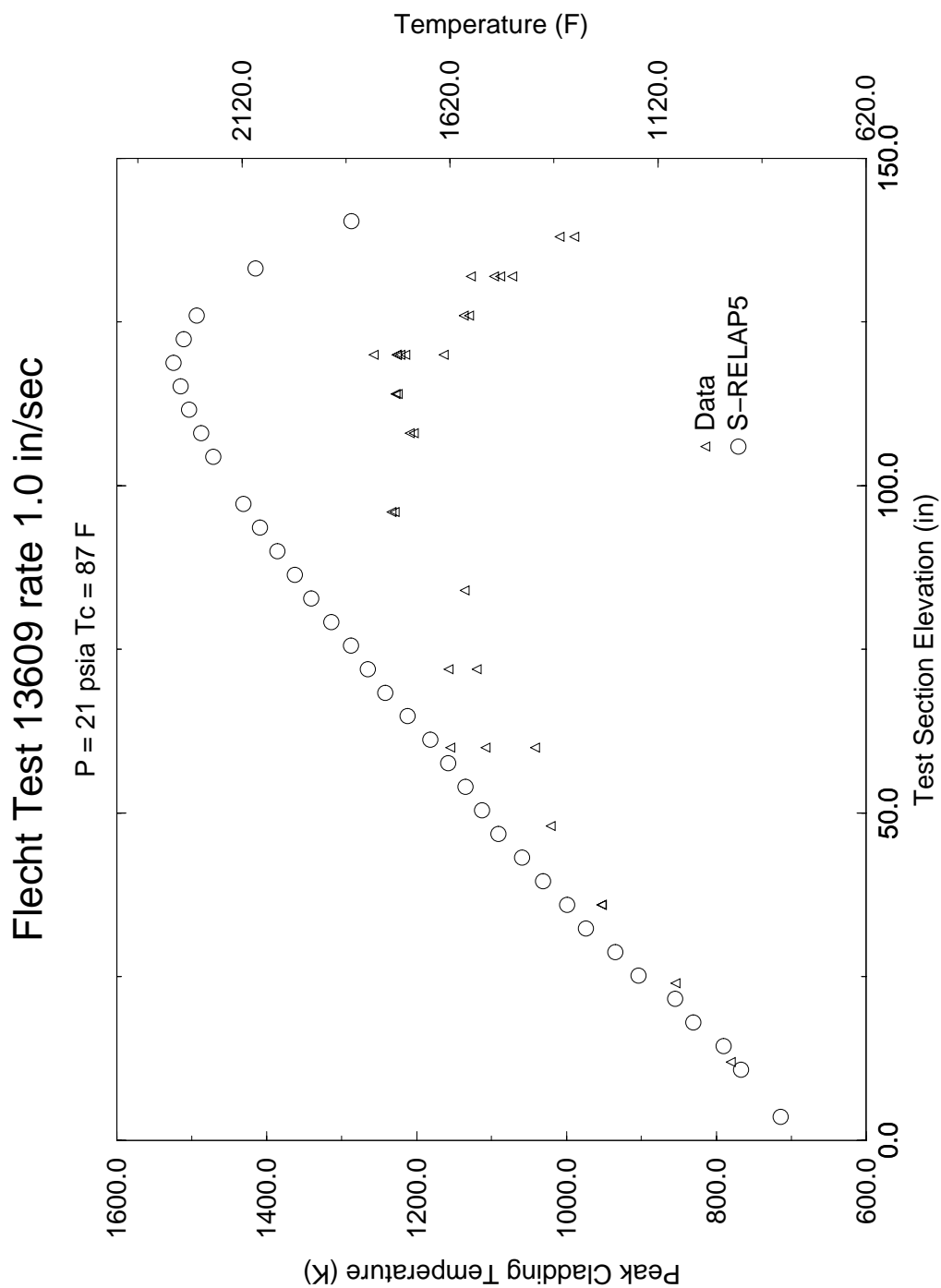


**Figure 4.41 Maximum Clad Temperature at All Measured Elevations,
FLECHT Skewed Test 13609**

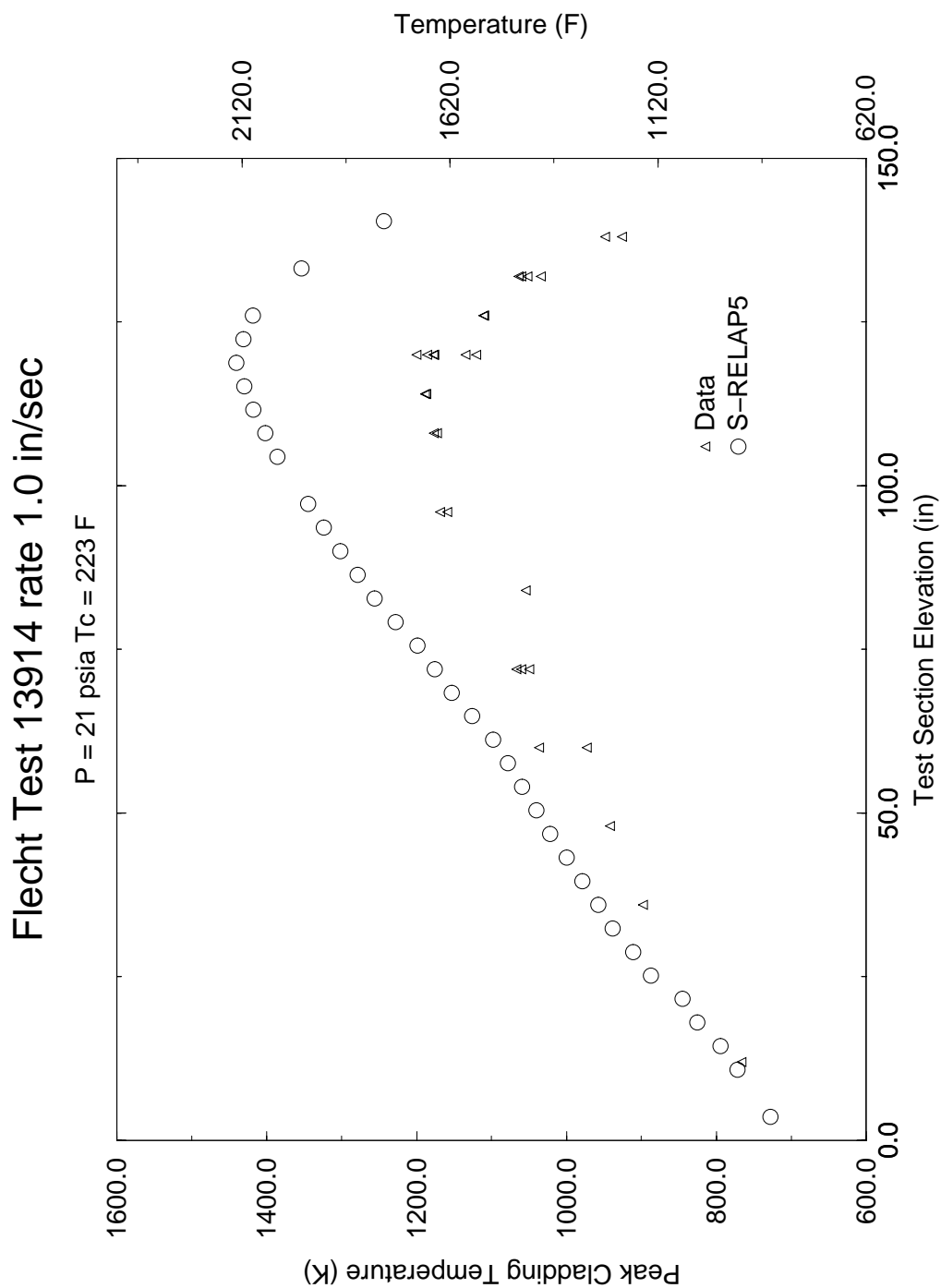


**Figure 4.42 Maximum Clad Temperature at All Measured Elevations,
FLECHT Skewed Test 13914**

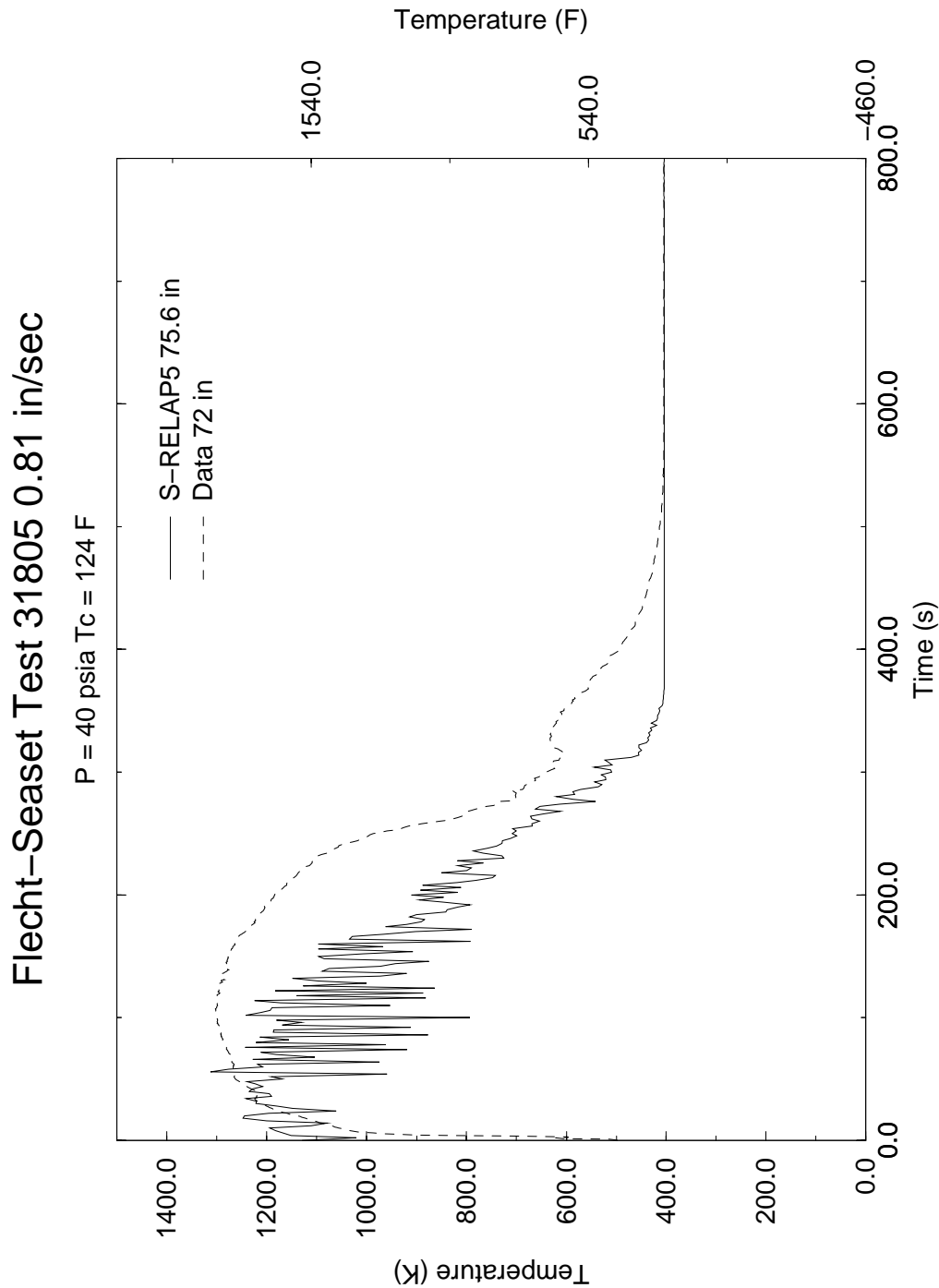


Figure 4.43 Steam Temperatures Calculated at 75.6 in and Measured at 72 in, FLECHT SEASET Test 31805

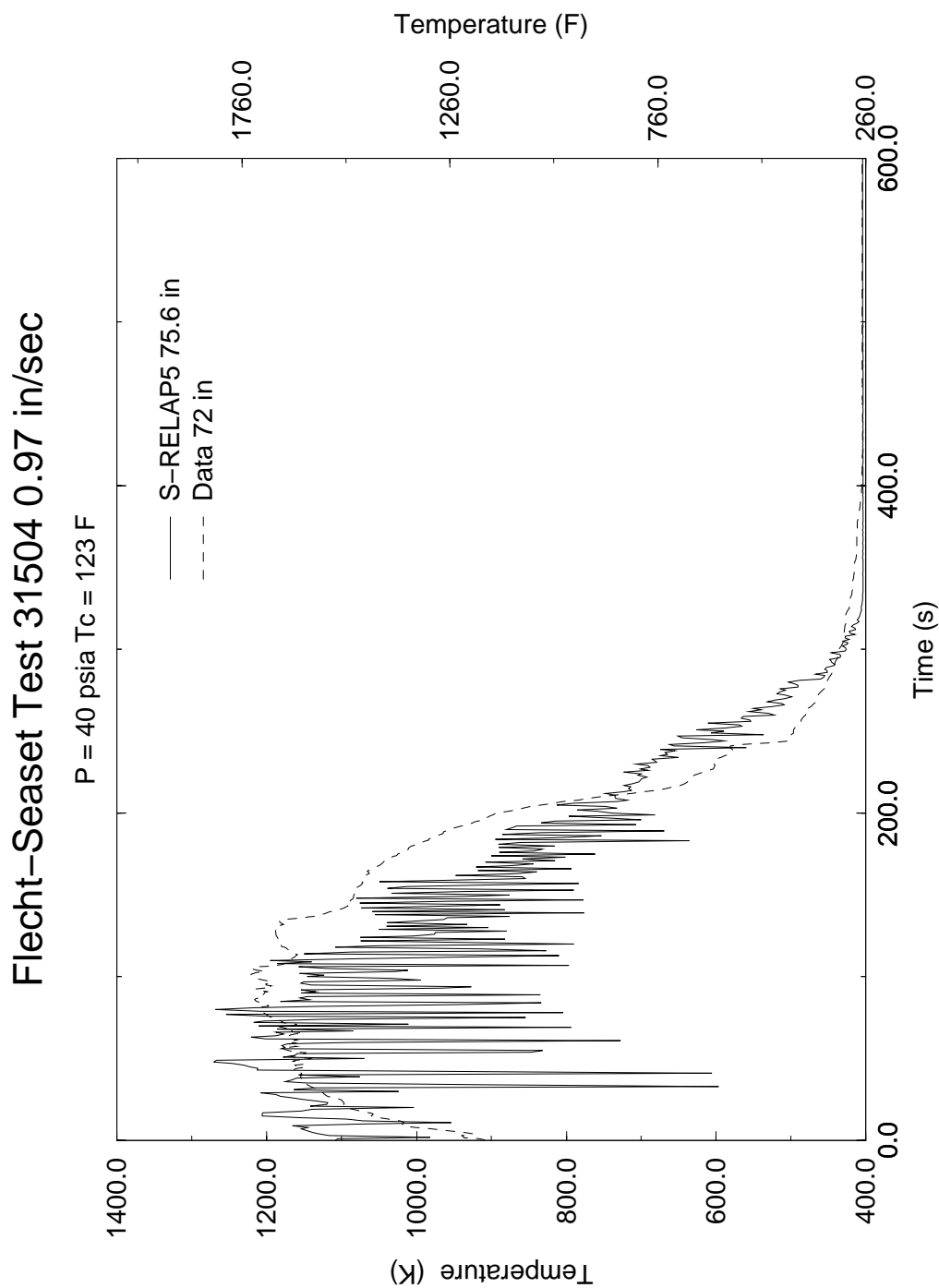


Figure 4.44 Steam Temperatures Calculated at 75.6 in and Measured at 72 in, FLECHT SEASET Test 31504

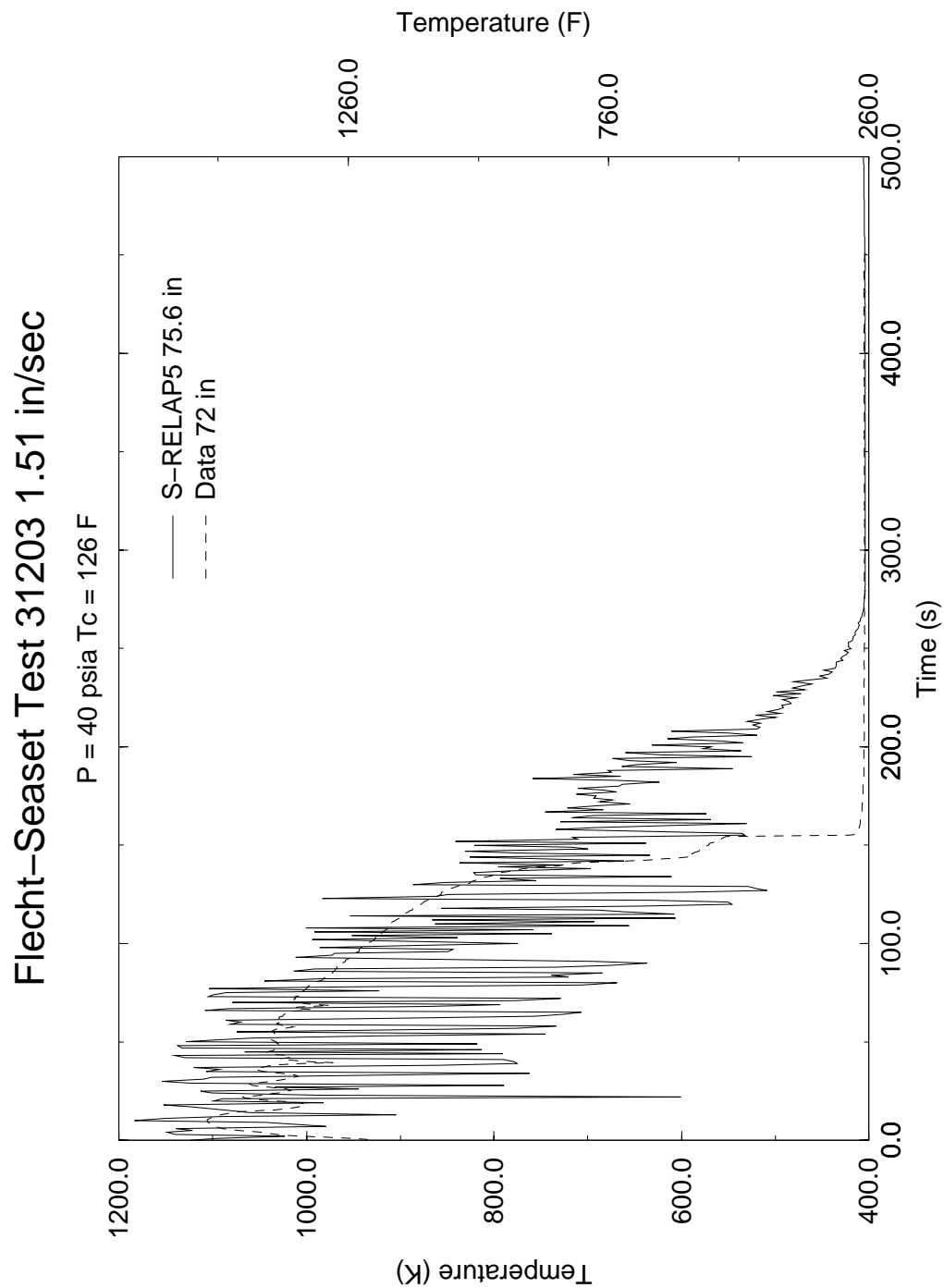


Figure 4.45 Steam Temperatures Calculated at 75.6 in and Measured at 72 in, FLECHT SEASET Test 31203

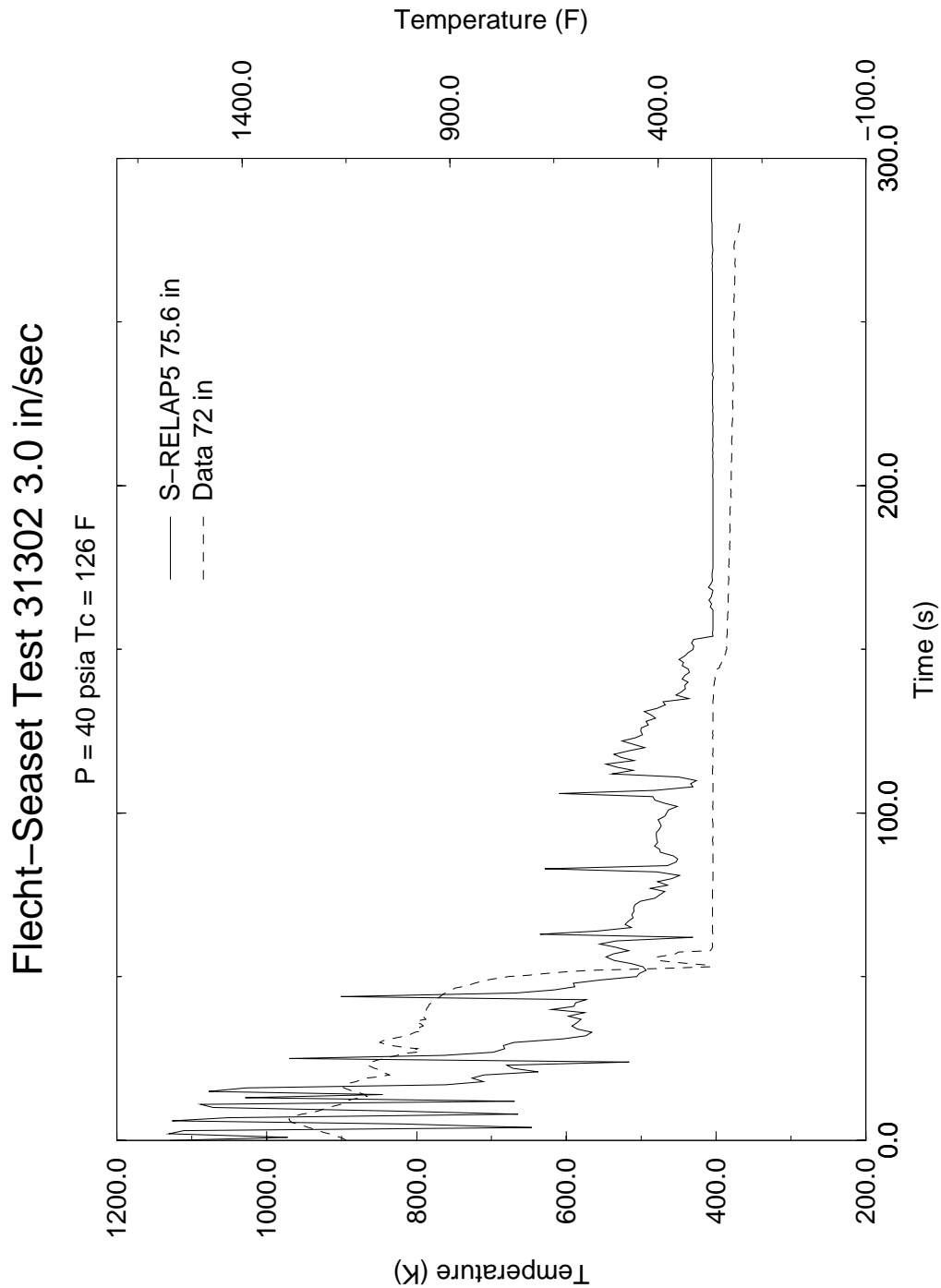


Figure 4.46 Steam Temperatures Calculated at 75.6 in and Measured at 72 in, FLECHT SEASET Test 31302

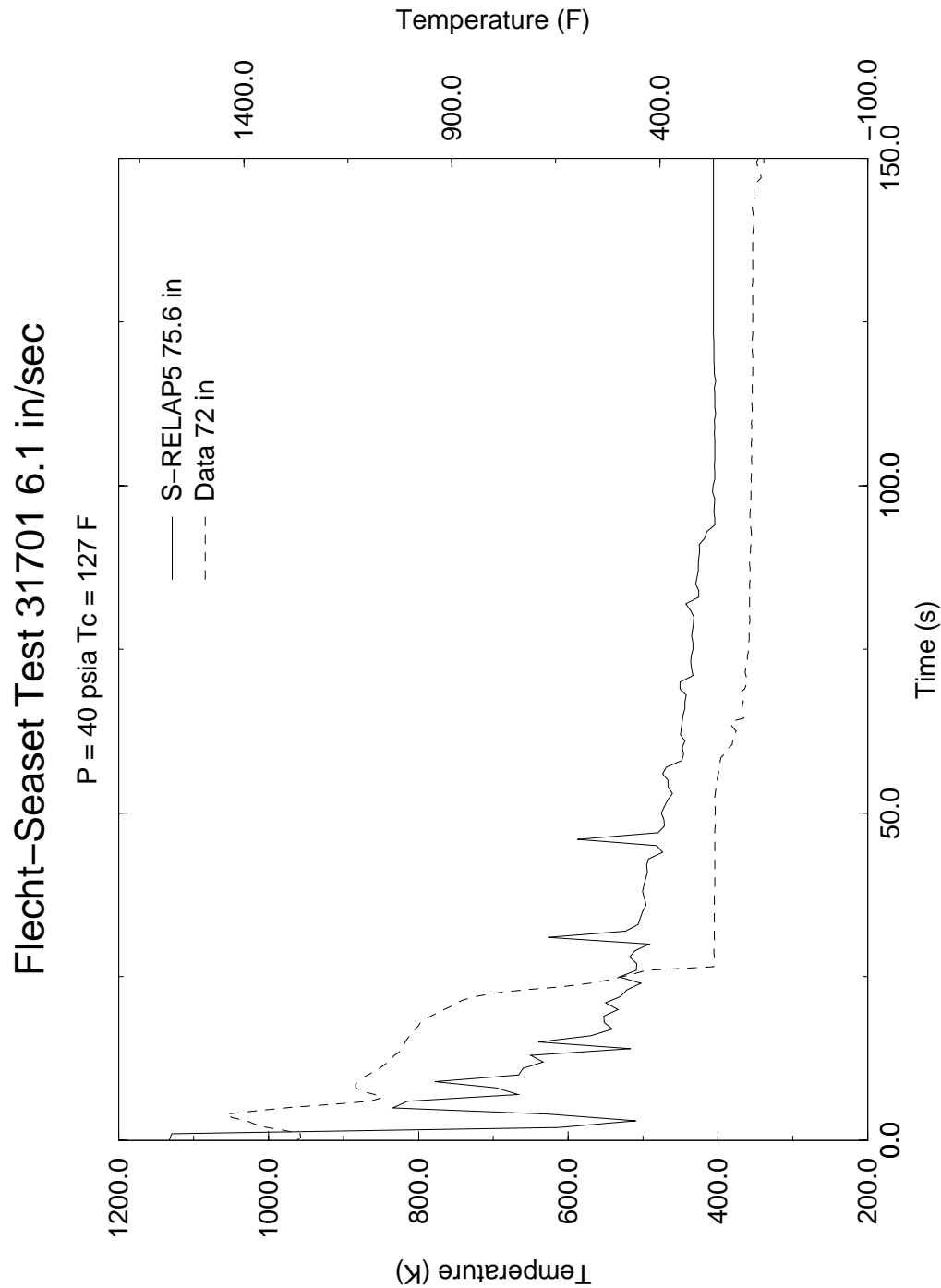


Figure 4.47 Steam Temperatures Calculated at 75.6 in and Measured at 72 in, FLECHT SEASET Test 31701

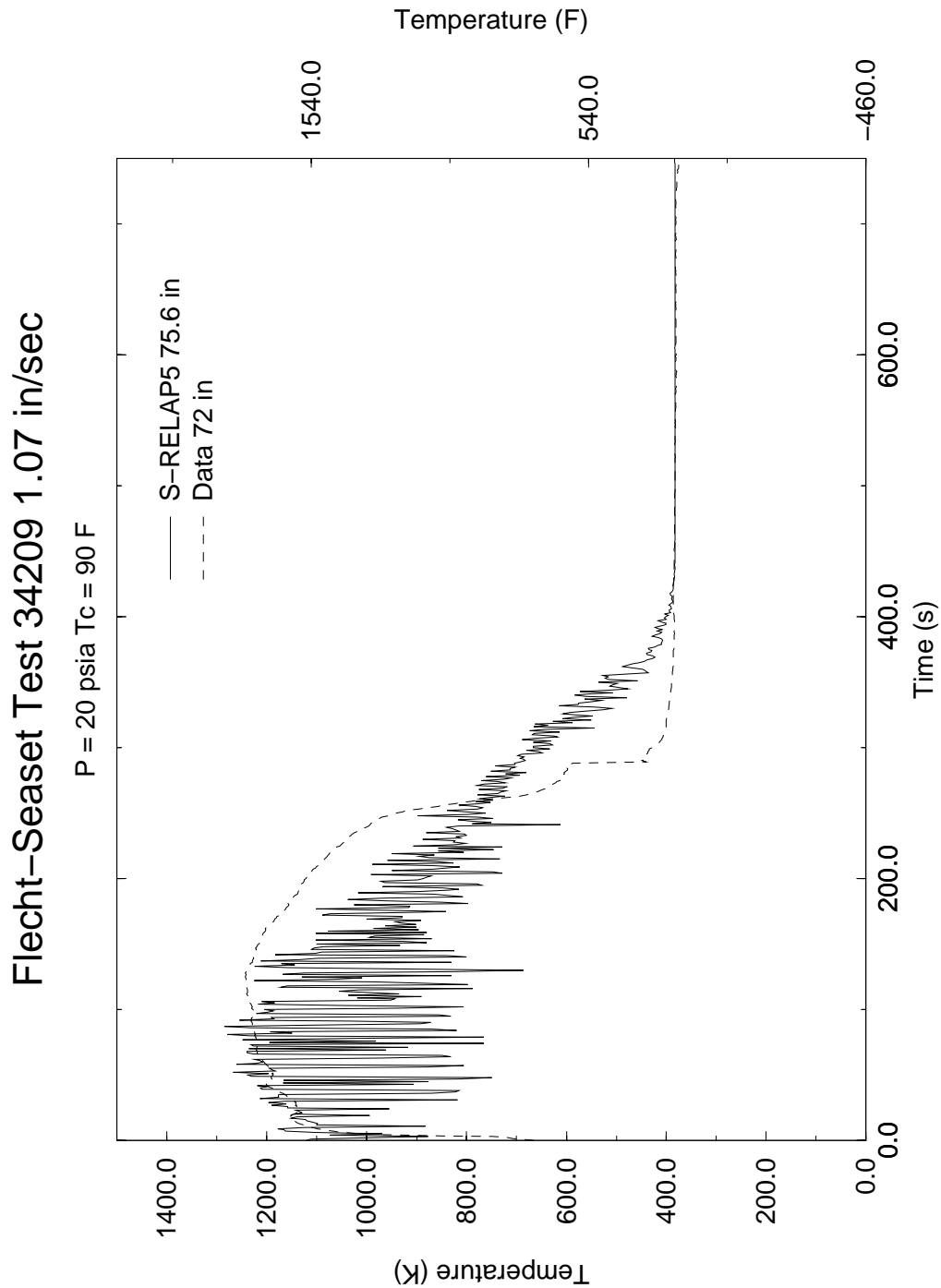


Figure 4.48 Steam Temperatures Calculated at 75.6 in and Measured at 72 in, FLECHT SEASET Test 34209

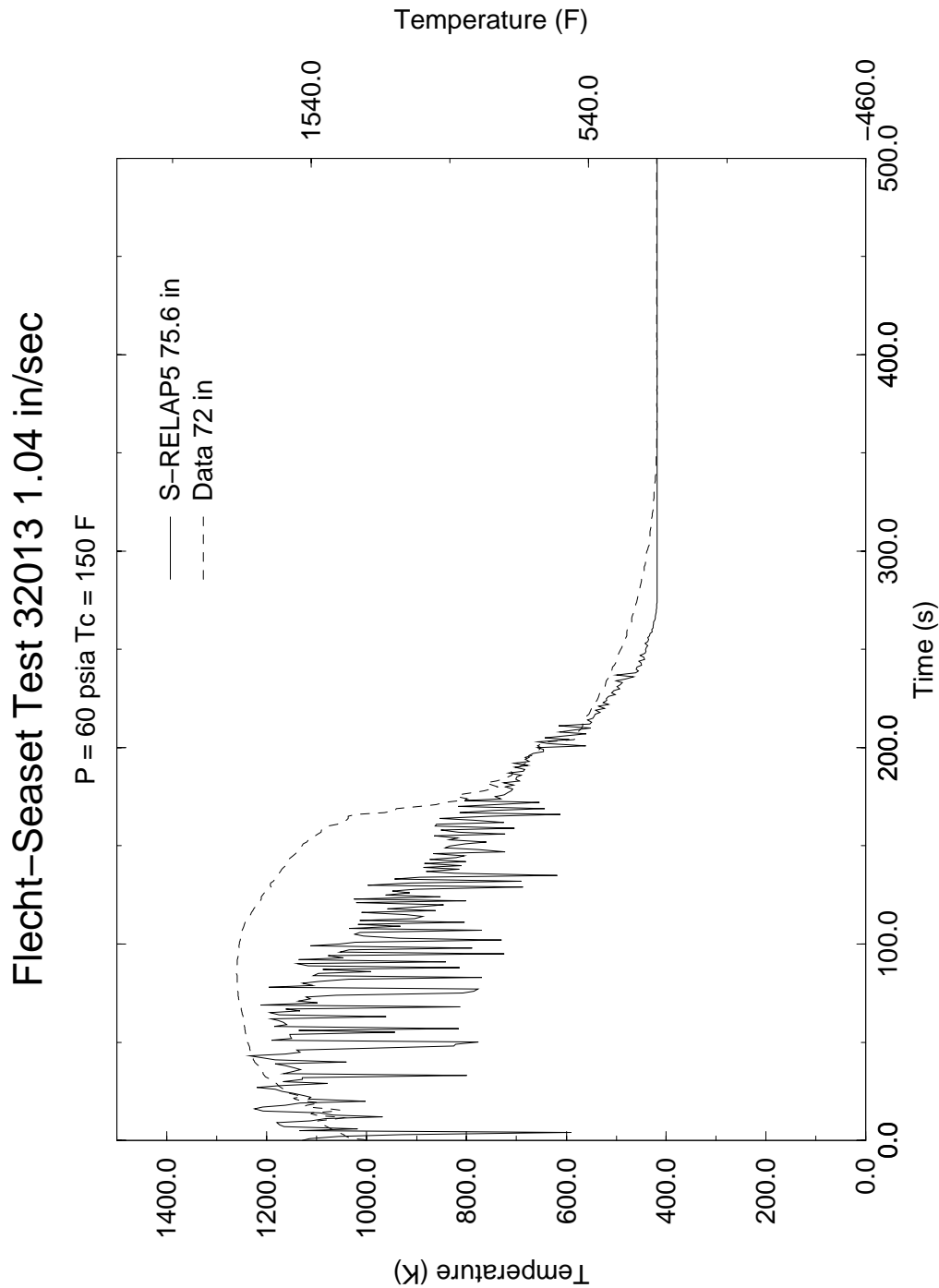


Figure 4.49 Steam Temperatures Calculated at 75.6 in and Measured at 72 in, FLECHT SEASET Test 32013

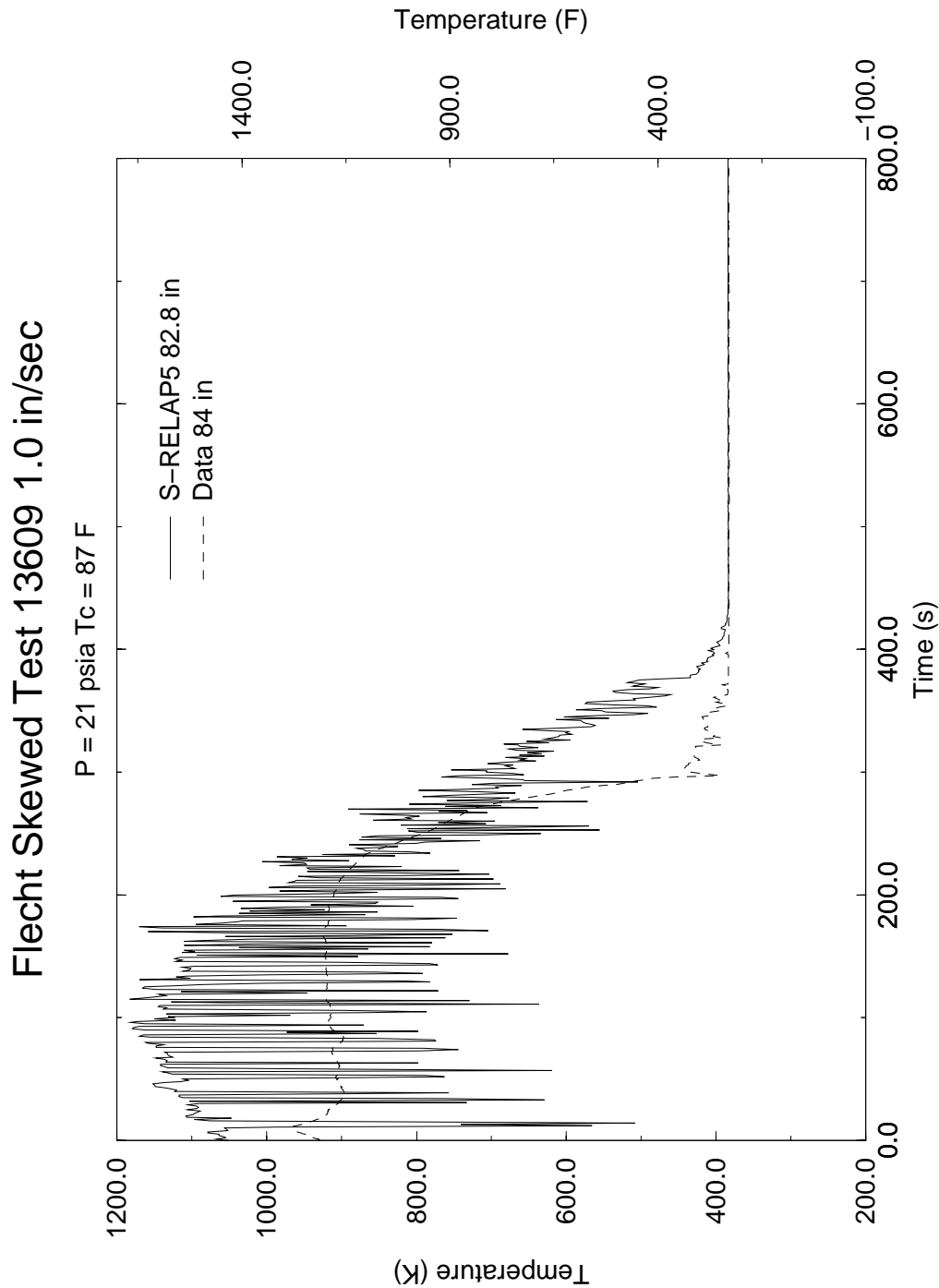


Figure 4.50 Steam Temperatures Calculated at 82.8 in and Measured at 84 in, FLECHT Skewed Test 13609

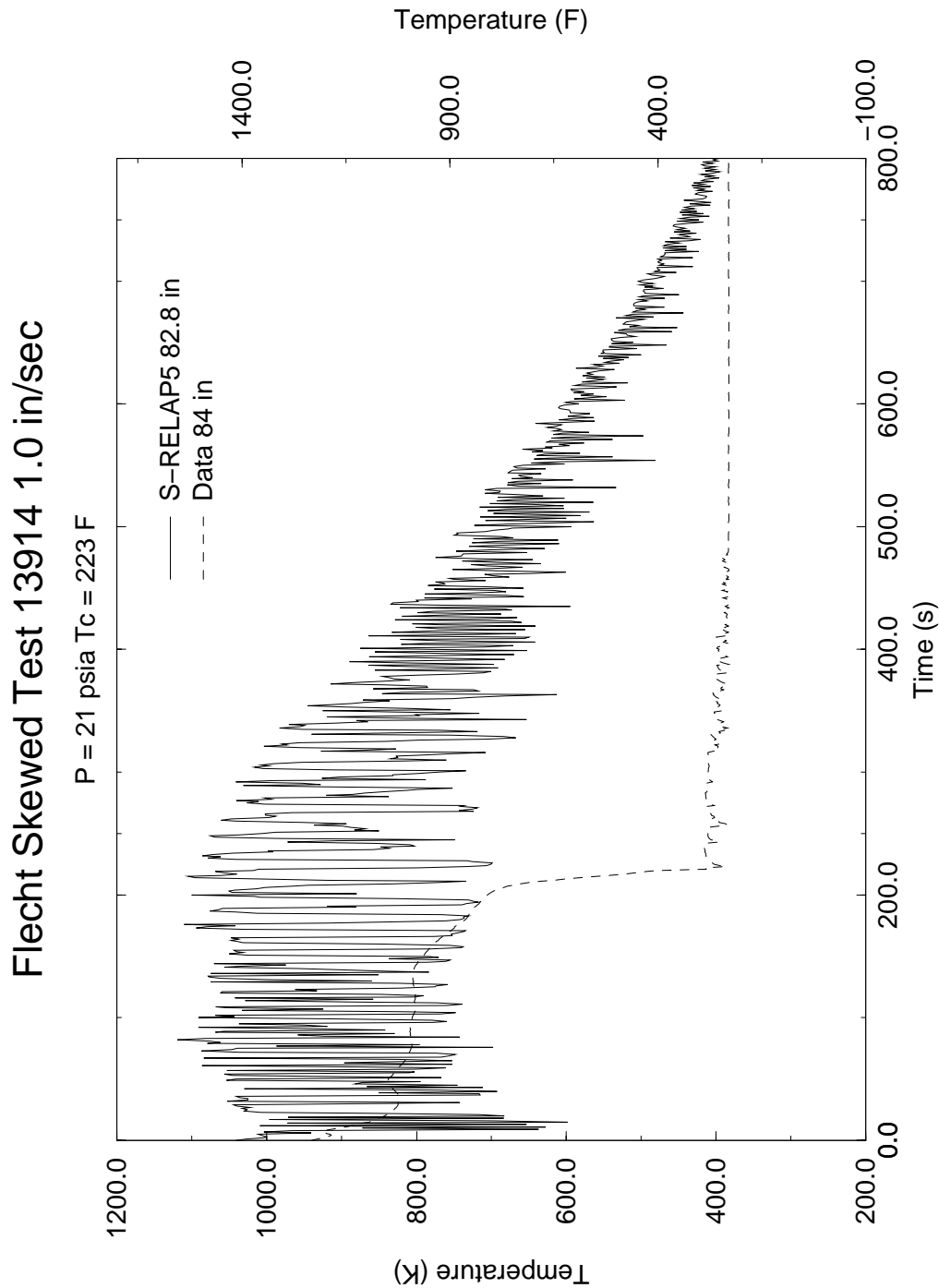


Figure 4.51 Steam Temperatures Calculated at 82.8 in and Measured at 84 in, FLECHT Skewed Test 13914

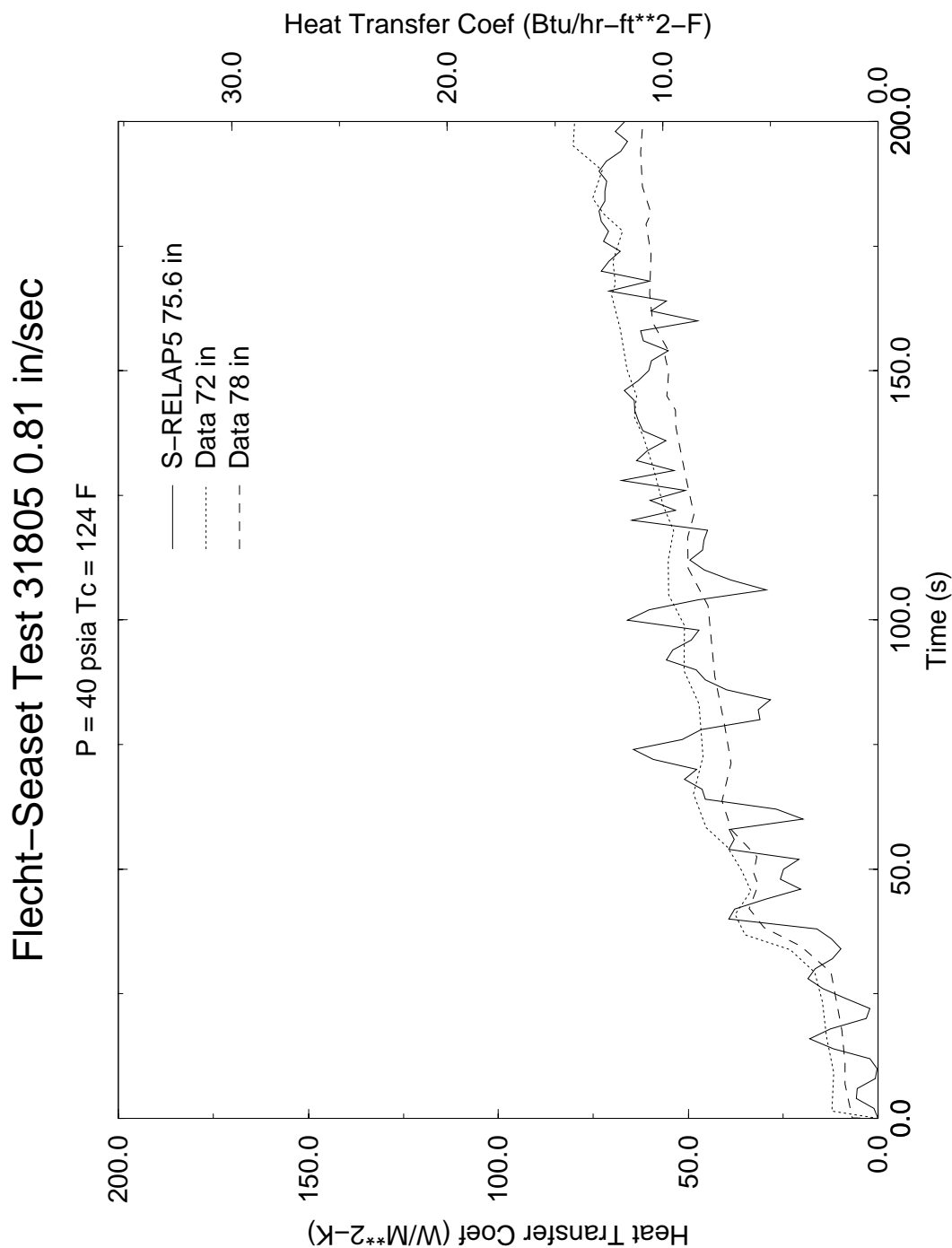


Figure 4.52 Comparison of Calculated and Measured Heat Transfer Coefficient, FLECHT SEASET Test 31805

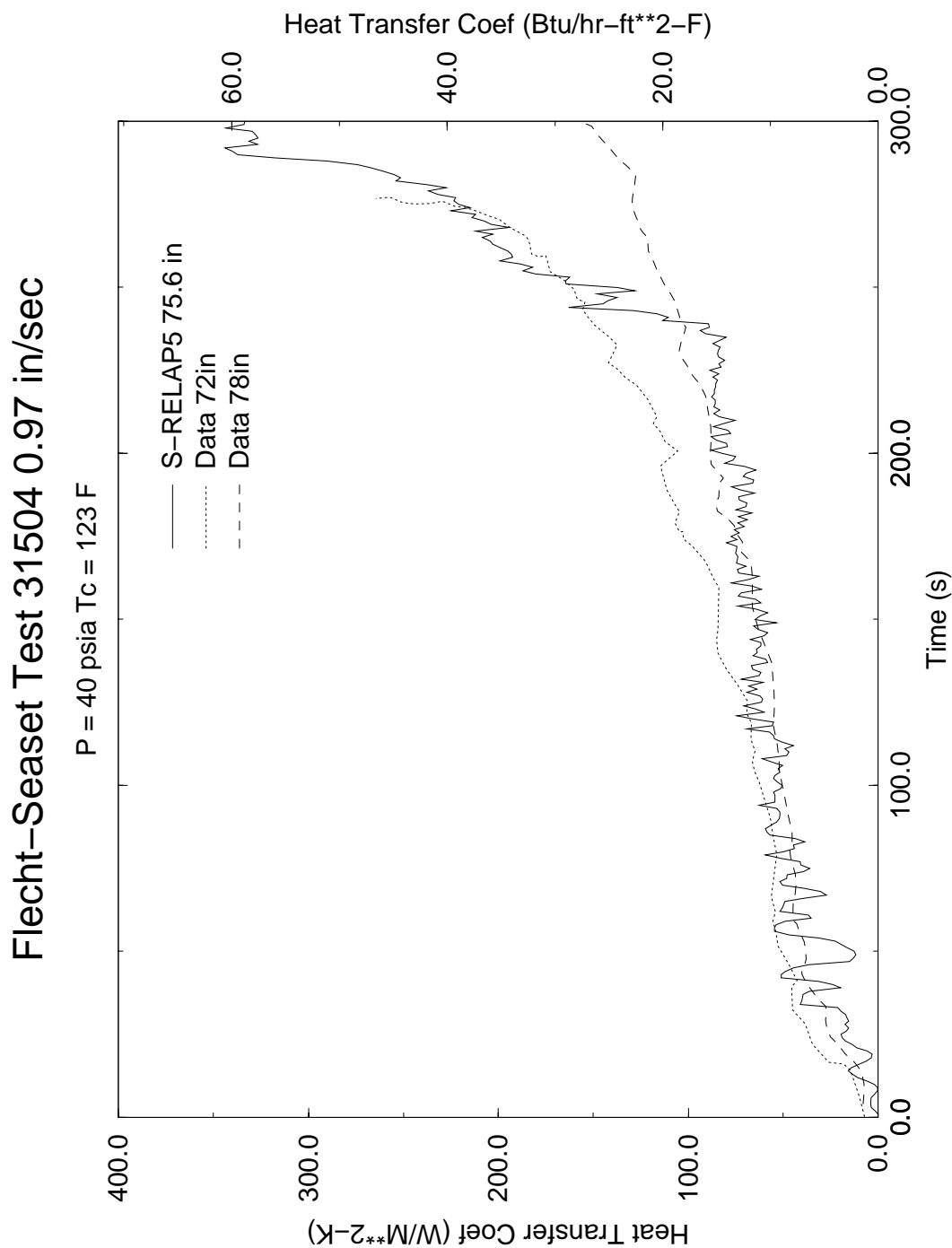


Figure 4.53 Comparison of Calculated and Measured Heat Transfer Coefficient, FLECHT SEASET Test 31504

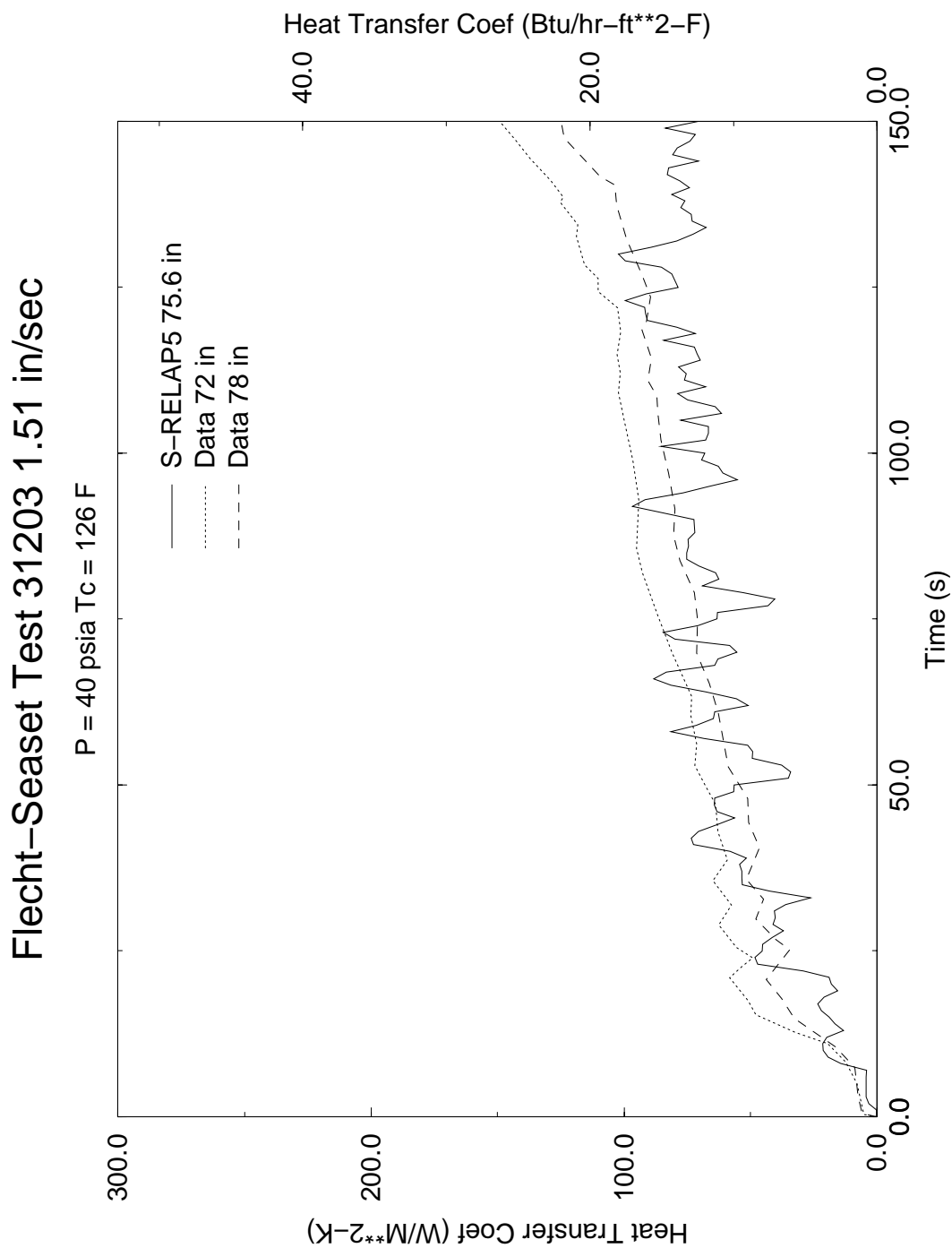


Figure 4.54 Comparison of Calculated and Measured Heat Transfer Coefficient, FLECHT SEASET Test 31203

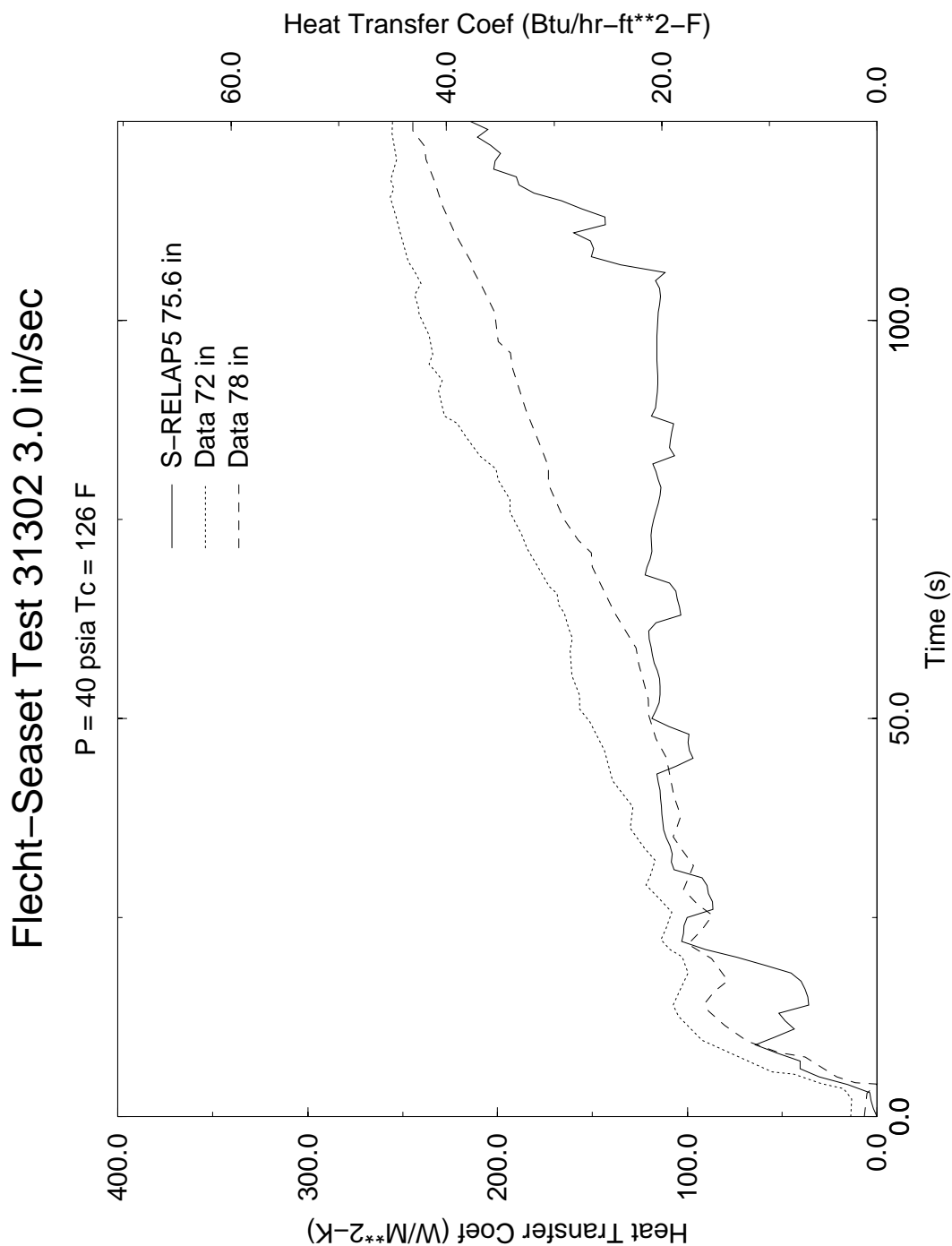


Figure 4.55 Comparison of Calculated and Measured Heat Transfer Coefficient, FLECHT SEASET Test 31302

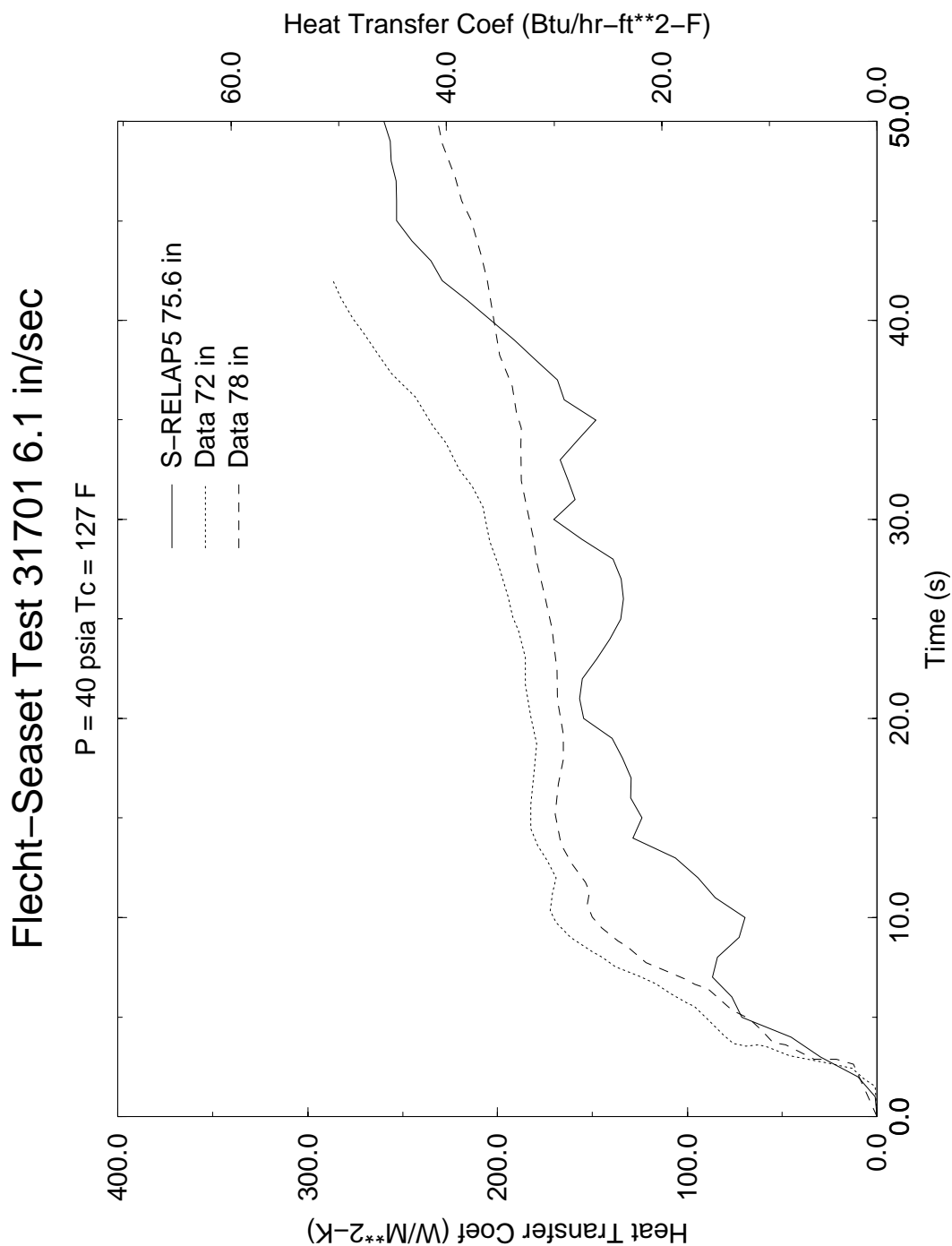


Figure 4.56 Comparison of Calculated and Measured Heat Transfer Coefficient, FLECHT SEASET Test 31701

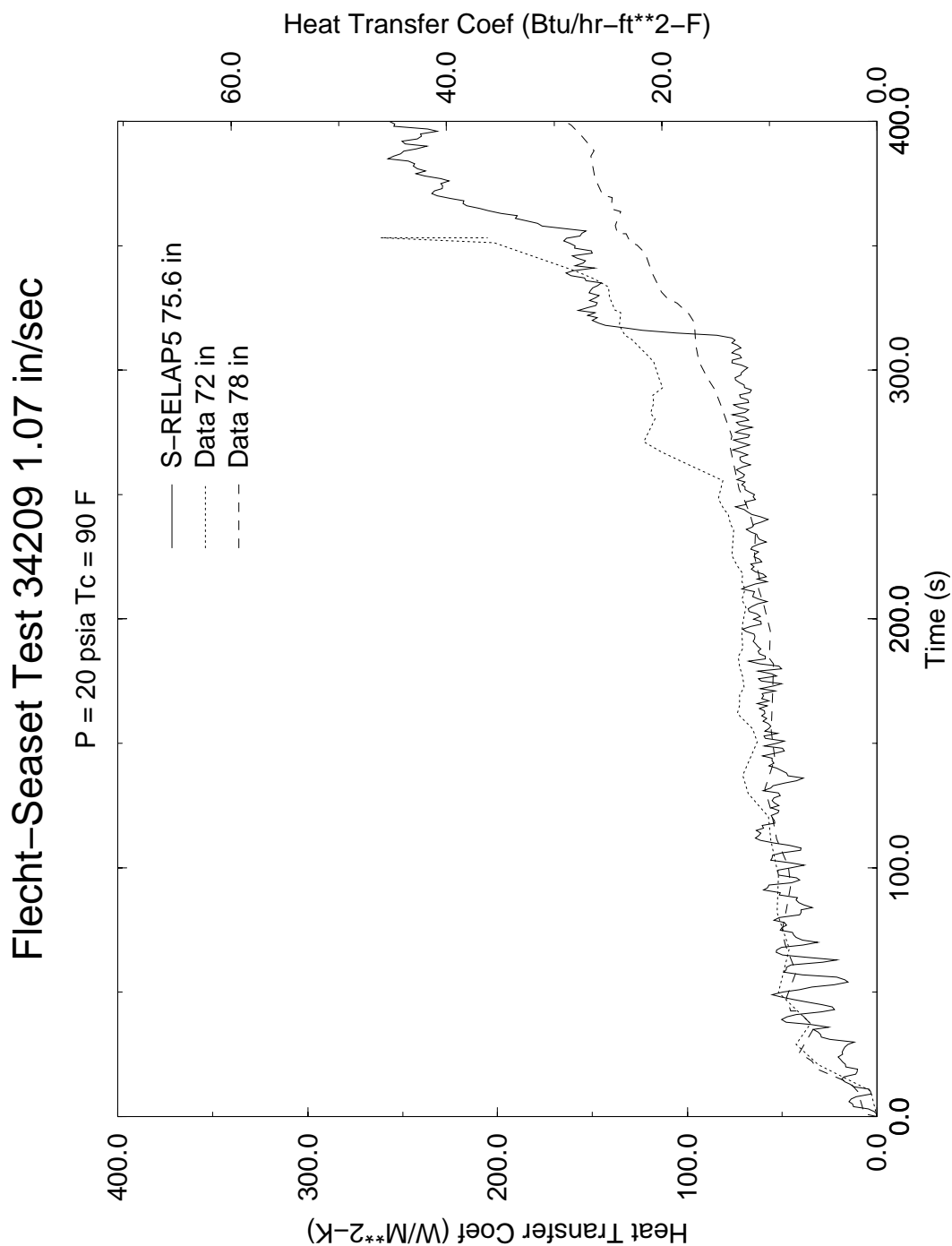


Figure 4.57 Comparison of Calculated and Measured Heat Transfer Coefficient, FLECHT SEASET Test 34209

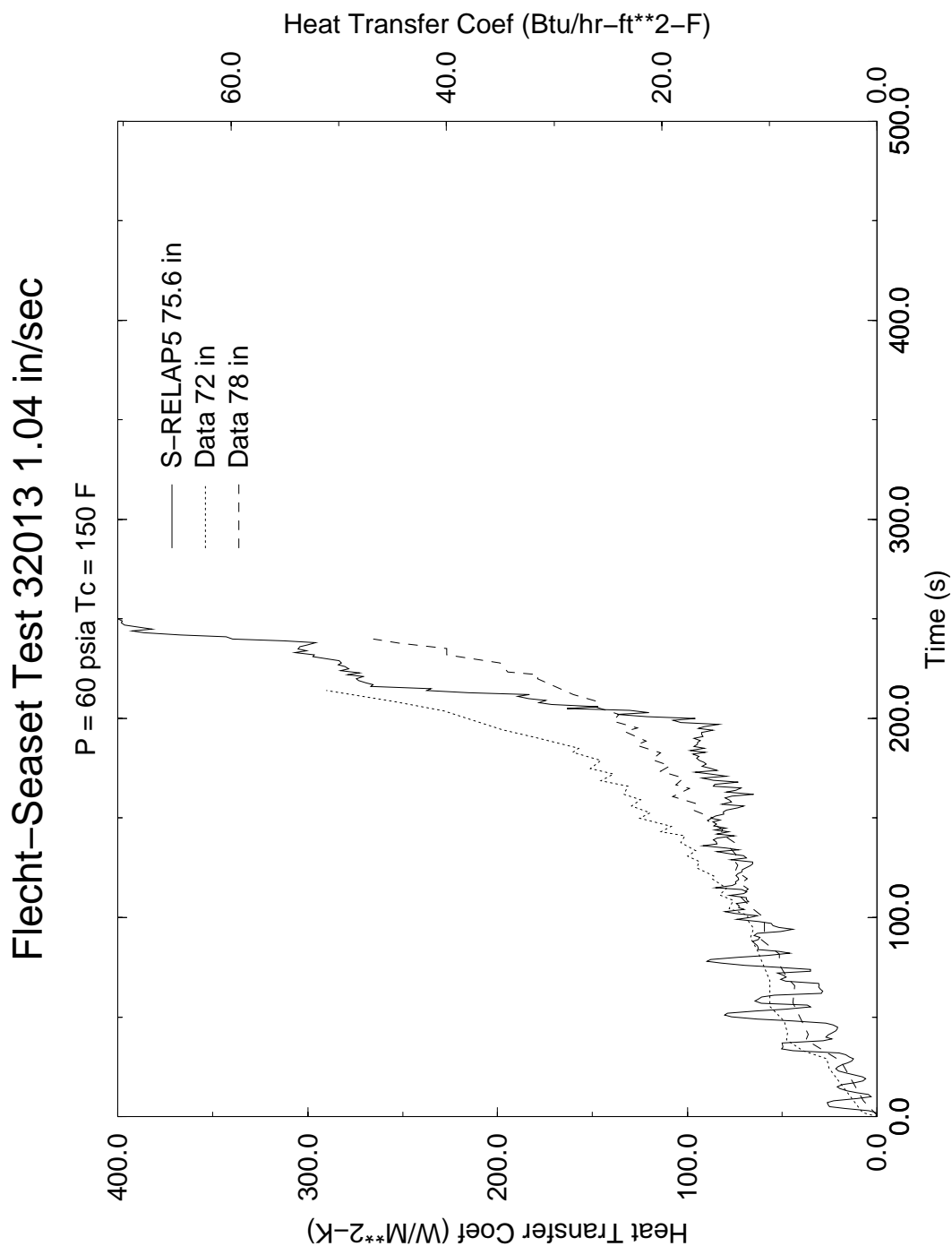


Figure 4.58 Comparison of Calculated and Measured Heat Transfer Coefficient, FLECHT SEASET Test 32013

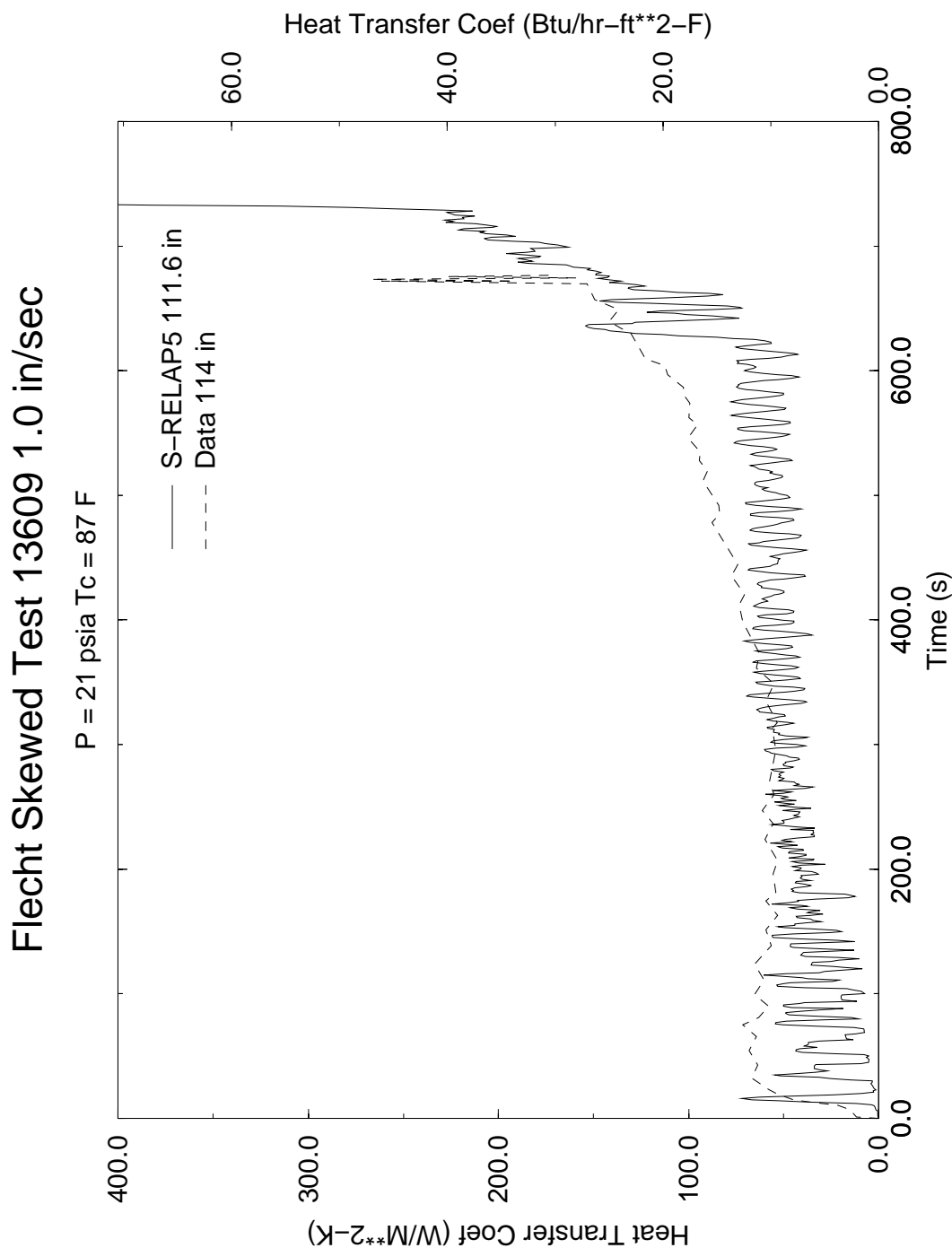


Figure 4.59 Comparison of Calculated and Measured Heat Transfer Coefficient, FLECHT Skewed Test 13609

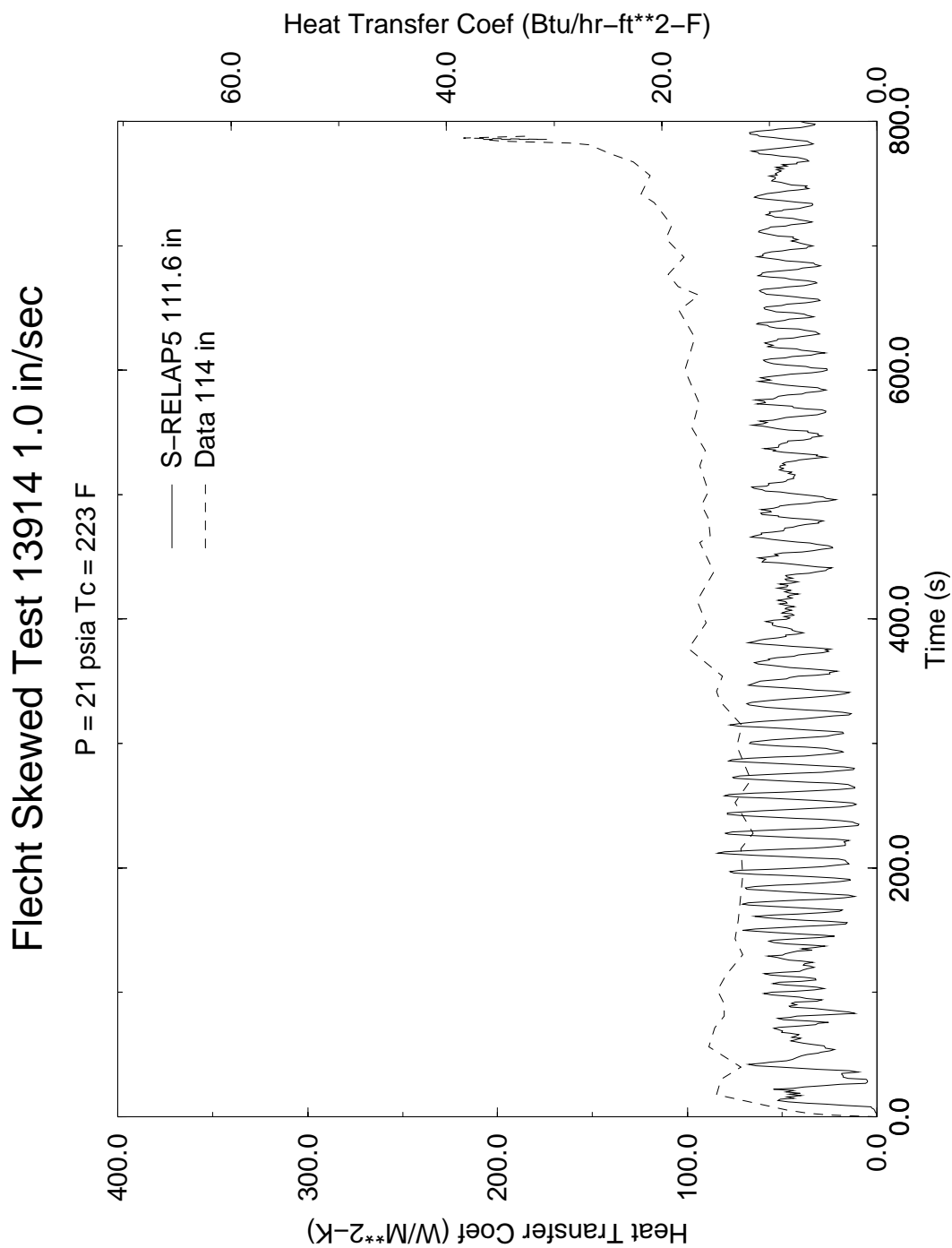
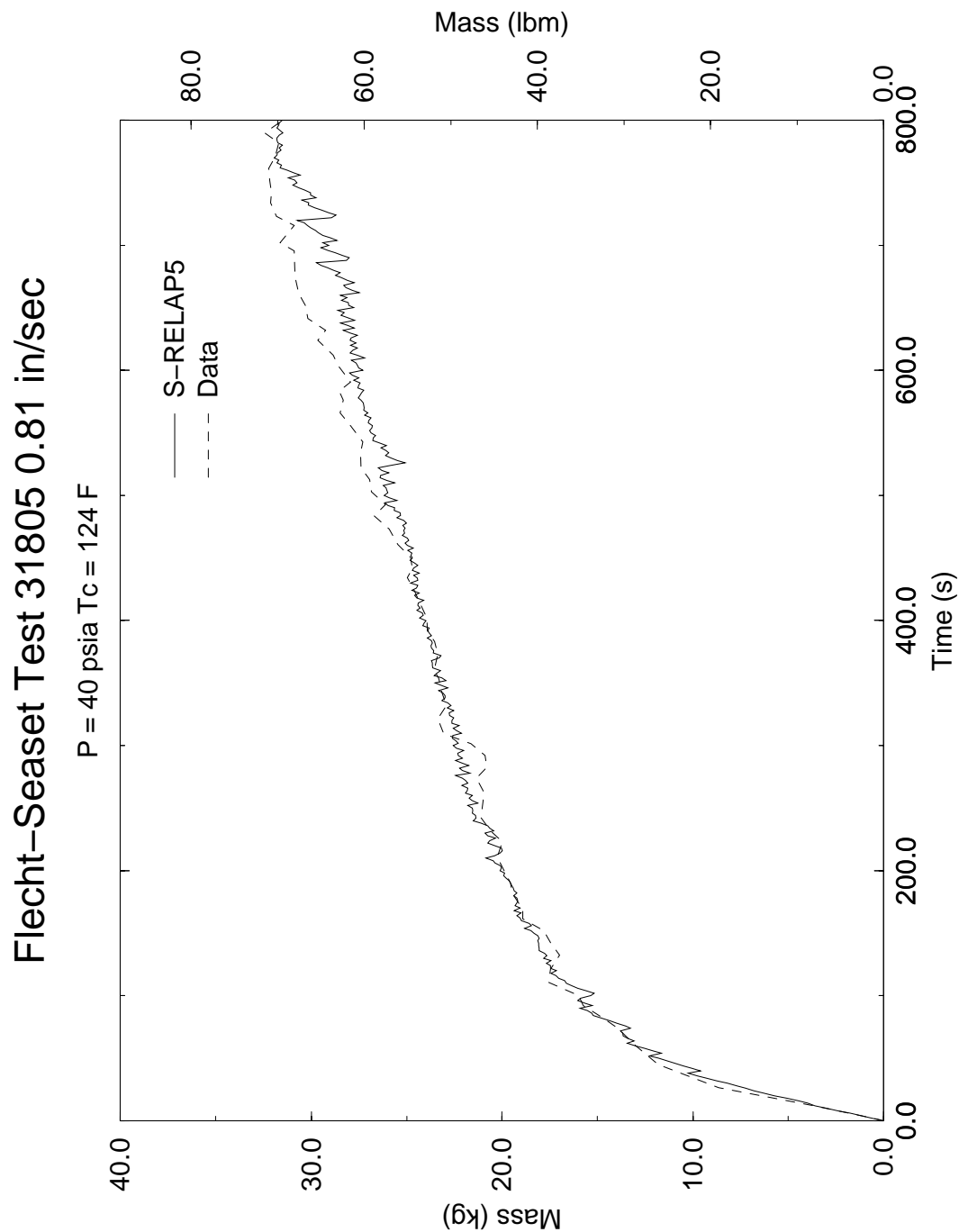


Figure 4.60 Comparison of Calculated and Measured Heat Transfer Coefficient, FLECHT Skewed Test 13914



**Figure 4.61 Accumulated Water Mass in the Test Section, FLECHT
SEASET Test 31805**

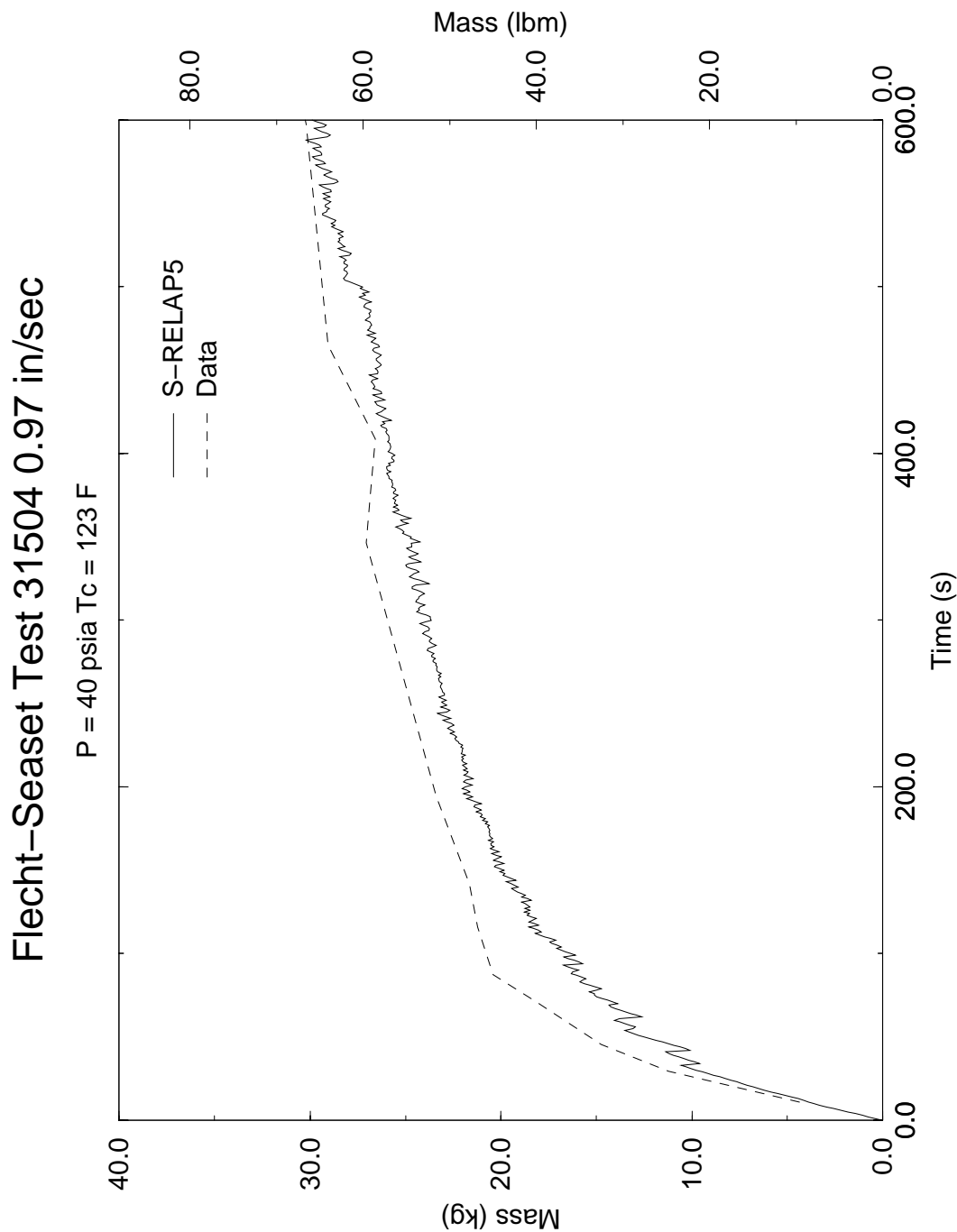


Figure 4.62 Accumulated Water Mass in the Test Section, FLECHT SEASET Test 31504

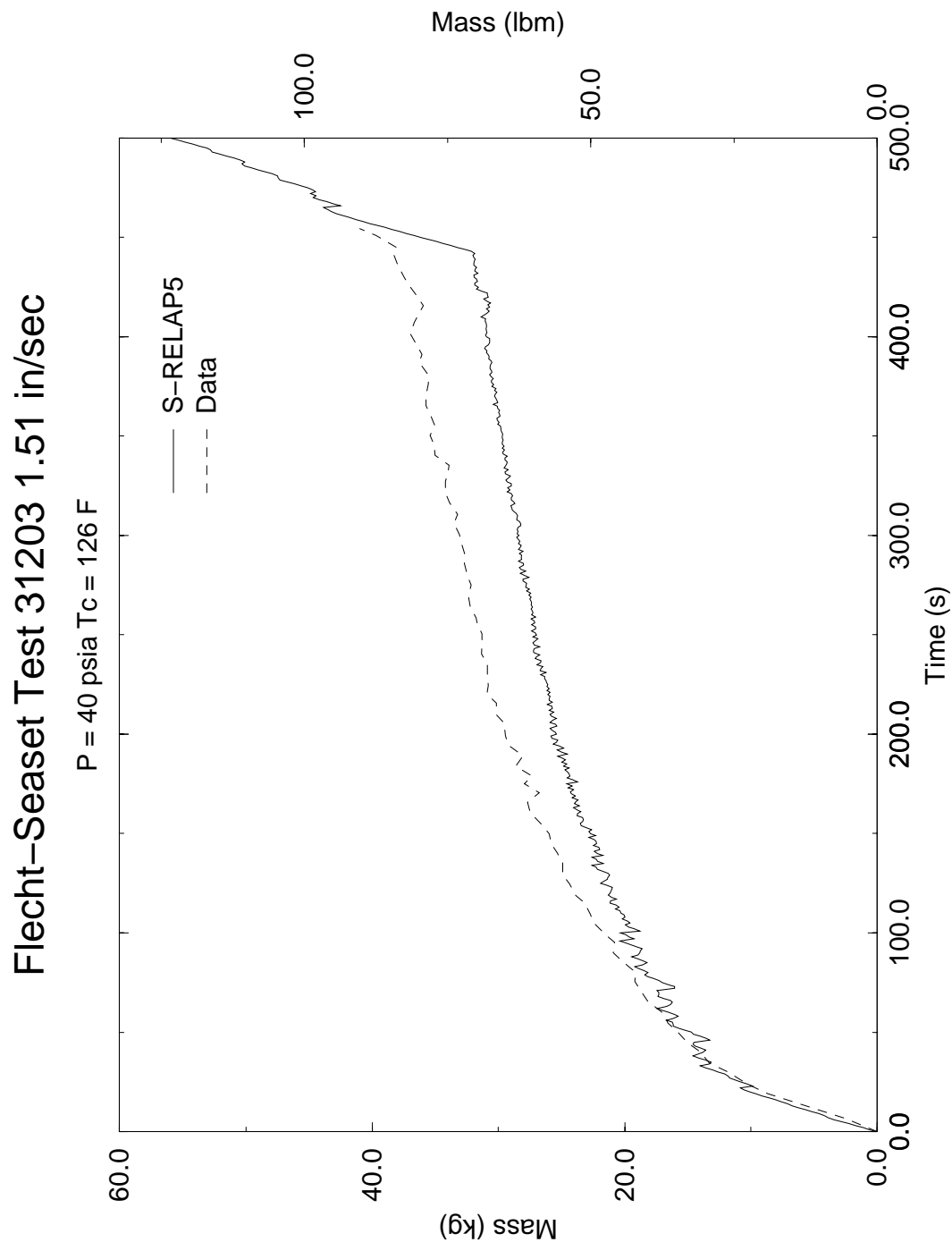


Figure 4.63 Accumulated Water Mass in the Test Section, FLECHT SEASET Test 31203

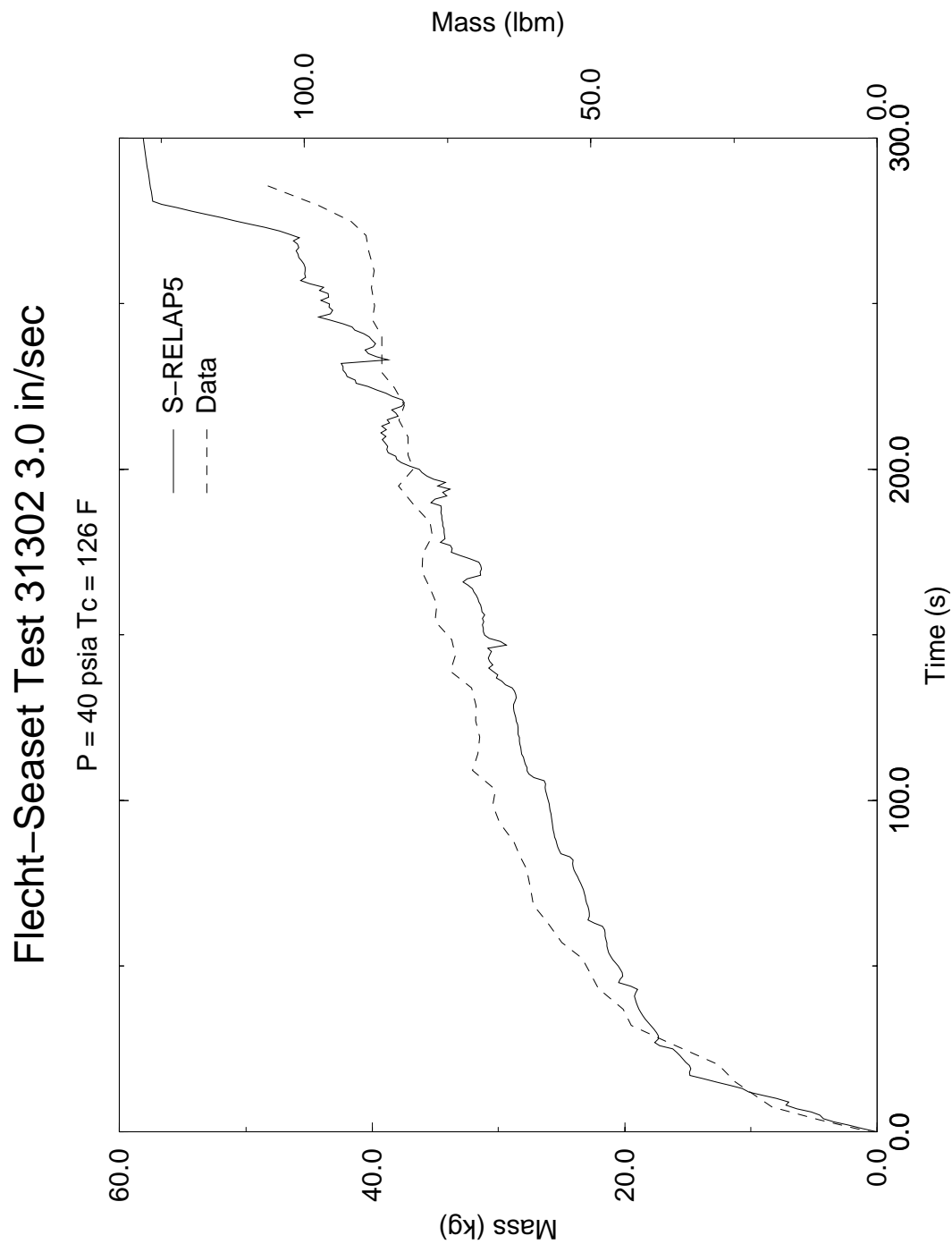
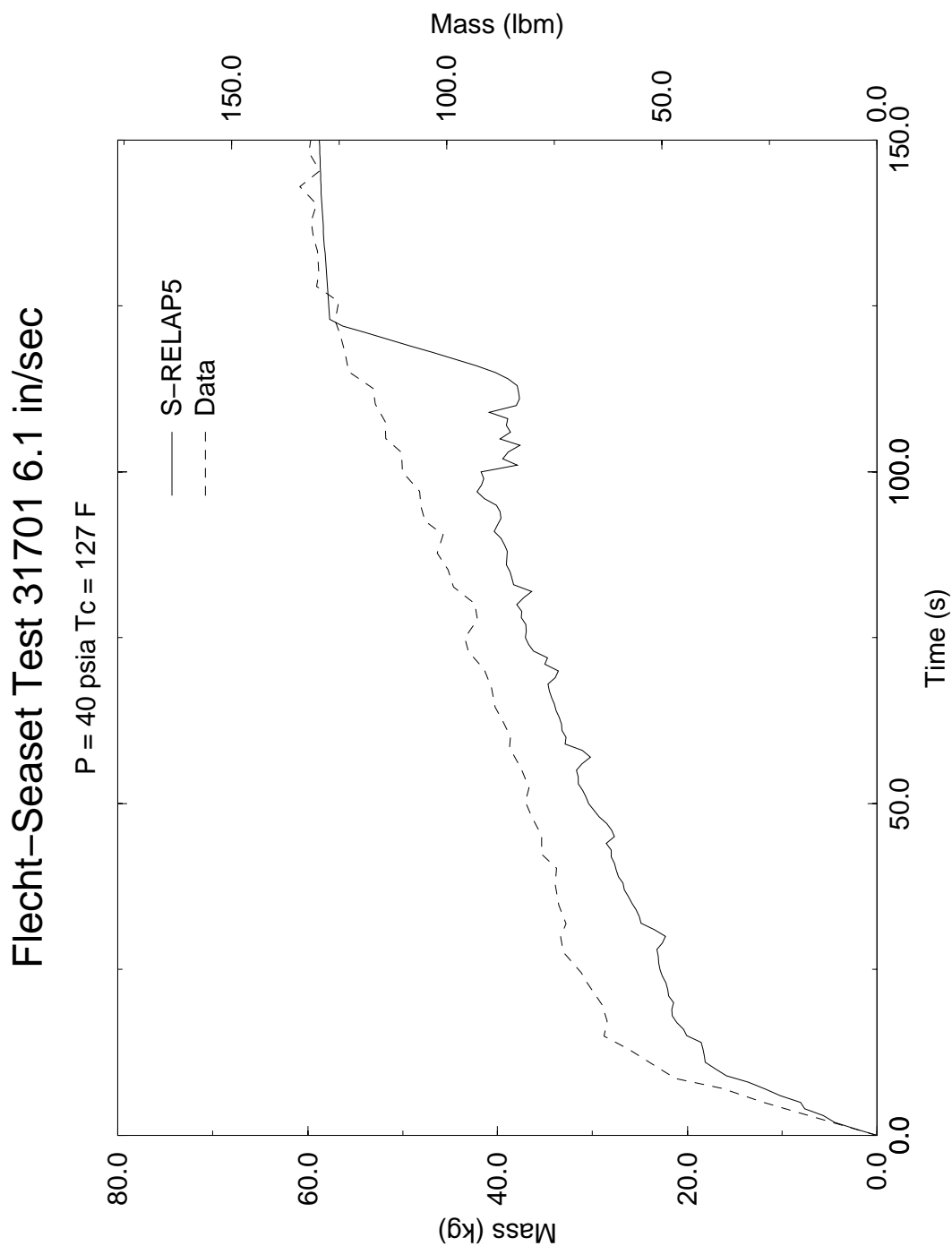


Figure 4.64 Accumulated Water Mass in the Test Section, FLECHT SEASET Test 31302



**Figure 4.65 Accumulated Water Mass in the Test Section, FLECHT
SEASET Test 31701**

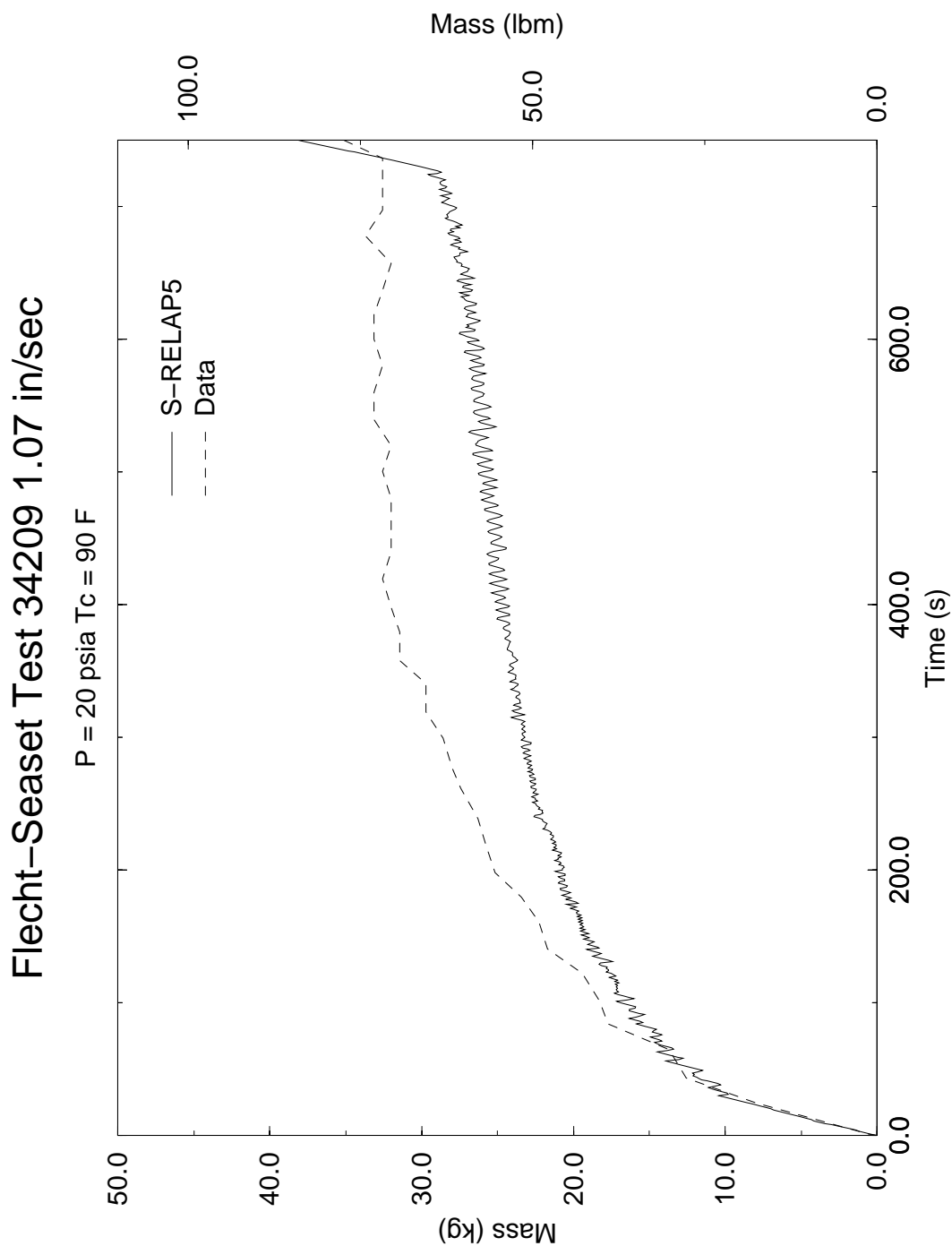


Figure 4.66 Accumulated Water Mass in the Test Section, FLECHT SEASET Test 34209

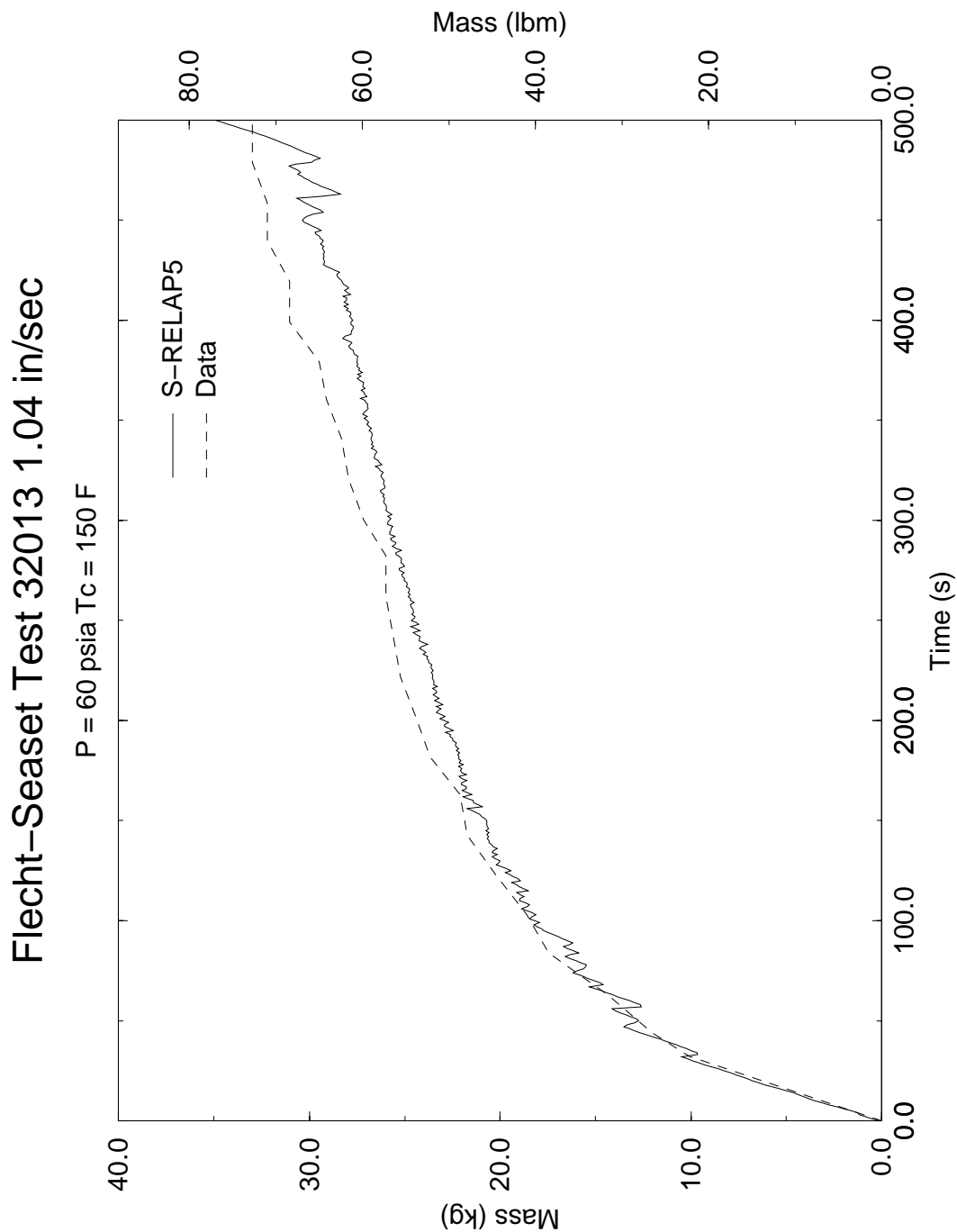


Figure 4.67 Accumulated Water Mass in the Test Section, FLECHT SEASET Test 32013

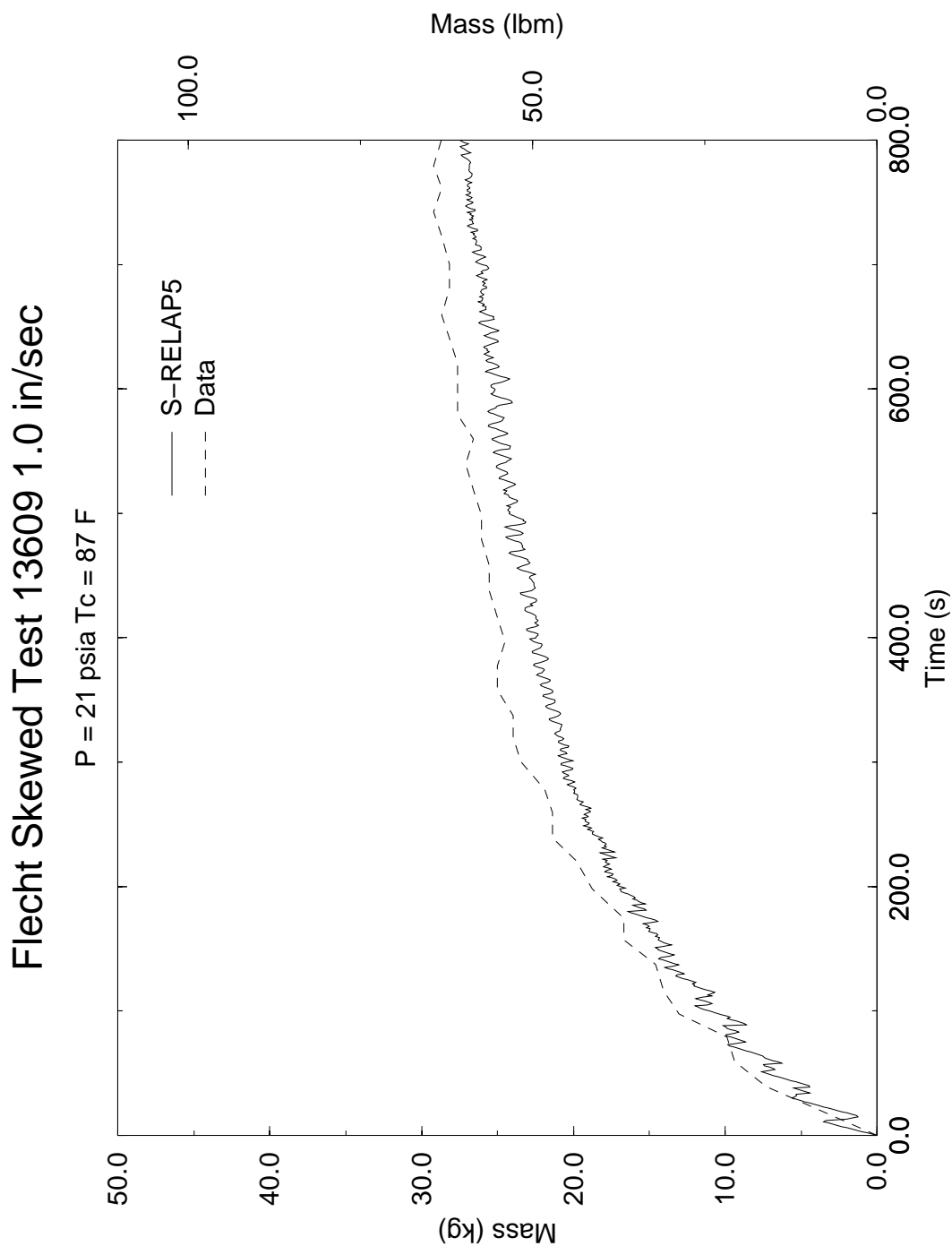


Figure 4.68 Accumulated Water Mass in the Test Section, FLECHT Skewed Test 13609

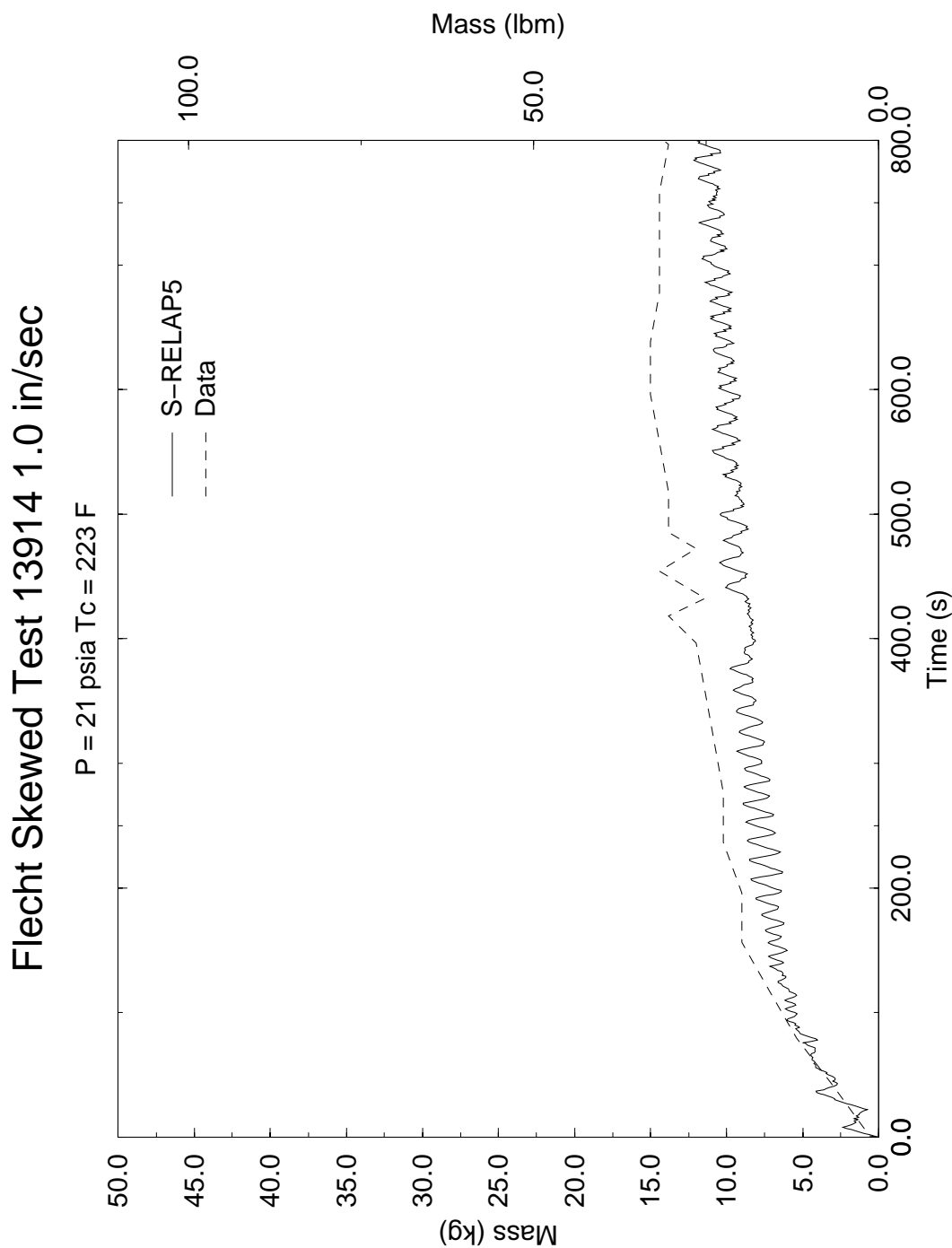
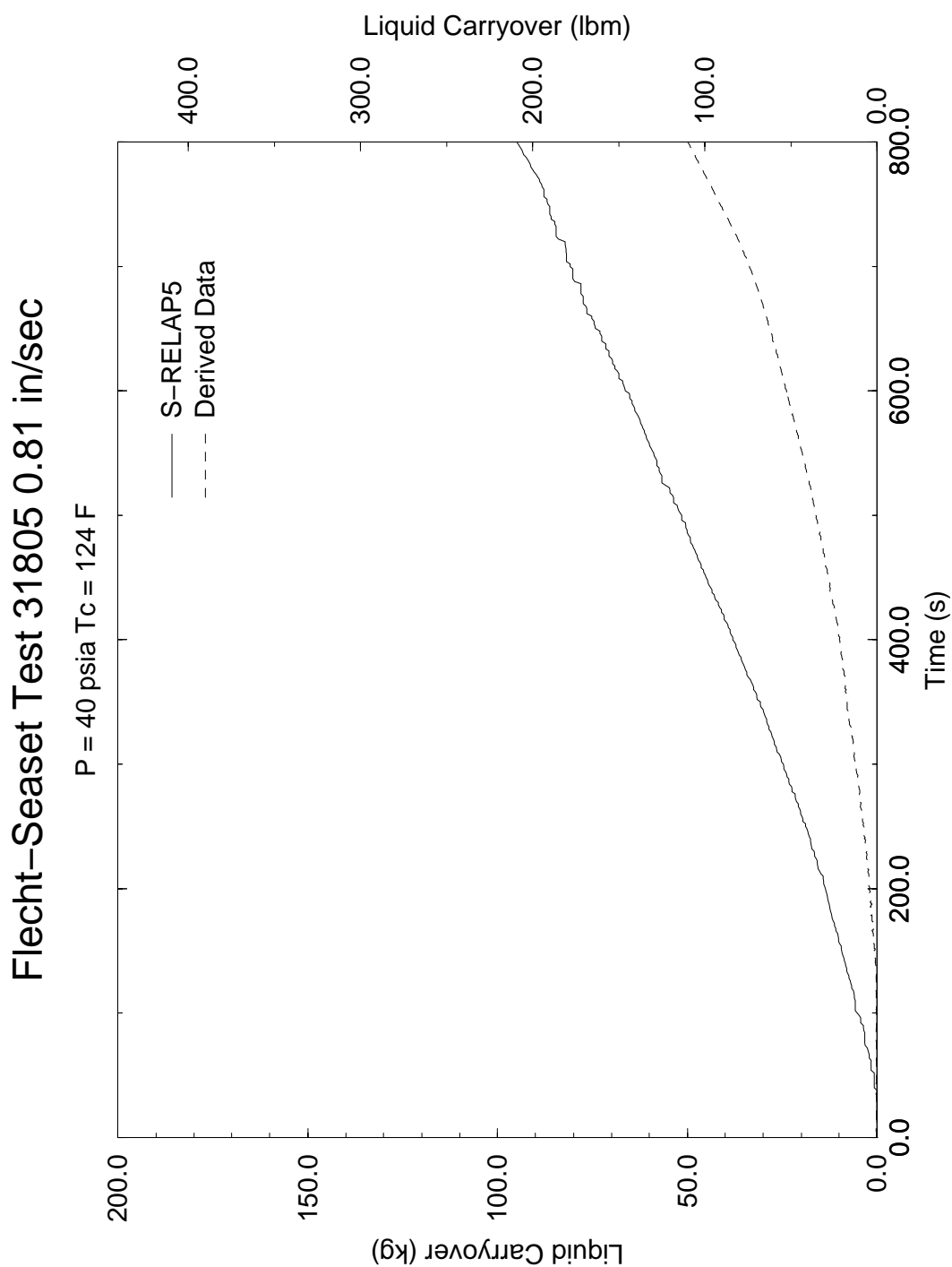
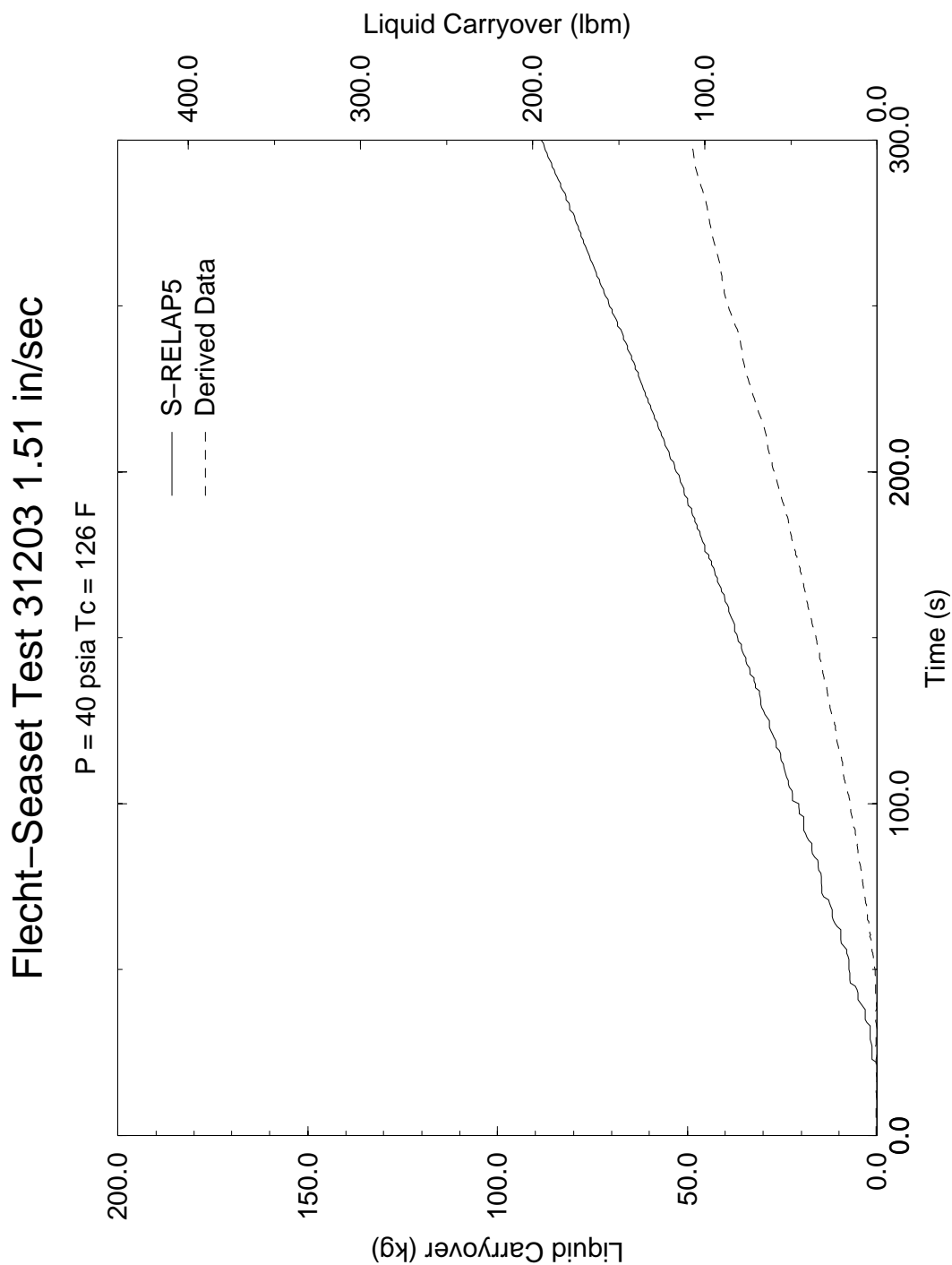


Figure 4.69 Accumulated Water Mass in the Test Section, FLECHT Skewed Test 13914



**Figure 4.70 Total Liquid Carryover From Test Assembly, FLECHT
SEASET Test 31805**



**Figure 4.71 Total Liquid Carryover From Test Assembly, FLECHT
SEASET Test 31203**

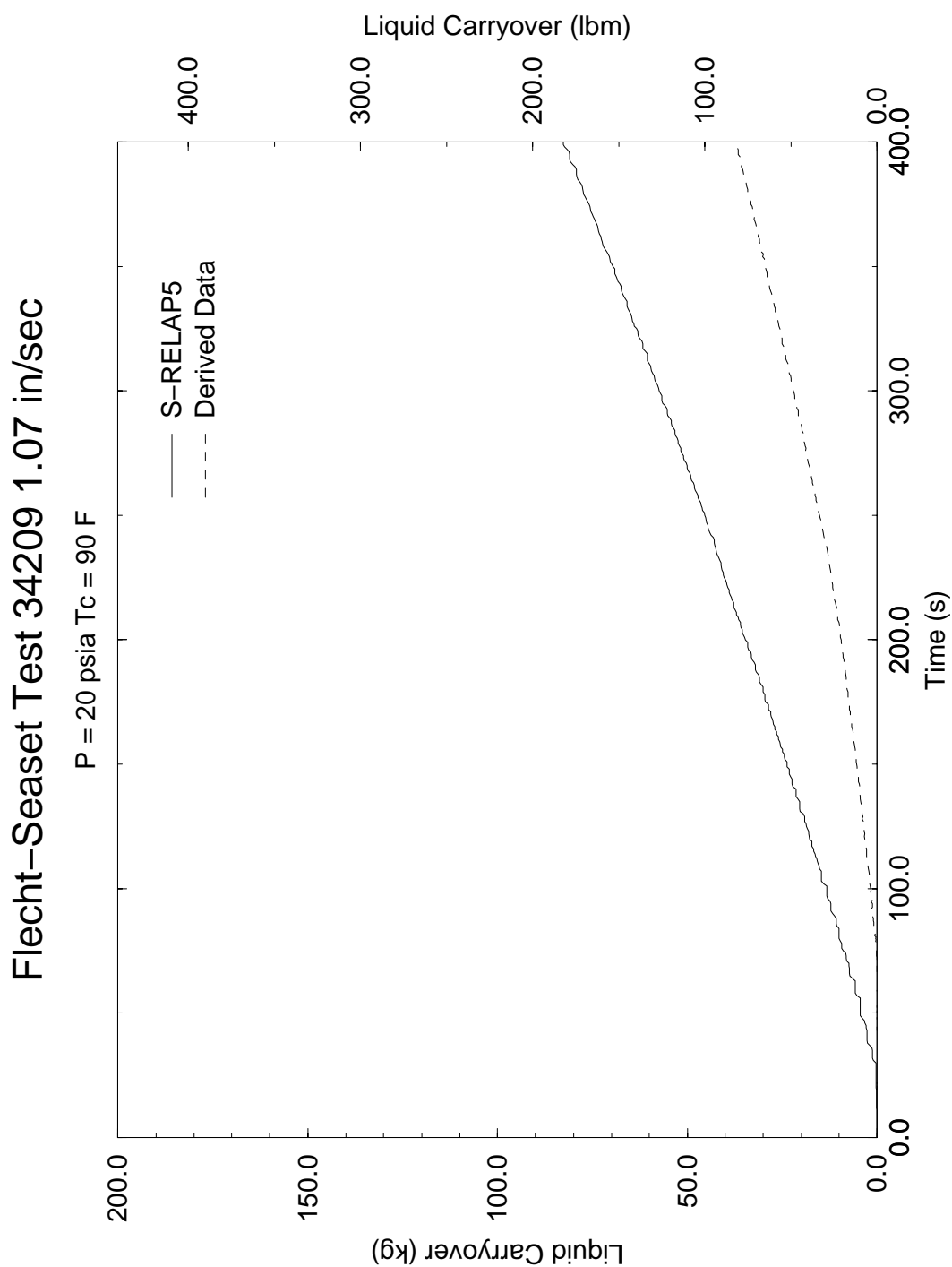


**Figure 4.72 Total Liquid Carryover From Test Assembly, FLECHT
SEASET Test 34209**

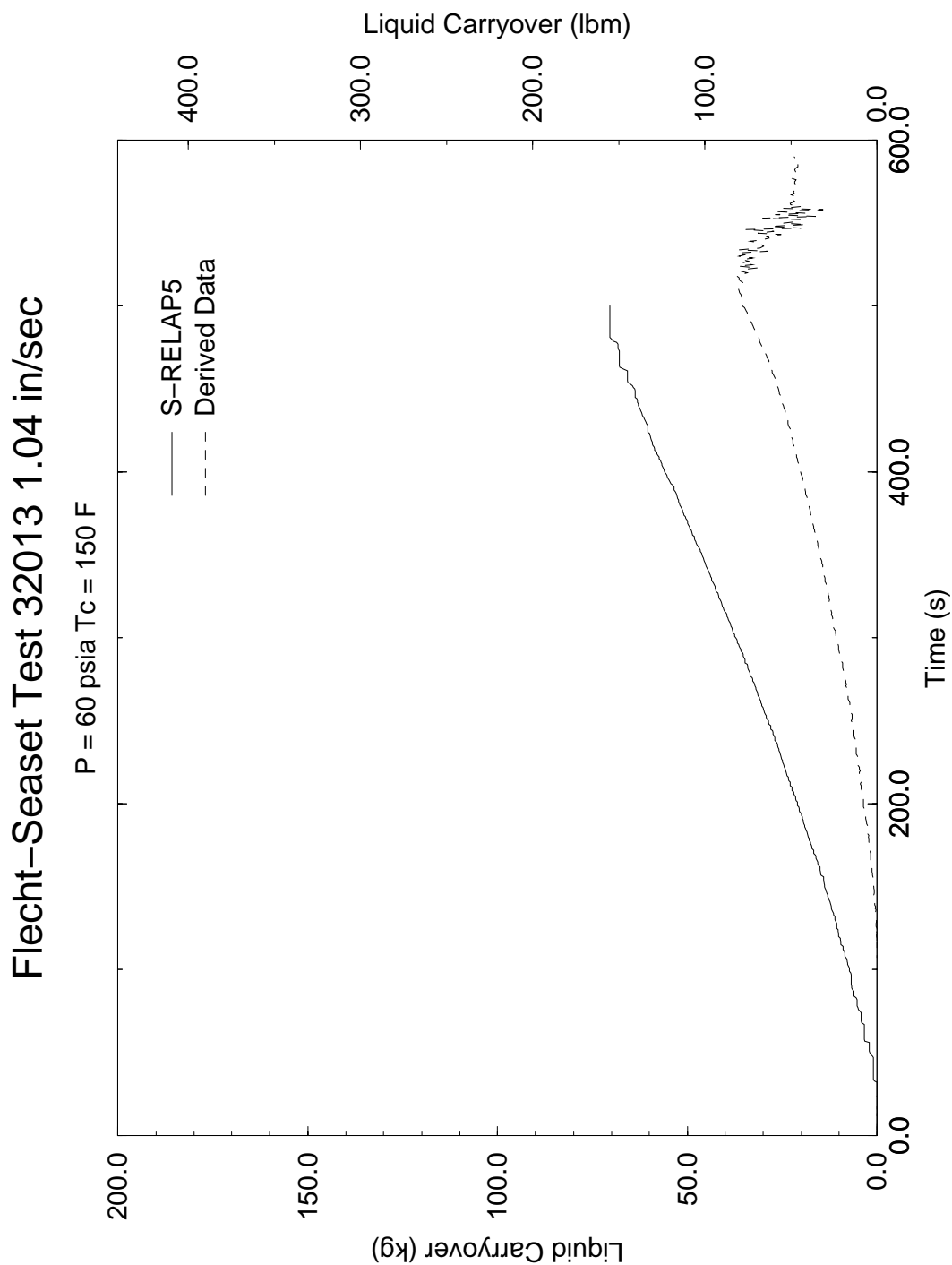


**Figure 4.73 Total Liquid Carryover From Test Assembly, FLECHT
SEASET Test 32013**

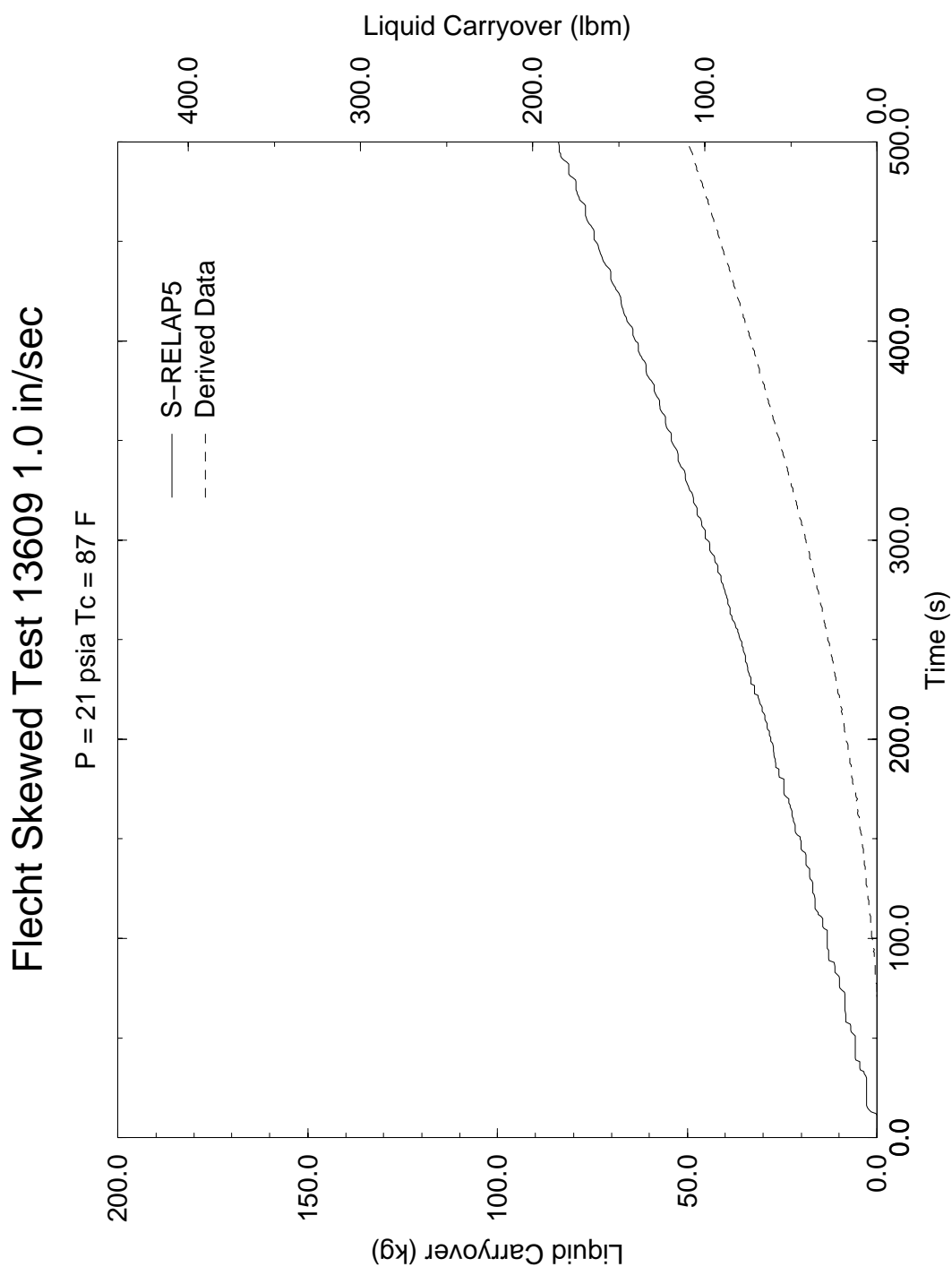


Figure 4.74 Total Liquid Carryover From Test Assembly, FLECHT Skewed Test 13609

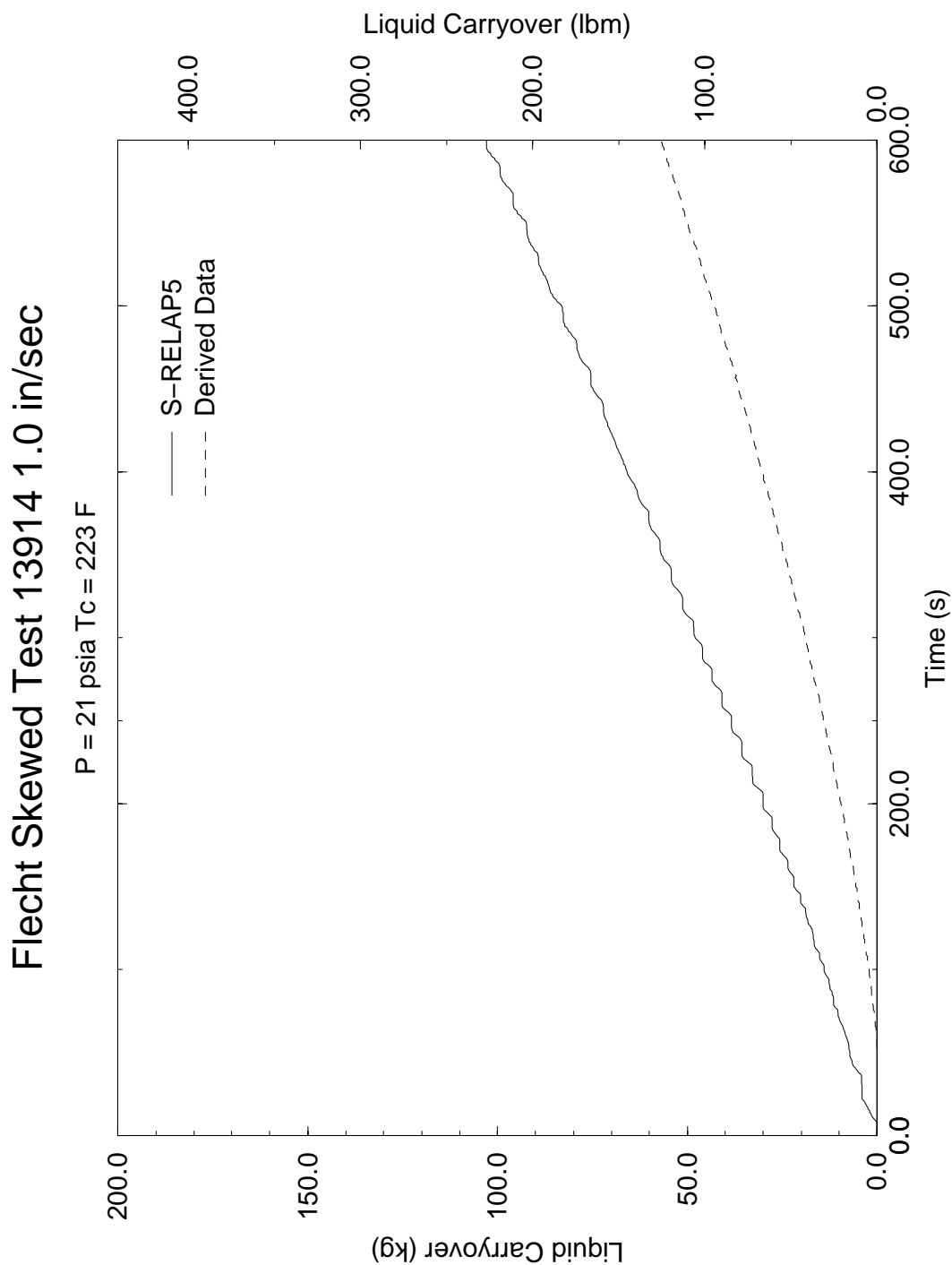


Figure 4.75 Total Liquid Carryover From Test Assembly, FLECHT Skewed Test 13914

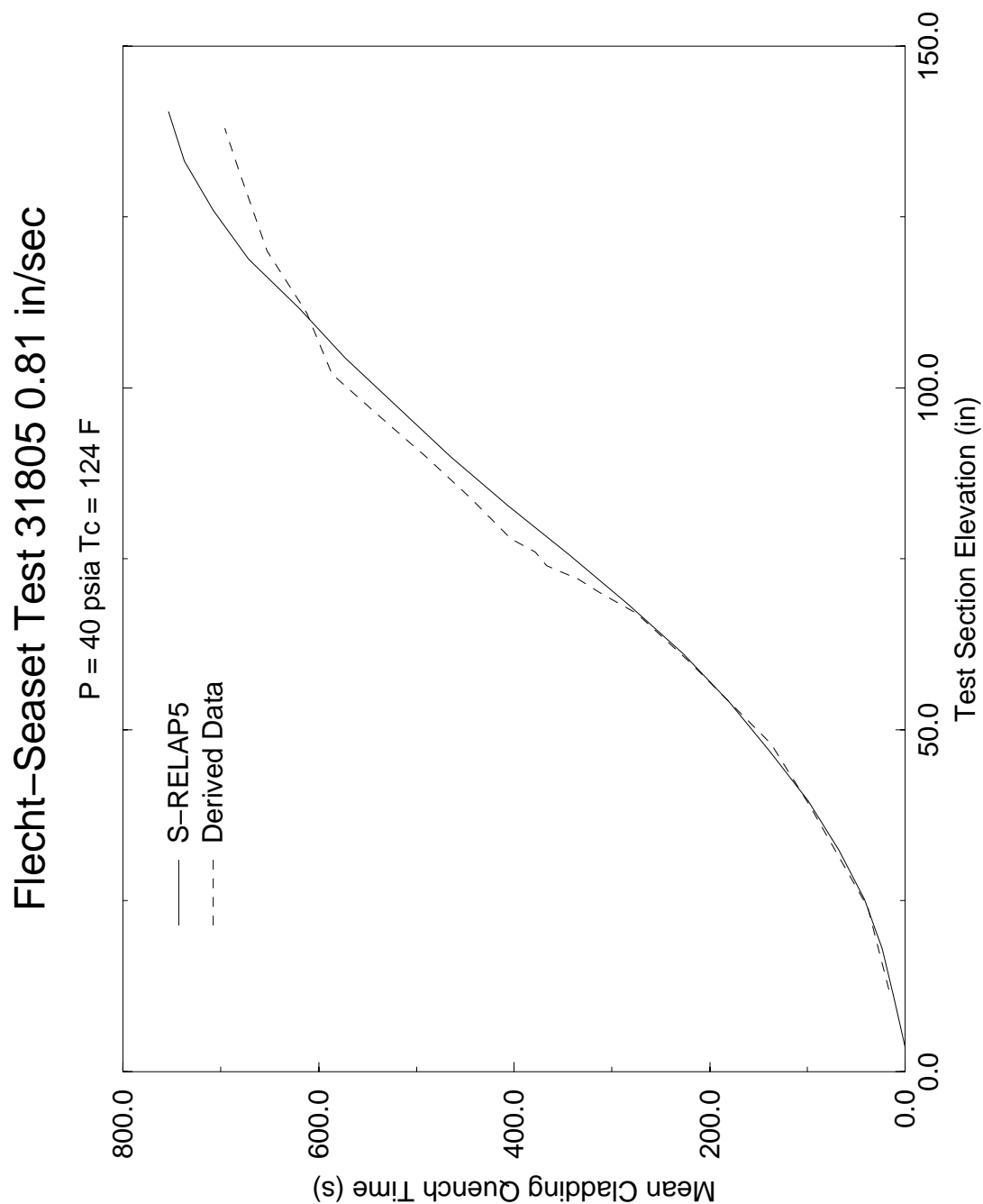


Figure 4.76 Average Rod Quench Time, FLECHT SEASET Test 31805

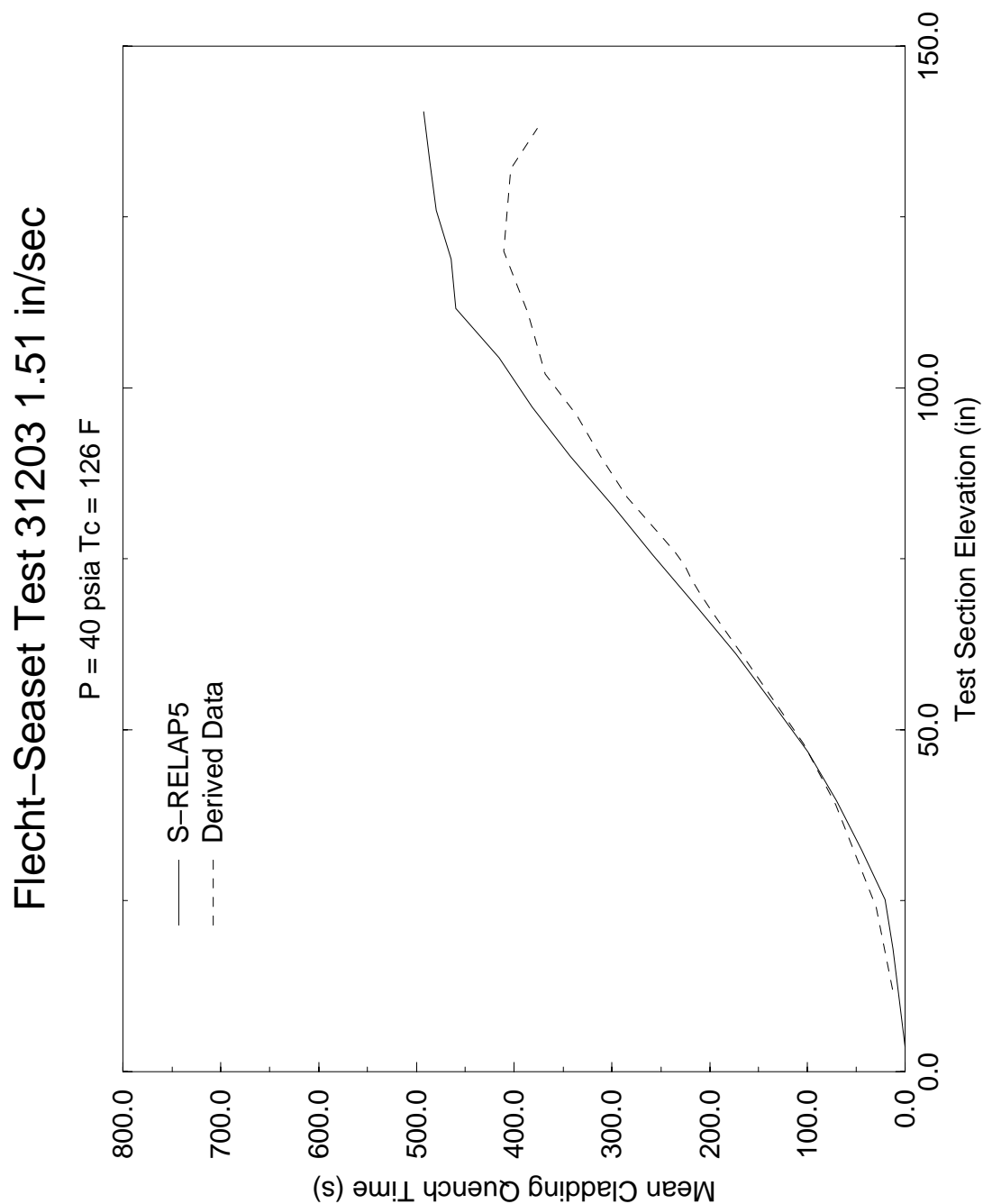


Figure 4.77 Average Rod Quench Time, FLECHT SEASET Test 31203

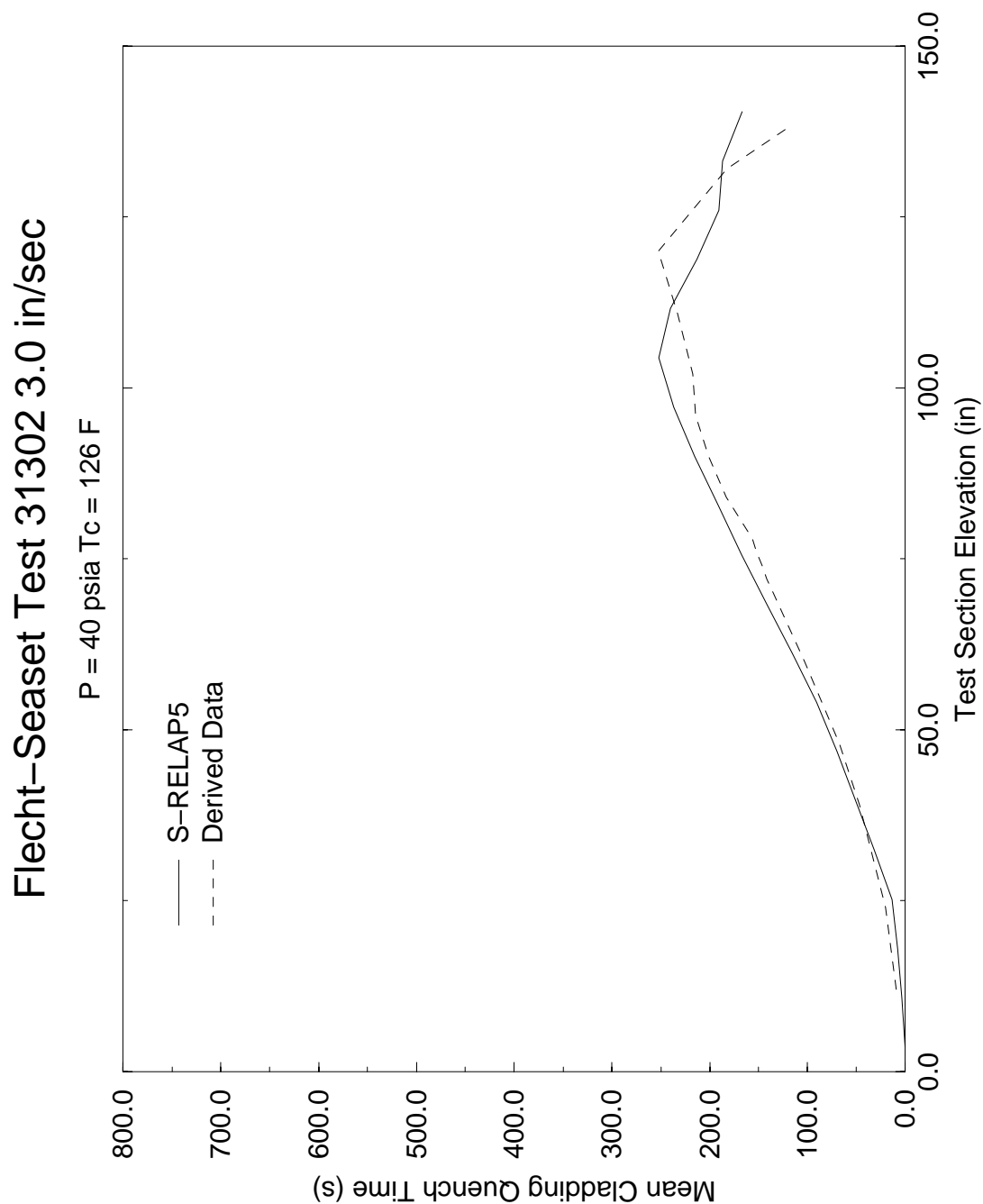


Figure 4.78 Average Rod Quench Time, FLECHT SEASET Test 31302

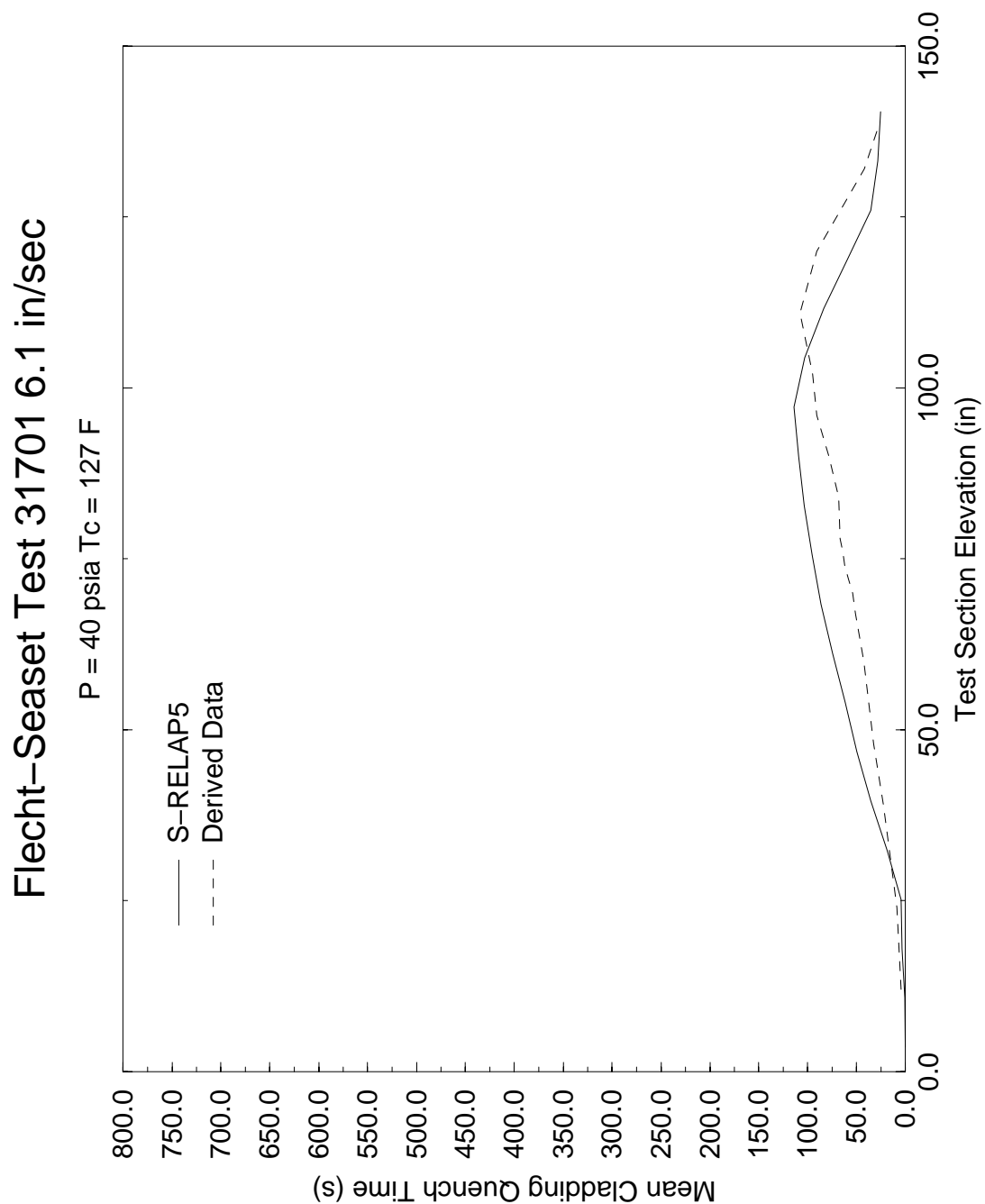


Figure 4.79 Average Rod Quench Time, FLECHT SEASET Test 31701

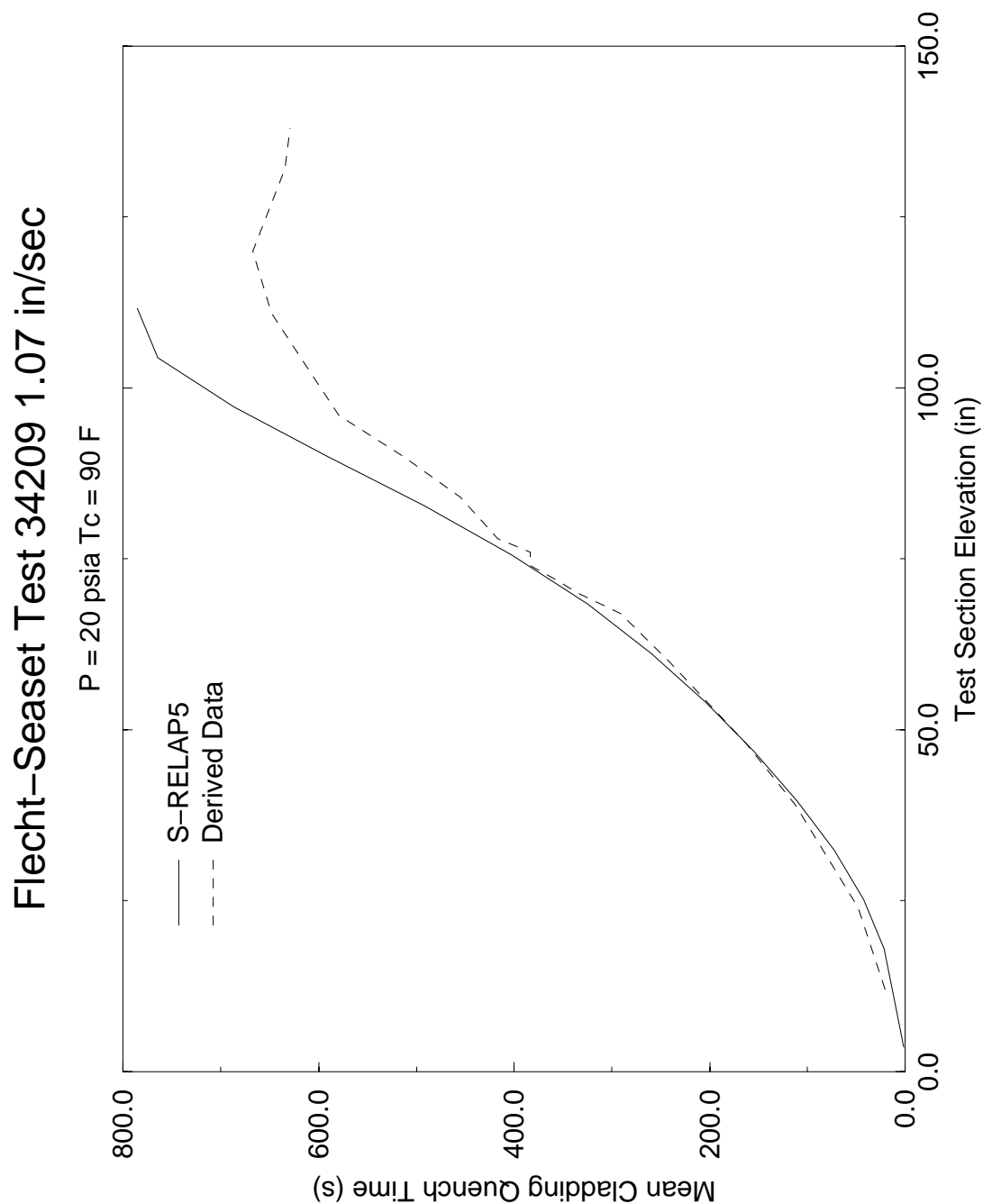


Figure 4.80 Average Rod Quench Time, FLECHT SEASET Test 34209

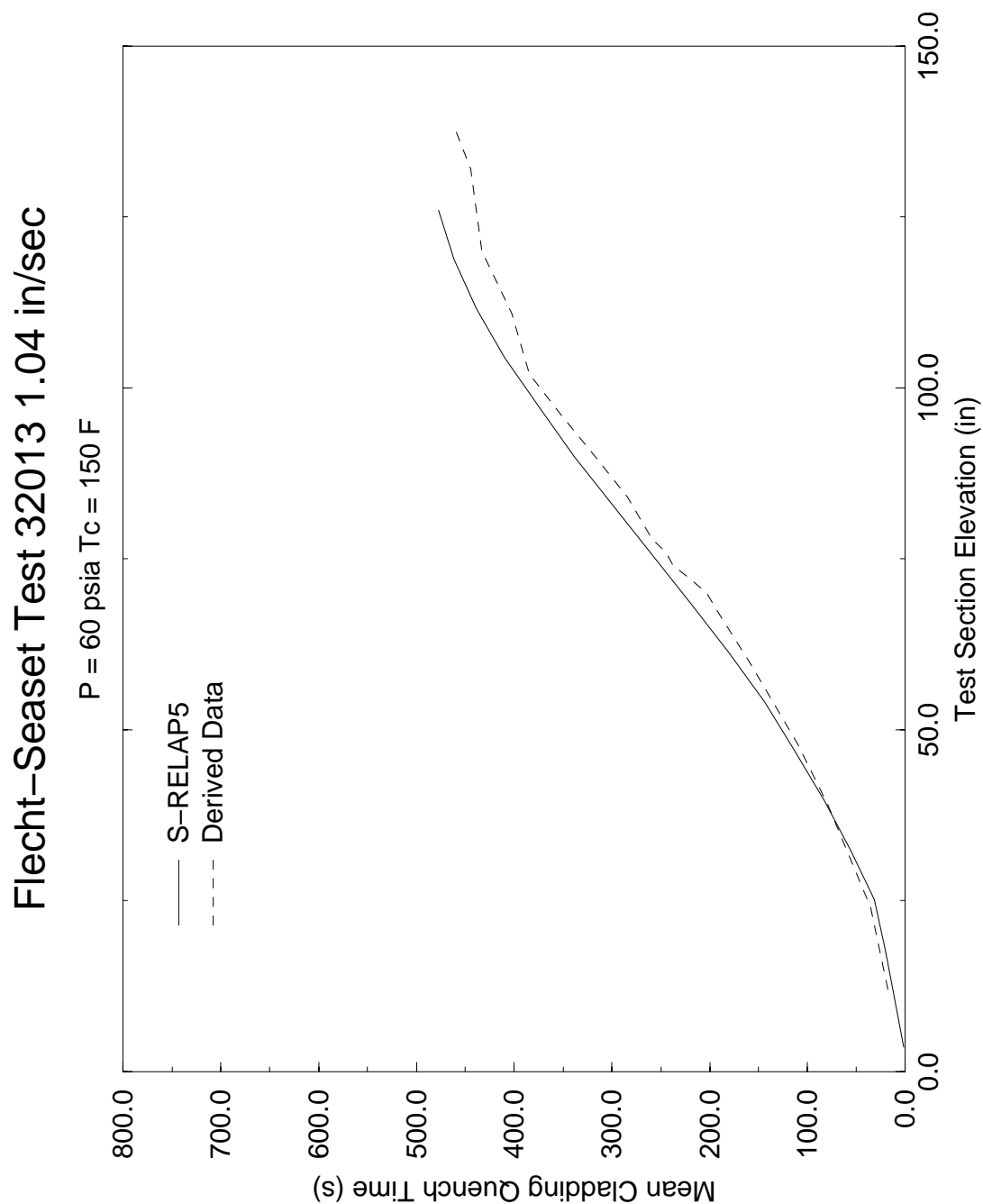
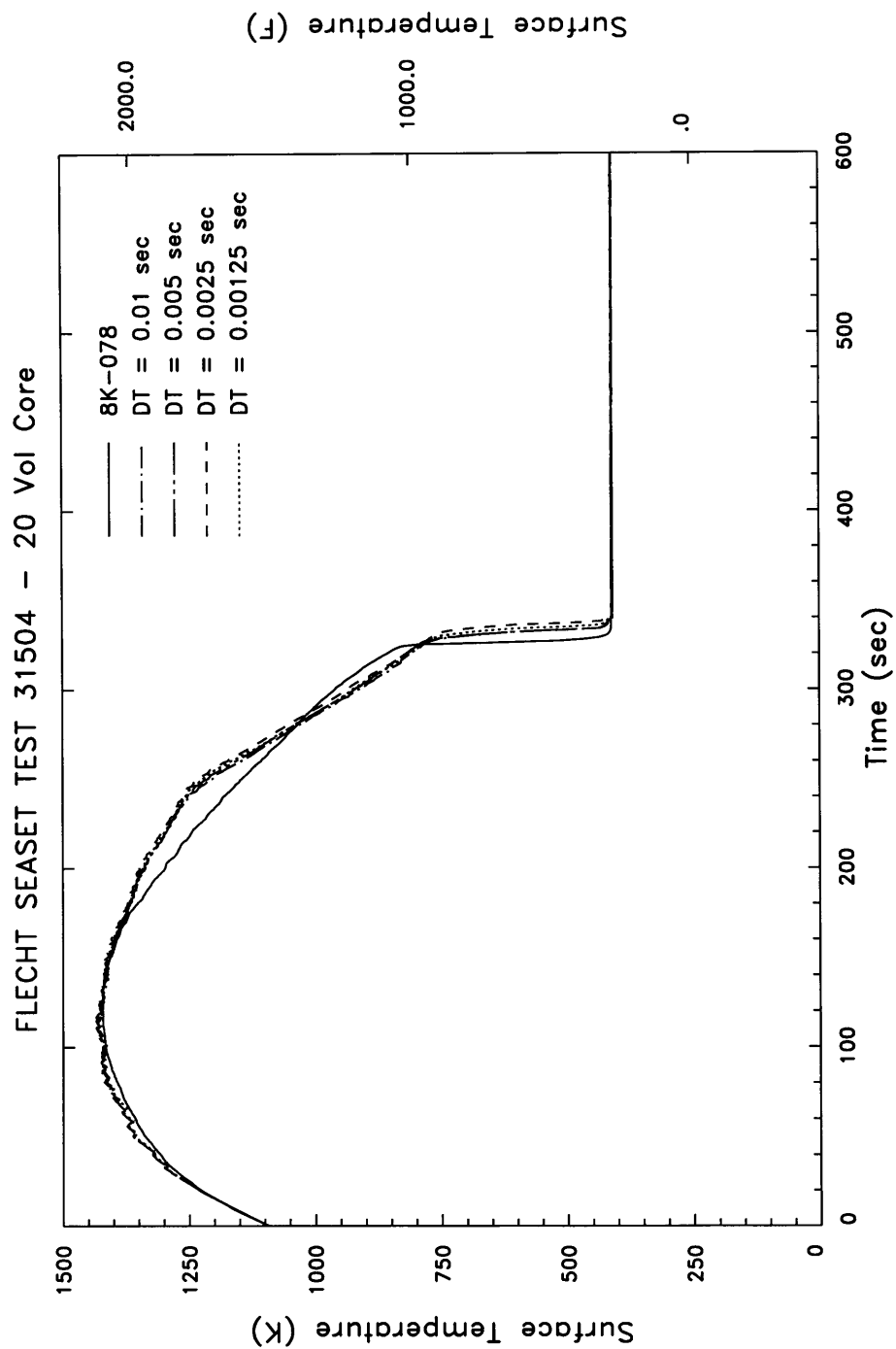


Figure 4.81 Average Rod Quench Time, FLECHT SEASET Test 32013



**Figure 4.82 Calculated Rod Surface Temperatures at 79 in for the
20-Volume Test Section Cases With Various Time-Step Sizes,
FLECHT SEASET Test 31504**

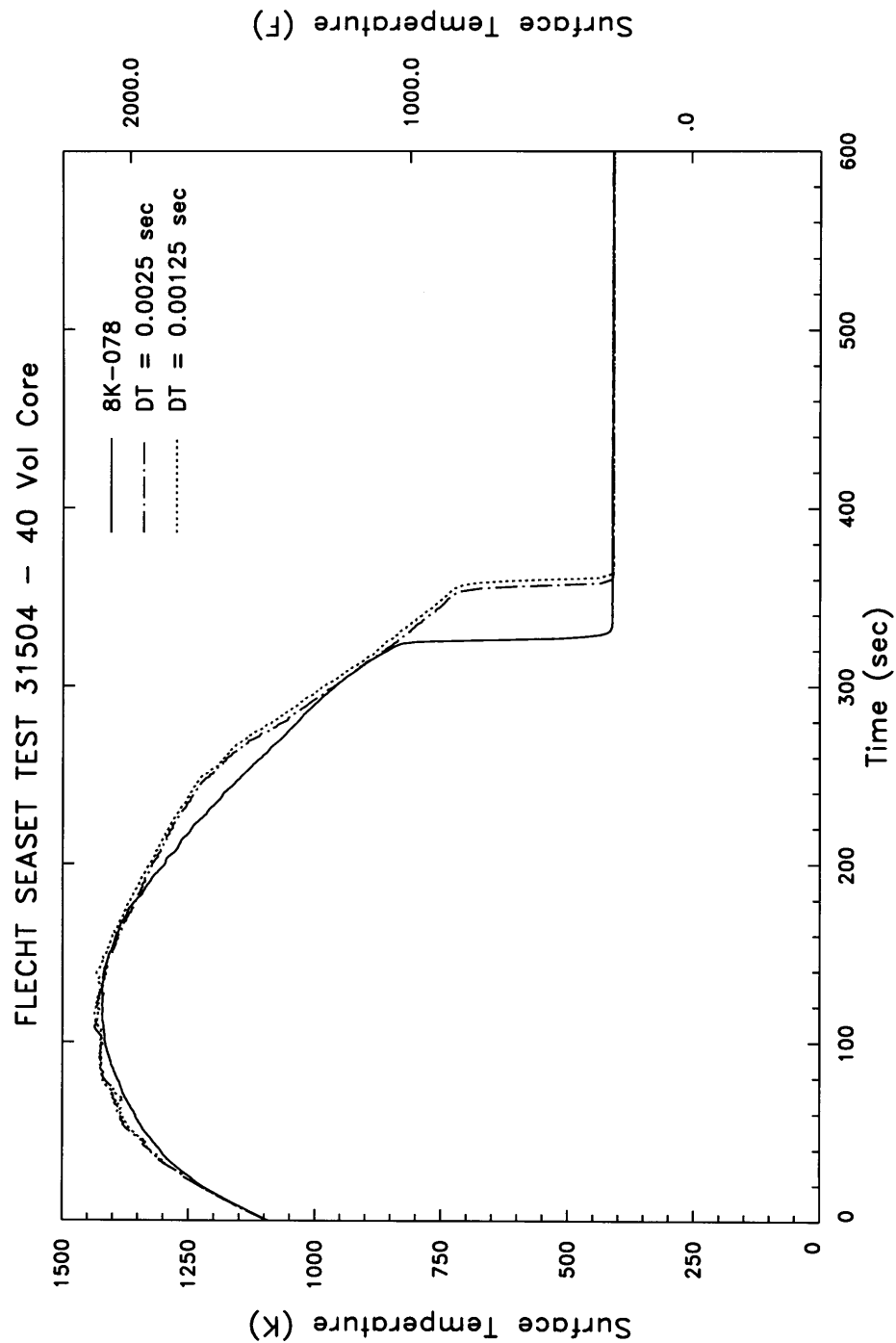
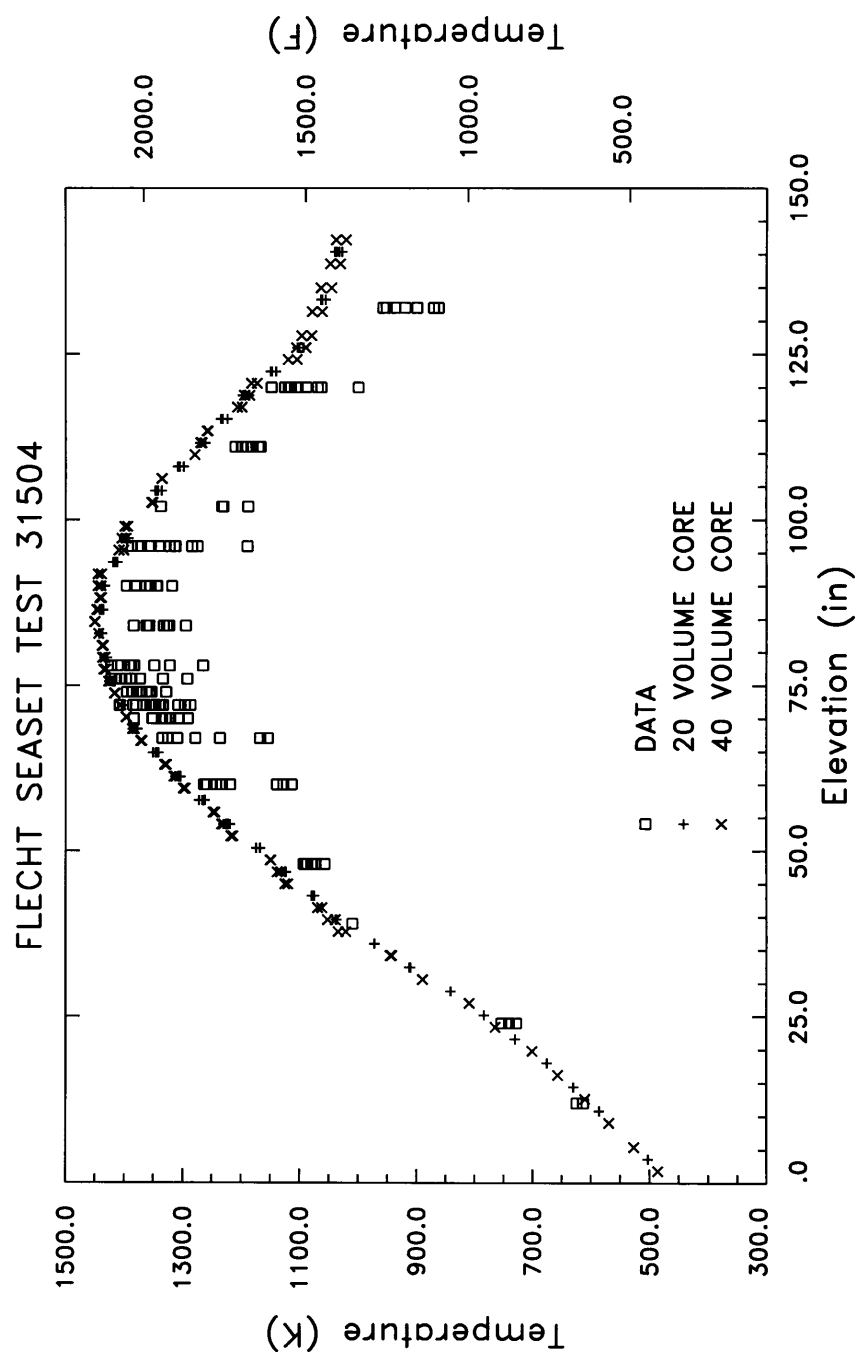
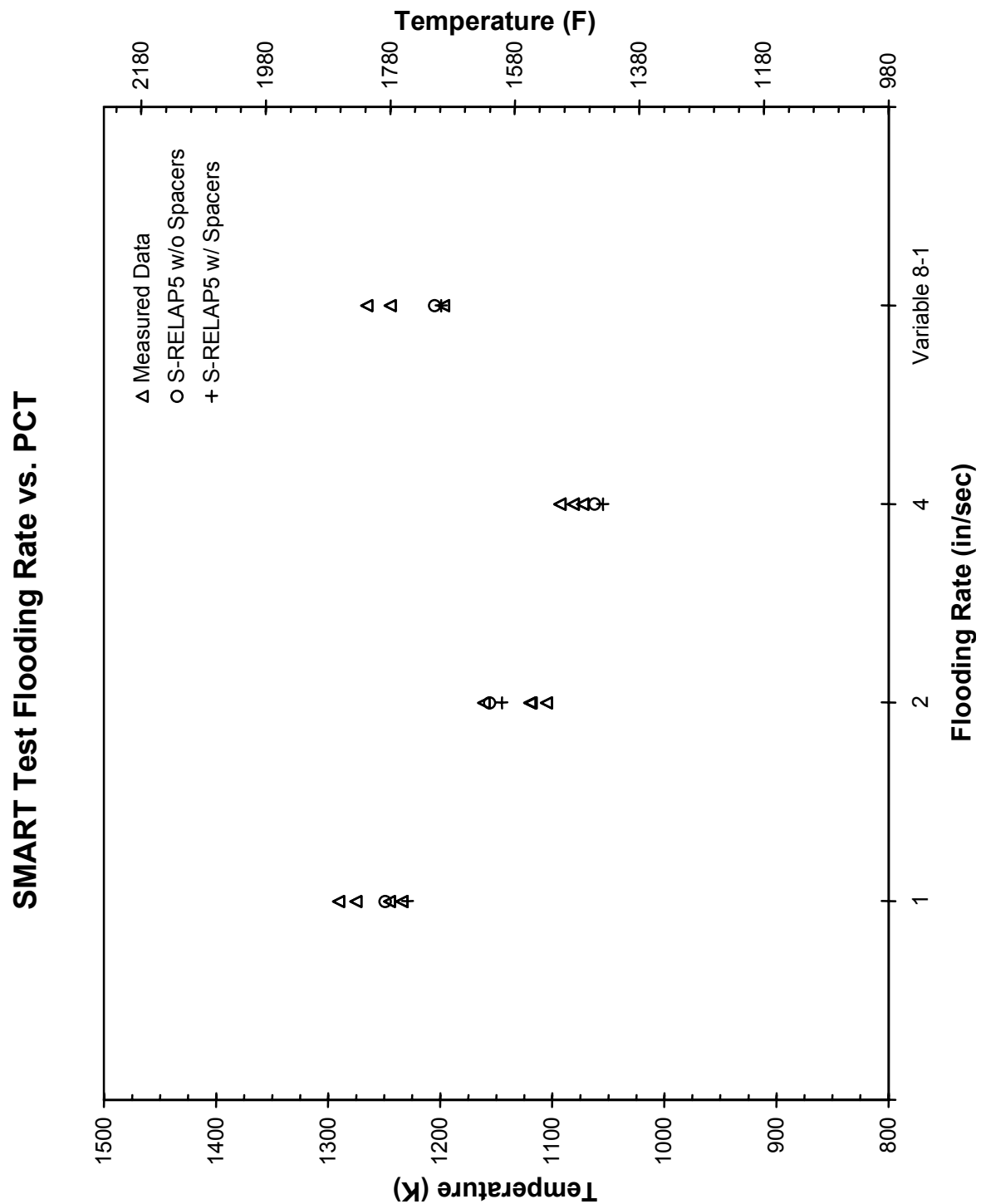


Figure 4.83 Calculated Rod Surface Temperatures at 79 in for the 40-Volume Test Section Cases With Various Time-Step Sizes, FLECHT SEASET Test 31504



**Figure 4.84 Maximum Cladding Temperatures vs. Axial Elevation,
FLECHT SEASET Test 31504**



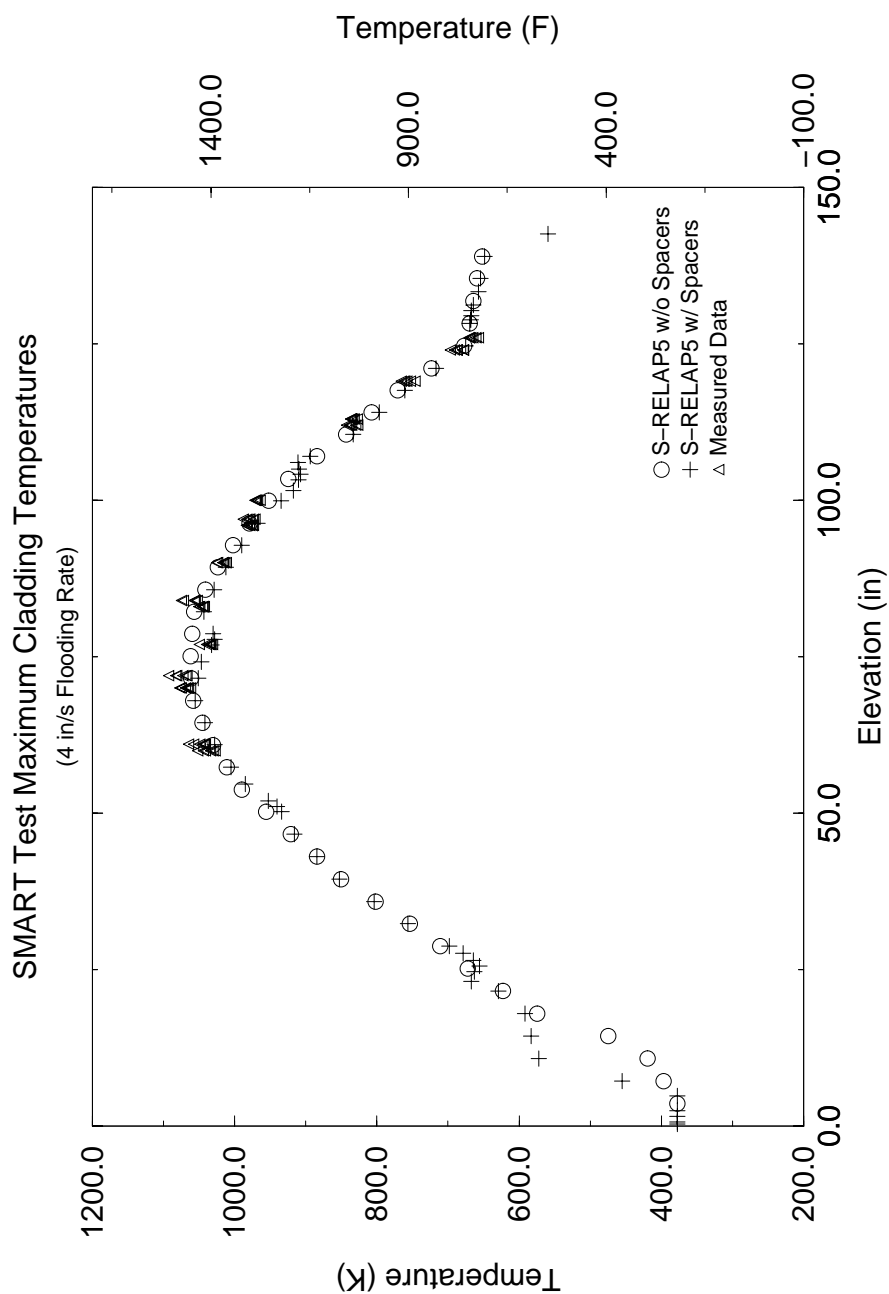
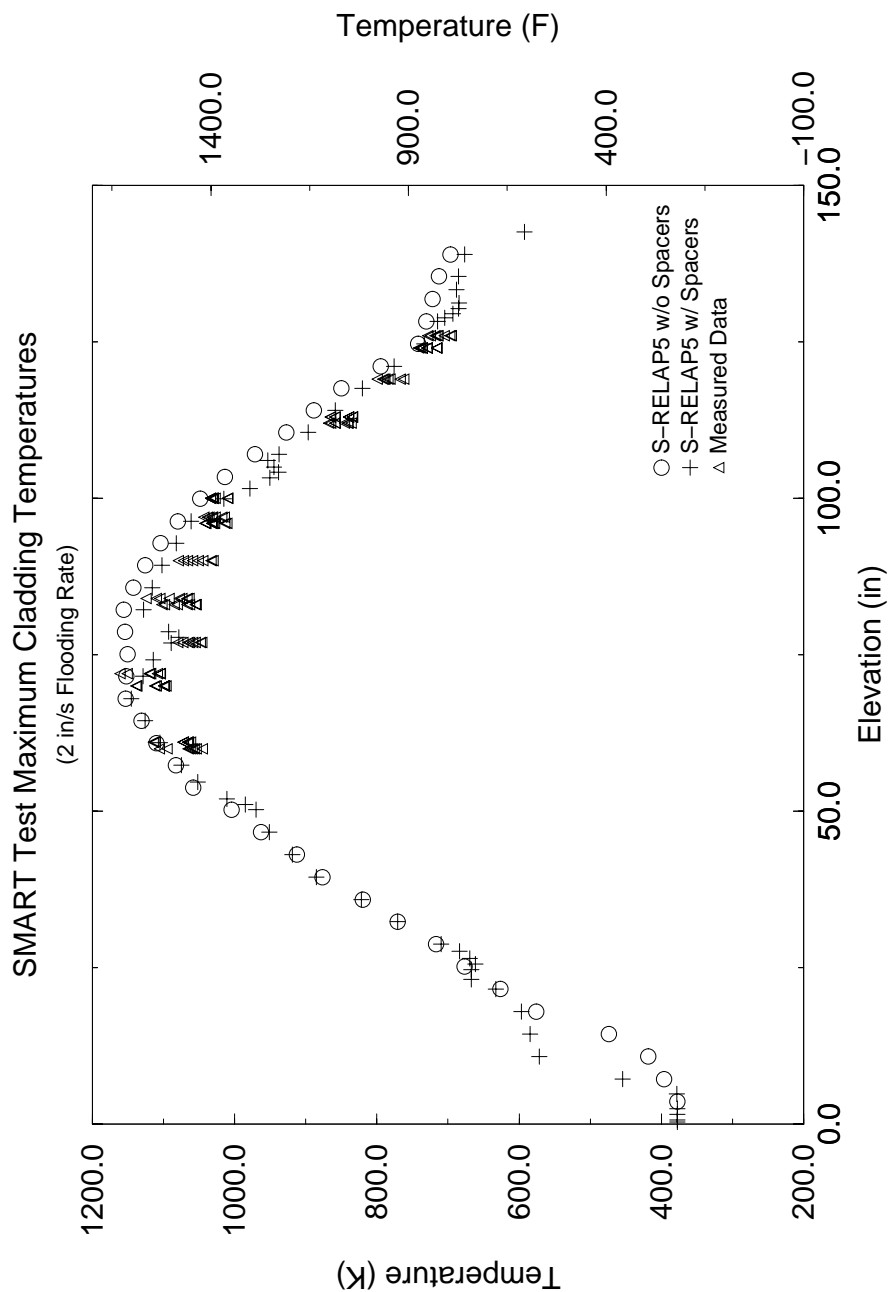


Figure 4.86 MCT vs. Elevation Comparison to Data for 4-in/s-Flooding-Rate Test, PDTF SMART



**Figure 4.87 MCT vs. Elevation Comparison to Data for
2-in/s-Flooding-Rate Test, PDTF SMART**

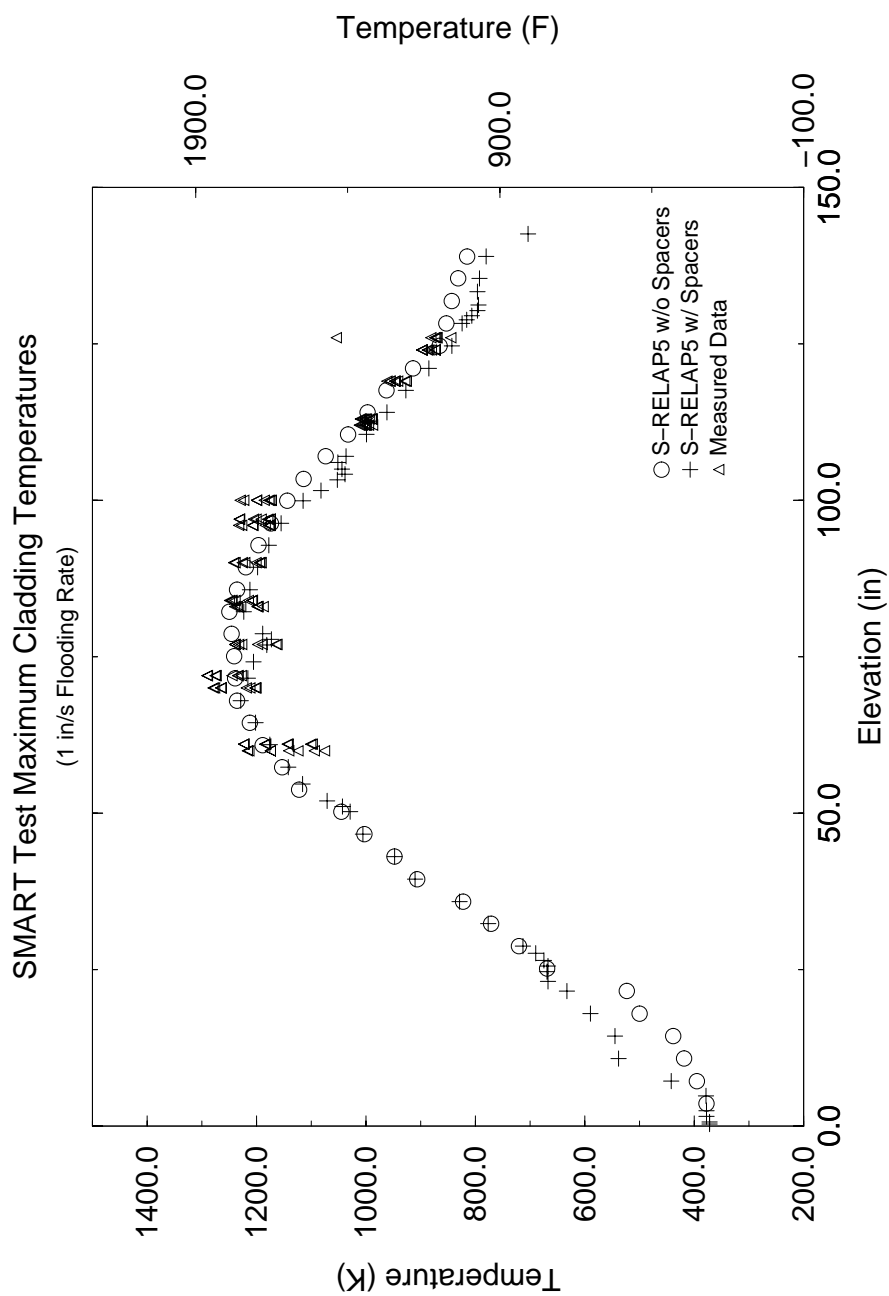
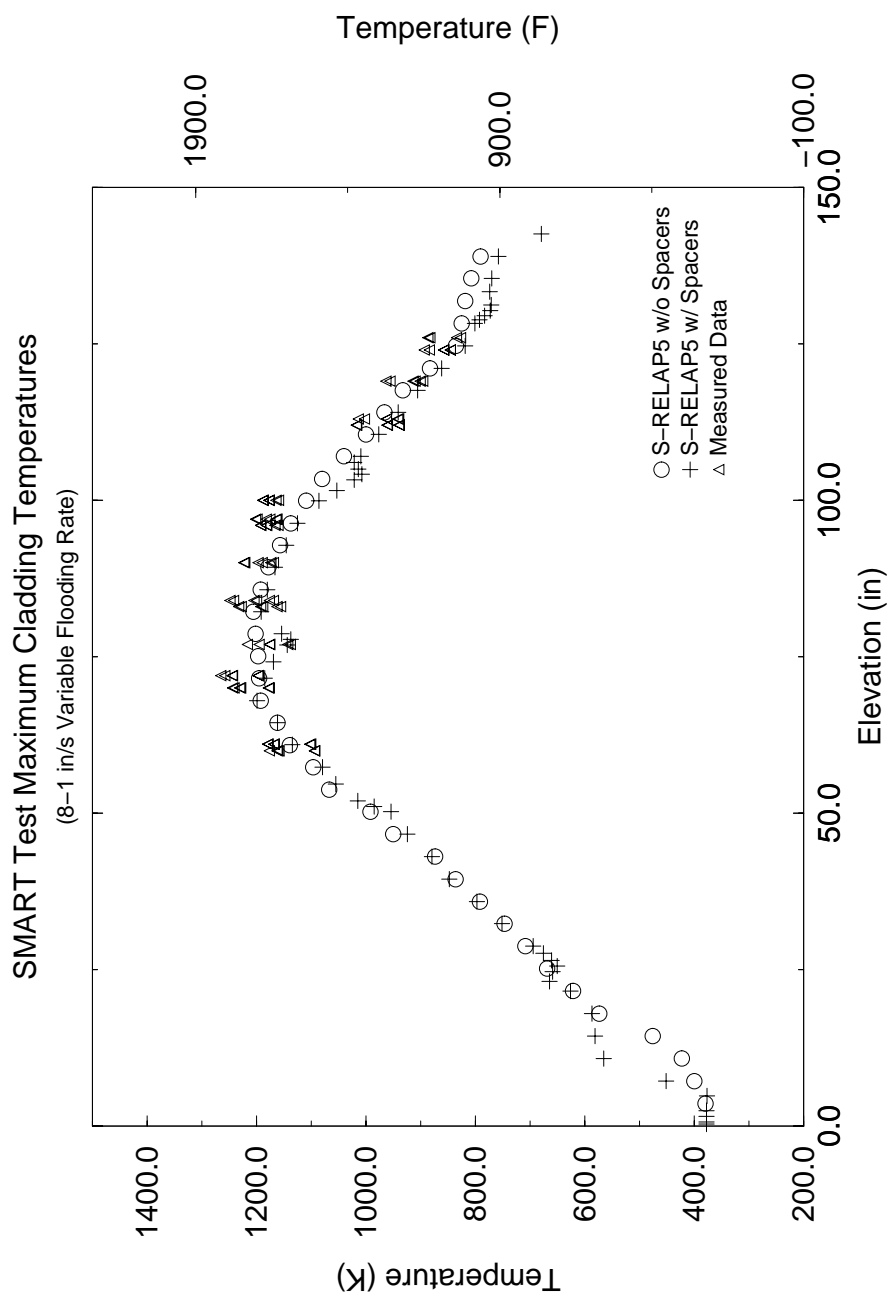


Figure 4.88 MCT vs. Elevation Comparison to Data for 1-in/s-Flooding-Rate Test, PDTF SMART



**Figure 4.89 MCT vs. Elevation Comparison to Data for
Variable-Flooding-Rate Test, PDTF SMART**

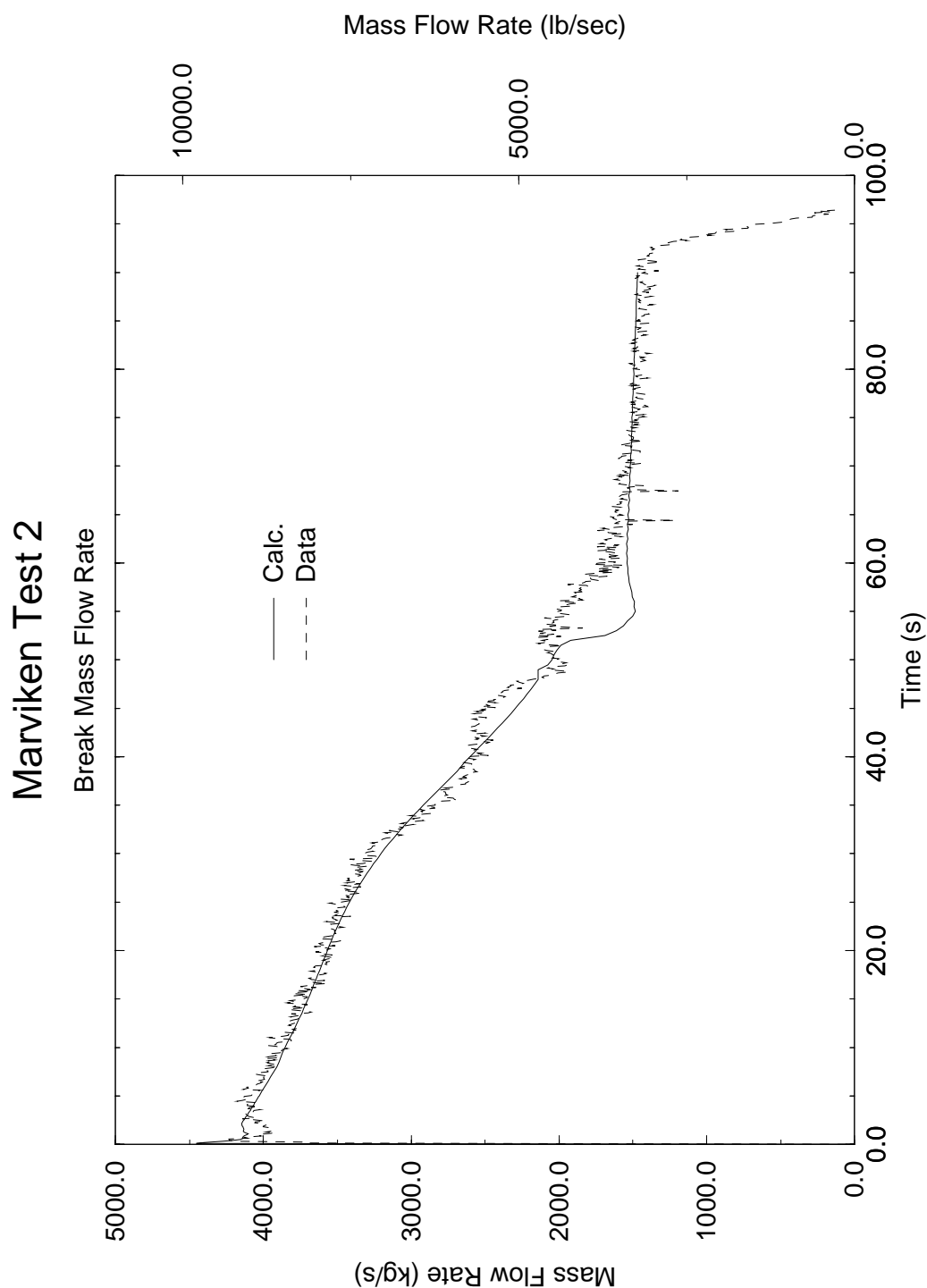


Figure 4.90 Comparison of Break Mass Flow Rates, Marviken Test 2

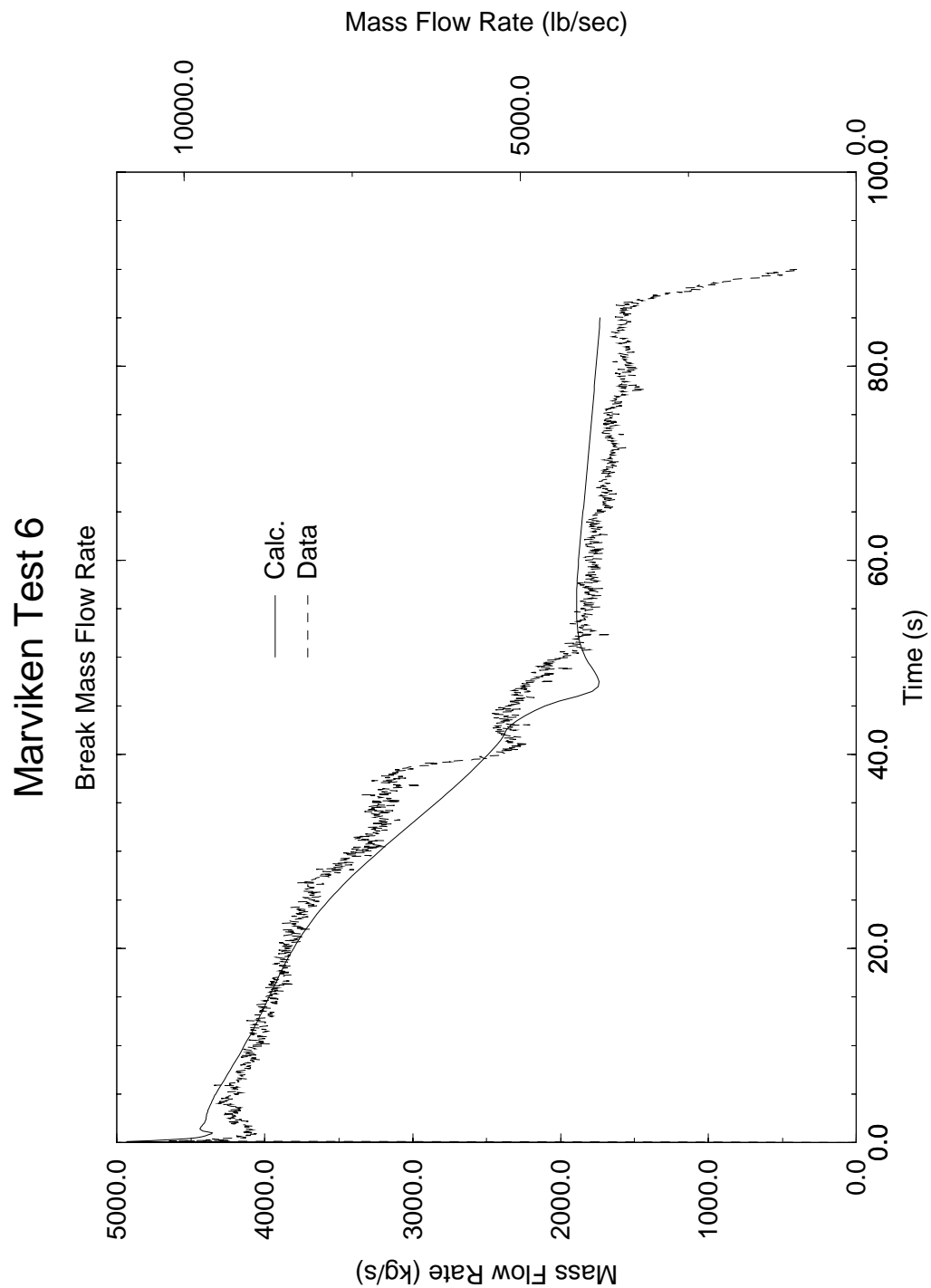


Figure 4.91 Comparison of Break Mass Flow Rates, Marviken Test 6

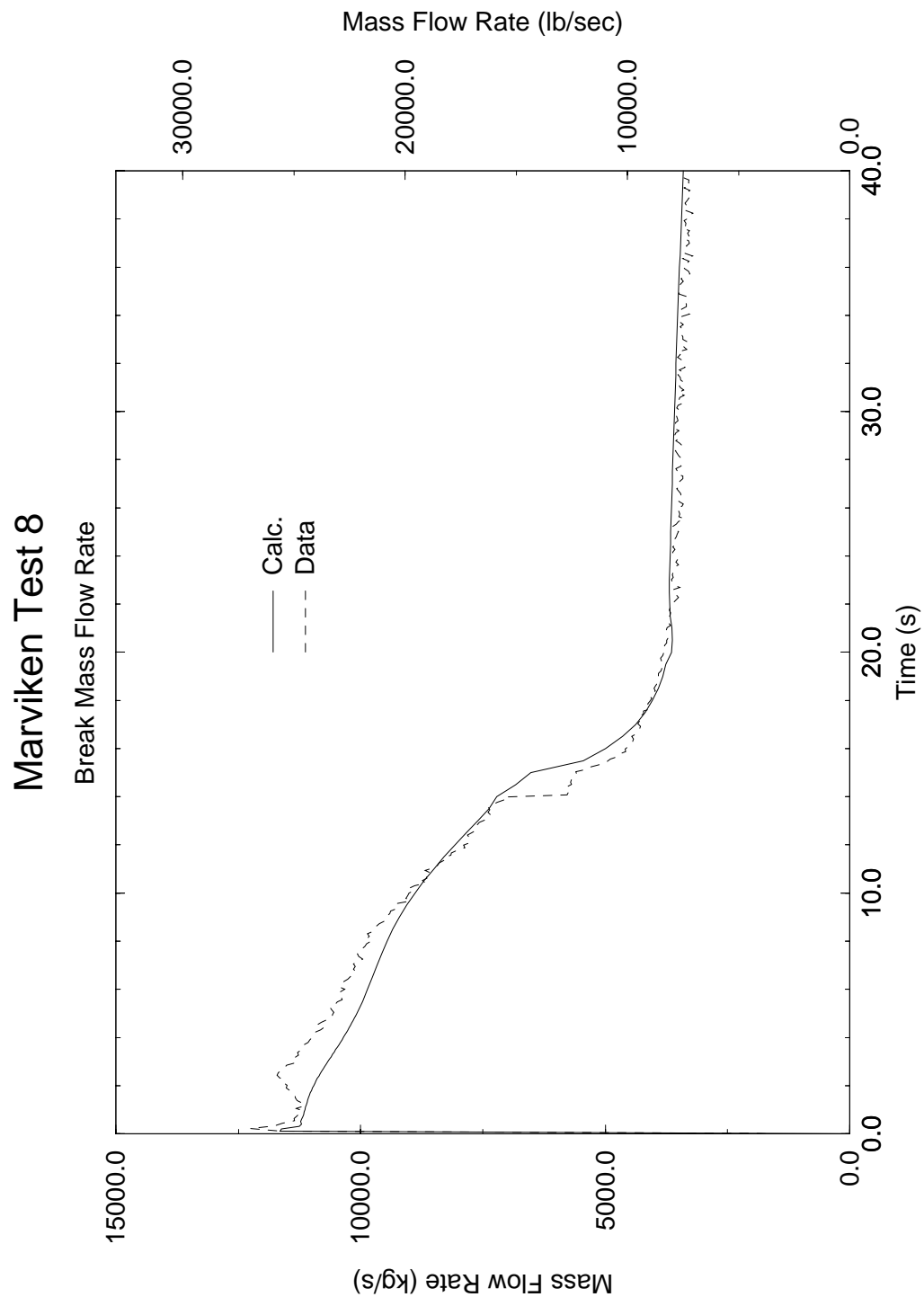


Figure 4.92 Comparison of Break Mass Flow Rates, Marviken Test 8

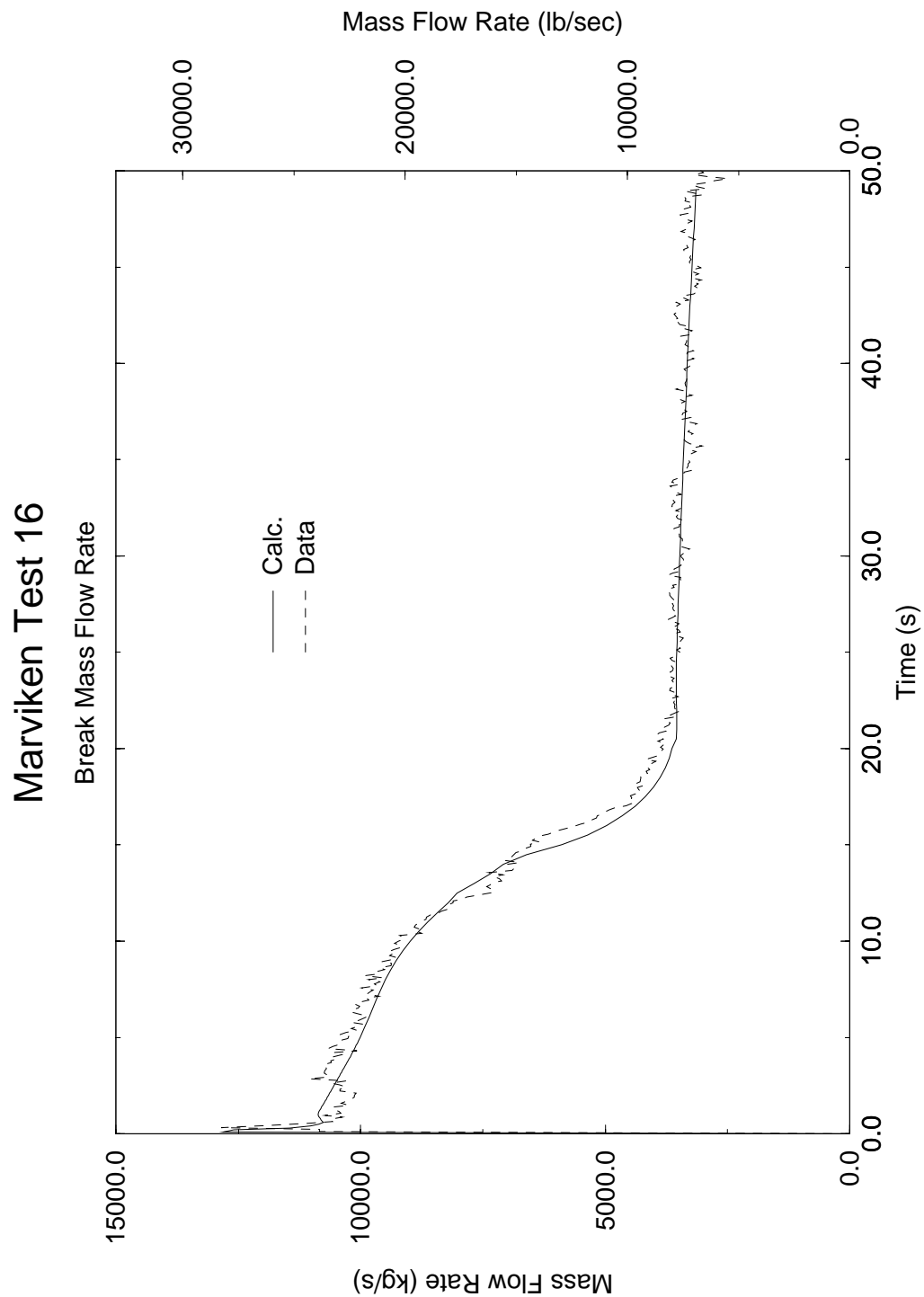


Figure 4.93 Comparison of Break Mass Flow Rates, Marviken Test 16

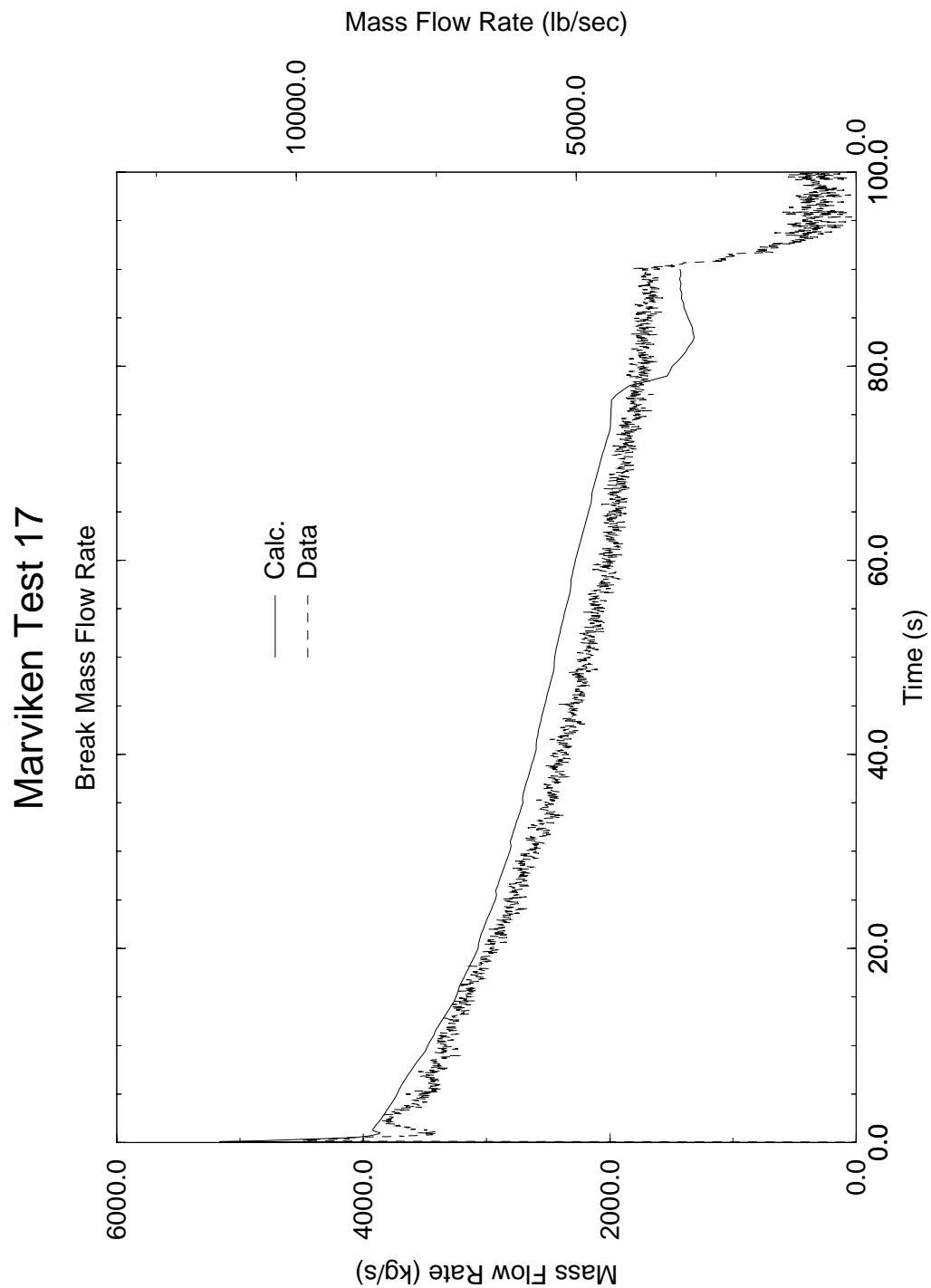


Figure 4.94 Comparison of Break Mass Flow Rates, Marviken Test 17

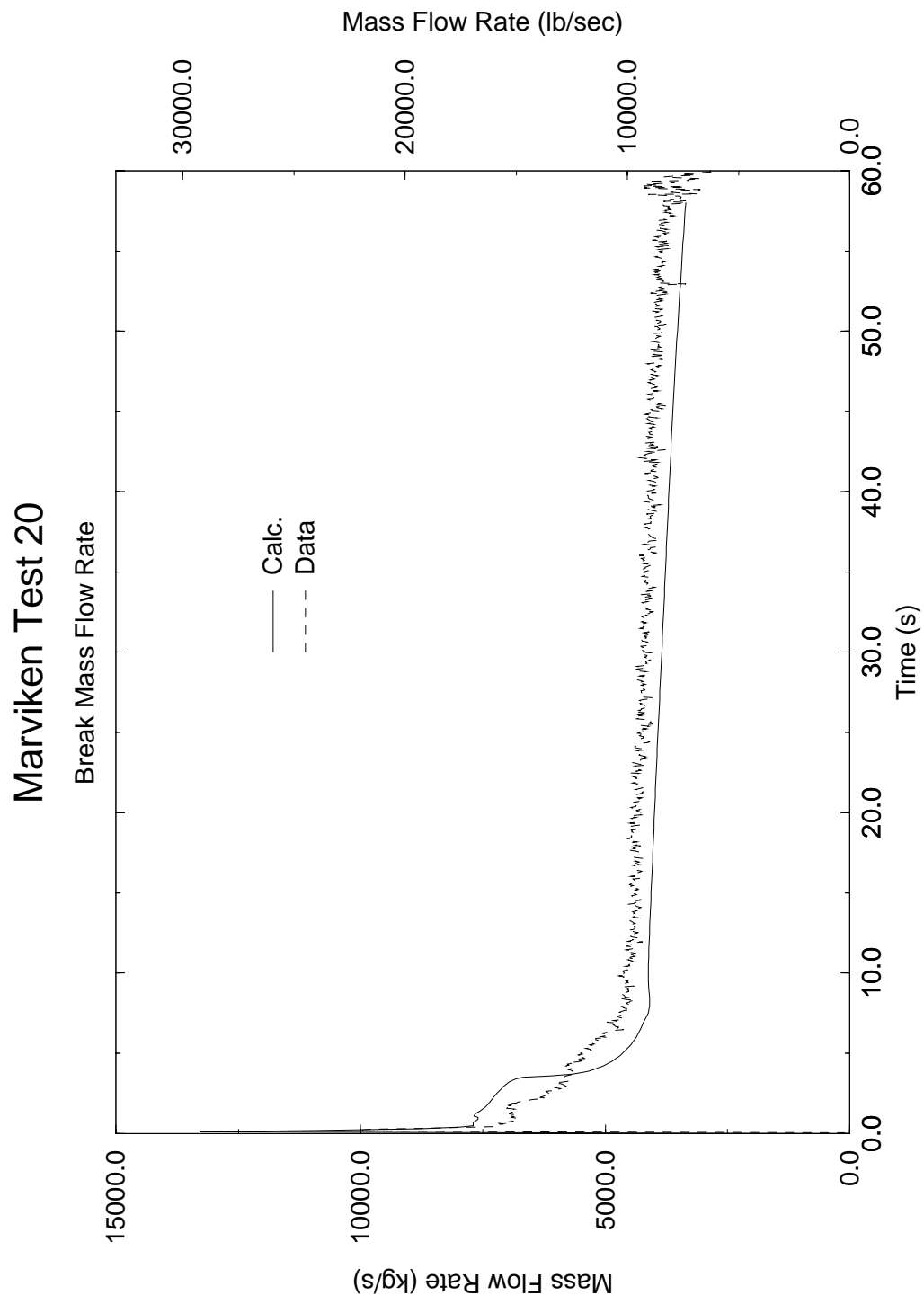


Figure 4.95 Comparison of Break Mass Flow Rates, Marviken Test 20

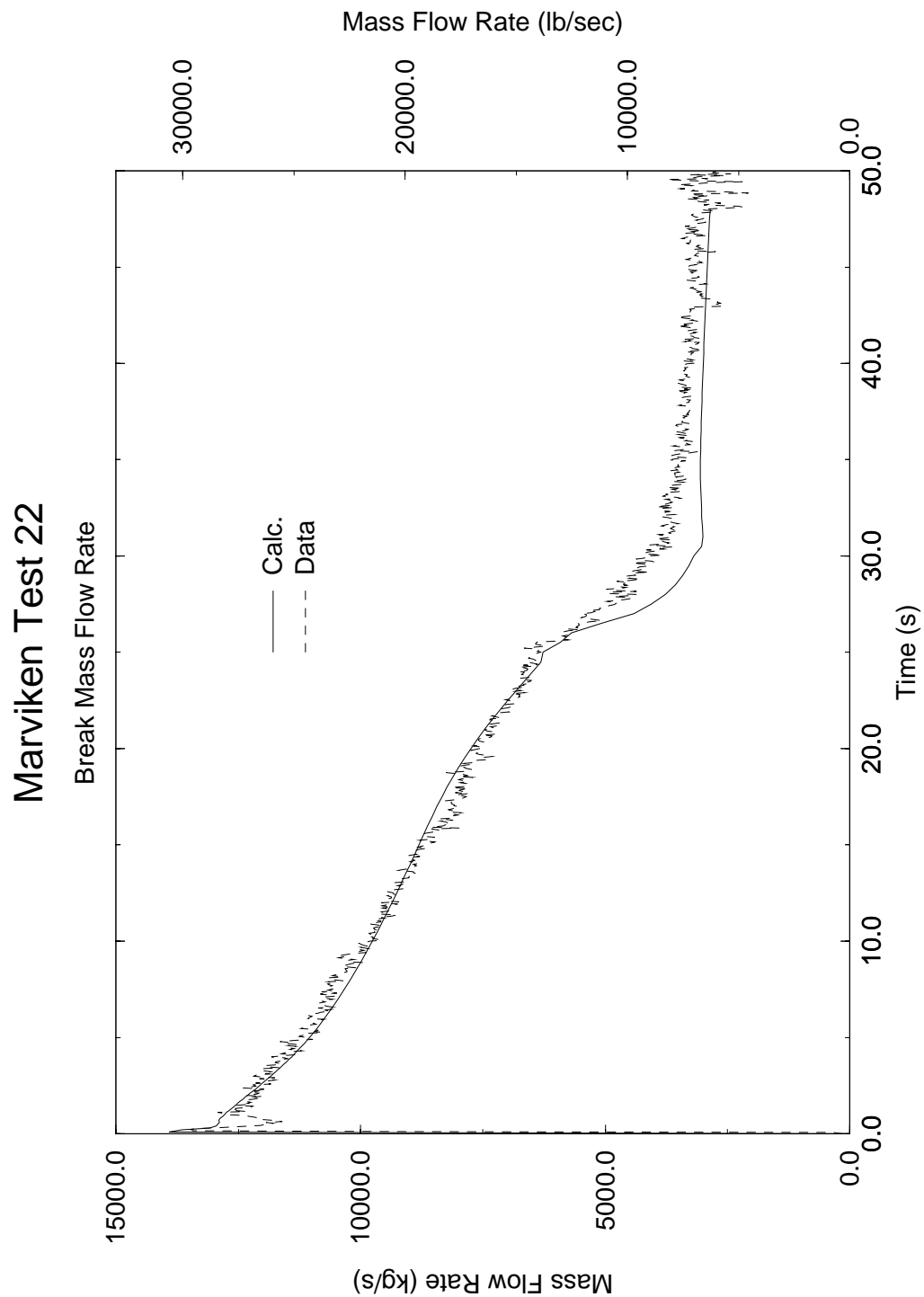


Figure 4.96 Comparison of Break Mass Flow Rates, Marviken Test 22

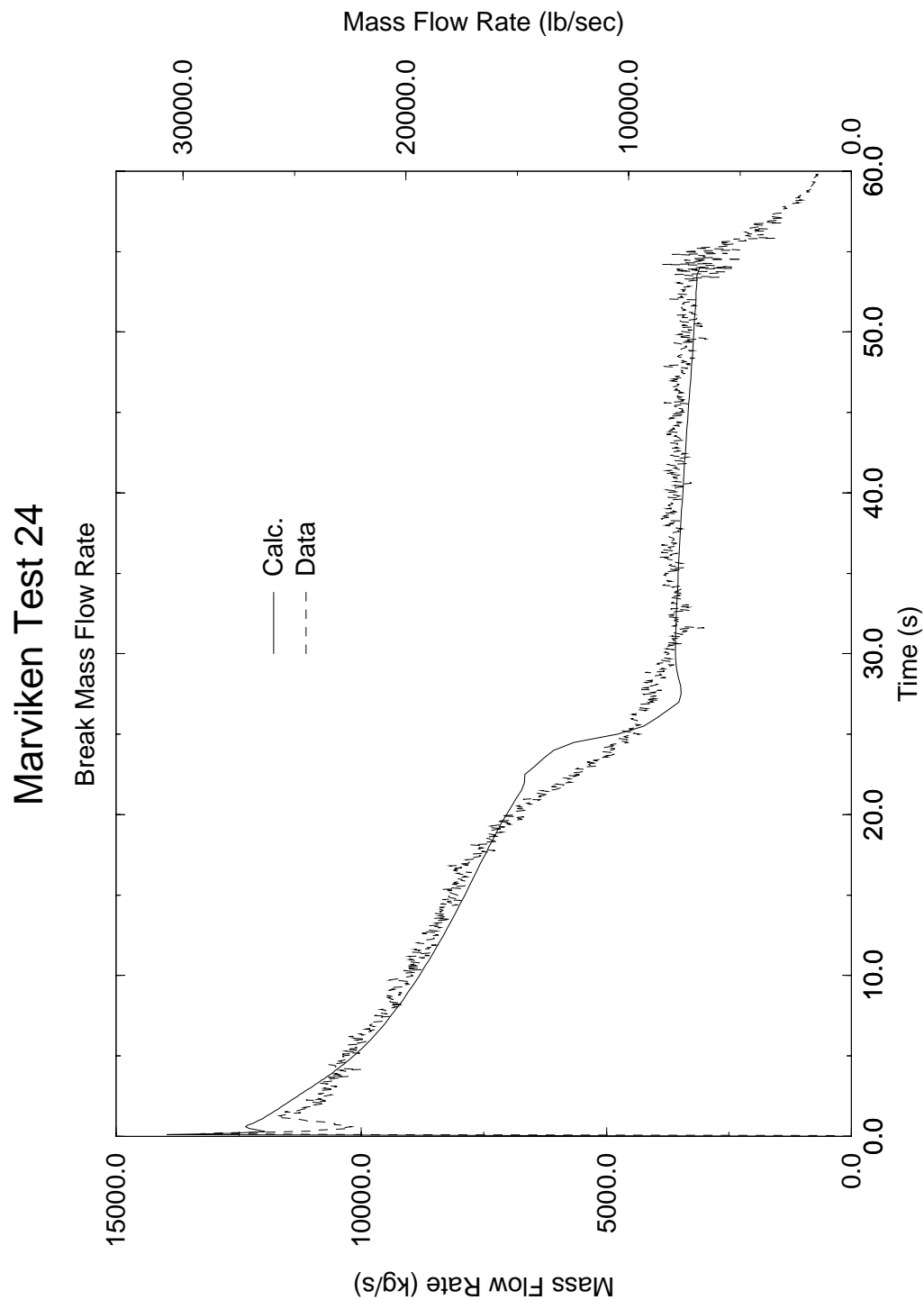


Figure 4.97 Comparison of Break Mass Flow Rates, Marviken Test 24

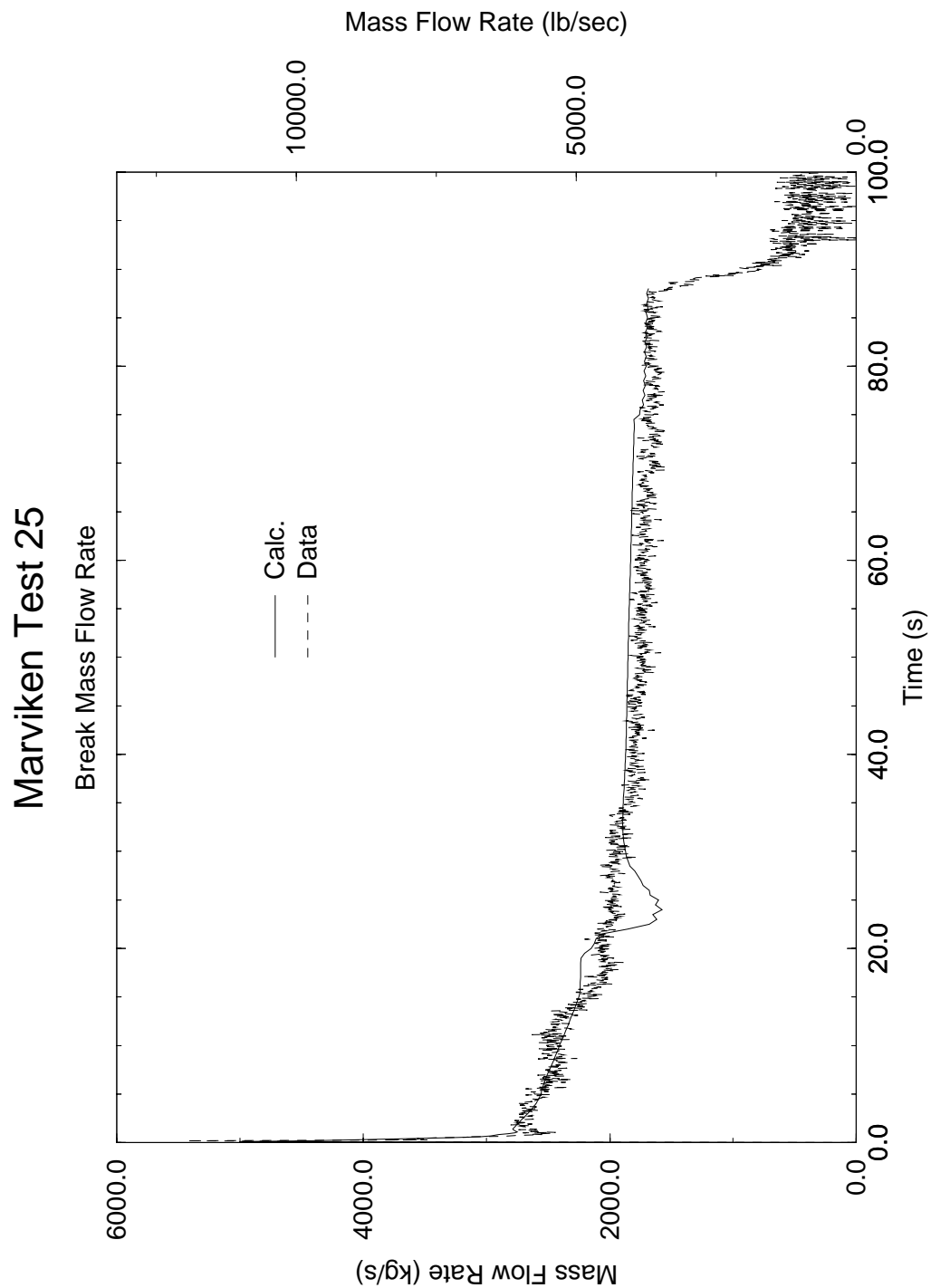
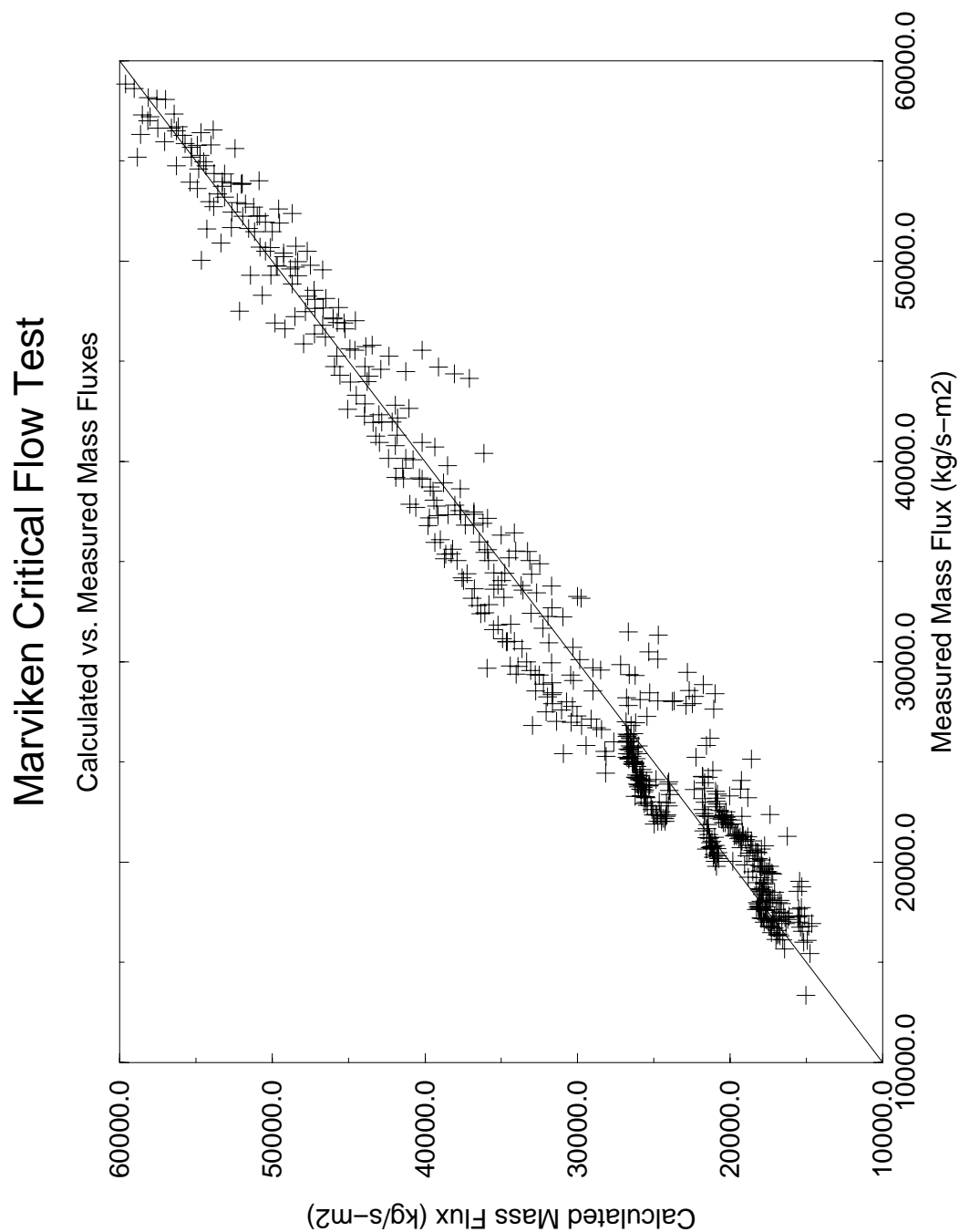


Figure 4.98 Comparison of Break Mass Flow Rates, Marviken Test 25



**Figure 4.99 Comparison of Calculated and Measured Mass Fluxes
(All Nine Marviken Tests)**

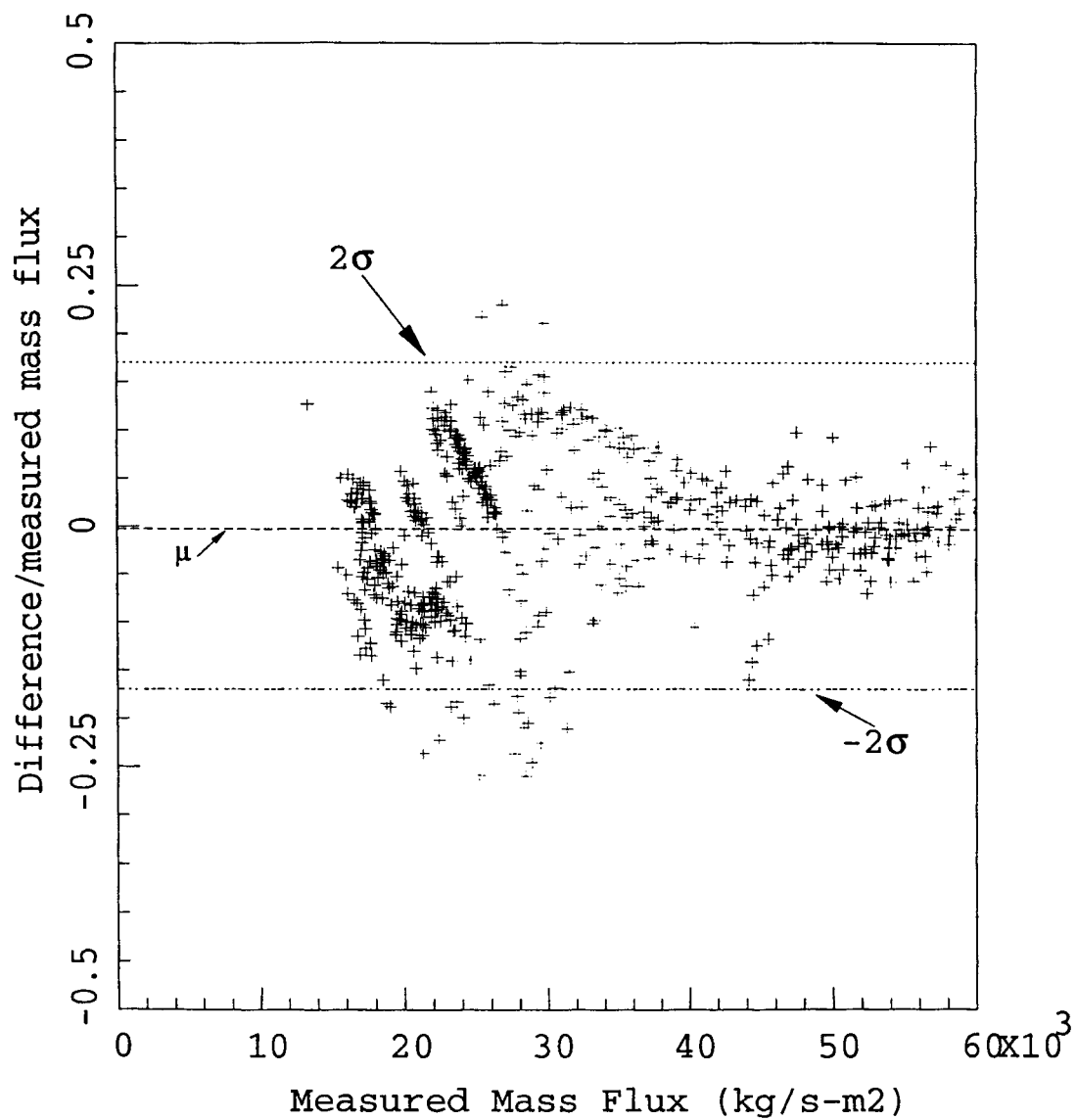


Figure 4.100 Break Flow Uncertainty, Marviken Tests

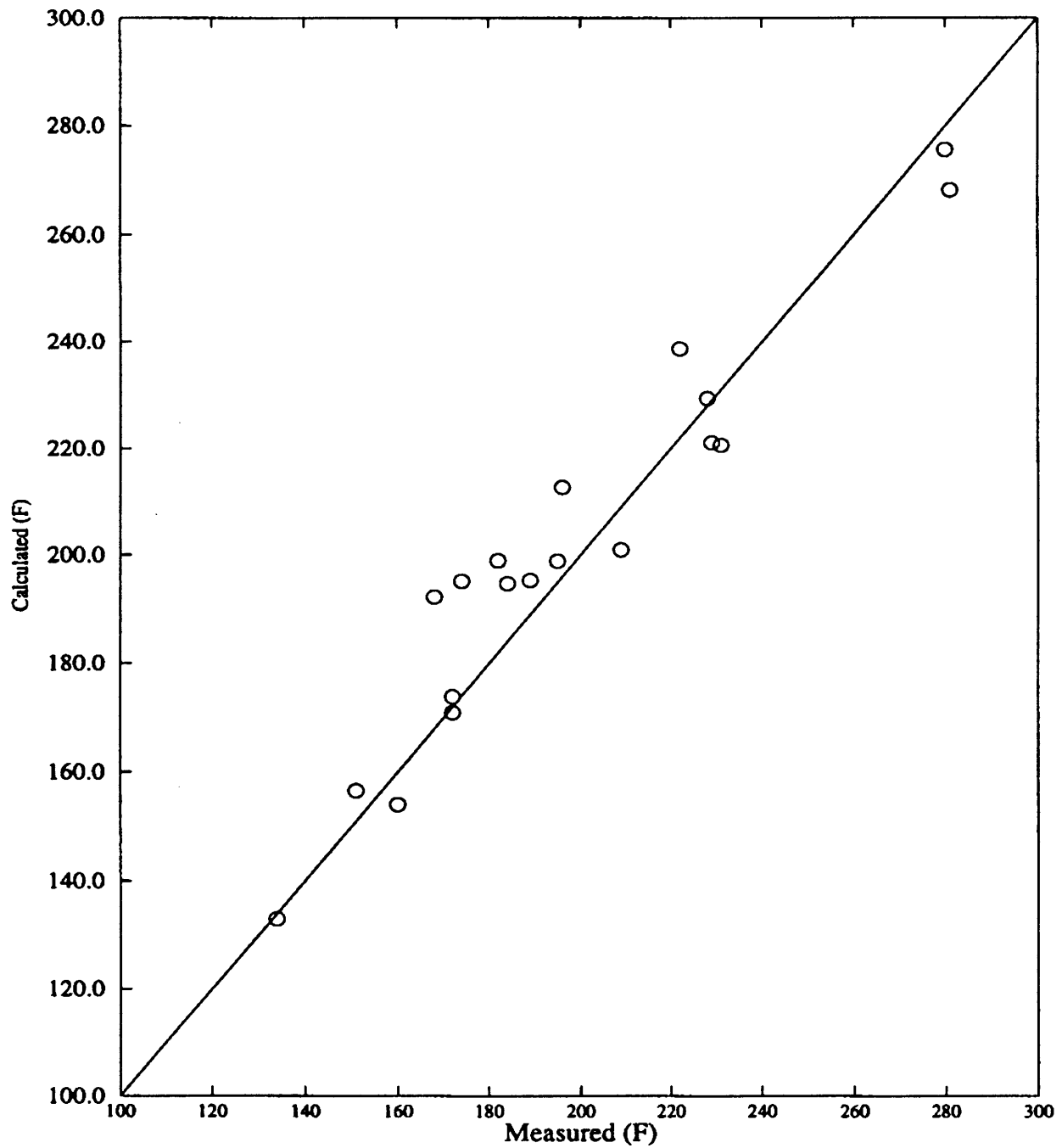
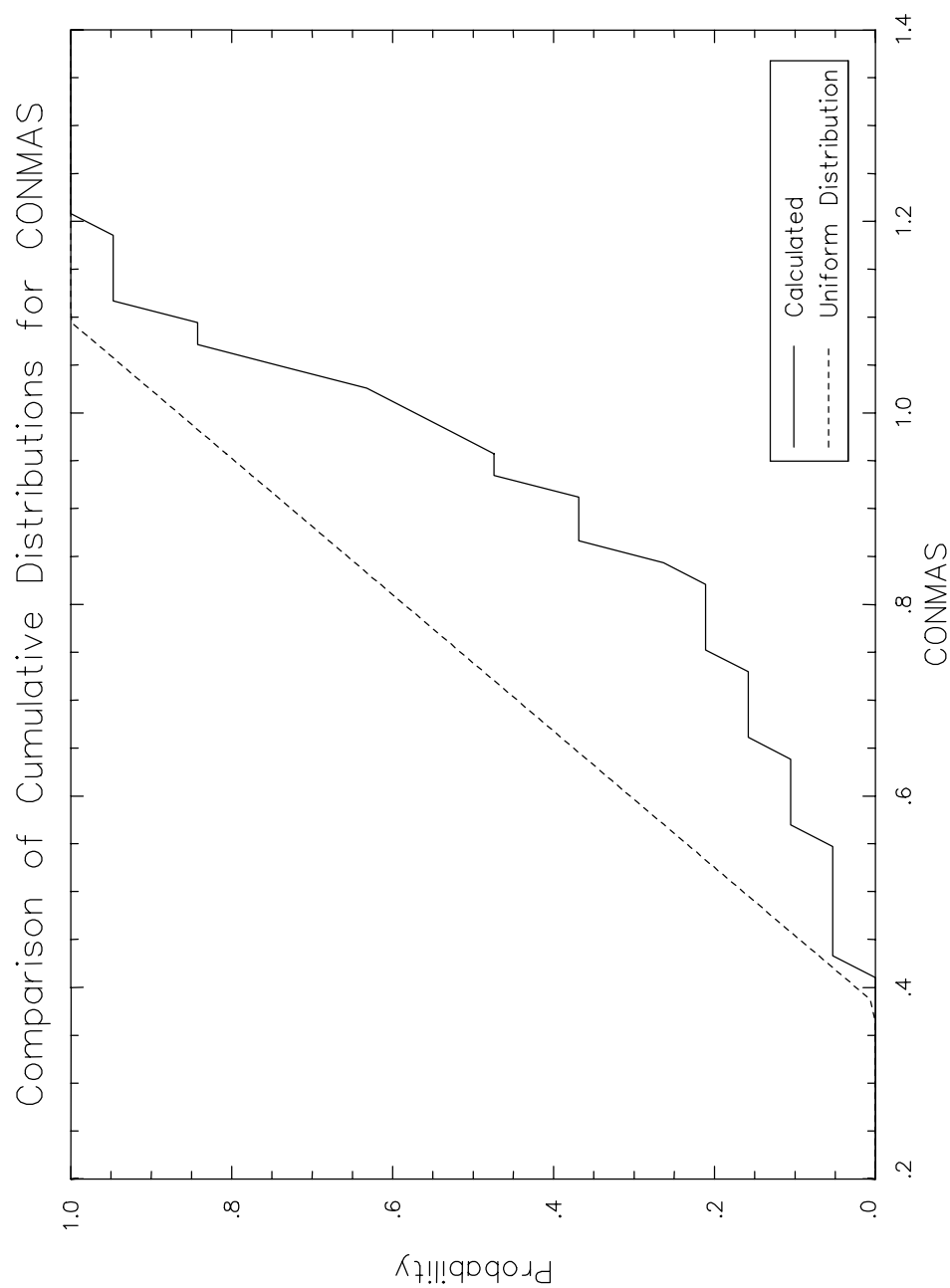


Figure 4.101 Comparison of Calculated and Measured Effluent Temperature for the Plant-Specific Model, Westinghouse/EPRI



**Figure 4.102 Cumulative Distribution Plots for CONMAS,
Westinghouse/EPRI**

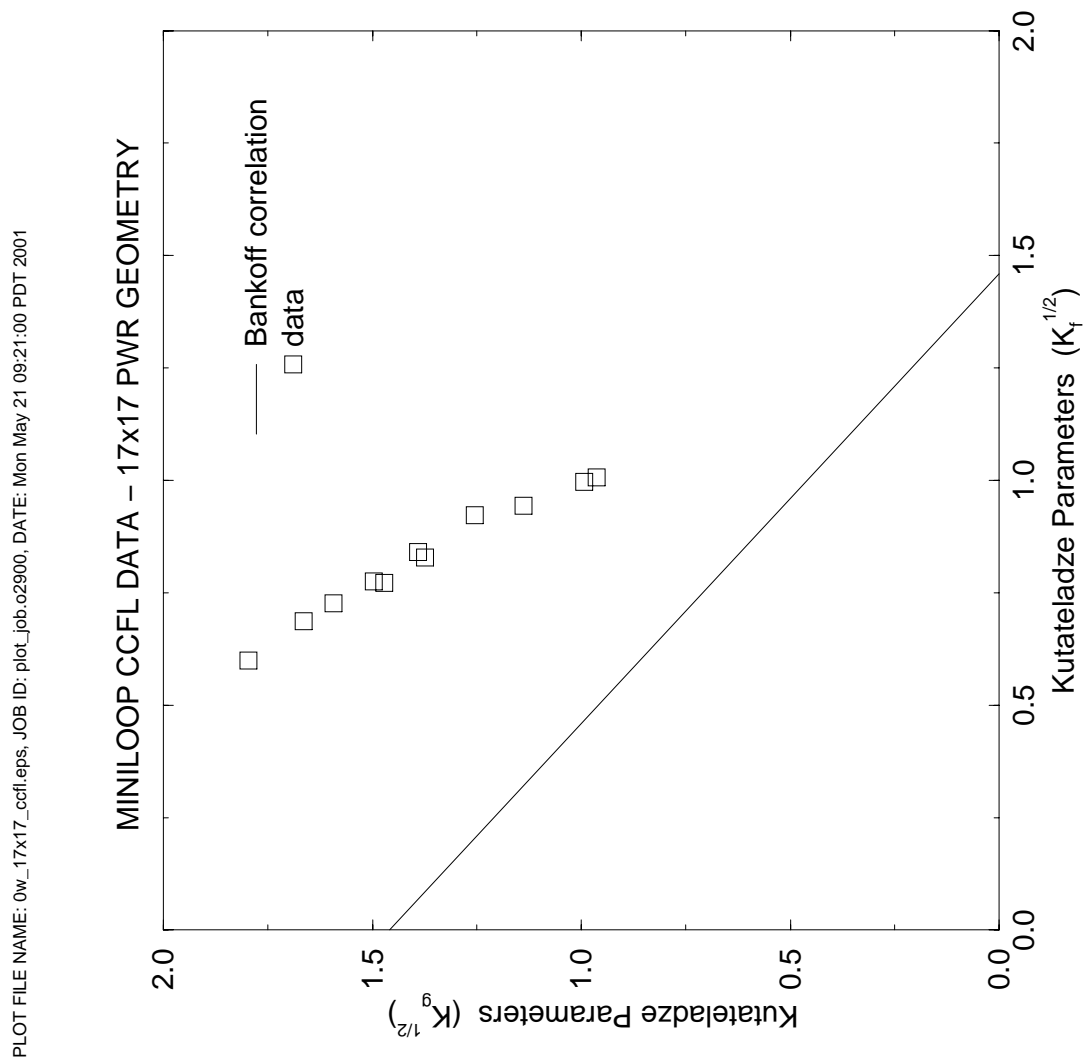


Figure 4.103 Comparison Between Mini-Loop CCFL Data of a Westinghouse 17 x 17 UTP and Bankoff

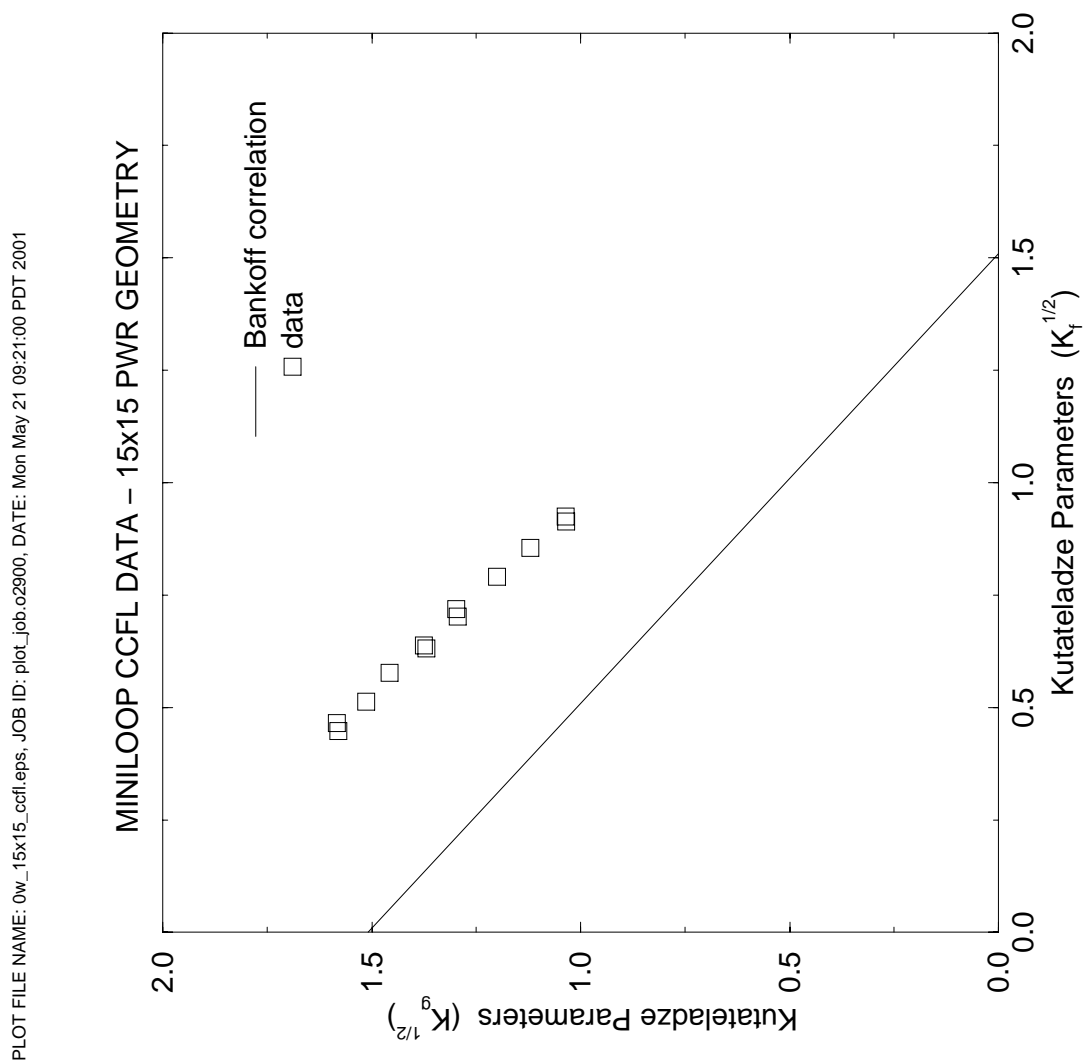


Figure 4.104 Comparison Between Mini-Loop CCFL Data of a Westinghouse 15 x 15 UTP and Bankoff

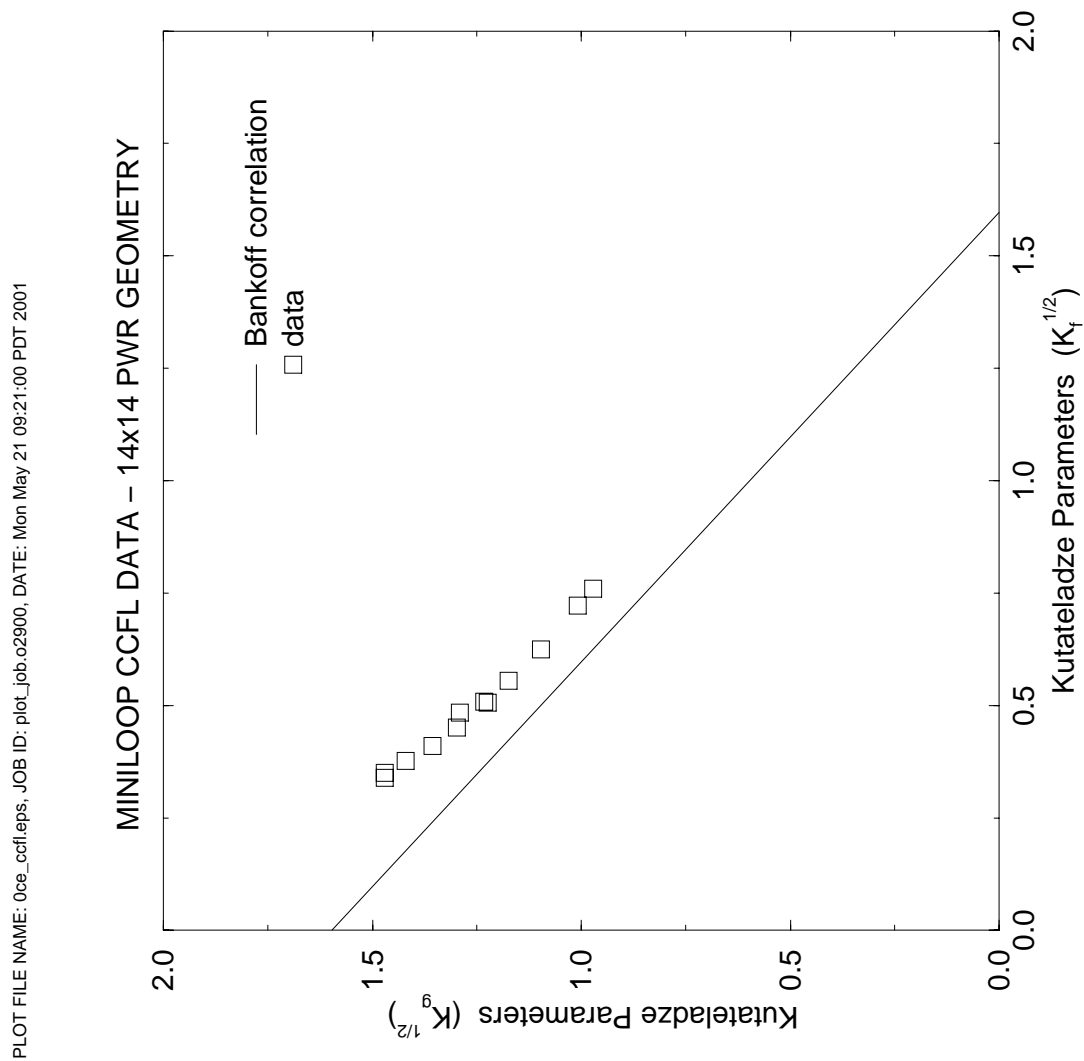
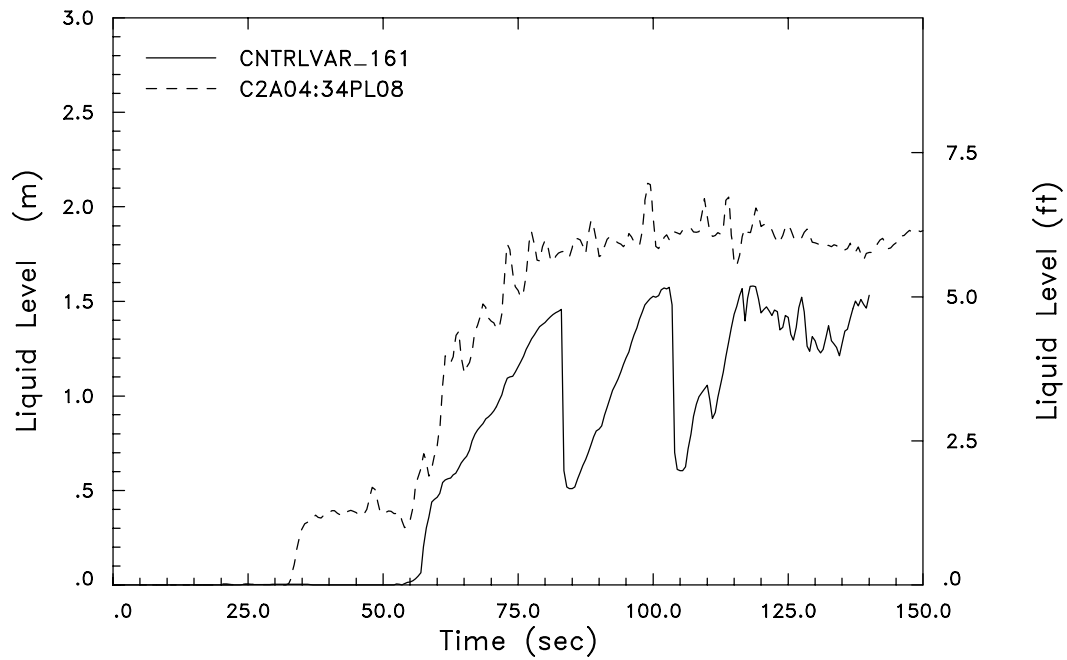
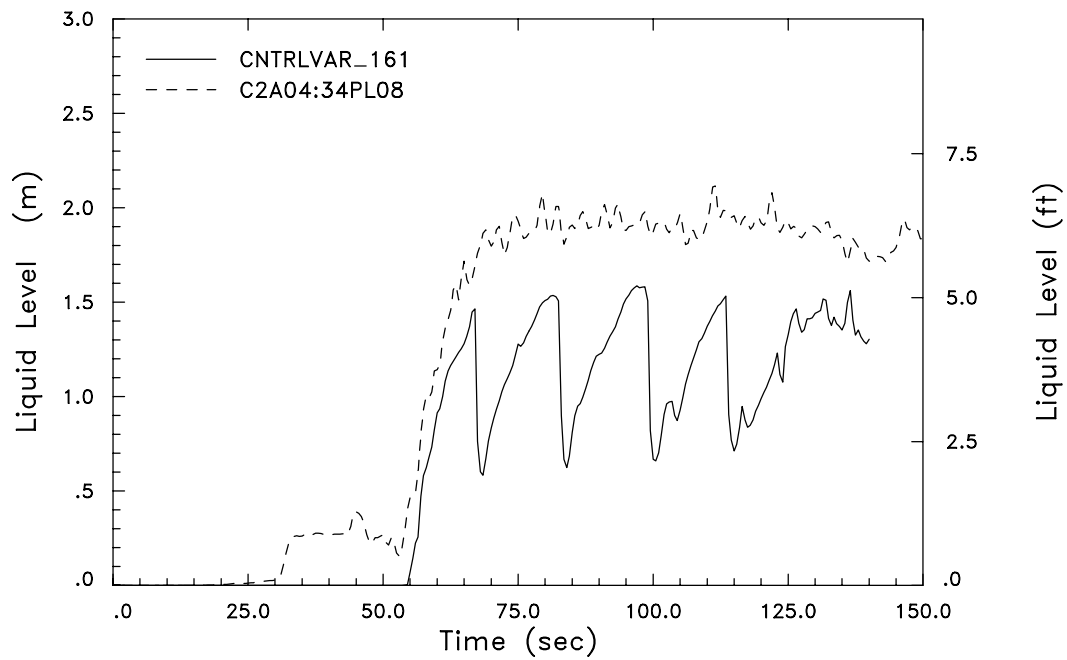


Figure 4.105 Comparison Between Mini-Loop CCFL Data of a Combustion Engineering 14 x 14 UTP and Bankoff



**Figure 4.106 Lower Plenum Liquid Level Comparison
UPTF Test 6 – Run 131**



**Figure 4.107 Lower Plenum Liquid Level Comparison
UPTF Test 6 – Run 132**

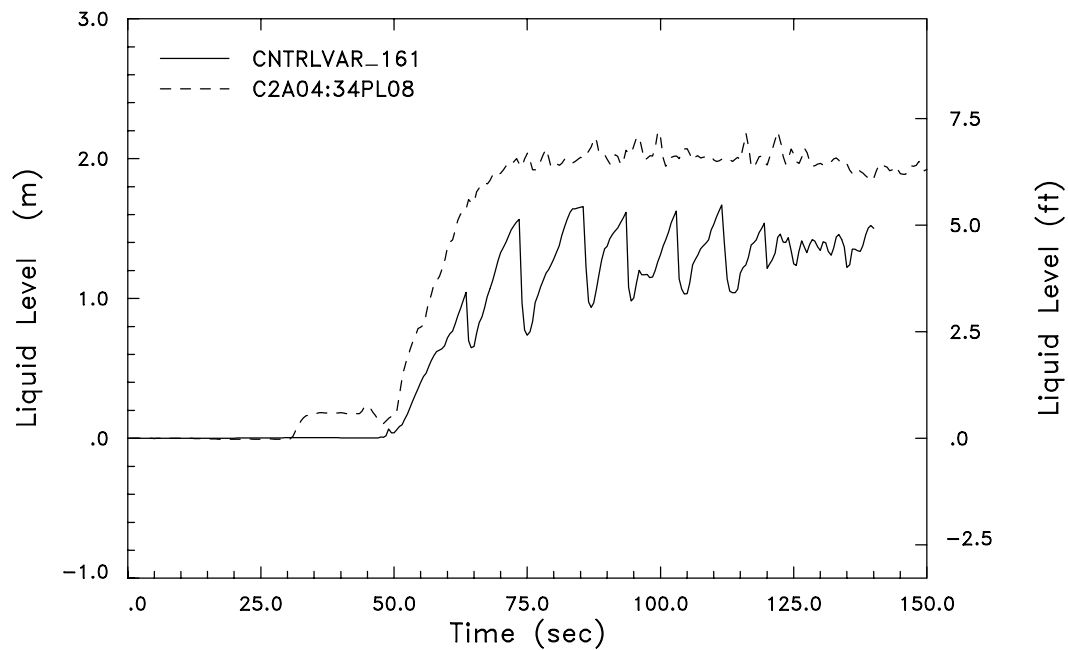


**Figure 4.108 Lower Plenum Liquid Level Comparison
UPTF Test 6 – Run 133**

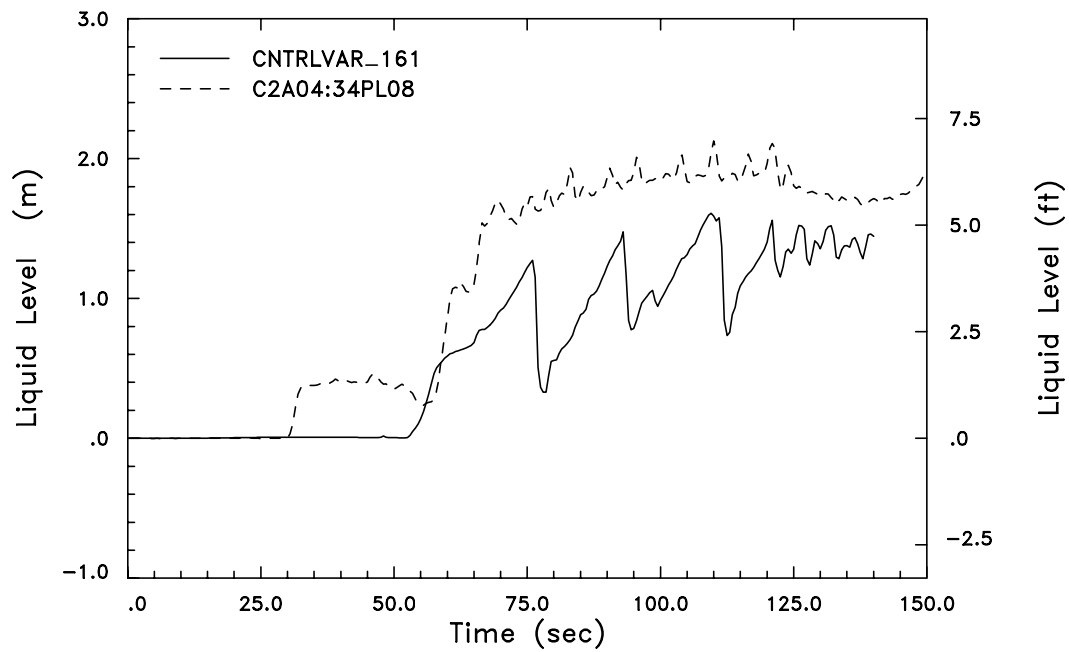


**Figure 4.109 Lower Plenum Liquid Level Comparison
UPTF Test 6 – Run 135**

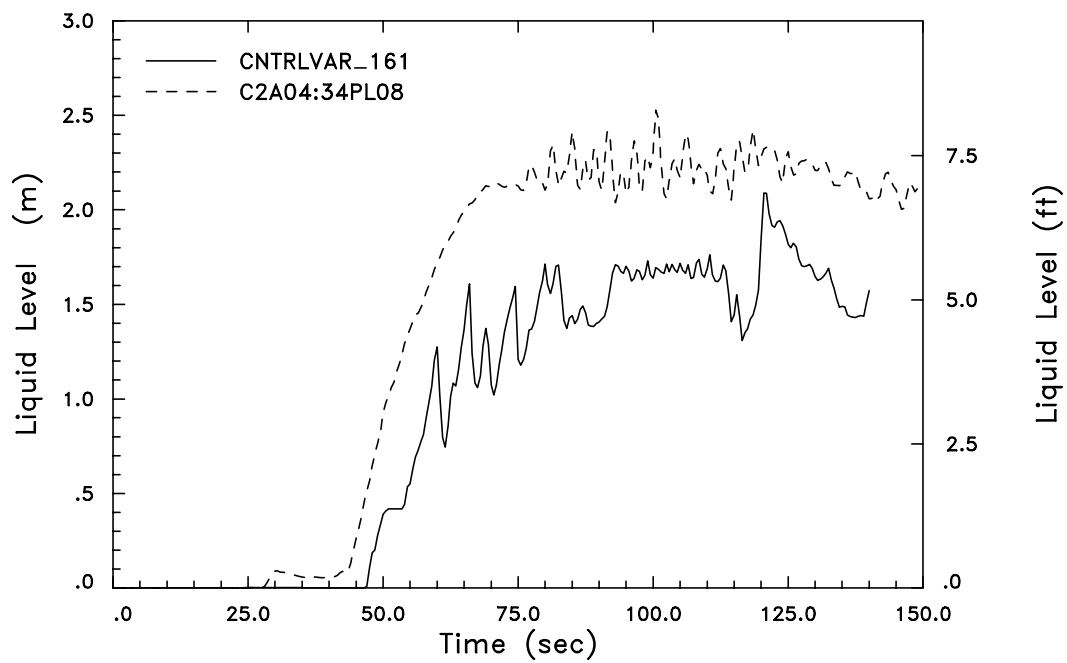


**Figure 4.110 Lower Plenum Liquid Level Comparison
UPTF Test 6 – Run 136**

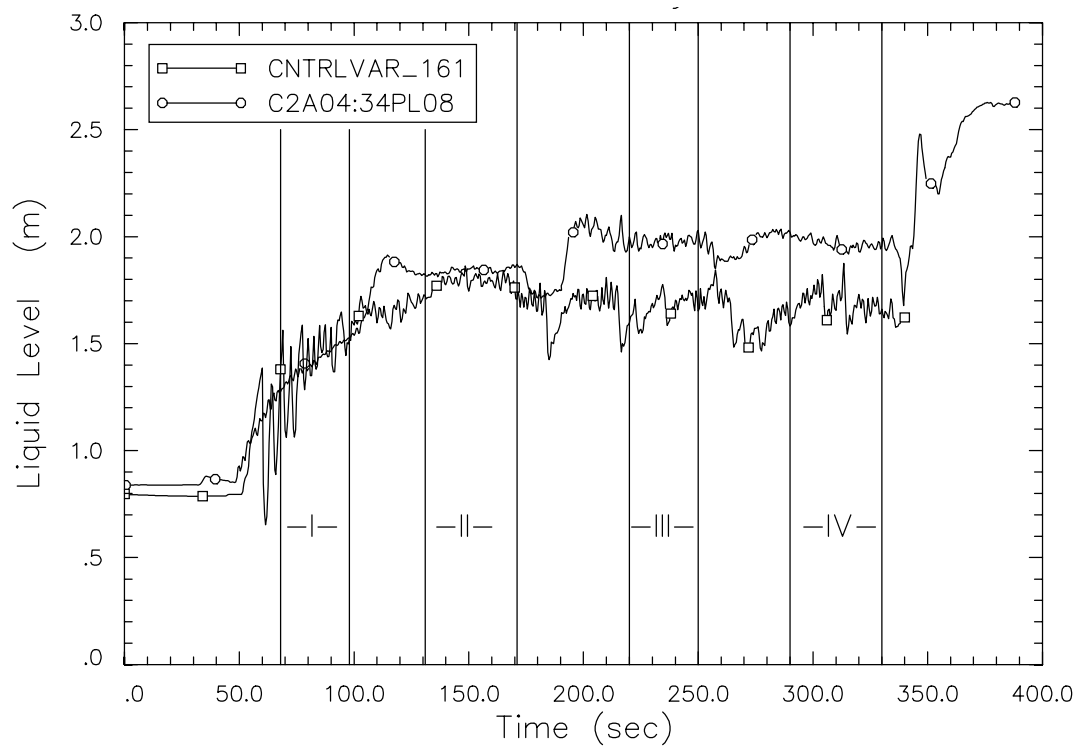


**Figure 4.111 Lower Plenum Liquid Level Comparison
UPTF Test 7 – Run 203**

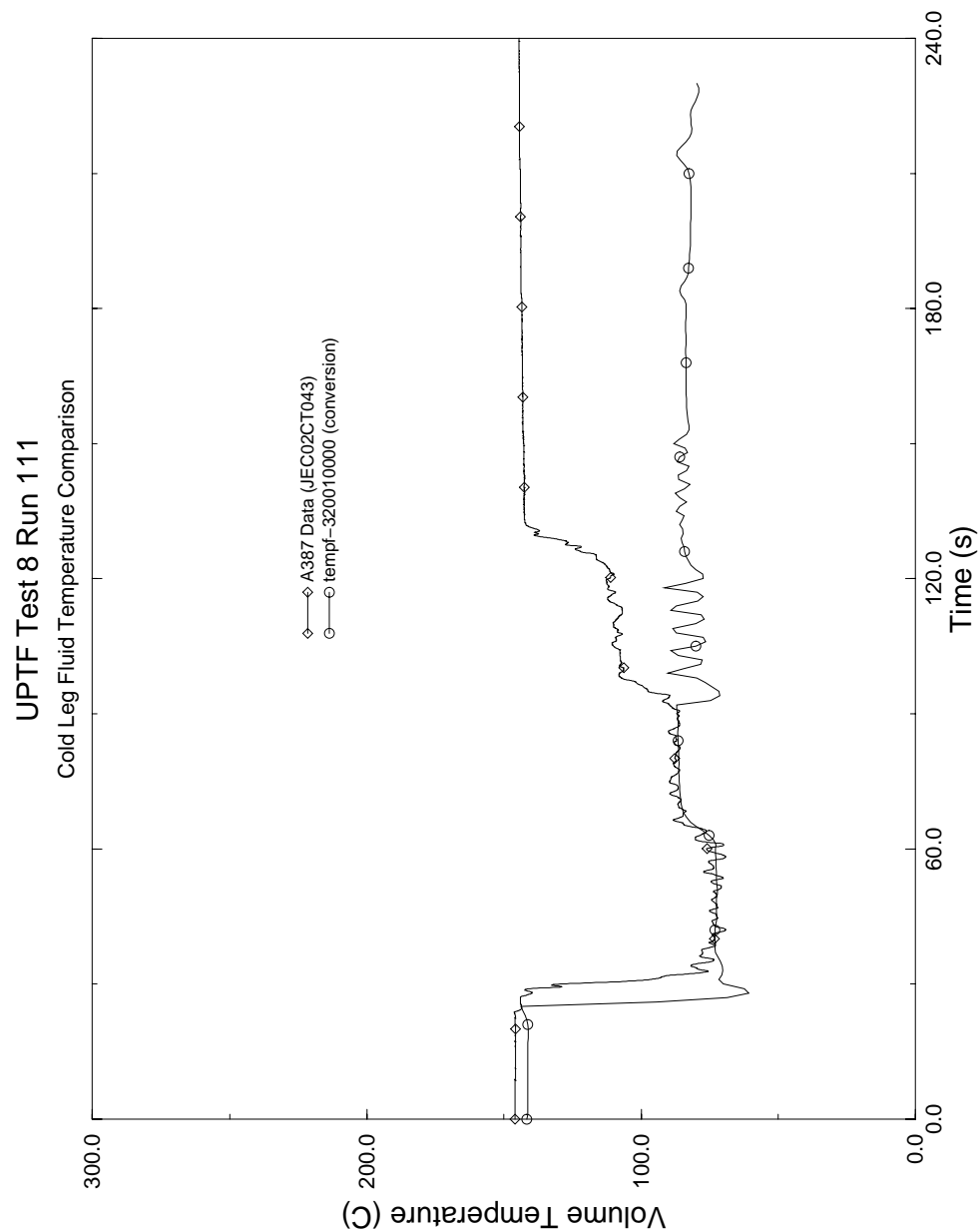


Figure 4.112 UPTF Data/S-RELAP5 Cold Leg Temperature Comparison, UPTF Test 8 Run 111

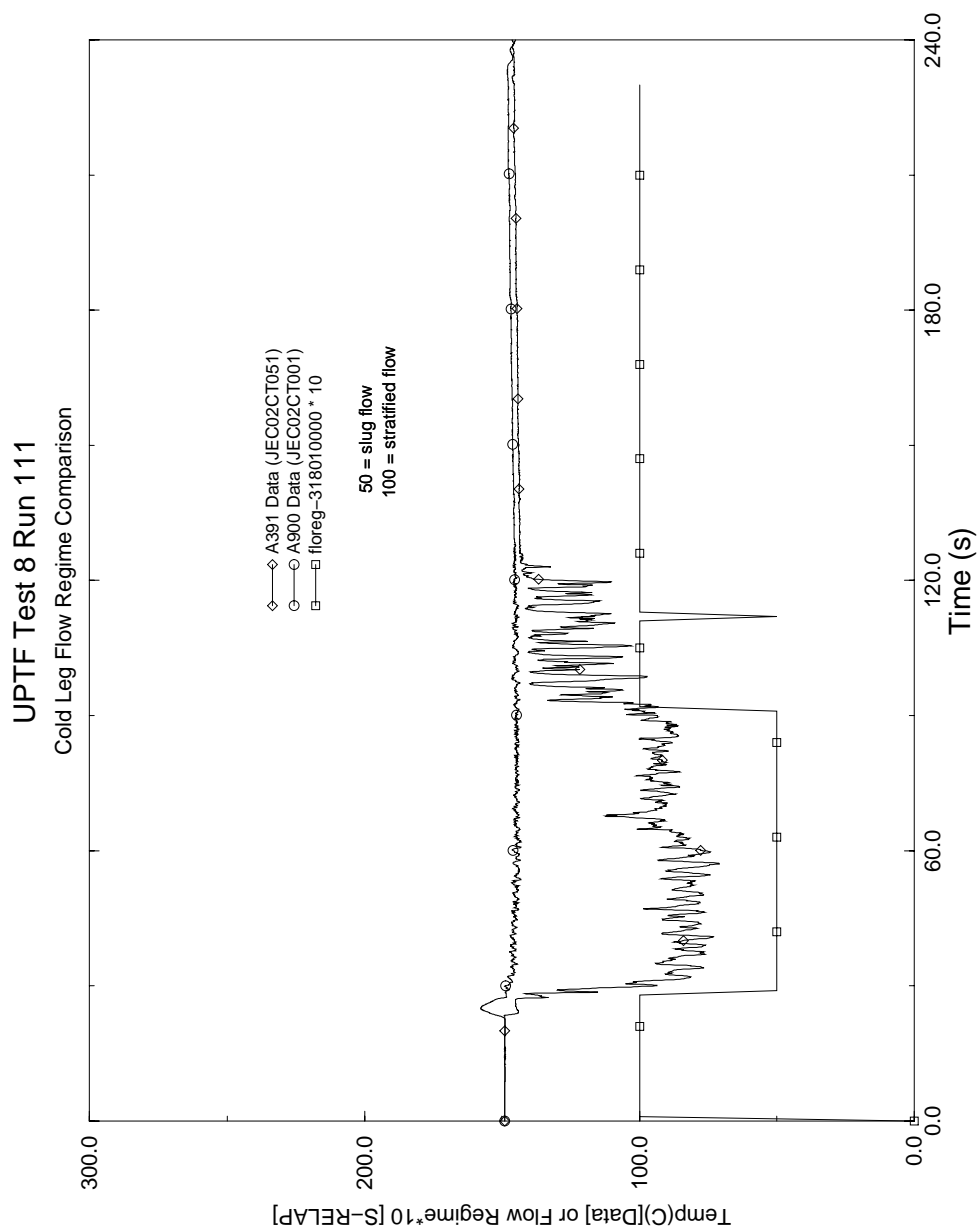


Figure 4.113 UPTF Data/S-RELAP5 Flow Regime Comparison, UPTF Test 8 Run 111

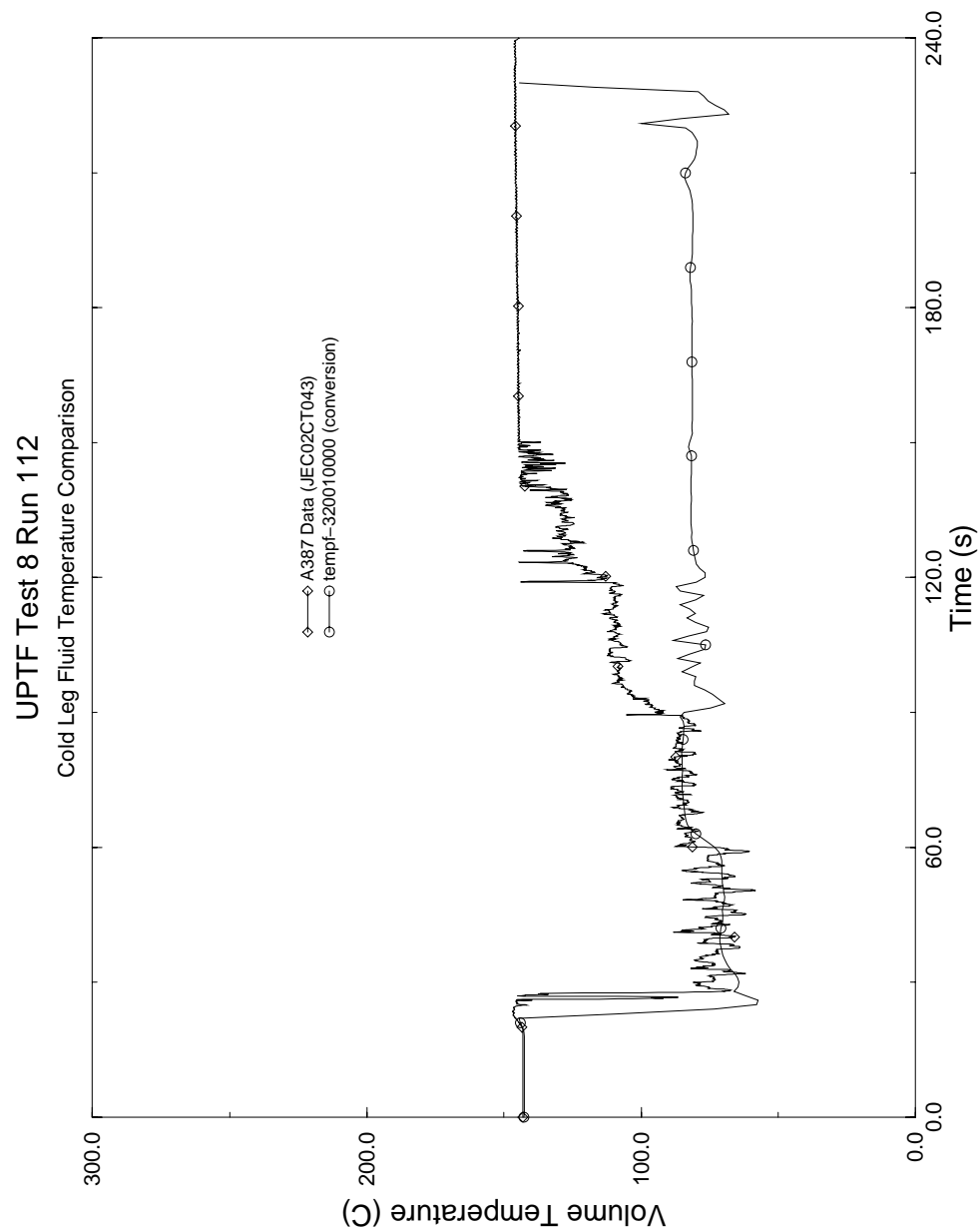


Figure 4.114 UPTF Data/S-RELAP5 Cold Leg Temperature Comparison, UPTF Test 8 Run 112

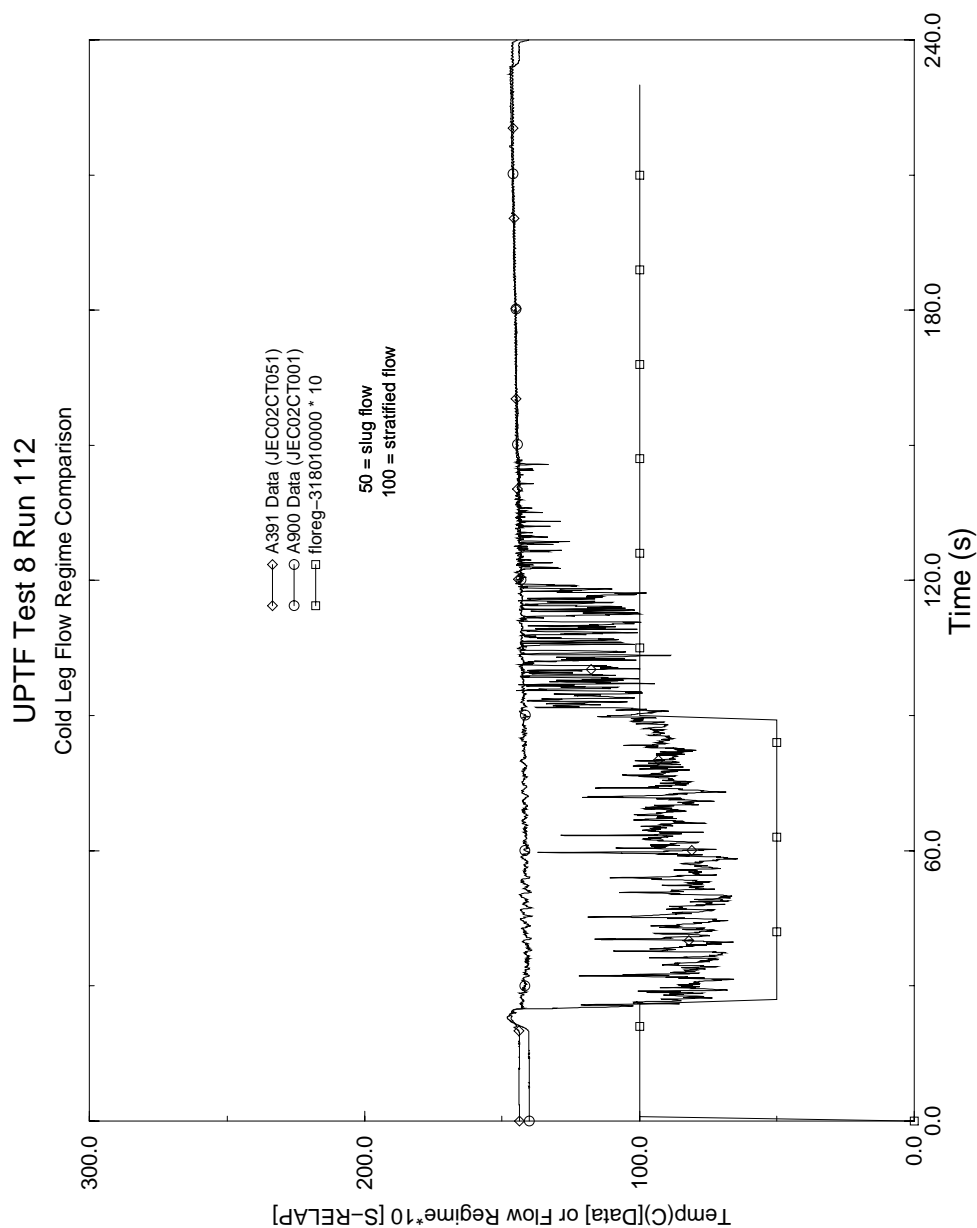
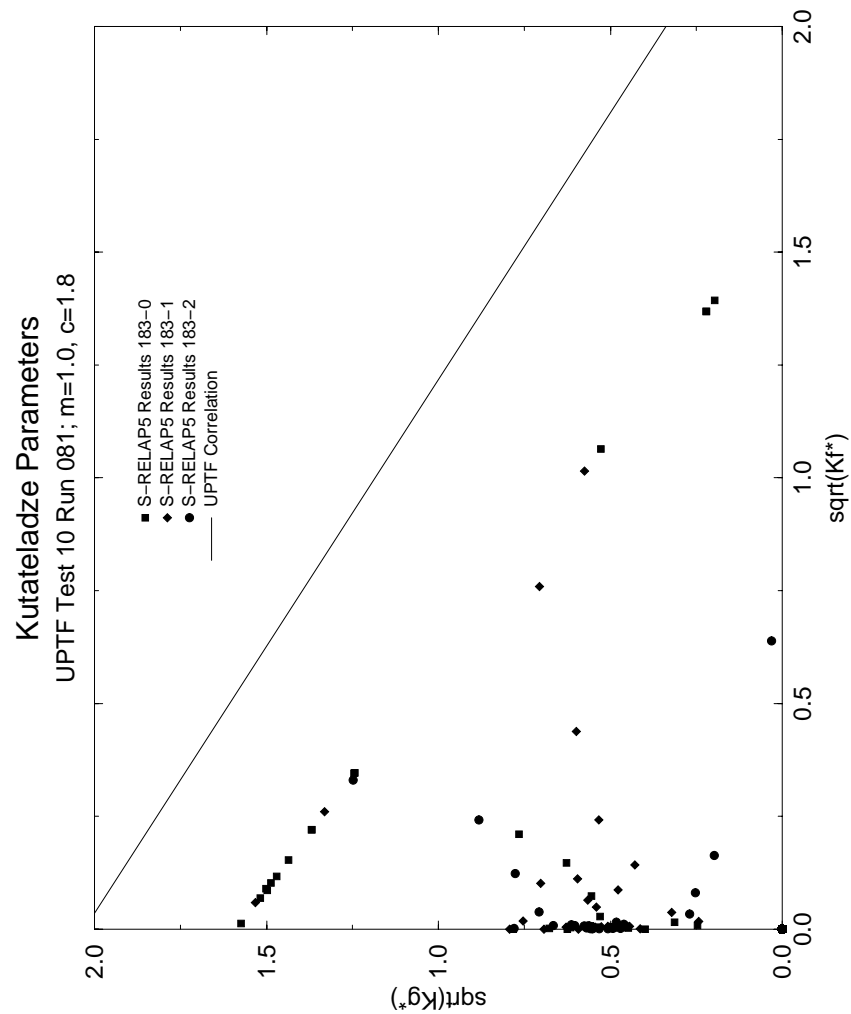


Figure 4.115 UPTF Data/S-RELAP5 Flow Regime Comparison, UPTF Test 8 Run 112



**Figure 4.116 Countercurrent Flow of Steam and Water
UPTF Test 10 Run 081**

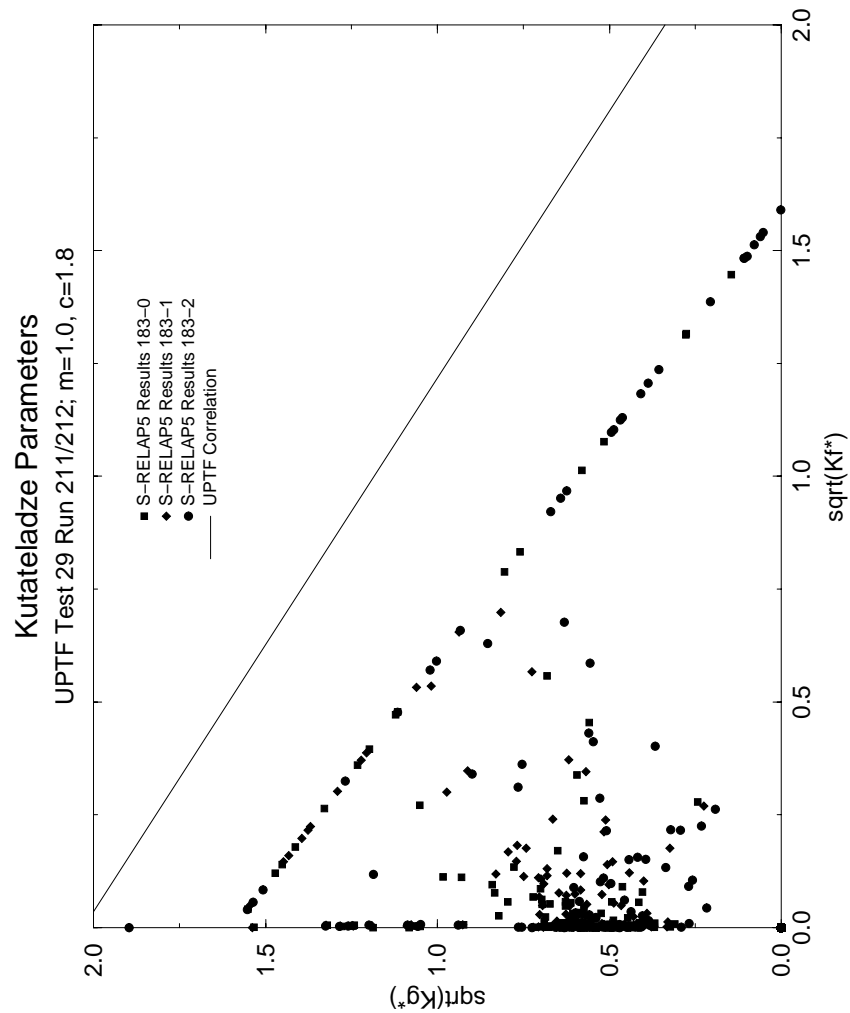
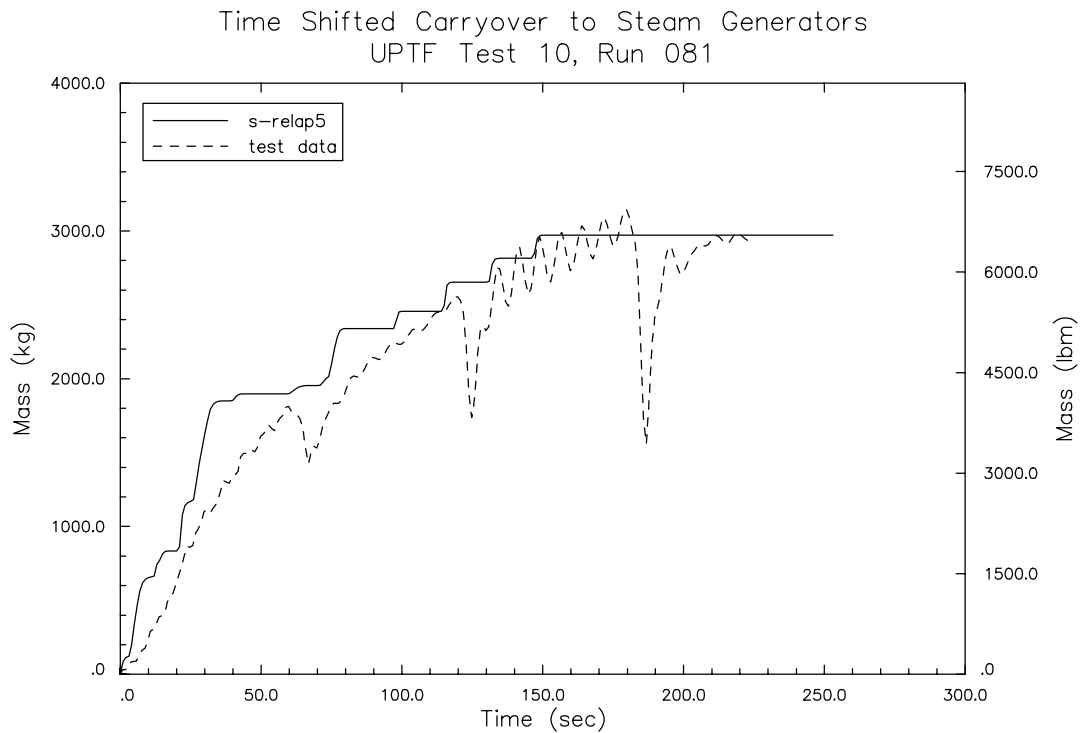
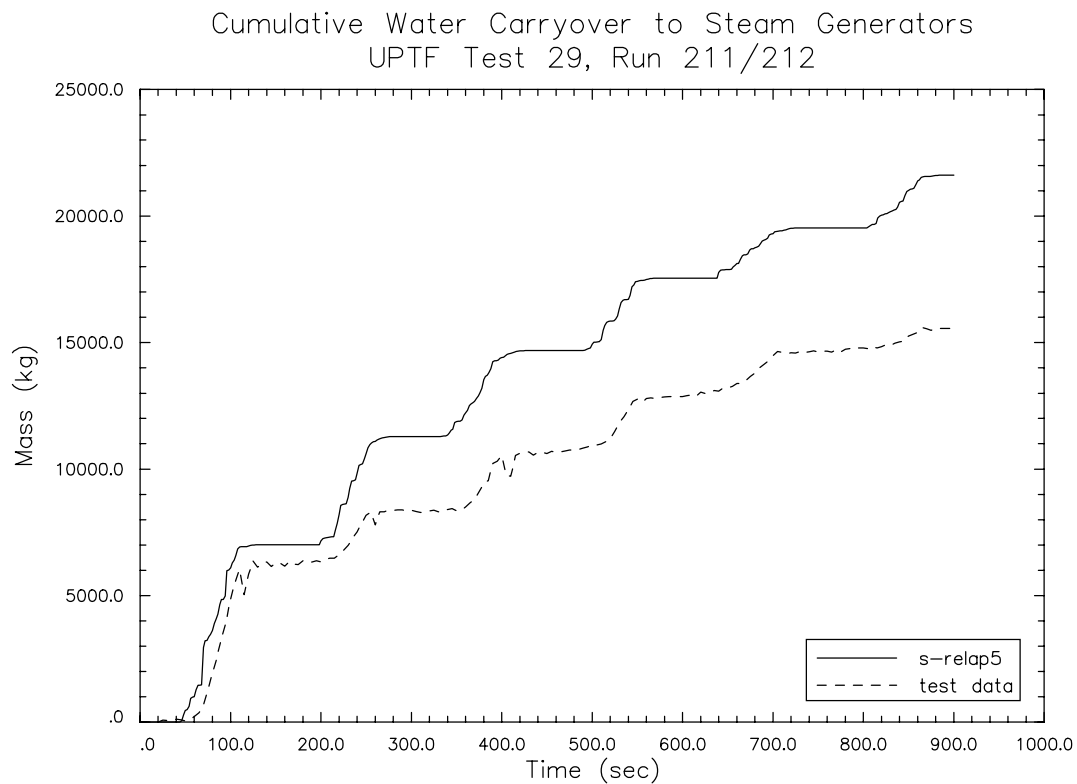


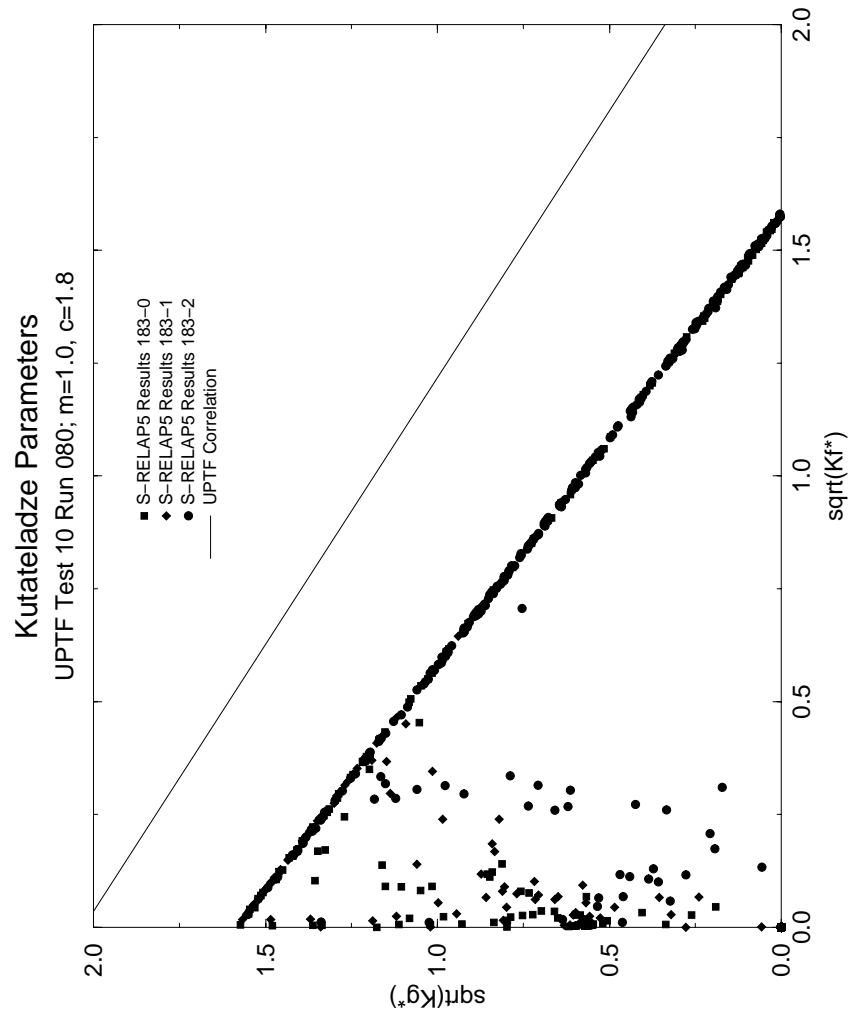
Figure 4.117 Countercurrent Flow of Steam and Water
UPTF Test 29 Run 212/211



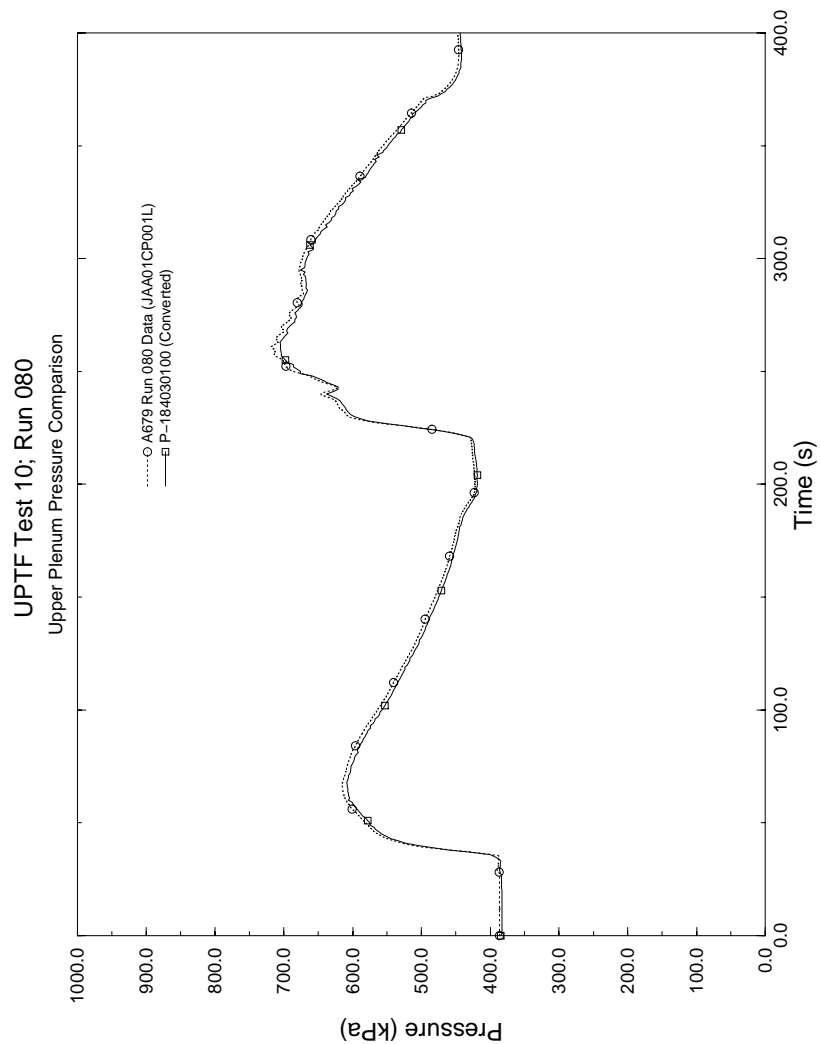
**Figure 4.118 Carryover to Steam Generators Test 10 Run 081
Beyond 150 sec.**



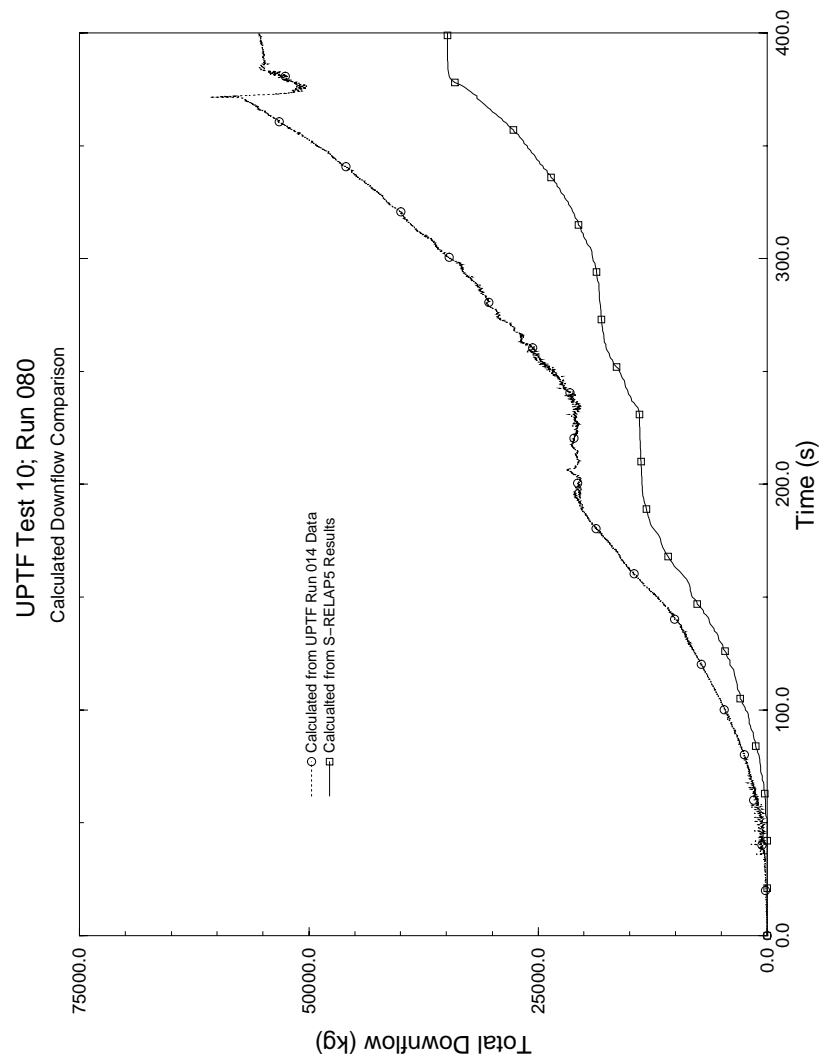
**Figure 4.119 Cumulative Water Carryover to Steam Generators
Test 29 Run 212/211**



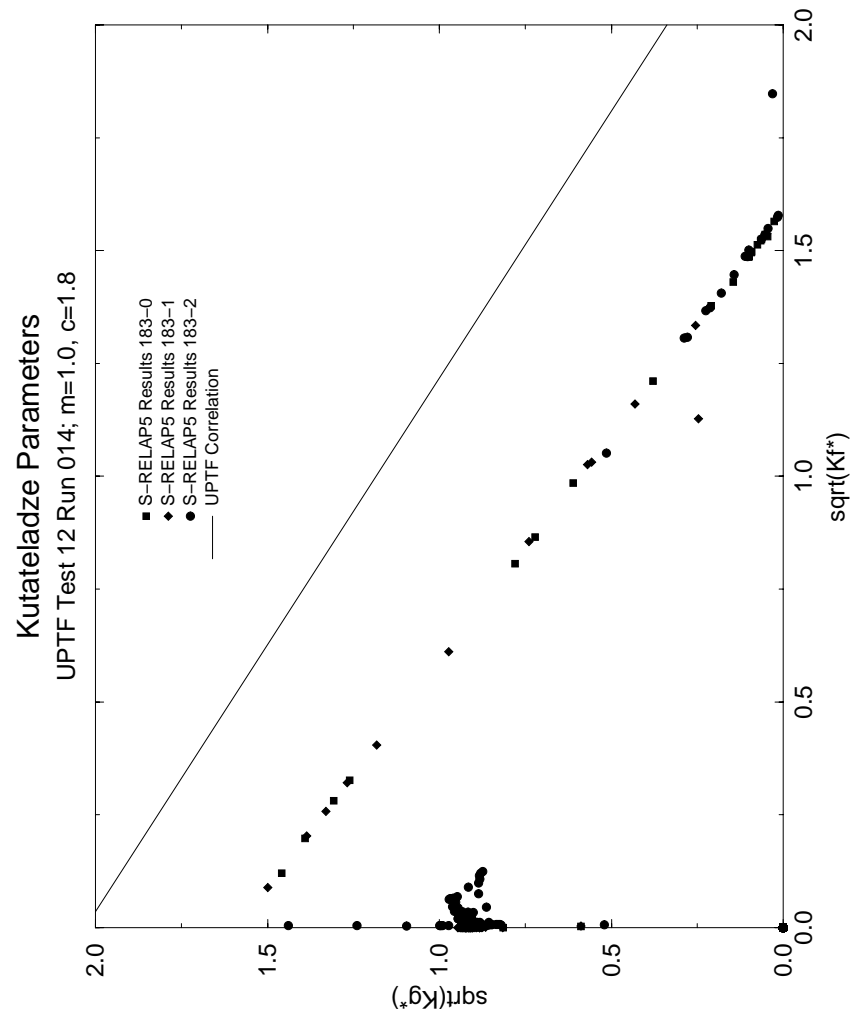
**Figure 4.120 Counter Current Flow of Steam and Water,
UPTF Test 10, Run 080**



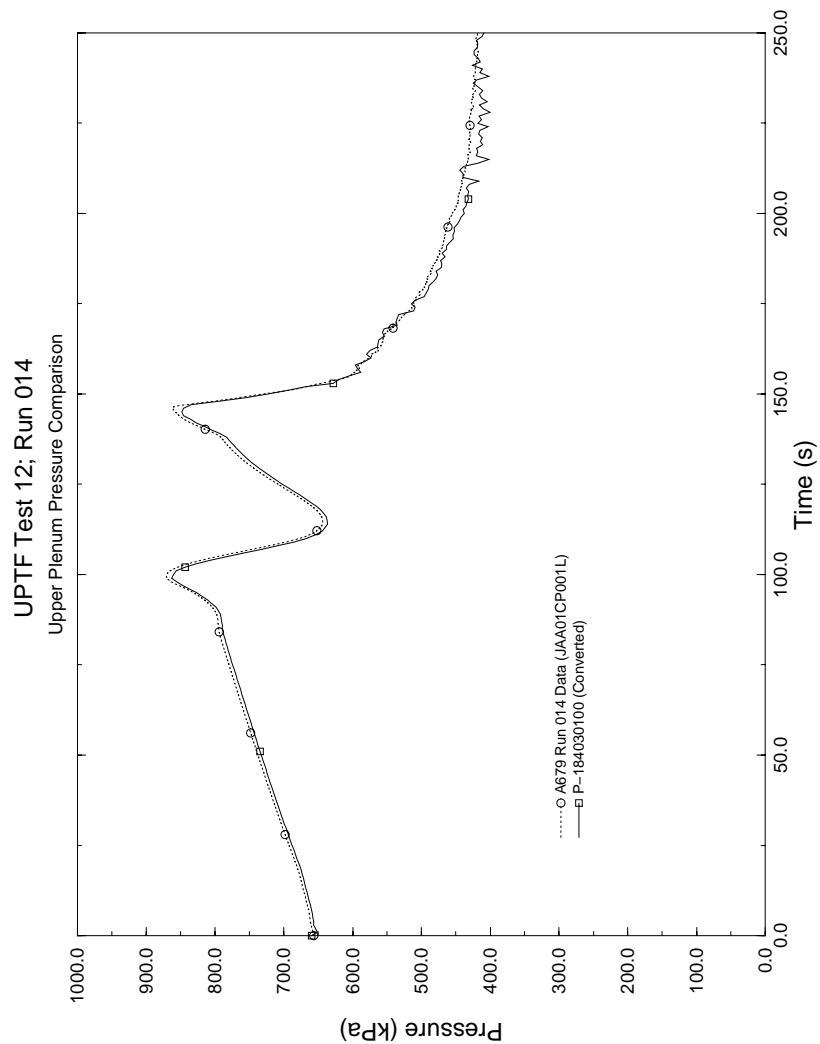
**Figure 4.121 Upper Plenum Pressure Comparison
Test 10, Run 080**



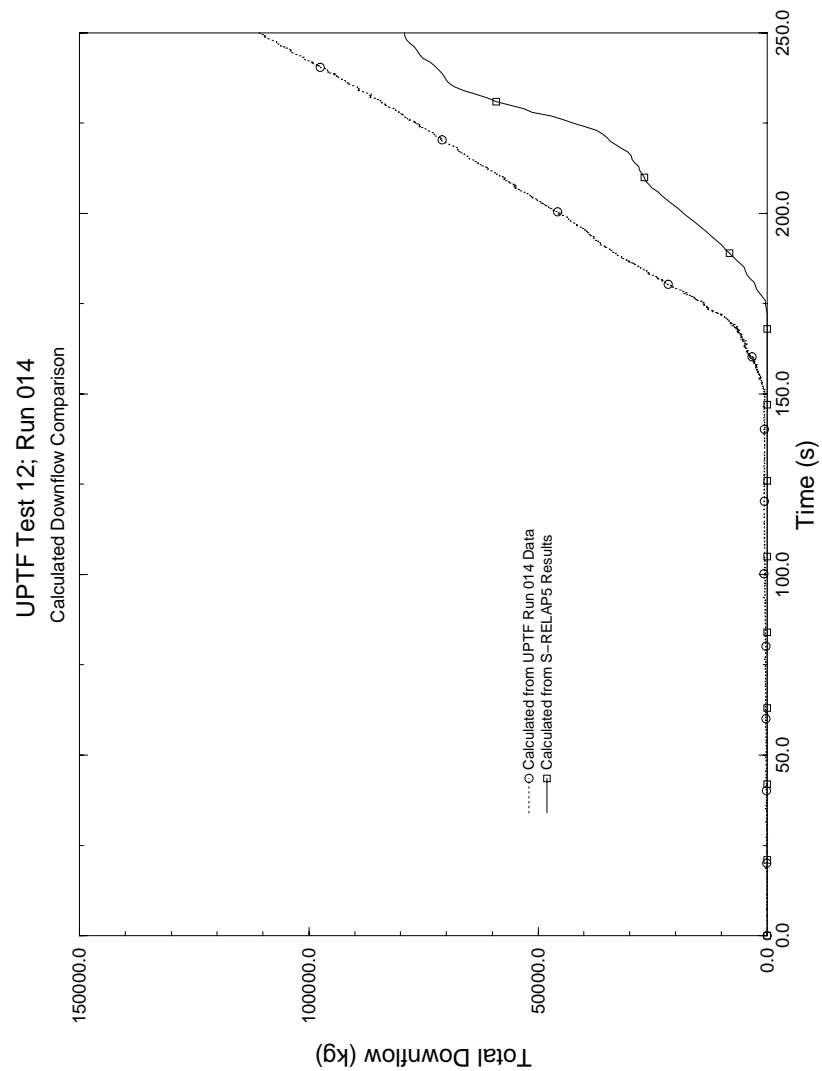
**Figure 4.122 Calculated Downflow Comparison UPTF Test 10,
Run 080 ($m=1.0$, $c=1.8$)**



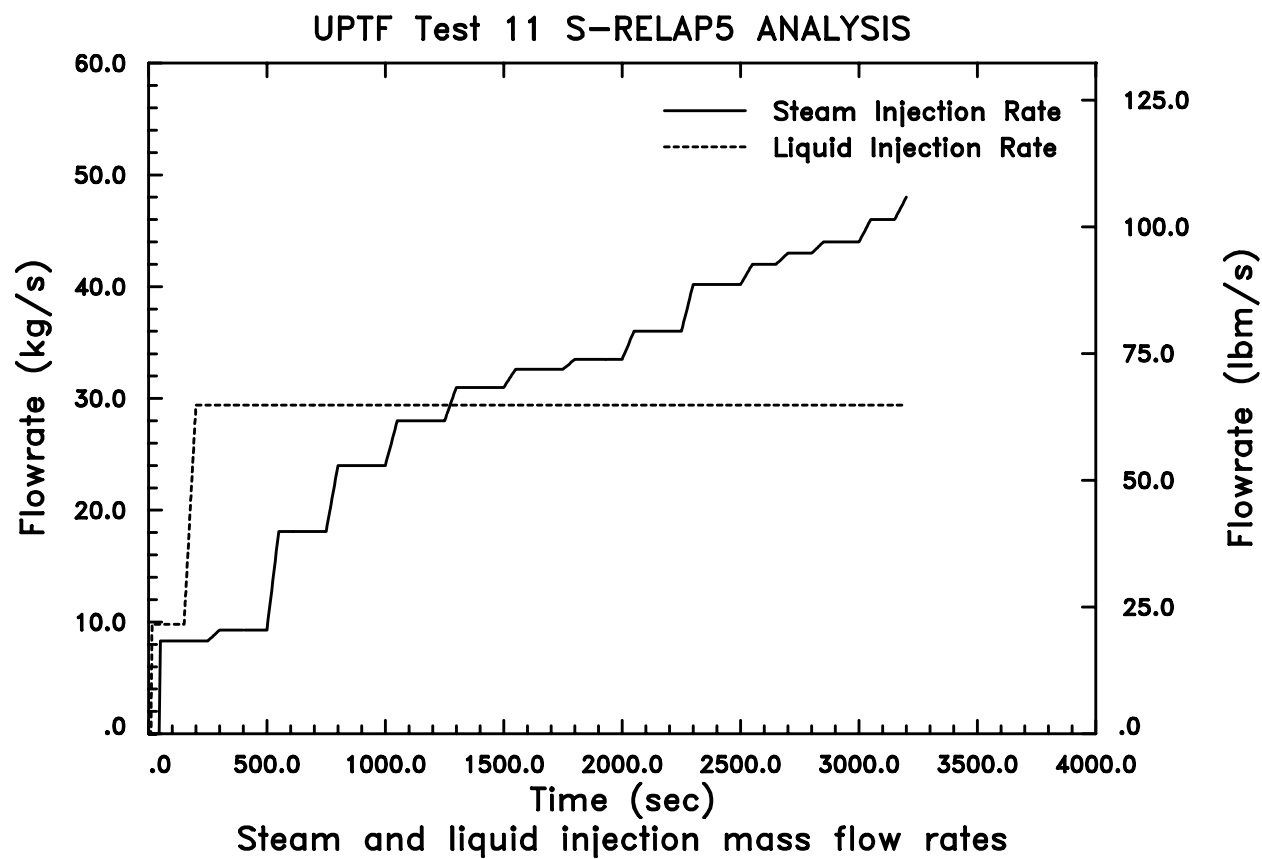
**Figure 4.123 Counter Current Flow of Steam and Water,
UPTF Test 12, Run 014**



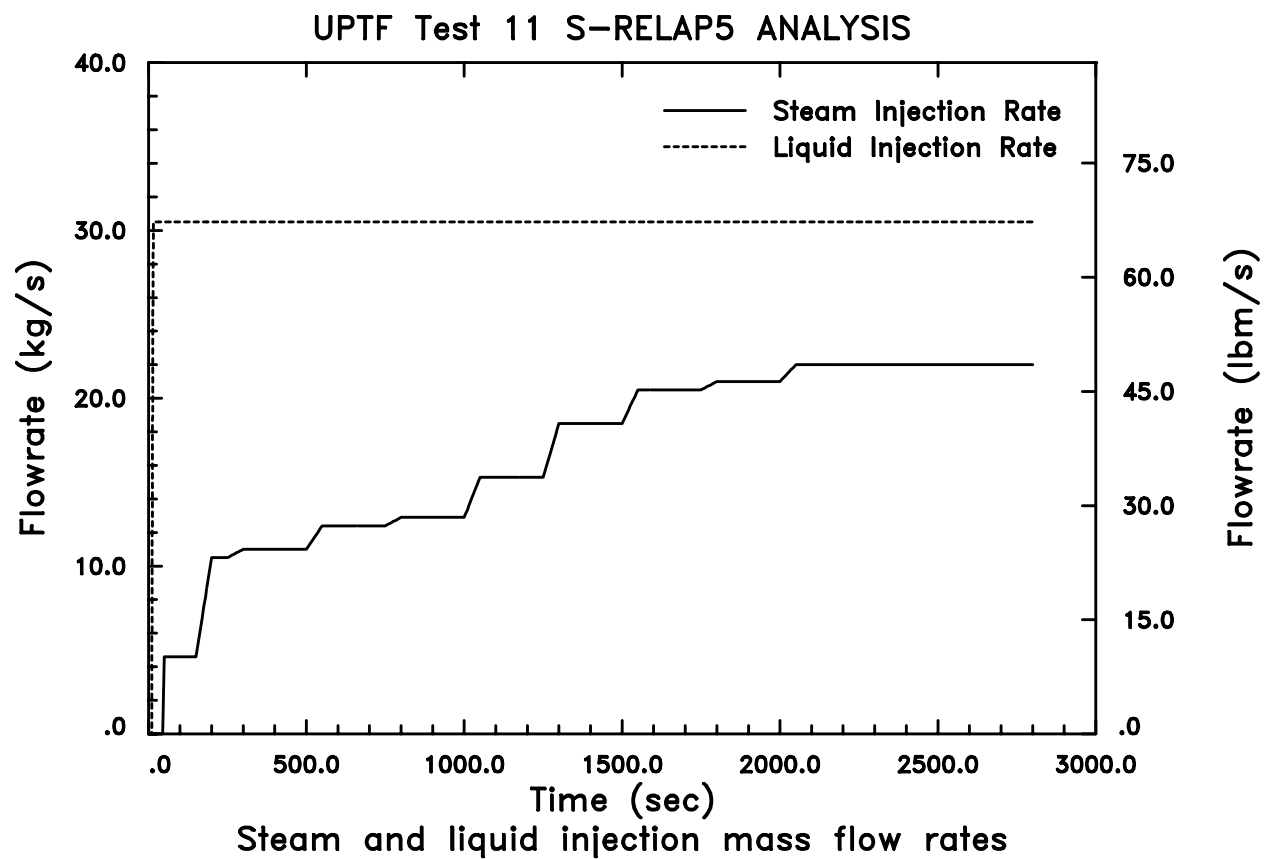
**Figure 4.124 Upper Plenum Pressure Comparison
UPTF Test 12, Run 014**



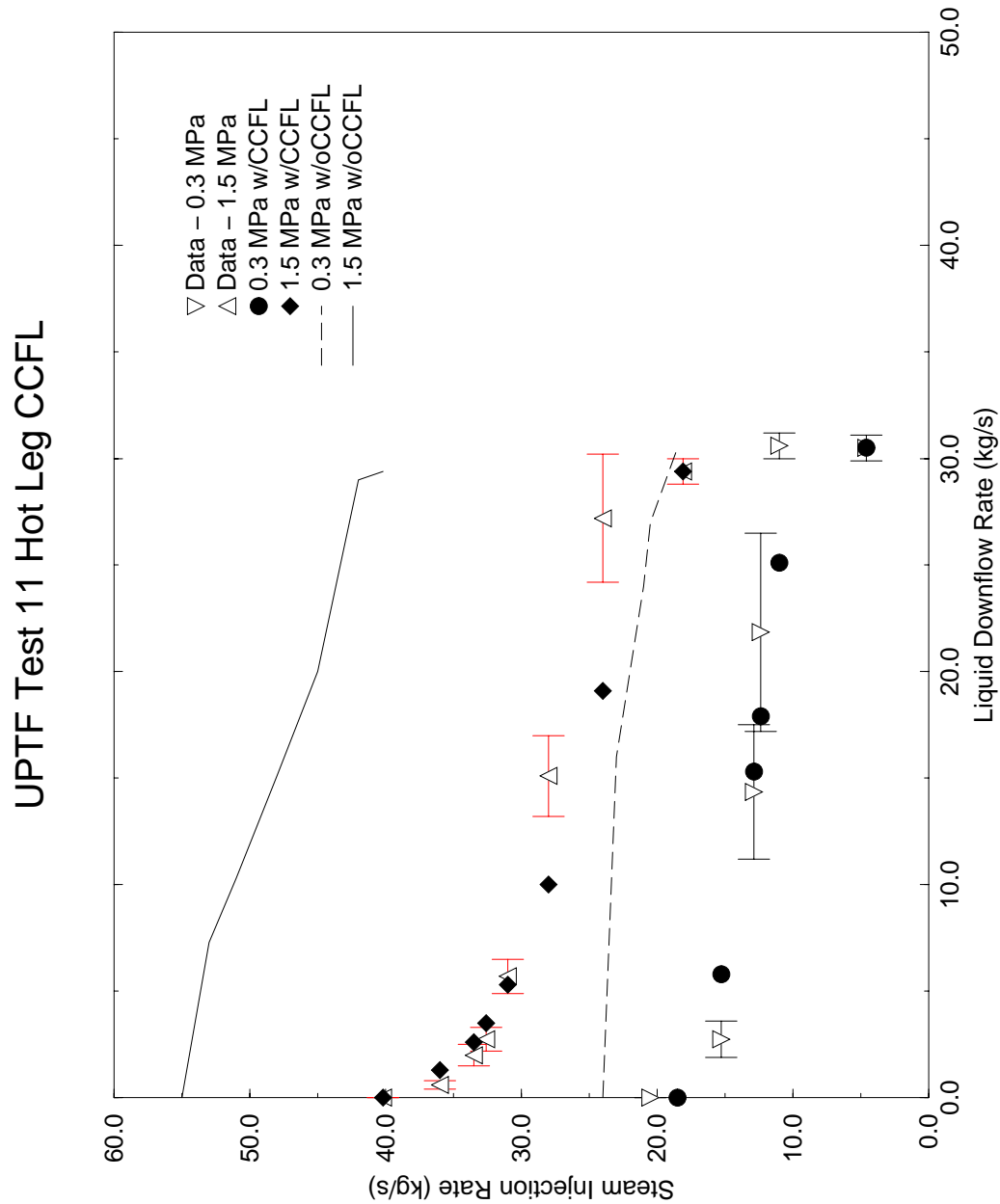
**Figure 4.125 Calculated Downflow Comparison UPTF Test 12,
Run 014 ($m=1.0$, $c=1.8$)**



**Figure 4.126 Steam and Water Injection Rates for UPTF Test 11
1.5 MPa Series**



**Figure 4.127 Steam and Water Injection Rates for UPTF Test 11
0.3 MPa Series**



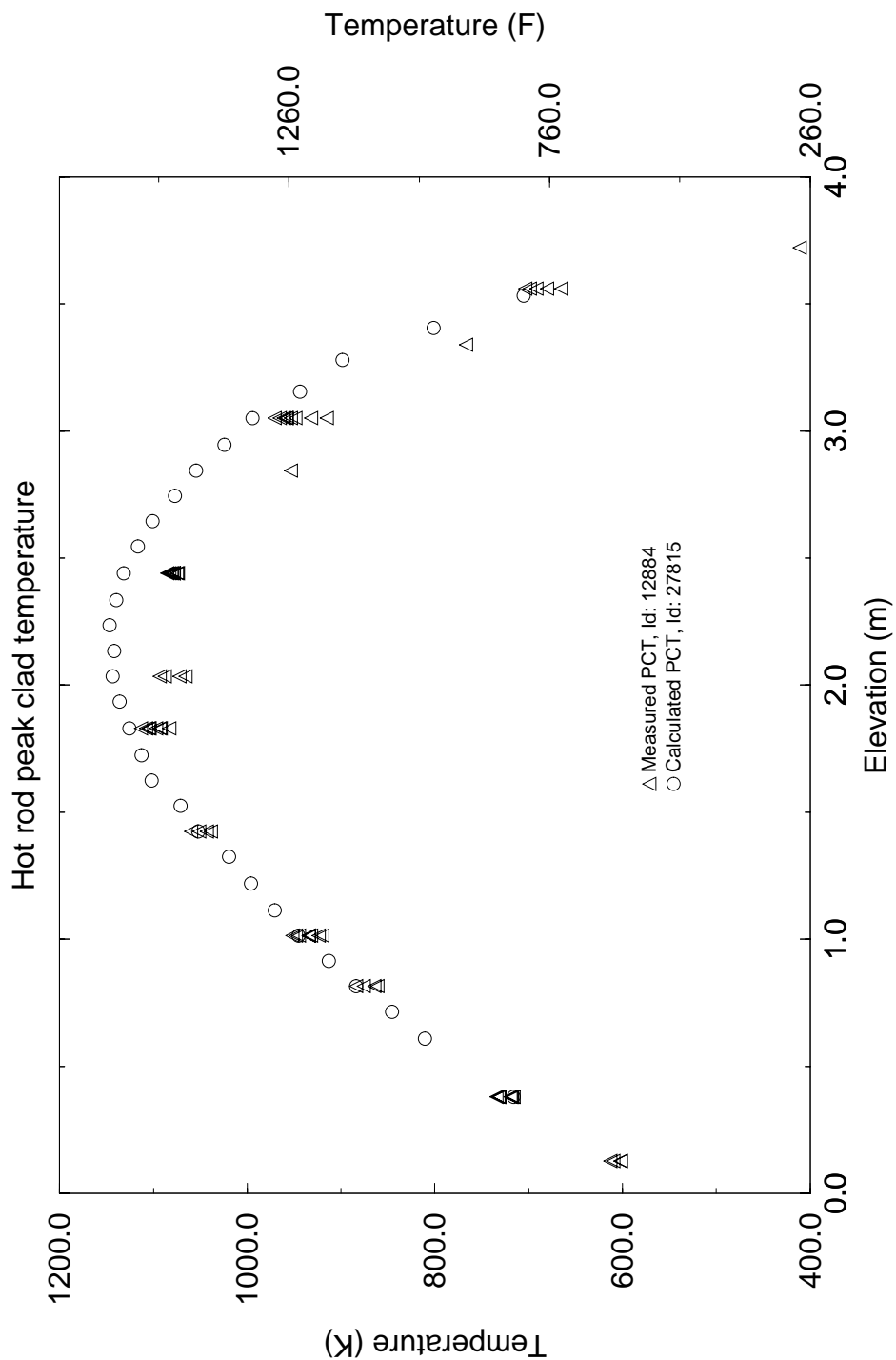


Figure 4.129 Comparison of Peak Surface Temperatures vs. Elevation for High Power Bundles, CCTF Test Run 54

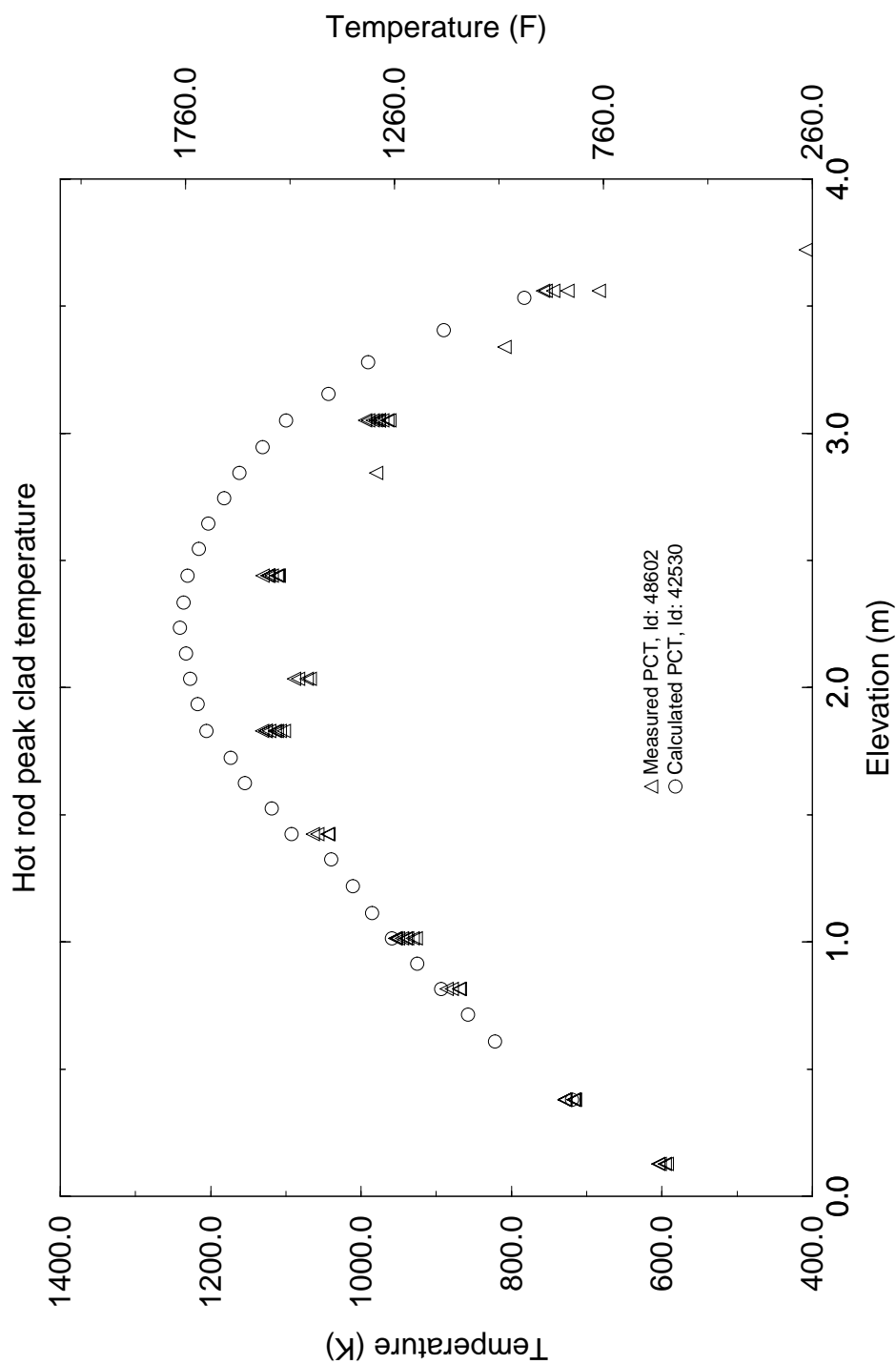


Figure 4.130 Comparison of Peak Surface Temperatures vs. Elevation for High Power Bundles, CCTF Test Run 62

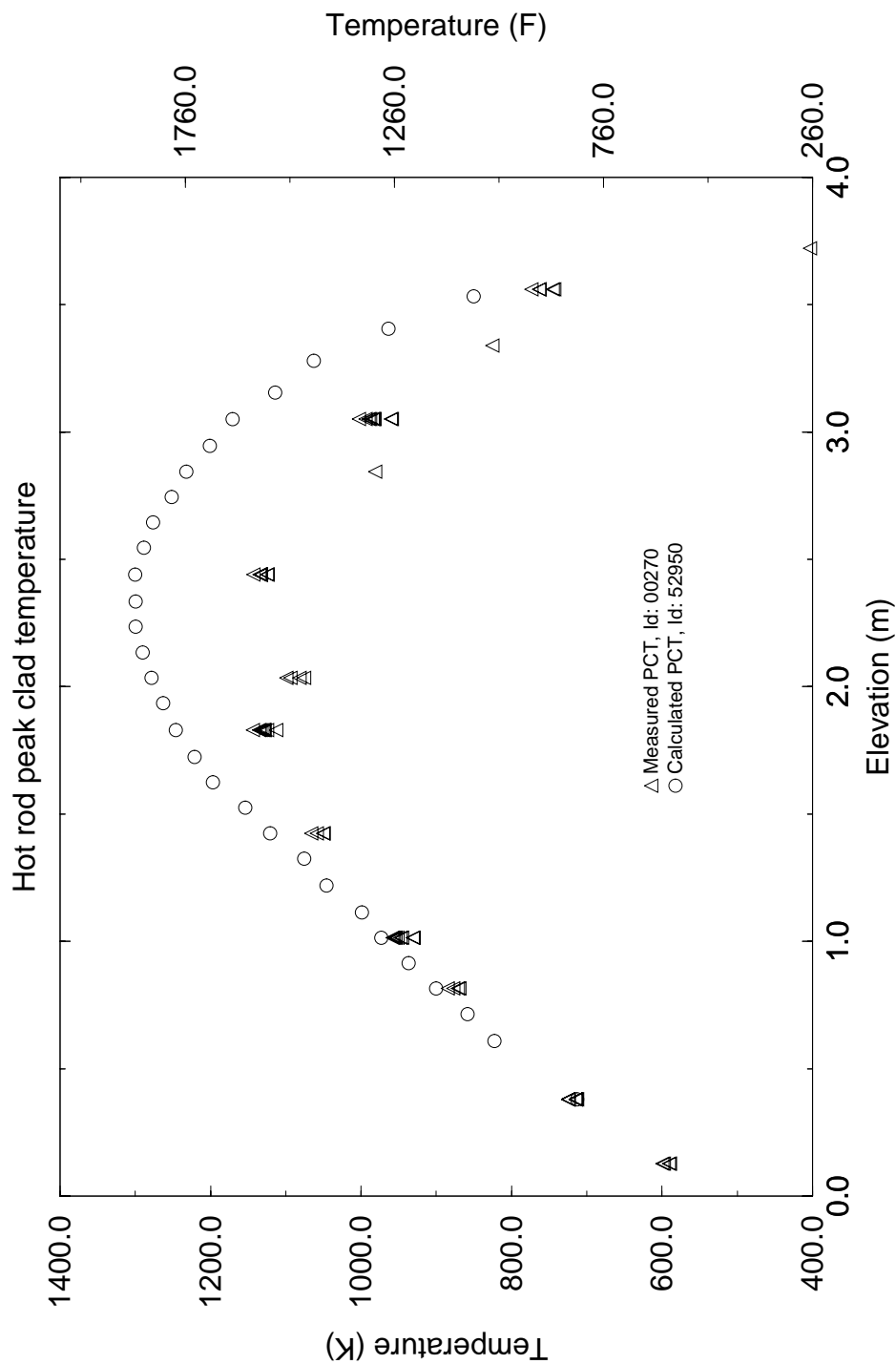


Figure 4.131 Comparison of Peak Surface Temperatures vs. Elevation for High Power Bundles for Test Run 67

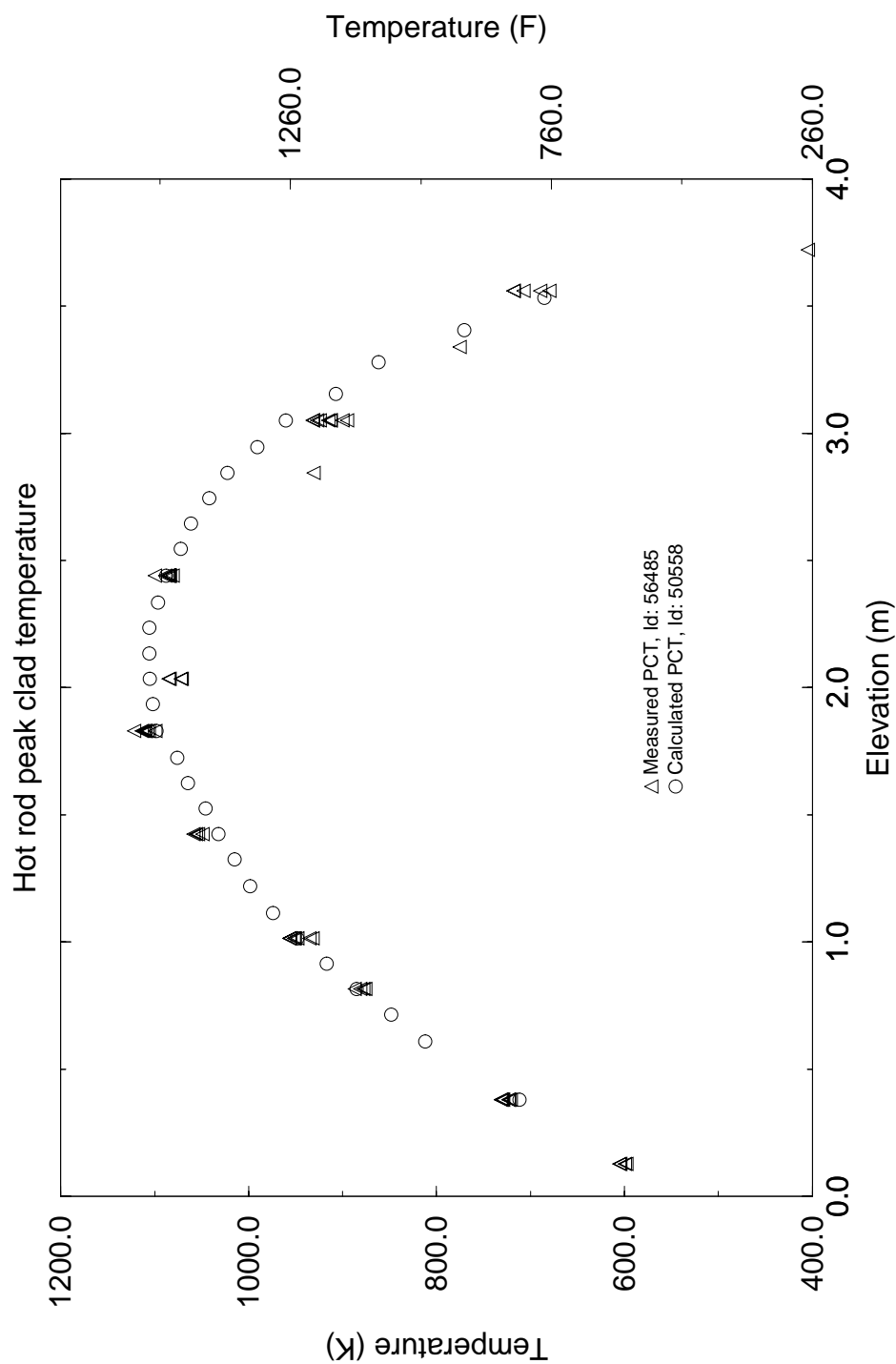


Figure 4.132 Comparison of Peak Surface Temperatures vs. Elevation for High Power Bundles, CCTF Test Run 68

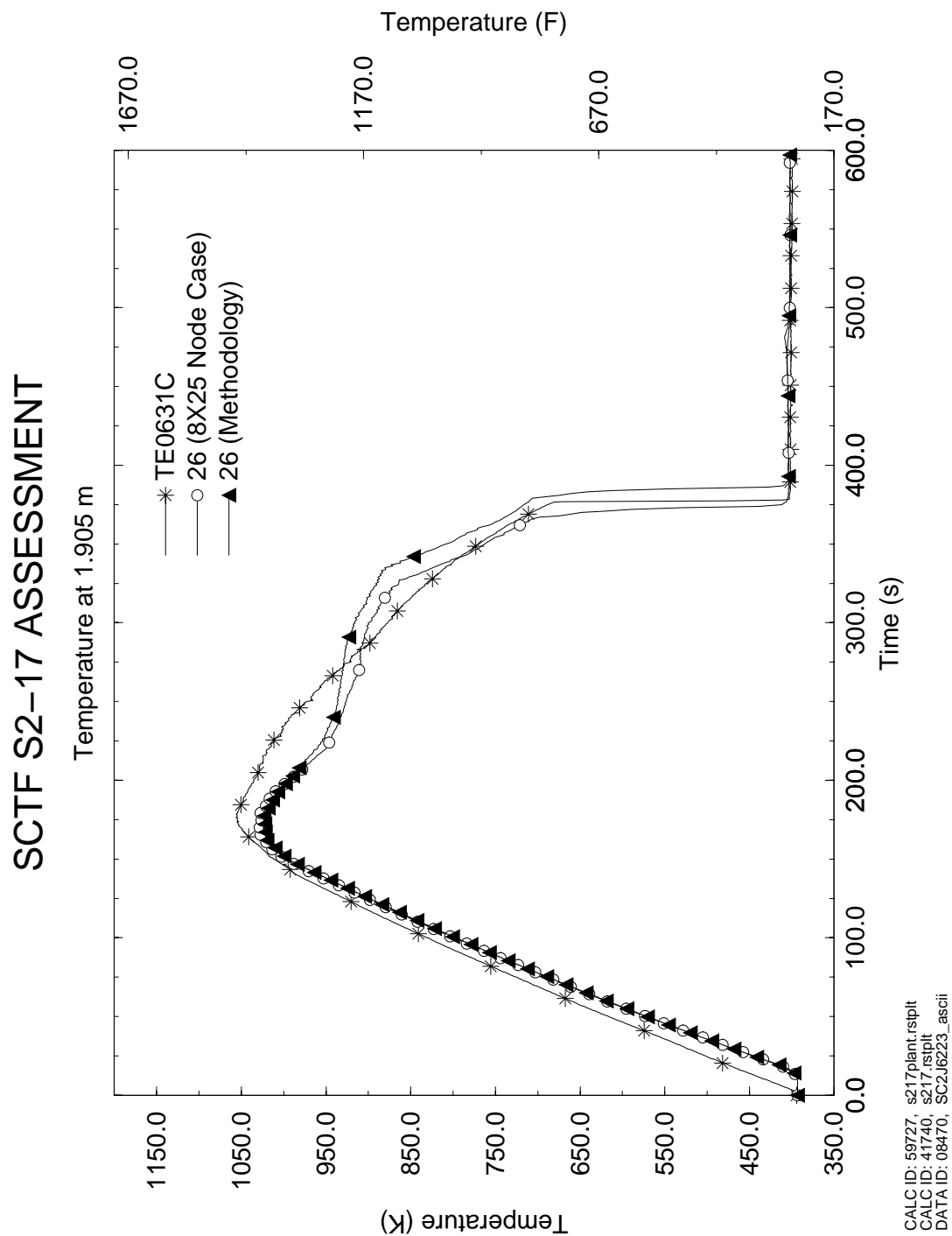


Figure 4.133 Temperature Comparison at 1.905 m, SCTF S2-17

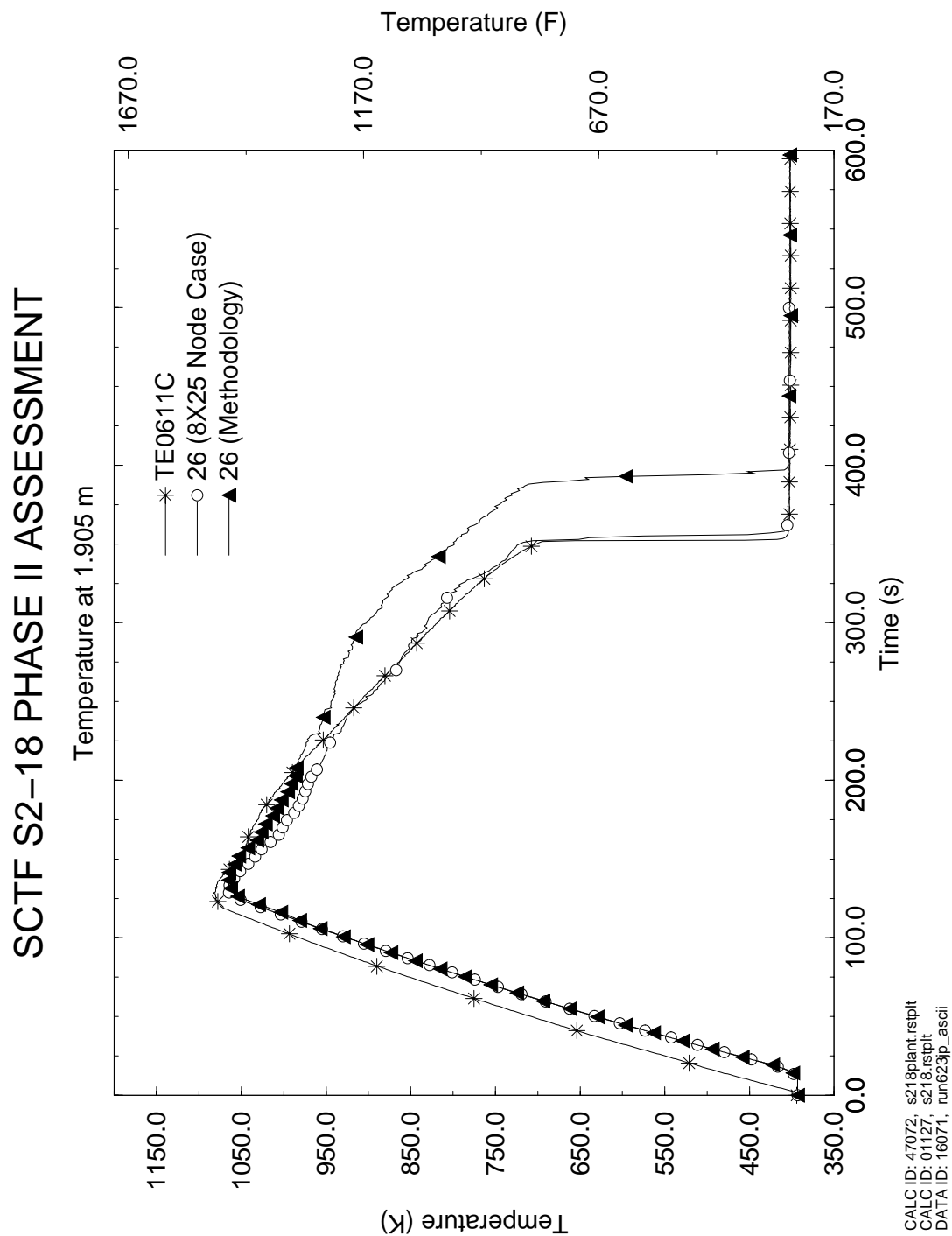


Figure 4.134 Temperature Comparison at 1.905 m, SCTF S2-18

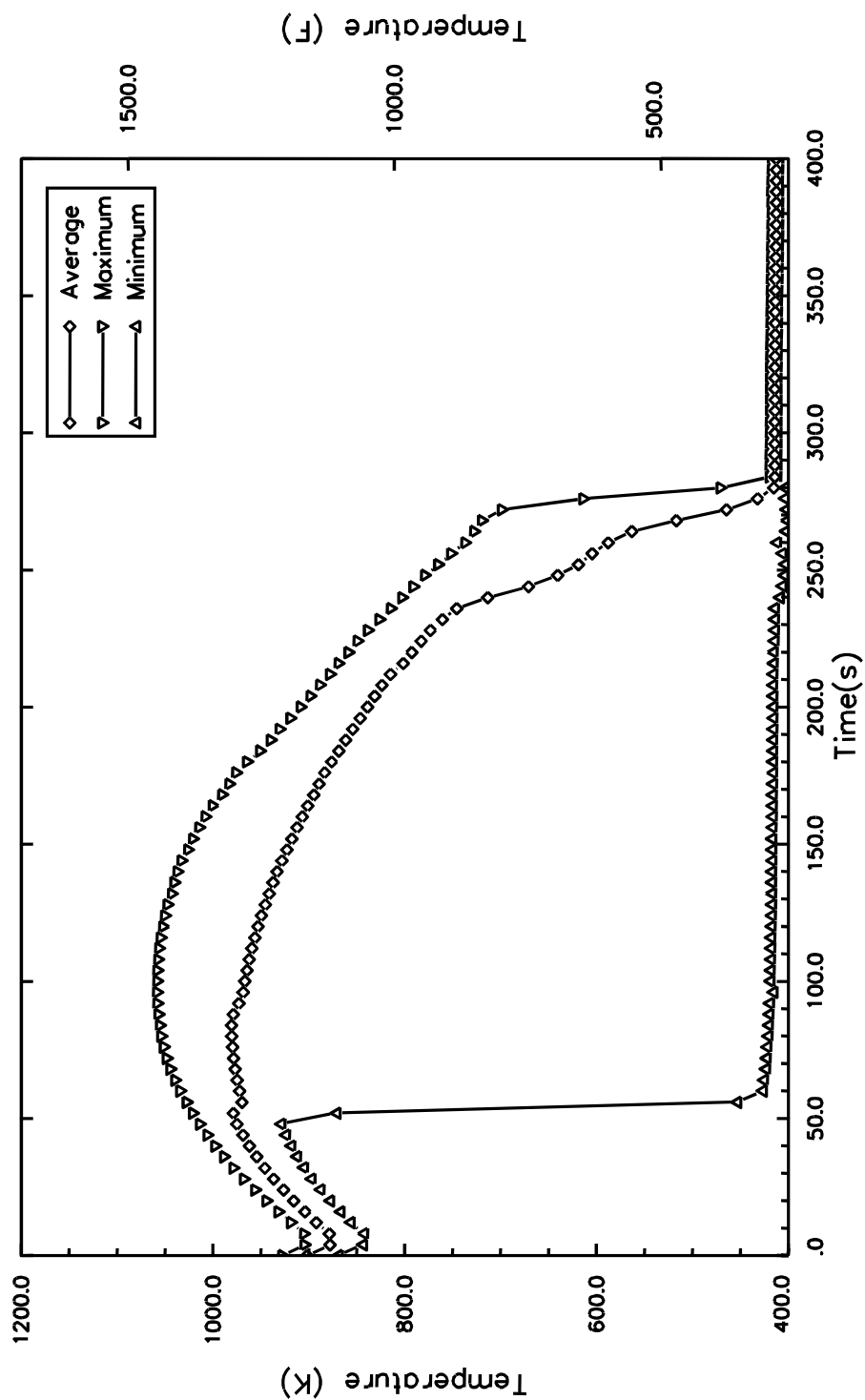


Figure 4.135 Thermocouple Variation Range at the PCT Elevation,
ACHILLES ISP 25

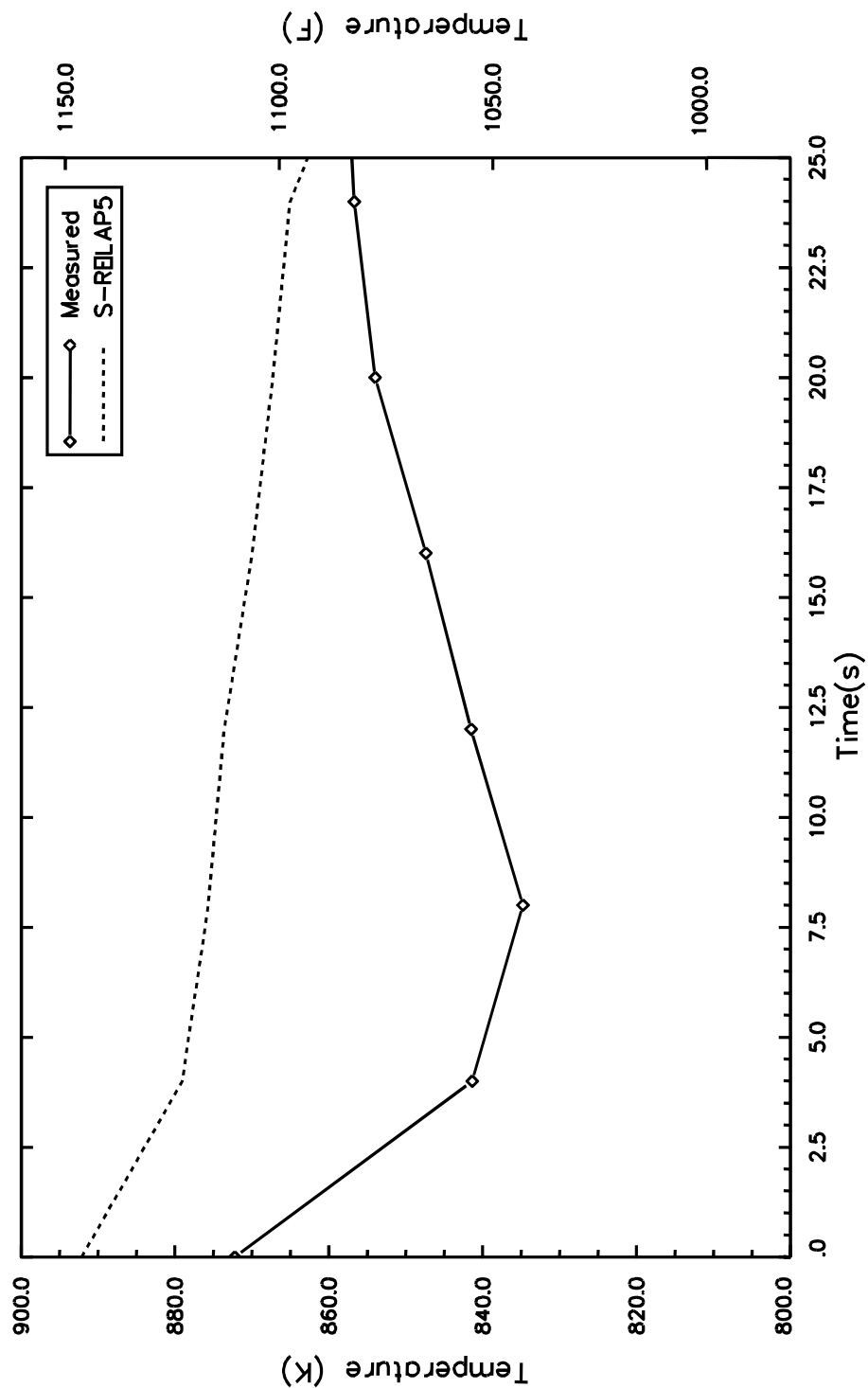


Figure 4.136 Nitrogen Insurge Impact at 1.08 m, ACHILLES ISP 25

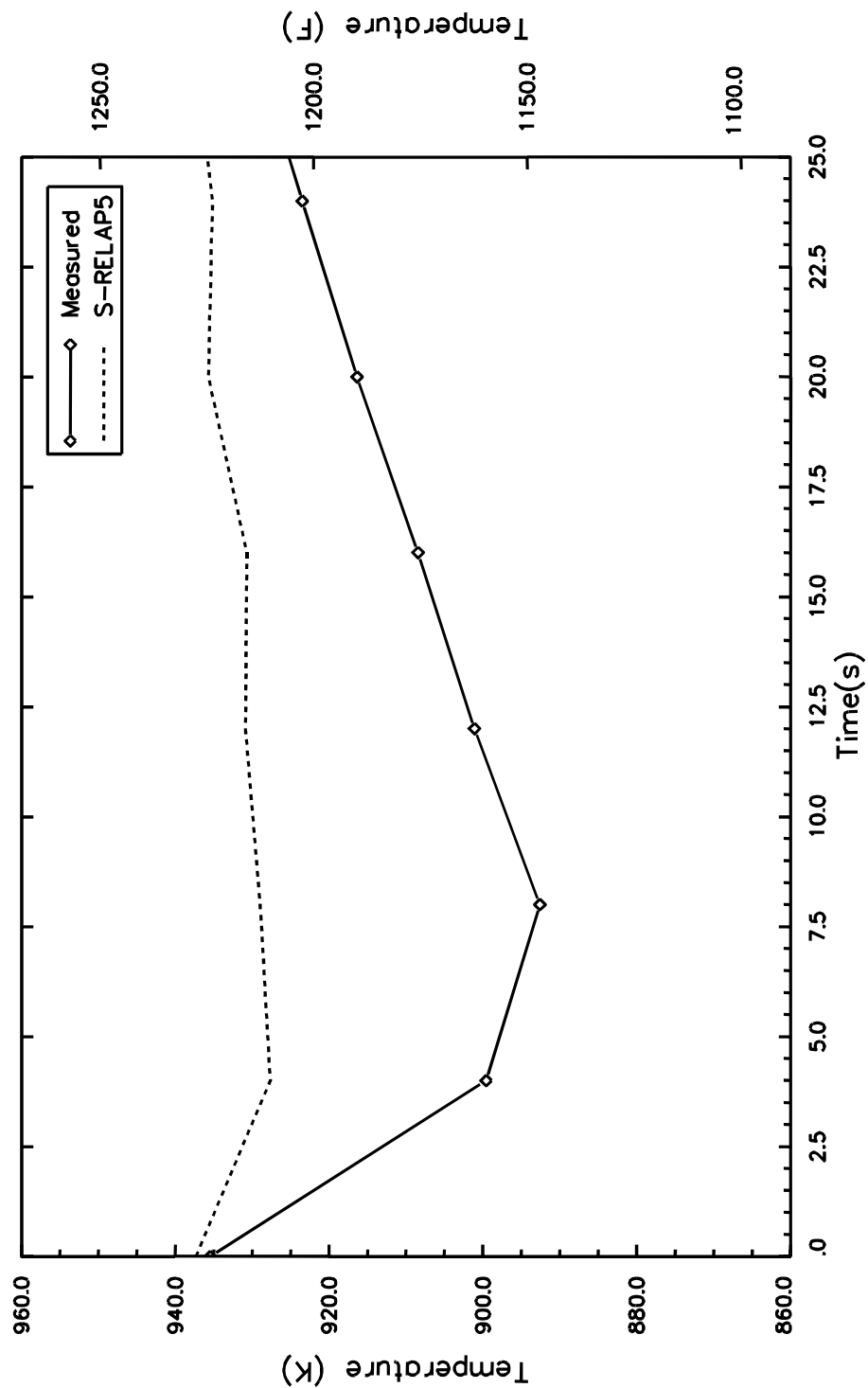


Figure 4.137 Nitrogen Insurge Impact at 1.81 m, ACHILLES ISP 25

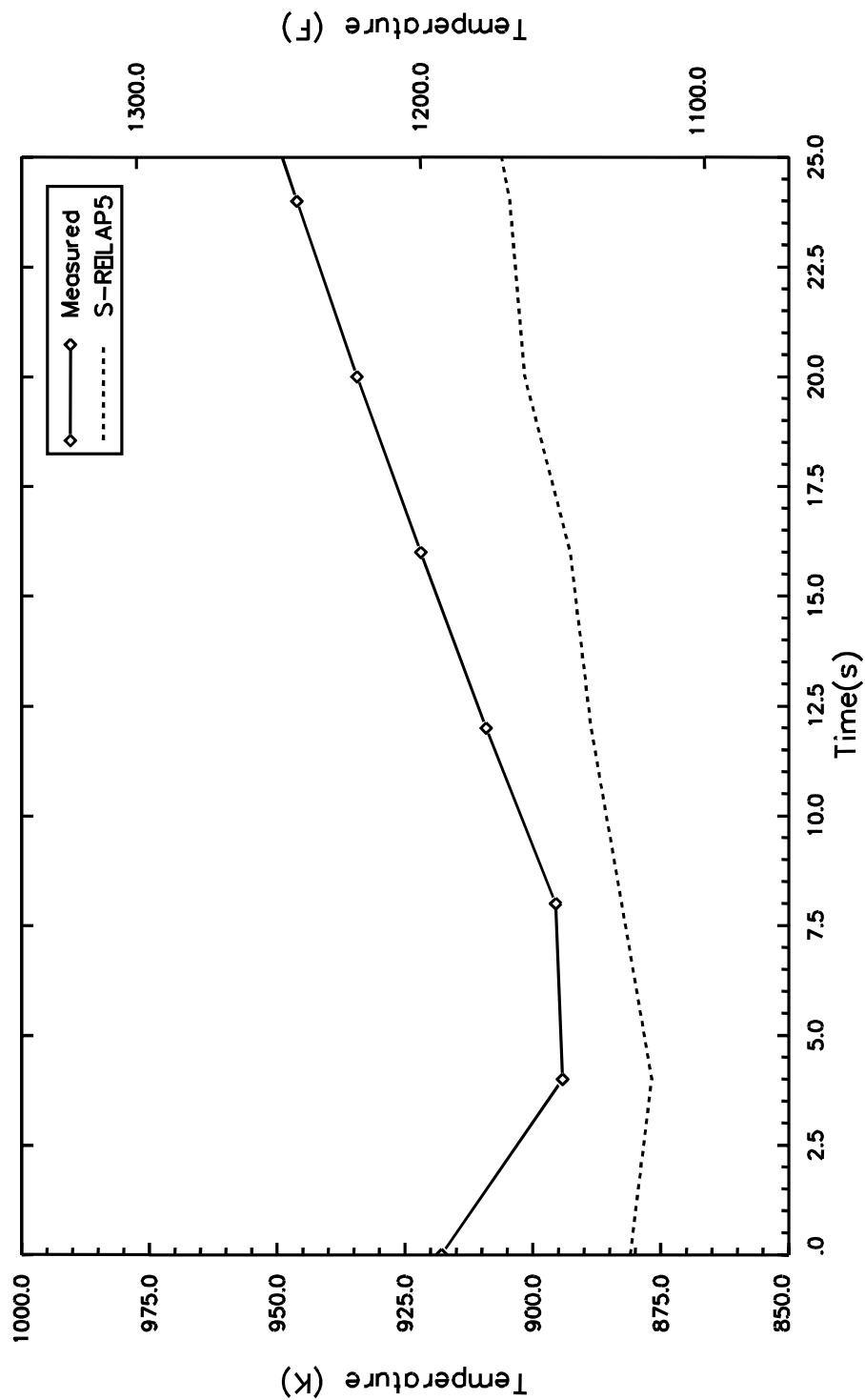


Figure 4.138 Nitrogen Insurge Impact at 2.13 m, ACHILLES ISP 25

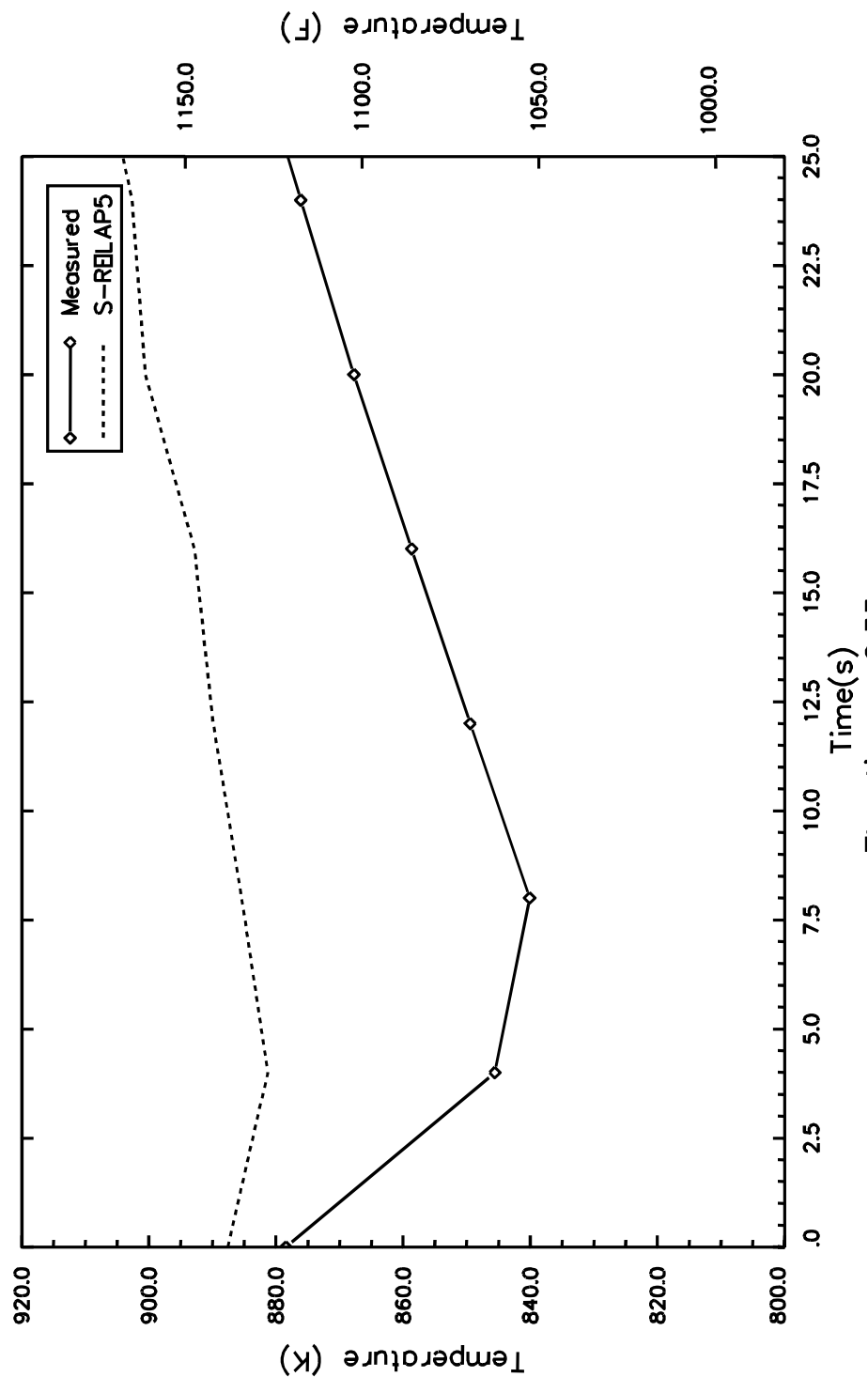


Figure 4.139 Nitrogen Insurge Impact at 2.33 m, ACHILLES ISP 25

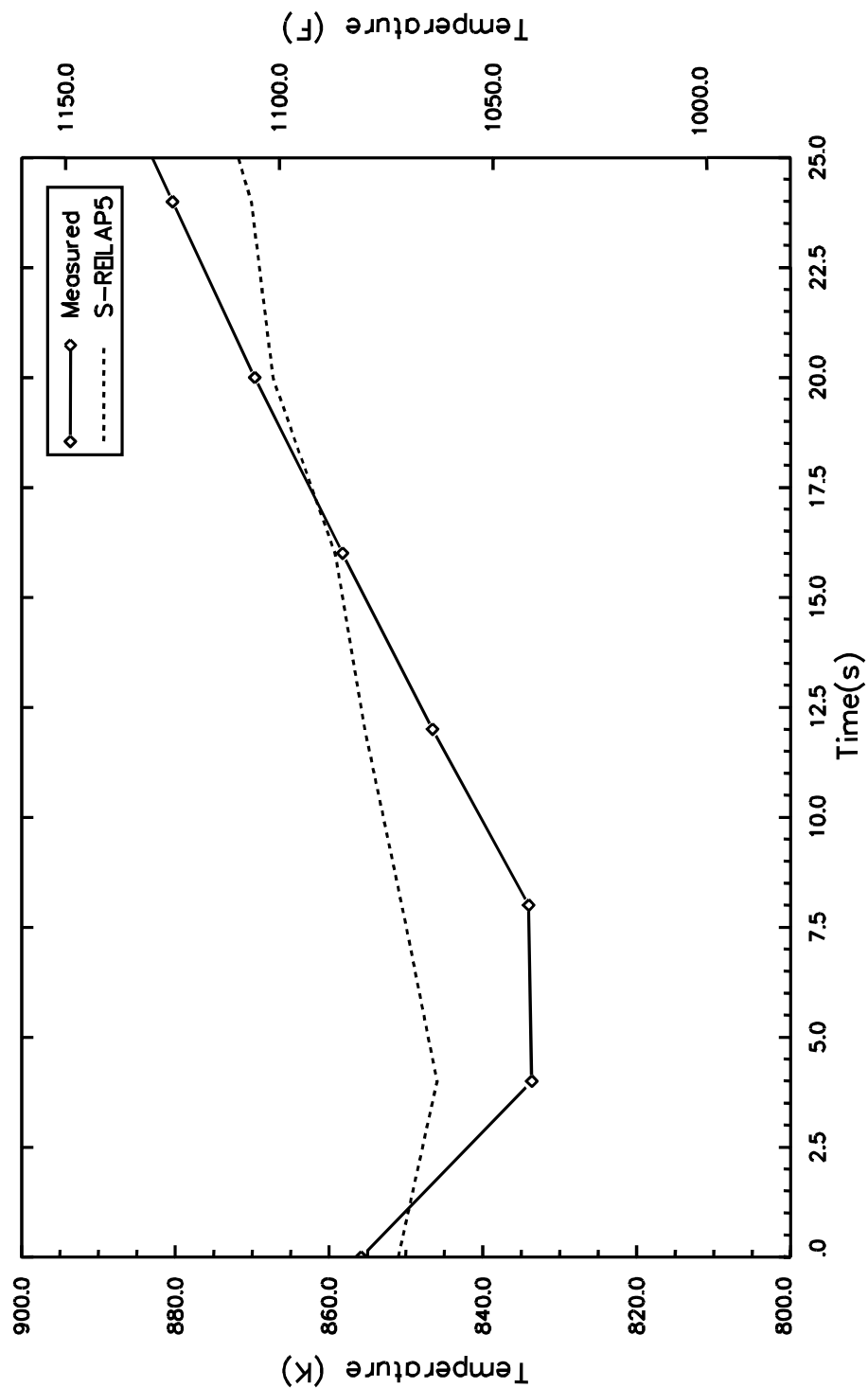


Figure 4.140 Nitrogen Insurge Impact at 2.65 m, ACHILLES ISP 25

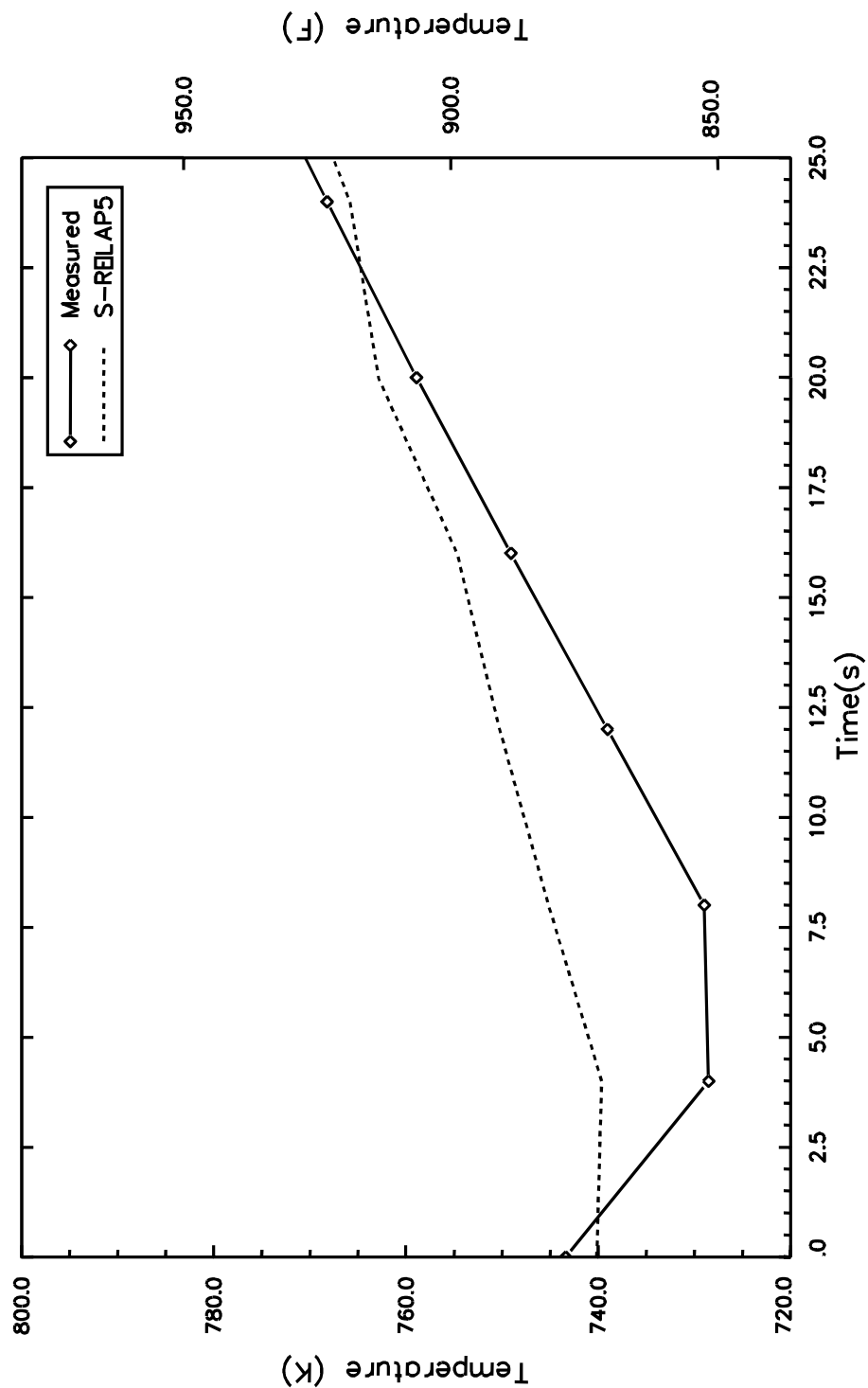


Figure 4.141 Nitrogen Insurge Impact at 3.18 m, ACHILLES ISP 25

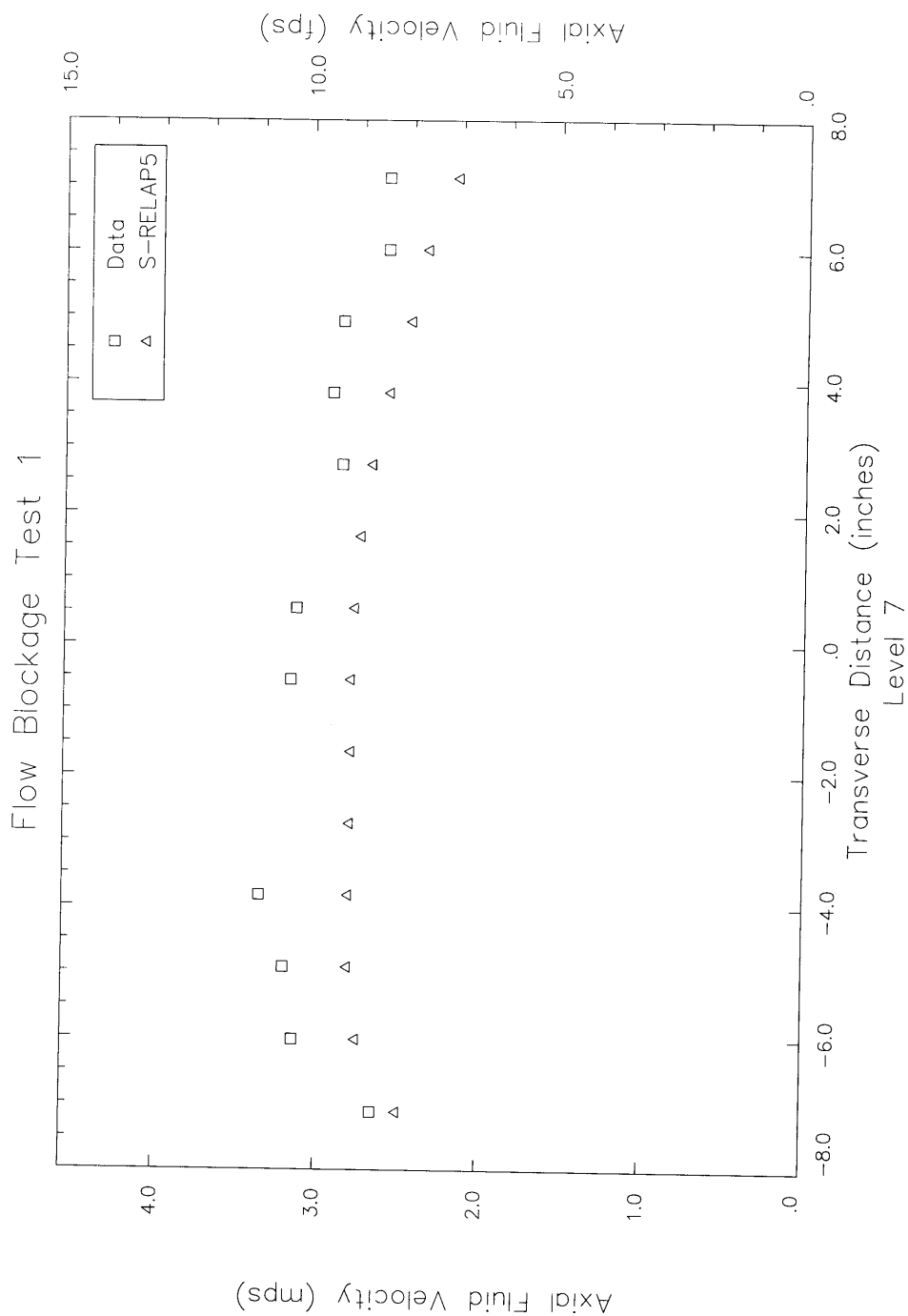


Figure 4.142 Axial Velocities at 32.5 Inches, Asymmetric Flow - Test 1

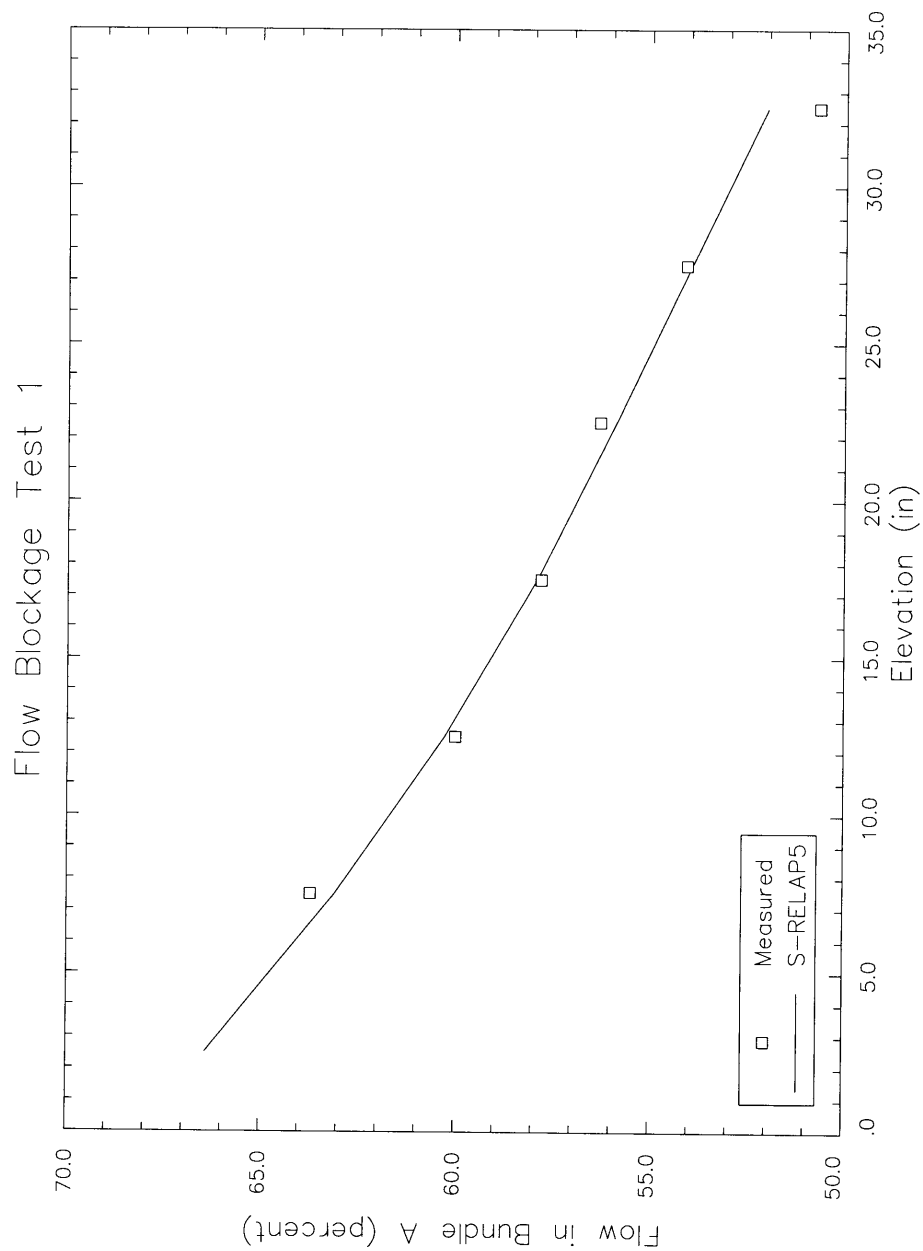


Figure 4.143 Axial Flow Fractions for Asymmetric Flow - Test 1

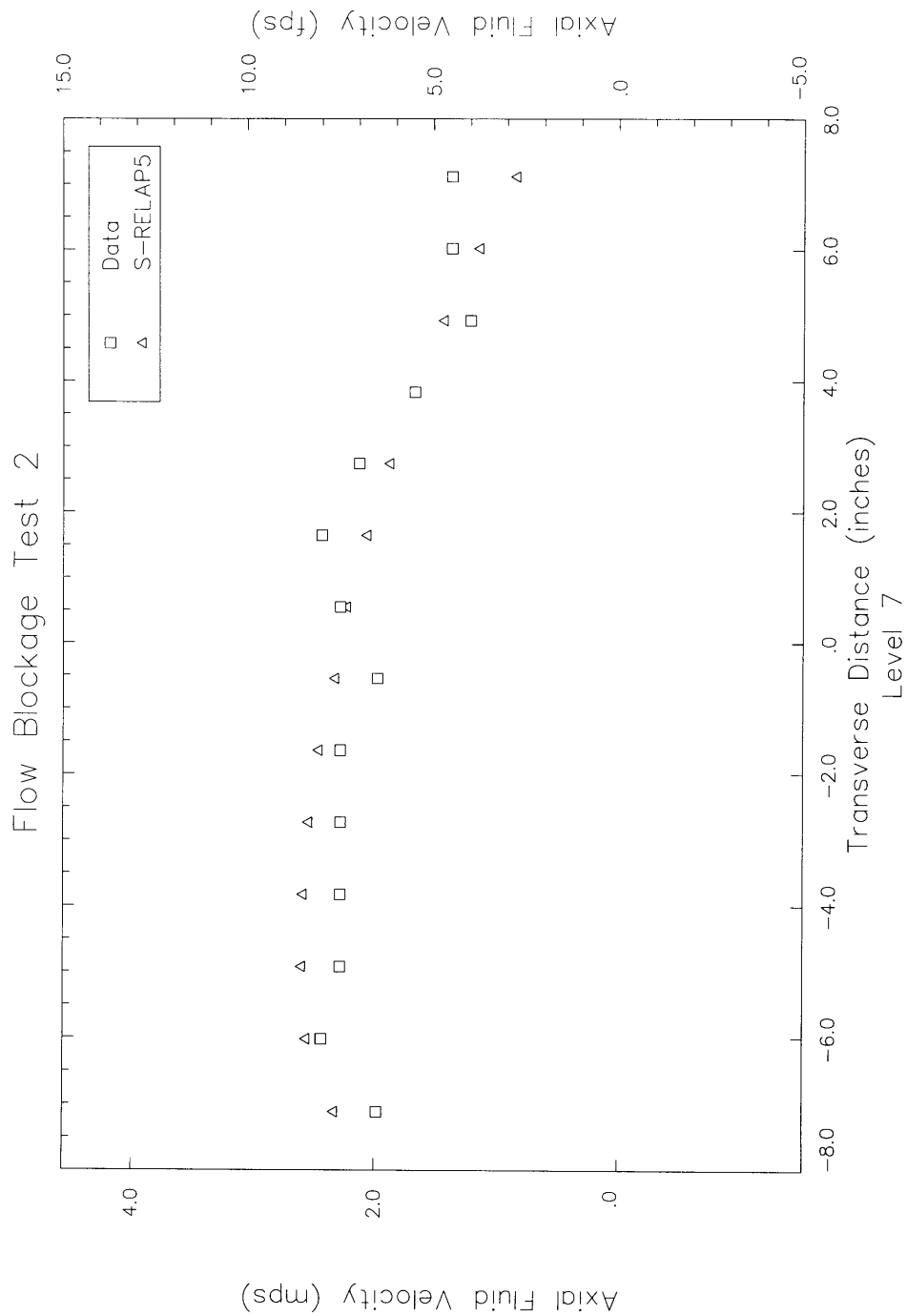


Figure 4.144 Axial Velocities at 32.5 Inches, for Asymmetric Flow - Test 2

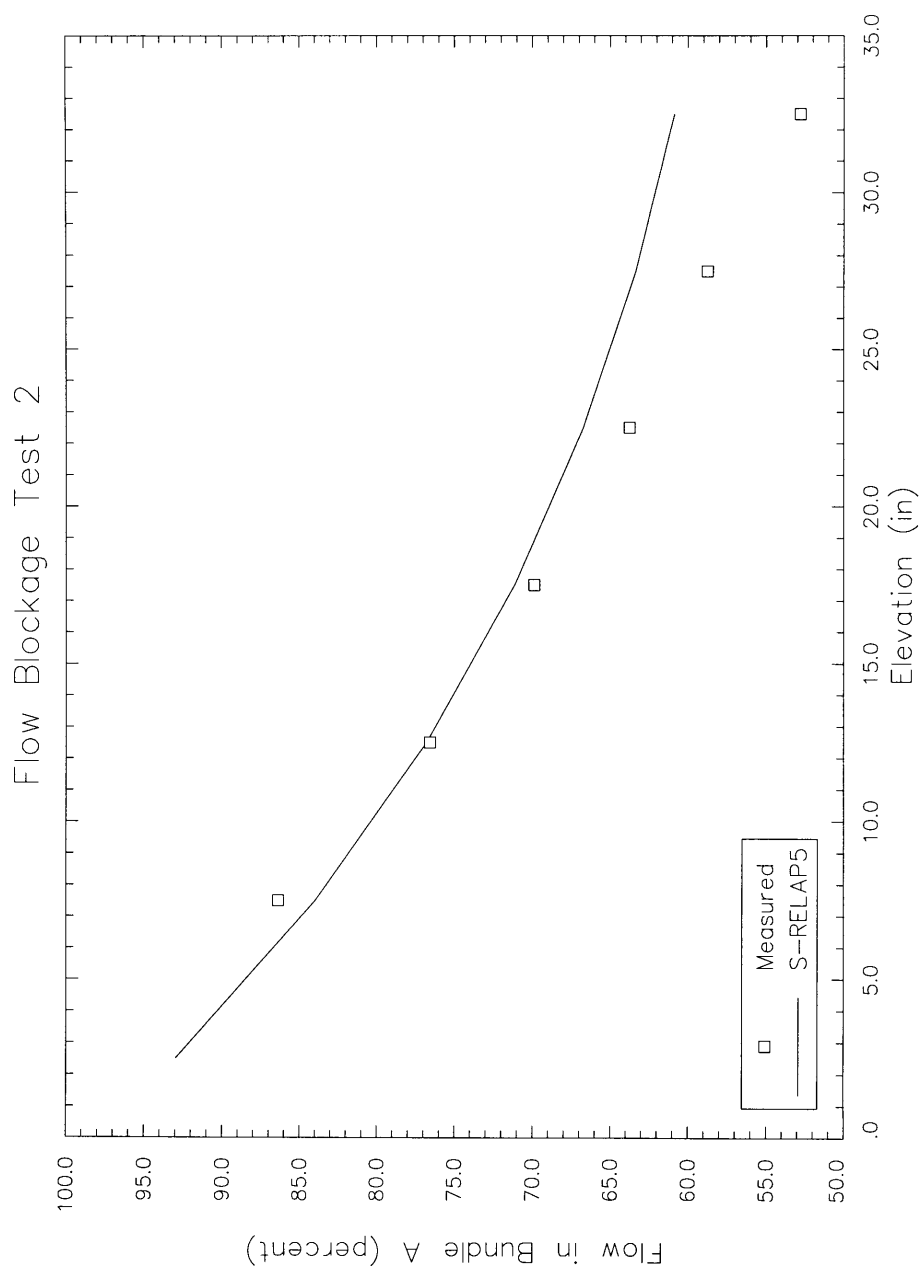


Figure 4.145 Axial Flow Fractions for Asymmetric Flow – Test 2

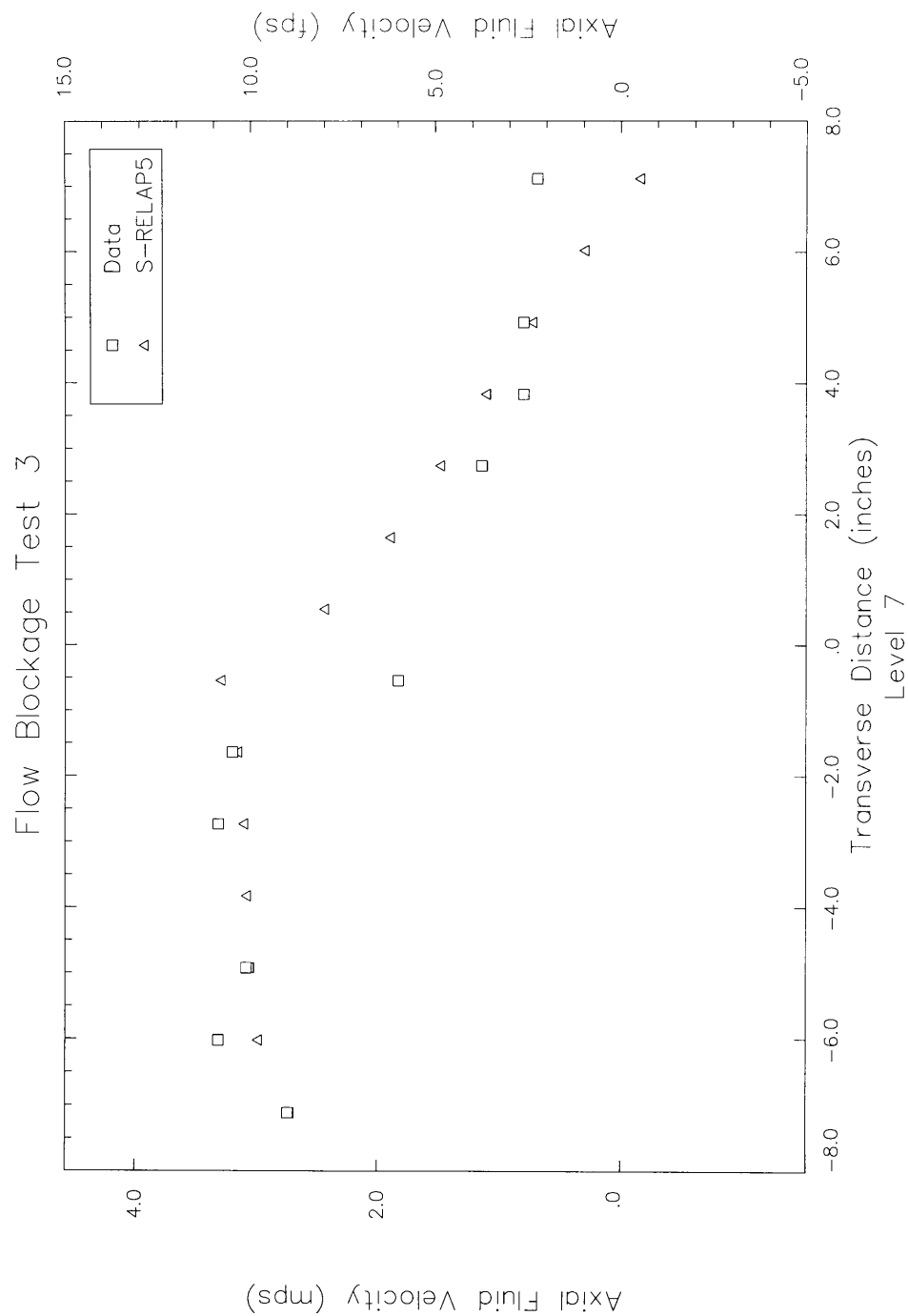


Figure 4.146 Axial Velocities at 32.5 Inches, for Asymmetric Flow - Test 3

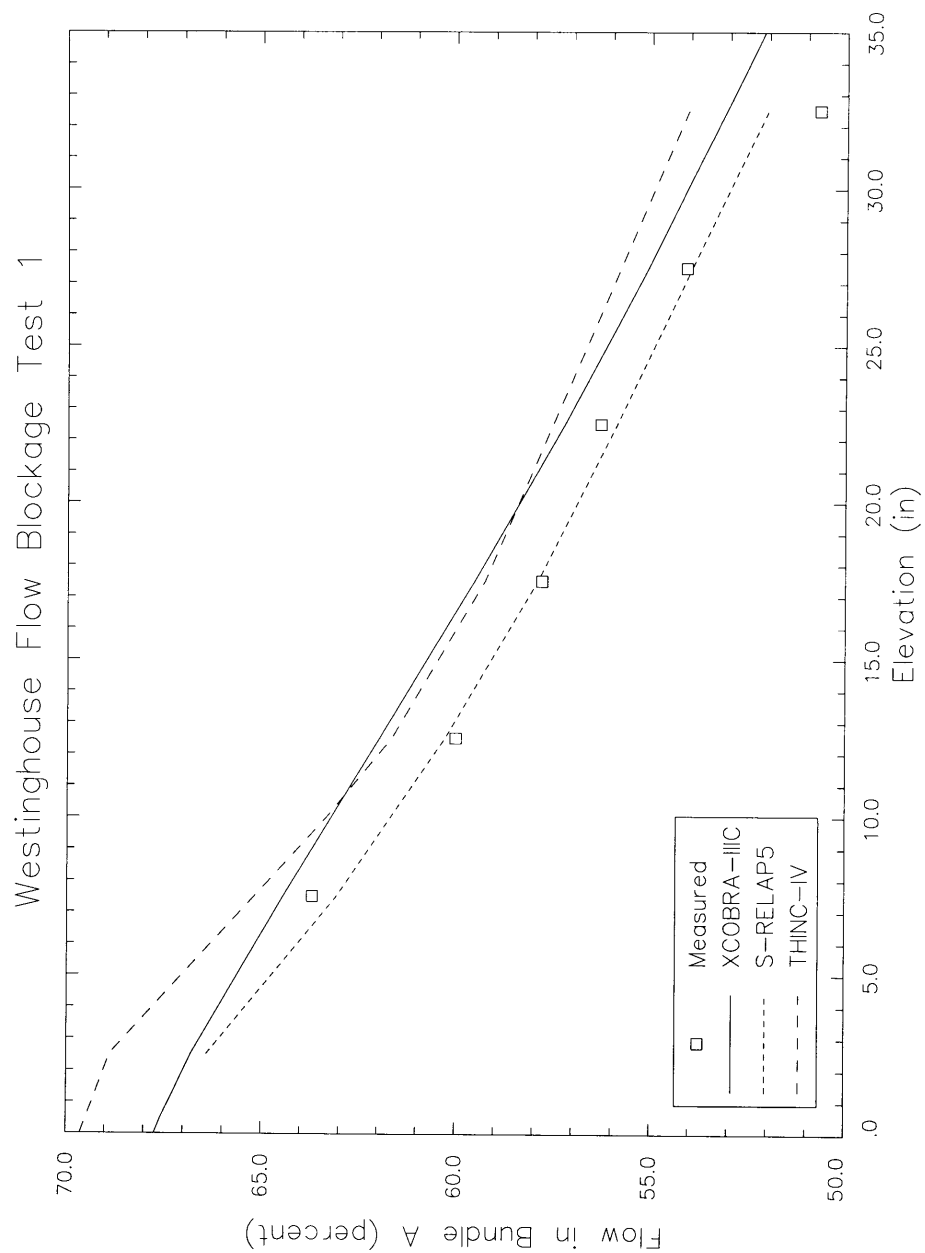
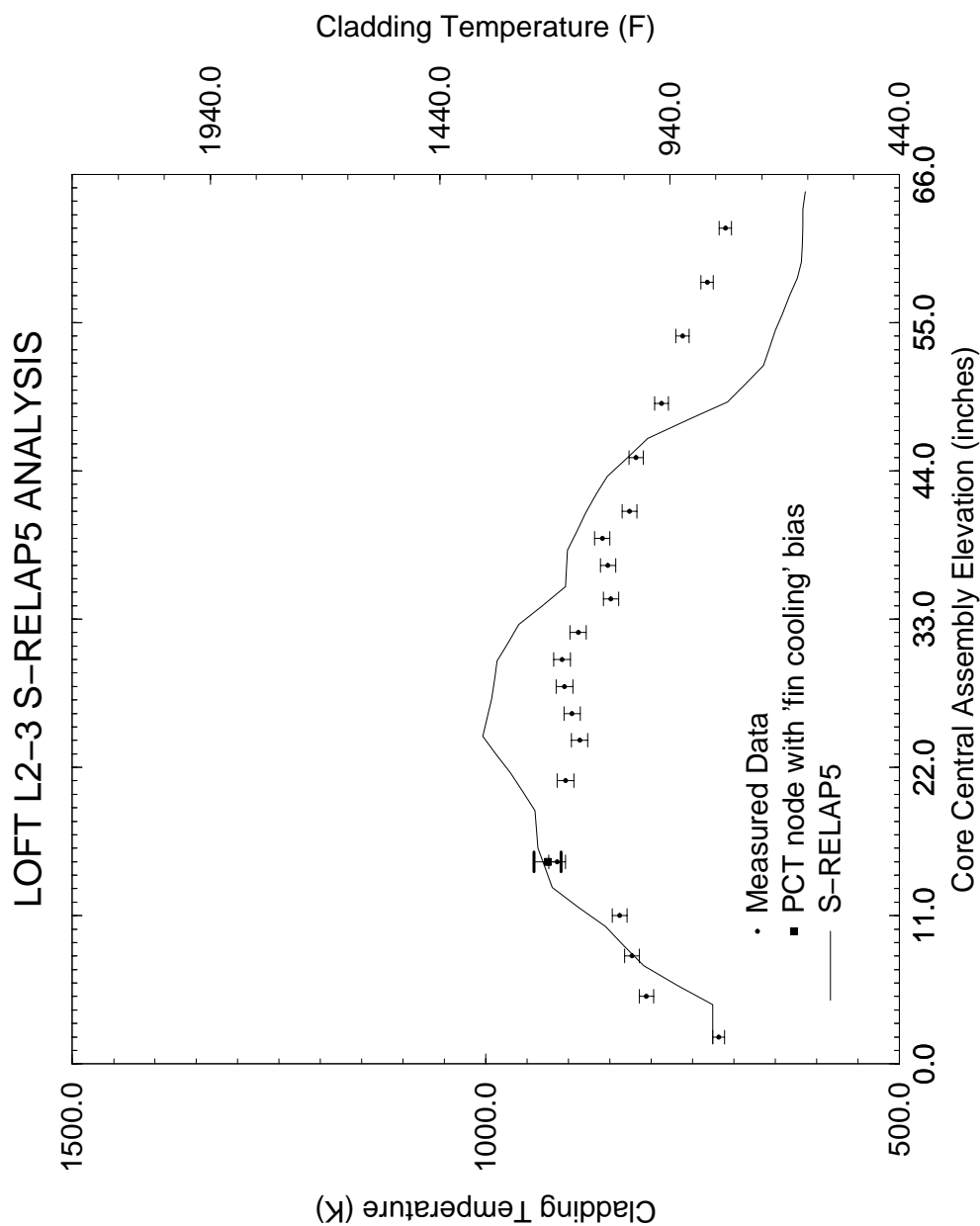


Figure 4.147 Comparison of S-RELAP5 with Design Codes for Asymmetric Flow - Test 1

LOFT L2-3 S-RELAP5 ANALYSIS PLOT FILE NAME: 012-3_pct_00.eps, JOB ID: make_pct_plot.o3570, DATE: Tue May 21 08:46:34 PDT 2002



**Figure 4.148 Comparison of PCTs Versus Core Elevations LOFT
Test L2-3 with S-RELAP5**

LOFT L2-5 S-RELAP5 ANALYSIS PLOT FILE NAME: 012-5_pct_00.eps, JOB ID: make_pct_plot.o3858, DATE: Tue Sep 10 15:04:54 PDT 2002

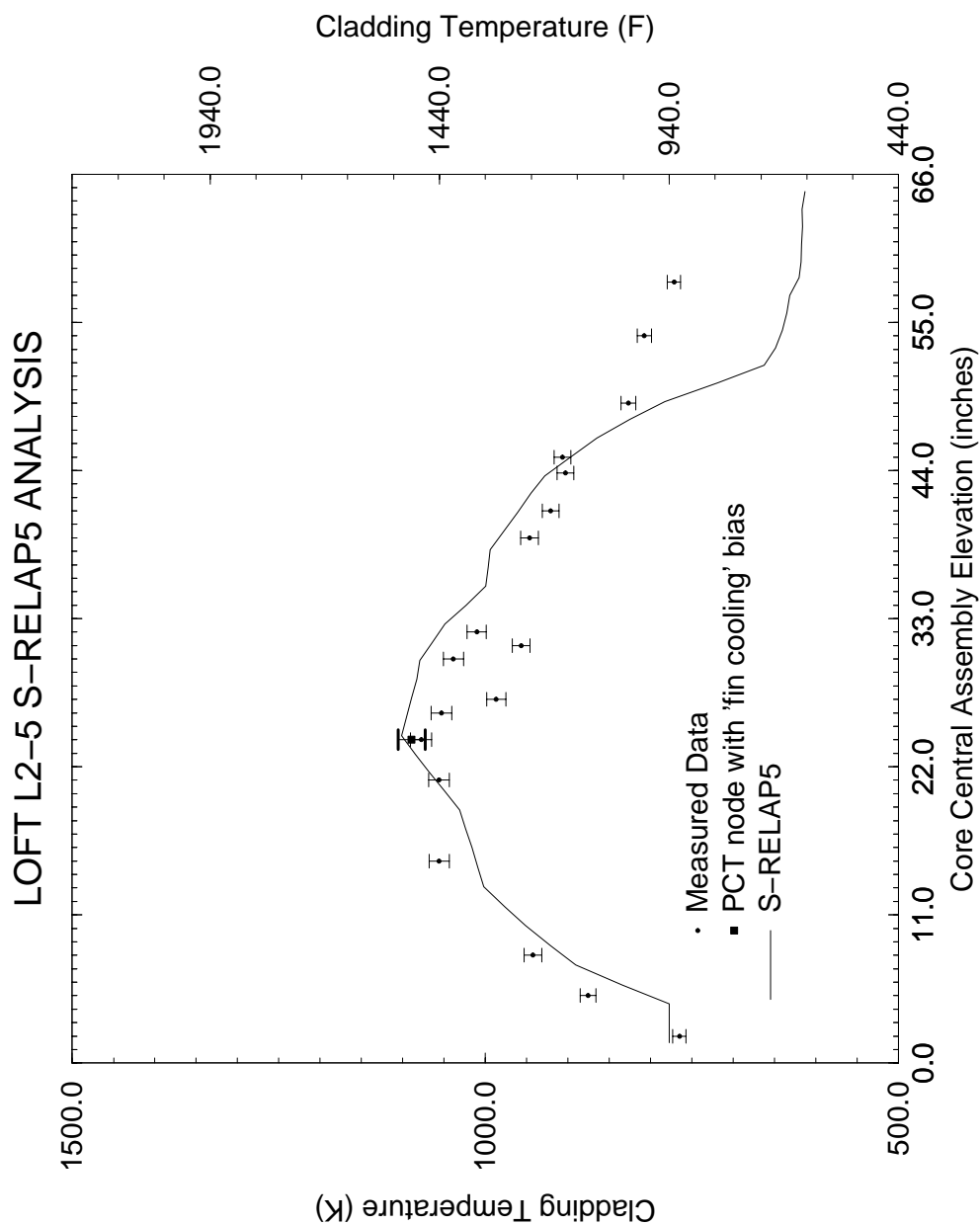


**Figure 4.149 Comparison of PCTs Versus Core Elevations LOFT
Test L2-5 with S-RELAP5**

LOFT LP-02-6 S-RELAP5 ANALYSIS PLOT FILE NAME: 012-6_pct_00.eps, JOB ID: make_pct_plot.03857, DATE: Tue Sep 10 15:04:09 PDT 2002

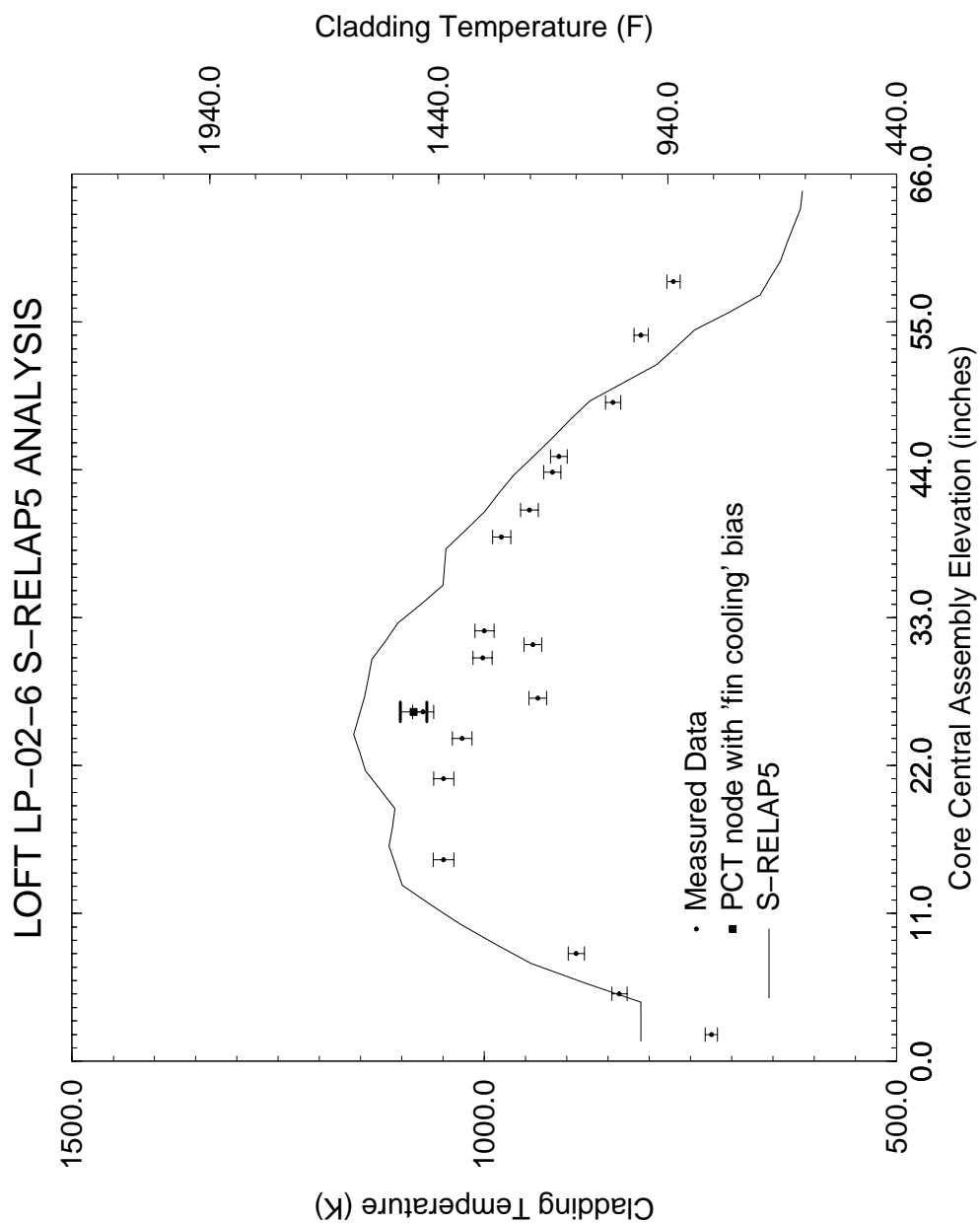


Figure 4.150 LOFT Test LP-02-6 Comparison of PCTs Versus Core Elevations

LOFT LP-LB-1 S-RELAP5 ANALYSIS PLOT FILE NAME: 0lb-1_pct_00.eps, JOB ID: make_pct_plot.o3587, DATE: Wed May 22 08:57:30 PDT 2002

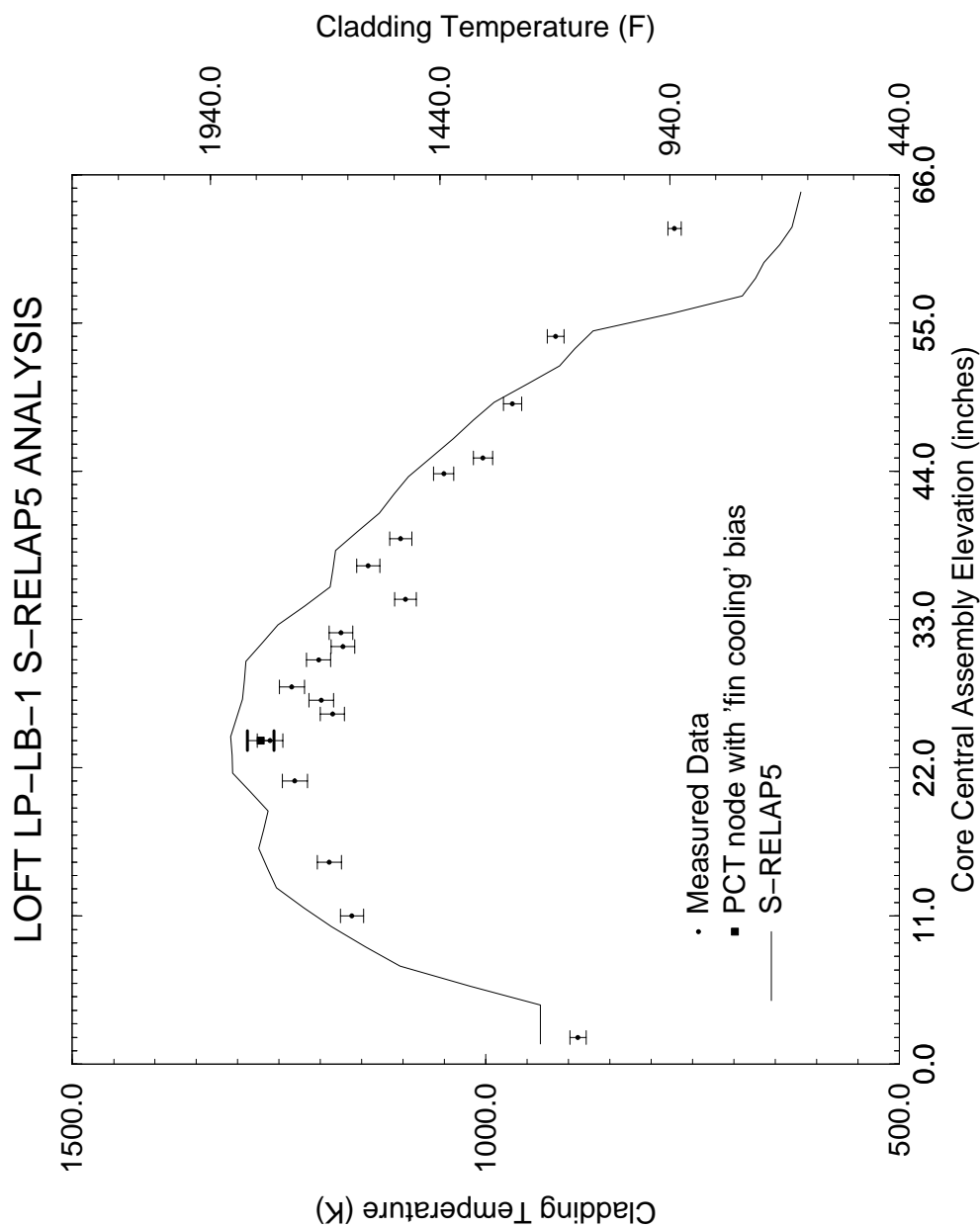


Figure 4.151 LOFT Test LP-LB-1 Comparison of PCTs Versus Core Elevations

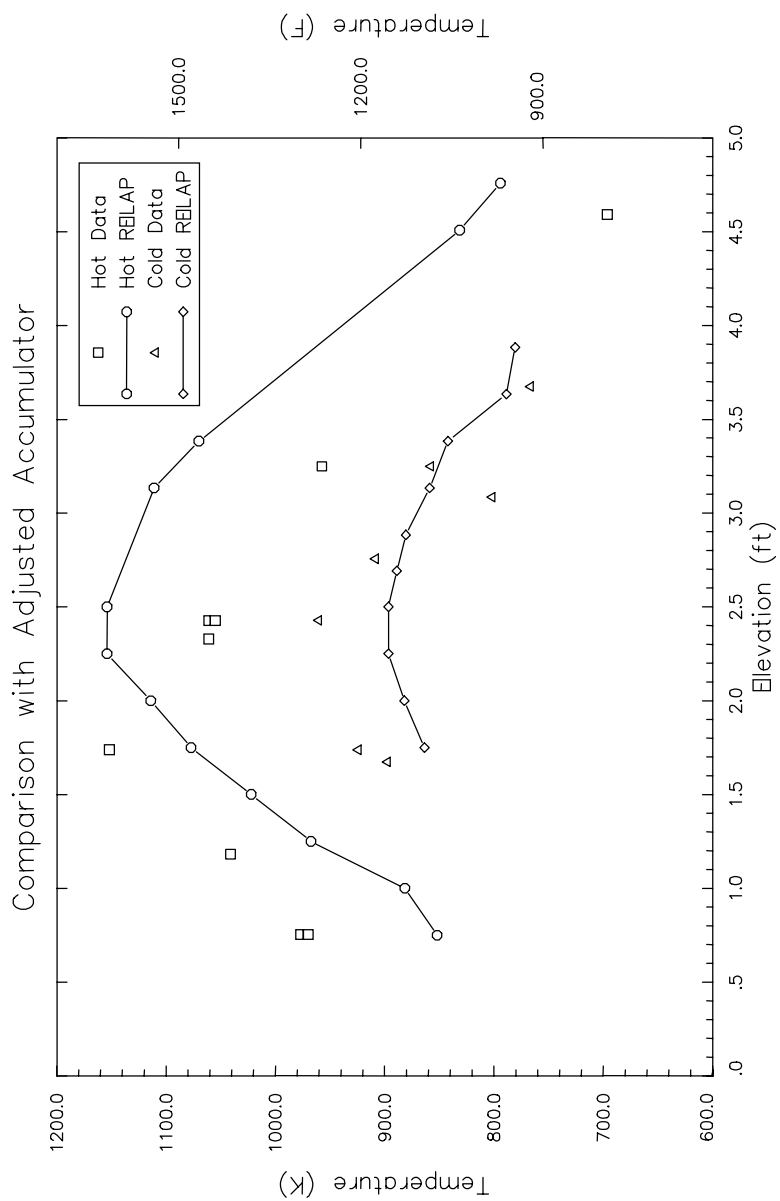
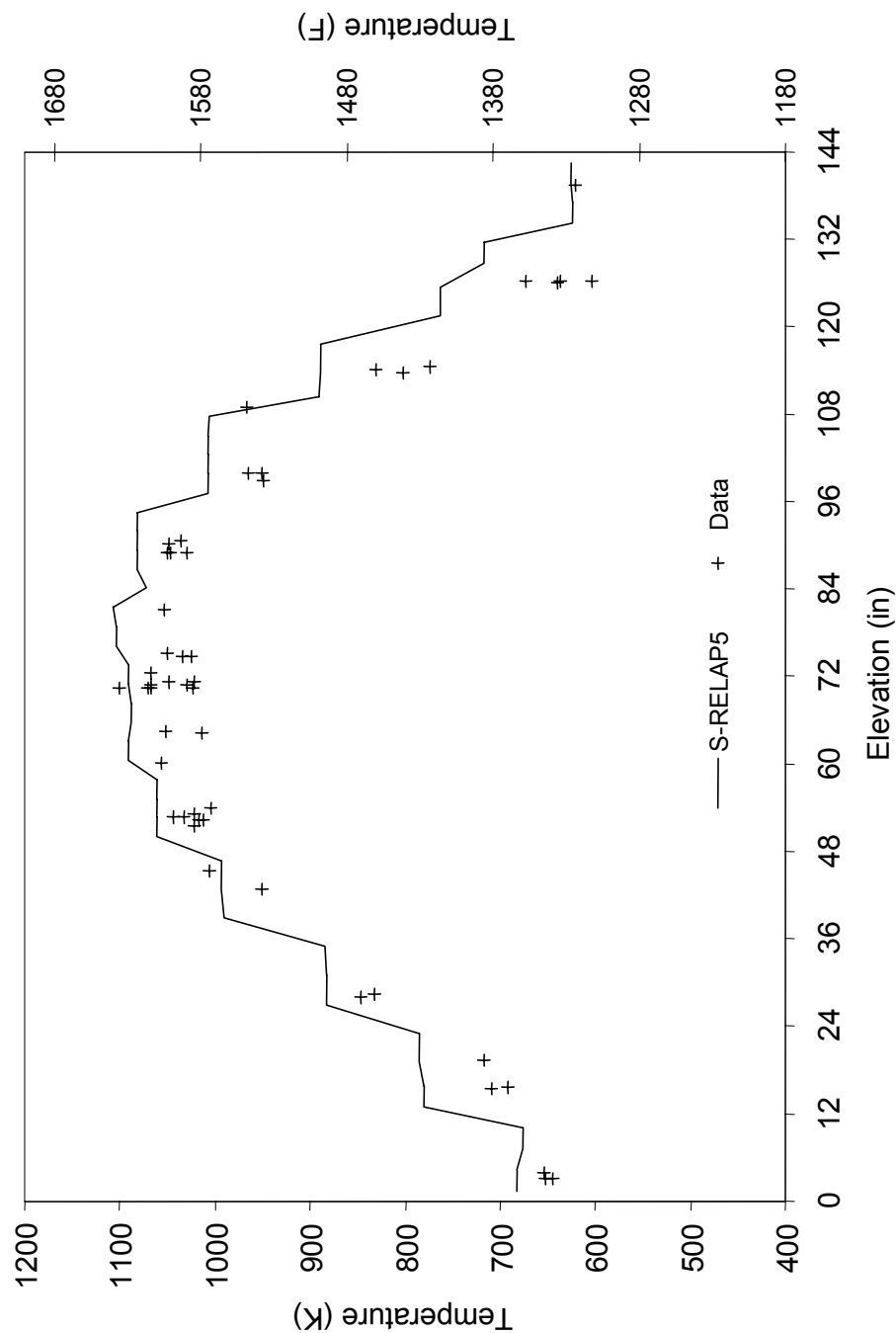


Figure 4.152 Assessment of Semiscale LBLOCA Test S-06-3, PCTs



**Figure 4.153 Assessment of Semiscale LBLOCA Test S-07-1,
PCTs versus Elevation**

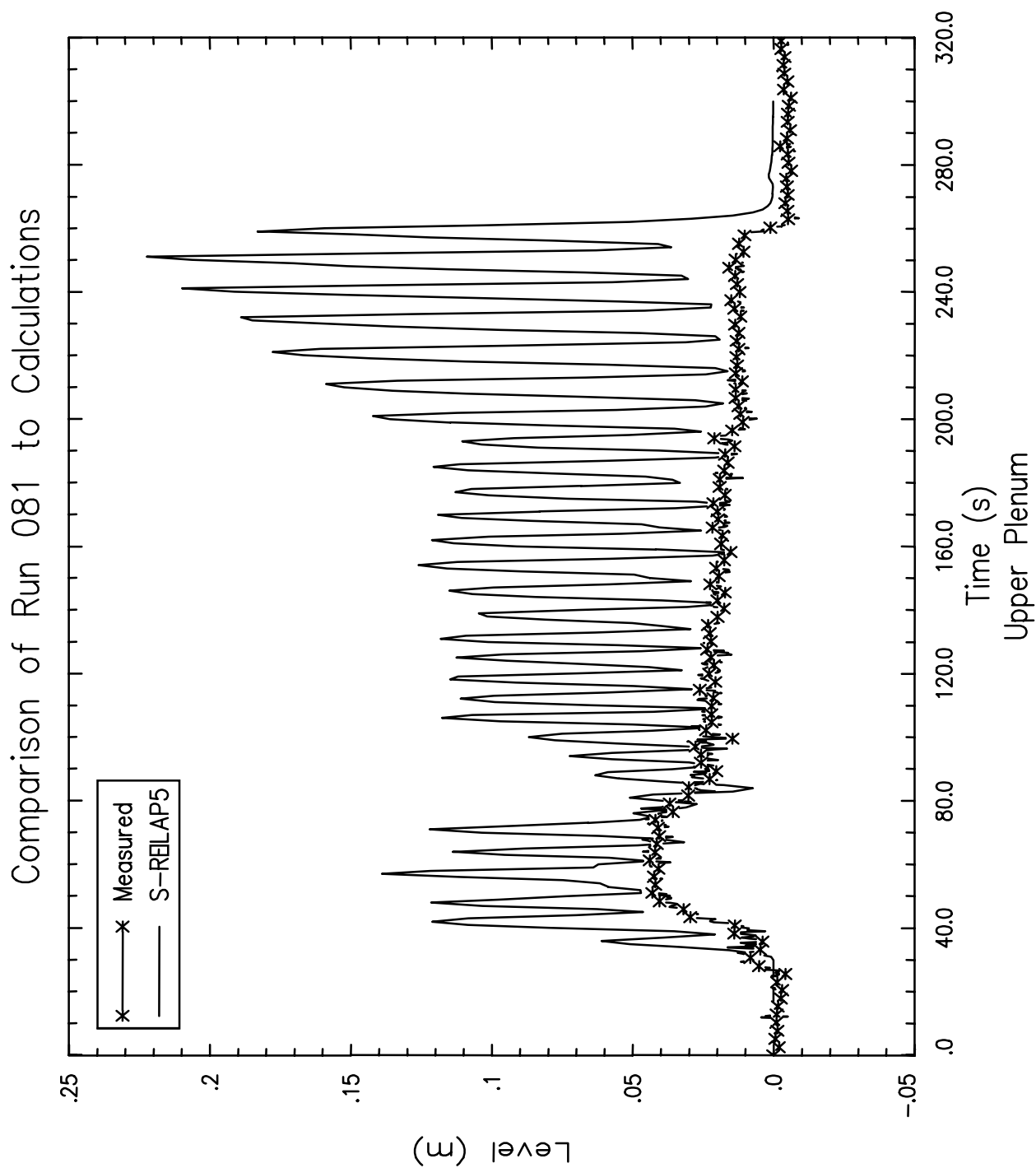


Figure 4.154 Upper Plenum Level, UPTF Test 10, Run 081

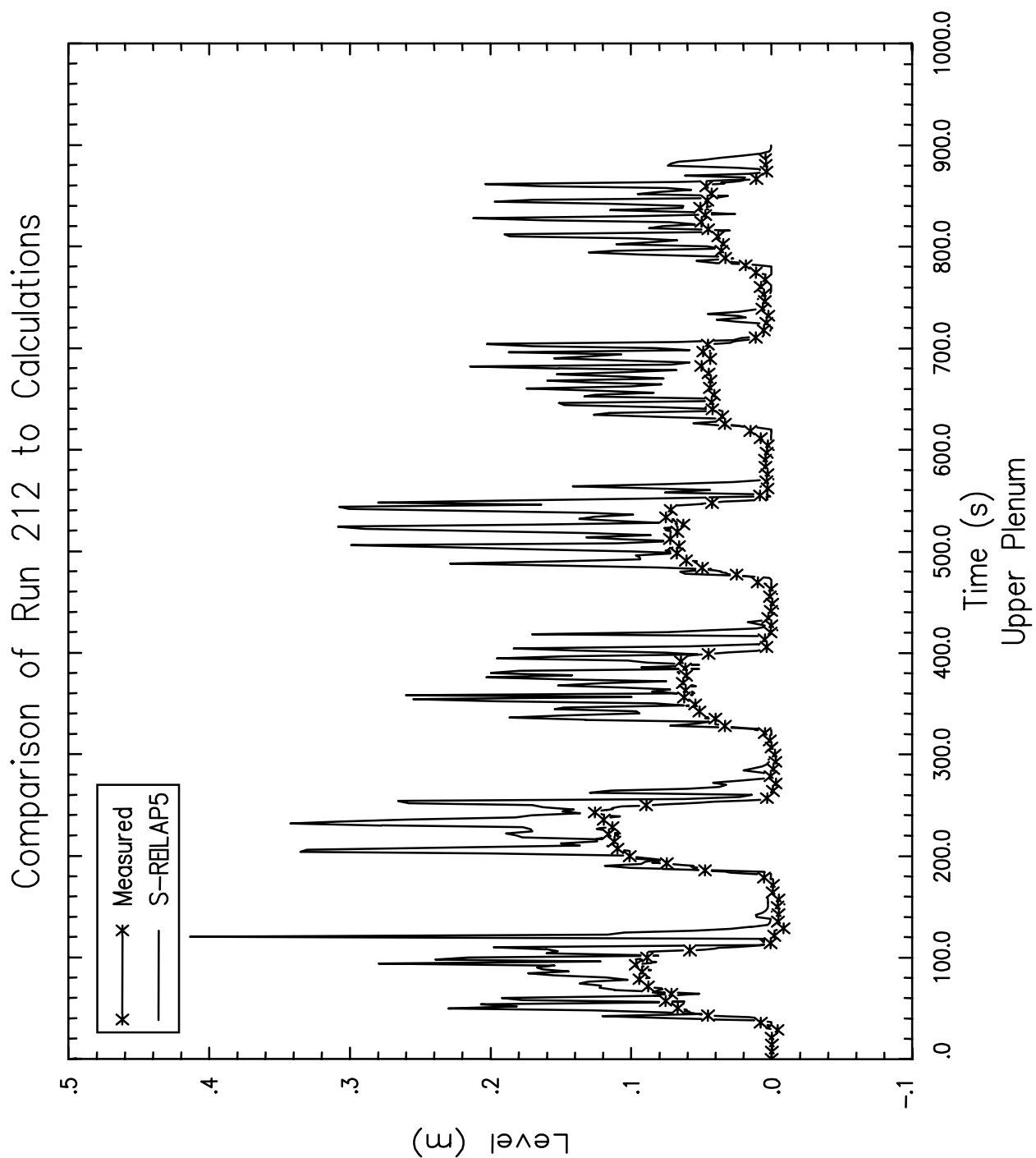


Figure 4.155 Upper Plenum Level, UPTF Test 29 Run 212/211

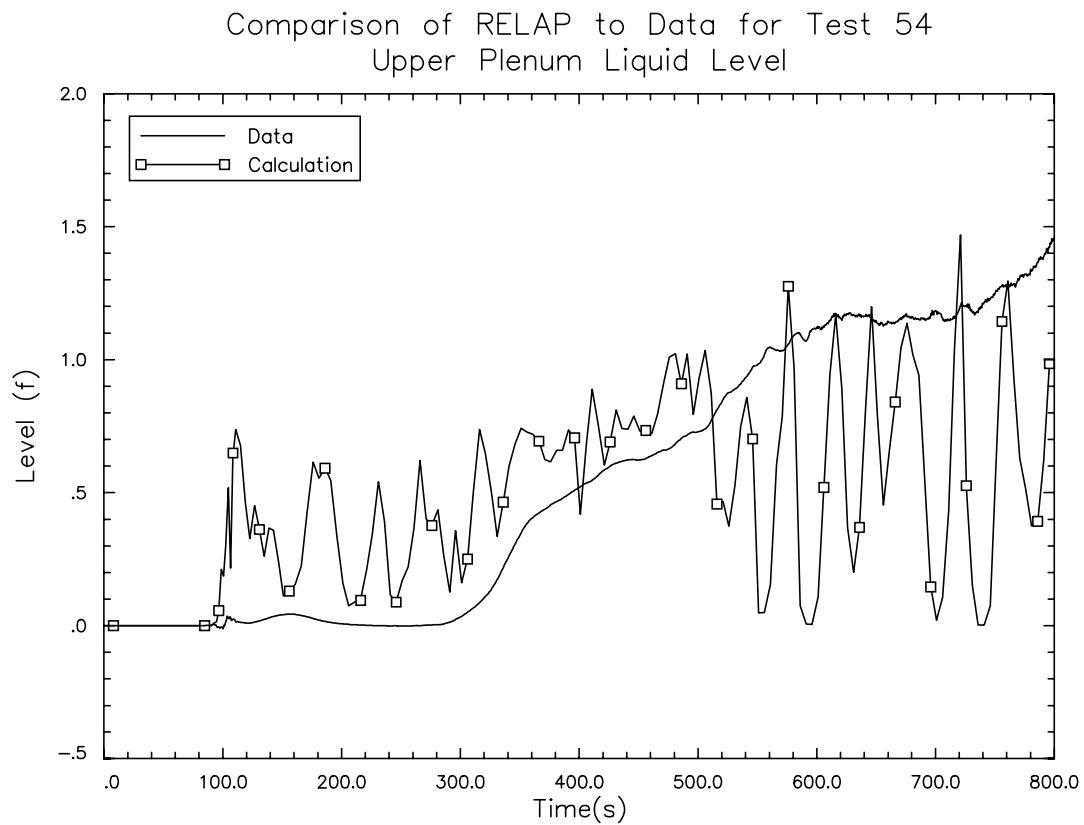


Figure 4.156 Liquid Level in Upper Plenum CCTF Test 54

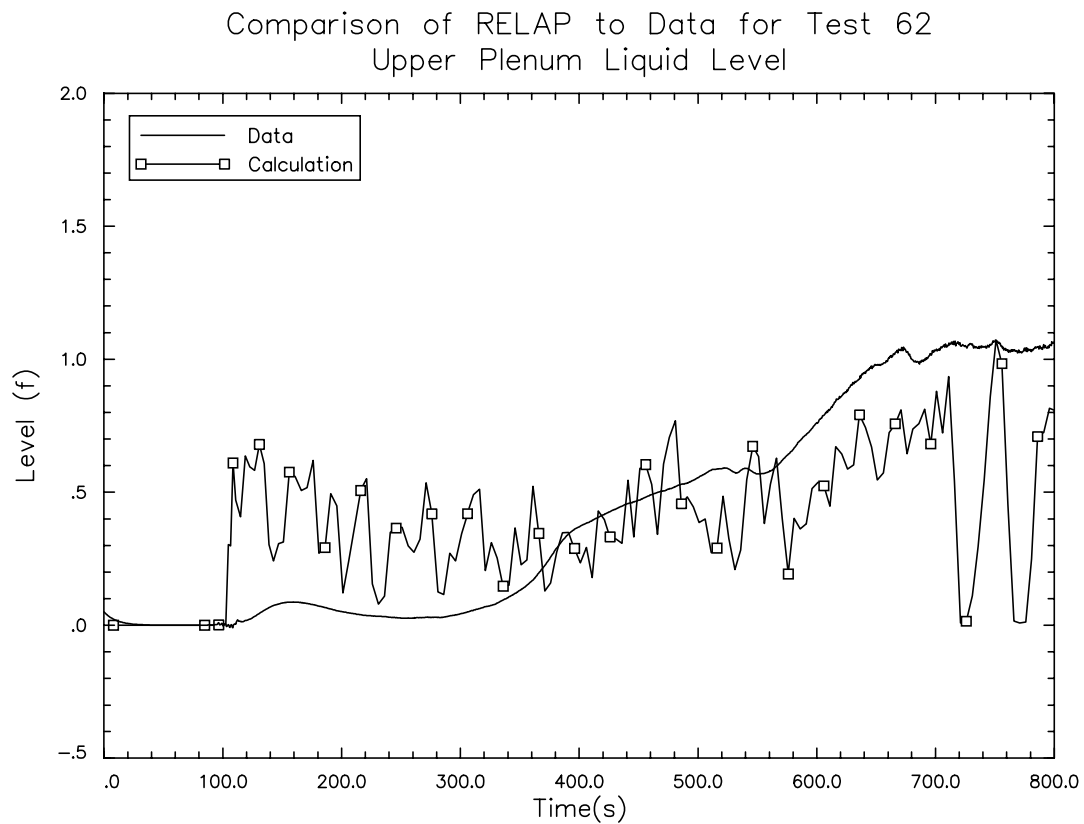


Figure 4.157 Liquid Level in Upper Plenum CCTF Test 62

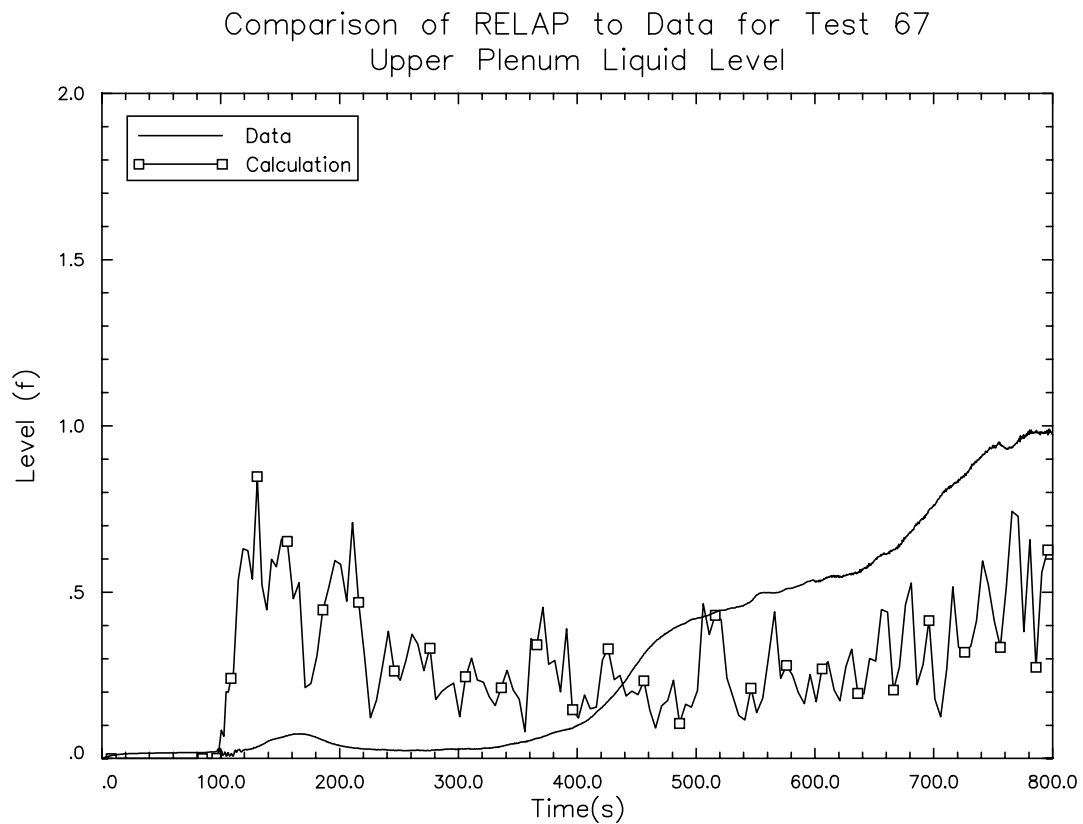


Figure 4.158 Liquid Level in Upper Plenum CCTF Test 67

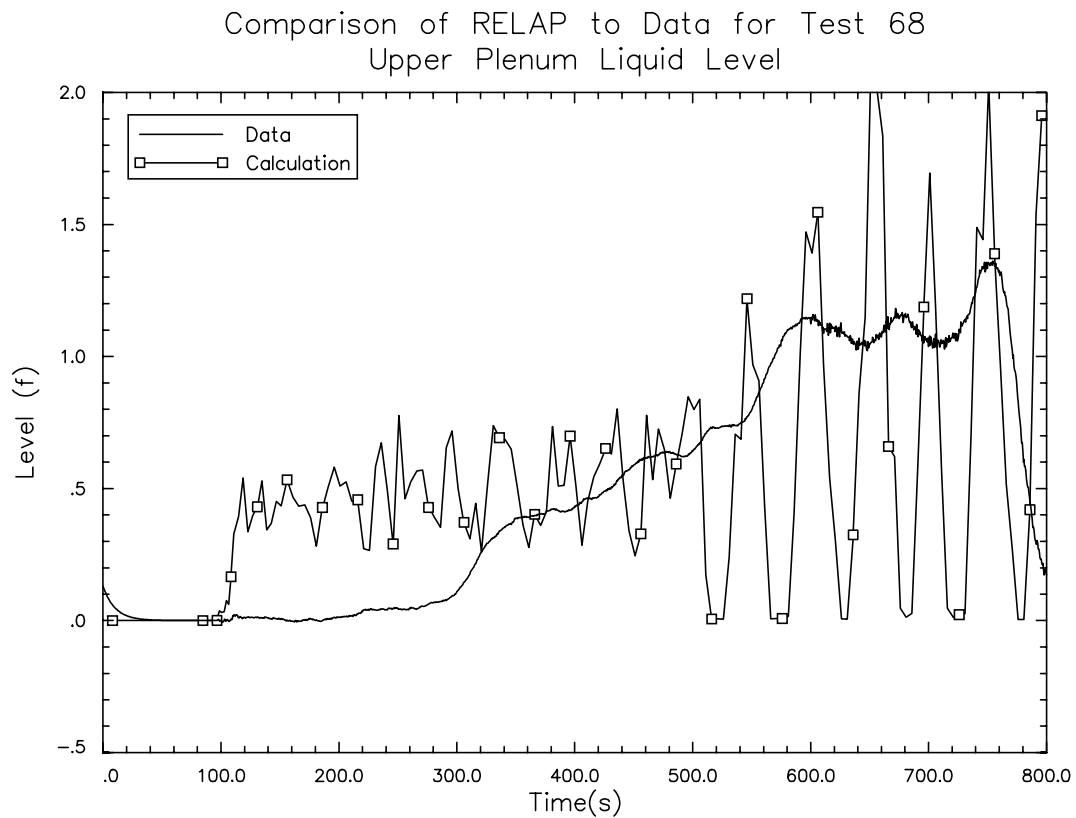


Figure 4.159 Liquid Level in Upper Plenum CCTF Test 68

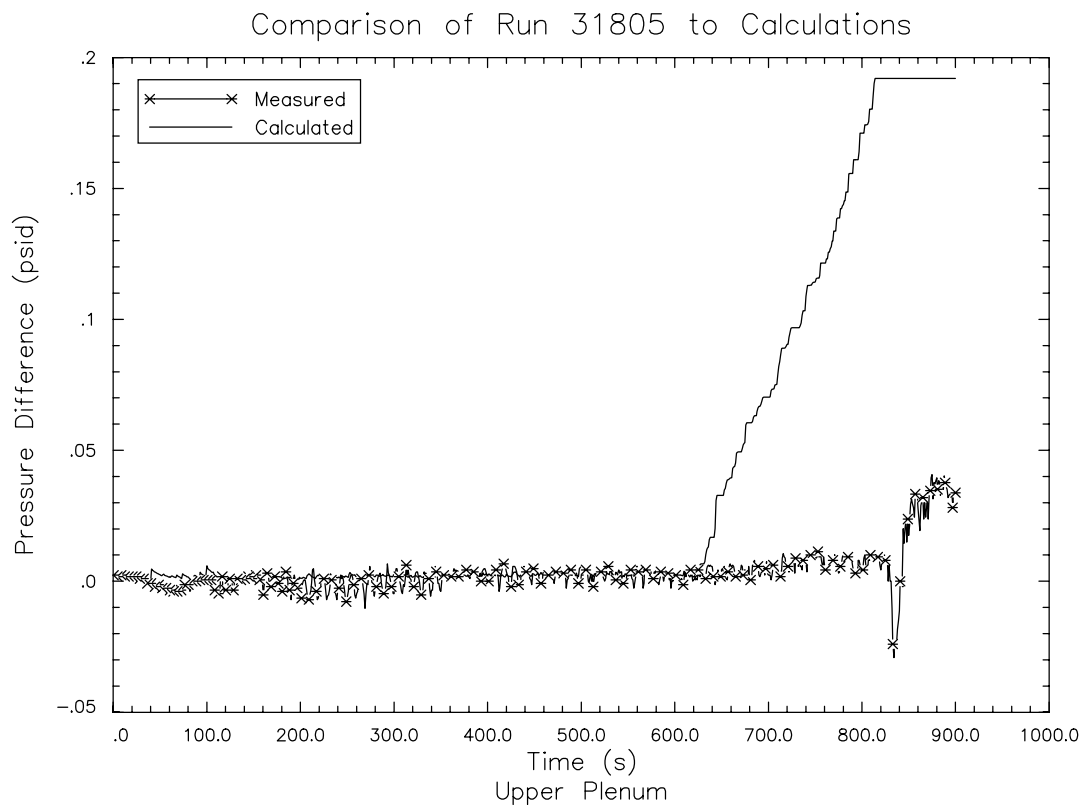


Figure 4.160 Upper Plenum Levels for FLECHT-SEASET Test 31805

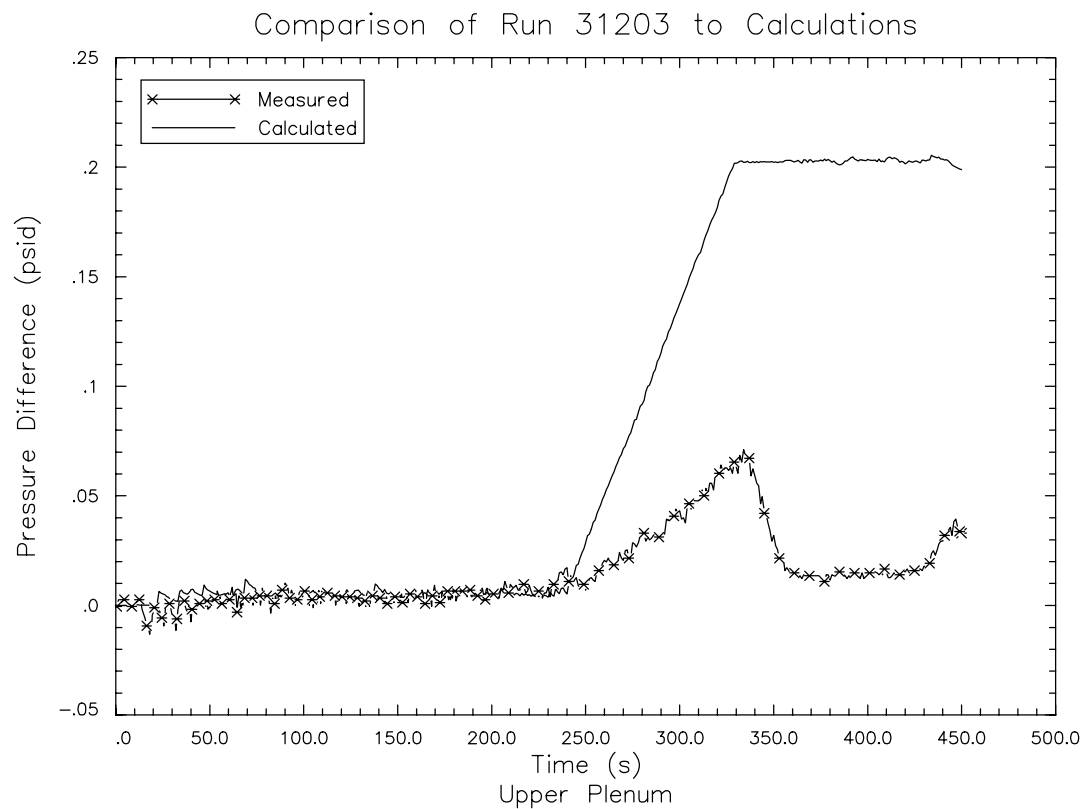


Figure 4.161 Upper Plenum Levels for FLECHT-SEASET Test 31203

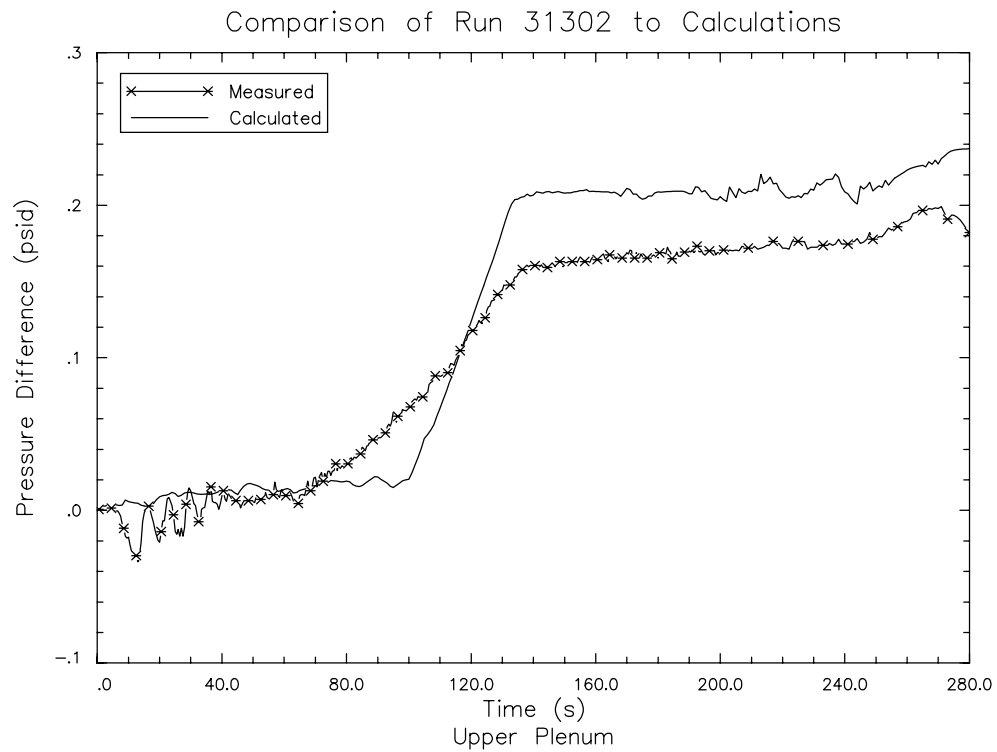


Figure 4.162 Upper Plenum Levels for FLECHT-SEASET Test 31302

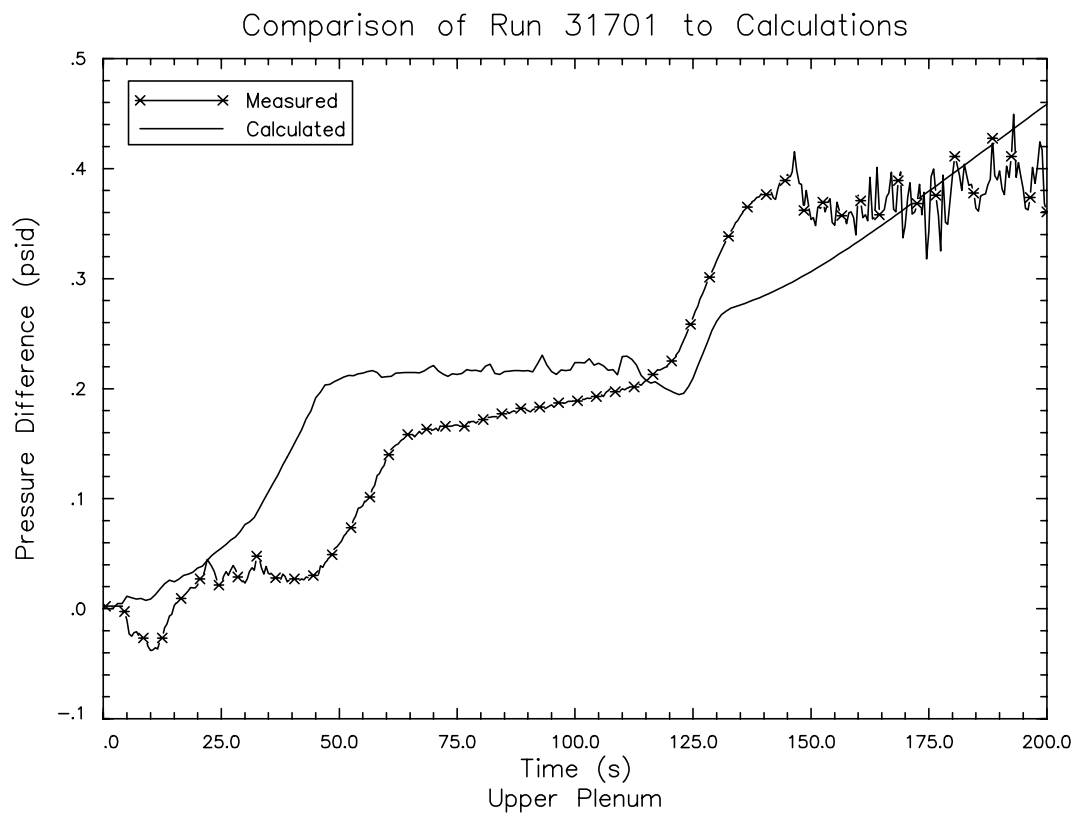


Figure 4.163 Upper Plenum Levels for FLECHT-SEASET Test 31701

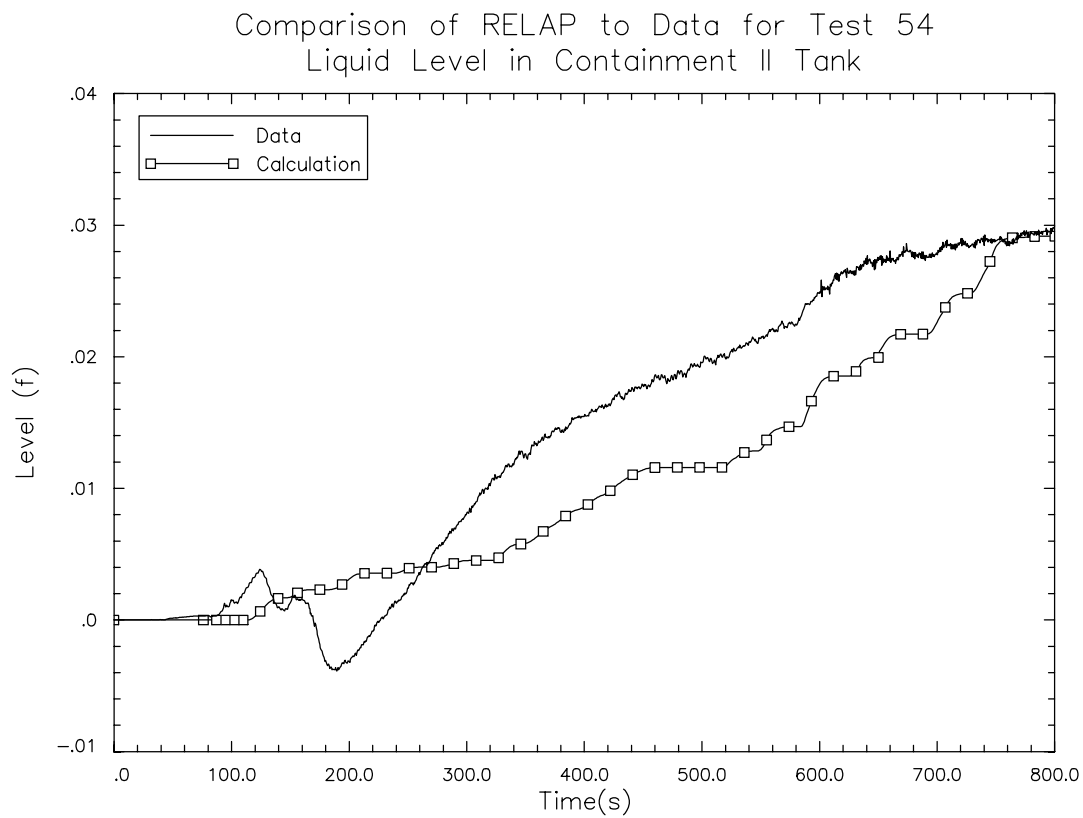


Figure 4.164 Comparison of Liquid Carryover for CCTF Test 54

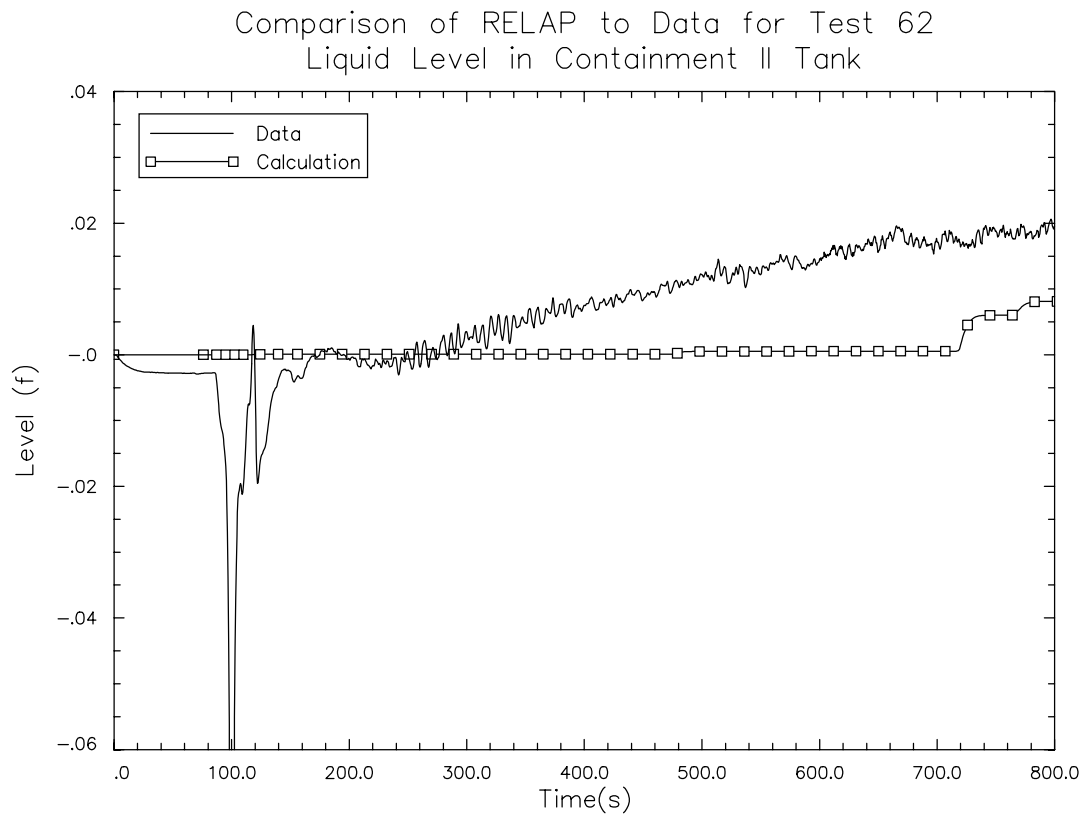


Figure 4.165 Comparison of Liquid Carryover for CCTF Test 62

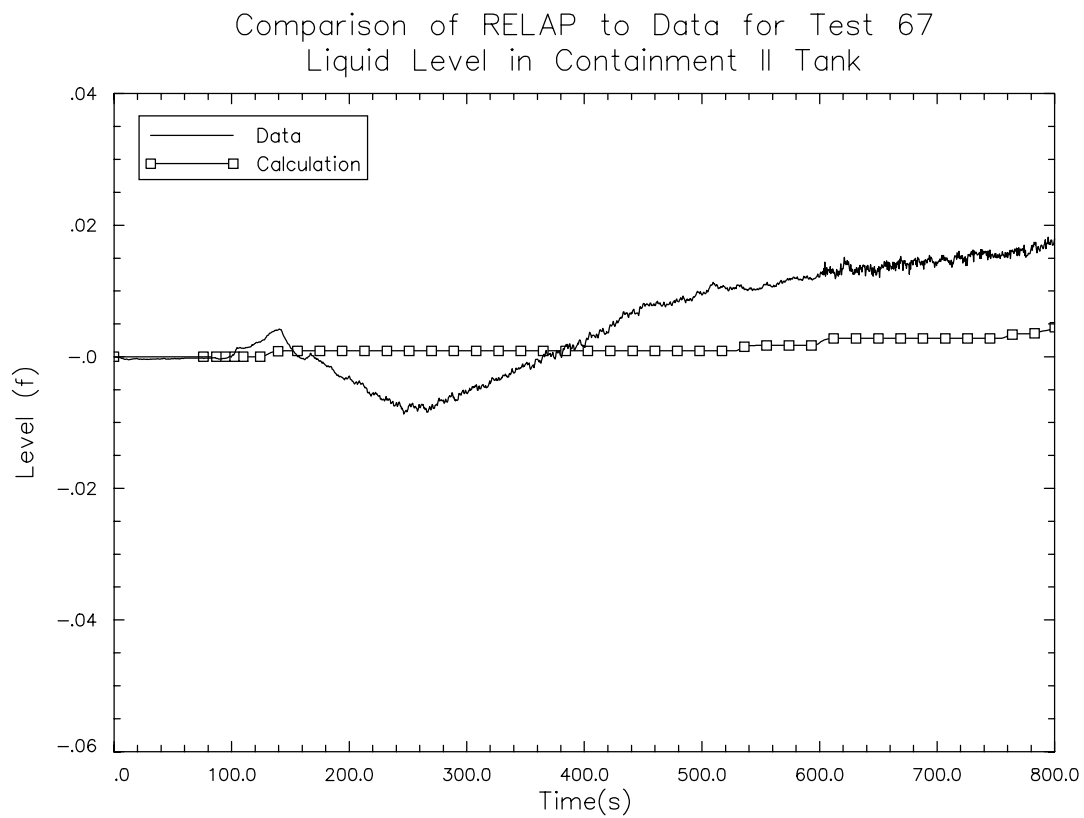


Figure 4.166 Comparison of Liquid Carryover for CCTF Test 67

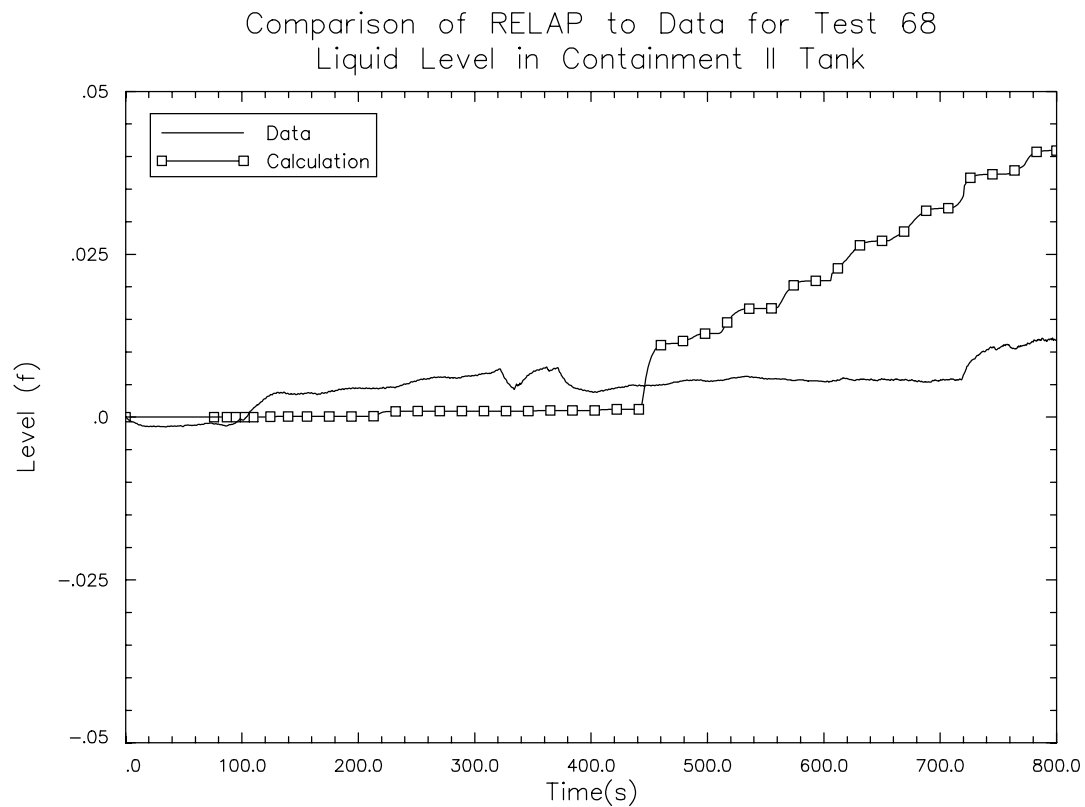


Figure 4.167 Comparison of Liquid Carryover for CCTF Test 68

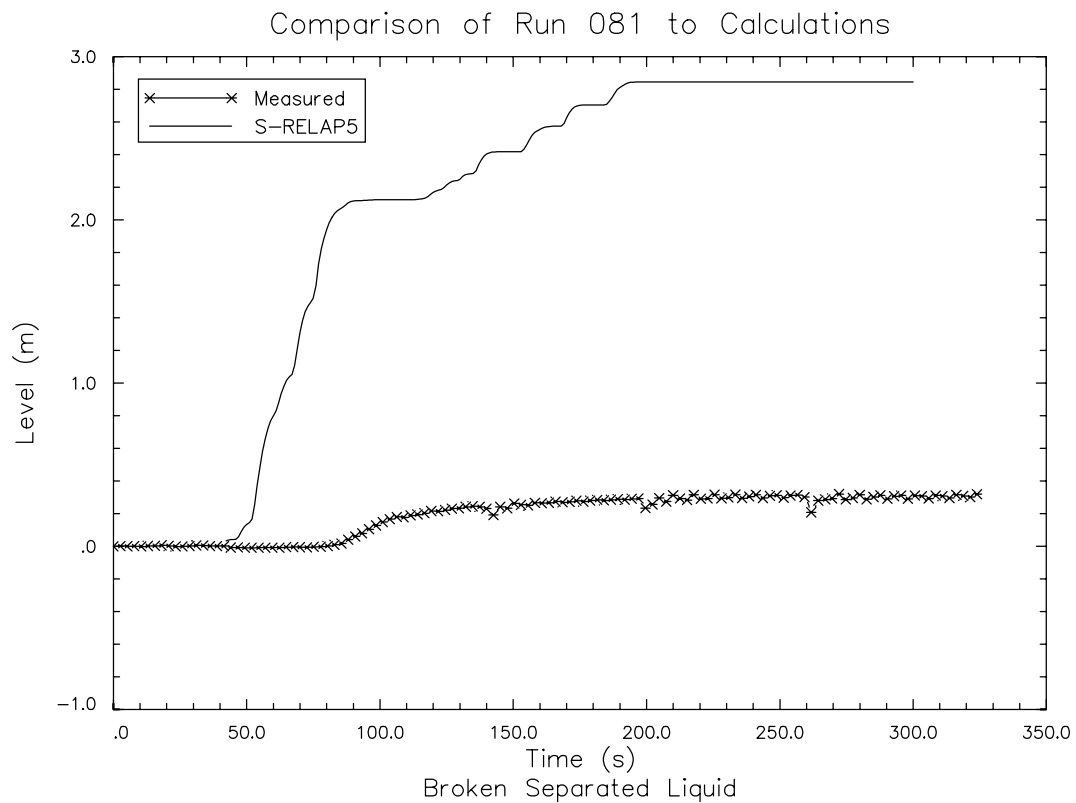


Figure 4.168 Level in Broken Loop Catch Tank - UPTF Test 081

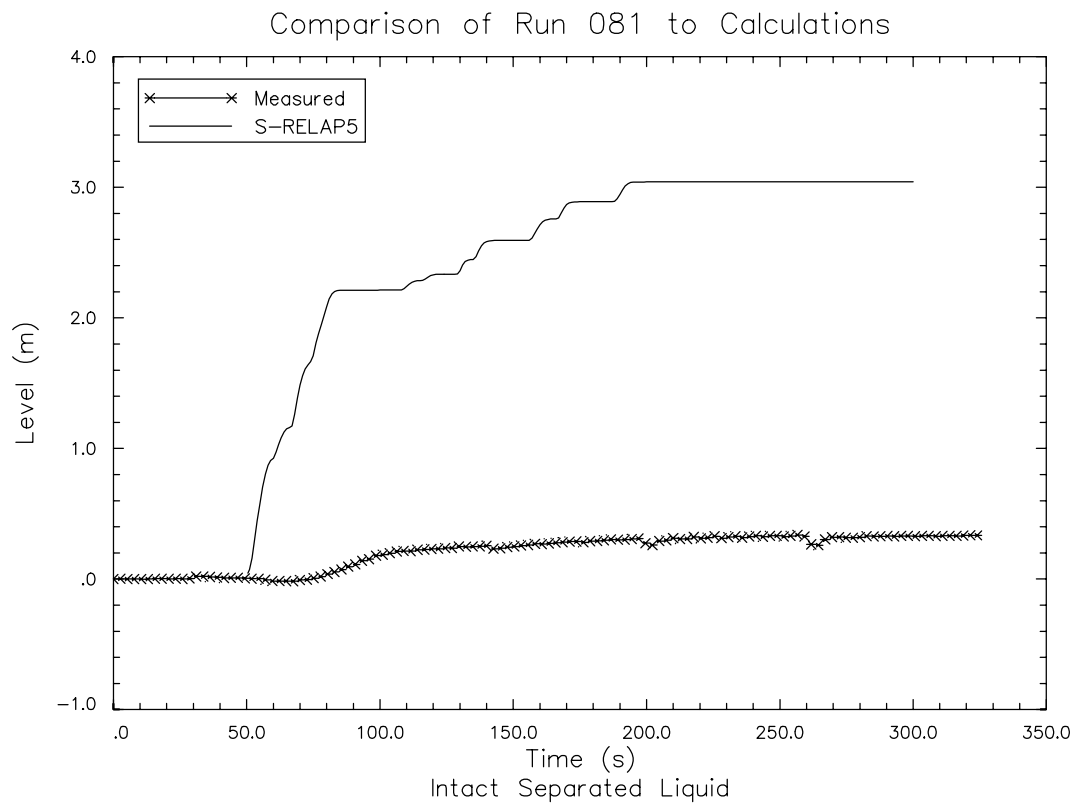


Figure 4.169 Level in Intact Loop Catch Tank - UPTF Test 081

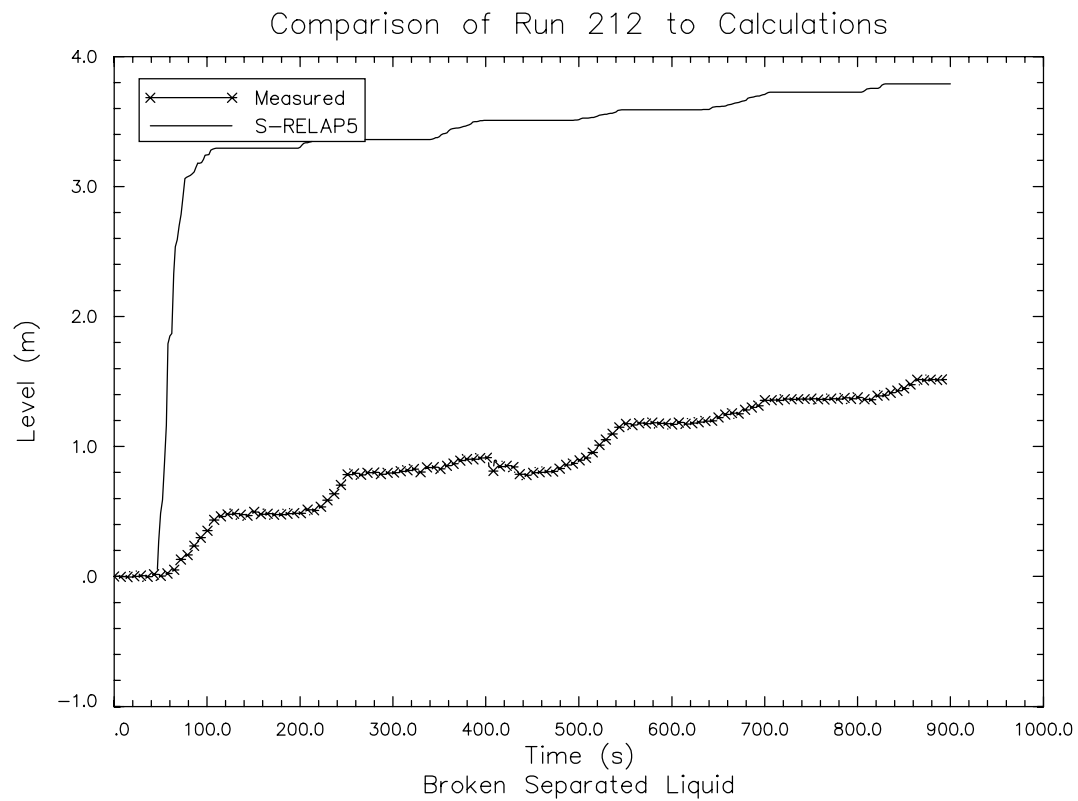


Figure 4.170 Level in Broken Loop Catch Tank - UPTF Test 212

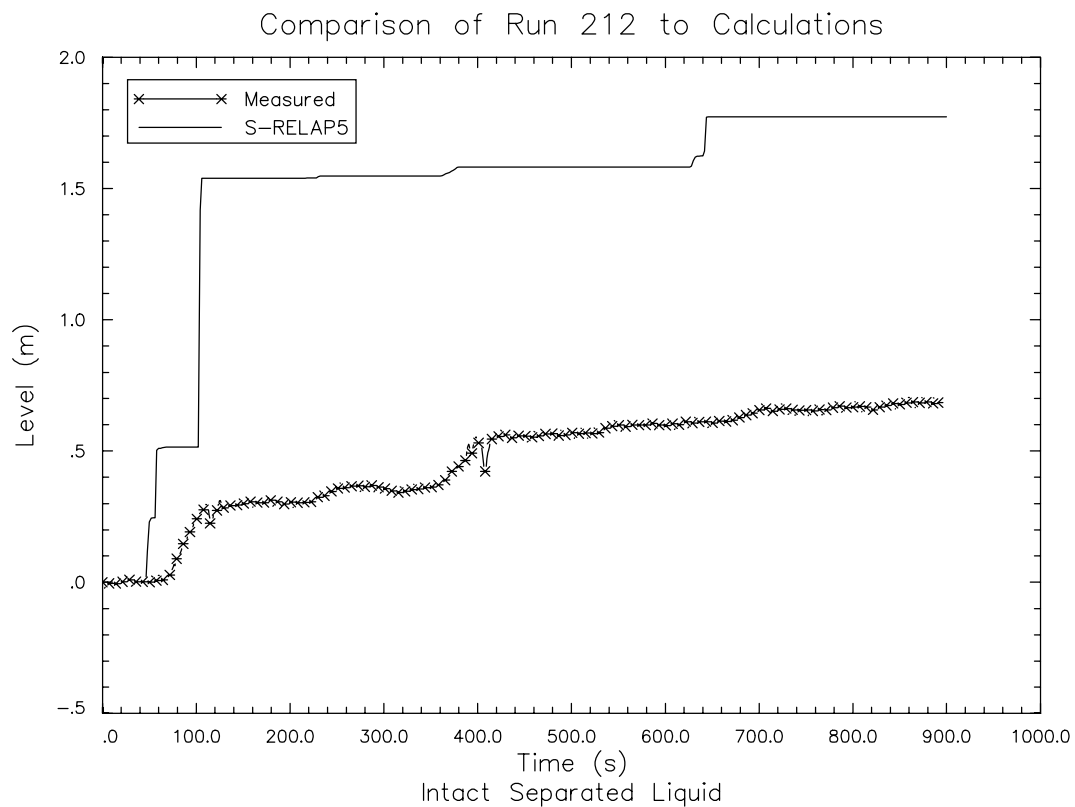
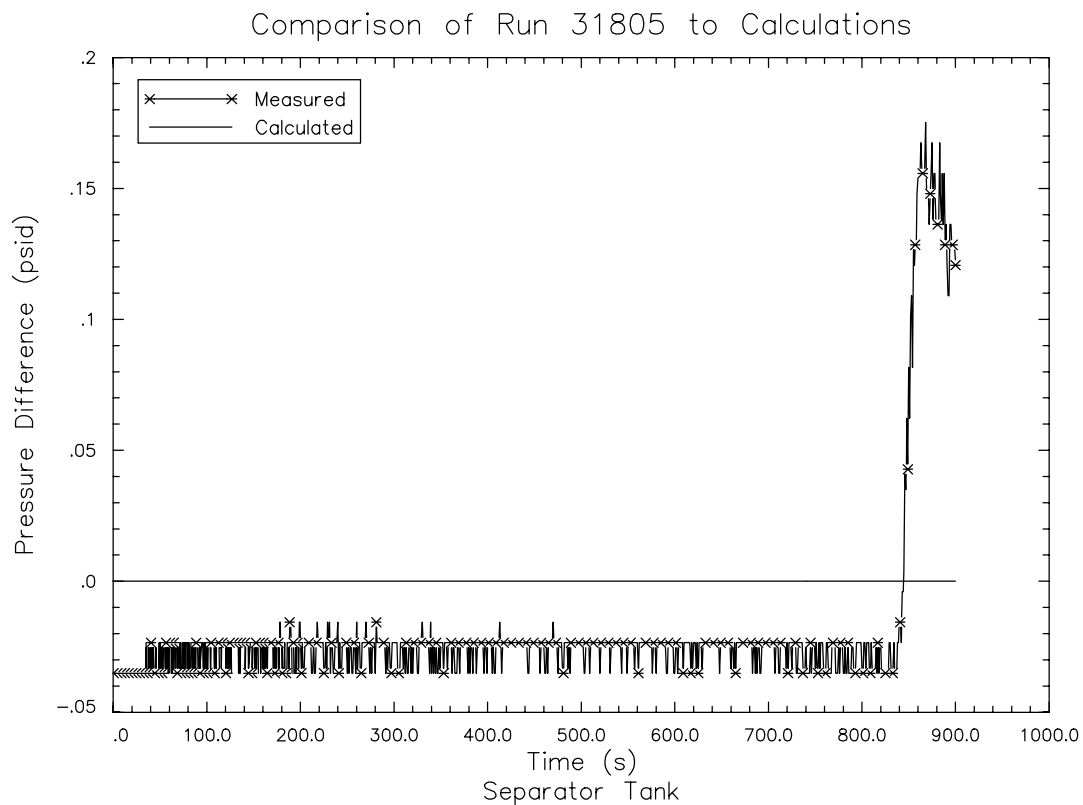
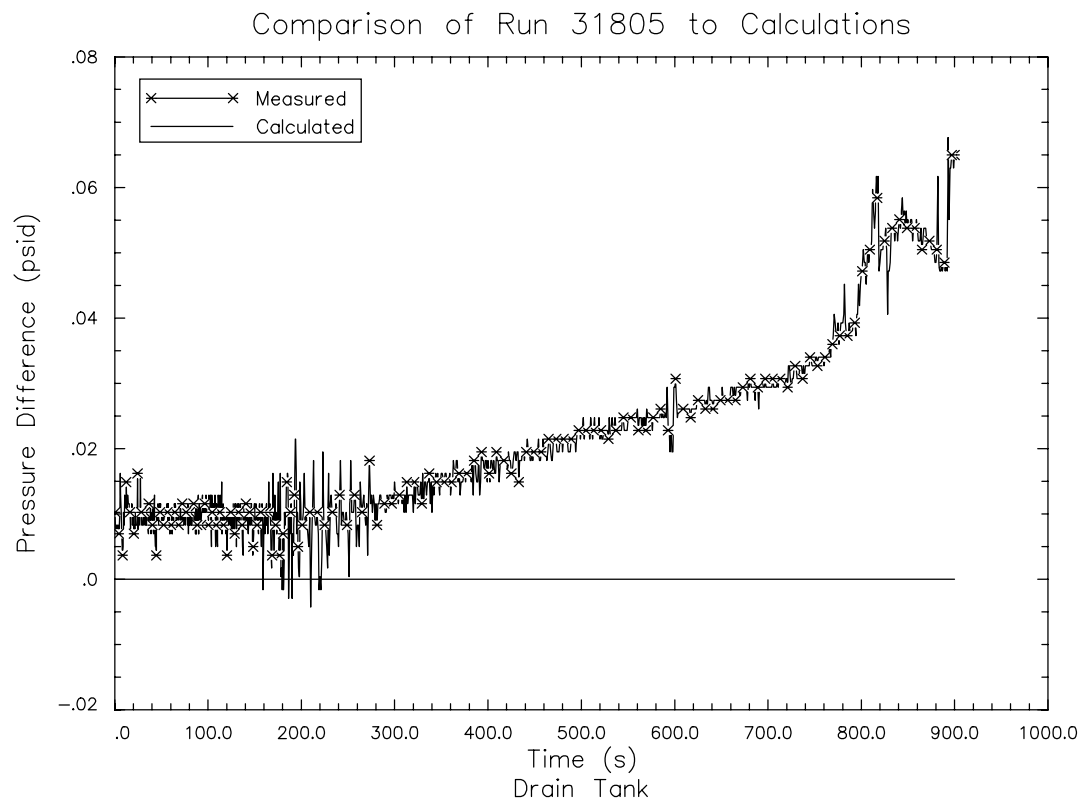


Figure 4.171 Level in Intact Loop Catch Tank - UPTF Test 212



**Figure 4.172 Level in Separator Tank for FLECHT-SEASET
Tests 31805**



**Figure 4.173 Level in Separator Drain Tank for FLECHT-SEASET
Tests 31805**

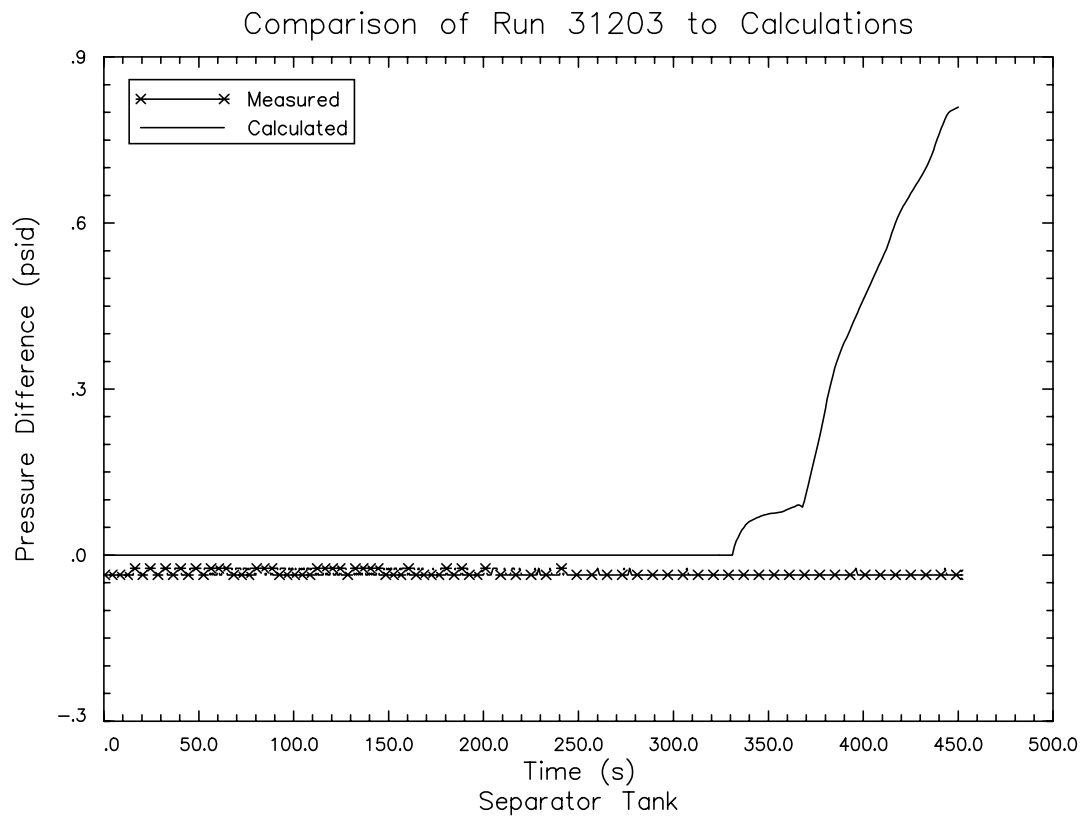


**Figure 4.174 Level in Separator Tank for FLECHT-SEASET
Tests 31203**

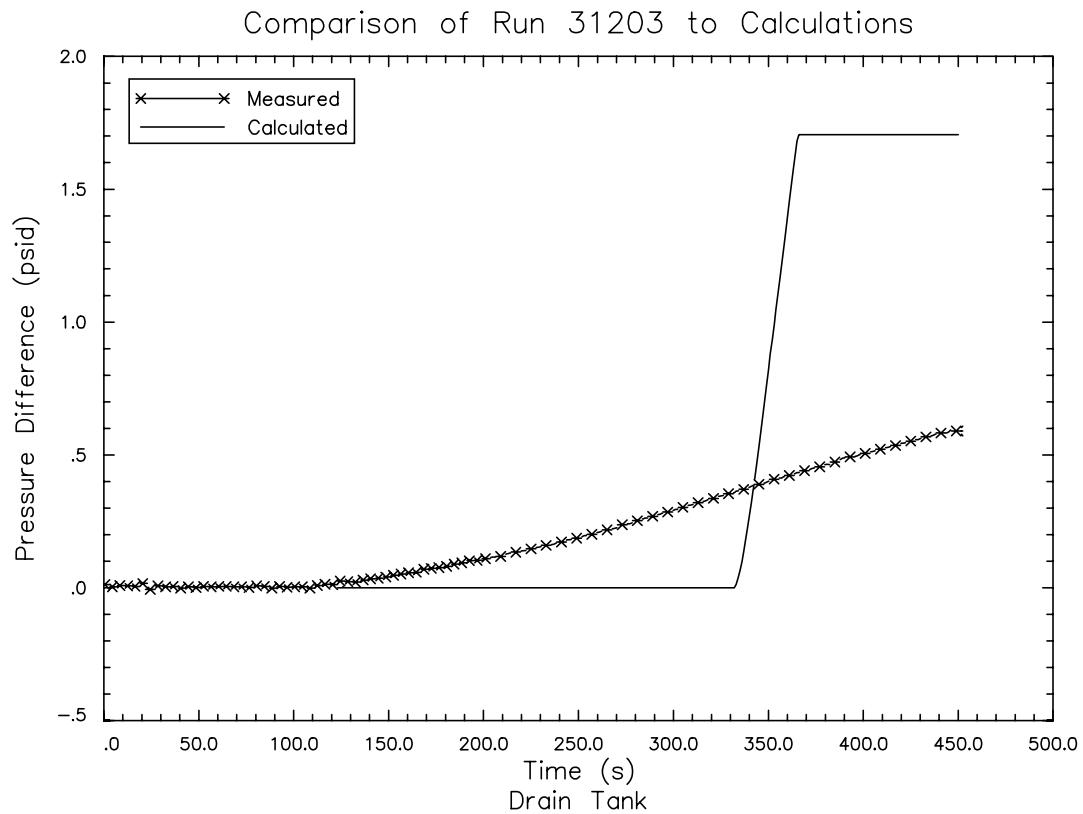


**Figure 4.175 Level in Separator Drain Tank for FLECHT-SEASET
Tests 31203**

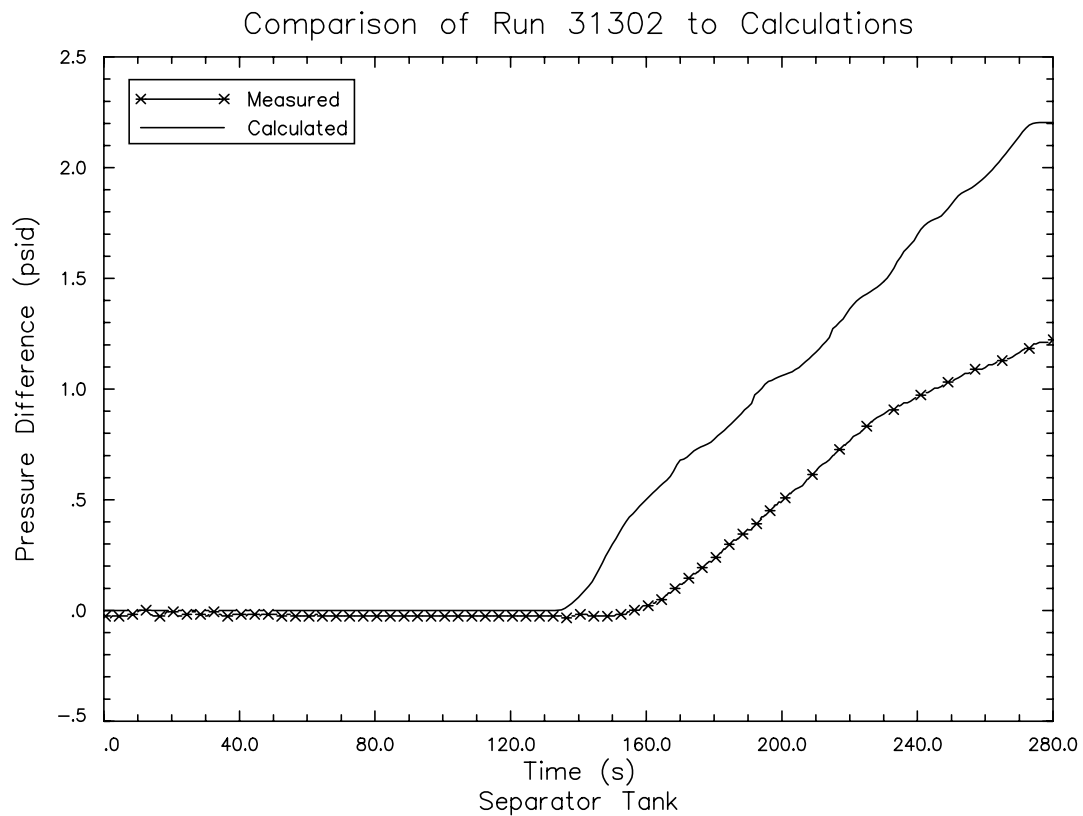


**Figure 4.176 Level in Separator Tank for FLECHT-SEASET
Tests 31302**

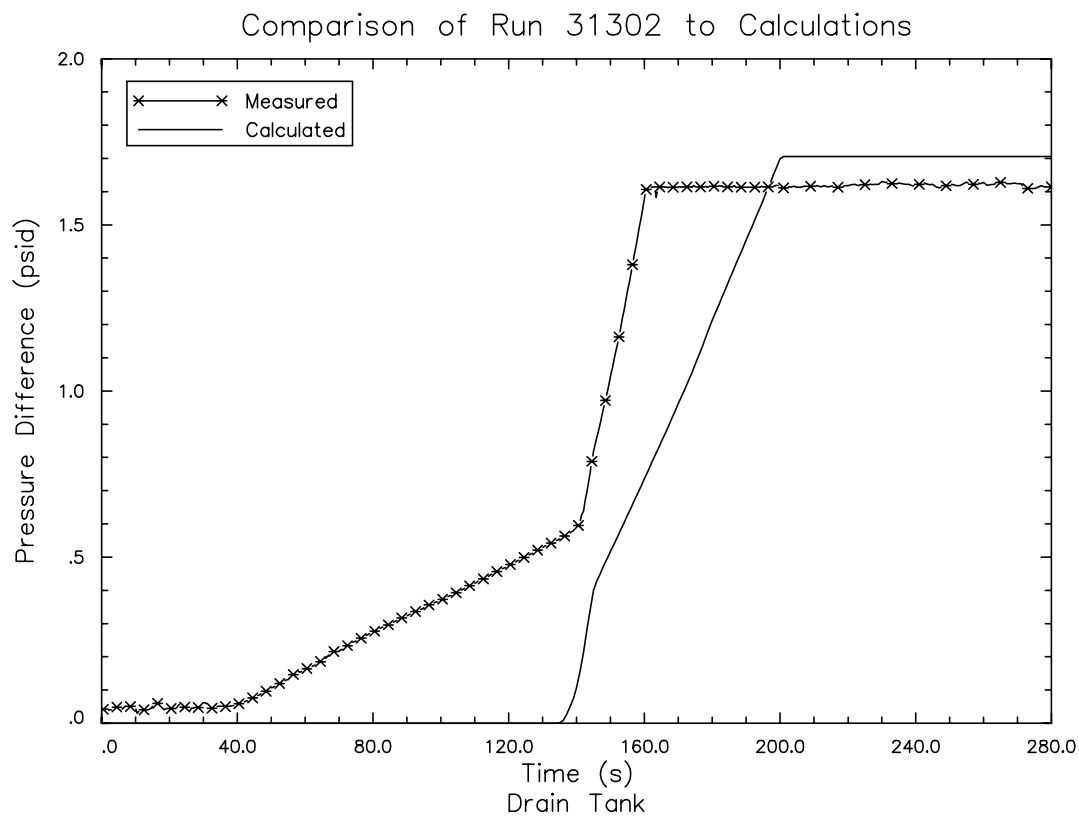


**Figure 4.177 Level in Separator Drain Tank for FLECHT-SEASET
Tests 31302**

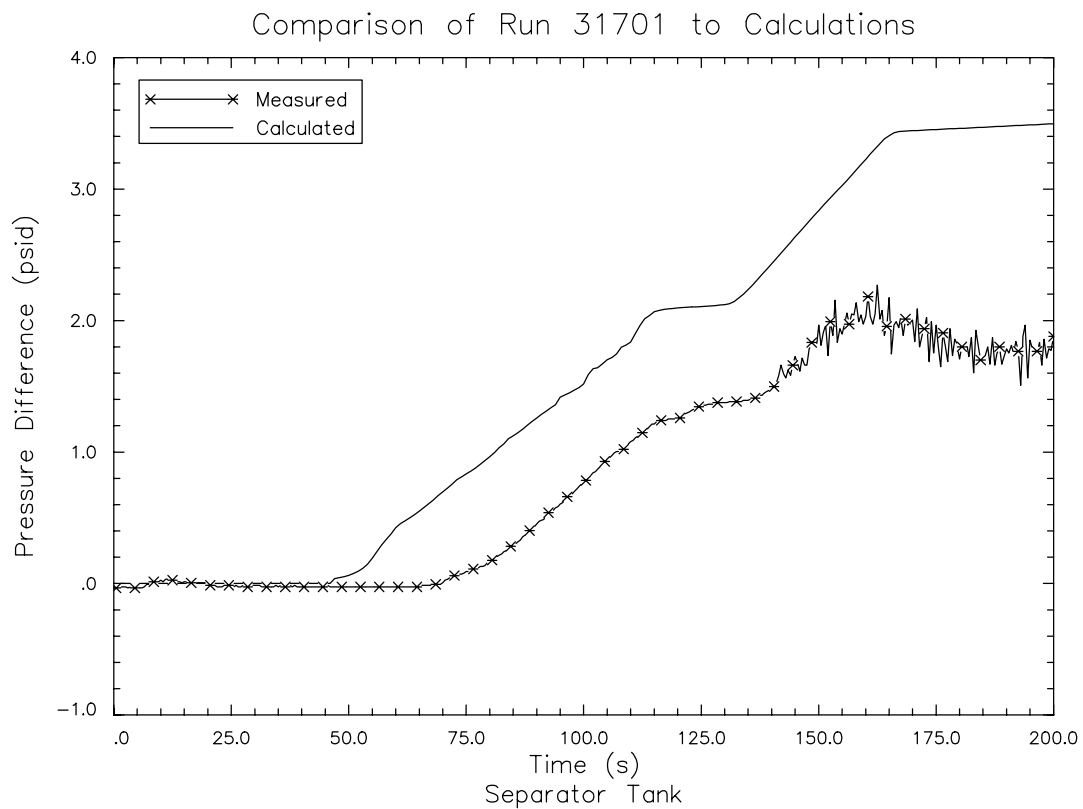


**Figure 4.178 Level in Separator Tank for FLECHT-SEASET
Tests 31701**

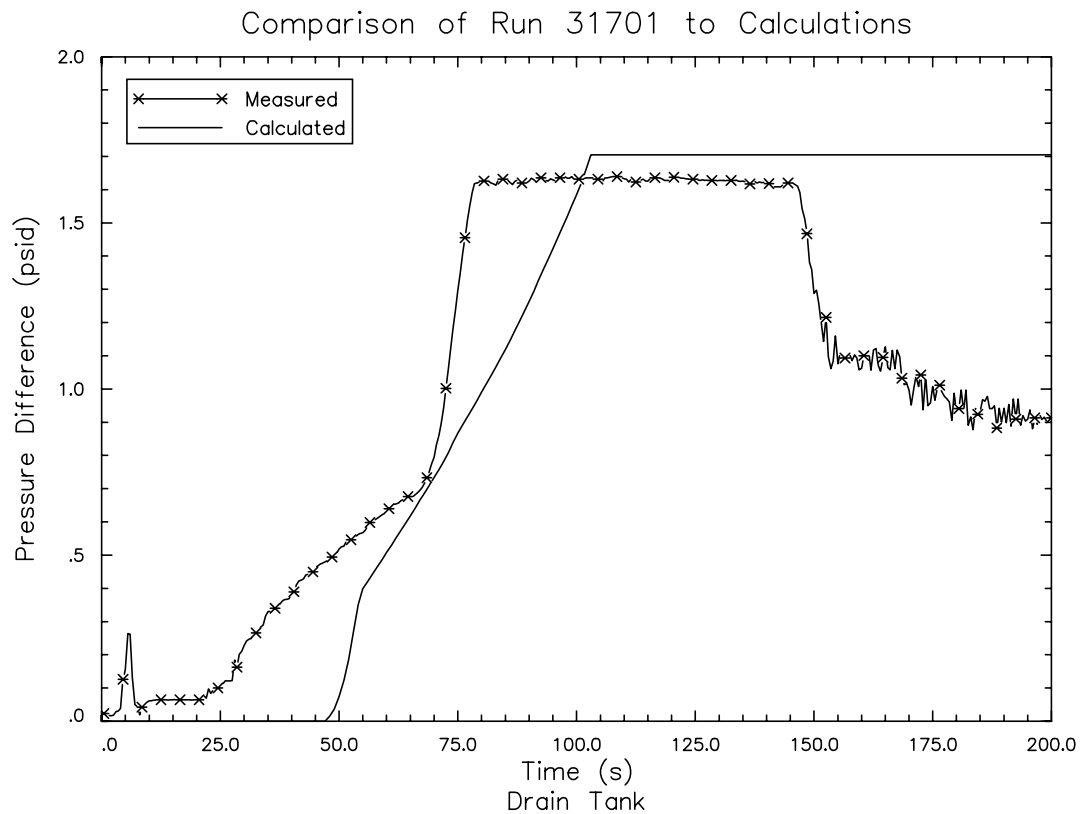


**Figure 4.179 Level in Separator Drain Tank for FLECHT-SEASET
Tests 31701**

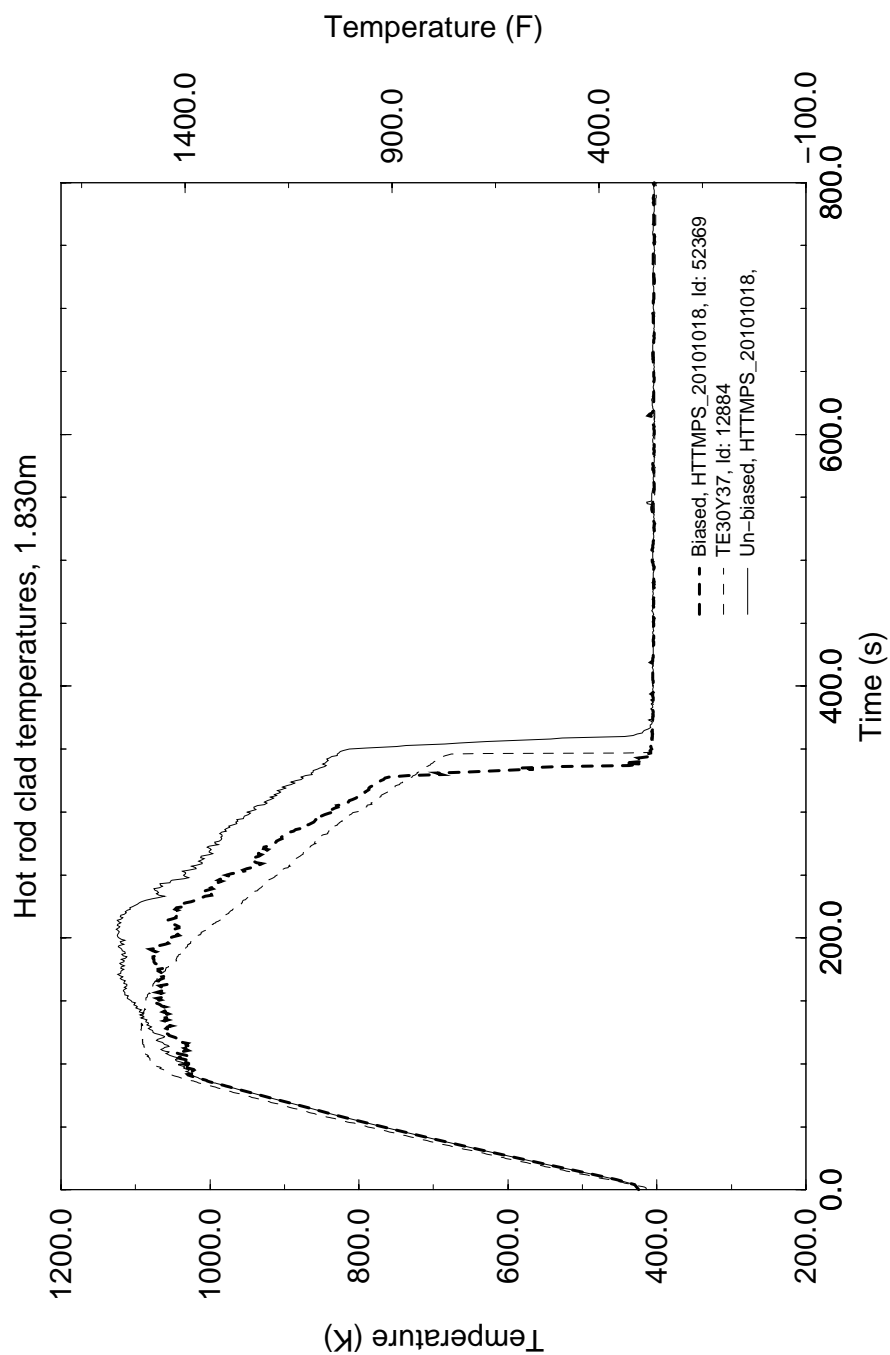
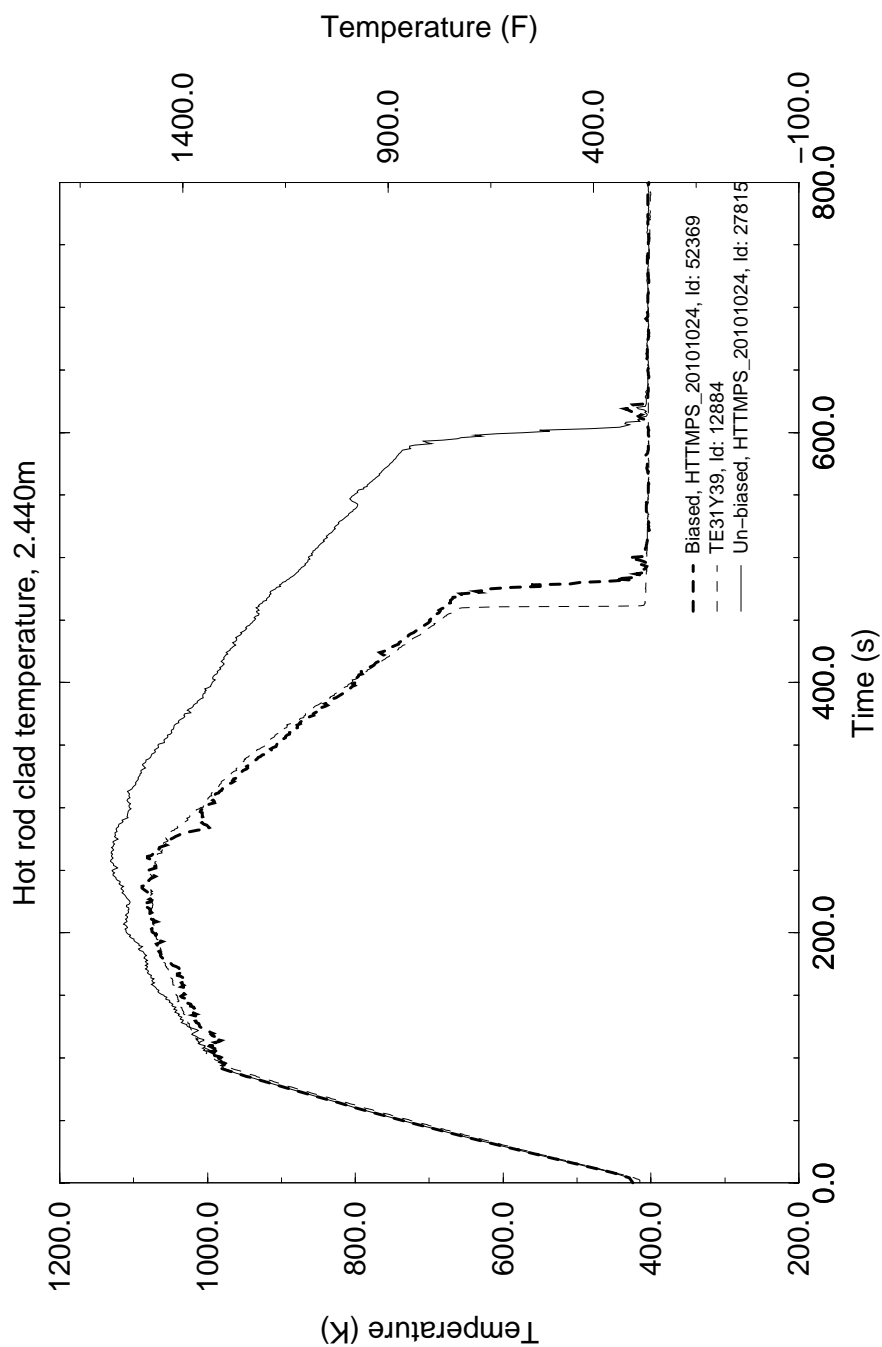


Figure 4.180 CCTF TEST 54 Temperatures at Measured PCT Node



**Figure 4.181 CCTF TEST 54 Temperatures Near Calculated
PCT Node**

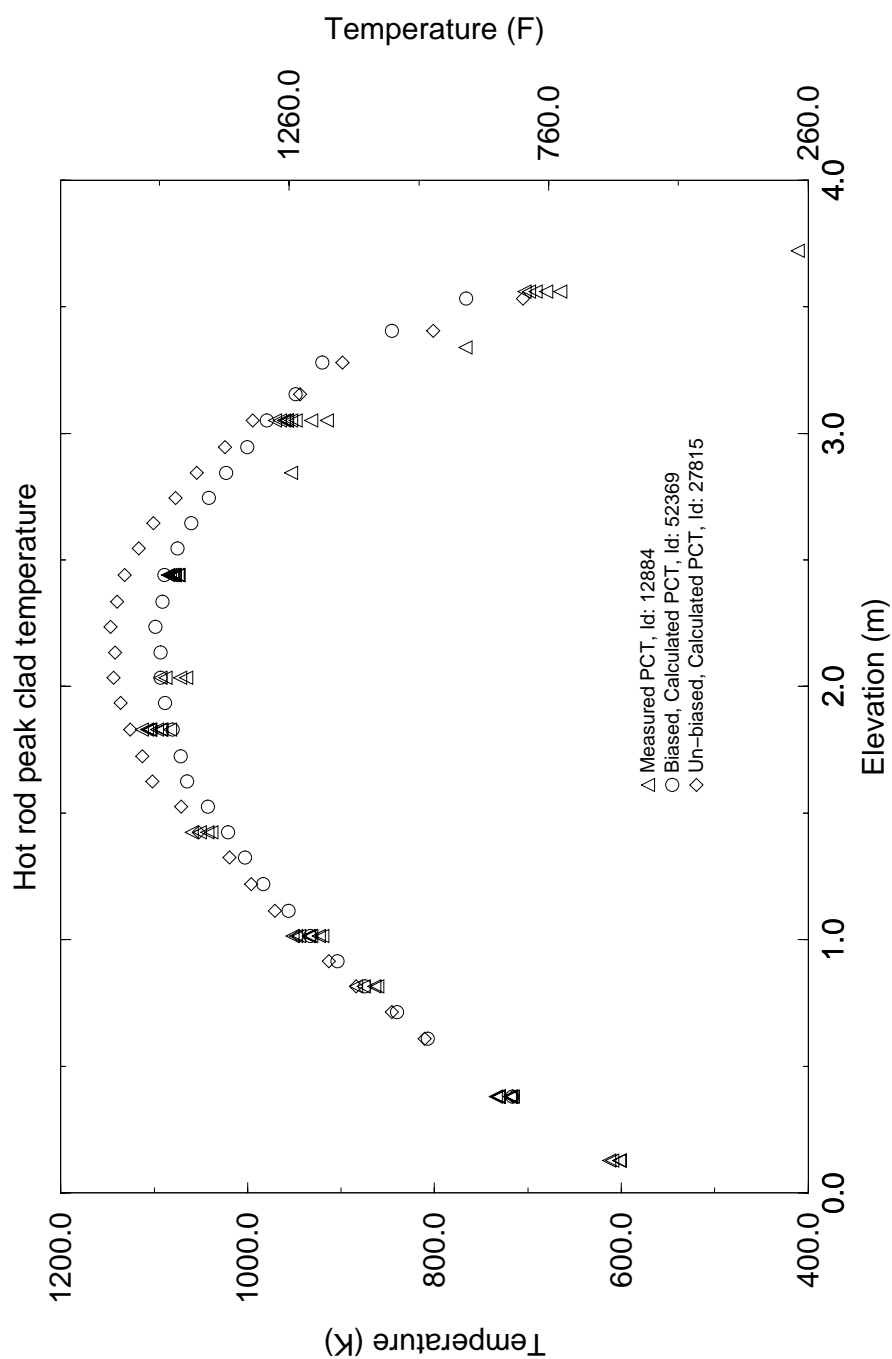


Figure 4.182 CCTF TEST 54 PCT Profile

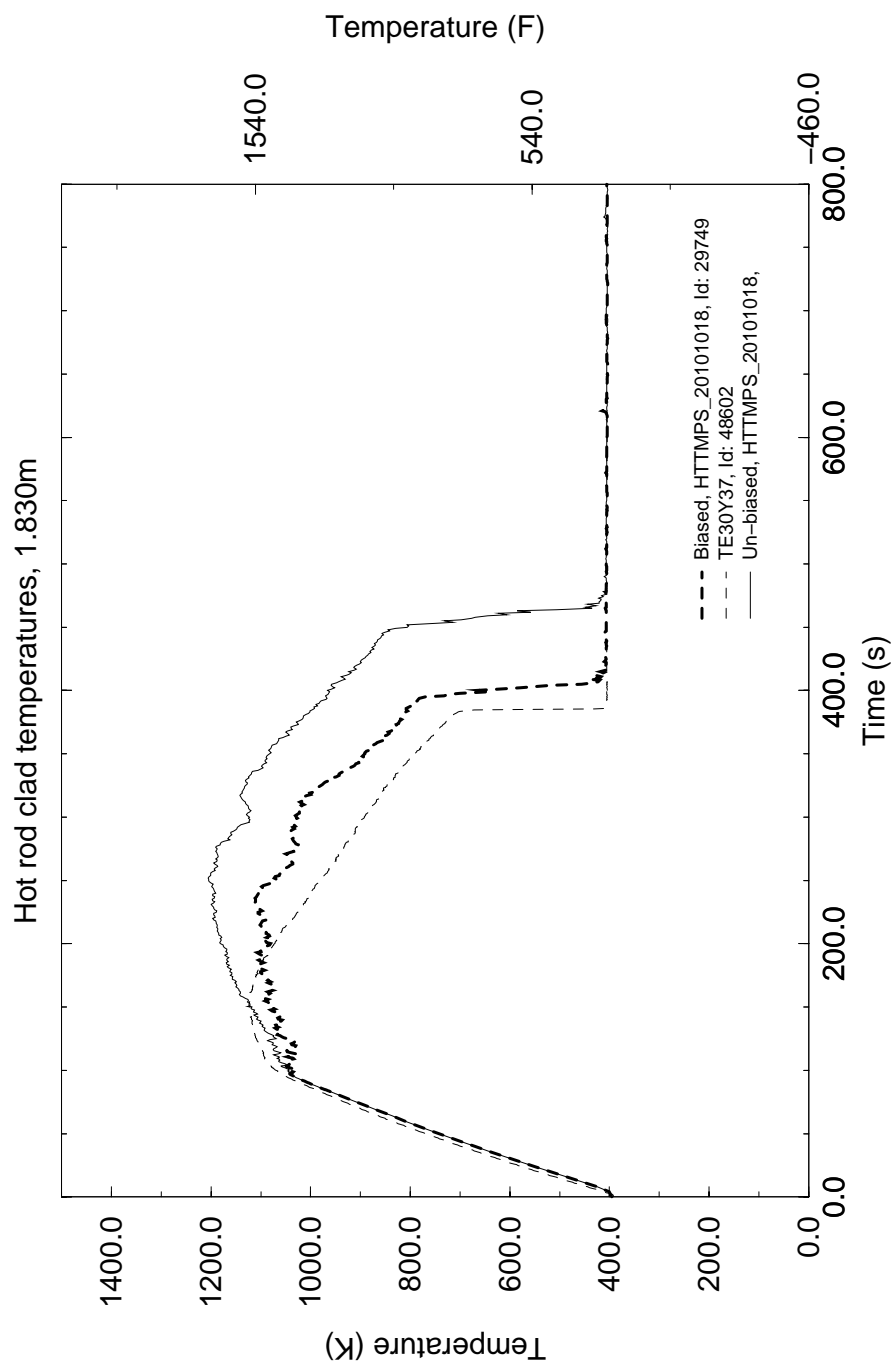


Figure 4.183 CCTF TEST 62 Temperatures at Measured PCT Node

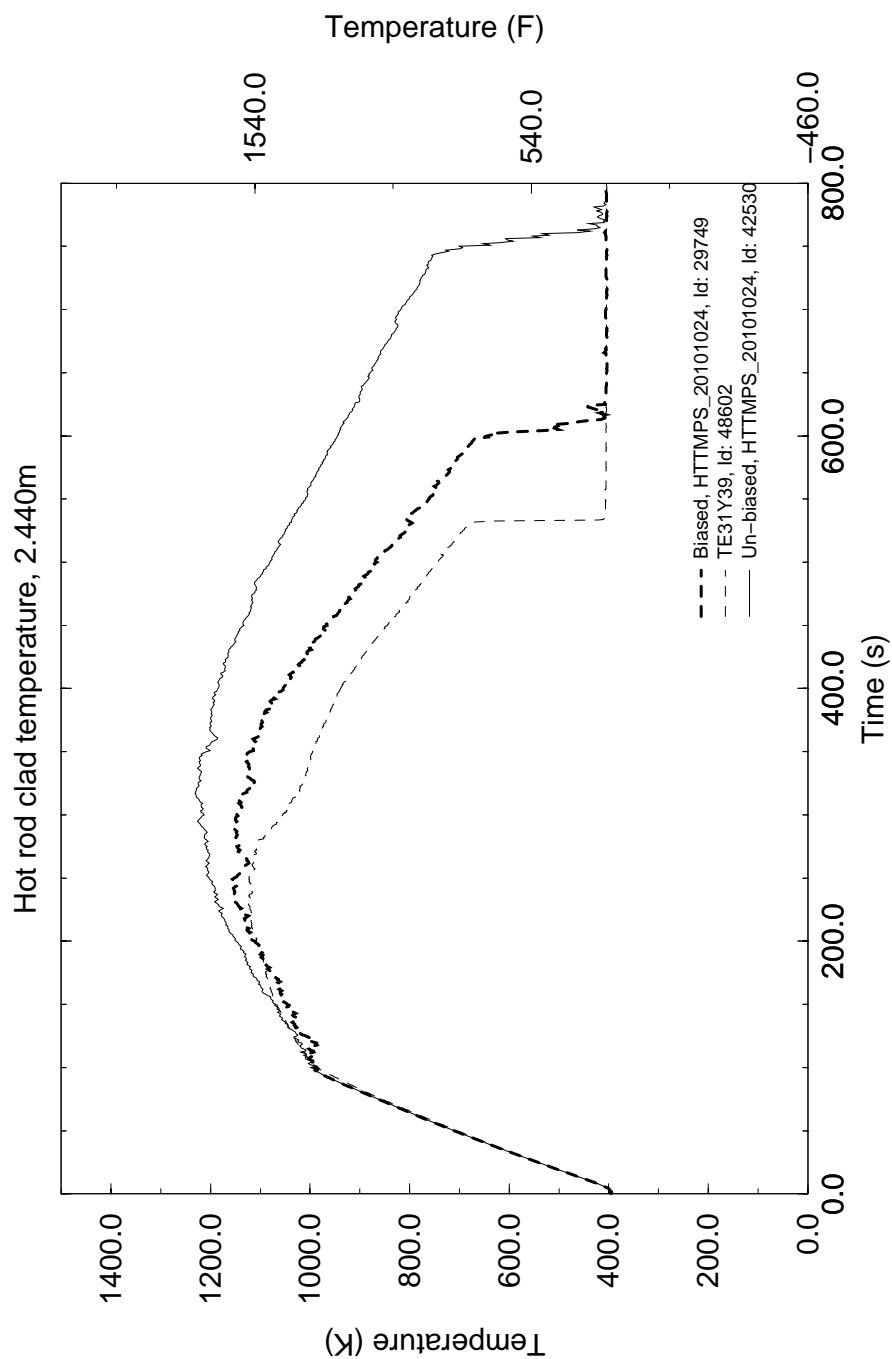


Figure 4.184 CCTF TEST 62 Temperatures Near Calculated PCT Node

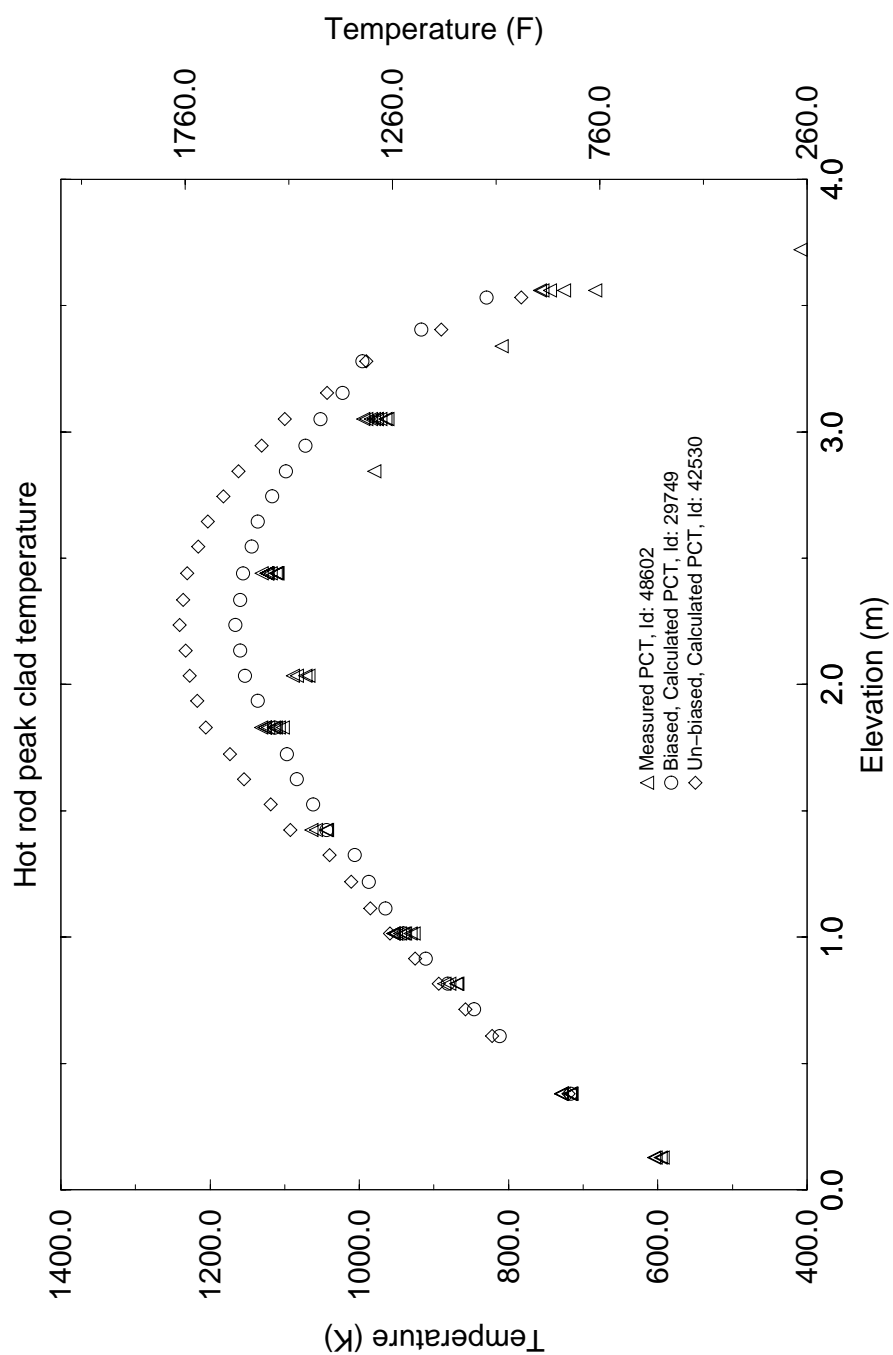


Figure 4.185 CCTF TEST 62 PCT Profile

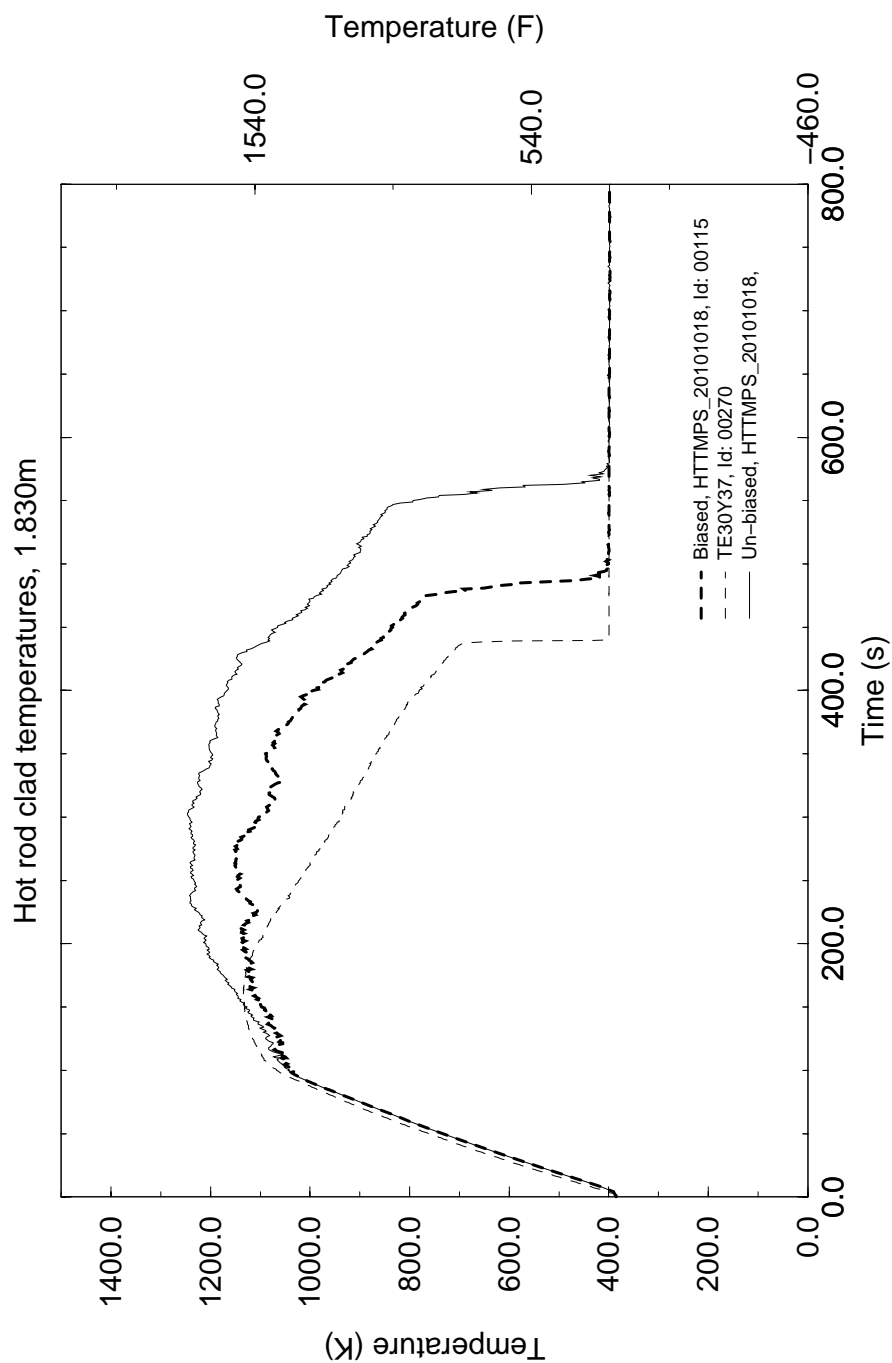
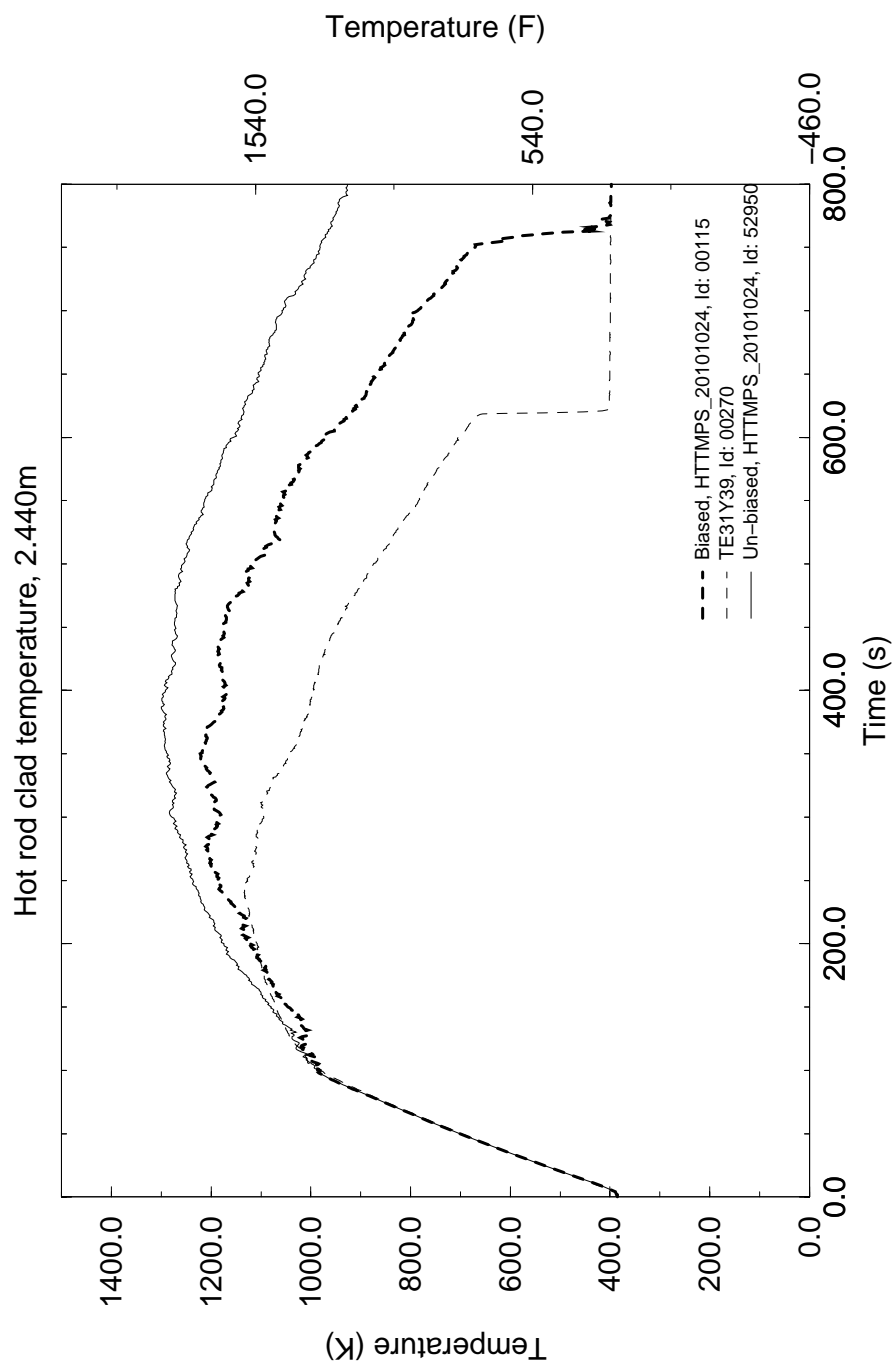


Figure 4.186 CCTF TEST 67 Temperatures at Measured PCT Node



**Figure 4.187 CCTF TEST 67 Temperatures Near Calculated
PCT Node**

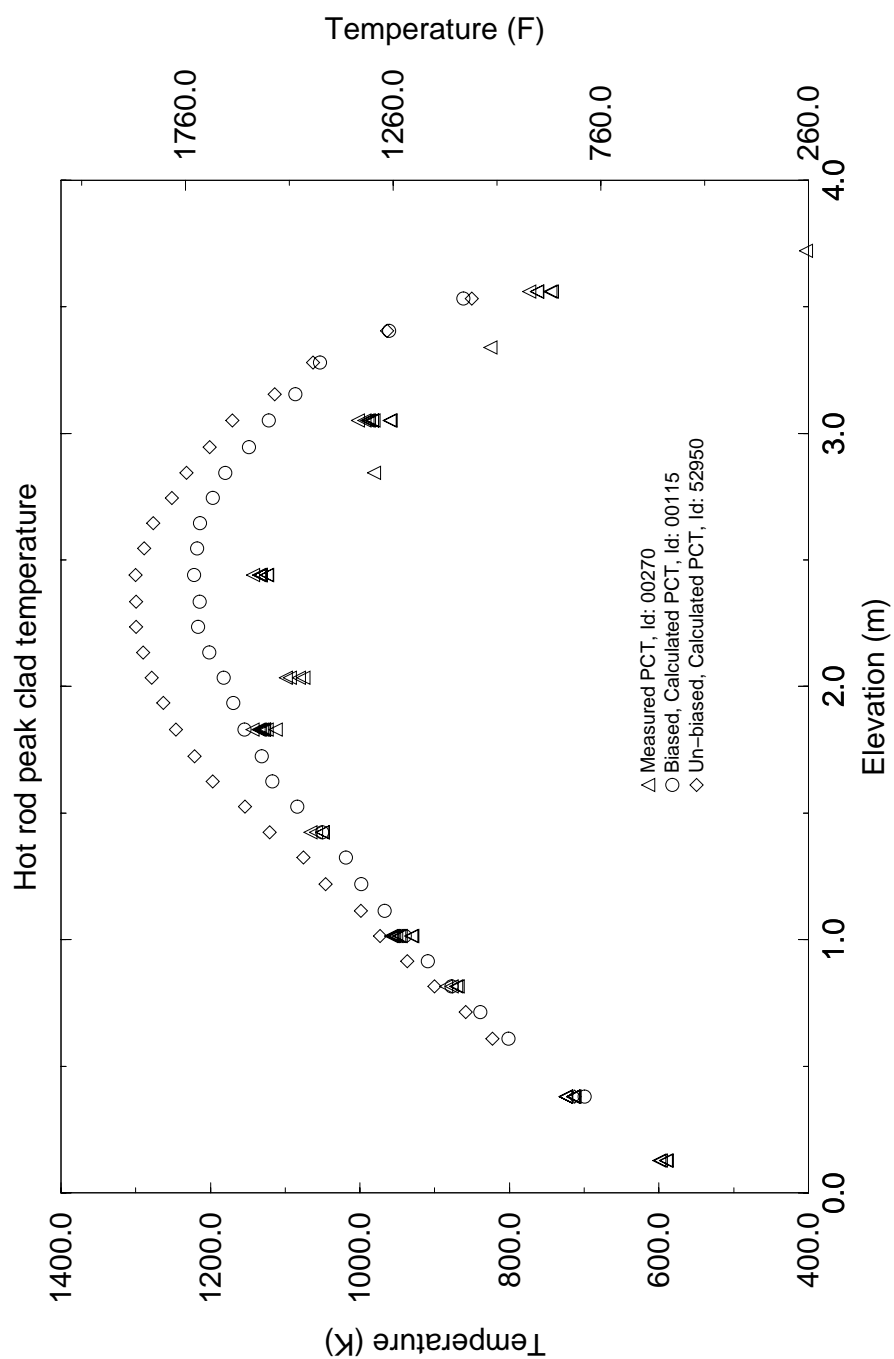


Figure 4.188 CCTF TEST 67 PCT Profile

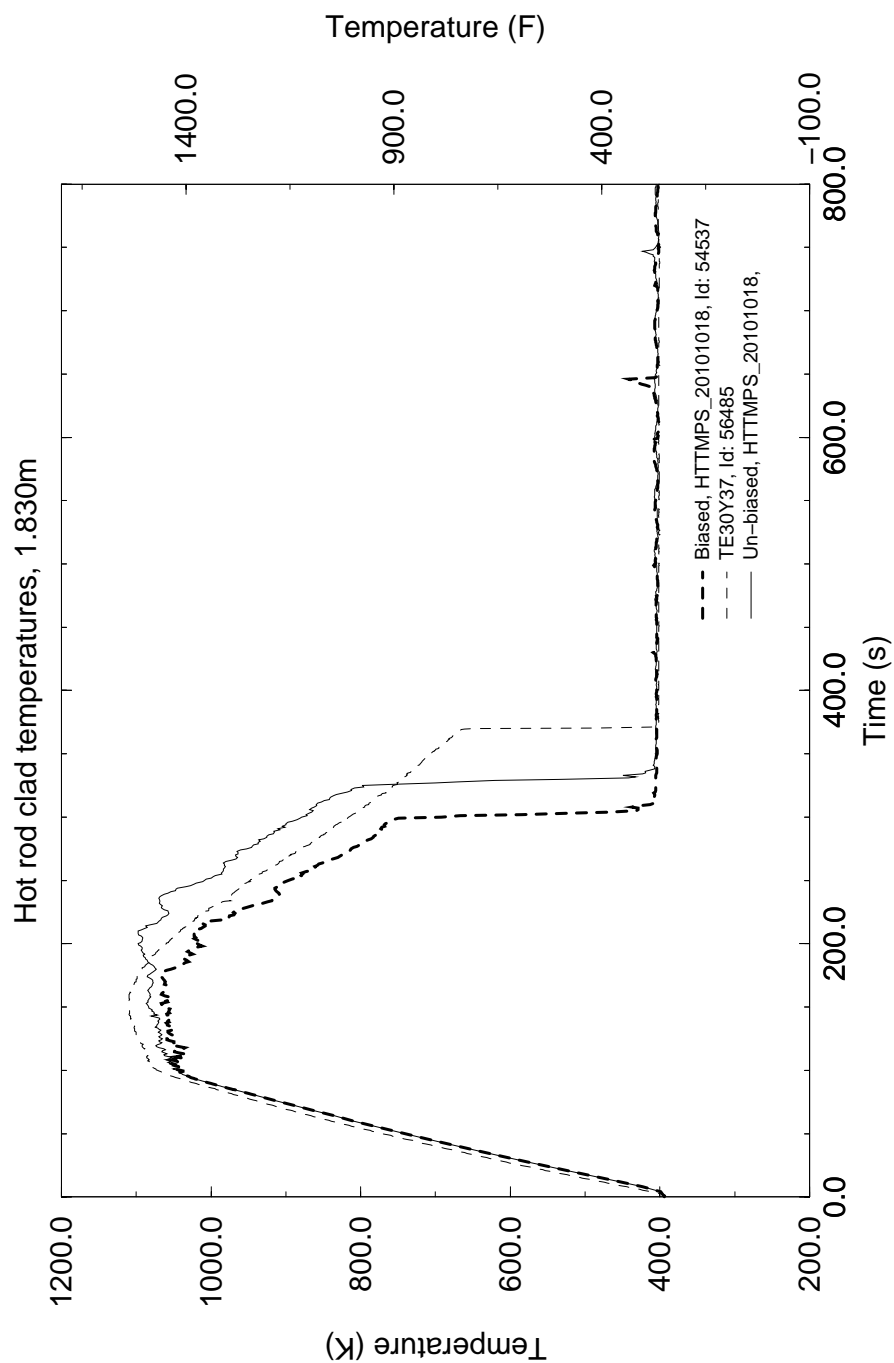
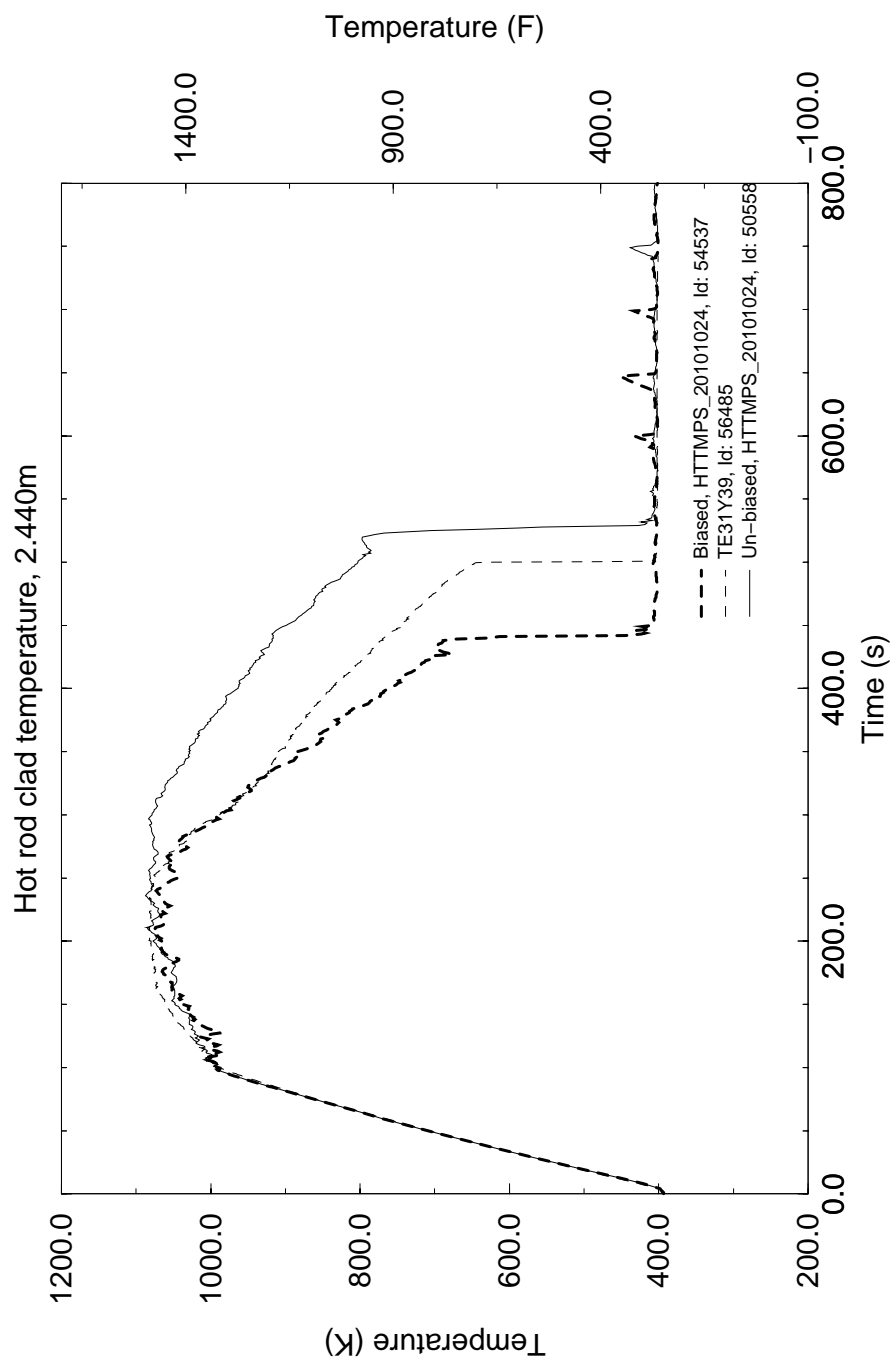


Figure 4.189 CCTF TEST 68 Temperatures at Measured PCT Node



**Figure 4.190 CCTF TEST 68 Temperatures Near Calculated
PCT Node**

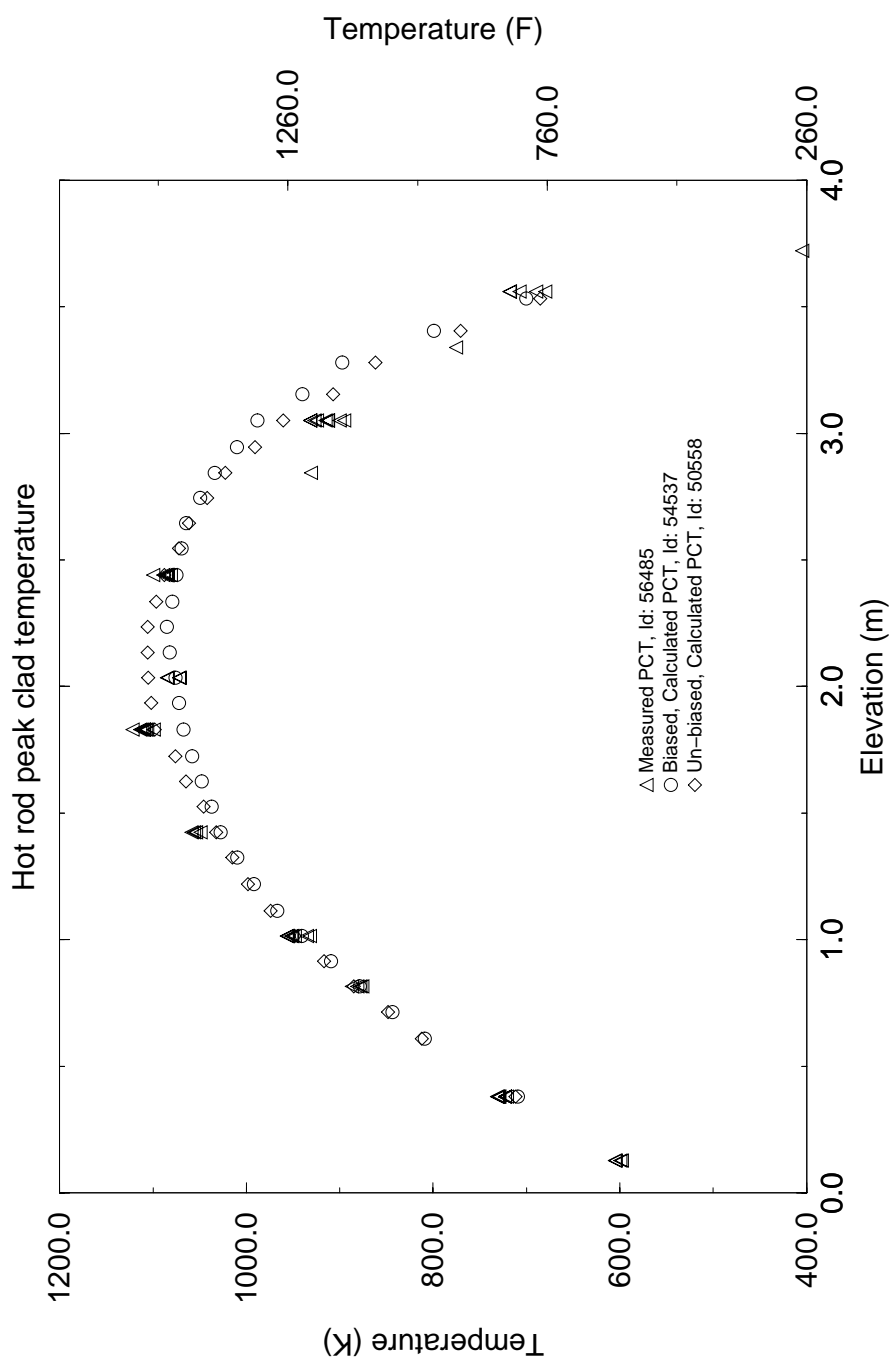


Figure 4.191 CCTF TEST 68 PCT Profile

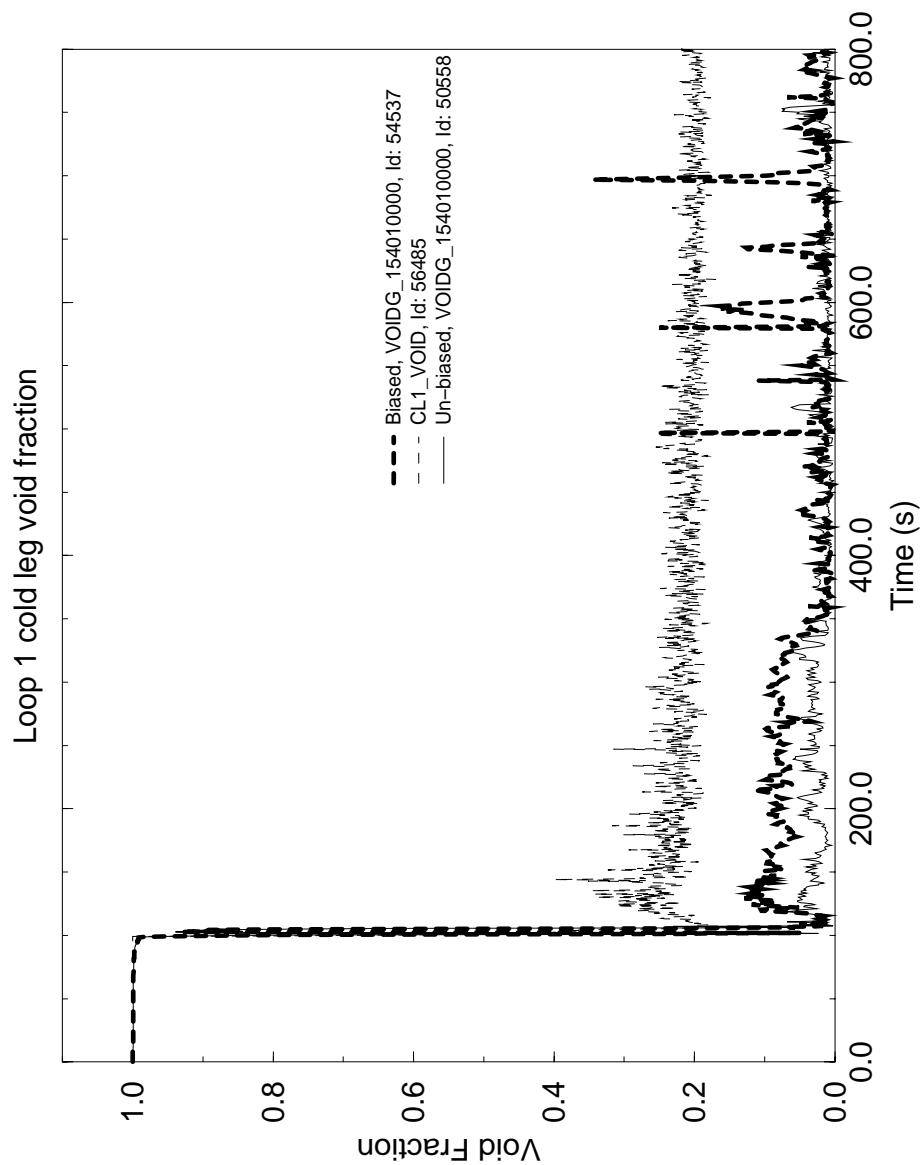


Figure 4.192 CCTF TEST 68 Intact Loop Cold Leg Void Fraction

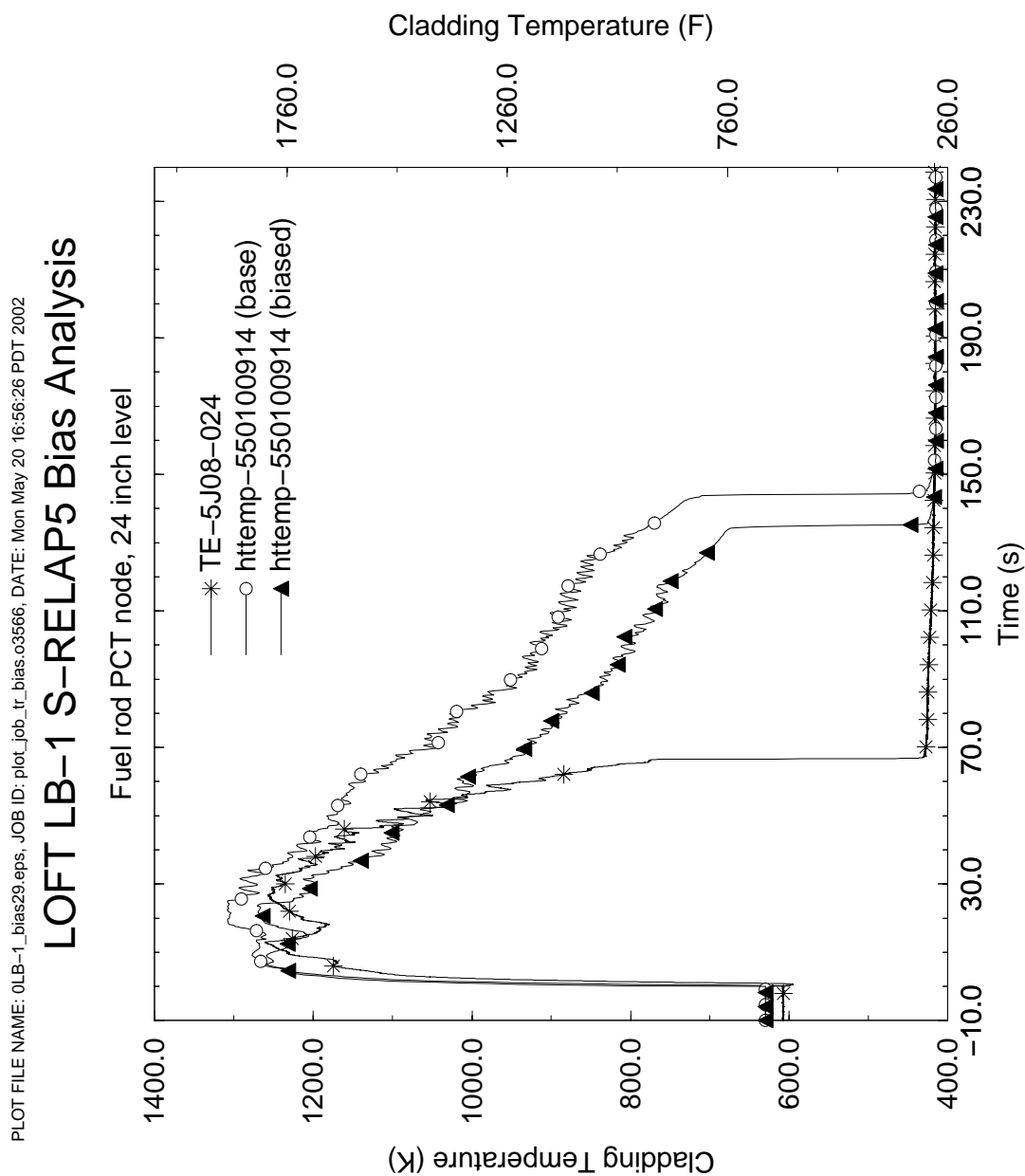


Figure 4.193 LOFT LP-LB-1 Temperatures at Measured PCT Node

LOFT LP-LB-1 S-RELAP5 ANALYSIS PLOT FILE NAME: 0lb-1_pct_00.eps, JOB ID: make_pct_plot_bias.o3588, DATE: Wed May 22 08:58:28 PDT 2002

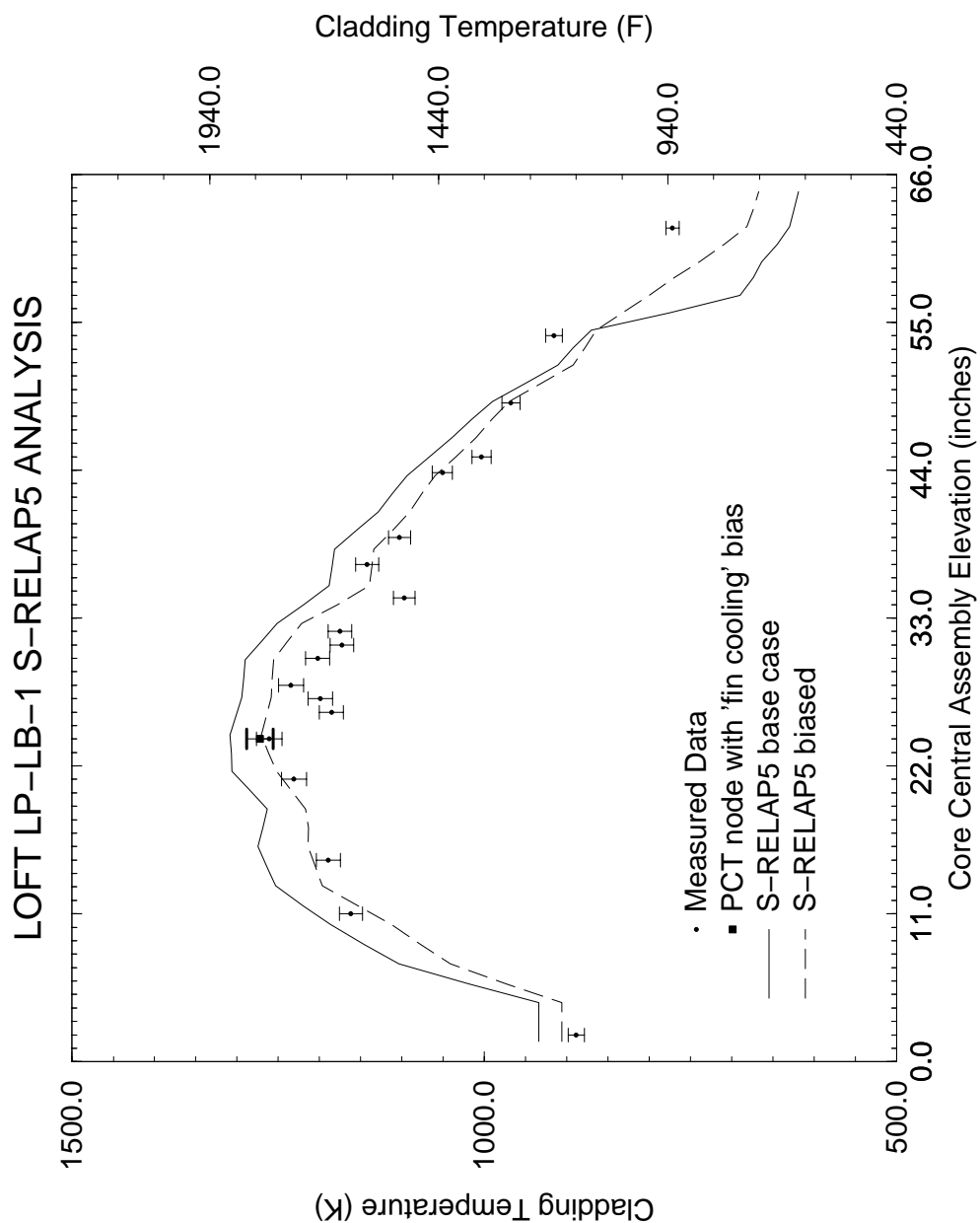


Figure 4.194 LOFT LP-LB-1 PCT Profile

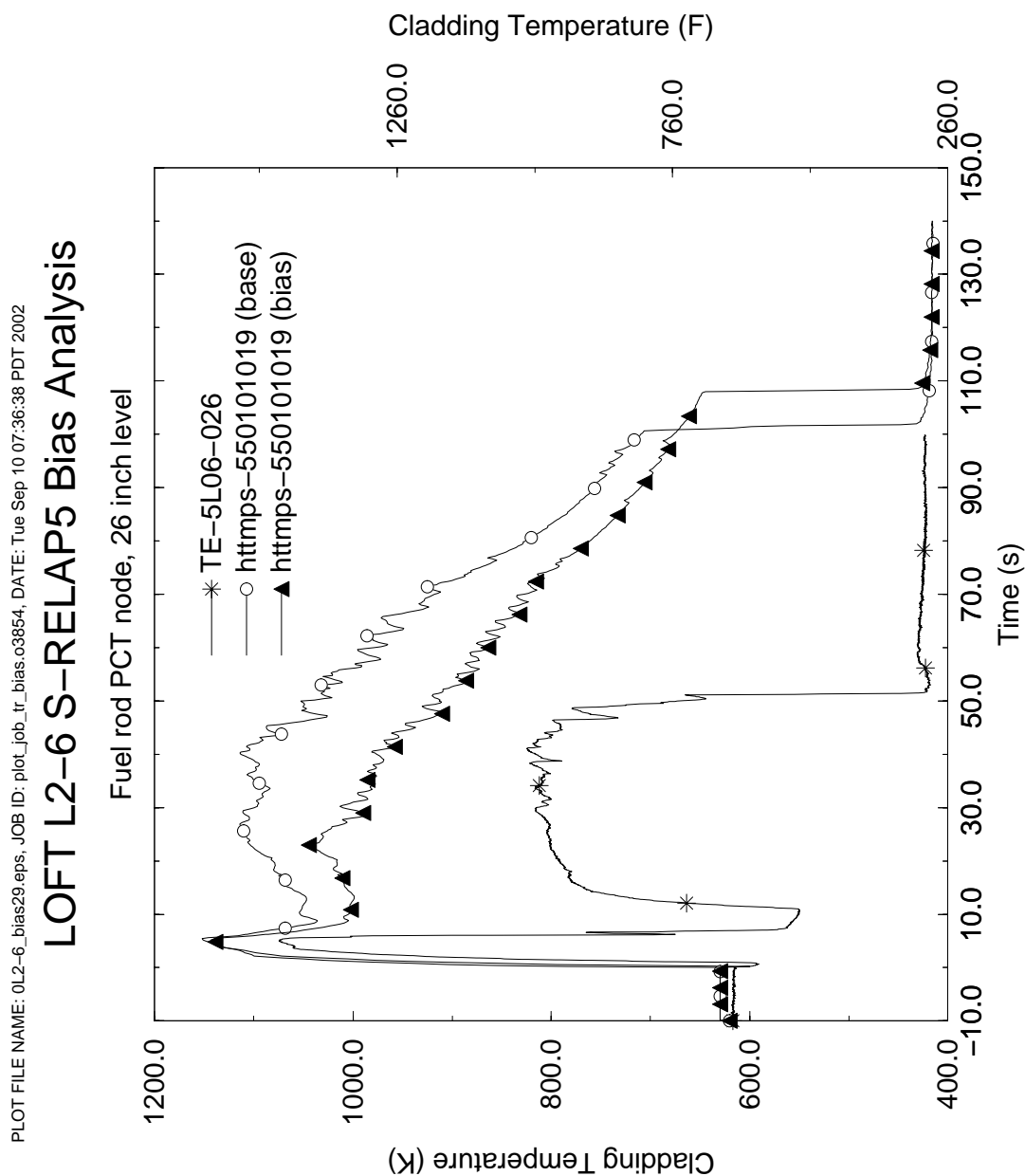


Figure 4.195 LOFT LP-02-6 Temperatures at Measured PCT Node

LOFT LP-02-6 S-RELAP5 ANALYSIS PLOT FILE NAME: 012-6_pct_00.eps, JOB ID: make_pct_plot_bias.o3856, DATE: Tue Sep 10 10:22:30 PDT 2002

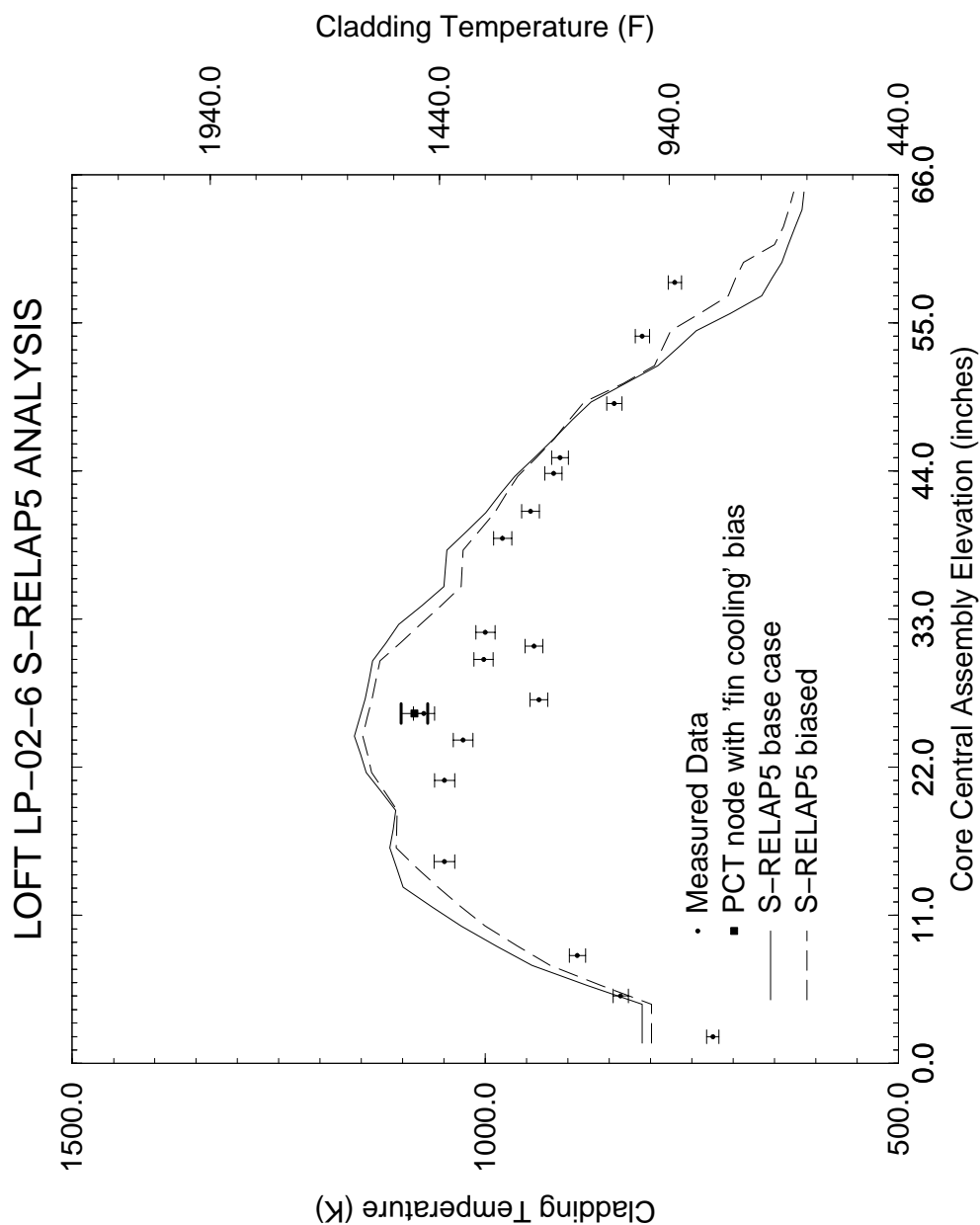


Figure 4.196 LOFT LP-02-6 PCT Profile

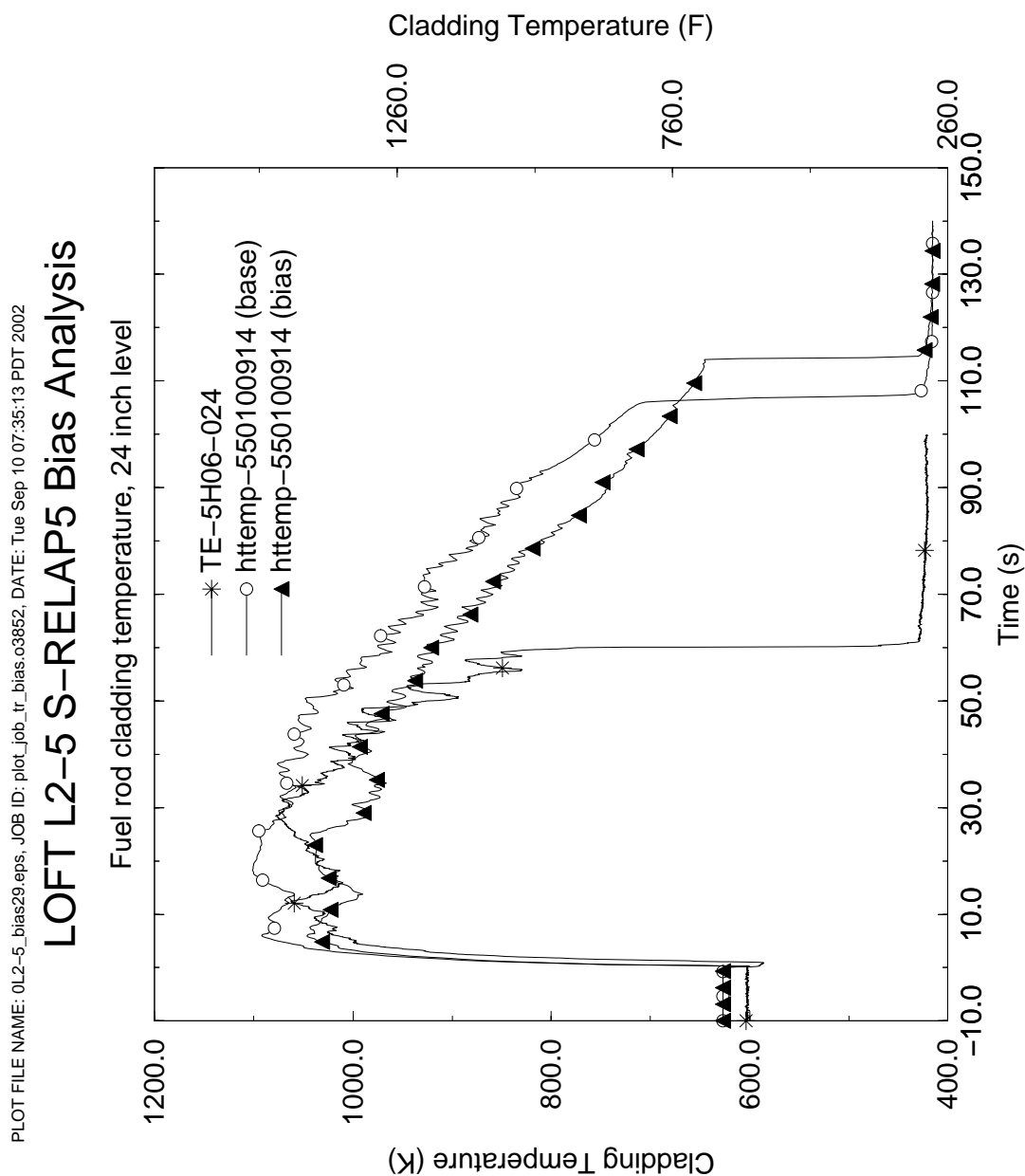


Figure 4.197 LOFT L2-5 Temperatures at Measured PCT Node

LOFT L2-5 S-RELAP5 ANALYSIS PLOT FILE NAME: 012-5_pct_00.eps, JOB ID: make_pct_plot_bias.o3859, DATE: Tue Sep 10 15:05:32 PDT 2002

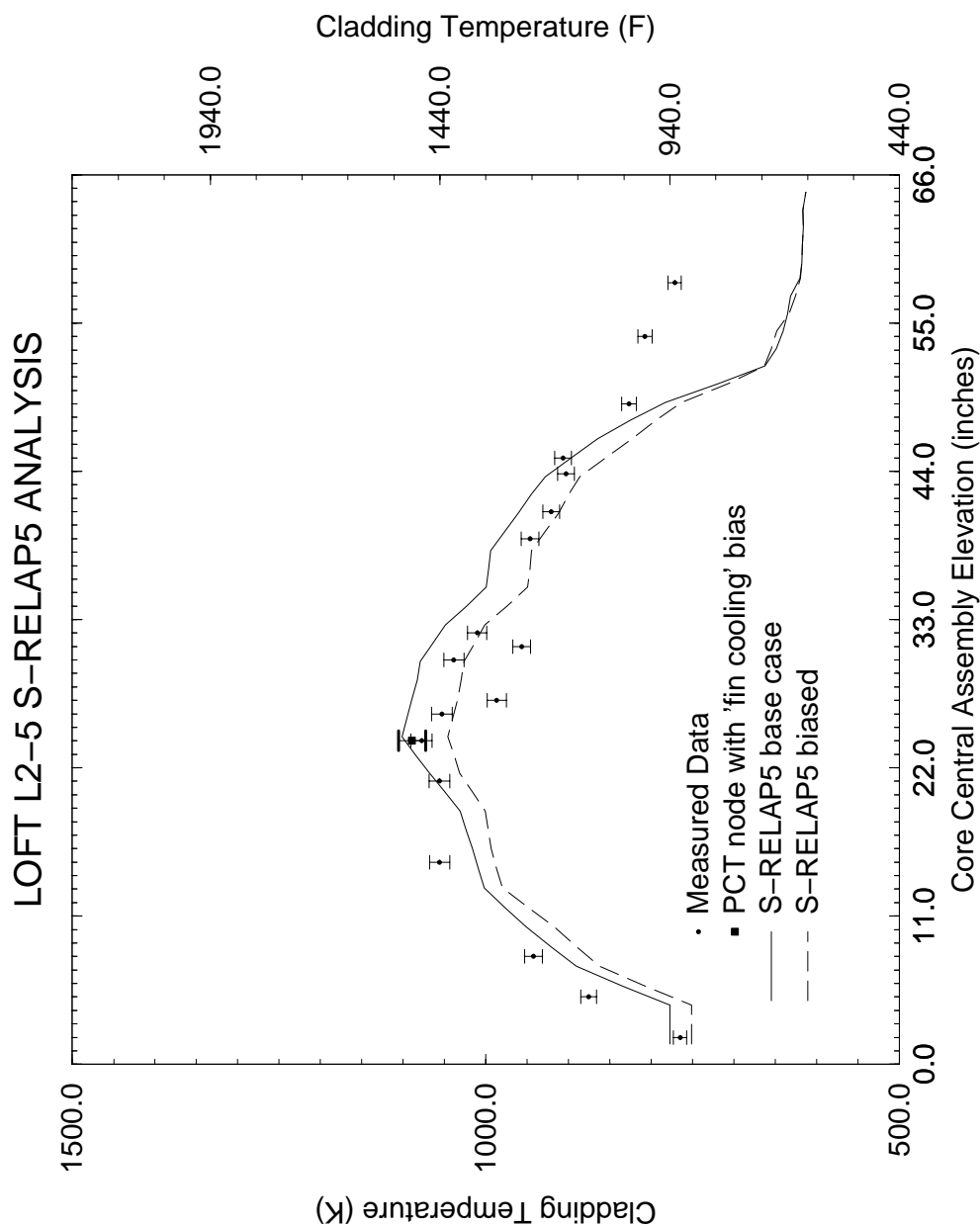


Figure 4.198 LOFT L2-5 PCT Profile

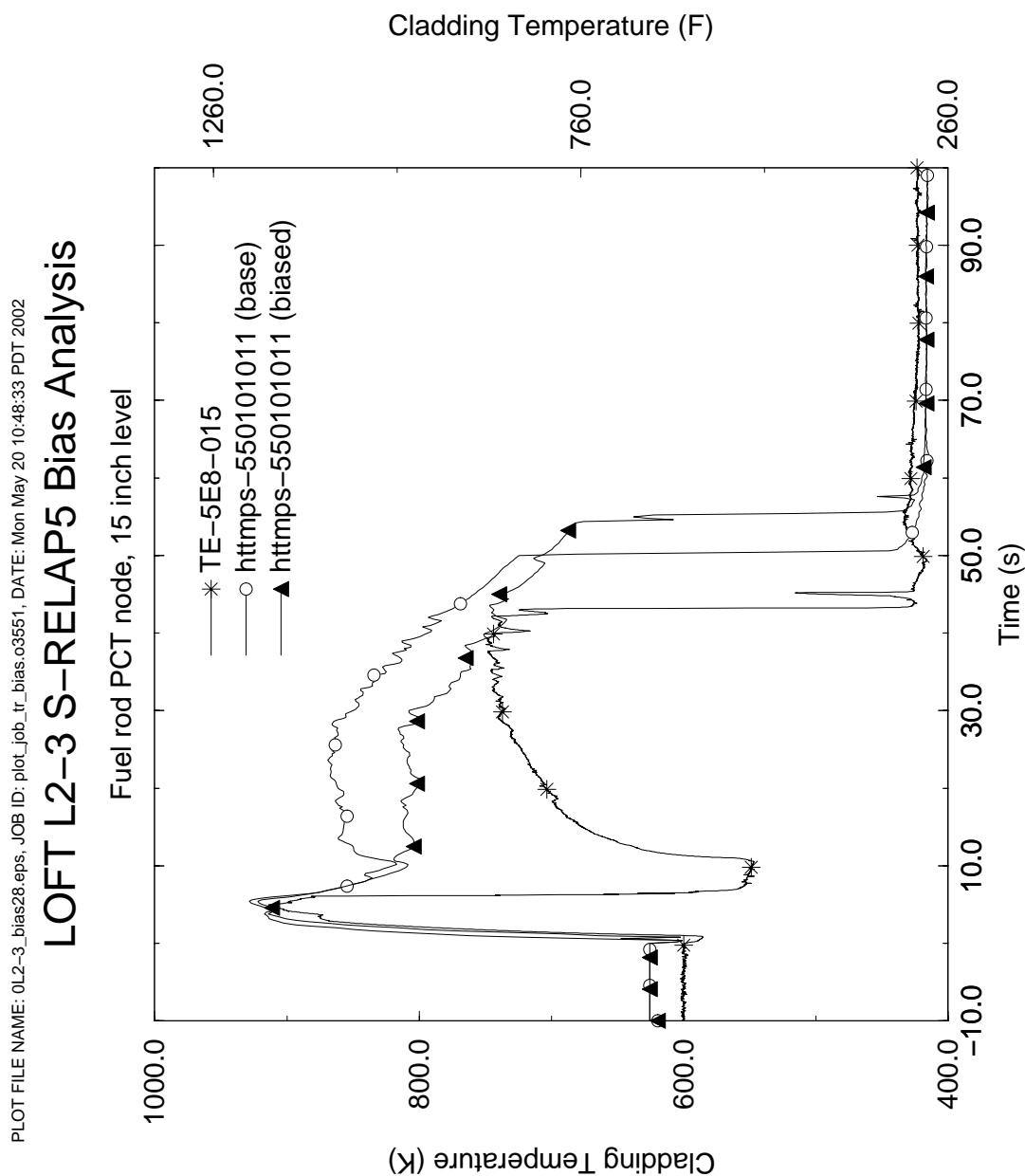


Figure 4.199 LOFT L2-3 Temperatures at Measured PCT Node

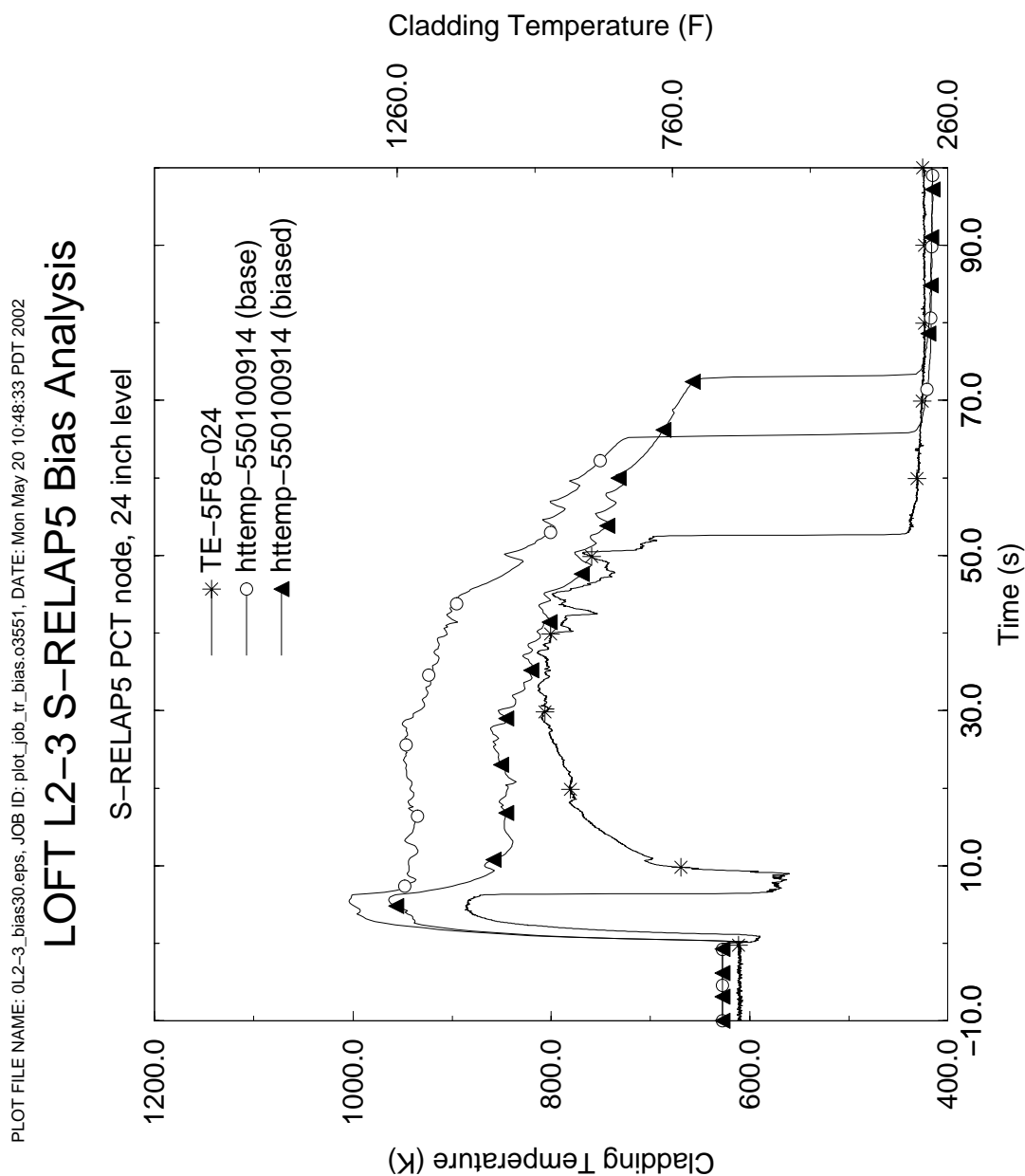


Figure 4.200 LOFT L2-3 Temperatures at Calculated PCT Node

LOFT L2-3 S-RELAP5 ANALYSIS PLOT FILE NAME: 012-3_pct_00.eps, JOB ID: make_pct_plot_bias.o3571, DATE: Tue May 21 08:48:21 PDT 2002

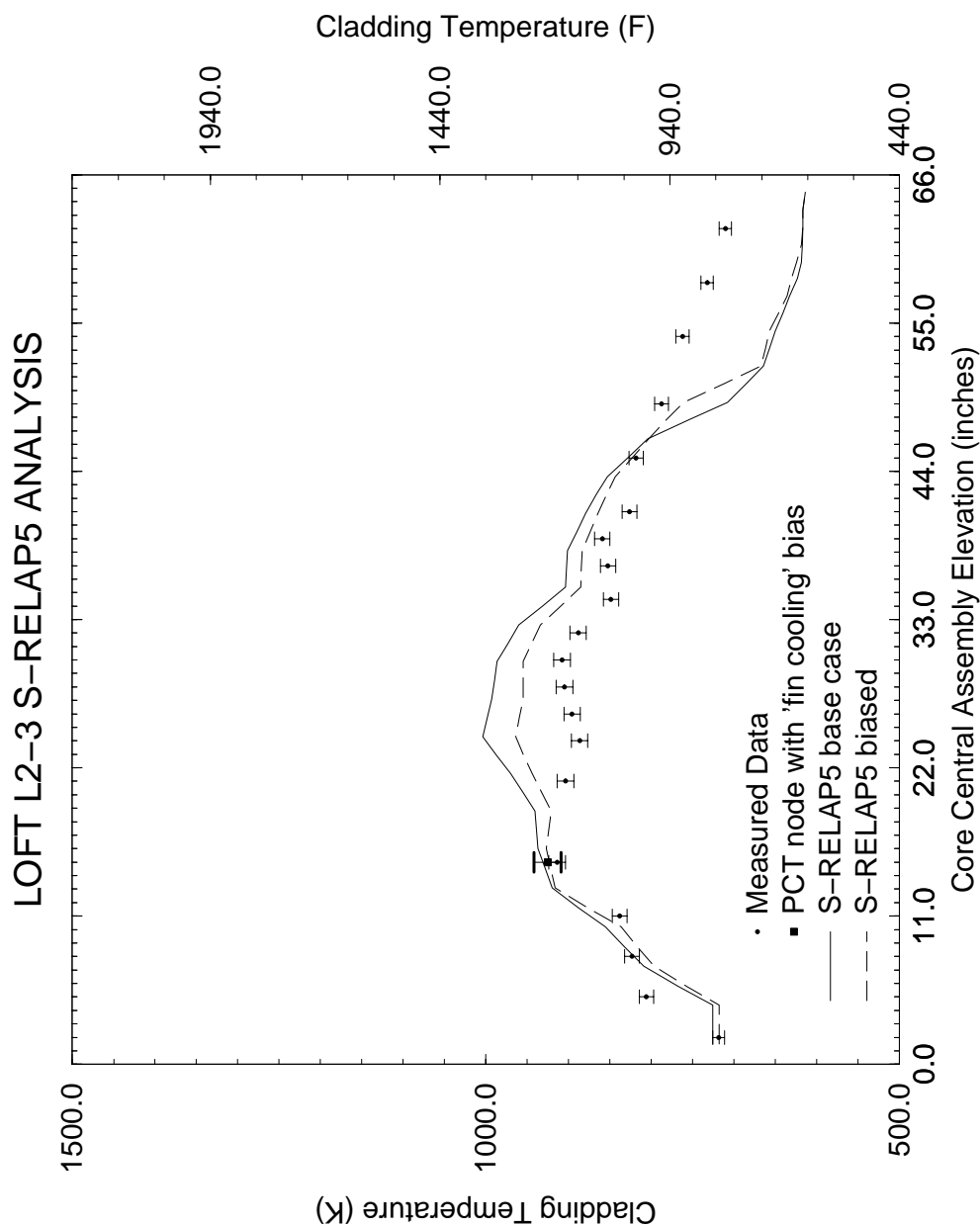


Figure 4.201 LOFT L2-3 PCT Profile

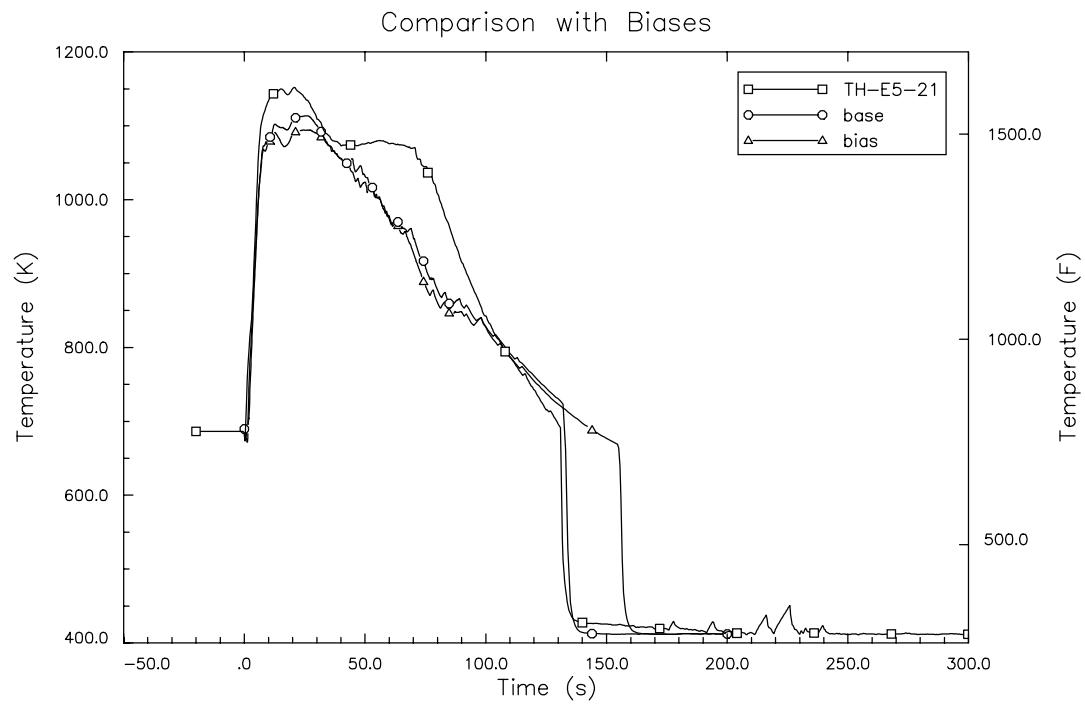


Figure 4.202 Semiscale S-06-3 Temperatures at Measured PCT Node

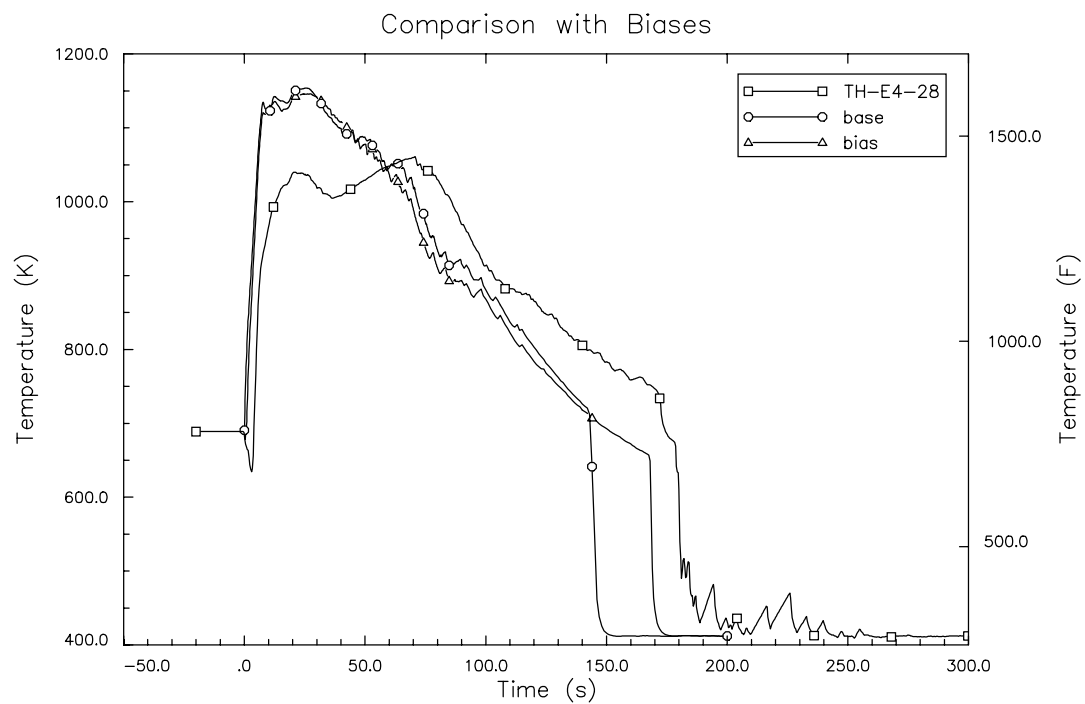


Figure 4.203 Semiscale S-06-3 Temperatures at Calculated PCT Node

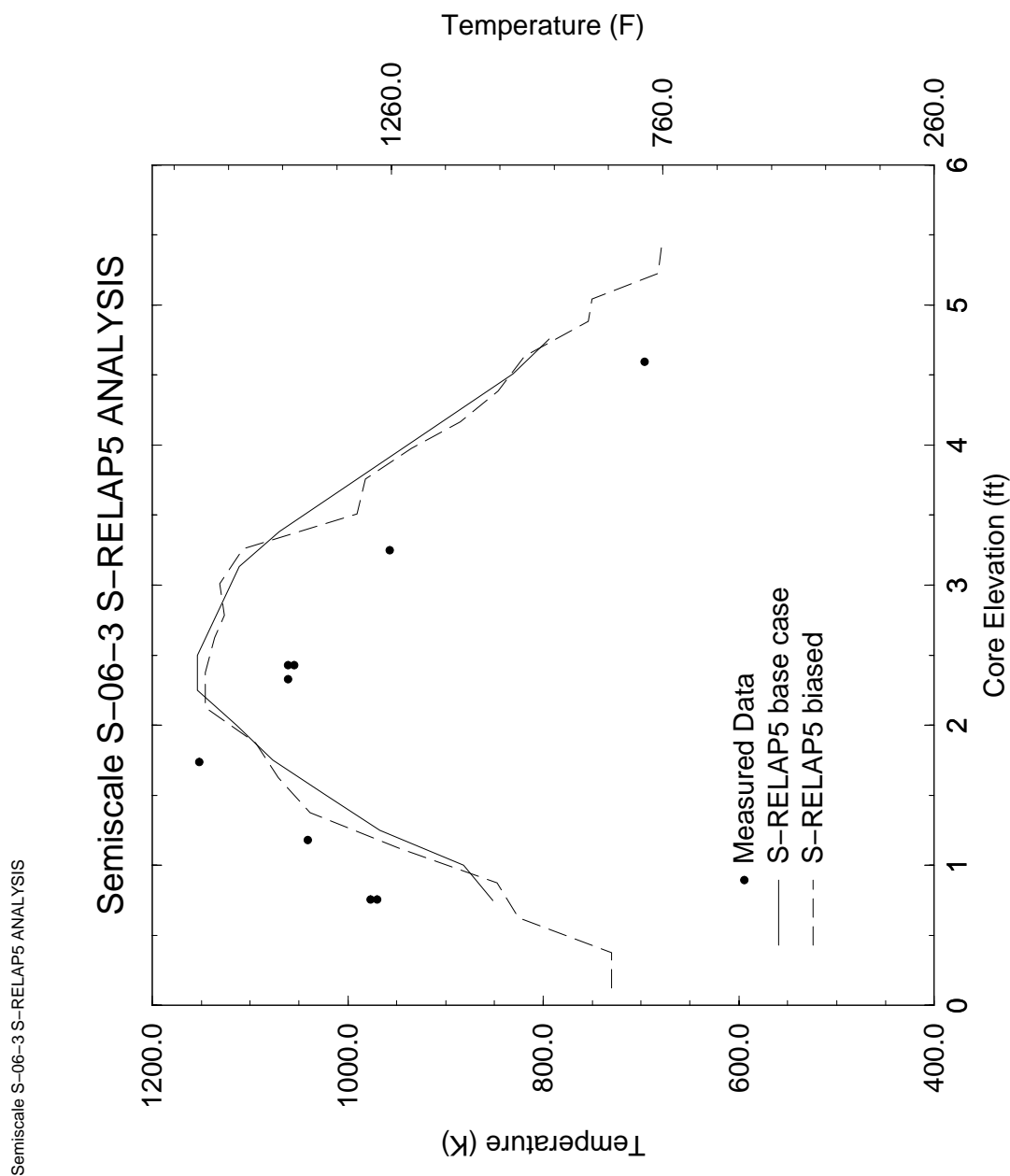


Figure 4.204 Semiscale S-06-3 PCT Profile

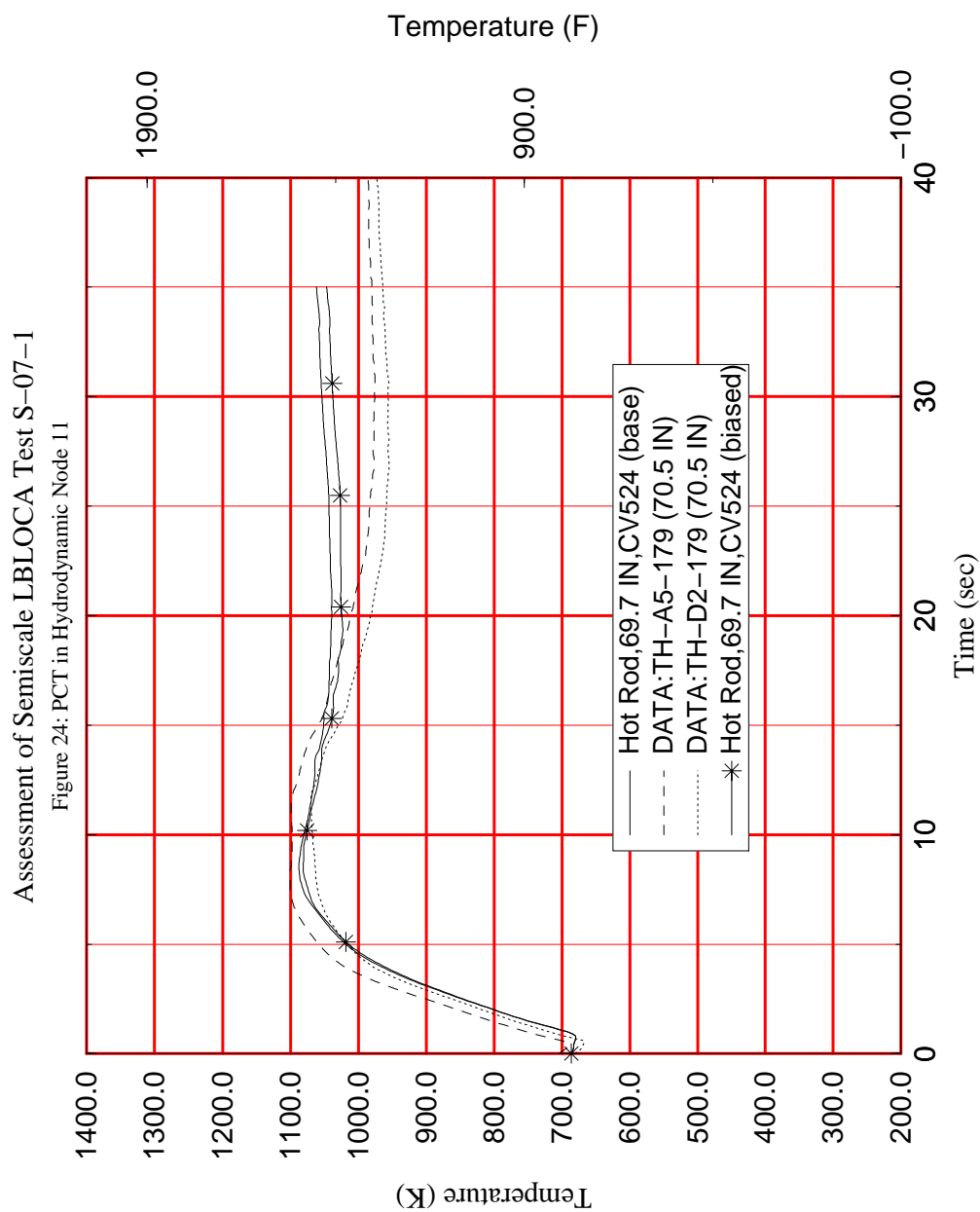


Figure 4.205 Semiscale S-07-1 Temperatures at Measured PCT Node

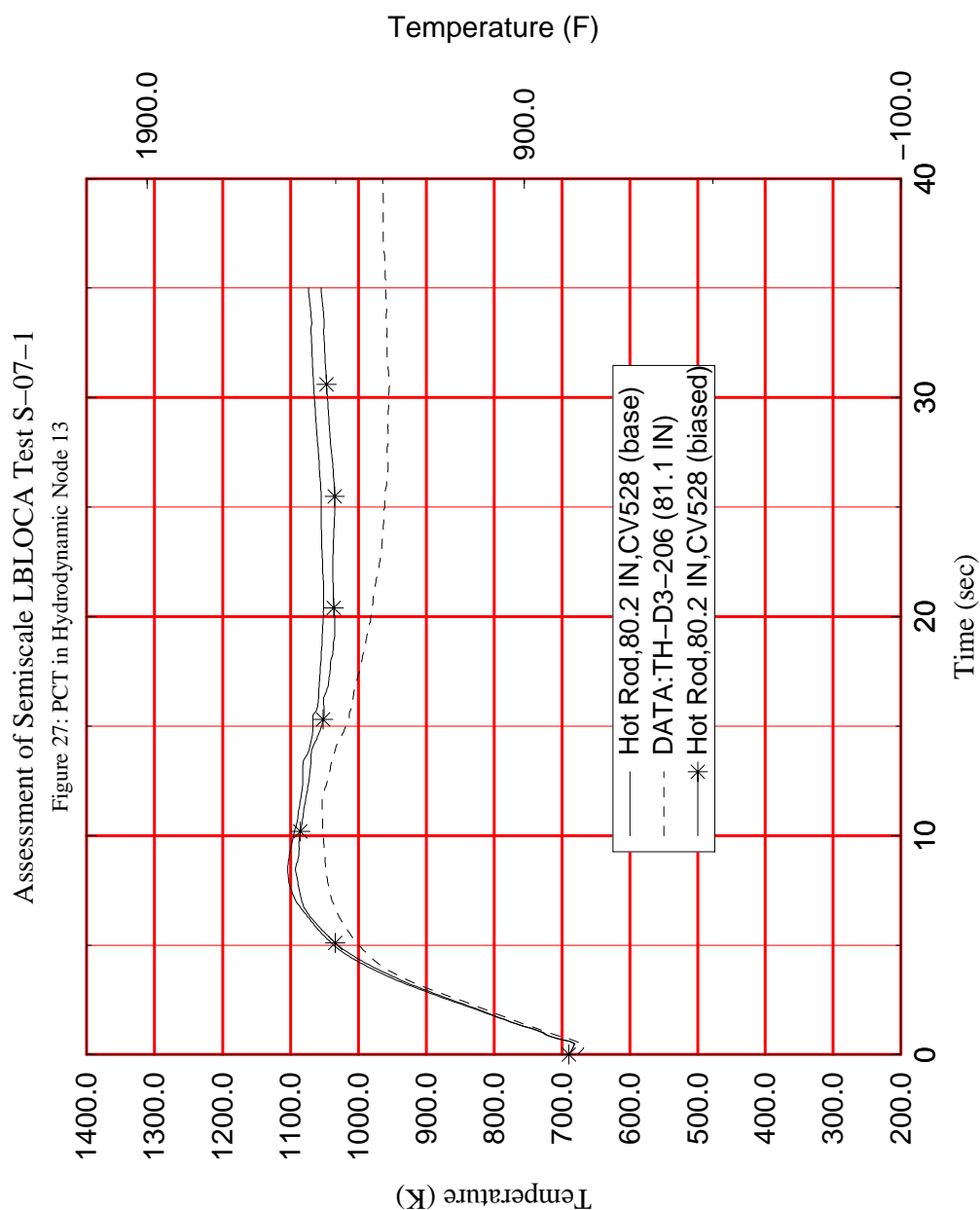


Figure 4.206 Semiscale S-07-1 Temperatures at Calculated PCT Node

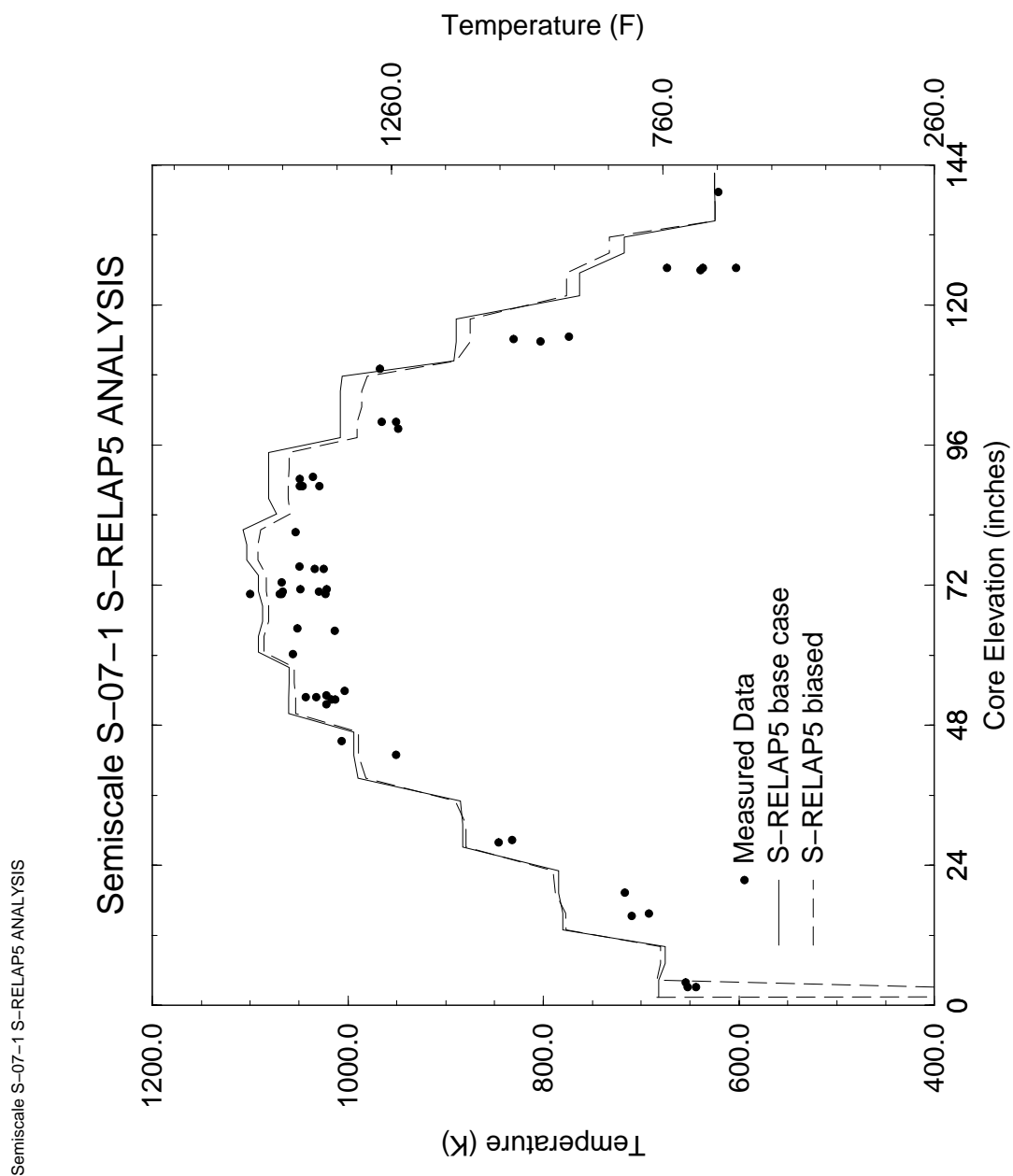


Figure 4.207 Semiscale S-07-1 PCT Profile

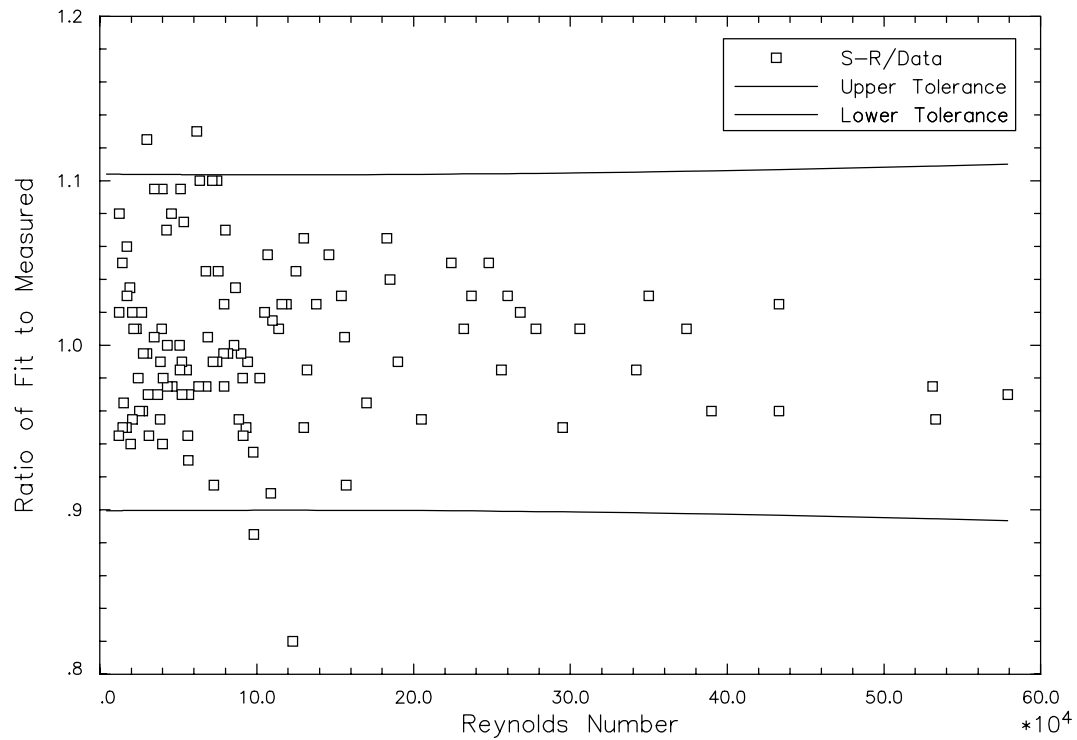


Figure 4.208 Sleicher-Rouse HTC for Steam Compared to Data

5.0 Sensitivity and Uncertainty Analysis

The objective of this section is to provide a statement of acceptability for each of the licensing criteria for the specified event. This is accomplished by evaluating the impact of the initial reactor state at the initiation of the specified event and determining a combined uncertainty statement. This combined uncertainty statement must address the biases and uncertainties in the important PIRT phenomena and the operating state of the NPP at the initiation of the event.

5.1 *Determination of Effect of Reactor Input Parameters and State (CSAU Step 11)*

The dynamics of a NPP may be characterized by design, phenomenological, and process (or operational) parameters. Design parameters are fixed values, such as a pipe diameter. Uncertainties associated with using design and phenomenological parameters are addressed by maintaining strict adherence to nodalization and identifying phenomenological uncertainties from code assessment studies applying well-defined nodalization guidelines. This is discussed in Sections 4.2 and 4.3, describing CSAU Steps 8 and 9. In contrast, process parameters characterize the state of operation and are, to various degrees, controllable by plant operators. Realistic variations can be expected in these parameters and uncertainty may be quantified with experimental and/or analytical studies.

5.1.1 Determining Important Process Parameters

From an operational standpoint, the NPP operating state is a function of the time in cycle (via burnup and power distribution) and the actual conditions present in the various NPP components. The deterministic approach to supporting the allowed variations in the NPP is to identify conservative bounds that are applied during safety analysis. Considering the complex nature of a NPP, such a declaration of conservatism can be given based only on the first order expectation of the effect of the given parameter on key LOCA parameters (e.g., PCT). Competing or compensating effects are possible; however, addressing these issues can be a challenging task in deterministic safety analysis. In contrast, treating these process parameters statistically accounts for higher order behavior by including all possible combinations in the sample space.

As part of the FRA-ANP RLBLOCA methodology development, a review was performed to identify the NPP parameters that are to be addressed in the performance of a LBLOCA

analysis. The identified parameters are provided in Table 5.1. The basis for inclusion in this list comes from three sources: PIRT, plant-specific technical specifications, and utility requests.

Determination of which process parameters to treat statistically begins with identifying the relationship a particular parameter has to any PIRT phenomenon. Table 5.2 lists process parameters determined to be important based on their potential influence to the moderate-to-high ranked phenomena given in Table 3.4. Process parameters that may only influence low ranked phenomena also should be included if an explicit limit is stated in a plant's technical specifications. Finally, utility requests may require the addition of still more process parameters. Such requests may be asked for support of plant procedures not explicitly mentioned in the technical specifications. To support the PIRT, the technical specifications, and any utility requests, these parameters will be explicitly treated by the RLBLOCA methodology. The preferred method for treating these parameters is statistically; however, conservative methods also can be used in the absence of adequate data to support a statistical approach.

5.1.2 Role of Sensitivity Studies

Quantifying the effect of individual process parameters is [

] Nonetheless, sensitivity studies on the

parameters given in Table 5.1 have been performed and included in the histogram presented in Figure 4.2. The primary value of these calculations is to establish a perspective on the level of importance a safety analysis team might give in quantifying process parameter uncertainties. For example, having insufficient information to support adequately describing a highly sensitive parameter may reduce the margin for key LBLOCA parameters such as PCT; while a conservative or bounding value may be easily justified for a parameter producing little sensitivity in the PCT. Table 5.3 ranks the results from a set of sensitivities performed for process parameters on both 3- and 4-loop PWRs (highest to lowest). The list is abbreviated to include only those parameters having significant sensitivity on PCT (i.e., >50 F).

Sensitivity studies also may be used to justify not treating a parameter statistically. Parameters not treated statistically fall into two categories: those to be treated conservatively or those that are judged to be not significant. Parameters can be demonstrated to be insignificant by

sensitivity studies and/or by their relationship to low-ranked PIRT parameters. Conservatism should be demonstrated by sensitivity studies. The analysis team chooses which parameters to treat conservatively.

5.1.3 Quantifying Statistical Quantities

For the FRA-ANP RLBLOCA methodology there are a number of plant specific parameters which are treated statistically.

5.1.3.1 General

The identified process parameters shown in Table 5.1 are allowed to vary within a prescribed range throughout an operational cycle. The constraints on these ranges may be defined from a plant's technical specifications, some physical or operational limitation, or a utility request. For example, the accumulator pressure is allowed to vary within a prescribed operating range based on a plant's technical specification. Similarly, containment temperature is usually constrained by technical specification on high temperature; however, no limit may be expressed for the low-temperature range, which may come from plant data or by other means.

While process parameters are expected to vary with plant operation, design constraints, given in the form of plant technical specifications, will provide a one- or two-sided limit on the variation. It should be noted that not all process parameters such as fuel state are explicitly constrained by technical specifications. For those operational parameters such as fuel state, other parameters having a direct effect on the operational parameter of consideration are constrained by the plant Technical Specifications (e.g., power peaking for the fuel state).

Inherent in the FRA-ANP RLBLOCA methodology is [

] To treat a parameter statistically, the parameter uncertainty must be quantified in terms of biases and distributions. Quantifying this uncertainty with plant data is the best approach. At most plants, histories of core power, RCS flow rate, core inlet temperature, pressurizer and accumulator parameters, containment temperature, and diesel start times are available. In some instances, parameter uncertainties may need to consider two components of uncertainty: operational range and measurement. Operational uncertainty is defined as the true fluctuation of the parameter during normal

operation. Measurement uncertainty addresses the error associated with measuring the parameter.

From analysis of plant data, the statistical distribution and uncertainty can be quantified. While measurement uncertainty is most often characterized by a normal distribution, no particular uncertainty distribution is expected describing operational variations. The choice of distribution may have implications as to how a utility manages the process parameter of interest. For example, using a uniform distribution may be attractive to a utility in that it will support the most flexibility in how they control a given parameter. Conversely, uniform distributions may be more conservative in that equal likelihood is given for values that reduce operation margin.

Other distributions will be considered if supported by the data. Additionally, it is not likely that a parameter limited by a plant's technical specification will coincide with limits identified by plant data. Technical specifications often bound the nominal operational range. In this situation, the statistical distribution on measurement uncertainty may be adjusted to ensure that the Technical Specification limits are included in the parameter's sample space.

An assessment of plant data provided for key process parameters has been performed for an existing 3-loop NPP. Table 5.4 summarizes the results of this assessment in terms of statistical distributions. In applications to other plants, such distributions may be different.

5.1.3.2 Treatment of Time in Cycle

The time in cycle establishes the fuel rod properties and the lower bound for the global power peaking factor, F_q . [

] Power history calculations are performed using an NRC approved methodology (References 64 and 65). Typically, fuel rod data for 20 to 40 burnup steps are explicitly written from a cycle power history calculation. Fuel rod data is provided for the life of a fuel rod; however, sensitivity studies have been performed that show only fresh fuel assemblies are limiting (Appendix B).

In contrast to a traditional safety analysis, which assumes conservative fuel rod models consistent with Appendix K requirements, [

1.]
2. []
3. []
4. []

The data produced by this method is used primarily to develop input for the RODEX3A code.

[]

5.1.3.3 Treatment of Axial and Radial Power Shapes

To support a plant's technical specification for the core peaking factor, F_q , the axial power shape must be adjusted from the nominal axial power shape extracted for the limiting fuel rod. During normal operation, F_q will most likely occur relatively near the nominal F_q represented in the power history files. []

[]

[

]

[

]

[

]

- []
- []
- []
- []
- []
- []
- []

5.1.4 Supporting Ranges Without Data

As shown in Table 5.1, some parameters lack explicit definition (technical specifications or data). For parameters for which no plant data is available, ranges may be established based on physical constraints or by analytical methods. Examples of physical limits include ranging the vessel upper head temperature to a maximum value of the hot leg temperature or ranging the diesel start delay on the LPSI pumps to a time corresponding to when RCS pressure drops below the back pressure delivered by the LPSI pumps. It may also be demonstrated that a particular parameter has a limited range of influence based on a set of sensitivity studies.

5.1.5 Reporting of Treatment of Process Parameters

Many decisions are required to establish plant specific treatment of process parameters. Such decisions must be reported or referenced when issuing a safety analysis report. Because the ranges and statistical description of the behavior of plant parameters may vary from plant to plant, the safety analysis report will require an explicit discussion of the treatment of key process parameters. If no changes are made in the treatment of process parameters for subsequent analyses, the earlier report may be referenced.

5.2 ***Performance of NPP Sensitivity Calculations (CSAU Step 12)***

5.2.1 Statistical Approach

[

]

[

]

[

]

[]

[]

[]

[]

[]

[]

[]

[]

[]

[

]

[

]

[

]

[

]

[

]

5.2.2 Application of Methodology

The FRA-ANP RLBLOCA methodology is a statistics-based methodology; therefore, the application does not involve the evaluation of different deterministic calculations. [

] The methodology results in a bounding value with 95% probability and 95% confidence in the PCT.

The PCT criterion is shown to be met with at least 95% probability and 95% confidence by comparing the 95/95 PCT value to the PCT criterion. Regulatory Guide 1.157 states that it is not necessary to explicitly consider the probability of meeting the other 10 CFR 50.46 criteria due to the strong dependence of the other criteria on PCT. Demonstration that the PCT

criterion is met with 95% probability and 95% confidence shows that the other criteria are also met with high probability as required by the regulation. In order to define values for peak local oxidation and total core oxidation, these values will be reported from the 95/95 PCT case.

Application of this methodology relies on two computer codes: RODEX3A and S-RELAP5. All key LBLOCA parameters are calculated from S-RELAP5; RODEX3A is used to generate the initial fuel properties to be used by the fuel performance models in S-RELAP5. Performance of the RLBLOCA calculations relies on three analyst-created code input files describing the fuel, plant thermal-hydraulics, and containment thermal-hydraulics. The fuel model input is processed by the RODEX3A code, which will produce a binary file describing fuel properties. This file will be processed by S-RELAP5 during the steady-state initialization. During steady-state initialization, S-RELAP5 will process only the RODEX3A binary output file and the steady-state plant model input. The LBLOCA calculation is an S-RELAP5 "Restart" calculation. It relies only on the steady-state restart file, the S-RELAP5 LBLOCA transient input file, and the containment model input. The containment model input is similar to the original ICECON code (Reference 14), which evolved from the CONTEMPT code (Reference 20). Reportable LBLOCA parameters can be retrieved from the S-RELAP5 transient output file. Figure 5.1 depicts the calculational framework.

5.2.3 New RLBLOCA Analyses

- []
- []
- []
- []
- []

5.2.4 Ranging Uncertainty

[] For this reason the RLBLOCA analyst must have available a validated random number generator. The most common type of random number generator available on most UNIX workstations produces a

floating point value between zero and one. The random number generator provides sample values uniformly distributed.

Random number generators require that a random number seed be defined before processing the random number function. Most random number generators use a default random number seed when no seed is provided. The RLBLOCA methodology does not provide a random number seed and relies on the random number generator to pick the seed. The random number seed is recorded, in order allow reproduction of the of random numbers. This provides calculation traceability and a mechanism for reproducing a set of calculations.

Given that the random number generator provides uniformly distributed values between 0 and 1, other probability distributions must be mapped from these distributions. For this methodology, the common probability distributions applied to parameter uncertainty ranges are binary, uniform between two arbitrary numbers, and normal. A typical uniform random number generator produces values, r , ranging from 0 to 1.

A uniform probability distribution function ensures an equal probability of selecting any given value over the range of interest. Using the uniform random number generator, a sample, z , from a uniform probability distribution function ranging between two points, a and b , is defined as

$$z = a + (b - a) \cdot r$$

A normal probability distribution function is the natural limit to the combination of many random events. Using the uniform random number generator; two samples, z_1 and z_2 , for a normal probability distribution function can be created from two samples from a uniform distribution, r_1 and r_2 (Reference 70)

$$z_1 = \eta + \sigma \cdot \cos(2 \cdot \pi \cdot r_1) \cdot \sqrt{-2 \cdot \ln(r_2)}$$

and

$$z_2 = \eta + \sigma \cdot \sin(2 \cdot \pi \cdot r_1) \cdot \sqrt{-2 \cdot \ln(r_2)}$$

where η and σ are the mean and standard deviation of the normal distribution, respectively.

Similarly, other distributions can be related to a uniform random distribution, so that a variety of probability distributions can be treated in the LBLOCA calculation.

5.2.5 Parameter Initialization

The key parameters identified for ranging have been summarized previously in Tables 4.1 and 5.2. Table 5.6 presents these parameters as they relate to computer code input.

5.2.6 Calculation Order

[

] The key results are the PCT, maximum cladding nodal oxidation, and total core wide oxidation.

5.2.7 Subsequent RLBLOCA Analyses

[

]

[

]

5.3 ***Determination of combined Bias and Uncertainty (CSAU Step 13)***

This section presents the results of a sample RLBLOCA analysis for a W 4-loop plant. An actual licensing analysis is in progress for a W 3-loop plant and will be submitted by the utility following the utilities review and acceptance of the analysis (Reference 16).

This 4-loop sample problem was performed in accordance with the calculation framework shown in Figure 5.1 as described above and in more detail in Reference 13. The base input models for the fuel rod and NPP were developed as described above and in conformance with Reference 12. The input for the fuel rod code was developed based on an existing FRA-ANP

17x17 fuel assembly with 0.955 cm (0.376 in) fuel rods. The input for the NPP was developed based on information which was obtained for several different 3 and 4-loop plants and consequently can only be considered as representative of a 4-loop plant. However, the NPP input model is adequate to demonstrate the application of the FRA-ANP RLBLOCA methodology described in this report.

The parameters treated statistically are listed in Table 5.6 and the values for the specific parameters and ranges addressed are given in Table 5.7. The distributions assumed for this sample problem are those given in Table 5.4. [

] The results of these calculations are presented in Figures 5.2 through 5.28.

Figures 5.2 through 5.16 present scatter plots for the more important phenomena/parameters in the analysis. These scatter plots are provided to demonstrate that the methodology does select input which covers the phenomena/parameter ranges and associated distributions. In general, it is difficult to see the PCT dependence of an individual parameter from these scatter plots. This is primarily due to the fact that there are several major parameters and a conservative combination of these parameters is required to obtain the higher values of PCT. Based on this the following paragraphs will concentrate on a discussion of the LBLOCA criteria as addressed by the analysis.

[

]

[

]

[

]

[

]

[

]

[

]

[

]

[

]

[

]

[

]

5.4 ***Determination of Total Uncertainty (CSAU Step 14)***

[] the biases and uncertainties determined during the code assessments are either directly addressed in the statistical analysis or demonstrated to be a code conservatism which adds an additional unquantified conservatism to the reported results. The final results for the 4-loop sample problem can be summarized as follows:

- The 95/95 calculated PCT was 1686 F which compares to the criterion for maximum PCT of 2200°F.
- The maximum nodal oxidation for the 95/95 PCT case was 0.8% which compares to the criterion for maximum nodal oxidation of 17%.
- The maximum total oxidation for the 95/95 PCT case was 0.02% which compares to the criterion for maximum total core oxidation of 1%.

Based on these results, it is concluded that the LBLOCA analysis for the sample W 4-loop plant meets the criteria for the LBLOCA event.

With respect to the identification of the degree of conservatism in the analysis, a comparison can be made to the 50/50 probability value for the PCT. The 50/50 PCT at 1375°F is 311°F less than the 95/95 PCT.

**Table 5.1 NPP Parameters for Consideration in the Performance of a
Realistic LBLOCA Analysis**

Table 5.2 Relationship of PIRT to Operational Parameters

Table 5.3 Ranked Importance of Process Parameters Relative to Plant Type

Table 5.4 Statistical Distributions Used for a Sample 3-Loop PWR

**Table 5.5 Number of Observations Required for a Desired
Tolerance: Non-Parametric Methods**

Table 5.6 Relationship of Uncertainty Parameters to Computer Code Input

**Table 5.7 Plant Operating Range and Fuel Design Supported by the
LOCA Analysis**

	<i>Event</i>	<i>Operating Range</i>
1.0	<i>Plant Physical Description</i>	
	<i>1.1 Fuel</i>	
	a) <i>Cladding outside diameter</i>	0.376 in.
	b) <i>Cladding inside diameter</i>	0.328 in.
	c) <i>Cladding thickness</i>	0.024 in.
	d) <i>Pellet outside diameter</i>	0.3215 in.
	e) <i>Pellet density</i>	95 % of theoretical
	f) <i>Active fuel length</i>	144 in.
	g) <i>Maximum rod-average exposure</i>	62,000 MWd/MTU
	<i>1.2 RCS</i>	
	a) <i>Flow resistance</i>	Analysis
	b) <i>Pressurizer location</i>	Analysis assumes location giving most limiting PCT
	c) <i>Hot assembly location</i>	Anywhere in core
	d) <i>Hot assembly type</i>	17x17
	e) <i>SG tube plugging</i>	≤ 10%
2.0	<i>Plant Initial Operating Conditions</i>	
	<i>2.1 Reactor Power</i>	
	a) <i>Core average linear heat generation rate</i>	Core power ≤ 102% of 3250 MWt
	b) <i>Peak linear heat generation rate</i>	≤ 2.62* (normalized)
	c) <i>Hot rod average linear heat generation rate</i>	≤ 1.8† (normalized)
	d) <i>Hot assembly linear heat generation rate</i>	< 1.731‡ (normalized)
	e) <i>Hot assembly burnup</i>	≤ 62000 MWD/MTU
	f) <i>MTC</i>	≤ 0 at HFP
	g) <i>HFP boron</i>	Normal letdown
	<i>2.2 Fluid Conditions</i>	
	a) <i>Loop Flow</i>	122.6 Mlb/hr ≤ M ≤ 142.1 Mlb/hr
	b) <i>Core Inlet Temperature</i>	550.0 ≤ T ≤ 556.6 °F

* Includes 5% measurement uncertainty and 3% manufacturing uncertainty.

† Includes 4% measurement uncertainty.

‡ Value equivalent to hot rod peaking factor without 4% uncertainty.

Table 5.7 Plant Operating Range Supported by the LOCA Analysis (*continued*)

	<i>Event</i>	<i>Operating Range</i>
	<i>c) Upper Head Temperature</i>	<i>< Core Outlet Temperature</i>
	<i>d) Pressurizer Pressure</i>	<i>$P \geq 2175$ psig</i>
	<i>e) Pressurizer Level</i>	<i>$48.2\% \leq L \leq 58.2\%$</i>
	<i>f) Accumulator Pressure</i>	<i>$600 \leq P \leq 660$ psig</i>
	<i>g) Accumulator Volume</i>	<i>$929 \leq V \leq 945$ ft³</i>
	<i>h) Accumulator Temperature</i>	<i>$80 \leq T \leq 130$ °F (coupled to containment temperature)</i>
	<i>i) Accumulator fL/D</i>	<i>Current line configuration</i>
	<i>j) Minimum ECC boron</i>	<i>≥ 2925 ppm</i>
3.0	<i>Accident Boundary Conditions</i>	
	<i>a) Break location</i>	<i>Any RCS piping location</i>
	<i>b) Break type</i>	<i>Double-ended guillotine or split</i>
	<i>c) Break size (relative to cold leg pipe)</i>	<i>$0.05 \leq A \leq 0.5$ full pipe area (split) $0.5 \leq A \leq 1.0$ full pipe area (guillotine)</i>
	<i>d) Offsite power</i>	<i>On or Off</i>
	<i>e) Safety injection flow</i>	<i>Current per loop pump delivery (same as used in current Robinson Appendix K methodology)</i>
	<i>f) Safety injection temperature</i>	<i>≤ 100 °F</i>
	<i>g) Safety injection delay</i>	<i>≤ 20.5 seconds (with offsite power) ≤ 40 seconds (without offsite power)</i>
	<i>h) Containment pressure</i>	<i>Bounding current configuration</i>
	<i>i) Containment temperature</i>	<i>$80 \leq T \leq 130$ °F</i>
	<i>j) Containment sprays</i>	<i>≥ 8 seconds</i>
	<i>k) Single failure</i>	<i>1 LPSI, 1 HPSI</i>

**Table 5.8 Summary of Major Parameters
Describing Limiting PCT Case (Case 22)**

Time (hrs)	5850
Core Power (MW)	3297
Core Peaking (FQ)	2.44
Radial Peak (Fdh)	1.8000
Axial Offset	-0.163
Local Peaking (FI)	1.098
Break Type	DEGB
Break Size (ft ²)	3.72 (~90%)
Offsite Power Availability	No
Diesel Start (s)	40.0
Decay Heat Multiplier	0.968

Table 5.9 Summary of Results for the Limiting PCT Case (22)

<i>PCT</i>	
<i>Temperature</i>	<i>1686 °F</i>
<i>Time</i>	<i>34 seconds</i>
<i>Elevation</i>	<i>9.4 ft</i>
<i>Metal-Water Reaction</i>	
<i>% Oxidation Maximum</i>	<i>0.8 %</i>
<i>% Total Oxidation</i>	<i>0.022 %</i>
<i>Total Hydrogen</i>	<i>0.5 lb</i>



Figure 5.1 Calculation Framework

Figure 5.2 [

]

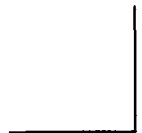


Figure 5.3 []

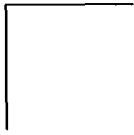


Figure 5.4 [

]



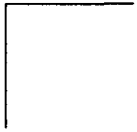


Figure 5.5 [

]

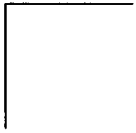


Figure 5.6 [

]



Figure 5.7 [

]

Figure 5.8 [

]

Figure 5.9 [

]

Figure 5.10 [

]

Figure 5.11 [

]

Figure 5.12 [

]

Figure 5.13 [

]

Figure 5.14 [

]



Figure 5.15 [

]

Figure 5.16 [

]



Figure 5.17 []

Figure 5.18 []



Figure 5.19 [

]

Figure 5.20 []

Figure 5.21 [

]

Figure 5.22 []

Figure 5.23 [

]

Figure 5.24 [

]

Figure 5.25 [

]

Figure 5.26 [

]

6.0 References

- 1) "Emergency Core Cooling Systems; Revisions to Acceptance Criteria," Federal Register, Vol. 53, No. 180, September 16, 1988, 10 CFR Part 50.
- 2) "Compendium of ECCS Research for Realistic LOCA Analysis," NUREG/1230, USNRC, December 1988.
- 3) "Best-Estimate Calculations of Emergency Core Cooling System Performance," Regulatory Guide 1.157, May 1989.
- 4) "Quantifying Reactor Safety Margins, Application of Code Scaling, Applicability, and Uncertainty Evaluation Methodology to a Large Break, Loss-of-Coolant Accident," NUREG/CR-5249, December 1989.
- 5) EMF-2102(P), Revision 0, S-RELAP5 Code Verification and Validation document
- 6) ANF-90-145(P)(A), *RODEX3 Fuel Rod Thermal-Mechanical Response Evaluation Model*, Volume 1, "Theoretical Manual," and Volume 2, "Thermal and Gas Release Assessments," April 1996.
- 7) EMF-1557(P) Revision 4, *RODEX3A: Theory and User's Manual*, November 2000.
- 8) EMF-2417(P) Revision 0, *RODEX3A Code Verification and Programmers Guide for Version USEP98*, July 2000.
- 9) EMF-2100(P) Revision 4, *S-RELAP5 Models and Correlations Code Manual*, January 2001.
- 10) EMF-2101(P) Revision 2, *S-RELAP5 Programmers Guide*, January 2001.
- 11) EMF-CC-097(P) Revision 7, *S-RELAP5 Input Data Requirements*, August 2000.
- 12) EMF-2054(P) Revision 2, *Code Input Development Guidelines for Realistic Large Break LOCA Analysis of a Pressurized Water Reactor*, July 2001.
- 13) EMF-2058, Revision 1, *S-RELAP5 Realistic Large Break LOCA Analysis Guideline*, July 2001
- 14) EMF-CC-039(P) Revision 2, *ICECON Code User's Manual: A Computer Program Used to Calculate Containment Back Pressure for LOCA Analysis (Including Ice Condenser Plants)*, March 1999.
- 15) EMF-CC-039(P) Revision 2 Supplement 1, *ICECON Code User's Manual: A Computer Program Used to Calculate Containment Back Pressure for LOCA Analysis (Including Ice Condenser Plants)*, December 1999.
- 16) EMF-2057, Revision 0, H. B. Robinson Unit 2 Nuclear Plant Realistic Large Break LOCA/ECCS Analysis, August 2001

- 17) NUREG-0800, U.S. Nuclear Regulatory Commission Standard Review Plan
- 18) NUREG/CR-4312, EGG-2396, Revision 1, RELAP5/MOD2 code Manual, Volume 1: Code Structure, Systems Models, and Solution Methods, March 1987
- 19) NUREG/CR-5535, INEL-95/0174, RELAP5/MOD3 Code Manual, August 1995
- 20) TID-4500, ANCR-1219, CONTEMPT-LT – A computer Program for Predicting Containment Pressure-Temperature Response to a Loss-Of-Coolant Accident, June 1975
- 21) EMF-2328 (P)(A), *PWR Small Break LOCA Evaluation Model, S-RELAP5 Based*, January 2000.
- 22) D. Fletcher and R. R. Schultz, RELAP5/MOD3 Code Manual, User's Guidelines, Volume 5, NUREG/CR-5535, January 1992.
- 23) R. R. Schultz, RELAP5-3D Code Manual, User's Guidelines, INEEL-EXT-98-00834, February 2001.
- 24) S. Shieh, V. H. Ransom, R. Krishnamurthy, RELAP5/MOD3 Code Manual, Validation of Numerical Techniques in RELAP5/MOD3, Volume 6, NUREG/CR-5535, August 1994.
- 25) J. V. Cathcart and R.E. Pawel, Zirconium Metal-Water Oxidation Kinetics: IV. Reaction Rate Studies, ORNL/NUREG-17, August 1977.
- 26) ANSI/ANS-5.1-1979, "American National Standard for Decay Heat Power in Light Water Reactors," approved August 29, 1979.
- 27) J. P. Unik and J.E. Gindler, "A Critical Review of the Energy Released in Nuclear Fission," ANL-7748, Argonne National Laboratory, Chemistry Division, March 1971.
- 28) "Comparisons of Thermal-Hydraulic Phenomena During Isothermal Loss-Of-Coolant Experiments and Effect of Scale in LOFT and SEMISCALE MOD-1," NURGE/CR-0410, December 1978.
- 29) "Similarity Analysis and Scaling Criteria for LWRs Under Single-Phase and Two-Phase Natural Circulation," NUREG/CR-3267, March 1983.
- 30) "UPTF: Program and System Description," U9 414/88/023, Siemens AG, KWU Group (Erlangen), November 1988.
- 31) Sleicher, C.A. and M.W. Rouse, "A Convenient Correlation for Heat Transfer to Constant and Variable Property Fluids in Turbulent Pipe Flow," International Journal of Heat and Mass Transfer, Volume 18, pp. 677-683, 1975.
- 32) Holman, J.P., *Heat Transfer*, 5th Edition, McGraw-Hill, New York, 1981.
- 33) Gebhart, B., *Heat Transfer*, 2nd Edition, McGraw-Hill, New York, 1971.

- 34) "ASME Steam Tables," Sixth Edition, ASME, New York, 1997.
- 35) Bird, R.B., W.E. Stewart and E.N. Lightfoot, *Transport Phenomena*, John Wiley and Sons, Inc., New York, 1960.
- 36) Dittus, F.W. and L.M.K. Boelter, "Heat Transfer in Automobile Radiators of the Tubular Type," *Publications in Engineering*, Volume 2, pp. 443-461. University of California, Berkeley, 1930.
- 37) Chen, J.C., R.K. Sundaram, F.T. Ozkaynak, "A Phenomenological Correlation for Post-CHF Heat Transfer," NUREG-0237, June 1977.
- 38) Forslund, R.P. and W.M. Rohsenow, "Dispersed Flow Film Boiling," *Journal of Heat Transfer*, Volume 90 (6), pp. 399-407, 1968.
- 39) Bromley, L.A., "Heat Transfer in Stable Film Boiling," *Chemical Engineering Progress*, Volume 46, pp. 221-227, 1950.
- 40) Berenson, P.J., "Film Boiling Heat Transfer from a Horizontal Surface," *Journal of Heat Transfer*, pp. 351-358, 1961.
- 41) Sun, K.H., J.M. Gonzales-Santalo and C.L. Tien, "Calculations of Combined Radiation and Convection Heat Transfer in Rod Bundles Under Emergency Cooling Conditions," *Journal of Heat Transfer*, pp. 414-420, 1976.
- 42) "FLECHT-SEASET Program, PWR FLECHT SEASET Unblocked Bundle, Forced and Gravity Reflood Task Data Evaluation and Analysis Report," NUREG/CR-2256, EPRI NP-2013, WCAP-8891, November 1981.
- 43) Taylor, D.D. et al, "TRAC-BD1/MOD1: An Advanced Best Estimate Computer Program for Boiling Water Reactor Transient Analysis, Volume 1: Model Description," NUREG/CR-3633, EGG-2294, April 1984.
- 44) "Dispersed Flow Film Boiling in Rod Bundle Geometry – Steady State Heat Transfer Data and Correlation Comparisons," NUREG/CR-2435, ORNL-5822, Oak Ridge National Laboratory, March 1982.
- 45) "An Analysis of Transient Film Boiling of High-Pressure Water in a Rod Bundle," NUREG/CR-2469, ORNL/NUREG-85, Oak Ridge National Laboratory, March 1982.
- 46) "Experimental Investigations of Bundle Boiloff and Reflood Under High-Pressure Low Heat Flux Conditions," NUREG/CR-2455, ORNL-5846, Oak Ridge National Laboratory, April 1982.
- 47) "ORNL Small-Break LOCA Heat Transfer Test Series I: High-Pressure Reflood Analysis," NUREG/CR-2114, ORNL/NUREG/TM-446, Oak Ridge National Laboratory, August 1981.
- 48) Loftus, M.J. et al, "PWR FLECHT-SEASET Unblocked Bundle, Forced and Gravity Reflood Task Data Report," NUREG/CR-1532, Volumes 1 and 2, June 1980.

- 49) "Data Report on Large Scale Reflood Test-43 – CCTF CORE-II Shakedown Test C2-SH2 (Run 054)," JAERI-memo 58-155, Japan Atomic Energy Research Institute, May 1983
- 50) Holmes, B.J, "I25 Comparison Report," NEA/CSNI/R(91)1, AEA-TRS-1043, February 1991.
- 51) Trapp, J.A. and V.H. Ransom, "A Choked-Flow Calculation Criterion for Nonhomogeneous, Nonequilibrium Two-Phase Flows," *International Journal of Multiphase Flow*, Volume 8, pp. 669-681, 1992.
- 52) "Upper Plenum Test Facility – UPTF – Test No. 10: Tie Plate Countercurrent Flow Test," U9 316/88/3, March 1988.
- 53) "Upper Plenum Test Facility – UPTF – Test No. 29: Entrainment/Deentrainment Test," E314/90/19, November 1990.
- 54) "Pump Two-Phase Performance Program," EPRI NP-1556, Volumes 1 through 8, September 1980.
- 55) "Mixing of ECC Water with Steam: 1/3 Scale Test and Summary," EPRI Report EPRI-294-2, June, 1975.
- 56) Carpenter, E.F. and A.P. Colburn, "The Effect of Vapor Velocity on Condensation Inside Tubes," *Proceedings of General Discussion on Heat Transfer, Institute of Mechanical Engineering/American Society of Mechanical Engineers*, pp. 20-26, 1951.
- 57) Collier, J.G., *Convective Boiling and Condensation*, 2nd Edition, McGraw-Hill, New York, 1981.
- 58) "Quick Look Report - UPTF - Test No. 6, Downcomer Countercurrent Flow Test," U9 316/89/2, Siemens AG UB KWU, March 1989.
- 59) "Experimental Data Report - UPTF - Test No. 6, Downcomer Countercurrent Flow Test," U9 316/88/18, Siemens AG UB KWU, March 1989.
- 60) "Quick Look Report - UPTF - Test No. 7, Downcomer Countercurrent Flow Test," E314/90/003, Siemens AG KWU, March 1990.
- 61) "Experimental Data Report - UPTF - Test No. 7, Downcomer Countercurrent Flow Test," U9 316/89/14, Siemens AG UB KWU, July 1989.
- 62) "Upper Plenum Test Facility, Test No. 8 Cold/Hot Leg Flow Pattern Test Quick Look Report," U9 316/88/11, Siemens AG, Erlangen Germany, September 1988.
- 63) "Upper Plenum Test Facility, Test No. 8 Cold/Hot Leg Flow Pattern Test Experimental Data Report," U9 316/88/12, Siemens AG, Erlangen Germany, September 1988.
- 64) XN-75-27(A), "Exxon Nuclear Neutronic Design Methods for Pressurized Water Reactors," Exxon Nuclear Company

- 65) EMF-96-029(P)(A), Reactor Analysis System for PWRs, January 1997.
- 66) Wilks, S.S., "Determination of Sample Sizes for Setting Tolerance Limits," Ann. Math. Stat., Vol. 12, pp. 91-96, 1941.
- 67) Somerville, P.N., "Tables for Obtaining Non-Parametric Tolerance Limits," Ann. Math. Stat., Vol. 29, No. 2, pp 599-601, June 1958.
- 68) "An Acceptable Model and Related Statistical Methods for the Analysis of Fuel
Densification," Regulatory Guide 1.126, Revision 1, U.S. Nuclear Regulatory
Commission, March 1978.
- 69) Abramowitz, M. and I. Stegun, "Handbook of Mathematical Functions with Formulas,
Graphs, and Mathematical Tables," National Bureau of Standards, Applied Mathematics
Series 55, 1966.
- 70) Box, G.E.P, M.E. Muller, "A note on the generation of random normal deviates," Annals
Math. Stat, V. 29, pp. 610-611 (1958).

Appendix A Overview of Base Case and Sensitivity Studies

A.1 Base Case Analyses Description

To demonstrate the range of applicability of the models used in the various sensitivity studies, four base case analyses are characterized in this Appendix. These are:

- 3-loop PWR, worst break, worst single failure, nominal (100%) core power, and plant technical specifications on rod power, and cosine power shape, no RODEX3A.
- 3-loop PWR, worst break, worst single failure, nominal (100%) core power, and plant technical specifications on rod power, and cosine power shape, no RODEX3A, no accumulator N₂.
- 3-loop PWR, worst break, worst single failure, high core power, and plant technical specifications on rod power, and top skewed power shape, no RODEX3A, no accumulator N₂.
- 4-loop PWR, worst break, worst single failure, high core power, and plant technical specifications on rod power, and top skewed power shape, no RODEX3A, no accumulator N₂.

The 3-loop PWR is an operating plant owned by a FRA-ANP customer with a 15x15 fuel design. The 4-loop PWR does not represent any particular 4-loop plant; however, it has the general dimensions typical of 4-loop PWRs. Those code models which may disguise the phenomena of interest for a given sensitivity study or add a computational burden to the problem have been removed for sensitivity study purposes only. These include the RODEX3A fuel model and accumulator nitrogen. With regard to RODEX3A, incorporation of the fuel model significantly increases calculation run times. A special suite of fuel rod studies was performed using the RODEX3A code. The key findings of these calculations are discussed in some detail in Appendix B. Accumulator nitrogen is neglected by using a valve at the accumulator exit that shuts off nitrogen flow as the accumulator completes discharging. The transport of the nitrogen has been shown to amplify code variability during late reflood, possibly disguising the effect of certain parameters expected to influence late reflood PCTs.

For these four base case input models, the plant and containment nodalization follow the governing guidelines issued at the time of model development (see References 15 and 16). Based on sensitivity studies using these input models only a few minor details have changed in the most recent revision of the guidelines.

A.2 *LBLOCA Calculation and Event Description*

From earlier sensitivity studies, the worst break size and worst single failure were identified. These parameters have been carried through most of the sensitivity studies performed during methodology development. The base case transients are well characterized by the event summary given in Table A.1. Figures A.1 through A.4 show the PCT trends for the 3-loop nominal power case with nitrogen and a 3-loop nominal power, 3-loop high power, and 4-loop high power case modeled without accumulator nitrogen release. The plots identify two cases: "Base" and "Case 7". In the suite of sensitivity studies, case 7 was designed to be identical to the base case so that the results from these two calculations would overlay. This provided a check on the sensitivity study process.

In general, the four base cases have very similar trends. The LBLOCA is initiated at time 0.0 s by a postulated large rupture of the reactor coolant system (RCS) primary piping. The worst break size for the 3-loop model is the 70% DEGB and for the 4-loop model, it is the 100% DEG. Based on deterministic studies, the worst break location was identified as being in the cold leg piping between the reactor coolant pump and the reactor vessel for the RCS loop containing the pressurizer. The break initiates a rapid depressurization of the RCS. A reactor trip signal is issued at about 0.7 s when the low pressurizer pressure trip setpoint is reached; however, reactor trip and scram are conservatively neglected in the analysis. The reactor initially shutdowns by coolant voiding in the core region.

For these break sizes, a rapid depressurization occurs, along with a core flow stagnation and reversal. This causes the fuel rods to experience departure from nucleate boiling (DNB) within a few seconds of the break. Subsequently, the limiting fuel rods dissipate heat via the film and transition boiling heat transfer regimes. The coolant voiding presents a strong negative reactivity contribution to the nuclear reaction and core fission ends. As heat transfer from the fuel rods is reduced, the cladding temperature rises.

Within the first few seconds, coolant in all regions of the RCS begins to flash. At the break plane, the loss of subcooling in the coolant results in substantially reduced break flow. This reduces the depressurization rate, and for the 4-loop leads to a period of positive core flow. The 3-loop result shows reduced downflow as the reactor coolant pumps in the intact loops continue to supply water to the vessel. Cladding temperatures are reduced from this blowdown cooling period in the 4-loop calculation; while, the 3-loop only shows a reduction in the rate of heatup.

This positive core flow or reduced downflow period ends as two-phase conditions occur in the reactor coolant pumps, reducing their effectiveness. Once again, the core flow reverses as most of the vessel mass flows out through the broken cold leg.

The mitigation of the LBLOCA begins when the safety injection actuation signal (SIAS) is issued. This occurs from high containment pressure. A worst single failure be considered for ECCS safety analysis. This single failure is assumed to be the loss of one low-pressure safety injection pump. The on-time start of containment spray and fan coolers is also assumed.

The RCS pressure falls below the accumulator pressure within 13 s. When this happens, fluid from the accumulators is injected into the cold legs. In the early delivery of accumulator water, high pressure and high break flow drive some of this fluid to bypass the core. Core heat transfer remains poor and the fuel rod cladding temperatures increased. As RCS and containment pressures equilibrate (around 25 s), ECCS water begins to fill the lower plenum and eventually lower portions of the core; thus, core heat transfer improves and cladding temperatures decrease.

Around 55 s, the relatively large volume of accumulator water is exhausted and core recovery must rely only on LPSI pump delivery of coolant. At this time (shown only for the case given in Figure A.1), the nitrogen gas used to pressurize the accumulator is transported out of the ECCS and RCS through the break. This may result in a short period of improved core heat transfer as the nitrogen gas displaces water in the downcomer into the core. After the accumulators have been exhausted, the LPSI coolant may (3-loop, nominal power cases) or may not (high power cases) be able to sustain cooling given the core decay heat and higher steam temperatures created by quenching of the lower portions of the core. The peak fuel rod cladding temperatures may increase for a short period until more energy is removed from the core from LPSI pump delivery and decay heat is reduced. Steam generated from fuel rod rewet entrains liquid and passes through the vessel upper plenum, the hot legs, the steam generator, and the

reactor coolant pump before it is vented out the break. The resistance of this flow path to the steam flow is balanced by the driving force of water filling the downcomer. This resistance acts to retard the progression of the core reflood and postpones core wide cooling. Eventually (within a couple of minutes of the accident), the core reflood progresses sufficiently to ensure core wide cooling. Full core quench will come in a matter of minutes after core wide cooling. Long-term cooling is then sustained with the residual heat removal system.

A.3. Sensitivity Studies Overview

Many sensitivity studies were performed in the development of the FRA-ANP RLBLOCA methodology. A detailed discussion of each study is not practical. It is important to present the evolution of these studies in order to demonstrate a pedigree for the methodology and to define ranges of applicability for these sensitivity studies. Table A.2 outlines classes of sensitivity studies that have been performed, explains the objective of these calculations, and presents general conclusions drawn from these calculations.

The basic philosophy in performing the earliest sensitivity studies was to first identify a best-estimate, "worst" case model. These models were characterized by a worst break size, worst single failure and plant technical specifications for hot rod power. Power distributions resembled a cosine shape. The 3-loop, nominal power cases conform to this description. This approach was considered to provide a bounding result to a "nominal" LBLOCA. It was later recognized that some of these assumptions may not extrapolate to even more limiting conditions. In consideration of this possibility, studies were performed at high powers and with top skewed power profiles to examine sensitivities near the criterion on peak clad temperature. For this reason, the high powered, 3- and 4-loop models were prepared and executed.

The results from the sensitivity studies sometimes deviated from the descriptions given in Section A.2. Underlining each of these studies are various assumptions about nodalization, the modeling of particular phenomena, runtime sequence, and plant state (nominal vs. "limiting" conditions). As the methodology developed, such issues evolved and are now reflected in the guidelines for performing RLBLOCA analyses (References 15 and 16). In general, quantitative results only represent one component of what may be defined as a "good" or "bad" result. In evaluating results, qualitative trends and deviations from the base cases have also been considered,

- "Is the expected sensitivity present?"
 - "If not, is this important?"
 - "If so, how do I capture this in a guideline?"

To answer this and other questions, the CSAU methodology recommends that the PIRT be considered. This has been followed during the methodology development.

**Table A.1 Base Case Large Break LOCA Approximate Sequence of
Events Table**

Event	<u>W</u> 3-loop Times, sec	<u>W</u> 3-loop HP Times, sec	<u>W</u> 4-loop HP Times, sec
Analysis Initiated	0.00	0.00	0.00
Break Opened	0.0	0.0	0.0
Safety Injection Signal	<1	<1	<1
Broken Loop Accumulator/ SIT Flow Initiated	8	8	8
Intact Loop Accumulator/ SIT Flow Initiated	13	13	13
End of Bypass/Beginning of Refill	25	25	25
Broken Loop Accumulator/ SIT Empties	55	55	55
Beginning of Reflood	30	30	30
Intact Accumulator/ SIT Empties	55, 57	55, 57	55, 57
PCT Occurred	28	140	111

Table A.2 Sensitivity Studies Performed for Methodology

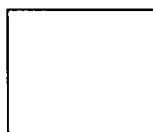


Table A.2 Sensitivity Studies Performed for Methodology

Table A.2 Sensitivity Studies Performed for Methodology

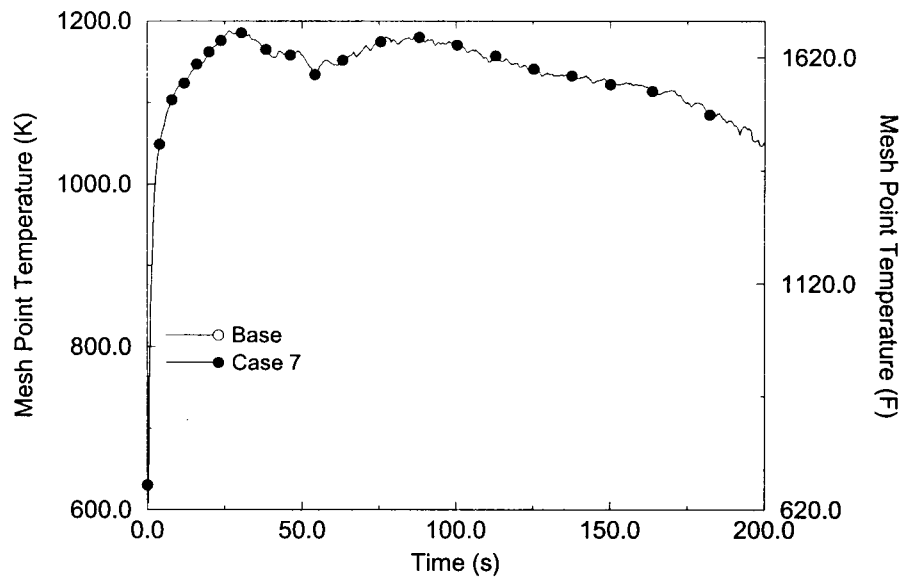


Figure A.1 PCT independent of elevation for 3-loop plant at nominal power with accumulator nitrogen effects

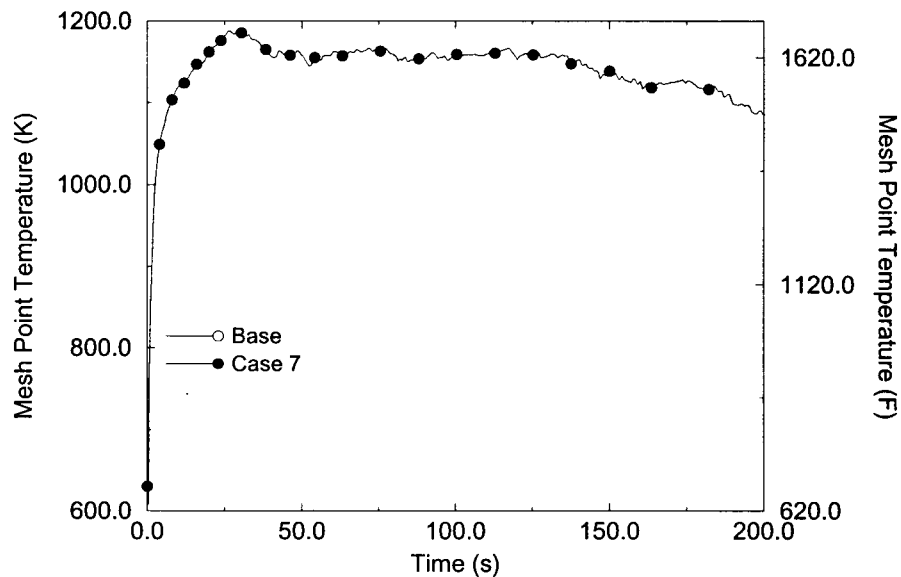


Figure A.2 PCT independent of elevation for the 3-loop plant at nominal power with accumulator nitrogen effects

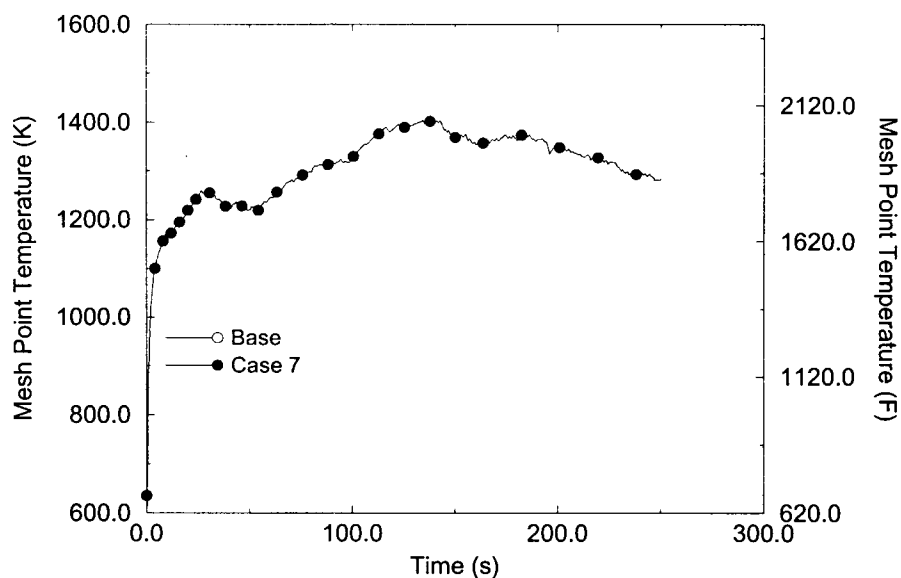


Figure A.3 PCT independent of elevation for the 3-loop plant at high power without accumulator nitrogen effects

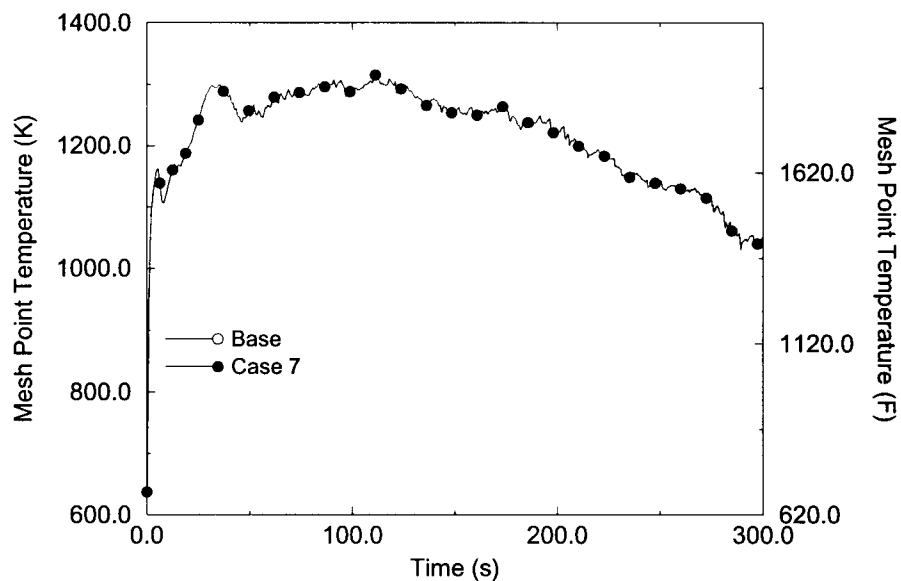


Figure A.4 PCT Independent of Elevation for the 4-loop Plant at High Power Without Accumulator Nitrogen Effects

Appendix B Conservatism

Among the major assumptions stated for the FRA-ANP RLBLOCA methodology are declarations of adopted conservatism. Such declarations are not always physically intuitive. In these instances, sensitivity studies have been performed to arrive at the stated conclusions. In this appendix, selections of calculations are presented to support some of the statements of conservatism presented in this methodology document.

B.1 Analysis for Fresh Fuel Assemblies Only

Only fresh fuel assemblies are specifically analyzed in the RLBLOCA methodology. By considering "Time-in-Cycle" as an uncertainty parameter, identification of a limiting hot rod and hot assembly is required. The motivation for this limitation is the necessity for a strategy that demonstrates that the methodology realistically supports the limiting conditions during an operation cycle. Core loading experience supports the premise that fresh fuel assemblies tend to give limiting peak assembly powers during a cycle. Cycle-to-cycle burnup will have two effects on PCT: reduced power and stored energy. Both of these factors are highly-ranked phenomena based on the PIRT given in Table 3.4 and their reduction will contribute to lower PCTs. However, the criterion for identifying the hot rod is based on the maximum core peaking factor F_q . F_q will fluctuate during a cycle creating the opportunity for burned or gadolinia bearing fuel assemblies to become limiting. This sensitivity study examined the question of whether this fluctuation in F_q creates the possibility that second or third cycle fuel could be limiting.

To evaluate the position that fresh fuel is limiting, a series of deterministic sensitivity studies was performed using models representing 3- and 4-Loop PWRs with 15x15 and 17x17 fuel designs, respectively. The validation strategy was to examine PCT sensitivity at BOC, MOC, and EOC for fresh and once burnt fuel for a 3-loop and 4-loop PWR. The analysis presented in this section was performed similar to the RLBLOCA methodology that sets the limiting rod at the technical specification limit for radial power peaking ($F_{\Delta h}$) including uncertainties.

Following the methodology as described in Section 5.1.3.2, RODEX3A and S-RELAP5 input was created describing the fuel conditions and power distributions at various times in life. To eliminate the contribution of radial power dependency on burnup, all calculations were performed with the same radial power distribution used in the base cases (see Appendix A).

Assembly lifetime was assumed to extend to two operational cycles. The calculations were performed as described in Section A.2. with the addition of the RODEX3A fuel rod models. Tables B.1. and B.2 show the results from the studies for the 3- and 4-loop PWRs, respectively. Figures B.1. and B.2. show the PCT traces comparing the results of cycle 1 BOC (BOC1) vs. cycle 2 BOC, MOC, and EOC for the two plant types. As shown in the tables and figures, the PCT calculations using fresh fuel, cycle 1 fuel, generally bounds the once burnt, cycle 2 results.

By using the same radial power distribution in each case, the only two differences between the calculations are fuel rod material properties and axial shape. Examination of the power shapes show that case-to-case differences are subtle for the BOC and MOC cases; thus, supporting the conclusion that the material property differences have the most influence the results. The material property changes reduce stored energy. This effect on stored energy is best observed during the blowdown and refill phases of the LBLOCA as can be observed in Figures B.1 and B.2. The axial shapes for the EOC cases show some differences in the PCT location. The EOC2 case has a higher power peak in the top portion of the core. This explains why the PCT calculated in the EOC2 cases in the 3- and 4-loop calculations is greater than the EOC1. The small differences shown in PCT is inconsequential, because the once burned fuel at EOC is not likely to be near the $F\Delta h$ technical specification limits. Thus, the higher PCTs for the EOC2 fuel compared to the EOC1 fuel, clearly are driven by unrealistic increasing the EOC2 fuel power.

The conclusion drawn from this study is that because of the reduction in power and stored energy with burnup, fuel assemblies residing in the core for more than one cycle will not be limiting. For this reason, the FRA-ANP RLBLOCA methodology has chosen to only analyze fresh fuel assemblies.

B.2 Analysis without Clad Swelling and Rupture

Cladding swelling and rupture is a possibility whenever fuel temperatures are highly elevated. Before rod failure, the cladding is expected to swell like a balloon. At some point, the material stresses within the cladding will yield to the internal pressure and the fuel rod will fail. Cladding temperatures will be influenced by three additional conditions as a result of swelling and rupture. These are increased cladding surface area, increased gap size, and reduced assembly flow area or blockage. With regard to PCT, these are competing effects. The larger surface area and gap size will act to reduce cladding temperatures; however, flow blockage may prevent rod

locations above the rupture point from receiving coolant and increase temperatures above the rupture location.

Cladding swelling and rupture is a required model for 10CFR50 Appendix K analysis. NUREG-630, "Cladding Swelling and Rupture Models," outlines acceptable models for describing swelling and rupture. The S-RELAP5 code used within the FRA-ANP RLBLOCA methodology has the same cladding swelling and rupture model used in existing FRA-ANP Appendix K licensing methodologies (model based on those described in NUREG-630). Experience with Appendix K methodologies has shown that the use of swelling and rupture models produce less conservative PCTs than when neglecting this phenomenon. To assess how this model performs with the FRA-ANP RLBLOCA methodology, a sensitivity study was performed for both a 3- and 4-loop PWR with 15x15 and 17x17 fuel designs, respectively.

Figures B.3 and B.4 show the PCT sensitivity to fuel rupture. In both instances, the case modeling fuel rupture shows a significant decrease in rod temperature. This is evidence that despite the blockage effect, the increased fuel rod surface area and the increased thermal resistance across the fuel-cladding gap resulting from swelling provides the dominant influence on the temperature transient. By the RLBLOCA methodology not treating rod swelling and rupture, the phenomena is conservatively bounded.

B.3. Radial Power Distributions

[

]

- []
- []
- []
- []

[

]

A set of ten radial power cases were designed for this study. These cases were analyzed using the 3-loop plant model. This same study was also performed for the 4-loop plant; however, results from that study showed little sensitivity since the transient in the 4-loop plants experiences quicker mitigation. The ten cases are summarized in the table below. The abbreviation HA identifies the hot assembly, SA identifies the surrounding assemblies, AA identifies the average assemblies, and CA identifies the cold assemblies. Those cases identified as "High" power had the core powers raised so that predicted peak cladding temperature results would be near the criterion. Given the original base case (HA>SA>AA>CA), averaging the peaking factors as defined in the table was all that was necessary to derive the other cases. The one exception is the HA>SA = AA>>CA. In this case the cold assembly power was assumed to be 20% less than the base case value.

Radial Configuration	Power
HA>SA>AA>CA (base)	Nominal
HA>SA=AA=CA	Nominal
HA>SA=AA>CA	Nominal
HA>SA=AA>>CA	Nominal
HA>SA>AA=CA	Nominal
HA>SA>AA>CA	High
HA>SA=AA=CA	High
HA>SA=AA>CA	High
HA>SA=AA>>CA	High
HA>SA>AA=CA	High

Figures B.5 and B.6 show the results from this study for the high power cases and the nominal power cases, respectively. In a separate study examining the effect of accumulator nitrogen on code variability, this same set of ten cases was redone. Figures B.7 and B.8 show the results. For the two plots showing the high power results, the case HA>SA=AA=CA stands out as having the highest PCT. While the most peaked case, HA>SA>AA>CA, does not show a second reflood peak in either case. At the nominal power, the trends are less pronounced.

[

]

B.4. Pump Two-Phase Degradation

During a LOCA event in a PWR, the reactor coolant will reach saturation conditions and a two-phase mixture of steam and water will circulate through the coolant loops and through the reactor coolant pumps (RCPs). The LOCA will result in pump operation far from rated conditions for single-phase fluid flow and may induce reverse flow and a negative pressure differential. In a large break LOCA, this period occurs for a brief time shortly after the break opens. The head generated by RCPs during this period can significantly enhance heat transfer in the core and may limit the rise in cladding temperature and, in some cases, actually reduce cladding temperatures during this period. Most safety analysis conservatively assumes RCP trip to reduce the effectiveness of the pumps to enhance heat transfer during blowdown.

The LBLOCA PIRT developed for the FRA-ANP RLBLOCA methodology ranks pump two-phase degradation as high. For this reason, sensitivity studies were performed examining the effect of a more severe degradation model on PCTs. As shown in Figures B.9 and B.10, the two-phase degradation of the Semiscale pump bound the two-phase characteristic of other well known pump experimental programs (figures come from NUREG-1230, "Compendium of ECCS Research for Realistic LOCA Analysis," Reference 2).

The Semiscale pump model can be defined for an S-RELAP5 RLBLOCA calculation through input. The S-RELAP5 pump model describes pump behavior by single-phase homologous curves, two-phase, fully degraded homologous curves, and void-dependent degradation multipliers for head and torque. The head across the pump is computed as:

$$H_{2\phi} = H_{1\phi} + M(\alpha)[H_{DEGRAD} - H_{1\phi}]$$

where $H_{2\phi}$, $H_{1\phi}$, H_{DEGRAD} and $M(\alpha)$ are two phase head, single-phase head, fully degraded head and degradation multiplier (a function of void fraction), respectively. A similar description is used for predicting the hydraulic torque for the pump.

In the sensitivity studies the single-phase homologous curves ($H_{1\phi}$) used for all cases are supplied by the default Westinghouse pump data that is coded in S-RELAP5. The model describing two-phase degradation (H_{DEGRAD} and $M(\alpha)$) is entered as tabular input to S-RELAP5. For the base case, the default EPRI-CE data (Reference 59) for two-phase degradation is specified. The sensitivity study examined replacing the EPRI-CE degradation model with the Semiscale degradation model. The degradation model is only applied when two-phase conditions are present in the pump. During the rapid blowdown resulting from a LBLOCA, this period lasts about 10-15s following the break.

The PCT results, relative to the three base cases without accumulator nitrogen, are shown in Figures B.13 - B.15 (extracted for the time period of interest). For the 3-loop plant cases, no sensitivity is evident. This is the expected result, since the break size chosen was selected to minimize the enhanced blowdown heat transfer provided by the pumps. The 4-loop plant case does show an increase in the blowdown peak PCT of about 18 °F (10 K).

The PCT change of 18 °F well within the expected variability of the results which is about 30 °F (see Appendix C). In hindsight the pump degradation does not appear to be as significant of a parameter as originally anticipated. This result is consistent with the original work performed on the CSAU methodology (Reference 4). Since it has been demonstrated that increased pump degradation is not an important PIRT phenomena, the best-estimate EPRI-CE degradation model will be used in the RLBLOCA methodology.

Table B.1 Key results for burnup studies for a 3-loop PWR at tech-spec radial power

Case #	Case	PCT Temp (F)	Delta Temp	Calc F_Q
1	BOC1 (base case)	1662.8	0.0	2.091
2	MOC1	1676.5	13.7	2.180
3	EOC1	1533.7	-129.1	2.086
4	BOC2	1500.3	-162.5	2.144
5	MOC2	1580.4	-82.4	2.106
6	EOC2	1564.4	-98.4	2.088

Table B.2 Key results for burnup studies for a 4-loop PWR at tech-spec radial power

Case #	Case	PCT Temp (F)	Delta Temp	Calc F_Q
1	BOC1 (base case)	1469.9	0.0	1.982
2	MOC1	1466.1	-3.8	2.122
3	EOC1	1318.1	-151.8	2.054
4	BOC2	1415.8	-54.1	2.029
5	MOC2	1351.7	-118.2	2.016
6	EOC2	1334.5	-135.4	1.998

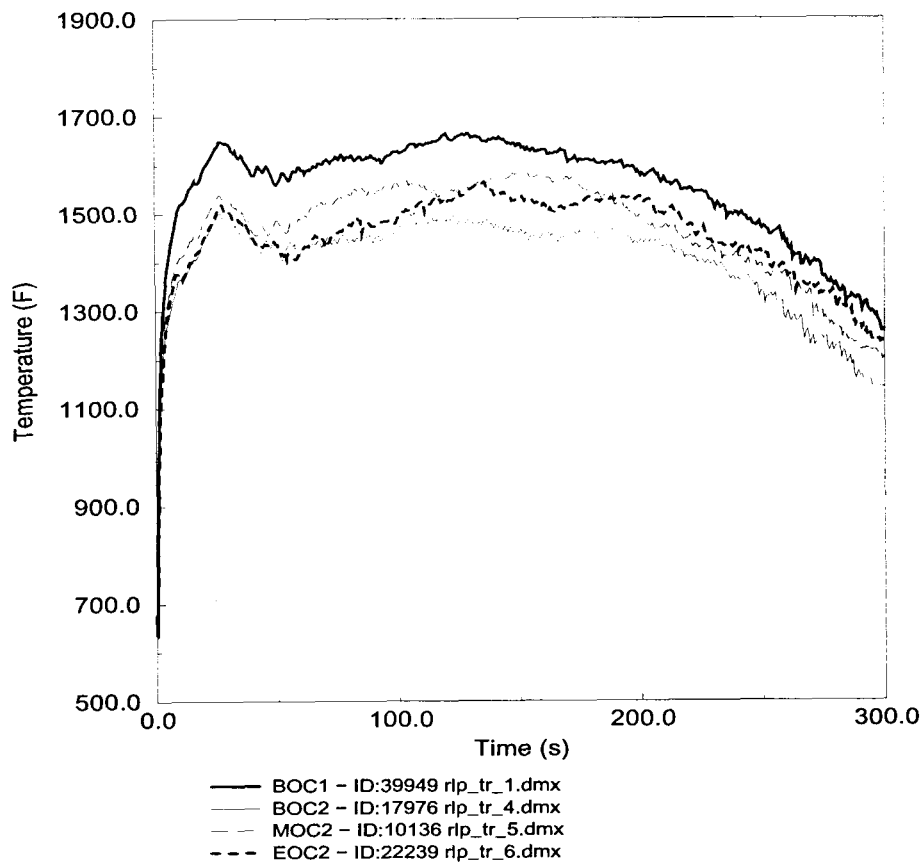


Figure B.1 PCT traces comparing a fresh fuel assembly at BOC to once burnt fuel at BOC, MOC, and EOC (3-loop, tech-spec power).

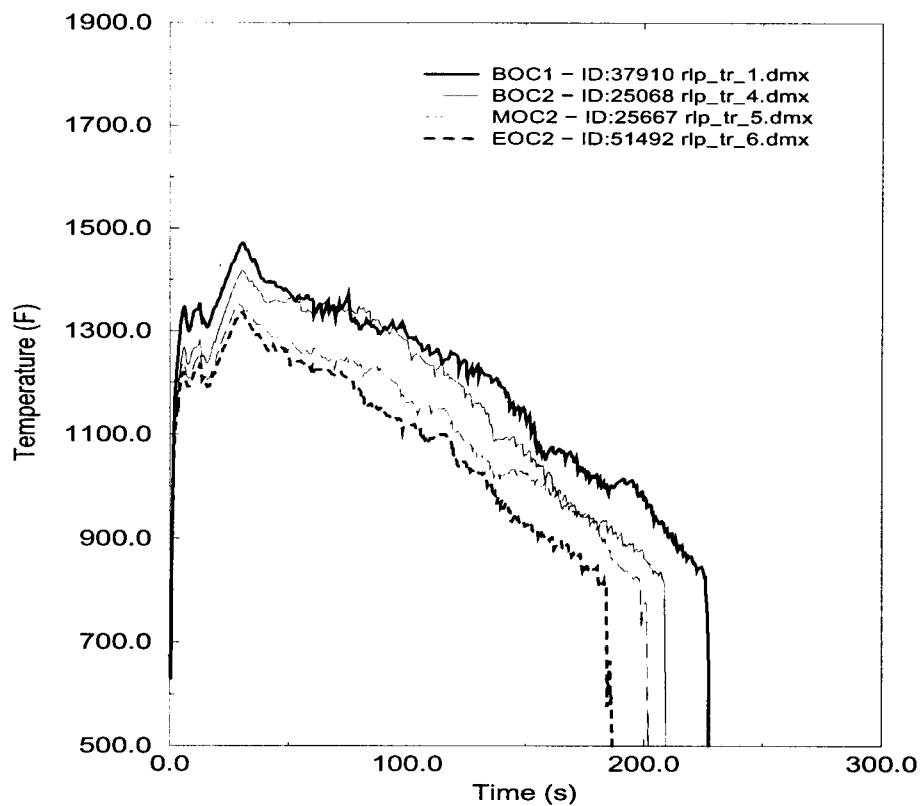


Figure B.2 PCT traces comparing a fresh fuel assembly at BOC to once burnt fuel at BOC, MOC, and EOC (4-loop, tech-spec power).

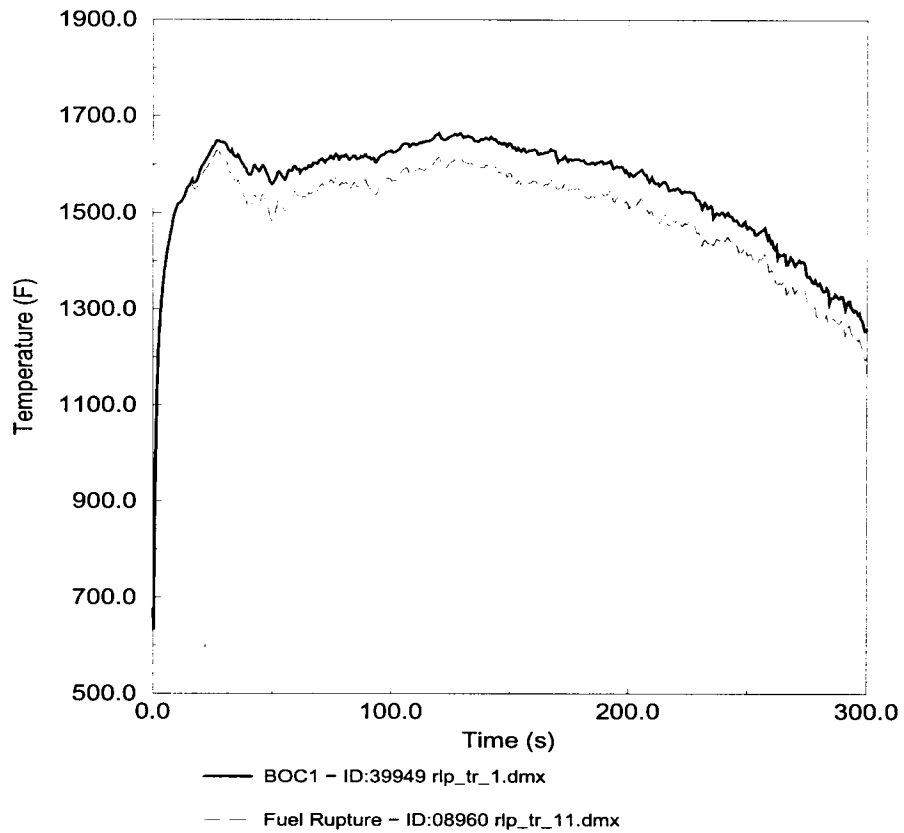


Figure B.3 Influence of fuel rupture on PCT (3-loop, tech-spec power)

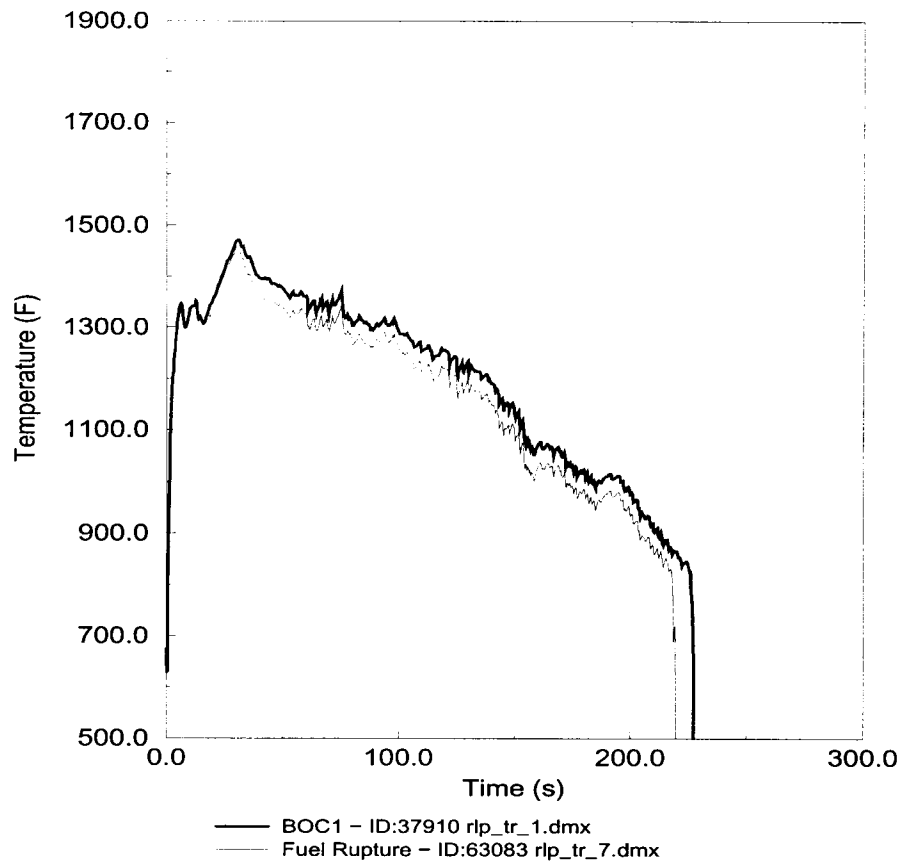


Figure B.4 Influence of fuel rupture on PCT (4-loop, tech-spec power)

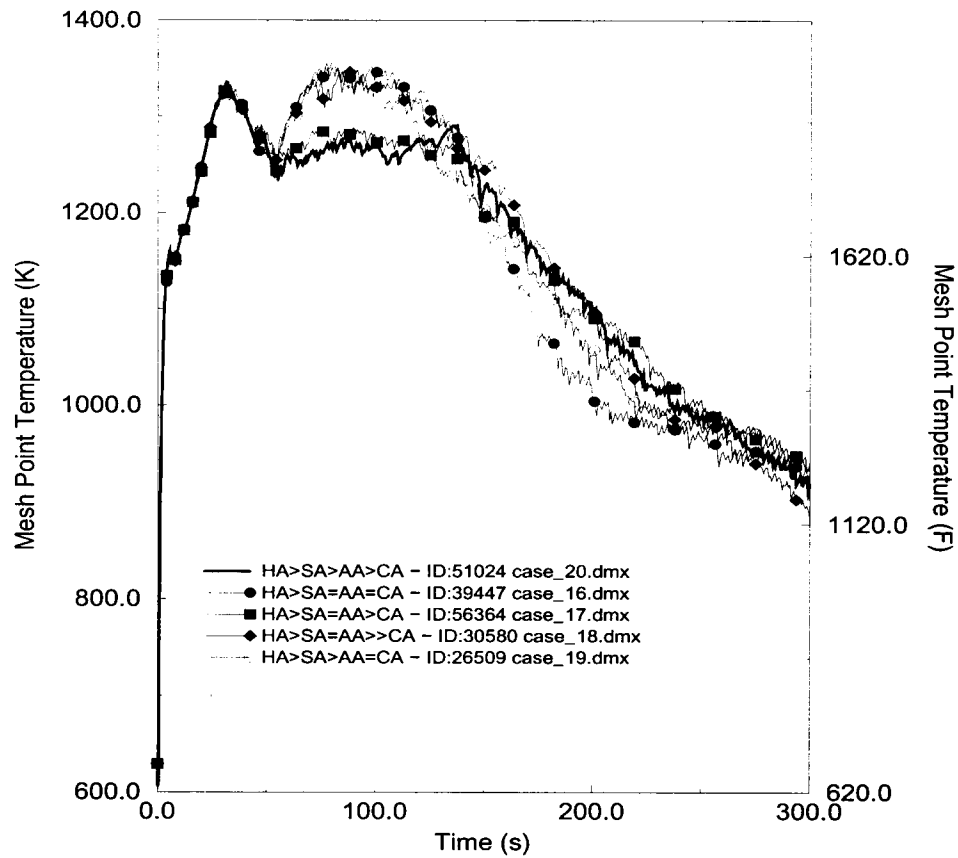


Figure B.5 PCTs from radial power sensitivity studies at high power

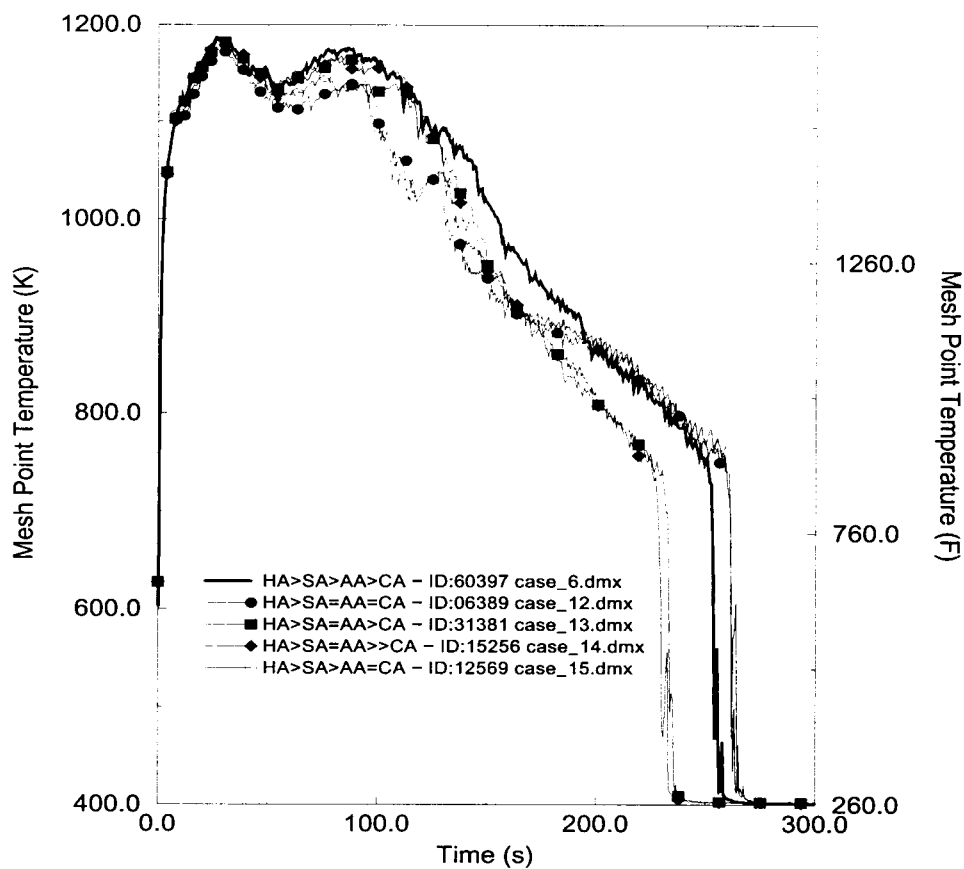
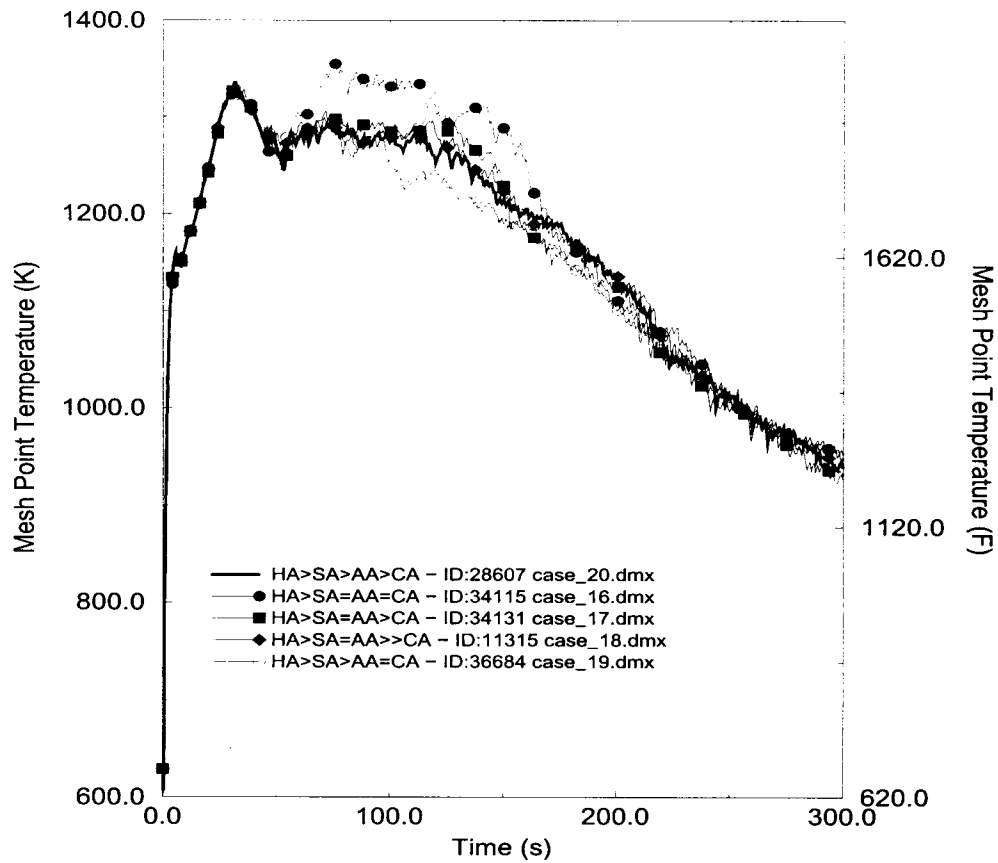
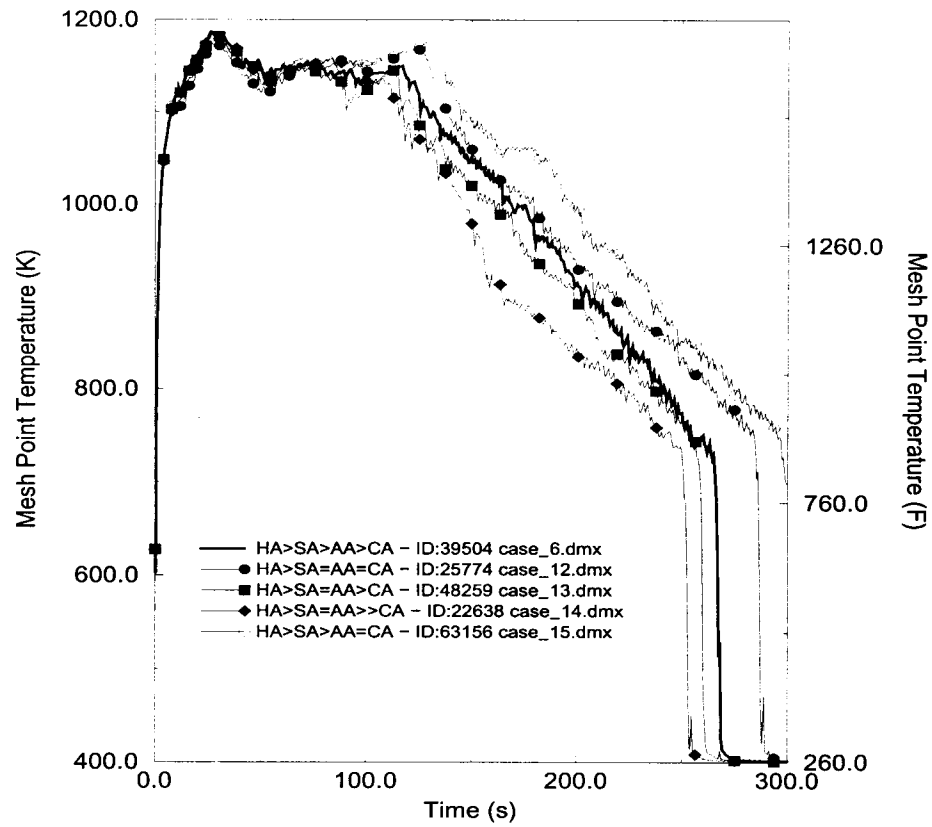


Figure B.6 PCTs from radial power sensitivity studies at nominal power



**Figure B.7 PCTs from radial power sensitivity studies at high power
(accumulators valved out)**



**Figure B.8 PCTs from radial power sensitivity studies at nominal power
(accumulators valved out)**

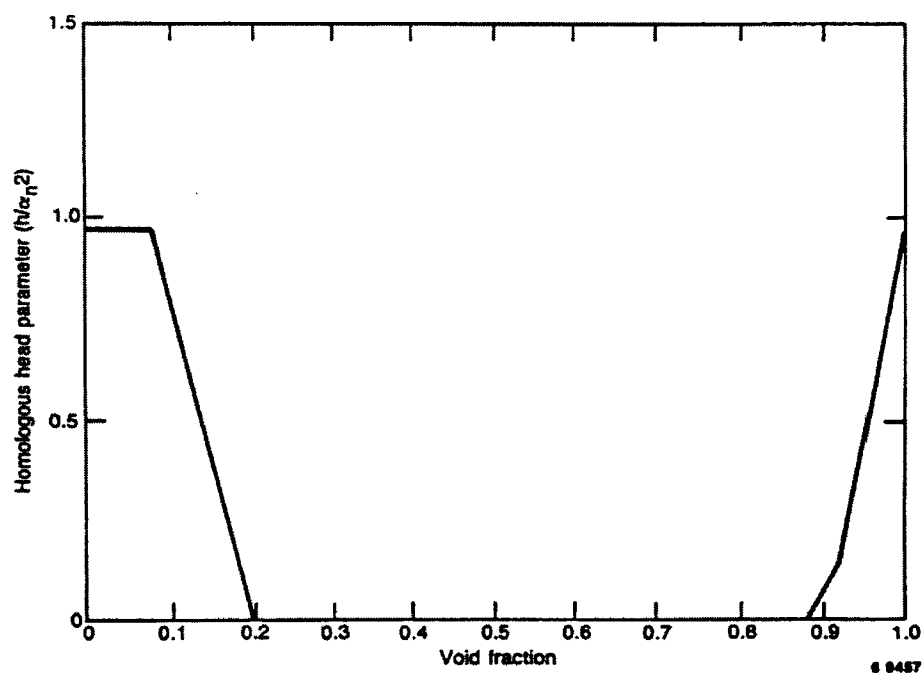


Figure B.9 Two-phase head multiplier for Semiscale pump model

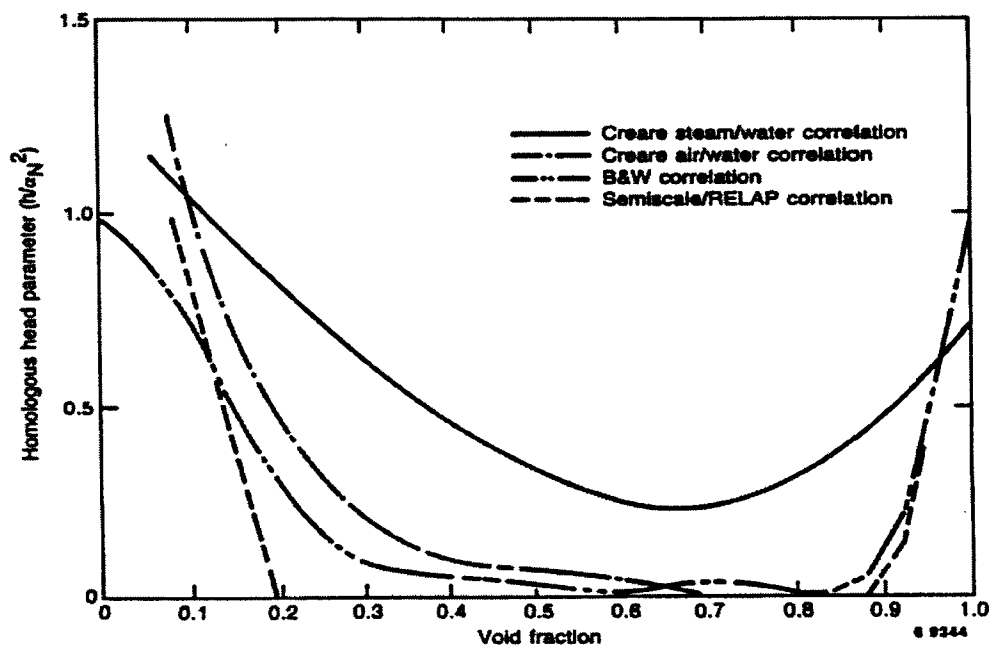


Figure B.10 Two-phase head multiplier for Semiscale pump model compared to other pump models

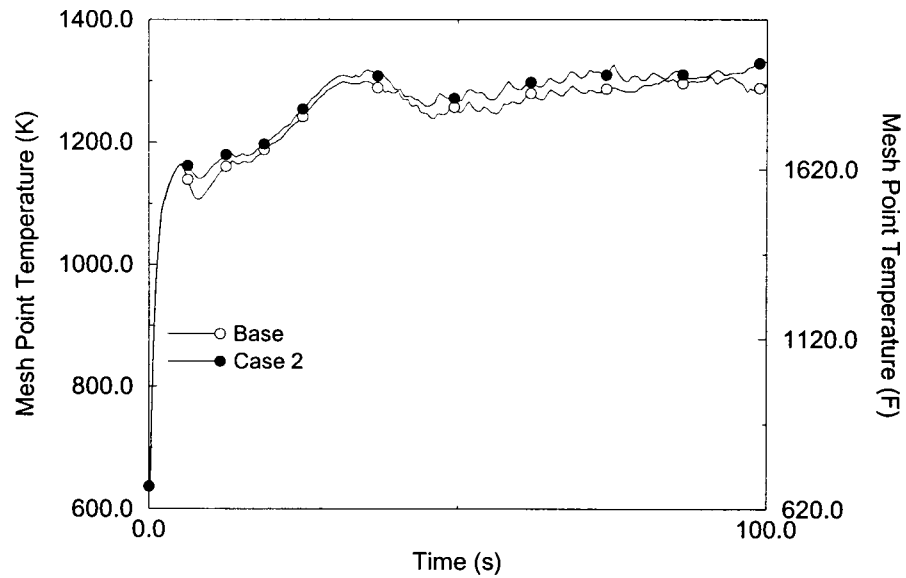


Figure B.11 Effect of Semiscale pump two-phase degradation model on PCT for 4-loop plant at high power

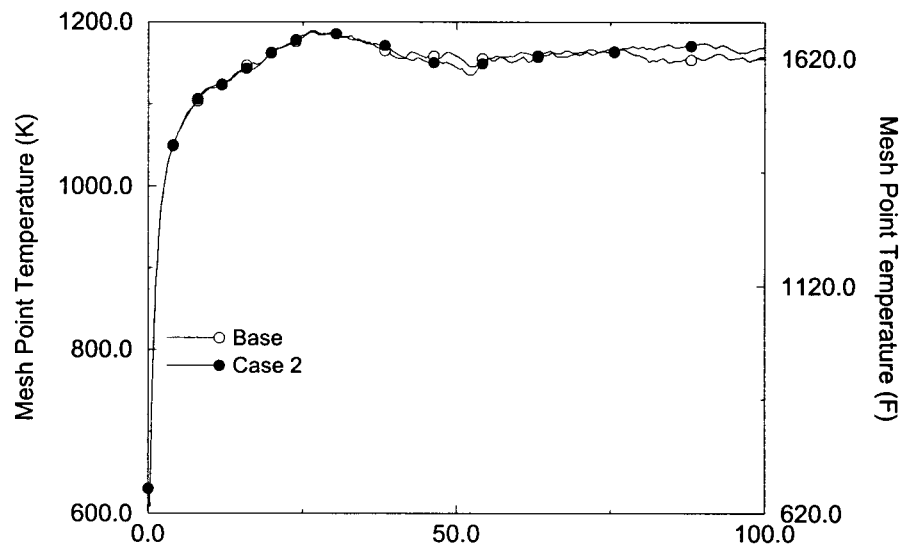
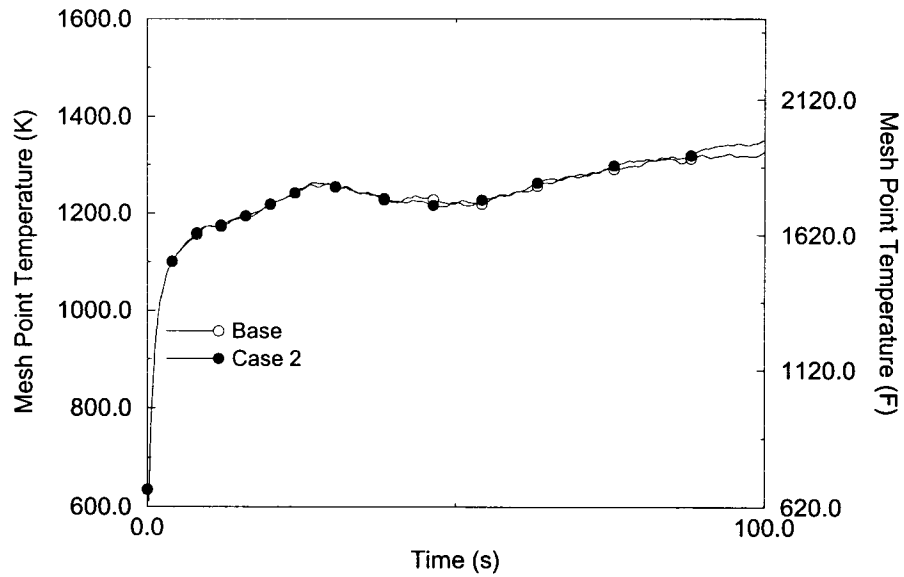


Figure B.12 Effect of Semiscale pump two-phase degradation model on PCT for 3-loop plant at nominal power



**Figure B.13 Effect of Semiscale pump two-phase degradation model
on PCT for 3-loop plant at high power**

Appendix C Time Step Sensitivity

Appendix K methodologies require that computer program solution convergence be demonstrated by studies of system modeling or noding and calculation time steps. [

]

This sensitivity study was performed by randomly varying time steps over a range from the base case time step set to about 20% larger. Four time step ranges were used to cover the main phases of the LBLOCA: blowdown (0-25 s), early reflood (25-60 s), late reflood (60-160 s), and cool down (>160 s). Each time step range was varied independently. Figure B.16 shows the results from these 14 calculations. Early in the event, S-RELAP5 shows very good agreement for all 14 cases. As the accumulators discharge, there is some noticeable divergence in the results. This is the result of downcomer boiling which can be exacerbated by the accumulator nitrogen passing through the system.

[

]

The cause of the variability, downcomer boiling, has been investigated. Downcomer boiling along the sector adjacent to the broken loop contributes to liquid holdup. This liquid holdup is vulnerable to entrainment out the break from pressure oscillations driven by condensation or the transport of the accumulator nitrogen bubble. The amount of mass held up does vary significantly and a large amount of coolant may be unphysically lost when a pressure spike occurs.

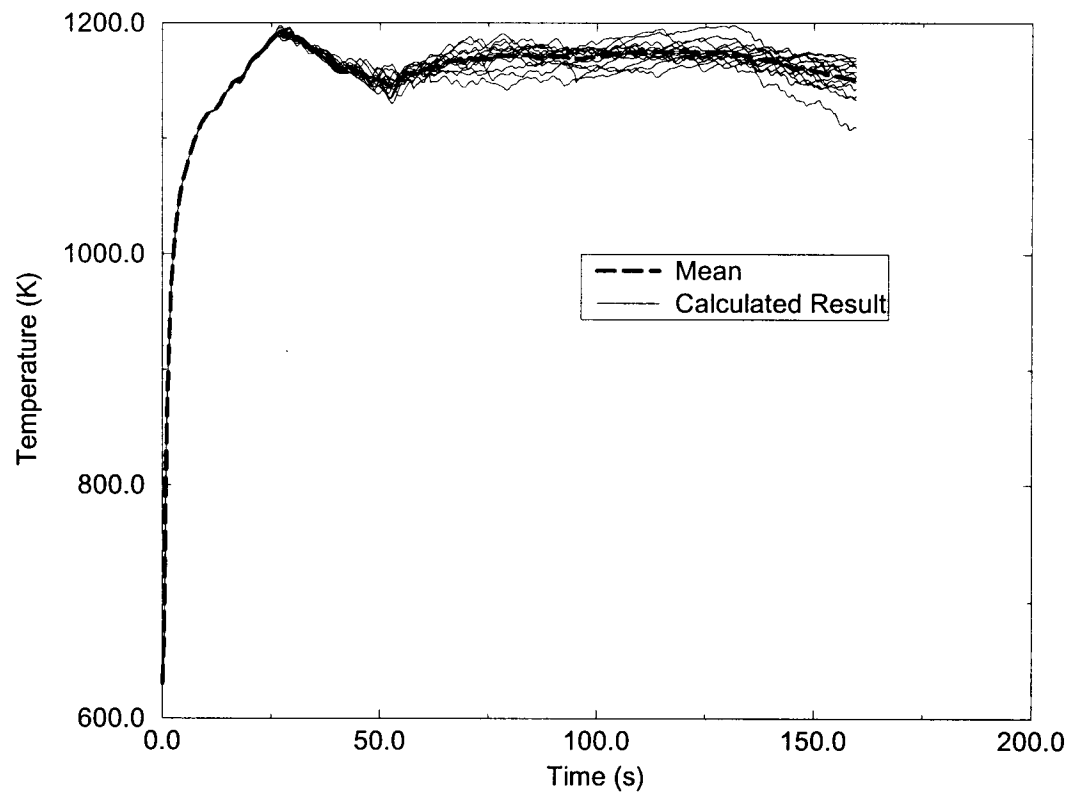


Figure C.1 PCT results from time step sensitivities performed for base case LBLOCA on 3-loop plant at nominal power

Appendix D Sample Westinghouse 3-Loop PWR Licensing Analysis

D.1 Introduction

This appendix describes a RLBLOCA analysis of a postulated large-break loss-of-coolant accident (LBLOCA) for a sample Westinghouse 3-loop PWR operating with Framatome ANP, Inc. (FRA-ANP) fuel.

The analysis is designed to support operation for a typical reload cycle. It also applies to subsequent cycles, unless changes in the technical specifications, core operating limits report, fuel design, plant hardware, or plant operation cause model input revisions.

The non-parametric statistical methods inherent in the FRA-ANP RLBLOCA methodology provide for the consideration of a full spectrum of break sizes, break configuration (Guillotine or Split Break), axial shapes, and plant operational parameters. A conservative single failure assumption is applied in which the negative effects of both the Loss of a low pressure safety injection pump and the loss of a diesel generator are simulated. The effects of Gadolinia-bearing fuel rods and peak fuel rod exposures are also considered.

D.2 Summary

The limiting peak cladding temperature (PCT) analysis is based on the parameter specification given in Table D.2.1, based on a set of 59 calculations. The PCT for that limiting case was calculated to be 1853°F.

The analysis assumes full-power operation at 2300 MW_t (plus uncertainties), a steam generator tube plugging level of up to 10% in any generator, a total peaking factor (F_Q) of 2.62 including uncertainties, and a nuclear enthalpy rise factor ($F_{\Delta H}$) of 1.80 (including 4% uncertainty). This analysis also addresses typical operational ranges or technical specification limits (which ever is applicable) with regard to pressurizer pressure and level; accumulator pressure, temperature (containment temperature), and level; core inlet temperature; core flow; containment pressure and temperature; and refueling water storage tank temperature.

The FRA-ANP RLBLOCA methodology explicitly analyzes only fresh fuel assemblies. A deterministic analysis has been performed to demonstrate that previously burnt fuel will not be limiting. This analysis accounts for peak rod average exposures of up to 62,000 MWd/MTU which corresponds to a maximum assembly burnup of 57,000 MWd/MTU. The analysis demonstrates that the 10 CFR 50.46(b) criteria listed in Section D.3 are satisfied.

Table D.2.1 Summary of Major Parameters for Limiting Transient

Time in Cycle (hrs)	4181
Burnup (MWd/MTU)	6800
Core Power (MW)	2301
Core Peaking (FQ)	2.28
Radial Peak (Fdh)	1.80
Axial Offset	-0.09
Local Peaking (FI)	1.144
Break Type	DEGB
Break Size (ft ²)	2.69 (~66%)
Offsite Power Availability	No
Decay Heat Multiplier	0.974

D.3 Analysis

The purpose of the analysis is to verify typical technical specification peaking factor limits and the adequacy of the emergency core cooling system (ECCS) by demonstrating that the following 10 CFR 50.46(b) criteria are met:

- The calculated maximum fuel element cladding temperature shall not exceed 2200°F.
- The calculated total oxidation of the cladding shall nowhere exceed 0.17 times the total cladding thickness before oxidation.
- The calculated total amount of hydrogen generated from the chemical reaction of the cladding with water or steam shall not exceed 0.01 times the hypothetical amount that would be generated if all of the metal in the cladding cylinders surrounding the fuel excluding the cladding surrounding the plenum volume, were to react.
- Calculated changes in core geometry shall be such that the core remains amenable to cooling.

Section D.3.1 of this report describes the postulated LBLOCA event. Section D.3.2 describes the models used in the analysis. Section D.3.3 describes the 3-loop PWR plant and summarizes the system parameters used in the analysis. Section D.3.4 summarizes the results of the RLBLOCA analysis.

D.3.1 Description of the LBLOCA Event

A LBLOCA is initiated by a postulated large rupture of the Reactor Coolant System (RCS) primary piping. Based on deterministic studies, the worst break location is in the cold leg piping between the reactor coolant pump and the reactor vessel for the RCS loop containing the pressurizer. The break initiates a rapid depressurization of the RCS. A reactor trip signal is initiated when the low pressurizer pressure trip setpoint is reached; however, reactor trip is conservatively neglected in the analysis. The reactor is shut down by coolant voiding in the core.

The plant is assumed to be operating normally at full power prior to the accident. The large cold leg break is assumed to open instantaneously. For this break, a rapid depressurization occurs, along with a core flow stagnation and reversal. This causes the fuel rods to experience departure from nucleate boiling (DNB). Subsequently, the limiting fuel rods are cooled by film and transition boiling heat transfer. The coolant voiding creates a strong negative reactivity effect, and core fission ends. As heat transfer from the rods is reduced, the cladding temperature rises.

Coolant in all regions of the RCS begins to flash. At the break plane, the loss of subcooling in the coolant results in substantially reduced break flow. This reduces the depressurization rate, and may also lead to a period of positive core flow or reduced downflow as the reactor coolant pumps in the intact loops continue to supply water to the vessel. Cladding temperatures may be reduced, and some portions of the core may rewet during this period.

This positive core flow or reduced downflow period ends as two-phase conditions occur in the reactor coolant pumps, reducing their effectiveness. Once again, the core flow reverses as most of the vessel mass flows out through the broken cold leg.

Mitigation of the LBLOCA begins when the safety injection actuation signal (SIAS) is tripped. This signal is initiated by either high containment pressure or low pressurizer pressure. Regulations require that a worst single failure be considered for ECCS safety analysis. This single failure has been determined to be the loss of one ECCS train, including one high-pressure safety-injection (HPSI) pump (delivered to an intact loop cold leg) and one low-pressure safety injection pump (LPSI) pump. The FRA-ANP RLBLOCA methodology conservatively assumes an on-time start and normal lineups of the containment spray and fan

coolers to conservatively reduce containment pressure and increase break flow. Hence, the analysis assumes that one HPSI pump, one LPSI pump, two containment spray pumps, and four fan coolers are operating.

When the RCS pressure falls below the accumulator pressure, fluid from the accumulators is injected into the cold legs. In the early delivery of accumulator water, high pressure and high break flow will drive some of this fluid to bypass the core. During this bypass period, core heat transfer remains poor and fuel rod cladding temperatures increase. As RCS and containment pressures equilibrate, ECCS water begins to fill the lower plenum and eventually the lower portions of the core; thus, core heat transfer improves and cladding temperatures decrease.

Eventually, the relatively large volume of accumulator water is exhausted and core recovery must rely on LPSI coolant delivery alone. As the accumulators empty, the nitrogen gas used to pressurize the accumulators exits through the break. This gas release may result in a short period of improved core heat transfer as the nitrogen gas displaces water in the downcomer. After the nitrogen gas has been expelled, the ECCS temporarily may not be able to sustain full core cooling because of the core decay heat and the higher steam temperatures created by quenching in the lower portions of the core. Peak fuel rod cladding temperatures may increase for a short period until more energy is removed from the core by the low pressure safety injection and the decay heat continues to fall. Steam generated from fuel rod rewet will entrain liquid and pass through the core, vessel upper plenum, the hot legs, the steam generator, and the reactor coolant pump before it is vented out the break. The resistance of this flow path to the steam flow is balanced by the driving force of water filling the downcomer. This resistance may act to retard the progression of the core reflood and postpone core wide cooling. Eventually (within a few minutes of the accident), the core reflood will progress sufficiently to ensure core wide cooling. Full core quench occurs within a few minutes after core wide cooling. Long term cooling is then sustained with the low pressure safety injection.

D.3.2 Description of Analytical Models

The RLBLOCA methodology is documented in EMF-2103, "Realistic Large Break LOCA Methodology," (Reference D.1). The methodology follows the Code Scaling, Applicability, and Uncertainty (CSAU) evaluation methodology (Reference D.2). This method outlines an approach for defining and qualifying a best-estimate thermal-hydraulic code and quantifies the uncertainties in a LOCA analysis.

The RLBLOCA methodology consists of the following computer codes:

- RODEX3A for computation of the initial fuel stored energy, fission gas release, and fuel-cladding gap conductance.
- S-RELAP5 for the system calculation.

The governing two-fluid (plus noncondensibles) model with conservation equations for mass, energy, and momentum transfer is used. The reactor core is modeled in S-RELAP5 with heat generation rates determined from reactor kinetics equations (point kinetics) with reactivity feedback, and with actinide and decay heating.

The two-fluid formulation uses a separate set of conservation equations and constitutive relations for each phase. The effects of one phase on another are accounted for by interfacial friction and heat and mass transfer interaction terms in the equations. The conservation equations have the same form for each phase; only the constitutive relations and physical properties differ.

The modeling of plant components is performed by following guidelines developed to ensure accurate accounting for physical dimensions and that the dominant phenomenon expected during the LBLOCA event are captured. The basic building block for modeling is the hydraulic volume for fluid paths and the heat structure for a heat transfer surface. In addition, special purpose components exist to represent specific components such as the pumps or the steam generator separators. All geometries are modeled at the resolution necessary to best resolve the flow field and the phenomena being modeled within practical computational limitations.

A typical calculation using S-RELAP5 begins with the establishment of a steady-state, initial condition with all loops intact. The input parameters and initial conditions for this steady-state calculation are chosen to reflect plant technical specifications or to match measured data. Specific parameters are discussed in Section D.3.3.

Following the establishment of an acceptable steady-state condition, the transient calculation is initiated by introducing a break into one of the loops. The evolution of the transient through blowdown, refill, and reflood is computed continuously using S-RELAP5. Containment pressure is also calculated by S-RELAP5.

The methods used in the application of S-RELAP5 to the large break LOCA are described in Reference D.1. A detailed assessment of this computer code was made through comparisons to experimental data. These assessments were used to develop quantitative estimates of the code's ability to predict key physical phenomena in a PWR large break LOCA. The final step of the best-estimate methodology is to combine all the uncertainties related to the code and plant parameters and estimate the PCT at 95% probability. The steps taken to derive the PCT uncertainty estimate are summarized below:

1. Base Plant Input File Development

First, base RODEX3A and S-RELAP5 input files for the plant (including the containment input file) are developed. Code input development guidelines are applied to ensure that the model nodalization is consistent with the model nodalization used in the code validation (Reference D.3).

2. Sampled Case Development

The non-parametric statistical approach requires that many "sampled" cases be created and processed. For every set of input created, each "key LOCA parameter" is randomly sampled over a range established through code uncertainty assessment or expected operating limits (provided by plant technical specifications or data). Those parameters considered "key LOCA parameters" are listed in Table D.3.1. This list includes both parameters related to LOCA phenomena (based on the PIRT provided in Reference D.1) and to plant operating parameters.

3. Determination of Adequacy of ECCS

The RLBLOCA methodology uses a non-parametric statistical approach to determine the value of PCT at the 95% probability level with 95% confidence. The values for peak local oxidation and total core oxidation are reported from the 95/95 PCT case. The adequacy of the ECCS is demonstrated when these results satisfy the criteria set forth in D.3.

D.3.3 Plant Description and Summary of Analysis Parameters

The plant analysis presented in this appendix is a Westinghouse designed pressurized water reactor (PWR), which has three loops, each with a hot leg, a U-tube steam generator, and a cold leg with a RCP. The RCS also includes one pressurizer. The ECCS includes one

accumulator/LPSI and one HPSI injection path per RCS loop. The HPSI and LPSI feed into common headers which are connected to the accumulator lines.

The S-RELAP5 model explicitly describes the RCS, reactor vessel, pressurizer, and ECCS back to the common LPSI header and accumulators. This model also describes the secondary-side steam generator that is instantaneously isolated (closed MSIV and feedwater trip) at the time of the break. A symmetric steam generator tube plugging level up to 10% per steam generator was assumed.

As described in the FRA-ANP RLBLOCA methodology, many parameters associated with LBLOCA phenomenological uncertainties and plant operation ranges are sampled. A summary of those parameters sampled is given in Table D.3.1. The LBLOCA phenomenological uncertainties are provided in Reference D.1. Values for process or operational parameters, including ranges of sampled process parameters, and fuel design parameters used in the analysis are given in Table D.3.2. Plant data is analyzed to develop uncertainties for the process parameters sampled in the analyses. Table D.3.3 presents a summary of the uncertainties used in the analyses. Two parameters (refueling water storage tank (RWST) temperature and diesel start time) are set at a conservative bounding values for all calculations. Where applicable, the sampled parameter ranges are based on technical specification limits. Plant data are used to define range boundaries for loop flow (high end) and containment temperature (low end).

D.3.4 Realistic Large Break LOCA Results

A set of fifty-nine calculations were performed sampling the parameters listed in Table D.3.1. The limiting PCT case (1853 °F) was number 41, which is characterized in Table D.2.1 and Table D.3.4. The limiting maximum oxidation is 1.3% and total oxidation is .041%. The fraction of total hydrogen generated was not directly calculated; however, it is conservatively bounded by the calculated total percent oxidation which is well below the 1 percent limit. A nominal 50/50 PCT case was identified as case 24. The nominal PCT is 1500 °F. This result can be used to quantify the relative conservatism in the 95/95 result. In this analysis, it is 353 °F.

The hot fuel rod results, event times and analysis plots for the limiting PCT case are shown in Table D.3.4, Table D.3.5, and in Figures D.3.1 through D.3.15. Figure D.3.1 shows linear scatter plots of the key parameters sampled for the 59 calculations. Parameter labels appear to the left of each individual plot. These figures show the parameter ranges used in the analysis. Figures D.3.2 and D.3.3 show PCT scatter plots vs. the time of PCT and vs. break size from the 59 calculations. Figures D.3.4 through D.3.15 show key parameters from the S-RELAP5 calculation. Figure D.3.4 is the plot of PCT independent of elevation. It includes an overlay plot of the elevation of the PCT location.

Table D.3.1 Sampled LBLOCA Parameters

Phenomenological
Time in cycle (peaking factors, axial shape, rod properties, burnup)
Break type (guillotine vs. split)
Break size
Critical flow discharge coefficients (break)
Decay heat
Critical flow discharge coefficients (surge line)
Initial upper head temperature
Pump 2-phase degradation
Film boiling heat transfer
Dispersed film boiling heat transfer
Critical heat flux
T _{min} (intersection of film and transition boiling)
Initial stored energy
Downcomer hot wall effects
Steam generator interfacial drag
Condensation interphase heat transfer
Metal-water reaction
Plant ^a
Offsite power availability
Core power
Pressurizer pressure
Pressurizer level
Accumulator pressure
Accumulator level
Accumulator temperature
Containment temperature
Containment volume
Initial flow rate
Initial operating temperature
RWST temperature
Diesel start (for loss of offsite power only)

^a Uncertainties for plant parameters are based on typical plant-specific data with the exception of "Offsite power availability" which is specified in Reference D.3.

Table D.3.2 Plant Operating Range Supported by the LOCA Analysis

	Event	Operating Range
1.0	Plant Physical Description	
	1.1 Fuel	
	a) Cladding outside diameter	0.424 in.
	b) Cladding inside diameter	0.364 in.
	c) Cladding thickness	0.030 in.
	d) Pellet outside diameter	0.357 in.
	e) Pellet density	95 % of theoretical
	f) Active fuel length	144 in.
	g) Maximum rod-average exposure	62,000 MWd/MTU
	1.2 RCS	
	a) Flow resistance	Analysis
	b) Pressurizer location	Analysis assumes location giving most limiting PCT
	c) Hot assembly location	Anywhere in core
	d) Hot assembly type	15x15
	e) SG tube plugging	≤ 10%
2.0	Plant Initial Operating Conditions	
	2.1 Reactor Power	
	a) Core average linear heat generation rate	Core power ≤ 102% of 2300 MWt
	b) Peak linear heat generation rate	≤ 2.62 ^a (normalized)
	c) Hot rod average linear heat generation rate	≤ 1.8 ^b (normalized)
	d) Hot assembly linear heat generation rate	< 1.731 ^c (normalized)
	e) Hot assembly burnup	≤ 62000 MWD/MTU
	f) MTC	≤ 0 at HFP
	g) HFP boron	Normal letdown
	2.2 Fluid Conditions	
	a) Loop flow	97.3 Mlb/hr ≤ M ≤ 113 Mlb/hr
	b) Core inlet temperature	541.6 ≤ T ≤ 553.6 °F ^d

^a Includes 5% measurement uncertainty and 3% manufacturing uncertainty.

^b Includes 4% measurement uncertainty.

^c Value equivalent to hot rod peaking factor without 4% uncertainty.

^d Measurement uncertainty bounds an uncertainty of ±4 °F.

Table D.3.2 Plant Operating Range Supported by the LOCA Analysis (continued)

	Event	Operating Range
	c) Upper head temperature	< Core Outlet Temperature
	d) Pressurizer pressure	$P \geq 2205 \text{ psig}^{a,b}$
	e) Pressurizer level	$43.3\% \leq L \leq 63.3\%^b$
	f) Accumulator pressure	$600 \leq P \leq 660 \text{ psig}$
	g) Accumulator volume	$825 \leq V \leq 841 \text{ ft}^3$
	h) Accumulator temperature	$80 \leq T \leq 130 \text{ }^\circ\text{F}$ (coupled to containment temperature)
	i) Accumulator fL/D	As-Built piping configuration
	j) Minimum ECCS boron	$\geq 1950 \text{ ppm}$
3.0	Accident Boundary Conditions	
	a) Break location	Any RCS piping location
	b) Break type	Double-ended guillotine or split
	c) Break size (relative to cold leg pipe)	$0.05 \leq A \leq 0.5$ full pipe area (split) $0.5 \leq A \leq 1.0$ full pipe area (guillotine)
	d) Worst single failure	Loss of one LPSI and one HPSI
	e) Offsite power	On or Off
	f) Low pressure safety injection flow	Bounding minimum of current pump delivery ^c
	g) High pressure safety injection flow	Bounding minimum of current pump delivery ^d
	h) Safety injection temperature	$\leq 100 \text{ }^\circ\text{F}$
	i) Safety injection delay	≤ 20.5 seconds (with offsite power) ≤ 40 seconds (without offsite power)
	j) Containment pressure	Bounding current configuration
	k) Containment temperature	$80 \leq T \leq 130 \text{ }^\circ\text{F}$
	l) Containment sprays	≥ 8 seconds

^a Considers both representative plant data and includes ± 30 psi measurement uncertainty.

^b Parameters sampled with a normal distribution have no hard limit, the technical specification is given with the understanding that the sample-space for the parameter bounds the technical specification.

^c Current LPSI pump delivery curves used in calculation provide for a 25 ft plus 5% degradation. Flow splits are calculated by S-RELAP5.

^d The average HPSI pump delivery to two intact RCS loops from a single HPSI pump is used in the analysis. This assumption reduces the expected HPSI flow to the RCS by 50%; however, it will bound the expected flow splits which are not calculated by S-RELAP5.

Table D.3.3 Statistical Distributions Used for Process Parameters

Parameter	Operational Uncertainty Distribution	Parameter Range	Measurement Uncertainty Distribution	Standard Deviation
Core Power (%)	Uniform	99.0 - 101.0	Normal	0.61
Pressurizer Pressure (psig)	Uniform	2220 - 2240	Normal	18.2
Pressurizer Level (%)	Uniform	50 - 56	Normal	4.3
Accumulator Volume (ft ³)	Uniform	825 - 841	N/A	N/A
Accumulator Pressure (psig)	Uniform	600 - 660	N/A	N/A
Containment/Accumulator Temperature (°F)	Uniform	80 - 130	N/A	N/A
Containment Volume (x10 ⁶ ft ³)	Uniform	1.95 - 2.23	N/A	N/A
Initial Flow Rate (Mlbm/hr)	Uniform	97.3 - 113	N/A	N/A
Initial Operating Temperature (°F)	Uniform	541.6 - 553.6	N/A	N/A
RWST Temperature (°F)	Point	100	N/A	N/A
Offsite Power Availability ^a	Binary	0,1	N/A	N/A
Diesel Start for Containment Cooling (s)	Point	8	N/A	N/A
Diesel Start for SI Start (s) ^b	Point	32	N/A	N/A

^a No data is available to quantify the availability of offsite power. During normal operation, offsite power is available. Since the loss of offsite power is typical more conservative (some loss in coolant pump capacity), it is assumed that there is a 50% probability the offsite power is unavailable, see Reference D.3.

^b Add 8 s for HPSI pump start up and 12 s for LPSI start up (additional load sequencing, 10 s, and pump acceleration, 2 s).

Table D.3.4 Summary of Results for the Limiting PCT Case

Case #	41
PCT	
Temperature	1853 °F
Time	87.3 seconds
Elevation	~8.7 ft
Metal-Water Reaction	
% Oxidation Maximum	1.3 %
% Total Oxidation	0.041 %
Total Hydrogen	0.78 lb

Table D.3.5 Calculated Event Times for the Limiting PCT Case

Event	Time (sec)
Begin Analysis	0.0
Break Opens	0.0
RCP Trip	0.0
SIAS Issued	0.5
Start of Broken Loop Accumulator Injection	9
Start of Intact Loop Accumulator Injection	13
End of Bypass	23
Start of HHSI	40
Beginning of Core Recovery (Beginning of Reflood)	31
LHSI Available	45
Broken Loop Accumulator Empties and LHSI Delivery Begins	54
Intact Loop Accumulator Empties and LHSI Delivery Begins (Loop 2 and 3, respectively)	55.5, 53
PCT Occurs (1853°F)	87.3

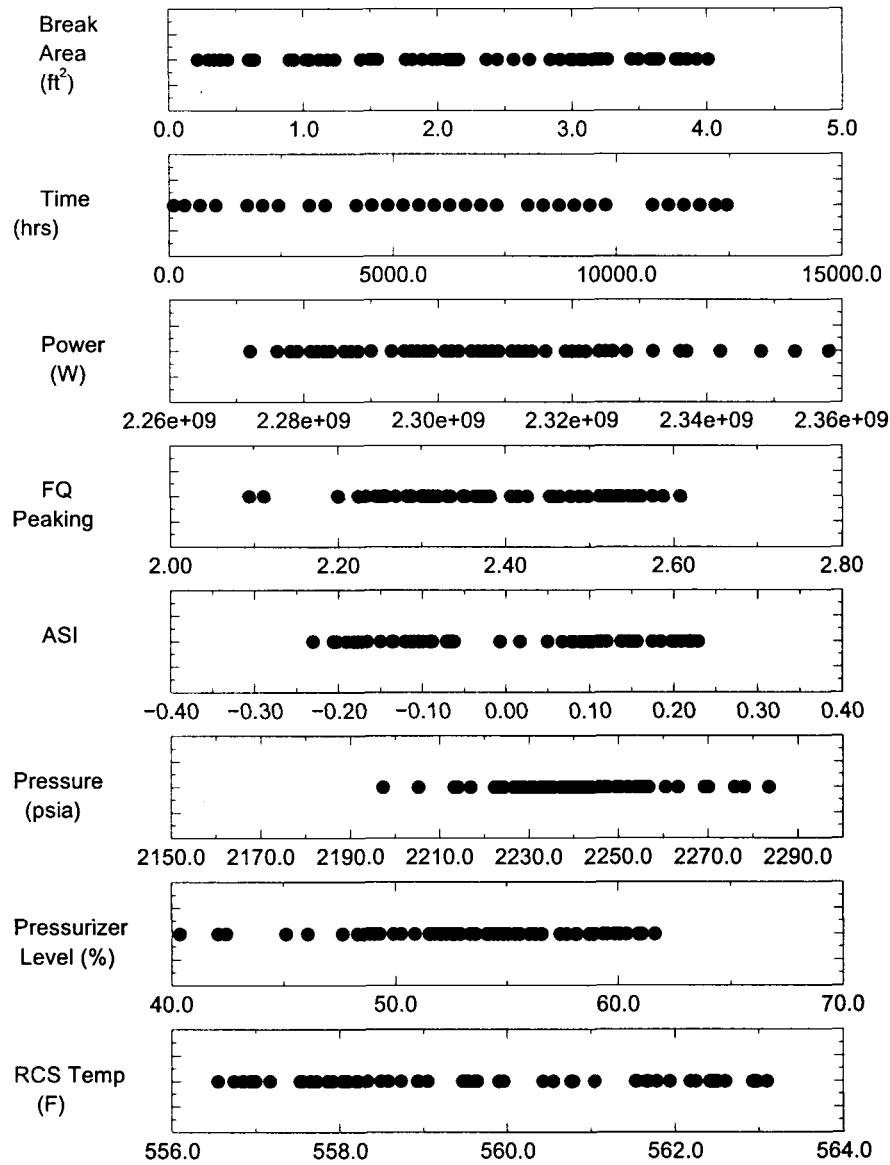


Figure D.3.1 Scatterplot of Operational Parameters

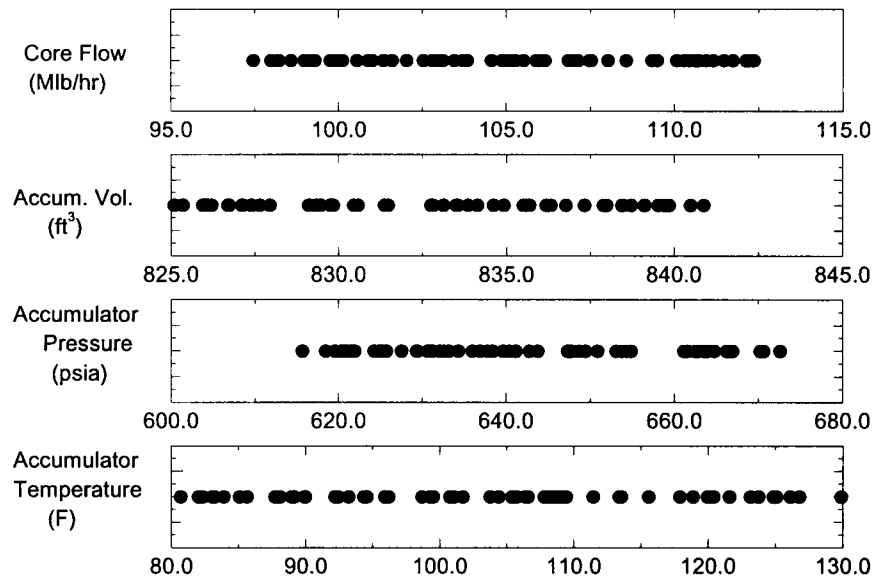


Figure D.3.1 Scatterplot of Operational Parameters (continued)

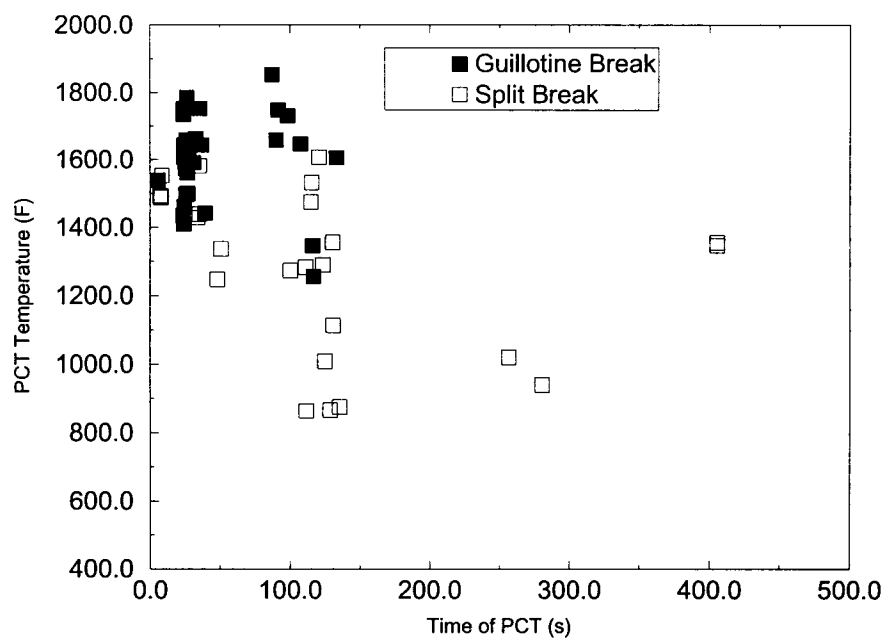


Figure D.3.2 PCT vs PCT Time Scatterplot from 59 Calculations

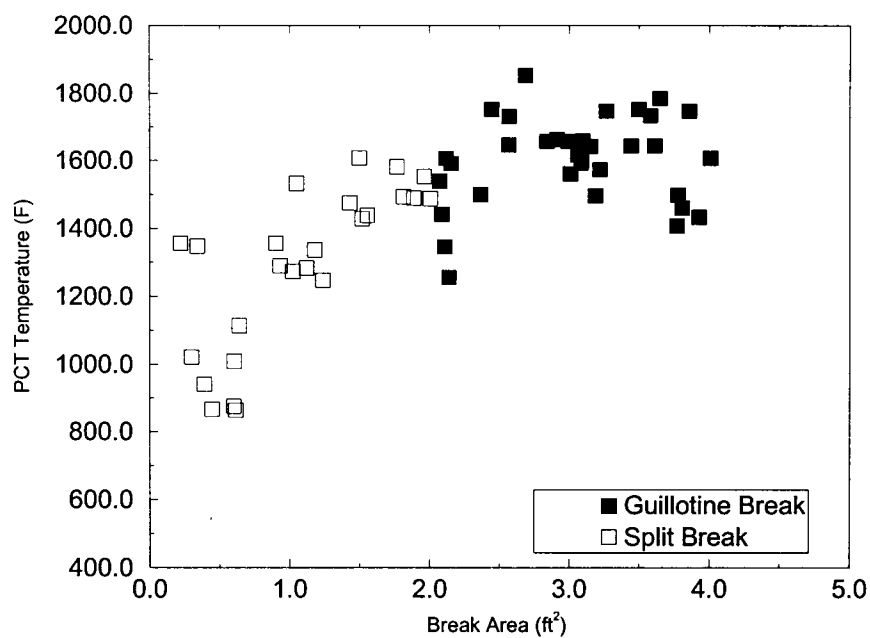


Figure D.3.3 PCT vs. Break Size Scatterplot from 59 Calculations

PCT Independent of Location

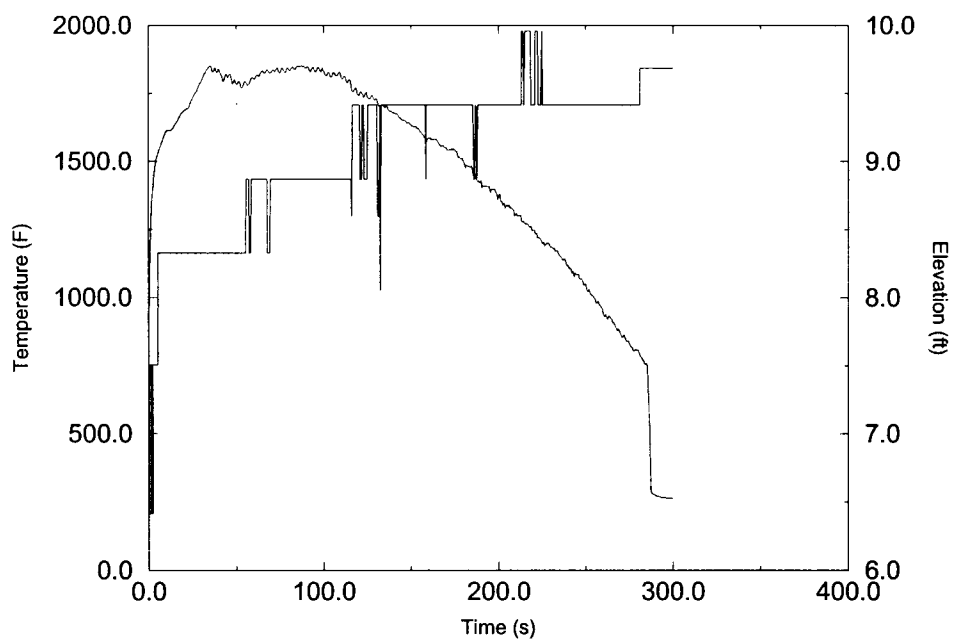


Figure D.3.4 Peak Cladding Temperature and Elevation for Limiting Break

Hot Rod Surface Temperature

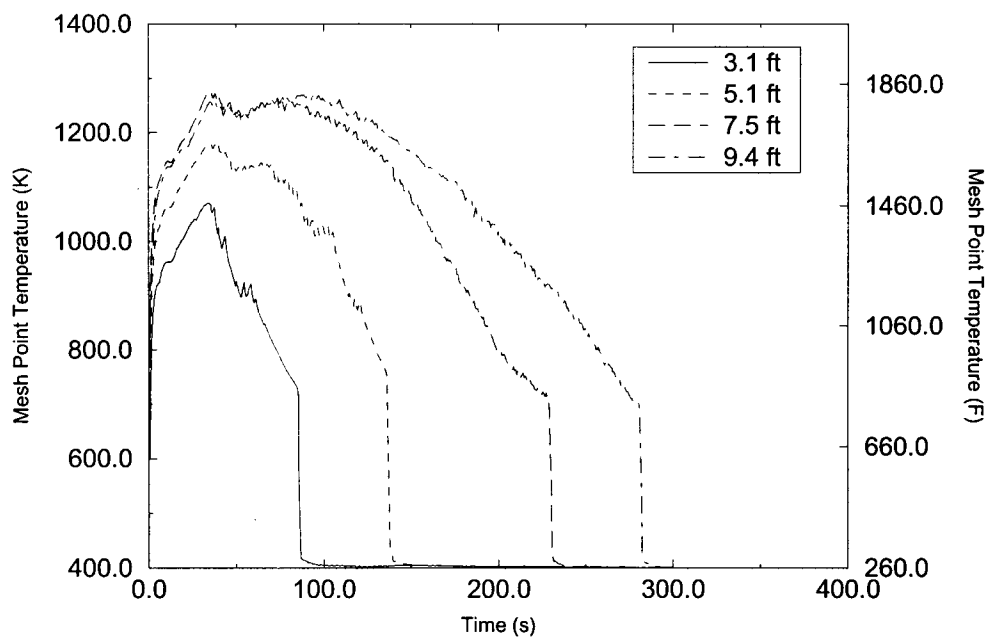


Figure D.3.5 Cladding Temperatures at Select Locations for the Limiting Break

Break Flow

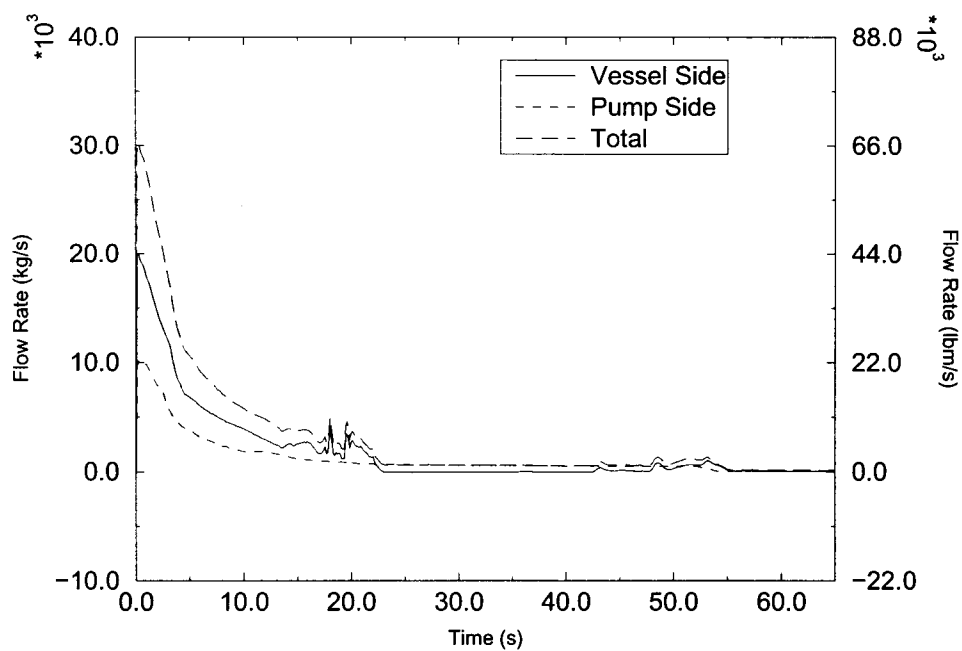


Figure D.3.6 Break Flow for the Limiting Break

Core Inlet Mass Flux

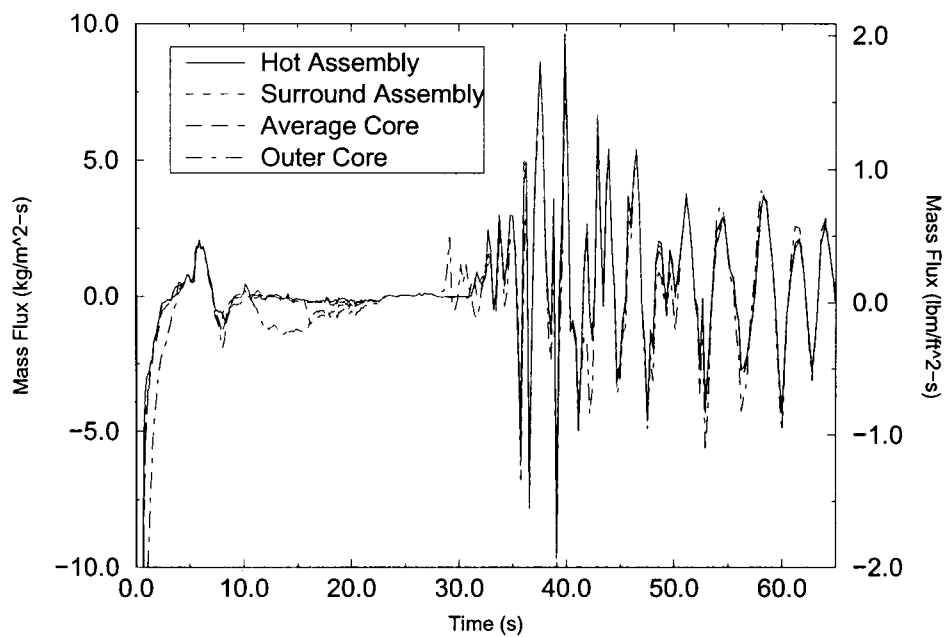


Figure D.3.7 Early Core Inlet Flow for Limiting Break

Core Outlet Mass Flux

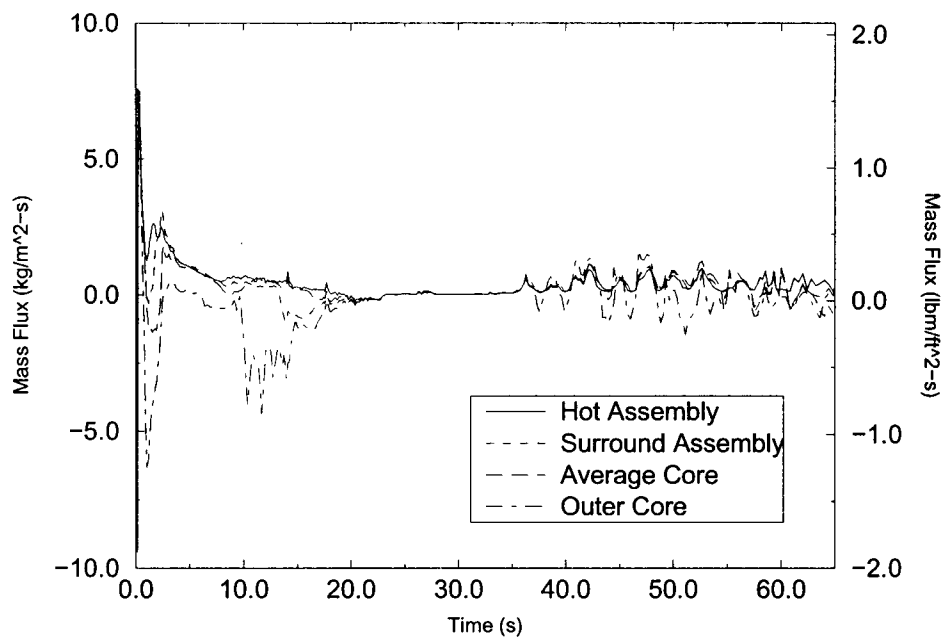


Figure D.3.8 Core Outlet Flow for Limiting Break

Pump Void Fraction

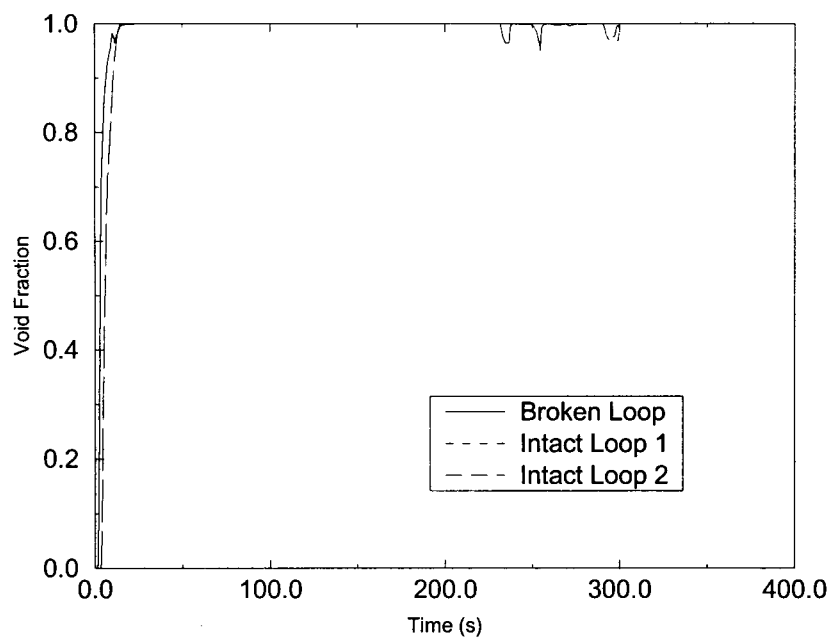
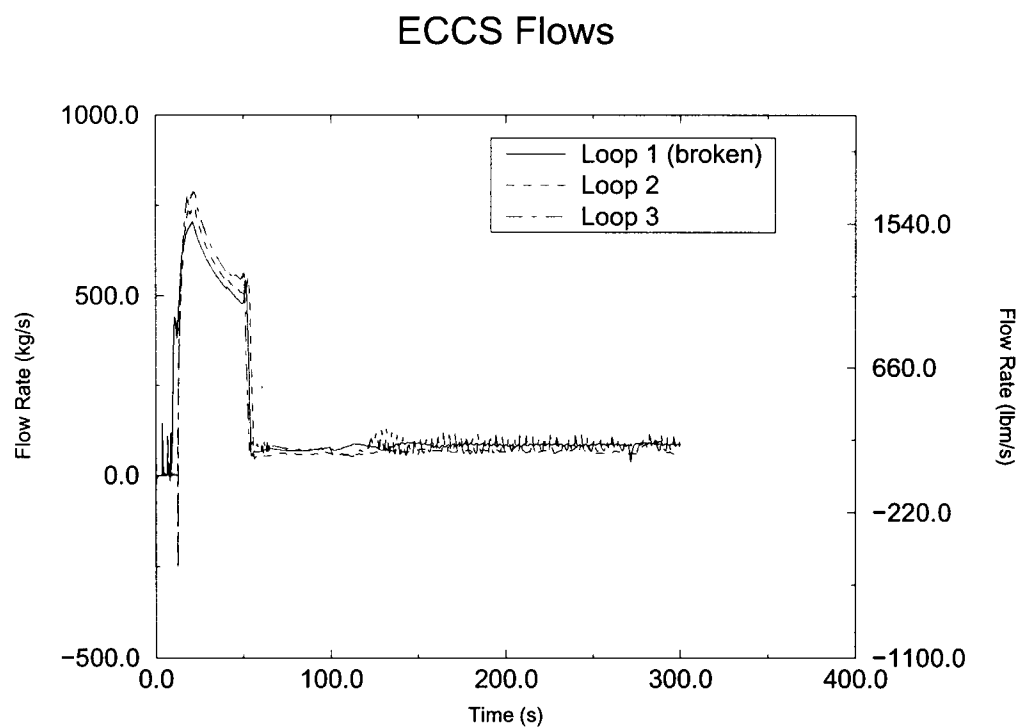


Figure D.3.9 Void Fraction at RCS Pumps for Limiting Break



**Figure D.3.10 ECCS Flows (includes Accumulator, HPSI and LPSI)
for Limiting Break**

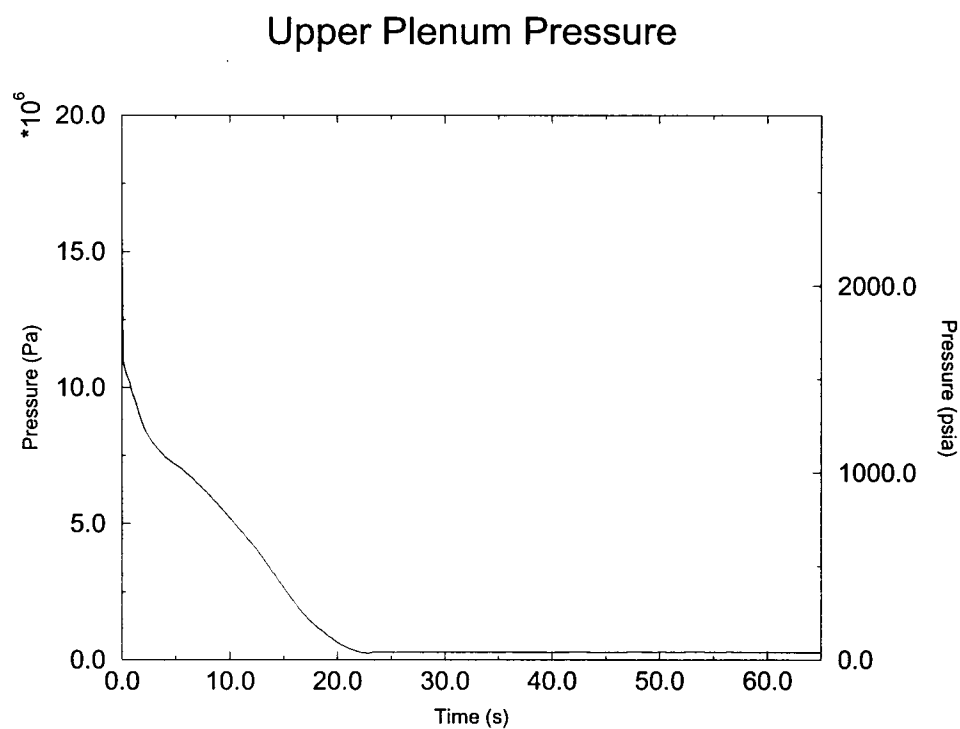


Figure D.3.11 System Pressure for Limiting Break

Downcomer Liquid Level

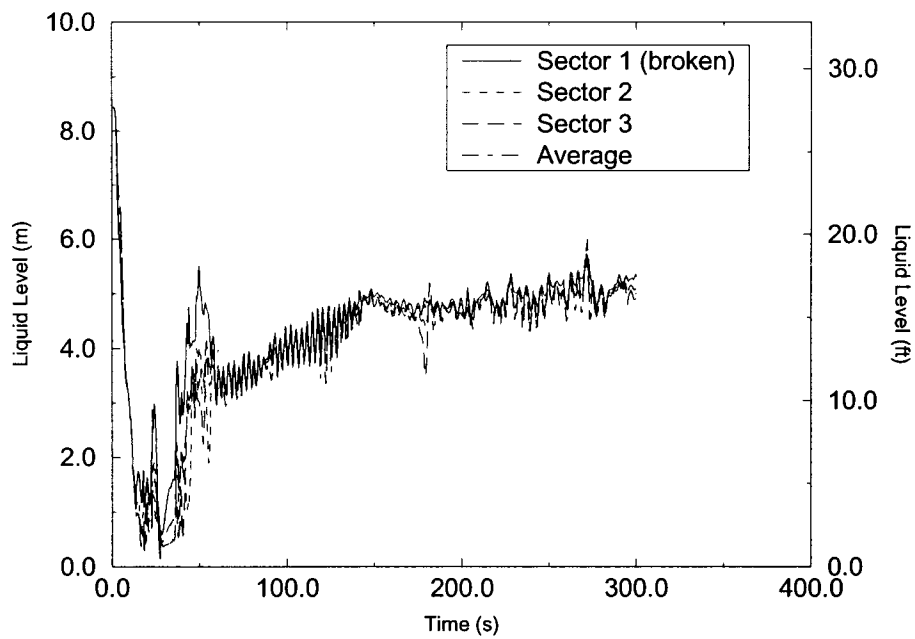


Figure D.3.12 Collapsed Liquid Level in the Downcomer for Limiting Break

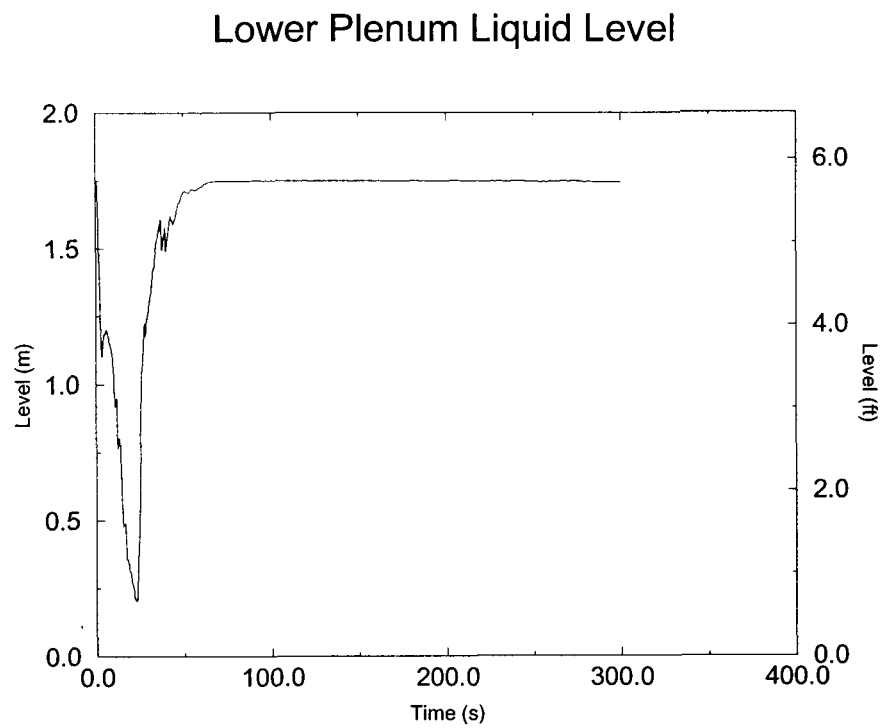


Figure D.3.13 Collapsed Liquid Level in the Lower Plenum for the Limiting Break

Core Liquid Level

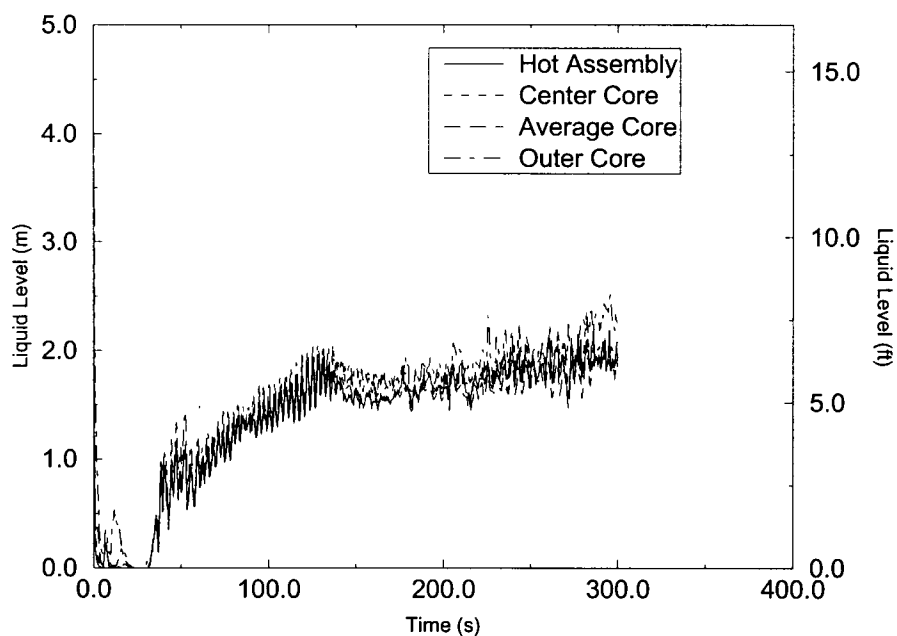


Figure D.3.14 Collapsed Liquid Level in the Core for the Limiting Break

Containment and Loop Pressures

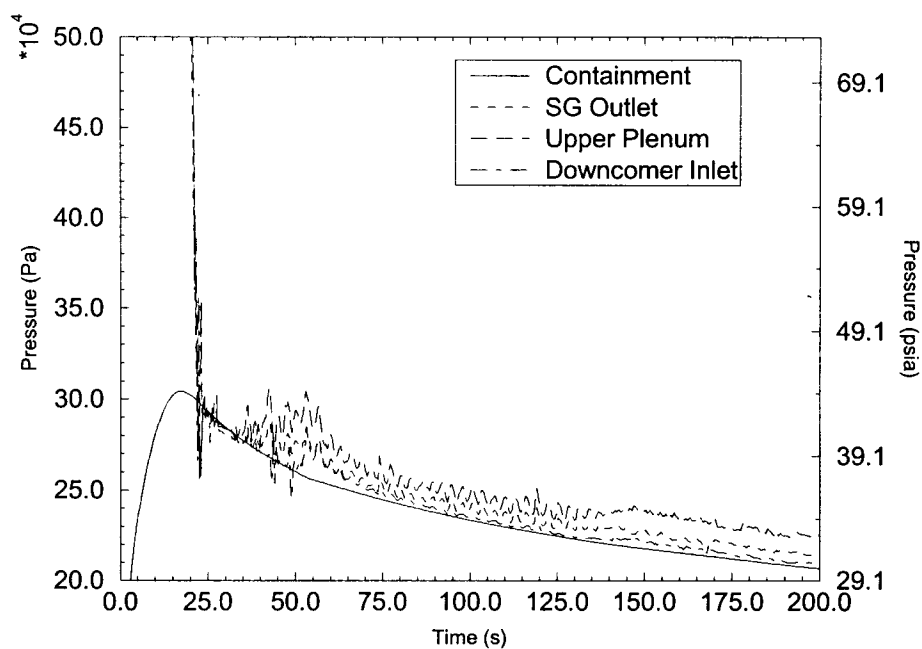


Figure D.3.15 Containment and Loop Pressures for Limiting Break

D.4 Conclusions

The results of the RLBLOCA analysis show that the limiting case has a PCT of 1853°F and a maximum oxidation thickness and hydrogen generation that fall well within regulatory requirements.

The analysis supports operation at a power level of 2300 MWt (plus 2% uncertainty), a steam generator tube plugging level of up to 10% in any generator, a total peaking factor (F_Q^T) of 2.62 and a nuclear enthalpy rise factor ($F_{\Delta H}$) of 1.80 with no axially-dependent power peaking limit. The analysis supports peak rod average exposures of up to 62,000 MWd/MTU corresponding to a maximum assembly burnup of 57,000 MWd/MTU.

D.5 References

- D.1. EMF-2103(P) Revision 0, *Realistic Large Break LOCA Methodology*, Framatome ANP Richland, Inc., August 2001.
- D.2. Technical Program Group, *Quantifying Reactor Safety Margins*, NUREG/CR-5249, EGG-2552, October 1989.
- D.3. EMF-2058(P) Revision 1, *S-RELAP5 Realistic Large Break LOCA Analysis Guidelines*, Framatome ANP Richland, Inc., August 2001.

Appendix E Incorporation of M5 Cladding Properties

E.1 Introduction

This Appendix describes the implementation of the Nuclear Regulatory Commission (NRC) approved M5 cladding material properties (References E.1 and E.2) into the Framatome ANP, Inc. (FRA-ANP) realistic large break loss-of-coolant accident (RLBLOCA) methodology. For most cladding material properties an approved model from Reference E.1 or E.2 was available and incorporation of these properties into the RLBLOCA methods was straightforward. However, some properties that were needed for the RLBLOCA methodology, were either not available in the approved documents, required a range of applicability that extended outside the approved range, or required a new correlation for model specific usage. These properties include creep, free growth, thermal expansion, emissivity and elastic modulus.

Both the S-RELAP5 (Section 3.4.2) code and the RODEX3A (Section 3.4.1) code required modifications to integrate the approved M5 cladding material properties in the FRA-ANP RLBLOCA methodology. Some M5 material properties were available in a form that was more detailed than the current Zircaloy representation. As a result, some M5 cladding properties have been incorporated using a more detailed representation than was previously used for Zircaloy cladding. No modifications to the base methodology were required for the inclusion of the M5 properties.

M5 is a proprietary variant of Zr1Nb that has desirable high burnup performance. It provides significant improvements in corrosion, hydrogen pick-up, axial growth and diametral creep relative to Zircaloy.

E.2 Summary

M5 cladding specific material properties have been incorporated into the FRA-ANP RLBLOCA methodology for the purpose of analyzing LBLOCA transients when M5 clad fuel rods are present. A RLBLOCA analysis was performed to investigate the sensitivity of PCT and oxidation when M5 is substituted for Zircaloy using identical boundary conditions and initial fuel geometry. The analysis shows that no unique phenomenological differences are introduced with the M5 cladding. However, differences in cladding properties result in some variation in

PCT and oxidation. Initial fuel rod stored energy was the primary contributor to variations in PCT and oxidation.

Differences in cladding material properties (particularly creep and thermal expansion) cause differences in the fuel pellet behavior at any particular burnup by affecting the gap width and therefore pellet temperature and pellet-cladding interaction. The resulting differences in fuel rod conditions produce initial fuel centerline temperatures at peak power up to 200°F greater for M5 rods. Additionally, since the cladding thermal expansion is larger for M5 than Zircaloy, the pellet-cladding gap may be larger for M5 rods during the LOCA event. A larger gap presents a greater thermal resistance to removal of the stored energy in the pellet. The larger initial stored energy will impact PCT. The mean impact on the PCT and oxidation was determined to be relatively small (6.3°F on PCT and 0.0083% on oxidation). The maximum change in PCT for a M5 cladding statistical case was +40°F and the maximum change in oxidation was +0.04%.

E.3 Incorporation of M5 Cladding Properties in RODEX3A

E.3.1 Summary of Cladding Related Models in the Fuel Performance Evaluation Model


E.3.1.1 M5 Cladding Creep Correlation

Cladding creep is dependent on the stress history of the cladding wall, including the internal gas pressure, the coolant pressure, and the fuel-cladding mechanical contact forces, as well as the temperature and irradiation histories. The form of the creep model used in RODEX3A for M5 cladding is identical to that used for Zircaloy cladding (References E.3 and E.4). Only model constants have been adjusted to represent M5 cladding creep behavior reported in Reference E.1 and E.2. The previously defined M5 model for creep was not used in RODEX3A because the previously approved model (Reference E.1) was not compatible with RODEX3A.

The generalized creep rate ($\dot{\epsilon}_c$, h^{-1}) is the sum of the thermal ($\dot{\epsilon}_p$, h^{-1}) and irradiation ($\dot{\epsilon}_l$, h^{-1}) components:

$$\dot{\epsilon}_c = \dot{\epsilon}_l + \dot{\epsilon}_p \quad (E.3.1)$$

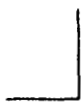
The thermal and irradiation creep component rates are evaluated using



(E.3.2)

(E.3.3)

(E.3.4)



(E.3.5)

where



The radial creep deformation is calculated in the same manner as for Zircaloy rods. [

] The radial
creep deformation and axial creep strain at the end of a time step increment (Δt) are then given
by

(E.3.6)

(E.3.7)

The details of this process are described in Reference E.3.

The values of the creep model constants used for M5 cladding are

All of these values are identical to those used for Zircaloy-4 cladding except for []. [], were calculated for M5 cladding based on creep anisotropy measurements. The value of [] was determined by benchmarking the overall RODEX3A creep model against M5 radial creep measurements from fuel irradiation test data. The results of the creep benchmarks are presented in Section E.3.2

E.3.1.2 M5 Cladding Free Growth Correlation

The M5 irradiation induced cladding free growth contributes to the total fuel rod growth calculation in RODEX3A. Cladding free growth for M5 was not reported separately from total fuel rod growth in previous FRA-ANP submittals. For incorporation into RODEX3A, however, this model is described.

The irradiation induced free growth of M5 contributes a small part to the fuel rod elongation with the remainder coming from axial creep. The model which is implemented in RODEX3A for irradiation induced cladding free growth of M5 is based on data obtained at []

(Reference E.5). The experiments were conducted in the SILOE test reactor by the Commissariat à l'Energie Atomique (CEA) to determine the free growth behavior under irradiation of M5 clad tubes. The data were fit using the least squares method to obtain the following free growth correlation.

$$\frac{\Delta L}{L_0} = \frac{1}{100} \left(\frac{T}{T_0} \right)^n \quad (E.3.8)$$

where $\frac{\Delta L}{L_0}$ = elongation (%)

T = temperature (K)

10

11

7

Framatome ANP, Inc.

E.3.1.4 M5 Cladding Zirconium Oxide Thermal Conductivity

The Zirconia thermal conductivity values (W/m-K) on M5 cladding is taken from the NRC approved Reference E.2, Equations 10-31 through 10-33:



(E.3.12)



where S is the thickness (m) of the oxide layer and T is temperature (K). The thermal conductivity is dependent on the temperature and the thickness of the oxide layer.

E.3.1.5 M5 Cladding Specific Heat

Specific heat is not used in the RODEX3A code. RODEX3A calculations assume quasi-steady thermal conditions for each burnup interval so specific heat is not required.

E.3.1.6 M5 Cladding Density

Cladding density is not used in the RODEX3A code. Cladding density would be multiplied by specific heat to provide volumetric heat capacity. However, since RODEX3A assumes quasi-steady state heat transfer, volumetric heat capacity is not required.

E.3.1.7 M5 Cladding Thermal Expansion

The integral coefficient of thermal expansion is based on the model approved by the NRC in Reference E.1, Appendix I and Section K-2.4. The α and β phase expansion rates approved in Reference E.1 are from work by Le Blanc and Jouen (Reference E.5) and measured data. Expansion rate coefficients for the current model follow those presented in References E.1 and E.2 except that the α phase expansion coefficient in the axial direction has been rounded down from [] to provide one value for the different components of an all M5 fuel assembly.

The SER for Reference E.1 states that the transition range in the approved model begins at a temperature that is about 60°C too low. In response to this observation, the transition region has been modified. For the $\alpha + \beta$ domain, the transition range will begin at [] as determined by Lofaro (Reference E.5). The previous transition range was [].

As presented in Reference E.1, Le Blanc and Jouen (Reference E.5) determined the relative contractions extrapolated to 850°C corresponding to $\alpha \rightarrow \beta$ phase transformation in the [] directions. These values allow calculation of the intersection with the Y-axis of the linear equation representing the β domain between []. The $\alpha + \beta$ thermal expansion equation is then obtained by constructing a linear connection between the α and β laws. Figure E.3.2 presents the Reference E.1 model compared to the current model. The current model is defined as follows:

The thermal expansion strain (in/in) in the axial direction is represented by (assuming a reference temperature of 20°C):

$$\epsilon_{axial} = \epsilon_{\alpha} + \frac{\epsilon_{\beta} - \epsilon_{\alpha}}{T - T_{trans}} (T - T_{trans}) \quad (E.3.13)$$

The thermal expansion strain (in/in) in the tangential direction is represented by:

$$\epsilon_{tangential} = \epsilon_{\alpha} + \frac{\epsilon_{\beta} - \epsilon_{\alpha}}{T - T_{trans}} (T - T_{trans}) \quad (E.3.14)$$

The thermal expansion strain (in/in) in the radial direction is represented by:

$$\left(\frac{1}{E} \right) = \left(\frac{1}{E_0} \right) \left(1 - \frac{T - T_0}{T_0} \right) \quad (E.3.15)$$

where T is temperature (°C).

Uncertainty in the α phase is []. Uncertainty is [] for the $\alpha \rightarrow \beta$ domain and for the β phase. The temperature in all LOCA applications is below the upper limit of []. Radial thermal expansion is associated with the change in thickness of the cladding due to thermal expansion and is only a small contributor to total thermal expansion in the radial direction; it is not considered in the approved RODEX3A cladding thermal expansion model.

E.3.1.8 M5 Cladding Elastic Modulus

The Young's modulus for cladding elastic deformation is taken from the NRC approved Reference E.2, Equation 10-54. The equation for Young's modulus (Pa) is as follows:

$$E = E_0 \left(1 - \frac{T - T_0}{T_0} \right) \quad (E.3.16)$$

where T is cladding temperature (K). The above equation is valid between [] with an uncertainty of [] (Reference E.5).

E.3.1.9 M5 Cladding Poisson's Ratio

Poisson's Ratio is taken from the NRC approved Reference E.1, Page I-75. As described in the reference, a [].

E.3.1.10 M5 Cladding Emissivity

Emissivity is used in the RODEX3A fuel model in calculating the small radiation component of the internal gap conductance. The emissivity correlation approved in Reference E.1, page I-73 is for high temperature oxidized applications []. RODEX3A calculations are typically performed at cladding temperatures below 400°C. At low temperatures and low oxidation, the emissivity of zirconium alloys is smaller. The data produced by Murphy and Havelock (Reference E.5) for Zr – 2.5% Nb alloy between 100°C and 400°C can be fitted by a

degree 2 polynomial (Figure E.3.3) to develop a low temperature low oxidation correlation. This correlation is implemented in RODEX3A for low temperatures. To provide a smooth transition, between the high temperature and low temperature correlations, the range of the low temperature correlation is extended upward and the range of the high temperature correlation is extended downward to the crossover point of the two correlations []. The combined correlation over the entire temperature range can be seen in Figure E.3.4.

Therefore, the emissivity (ϵ) for M5 is given by

$$\epsilon = \begin{cases} \epsilon_{low} & T \leq T_{crossover} \\ \epsilon_{high} & T > T_{crossover} \end{cases} \quad (E.3.17)$$

$$\epsilon_{low} = \epsilon_{low,ref} \left(\frac{T}{T_{ref}} \right)^n \quad (E.3.18)$$

where T is temperature ($^{\circ}\text{C}$). In case of a cladding temperature lower than []. The use of a lower internal cladding emissivity value at low temperatures in RODEX3A minimizes gap conductance and maximizes stored energy at the beginning of the LBLOCA transient.

E.3.1.11 M5 Cladding Corrosion

The pre- and post-transition M5 cladding corrosion models presented in the NRC approved Reference E.2, Pages 8-7 through 8-9 and Equations 8-14 and 8-16, are implemented in RODEX3A. The pre-transition equation used in RODEX3A is []:

$$\dot{m}_{cor} = \begin{cases} \dot{m}_{cor,pre} & T \leq T_{transition} \\ \dot{m}_{cor,post} & T > T_{transition} \end{cases} \quad (E.3.19)$$

and the post-transition equation is:

where



where

The RODEX3A calculations are performed at normal reactor operating conditions. The temperature of the cladding during normal operating conditions is not high enough for significant metal-water reaction to take place. Therefore, only cladding corrosion models are used to

determine cladding oxidation in the RODEX3A code. A separate high temperature M5/Steam reaction kinetics model is not required.

E.3.1.14 M5 Cladding Swelling and Rupture / Blockage

The RODEX3A code is used to calculate burnup dependent fuel behavior at normal reactor operating conditions. Under these conditions, swelling and rupture / blockage will not occur and therefore no swelling and rupture / blockage model is implemented in the RODEX3A code.



Figure E.3.1 Free Growth Under Irradiation



Figure E.3.2 Integral Thermal Expansion for M5 Cladding



**Figure E.3.3. Emissivity of Non-Oxidized Samples Between 100°C
and 400°C**



**Figure E.3.4 Internal Emissivity of M5 Cladding Used in RLBLOCA
Methodology**

E.3.2 Creep Benchmark Calculations

E.3.2.1 Introduction

Cladding creep is one of the most important M5 cladding properties incorporated into RODEX3A because of its difference from Zircaloy creep and its resultant impact on fuel rod thermal performance and temperature calculations. The previously defined M5 model for creep was not used in RODEX3A because the previously approved model (Reference E.1) was not compatible with RODEX3A. Therefore, it is necessary to benchmark the modified RODEX3A cladding creep model against radial creep measurements from M5 irradiation test data.

Data from [] M5 clad fuel rods are used to benchmark the radial cladding creep calculated by RODEX3A. The rods are listed in Table E.3.1. Each of the rods has identical design parameters that are provided in Table E.3.2.

The rods were irradiated in [

] The radial creep has been measured at 12 axial locations for each of the cycle 1 and 2 rods and at 10 axial locations for each of the cycle 3 rods. These are the same rods referred to in Appendices I and J of Reference E.1 and in Section 7 of Reference E.2. The calculated burnups differ slightly from those reported in Reference E.1, since the power history input used for RODEX3A was obtained independently.

Table E.3.1 M5 Creep Benchmark Rods



Table E.3.2 Benchmark Rod Design Parameters



E.3.2.2 Creep Benchmark Results

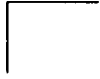
The radial cladding creep results calculated by RODEX3A are shown in Table E.3.3 along with the measured values. Figure E.3.5 also compares the calculated results to the measured values. Figure E.3.6 compares the calculated and measured creep values as a function of local

burnup. The figures demonstrate that the RODEX3A creep prediction gives acceptable agreement with the measured data.

The agreement between the measured data and the RODEX3A model results was further evaluated by calculating the mean and standard deviation of the differences. Since the third cycle data are significantly influenced by pellet cladding interaction, the data are evaluated both with and without the cycle three creep data. The statistical results are shown in Table E.3.4. The average error is less than [], and the standard deviation of the calculated creep error is less than []. This standard deviation implies a 2σ uncertainty range of approximately [] for the calculated cladding radial creep. These results are comparable to Zircaloy results and further demonstrates that the RODEX3A cladding creep model is adequate.

Table E.3.3 M5 Radial Creep Benchmark Results

Table E.3.4 M5 Benchmark Results Statistics



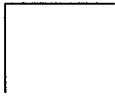


**Figure E.3.5 Calculated M5 Cladding Radial Creep Compared to
Measured Creep**



**Figure E.3.6 Calculated and Measured Radial Creep vs. Local
Burnup**

E.4 Incorporation of M5 Properties in S-RELAP5

E.4.1 Summary of Cladding Related Models in the Thermal-Hydraulic Performance Evaluation Model

E.4.1.1 M5 Cladding Creep Correlation

Cladding creep is a burnup dependent parameter. The duration of an S-RELAP5 LBLOCA calculation is sufficiently short to hold burnup dependent parameters constant. Therefore, cladding creep is not calculated in the S-RELAP5 code.

E.4.1.2 M5 Cladding Free Growth Correlation

Cladding irradiation induced free growth is a burnup dependent parameter. The duration of an S-RELAP5 LBLOCA calculation is sufficiently short to hold burnup dependent parameters constant. Therefore, cladding free growth is not calculated in the S-RELAP5 code.

E.4.1.3 M5 Cladding Thermal Conductivity

The thermal conductivity model for M5 cladding described in Section E.3.1.3 is also used in the S-RELAP5 code.

E.4.1.4 M5 Cladding Oxide Thermal Conductivity

The thermal conductivity model for M5 cladding oxide described in Section E.3.1.4 is also used in the S-RELAP5 code.

E.4.1.5 M5 Cladding Specific Heat

The specific heat (J/kg-K) values for M5 cladding are approved in Reference E.1, Page I-72 as follows:

(E.4.1)

Volumetric heat capacity is determined by the product of the density and the specific heat.

E.4.1.6 M5 Cladding Density

The density of M5 Cladding is taken from the NRC approved Reference E.1, page I-70 :



(E.4.2)

The density is used in the conduction equation to calculate the mass in the cell. Since the mass in a cell (mesh interval or node) and the cell dimensions do not change in the conduction solution scheme, the density used is that at room temperature. The use of temperature-dependent or phase-dependent density is not appropriate.

E.4.1.7 M5 Cladding Thermal Expansion

The thermal expansion model for M5 cladding described in Section E.3.1.7 is also used in the S-RELAP5 code.

E.4.1.8 M5 Cladding Elastic Modulus

The approved elastic modulus model for M5 cladding described in Section E.3.1.8 is also used in the S-RELAP5 code. In S-RELAP5 applications, however, Equation E.3.16 is assumed to be applicable to all temperatures of interest. The following table compares the elastic modulus values of M5 from Equation E.3.16 and those for Zircaloy used in S-RELAP5 (Equation 7.127 of Reference E.6). The comparison shows that extension of Equation E.3.16 to the entire LOCA temperature range is within [] of the Zircaloy Young's modulus which is within the standard error of the Zircaloy correlation (6400 MPa). Therefore, the range extension is acceptable.

Table E.4.1 Comparison of Young's Modulus for M5 and Zircaloy Cladding



E.4.1.9 M5 Cladding Poisson's Ratio

Poisson's ratio for M5, [], described in Section E.3.1.9 is also used in S-RELAP5.

E.4.1.10 M5 Cladding Emissivity

Emissivity is used in the RODEX3A fuel model in S-RELAP5 to calculate the radiation component of the internal gap conductance. For this purpose, S-RELAP5 uses the same values as described in Section E.3.1.10. S-RELAP5 also calculates rod external radiation to the coolant. For this purpose S-RELAP5 uses the emissivity defined in Section 4.8 of Reference E.6. The value that is used is [] and is the same for both Zircaloy and M5 cladding. This value is based on the analysis of core cooling for BWR rod bundles. Using an external emissivity of [] is conservative relative the recommended value for M5 of [] in Reference E.1, page I-73 and maintains consistency with the treatment of Zircaloy cladding. [].

E.4.1.11 M5 Cladding Corrosion

Low temperature cladding corrosion is not calculated in S-RELAP5. The large break LOCA transient calculation performed by S-RELAP5 occurs over a short time period compared to the burnup calculation in RODEX3A and produces high cladding temperatures. When high temperatures occur, corrosion is accelerated and the low temperature corrosion models are no longer valid. At the high cladding temperatures predicted in the S-RELAP5 calculation, a special high temperature M5/steam reaction kinetics model is needed. Section E.4.1.13 describes the high temperature M5/steam reaction kinetics model used in S-RELAP5

E.4.1.12 M5 Cladding Hydrogen Pick-up

Cladding hydrogen pick-up is not calculated in S-RELAP5. The cladding hydrogen pick-up model described in Section E.3.1.12 is associated with low temperature cladding corrosion. The large break LOCA transient calculation performed by S-RELAP5 produces high cladding temperatures, where corrosion is accelerated and where the low temperature corrosion models are no longer valid. A special high temperature M5/steam reaction kinetics model is then required as described in Section E.4.1.13. Since the criteria for LBLOCA do not set limits on

hydrogen pick-up but only on cladding oxidation, the high temperature M5/steam reaction kinetics model only considers oxidation and not hydrogen pick-up.

E.4.1.13 High Temperature M5/Steam Reaction Kinetics

Metal-water reaction kinetics in S-RELAP5 for realistic LBLOCA are calculated using the Cathcart-Pawel model (Reference E.7) described in Section 7.4 of Reference E.6. The same method is used for both Zircaloy and M5 cladding. Figure E.4.1 shows a comparison of measured cladding weight gain to predicted cladding weight gain for M5 cladding using Cathcart-Pawel. [

]

The M5 cladding oxidation tests were performed in the CINOG facility (CINétique d'Oxydation á Grenoble) and reported in Reference E.8. [

]

[

] This M5 cladding oxidation test is the same as that described in NRC approved Reference E.1, Appendix D and Section I.25. [

]

E.4.1.14 M5 Cladding Swelling and Rupture / Blockage

The realistic LBLOCA model does not calculate swelling and rupture / blockage. Therefore, no swelling and rupture / blockage model for M5 cladding is implemented in S-RELAP5 for realistic LBLOCA application.



**Figure E.4.1 Alloy M5 High Temperature Metal-Water Reaction Data
Comparison with Cathcart-Pawel Model Predictions**

E.4.2 3-Loop Sample Problem with M5 Cladding

To evaluate peak cladding temperature (PCT) and oxidation sensitivity to M5 properties, a fuel rod with M5 cladding was modeled in the RLBLOCA analysis presented in Appendix D. The scope of this analysis was to compare PCT and oxidation predictions between hot rods modeled with Zircaloy and M5 cladding and to identify the major phenomenological contributors for any differences observed. It is not expected that the introduction of M5 cladding will produce fuel stored energy, PCT and maximum oxidation for M5 rods that is significantly different from Zircaloy rods. These expectations are confirmed by the analysis.

The 3-loop sample problem presented in Appendix D modeled two geometrically identical hot rods – one with Zircaloy cladding and one with M5 cladding. These two hot rods were modeled in the thermally-decoupled condition as specified for this RLBLOCA methodology (see Reference E.9). Since both of these fuel rod models were decoupled, differences in PCT and oxidation reflect only the differences in material properties.

To identify any differences in behavior between the use of M5 and Zircaloy cladding, the limiting values for the key acceptance criteria must be compared. Any difference in cladding material properties between the two base models can alter the analytical results. The analytical results show that the limiting PCT and oxidation calculations (cases 41 and 16) are the same for both materials. The limiting PCT was calculated to be 1861°F (vs. 1853°F for the Zircaloy rod) and the limiting oxidation was calculated to be 1.50% (vs. 1.49% for the Zircaloy clad rod). Figure E.4.2 shows excellent PCT agreement between the M5 and Zircaloy rod over the course of the transient.

Examination of the results from all 59 calculations show that the steady-state cladding temperatures are identical between the two hot rod models; however, fuel centerline temperatures for the M5 rod at the peak power location can be up to 200°F higher.* This variation is attributed to differences in cladding creep and tangential thermal expansion, which influence the fuel-cladding gap thickness. The PCT differences span from about -10°F to 40°F with the mean 6.3°F. Since the maximum oxidation is highly correlated to cladding temperature, it has a similar trend, spanning from - 0.005% to 0.04% with a mean of 0.0083%.

* Centerline temperatures will be dependent on both material properties *and* local power factors. Actual rod-averaged changes in centerline temperature will be much lower.

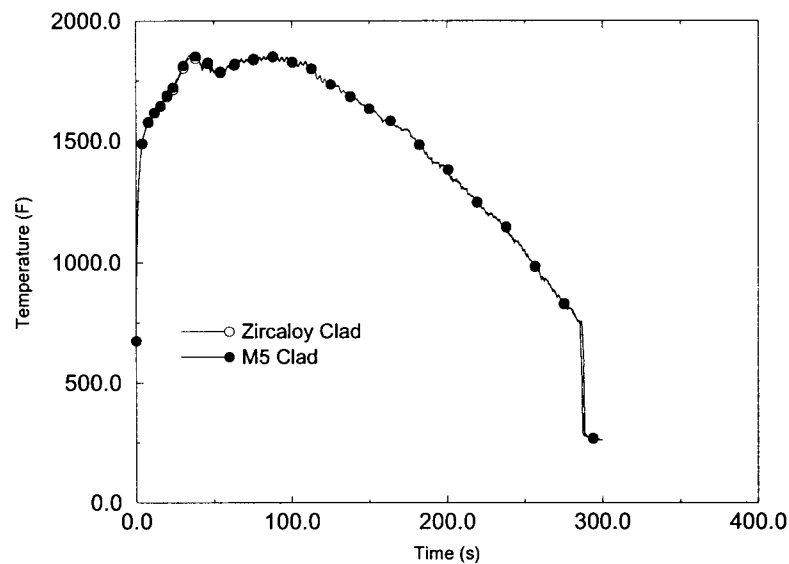


Figure E.4.2 M5 PCT and Zircaloy PCT from the Limiting PCT Calculation

E.5 References

- E.1. BAW-10227P-A, *Evaluation of Advanced Cladding and Structural Material (M5) in PWR Reactor Fuel*, Framatome Cogema Fuels, February 2000.
- E.2. BAW-10231P-A, *COPERNIC Fuel Rod Design Computer Code*, Framatome Cogema Fuels. (Note: the SER was issued on April 18th 2002 but the approved document has not yet been released)
- E.3. EMF-1557(P) Rev. 4, *RODEX3A: Theory and Users Manual*, May 2001 (Rev. 5 is pending).
- E.4. ANF-90-145(P)(A) Vols. I and II, Rev. 0, including Supplement 1, *RODEX3 Fuel Rod Thermal-Mechanical Response Evaluation Model*, April 1992.
- E.5. FTG-38-1287806-00(P), "Fuel Materials Manual Basic Properties of M5 Cladding Tube," FTG, August 1999.
- E.6. EMF-2100(P) Revision 4, *S-RELAP5 Models and Correlation Code Manual*, Framatome ANP Richland, Inc, May 2001.

- E.7. J. V. Cathcart, et. Al., *Reaction Rate Studies, IV, Zirconium Metal-Water Oxidation Kinetics*, ORNL/NUREG-17, August 1977.
- E.8. FTG- 57-1210849-00P, "CINOG Oxidation and Quench Embrittlement Results," FTG, October 1997.
- E.9. EMF-2054(P) Revision 2, *Code Input Development Guidelines for Realistic Large Break LOCA Analysis of a Pressurized Water Reactor*, Framatome ANP Richland, Inc., July 2001.

Revised Pages

These pages were revised in content as a result of NRC review.
Pages that were changed due to renumbering of pages or tables
and figures are not shown here.

the realistic LBLOCA event. Actual NPP operating conditions and typical technical specifications were assessed to identify allowed operating conditions. Sensitivity studies were performed using the selected NPP model to determine those parameters that impact the realistic LBLOCA event. For the most important parameters additional plant data were obtained, where available, so that actual operational data distributions could be determined.

[

] The identification of the parameters and the results of the parameter studies are provided in Tables 5.1-5.4 and Section 5.1.

The methodology for determination of the combined biases and uncertainties and the development of a final statement of probability for the limiting criteria are addressed in Section 5.2. To perform these last two CSAU steps, [

]

[

] A licensing analysis for a 3-loop (W) designed plant is provided in Reference 16. Section 5.4 provides the final statement of overall conformance to the licensing criteria.

measured temperatures below the 15-in elevation, much greater than the measurements from 15-in to 44-in elevation, and much lower than measurements above the 44-in elevation. The comparison can be considered acceptable because the calculated temperature trends followed the data trends, although the magnitudes did not compare well, and the calculated temperatures were overpredicted for the high power region. The highest PCT of 942 K (1236 F) was measured at the 15-in elevation while the calculated PCT was 1006 K (1351 F).

4.3.2.1.5 LOFT Test L2-5 Assessment

Test L2-5 was the third LBLOCA test conducted in the LOFT facility in which the reactor core power provided the primary heat source. The test represented a hypothetical cold leg guillotine break that simulated a double-ended, offset, shear break in a commercial (1000 MWe) 4-loop PWR. The test was initiated at 75% thermal power (36 MWt) and a 12.22 kW/ft maximum LHGR.

Operation of the LOFT PCPs differs from a typical PWR in that the LOFT pump rotors are electromagnetically coupled to their flywheel system. It is normal during LOFT tests to uncouple the pumps from their flywheels whenever the pump speed falls below 750 rpm (78.54 rad/s). During the L2-5 test, the two PCPs were tripped at 1 second and disconnected from their flywheels. This provided a rapid pump coast down. This operation of the pumps reduced the flow into the vessel to less than the flow to the break, thus preventing an early bottom-up fuel rod rewet. These simulated conditions are more typical of a 3-loop PWR than a 4-loop PWR. LOFT pumps normally coast down while connected to their flywheels that were designed to represent the normal pump coast down of commercial W 4-loop PWRs.

The Test L2-5 HPIS flow is 58% of Test L2-3 HPIS flow and is 75% of Test LP-02-6 HPIS flow because an improper small break HPIS flow condition was inadvertently specified for Test L2-5. The injections of high and low pressure ECCSs were delayed to 23.9 and 37.32 seconds, respectively, to simulate the expected delay in starting up the emergency power diesel generator to run the ECCS.

Before the transient started, the power level in the reactor core was steadily increased, then held at $36 \text{ MW} \pm 1.2 \text{ MW}$ for about 28 hours. This ensured that an appropriate decay heat power level would be obtained once the control rods were inserted into the reactor core. Test conditions before the beginning of the L2-5 test were as follows.

leg and 558.0 K for the hot leg come very close to measured values considering the large error bands quoted for the measured data, namely $554.3 \text{ K} \pm 4.2 \text{ }^{\circ}\text{K}$ for the cold leg and $561.9 \text{ K} \pm 4.3 \text{ }^{\circ}\text{K}$ for the hot leg. The desired steady-state conditions were successfully achieved and the calculation accurately reached the L2-5 test initial conditions.

For the transient calculation, a short steady-state calculation before the break opening is carried out to ensure that the steady-state initial condition is properly maintained when switching from the steady-state input model to the transient simulation. The calculation for this analysis is a simulation of Test L2-5 from 10 seconds before the break initiation at 0 seconds up to 140 seconds. This time interval was chosen because the important phenomena and significant events of Test L2-5 occurred during this period.

The assessment of S-RELAP5 to predict each of the important LOCA phenomena is presented in detail in Reference 5. Figure 4.149 depicts the final comparison of the calculated and measured PCT versus core elevation. In this figure, the PCT is referred to as a maximum cladding surface temperature, either calculated or measured at the various locations, during the LOCA transient history. The comparison generally shows very good agreement and the differences between the calculated and measured PCT in the high power region between 15-in to 44-in elevations are quite small. Calculations and measurements both show a plateau region between the 15-in and 28-in elevations where maximum PCT occurs. The highest PCT of 1105.4 K (1530.1 F) was measured at the 24-in elevation and the calculated PCT was 1106 K (1531 F).

4.3.2.1.6 LOFT LP-02-6 Assessment

LOFT LP-02-6 was the fourth LOFT nuclear powered core LBLOCA test conducted with pressurized nuclear fuel rods and with a specification of minimum U.S. ECC injection rates. The maximum LHGR of 14.87 kW/ft was above the typical technical specifications currently used for licensing analyses of PWR fuel rods with the same approximate pellet diameter used in a 15 x 15 fuel pin array. Test LP-02-6 represented an NRC "design basis accident" test and was supposed to run at 100% power, 50 MWt, but because of questions concerning the integrity of the pressurized fuel rods in the central hot assembly, the power level was reduced to mitigate possible safety problems. LP-02-6 is an important LBLOCA test for code assessment because it addresses the issues relating to safety margins associated with the response of a PWR to the NRC "design basis accident" scenario, including delayed minimum ECC safeguards.

agree quite well and the calculated initial conditions are generally within the uncertainty band of the measured quantities. The calculated initial broken loop temperature of 557.6 K for the cold leg and 558.3 K for the hot leg come very close to measured values considering the large error bands quoted for the measured data, namely $553.0 \text{ K} \pm 6.0 \text{ }^{\circ}\text{K}$ for the cold leg and $560.0 \text{ K} \pm 6.0 \text{ }^{\circ}\text{K}$ for the hot leg. The desired steady-state conditions were achieved and the calculation accurately reached the LP-02-6 test initial conditions.

A short, steady-state calculation before the break opening is carried out to ensure that the steady-state initial condition is properly maintained when switching from the steady-state input model to the transient simulation. The calculation for this analysis is a simulation of Test LP-02-6 from 10 seconds before the break initiation at 0 second up to 140 seconds. This time interval was chosen because the important phenomena and significant events of Test LP-02-6 occurred during this period.

The assessment of S-RELAP5 to predict each of the important LOCA phenomena for LOFT LP-02-6 is presented in detail in Reference 5. Figure 4.150 compares the calculated and measured PCT versus core elevation. This figure refers to the PCT as a maximum cladding surface temperature, either calculated or measured at the various elevations, during the LOCA transient history. The comparison shows that the code overpredicted the measured temperatures except at the low power region near the core exit. The greatest differences between the calculated and measured PCT occur in the high power region between the 15 in and 44 in elevations. The highest PCT of 1104.8 K (1529 F) was measured at the 26-in elevation. The comparison shows that the calculated PCT of 1159.6 K (1627.6 F) is in good agreement with data and conservatively exceeds the measured PCT in the high power core region.

4.3.2.1.7 LOFT Test LP-LB-1 Assessment

The fifth LOFT LOCE, Test LP-LB-1, simulated a hypothetical double-ended cold leg guillotine break initiated from conditions representative of a PWR operating near its licensing limits. The initial core power was near the facility design limit of 50 MWt with maximum LHGR of 15.8 kW/ft. Included in the test's boundary conditions were loss-of-offsite power coincident with the LOCE, a rapid PCP coastdown, and a minimum safeguard ECCS injection assumption from a European PWR. To minimize possible fuel pin damage, all of the fuel rods in the core were initially unpressurized.

From Reference 5, a bias of $11.4^{\circ}\text{K} \pm 16.2^{\circ}\text{K}$ ($20.5^{\circ}\text{F} \pm 29.2^{\circ}\text{F}$) should be applied to the measured PCT to account for the 'fin cooling' effects on the surface mounted thermocouples. Thus, the reportable PCT for LOFT LP-LB-1 is 1284.0 K (1851.5 F).

A steady-state initialization calculation was performed to reach the desired steady-state conditions for initiating the LOCA calculation. The calculated and measured initial conditions agree quite well and the calculated initial conditions are generally within the uncertainty band of the measured quantities. The calculated initial broken loop temperature of 560.0 K for the cold leg and 558.3 K for the hot leg come very close to measured values considering the large error bands quoted for the measured data, namely $552.0 \text{ K} \pm 6.0 \text{ K}$ for the cold leg and $561.0 \text{ K} \pm 6.0 \text{ K}$ for the hot leg. The desired steady-state conditions were achieved and the calculation accurately reached the LP-LB-1 test initial conditions.

A short steady-state calculation before the break opening is carried out to ensure that the steady-state initial condition is properly maintained when switching from the steady-state input model to the transient simulation. The calculation for this analysis is a simulation of Test LP-LB-1 from 10 seconds before the break initiation at 0 second up to 240 seconds. This time interval was chosen because, although most the important phenomena and significant events of Test LP-LB-1 occur before 100 seconds, the quenching of the core occurred much later in the calculation.

The assessment of S-RELAP5 to predict each of the important LOCA phenomena for LOFT test LP-LB-1 is presented in detail in Reference 5. Figure 4.151 compares the calculated and measured PCT versus core elevation. In this figure, the PCT is referred to as a maximum cladding surface temperature, either calculated or measured at the various elevations, during the LOCA transient history. The comparison shows that S-RELAP5 overpredicted temperatures in the high power region up to the 44-in elevation, and slightly underpredicted temperatures above 44 in. The measured PCT is 1284.0 K (1851.5 °F) at the 24-in elevation. That measurement includes a bias and uncertainty of $11.4^{\circ}\text{K} \pm 16.2^{\circ}\text{K}$ ($20.5^{\circ}\text{F} \pm 29.2^{\circ}\text{F}$) caused by the fin cooling effects on the surface mounted thermocouple. The calculated maximum PCT of 1329 K (1932 F) also occurred at the 24-in core level and is in good agreement with the measured PCT. Based on Figure 4.151, the PCT at any elevation is within approximately 20% of the data, which is reasonable agreement.

with higher flows (54 and 68) the predicted levels are either conservative or in reasonable agreement.

For the UPTF tests, the liquid is separated in the steam generator simulator. For the two tests, the calculated liquid accumulating in the catch tanks is quite conservative (See Figures 4.168 through 4.171).

For the FLECHT-SEASET tests, there is no steam generator. The hot-leg piping terminates in a separator, which has a tank with a pipe in the bottom leading to a drain tank. Figures 4.172 through 4.179 compare the calculated levels in the separator tank and the separator drain tank with the measured levels. Because of the tendency of the model to hold a larger quantity of liquid in the upper plenum initially than would be indicated by measurements (See Section 4.3.3.1.4), the calculated carry-over to the separator is delayed. The bottom line for these figures is that the calculation has the liquid carried over to these tanks arriving slightly later than the measurements would indicate, with the overall carry-over from the calculation being greater. This latter point shows that the liquid entrained and carried over by the hot-leg model is conservative.

4.3.3.1.7 Two Phase Pump Degradation

The pump two phase degradation is addressed in the methodology as a conservative input. Based on the sensitivity study described in Appendix B for a limiting break on both a 3-loop and a 4-loop plant, it is shown that this is not an important phenomenon for the limiting LBLOCA case. The use of the Semiscale two-phase degradation instead of the CE/EPRI two-phase degradation model produced essentially no impact on the 3-loop results and only an 18 F (10 K) for the 4-loop plant. However, it was shown that the use of the Semiscale pump degradation curves does provide a conservative bias to the model, so it was adopted as a minor conservatism.

4.3.3.1.8 Pump Differential Pressure Loss

The pump differential pressure loss is addressed in the methodology strictly as a best estimate. The S-RELAP5 code has the ability to input the pump specific homologous curves for the NPP being analyzed and this option is used. The homologous curves for the specific NPP pumps are obtained from the utility and, if plant data is available, a pump coast down is modeled to ensure that the curves are consistent with the plant data.

]

The probability density functions are defined by the following two equations. The coefficients for the equations vary depending on whether they are to be applied to FILMBL (low void fraction) or FRHTC (high void fraction).

[

]

[

]

These are given in Table 4.20.

4.3.3.2.6 Tmin

A set of seven FLECHT SEASET tests was used to evaluate the trends in Tmin at low pressure. Quench temperatures improve at higher pressures; hence, a Tmin uncertainty based on low pressure data was expected to bound high pressure data. This was validated with data from ROSA/TPTF, the ORNL/THTF and the Westinghouse G1/G2 tests. Examination of FLECHT SEASET data showed that based on observable conservatisms, only the 3 in/s reflood rate test (Test #31302) was necessary to evaluate a bounding Tmin uncertainty (Reference 5).

From the FLECHT SEASET data and from an evaluation of code uncertainty with regard to how the LBLOCA multiplier relates to Tmin, [

] The uncertainty evaluation has been

demonstrated to be a conservative bounding distribution relative to other datasets. As this value was based solely on data at 40 psia (2.76 bar), a penalty bias was included to cover the possibility of the system pressure falling below this value. The hydrodynamic film instability theory of Berenson was used to develop this pressure bias (Reference 5).

4.3.3.2.7 Break Flow

Break flow is a function of break area and critical flow uncertainty. [

region was tested at full scale in the UPTF, as were the hot legs and the steam generator inlet plenum. The steam generator tubing geometry is prototypic in the CCTF (although the number of tubes is smaller). All these tests in the three facilities collected water carried over from the core under conditions representing the reflood phase of the LBLOCA and all three have additional collapsed liquid level measurements. As presented in Section 4.3, a study on carryover to the steam generator was performed using the CCTF. From that study, a bias on interfacial drag was determined to conservatively bound this phenomenon. The results of the CCTF (with bias), UPTF, and FLECHT-SEASET evaluations indicate that S-RELAP5 overpredicts the entrainment of liquid from the test bundle (Section 5.6 and Reference 5). While each test by itself has some deficiencies in terms of simulating a PWR and in terms of scale, the combination of the three tests provides a substantial basis for evaluating modeling of the drag between the two phases during reflood at full scale.

4.4.2.2.5 Pump Scaling

The S-RELAP5 code has normalized single phase homologous curves for a full scale W reactor coolant pump as code default. The use of full scale data for the pump makes code scaling moot for the pump. These homologous curves are set to applicable values by entering plant specific values for rated head, torque, moment of inertia, etc.. The coastdown of the pump is driven by the torque and moment of inertia of the rotating mass. The torque includes the effects of friction and back EMF (pump torque) and of the loop pressure losses (hydraulic torque). The single phase pump head and torque curves are adjusted for two-phase degradation based on experimental data. The EPRI two-phase degradation data (Reference 54) is based on pumps that are similar to PWR coolant pumps and represent best estimate parameters. However, as a result of the sensitivity studies performed, the Semiscale two-phase degradation data produced a slightly conservative PCT and is used in the RLBLOCA methodology.

4.4.2.2.6 Cold Leg Condensation

Cold leg condensation was evaluated at a scaled EPRI test facility (Reference 55) to determine the accuracy of the calculated interfacial heat transfer between the ECC water and the steam in the cold leg. The principal portion of the test apparatus was the simulated cold leg, which was fabricated from straight pipe with an ID of 10.42 in. Two injection points were provided so that the pipe lengths downstream of the injection point approximated either a typical PWR cold leg scaled down to about one-third or the full length of the cold leg. The cold leg pipe length

Table 4.1 Parameters Perturbed for PIRT Sensitivity Studies (*Continued*)

Table 4.18 Important PIRT Phenomena and Methodology Treatment



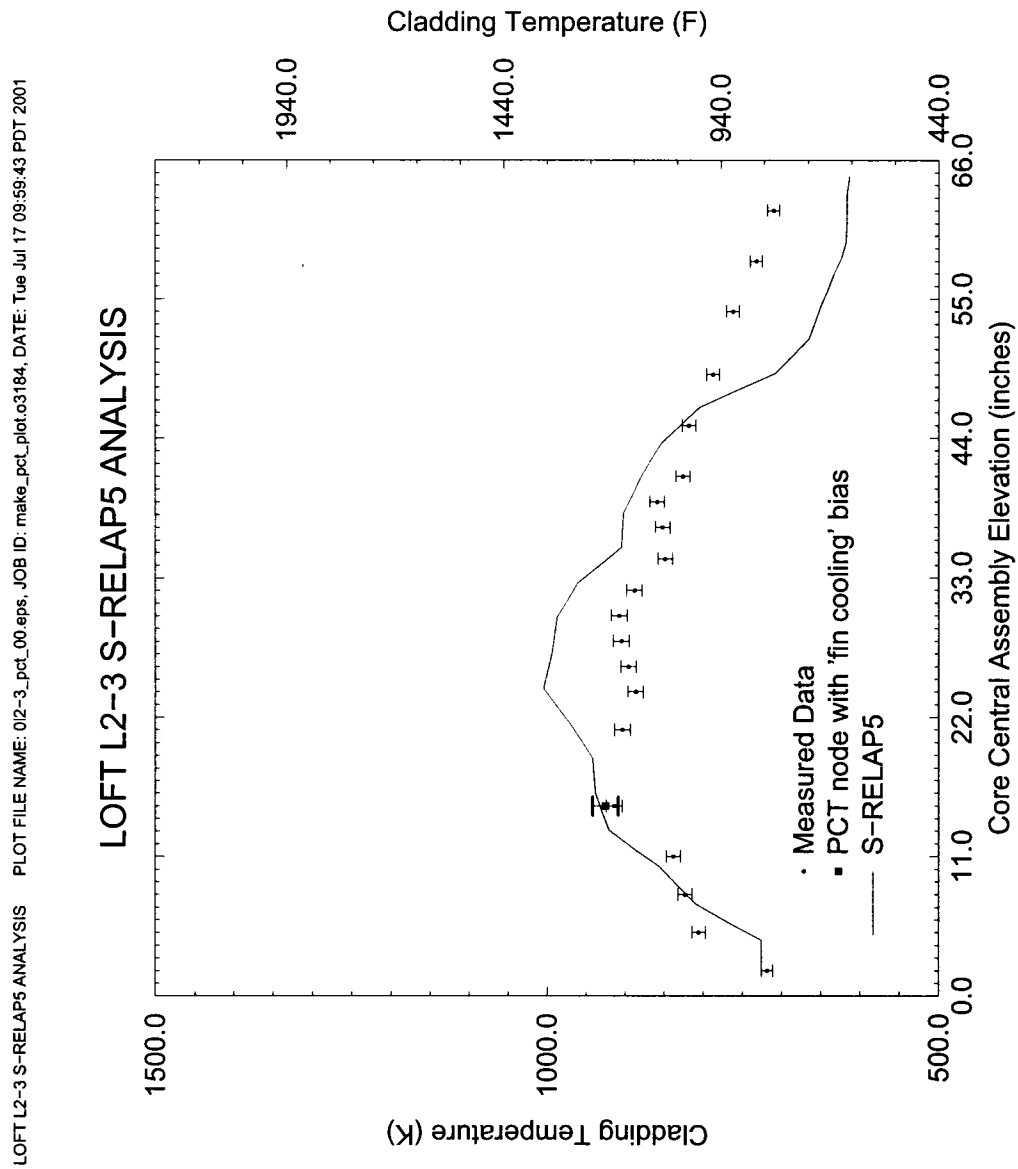


**Figure 4.148 Comparison of PCTs Versus Core Elevations LOFT
Test L2-3 with S-RELAP5**

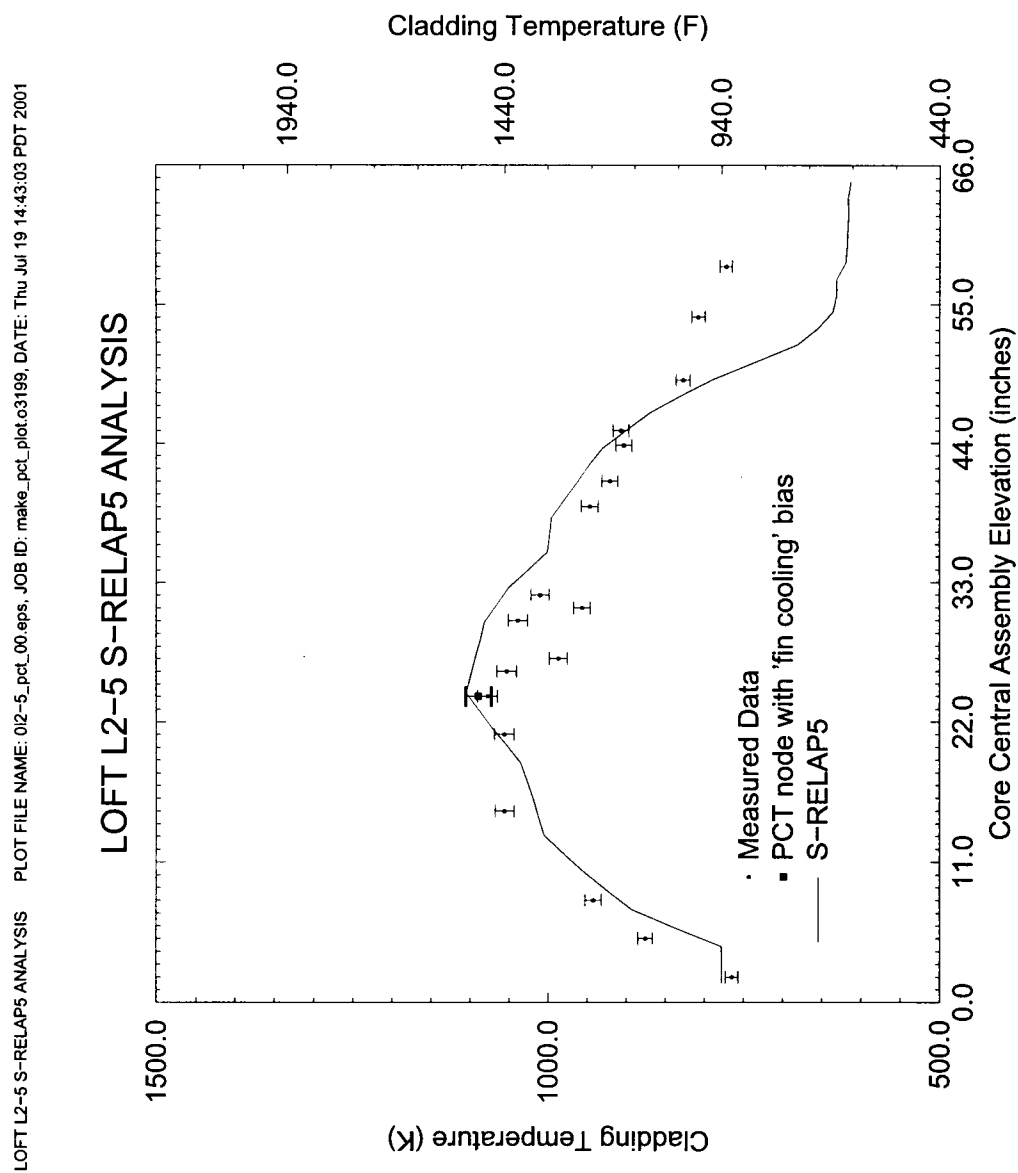


Figure 4.149 Comparison of PCTs Versus Core Elevations LOFT
Test L2-5 with S-RELAP5

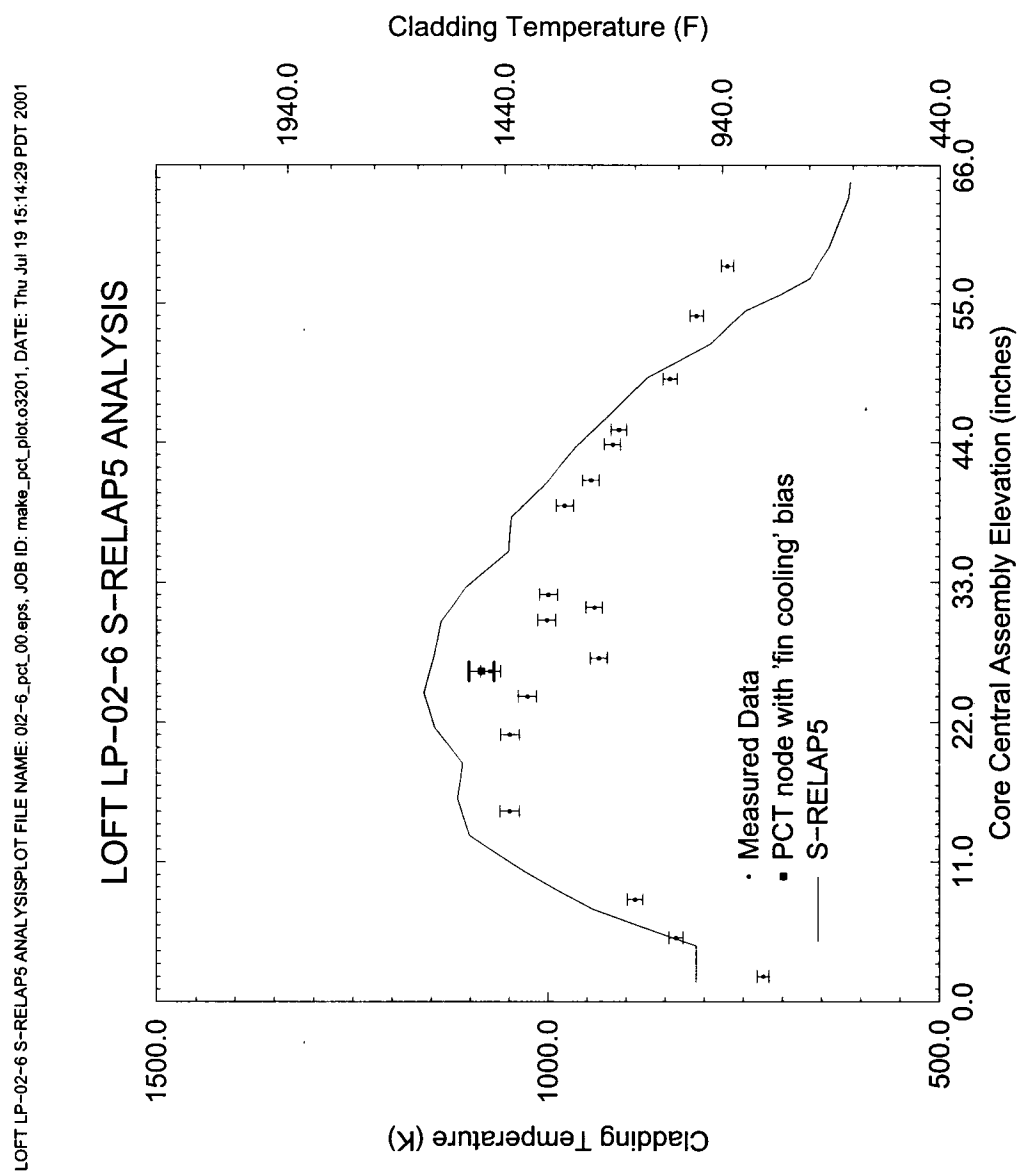


Figure 4.150 LOFT Test LP-02-6 Comparison of PCTs Versus Core Elevations

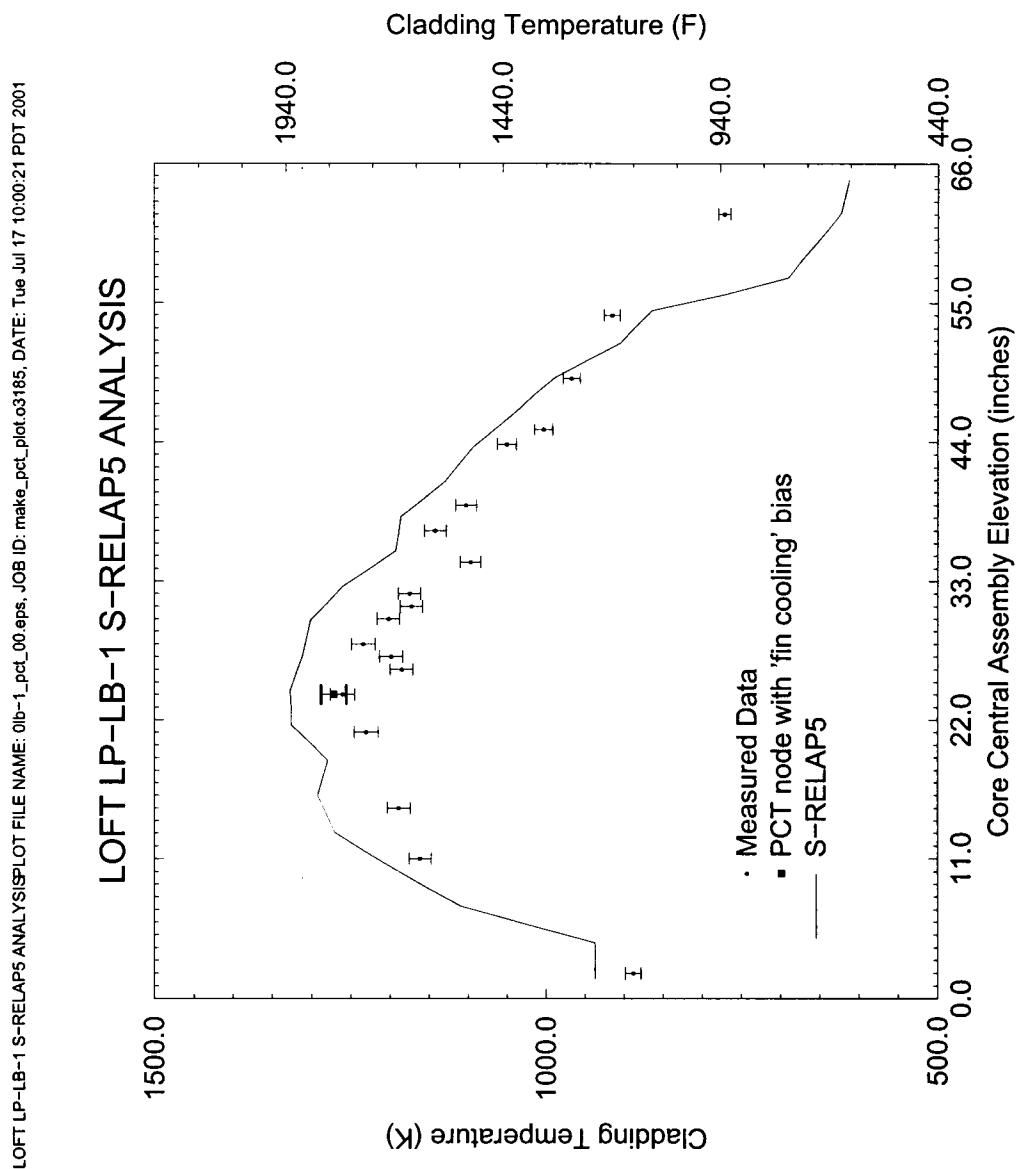


Figure 4.151 LOFT Test LP-LB-1 Comparison of PCTs Versus Core Elevations

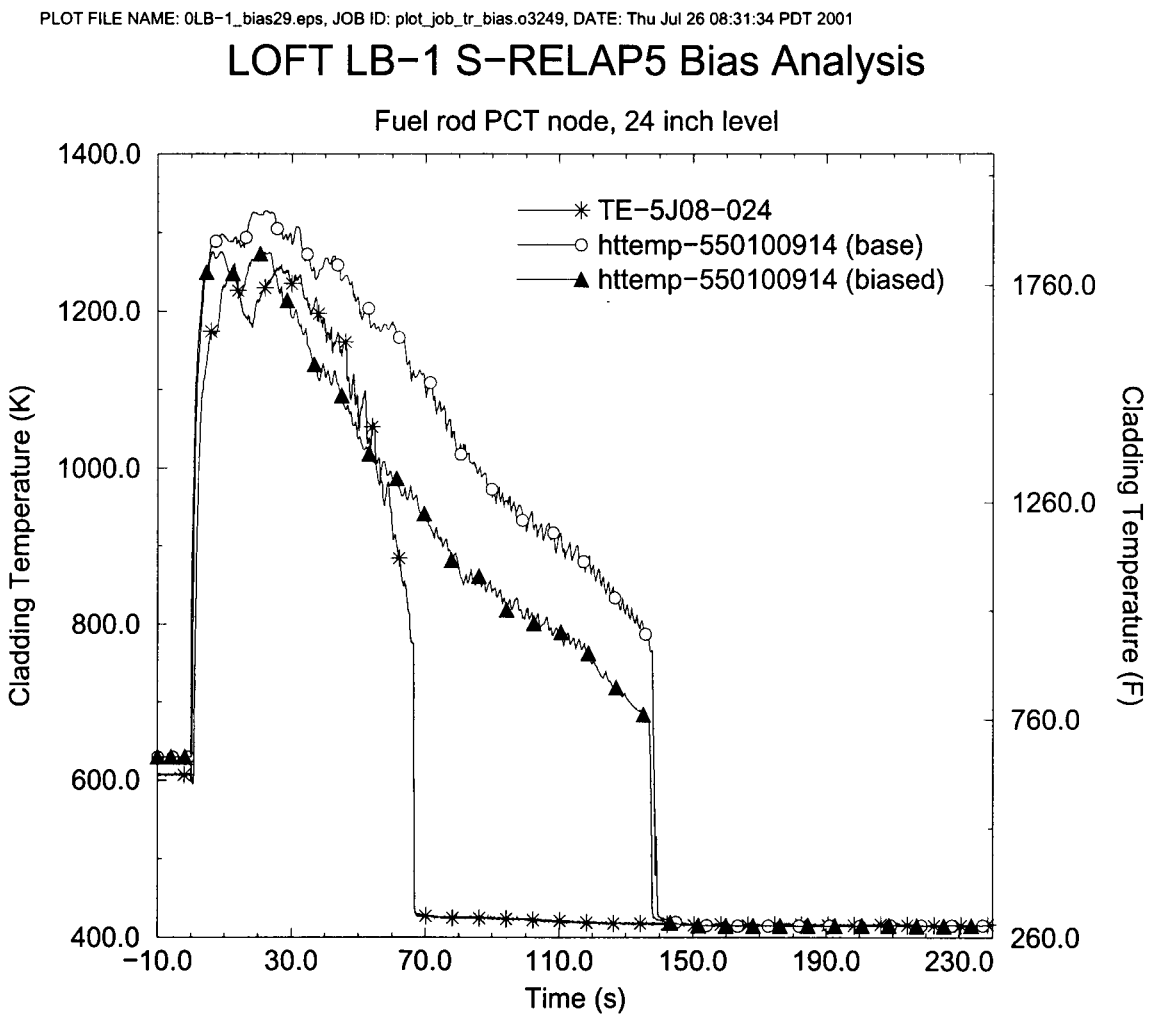


Figure 4.193 LOFT LP-LB-1 Temperatures at Measured PCT Node

LOFT LP-LB-1 S-RELAP5 ANALYSIS PLOT FILE NAME: 0lb-1_pct_00.eps, JOB ID: make_pct_plot_bias.o3250, DATE: Thu Jul 26 16:35:25 PDT 2001

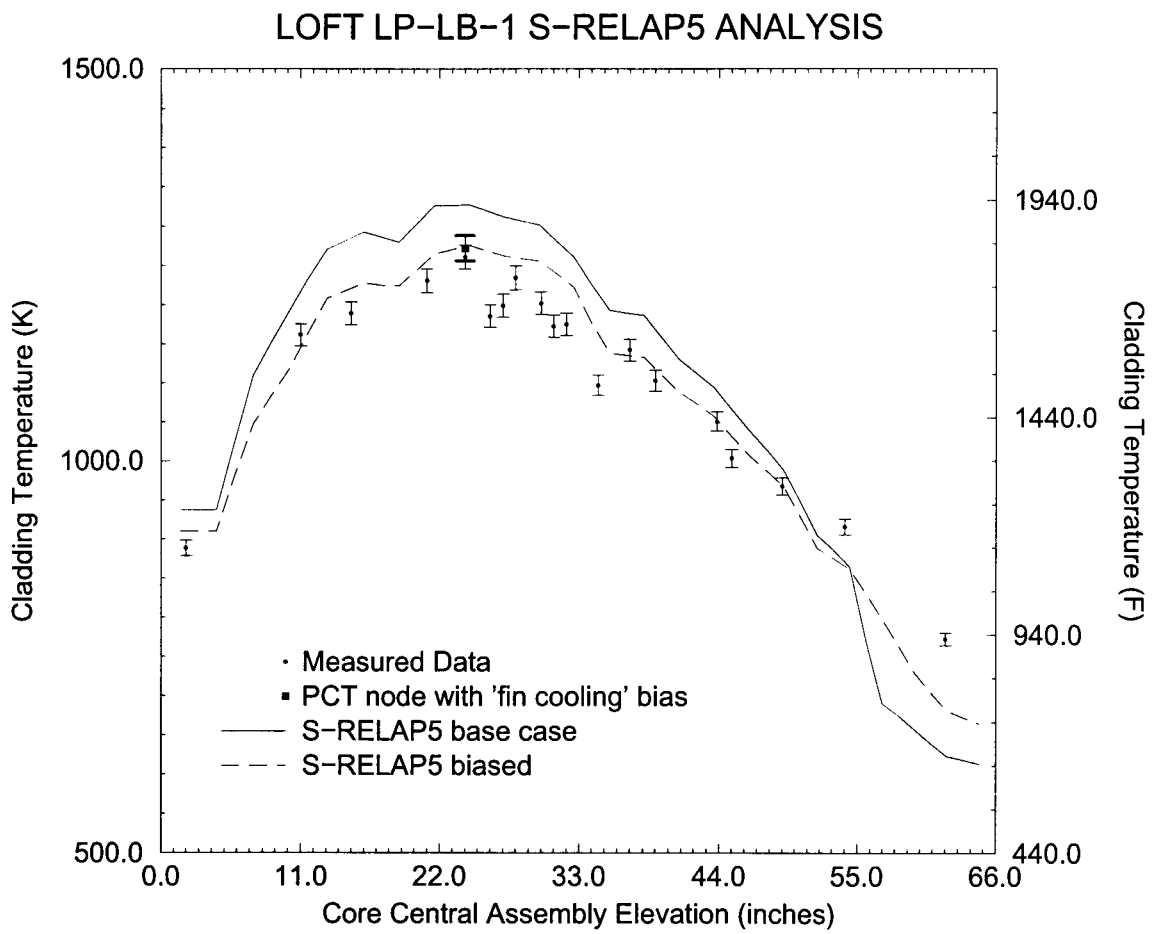


Figure 4.194 LOFT LP-LB-1 PCT Profile

PLOT FILE NAME: 0L2-6_bias29.eps, JOB ID: plot_job_tr_bias.o3248, DATE: Thu Jul 26 08:29:58 PDT 2001

LOFT L2-6 S-RELAP5 Bias Analysis

Fuel rod PCT node, 26 inch level

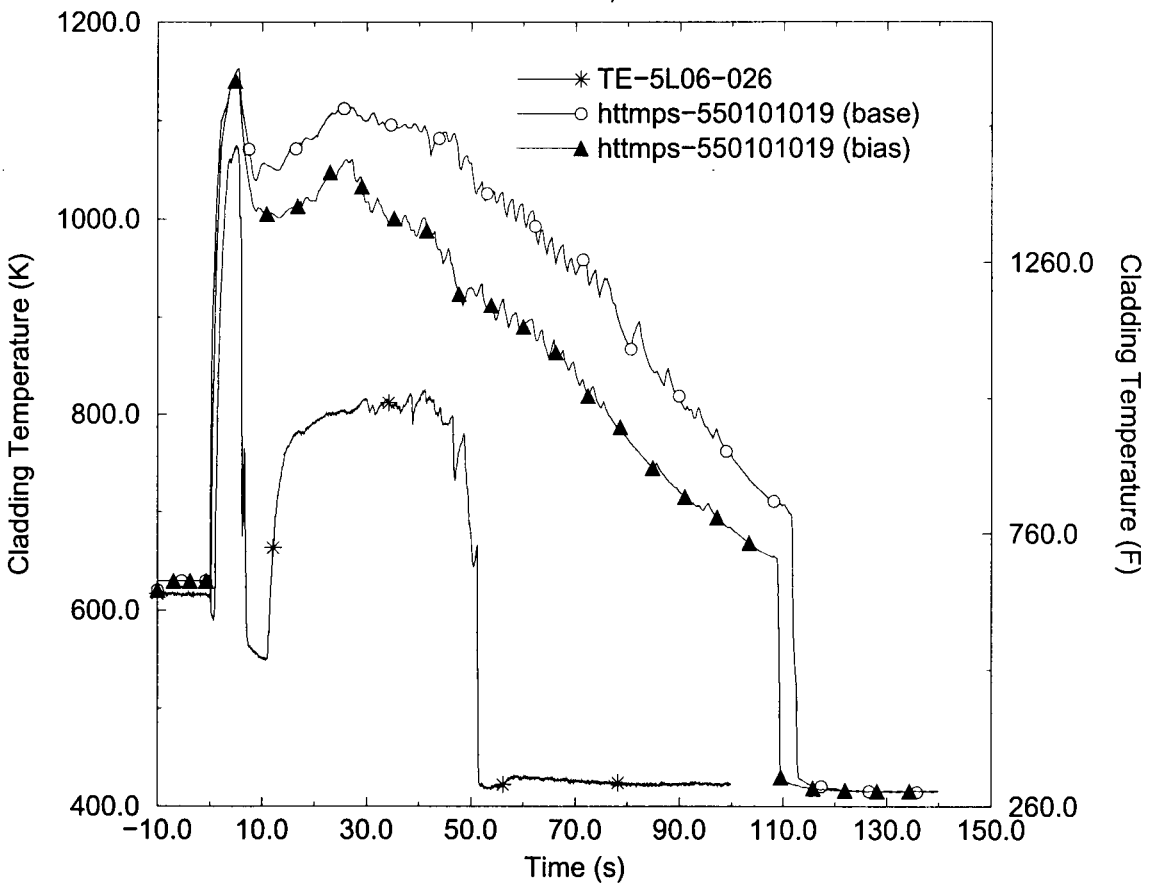


Figure 4.195 LOFT LP-02-6 Temperatures at Measured PCT Node

LOFT LP-02-6 S-RELAP5 ANALYSIS PLOT FILE NAME: 012-6_pct_00.eps, JOB ID: make_pct_plot_bias.o3251, DATE: Thu Jul 26 16:35:49 PDT 2001

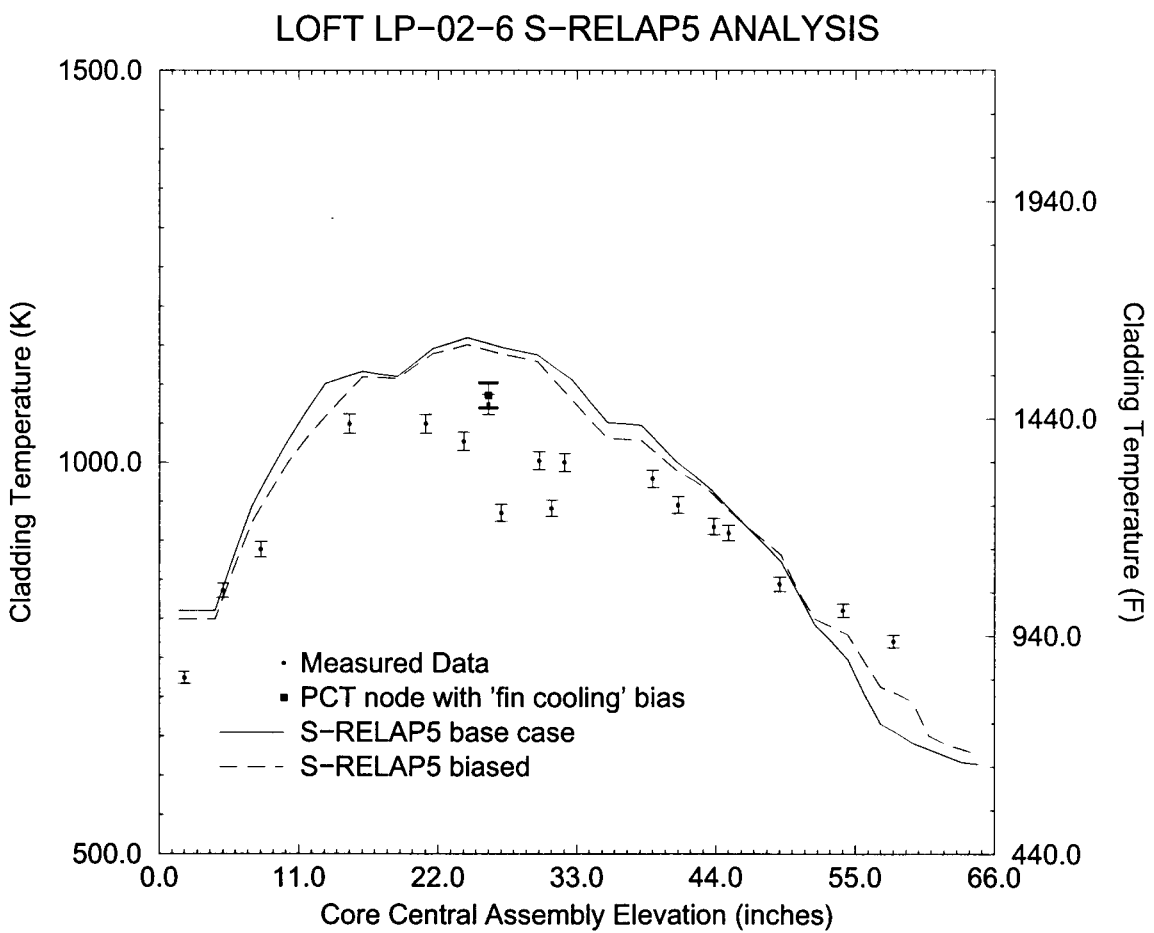


Figure 4.196 LOFT LP-02-6 PCT Profile

PLOT FILE NAME: 0L2-5_bias29.eps, JOB ID: plot_job_tr_bias.o3247, DATE: Thu Jul 26 08:28:09 PDT 2001

LOFT L2-5 S-RELAP5 Bias Analysis

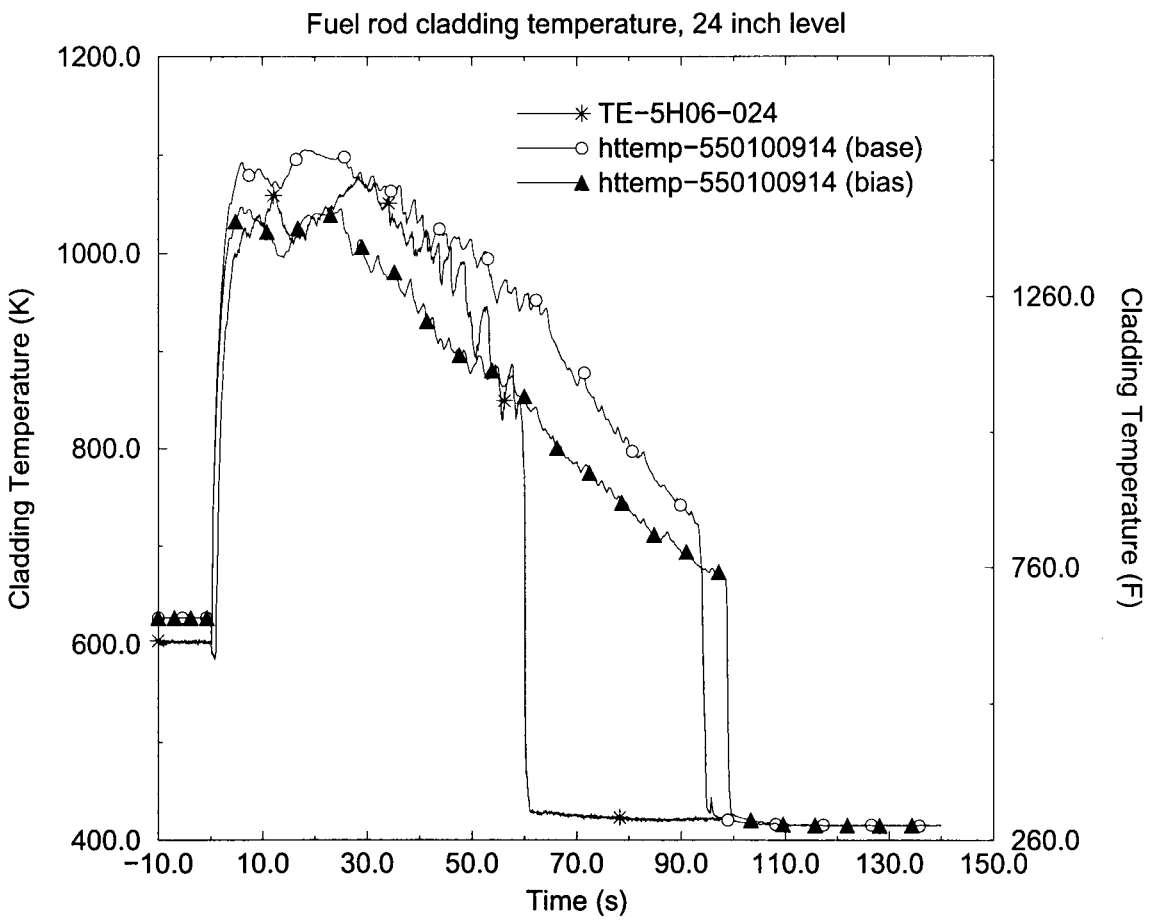


Figure 4.197 LOFT L2-5 Temperatures at Measured PCT Node

LOFT L2-5 S-RELAP5 ANALYSIS PLOT FILE NAME: 012-5_pct_00.eps, JOB ID: make_pct_plot_bias.o3252, DATE: Thu Jul 26 16:36:13 PDT 2001

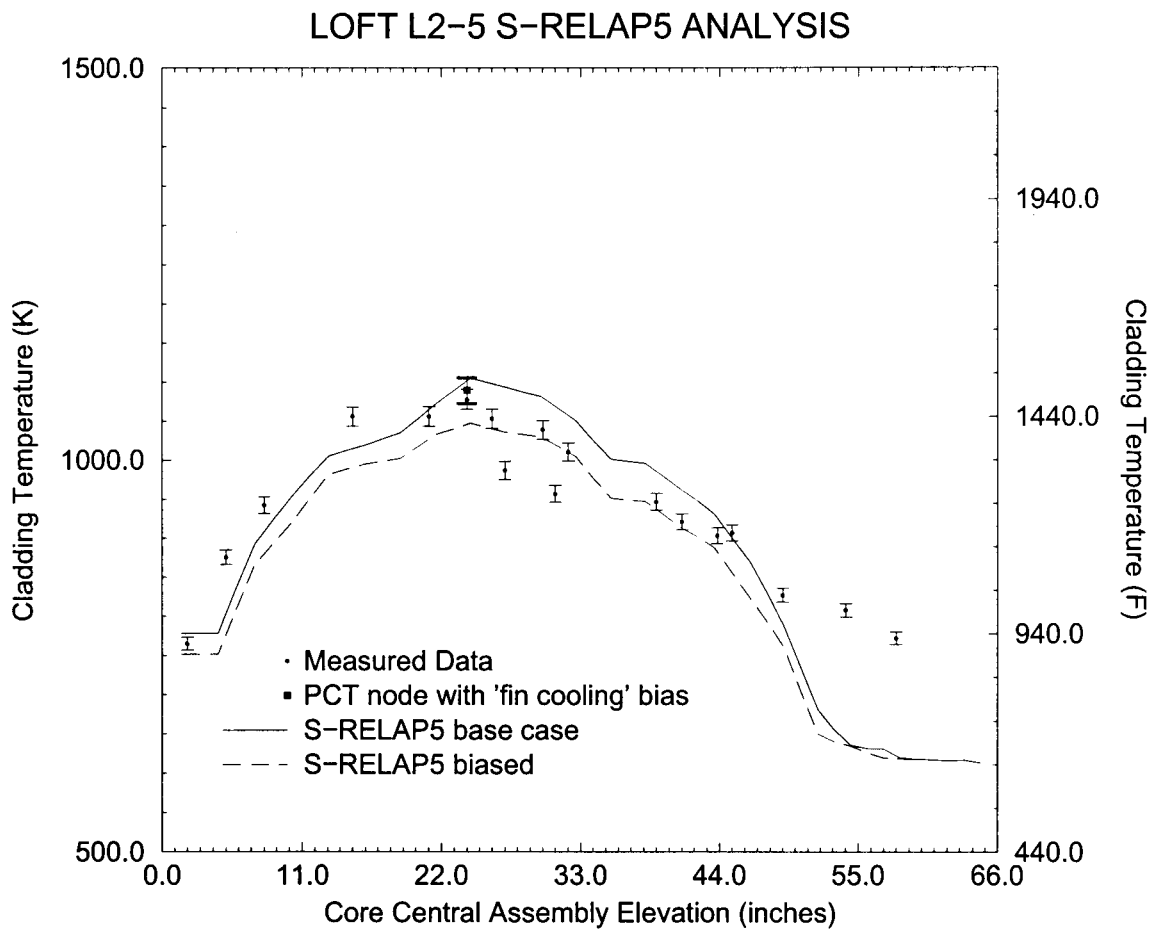


Figure 4.198 LOFT L2-5 PCT Profile

PLOT FILE NAME: 0L2-3_bias28.eps, JOB ID: plot_job_bias.o3246, DATE: Thu Jul 26 08:27:05 PDT 2001

LOFT L2-3 S-RELAP5 Bias Analysis

Fuel rod PCT node, 15 inch level

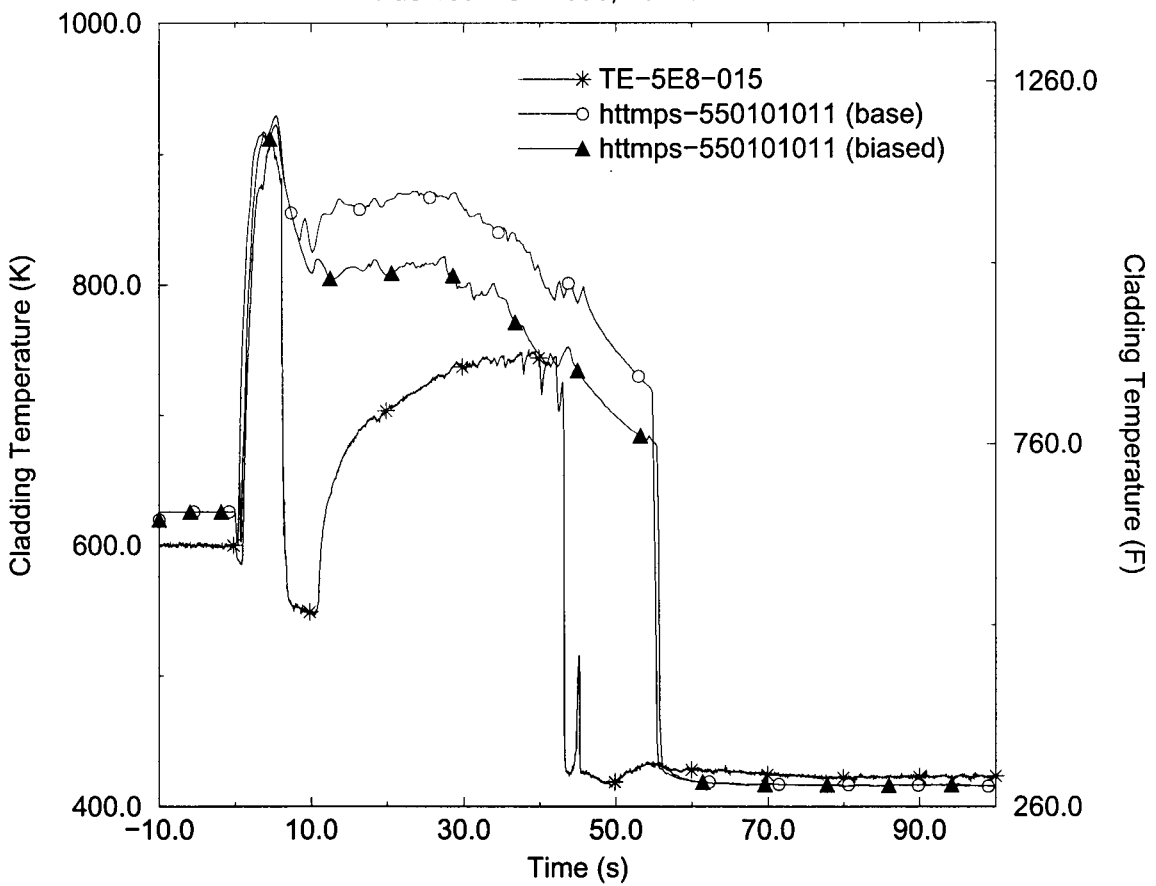


Figure 4.199 LOFT L2-3 Temperatures at Measured PCT Node

PLOT FILE NAME: 0L2-3_bias30.eps, JOB ID: plot_job_bias.o3246, DATE: Thu Jul 26 08:27:05 PDT 2001

LOFT L2-3 S-RELAP5 Bias Analysis

S-RELAP5 PCT node, 24 inch level

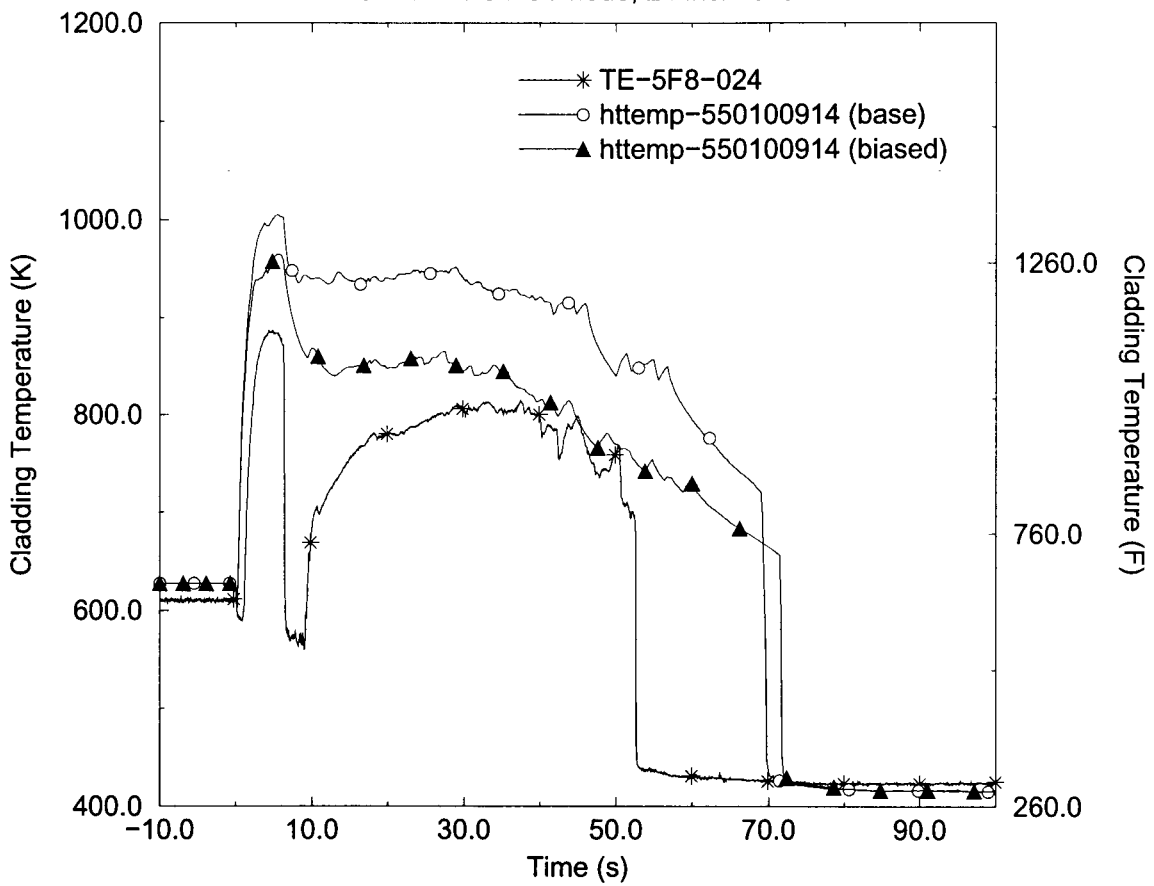


Figure 4.200 LOFT L2-3 Temperatures at Calculated PCT Node

LOFT L2-3 S-RELAP5 ANALYSIS PLOT FILE NAME: 012-3_pct_00.eps, JOB ID: make_pct_plot_bias.o3253, DATE: Thu Jul 26 16:40:49 PDT 2001

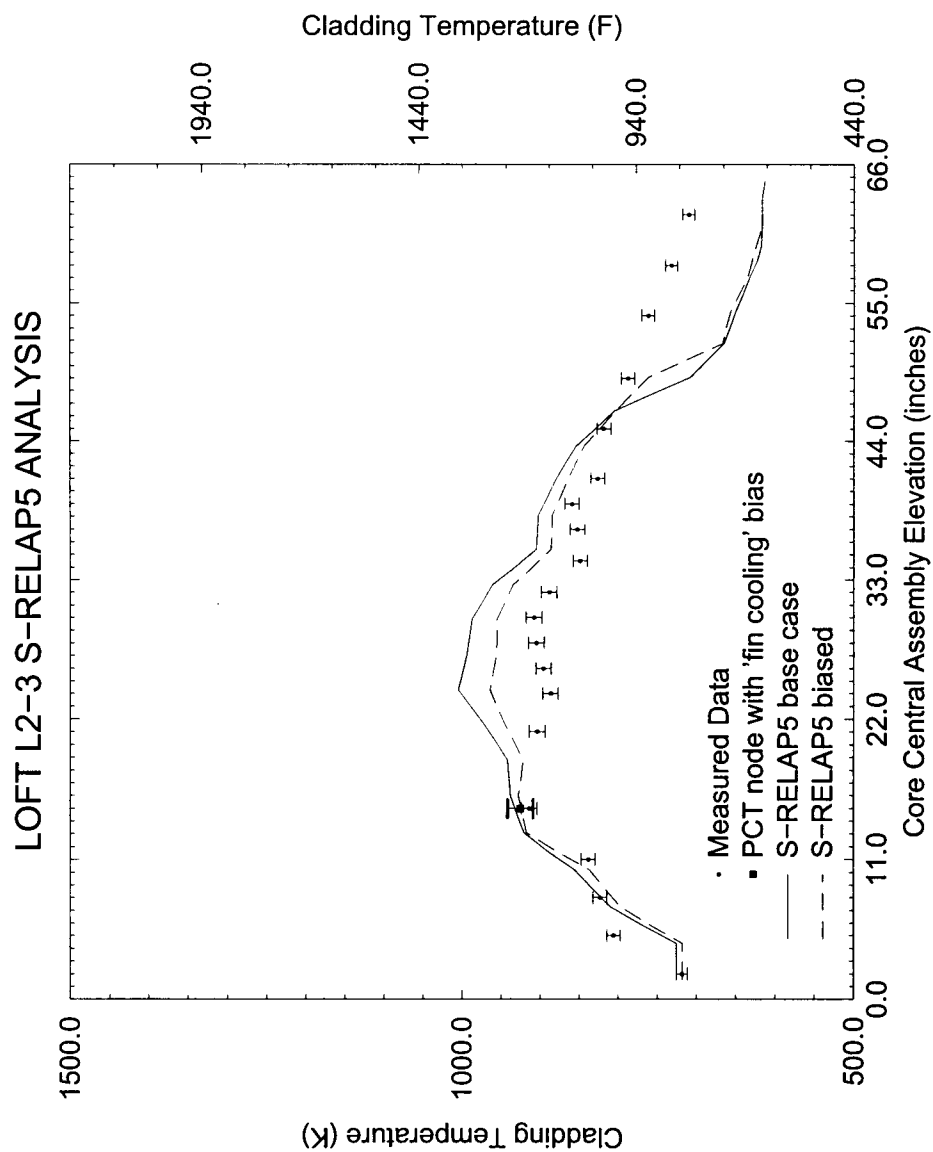


Figure 4.201 LOFT L2-3 PCT Profile

]

[

]

5.2.2 Application of Methodology

The FRA-ANP RLBLOCA methodology is a statistics-based methodology; therefore, the application does not involve the evaluation of different deterministic calculations. [

] The methodology results in a bounding value with 95% probability and 95% confidence in the PCT, total metal water reaction, and total core oxidation.

Application of this methodology relies on two computer codes: RODEX3A and S-RELAP5. All key LBLOCA parameters are calculated from S-RELAP5; RODEX3A is used to generate the initial fuel properties to be used by the fuel performance models in S-RELAP5. Performance of the RLBLOCA calculations relies on three analyst-created code input files describing the fuel, plant thermal-hydraulics, and containment thermal-hydraulics. The fuel model input is processed by the RODEX3A code, which will produce a binary file describing fuel properties. This file will be processed by S-RELAP5 during the steady-state initialization. During steady-state initialization, S-RELAP5 will process only the RODEX3A binary output file and the steady-state plant model input. The LBLOCA calculation is an S-RELAP5 "Restart" calculation. It relies only on the steady-state restart file, the S-RELAP5 LBLOCA transient input file, and the containment model input. The containment model input is similar to the original ICECON code

Figures 5.2 through 5.16 present scatter plots for the more important phenomena/parameters in the analysis. These scatter plots are provided to demonstrate that the methodology does select input which covers the phenomena/parameter ranges and associated distributions. In general, it is difficult to see the PCT dependence of an individual parameter from these scatter plots. This is primarily due to the fact that there are several major parameters and a conservative combination of these parameters is required to obtain the higher values of PCT. Based on this the following paragraphs will concentrate on a discussion of the LBLOCA criteria as addressed by the analysis.

[

]

[

]

[

]

[

]

[

]

[

]

[

]

[

]

[

]

[

]

[

]

[

]

[

]

5.4 ***Determination of Total Uncertainty (CSAU Step 14)***

[

to the reported results. The final results for the 4-loop sample problem can be summarized as follows:

- The 95/95 calculated PCT was 1686 F which compares to the criterion for maximum PCT of 2200°F.
- The 95/95 calculated maximum nodal oxidation was 1.1% which compares to the criterion for maximum nodal oxidation of 17%.
- The 95/95 calculated maximum total oxidation was 0.02% which compares to the criterion for maximum total core oxidation of 1%.

Based on these results, it is concluded that the LBLOCA analysis for the sample W 4-loop plant meets the criteria for the LBLOCA event.

With respect to the identification of the degree of conservatism in the analysis, a comparison can be made to the 50/50 probability values for the PCT, maximum nodal oxidation, and the maximum total core oxidation. This comparison is provided in Table 5.12. As indicated in this table the 50/50 PCT at 1375°F is 311°F less than the 95/95 PCT. The 50/50 total core oxidation at 0.003% is nearly an order of magnitude less than the 95/95 value while the 50/50 maximum nodal oxidation at 0.34% is nearly one fourth that of the 95/95 value.

Table 5.6 Relationship of Uncertainty Parameters to Computer Code Input

In the sensitivity studies the single-phase homologous curves ($H_{1\phi}$) used for all cases are supplied by the default Westinghouse pump data that is coded in S-RELAP5. The model describing two-phase degradation (H_{DEGRAD} and $M(\alpha)$) is entered as tabular input to S-RELAP5. For the base case, the default EPRI-CE data (Reference 59) for two-phase degradation is specified. The sensitivity study examined replacing the EPRI-CE degradation model with the Semiscale degradation model. The degradation model is only applied when two-phase conditions are present in the pump. During the rapid blowdown resulting from a LBLOCA, this period lasts about 10-15s following the break.

The PCT results, relative to the three base cases without accumulator nitrogen, are shown in Figures B.11 - B.13 (extracted for the time period of interest). For the 3-loop plant cases, no sensitivity is evident. This is the expected result, since the break size chosen was selected to minimize the enhanced blowdown heat transfer provided by the pumps. The 4-loop plant case does show an increase in the blowdown peak PCT of about 18 °F (10 K).

The PCT change of 18 °F well within the expected variability of the results which is about 30 °F (see Appendix C). In hindsight the pump degradation does not appear to be as significant of a parameter as originally anticipated. This result is consistent with the original work performed on the CSAU methodology (Reference 4). Since it has been demonstrated that increased pump degradation is slightly conservative, the Semiscale two-phase degradation has been adopted for FRA-ANP RLBLOCA analyses.

The methods used in the application of S-RELAP5 to the large break LOCA are described in Reference D.1. A detailed assessment of this computer code was made through comparisons to experimental data. These assessments were used to develop quantitative estimates of the code's ability to predict key physical phenomena in a PWR large break LOCA. The final step of the best-estimate methodology is to combine all the uncertainties related to the code and plant parameters and estimate the PCT at 95% probability. The steps taken to derive the PCT uncertainty estimate are summarized below:

1. Base Plant Input File Development

First, base RODEX3A and S-RELAP5 input files for the plant (including the containment input file) are developed. Code input development guidelines are applied to ensure that the model nodalization is consistent with the model nodalization used in the code validation (Reference D.3).

2. Sampled Case Development

The non-parametric statistical approach requires that many "sampled" cases be created and processed. For every set of input created, each "key LOCA parameter" is randomly sampled over a range established through code uncertainty assessment or expected operating limits (provided by plant technical specifications or data). Those parameters considered "key LOCA parameters" are listed in Table D.3.1. This list includes both parameters related to LOCA phenomena (based on the PIRT provided in Reference D.1) and to plant operating parameters.

3. Determination of Adequacy of ECCS

The RLBLOCA methodology uses a non-parametric statistical approach to determine values of PCT, total oxidation, and total hydrogen at the 95% probability level with 95% confidence. The adequacy of the ECCS is demonstrated when these results satisfy the criteria set forth in D.3.

D.3.3 Plant Description and Summary of Analysis Parameters

The plant analysis presented in this appendix is a Westinghouse designed pressurized water reactor (PWR), which has three loops, each with a hot leg, a U-tube steam generator, and a cold leg with a RCP. The RCS also includes one pressurizer. The ECCS includes one

accumulator/LPSI and one HPSI injection path per RCS loop. The HPSI and LPSI feed into common headers which are connected to the accumulator lines.

The S-RELAP5 model explicitly describes the RCS, reactor vessel, pressurizer, and ECCS back to the common LPSI header and accumulators. This model also describes the secondary-side steam generator that is instantaneously isolated (closed MSIV and feedwater trip) at the time of the break. A symmetric steam generator tube plugging level up to 10% per steam generator was assumed.

As described in the FRA-ANP RLBLOCA methodology, many parameters associated with LBLOCA phenomenological uncertainties and plant operation ranges are sampled. A summary of those parameters sampled is given in Table D.3.1. The LBLOCA phenomenological uncertainties are provided in Reference D.1. Values for process or operational parameters, including ranges of sampled process parameters, and fuel design parameters used in the analysis are given in Table D.3.2. Plant data is analyzed to develop uncertainties for the process parameters sampled in the analyses. Table D.3.3 presents a summary of the uncertainties used in the analyses. Two parameters (refueling water storage tank (RWST) temperature and diesel start time) are set at a conservative bounding values for all calculations. Where applicable, the sampled parameter ranges are based on technical specification limits. Plant data are used to define range boundaries for loop flow (high end) and containment temperature (low end).

D.3.4 Realistic Large Break LOCA Results

A set of fifty-nine calculations were performed sampling the parameters listed in Table D.3.1. The limiting PCT case (1853 °F) was number 41, which is characterized in Table D.2.1 and Table D.3.4. The limiting maximum oxidation (1.49 %) and total oxidation (0.045 %) results came from cases 16 and 27. These calculations are characterized in Tables D.3.5 and D.3.6. The fraction of total hydrogen generated was not directly calculated; however, it is conservatively bounded by the calculated total percent oxidation which is well below the 1 percent limit. A nominal 50/50 PCT case was identified as case 24. The nominal PCT is 1500 °F. This result can be used to quantify the relative conservatism in the 95/95 result. In this analysis, it is 353 °F.

The hot fuel rod results, event times and analysis plots for the limiting PCT case are shown in Table D.3.4, Table D.3.7, and in Figures D.3.1 through D.3.16. Figure D.3.1 shows linear scatter plots of the key parameters sampled for the 59 calculations. Parameter labels appear to the left of each individual plot. These figures show the parameter ranges used in the analysis. Figures D.3.2 and D.3.3 show PCT scatter plots vs. the time of PCT and vs. break size from the 59 calculations. Figure D.3.4 shows the maximum oxidation vs. PCT for the 59 calculations. Figures D.3.5 through D.3.16 show key parameters from the S-RELAP5 calculation. Figure D.3.5 is the plot of PCT independent of elevation. It includes an overlay plot of the elevation of the PCT location.

Distribution

E-mail

J. S. Holm